RADIATION SHIELDING

Analysis and Design Principles As Applied to Nuclear Defense Planning

TR 40
NOVEMBER 1966

TR 40
NOVEMBER 1966

RADIATION SHIELDING

Analysis and Design Principles
As Applied to Nuclear Defense Planning

Prepared by

OFFICE OF CIVIL DEFENSE

and

KANSAS STATE UNIVERSITY

For sale by the Superintendent of Documents, U.S. Government Printing Office
Washington, D.C., 20402 - Price $6

RADIATION SHIELDING

Analysis and Design Principles
As Applied to Nuclear Defense Planning

•

WILLIAM R. KIMEL, Editor-in-Chief
Professor and Head, Dept. of Nuclear Engineering, Kansas State University

•

List of Contributors

L.V. SPENCER, Professor of Physics, Dep't. of Mathematics & Physics
Ottawa University, Ottawa, Kansas
and Consultant, National Bureau of Standards

JOHN C. LeDOUX, Cdr. U.S. Navy Civil Engineer Corps

ARTHUR B. CHILTON, Professor of Civil Engineering and of Nuclear Engineering
University of Illinois, Urbana, Illinois

CHARLES EISENHAUER, National Bureau of Standards
U.S. Dep't. of Commerce, Wash. D.C.

ACKNOWLEDGEMENT

This publication is a compilation of lectures and papers presented at the Kansas State University Summer Institutes on Fundamental Radiation Shielding Problems as Applied to Nuclear Defense Planning. These institutes were conducted during the summers of 1962, 1963, and 1965 under the direction of Dr. William R. Kimel, Professor and Head, Department of Nuclear Engineering, Kansas State University. The institues formed a part of the Faculty Development Program initiated by the Office of Civil Defense to acquaint college and university faculty members with the analysis and design principles of radiation shielding.

I am indebted to the authors of these papers who spent much valuable time in preparing their material for publication. A special debt of gratitude, however, is owed to members and former members of my staff (Mr. Robert Berne, AIA; Cdr. Jack C. LeDoux, PE; Mr. Flory J. Tamanini, PE; Mr. Henry S. Wakabayashi, PE; and Mr. Seymour Wengrovitz, PE) who were instrumental in overcoming innumerable difficulties during the first few years of operation to make the Summer Institute Program a success.

James E. Roembke, Director
Architectural & Engineering
Services Division
Office of Civil Defense
October 12, 1966

RADIATION SHIELDING

Analysis and Design Principles

As Applied to Nuclear Defense Planning

VOL. I: GAMMA RAY SHIELDING THEORY

L. V. Spencer

VOL. II: ENGINEERING ANALYSIS - BASIS AND METHODS

J. C. LeDoux

VOL. III: ENGINEERING ANALYSIS - BASIS AND METHODS

J. C. LeDoux

VOL. IV: EXPERIMENTAL PROGRAM

Arthur B. Chilton, et al.

VOL. V: DEVELOPMENT OF THE ENGINEERING METHOD AND SOME SIMPLIFIED METHODS OF STRUCTURE SHIELDING ANALYSIS

Charles Eisenhauer

This set of volumes was prepared in connection with the 1962, 1963 and 1965 Kansas State University - Office of Civil Defense, Summer Institutes on Fundamental Radiation Shielding Problems as Applied to Nuclear Defense Planning.

Vol. I

GAMMA RAY SHIELDING THEORY

L. V. Spencer

National Bureau of Standards*

*Work partly done at Ottawa University, Ottawa, Kansas

CONTENTS

1. Introductry Comments

This manuscript summarizes 40 or more lectures on gamma ray penetration theory presented in the summers of 1962, 1963, and 1965 at the Summer Institute on Fundamental Radiation Shielding Problems as Applied to Nuclear Defense Planning, held at Kansas State University.

a) Fallout radiation shielding. At present radiation shielding, as an engineering and research specialty, has four major subdivisions:

reactor shielding,

space shielding,

accelerator shielding, and

weapons shielding.

Each shielding area has its own flavor and its own peculiar problems. But the extent to which the mathematical methods and experimental techniques are shared among them is noteworthy; and the emergence of a shielding specialty under the more general heading of "nuclear engineering" is a direct result.

Our attention is here directed to shielding against the gamma rays from radioactive fallout, which is only part of "weapons shielding." But the mathematical methods are largely applicable to problems of shielding against gamma rays and neutrons given off initially in a nuclear explosion. Further,

the carry-over into problems of shielding against the radiations of reactors, accelerators, and outer space is substantial.

In the study of weapons shielding problems, a very serious question has always been the extent to which we can avoid problems of classified information. Three devices have made this possible in fallout radiation studies: First, by concentrating on general methods rather than specific devices, we avoid weapons design information. The feasibility of this traces to the dominant influence of the delayed gamma radiation produced by mixed fission products, which radiation is relatively independent of the design of nuclear weapons. Second, we study schematized problems primarily, in which the source and shield configurations have been standardized. We do not, for example, concern ourselves with the weapons phenomenology, the mechanics of the transportation of debris, or with the time sequence which precedes the positioning of a radiation source. In the third place, we try to avoid questions of absolute intensity by discussing shielding in relative terms, that is, relative to a standard "unshielded detector."

Other questions than these are not ignored, but limitation of our attention in this way still leaves a vast area for work in which problems of classified data are minor.

I should probably state at the outset two or three of the assumptions fundamental to most existing studies of shielding against fallout gamma rays. We assume that horizontal variations in the amount of fallout are negligible. Further, surfaces are assumed to receive an amount of fallout

proportional to the horizontal projection of their area. Thus, the two roofs in the sketch of Fig. I-1.1, having quite different exposed areas but the same area in horizontal projection, would receive the same total amount of fallout.

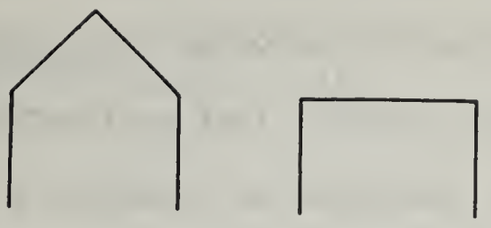

Fig. I-1.1. Structures occupying equal area horizontally.

We assume that fallout is not suspended in trees and shrubs. There is some experimental and a little theoretical information supporting this assumption when exposed surfaces are dry.[26] I know of no information on this subject should the surfaces be wet.

Regarding the standard "unshielded detector" in terms of which we measure protection, we use the exposure[21] measured by a detector three feet from an infinite source plane in an infinite, homogeneous medium of air at standard temperature and pressure. Such a standard turns out to be a fairly good approximation to the exposure measured at waist level above the ground in a large open field supporting a similar radiation source.[36]

b) Gamma Ray Penetration Theory. Part of the following material has to do directly with gamma ray penetration and part deals with related numerical methods. The latter is intended to relieve the penetration theory of digressions into mathematical topics. I am assuming an audience which is, say, mid-physics graduate school level of sophistication in mathematics. Some of this supplementary material will be unfamiliar and not easily referenced. I have included a summary of lecture material on Monte

Carlo methods given at the Summer Institute by Dr. Martin J. Berger. It is a brief, but comparatively complete, introduction to the subject.

The theory of gamma ray penetration as presented here is patterned after the monograph Penetration and Diffusion of X Rays, by Fano, Spencer and Berger.[15] That publication contains many things not directly pertinent to questions of radiation protection so that a shortened discussion, directed to radiation shielding but covering much of the same ground, may be very useful. Some of the material to be presented is in Ref. 15 only by implication, and we present here the only detailed exposition of which I am aware.

A second general reference for these lectures is the NBS Monograph on Structure Shielding against Fallout Radiation from Nuclear Weapons.[36] This is not a presentation of theory, but a summary application of theoretical data to elementary shielding configurations. The penetration theory given here includes methods used to calculate the data of that publication.

Other texts giving the general theory of radiation penetration are, for example, Goldstein,[48] Weinberg and Wigner,[44] and Davison.[49]

A. INGREDIENTS OF GAMMA RAY TRANSPORT THEORY

2. Radiation Sources*

Gamma rays from radioactive fallout, the so-called "fallout gamma rays," originate in two ways: Fission fragments remain radioactive; these ordinarily produce the dominant part of fallout radiation. Alternately, fallout gamma rays may be produced by nuclei from the bomb or nearby ground which have captured neutrons. We plan to say little about the latter case of neutron induced activities: Experimentation indicates that three isotopes tend to be of greatest importance.[28] Mn^{56} gives a significant contribution within a few hours of detonation. Na^{24} may be significant during the period from half a day to one or two days after detonation. Np^{239}, perhaps the most important though of relatively low spectral energy, is apt to be significant several days following detonation.

The fission fragments from a nuclear explosion are distributed according to a well-known type of yield curve: The abscissa on this sketch gives atomic number, which measures the nuclear charge, and the vertical axis gives relative numbers of fragments with a giv-

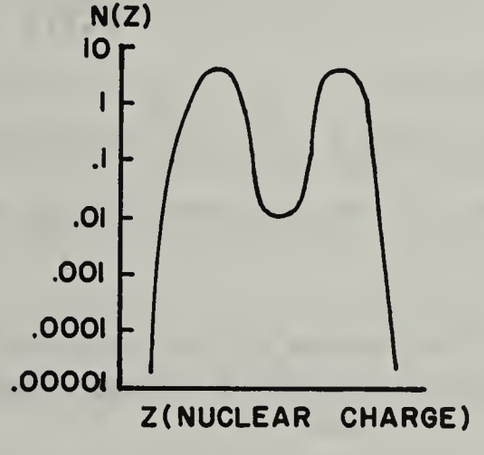

Fig. I-2.1. Qualitative sketch of a fission yield curve.

*See, e.g., Ref. 44 for a general discussion of the fission process.

en charge. The two humps include many different nuclear types. Each type of fission-fragment nucleus undergoes a sequence of disintegrations, producing a series of daughter products. Many chains of radioactive nuclei result, which build up and die off with time according to characteristic decay constants.

As a result of decay processes for the many nuclear chains, each starting from a fragment of uranium or plutonium nucleus, there exist at any time t a number of atoms of nuclear charge Z. We will use $N_i(Z,t)$ to indicate this distribution of nuclear types.* It would be proportional to the number of atoms undergoing fission, and $\sum_i N_i(Z,0)$ would be the yield curve of the fission process.

Each nuclear type has a characteristic probability per unit time for emitting photons of discrete energies E_j, which will be designated $p_i(Z,E_j)$. If we then refer to the photon spectrum emitted by the material at time t as $S(E,t)$, a formal expression for this spectrum may be written, namely

$$S(E,t) = \sum_{Z,i,j} N_i(Z,t)\, p_i(Z,E_j)\, \delta(E-E_j), \qquad \text{(I-2.1)}$$

where $\delta(E-E_j)$ is the Dirac function and indicates the concentration of photons at the discrete set of energies E_j.

---

*Each value of the nuclear charge would include nuclei of different masses and different energy states, i.e.,many nuclear types, each designated by a value of i.

Although this formal representation of the spectrum is easily written down, no one has ever, to my knowledge, calculated it in this form. There are literally thousands of lines in the spectrum, and to reduce the representation to manageable size, integrals S_k are calculated over finite energy regions, i. e.,

$$S_k = \int_{E_k}^{E_{k+1}} S(E,t)\, dE = \sum_{Z,i,j} N_i(Z,t)\, p_i(Z,E_j) ,$$

$$E_k \leq E_j < E_{k+1} . \qquad \text{(I-2.2)}$$

Anne Nelms and John Cooper, of NBS, did one of the early calculations of this type for the project which later produced NBS Monograph #42.[32] They used data for $N_i(Z,t)$ from calculations of R. C. Bolles and N. E. Ballou,[5] together with data for $p_i(Z,E_j)$ from a compilation by Carl Miller.[31]

An independent calculation using the same two reference sources has been made by P. J. Dolan,[10] and a more recent calculation of the same type has been made by R. Björnerstedt.[4] This last calculation was based on more recent calculations of $N_i(Z,t)$ and data for $p_i(Z,E_j)$ by the same group in Sweden, and is probably the best available source of information about the spectrum of gamma rays from fission products.

A number of differences between these theoretical spectra should be noted other than the data used in their calculations. Nelms and Cooper used a set of energy "boxes," i. e., E_k values, which are approximately equal in size in the variable log E, rather than E. This reduced the

number of spectral source energies for later penetration calculations to about 24. Both Dolan and Björnerstedt used E_k values equally spaced in E; Dolan used a particularly fine mesh, with well over 100 energy boxes.

One of the problems in determining spectra for fallout gamma rays is "fractionation." Heavier fallout particles reach the ground relatively nearer the burst point, and this has some effect on the distribution of fission products present in the debris at different locations relative to the burst point. Further, some fission product materials do not appear in the debris in the concentration expected. This is because some of the daughter atoms in some of the decay chains are either gaseous or very volatile. The calculations of Nelms and Cooper, as well as those of Dolan, removed some components which were expected or known to be affected in this way. The calculations of Björnerstedt ignored this effect completely. It should be noted that attempts to take fractionation into account represent at best a sort of "shot in the dark." The phenomenon is very complicated, space dependent, and only crudley known.

C. S. Cook has compared experimental fallout spectra with the calculated spectra of Dolan and the spectra of Nelms and Cooper.[7] He concludes that after corrections to take into account Neptunium present in the fallout, the theoretical and experimental spectra have shapes which are generally similar, but that specific differences are too large to be accounted for by known sources of error. He feels that the state of affairs reflects inadequate knowledge about fractionation.

We might express the results of comparisons between different theo-

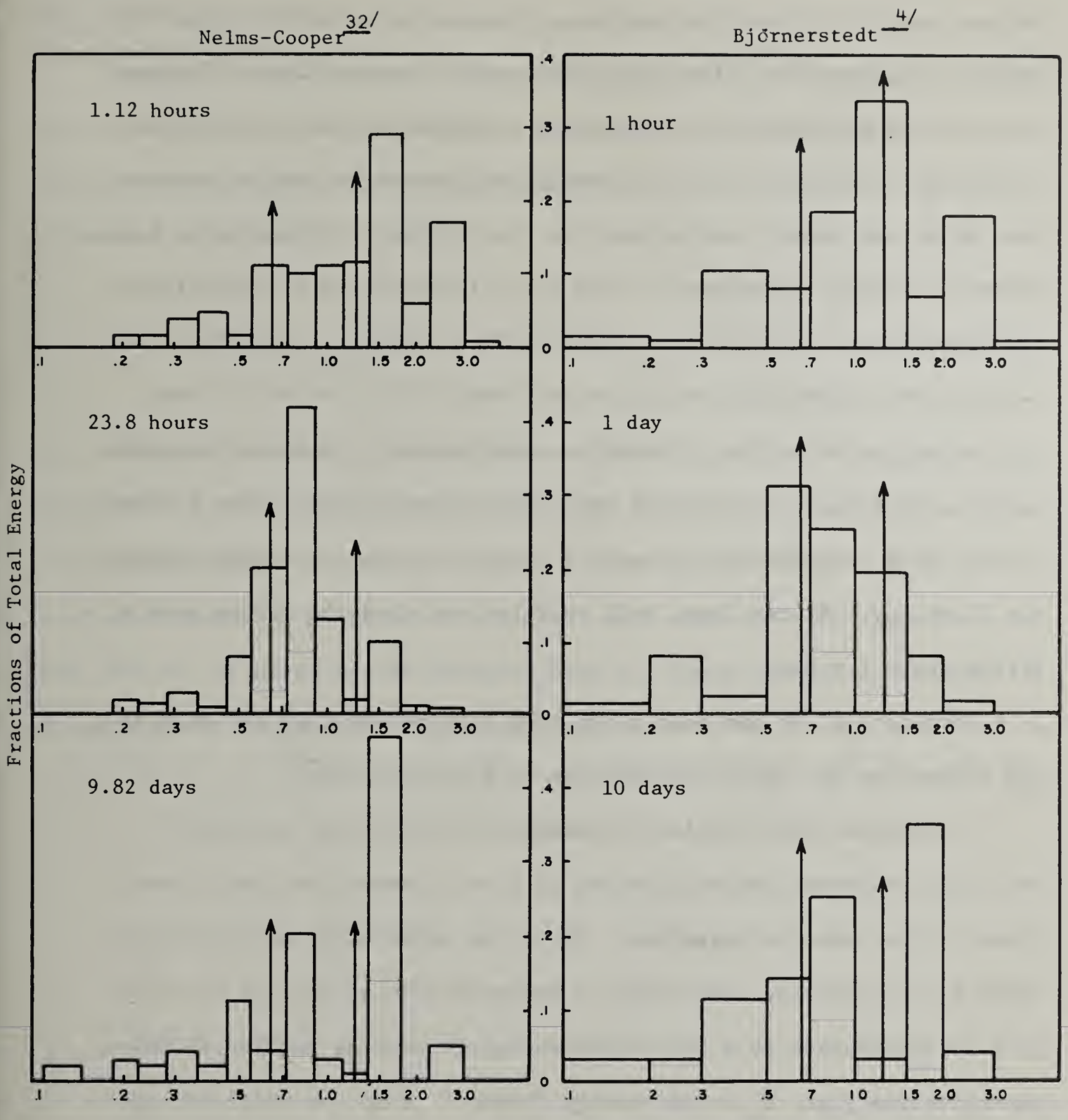

Fig. I-2.2. Comparison of theoretical spectra for gamma rays from fission products at different times after fission. Nelms and Cooper take some account of fractionation. The arrows indicate the positions of Cs-137 and Co-60. The sum of the ordinates for each case adds to unity, so that the ordinates indicate fractions of the total energy.

retical spectra in much the same way. Shapes and trends are generally similar, but specific differences are larger than one likes. To some extent, these differences are traceable to different assumptions about fractionation. In Fig. I-2.2 a comparison is made between a spectrum from Nelms and Cooper, and a spectrum from Björnerstedt which has been chosen to roughly correspond. This will illustrate both similarities and differences which one encounters in these spectra. Note that the 1-hour curves show heavy contributions from a little below 0.5 Mev all the way up to 3.0 Mev. There is a gap above 1.0 Mev which appears in both. The 1-day curves both show heavy contributions below 1.0 Mev, so that both calculations indicate a decrease in photon energy during the first day. At ten days, both calculations show the strong peak a little above 1.5 Mev.

Fortunately, it has been shown that both penetration and scattering properties are rather insensitive to spectral shape.[36]

To conclude this initial discussion, we should say something about the radiation source function as it will enter into our discussions of the transport equation. First, we might note that for calculations we generally assume that a spectrum such as that of Equation (I-2.2) corresponds to a set of monoenergetic sources located at representative energies $\bar{E}_k$ in the energy "boxes." Thus, we write our spectrum in the form

$$S(E,t) = \sum_k S_k \, \delta(E - \bar{E}_k) \quad . \qquad \text{(I-2.3)}$$

Units of $S(E,t)$ might be number of photons/Mev·sec.

Complete specification of a source function requires that the angular distribution of photon emission and the space distribution of the source be given also. This means that a source function will in general be written

$$S(E;\theta,\phi;x,y,z;t) \quad , \tag{I-2.4}$$

with units such as number of photons/Mev·sec·steradian·cm^3. It will correspond to the emission spectrum per unit solid angle along the direction with polar coordinates (θ,ϕ), and per unit volume at the point with cartesian coordinates (x,y,z). Note that the source spectrum $S(E,t)$ is given by the integral over all space and all directions of emission of the function $S(E;\theta,\phi;x,y,z;t)$.

3. Interactions

a) Total Interaction Probabilities. As radiation from a source moves away through the surrounding material, the nature of the penetration process is determined by the interactions which occur, and we next wish to discuss these interactions.

Interactions are chance events. When a gamma ray photon moves through a material, there will be probabilities $p_1, p_2, \ldots,$ that interactions of different types $1,2,\ldots,$ may occur, per unit path length traveled. These probabilities are not correlated, and therefore they may be added to obtain the total probability per unit path length that an interaction of some type occurs. The total probability per unit path length for occurrence of some kind of interaction is usually designated by μ. It depends on the material through which the photons travel and on the energy of the photons. We indicate this by writing $\mu(E,Z)$, where Z is used in the generic sense to indicate any type of material, even mixtures.

Gamma rays travel in straight lines between interactions. Fig. I-3.1 is a sketch representing a gamma ray originating at 0 and undergoing an interaction after traveling a distance x_o.

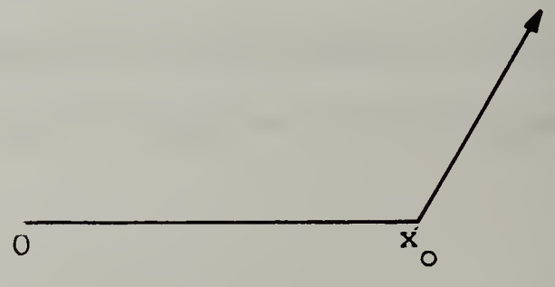

Fig. I-3.1

Let $p(x)$ be the probability that a gamma ray will have no interaction for a distance x along its trajectory. If we divide this dis-

tance into two segments, $x = x_1 + x_2$, we note that $p(x)$ must be of the form

$$p(x) = p(x_1)\, p(x_2),$$

since no interaction for a distance x, means no interaction for x_1, followed by no interaction for x_2. The probabilities $p(x_1)$ and $p(x_2)$ are uncorrelated and must have the functional form of $p(x)$.

This simple product relationship implies that $p(x)$ must be of the form

$$p(x) = e^{-Bx},$$

since the exponential is the functional form possessing this property. To determine B, we examine the case of a very small path length, Δx. Since $1 - p(x)$ represents the probability for an interaction, and

$$1 - p(\Delta x) = 1 - e^{-B\Delta x} \simeq B\Delta x,$$

we find that B is probability per unit path length for occurrence of an interaction. We identify B with μ and write

$$p(x) = e^{-\mu x}. \qquad \text{(I-3.1)}$$

The related quantity, probability that an interaction occurs between x

and $x + \Delta x$, is clearly

$$p(x)\,[1 - p(\Delta x)] = \mu \Delta x\, e^{-\mu x} . \qquad \text{(I-3.2)}$$

We now consider a source which produces a large number, N_o, of photons of identical energy. The number N escaping an interaction for a path length at least as long as x should be

$$N = N_o p(x) = N_o e^{-\mu x} . \qquad \text{(I-3.3)}$$

If these photons form a narrow beam traveling away from the source, any interaction will in principle remove the photon from the beam. We thus expect exponential attenuation of such narrow beams.

The coefficient μ is usually referred to as the "linear attenuation coefficient." Its reciprocal, the average distance traveled before an interaction, is the familiar "mean free path," which will be here designated by ℓ. In the table below, values of ℓ for 1 Mev photons are listed; this energy being typical for components of the gamma rays from fission fragments:*

Table I-3.1. Typical Values for Mean Free Path

Material	ℓ (ft.)	ℓ (lbs/ft^2)
Concrete	0.22	32.3
Wood	0.89	30.4
Air	430.0	32.3
Lead	0.04	29.9

The English units are used; note that the metric units, g/cm^2, would

*For extensive tabulations, see Refs. 9, 19.

give values only about half as large as those of the third column. In any case, the conclusions to be drawn do not depend on precise values.

There are several interesting things which can be said on the basis of this table. Most important from the point of view of protection are comments about room and building dimensions. Typical dimensions for rooms might range from 15 ft. to 50 ft. In any case, the mean free path in air is in order of magnitude larger than this. On the other hand, the mean free path in concrete and wood is at least an order of magnitude smaller. Because of these facts, two approximations become very attractive and useful. If air has such a large mean free path, what will happen inside buildings? The gamma rays emerging from one wall will go unimpeded across to another wall, in nearly all cases. We can therefore perform realistic calculations for structures which omit any effects of air. While the presence of air <u>can</u> be very important, this will not usually be so <u>inside</u> structures.

On the other hand, concrete and wood have mean free paths that are so short--less than a foot--that it is possible to do realistic calculations of the penetration through walls by assuming that gamma rays do not move laterally inside the walls. They can be considered to reemerge either at the point of entry or at the opposite point on the other side of the wall. This also means that we need not be much concerned about corner and edge effects, which will involve only that small fraction of all the entering gamma rays which penetrate within a few inches of the edge or corner.

The last column of this table also exhibits an interesting feature.

The mean free path is inversely proportional to the density of the material; but we often scale out the density, as has been done here. The values then turn out to be closely comparable. The difference for wood, as compared with concrete and air, is due to the hydrogen in the wood: the values depend on the ratio of atomic mass (expressed by A) to the number of atomic electrons (expressed by Z). The value of this ratio averaged over the constituent elements of wood is about 6% smaller than for concrete or air because of the hydrogen content. The fact that Pb has nearly the same value as the other materials is due to the combination of effects: the A/Z ratio is substantially larger for lead than for concrete, and this would tend to increase the mean free path. Counteracting this is a substantial probability, per unit path length in Pb, for photoelectric interactions, an additional contribution that is lacking for the materials with lower Z. This lowers the value relative to the other materials. The two effects nearly compensate one another.

The fact that lead is so expensive, while being so nearly comparable to more common materials, rules out the possibility of using lead as a standard construction material for shelters. Note, however, that lead has a strong differential effect against low energy gamma rays and may be particularly useful under special circumstances as a shield against gamma rays which have lost much of their original photon energy.

b) Differential Interaction Probabilities.* Many different types of interactions contribute to the attenuation coefficient; but of all the different kinds of interaction which are possible, three are dominant.

*For a general treatment see Ref. 20, and for a summary discussion see Ref. 15.

These three combine additively, as mentioned, and are photoelectric absorption (μ_{ph}), Compton scattering (μ_{KN}), and the production of positron-electron pairs (μ_{pp}). For our purpose, all other interaction types are small enough to be neglected, so that we may write

$$\mu = \mu_{ph} + \mu_{KN} + \mu_{pp} \quad . \tag{I-3.4}$$

For a chart of the different possible interaction types, you can refer to Ref. 15, p. 663.

A few comments will be made about each of the most important types of interaction, but before doing so, we note that photon energy and photon wave length are essentially reciprocals of each other. The photon wave length, which will be designated by λ, can be written

$$\lambda = \frac{mc^2}{E} \quad , \tag{I-3.5}$$

where mc^2 is the rest energy of an electron. When this definition is made, the wave length is said to be in Compton units.

Recall also the relationship between interaction probability per unit path length and interaction cross section. In general, for a given element of atomic number A,

$$\mu = \frac{N_A}{A} \rho\sigma \ \text{cm}^{-1} \quad , \qquad \text{or} \qquad \frac{\mu}{\rho} = \frac{N_A}{A} \sigma \ \text{cm}^2/\text{g} \quad , \tag{I-3.6}$$

where N_A is Avogadro's number, ρ is the density, and σ is the

cross section. The combination N_A/A gives atoms per gram. A suitable linear combination of terms of this type will give μ for mixtures and compounds.

In a photoelectric interaction, the gamma ray disappears and its energy is given to an atom. The total probability of such an interaction can be considered the sum of the separate probabilities that the interaction occur with the different atomic electrons. Since we are not here interested in a detailed expression of great accuracy, it will be adequate to focus attention on an approximate form (σ_K) for the two K-shell electrons only. Evaluation by Born approximation gives the following result:[20]

$$\sigma_K = \sigma_{Th}\, 4\sqrt{2}\, \lambda^{3.5} \frac{Z^5}{137^4}, \qquad \text{(I-3.7)}$$

where the constant σ_{Th} is called the Thomson cross section, and is given by

$$\sigma_{Th} = \frac{8\pi}{3} (e^2/mc^2)^2$$

In the expression for μ, the combination of constants $N_A\sigma_{Th}$ occurs. It is useful to remember that

$$N_A\sigma_{Th} = .4 \ \text{cm}^2/\text{mole} \qquad \text{(I-3.8)}$$

almost precisely. The higher shell electrons make a contribution also, so that the total photoelectric cross section per atom is somewhat larger than σ_K, but the trends with Z and with λ are not changed.

Note that with increasing energy this cross section becomes small rapidly, since λ decreases as the energy increases. The fact that σ_K is proportional to Z^5 means that at any given energy this cross section is much more important at large than small values of Z. In small-Z materials the photoelectric cross section is therefore important only at low energies, as has already been noted. In materials with lower Z than Fe, interactions of this type are important only below, say .1 Mev, while for materials with smaller Z values than 13 (Al), such interactions are important only below about .05 Mev. For Pb ($Z = 82$), photoelectric interactions are important at all energies up to, and somewhat above, 1 Mev.

Turning to Compton scattering interactions, in which gamma rays give only part of their energy to electrons, we first write the differential cross section per electron, namely*

$$d\sigma_{KN} = \frac{3}{16\pi}\,\sigma_{Th}\,(\lambda'/\lambda)^2\,[\lambda/\lambda' + \lambda'/\lambda - 2(\lambda - \lambda') + (\lambda' - \lambda)^2] \times \delta(\cos\theta - 1 + \lambda - \lambda')\,d\Omega\,d\lambda \quad . \qquad \text{(I-3.9)}$$

Here, λ' and λ are gamma-ray wavelenghts before and after scatter, respectively, and $d\Omega$ is a differential solid angle encompassing the

---

*At this point our discussion is oversimplified in that known corrections to the simple expression given here are ignored. Such corrections have not as yet appeared to be important in the penetration process, perhaps because of some tendency for the omission to compensate for relatively unimportant interaction types also omitted.

deflection angle θ between photon trajectories before and after the interaction. The Dirac delta function expresses the Compton relationship between wave length change and deflection angle, namely

$$1 - \cos\theta = \lambda - \lambda' \qquad \text{(I-3.10)}$$

We might observe from this that a scattering interaction with a deflection of 90° will increase the wave length by one Compton unit, while an interaction with a deflection through 180° will increase the wave length by two Compton units. Correspondingly, gamma rays which have had such interactions retain photon energies below approximately .5 Mev and .25 Mev, respectively.

The total cross section for Compton scattering can be calculated from Equation (I-3.9) by integration over all deflection angles and over all possible scattered wave lengths. The integration over deflection angles removes the Dirac delta function and gives the familiar form referred to as the differential Klein-Nishina cross section. The wave length integration is also elementary, and the resulting expression is called the integral Klein-Nishina cross section. The relevant comments about this total cross section can be made from a simple form valid at high energies and small wave lengths, namely

$$\sigma_{KN} = \frac{3}{8} Z \sigma_{Th} \lambda' \log\frac{3.28}{\lambda'} \quad , \qquad \lambda << 1. \qquad \text{(I-3.11)}$$

Here the subscript KN refers to Klein-Nishina and should not be confused

with the subscript K, referring to K-shell electrons. The factor Z in the expression is introduced because all (Z) electrons of the atom are assumed to contribute like terms.

The total cross section for Compton scattering changes much more slowly with wave length (or energy) than the σ_K. This statement is true also at lower energies, where the expression given is not applicable. It is also apparent that σ_{KN} changes more slowly with Z than does σ_K.

At high energies, then, the photoelectric cross section tends to become very small, and the Compton scattering cross section becomes dominant. Likewise, at a fixed energy, if Z is decreased, the relative importance of photoelectric interactions decreases.

The cross section for producing electron-positron pairs is often important, though this is not so much the case for our problems. This interaction does not occur at photon energies below about 1 Mev. At higher energies it increases; but in small-Z materials it tends to remain small up to energies greater than those of fallout gamma rays. Because the gamma ray photon disappears as a result of such interactions, the effect on penetration is very similar to that produced by photoelectric interactions. For this reason, one often tends to distinguish between "scattering" and "absorbing" interactions, with the latter including pair production as well as photoelectric effects.*

Before leaving the subject, some further comments about possible oversimplifications may be useful. In addition to a simplified form for the scattering cross section, the phenomenon of polarization has been altogether neglected. Gamma ray photons become polarized as a re-

*These comments ignore the .51 Mev gamma rays due to annihilation of electron-positron pairs. This radiation can be important in backscattering phenomena, and leads to slight underestimates of penetration.

sult of scattering interactions just as light, scattering from small dust particles in the atmosphere, becomes polarized. As a consequence of polarization, gamma-ray photons tend to maintain directions along the plane of their first substantial scattering interaction. This tendency has a small effect on penetration, and also some effect on backscattering from a wall. It may show up in comparisons between theoretical and experimental albedos. Because for the most part the effect is confined to gamma rays of low energy, we can safely omit all consideration of it in problems of penetration.

A simple, but indicative, integral over the differential scattering cross section is the following:

$$\frac{\int_{\lambda'+1}^{\lambda'+2} \int_{4\pi} d\sigma_{KN}\, \lambda^{-1}}{\int_{\lambda'}^{\lambda'+2} \int_{4\pi} d\sigma_{KN}\, \lambda^{-1}} \quad . \tag{I-3.12}$$

According to the integration limits, the numerator is proportional to the average energy of gamma rays scattered through angles larger than 90°, while the denominator is proportional to the average energy of gamma rays scattered through any angle, in a single interaction. The ratio is a rough measure of the size of the "energy albedo," the fraction of energy which backscatters from a wall.* For 1 Mev photons, the ratio is approximately .2.

The smallness of this ratio is much more important than might appear

---

*We refer to the fraction backscattered for energy, photon number, or dose, as various albedos: energy albedo, number albedo, or dose albedo.

at first. This simple calculation indicates that the "energy albedo" is expected to be small, about an order of magnitude less than the incident energy. This, in turn, means that in buildings, the radiation penetrating through a wall directly to the detector, without backscattering from other walls, is much the largest contribution to the dose, much larger than contributions backscattered from one or more walls. It should thus prove reasonably accurate to perform calculations that treat the backscattering as a small correction to the contribution coming directly through each wall. Moreover, one can proceed with some confidence to perform wall-by-wall analysis of structure shielding.

4. Radiation Flux

a) Definitions. One basic problem is to provide an adequate and useful description of a radiation field. We might conceive of a radiation field more or less as in the following sketch, in which the arrows represent gamma-ray photons traveling in all directions through different regions of space.

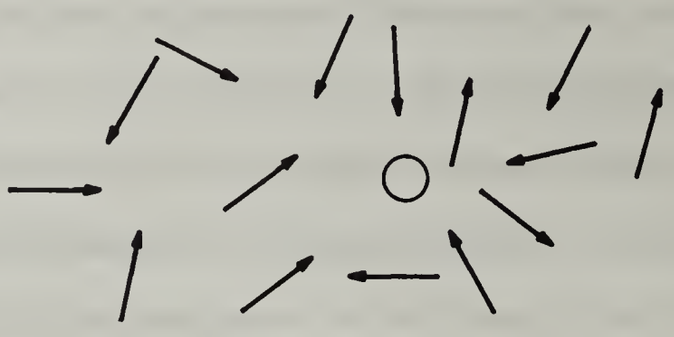

Fig. I-4.1

As indicated by the small circle, a probe is introduced to sample the field. This probe is small so that the characteristics of the radiation are uniform over the region of space which the probe is to occupy, and also so that the presence of the probe doesn't modify the radiation field appreciably. In shape, the probe is spherical, so that it presents the same shape and apparent size regardless of the direction from which it is approached. Ideally the probe is capable of registering the characteristics of each photon which passes through it. Photons not passing through the probe are not recorded. Thus, from the total set of photons, a subset is selected which passes through the probe, and which we might indicate by the following sketch.

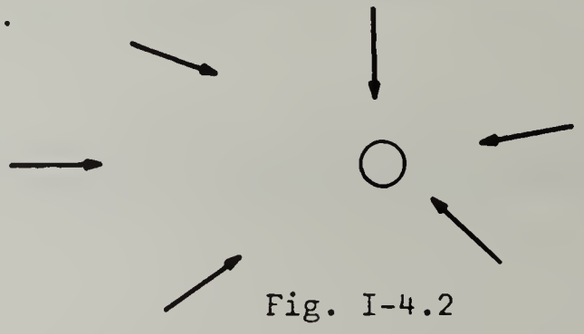

Fig. I-4.2

Note that each photon in the sketch is traveling on a collision course with some part of the probe--its center, its edge, or some other part.

The photons which strike the probe are characterized by energy, direction, and the time they strike. The probe itself is characterized by its cross-sectional area, which we call a, and its location, which we designate by a set of Cartesian coordinates, x, y, z. To classify photons by direction, we choose an arbitrary polar axis extending out from the center of the probe, and an arbitrary azimuthal reference half-plane, as in Fig. I-4.3. Radial lines from the center of the probe can be identified by an obliquity angle θ relative to the reference axis, and an azimuthal angle ϕ between reference half-plane, and the half-plane from the polar axis containing the radial line.

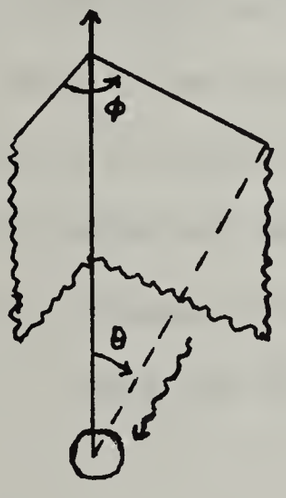

Fig. I-4.3

Each photon trajectory passing through some part of the probe is then identified by the angles θ,ϕ of the radial line starting at the center of the probe and lying parallel to the photon trajectory. To render θ and ϕ unique, we must specify that we will either choose consistently the radial line back along the path of approach, or the radial line parallel to the direction of motion of the photon. Both are used; in Figure I-4.3 the first possibility is indicated.

With a classification system for direction, and some mechanism for identifying photon energy, we simply count the number of photons passing through the detector with energies between E and $E + dE$, with directions in a differential solid angle $d\Omega$ in which the direction θ,ϕ lies, in the time interval between t and $t + dt$. This number will be proportional to dE, $d\Omega$, and dt, and will be indicated by

$$N(E;\theta,\phi;x,y,z;t)dE\ d\Omega\ dt\ .$$

Finally, we note that the number of photons passing through the probe will increase or decrease as the size of the probe is increased or decreased. For small probes there will be a proportionality between N and the size of "target" presented by the probe, as measured by its cross-sectional area a. The fundamental quantity which we call the flux, or number flux, and designate by N, is the ratio

$$N(E;\phi,\theta;x,y,z;t) = \frac{1}{a} N\ .$$

It clearly has the units

$$\frac{\text{Number of Photons}}{\text{Energy}\cdot\text{Steradian}\cdot\text{Area}\cdot\text{Second}}\ .$$

If one integrates N over energy and direction, the result is commonly called the "total flux," or "total number flux." To avoid some resulting confusion, N and its integral over energy or direction, but not both,

are commonly referred to as the "differential" flux or number flux.

To prepare the way for future discussions, we consider also the case of a probe which is not spherical, but shaped like a small flat plate of area a, oriented so that the plane of the detector is perpendicular to a unit vector $\vec{k}$, as in Figure I-4.4. In this case the target presented by the probe clearly depends on the direction of approach. Further, it is advantageous to choose $\vec{k}$ as the reference polar axis in classifying photon directions.

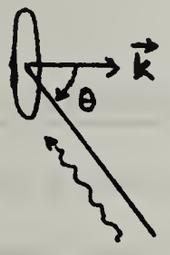

Fig. I-4.4

The number of photons passing through this detector will be indicated by

$$N'(E;\theta,\phi;x,y,z;t)dEd\Omega dt \ .$$

Since the target size is proportional to $|\cos\theta|$, we find that

$$\frac{1}{a}N' = |\cos\theta|\frac{1}{a}N = |\cos\theta|N(E;\theta,\phi;x,y,z;t) \ .$$

The quantity $|\cos\theta|N$ is often referred to as the <u>current</u>, as distinguished from the <u>flux</u>, N.*

---

* A quantity often calculated is $\cos\theta N$, i. e.,with $\cos\theta$ permitted to be negative as well as positive, and on occasion this has been called the current. If this quantity should be referred to later in this manuscript, it will be called the "signed current."

The current depends on the direction of $\vec{k}$. Normally one speaks about current in connection with some flat surface, and with the detector plane oriented parallel to the surface. The direction of $\vec{k}$ is then normal to the surface. One may distinguish between the current into, and the current out from, the surface, each referring only to those values of θ which correspond to photons going "into," or "out from," the surface.

b) Detector Response to Radiation from a Wall. Next let us consider a flat wall or wall section and a nearby detector measuring radiation which emerges from the wall and passes through the detector. Our purpose is to express the detector response in terms of radiation flux at the wall surface and also radiation current through the wall surface. The comparison is both interesting and useful.

In Figure I-4.5, the detector position is measured in a rectangular coordinate system and found to be (x,y,z). A small surface element of the wall surface S is located at (x',y',z') , and its size is dA . In our sketch, this surface element is drawn with exaggerated size; it is to be thought of as very small. The (spherical) detector has cross-sectional area a .

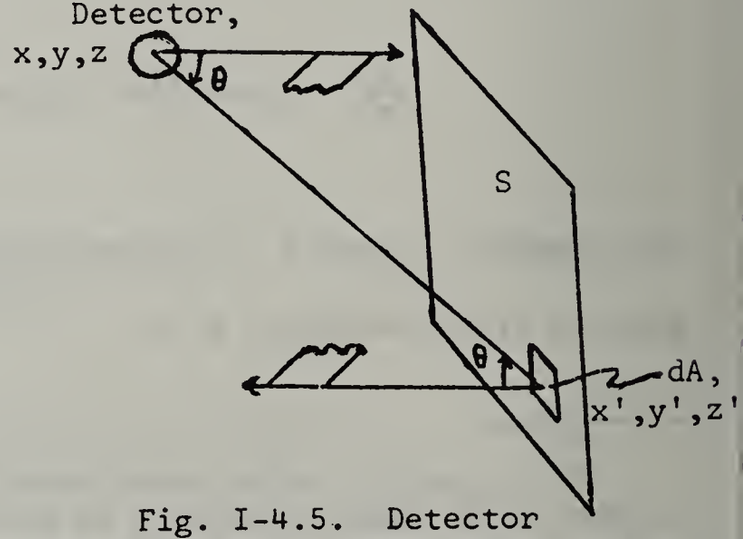

Fig. I-4.5. Detector and radiating surface.

Two reference systems are natural to this configuration: the polar axis for classification of pho-

ton directions at the detector points towards and perpendicular to the wall; and photon directions are measured by radial lines opposite the direction of photon movement and therefore pointing from detector to wall. On the other hand, at the surface a polar reference axis points perpendicular to, and away from, the wall, and photon directions are measured by lines drawn from dA in the direction of photon movement.

At the detector, an azimuthal reference half-plane is selected; and at the surface S, the azimuthal reference half-plane is chosen parallel to, and extending in the opposite direction from, the one for the detector. All this is displayed in Figure I-4.5.

We call the flux at the surface element $N(E;\theta',\phi';x',y',z')$. As indicated it is a function of photon energy, direction, and the position of dA. Specific reference to the time has been omitted, as it is irrelevant for our present purpose. We first write down an expression for the number of photons passing through dA, with energies E lying in dE, and directions θ',ϕ' lying in a solid angle element $d\Omega'$. Since dA behaves like a flat detector, the quantity we wish is given by

$$\cos\theta' N(E;\theta',\phi';x',y',z')dEd\Omega dA.$$

Next we determine the number of photons passing through both dA and the detector. This must be the following integral over directions intercepting some part of the detector:

$$\int_{\Omega_{\text{detector}}} d\Omega' \cos\theta' N(E;\theta',\phi';x',y',z')dEdA.$$

While this is the number passing through the detector, it is not the flux passing through the detector. We must divide by the cross-sectional area a of the detector to obtain flux:

$$dN = \frac{1}{a} \int_{\Omega_{detector}} d\Omega' \cos\theta' N(E;\theta',\phi';x',y',z') dE dA .$$

This flux is called dN because it is proportional to dE and dA. If we omit the factor dE, and integrate over the complete wall surface S, we obtain the flux N_S at the detector position from all parts of S,

$$N_S(E) = \frac{1}{a} \int_S dA \int_{\Omega_{detector}} d\Omega' \cos\theta' N(E;\theta',\phi';x',y',z') .$$

If $\Omega_{detector}$ is very small, the argument is essentially a constant for the integration over directions, since θ',ϕ' can then change only slightly. Noting that

$$\Omega_{detector} = \frac{a}{r^2}$$

and that

$$(\theta',\phi')_{\text{surface reference system}} = (\theta,\phi)_{\text{detector reference system}}$$

we write

$$N_S(E;x,y,z) = \frac{1}{a}\int_S dA\Omega_{detector}\cos\theta' N(E;\theta',\phi';x,y,z)$$

$$= \frac{1}{r^2}\int_S dA\cos\theta N(E;\theta,\phi;x',y',z'). \qquad \text{(I-4.1)}$$

Finally, observing that the solid angle subtended by dA at the detector is

$$d\Omega = \frac{dA\cos\theta}{r^2} ,$$

we write

$$N_S(E;x,y,z) = \int_S d\Omega\ N[E;\theta,\phi;x'(\theta,\phi),y'(\theta,\phi),z'(\theta,\phi)]. \qquad \text{(I-4.2)}$$

In this final expression, the angular distribution may or may not vary from point to point on S. If the flux at S is independent of position, the detector flux is given simply by an integral over the emergent angular distribution. But if the flux at S depends on position, the integrand must be evaluated at the point x',y',z' intercepted by the θ,ϕ radial line from the detector. Nearly all shielding calculations thus far have used the assumption that emergent angular distributions are position independent.

Comparison of Equation (I-4.1) with Equation (I-4.2) makes it clear that we can adopt a point of view which looks from the surface S outwards, utilizing a polar axis pointing away from the surface and identifying photon directions with photon movement. It is then natural to

identify the flux at the detector with a surface integral over emergent current. Alternately, we can adopt a point of view which looks from the detector towards the surface, utilizing a polar axis pointed towards the surface and identifying θ,ϕ with the reverse of the direction of photon movement. It is then natural to describe the flux at the detector in terms of an integral over emergent flux at S.

The two points of view are completely equivalent. Discussions of structure shielding mostly utilize the latter point of view.

5. Derivation of the Transport Equation

There are many different derivations of the transport equation. The one to be presented here is detailed, rather pedestrian, and not highly intuitive; in fact, it has been chosen largely for these characteristics. The quantity basic to this derivation is not the number flux but the number density, a related quantity; and we begin by establishing this relationship.

We first consider a radiation field, and a small spherical volume, rather like the spherical probe of Figure I-4.1, within this field. The magnitude of the cross-sectional area of the small sphere can again be designated a, and the magnitude of the enclosed volume by V. If the sphere contains the point x,y,z, the number of photons having energies within dE at E and directions within $d\Omega$ at θ,ϕ, which are incident on the surface of this sphere in the time interval dt, is

$$aN(E;\theta,\phi;x,y,z;t)dEd\Omega dt \quad .$$

If these photons remain inside the sphere for an average time interval which we designate $\langle t \rangle$, the number of photons of this type in the spherical volume will be

$$\int_{t}^{t+\langle t \rangle} dt' aN(E;\theta,\phi;x,y,z;t')dEd\Omega \approx a\langle t \rangle N(E;\theta,\phi;x,y,z;t)dEd\Omega \quad .$$

We divide this number by the volume of the sphere to obtain the number per unit volume, or <u>density</u>, of photons of this type at x,y,z at time t

The density function we wish to use will be designated $n(E;\theta,\phi;x,y,z;t)$, and is given by

$$n(E;\theta,\phi;x,y,z;t)dEd\Omega = \frac{a}{V}\langle t\rangle N(E;\theta,\phi;x,y,z;t)dEd\Omega .$$

But V is simply a, multiplied by the average chord length across the sphere; therefore, $V/a\langle t\rangle$ is the ratio of average distance to average time for traversal of the sphere, which must equal the photon velocity, c. Thus we have,

$$n(E;\theta,\phi;x,y,z;t) = \frac{1}{c}N(E;\theta,\phi;x,y,z;t) . \qquad \text{(I-5.1)}$$

For neutrons and other particles, c must be replaced by the particle speed, v, which will in general depend on E. With this modification, the entire derivation applies equally well to any type of particle; and we therefore use $v(E)$ rather than c in the following discussion, while referring to "particles," a generic term including photons.

In a small time interval δt, particles traveling with velocity $v(E)$ will move a distance $v\delta t$. If this path length is very short, the particles may or may not have some kind of interaction in $v\delta t$. Multiple interactions during δt will have vanishing probability. We assume that interactions occur instantaneously, so that occurrence or non-occurrenceof an interaction is definite in any finite time interval.

The probability for some kind of interaction is $\mu v\delta t$, where μ is the total interaction probability per unit path length as defined in

section 3, a quantity we also refer to as the attenuation coefficient in the case of gamma rays. The probability of no interaction is $(1 - \mu v \delta t)$. Some interactions cause particles to change direction and energy. We take note of the probability for particles of energy E' and direction θ', ϕ' to scatter in $v(E')\delta t$ in such a way as to transfer to E lying within dE and θ, ϕ lying within $d\Omega$. This will be written

$$k(E', \theta', \phi'; E, \theta, \phi) dE d\Omega v(E') \delta t .$$

To derive the transport equation we consider the number of particles in a volume element dV at x, y, z, with energies in dE at E and directions in $d\Omega$ at θ, ϕ, at a time $t + \delta t$. This number can be written

$$n(E; \theta, \phi; x, y, z; t) dE d\Omega dV ;$$

and we can estimate it in terms of the particle density at the slightly earlier time t. There are three main contributions: a) particles of the indicated energy and direction which move without interaction during δt, so as to be in dV at the indicated time; b) particles undergoing an interaction in δt which gives them the indicated energy and directions, and whose dog-leg path puts them in dV at the indicated time; and c) particles "born" during δt with the indicated energy and direction and moving into dV at the indicated time. The first contribution will be called the "convection" term; the second will be referred to as the "scatter" term; and the third will be called the "source" term. We discuss each in turn.

a) The Convection Term. At time t these particles occupy a volume of the same size as dV, located at $x - v_x\delta t$, $y - v_y\delta t$, $z - v_z\delta t$, where v_x, v_y, v_z are the velocity components parallel to the three Cartesian axes. The number of such particles, multiplied by the probability of no interaction, gives the size of the contribution:

$$(1 - \mu v\delta t)n(E;\theta,\phi;x - v_x\delta t, y - v_y\delta t, z - v_z\delta t;t)dEd\Omega dV.$$

b) The Scatter Term. This is somewhat complicated. Particles start with energy E' and direction θ',ϕ' and scatter to energy E and direction θ,ϕ within the small interval δt. Thus, they have paths looking something like the following.

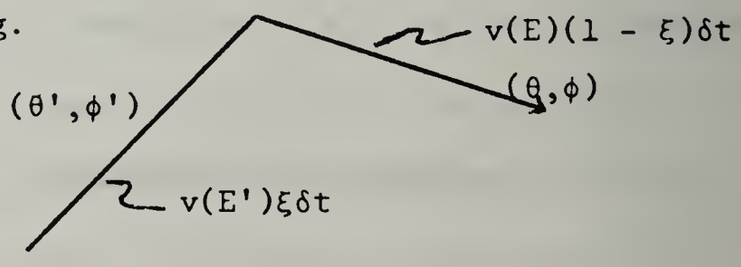

Figure I-5.1

The time interval δt is divided into a part $\xi\delta t$ before the scatter and the remainder $(1 - \xi)\delta t$ after scatter, where $0 \leq \xi \leq 1$. Consider those particles whose scattering from E',θ',ϕ' to E,θ,ϕ occurs within the sub-interval between $\xi\delta t$ and $(\xi + \delta\xi)\delta t$. At time t these particles are in a volume of the same size and shape as dV, but located at the point with coordinates

$x - v_x(E')\xi\delta t - v_x(E)(1 - \xi)\delta t$, which we abbreviate $x_\xi(E',E)$,

$y - v_y(E')\xi\delta t - v_y(E)(1 - \xi)\delta t$, which we abbreviate $y_\xi(E',E)$,

$z - v_z(E')\xi\delta t - v_z(E)(1 - \xi)\delta t$, which we abbreviate $z_\xi(E',E)$.

The number of particles is

$$d\xi\{v(E')\delta t k(E',\theta',\phi';E,\theta,\phi)dEd\Omega\}$$

$$\times \{dE'd\Omega'dVn(E';\theta',\phi';x_\xi(E',E),y_\xi(E',E),z_\xi(E',E);t + \xi\delta t)\} .$$

The scatter term which we require is simply the sum over all values of ξ,E',θ',ϕ' of such contributions, i. e.,

$$\int_0^1 d\xi \int_E^\infty dE' \int_{4\pi} d\Omega' \; k(E',\theta',\phi';E,\theta,\phi)$$

$$\times v(E')n(E';\theta',\phi';x_\xi(E',E),y_\xi(E',E),z_\xi(E',E);t + \xi\delta t)dEd\Omega dV\delta t .$$

c) The Source Term. We assume the existence of a particle source S, which generates the following number of particles per unit volume per unit time, with energies in dE at E, and with directions in $d\Omega$ at θ,ϕ :

$$S(E;\theta,\phi;x,y,z;t)dEd\Omega .$$

We face the same situation here as in the case of the scatter term. The source emits particles all during the time interval δt. The particles which end in dV at $t + \delta t$ can be classified according to subinterval. In particular, those emitted between $\xi\delta t$ and $(\xi + d\xi)\delta t$ originated in a volume similar to dV and located at

$$x - v_x(E)(1 - \xi)\delta t \text{ , which we abbreviate } x_\xi(E) ,$$

$y - v_y(E)(1 - \xi)\delta t$, which we abbreviate $y_\xi(E)$,

$z - v_z(E)(1 - \xi)\delta t$, which we abbreviate $z_\xi(E)$.

The number generated by the source during $d\xi\,\delta t$, and located in dV at $t + \delta t$, is

$$d\xi\delta t\{S(E;\theta,\phi;x_\xi(E),y_\xi(E),z_\xi(E);t + \xi\delta t)dEd\Omega dV\} ,$$

and the total scatter term is therefore

$$\int_0^1 d\xi S(E;\theta,\phi;x_\xi(E),y_\xi(E),z_\xi(E);t + \xi\delta t)dEd\Omega dV\delta t .$$

d) The Equation. Combining all the terms together into an equation, we obtain quite a long expression. To maintain some clarity, we will not re-write the scatter and source terms in the following expression, but merely indicate their presence:

$$n(E;\theta,\phi;x,y,z;t + \delta t)dEd\Omega dV =$$
$$(1 - \mu v\delta t)n(E;\theta,\phi;x - v_x\delta t,y - v_y\delta t,z - v_z\delta t;t)dEd\Omega dV$$
$$+ \text{Scatter term} + \text{Source term} . \qquad \text{(I-5.2)}$$

To turn this expression into a differential equation, we expand the convection term and the term on the left side of the equation in powers of δt , these being the only terms not containing δt as a factor:

$$n(E;\theta,\phi;x,y,z;t+\delta t) = n(E;\theta,\phi;x,y,z;t) + \delta t\frac{\partial n}{\partial t} + O(\delta t^2) ,$$

$$n(E;\theta,\phi;x-\delta tv_x,y-\delta tv_y,z-\delta tv_z;t) = n(E;\theta,\phi;x,y,z;t)$$
$$- \delta t\frac{\partial n}{\partial x}v_x - \delta t\frac{\partial n}{\partial y}v_y - \delta t\frac{\partial n}{\partial z}v_z + O(\delta t^2) .$$

Inserting the expansions into our equation, we obtain

$$\left\{\frac{\partial n}{\partial t}\delta t + \left(\frac{\partial n}{\partial x}v_x + \frac{\partial n}{\partial y}v_y + \frac{\partial n}{\partial z}v_z\right)\delta t + \mu vn\delta t + O(\delta t^2)\right\}dEd\Omega dV$$
$$= \int_0^1 d\xi \int_E^\infty dE' \int_{4\pi} d\Omega' kvn(E';\theta',\phi';x_\xi(E',E),y_\xi(E',E),z_\xi(E',E);t+\xi\delta t)dEd\Omega dV\delta t$$
$$+ \int_0^1 d\xi S(E;\theta,\phi;x_\xi(E),y_\xi(E),z_\xi(E);t+\xi\delta t)dEd\Omega dV\delta t .$$

If we now divide all terms in the equation by δt, and take the limit as $\delta t \to 0$, we find that in both scatter and source terms, $x_\xi, y_\xi, z_\xi \to x,y,z$, so that

$$\left\{\frac{\partial n}{\partial t} + \frac{\partial n}{\partial x}v_x + \frac{\partial n}{\partial y}v_y + \frac{\partial n}{\partial z}v_z + \mu vn\right\}dEd\Omega dV$$
$$= \int_0^1 d\xi \int_E^\infty dE' \int_{4\pi} d\Omega' kv(E')n(E';\theta',\phi';x,y,z;t)dEd\Omega dV$$
$$+ \int_0^1 d\xi S(E;\theta,\phi;x,y,z;t)dEd\Omega dV . \qquad \text{(I-5.3)}$$

In this limit both integrands are seen to be independent of ξ. We can therefore easily perform the ξ integrations. If this is done, and if we remove the differential factors, we obtain

$$\frac{\partial n}{\partial t} + \frac{\partial n}{\partial x}v_x + \frac{\partial n}{\partial y}v_y + \frac{\partial n}{\partial z}v_z + \mu vn = S(E;\theta,\phi;x,y,z;t)$$
$$+ \int_E^\infty dE' \int_{4\pi} d\Omega' k(E',\theta',\phi';E,\theta,\phi)v(E')n(E';\theta',\phi';x,y,z;t) . \qquad \text{(I-5.4)}$$

Next, we note that v_x/v, v_y/v, and v_z/v are the cosines of a unit vector which points in the direction of motion of the particles. We designate this vector $\vec{\omega}$. Recalling the relation $vn = N$ between density function and flux, we can rewrite Equation (I-5.4) in the simpler form

$$\frac{1}{v(E)}\frac{\partial N}{\partial t} + \vec{\omega}\cdot\nabla N + \mu N(E;\theta,\phi;x,y,z;t) = S(E;\theta,\phi;x,y,z;t)$$
$$+ \int_E^\infty dE' \int_{4\pi} d\Omega' k(E',\theta',\phi';E,\theta,\phi) N(E';\theta',\phi';x,y,z;t) \ . \qquad \text{(I-5.5)}$$

The first term in this equation has little significance for shielding calculations because radiation sources change little over photon lifetimes. We therefore assume that N is effectively time-independent. The first term then vanishes, and we arrive at the form of the transport equation on which our attention will be focused in further discussions, namely*

$$\vec{\omega}\cdot\nabla N + \mu N(E;\theta,\phi;x,y,z) = S(E;\theta,\phi;x,y,z)$$
$$+ \int_E^\infty dE' \int_{4\pi} d\Omega' k(E',\theta',\phi';E,\theta,\phi) N(E';\theta',\phi';x,y,z) \ . \qquad \text{(I-5.6)}$$

The source function in Eq. (I-5.6) might be a delayed fission-product gamma-ray source function, such as was discussed in section 2. Alternately, it might be a Co-60 source, a Cs-137 source, or something else.

The coefficient $\mu(E)$ was discussed in section 3. The function $k(E',\theta',\phi';E,\theta,\phi)$ is written here in somewhat more general form than necessary We assume it to be proportional to the Klein-Nishina function, Eq. (I-3.9).

---

*We omit t henceforth and may or may not indicate explicitly in later discussions that N and S are sec^{-1}.

There is no point in rewriting the expression here, but it should be noted that

$$k(E',\theta',\phi';E,\theta,\phi) = k(E',E,\cos\Theta)$$

where

$$\cos\Theta = \cos\theta\cos\theta' + \sin\theta\sin\theta'\cos(\phi - \phi') \; . \qquad \text{(I-5.7)}$$

That is to say, the function k depends on initial and final directions only through the cosine of the deflection angle Θ. The origin and interpretation of Equation (I-5.7) can be found in any treatise on spherical trigonometry.

6. Linearity, Superposition Properties, and Boundary Conditions

The first thing we note about Equation (I-5.6), and also the more general time-dependent form of the transport equation, is the fact that it is a linear equation. We designate the combination of integral and differential operators by L :

$$LN = \left\{\vec{\omega}\cdot\nabla N + \mu N - \int_E^\infty dE' \int_{4\pi} d\Omega' k(E',E,\cos\theta) N(E',\theta',\phi',x,y,z)\right\} .$$

Equation (I-5.6) then simply reads

$$LN = S . \qquad \text{(I-6.1)}$$

Because of linearity, the superposition principle holds for solutions of the transport equation. That is, if $N_i, i = 1,2,\ldots,$ are solutions of the equation

$$LN = S_i ,$$

where the S_i, $i = 1,2,\ldots,$ are different source functions, then the equation

$$LN = \sum_i a_i S_i , \qquad a_i \text{ constant} ,$$

has the solution $N = \sum_i a_i N_i$. The finite or infinite sums referred to

here may be replaced by integrals over any parameter or combination of parameters independent of the variables on which N and S depend.

It is extremely convenient to represent complex spectra and source configurations in terms of superpositions of very elementary source types. The most useful elementary source types for this purpose will be discussed in section 12.

In principle an equation of this type can have solutions corresponding to the homogeneous equation (sourceless, $S = 0$), as well as solutions corresponding to a given source S. Therefore, the solutions corresponding to a given source S are not necessarily unique, since solutions to the homogeneous equation may be added to any solution for a given source S to produce a different solution for the same source. In these problems as in problems of other linear systems, boundary conditions are necessary to remove this possible ambiguity and insure that a particular solution to the transport equation corresponds to a given physical situation. The boundary conditions also take care of the related problem of insuring that there are no sources of radiation in the configuration other than the sources we choose to insert.

Three cases commonly arise, of which only the first will be much referred to beyond a few comments here. In this first case the medium is infinite and contains a source which is confined to a given region within the medium. A simple example would be a source located at a point, or in a small volume somewhere in the medium. For this type of problem the boundary conditions are very simple: as one considers points farther and farther from the source region, the flux must decrease

in a regular way towards the limit zero,

$$\lim_{r\to\infty} N = 0 ,$$

where r represents distance from the source region. The photons all eventually interact, lose their energy, and disappear. If this limit differs from zero, it means that photons are somehow being fed into the problem from infinity.

A second common case involves a finite medium with an internal source. A simple example of this might be a sphere of material containing a distributed radioactive source, suspended in vacuum. Here again the boundary condition is simple: there must be no photons incident on the sphere from outside. That is to say, the flux N at the boundary must be zero for all photon directions corresponding to incidence on the surface. (The magnitude of N at the boundary, for directions corresponding to exit from the sphere, will not, in general, be zero.)

This case can be modified by placing a source of photons outside the sphere. It is clear that this would make the following change in the boundary conditions: the value of N at the boundary, corresponding to directions of entrance into the sphere must just be that produced by the (known) exterior source.

There is a third case which occurs, that of two adjacent, but different media, as indicated in the sketch of Figure I-6.1. The flux

in the first medium is indicated by N_1, while the flux in the second medium is indicated by N_2. The boundary condition at the interface is fairly obvious. Assuming no concentration of source at the interface,

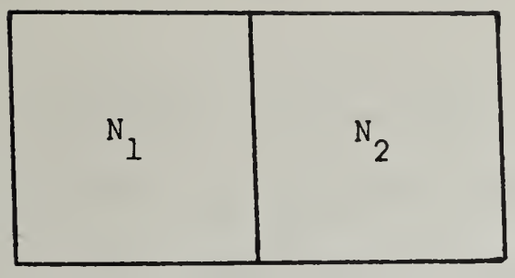

Figure I-6.1

the limiting value of the flux N_1, as the interface is approached from the left, must equal the limiting value of the flux N_2, as the interface is approached from the right. Calculations for the two regions must in principle be done jointly, because this boundary condition links together the transport equations for the two regions.

If there is a concentration of source at an interface between two different media or regions, the boundary conditions change again, so that the two limits just mentioned need not agree, and the flux will in general be discontinuous. But the discontinuity in the flux must then be precisely that produced by the (known) source at the interface.

B. ELEMENTARY THEOREMS ABOUT THE TRANSPORT EQUATION

7. Fano's Theorem

There are several elementary theorems associated with the transport equation which are easy to prove. The first is due to Fano, though it had often been assumed to hold before his formal proof was published:[11/]

Theorem 1: In an infinite medium in which the material is everywhere the same except for variations in density, if there is a source of radiation which is everywhere proportional to the local density in strength, but otherwise everywhere the same in spectrum and angular distribution, the radiation flux, spectrum, and angular distribution in no way depend on position.

The configuration of interest is one in which a medium extends to infinity in all directions, but contains blobs of different densities. Figure I-7.1 suggests high density blobs in a low-density medium. We are trying to suggest by this sketch that such configurations can be very complicated indeed.

Figure I-7.1

If the medium is everywhere the same, except for changes of the density, ρ, then $\frac{1}{\rho}\mu$ and $\frac{1}{\rho}k(E',E,\cos\theta;x,y,z)$ are independent of position. and a source S proportional to the local density has the property that S/ρ is also independent of position.

To prove the theorem, we first write down the transport equation,

$$\vec{\omega}\cdot\nabla N + \mu(E;x,y,z)N = \int_E^\infty dE' \int_{4\pi} d\Omega' k(E',E,\cos\theta;x,y,z)N(E';\theta',\phi';x,y,z)$$

$$+ S(E;\theta,\phi;x,y,z) \ . \qquad \text{(I-7.1)}$$

Next, we divide each term in this equation by the local density, evaluated at the same point, (x,y,z), appearing throughout the equation:

$$\frac{1}{\rho}\vec{\omega}\cdot\nabla N + \frac{1}{\rho}\mu(E;x,y,z)N = \int_E^\infty dE' \int_{4\pi} d\Omega' \frac{1}{\rho}k(E',E,\cos\theta;x,y,z)N(E';\theta',\phi';x,y,z)$$

$$+ \frac{1}{\rho} S(E;\theta,\phi;x,y,z) \ . \qquad \text{(I-7.2)}$$

Finally, we assume that the solution of this equation is of the form

$$N = N(E;\theta,\phi) \ , \qquad \text{(I-7.3)}$$

with no dependence on position whatever. If we make this assumption, the space derivatives of N vanish, so that $\nabla N = 0$, and the equation which results is

$$\left\{\frac{1}{\rho}\mu\right\}N = \int_E^\infty dE' \int_{4\pi} d\Omega' \left\{\frac{1}{\rho}k\right\}N(E';\theta',\phi') + \left\{\frac{1}{\rho}S\right\} \ . \qquad \text{(I-7.4)}$$

In this equation, if the bracketed terms are not disassociated, there appears no factor of any kind which contains a space variable. This confirms our assumption about N, and further gives a simpler equation from which N can be determined, an equation identical with that corresponding to a uniformly distributed source in an infinite, homogeneous medium. The theorem is thereby established.

The generality of this theorem is great, because no expression for the source has been assumed, and no description of the configuration has been required.

8. A Corollary to Fano's Theorem

There is a corollary to this theorem which probably deserves a formal statement also, because it is so frequently referred to informally. It involves a number of integral quantities very useful in the theory of radiation dosimetry. Among these are the so-called "kerma," the "exposure," and the "absorbed dose" in a medium. All are defined and described in the 1962 edition of Handbook 84, Radiation Quantities and Units, published by the National Bureau of Standards.[21] All the quantities relate to the degradation of the energy represented by the gamma-ray flux. The various types of gamma-ray interactions not only have the effect of destroying photons or lowering their photon energy; they also result in the production of fast electrons (and X-rays).

The fast electrons produced as a result of gamma ray interactions represent the source for an electron penetration problem which has close similarities to the gamma-ray penetration problem which is our main concern. Electrons thus produced interact with atoms in various ways and distribute energy among many electrons of lower kinetic energy, as well as in the formation of ions, and in atomic excitations. The kinetic energy of fast electrons is thus eventually changed into the energy of excited atoms, ions, chemical changes, optical radiation, and heat.

a) Definitions

The kerma is described as the sum of the initial kinetic energies of all the charged particles liberated by indirectly ionizing particles in a volume element of the specified material divided by the mass of the matter within the volume element. That is to say, the kerma refers to the energy transferred from the gamma ray flux to the kinetic

energy of free electrons. A formal expression for this quantity, and the other quantities also, can be written down with the aid of a few definitions. Suppose that

1) $K(E',T;\vec{\omega}'\cdot\vec{\omega};x,y,z)dTd\Omega$ is the probability, per unit path length, that a photon of energy E' and direction $\vec{\omega}'$ produces an electron with kinetic energy T in dT, and direction $\vec{\omega}$ in the solid angle differential $d\Omega$,

2) $K_{air}(E',T,\vec{\omega}'\cdot\vec{\omega})dTd\Omega$ is the same type of probability per unit path length for gamma rays in air under standard conditions,

3) $K_e(T,\Delta,x,y,z)$ is the average energy transferred by fast electrons of kinetic energy T, to slow electrons of kinetic energy less than Δ, per unit path length travelled by the fast electrons,

4) $N_e(T;\theta,\phi;x,y,z)dTd\Omega$ is the flux of electrons with kinetic energy T in dT, and direction (θ,ϕ) in $d\Omega$, at the position (x,y,z),

5) $S_e(T;\theta,\phi;x,y,z)dTd\Omega$ is the number of electrons with kinetic energies T in dT, direction (θ,ϕ) in $d\Omega$, generated per unit volume per second by the atomic interactions of gamma rays, and

6) $S_{e,air}(T;\theta,\phi;x,y,z)dTd\Omega$ is the same quantity, but corresponding to fast electrons produced in air by gamma ray interactions.

If we designate the gamma ray flux by $N(E;\theta,\phi;x,y,z)$, as formerly, the two electron source functions are seen to be

$$S_e(T;\theta,\phi;x,y,z)dTd\Omega = \int_T^\infty dE' \int_{4\pi} d\Omega' N(E';\theta',\phi';x,y,z)K(E',T,\vec{\omega}'\cdot\vec{\omega};x,y,z)dTd\Omega$$
$$(\text{electrons/cm}^3/\text{sec}), \qquad \text{(I-8.1)}$$

and

$$S_{e,air}(T;\theta,\phi;x,y,z)dTd\Omega = \int_T^\infty dE' \int_{4\pi} d\Omega' N(E';\theta',\phi';x,y,z) K_{air}(E',T,\vec{\omega}'\cdot\vec{\omega}) dTd\Omega$$

$$(\text{electrons/cm}^3\cdot\text{sec}) . \qquad \text{(I-8.2)}$$

The energy D transferred to slow electrons of kinetic energy less than Δ may be formally written

$$D(\Delta;x,y,z) = \int_\Delta^\infty dT \int_{4\pi} d\Omega N_e(T;\theta,\phi;x,y,z) \frac{1}{\rho} K_e(T,\Delta;x,y,z)$$

$$+ \int_0^\Delta dTT \int_{4\pi} d\Omega \frac{1}{\rho} S_e(T;\theta,\phi;x,y,z) \qquad (\text{Mev/g-sec}) . \qquad \text{(I-8.3)}$$

The kerma rate can be formally described by the expression

$$\text{kerma rate} = \int_0^\infty dT \int_{4\pi} d\Omega T \frac{1}{\rho} S_e(T;\theta,\phi;x,y,z)$$

$$(\text{Mev/g}\cdot\text{sec}) . \qquad \text{(I-8.4)}$$

The exposure, formerly referred to as the "exposure dose," is the energy transferred from the gamma ray flux, in air, to the kinetic energy of fast electrons per unit mass of air.* A formal expression for the exposure rate is

$$\text{exposure rate} = \int_0^\infty dT \int_{4\pi} d\Omega T \frac{1}{\rho_a} S_{e,air}(T;\theta,\phi;x,y,z) ,$$

$$(\text{Mev/g}\cdot\text{sec}) , \qquad \text{(I-8.5)}$$

where ρ_a is the density of air.

Finally, the absorbed dose is the energy imparted by ionizing radiation to the matter in a volume element divided by the mass of the matter in the volume element. For our purpose, the

---

*The official definition refers to charge rather than energy released in matter. The proportionality is discussed in b).

volume and surface area of the element will be designated $\underline{V}$ and $\underline{A}$, respectively; and the point (x,y,z) is within the volume element.* An expression for the absorbed dose rate (designated ADR) in the volume element is

$$ADR = M_V^{-1} \int_0^\infty dE E \int_{4\pi} d\Omega \left\{ \int_V dV' S(E;\theta,\phi;x',y',z') \right.$$

$$\left. - \int_A d\vec{A}' \cdot \vec{\omega} [N(E;\theta,\phi;x',y',z') + N_e(E;\theta,\phi;x',y',z')] \right\}, \quad \text{(I-8.6)}$$

where the mass of the volume element is M_V and the gamma ray source is S. This expression is the difference between energy injected into the volume element and energy leaving the volume element. The volume integral represents energy input by the (γ-ray) source. The surface integral is negative because of the convention that $\vec{dA}'$ points away from the volume element; the contribution must be positive if $\vec{\omega}$, the direction of travel of the radiation, points toward the volume element. Energy can enter or leave in the form of photons or electrons.

Equation (I-8.6) is not very suitable for calculational purposes. A useful approximation which can be highly accurate is provided by the function $\underline{D}$ of (I-8.3):

$$D(\Delta_0;x,y,z) \tilde{\approx} ADR. \quad \text{(I-8.7)}$$

The energy Δ_0 is a cut-off below which it is possible to assume no

---

*By choosing the volume element small (but not vanishing) it is possible to refer without ambiguity to the "dose absorbed at the point x,y,z."

further transport of energy by either electrons or gamma rays. Either of two concepts can lead to specification of a value for this parameter:

1) Δ_0 can be related to the energy required for an electron, say to travel across the mean diameter of the volume element. Electrons with kinetic energies substantially below this value will mostly dissipate their total energy within the volume and hence they can be assumed to dissipate their energy at the point where they are formed, and

2) Δ_0 can be assigned a value such that the associated distances of travel of photons and electrons are small compared with the distances required for significant changes in photon and electron fluxes at the energy Δ_0. Two types of spatial variations should be considered separately: the variations which occur in the radiation spectra before pseudo-equilibrium* is established; and the variations of the total intensity of the beam with distance of penetration. If pseudo-equilibrium holds below Δ_0, and if the total flux is effectively constant over distances the size of electron ranges and photon mean free paths at Δ_0, then radiation at lower energies can be assumed to dissipate energy at the point of generation.

Use of $D(\Delta_0;x,y,z)$ to estimate the absorbed dose bypasses the self-contradiction inherent in the phrase "dose absorbed at the point x,y,z."

b) The Corollary

With these formal statements to indicate more precisely the content of the terms, we can state the corollary to Fano's theorem:

Theorem 2: In an infinite medium in which the material is everywhere

---

*See section 21.

the same except for variations of density, if there is a source of radiation which is everywhere proportional to the local density in strength, but otherwise everywhere the same in spectrum and angular distribution, the kerma, the exposure, and the absorbed dose are everywhere the same and equal to the values which would exist without the density variations.

The argument is a direct application of Fano's theorem. Under the conditions assumed, the flux of gamma rays N is space independent, according to Fano's theorem. This means that the position dependence of S_e will be determined by the position dependence of $K(E',T;\vec{\omega}'\cdot\vec{\omega};x,y,z)$. But if only density changes occur, this function will be strictly proportional to the local density. This means that S_e is proportional to the local density. The integrand of Equation (I-8.4) is then position independent, as is the kerma rate and its time integral, the kerma.

The fact that S_e is proportional to the local density means that the electron penetration problem for which this is the source satisfies the conditions of Fano's theorem. All the electron interactions which appear in the electron transport equation are proportional to the local density.* Thus, Fano's theorem applies to the electron flux, N_e, which must be position independent. On the other hand the factor $K_e(T,\Delta;x,y,z)$ in the integrand of Equation (I-8.3) is determined by the interaction probabilities, and must be proportional to the local density. As a result of the factor $(1/\rho)$, the integral quantity $D(\Delta;x,y,z)$ must, in fact, be position independent. But then the approximate absorbed dose rate,

*Strictly speaking, this is not quite correct. Small corrections to the electron stopping powers, which depend in a complicated way on density, are known to exist.

$D(\Delta_0;x,y,z)$, must be position independent.

To show that the absorbed dose rate as given by Equation (I-8.6) is position independent, we observe that since both N and N_e are position independent,the surface integral must vanish regardless of the choice of volume element. Since S is proportional to the local density, the volume integral must be proportional to M_V, and the right side of (I-8.6) is Mev/g/sec produced by the source, which was assumed to be independent of position. Because energy is conserved while being degraded, the total energy transferred to electrons which achieve kinetic energies less than Δ_0 must equal the energy produced by the source. Therefore, when Fano's theorem holds, (I-8.7) is exact and is independent of Δ_0.

Finally, we note that $S_{e,air}$, as given by Equation (I-8.2), is position independent. Therefore, the exposure rate as given by Equation (I-8.5) is position independent.

To complete the discussion, a few more comments should be made: If the medium is infinite, so that no leakage through boundaries is possible, energy produced by the gamma ray source is equal to the kerma, which must be equal to the absorbed dose, due to energy conservation.

Further, the expressions for kerma, exposure, and absorbed dose which we have used are neither in the most commonly used units used for these quantities, nor are they in the simplest possible form. A unit for absorbed dose is the rad, which corresponds to 100 ergs/g.* Equation (I-8.3) can be multiplied by a conversion factor,

*There appears to be a movement towards elimination of the rad, which is not officially approved as a unit for kerma.

$(10^{-2}$g-rad/erg)×(# ergs/Mev) , to make this change. The common unit for the exposure is the roentgen. To obtain exposure rate in roentgens per second, Equation (I-8.5) should be multiplied by the factor

$$\frac{e \text{ (coulombs/ion)}}{2.58\times10^{-7} \text{ (coulombs/g,roentgen)}\times W\text{(Mev/ion pair)}} ,$$

where e is the electronic charge, and W, an average energy expended by fast electrons per ion pair formed, is about 32.5 electron volts in air.

c) Expressions for the Kerma and Exposure

To illustrate a simpler form for the kerma and the exposure, consider the integral

$$\text{kerma rate} = \int_0^\infty dT \int_{4\pi} d\Omega \int_T^\infty dE' \int_{4\pi} d\Omega' N(E';\theta',\phi';x,y,z) \frac{1}{\rho} TK(E',T;\vec{\omega}'\cdot\vec{\omega};x,y,z) . \quad \text{(I-8.7)}$$

The two solid angle integrals can be performed to give

$$K_0(E',T;x,y,z) = \int_{4\pi} d\Omega K(E',T,\vec{\omega}'\cdot\vec{\omega};x,y,z) ,$$

and

$$N_0(E';x,y,z) = \int_{4\pi} d\Omega' N(E';\theta',\phi';x,y,z) ,$$

where the subscript indicates the integral over all angles. The two energy integrals which remain can be interchanged by noting that the region of integration corresponds to the shaded portion of the sketch in Figure I-8.1 . The resulting expression may be written in the form

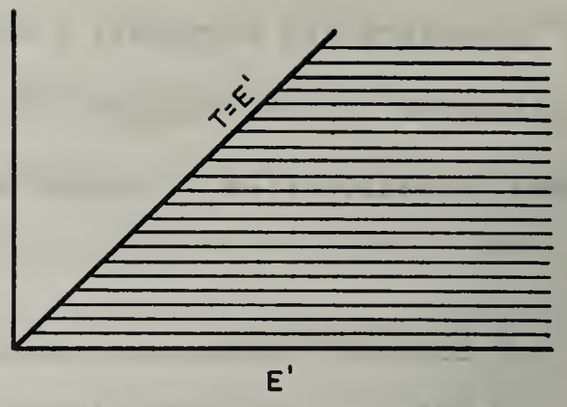

Figure I-8.1

$$\text{kerma rate} = \int_0^\infty dE'E'N_0(E';x,y,z)\left\{\frac{1}{\rho}\frac{1}{E'}\int_0^{E'} dTTK_0(E',T;x,y,z)\right\} . \quad \text{(I-8.8)}$$

The quantity in curly brackets, which depends only on the interaction probabilities of the material, is called the mass energy transfer coefficient. In Reference 15 , this quantity was indicated by μ_D . Tabulations have been made of this quantity by Rosemary Berger and others.[3]

The same reduction can be performed on the expression for exposure, which takes the form

$$\text{exposure rate} = \int_0^\infty dE'E'N_0(E';x,y,z)\mu_d(E') , \quad \text{(I-8.9)}$$

where

$$\mu_d(E') = \frac{1}{\rho_{air}}\frac{1}{E'}\int_0^{E'} dTTK_{0,air}(E',T) . \quad \text{(I-8.10)}$$

Tabulations of μ_d , the mass energy transfer coefficient for air, are also to be found in Mrs. Berger's tables.[3]

9. Application to Cavity Ionization Chambers

Fano's theorem and corollary have applications to the theory of cavity ionization chambers; and we therefore digress in order to present the fundamental concept of those detectors.

Cavity ionization chambers consist of a hollow container filled with gas. Different selections of wall material and gas give rise to the three cases indicated in Figure I-9.1 . The walls of the container are metal, and form one electrode of a condenser. The other electrode is a thin wire extending into the cavity and insulated from the walls.

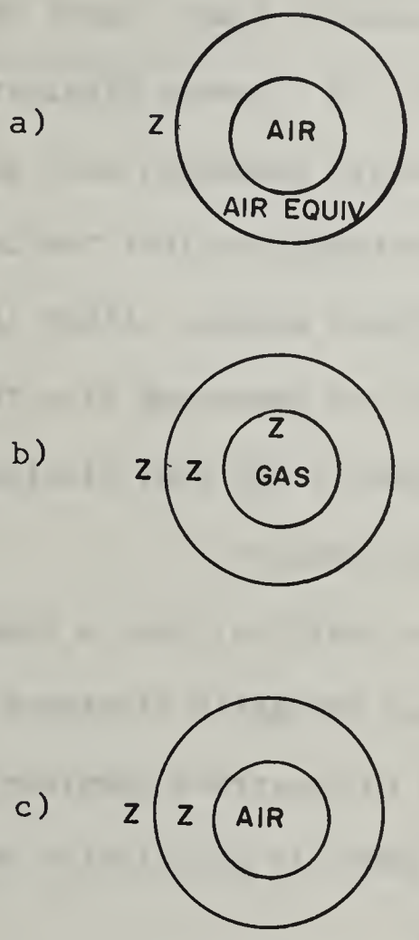

Figure I-9.1

Fast electrons produced by gamma-ray interactions in the cavity walls sweep across the cavity and dissipate energy in the form of (a) atomic transitions and (b) ion pairs. The quantity actually measured by the detector is charge, that is, the number of ion pairs formed in the cavity. It is an experimental fact, which is far from obvious, that regardless of the kinetic energy of the fast electrons, the ratio of the total energy dissipated by the fast electrons to the energy which goes into the formation of ion pairs is a constant for any one medium:

$$\frac{(\text{Energy})_{\text{ion pairs}}}{(\text{Energy})_{\text{ion pairs}} + (\text{Energy})_{\text{atomic trans.}}} = \text{Constant} . \qquad \text{(I-9.1)}$$

Because of this there exists a proportionality between total energy per gram dissipated and charge measured, a proportionality expressed by the constant W, energy dissipated per ion pair formed.*

Cavity chambers, such as those sketched in Figure I-9.1, should be thin enough so that the incident gamma-ray flux passes through without appreciable change, either in spectrum or flux strength. If this criterion is met, the gamma-ray flux throughout the detector is essentially position independent, and fast electrons will everywhere be produced in proportion to local density.

In addition, such a chamber should have walls thick enough so that the most energetic electrons produced by the gamma ray interactions are unable to penetrate completely through. This requirement puts the gas, as it were, in an infinite medium as far as electron penetration is concerned.

If these two conditions can be satisfied simultaneously, Fano's theorem and corollary apply. One can then say that energy absorbed per gram of gas in chambers a) and b) of Figure I-9.1 is representative of the energy absorbed per gram of wall material. One can further say that the ionization measured in chamber b) is proportional both to energy absorbed and kerma, and that the ionization measured in chamber a) is proportional to the exposure. Chamber a) does not measure kerma or absorbed dose in the medium Z.

*Note that the value of W depends on the medium.

The second case, b) , is simple, but often difficult to realize. Case c) illustrates one type of mixed situation which is fairly easy to realize but not simple. This case calls for a substantial additional theory, because Fano's theorem does not apply. Such a theory exists; its importance is due to the fact that in practice the cavity walls and the cavity gas are hardly ever equivalent at all energies. [37]

10. Theorem on Plane Density Variations

Next we consider configurations in which the medium has density variations, but with the density a constant on parallel planes. The best-known problem of this type is the ground-air interface, with the ground considered to be equivalent to compressed air of the same density. Other configurations of this type have importance also.

The restriction to density variations would allow us to apply Fano's theorem if the radiation source were everywhere proportional to the local density. We do not make this assumption, but instead, we make the assumption that the radiation source is constant on planes parallel to the planes of constant density. The theorem is as follows:

Theorem 3: In an infinite medium in which the material is everywhere the same except for plane density variations, if there is a source of radiation which is likewise constant along planes of constant density, the radiation flux equals that in a corresponding problem with constant density $(\bar{\rho})$. The radiation source strength, spectrum, and angular distribution, per unit mass of material, must be the same in the two cases at distances $z,\bar{z}$ from the two reference planes, with

$$\int_0^z \rho(z'')dz'' = \bar{\rho}\,\bar{z} ,$$

and the comparison between fluxes must likewise be made at distances corresponding in this way.

We are contrasting two cases, one in which the density has everywhere the value $\bar{\rho}$, and the other with a variable density function

of the type $\rho(z)$. The argument is like that used in the proof of Fano's theorem. The parts of the gradient term involving derivatives with respect to x and y are zero, and the transport equations for the two cases may be written

$$\frac{1}{\rho(z)}\cos\theta\frac{\partial N}{\partial z} + \frac{1}{\rho}\mu N(E;\theta,\phi;z) = \int_E^\infty dE' \int_{4\pi} d\Omega' \frac{1}{\rho}k(E',E,\cos\theta;z)N(E';\theta',\phi';z) + \frac{1}{\rho}S(E;\theta,\phi;z) ,$$

$$\frac{1}{\bar{\rho}}\cos\theta\frac{\partial \bar{N}}{\partial \bar{z}} + \frac{1}{\bar{\rho}}\bar{\mu}\bar{N}(E;\theta,\phi;\bar{z}) = \int_E^\infty dE' \int_{4\pi} d\Omega' \frac{1}{\bar{\rho}}\bar{k}(E',E,\cos\theta)\bar{N}(E';\theta',\phi';\bar{z}) + \frac{1}{\bar{\rho}}\bar{S}(E;\theta,\phi;\bar{z}) ,$$

(I-10.1)

where $\cos\theta$ is the photon obliquity relative to the z-axis. We have divided all terms in both equations by the density, because we expect to use the position independence of the functions $\frac{1}{\rho(z)}\mu(E,z)$ and $\frac{1}{\rho(z)}k(E',E,\cos\theta;z)$.

Next, we define new variables $\tau(z)$ and $\bar{\tau}(\bar{z})$,

$$\tau(z) = \int_0^z dz'\rho(z') ,$$

$$\bar{\tau}(\bar{z}) = \int_0^{\bar{z}} d\bar{z}'\bar{\rho} = \bar{\rho}\,\bar{z} . \qquad \text{(I-10.2)}$$

In terms of these mass thickness variables, the two transport equations may be re-written as follows:

$$\cos\theta\frac{\partial N}{\partial \tau} + \left(\frac{\mu}{\rho}\right)N(E;\theta,\phi;\tau) = \int_E^\infty dE' \int_{4\pi} d\Omega' \frac{1}{\rho}k(E',E,\cos\theta;\tau)N(E';\theta',\phi';\tau) + \frac{1}{\rho}S(E;\theta,\phi;\tau) ,$$

$$\cos\theta\frac{\partial\bar{N}}{\partial\bar{\tau}} + \left(\frac{\bar{\mu}}{\bar{\rho}}\right)\bar{N}(E;\theta,\phi;\bar{\tau}) = \int_E^\infty dE' \int_{4\pi} d\Omega' \frac{1}{\bar{\rho}}\bar{k}(E',E,\cos\Theta;\bar{\tau})\bar{N}(E';\theta',\phi';\bar{\tau}) + \frac{1}{\bar{\rho}}\bar{S}(E;\theta,\phi;\bar{\tau}) ,$$

(I-10.3)

where the functional dependence of N and S on z in the first equation is obtained by replacing z by its equivalent function of τ, and likewise for the second equation.

It is clear that the two equations are precisely the same, except possibly for the source term, since $\frac{\mu}{\rho}$ and $\frac{k}{\rho}$ in the first equation are not only independent of position, but numerically equal to $\frac{\bar{\mu}}{\bar{\rho}}$ and $\frac{\bar{k}}{\bar{\rho}}$, respectively. If, therefore, the source terms are such that

$$S(E;\theta,\phi;\tau) = \frac{\rho}{\bar{\rho}}\bar{S}(E;\theta,\phi;\tau) , \qquad \text{(I-10.4)}$$

the two equations will be identical in all respects, except that τ appears in one equation wherever $\bar{\tau}$ appears in the other. Further, if the media in the two cases extend to infinity in the sense that

$$\lim_{|z|\to\infty} |\tau| = \lim_{|z|\to\infty} |\bar{\tau}| = \infty , \qquad \text{(I-10.5)}$$

the boundary conditions will be the same in the two cases. It is therefore clear that

$$N(E;\theta,\phi;\tau) = \bar{N}(E;\theta,\phi;\bar{\tau}) . \qquad \text{(I-10.6)}$$

This completes the proof.

To illustrate this theorem, we compare two problems in which the source is confined to a plane and uniform over the plane, but has the same strength in both cases. In one problem the density, $\rho(z)$, varies; in the other the density, $\bar{\rho}$, is constant. The source is located at $z = 0$ in the first problem and at $\bar{z} = 0$ in the second. We define

$$\tau(z) = \int_0^z dz'\rho(z') ,$$

$$\bar{\tau}(\bar{z}) = \int_0^{\bar{z}} dz'\bar{\rho} = \bar{\rho}\bar{z} . \qquad \text{(I-10.7)}$$

Using the Dirac delta function to represent a concentrated source, we write expressions for the (equal strength) sources:

$$S(E;\theta,\phi;\tau) = S(E;\theta,\phi)\delta[z(\tau)] ,$$

$$\bar{S}(E;\theta,\phi;\bar{\tau}) = S(E;\theta,\phi)\delta[\bar{z}(\bar{\tau})] . \qquad \text{(I-10.8)}$$

But since

$$\int_{-\infty}^{z} \delta(z')dz' = \int_{-\infty}^{\tau(z)} \delta[z'(\tau)] \frac{dz'}{d\tau} d\tau = \int_{-\infty}^{\tau} \delta(\tau)d\tau ,$$

we write

$$\delta(\tau) = \delta(z) \frac{dz}{d\tau} = \delta(z) \frac{1}{\rho(z)} ,$$

$$\delta(\bar{\tau}) = \delta(\bar{z}) \frac{1}{\bar{\rho}} , \qquad \text{(I-10.9)}$$

so that

$$S(E;\theta,\phi;\tau) = S(E;\theta,\phi)\rho\delta(\tau) ,$$

$$\overline{S}(E;\theta,\phi;\overline{\tau}) = S(E;\theta,\phi)\overline{\rho}\delta(\overline{\tau}) ,$$

and the condition (I-10.4) is obviously satisfied.

It follows from the arguments used here that it is possible to construct equivalent configurations in which plane layers of <u>different</u> materials occur. The two conditions necessary for equivalence are (I-10.9) and the requirement that for $z,\overline{z}$ such that

$$\tau(z) = \overline{\tau}(\overline{z}) ,$$

the same material occurs in the configurations being compared. If these conditions are satisfied, the density functions $\rho(z)$, $\overline{\rho}(\overline{z})$ can be arbitrary.

11. The Scaling Theorem

The last theorem is as well-known as the others, and so intuitively obvious that we include it with some hesitation. In it we compare two configurations, calling them "A" and "B".

When two points, one in A and the other in B, differ in that the coordinates of the point in B are those of the point in A multiplied by a basic scaling parameter ξ, we say that the points are "corresponding points". The two configurations are then comparable in the following sense:

a) All interfaces in A occur also in B at corresponding points.,

b) The material at corresponding points in A and B is always the same except that the density of this material in B is greater (or less) by a factor $\frac{1}{\xi}$, and

c) The radiation sources in the two problems are identical in spectrum, angular distribution, and spatial distribution, but the source in B is greater (or less) by a factor ξ^2 in each corresponding volume element. If A and B have these relationships, we will refer to them (here) as "similar" configurations. The scaling theorem can then be stated as follows:

Theorem 4. The radiation flux is identically the same at corresponding points in two or more similar configurations.

The proof can be obtained by comparing transport equations, as in the preceding theorem. The following relations have been stated or implied as holding at corresponding points:

$$x_B = \xi x_A \ , \quad y_B = \xi y_A \ , \quad z_B = \xi z_A \ ,$$

$$\mu_B = \frac{\mu_A}{\xi} \ , \quad k_B = \frac{k_A}{\xi} \ ,$$

$$S_B dx_B dy_B dz_B = \xi^2 S_A dx_A dy_A dz_A \ . \tag{I-11.1}$$

It is also clear that

$$\nabla_B = (\vec{i}\frac{\partial}{\partial x_B} + \vec{j}\frac{\partial}{\partial y_B} + \vec{k}\frac{\partial}{\partial z_B}) = \frac{1}{\xi}(\vec{i}\frac{\partial}{\partial x_A} + \vec{j}\frac{\partial}{\partial y_A} + \vec{k}\frac{\partial}{\partial z_A})$$

$$= \frac{1}{\xi}\nabla_A \ . \tag{I-11.2}$$

Transport equations for the two configurations are as follows:

$$\vec{\omega}\cdot\nabla_A N_A + \mu_A N_A = \int_E^\infty dE' \int_{4\pi} d\Omega' k_A(E',E,\cos\Theta;x_A,y_A,z_A) N_A(E';\theta',\phi';x_A,y_A,z_A)$$
$$+ S_A(E;\theta,\phi;\ x_A,y_A,z_A)$$

$$\vec{\omega}\cdot\nabla_B N_B + \mu_B N_B = \int_E^\infty dE' \int_{4\pi} d\Omega' k_B(E',E,\cos\Theta;x_B,y_B,z_B) N_B(E';\theta',\phi';x_B,y_B,z_B)$$
$$+ S_B(E;\theta,\phi;x_B,y_B,z_B) \ . \tag{I-11.3}$$

But the second equation can be written in the form

$$\frac{1}{\xi}\vec{\omega}\cdot\nabla_A N_B + \frac{1}{\xi}\mu_A N_B = \int_E^\infty dE' \int_{4\pi} d\Omega' \frac{1}{\xi} k_A(E',E,\cos\Theta;x_A,y_A,z_A) N_B(E';\theta',\phi';x_B,y_B,z_B)$$
$$+ \frac{1}{\xi} S_A(E;\theta,\phi;x_A,y_A,z_A) \tag{I-11.4}$$

The boundary conditions at corresponding points must be the same, and it is clear that

$$N_B(E;\theta,\phi;x_B,y_B,z_B) = N_A(E;\theta,\phi;x_A,y_A,z_A) \ . \qquad \text{(I-11.5)}$$

This is the basis for the experimental work with scale models which has been informative and useful.

C. TRANSFORMATIONS OF THE TRANSPORT EQUATION

12 Applications of Superposition

In this and the next few sections, we discuss forms of the transport equation which lend themselves to analysis more easily than, for example, Equation (I-5.6). Here we examine some of the elementary source types which are useful because they can be used in various linear combinations to represent more complicated sources of interest.

Recall that the linearity of the transport equation has as a consequence that a representation of a source function S as

$$S = \sum_i a_i S_i \qquad \text{(I-12.1)}$$

implies that the solution of the transport equation, N, has the form

$$N = \sum_i a_i N_i \ , \qquad \text{(I-12.2)}$$

where the N_i are solutions corresponding to the S_i. This holds also when the source is an integral over some parameter ξ, rather than a sum. Thus

$$S = \int d\xi f(\xi) S(\xi) \qquad \text{(I-12.3)}$$

implies that

$$N = \int d\xi f(\xi) N(\xi) \ , \qquad \text{(I-12.4)}$$

where $f(\xi)$ is arbitrary and $N(\xi)$ is the solution corresponding to the source $S(\xi)$. We will consider what this means for each of the variables of the source function in turn.

a) Energy. Considering first the energy dependence, $S = S(E)$, and not bothering to write in the other variables, we observe that

$$S(E) = \int_0^\infty dE_0 S(E_0)\delta(E - E_0) , \qquad \text{(I-12.5)}$$

where $\delta(E - E_0)$ is the Dirac delta function. This demonstrates the superposition possibilities of the delta-function source. Such sources can be combined to give any polychromatic source of interest.

This is about the only type of elementary energy dependence used for superpositions. In principle, sources which are harmonic in the energy variable, as well as exponential and power functions and many other possibilities, could be used; but so far none but the delta function has proven convenient for this purpose.

b) Direction. There are two common choices of elementary angular functions. First we consider monodirectional sources, which have the mathematical form

$$\delta(\cos\theta - \cos\theta_0)\delta(\phi - \phi_0) = \delta(\vec{\omega} - \vec{\omega}_0) . \qquad \text{(I-12.6)}$$

Here we have indicated a shorthand notation often used in Reference 15 which we will use to shorten some of the mathematical expressions. Superposition possibilities of monodirectional sources are demonstrated by the

expression

$$S(\theta,\phi) = \int_{4\pi} d\Omega_0 S(\theta_0,\phi_0)\delta(\cos\theta - \cos\theta_0)\delta(\phi - \phi_0) \ , \qquad \text{(I-12.7)}$$

where $S(\theta_0,\phi_0)$ is arbitrary.

The other useful type of elementary function is the harmonic source, with an angular dependence of the form*

$$Y_\ell^m(\theta,\phi) = (-1)^m\left[\frac{2\ell+1}{4\pi}\frac{(\ell-m)!}{(\ell+m)!}\right]^{\frac{1}{2}} P_\ell^m(\cos\theta)e^{im\phi} \ , \qquad \text{(I-12.8)}$$

where $P_\ell^m(\cos\theta)$ is the associated Legendre polynomial,

$$P_\ell^m(x) = \frac{(-1)^m}{2^\ell \ell!}(1-x^2)^{\frac{m}{2}}\left\{\frac{d}{dx}\right\}^{\ell+m}(x^2-1)^\ell \ ,$$

$$P_\ell^{-m}(x) = (-1)^m \frac{(\ell-m)!}{(\ell+m)!} P_\ell^m(x) \ . \qquad \text{(I-12.9)}$$

Possibilities for using these functions for superpositions result from the fact that arbitrary functions $S(\theta,\phi)$ can be represented in the series form

$$S(\theta,\phi) = \sum_{\ell=0}^{\infty}\sum_{m=-\ell}^{\ell} S_\ell^m Y_\ell^m(\theta,\phi) \ , \qquad \text{(I-12.10)}$$

---

*See Ref. 30, pages 159 ff and 197.

a special case of Equation (I-12.1), since the S_ℓ^m are independent of θ and ϕ.

c) Space. In regards to the space variables, several choices of elementary functions have been made. Perhaps the most obvious choice is again the delta-function source, here representing a source concentrated at a point in space,

$$\delta(x - x_0)\delta(y - y_0)\delta(z - z_0) = \delta(\vec{r} - \vec{r}_0), \tag{I-12.11}$$

where the right side again introduces a shorthand notation. Usefulness of superpositions of this type is demonstrated by the integral

$$S(x,y,z) = \int_{\text{All space}} \int \int dx_0 dy_0 dz_0 S(x_0,y_0,z_0)\delta(x - x_0)\delta(y - y_0)\delta(z - z_0) , \tag{I-12.12}$$

where $S(x_0,y_0,z_0)$ is any function of the space variables.

A second type of function which should be mentioned is the exponential function $e^{i\vec{q}\cdot(\vec{r}-\vec{r}_0)}$ The possibility of representing general functions of the space variables in this way is clear from the expression

$$\begin{aligned}\delta(x - x_0)\delta(y - y_0)\delta(z - z_0) &= \{\tfrac{1}{2\pi}\textstyle\int_{-\infty}^{\infty} dq_x e^{iq_x(x-x_0)}\}\{\tfrac{1}{2\pi}\int_{-\infty}^{\infty} dq_y e^{iq_y(y-y_0)}\} \\ &\quad \times \{\tfrac{1}{2\pi}\textstyle\int_{-\infty}^{\infty} dq_z e^{iq_z(z-z_0)}\} \\ &= \frac{1}{(2\pi)^3}\int_{\text{All q space}} \int \int dq_x dq_y dq_z e^{i[q_x(x-x_0)+q_y(y-y_0)+q_z(z-z_0)]} \\ &= \frac{1}{(2\pi)^3}\int_{\text{All q}} d\tau_q e^{i\vec{q}\cdot(\vec{r}-\vec{r}_0)}\end{aligned} \tag{I-12.13}$$

where $\vec{q} = \vec{i}q_x + \vec{j}q_y + \vec{k}q_z$, $d\tau_q = dq_x dq_y dq_z$. If the product of delta functions in the integrand of Equation (I-12.12) is replaced by the Fourier integral on the right of Equation (I-12.13), we obtain

$$S(x,y,z) = \int d\tau_0 S(x_0,y_0,z_0) \frac{1}{(2\pi)^3} \int d\tau_q e^{i\vec{q}\cdot(\vec{r}-\vec{r}_0)} ,$$

$$= \frac{1}{(2\pi)^3} \int d\tau_q e^{i\vec{q}\cdot\vec{r}} \int d\tau_0 S(x_0,y_0,z_0) e^{-i\vec{q}\cdot\vec{r}_0} ,$$

$$= S(\vec{r}) = \frac{1}{(2\pi)^3} \int d\tau_q e^{i\vec{q}\cdot\vec{r}} S(\vec{q}) , \qquad \text{(I-12.14)}$$

where $S(q_x,q_y,q_z)$ is the Fourier transform of S . The Fourier integral, Equation (I-12.14), demonstrates the superposition possibilities of this type of function.

From our point of view, the most important elementary function for use in representing space distributions is the function

$$\delta(\vec{q}\cdot\vec{r} - s) , \qquad \text{(I-12.15)}$$

which represents a source uniformly distributed on a plane in space. Its generality is not obvious, but can be demonstrated by a simple extension of Equation (I-12.14). We write

$$e^{i\vec{q}\cdot\vec{r}} = \int_{-\infty}^{\infty} ds e^{is} \frac{1}{q} \delta[\frac{1}{q}(\vec{q}\cdot\vec{r} - s)] \qquad \text{(I-12.16)}$$

and insert the expression on the right into Equation (I-12.14), replacing

the exponential function. The resulting expression,

$$S(x,y,z) = \frac{1}{(2\pi)^3} \int_{\text{All } q} d\tau_q \int_{-\infty}^{\infty} ds e^{is} \frac{1}{q} S(\vec{q}) \delta[\frac{1}{q}(\vec{q}\cdot\vec{r} - s)] \ , \qquad \text{(I-12.17)}$$

shows the manner in which arbitrary functions of the spatial variables can be represented as superpositions of the functions (I-12.15).

The planes $\vec{q}\cdot\vec{r} = s$ are oriented in many different directions. This is not particularly a drawback, because it is possible to identify any of these planes as the reference plane $z = 0$. for purposes of solution of the transport equation and transform it, with the corresponding solution, as needed for Equation (I-12.17). That is to say, we can obtain solutions $N(z)$ to transport equations with source functions proportional to $\delta(z)$. In accordance with Equation (I-12.17) , the flux $N(x,y,z)$ for problems with source functions $S(x,y,z)$ is given by

$$N(x,y,z) = \frac{1}{(2\pi)^3} \int d\tau_q \int_{-\infty}^{\infty} ds e^{is} \frac{1}{q} S(\vec{q}) N[\frac{1}{q}(\vec{q}\cdot\vec{r} - s)]$$

$$= \frac{1}{(2\pi)^3} \int d\tau_q \int_{-\infty}^{\infty} dt e^{i(\vec{q}\cdot\vec{r} - qt)} S(\vec{q}) N(t)$$

$$= \frac{1}{(2\pi)^3} \int d\tau_q e^{i\vec{q}\cdot\vec{r}} S(\vec{q}) \Phi(q) \ , \qquad \text{(I-12.18)}$$

where $\Phi(q)$ is the Fourier transform of $N(z)$. Note that the direction normal to the source plane is here identified with the direction $\vec{q}/q$, and that Φ may depend on $\vec{q}$ through use of $\vec{q}/q$ as reference axis for the photon direction of motion.

d) Combinations. The various elementary functions mentioned so far can be combined in a great many ways. We do not have occasion to refer to them all, and so must omit some that are very important. Three source types will be the subject of much of our later discussion: first we should mention a monoenergetic, isotropic source which is concentrated at point in space, the so-called point isotropic (PTI) source,

$$S^{PTI}(E;\theta,\phi;x,y,z) = \frac{1}{4\pi}\delta(E - E_0)\delta(x)\delta(y)\delta(z)$$

$$= \frac{1}{16\pi^2 r^2}\delta(E - E_0)\delta(r) , \qquad r = \sqrt{x^2 + y^2 + z^2} \ . \tag{I-12.19}$$

A source of this type producing one photon/Mev·steradian cm^3, or this strength per second, will be called a unit source, since integration over energy, direction, and space gives unity.

Closely related to the point isotropic source is the so-called plane isotropic source (PLI), which we here consider to be monoenergetic as well,

$$S^{PLI}(E;\theta,\phi;x,y,z) = \frac{1}{4\pi}\delta(E - E_0)\delta(z) \ . \tag{I-12.20}$$

The strength of a unit source of this type is, for example, one photon/Mev·steradian produced per cm^2 area of the source plane, per cm thickness of the source plane. (We consider the source plane to be of vanishing thickness, and the product of source strength times source thickness to be

finite, i. e., one/Mev·steradian·cm^2.) Again the time variable can either be included or omitted, since time variations play no part in the transport equation.

Finally, the plane oblique source (PLO) should be mentioned, and again we consider the case of greatest interest to be monoenergetic:

$$S^{PLO}(E;\theta,\phi;x,y,z) = \frac{1}{2\pi}\delta(E - E_0)\delta(z)\delta(\cos\theta - \cos\theta_0) \quad . \qquad \text{(I-12.21)}$$

In the case of the plane oblique source, we assume that there is no azimuth dependence, in contrast to the monodirectional source of Equation (I-12.6). Sometimes the source which we here describe as "oblique" is called a "conical" source.

A special case of the plane oblique source is the plane normal source (PLN), for which $\cos\theta_0 = 1$,

$$S^{PLN}(E;\theta,\phi;x,y,z) = \frac{1}{2\pi}\delta(E - E_0)\delta(z)\delta(\cos\theta - 1) \quad . \qquad \text{(I-12.22)}$$

Units for the plane oblique source are the same as for the plane isotropic source.

e) Relationships. In conclusion, we call attention to the most useful relationships between types of sources just specified, namely

$$S^{PLI} = \int_{-\infty}^{\infty} dx \int_{-\infty}^{\infty} dy S^{PTI} \quad , \qquad \text{(I-12.23)}$$

as can be seen from Equation (I-12.11), and

$$S^{PLI} = \frac{1}{2}\int_{-1}^{1} d\cos\theta_0 S^{PLO} , \qquad \text{(I-12.24)}$$

as can be seen from Equation (I-12.21). These are the basis for relationships between flux distributions to be discussed later.

13. The Fourier Transformation

a) Plane Source in an Infinite Homogeneous Medium. The Fourier transform of the transport equation is a useful point of departure for a number of general studies, particularly of the radiation flux at great distances from the source. Only the case of an infinite homogeneous medium will be considered, and the simplicity and generality of the case of a radiation source uniformly distributed along a plane encourages us to concentrate attention on this case. The transport equation then has the form

$$\cos\theta\frac{\partial N}{\partial z} + \mu(E)N(E,\theta,\phi,z) = \int_E^\infty dE' \int_{4\pi} d\Omega' k(E',E,\cos\Theta)N(E',\theta',\phi',z) + S(E,\theta,\phi)\delta(z) . \tag{I-13.1}$$

We multiply each term of this equation by e^{-iqz}, and integrate over all z. Thus treated, the second term gives

$$\int_{-\infty}^{\infty} dz e^{-iqz}\mu(E)N(E,\theta,\phi,z) = \mu(E)\Phi(E,\theta,\phi,-iq) , \tag{I-13.2}$$

where

$$\Phi(E,\theta,\phi,-iq) = \int_{-\infty}^{\infty} dz e^{-iqz}N(E,\theta,\Phi,z) . \tag{I-13.3}$$

The convection term requires integration by parts:

$$\int_{-\infty}^{\infty} dz e^{-iqz}\cos\theta\frac{\partial N}{\partial z} = \cos\theta N(E,\theta,\phi,z)e^{-iqz}\Big]_{-\infty}^{\infty} + iq\int_{-\infty}^{\infty} dz e^{-iqz}\cos\theta N = +iq\cos\theta\Phi(E,\theta,\phi,-iq). \tag{I-13.4}$$

We have applied here the boundary condition $\lim_{|z|\to\infty} N(E,\theta,\phi,z) = 0$. The scattering term transforms as follows:

$$\int_{-\infty}^{\infty} dz e^{-iqz} \int_{E}^{\infty} dE' \int_{4\pi} d\Omega' k(E',E,\cos\theta) N(E',\theta',\phi',z) = \int_{E}^{\infty} dE' \int_{4\pi} d\Omega' k(E',E,\cos\theta) \Phi(E',\theta',\phi',-iq). \tag{I-13.5}$$

Lastly, the source term becomes

$$\int_{-\infty}^{\infty} dz e^{-iqz} S(E,\theta,\phi)\delta(z) = S(E,\theta,\phi) . \tag{I-13.6}$$

Putting all terms together, our transformed equation has the form

$$(\mu + iq\cos\theta)\Phi(E,\theta,\phi,iq) = \int_{E}^{\infty} dE' \int_{4\pi} d\Omega' k(E',E,\cos\theta)\Phi(E',\theta',\phi',-iq) + S(E,\theta,\phi) . \tag{I-13.7}$$

Or, writing $p = -iq$, we may prefer the form

$$(\mu - p\cos\theta)\Phi(E,\theta,\phi,p) = \int_{E}^{\infty} dE' \int_{4\pi} d\Omega' k(E',E,\cos\theta)\Phi(E',\theta',\phi',p) + S(E,\theta,\phi) . \tag{I-13.8}$$

Note that Equation (I-13.7) could alternately have been obtained by choosing an appropriate exponential spatial distribution for the source,

$$S(E,\theta,\phi)e^{iqz},$$

and then assuming that the spatial distribution of the radiation flux must

follow the same distribution.

It is quite important to observe that in terms of p, Equation (I-13.3) is

$$\Phi(E,\theta,\phi,p) = \int_{-\infty}^{\infty} dz e^{pz} N(E,\theta,\phi;z) \quad . \tag{I-13.9}$$

For real and positive values of p,, the exponential function in the integrand is very large for z positive and large. Indeed, the main contributions to this integrand come from such a z region. We therefore associate real, positive p values with large positive z values.

b) Integral Form of the Transport Equation.

While on the subject, we use Equation (I-13.7) to write the transport equation in integral form. If we divide by the factor multiplying Φ on the left side of the equation, and observe that

$$\frac{1}{\mu+iq\cos\theta} = \int_0^\infty ds e^{-s(\mu+iq\cos\theta)} ,$$

we see that this equation may be written

$$\Phi(E,\theta,-iq) = \int_0^\infty ds e^{-s(\mu+iq\cos\theta)} \left\{ \int_E^\infty dE' \int_{4\pi} d\Omega' k(E',E,\cos\theta)\Phi(E',\theta',-iq) + S(E,\theta) \right\}. \quad \text{(I-13.10)}$$

Taking the inverse Fourier transformation, we obtain

$$N(E,\theta,z) = \frac{1}{2\pi}\int_{-\infty}^{\infty} dq e^{+iqz} \Phi(E,\theta,-iq)$$

$$= \int_0^\infty ds e^{-\mu s} \left\{ \int_E^\infty dE' \int_{4\pi} d\Omega' k(E',E,\cos\theta) N(E',\theta',z-s\cos\theta) + S(E,\theta)\delta(z-s\cos\theta) \right\}. \quad \text{(I-13.11)}$$

If we carry out the integral over the source term, we obtain the more familiar form*

$$N(E,\theta,z) = \int_0^\infty ds e^{-\mu s} \int_E^\infty dE' \int_{4\pi} d\Omega' k(E',E,\cos\theta) N(E',\theta',z-s\cos\theta)$$

$$+ S(E,\theta) \frac{e^{-\mu\, z/\cos\theta}}{|\cos\theta|} h(z/\cos\theta) . \quad \text{(I-13.12)}$$

*Note that $h(x) = \begin{cases} 1, & x \geq 0 \\ 0, & x < 0 \end{cases}$.

In conclusion, one may observe that if Equation (I-13.10) is used in connection with (I-12.18), analogous expressions for other source configurations can be obtained.

14. The Legendre Expansion

To discuss the Legendre expansion of the transport equation, it is essential to know some of the elementary properties of Legendre functions. For this purpose any standard treatise should be adequate; but since we only use a few fundamental expressions, it would not be amiss to list these prior to their application. We will make use of the Y_ℓ^m functions defined by Equation (I-12.8), which have the properties listed below. Note that $\bar{Y}_\ell^m$ is the complex conjugate of Y_ℓ^m.

ORTHOGONALITY:

$$\int_{4\pi} d\Omega \bar{Y}_{\ell'}^{m'}(\theta,\phi)\, Y_\ell^m(\theta,\phi) = \delta_{\ell\ell'}\delta_{mm'} \qquad \text{(I-14.1)}$$

EXPANSION OF FUNCTIONS:

$$F(\theta,\phi) = \sum_{\ell=0}^{\infty} \sum_{m=-\ell}^{\ell} \left\{\frac{2\ell+1}{4\pi}\right\}^{1/2} F_\ell^m Y_\ell^m(\theta,\phi)\ , \qquad \text{(I-14.2)}$$

where

$$F_\ell^m = \left\{\frac{4\pi}{2\ell+1}\right\}^{1/2} \int_{4\pi} d\Omega \bar{Y}_\ell^m(\theta,\phi) F(\theta,\phi) \qquad \text{(I-14.3)}$$

ADDITION FORMULA:

$$Y_\ell^0(\Theta) = \sqrt{\frac{4\pi}{2\ell+1}} \sum_{m=-\ell}^{\ell} \bar{Y}_\ell^m(\theta',\phi') Y_\ell^m(\theta,\phi)\ , \qquad \text{(I-14.4)}$$

where $\cos\Theta = \cos\theta'\cos\theta + \sin\theta'\sin\theta\cos(\phi-\phi')$. Combination of Equations

(I-14.2) and (I-14.4) gives the

FOLDING RULE:*

$$\int_{4\pi} d\Omega \bar{Y}_\ell^m(\theta,\phi)F(\Omega) = F_\ell \bar{Y}_\ell^m(\theta',\phi') \ , \qquad \text{(I-14.5)}$$

where

$$F_\ell = \sqrt{\frac{4\pi}{2\ell+1}} \int_{4\pi} d\Omega \bar{Y}_\ell^0(\Omega)F(\Omega) \ . \qquad \text{(I-14.6)}$$

Lastly we record the

RECURSION FORMULA:

$$\cos\theta Y_\ell^m(\theta,\phi) = \left\{\frac{(\ell+1)^2-m^2}{(2\ell+1)(2\ell+3)}\right\}^{1/2} Y_{\ell+1}^m + \left\{\frac{\ell^2-m^2}{(2\ell+1)(2\ell-1)}\right\}^{1/2} Y_{\ell-1}^m \ . \qquad \text{(I-14.7)}$$

With these expressions it is a simple matter to apply the Legendre expansion to the transport equation, as given in Equation (I-13.1):

$$\int_{4\pi} d\Omega \left\{\frac{4\pi}{2\ell+1}\right\}^{1/2} \bar{Y}_\ell^m(\theta,\phi)\left\{\cos\theta\frac{\partial N}{\partial z} + \mu N - \int_E^\infty dE' \int_{4\pi} d\Omega' kN - S\delta(z)\right\} \ . \qquad \text{(I-14.8)}$$

According to (I-14.3), the second and fourth terms of this integral are μN_ℓ^m and $S_\ell^m\delta(z)$, respectively. Applying (I-14.7) to the first term we see that it has the form

$$\left\{\frac{4\pi}{2\ell+1}\right\}^{1/2}\left\{\left[\frac{(\ell+1)^2-m^2}{(2\ell+1)(2\ell+3)}\right]^{1/2}\left[\frac{2\ell+3}{4\pi}\right]^{1/2}\frac{\partial N_{\ell+1}^m}{\partial z} + \left[\frac{\ell^2-m^2}{(2\ell+1)(2\ell-1)}\right]^{1/2}\left[\frac{2\ell-1}{4\pi}\right]^{1/2}\frac{\partial N_{\ell-1}^m}{\partial z}\right\}$$

$$= \frac{1}{2\ell+1}\left\{\sqrt{(\ell+1)^2-m^2}\ \frac{\partial N_{\ell+1}^m}{\partial z} + \sqrt{\ell^2-m^2}\ \frac{\partial N_{\ell-1}^m}{\partial z}\right\} \ .$$

*This is not a commonly used name.

Applying the folding rule (I-14.5) to the third term, we make the following calculation, after changing the order of integrations:

$$\int_E^\infty dE' \left\{\frac{4\pi}{2\ell+1}\right\}^{1/2} \int_{4\pi} d\Omega' N(E',\theta',\phi',z) \int_{4\pi} d\Omega \bar{Y}_\ell^m(\theta,\phi) k(E',E,\cos\Theta)$$

$$= \int_E^\infty dE' \left\{\frac{4\pi}{2\ell+1}\right\}^{1/2} \int_{4\pi} d\Omega' N(E',\theta',\phi',z) k_\ell(E',E) \bar{Y}_\ell^m(\theta',\phi')$$

$$= \int_E^\infty dE' k_\ell(E',E) N_\ell^m(E',z) \ . \qquad \text{(I-14.9)}$$

Putting all these results together, we obtain the transformed equation,

$$\frac{\sqrt{(\ell+1)^2-m^2}}{2\ell+1} \frac{\partial N_{\ell+1}^m}{\partial z} + \frac{\sqrt{\ell^2-m^2}}{2\ell+1} \frac{\partial N_{\ell-1}^m}{\partial z} + \mu(E) N_\ell^m(E,z)$$

$$= \int_E^\infty dE' k_\ell(E',E) N_\ell^m(E',z) + S_\ell^m(E)\delta(z) \ . \qquad \text{(I-14.10)}$$

This is essentially a recursion system linking together coefficients with adjacent values, in sets of three. The remarkable feature of this expression is the fact that no corresponding linkage exists between different m values. This azimuthal index is the same for all terms, so that a complete separation of the azimuthal variable has been accomplished.

For future reference, we list expressions for $k_\ell(E',E)$ and for the $S_\ell(E)$ expressions pertaining to the three major source types previously mentioned. Referring to Equation(I-3.9) and Equation (I-14.6), we see that $k_\ell(E',E)$ involves the integral

$$\sqrt{\frac{4\pi}{2\ell+1}} \int_{4\pi} d\Omega \bar{Y}_\ell^0(\theta) \frac{1}{2\pi} \delta(\cos\theta - 1 + \lambda - \lambda') = \int_{4\pi} d\Omega P_\ell(\cos\theta) \frac{1}{2\pi} \delta(\cos\theta - 1 + \lambda - \lambda')$$

$$= P_\ell(1 - \lambda + \lambda') , \qquad \text{(I-14.11)}$$

and thus has the value

$$k_\ell(E', E) = (N_A \sigma_{Th} Z/A) \frac{3}{8} (\lambda'/\lambda)^2 [\lambda/\lambda' + \lambda'/\lambda - 2(\lambda - \lambda') + (\lambda - \lambda')^2] P_\ell(1 - \lambda + \lambda') \frac{d\lambda}{dE} ,$$

(I-14.12)

where $\lambda = mc^2/E$ and $\lambda' = mc^2/E'$.

Referring to Equations (I-12.19), (I-12.20), and (I-12.21) we see that

$$S^{PLI}(E) = \sqrt{\frac{4\pi}{2\ell+1}} \int_{4\pi} d\Omega \bar{Y}_\ell^0(\theta) \frac{1}{4\pi} \delta(E_0 - E) ,$$

$$= \delta(E_0 - E) \frac{1}{\sqrt{2\ell+1}} \int_{4\pi} d\Omega \bar{Y}_\ell^0(\theta) \bar{Y}_0^0(\theta) ,$$

$$= \delta(E_0 - E) \delta_{\ell 0} . \qquad \text{(I-14.13)}$$

Further,

$$S_\ell^{PLO}(E) = \sqrt{\frac{4\pi}{2\ell+1}} \int_{4\pi} d\Omega \bar{Y}_\ell^0(\theta) \frac{1}{2\pi} \delta(E - E_0) \delta(\cos\theta - \cos\theta_0) ,$$

$$= \sqrt{\frac{4\pi}{2\ell+1}} \bar{Y}_\ell^0(\theta_0) \delta(E - E_0) ,$$

$$= P_\ell(\cos\theta_0) \delta(E - E_0) , \qquad \text{(I-14.14)}$$

and, as a special case,

$$S_{\ell}^{PLN}(E) = \delta(E - E_0) \ , \qquad \text{(I-14.15)}$$

since $P_{\ell}(1) = 1$.

15. The Moment Transformation

a) Transformation of the Transport Equation.

Many calculations of flux distributions utilize spatial moments, and we therefore next derive the recursion relation for these integral quantities. The most direct way of doing this is the multiplication of each term in Equation (I-13.1) by a power of z, say z^ν, $\nu>0$, and integration of the resulting terms. For later reference we will generalize to powers of (αz) rather than z, with α an arbitrary parameter. The second term of Equation (I-13.1) then gives

$$\int_{-\infty}^{\infty} dz(\alpha z)^\nu \mu(E)N(E,\theta,\phi,z) = \mu(E)N(E,\theta,\phi,\nu), \qquad \text{(I-15.1)}$$

where

$$N(E,\theta,\phi,\nu) = \int_{-\infty}^{\infty} dz(\alpha z)^\nu N(E,\theta,\phi,z) \ . \qquad \text{(I-15.2)}$$

The convection term, with integration by parts, gives

$$\int_{-\infty}^{\infty} dz(\alpha z)^\nu \cos\theta \frac{\partial N(E,\theta,\phi,z)}{\partial z} = (\alpha z)^\nu \cos\theta N(E,\theta,\phi,z)\Big]_{-\infty}^{\infty} - \alpha\nu \int_{-\infty}^{\infty} dz(\alpha z)^{\nu-1} \cos\theta N(E,\theta,\phi,z)$$

$$= -\alpha\nu\cos\theta N(E,\theta,\phi,\nu-1) \ . \qquad \text{(I-15.3)}$$

The scattering and source terms turn out to be

$$\int_{-\infty}^{\infty} dz(\alpha z)^\nu \int_E^{\infty} dE' \int_{4\pi} d\Omega' k(E',E,\cos\theta)N(E',\theta',\phi',z) = \int_E^{\infty} dE' \int_{4\pi} d\Omega' k(E',E,\cos\theta)N(E',\theta'\phi',\nu)$$

and

$$\int_{-\infty}^{\infty} dz(\alpha z)^\nu S(E,\theta,\phi)\delta(z) = S(E,\theta,\phi)\delta_{\nu 0} \ .$$

Here the factor $\delta_{\nu 0}$ is the Kronecker delta, which vanishes for $\nu \neq 0$ and is unity for $\nu = 0$.

Combining all terms, we have the equation

$$-\alpha\nu\cos\theta N(E,\theta,\phi,\nu-1) + \mu(E)N(E,\theta,\phi,\nu) = \int_E^\infty dE' \int_{4\pi} d\Omega' k(E',E,\cos\theta)N(E',\theta',\phi',\nu)$$

$$+ S(E,\theta,\phi)\delta_{\nu 0} , \qquad \text{(I-15.4)}$$

which is a recursion system joining moments which differ in ν values by unity. The chain of moments can be calculated providing any single moment is known. Determination of the moment $\nu = 0$ turns out to be feasible because the first term of Equation (I-15.4) then does not appear, while the last term, a known function, is present. This means that values of $N(E,\theta,\phi,\nu)$, for which ν is a positive integer, can in principle be determined chainwise.

If we restrict our attention to positive integer values of ν , we find that Equation (I-15.4) can be derived from Equation (I-13.8). To accomplish this we write $\Phi(E,\theta,\phi,p)$ as a power series in p , and anticipate the result by identifying the expansion coefficients as $N(E,\theta,\phi,i)$:

$$\Phi(E,\theta,\phi,p) = \sum_{i=0}^{\infty} N(E,\theta,\phi,i)\frac{p^i}{\alpha^i i!} . \qquad \text{(I-15.5)}$$

Collecting all terms which multiply p^m , and equating to zero, we obtain Equation (I-15.4), thus confirming Equation (I-15.5). This result also follows by expansion of Equation (I-13.3) in powers of $p = -iq$.

b) The Combined Moment-Legendre Transformation.

The moment transformation can be applied to Equation (I-14.10), with almost no modification of the preceding argument. Writing n in place of ν to indicate that we restrict our attention to (positive) integer values, we obtain the equation

$$-\alpha n\left\{\frac{\sqrt{(\ell+1)^2-m^2}}{2\ell+1} N^m_{n-1,\ell+1}(E) + \frac{\sqrt{\ell^2-m^2}}{2\ell+1} N^m_{n-1,\ell-1}(E)\right\} + \mu(E)N^m_{n\ell}(E)$$

$$= \int_E^\infty dE' k_\ell(E',E)N^m_{n\ell}(E') + S^m_\ell(E)\delta_{n0} \,. \qquad \text{(I-15.6)}$$

This is a particularly simple recursive system. Note that when $\ell = |m|$, the second term vanishes. Figure I-15.1 shows the relationship of the coefficients in Equation (I-15.6), if m has a fixed value. The top row in the diagram, with $n = 0$, is particularly simple in that the factor n removes the linkage terms of the equation.

n \ ℓ-|m|	0	1	2	3	4
0					
1					
2					
3			$N^m_{n-1,\ell-1}$		$N^m_{n-1,\ell+1}$
4				$N^m_{n\ell}$	
5					
6					

Fig. I-15.1. Linkage system for the Moment-Legendre Transformation.

16. The Relationship between Point Isotropic and Plane Isotropic Sources.

We are now in a position to discuss the flux generated by a plane isotropic source, as a superposition of flux distributions for point isotropic sources. As stated in section 12, it is possible also to consider the point isotropic source as a superposition of plane sources; but this turns out to be more complicated and less useful, and we concentrate primarily on the former.

a) Plane Isotropic as a Superposition of Point Isotropic Sources.

The basic rule of combination must be the same as the superposition rule for the sources, Equation (I-12.23). But the flux distributions N^{PTI} and N^{PLI} depend also on photon direction; and this introduces an additional complication. If we indicate the photon direction by the unit vector $\vec{\omega}$, and use as polar axis for the plane source a unit vector $\vec{k}$ perpendicular to the source plane, the flux depends on the angle θ between the two vectors and can be written as a Legendre series, as in Equation (I-14.10), which we repeat here:

$$N^{PLI}(E,\theta,z) = \sum_{\ell=0}^{\infty} \sqrt{\frac{2\ell+1}{4\pi}}\, N_{\ell}^{PLI}(E,z) Y_{\ell}^{0}(\theta) \ , \qquad \text{(I-16.1)}$$

where $\cos\theta = \vec{\omega}\cdot\vec{k}$.

In the case of the point isotropic source there is no reference direction fixed in the configuration which makes a suitable polar axis for photon directions. Accordingly, the reference polar axis is commonly taken to be the radial line from source to photon position, as sketched

in Figure I-16.1. This means that while the photon directions are not dependent on position, the reference system for the direction coordinates is position dependent. The flux in the PTI source configuration can be written as a Legendre series very similar to Equation (I-16.1), namely

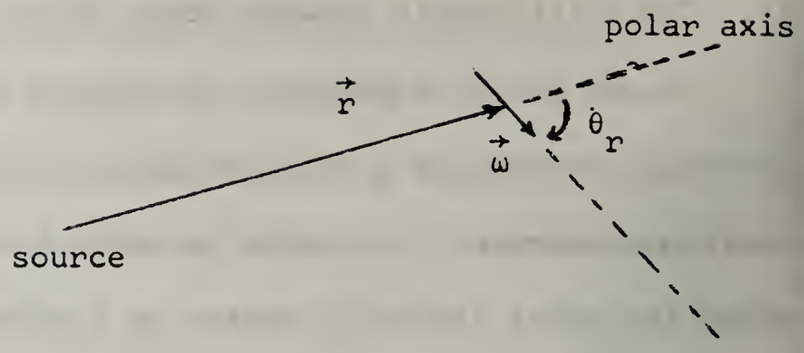

Fig. I-16.1

$$N^{PTI}(E,\theta_r,r) = \sum_{\ell=0}^{\infty} \sqrt{\frac{2\ell+1}{4\pi}}\, N^{PTI}(E,r) Y_\ell^0(\theta_r) , \qquad \text{(I-16.2)}$$

where $\cos\theta_r = \vec{\omega}\cdot\vec{u}$, with $\vec{u} = \vec{r}/r$.

Now, the three vectors $\vec{\omega}$, $\vec{k}$, and $\vec{u}$ define a spherical triangle, as shown in Figure I-16.2. (Recall that $\vec{r} \cdot \vec{k} = z$). An azimuthal angle, η , has been identified. The law of cosines holds for this spherical triangle, and Equation (I-14.5) can be applied to functions of θ and θ_r .

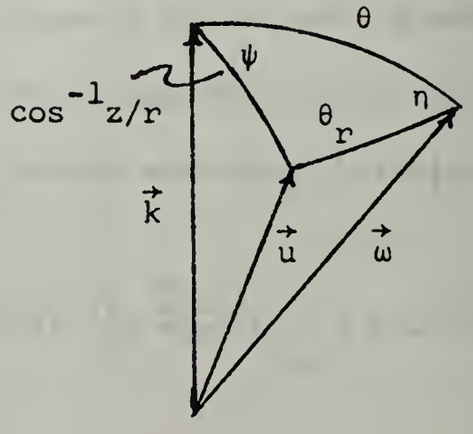

Fig. I-16.2

The basic relation between the fluxes must be

$$N^{PLI}(E,\theta,z) = \int_{-\infty}^{\infty} dx \int_{-\infty}^{\infty} dy N^{PTI}(E,\theta_r,r) , \qquad \text{(I-16.3)}$$

because of Equation (I-12.23).

Of far more interest is the expression relating coefficients of the corresponding Legendre series. This can be obtained by multiplying both sides of Equation (I-16.3) by $\sqrt{\frac{4\pi}{2\ell+1}}\,\bar{Y}_\ell^0(\theta)$, integrating, and using the relation shown in Equation (I-14.5):

$$N_\ell^{PLI}(E,z) = \int_{-\infty}^{\infty}dx\int_{-\infty}^{\infty}dy\sqrt{\frac{4\pi}{2\ell+1}}\int_{4\pi}d\Omega\bar{Y}_\ell^0(\theta)N^{PTI}(E,\theta_r,r)\ ,$$

$$= \int_{-\infty}^{\infty}dx\int_{-\infty}^{\infty}dyN_\ell^{PTI}(E,r)\sqrt{\frac{4\pi}{2\ell+1}}\,\bar{Y}_\ell^0(\cos^{-1}z/r)\ . \qquad \text{(I-16.4)}$$

Finally, changing to plane polar coordinates (ρ,ϕ) for the remaining integrations and noting from Fig. I-16.3 that $r^2 = z^2 + \rho^2$ implies

$$dxdy = \rho d\rho d\phi = rdrd\phi, \qquad \text{(I-16.5)}$$

we simplify Equation (I-16.4) to the form

$$N_\ell^{PLI}(E,z) = 2\pi\int_{|z|}^{\infty}rdrP_\ell(z/r)N_\ell^{PTI}(E,r)\ . \qquad \text{(I-16.6)}$$

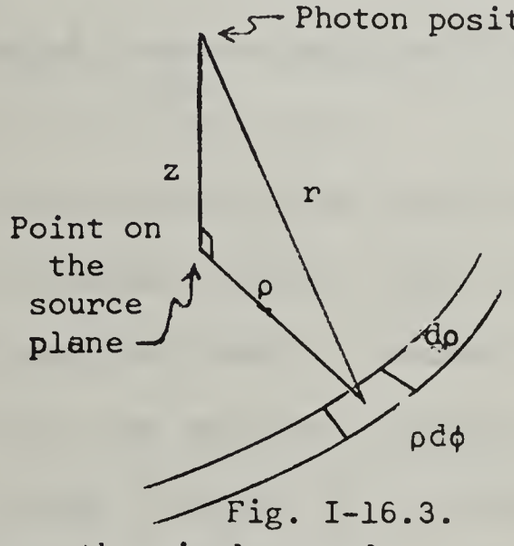

Fig. I-16.3.

Calculation of moments of this expression gives the simple result

$$N_{n\ell}^{PLI}(E) = \int_{-\infty}^{\infty}dz\ z^n 2\pi\int_{|z|}^{\infty}rdrP_\ell(\frac{z}{r})N_\ell^{PTI}(E,r) \qquad \text{(I-16.6')}$$

$$= \int_0^{\infty}dr\ r^n[4\pi r^2N_\ell^{PTI}(E,r)]\int_0^1 d(z/r)(z/r)^nP_\ell(z/r) = N_{n\ell}^{PTI}(E)C_{n\ell}\ ,$$

where the $C_{n\ell}$ are numbers further described in section 22.

b) Point Isotropic as a Superposition of Plane Isotropic Sources.

For reference purposes we derive a general expression for the point isotropic source in terms of plane isotropic sources. To this end we note from Equations (I-12.13) and (I-12.16) that the point source can be written as the following superposition of plane sources:

$$\delta(x - x_0)\delta(y - y_0)\delta(z - z_0) = \frac{1}{(2\pi)^3}\int d\tau_q e^{-i\vec{q}\cdot\vec{r}_0} e^{i\vec{q}\cdot\vec{r}}\int_{-\infty}^{\infty} dt e^{-i\vec{q}\cdot(t\vec{k})}\delta(t),. \tag{I-16.7}$$

where $\vec{q} = q\vec{k}$. From the special case $x_0 = y_0 = z_0 = 0$, we obtain

$$\delta(x)\delta(y)\delta(z) = \delta(\vec{r}) = \frac{1}{(2\pi)^3}\int d\tau_q e^{i\vec{q}\cdot\vec{r}}\int_{\infty}^{\infty} dt e^{-itq}\delta(t) . \tag{I-16.8}$$

We therefore write

$$N^{PTI}(E,\theta_r,r) = \frac{1}{(2\pi)^3}\int d\tau_q e^{i\vec{q}\cdot\vec{r}}\int_{\infty}^{\infty} dt e^{-itq} N^{PLI}(E,\theta,t) . \tag{I-16.9}$$

As indicated in the integrand of Equation (I-16.7), we consider the vector $(t\vec{k})$, which is parallel to $\vec{q}$, and which has magnitude equal to the distance t from the plane $\delta(t)$, to be perpendicular to this plane. Accordingly, the polar axis with respect to which θ is measured is parallel to $\vec{q}$, so that $\cos\theta = \vec{\omega}\cdot\vec{k}$.

Equation (I-16.9) can be transformed into an equation analogous to Equation (I-16.6) relating corresponding Legendre polynomial coefficients. We multiply Equation (I-16.9) by $\sqrt{\frac{4\pi}{2\ell+1}}\,\bar{Y}_\ell^0(\theta_r)$, note by Figure I-16.2 that $\vec{q}\cdot\vec{r} = qr[\cos\theta_r\cos\theta + \sin\theta_r\sin\theta\cos\eta]$, and apply the transformation of Equation (I-14.5) :

$$N_\ell^{PTI}(E,r) = \frac{1}{(2\pi)^3}\int d\tau_q\left\{\sqrt{\frac{4\pi}{2\ell+1}}\int d\Omega \bar{Y}_\ell^0(\theta_r)e^{i\vec{q}\cdot\vec{r}}\right\}\int_{\infty}^{\infty} dt e^{-itq} N^{PLI}(E,\theta,t)$$

$$= \frac{1}{(2\pi)^3}\int d\tau_q\sqrt{\frac{4}{2\ell+1}}\left[\sqrt{\frac{2\pi}{qr}}\, i^\ell J_{\ell+1/2}(qr)\bar{Y}_\ell^0(\theta)\right]\int_{\infty}^{\infty} dt e^{-itq} N^{PLI}(E,\theta,t$$

$$= \frac{1}{(2\pi)^2} \int_0^\infty q^2 dq \left[\sqrt{\frac{2\pi}{qr}}\, i^\ell J_{\ell+1/2}(qr)\right] \int_{-\infty}^{\infty} dt e^{-itq} \sqrt{\frac{4\pi}{2\ell+1}}$$

$$\times \int d\Omega_q \bar{Y}_\ell^0(\theta) N^{PLI}(E,\theta,t)$$

$$= \frac{i^\ell}{(2\pi)^2} \int_0^\infty q^2 dq \sqrt{\frac{2\pi}{qr}}\, J_{\ell+1/2}(qr) \int_{-\infty}^{\infty} dt e^{-itq} N_\ell^{PLI}(E,t) \ . \qquad \text{(I-16.10)}$$

We have used here a well-known integral representation for the Bessel function.*

This expression can be put in a variety of alternate forms, which we shall not use, and therefore have no reason to investigate here.

---

* See, for example, p. 50, Bessel Functions, G. N. Watson, (MacMillan, 1948 edition.)

17. The Transport Equation in Dimensionless Variables.

From some points of view, the natural energy variable to use in gamma ray calcuations is the photon wavelength in Compton units, which we have been designating λ. This suggests that other variables may be made dimensionless by introduction of appropriate scale factors, and that there may result a particularly general but simple form for this equation.

The change from photon energy to photon wavelength is easily accomplished by multiplying each term in Equation (I-13.1) by $dE/d\lambda$ and defining

$$N(\lambda,\theta,z) = -N(E,\theta,t)dE/d\lambda,$$

$$k(\lambda',\lambda,\cos\theta) = -k(E',E,\cos\theta)(dE/d\lambda),$$

$$S(\lambda,\theta) = -S(E,\theta)dE/d\lambda . \qquad \text{(I-17.1)}$$

The resulting equation is

$$\cos\theta\frac{\partial N}{\partial z} + \mu(\lambda)N(\lambda,\theta,z) = \int_0^{\lambda} d\lambda' \int_{4\pi} d\Omega' k(\lambda',\lambda,\cos\theta)N(\lambda',\theta',z) + S(\lambda,\theta)\delta(z) . \qquad \text{(I-17.2)}$$

A further step now turns out to be advantageous, that of changing the dependent variable from flux per unit wave length, N, to a new variable

$$I(\lambda,\theta,z) = \lambda N(\lambda,\theta,z) . \qquad \text{(I-17.3)}$$

It is very easily seen from Equation (I-17.1) that

$$I = -EN(E,\theta,z)\frac{d \log E}{d \log \lambda} = EN(E,\theta,z) , \qquad \text{(I-17.4)}$$

so that the variable I, interpreted as a function of photon energy is essentially an "energy flux." But the primary advantage to the use of this quantity is a resultant "smoothing" of the kernel in the scattering integral. If we multiply Equation (I-17.2) by λ, the equation takes the form

$$\cos\theta \frac{\partial I}{\partial z} + \mu(\lambda)I(\lambda,\theta,z) = \int_0^{\lambda} d\lambda' \int_{4\pi} d\Omega' \frac{\lambda}{\lambda'} k(\lambda',\lambda,\cos\Theta)I(\lambda',\theta',z) + \lambda S(\lambda,\theta)\delta(z) \ . \tag{I-17.5}$$

The additional factor in the integrand is quite effective in countering some of the variations of the scattering function, as will be seen.

Next, to de-dimensionalize the space variable, we divide each term in the transport equation by a constant,

$$\alpha = N_A \sigma_{Th} \frac{Z}{A} \rho \quad , \tag{I-17.6}$$

where ρ is the density, and we still use σ_{Th} to refer to the Thomson cross section. Recalling again that $\delta(z) = \alpha\delta(\alpha z)$, the equation becomes

$$\cos\theta \frac{\partial I}{\partial(\alpha z)} + \left[\frac{\mu(\lambda)}{\alpha}\right] I(\lambda,\theta,z) = \int_0^{\lambda} d\lambda' \int_{4\pi} d\Omega' \left\{\frac{\lambda}{\lambda'} \frac{1}{\alpha} k(\lambda',\lambda,\cos\Theta)\right\} I(\lambda',\theta',z)$$

$$+ \lambda S(\lambda,\theta)\delta(\alpha z) \ . \tag{I-17.7}$$

Finally, we re-define the variables of this equation as follows

$$\bar{z} = \alpha z \ ,$$

$$\bar{\mu} = \mu/\alpha \ ,$$

$$K(\lambda',\lambda,\cos\Theta) = \frac{\lambda}{\lambda'} \frac{1}{\alpha} k(\lambda',\lambda,\cos\Theta) = K_0(\lambda',\lambda) \frac{1}{2\pi} \delta(\cos\Theta - 1 + \lambda - \lambda') \ ,$$

with*

$$K_0(\lambda',\lambda) = \frac{3}{8}\frac{\lambda'}{\lambda}\left\{\frac{\lambda}{\lambda'} + \frac{\lambda'}{\lambda} - 2(\lambda - \lambda') + (\lambda - \lambda')^2\right\}h[2 - (\lambda-\lambda')] \ . \tag{I-17.8}$$

We use the same letters as before to designate distance and total attenuation coefficient. Observe that $\overline{\mu z} = \mu z$, so that distance in mean free paths is unchanged.

Finally, we divide all terms by the number of photons generated per cm^2 of the source plane and absorb the factor into I and S . In the resulting equation,

$$\cos\theta \frac{\partial I}{\partial \overline{z}} + \overline{\mu}(\lambda)I(\lambda,\theta,\overline{z}) = \int_0^{\lambda} d\Omega' \int_{4\pi} d\Omega' K(\lambda',\lambda,\cos\theta)I(\lambda',\theta',\overline{z}) + \lambda S(\lambda,\theta)\delta(\overline{z}) \ , \tag{I-17.9}$$

all quantities are then dimensionless.

---

*Note that $h(x) = \begin{cases} 1, & x \geq 0 \\ 0, & x < 0 \end{cases}$.

18. The Small Angle Approximation and the Fourier-Bessel Transformation.

Studies of the gamma-ray flux very far away from the radiation source make use of the fact that those gamma rays which manage to penetrate great distances must have had trajectories oriented away from the source throughout most of their travel. A correlation is expected between direction and depth of penetration: the deeper the penetration, the more important are these photon directions.

More specifically, suppose we consider the case of radiation originating on the plane $z = 0$. The relevant transport equation is either Equation (I-13.1) or the dimensionless Equation (I-17.9). It will be a little simpler to use the latter, and for our purpose the spatial Fourier transformation is useful. The transformed version of Equation (I-17.9) is

$$(\mu - p\cos\theta)\Phi(\lambda,\theta,p) = \int_0^{\lambda} d\lambda' \int_{4\pi} d\Omega' K(\lambda',\lambda,\cos\Theta)\Phi(\lambda',\theta,p) + \lambda S(\lambda,\theta) , \tag{I-18.1}$$

where we use Φ to represent the Fourier transform of $I(\lambda,\theta,z)$ (as well as $N(E,\theta,z)$) since no confusion is expected to result.

As discussed at the end of section 13a, positive p values in Equation (I-18.1) can be associated with positive z values. At positive z, "directly away from the source" means the direction $\theta = 0$, $\cos\theta = 1$. The expected importance of angles $\theta \approx 0$ makes it reasonable to use a simplified treatment which is accurate for small θ, even if the flux for large values of θ is distorted in this treatment.

Such a treatment is the so-called "small-angle approximation," in

which the trigonometric functions are approximated by

$$\cos\theta \approx 1 - \frac{\theta^2}{2} ,$$

$$\sin\theta \approx \theta , \qquad \text{(I-18.2)}$$

and therefore

$$\cos\Theta = \cos\theta\cos\theta' + \sin\theta\sin\theta'\cos(\phi - \phi')$$

$$\approx [1 - \frac{\theta^2}{2}][1 - \frac{\theta'^2}{2}] + \theta\theta'\cos(\phi - \phi')$$

$$\approx 1 - \frac{\theta^2}{2} - \frac{\theta'^2}{2} + \theta\theta'\cos(\phi - \phi') . \qquad \text{(I-18.3)}$$

If θ,ϕ are taken to be polar coordinates in a plane, with values of θ permitted on the range $0 \leq \theta < \infty$, Equation (I-18.3) can be written in the attractive form

$$\cos\Theta \approx 1 - \frac{1}{2}(\vec{\theta} - \vec{\theta}')^2 , \qquad \text{(I-18.4)}$$

where $\vec{\theta}$ and $\vec{\theta}'$ are position vectors of points in this plane with coordinates (θ,ϕ) and (θ',ϕ'), respectively.

To carry the discussion further, we use the expression for the scattering function and specialize to the plane isotropic, monoenergetic source, as given in Equation (I-17.8) and Equation (I-12.19). In small angle approximation these have the form

$$K(\lambda',\lambda,\Theta) \approx K_0(\lambda',\lambda)\frac{1}{2\pi}\delta[\frac{1}{2}(\vec{\theta} - \vec{\theta}')^2 - (\lambda - \lambda')] , \qquad \text{(I-18.5)}$$

$$\lambda S^{PLI}(\lambda,\theta) = \frac{1}{4\pi}\lambda\delta(E - E_0)dE/d\lambda ,$$

$$= \frac{1}{4\pi}\lambda_0\delta(\lambda - \lambda_0) , \qquad \text{(I-18.5)}$$

so that the transport equation for this case in small angle approximation is

$$[(\mu-p) + p\frac{\theta^2}{2}]\Phi(\lambda,\theta,p) = \int_0^{\lambda}d\lambda'\int_0^{\infty}\theta'd\theta'\int_0^{2\pi}d\phi' K_0(\lambda',\lambda)\frac{1}{2\pi}\delta[\frac{1}{2}(\vec{\theta}-\vec{\theta}')^2 - (\lambda-\lambda')]$$

$$\times \Phi(\lambda',\theta',p) + \frac{\lambda_0}{4\pi}\delta(\lambda-\lambda_0) . \qquad \text{(I-18.6)}$$

where $d\Omega' = -d\cos\theta' d\phi \approx -d(1-\frac{\theta'^2}{2})d\phi'$, and the integral covers the whole θ' plane.

The Legendre expansion is not suitable for the direction variables of this approximate equation. If we wish to transform the direction variables in a natural way we multiply the terms of the equation by

$$e^{i(\theta_x\sigma_x + \theta_y\sigma_y)} = e^{i(\vec{\theta}\cdot\vec{\sigma})} , \qquad \text{(I-18.7)}$$

where σ_x and σ_y are two constants, and integrate over the whole θ plane to obtain an equation for the function

$$\Phi(\lambda,\sigma,p) = \int_{-\infty}^{\infty}d\theta_x\int_{-\infty}^{\infty}d\theta_y e^{i(\theta_x\sigma_x + \theta_y\sigma_y)}\Phi(\lambda,\theta,p) \qquad \text{(I-18.8)}$$

$$= \int_0^{\infty}\theta d\theta\int_0^{2\pi}d\phi e^{i\vec{\theta}\cdot\vec{\sigma}}\Phi(\lambda,\theta,p) . \qquad \text{(I-18.9)}$$

By writing the arguments in each expression, we should be able to avoid confusion which might arise by using the Φ symbol once again.

This is the Fourier-Bessel transformation, the appropriateness of the name being apparent in the following form:

$$\Phi(\lambda,\sigma,p) = \int_0^\infty \theta d\theta \Phi(\lambda,\theta,p) \int_0^{2\pi} d\phi e^{i\theta\sigma\cos\phi}$$

$$= 2\pi \int_0^\infty \theta d\theta \Phi(\lambda,\theta,p) J_0(\theta\sigma) \ . \qquad \text{(I-18.10)}$$

Each term in Equation (I-18.6) requires a special discussion. In the first term we must use the differential equation satisfied by $J_0(\theta\sigma)$ to evaluate the integral:

$$2\pi \int_0^\infty \theta d\theta \left[p\frac{\theta^2}{2}\right] J_0(\theta\sigma)\Phi(\lambda,\theta,p) = 2\pi \int_0^\infty \theta d\theta \frac{p}{2}\left[-\frac{1}{\sigma}\frac{\partial}{\partial\sigma}\sigma\frac{\partial}{\partial\sigma}\right] J_0(\sigma\theta)\Phi(\lambda,\theta,p) \ ,$$

$$= -\frac{p}{2}\left[\frac{1}{\sigma}\frac{\partial}{\partial\sigma}\sigma\frac{\partial}{\partial\sigma}\right] 2\pi \int_0^\infty \theta d\theta J_0(\sigma\theta)\Phi(\lambda,\theta,p) \ ,$$

$$= -\frac{p}{2}\frac{1}{\sigma}\frac{\partial}{\partial\sigma}\sigma\frac{\partial}{\partial\sigma}\Phi(\lambda,\sigma,\phi) \ . \qquad \text{(I-18.11)}$$

In the final term we can use the two-dimensional form of Equation (I-12.13). Thus

$$\int_{-\infty}^{\infty} d\theta_x e^{i\theta_x\sigma_x} \int_{-\infty}^{\infty} d\theta_y e^{i\theta_y\sigma_y} \left\{\frac{\lambda_0}{4\pi}\delta(\lambda-\lambda_0)\right\} = \left\{\frac{\lambda_0}{4\pi}\delta(\lambda-\lambda_0)\right\}(2\pi)^2\delta(\sigma_x)\delta(\sigma_y) \ ,$$

$$= \left\{\frac{\lambda_0}{4\pi}\delta(\lambda-\lambda_0)\right\} 2\pi\delta\left(\frac{\sigma^2}{2}\right) \ . \ ^* \qquad \text{(I-18.12)}$$

---

* Note that $\delta(\sigma_x)\delta(\sigma_y)$ and $(2\pi)^{-1}\delta(\frac{\sigma^2}{2})$ are equivalent expressions.

The scattering term can be most easily transformed by use of a property of the Fourier-Bessel transformation analogous to Equation (I-14.5). If $F(\theta)$ is an arbitrary function,

$$\int_{-\infty}^{\infty} d\theta_x \int_{-\infty}^{\infty} d\theta_y e^{i(\vec{\theta}\cdot\vec{\sigma})} F(|\vec{\theta}-\vec{\theta}'|) = \int_{-\infty}^{\infty} d(\theta_x-\theta'_x) \int_{-\infty}^{\infty} d(\theta_y-\theta'_y) e^{i(\vec{\theta}'\cdot\vec{\sigma}) + i(\vec{\theta}-\vec{\theta}')\cdot\vec{\sigma}} F(|\vec{\theta}-\vec{\theta}'|) .$$

Writing $\vec{t} = \vec{\theta} - \vec{\theta}'$, this becomes

$$\int_{-\infty}^{\infty} d\theta_x \int_{-\infty}^{\infty} d\theta_y e^{i(\vec{\theta}\cdot\vec{\sigma})} F(|\vec{\theta}-\vec{\theta}'|) = \int_{-\infty}^{\infty} dt_x \int_{-\infty}^{\infty} dt_y e^{i(\vec{\theta}'\cdot\vec{\sigma}) + i(\vec{t}\cdot\vec{\sigma})} F(t)$$

$$= e^{i\vec{\theta}'\cdot\vec{\sigma}} \int_0^{\infty} t\,dt \int_0^{2\pi} d\psi e^{it\sigma\cos\psi} F(t)$$

$$= e^{i\vec{\theta}'\cdot\vec{\sigma}} F(\sigma) , \qquad \text{(I-18.13)}$$

where, following the convention of Equation (I-18.10), $F(\sigma)$ is the transform of $F(t)$.

Applying this relation to the scattering integral, we obtain

$$\int_{-\infty}^{\infty} d\theta_x \int_{-\infty}^{\infty} d\theta_y e^{i(\vec{\theta}\cdot\vec{\sigma})} \int_0^{\lambda} d\lambda' \int_{-\infty}^{\infty} d\theta'_x \int_{-\infty}^{\infty} d\theta'_y K_0(\lambda',\lambda) \frac{1}{2\pi} \delta[\tfrac{1}{2}(\vec{\theta}-\vec{\theta}')^2-(\lambda-\lambda')] \Phi(\lambda',\theta',p)$$

$$= \int_0^{\lambda} d\lambda' K_0(\lambda',\lambda) \int_{-\infty}^{\infty} d\theta'_x \int_{-\infty}^{\infty} d\theta'_y \Phi(\lambda',\theta',p) \left\{ \int_{-\infty}^{\infty} d\theta_x \int_{-\infty}^{\infty} d\theta_y e^{i(\vec{\theta}\cdot\vec{\sigma})} \frac{1}{2\pi} \delta[\tfrac{1}{2}(\vec{\theta}-\vec{\theta}')^2-(\lambda-\lambda')] \right\} ,$$

$$= \int_0^{\lambda} d\lambda' K_0(\lambda',\lambda) \left\{ \int_{-\infty}^{\infty} d\theta'_x \int_{-\infty}^{\infty} d\theta'_y \Phi(\lambda',\theta',p) e^{i\vec{\theta}'\cdot\vec{\sigma}} \right\} \left\{ \int_0^{\infty} t\,dt J_0(t\sigma) \delta[\frac{t^2}{2} - (\lambda-\lambda')] \right\} ,$$

$$= \int_0^{\lambda} d\lambda' K_0(\lambda',\lambda) \Phi(\lambda',\sigma,p) J_0[\sigma\sqrt{2(\lambda-\lambda')}] . \qquad \text{(I-18.14)}$$

Combining the different terms, now, we can write the complete equation,

$$[(\mu-p)-\frac{p}{2}\frac{1}{\sigma}\frac{\partial}{\partial\sigma}\sigma\frac{\partial}{\partial\sigma}]\Phi(\lambda,\sigma,p) = \int_0^{\lambda} d\lambda' K_0(\lambda',\lambda)\Phi(\lambda',\sigma,p)J_0[\sigma\sqrt{2(\lambda-\lambda')}]$$

$$+ \frac{1}{2}\lambda_0\delta(\lambda-\lambda_0)\delta(\frac{\sigma^2}{2}) \; . \qquad \text{(I-18.15)}$$

This equation offers an interesting contrast to the corresponding equation in which the more accurate Legendre equation is used and no small angle approximation is involved. The two equations can be made to correspond, term by term, with the discrete variable $(\ell + \frac{1}{2})$ playing the role in the more exact equation which σ plays in Equation (I-18.15).

19. Discussion of General Methods

Solutions to the transport equation have always leaned heavily on methods for obtaining limited amounts of specialized information.

One such method is the orders of scattering calculation, which will be discussed in the next section. In principle this type of calculation is perfectly general, and the information generated is exact. In practice the method is most useful in producing accurate information about radiation which has not been scattered, or which has been scattered only once or twice. Such information about the low orders of scattering is very useful: multiple scattering tends to smooth out irregularities in flux distributions. The irregular or discontinuous features of the flux distributions are contributed by components with low orders of scattering. Thus we learn the irregular features of the flux distributions by such orders-of-scattering analysis.

Other general methods permit the study of very deep penetrations. Some of these methods are likewise general and could yield information about the flux of radiation at any depth; but the power of this type of analysis is most felt in connection with the study of approximate equations which are correct only in the deep penetration limit. Information produced in such studies has several applications: occasionally the deep penetration studies represent the answer to a specific problem. Knowledge of the deep penetration trends has been used as a test of Monte Carlo methods,

and as a source of functional approximations in moments methods. Finally, the contrast between low orders of scattering results and deep penetration results gives a great deal of physical information about the penetration process, which involves transition between the two cases.

A third method which yields exact, but limited information, is the numerical calculation of spatial moments. In principle the method can be used to calculate any number of moments with arbitrary accuracy. In practice it is not feasible to determine more than, say, six to twelve moments of a flux distribution. Of these moments, only those that describe the integral over all space have an independent physical interpretation of sufficient interest to warrant special study.

The three types of partial information just mentioned complement one another very well. We obtain some of our best knowledge about flux distributions when we combine them. Methods for doing this are discussed in Part E of this manuscript.

20. Orders-of-Scattering Calculations

a) Discussion. A formal solution to the transport equation by orders of scattering can be obtained in a simple and straightforward manner. We write Eq. (I-13.1) in the form

$$\cos\theta\frac{\partial N}{\partial z} + \mu N = TN + S(E,\theta,\phi)\delta(z), \tag{I-20.1}$$

where the integral operator T is given by

$$TN(E,\theta,\phi,z) = \int_E^\infty dE' \int_{4\pi} d\Omega' k(E',E,\cos\Theta) N(E',\theta',\phi',z). \tag{I-20.2}$$

Next, we write the flux as the sum of terms corresponding to different orders of scattering,

$$N(E,\theta,\phi,z) = \sum_{i=0}^{\infty} N^{(i)}(E,\theta,\phi,z) \tag{I-20.3}$$

so that Eq. (I-20.1) becomes

$$\sum_{i=0}^{\infty} \left\{\cos\theta\frac{\partial N^{(i)}}{\partial z} + \mu N^{(i)}\right\} = \sum_{i=0}^{\infty} TN^{(i)} + S(E,\theta,\phi)\delta(z). \tag{I-20.4}$$

We relate the individual terms on left and right sides of (I-20.4) by the following simple rule:

$$\begin{aligned} \cos\theta\frac{\partial N^{(o)}}{\partial z} + \mu N^{(o)} &= S(E,\theta,\phi)\delta(z), \\ \cos\theta\frac{\partial N^{(i)}}{\partial z} + \mu N^{(i)} &= TN^{(i-1)}, \quad i \geq 1. \end{aligned} \tag{I-20.5}$$

These differential equations can now be solved recursively for all values of i.

Actually, however, we do not need to make a new effort to solve Eqs. (I-20.5). The same result is reached by applying iteration to Eq. (I-13.12), the integral form of the transport equation, or to its Fourier transform, Eq. (I-13.10). The result is

$$N^{(o)} = S(E,\theta,\phi)\frac{e^{-\mu z/\cos\theta}}{|\cos\theta|}h(z/\cos\theta), \quad h(x) = \begin{cases} 1, x\geq 0 \\ o, x<0, \end{cases}$$

$$N^{(i)} = \int_o^\infty ds e^{-\mu s} T N^{(i-1)}(E',\theta',\phi',z-s\cos\theta) \ , \ i\geq 1. \qquad \text{(I-20.6)}$$

We have already mentioned that the low orders of scattering contribute the sharp features to the penetration curves. This is evident in (I-20.6). If all photons travel initially with obliquities $\theta<\pi/2$, that is towards increasing z, $N^{(o)}$ will be discontinuous at $z = 0$ for arbitrary E,θ,ϕ. This discontinuity will persist through both angle and energy integrations and will characterize the spatial distribution of the dose due to unscattered photons. Further, because the total radiation beam is made up of the sum of the different orders of scattering, a discontinuity in the unscattered component will be introduced, unchanged in magnitude or position, into the total beam.

Since each order of scattering is obtained from the next lower by integration, the sharp features tend to be washed out step by step in the higher order components. Thus, a discontinuity in the $N^{(o)}$ implies a slope discontinuity in the $N^{(1)}$, and a corresponding discontinuity in the second spatial derivative of the $N^{(2)}$, etc.

Because low orders of scattering are often amenable to analysis, at least insofar as the discontinuous feature is concerned, we often wish to introduce these low orders of scattering--or their discontinuous features--

analytically into a distribution. This is apt to lead to a requirement for the moments of the $N^{(i)}$ for small i. Equations satisfied by these quantities can be obtained by applying moment and Legendre expansions to Eqs. (I-20.5). If we disregard the ϕ dependence and define

$$N_{n\ell}^{(i)}(E) = \int_{-\infty}^{\infty} dz(\alpha z)^n \sqrt{\frac{4\pi}{2\ell+1}} \int_{4\pi} d\Omega \bar{Y}_\ell^o(\cos\theta) N^{(i)}(E,\theta,z), \qquad \text{(I-20.7)}$$

the moment equations are (see (I-15.4), (I-14.18), and (I-14.20))

$$\mu N_{n\ell}^{(o)}(E) = S_\ell(E)\delta_{no} + \frac{n\alpha}{2\ell+1}\left\{(\ell+1)N_{n-1,\ell+1}^{(o)}(E) + \ell N_{n-1,\ell-1}^{(o)}(E)\right\},$$

$$\mu N_{n\ell}^{(i)}(E) = \int_E^{\infty} dE' k_\ell(E',E) N_{n\ell}^{(i-1)}(E') + \frac{n\alpha}{2\ell+1}\left\{(\ell+1)N_{n-1,\ell+1}^{(i)}(E) + \ell N_{n-1,\ell-1}^{(i)}(E)\right\}. \qquad \text{(I-20.8)}$$

b) Special cases. Eq. (I-20.6) gives the unscattered component for plane sources in general. But to obtain even one more component analytically it is necessary to specialize, for example, to a monoenergetic and monodirectional source. If in (I-20.6) we write

$$S(E,\theta,\phi) = \delta(E-E_o)\delta(\cos\theta-\cos\theta_o)\delta(\phi), \qquad \text{(I-20.8)}$$

straightforward calculation yields

$$N^{(1)} = \int_o^{\infty} ds e^{-\mu s} \int_E^{\infty} dE' \int_{4\pi} d\Omega' k(E',E,\cos\theta)\delta(E'-E_o)\delta(\cos\theta'-\cos\theta_o)\delta(\phi') \frac{e^{-\mu(E')(z-s\cos\theta)/\cos\theta'}}{|\cos\theta'|} h\left(\frac{z-s\cos\theta}{\cos\theta'}\right)$$

$$= k[E_o,E,\cos\theta_o] \frac{1}{|\cos\theta_o|} \int_o^{\infty} ds \exp\{-\mu(E)s - \mu(E_o)(z-s\cos\theta)/\cos\theta_o\} h\left(\frac{z-s\cos\theta}{\cos\theta_o}\right),$$

where $\cos\theta_o = \cos\theta_o\cos\theta + \sin\theta_o\sin\theta\cos\phi$. This leads to

$$N^{(1)} = k[E_o,E,\cos\theta]\frac{1}{\mu\cos\theta_o-\mu_o\cos\theta}\left(e^{\frac{-\mu_o z}{\cos\theta_o}} - e^{-\mu z/\cos\theta}\right), \text{ for } z,\cos\theta_o,\cos\theta>0,$$

$$= k[E_o,E,\cos\theta]\frac{1}{\mu\cos\theta_o-\mu_o\cos\theta}e^{-\mu_o z/\cos\theta_o}, \text{ for } z,\cos\theta_o>0 \text{ and } \cos\theta<0,$$

$$= k[E_o,E,\cos\theta]\frac{1}{\mu\cos\theta_o-\mu_o\cos\theta}e^{-\mu z/\cos\theta}, \text{ for } \cos\theta_o>0 \text{ and } z,\cos\theta<0.$$

(I-20.9)

The unscattered flux due to a plane isotropic source is an immediate consequence of Eq. (I-20.6) if we take $S(E,\theta,\phi) = S(E)/4\pi$. We then have

$$N^{(o)}_{PLI} = \frac{1}{4\pi}S(E)e^{-\mu(E)z/\cos\theta}\left|\frac{1}{\cos\theta}\right|h(z/\cos\theta). \qquad \text{(I-20.10)}$$

It is instructive to calculate the unscattered flux from a point isotropic source by superposition of plane sources. If we refer back to (I-12.18) and recall that for a point source, $S(\vec{q}) = 1$, we obtain using (I-20.10)

$$N^{(o)}_{PTI} = \frac{1}{(2\pi)^3}\int d\tau_q e^{i\vec{q}\cdot\vec{r}}\frac{\frac{1}{4\pi}S(E)}{\mu + i\vec{q}\cdot\vec{\omega}},$$

where $\vec{q}\cdot\vec{\omega}$ in the denominator replaces $q(\cos\theta)$, because of the identification of the normal to the source plane with the direction of $\vec{q}$. Recalling that

$$\frac{1}{\mu+i\vec{q}\cdot\vec{\omega}} = \int_0^\infty ds e^{-s(\mu+i\vec{q}\cdot\vec{\omega})}$$

we rewrite this expression as follows:

$$N_{PTI}^{(o)} = \frac{1}{4\pi} S(E) \int_o^\infty ds e^{-\mu s} \frac{1}{(2\pi)^3} \int d\tau_q \, e^{i\vec{q}\cdot(\vec{r}-s\vec{\omega})}$$

$$= \frac{1}{4\pi} S(E) \int_o^\infty s^2 ds \frac{e^{-\mu s}}{s^2} \delta(\vec{r}-s\vec{\omega}).$$

The Dirac delta function has the consequence that $s\vec{\omega} = \vec{r}$, which in turn means that $s = |\vec{r}| = r$, so that the $\underline{s}$-dependent factor may be removed from the integrand, and

$$N_{PTI}^{(o)} = \frac{1}{4\pi} S(E) \frac{e^{-\mu r}}{r^2} \int_o^\infty s^2 ds \delta(\vec{r}-s\vec{\omega}).$$

The remaining integral identifies the photon direction $\vec{\omega}$ with $|\frac{\vec{r}}{\vec{r}}|$. Since this integral factor must clearly give

$$\int d\Omega \int_o^\infty s^2 ds \delta(\vec{r}-s\vec{\omega}) = 1,$$

we may replace it with $\frac{1}{2\pi} \delta(\omega_r - 1)$, where $\omega_r = \vec{\omega} \cdot |\frac{\vec{r}}{\vec{r}}|$, which also integrates to unity and identifies the photon direction with the outward radial direction from the source. In conclusion,

$$N_{PTI}^{(o)} = S(E) \frac{1}{2\pi} \delta(\omega_r - 1) \frac{1}{4\pi r^2} e^{-\mu r} \qquad \text{(I-20.11)}$$

An expression for $N_{PTI}^{(1)}$ can be obtained by a similar, though more involved calculation; but it is much easier to calculate this quantity by other methods.

21. Analysis of Deep Penetration Trends*

The study of the deep penetration of gamma rays can proceed by use of approximations not valid at moderate penetrations. Hence, calculations of this type are difficult to generalize and yield partial, though extremely valuable, information.

There are common misconceptions about deeply penetrating radiations. On the one hand many people assume that the spectrum undergoes a progressive softening as the high energy radiations are degraded by scattering interactions. This fails to take account of the opposite tendency for the low-energy spectral components to be removed because they are less penetrating than the radiations which retain their high energy.

There is often another assumption that the spectrum achieves an equilibrium shape at some depth and does not change thereafter. This is more nearly the case than the concept of progressive softening, but it fails to take account of spectral regions near the most penetrating photon energy which are not in equilibrium. It is true that some energy regions come to relative equilibrium quickly, the faster the less penetrating the spectral region. Thereafter these regions retain a characteristic spectral shape, but the region as a whole may not be in equilibrium with other, much more penetrating spectral components.

Near the most penetrating component, there will exist at any penetration a non-equilibrium region. With increasing penetration this region narrows, and spectral variations across it increase.

All of these tendencies are illustrated in Refs. 16 and 35 .

Calculations for a plane isotropic source can make use of the small angle approximation and, correspondingly, the Fourier-Bessel transform of

*For a recent summary discussion, see Ref. 13 . The first analysis of this type is apparently due to Wick (Ref. 45).

the transport equation, (I-18.15),

$$[\mu - p - \frac{p}{2}\frac{1}{\sigma}\frac{\partial}{\partial\sigma}\sigma\frac{\partial}{\partial\sigma}]\Phi(\lambda,\sigma,p) = \int_{\lambda_o}^{\lambda} d\lambda' K_o(\lambda',\lambda) J_o(\sigma\sqrt{2(\lambda-\lambda')})\Phi(\lambda',\sigma,p) \qquad \text{(I-21.1)}$$

$$+ \frac{1}{2}\lambda_o \delta(\lambda-\lambda_o)\delta(\sigma^2/2).$$

a) Reduction to a Partial Differential Equation.

For an illustrative calculation, we will consider only the case in which the most penetrating photons are those produced by a (monoenergetic) source at λ_o, and the attenuation coefficient, $\mu(\lambda)$, increases linearly near λ_o:

$$\mu(\lambda) \doteq \mu_o + (\lambda-\lambda_o)\dot{\mu}_o. \qquad \text{(I-21.2)}$$

We assume at the outset that deep penetration implies a limitation to small-energy-loss scattering interactions, and will in any case confine our attention to wavelengths near λ_o, where the transition to spectral equilibrium is expected to occur. Both aspects of the problem suggest the approximation

$$K_o(\lambda',\lambda) \simeq K_o(\lambda,\lambda) = C. \qquad \text{(I-21.3)}$$

A more detailed study would show that this "approximation" does not disturb the limiting trends, and in this sense it is a simplification rather than an approximation.

Equation (I-21.1) now takes the form

$$[\dot{\mu}_o(\lambda-\lambda_o) + (\mu_o-p) - \frac{p}{2}\frac{1}{\sigma}\frac{\partial}{\partial\sigma}\sigma\frac{\partial}{\partial\sigma}]\Phi(\lambda,\sigma,p) = C\int_{\lambda_o}^{\lambda} d\lambda' J_o(\sigma\sqrt{2(\lambda-\lambda')})\Phi(\lambda',\sigma,p)$$

$$+ \frac{1}{2}\lambda_o\delta(\lambda-\lambda_o)\delta(\sigma^2/2). \qquad \text{(I-21.4)}$$

A Laplace transformation will reduce this to a recognizable partial differential equation. To accomplish this, each term is multiplied by $\exp[-\eta(\lambda-\lambda_o)/(\mu_o-p]$ and an integration is performed over $(\lambda-\lambda_o)$. To conserve symbols, we write

$$\Phi(\eta,\sigma,p) = \int_{\lambda_o}^{\infty} d\lambda\Phi(\lambda,\sigma,p)\exp[-\eta(\lambda-\lambda_o)/(\mu_o-p)]. \qquad \text{(I-21.5)}$$

Then we find that

$$\int_{\lambda_o}^{\infty} d\lambda\ (\lambda-\lambda_o)\Phi\exp[-\eta(\lambda-\lambda_o)/(\mu_o-p)] = -\frac{\partial}{\partial\eta}\Phi(\eta,\sigma,p)(\mu_o-p),$$

$$\int_{\lambda_o}^{\infty} d\lambda\delta(\lambda-\lambda_o)\exp[-\eta(\lambda-\lambda_o)/(\mu_o-p)] = 1.$$

Our last calculation, that of

$$\int_{\lambda_o}^{\infty} d\lambda\int_{\lambda_o}^{\lambda} d\lambda'\Phi(\lambda',\sigma,p)J_o(\sigma\sqrt{2(\lambda-\lambda')})\exp[-\eta(\lambda-\lambda_o)/(\mu_o-p)],$$

can be simplified by reference to Fig. I-21-1, where the shaded area denotes the region of integration. Changing the order of the integrals, we find that this double integral becomes

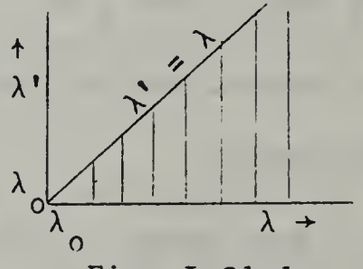

Fig. I-21.1.

$$\int_{\lambda_o}^{\infty} d\lambda \int_{\lambda_o}^{\lambda} d\lambda' \{\ \} = \int_{\lambda_o}^{\infty} d\lambda' \int_{\lambda'}^{\infty} d\lambda \{\ \} \qquad \text{(I-21.6)}$$

$$= \int_{\lambda_o}^{\infty} d\lambda' \{\phi(\lambda',\sigma,p) e^{-\mu \frac{(\lambda'-\lambda_o)}{\mu_o - p}}\} \int_{o}^{\infty} d(\lambda-\lambda') \{J_o(\sigma\sqrt{2(\lambda-\lambda')}) e^{-\eta \frac{(\lambda-\lambda')}{\mu_o - p}}\}.$$

The two integrations can be performed independently. Consulting a table of Laplace transforms to evaluate the integral over J_o, we obtain for the complete expression

$$\Phi(\eta,\sigma,p) \frac{(\mu_o - p)}{\eta} \exp[-\frac{\sigma^2}{2\eta}(\mu_o - p)].$$

Putting all results together, we write the transformed equation as follows:

$$[-(\mu_o - p)\dot{\mu}_o \frac{\partial}{\partial \eta} + (\mu_o - p) - \frac{n}{2} \frac{1}{\sigma} \frac{\partial}{\partial \sigma} \sigma \frac{\partial}{\partial \sigma}] \Phi(\eta,\sigma,\eta) = C(\frac{\mu_o - p}{\eta}) \Phi e^{-\frac{\sigma^2}{2\eta}(\mu_o - p)} + \frac{1}{2}\lambda_o \delta(\sigma^2/2).$$

(I-21.7)

This equation is equivalent to (I-21.4).

b) Separation of Variables.

Before proceeding to analyze the equation, we take advantage of a natural scaling property by replacing σ with the variable s,

$$s = \sigma \sqrt{\frac{\mu_o - p}{\eta}} . \qquad \text{(I-21.8)}$$

Since

$$\frac{\partial}{\partial \eta} \Phi(\eta,\sigma,p) = (\frac{\partial}{\partial \eta} + \frac{\partial s}{\partial \eta} \frac{\partial}{\partial s}) \Phi(\eta,s,p),$$

we can rewrite the equation in terms of s in simpler form,

240-816 O-67—9

$$\{-(\mu_o-p)\dot{\mu}_o(\frac{\partial}{\partial\eta}-\frac{s}{2\eta}\frac{\partial}{\partial s})+(\mu_o-p)-\frac{p}{2}\frac{(\mu_o-p)}{\eta}\frac{1}{s}\frac{\partial}{\partial s}s\frac{\partial}{\partial s}\}\Phi(\eta,s,p)$$

$$=C(\frac{\mu_o-p}{\eta})\Phi e^{-s^2/2}+(\frac{\mu_o-p}{\eta})\frac{1}{2}\lambda_o\delta(s^2/2). \qquad \text{(I-21.9)}$$

Deep penetrations correspond to p near μ_o. We therefore replace the factor p by μ_o in the last term on the left of (I-21.9). Then, removing from all terms the factor $(\mu_o-p)/\eta$, we group the terms as follows:

$$[-\dot{\mu}_o\,\eta\frac{\partial}{\partial\eta}+\eta]\Phi+[\dot{\mu}_o\frac{s}{2}\frac{\partial}{\partial s}-\frac{\mu_o}{2}\frac{1}{s}\frac{\partial}{\partial s}s\frac{\partial}{\partial s}-Ce^{-s^2/2}]\Phi$$

$$=\frac{1}{2}\lambda_o\delta(s^2/2). \qquad \text{(I-21.10)}$$

Separation of the variables s and η is clearly evident in this partial differential equation; and the second set of terms identifies an appropriate type of expansion, in terms of eigenfunctions of the equation

$$[\dot{\mu}_o\frac{s}{2}\frac{d}{ds}-\frac{\mu_o}{2}\frac{1}{s}\frac{d}{ds}s\frac{d}{ds}-Ce^{-s^2/2}]\psi=-\kappa\dot{\mu}_o\psi. \qquad \text{(I-21.11)}$$

We therefore represent Φ as the sum

$$\Phi(\eta,s,p)=\sum_{n=0}^{\infty}a_n(\eta,p)\psi_n(s), \qquad \text{(I-21.12)}$$

and insert this representation into Eq. (I-21.10), to obtain the equation

$$\sum_{n=0}^{\infty}[-\dot{\mu}_o\eta\frac{\partial}{\partial\eta}+\eta-\kappa_n\dot{\mu}_o]a_n(\eta,p)\psi_n(s)=\frac{1}{2}\lambda_o\delta(s^2/2). \qquad \text{(I-21.13)}$$

We next multiply this equation by $s\psi_k^\dagger(s)$, where $\psi_k^\dagger$ is adjoint to $\psi_k(s)$, and integrate over the range $s \geq 0$.* Assuming the $\psi_n(s)$ to be normalized so that

$$\int_0^\infty s\,ds\,\psi_k^\dagger(s)\psi_n(s) = \delta_{kn},$$

we obtain

$$\left[-\dot{\mu}_o \eta \frac{d}{d\eta} + \eta - \kappa_k \dot{\mu}_o\right] a_k(\eta,p) = \frac{1}{2}\lambda_o d_k^\dagger, \qquad \text{(I-21.14)}$$

where

$$d_k = \psi_k(0);\ d_k^\dagger = \psi_k^\dagger(0). \qquad \text{(I-21.15)}$$

Eq. (I-21.14) is an elementary differential equation, which can be solved by standard methods. An integrating factor is

$$\eta^{-1+\kappa_k} e^{-\eta/\dot{\mu}_o},$$

so that

$$\frac{d}{d\eta}\left\{-\dot{\mu}_o \eta^{\kappa_k} e^{-\eta/\dot{\mu}_o} a_k\right\} = \frac{1}{2}\lambda_o d_k^\dagger \eta^{-1+\kappa_k} e^{-\eta/\dot{\mu}_o},$$

and, correspondingly,

$$a_k = \frac{1}{2}\frac{\lambda_o d_k^\dagger}{\dot{\mu}_o}\int_\eta^\infty \frac{d\eta'}{\eta'} e^{-(\eta'-\eta)/\dot{\mu}_o}\left(\frac{\eta}{\eta'}\right)^{\kappa_k}. \qquad \text{(I-21.16)}$$

---

*See, for example, section 38.

c) Inversion of the Transforms.

Finally we wish to use this solution to calculate the total flux, integrated over all angles. Referring to Eq. (I-18.9), we see that the integral over all angles corresponds to $\sigma = 0$, which, by Eq. (I-21.8) corresponds to $s = 0$. By Eqs. (I-21.12) and (I-21.16) we must therefore evaluate the inverse transforms of

$$\Phi(\eta,o,p) = \sum_{n=o}^{\infty} a_n(\eta,p)\psi_n(o), \tag{I-21.17}$$

that is,

$$I_o(\lambda,z) = \frac{1}{2\pi i}\int dp e^{-pz}\frac{1}{2\pi i}\int d\left(\frac{\eta}{\mu_o-p}\right)e^{\eta(\lambda-\lambda_o)/(\mu_o-p)}\sum_{n=o}^{\infty} d_n a_n(\eta,p). \tag{I-21.18}$$

The inversion integrals can be most easily evaluated by utilizing a new variable in place of η',

$$u = \frac{\eta'-\eta}{\eta}\frac{(\mu_o-p)}{\dot{\mu}_o}, \tag{I-21.19}$$

in terms of which we may write

$$d_n a_n = d_n^{\dagger} d_n \frac{\lambda_o}{2(\mu_o-p)}\int_o^{\infty} du\, e^{-u\eta/(\mu_o-p)}\left\{1+\frac{u\dot{\mu}_o}{\mu_o-p}\right\}^{\kappa_n-1}$$

so that if we write $\tau = \frac{\eta}{\mu_o-p}$,

$$\frac{1}{2\pi i}\int d\left(\frac{\eta}{\mu_o-p}\right)\exp\left\{\left(\frac{\eta}{\mu_o-p}\right)(\lambda-\lambda_o)\right\}\Phi(\eta,o,p) \tag{I-21.20}$$

$$= \sum_{n=o}^{\infty} d_n^{\dagger} d_n \frac{\lambda_o}{2(\mu_o-p)}\frac{1}{2\pi i}\int d\tau\, e^{\tau(\lambda-\lambda_o)}\int_o^{\infty} du\, e^{-\tau u}\left\{1+\frac{u\dot{\mu}_o}{\mu_o-p}\right\}^{-1+\kappa_n}$$

The double integral on the right of this last equation is recognizable as a Laplace transformation followed directly by its inverse. Evaluation of the double integrals is therefore immediately accomplished: we merely replace them by the integrand, with $u = \lambda - \lambda_o$.

We are then left with the expression

$$I_o(\lambda,z) = \frac{1}{2\pi i}\int dp e^{-pz} \sum_{n=o}^{\infty} d_n^\dagger d_n \frac{\lambda_o}{2} \frac{1}{(\mu_o - p)} \left\{1 + \frac{\dot{\mu}_o(\lambda-\lambda_o)}{\mu_o - p}\right\}^{-1+\kappa_n}$$

$$= \frac{\lambda_o}{2} \sum_{n=o}^{\infty} d_n^\dagger d_n \frac{1}{2\pi i}\int dp e^{-pz} \frac{(\mu-p)^{\kappa_n - 1}}{(\mu_o - p)^{\kappa_n}} \quad . \qquad \text{(I-21.21)}$$

This type of integral can be performed analytically; it yields confluent hypergeometric functions. But our purpose is well served if instead we perform a simple approximate calculation. If $(\lambda-\lambda_o)$ is sufficiently large we may write

$$(\mu - p) \simeq (\mu - \mu_o), \qquad \text{(I-21.22)}$$

and remove the numerator of the integrand from the integral. Then the calculation gives a particularly simple result:

$$I_o(\lambda,z) \simeq \frac{\lambda_o}{2} \sum_{n=o}^{\infty} d_n^\dagger d_n (\mu-\mu_o)^{\kappa_n - 1} e^{-\mu_o z} \frac{1}{2\pi i}\int dp e^{(\mu_o - p)z} (\mu_o - p)^{-\kappa_n}$$

$$\simeq \frac{\lambda_o}{2} \sum_{n=o}^{\infty} \frac{d_n^\dagger d_n}{[\kappa_n - 1]!} e^{-\mu_o z} [(\mu-\mu_o)z]^{\kappa_n - 1} \quad . \qquad \text{(I-21.23)}$$

The eigenvalues, κ_n, <u>decrease</u> with increasing n. This means that the terms in the sum have widely differing values for large <u>z</u>, the largest being the first (n = 0) term. Neglecting the others by comparison, we see that

$$I_o(\lambda,z) \simeq \frac{\lambda_o}{2} \frac{d_o^\dagger d_o}{[\kappa_o-1]!} [(\mu-\mu_o)z]^{\kappa_o-1} e^{-\mu_o z}, \qquad \text{(I-21.24)}$$

(Plane Isotropic Source).

d) Comparison with the Plane Normal Source Case and Further Discussion.

Before commenting on this result, which applies to plane isotropic sources, we will identify the changes which make the analysis apply to plane normal sources. For this source type, the source term in Eqs. (I-21.4), and (I-21.7) should be changed by omission of the factor $\frac{1}{2}\delta(\sigma^2/2)$. The source term in Eq. (I-21.9) should be simply λ_o, and in Eqs. (I-21.10) and (I-21.13) it should be $\lambda_o\eta/(\mu_o-p)$. In Eq. (I-21.14) the factor $d_k^\dagger$ should be replaced by $2d_k^\dagger A_k \eta/(\mu_o-p)$, where

$$A_k = \int_o^\infty sds \frac{\psi_k^\dagger(s)}{\psi_k^\dagger(o)} . \qquad \text{(I-21.25)}$$

In Eq. (I-21.16), the factor $d_k^\dagger$ should be replaced by $2d_k^\dagger A_k/(\mu_o-p)$, and the factor $\frac{1}{\eta^\dagger}$ should be removed from the integrand. In Eqs. (I-21.20) and (I-21.21), the factor $d_n^\dagger$ should be replaced by $2d_n^\dagger A_n \frac{\partial}{\partial\lambda}$, and the integrand should have the exponent κ_n. Skipping to the final result, instead of (I-21.24), we arrive at the expression

$$I_o(\lambda,z) \simeq \lambda_o \frac{d_o^\dagger d_o A_o}{(\kappa_o)!} \frac{\partial}{\partial\lambda} [(\mu-\mu_o)z]^{\kappa_o} e^{-\mu_o z}, \qquad \text{(I-21.26)}$$

(Plane Normal Source).

Note that the spectrum given by (I-21.26) is essentially that of Eq. (I-21.24), while the spatial trend is increased by a factor of z.

Both observations are more general than the assumptions basic to the preceding calculations. We expect the spectral region which has attained relative equilibrium to be independent of details of the source shape, and we expect the plane normal source quite generally to have the same trend as the point isotropic source without the inverse square factor, but since the plane isotropic source is obtained from the point isotropic source by integration, as shown in Eq. (I-16.6),

$$I_o^{PLI}(\lambda,z) = \frac{1}{2}\int_z^\infty \frac{dr}{r}\{4\pi r^2 I_o^{PTI}(\lambda,r)\}, \qquad \text{(I-21.27)}$$

we expect that the plane isotropic source will always give a trend which differs by one power of the penetration variable from that of both the plane normal source and the point isotropic source without the inverse square factor.

The exponent κ_o in Eq. (I-21.26) can be calculated by standard eigenvalue techniques. It turns out to be of the order of unity for low-Z materials and photon energies near 1 Mev.

Eqs. (I-21.24) and (I-21.26) do not describe the spectrum in the non-equilibrium region, which undergoes a sharp transition to values expressive of a different spatial trend at $\lambda = \lambda_o$. The more accurate solution which uses confluent hypergeometric functions is able, in principle, to describe the non-equilibrium region; but the calculations involve other terms in the sum of Eq. (I-21.21).

This same type of analysis is applicable for the case $\dot{\mu}_o < 0$, and analogous studies have been made for the cases in which $\mu(\lambda)$ is constant or has a minimum value for some $\lambda > \lambda_o$. [12/]

22. Calculation of Spatial Moments of Legendre Coefficients

a) Formal Development: PLI Monoenergetic Source

At this point the calculation of spatial moments of Legendre coefficients is an exercise of the analytical machinery developed in many of the preceding sections. Considering first the PLI monoenergetic source of Equation (I-12.20), we write the equation in dimensionless variables, Equation (I-17.9), using Equation (I-17.1):

$$\cos\theta\frac{\partial I}{\partial \bar{z}} + \bar{\mu}(\lambda)I(\lambda,\theta,\bar{z}) = \int_0^{\lambda} d\lambda' \int_{4\pi} d\Omega' K(\lambda',\lambda,\cos\theta)I(\lambda',\theta',\bar{z}) + \lambda\left\{\frac{1}{4\pi}\,\delta(E-E_0)\delta(\bar{\mathbf{z}})\right\}\frac{dE}{d\lambda} . \qquad \text{(I-22.1)}$$

Recall that $\bar{\mu}$ and $\bar{z}$ are simply attenuation coefficient and distance in dimensionless units, and note that we may write $\delta(\lambda-\lambda_0)$ for $\delta(E-E_0)\frac{dE}{d\lambda}$.

To this equation we next apply moment and Legendre transformations. If the "coefficient-moment" is defined in accordance with Equations (I-14.3) and (I-15.2) to be

$$I_{n\ell}(\lambda) = \int_{-\infty}^{\infty} d\bar{z}(\bar{\mu}_0\bar{z})^n\left\{\frac{4\pi}{2\ell+1}\right\}^{1/2} \int_{4\pi} d\Omega \bar{Y}_\ell^o(\theta)I(\lambda,\theta,\bar{z}) , \qquad \text{(I-22.2)}$$

where $\bar{\mu}_0 = \bar{\mu}(\lambda_0)$, the equations satisfied by the $I_{n\ell}$'s can be immediately written down from Equation (I-15.6), using $\alpha = \bar{\mu}_0$ and $m = 0$:

$$\bar{\mu}(\lambda)I_{n\ell}(\lambda) = \int_{\lambda_0}^{\lambda} d\lambda' K_\ell(\lambda',\lambda)I_{n\ell}(\lambda') + \bar{\mu}_0\frac{n}{2\ell+1}\left[(\ell+1)I_{n-1,\ell+1} + \ell I_{n-1,\ell-1}\right] + \lambda_0\delta(\lambda-\lambda_0)\delta_{n0}\delta_{\ell 0} . \qquad \text{(I-22.3)}$$

where

$$K_\ell(\lambda',\lambda) = K_0(\lambda',\lambda)P_\ell(1-\lambda+\lambda'), \qquad \text{(I-22.4)}$$

and $K_0(\lambda',\lambda)$ is given by Equation (I-17.8) .

We are primarily interested in the numerical solution of this set of equations; but they are not yet in suitable form because the last term is singular. The difficulty is essentially confined to the unscattered component of the photon flux, and can be removed by replacing Equation (I-22.3) with the corresponding equation which describes only the scattered photons. We write

$$I_{n\ell}(\lambda) = I^{(s)}_{n\ell} + I^{(o)}_{n\ell} , \qquad \text{(I-22.5)}$$

where the superscripts refer, respectively, to scattered photons and photons that have as yet been scattered zero times. We insert this expression in the preceding equation to obtain an equation which is equivalent to the two equations below (see Equation (I-20.8)):

$$\bar{\mu}(\lambda)I^{(o)}_{n\ell} = (1-\delta_{n0})\bar{\mu}_0 \frac{n}{2\ell+1}[(\ell+1)I^{(o)}_{n-1,\ell+1} + \ell I^{(o)}_{n-1,\ell-1}]$$

$$+ \lambda_0\delta(\lambda-\lambda_0)\delta_{n0}\delta_{\ell 0} ; \qquad \text{(I-22.6)}$$

$$\bar{\mu}(\lambda)I^{(s)}_{n\ell} = \int_{\lambda_0}^{\lambda} d\lambda' K_\ell(\lambda',\lambda)I^{(s)}_{n\ell}(\lambda') + \bar{\mu}_0 \frac{n}{2\ell+1}[(\ell+1)I^{(s)}_{n-1,\ell+1} + \ell I^{(s)}_{n-1,\ell-1}]$$

$$+ \int_{\lambda_0}^{\lambda} d\lambda' K_\ell(\lambda',\lambda)I^{(o)}_{n\ell}(\lambda') . \qquad \text{(I-22.7)}$$

The equations for the unscattered component are easily solved. We note that $I^{(o)}_{n\ell}$ has the form

$$I^{(o)}_{n\ell} = \lambda_0 \delta(\lambda-\lambda_0) \frac{n!}{\bar{\mu}_0} C_{n\ell} , \qquad \text{(I-22.8)}$$

where the $C_{n\ell}$ are constants obeying the linkage equations

$$C_{n\ell} = (1-\delta_{n0})\left[\frac{\ell+1}{2\ell+1} C_{n-1,\ell+1} + \frac{\ell}{2\ell+1} C_{n-1,\ell-1}\right] + \delta_{n0}\delta_{\ell 0} . \qquad \text{(I-22.9)}$$

The nature of these numbers is apparent if we refer to the analytic form of the unscattered flux from a plane isotropic source, as given by Equation (I-20.6):*

$$I^{(o)}(\lambda,\theta,\bar{z}) = \lambda_0 \delta(\lambda-\lambda_0) \frac{1}{4\pi} \frac{e^{-\bar{\mu}_o \bar{z}/\cos\theta}}{|\cos\theta|} h(\bar{z}/\cos\theta) . \qquad \text{(I-22.10)}$$

If we apply moment and Legendre expansions to this distribution we obtain a very simple result:

$$I^{(o)}_{n\ell} = \left\{\frac{4\pi}{2\ell+1}\right\}^{1/2} \int_{4\pi} d\Omega \bar{Y}^o_\ell(\theta) \int_{-\infty}^{\infty} d\bar{z} (\bar{\mu}_0 \bar{z})^n I^{(o)}(\lambda,\theta,\bar{z})$$

$$= \lambda_0 \delta(\lambda-\lambda_0) \frac{1}{\bar{\mu}_0} \frac{1}{4\pi} \int_{4\pi} d\Omega P_\ell(\cos\theta) \int_{-\infty}^{\infty} dx\, x^n \frac{e^{-x/\cos\theta}}{|\cos\theta|} h(x/\cos\theta)$$

$$= \lambda_0 \delta(\lambda-\lambda_0) \frac{n!}{\bar{\mu}_0} \int_0^1 d\cos\theta P_\ell(\cos\theta)(\cos\theta)^n \quad ;$$

and from this it is clear that $n!\, C_{n\ell}$ is the moment-Legendre transformation

---

*Note that $h(x) = \begin{matrix} 1, x \geq 0 \\ 0, x < 0 \end{matrix}$.

of the distribution $|\cos\theta|^{-1}\exp[-x/\cos\theta]h(x/\cos\theta)$, with $C_{n\ell}$ given by

$$C_{n\ell} = \int_0^1 du u^n P_\ell(u) \ . \qquad \text{(I-22.11)}$$

Note that these numbers are identical with the numbers of Equation (I-16.6'). Table I-22.1 lists a set of these numbers.

n \ ℓ	0	1	2	3	4	5	6	7
0	1							
1		1/3						
2	1/3		2/15					
3		1/5		6/105				
4	1/5		4/35		8/315			
5		1/7		4/63		8/693		
6	1/7		2/21		8/231		16/3003	
7		1/9		2/33		8/429		16/6435
8	1/9		8/99		16/429		64/6435	
9		1/11		8/143		16/715		
10	1/11		18/143		48/1287			
11		1/13		6/117				
12	1/13		4/65					
13		1/15						
14	1/15							
15								
16	1/17							
17								
18	1/19							

Table I-22.1. Some $C_{n\ell}$ values.

With these results we are in a position to evaluate the final (source) term in Equation (I-22.7), which gives

$$\int_{\lambda_0}^{\lambda} d\lambda' K_\ell(\lambda',\lambda)\lambda_0\delta(\lambda'-\lambda_0)\frac{n!}{\bar{\mu}_0^n}C_{n\ell} = \lambda_0 K_\ell(\lambda_0,\lambda)\frac{n!}{\bar{\mu}_0^n}C_{n\ell} \ . \qquad \text{(I-22.12)}$$

At this point we are ready to discuss the numerical analysis; but

rather than proceed next in this direction we repeat the foregoing analysis for PLane "mon-Obliquity" sources.

b) Formal Development: PLO Monoenergetic Sources

For this source type we must replace the final term in Equation (I-22.1) with the expression

$$\lambda_0 \delta(\lambda-\lambda_0)\delta(\bar{z})\,\frac{1}{2\pi}\,\delta(\cos\theta-\cos\theta_0)\ ,$$

where θ_0 is the obliquity angle of the source, and we assume no azimuth dependence.* If the coefficient-moments are defined as in Equation (I-22.2), the final term in Equation (I-22.3) must be replaced by

$$\lambda_0 \delta(\lambda-\lambda_0)\delta_{n0}P_\ell(\cos\theta_0)\ ,$$

and Equation (I-22.6) is replaced by

$$\bar{\mu}(\lambda)I^{(o)}_{n\ell} = (1-\delta_{n0})\bar{\mu}_0\,\frac{n}{2\ell+1}\,[(\ell+1)I^{(o)}_{n-1,\ell+1} + \ell I^{(o)}_{n-1,\ell-1}]$$

$$+\ \lambda_0 \delta(\lambda-\lambda_0)\delta_{n0}P_\ell(\cos\theta_0)\ . \qquad \text{(I-22.13)}$$

It follows from the recursion formula

$$\cos\theta_0 P_\ell(\cos\theta_0) = \frac{1}{2\ell+1}\,[(\ell+1)P_{\ell+1}(\cos\theta_0) + \ell P_{\ell-1}(\cos\theta_0)]$$

---

*This source type is sometimes loosely referred to as mono-directional or oblique.

that the solution to Equation (I-22.13) is

$$I_{n\ell}^{(o)} = \lambda_0 \frac{\delta(\lambda-\lambda_0)n!(\cos\theta_0)^n P_\ell(\cos\theta_0)}{\bar{\mu}_0} . \qquad \text{(I-22.14)}$$

Correspondingly, the source term for Equation (I-22.7) is given by

$$\int_{\lambda_0}^{\lambda} d\lambda' K_\ell(\lambda',\lambda)\lambda_0\delta(\lambda'-\lambda_0)(\cos\theta_0)^n P_\ell(\cos\theta_0) = \lambda_0 \frac{K_\ell(\lambda_0,\lambda)}{\bar{\mu}_0}(\cos\theta_0)^n P_\ell(\cos\theta_0) . \qquad \text{(I-22.15)}$$

One can perhaps more easily obtain this result from the analytic expression for the source space-angle distribution.

c) Numerical Solution of the Equation for $I_{00}(\lambda)$.

The methods for numerical solution of all these equations are well illustrated by application to the special case $n = \ell = 0$, which has a typical form. Note that this equation is the same for all the source types just considered:

$$\bar{\mu}(\lambda)I_{00}^{(s)}(\lambda) = \int_{\lambda_0}^{\lambda} d\lambda' K_0(\lambda',\lambda)I_{00}^{(s)}(\lambda') + \lambda_0 K_0(\lambda_0,\lambda)/\bar{\mu}_0 . \qquad \text{(I-22.16)}$$

.

The final term in this equation is a smooth, non-singular, well-behaved, finite function for $\lambda_0 \leq \lambda \leq \lambda_0 + 2$. At $\lambda = \lambda_0 + 2$ this function drops abruptly to zero, and it remains zero for all values $\lambda > \lambda_0 + 2$.

Applying numerical integration concepts, such as outlined in Part G, we assume that the integral in Equation (I-22.16) can be approximately evaluated as a sum with the use of appropriate integration weights. We establish a set of values $\lambda_0, \lambda_1, \ldots$ at which the function $I_{00}(\lambda)$

is to be evaluated, choosing equal spacings for convenience. To the accuracy of the basic integration formula, as applied here, we may replace Equation (I-22.6) by

$$\bar{\mu}(\lambda_n)I_{00}^{(s)}(\lambda_n) = \sum_{i=0}^{n} w_i K_0(\lambda_i,\lambda_n)I_{00}^{(s)}(\lambda_i) + \lambda_0 K(\lambda_0,\lambda_n)/\bar{\mu}_0 \ , \qquad \text{(I-22.17)}$$

where the w_i are appropriate integration weights, perhaps those developed in section 35c. Solving for $I_{00}(\lambda_n)$ we obtain

$$I_{00}^{(s)}(\lambda_n) = \{\bar{\mu}(\lambda_n) - w_n K_0(\lambda_n,\lambda_n)\}^{-1}\{\sum_{i=0}^{n-1} w_i K_0(\lambda_i,\lambda_n)I_{00}^{(s)}(\lambda_i) + \lambda_0 K(\lambda_0,\lambda_n)/\bar{\mu}_0\} \ . \qquad \text{(I-22.18)}$$

The result here is determined, providing $I_{00}(\lambda_i)$ is known for $0 \leq i < n$. This will be true if the solution progresses always from n to $n + 1$ and if $I_{00}(\lambda_0)$ can be determined. But for $\lambda = \lambda_0$, the scattering integral is precisely zero, so that

$$I_{00}^{(s)}(\lambda_0) = \lambda_0 \frac{K_0(\lambda_0,\lambda_0)}{[\bar{\mu}(\lambda_0)]^2} \ . \qquad \text{(I-22.19)}$$

Two problems may present themselves in such a calculation. First, it is possible that due to the chain nature of the solution small errors may build up, so that the calculation proves basically unstable. All experience gained thus far indicates that for gamma-ray and neutron calculations this does not happen.

Second, the discontinuity in the function $K_0(\lambda_0,\lambda)$ at $\lambda = \lambda_0 + 2$ will be reflected in the function $I_{00}(\lambda)$ in the form of a corresponding

discontinuity at the same wavelength. But then the integrand of Equation (I-22.16) is discontinuous at this wavelength and we must proceed with caution. Strictly speaking, the integration should be performed in two pieces, by writing

$$\int_{\lambda_0}^{\lambda} d\lambda' K_0(\lambda',\lambda) I_{00}^{(s)}(\lambda') = \int_{\lambda-2}^{\lambda_0+2} + \int_{\lambda_0+2}^{\lambda} , \qquad \text{(I-22.20)}$$

and by assigning $I_{00}^{(s)}$ appropriate left and right limits in the two integrals. This has usually been done. but in the calculations which produced the data of Ref. 36 , a sufficiently fine mesh was used to encourage neglect of this problem. This turned out to be feasible not only because of the fine mesh but also because the problem arises only at such low photon energies that the error is innocuous.

The network of Equations (I-22.7) can be solved numerically, in proper sequence, each equation in turn being evaluated by exactly the same integration procedure which is applied to the appropriate (known) source function and $K_\ell(\lambda',\lambda)$. Each has the same problem of a discontinuity at $\lambda_0 + 2$.

d) <u>A Conservation Rule for the $I_{00}(\lambda)$.</u>

In section 8 we noted that the energy produced by the gamma ray source must equal the kerma for the medium. This gives a useful relation between source and solution of the $n = \ell = 0$ equation of (I-22.3). The kerma is given by integrating $I_{00}(\lambda)$ multiplied by the mass energy transfer coefficient, μ_D , as tabulated, for example, in Ref. 3 . On the other hand, the energy produced by the source can be obtained by

integration over the source function. We therefore have the equation*

$$\int_0^{E_0} dE[I_{00}^{(o)}(\lambda) + I_{00}^{(s)}(\lambda)]\,\bar{\mu}_D(E) = \int_0^{E_0} dE\lambda_0\delta(\lambda-\lambda_0) , \qquad \text{(I-22.21)}$$

or, evaluating the integrals over the delta functions,

$$\int_0^{E_0} dE I_{00}^{(s)}(\lambda)\bar{\mu}_D(E) = E_0\left[1 - \frac{\bar{\mu}_D(E_0)}{\bar{\mu}_0}\right] . \qquad \text{(I-22.22)}$$

Here $\bar{\mu}_D = \mu_D/\alpha$, so that $(\bar{\mu}_D/\bar{\mu}_0) = (\mu_D/\mu_0)$. This relation provides an extremely useful check on the consistency of the functions used in these calculations, and also on the accuracy of the calculation itself.

No analogous rule for other coefficient-moments is known. Because the argument applies to more general source types, it is in principle possible to make extensions of this rule, providing that functions analogous to $\bar{\mu}_D$ are defined for $\ell > 0$. Such extensions have not been made and are probably not very useful.

e) An Elementary FORTRAN Routine for Evaluating Coefficient-Moments

For its pedagogical value, we give an extremely simple routine for solving integral equations of the type Equation (I-22.7). In spite of the additional complexity introduced by two integration regions which join at the discontinuity, we have included this feature in the code. The utility subroutines called must be those of section 36, or equivalent to them. The subroutine MØMENT only performs solutions for a single λ value. It must be operated cyclically by a control routine. The subroutine ELISTS reads

*Note that I_{00} represents an integral over $\bar{z}$, hence the use of $\bar{\mu}_D$.

the basic cross section data and interpolates to set up tables for use in the calculation. The subroutine INPUTB reads the data which establishes a pattern of coefficient-moments to be calculated, and determines linkage coefficients and $C_{n\ell}$ values. The control routine is relatively complicated because it must cycle MØMENT properly and do routine operations connected with this.

Returning to MØMENT: this subroutine is essentially a transcription of the numerical procedure outlined in c) of this section. The first part of the code, to the second order beyond 20, is concerned with proper indexing of the integration in view of the use of two integration regions if the discontinuity is within the integration range. The second part of the code, to order 45, tabulates the Klein-Nishina cross section multiplied by the integration weights, for the λ value being calculated. This tabulation is utilized for all coefficient-moments which have the same value of $\underline{n}$. The subroutine assumes that a table of Legendre polynomials $P_\ell(1-\lambda_n+\lambda_i)$ is available.

The final part of the code, which begins with order 45, effects solutions for all ℓ values which are to be calculated for the moment $\underline{n}$.

```
C     *     *     *     *     *     *     *

      SUBRØUTINE MØMENT(XLAM,XMU,ALPH,ND,LAM,LS,CNL,LNØ,PL,SØL)
      DIMENSIØN XLAM(500),XMU(500),W(500),XK(500),PL(12,300),
     1 SØL(2,10,500),LS(10,3),CNL(10,3)
```

XLAM is the list of wavelength values (assumed equally spaced) for which a solution may be attempted. LAM is the index of the wavelength value for which the calculation is to proceed. XMU is a list of attenuation coefficient values, one for each XLAM value. ALPH is the distance scale factor assumed, usually XLAM(1).

We assume that XLAM has two identical entries at the discontinuity, the second corresponding to the limit approached from larger λ. ND is the index of the second value.

Array interpretations: LS(I,1) is the ℓ value for which solutions are sought; LS(I,2) is an index identifying $I_{n-1,\ell-1}$; and LS(I,3) is the corresponding index for $I_{n-1,\ell+1}$. CNL(I,1) is the appropriate C_n value for the I'th ℓ value. CNL(I,2) is the linkage coefficient multiplying $I_{n-1,\ell-1}$ (usually $\ell/(2\ell+1)$). Likewise CNL(I,3) is the linkage coefficient multiplying $I_{n-1\ \ell+1}$ (usually $\ell+1/(2\ell+1)$).

XK is the list of kernel values appropriate to LAM. multiplied by appropriate integration weights. PL(L,j) is the Legendre polynomial $P_{L-1}(1-\lambda_j+\lambda_1)$; and we assume that this array has been computed.

SØL(1,IP,J) is the solution list for the IP'th ℓ value, for the N-1'st moment. SØL(2,I,J) is the solution list for the I'th ℓ value, calculated for the N'th moment.

```
   NDP=ND-1
```

This generates the index of the first discontinuity wavelength. Our first task is to see if the integration overlaps the discontinuity or lies completely to larger or smaller wavelengths.

```
   IF(LAM-NDP)  10,10,5
 5 IF(LAM-2*NDP) 15,20,20
10 NB=1
   NØ1=LAM
   NØ2=0
   GØ TØ 25
```

Here NØ1 is the number of XLAM values in the integration, and NB is the first index of the XLAM list involved in the integration. The total calculation falls on the small wavelength side of the discontinuity.

```
15 NB=LAM-NDP
   NØ1=ND-NB
   NØ2=NB
   GØ TØ 25
```

NB and ND give initial XLAM indices for the two integrations; and NØ1 and NØ2 are the (respective) numbers of wavelengths for these two integrations.

```
20 NB=LAM-NDP+1
   NØ1=NDP
   NØ2=0
```

Here the whole calculation is on the large wavelength side of the discontinuity, and only one integration region is necessary.

```
25 CALL IWATE(1,NØ1,XLAM(NB),W)
   IF(NØ2) 30,30,40
40 CALL IWATE(1,NØ2,XLAM(ND),W(NØ1+1))
```

It should be clear in these last three orders that if there are two integration regions, the weights adjoin in the list. Note that if LAM=ND, only one weight, namely zero, will be calculated by order 40.

```
30 DØ 35 I=NB,LAM
   DEL=XLAM(LAM)-XLAM(I)
   RAT=XLAM(I)/XLAM(LAM)
   IP=I-NB+1
35 XK(I)=.375*RAT*(RAT+1./RAT-2.*DEL+DEL**2)*W(IP)
```

This completes preparation of the XK list.

```
45 DØ 60 I=1,LNØ
```

This begins the main calculation loop, over different ℓ values.

Next we must prepare indices for the main calculation. The next three orders give simple names to several indices. The fourth order clears the SUM cell for cumulation.

```
   L=LS(I,1)
   LHI=LS(I,3)
   LLØ=LS(I,2)
   SUM=0.
```

The next four orders, which are probably unnecessary, keep LHI and LLØ in the normal range (i.e. >0.) Either index vanishes or goes negative only if the corresponding linkage term is missing, in which case the value assigned to the index is immaterial.

```
   IF(LHI) 41,41,42
41 LHI=1
42 IF(LLØ) 43,43,44
43 LLØ=1
44 LAMP=LAM-1
   IF(LAMP) 52,52,46
```

Now we are ready for the integration loop, which includes contributions up to LAMP rather than LAM. One of the problems

in this loop is to calculate the correct PL index, taking into account the double XLAM value at the discontinuity.

```
   46 DØ 50 J=NB,LAMP
      JP=LAM-J+1
      IF(NØ2) 47,50,47
   47 IF(J-ND) 48,50,50
   48 JP=JP-1
   50 SUM=SUM+XK(J)*PL(L+1,JP)*SØL(2,I,J)
```

Note that the PL values are stored so that PL(L,1) corresponds to zero wavelength increment, i.e. to zero angular deflection. Next we must add both linkage terms. A factor $\underline{n}$, which might have been included, has been omitted, with the result that the moments being calculated are reduced by n!.

```
   52 SUM=SUM+ALPH*(CNL(I,3)*SØL(1,LHI,LAM)+CNL(I,2)*SØL(1,LLØ,LAM))
```

If LAM$\leq$NDP, a source term must be added. If LAM=1 we must take account of the fact that since W(1)=0, XK(1)=0, hence a special calculation.

```
      IF(LAM-NDP) 53,53,57
   53 IF(LAM-1) 54,54,55
   54 SUM=SUM+.75*XLAM(1)*CNL(I,1)/XMU(1)
      GØ TØ 57
   55 SUM=SUM+XK(1)*XLAM(1)*PL(L+1,LAM)*CNL(I,1)/W(1)/XMU(1)
```

Order 55 is the main integration order. We complete the calculation by solving for the new coefficient-moment value. Note that XK(LAM) vanishes if LAM=1 or if LAM=ND.

```
   57 SØL(2,I,LAM)=SUM/(XMU(LAM)-XK(LAM))
   60 CØNTINUE
      RETURN
      END
C     *     *     *     *     *     *     *
```

The first part of ELISTS is concerned with establishing the basic list of energies at which solution is to be effected. Beginning two orders before order 3, cross section data of two kinds is read and then interpolated at the energy values of the calculation. (Note that CX refers to the attenuation coefficients, while CEX refers to the energy absorption data for calculating dose.) Following this the Legendre polynomials are tabulated, and further indexing takes place.

```
C     *     *     *     *     *     *     *
      SUBRØUTINE ELISTS(INDEX,ALPH,XLAM,CXLM,CLXLM,PL)
      DIMENSIØN INDEX(6),ECX(50),CX(50),ECLX(50),CLX(50),XLAM(500),
     1 CXLM(500),CLXLM(500),PL(12,300)
```

INDEX contains NLAMP, the no. of wavelengths;
NDP, the no. of wavelengths in an interval of 2;
NCX, the no. of tabulated cx values (cx means cross section);
NCEX, the no. of tabulated energy cx values;
NNØ, the number of N values;
LMAX, the maximum L value;
in this order. ALPH is the assumed reciprocal mean free path. XLAM is the list of wavelength values, doubled at the discontinuity. CXLM is the corresponding cx list; and CLXLM is the corresponding energy cx list.

```
      PRINT 100
  100 FØRMAT(1HO)
```

This spacing order skips two lines.

```
      PRINT 101
  101 FØRMAT(6H INDEX)
```

Under this heading, INDEX values are listed.

```
      READ 1,(INDEX(I),I=1,6)
      PRINT1,(INDEX(I),I=1,6)
    1 FØRMAT(12I6)
```

Input data is printed immediately after being read to give a permanent record, and to assure that it was properly read.

```
      PRINT 100
      PRINT 102
  102 FØRMAT(27H    ALPH  XLAM(1)     XSCALE)
      READ 2,ALPH,XLAM(1),XSCALE
      PRINT2,ALPH,XLAM(1),XSCALE
    2 FØRMAT(8F9.4)
```

XSCALE is a conversion coefficient which changes the attenuation coefficient data to dimensionless units. We assume that ALPH has already been scaled in this manner.

Our first job is to set up explicitly some coefficients needed for the energy lists.

```
      NDP=INDEX(2)
      FN=NDP-1
      DEL=2./FN
```

```
    ND=NDP+1
    NLAMP=INDEX(1)
    NCX=INDEX(3)
    NCEX=INDEX(4)
    LMAX=INDEX(6)
```

Next we must read in the basic cross section tables. Recall that ECX and ECEX are energy lists for the CX and CEX tables, respectively.

```
    PRINT 100
    PRINT 103
103 FØRMAT(19H CROSS SECTION DATA)
    READ 2,(ECX(I),I=1,NCX)
    PRINT2,(ECX(I),I=1,NCX)
    PRINT 100
    READ 2,(CX(I),I=1,NCX)
    PRINT2,(CX(I),I=1,NCX)
    PRINT 100
    READ 2,(ECEX(I),I=1,NCEX)
    PRINT2,(ECEX(I),I=1,NCEX)
    PRINT 100
    READ 2,(CEX(I),I=1,NCEX)
    PRINT2,(CEX(I),I=1,NCEX)
    PRINT 100
```

Interpolations are to be performed in logarithms. Therefore we next replace tables and scale factor by the logs of the numbers.

```
    XSCALE=LØGF(XSCALE)
    DØ 200 I=1,NCX
    ECX(I)=LØGF(ECX(I))
200 CX(I)=LØGF(CX(I))-XSCALE
    DØ 210 I=1,NCEX
    ECEX(I)=LØGF(ECEX(I))
210 CEX(I)=LØGF(CEX(I))
```

We are now ready for the main loop, which establishes the energy and cross-section lists, the latter by interpolation. It is also advantageous to construct the PL array at this time.

```
    DØ 10 I=1,NLAMP
    FI=I
    DELP=DEL*(FI-1.)
    XLAM(I)=XLAM(1)+DELP
    E=LØGF(.511/XLAM(I))
    CALL INTRP(NCX,ECX,CX,3,E,CXLM(I))
    CXLM(I)=EXPF(CXLM(I))
    CALL INTRP(NCEX,ECEX,CEX,3,E,CEXLM(I))
    CEXLM(I)=EXPF(CEXLM(I))/(XLAM(I)**2)
```

This last order weights the energy cross sections with λ^{-2}, in anticipation of the integration to obtain dose. (Recall that $dE=d\lambda/\lambda^2$ in mc^2 units.)

Next we cycle the calculation of Legendre polynomials.

```
      IF(I-NDP) 8,8,10
    8 PL(1,I)=1.
      X=1.-DELP
      PL(2,I)=X
      DØ 9 J=3,LMAX
      FJ=J-1
    9 PL(J,I)=(2.-1./FJ)*X*PL(J-1,I)-(1.-1./FJ)*PL(J-2,I)
   10 CØNTINUE
```

Finally, we must correct the energy list to provide two identical values at the discontinuity. This is accomplished by moving values to an index increased by unity, beginning with the values at NLAMP.

```
      IF(NLAMP-NDP) 30,30,15
   15 NLAM=NLAMP+1
      DØ 20 I=NDP,NLAMP
      IP=NLAMP-I+NDP
      XLAM(IP+1)=XLAM(IP)
      CXLM(IP+1)=CXLM(IP)
   20 CEXLM(IP+1)=CEXLM(IP)
   30 PRINT 104
  104 FØRMAT(20H CRØSS SECTIØN TABLE)
      PRINT 4,(XLAM(I),CXLM(I),CEXLM(I),I=1,NLAM)
    4 FØRMAT(f8.3,2F9.4)
```

After recording the tabular cross section data, we record the Legendre polynomial data.

```
      PRINT 100
      PRINT 105
  105 FØRMAT(20H LEGENDRE PØLYNØMIAL)
      DØ 130 J=1,NDP
  130 PRINT 5,XLAM(J),(PL(I,J),I=1,LMAX)
    5 FØRMAT(F8.3,12F9.5)
      PRINT 100
      RETURN
      END
C     *     *     *     *     *     *     *
```

The next subroutine, INPUTB, was designed to control in an elementary way any combination of linkages which could possibly be of interest, by means of a card deck specifying order and linkage pattern for the calculation. Despite an appearance of clumsiness, the procedure works well in practice.

```
C     *     *     *     *     *     *     *
      SUBRØUTINE INPUTB(LZRØ,MZRØ,NNL,N,L,LINKH,LINKL,CH,CL,CNL,K)
      DIMENSIØN N(60),L(60),LINKH(60),LINKL(60),CH(60),CL(60),CNL(60)
```

This subroutine reads data identifying the pattern of integral equations to be solved, and prepares lists of linkage indices and multiplicative coefficients required for the calculation. The arguments have the following interpretations:

LZRØ is the harmonic coefficient ℓ_0 of the source angular distribution; it is strictly for identification purposes;

MZRØ is the azimuthal coefficient m_0 (or m) of the source angular distribution;

NNL is the total number of n,ℓ combinations to be calculated;

N is a list of n values, in order of solution;

L is a list of ℓ values, in order of solution;

LINKH is the index of the $(\ell+1)$ linkage term, in the N and L lists;

LINKL is the corresponding index of the $(\ell-1)$ linkage term;

CH is $[(\ell+1)^2-m^2]^{1/2}/(2\ell+1)$; CL is $[\ell^2-m^2]^{1/2}/(2\ell+1)$;

CNL is $C_{n\ell}$, the coefficients which weight the single-scattering source term. (Note that these depend on ℓ_0 , which is zero for isotropic sources.

```
      PRINT 200
  200 FØRMAT (1HO)
      PRINT 210
  210 FØRMAT (30H   NLØ  LZRØ  MZRØ   NNL     K)
      READ 5,NLØ,LZRØ,MZRØ,NNL,K
      PRINT5,NLØ,LZRØ,MZRØ,NNL,K
    5 FØRMAT (12I6)
```

Having read in the control indices, we next read the pattern of coefficients defining the problem.

```
      PRINT 200
      IF(NNL) 21,21,8
    8 PRINT 220
  220 FØRMAT(24H     N     L LINKH LINKL)
      READ 5,(N(I),L(I),LINKH(I),LINKL(I),I=1,NNL)
      PRINT5,(N(I),L(I),LINKH(I),LINKL(I),I=1,NNL)
      PRINT 200
      PRINT 230
  230 FØRMAT(12H CNL FOR N=0)
      READ 19,(CNL(I),I=1,NLØ)
      PRINT19,(CNL(I),I=1,NLØ)
   19 FØRMAT (1P4E15.7)
```

The 1P in this last format moves the decimal point one Place to the right. We assume that N, L, etc. are ordered so that

all $\underline{\ell}$ values for a given $\underline{n}$ value are read before anything pertaining to the next $\underline{n}$ value is read. NLØ is the no. of ℓ_0's.

```
    PRINT 200
    DØ 103 I=1,NLØ
    CH(I)=0.
103 CL(I)=0.
```

The last three orders complete the subroutine's function for the n=0 coefficients. We next go into the main loop, which determines CH, CL, and CNL lists for the remaining coefficients.

```
    FM=MZRØ
    IF(NNL-NLØ) 21,21,105
105 NLØP=NLØ+1
    DØ 18 I=NLØP,NNL
    JH=LINKH(I)
    JL=LINKL(I)
    A=L(I)
    S=(A+1.)**2-FM**2
    T=A**2-FM**2
    B=0.
```

Note the limited range of I values. S and T are $(\ell+1)^2-m^2$ and ℓ^2-m^2, respectively. B is for cumulation purposes.

```
    IF(JH) 11,11,12
 11 CH(I)=0.
    GØ TØ 13
```

If a linkage term is missing, the corresponding CH value is set equal to zero. One knows that this is the case because LINKH and LINKL values are put equal to zero to indicate missing terms.

```
 12 CH(I)=SQRTF(S)/(2.*A+1.)
    B=CH(I)*CNL(JH)
 13 IF(JL) 14,14,16
 14 CL(I)=0.
    GØ TØ 18
 16 CL(I)=SQRTF(T)/(2.*A+1.)
    B=B+CL(I)*CNL(JL)
 18 CNL(I)=B
```

The five orders beginning just prior to 11, and the five orders beginning with 13, correspond and take care of upper and lower linkage cases in the same way. These 11 orders constitute the main calculation, and generate all three coefficient lists. We are now done; but it is useful to print out the lists.

```
      PRINT 240
  240 FØRMAT (24H     I    CH    CL   CNL)
      DØ 250 I 1,NNL
  250 PRINT 20,I,CH(I),CL(I),CNL(I)
   20 FØRMAT (I6,1P3E15.7)
      PRINT 200
   21 RETURN
      END
C     *     *     *     *     *     *     *
```

The CØNTRØL routine calls the subroutines, and to do this quite a bit of indexing must be included. The main indexing problem occurs because INPUTB produces a master list of coefficient-moments which is in the correct order of solution, but not broken into groups associated with different moments. On the other hand, MØMENT requires this subdivision, and it is accordingly provided in the CØNTRØL routine, as the first half of the main loop.

A separate ØUTPUT subroutine did not appear advantageous; so that all the output orders are in CØNTRØL. The last part of the main loop prints all the spectral data and calculates dose integrals. Printing of the dose integrals concludes the routine.

```
C     *     *     *     *     *     *     *
      CONTRØL
      DIMENSIØN INDEX(7),XLAM(500),CXLM(500),CEXLM(500),PL(12,300),
     1 N(60),L(60),LINKH(60),LINKL(60),CH(60),CL(60),CNLP(60),LS(10,3),
     2 CNL(10,3),XK(500),SØL(2,10,500),WT(500),TØT(20,10),LN(20),ILS(20)
```

Most of the lists and arrays are described in one of the subroutines. Note that we use CNLP rather than CNL in connection with INPUTB because CNL is being used with MØMENT. WT is a master list of integration weights for final calculation of the dose integrals. TØT is the array of dose integrals. LN is a list of the number of L values associated with each value of the moment number N (or NX).

```
      CALL ELISTS(INDEX,ALPH,XLAM,CXLM,CEXLM,PL)
      CALL INPUTB(LZRØ,MZRØ,NNL,N,L,LINKH,LINKL,CH,CL,CNLP,K)
```

These two orders set up all the energy lists, as well as the linkage lists. Both subroutines contain the necessary read and print orders. (The index K has been used when several calculations were cycled, as an indicator of the remaining number of calculations to be done. It is irrelevant here.)

We first set up explicit indices and establish the basic list of integration weights (i.e. WT).

```
      NLAM=INDEX(1)+1
      ND=INDEX(2)+1
      NNØ=INDEX(5)
      NDP=INDEX(2)
      CALL IWATE(1,NDP,XLAM(1),WT)
      IX=NLAM-NDP
      CALL IWATE(1,IX,XLAM(ND),WT(ND))
      DØ 5 I=1,NLAM
    5 CEXLM(I)=CEXLM(I)*WT(I)
```

The last two orders establish the list of multipliers for all the dose integrals. Next we begin our main loop.

```
      DØ 30 NX=1,NNØ
```

Recall that NX identifies a moment, and that NNØ is the number of moments to be calculated. The first thing we must do in this loop is construct the LS and CNL arrays for moment number NX.

```
      J=0
      DØ 10 I=1,NNL
      IF(N(I)+1-NX) 10,7,10
    7 J=J+1
      ILS(NX)=I
```

This last order records the largest I value for each NX.

```
      LS(J,1)=L(I)
      LS(J,2)=LINKL(I)
      LS(J,3)=LINKH(I)
      CNL(J,1)=CNLP(I)
      CNL(J,2)=CL(I)
      CNL(J,3)=CH(I)
   10 CØNTINUE
```

This completes the CNL array. But the LS(J,2) and LS(J,3) values are not at this point correct because they are indices in the full list of NNØ equations, rather than indices for the list of ℓ values for the (n-1)'st moment, as called for in MØMENT. We must now make this change and at the same time identify the number of ℓ values for the n'th moment.

```
      IF(NX-2) 14,14,11
   11 DØ 12 I=1,J
      LS(I,2)=LS(I,2)-ILS(NX-2)
   12 LS(I,3)=LS(I,3)-ILS(NX-2)
   14 LN(NX)=J
```

When NX is one, these LS values will be zero. When NX is two, the LS values don't need to be modified. Thereafter, all LS indices must be shifted, as indicated, to correspond to entries in the ℓ list for the (n-1)'st moment, which are indexed from one to LN(NX-1). Order 14 records the count of the DØ loop ending at order 10.

The next three orders solve the NX equations for all λ values.

```
      DØ 15 I=1,NLAM
      CALL MØMENT(XLAM,CXLM,ALPH,ND,I,LS,CNL,J,PL,SØL)
   15 CØNTINUE
      PRINT 200
  200 FØRMAT(1HO)
```

This order is to skip two lines. We first will record the results and then determine the dose integrals and store them.

```
      PRINT 210
  210 FØRMAT(5H N, L)
      NXX=NX-1
      PRINT 1,NXX,(LS(K,1),K=1,J)
    1 FØRMAT (12I6)
      PRINT 200
      PRINT 220
  220 FØRMAT(23H   XLAM, ENERGY MØMENTS)
      DØ 230 I=1,NLAM
  230 PRINT 2,XLAM(I),(SØL(2,K,I),K=1,J)
    2 FØRMAT(F7.3,1P7E15.7)
      PRINT 200
```

This completes the printing of the results for each wavelength. Next the integrals are performed and recorded.

```
    DØ 20 K=1,J
    TØT(NX,K)=0.
    DØ 20 I=1,NLAM
    TØT(NX,K)=TØT(NX,K)+CEXLM(I)*SØL(2,K,I)
 20 SØL(1,K,I)=SØL(2,K,I)
 30 CØNTINUE
```

The first order in the outer DØ loop ending at order 20 clears the cells for cumulation. The inner DØ loop is the integration. The final statement of the inner loop prepares the inhomogeneous terms for the next n value, calculations for which begin following end of the main loop at order 30.

Lastly, having finished all calculations, we must record the dose moments.

```
    PRINT 240
240 FØRMAT(13H DØSE MØMENTS)
    DØ 250 NX=1,NNØ
    NXX=NX-1
    J=LN(NX)
250 PRINT 3,NXX,(TØT(NX,K),K=1,J)
  3 FØRMAT(I7,1P7E15.7)
```

There is an implicit assumption in the use of this last format that no more than 7 values of ℓ will occur for any n. If this number is exceeded, the format must be changed.

```
    CALL ENDJØB
    END
```

E. CALCULATION OF FLUX DISTRIBUTIONS FOR ELEMENTARY SOURCES

23. Space Distributions for Isotropic Sources[15, 38]

a) Coefficient-Moments of the Exposure. The methods of the preceding section suffice to give coefficient-moments for the different spectral components, that is to say the $I_{n\ell}(\lambda)$. Having determined these basic quantities, we must face the problems of distribution construction. For the fallout radiation, it has been possible thus far to ignore spectral details and confine attention to the exposure integral

$$D(\theta,\bar{z}) = \frac{1}{E_0}\int_0^\infty dE\bar{\mu}_d(E)I\ [\lambda(E),\theta,\bar{z}] \qquad \text{(I-23.1)}$$

and its coefficient-moments. Further, the machine calculations for Ref. 36 were so organized that flux distributions were constructed only for monoenergetic sources. Distributions for the fallout spectra were calculated by superposition of many monoenergetic source results.

In this section we limit our attention to monoenergetic sources, and to the coefficient-moments of the exposure

$$D_{n\ell} = \int_{-\infty}^{\infty} d\bar{z}(\bar{\mu}_0\bar{z})^n \int_{4\pi} d\Omega P_\ell(\cos\theta)D(\theta,\bar{z}) \ . \qquad \text{(I-23.2)}$$

Table I-23.1 gives machine-calculated values for Cs137 in H_2O , that is for $\lambda_0 = 0.770$.* Spectral data was determined in the calculation, but has not been utilized. In any case the procedure which we use for the integral is applicable for the different spectral components, though for the latter an efficient and accurate calculation would probably require exact calculation

*All tables in this part of the manuscript give numbers to more digits than the accuracy of the data appears to require. This is partly because of the requirements of internal consistency in calculations based on the data. In general, space distributions calculated from such data are not accurate to better than a few percent nor angular distributions to better than ~ 10%.

Table I-23.1. Coefficient-moments for a Cs137 PLI source.

$\frac{1}{n!}D_{n\ell}$(PLI)

n \ ℓ	0	1	2	3	4	5	6	7	8	9
0	1.0084677									
1		.37870041								
2	1.0179735		.15673754							
3		.45161733		.065631703						
4	1.2192226		.21848422		.027936001					
5		.53417328		.10490143		.012107615				
6	1.4447422		.26803462		.050536350		.0053414515			
7		.62002221		.13570174		.024527591		.0023919494		
8	1.6791055		.31395984		.069481441		.012005140		.0010852974	
9		.70762030		.16281820		035956811		.0059167510		.00049745723
10	1.9183552		.35841645		.086223055		.018775529		.0029335079	
11		.79624855		.18801825		.046427097		.0098640711		
12	2.1605026		.40212124		.10157414		.025311067			
13		.8854301		.21207985		.056133195				
14	2.4042003		.44534137		.11599321					
15		.97482187		.23538834						
16	2.6484847		.48818120							
17		1.0641788								
18	2.8926760									

$D_{00}^{(o)}$ = .3818699 (Unscattered photons)

$\bar{\mu}_0$ = .3854

of the once-scattered component.

b) PTI Space Distributions. The coefficient-moments of Table I-23.1 describe a plane source. They can be transformed to moments for a point isotropic source by applying the general relationship of Equation (I-16.6').* Dividing the values of Table I-23.1 by the corresponding $C_{n\ell}$ values of Table I-22.1, we obtain the data for the PTI source in Table I-23.2.*

Table I-23.2. Coefficient-moments for a Cs137 point isotropic source.

$\frac{1}{n!} D_{n\ell}$ (PTI)

n \ ℓ	0	1	2	3	4
0	1.00847				
1		1.13610			
2	3.05392		1.17553		
3		2.25809		1.14855	
4	6.09611		1.91174		1.09998
5		3.73921		1.65220	
6	10.11320		2.81436		1.45924
7		5.58020		2.23908	
8	15.11195		3.88525		1.86297
9		7.78382		2.91038	
10			5.12536		2.31186
11				3.66636	

The most direct way to obtain space distributions is by means of expansions in the $U_n^{\ell}(r)$ polynomial systems described in Ref. 15 and in sections 40 and 41. The expansion coefficients are simple binomial combinations of the numbers in Table I-23.2 (see Equation (I-41.2):

$$A_{m\ell} = \sum_{j=0}^{m} (-)^j \binom{m}{j} \frac{D_{\ell+2j,\ell}}{(\ell+2j)!} , \quad m = \frac{1}{2}(n-\ell) . \qquad \text{(I-23.3)}$$

Evaluation of many of these coefficients yields the values of Table I-23.3.

*Note that the inverse square factor is removed from the PTI distributions, as can be seen in Equation (I-16.6').

Table I-23.3. Coefficients $A_{n\ell}$ of the $U_n^{\ell}(r)$ series.

n \ ℓ	0	1	2	3	4
0	1.00847	1.13610	1.17553	1.14855	1.09998
1	-2.04545	-1.12199	-.73621	-.50365	-.35926
2	.99674	.35913	.16641	.08323	.04447
3	.02184	-.00074	-.00186	-.00119	-.00069
4	.02860	.00192	-.00091	-.00093	

The convergence is highly gratifying, though its meaning in terms of the accuracy of the solution is not obvious.

To obtain space distributions, we now sum the series*

$$\hat{D}_{\ell}(r) = \mu_0 e^{-\mu_0 r} \sum_{j=0}^{(n-\ell)/2} A_{j\ell} U_j^{\ell}(\mu_0 r) \ . \qquad \text{(I-23.4)}$$

(The "hat" on $\hat{D}_{\ell}$ indicates approximation.) A few results of these calculations are in Table I-23.4. They were obtained using Table I-40.2 supplemented by calculations with Table I-40.3.

Table I-23.4. Values of $\mu_0^{-1} e^{\mu_0 r} \hat{D}_{\ell}(r)$, for $\mu_0 r = 0,1$.

$\mu_0 r$ \ ℓ	0	1	2	3	4	
0	.3742	.3744	.3806	.3815	.3919	
1	.5025	.2904	.2061	.1533	.1150	(scattered radiation only)

The results of the second row, pertaining to scattered radiation only, were

---

*Strictly speaking, to make this comparable with Equation (I-23.1), we should use $\bar{\mu}_0$ and $\bar{r}$ rather than μ_0 and r in this and following expressions. But this appears to be the best place to change back to dimensional quantities, making use of the fact that $\bar{\mu}_0 \bar{r} = \mu_0 r$.

calculated from the (approximate) expression

$$\mu_0^{-1} e^{1} \hat{D}_{\ell}^{(s)}(1) = \sum_{j=0}^{4} A_{j\ell} [U_n^{\ell}(1) - U_n^{\ell}(0)] \ . \qquad \text{(I-23.4')}$$

The terms here subtracted correspond to exponential penetration and describe the unscattered photons, which comprise the only component at $r = 0$. These calculations are not very accurate; note that not all the information of Table I-23.1 has been used. Nevertheless it is gratifying that for $r = 0$, the results for different ℓ values are so nearly the same, and so nearly equal to the exact value, .38187, corresponding to unscattered photons only.

An alternate approach to these calculations, which has actually been the one used in the computer programs, proceeds by evaluation of the M_{ij} matrix coefficients described in section 41, for different sizes of coefficient lists. The step from spatial moments to coefficients a_{ij} for the power series representation*

$$\hat{D}_{\ell}(r) = \mu_0 e^{-\mu_0 r} \sum_{i} a_{i\ell} (\mu_0 r)^i \qquad \text{(I-23.5)}$$

is then simply a series of matrix multiplications, one for each value of ℓ .

---

*Note that the inverse square factor is removed from the PTI distributions, as can be seen in Equation (I-16.6'). This expression must accordingly be divided by $4\pi r^2$, whereupon the units become essentially $(\text{volume})^{-1}$. Note that in Equation (I-23.1) an energy factor was removed.

Thus, if we apply the data of Table I-41.1 to the moments in Table I-23.2, we obtain the following power series coefficients:

Table I-23.5. Coefficients $a_{i\ell}$ for the series of Equation *I-23.5)

i \ ℓ	0	1	2	3	4
0	.366	.372	.380	.387	.394
1	.385	.248	.184	.140	.109
2	.130	.045	.020	.010	.005
3	-.000	.000	.000	.000	.000

Fig. I-23.1 illustrates trends of these coefficients.

c) PLI Space Distributions.

The advantage in using Equation (I-23.3) as an analytical representation of the distribution lies partly in the ease with which conversion to the plane isotropic case can be made. If we insert such an expression into the general transformation, Equation (I-16.6), it is immediately clear that functions

$$Q_{i\ell}(z,R) = \int_{|z|}^{R} \frac{dr}{r} r^{i} P_{\ell}(\frac{z}{r}) e^{-r} \qquad \text{(I-23.6)}$$

are required for calculation of plane isotropic data. The upper limit is here made finite so that these functions may be directly applicable to disc or ring shaped isotropic sources. It corresponds to the outer radius of a disc-shaped section of the source plane.

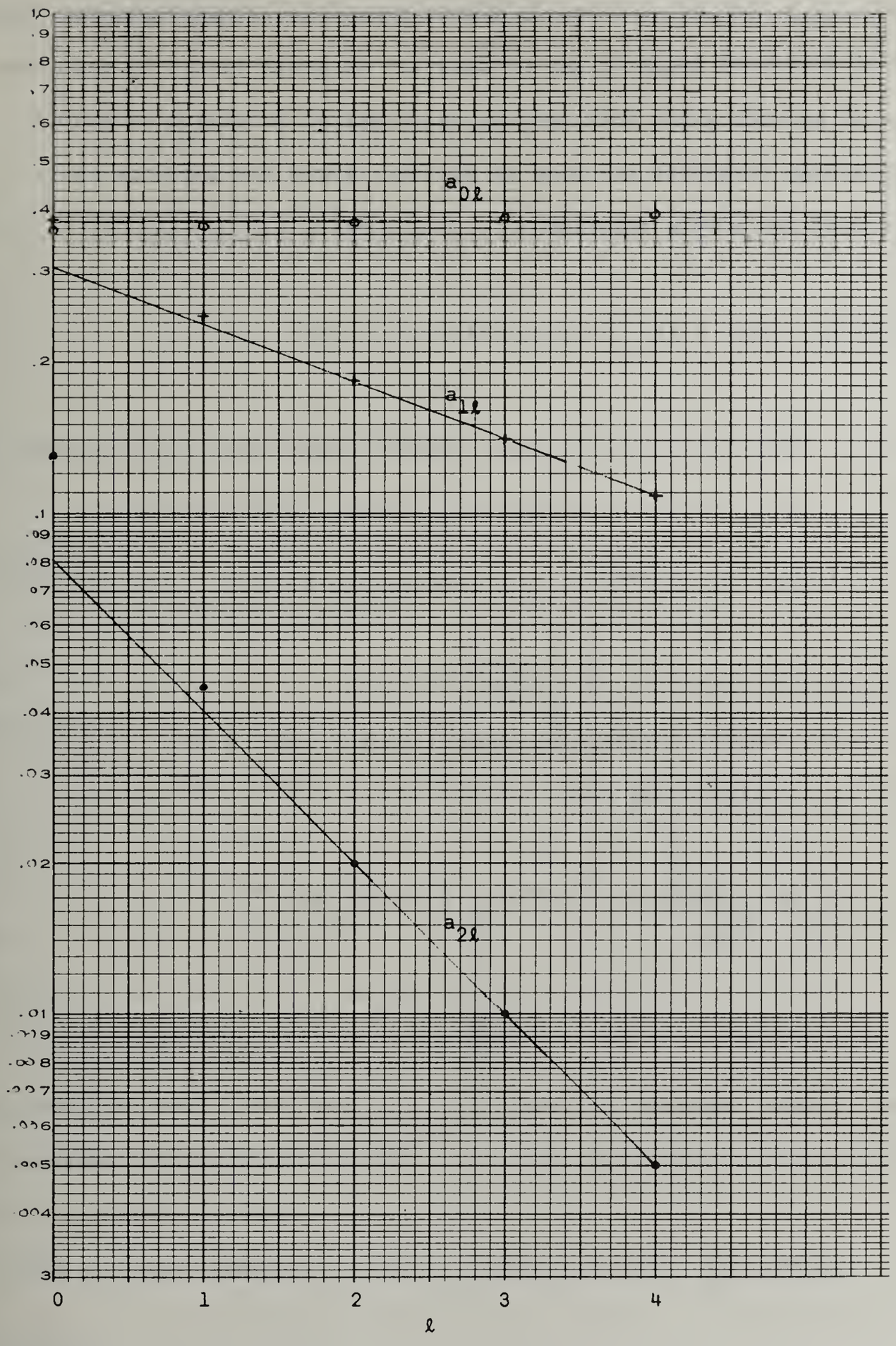

Fig. I-23.1. Illustrating the exponential trend of the $a_{i\ell}$ coefficients for scattered photons at $\mu_0 z = .01$. (Point isotropic Cs137 source.)

The $Q_{i\ell}$'s can be obtained by direct numerical integration; but the number of different index values of interest is great enough to encourage the use of methods which take maximum advantage of recursion relations. Such recursion relations are easy to derive: since the Legendre polynomials obey the simple relation

$$(\ell+1)P_{\ell+1}(z/r) + \ell P_{\ell-1}(z/r) = (2\ell+1)\frac{z}{r}P_{\ell}(z/r) ,$$

we find, by inserting this into the integral of Equation (I-23.6), the result

$$(2\ell+1)zQ_{i\ell}(z,R) = (\ell+1)Q_{i+1,\ell+1} + \ell Q_{i+1,\ell-1} . \qquad \text{(I-23.7)}$$

This is the most important relationship we need.

A second recursion relation, special to the case $\ell = 0$, can be obtained by integration by parts. Thus

$$Q_{i0} = \int_{|z|}^{R} dr\, r^{i-1}e^{-r} = -r^{i-1}e^{-r}\Big]_{|z|}^{R} + (i-1)\int_{|z|}^{R} dr\, r^{i-2}e^{-r}$$

$$= |z|^{i-1}e^{-|z|} - R^{i-1}e^{-R} + (i-1)Q_{i-1,0} . \qquad \text{(I-23.8)}$$

If three of these expressions, for (i+1), i, and (i-1), are combined, the remainder terms can be eliminated to give the following 4-term recursion:

$$Q_{i+1,0} - (|z|+R+i)Q_{i0} + [R|z|+(R+|z|)(i-1)]Q_{i-1,0} - R|z|(i-2)Q_{i-2,0} = 0 .$$

(I-23.8')

Finally, we note that

$$Q_{00}(z,R) = E_1(|z|) - E_1(R) ,$$

$$Q_{10}(z,R) = e^{-|z|} - e^{-R} ,$$

$$Q_{20}(z,R) = (|z|+1)e^{-|z|} - (R+1)e^{-R} . \qquad \text{(I-23.9)}$$

These special cases give us the start we need.

The application of the recursion formulae is clarified by reference to Figure I-23.2. The special cases Q_{00}, Q_{10}, and Q_{20} can be calculated directly. The recursion for $\ell = 0$ can then be used to obtain first Q_{i0} for $i = 3,4,\ldots$ and then for $i = -1,-2,\ldots$. Following this, the general recursion can be used to work out values for higher ℓ. But the diagonal structure of this recursion implies that the smallest required i value increases by unity each time that ℓ increases by unity, so that if, for example, $i = -5$ were the

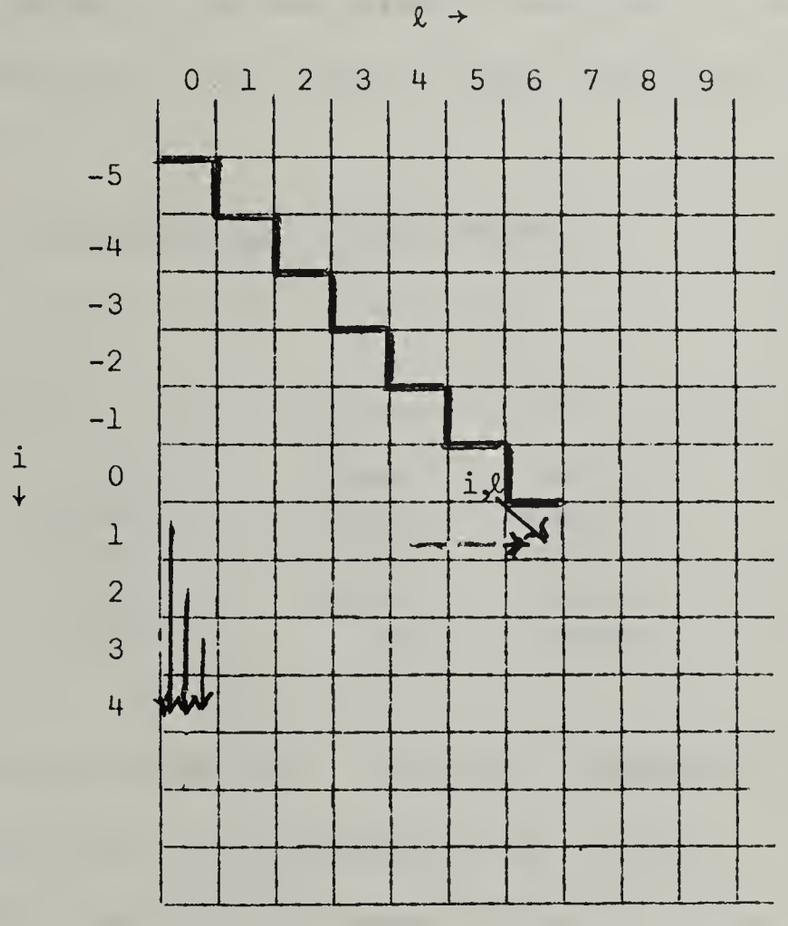

Fig. I-23.2. $Q_{i\ell}$ linkages.

smallest index for $\ell = 0$, then terms in the diagram below the jagged diagonal would be accessible to recursive calculation.

The space distributions require only terms with $i \geq 0$. Thus, we determine a triangle of values which are not directly useful in the calculation of distributions; but the number of entries in the triangle is apt to be comparable with the number of entries directly required.

Our experience is that the accuracy of the $Q_{i\ell}$'s does not decrease with multiple use of the recursion relations as described.

Dr. J. A. Diaz has written a machine program which applies the recursion system to the calculation of $Q_{i\ell}$'s for arbitrary penetration. Table I-23.6 gives illustrative results which he obtained for $\mu_0 z = .01$ mean free paths, quite a small value. One feature of this table is

Table I-23.6. $Q_{i\ell}$ values for $\mu_0 z = .01$.

i \ ℓ	0	1	2	3	4
0	4.0379	.94967	-1.2835	-.60355	.75496
1	.99005	.040379	- .48078	-.048312	.35002
2	.99995	.009005	- .49937	-.014613	.37368
3	2.0000	.099995	- .99988	-.014989	.74963
4	6.0000	.02	-2.9999	-.029998	2.2496

worth a comment: For odd ℓ the values are very much smaller than for even ℓ, due to proportionality of these terms to $\mu_0 z$. The formal expression for the PLI space distributions, written in terms of the $Q_{i\ell}$'s, is*

---

*When this expression is multiplied by the source strength (photons/area), the units become those of (volume)$^{-1}$.

$$\hat{D}_\ell(z) = \frac{1}{2}\mu_0 \sum_i a_{i\ell} Q_{i\ell}(\mu_0 z, \infty), \qquad \text{(I-23.10)}$$

where the $a_{i\ell}$ coefficients are the same quantities which appear in Equation (I-23.5). Illustrative values for $\hat{D}_\ell(z)$ can be obtained by combining numbers from Tables I-23.5 and I-23.6. This produces values given in Table I-25.1, from which the contribution of the unscattered component has been removed. Further discussion of the $\hat{D}_\ell$'s and their application to angular distributions is given in section 25.

24. Angular Distributions for Point Isotropic Sources

Assuming that calculations of spatial distributions of the various Legendre coefficients have been made, it is possible to determine angular distributions. We will restrict our attention in this section to the case of point isotropic sources, and focus on angular distributions of the exposure.*

One apparently obvious way to construct angular distributions is simply by summing the Legendre series,

$$\hat{D}(\theta_r, r) = \sum_{\ell=0}^{\infty} \frac{2\ell+1}{4\pi} \hat{D}_\ell(r) P_\ell(\cos\theta_r) \ , \qquad \text{(I-24.1)}$$

where θ_r is the angle between photon direction and the radial line from source to photon.

In practice, however, perhaps half a dozen values of ℓ are available, and in order to obtain suitable convergence, one might need, say, 20 or more terms. Therefore, the angular distributions one calculates by carrying out these sums are not accurate enough. The reason for the large number of terms is simple: the angular distribution for all values of r has a strong peak at $\cos\theta_r = 1$. Such an irregular feature always requires many terms of accurate description.

There is an additional difficulty which should be kept in mind: the Legendre coefficients have been determined by moment calculations; but

---

*The angular distributions of the different spectral components will be quite different from angular distributions of an integral over the spectrum; the procedures we discuss are not expected to be very useful in the differential case.

such calculations are only of an accuracy of, say, a few percent. There is a possibility that in the second construction errors of the first construction may be further multiplied.

Putting the accuracy problem aside, let us focus attention on the problem of convergence, using the data of Table I 23.5. The top row of values are easily interpreted. The angular distribution of the flux at the source is completely dominated by unscattered photons, all of which travel directly away from the source. Accordingly, the values of the top row must describe a delta-function and must, if calculated accurately, have values precisely equal to .3818699. The angular distribution can be written analytically in the form

$$D(\theta_r,0) = .3818699 \frac{\mu_0}{2\pi} \delta(\cos\theta_r - 1) . \qquad (I\text{-}24.2)$$

This angular distribution, attenuated exponentially, describes unscattered photons at all penetrations.

The main problem therefore can be restricted to the scattered photons, for which the coefficients of the second row of Table I-23.4 are typical.* These coefficients appear to form a succession in which the ratios of successive values are nearly constant. To see this more clearly, refer to Figure I-24.1, in which they are plotted on logarithmic paper. As can be seen there, the higher coefficients do indeed appear to lie more and more nearly on a straight line. This suggests a way in which we may be able to extrapolate to higher ℓ values. But for this purpose we would like to have analytic information about the function whose series is of

*In the discussion which follows, a feature of the singly scattered component is neglected, namely a singularity of the type θ^{-1} at $\theta = 0$.[47] In future calculations for shielding purposes an increase in accuracy can be obtained by exact calculation of this component.

$\mu_0^{-1} e^{1} \hat{D}_\ell(\mu_0 r = 1)$

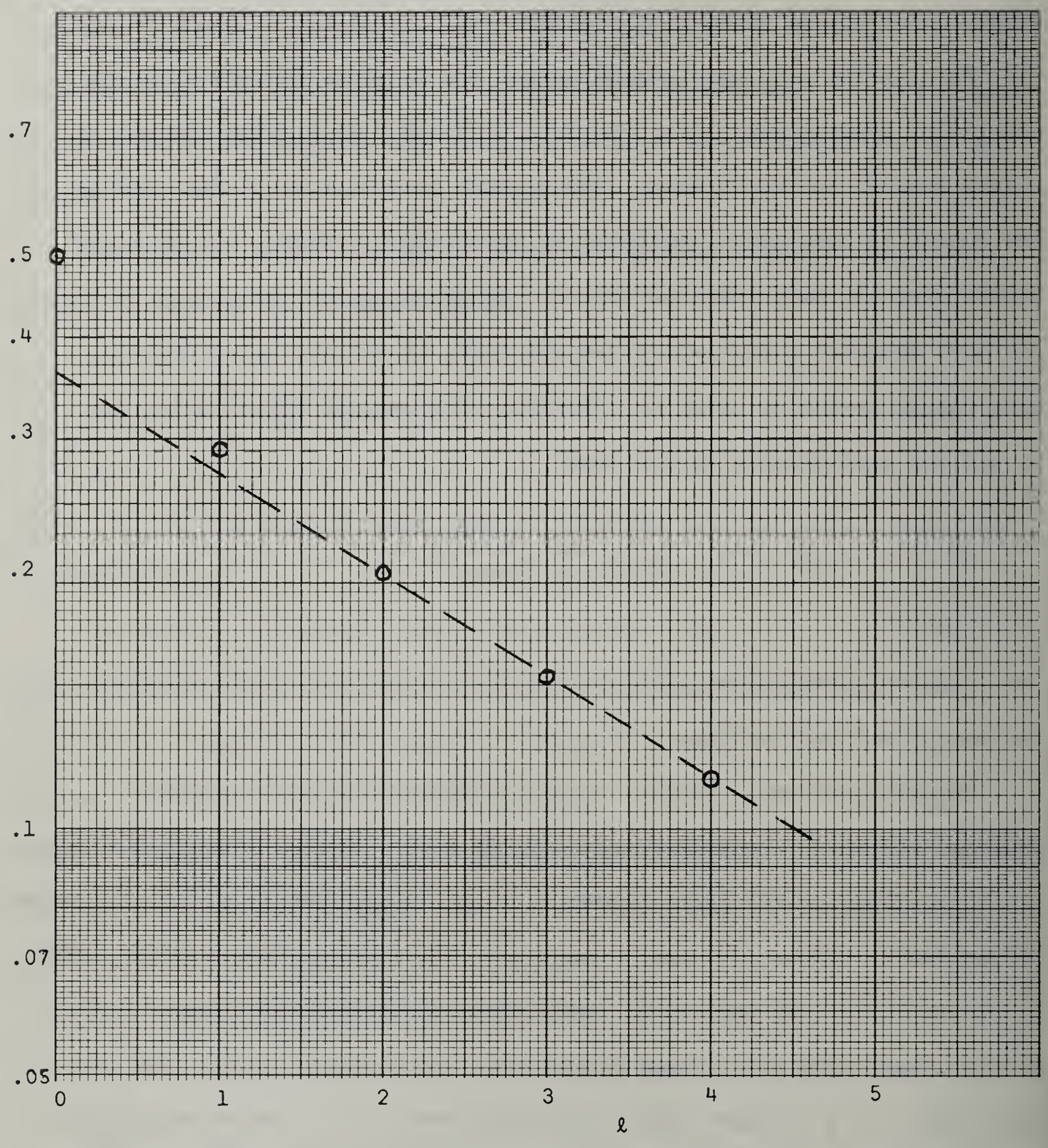

Fig. I-24.1. $\hat{D}_\ell$ coefficients at $\mu_0 r = 1$, scattered flux only. (Point isotropic Cs137 source).

the type

$$f(x) = \sum_{\ell=0}^{\infty} (\ell+1/2)e^{-b\ell}P_\ell(x) .$$

Tha nature of this function can be readily ascertained. If we start with the usual generating function for the Legendre polynomials,

$$\frac{1}{\sqrt{1-2x\alpha+\alpha^2}} = \sum_{\ell=0}^{\infty} \alpha^\ell P_\ell(x) ,$$

and replace α by e^{-b}, we obtain from differentiation with respect to b the expression

$$\frac{e^{b/2}\sinh b}{[2(\cosh b-x)]^{3/2}} = \sum_{\ell=0}^{\infty} (\ell+1/2)e^{-b\ell}P_\ell(x) . \qquad \text{(I-24.3)}$$

It is clear that when b is small the series on the right converges slowly, while at the same time the factor (cosh b - x) in the denominator on the left becomes small for x near unity. Thus, the function has a peak at x = 1, as we said must be the case for our angular distribution.

There are many ways in which this function can be used to obtain an approximate angular distribution. The procedure which was used to obtain data for Ref. 36 was of the following type: the angular distribution is represented formally by

$$\frac{2\pi}{\mu_0}e^{\mu_0 r}\hat{D}(\theta_r,r) = A\frac{e^{b/2}\sinh b}{[2(\cosh b-\cos\theta_r)]^{3/2}} + \sum_{\ell=0}^{4} (\ell+1/2)c_\ell P_\ell(\cos\theta_r) . \qquad \text{(I-24.4)}$$

The main term is the first; the final sum represents a correction. We

write this expression in the equivalent and suggestive form

$$\frac{2\pi}{\mu_0} e^{\mu_0 r} \hat{D}(\theta_r, r) = \sum_{\ell=0}^{4} (\ell+1/2)\{Ae^{-b\ell}+c_\ell\}P_\ell(\cos\theta_r) + \sum_{\ell=5}^{\infty} (\ell+1/2)Ae^{-b\ell}P_\ell(\cos\theta_r) . \tag{I-24.5}$$

Of the 7 undetermined constants in this expression, two may be specified arbitrarily if we only use the 5 coefficients of Table I-23.4. We therefore equate the c_2 and c_4 coefficients to zero. But then the following equations must hold:

$$\begin{aligned} Ae^{-2b} &= .2061, \\ Ae^{-4b} &= .1150. \end{aligned} \tag{I-24.6}$$

These guarantee that the approximation has correct values for the P_2 and P_4 coefficients. In Figure I-24.1 this means that the main term will have coefficients on a straight line through these two points (i.e. on the dashed line.) The choice of P_2 and P_4 coefficients was made because they are far enough out on the sequence to give a reasonably good extrapolation.* Solution of Equation (I-24.6) is elementary and gives the values A = .3694, b = .2917. Using these numerical values, the other coefficients can be obtained from the equations

$$c_\ell = \{\mu_0^{-1} e^{\mu_0 r} \hat{D}_\ell(r)\} - Ae^{-b\ell} .$$

Values obtained using Table I-23.4 are

---

*In the machine calculations, the coefficients of P_3 and P_5 were used, and the correction sum extended to P_7.

$$c_0 = .133 ,$$

$$c_1 = .0145 ,$$

$$c_3 = -.0007 .$$

The final expression for the (scattered flux).angular distribution is

$$\frac{2\pi}{\mu_0} e^{l} \hat{D}(\theta_r,\mu_0 r=1) = \frac{.02275}{[1.0428-\cos\theta_r]^{3/2}} + .0666 + .0218\cos\theta_r - .0024P_3(\cos\theta_r) .$$

Figure I-24.2 shows this angular distribution. The arrow at $\cos\theta_r = 1$ is intended to represent unscattered photons; its length means nothing here.

The correction terms are negligible in the region of the peak, but they tend to be important at $\cos\theta_r = -1$, and at neighboring angles which correspond to backscattering. The angular distributions published in Ref. 36 tend to have a "hook" at $\cos\theta_r = -1$, which is certainly spurious.

Another type of construction may not give greater accuracy, but it could provide some estimate of the errors involved in this type of calculations, and it is certainly possible to obtain more realistic results for backscattering angles. Perhaps the most obvious alternate method would utilize a representation of D_ℓ coefficients by a sum of exponentials, and the angular distribution by a sum of terms of the type of Equation (I-24.3).

This construction must be repeated for each penetration distance. Promising alternatives are discussed in the next section.

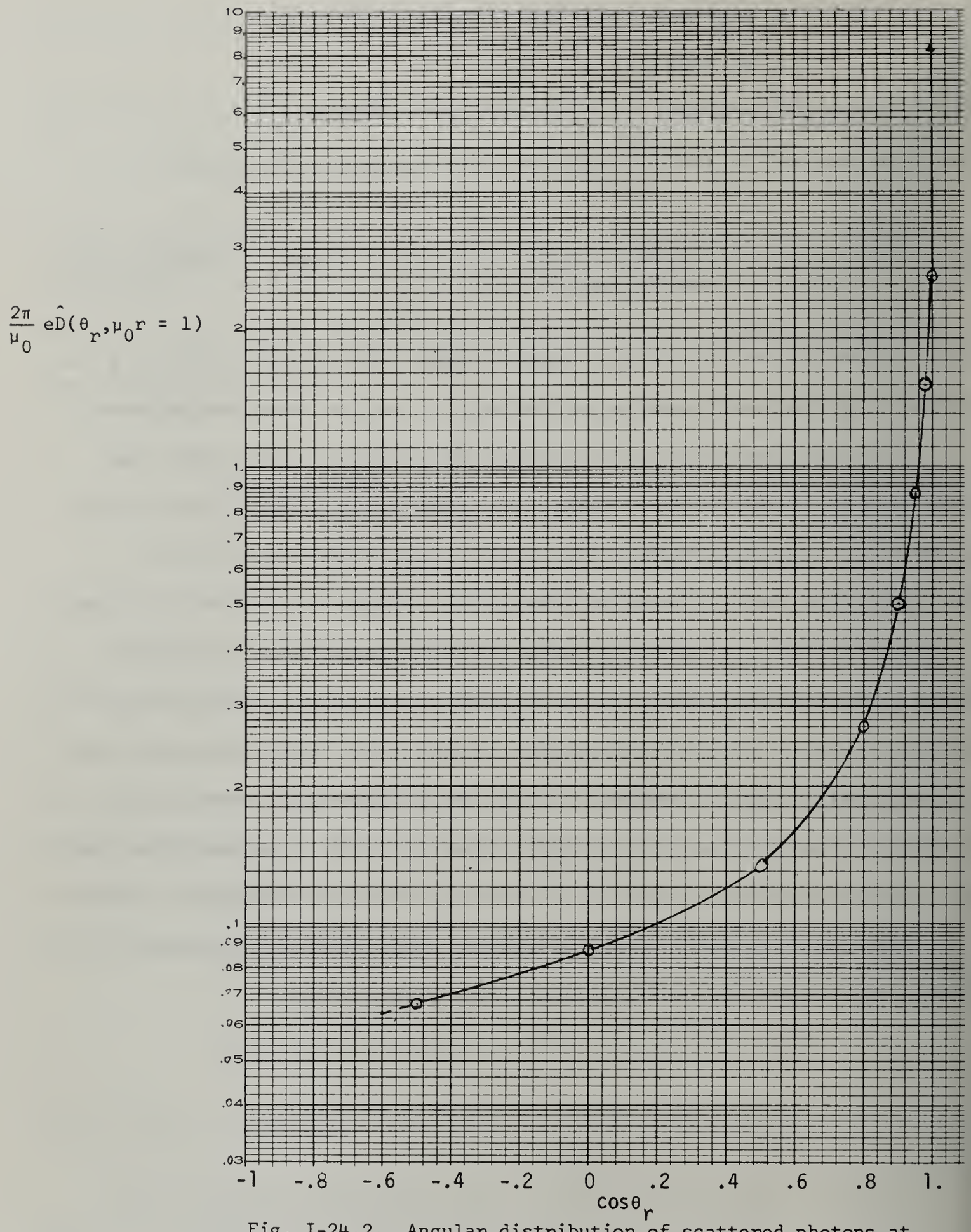

Fig. I-24.2. Angular distribution of scattered photons at $\mu_0 r = 1$, for a point isotropic Cs137 source in H_2O.

25. Angular Distributions for Plane Isotropic Sources*

As in the case of the point isotropic source, it is desirable to treat unscattered and scattered radiation in different ways. Referring to Table I-23.5 and Equation (I-23.10), we note that the strength of the unscattered component is given by $a_{0\ell}$ values, which are ideally all equal to .3818699 as noted in the preceding section. The form of the unscattered radiation is known (see Equation (I-20.10)), and we therefore deduce that

$$\hat{D}^{(o)}(z) = \frac{\mu_0}{4\pi} \frac{.3818699}{|\cos\theta|} e^{-\mu_0 z/\cos\theta} h(z/\cos\theta) , \qquad (I\text{-}25.1)$$

where $h(z/\cos\theta)$ is the unit function.

Next we calculate the Legendre coefficients for the scattered photons by evaluating the sum of Equation (I-23.10), with the omission of the $i = 0$ term. For illustrative purposes, we combine data from Tables I-23.5 and I-23.6 to obtain the following list.

Table I-25.1. Legendre coefficients for the angular distribution of scattered photons, at .01 mean free paths, from a plane isotropic Cs137 source in water.

ℓ	$\mu_0^{-1} \hat{D}_\ell^{(s)}$
0	.510
1	.0104
2	-.0985
3	-.0069
4	.04

Note that the odd coefficients have abnormally low values. The convergence can best be gauged by the sequence of even ℓ values.

To evaluate directly an angular distribution, we can simply evaluate

*For an early calculation see Ref. 11, and for experiments on actual fallout fields see Ref. 131 .

the Legendre sum,

$$\hat{D}^{(s)}(0,z) = \frac{1}{2\pi} \sum_{\ell} (\ell+1/2) \hat{D}_{\ell}^{(s)}(z) P_{\ell}(\cos\theta) \ , \qquad \text{(I-25.2)}$$

using this data. The resulting distribution will have a peak at or very near $\cos\theta = 0$. It will have a tendency to oscillate which will be most marked for $\cos\theta$ near ± 1 , where the distribution has its lowest values. This tendency to oscillate reflects the lack of convergence illustrated in Table I-25.1, and is spurious. When the scattered and unscattered components are combined, the irregularities of the scattered components are masked for positive $\cos\theta$ values, by the much larger contributions of unscattered photons. The irregularities appear in full strength only for backscattered (negative $\cos\theta$) values.

Calculations of this type, but using terms through $\ell = 7$, were made for the data of Ref. 36 . They are not entirely satisfactory, the more so because it should be possible to smooth out the spurious irregularities by suitable extrapolation of coefficient sequences. One method for doing this is suggested by the regularities of Table I-23.5. We have already observed that the top row of coefficients are all equal in principle, and it is clear that the next two rows are roughly exponential. This is exhibited in Figure I-23.1.

These simple trends suggest the possible use of functions in the plane isotropic case analogous to Equation (I-24.3). This is certainly feasible; but the pertinent functions are analytically representable as folding integrals which must be evaluated numerically. Once committed to numerical evaluation, however, alternative procedures must be examined. We propose

evaluation of angular distributions by the following process:

1) extrapolation of the $a_{i\ell}$ values to large ℓ by use of methods analogous to those of section 24, applied separately for different values of i;

2) evaluation of $Q_{i\ell}$'s by recursion for large ℓ values;

3) evaluation of $D_{\ell}^{(s)}(z)$ for perhaps 20 to 30 ℓ values, using Equation (I-23.10); and

4) calculation of the angular distribution by means of Equation (I-25.2), but with 20 to 30 terms in the sum rather than perhaps half a dozen.

It is possible to apply these same ideas to the $A_{n\ell}$ coefficients instead of the $a_{i\ell}$, since they also have basically exponential trends with increasing ℓ. The $A_{n\ell}$ values do not change, as do the $a_{i\ell}$, when more moments are used for a better approximation. A version of this procedure, using $A_{n\ell}$ coefficients, is being programmed for improvement of angular distributions for various isotropic source configurations.

26. Space Distributions for Plane Monodirectional Sources*

We will not be concerned with azimuthal variations of the flux in this section, but will assume that the source generates photons at fixed obliquity and equally for all azimuths. The use of "monodirectional" in the heading is therefore only justified by the fact that procedures illustrated by the special case can be applied generally to distributions produced by truly monodirectional sources.

Many of the features of these plane source distributions can be exhibited by reference to the unscattered and once-scattered components. We specialize the function $S(E,\theta,\phi)$ in Equation (I-20.6) to the form

$$S(E,\theta,\theta) = \frac{1}{2\pi}\,\delta(\cos\theta-\cos\theta_0)\delta(E-E_0)\ . \qquad \text{(I-26.1)}$$

The unscattered component is then

$$I^{(o)}(\lambda,\theta,\bar{z}) = \lambda_0\,\frac{1}{2\pi}\,\delta(\cos\theta-\cos\theta_0)\delta(\lambda-\lambda_0)\,\frac{1}{\cos\theta_0}\,e^{-\bar{\mu}_0\bar{z}/\cos\theta_0}h(\bar{z})\ , \qquad \text{(I-26.2)}$$

where h is the unit function, and the barred quantities are dimensionless as given in section 17. We will not bother to rewrite the once-scattered component, since the spatial trends are those given by Equation (I-20.9).

Now, for all initial angles θ_0, the unscattered component vanishes for negative z and has a discontinuity at the source plane. This feature persists through integrations over spectral energy and angular variables; it therefore characterizes $D^{(o)}(\theta,z)$ and $D^{(o)}(z)$.

Examination of Equation (I-20.9) shows that there is a slope

*For an early calculation see Ref. 15.

discontinuity at the source plane, for all spectral energies and all θ_0 and θ values. Further, for $\cos\theta > 0$, the flux is proportional to z for small, positive z values; while for $\cos\theta < 0$, the flux has different exponential trends on the two sides of the source plane. We expect the existence of a slope discontinuity to persist through different integrations over angle and energy. Likewise, the characteristics peculiar to forward-penetrating ($\cos\theta > 0$) and backward-penetrating ($\cos\theta < 0$) components will be features of integrals over those components.

Putting all this together with reference to the space distribution of the Legendre harmonics of the exposure angular distribution, we expect the features sketched in Figure I-26.1. Since the $\ell = 0$ coefficient is the integral over all angles, these comments apply to this most important case. Further, the arguments apply not only to the azimuth-independent case but also to the expansion coefficients $D_{\ell m}$ of the true monodirectional source.

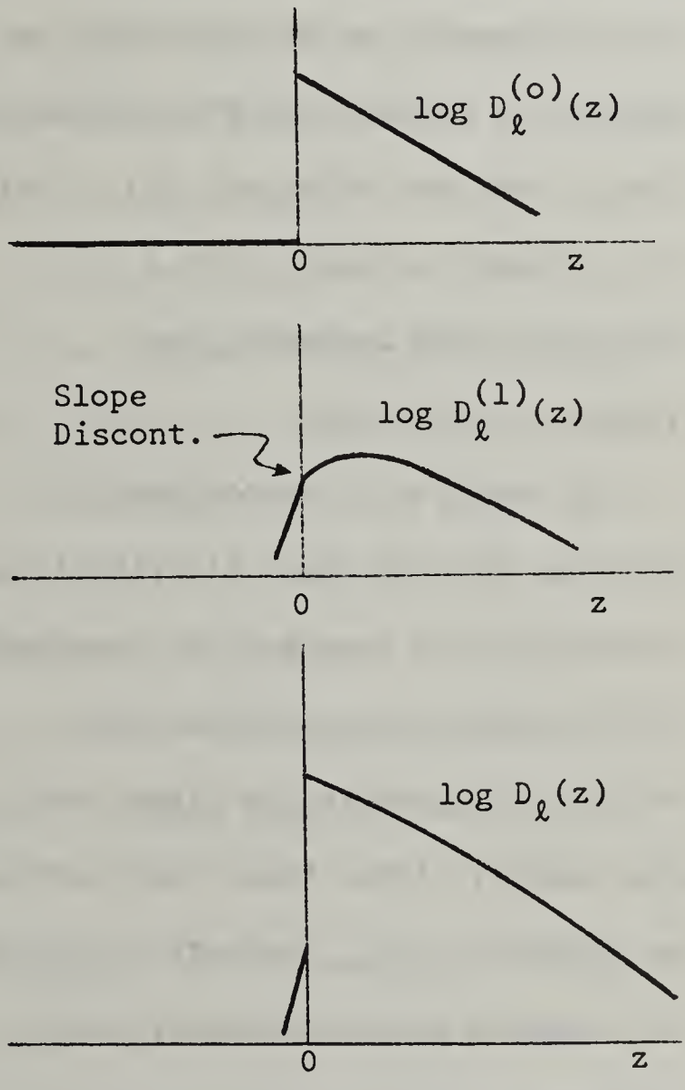

Fig. I-26.1. Spatial trends for Legendre coefficients for plane monodirectional sources.

It is clear from Equations (I-20.6) that the size of the discontinuity increases as

$\cos\theta_0$ decreases. At the same time, the strength of the negative z components increases relative to components at positive z. Finally, the intensity of all spectral components tends to be more concentrated near the source plane. All of these tendencies are exhibited in the data of Ref. 36.

The spatial moments, which are integrals over both negative and positive z, describe a complete distribution, say $D_\ell(z)$. The even moments have precisely the value of moments of a distribution $D_\ell^{(+)}(|z|)$, obtained by adding the backscattering to the forward scattering. Similarly, the odd moments can be considered as describing a distribution $D_\ell^{(-)}(|z|)$ obtained by subtracting the backscattered flux from the forward scattered flux at the same value of $|z|$. Both even and odd component distributions are sketched in Figure I-26.2. The dashed line indicates the original distribution.

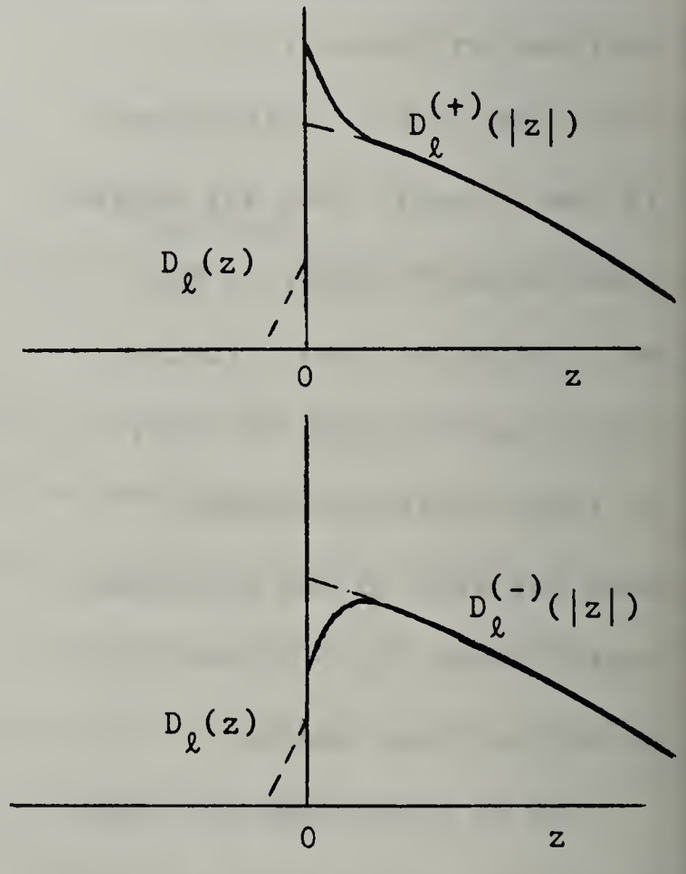

Fig. I-26.2. Even ($D^{(+)}$) and odd ($D^{(-)}$) components of space distribution.

In nearly all methods used to construct the PLM space distributions, calculations of even and odd component distributions are undertaken separately, each using <u>every other</u> available moment. After these constructions, one obtains $D(z)$, for both positive and negative penetrations, by superposition:

$$D_\ell(z) = \frac{1}{2}\left[D_\ell^{(+)}(|z|) + D_\ell^{(-)}(|z|)\right] , \quad z > 0 ;$$

$$D_\ell(z) = \frac{1}{2}\left[D_\ell^{(+)}(|z|) - D_\ell^{(-)}(|z|)\right] , \quad z < 0 . \qquad \text{(I-26.3)}$$

The construction of even and odd component distributions can be effected with the U_n^ℓ polynomial systems. The data of Ref. 16 was calculated in this way, or rather, in a manner equivalent to this. The difficulty with this construction procedure can be understood by making reference to Figure I-26.2. The distributions $D_\ell(z)$ obey an exponential trend for positive $\underline{z}$ which is quite different from that for negative $\underline{z}$; the latter is far more rapidly decreasing than the former except for $\cos\theta_0$ very small (grazing incidence). Consequently, an expansion in U_n^ℓ polynomials which represents the positive $\underline{z}$ case well with a few terms will require many terms to represent the negative $\underline{z}$ case. The superpositions $D_\ell^{(+)}$ and $D_\ell^{(-)}$ will therefore generally consist of a slowly converging series of small terms added to a rapidly converging series of large terms.

It was for this reason that the data of Ref. 16 was not given near the source plane, for the plane normal source configuration. The convergence was not adequate for the description of the backscattered part of the distribution, which appears as a "pip" or "well", as the case may be, for small $\underline{z}$.

The construction procedures which have proved most useful have been generally referred to as "function-fitting" methods, and are discussed in sections 42 and 43. In particular, the data of Refs. 36,39,40,41 has been obtained by assuming the forms

$$\hat{D}_0^{(+)}(z) = \mu_0 \sum_{i=1}^{4} \frac{\alpha_i}{\beta_i} e^{-\mu_0 z/\beta_i} ,$$

$$\hat{D}_0^{(-)}(z) = \mu_0 \sum_{i=1}^{4} \frac{\alpha_i}{\beta_i^2} e^{-\mu_0 z/\beta_i} . \qquad \text{(I-26.4)}$$

For both distribution types, β_0 is assigned the value $\cos\theta_0$ and β_1 has been used as an adjustable parameter normally given a value near .7 . The remaining six parameters in the expression for $D_0^{(+)}$ have been determined using six moment equations, as outlined in section 43.

One can see from Figure I-26.2 that $D_0^{(-)}$ has a value for $z = 0$ equal to the discontinuity at the source plane. Since this discontinuity is a feature of the unscattered component, its size is exactly known. One can incorporate the discontinuity correctly by determining the distribution $D_0^{(-)}$ from <u>five</u> moment equations, plus the requirement

$$\mu_0^{-1} \hat{D}_0^{(-)}(0) = \sum_{i=1}^{4} \frac{\alpha_i}{\beta_i^2} = D_{00}^{(o)} = \frac{\bar{\mu}_d(E_0)}{\bar{\mu}_0(E_0)} . \qquad \text{(I-26.5)}$$

The procedure for solving the resulting system of equations for the α_i and β_i values is again just that outlined in section 43.

To illustrate all this, we give data again for the case of Cs137. Two sets of moments are listed in Table I-26.1, corresponding to two values of $\cos\theta_0$. The parameter values giving even and odd component distributions for both cases are listed in Table I-26.2.

Table I-26.1. Coefficient-moments for plane monodirectional Cs137 sources in H_2O. ($\bar{\mu}_0$ = .3854).

n	$\frac{1}{n!} D_{n0}(PLS)$ $\cos\theta_0 = 1$	$\cos\theta_0 = .5$	
$D_{00}^{(o)}$	0.3818699	0.7637399	(Discontinuity)
0	1.0084677	1.0084677	
1	1.4586109	0.72930548	
2	2.2024530	0.86991361	
3	2.8817104	0.69998723	
4	3.7939434	0.81884550	
5	4.7044572	0.70423041	
6	5.7992881	0.78364308	
7	6.9359811	0.69913194	
8	8.2236733	0.74242435	
9	9.5807485	0.67626414	
10	11.068103	0.69288998	

Table I-26.2. Distribution parameters for two plane slant Cs137 sources in H_2O.

Even			Odd	
		$\cos\theta_0 = 1.0$		
α_i/β_i	β_i		α_i/β_i^2	β_i
-60.045188	1.		-15.083005	1.
-00.54834221	0.74161984		20.741507	0.74161984
17.175787	0.93287377		-18.509065	0.72843107
43.967109	1.0334424		13.232433	1.0630951
		$\cos\theta_0 = 0.5$		
-.23270104	0.5		4.4320127	0.5
-2.0783500	0.74161984		-1.3361580	0.74161984
2.0853296	0.65103604		-3.4916661	0.44897421
1.3830670	0.94611402		1.1595514	0.95612440

Note that for $\cos\theta_0 = 1$, exponential coefficients slightly larger than unity appear, corresponding more or less to the presence of a build-up factor.

It is also quite interesting that for $\cos\theta_0 = 0.5$, one of the exponential coefficients approaches unity, corresponding to spectral components which scatter without much loss of energy into a direction more or less perpendicular to the source plane.

There is some cause for concern that the terms which obviously dominate at large penetrations are somewhat different in even and odd distributions, and so cannot be expected to cancel completely. This is not very important, however, since the distance at which this would become noticeable in the back-penetration is such that the radiation flux would be almost negligible.

In general, the values of the multiplicative parameters are very unstable in the sense that they may vary greatly without changing the distribution very much. This is because the trend of the distribution depends on the combination of terms rather than any single term, except for great penetrations.

It is instructive to see the coefficients of the U_n^o polynomial expansion. Table I-26.3 gives results for $\hat{D}_0^{(+)}$, as calculated from Table I-26.1. The coefficients for $\cos\theta_0 = 1$ exhibit the expected feature of large, rapidly converging coefficients for the first few terms, followed by a much more slowly converging sequence of small terms.

Table I-26.3. Coefficients for the series $\hat{D}_0^{(+)} = \mu_0 e^{-\mu_0 z} \sum_{i=0}^{5} A_{i0} U_i^o(\mu_0 z)$, for PLS Cs137 sources in H_2O.

i	$A_{i0}, \cos\theta_0 = 1$	$A_{i0}, \cos\theta_0 = .5$
0	1.00847	1.00847
1	-1.19398	.13855
2	0.39751	.08749
3	-0.01635	.07162
4	-0.01116	.04974
5	-0.00698	.03016

The coefficients for $\cos\theta_0 = 0.5$ converge rather slowly, in a regular manner, following the first large coefficient. Note that the unscattered flux for this case has the exponential trend $e^{-\mu_0 z/.5}$, quite different from the exponential assumed for Table I-26.3. Accordingly, the terms of the series corresponding to Table I-26.3 undergo strong cancellations. It would probably be more accurate to use a more rapidly decreasing exponential, and this merely underscores the fact that the effective exponential behavior is difficult to specify.

F. ELEMENTARY MONTE CARLO CALCULATIONS

27. Schematized Problems and Particle Trajectories*

In a Monte Carlo calculation for a radiation problem, one essentially carries out an experiment with pencil or paper, or with an electronic computer, by simulating the actual physical process. The name "Monte Carlo" arises from the use of random numbers in such a theoretical experiment to determine a sequence of chance events.

Such a theoretical experiment has a number of advantages and disadvantages in comparison with an actual experiment. The chief advantage is that all variables are under control; one is not bothered with the problem of background counts or uncertain detector response. The schematized situation can be made as realistic as one desires. On the other hand, in comparison with an actual experiment one is working with sources of very low strength. Even with the most modern computers, Monte Carlo "experiments" use 10,000, or in an extreme case up to 100,000 particles. But this is extremely small when compared with the number of gamma rays which are emitted from a radiation source in a typical experiment. The main problem with Monte Carlo methods is the inevitable statistical error due to a low "counting rate."

The first phase of a Monte Carlo calculation is the determination of a schematized problem. While a Monte Carlo simulation can incorporate any amount of detail, an extremely realistic mock-up can be costly. So as a matter of practice, a compromise schematization may be established,

---

*This and the following 5 sections are revisions of material originally presented by Dr. Martin J. Berger, of the National Bureau of Standards, in four lectures given July 16 and 17, 1962.

and this may serve as the basis for solution of a large number of problems in a single Monte Carlo calculation. Great care must accordingly be exercised in setting up this calculation.

Certain features of these calculations are of a fairly universal character. For example the procedures for utilizing cross sections and the method of random sampling can be applied to any problem of interest. We wish to discuss these things in connection with the concept of a Monte Carlo case history. Nearly every aspect of the following discussion applies equally to neutrons and gamma rays, though our attention is focused on the latter.

Consider the path of a photon as it penetrates through some medium. Because many scatterings will occur, such a path is expected to zig-zag more or less as in Figure I-27.1. In this sketch the photon starts at B, where it is emitted with a given energy and a given direction. It has a free flight until there is an interaction. While the interaction can be either a scattering or an absorption, we assume that it is a scattering. The photon accordingly loses some energy and changes direction. This loss of energy with change of direction is a statistical process; that is, there is a probability distribution for different energy losses and changes of direction. After this first scattering the particle has another free

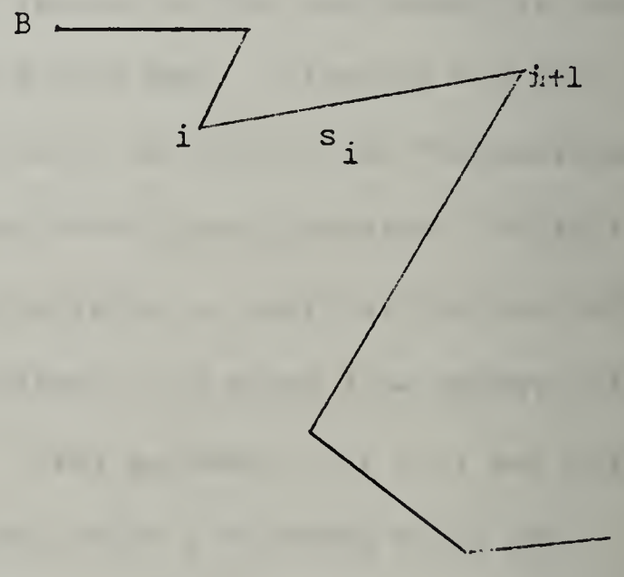

Fig. I-27.1. Trajectory of a photon

flight and makes another interaction, and so on.

Let us consider how to describe the state of the photon at any point along its path. One needs coordinates x,y,z to describe the position, coordinates θ,ϕ to describe the direction of motion, and an energy variable E. The state of the particle, which we shall refer to as α, might accordingly be written

$$\alpha = (x,y,z,E,\theta,\phi) ,$$

so that it depends on a total of six variables. An alternative representation of the photon direction utilizes a unit vector $\vec{u}$,

$$\vec{u} = (\sin\theta\cos\phi,\sin\theta\sin\phi,\cos\theta) ,$$

whose components are direction cosines.

A photon "trajectory" can be described by a sequence of states, $\alpha_0,\alpha_1,\alpha_2$, etc., up to some α_n, where α_0 is the initial state at emission by the source, α_1 is the state immediately after the first interaction, and so on to α_n, the final state before absorption or disappearance from the space or energy region of interest.

As already indicated, α_i is a statistical quantity whose distribution depends only on the immediately preceding state, α_{i-1}. That is, there exists a probability distribution of α_i conditional on α_{i-1} alone:

$$\psi(\alpha_i|\alpha_{i-1}).$$

This probability distribution, ψ, is given by the local cross section

for the particular radiation considered. To generate a chain of states which would correspond to a trajectory like that of Figure I-50.1, one would first pick an α_0 corresponding to initial conditions. Then one would pick an α_1 from the distribution $\psi(\alpha_1|\alpha_0)$, then α_2 from $\psi(\alpha_2,\alpha_1)$, and so on, each choice being made by random sampling except possibly the choice of α_0. The "case-history" of a photon can be expressed by the following array:

$$\begin{array}{cccc} x_0 & x_1 & \cdot\ \cdot\ \cdot & x_n \\ y_0 & y_1 & \cdot\ \cdot\ \cdot & y_n \\ z_0 & z_1 & \cdot\ \cdot\ \cdot & z_n \\ E_0 & E_1 & \cdot\ \cdot\ \cdot & E_n \\ \theta_0 & \theta_1 & \cdot\ \cdot\ \cdot & \theta_n \\ \phi_0 & \phi_1 & \cdot\ \cdot\ \cdot & \phi_n \end{array} .$$

We obtain such an array one column at a time.

The first question, then, is: given the coordinates of α_i, how can one determine the position of the next collision, x_{i+1},y_{i+1},z_{i+1}? If we represent the path length traveled by the photon after the i'th interaction as $\underline{s}$, then according to Equation (I-3.2) the probability for an interaction between $\underline{s}$ and $\underline{s} + \Delta s$ is just $e^{-\mu s}\mu\Delta s$, where μ is an attenuation coefficient. A procedure must therefore be established for picking $\underline{s}$ from this probability distribution. Once a value has been assigned to $\underline{s}$, the coordinates of the next interaction are given by

$$\begin{aligned} x_{i+1} &= x_i + s(\sin\theta_i\cos\phi_i) , \\ y_{i+1} &= y_i + s(\sin\theta_i\sin\phi_i) , \\ z_{i+1} &= z_i + s(\cos\theta_i) . \end{aligned} \qquad \text{(I-27.1)}$$

Note that the particle retains the values θ_i and ϕ_i acquired as a result of the i'th interaction until after the (i+1)'st interaction. Once the position of the (i+1)'st interaction is known, one must decide whether the case history should be terminated or not. This depends on the type of interaction next occurring. Ordinarily, μ refers to the total attenuation coefficient, that is the sum of attenuation coefficients for scattering (μ_s) and absorption (μ_a).* Then μ_s/μ is the probability that the history is continued, and correspondingly μ_a/μ is the probability that the interaction is an absorption, either photoelectric or pair production, in either case terminating the history.

Assuming a continuation of the case-history, we next wish to determine the new energy, E_{i+1}, from the Klein-Nishina cross section for scattering of gamma rays. Details of this calculation will be given a little later. For the moment we limit ourselves to the observation that because of the Compton relationship, (I-3.10), the deflection angles (together with E_i) determine E_{i+1}. Conversely, E_i together with the energy change determines Θ, the deflection angle.

In Figure I-27.2, O refers to the point of interaction, and OO' is an extension of the line of motion along which the photon approached O. Then Θ is the obliquity angle of the new path relative to OO'. In addition to Θ, there is an azimuthal

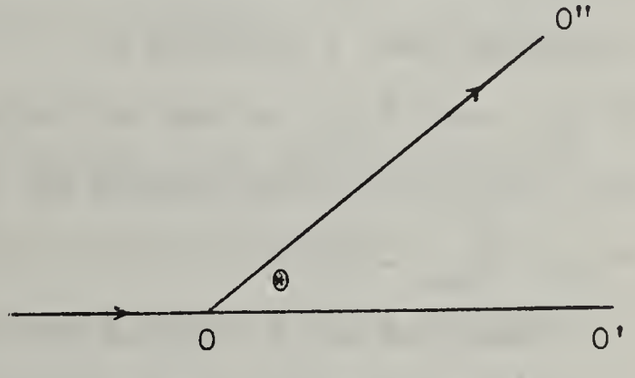

Fig. I-27.2. Deflection of a particle.

*Compare with Equation (I-3.4). The coefficient μ_s is there called μ_{KN}, and the coefficient μ_a is the sum $\mu_p + \mu_{pp}$.

deflection angle, Φ. This angle is randomly distributed between $-\pi$ and π, expressing the fact that 00" is equally likely to appear at any angle of rotation about 00'.*

Now, suppose that the direction of 00' is described by the polar coordinates θ_i, ϕ_i, and that both Θ and Φ have been determined for the next interaction. We wish to determine coordinates the new direction, θ_{i+1}, ϕ_{i+1}. This requires spherical trigonometry, because the two photon directions together with the reference polar axis define a spherical triangle as shown in Figure I-27.3. Here P is the location of the interaction; $\vec{k}$ is a unit vector in the direction of the reference polar axis; and $\vec{u}_i$ and $\vec{u}_{i+1}$ are photon directions before and after the interaction. If we surround P with a sphere of unit radius, rays extending from P parallel to $\vec{k}$, $\vec{u}_i$, and $\vec{u}_{i+1}$ cut the unit sphere at three points as shown, forming the triangle with side lengths at θ_i, θ_{i+1}, and Θ, and interior angles Φ and $\phi_{i+1} - \phi_i$.

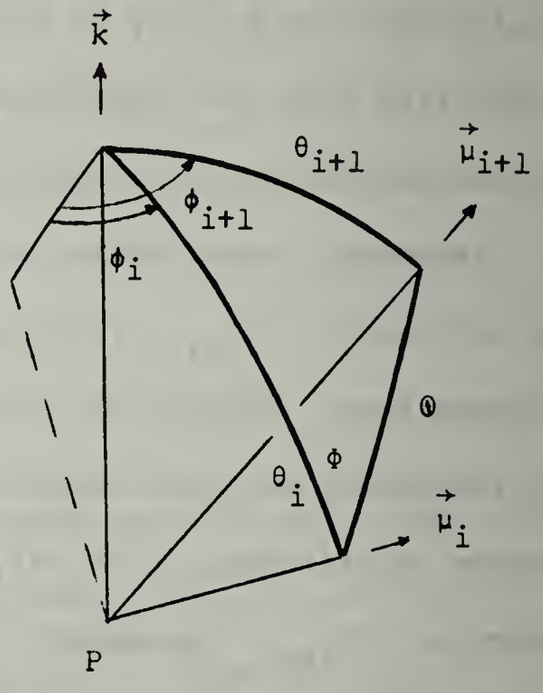

Fig. I-27.3. Spherical trigonometry of a particle deflectio

Using the Law of Cosines for spherical triangles, we see that

$$\cos\theta_{i+1} = \cos\theta_i\cos\Theta + \sin\theta_i\sin\Theta\cos\Phi \ . \qquad \text{(I-27.2)}$$

---

*This would not be true if polarization effects were included.

Since all angles on the right side are presumed known, the calculation of $\cos\theta_{i+1}$ can proceed and the Pythagorean theorem correspondingly gives $\sin\theta_{i+1}$. Next, the Law of Sines yields the relation

$$\sin(\phi_{i+1} - \phi_i) = \sin\theta_{i+1}\sin\Phi/\sin\Theta \ , \qquad \text{(I-27.3)}$$

Again, the calculation can proceed because all quantities on the right are known. Applying the Law of Cosines once again we can write

$$\cos\Theta = \cos\theta_i\cos\theta_{i+1} + \sin\theta_i\sin\theta_{i+1}\cos(\phi_{i+1} - \phi_i) \ , \qquad \text{(I-27.4)}$$

from which $\cos(\phi_{i+1} - \phi_i)$ can be calculated. Lastly the values of $\sin\phi_{i+1}$ and $\cos\phi_{i+1}$ can be deduced from trigonometric formulae:

$$\sin\phi_{i+1} = \sin(\phi_{i+1} - \phi_i)\cos\phi_i + \cos(\phi_{i+1} - \phi_i)\sin\phi_i$$

$$\cos\phi_{i+1} = \cos(\phi_{i+1} - \phi_i)\cos\phi_i - \sin(\phi_{i+1} - \phi_i)\sin\phi_i \ . \qquad \text{(I-27.5)}$$

An alternative procedure can be constructed using direction cosines; but it turns out to involve the same number of multiplications. The series of calculations just described, repeated over and over, takes much of the time required for the Monte Carlo calculation. It would be highly desirable to find a shorter procedure, but none seems to exist.

This completes a sketch of the procedure by which one constructs theoretical trajectories, except for the sampling procedures which are

discussed in the next section. In conclusion we might just indicate how this type of calculation could determine the radiation crossing a boundary. If the boundary permitted radiation to escape completely from the configuration, we could simply generate a large number of trajectories as if no boundaries existed and then count the trajectories which penetrate the first time to a position beyond the boundary.

28. Techniques for Random Sampling*

In the preceding section we have taken for granted the possibility of random sampling from various probability distributions. We next discuss some of the concepts and better known random sampling techniques.

a) Random and Pseudo-Random Numbers.

Suppose a quantity x is distributed according to $f(x)$, and an x value selected at random from the distribution is desired. The most straightforward approach would be preparation of a population of x's, containing different x values with appropriate frequencies, followed by a random selection. This is obviously a cumbersome procedure, since it means preparing a different population for each distribution. A much simpler approach which is ordinarily used instead is that of sampling from a single, canonical distribution,

$$f(x) = 1, \text{ for } 0 \leq x \leq 1 . \qquad \text{(I-28.1)}$$

An x value for another distribution then requires an appropriate transformation.

Numbers randomly selected from the probability distribution of Equation (I-28.1) are what we refer to as "random numbers." And it is difficult to discuss random numbers more precisely than this. They may have any value between zero and unity with equal likelihood; and furthermore, in a sequence of such numbers there should be no correlations whatsoever. Since all types of correlation are possible, this is not a simple matter. The strongest requirement of this type might be that of no correlation between successive numbers; but we could also focus on

*For a general discussion see Ref. 24 , Chapter 8.

correlations between each number and the tenth number beyond, or on the correlation between successive increases and decreases.

Furthermore, consider a very long random digit sequence. By mere chance the value 0.5 might occur. In fact, there is a finite probability for 0.5 to occur 100 times in a row. But use of 100 0.5 values in a row could be a very questionable thing to do. The point here is that even a long sequence of random numbers could be locally very nonrandom. This is a difficult subject conceptually, though the practical problems may not be very serious.

When such numbers are needed, it is possible to refer to extensive tables; but even though such tables are available, such a procedure would require valuable memory space in the computer. It is ordinarily preferable to generate the numbers as they are needed. A variety of deterministic rules have been derived for producing numbers which behave as if they were random and which are referred to as "pseudo-random" numbers. In spite of the contradiction involved in deriving "random" numbers deterministically, these procedures work well in practice.

One deterministic procedure has become so popular that it is now almost the only one widely used.[27/] A sequence y_n of pseudo-random numbers is defined by

$$y_{n+1} = (\lambda y_n + \mu)(\text{mod } p) . \qquad \text{(I-28.2)}$$

The meaning of this is as follows: $(\lambda y_n + p)$ is calculated and then divided by p. The remainder after division is taken to be y_{n+1}.

In the next step, y_{n+1} is used in the same way to calculate y_{n+2}. This recursion yields a chain of numbers $y_1, y_2, \ldots$, for each given y_0. It turns out that this type of sequence usually has a very long cycle; that is, it takes a very long sequence for repetition of the numbers to occur. Furthermore, if the remainder with respect to $\underline{p}$ is always used, none of the numbers is larger than $\underline{p}$, so that when divided by $\underline{p}$ they all lie between zero and unity. On the basis of empirical tests, these numbers appear to be reasonably uncorrelated.

For this type of sequence the correlation coefficient of two successive numbers, say y_n and y_{n+1}, can be shown to be [8]

$$\rho(y_n, y_{n+1}) = \frac{1 - 6(\mu/p)(1-\mu/p)}{\lambda} . \qquad \text{(I-28.3)}$$

From this one can see that if λ is a very large number, the correlation coefficient between successive y_n's is very small. In practice, λ is usually taken to be nearly as large an integer as a given machine can use.

To illustrate this, consider a specific sequence,

$$y_{n+1} = 5^k y_n \pmod{2^{35}} , \qquad \text{(I-28.4)}$$

where $\underline{k}$ is 13. Here the λ value is so large that the correlation coefficient is obviously very small. The value $p = 2^{35}$ is chosen because this is the largest number expressible on an IBM 7090. One can show that the sequence has 2^{33} numbers, and that it will either be a permutation of the sequence 1, 5, 9, ..., $2^{35} - 1$, or else a permutation of the sequence 3, 7, 11, ..., $2^{35} + 1$, depending on the

starting value y_0. If y_0 gives a remainder 1 when divided by 4, there occurs a permutation of the first sequence, and if y_0 has a remainder of 3 after division by 4, there occurs a permutation of the second sequence. Tests with up to 100,000 numbers of this type satisfy tests of randomness reasonably well.

For the preceding sequences, $\mu = 0$. It is sometimes advantageous to compute with $\mu \neq 0$. For example, if the determination of random numbers takes a large proportion of the time required for a given calculation, one might wish to choose a particularly fast procedure. Multiplication by $(2^\alpha + 1)$ is inherently faster than multiplication by 5^k because multiplication by a power of 2 in a binary computer represents a shift of the numbers in the machine by that many binary places, and usually shifting plus addition takes less time than multiplication. Furthermore, the shorter the shift (i.e., the smaller the α) the quicker the calculation. One pays here for speed with shorter cycle lengths and larger correlations. But in principle the size of the correlations can be controlled by proper choice of μ.

Following this type of procedure, Rotenberg found it possible to cut the time required to generate a random number in half, when using an IBM 704.* [34]

b) Sampling from Cumulative Probability Distributions.

Assuming for the moment the possibility of generating suitable pseudo-random numbers, the next problem is the determination of procedures by which one can determine $\underline{x}$ from an arbitrary probability distribution, f(x). One method for accomplishing this makes use of a change of variables

*Rotenberg's procedure has been criticized by Greenberger, Refs. 17, 18.

from $\underline{x}$ to $\underline{t}$, as follows:

$$\int_{-\infty}^{x} dx' f(x') = t = \int_{0}^{t} dt' 1. \qquad \text{(I-28.5)}$$

Clearly the probability that x lies between x_1 and $x_2 > x_1$ equals the probability that t lies between $t_1(x_1)$ and $t_2(x_2)$, where t is considered a random variable governed by a probability distribution $g(t)$, with

$$g(t) = 1, \quad 0 \leq t \leq 1. \qquad \text{(I-28.6)}$$

But $g(t) = 1$ is the canonical distribution which is sampled by selection of a random number, ρ. We therefore sample $\underline{x}$ according to $f(x)$ by defining $t = \rho$, inserting this value of $\underline{t}$ in Equation (I-28.5), and solving the resulting equation for $\underline{x}$. While this procedure is quite generally applicable, the determination of $\underline{x}(t)$ requires calculation of the inverse of a function which may be very complicated. This can be difficult at times.

As an example, let us consider the problem of sampling the probability distribution of photon path lengths,

$$f(s) = e^{-\mu s} \mu ds, \quad 0 \leq s < \infty. \qquad \text{(I-28.7)}$$

To simplify matters, we express the path length in units of mean free path, so that $\mu = 1$. The cumulative probability distribution may then be written

$$\int_s^\infty ds' e^{-s'} = t = e^{-s} . \qquad \text{(I-28.8)}$$

Inverting, and writing $t = \rho$, we obtain

$$s = -\log \rho . \qquad \text{(I-28.9)}$$

Here the inversion is comparatively simple, but even so one must calculate a logarithm for each s value, and this is a rather time-consuming machine operation.

One way to speed the evaluation of Equation (I-28.9) might be to make a large table of $\underline{s}$ values for numbers ρ_1, ρ_2, up to ρ_N , covering the range from zero to unity densely. For example, these numbers might be separated by intervals of, say, 1/1000, so that 1000 values of $\underline{s}$ would be stored in the computer. To determine an $\underline{s}$, a pseudo-random number would be generated, and by round-off (if necessary) would be converted to one of the 1000 indices, say ρ_k . The corresponding value of $-\log\rho_k$ would then be obtained by table look-up with this index.

Thus table look-up, an extremely fast machine operation, would replace the much slower computation of a logarithm. This obviously requires a computer with a large memory. But it should be remembered that if the computer memory is not large enough to permit full use of this procedure, there is still the possibility of combining table look-up and direct computation with interpolation, which is intermediate in speed.

c) Sampling by Rejection Techniques[43].

An alternative technique of great generality is called the "rejection" technique. It applies when the distribution is confined to a finite range.

To illustrate it let us assume, for simplicity, that x has values between zero and unity, while $f(x)$ has values between zero and L, as sketched in Figure I-28.1.

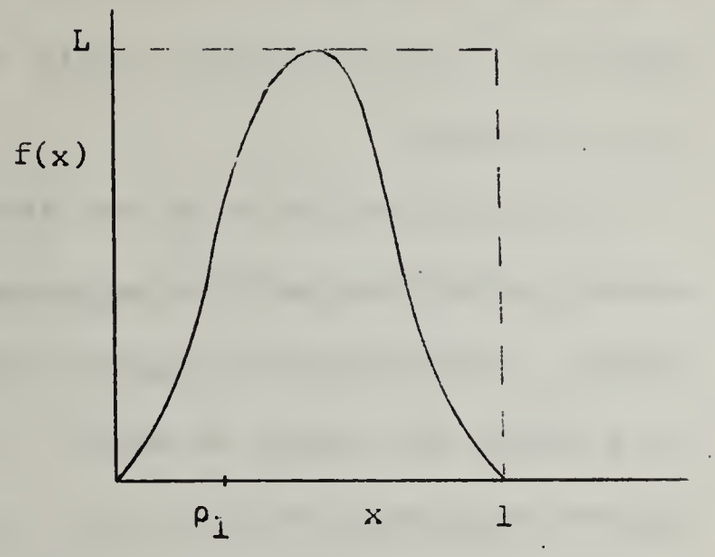

Fig. I-28.1. An illustration of rejection sampling.

The first step is the picking of a random number, ρ_1; this identifies an abscissa value. Another random number, ρ_2, then gives the ordinate value, $\rho_2 L$. Thirdly, an examination is made to determine whether the point $(\rho_1, \rho_2 L)$ is under the curve. If it is, $\rho_1 = x$ is the value selected; but if this point is above the curve, the process is started again. The probability $p(x_1)$ for success is

$$p(x_1) = \int_0^{f(x_1)/L} d\rho_2 = \frac{1}{L} f(x_1) \ . \qquad \text{(I-28.10)}$$

With this technique the sampling is guaranteed to be from the correct distribution, $f(x)$, if the numbers used are random. Points $(\rho_1, \rho_2 L)$ will be randomly located in a square with demensions $L \cdot 1$, as shown in Figure I-28.1. Since acceptance only occurs if the point is under the curve, the probability of acceptance is

$$\frac{1}{L} \int_0^1 dx f(x) \ .$$

But if $f(x)$ is a probability distribution, we can assume that it is

normalized to unity; this means that the area of acceptance is unity, and the efficiency of the procedure is $1/L$. When L is large, as would be the case for a peaked function $f(x)$, the rejection technique is inefficient -- it is necessary to pick many pairs of random numbers to obtain a selection.

A useful application of this technique occurs in the calculation of neutron deflections due to elastic scattering, in the center-of-mass system. The cross section data and therefore the probability distribution for a deflection through an angle θ , is usually given in the form of a Legendre polynomial series,

$$p(\theta) = \sum_{\ell} a_{\ell} P_{\ell}(\cos\theta) \ . \qquad \text{(I-28.11)}$$

For an isotropic distribution, this polynomial would reduce to a constant, and often the anisotropic distributions vary only by small amounts, looking perhaps like the sketch of Figure I-28.2. Since it is quite common to find cases in which the maximum value is not very great, the number of pairs which must be examined per selection is reasonably small. Some figures on this which may be typical are given in Table I-28.1.*

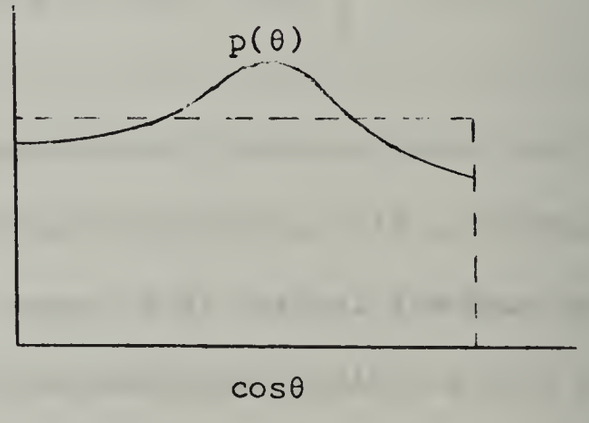

Fig. I-28.2. Slightly anisotropic angular distribution.

*Unpublished data due to M. J. Berger.

Table I-28.1. Elastic Scattering of Neutrons from Oxygen

Energy (Mev)	Average Number of Random Number Pairs Tried
14	6.8
9	4.3
3	2.3
0.3	1.03

At 14 Mev the distribution is quite anisotropic; but from .3 Mev down it is so nearly isotropic that the first pair of numbers tried will almost always result in a selection.

d) Special Sampling Methods: Sine, Cosine of a Random Angle.

There are many devices for sampling from specific distributions; a particularly useful compilation has been given by Kahn.[23] One amusing example is the problem of sampling from the distribution

$$f(x) = nx^{n-1} . \qquad \text{(I-28.12)}$$

Sampling from the cumulative distribution requires the time-consuming calculation of the n'th root of the random number and if n is moderately large, the efficiency of the rejection technique is low. Better and simpler than either is the following procedure: Pick n random numbers $\rho_1, \rho_2,$ up to ρ_n. The largest of these is distributed according to Equation (I-28.12). Since this requires determination of n random numbers, while the rejection technique would require $2n$ (i.e. n number pairs), the superiority is evident.

A very useful technique, which appears to be due to Von Neumann, can be used to determine the sine and/or cosine of a random angle. Suppose

one wishes to select a κ value from a distribution uniform between 0 and 2π, but the sine and cosine of the angle κ are the quantities of interest. Consider first a circular quadrant with unit radius, and a point chosen randomly in this area (Figure I-28.3). The point will determine an angle, which we refer to as α. Note that determination of the point requires two random numbers, one for the x coordinate and the second for the y coordinate. Then

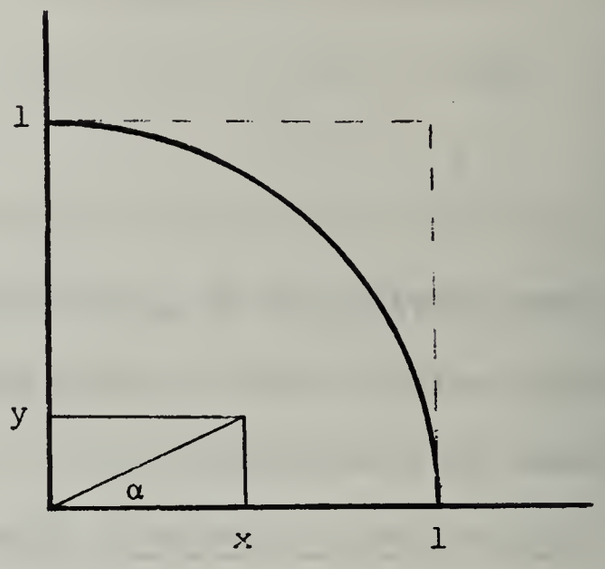

Fig. I-28.3. Random sampling of angles.

$$\cos\alpha = \frac{x}{\sqrt{x^2+y^2}} \quad ,$$

$$\sin\alpha = \frac{y}{\sqrt{x^2+y^2}} \quad . \qquad \text{(I-28.13)}$$

If the random numbers are both positive, the point will lie in the first quadrant. The condition

$$x^2 + y^2 \leq 1 \qquad \text{(I-28.14)}$$

must be satisfied because the points must lie in a circular area if α is to be random.

An unpleasant feature of Equation (I-28.13) is the necessity for

calculating a square root, which is time-consuming. To avoid this one can instead calculate the sine and cosine of the double angle,

$$\sin 2\alpha = \frac{xy}{x^2+y^2} ,$$

$$\cos 2\alpha = \frac{x^2-y^2}{x^2+y^2} . \qquad \text{(I-28.15)}$$

If α is distributed uniformly between 0° and 90°, 2α is distributed uniformly between 0° and 180°, and the square root calculation has been eliminated.

One more change is necessary to cover the full range 0° to 360°. Up to this point, both $\underline{x}$ and $\underline{y}$ have been chosen between zero and unity, so that $\sin(2\alpha)$ is always positive. To make it negative with equal probability, we replace $y = \rho_2$ with

$$y = 1 - 2\rho_2 . \qquad \text{(I-28.16)}$$

Defined in this way, $\underline{y}$ will be randomly selected between -1 and 1, if ρ_2 is random, and correspondingly, $\sin(2\alpha)$ will be positive or negative with equal likelihood, and we select these values for $\sin\kappa$ and $\cos\kappa$.

This is a fast procedure. Since the random points lie within a circle of area $\pi/4$, the efficiency is high, nearly .8. Only about one pair of random numbers in five must be thrown away.

Often with big computers there is no advantage in the use of clever procedures. Fast as the preceding method is, it is not nearly as fast as table look-up, which might perhaps be accomplished as follows: first,

$\cos \kappa$ and $\sin \kappa$ would be pre-tabulated at intervals of, say, one degree, beginning with 0.5° and extending up to, say, 179.5° if angles up to $\pi/2$ were desired. Let us call these lists CØS(N) and SIN(N), where N runs from 1 to 180. A random number between zero and one is now selected and multiplied by 180. The result, ordinarily a floating point number, is then "fixed." By this we mean calculation of the integer just below -- in FORTRAN notation this means the operation

```
N = XFIX(180.*R) ,                                    (I-28.17)
```

where R is the random number. Since the value of N as determined in this way can be any value between 0 and 179 with equal probability, the final step would be two table look-ups to determine $\cos \kappa$ and $\sin \kappa$,

```
cos κ = CØS(N+1) ,

sin κ = SIN(N+1) .                                    (I-28.18)
```

Each pair of values for $\sin \kappa, \cos \kappa$ thus requires only a single multiplication, and the fixing of a floating-point number to provide the index. It is therefore a very fast procedure and very simple; but it requires space for the tabular storage.

e) Distributions in Combination: The Klein-Nishina Function.

When two or more events are mutually exclusive, the probability that one of these events will occur is the sum of the probabilities of the different event types. Thus, if the probability that the next interaction will be photoelectric absorption, Compton scattering, or pair production

are written P_{ph}, P_{KN}, and P_{pp}, the total probability P that the next interaction will be one of these is

$$P = P_{ph} + P_{KN} + P_{pp} , \qquad \text{(I-28.19)}$$

and if these are the only interactions, $P = 1$.

So far we simply repeat the discussion of section 3. But suppose we recall that the total probability for a scattering interaction is the integral over all the different types of scatterings which can occur. That is to say,

$$P_{KN} = \int_{\lambda'}^{\lambda'+2} d\lambda \; p_{KN}(\lambda',\lambda) , \qquad \text{(I-28.20)}$$

where $p_{KN}(\lambda',\lambda)$ is a probability distribution. Then, having sampled to determine that the next interaction is a scattering, we must sample again from $\frac{p_{KN}}{P_{KN}}$ to determine the type of scattering -- i.e. the wavelength change.

The foregoing example makes clear a type of procedure which can be followed when a probability distribution $f(x)$ is written as the sum of two or more component distributions. If we write $f_0(x) = 0$,

$$f(x) = f_1(x) + f_2(x) + f_3(x) , \quad 0 \leq x \leq 1 , \text{ say,} \qquad \text{(I-28.21)}$$

where $f_1(x)$, $f_2(x)$, and $f_3(x)$ are properly normalized so that they can be considered probability distributions, then writing $\int_0^1 dx f_i(x) = F_i$ we may sample from $f(x)$ by selecting a random number, ρ , and when $F_{i-1} \leq \rho < F_i$, sampling $f_i(x)/F_i$.

When a given event occurs only if two or more component events occur

together, the probability is the product of the probabilities for component events. In the preceding paragraph we use this idea implicitly, because we may write

$$f_2(x) = F_2[f_2(x)/F_2] \; ; \qquad \text{(I-28.22)}$$

we sample $f_2(x)$ by first sampling F_2 and then upon success sampling $[f_2(x)/F_2]$, a probability distribution with unit total probability. Quite generally, if

$$f(x) = g(x)h(x) \qquad \text{(I-28.23)}$$

where g and h are both probability distributions, then we can sample $f(x)$ by demanding a successful sampling of both $g(x)$ and $h(x)$.

Figure I-28.4 illustrates a simple rejection technique which utilizes this idea. If we select random numbers ρ_2, ρ_3 and $\rho_1 = x$, then x is selected only if $\rho_2 < g(\rho_1)$ and $\rho_3 < h(\rho_1)$.

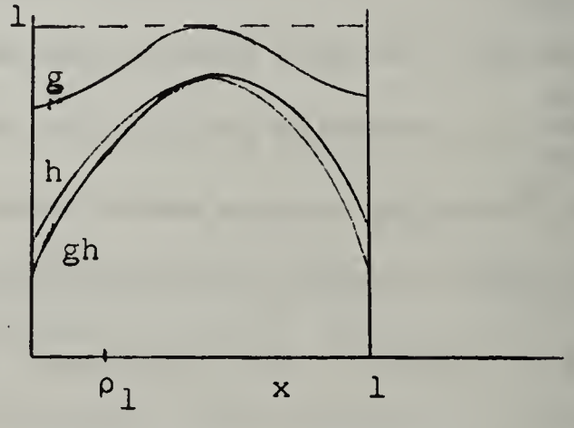

Fig. I-28.4. Sampling $f(x) = g(x)h(x)$.

Cumulative distribution methods can be applied to the same problem. Writing $G(x) = \int_0^x dx'g(x')$, we have

$$\int_0^x f(x')dx' = \int_0^x dx'g(x')h(x') = \int_0^G dG'h[x'(G')] \; . \qquad \text{(I-28.24)}$$

At this point it is clear that we can sample by selecting a random number,

ρ, writing $\rho = \int_0^G dG' h[x'(G')]$, solving for G, writing $G = \int_0^x dx' g(x')$, and finally solving for x.

The foregoing procedure is far too clumsy to be very useful except in special circumstances in which at least one of the inversions is easily performed. Much more flexible is a combination of rejection and cumulative-distribution sampling in which one selects ρ_1, then determines G_1 by inversion of

$$\rho_1 = \int_0^{G_1} dx' g(x') , \qquad \text{(I-28.25)}$$

and finally samples

$$f(x)dx = h[x(G)]dG \qquad \text{(I-28.26)}$$

by testing to see if a second random number, ρ_2, satisfies $\rho_2 \leq h[x(G_1)]$.

These techniques are nicely illustrated by a method for sampling the Klein-Nishina distribution devised by Kahn.[23/] He writes the Klein-Nishina distribution as follows:

$$k(\lambda',\lambda)d\lambda = \frac{3}{8}\frac{\lambda'^2}{\lambda^2}\left[\frac{\lambda'}{\lambda} + \frac{\lambda}{\lambda'} - 2(\lambda-\lambda') + (\lambda-\lambda')^2\right]d\lambda$$

$$= \frac{3}{8}\frac{1}{r^2}\left[\frac{1}{r} + r + (1-\lambda' r+\lambda')^2 - 1\right]d\lambda, \quad r = \frac{\lambda}{\lambda'} ,$$

$$= \frac{3}{16}\frac{9\lambda'+2}{(\lambda'+2)}\left\{\frac{\lambda'+2}{9\lambda'+2}\left(\frac{\lambda'}{2}\right)\left[4\left(\frac{1}{r} - \frac{1}{r^2}\right)\right]\right.$$

$$\left. + \frac{8\lambda'}{9\lambda'+2}\left(\frac{\lambda'+2}{2r^2}\right)\left[(\lambda'-\lambda' r+1)^2 + \frac{1}{r}\right]\right\}\frac{d\lambda}{\lambda'} .$$

The wavelength λ' describes the photon before scatter, and is constant during the sampling. The Klein-Nishina distribution is thus in the form

$$k(\lambda',\lambda)d\lambda = \text{Const.}\left\{\frac{\lambda'+2}{9\lambda'+2}\, g_1(\lambda)h_1(\lambda) + \frac{8\lambda'}{9\lambda'+2}\, g_2(\lambda)h_2(\lambda)\right\}d\left(\frac{\lambda}{\lambda'}\right) \qquad \text{(I-28.27)}$$

where

$$\frac{\lambda'+2}{9\lambda'+2} + \frac{8\lambda'}{9\lambda'+2} = 1 \ ,$$

$$\int_1^{1+2/\lambda'} d\left(\frac{\lambda}{\lambda'}\right)\, g_1(\lambda') = 1 \ ,$$

$$\int_1^{1+2/\lambda'} d\left(\frac{\lambda}{\lambda'}\right)\, g_2(\lambda') = 1 \ . \qquad \text{(I-28.28)}$$

If we rescale the wavelength variable appropriately, and assume that the total interaction probability is normalized to unity, we arrive at Kahn's procedure, given in detail in Figure I-28.5, below:

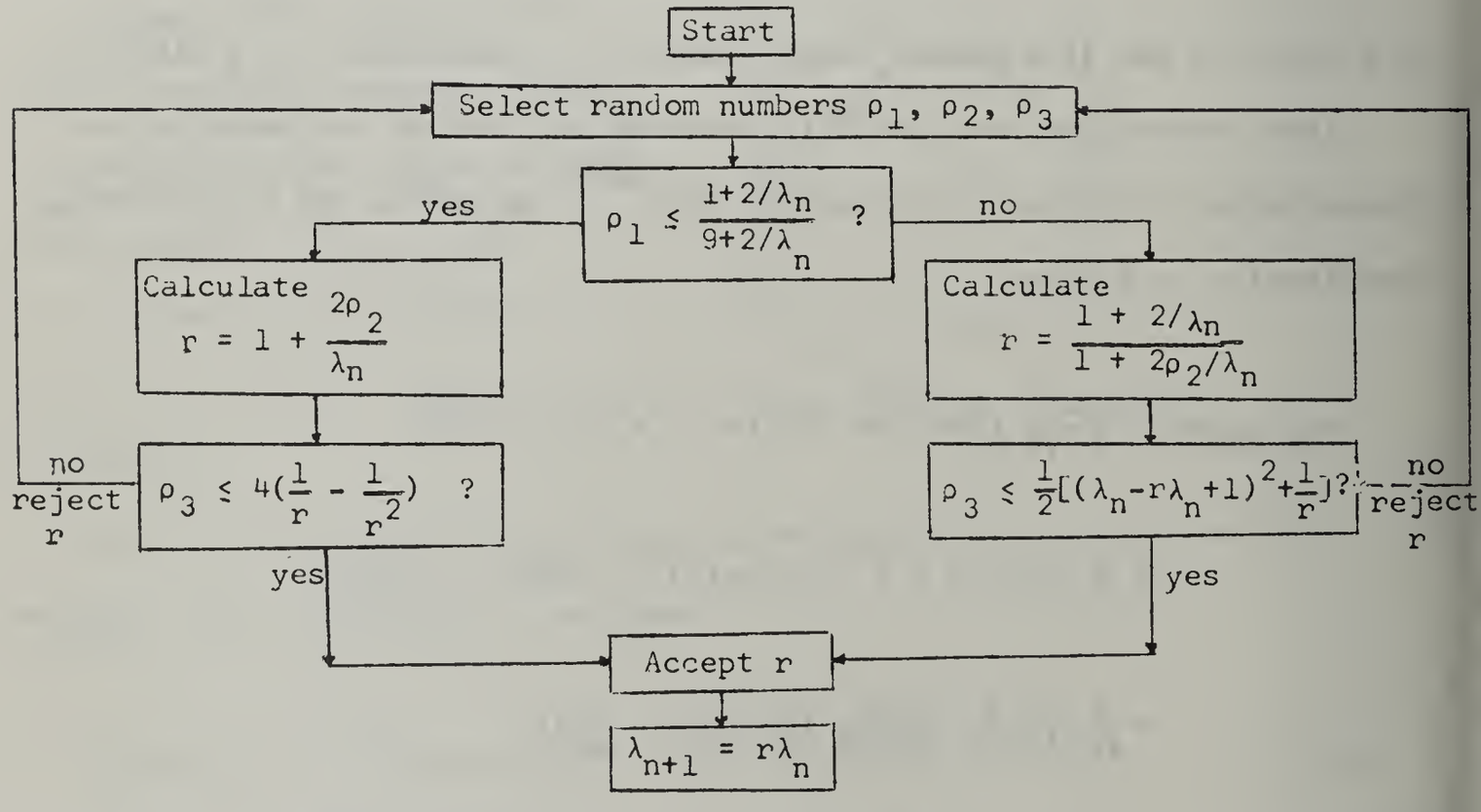

Fig. I-28.5. Flow diagram for Kahn's sampling procedure for the Klein-Nishina distribution. (λ_n, λ_{n+1} correspond to λ',λ.)

Note that $h_1 = 0$ and $h_2 = 1$, for $r = 1$. With increasing r, h_1 rises, achieving a maximum value of unity when $r = 2$, and then falling again. On the other hand, h_2 falls with increasing r and then may rise again but without the possibility of exceeding 1. Neither h_1 nor h_2 is normalized to unit total probability.

It can be shown that the average number of random number triplets required for success of this procedure is about 3 at 10 Mev and falls to a little above 1.5 below 1 Mev.

29. Importance Sampling and Other Special Procedures

a) Splitting, Exponential Transformation, and Other Procedures.

Thus far, all procedures have been more or less analogous to natural processes. It is possible to distort the sampling processes to advantage in many problems. Von Neumann's splitting technique is one of the simplest examples of this.

Suppose one wishes to calculate the penetration of gamma rays to great depths in a material. Since the gamma ray flux is known to decrease with a dominant exponential trend, the number of case histories would decrease similarly with increasing depth of penetration. This means that at 10 mean free paths, say, since $e^{-10} \sim 20{,}000$, one can anticipate the need for $\gtrsim 10^5$ case histories if no modification in sampling procedures is made.

According to the splitting procedure, the material would be divided into layers. Then, each time a photon makes the transition to a deeper layer, it would be "split" into two or more photons, each assigned a weight that correctly reflects its physical importance. If the splitting generates n photons, each "descendant" is assigned the weight 1/n, and each is followed individually. This provides a mechanism by which the photon population can increase exponentially to offset the natural exponential decline.

This procedure has been used successfully in slab penetration problems and can in principle be applied to more complicated configurations. For slab problems it is fairly clear that the splitting should just about offset the degradation, so that the flux stays more or less constant. For more complicated configurations it is more difficult to determine when to

have many descendants and when to have few. Unfortunately, a wrong guess at this point can produce extremely misleading and wrong results. One of the advantages in the study of slab and infinite medium problems is the existence of alternative procedures which can be used to check the choice of bias procedure.

Consider a problem of penetration through ducts. Here one might wish to bias in favor of particles which are scattered approximately by a right angle since these have the best possibility for a long path down another leg of the duct. But since one has little analytical knowledge of the penetration process, it would be somewhat difficult to introduce a suitable bias a priori. It might be as efficient to begin with an unbiased calculation and analyze the results in detail to see what is important. It might turn out that a photon which penetrates too far into the wall of the duct should be terminated, while a photon which makes a collision very close to the surface of the duct wall has an excellent chance of emerging. One might then decide to "split" a photon of the latter type. But this is all very loose; in fact one does not know how to introduce appropriate biasing techniques for duct penetration problems.

The fundamental difficulty with these modifications is that at the same time certain possible types of events are being enhanced, others are being discriminated against. Therefore it is necessary to be quite certain that the favored events include <u>all</u> the important cases. If, for example, one discriminates against events that turn out to contribute 25% of the scores, one expects the answer to be in error by as much as 25%, no matter how accurately the remaining 75% may be calculated.

A method which has been the subject of much study is called the exponential transformation.* If in the transport equation,

$$\cos\theta \frac{\partial N}{\partial z} + \mu N = \int kN \ , \qquad \text{(I-29.1)}$$

we let

$$N = Fe^{-cz} \ , \qquad \text{(I-29.2)}$$

where c is a constant and F is a function defined by this equation, we obtain an equation for F, instead of N:

$$\cos\theta \frac{\partial F}{\partial z} + (\mu - c\cos\theta)F = \int kF \ . \qquad \text{(I-29.3)}$$

In this equation the attenuation coefficient, μ, has been replaced by $(\mu - c\cos\theta)$. Now, suppose that c is positive and close in value to μ. Then, for particles with directions away from the source plane (θ small), the attenuation will be small, while for particles which penetrate back towards the source plane the value of $\cos\theta$ will be negative and the effective attenuation coefficient will be large.

This is a procedure which strongly favors long path lengths directly away from the source plane, while discriminating against photons which scatter back. From another point of view, instead of computing the quantity I, one computes Ie^{cz}. Thus the problem has been changed.

An alternative way of writing Equation (I-29.3) is

$$\cos\theta\frac{\partial F}{\partial z} + \mu F = \int kF + c\cos\theta F \ . \qquad \text{(I-29.4)}$$

---

*Some more recent papers on this are Refs. 6 and 50.

Here the new term is considered a type of photon source which is proportional to the flux. This idea, due to Chilton,* leads to an exponential approach which can also be viewed as a splitting procedure of special elegance and it turns out to be extremely successful in elementary configurations.

The nature of biased sampling is such that a bias for a specific result may be wrong for other, related questions. Thus, a bias which gives satisfactory results for very deep penetrations must give special weight to photons which have undergone a number of small-energy-loss collisions. But such a bias will usually have been applied on the basis of photon position -- not photon spectral energy. It may well lead to atypical spectral results at the same depth, and it may be quite unsuitable for use at moderate depths. One of the advantages which Chilton's method has is appropriateness for simultaneous calculations at a range of penetrations.

Note that a type of bias based on position (splitting) is not the sole possibility. The exponential transformation favors certain directions. It is also possible to modify the cross sections, or to favor certain energy loss sequences. In all cases, the method is investigated by comparison with independent and better understood calculations, usually in a particularly simple configuration. The practical theory of the choice of bias methods doesn't really exist, although in general one knows that it involves the study of functions adjoint to the flux.†

b) Survival Weights

It is not necessary to terminate a case history by determining that

---

*Reference 6. To make the source term positive, Chilton adds a term cF to both sides; he also takes c to be the smallest value of μ in the integration range.

†See section 38c.

an absorption interaction has occurred. Instead one can proceed as if every interaction were a scattering, but with each interaction changing an assigned "survival weight" appropriately. For example, the survival weight of a particle would be unity before occurrence of the first interaction. After the first interaction, the survival weight would be decreased by the factor μ_{KN}/μ, which is simply the probability of surviving the first interaction. A similar decrease would occur with each interaction, so that the survival weight w_n after $\underline{n}$ collisions would be

$$w_n = \prod_{i=1}^{n} \left(\frac{\mu_{KN}(\lambda_i)}{\mu(\lambda_i)}\right) , \qquad \text{(I-29.5)}$$

where λ_0, λ_1, ... are the successive wavelengths of the photon.

If this procedure is followed, it is necessary to specify a method for terminating case histories. One might, for example, terminate any case history when the survival weight decreases below a limiting value. Note that in the final score, each case history must be counted in proportion to its survival weight, so that this is a logical criterion to apply.

This type of calculation is apt to involve long case histories. On the other hand, it is almost the only method which permits the study of low energy spectra in high Z materials, where it is highly improbable for a photon to scatter to low energies.

c) Correlated Sampling

Correlated sampling involves two closely analogous Monte Carlo calculations, with an examination of the difference between them. Quite often it is possible to analyze a problem in such a way that the desired

information appears as a difference. For example, the study of boundary effects is basically the comparison of an infinite medium problem with a similar semi-infinite medium problem, as illustrated in Figure I-29.1.

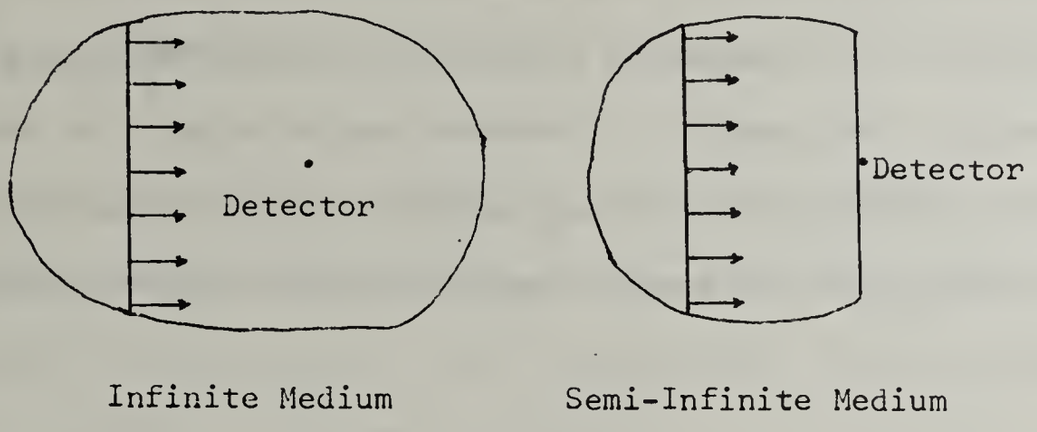

Fig. I-29.1. Example of comparative configurations suitable for correlated sampling.

Both have the plane source and the point detector, but in the semi-infinite medium case radiation can escape.

The difference between the two cases is not very great; the photons which escape would in some cases have made an additional contribution. One can therefore gain accuracy by studying the difference between calculations for the two cases. This requires use of exactly the same random numbers for corresponding events in the two problems. In the case above, angles, energies, and positions of corresponding case histories would be identical up to the escape of one of the photons across the boundary.

Another case in which correlated sampling is useful is a problem in which one investigates the effect of a change in cross sections. It occurs in certain neutron penetration studies, where the interaction

cross sections are not accurately known. Here again one applies in two calculations, with slightly differing cross section, the same random numbers for calculating deflections, path lengths, and particle energies.

In an example by Berger, neutron elastic scattering by oxygen was assumed in one calculation to have a realistic cross section, as accurate as known, while in the comparison calculation the scattering was assumed to be isotropic. The quantity of interest was the albedo, or rather the difference between corresponding albedos. It turned out that correlated sampling reduced the sample size required for a given accuracy by a factor of 4.

30. Estimation of Error .

Suppose that $p(x)$ is a probability function, normalized so that its integral is unity. The "expected value" of a second function of x, say $u(x)$, over the distribution $p(x)$ is defined and denoted by*

$$\langle u(x)\rangle_{p(x)} = \int_R dx u(x)p(x) , \qquad \text{(I-30.1)}$$

where R is the range of the variable x, and the subscript on the left is usually omitted unless there is danger of confusion. If $u(x)$ is a simple function such as $x, x^2, \ldots$ the simpler forms $\bar{x}, \overline{x^2}, \ldots$ will often be used instead of the bracket notation.

The expectation value is a linear operator, so that

$$\langle c_1 u_1(x) + c_2 u_2(x)\rangle = c_1\langle u_1(x)\rangle + c_2\langle u_2(x)\rangle . \qquad \text{(I-30.2)}$$

By the "variance" V_x and "standard deviation" σ_x of the variable x we mean

$$V_x = \overline{x^2} - \bar{x}^2 ,$$

$$\sigma_x = \sqrt{V_x} ; \qquad \text{(I-30.3)}$$

and by the "relative standard deviation" we mean

---

*The independent variable may be discrete, perhaps an index i. We would then have, for example

$$\langle u_i\rangle = \sum_i u_i p_i .$$

$$\frac{\sigma_x}{\bar{x}} = \sqrt{\frac{\overline{x^2} - \bar{x}^2}{\bar{x}^2}} \quad . \qquad \text{(I-30.3)}$$

With these definitions in mind, let us consider a simple albedo problem which will illustrate most of the concepts of error estimation. Photons are injected into a semi-infinite medium; and we wish to study the emergent radiation. To perform this study we first simply record whether or not any given photon emerges again across the interface. If we are simply counting photons to evaluate the "number albedo" we assign a weight $x = 1$ to emergent photons, and a weight $x = 0$ to non-emergent photons. Our probability distribution can be written in terms of Dirac delta functions,

$$p(x) = (1-A)\delta(x) + A\delta(x-1) \ , \qquad \text{(I-30.4)}$$

where $\underline{A}$ is the number albedo, that is the probability for emergence. Note that $\underline{A}$ will have a precise value; but that in ignorance of this value we attempt to measure it by random sampling procedures.

a) Expressions Involving the Variance .

The variance of our probability distribution can be written down directly. Since

$$\bar{x} = (1-A)\cdot 0 + A\cdot 1 = A \ ,$$

$$\overline{x^2} = (1-A)\cdot 0 + A\cdot 1 = A \ , \qquad \text{(I-30.5)}$$

the variance is

$$V_x = A - A^2 = A(1-A) \ . \qquad \text{(I-30.6)}$$

In our calculation, we inject $\underline{n}$ photons into the medium and weight

the photons $x_1, x_2, .., x_n$, where each of the x_i is zero or unity according to whether or not the i'th photon emerges or not. Our first task is then to measure the albedo, which we accomplish by averaging. This is because the expected value of the average is A:

$$\left\langle \frac{1}{n} \sum_{i=1}^{n} x_i \right\rangle = \frac{1}{n} \sum_{i=1}^{n} \langle x_i \rangle = \frac{1}{n} \sum_{i=1}^{n} A = \frac{1}{n} nA = A \ . \qquad \text{(I-30.7)}$$

It is extremely important to distinguish between the calculated average and its expected value: the former is simply an estimate of the latter and is not equal to it.

The main problem of error estimation has to do with determination of the difference which may exist between the albedo estimate (i.e. the calculated average over $\underline{n}$ case histories) and the albedo (i.e. the expected value of the average). The expected value of this difference is obviously zero; and we must therefore use some different measurement. Our choice is the calculated variance, which we write with a "hat" to indicate approximation:

$$\hat{V}_x = \frac{1}{n} \sum_{i=1}^{n} x_i^2 - \left\{ \frac{1}{n} \sum_{i=1}^{n} x_i \right\}^2 \ . \qquad \text{(I-30.8)}$$

The expected value of this quantity is

$$\langle \hat{V}_x \rangle = \left\langle \frac{1}{n} \sum_{i=1}^{n} x_i^2 - \frac{1}{n^2} \sum_{i=1}^{n} \sum_{j=1}^{n} x_i x_j \right\rangle$$

$$= \overline{x^2} - \frac{1}{n^2} \left\langle \sum_{i=1}^{n} x_i^2 + \sum_{i=1}^{n} x_i \left[\sum_{\substack{j=1 \\ j \neq i}}^{n} x_j \right] \right\rangle$$

$$= \overline{x^2} - \frac{1}{n^2}\left\{n\overline{x^2} + \left\langle \sum_{i=1}^{n} x_i \right\rangle \left\langle \sum_{\substack{j=1 \\ j\neq i}}^{n} x_j \right\rangle\right\}$$

$$= \overline{x^2} - \frac{1}{n^2}\left\{n\overline{x^2} + (n\bar{x})(n-1)\bar{x}\right\}$$

$$= \frac{n-1}{n}\left(\overline{x^2} - \bar{x}^2\right)$$

$$= \frac{n-1}{n} V_x \,. \qquad \text{(I-30.9)}$$

Thus, the calculated variance is a measure of the true variance. Moreover, the true variance can be used to estimate the "squared error,"

$$\left\{\frac{1}{n}\sum_{i=1}^{n} x_i - \bar{x}\right\}^2 ,$$

since the expectation value of this quantity is

$$\left\langle\left(\frac{1}{n}\sum_{i=1}^{n} x_i - \bar{x}\right)^2\right\rangle = \left\langle\frac{1}{n^2}\sum_{i=1}^{n}\sum_{j=1}^{n} x_i x_j - 2\bar{x}\,\frac{1}{n}\sum_{i=1}^{n} x_i + \bar{x}^2\right\rangle$$

$$= \left\langle\frac{1}{n^2}\left(\sum_{i=1}^{n} x_i^2 + \sum_{i=1}^{n} x_i \sum_{\substack{j=1 \\ j\neq i}}^{n} x_j\right)\right\rangle - 2\bar{x}\,\frac{1}{n}\sum_{i=1}^{n}\langle x_i\rangle + \bar{x}^2$$

$$= \frac{1}{n}\overline{x^2} + \frac{1}{n^2}\left\langle\sum_{i=1}^{n} x_i\right\rangle\left\langle\sum_{\substack{j=1 \\ j\neq i}}^{n} x_j\right\rangle - \bar{x}^2$$

$$= \frac{\overline{x^2}}{n} + \frac{1}{n^2}(n\bar{x})[(n-1)\bar{x}] - \bar{x}^2$$

$$= \frac{1}{n}\left(\overline{x^2} - \bar{x}^2\right) = \frac{1}{n} V_x \,. \qquad \text{(I-30.10)}$$

The square root of this quantity divided by $\bar{x}$ is dimensionless and is easier to interpret:

$$\frac{1}{\bar{x}}\sqrt{\left\langle\left(\frac{1}{n}\sum_{i=1}^{n} x_i - \bar{x}\right)^2\right\rangle} = \frac{1}{\sqrt{n}}\frac{\sqrt{V_x}}{\bar{x}} = \frac{1}{\sqrt{n}}\frac{\sigma_x}{\bar{x}} . \qquad \text{(I-30.11)}$$

Further, Equation (I-30.9) establishes our calculated variance as a measure of the true variance, and therefore our calculated standard deviation as a measure of σ_x . Thus*,

$$\frac{1}{\bar{x}}\sqrt{\left\langle\left(\frac{1}{n}\sum_{i=1}^{n} x_i - \bar{x}\right)^2\right\rangle} \approx \frac{1}{\sqrt{n}}\frac{\sqrt{\hat{V}_x}}{\left(\frac{1}{n}\sum_{i=1}^{n} x_i\right)} . \qquad \text{(I-30.12)}$$

Note that in the albedo problem the right hand side of Equation (I-30.11) is

$$\frac{1}{\sqrt{n}}\frac{\sqrt{A(1-A)}}{A} = \frac{1}{\sqrt{n}}\sqrt{\frac{1-A}{A}} ,$$

which is approximated by the right side of Equation (I-30.12).

The closeness with which the calculated averages approximate the expectation value for moderate-sized n values depends on the distribution function, as can be seen clearly in this example: The smaller the A value, the larger the relative standard deviation. Further, the larger the relative standard deviation, the farther from its true value the denominator

---

*Note that an improvement would result if we were to replace $\hat{V}_x$ here by $\frac{n}{n-1}\hat{V}_x$, because of Equation (I-30.9).

in (I-30.11) may be and the poorer our knowledge of what the relative standard deviation actually is. Further, we have <u>not</u> taken into account the statistical fluctuations in $\hat{V}_x$, which can only be gauged if one estimates higher moments such as x^4 .*

The discussion of the preceding paragraph applies generally to the use of the variance or derived quantities to estimate the error of a calculated average.

b) <u>Other Averages: The Energy Albedo</u>

The arguments of the preceding paragraphs are only slightly more complicated when applied to the problem of determining the fraction of the injected <u>energy</u> which emerges again, the "energy albedo." The appropriate probability distribution must express first the probability of emergence and then the probability, predicated on emergence, that the photon has energy between E and $E + dE$. That is to say, the probability distribution is the <u>product</u> of $p(x)$ as given by Equation (I-30.4) and another function, say $\varepsilon(E)$, such that

$$\int_0^\infty dE\varepsilon(E) = 1 . \qquad \text{(I-30.13)}$$

The function $\varepsilon(E)$ is essentially the spectrum of emergent photons. If we make the designation

$$\langle u(E) \rangle = \int_0^\infty dEu(E)\varepsilon(E) ,$$

---

*For these and other reasons the relative standard deviations in Monte Carlo calculations must be interpreted with great care. It can happen that the statistical distribution is so skew that it must be much more carefully investigated before one knows the meaning of a calculated σ value.

with use also of the simpler form $\overline{E^n}$ for $\langle E^n \rangle$, we find that

$$\langle xE \rangle = \int_0^1 dx \int_0^\infty dE(xE)p(x)\varepsilon(E) = A\overline{E}$$

$$\langle (xE)^2 \rangle = A\overline{E^2}$$

$$V_{xE} = A\overline{E^2} - A^2\overline{E}^2 . \qquad \text{(I-30.14)}$$

The relative standard deviation can be written

$$\frac{\sqrt{V_{xE}}}{\langle xE \rangle} = \sqrt{\frac{1-A}{A} + \frac{1}{A}\left(\frac{\overline{E^2}}{\overline{E}^2} - 1\right)} . \qquad \text{(I-30.15)}$$

This consists of two parts. One term, $(1-A)/A$, is due to the fluctuation of the number of reflected particles as can be seen from Equation (I-30.6). The term added to this arises from the fluctuations in the energy of the reflected particles; if they all came out with the same energy, $\overline{E^2}$ would be equal to $\overline{E}^2$, and the second term would vanish.

It turns out that the relative standard deviation is usually about twice the value due to number fluctuations alone. Thus, a calculation of average energy rather than average number is apt to have about twice the error associated with it; and this is often very useful information. This statement holds for transmission calculations as well as albedo calculations.

Note that expressions (I-30.7) through (I-30.12) apply to the calculation of energy averages and variances, if one generalizes the probability distribution and also understands that the quantity $\underline{x}$ must be re-interpreted as $\underline{xE}$.

c) Correlated Sampling.

Let us consider two albedo problems with slightly different cross sections. We wish to examine the difference between them by correlated sampling. Accordingly, a "case history" now consists of injection of a photon in each problem, with use of the same random numbers for the sampling of corresponding distributions in the two problems. If we assign a weight $x = 1$ to an emergent photon in the first problem, and $x' = 1$ to an emergent photon in the second problem, with weights $x = 0$ and $x' = 0$ to non-emergent photons in both problems, the probability distribution can be written

$$p(x,x') = A_{11}\delta(x-1)\delta(x'-1) + A_{10}\delta(x-1)\delta(x') + A_{01}\delta(x)\delta(x'-1) + A_{00}\delta(x)\delta(x') , \quad \text{(I-30.16)}$$

where the four coefficients are probabilities of emergence of 2, 1, and 0 photons, and their sum is unity.

It is not difficult to show that

$$V_{(x-x')} = V_x + V_{x'} - 2\sqrt{V_x V'_x}\,\rho_{xx'} \quad \text{(I-30.17)}$$

where

$$\rho_{xx'} = \frac{\langle xx' \rangle - \langle x \rangle \langle x' \rangle}{\sqrt{V_x V_{x'}}} \quad \text{(I-30.18)}$$

is the correlation coefficient, a parameter with the following properties: If $p(x,x')$ factors, so that the probability distributions for $\underline{x}$ and $\underline{x'}$

are independent, then $\rho_{xx'} = 0$. If $p(x,x')$ vanishes unless $x = x'$, it is quite clear that $\rho_{xx'} = 1$.*

According to Equation (I-30.17), the variance $V_{(x-x')}$ of the difference between results for the two problems can be made very small if the correlation coefficient approaches unity. In one of Dr. Berger's calculations of neutron albedo differences due to anistropy in the scattering angular distiibution, correlation coefficients $\rho = .66$ for the number albedo and $\rho = .77$ for the energy albedo were obtained. The effective sample size was increased by about factors of three and four, respectively, by the use of correlated sampling, in this case.

---

*Negative correlations, $-1 \leq \rho_{xx'} < 0$, are also possible, here if $x = 1 \Rightarrow x' = 0$ and $x = 0 \Rightarrow x' = 1$.

31. WALLSTREET: General Description*

a) The Schematization.

WALLSTREET applies to an idealization of regularly-shaped buildings bounding two opposite sides of an otherwise infinite fallout field, as shown in Figure I-31.1. The fallout field is a plane isotropic source of

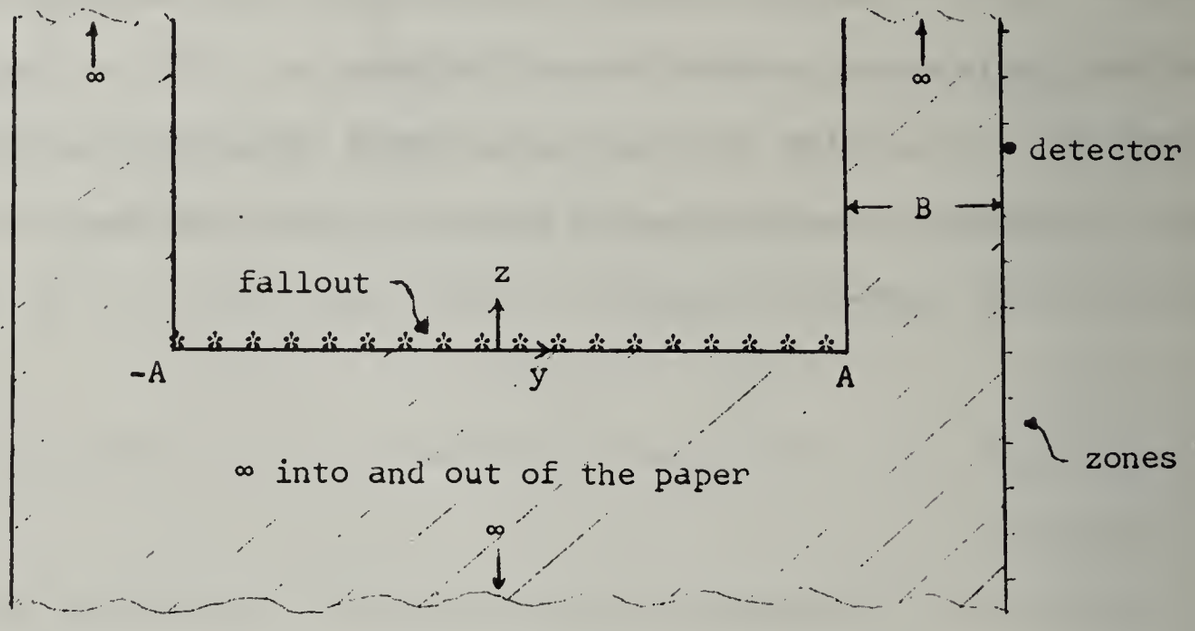

Fig. I-31.1. The walls and fallout-covered street of WALLSTREET.

gamma radiation. We wish to know the dose received by a detector behind one wall. Note that the problem could equally well be done with only one wall; but insertion of the second wall gives the advantage of symmetry. Note also that the problem is essentially two-dimensional; the y and z coordinates are indicated in Figure I-31.1, while walls and street extend to infinity in the x direction, without change.

The fallout field extends in y from -A to +A. The materials of walls

---

*Dr. Berger's program was written in the middle of June, 1962, at the time of a crisis in the stock market.

and street are alike, presumably concrete, though other materials could be used. Between the walls and above the street is another material, air. The distance A is large enough so that air scattering can be significant. If A is chosen large enough so that the walls do not interact significantly, the problem reduces to the one-wall case. On the other hand, if A is small air scattering will not be important but scattering back and forth between the walls will be significant.

One more simplifying assumption is made in the schematization, namely that beyond the walls there is no air. If a gamma ray penetrates through a wall it cannot return. In practice,backscattering is possible of course. But there is an advantage in having an "absorbing plane" in the problem in that the case histories will be terminated when this plane is crossed, thus shortening the computation. The calculation for the schematized problem will slightly underestimate the dose which would be measured if back-scattering were taken into account.

We indicate the thickness of the wall by B, and plan to perform calculations simultaneously for various wall thicknesses. The exterior surface of the wall is divided into zones according to height, and the number of such zones is specified arbitrarily. Provision is made also for zones which lie below the street level.

Our calculation is to determine the average dose in a given height zone, for a given wall thickness. The WALLSTREET program which accomplishes this consists of a control routine and four "outer" subroutines INPUT, PRELIM, HISTØR, and ØUTPUT. These call a number of "inner" subroutines, which in turn depend on two "utility" subroutines, RANDA and INTRP. RANDA

is a pseudo-random number generator, written in machine language, and INTRP is a general interpolation routine; and both are described in detail in section 36.

Generally speaking, machine programs are apt to be constructed from the inside out. Therefore, in the remainder of this section we comment on the code as a whole. In section 32 we describe the routines in detail, starting with the inner subroutines and working towards the control routine in more or less of a programmer's sequence.

b) Outline

Figure I-31.2 below gives a block diagram of WALLSTREET, with the different types of routines distinguished according to row. INPUT reads in the data; and PRELIM sets up the tables to be used in the calculation.

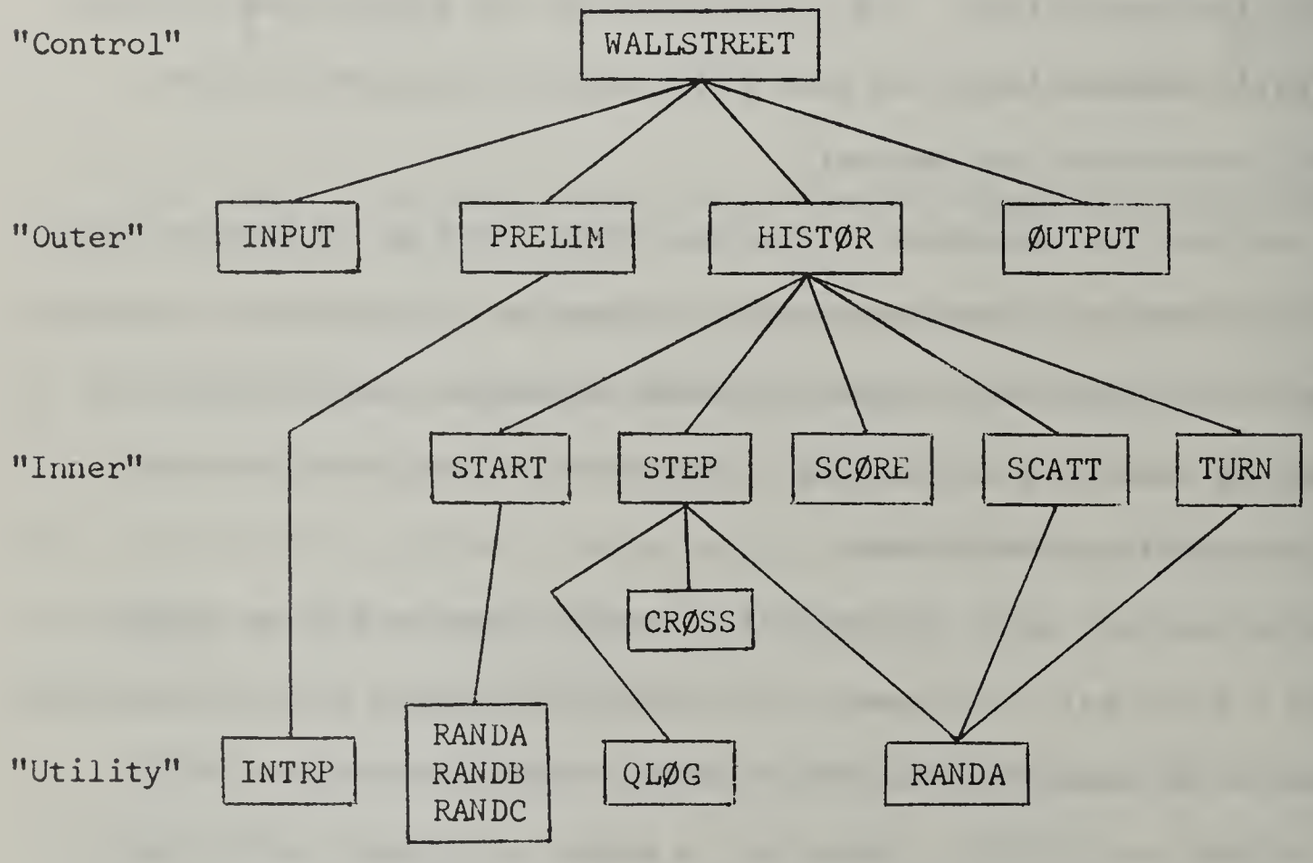

Fig. I-31.2. Diagram of WALLSTREET.

The heart of the program is the HISTØR routine, with its five inner subroutines. START sets up the initial conditions for each history. That is, it generates the initial position, initial direction, and initial energy of each gamma ray case history. STEP determines how far the photon will travel to the next collision; and this has complications due to the presence of two materials -- air and concrete. STEP makes use of CRØSS, which determines whether or not a boundary is crossed.

After this is a subroutine called SCØRE. If the photon penetrates beyond the walls, one must determine what contribution has been made to the detector response at a location outside the wall. After a SCØRE the photon is lost and the case history is terminated.

If there is no SCØRE, the program proceeds with a scattering routine called SCATT, which gives a new energy due to scattering, according to the Klein-Nishina cross section. This is followed by TURN, which gives new angular coordinates to the photon.

From TURN the program goes back to STEP and the sequence is repeated. When a case history is terminated, because of a SCØRE or because the wavelength exceeds the maximum permitted, a new START is made.

When a run is complete the cumulated scores are stored on tape. When the desired set of runs has been completed, the ØUTPUT is generated and the calculation comes to an end.

c) Symbols in Common Storage.

There are two ways of linking routines and subroutines together in the more recent versions of the FØRTRAN language. One way is by means of subroutine arguments; this has been used in section 22. By using the

address of a number, or the first number of a list, in a subroutine argument, you indicate where the variable to be used by the subroutine is located in the main program. This method has the advantage that subroutines can then be used without change in many programs. But it has the disadvantage that in complicated programs, with many arguments, it is tedious to write the arguments all down whenever a subroutine is called. In extreme cases a subroutine can depend on dozens of arguments. Even in WALLSTREET there are many variables. Furthermore, every time the computer makes use of a subroutine, some computation must be performed to identify the numbers in the main routine which are to be used in the subroutine; and this takes some computer time.

The other procedure makes use of CØMMØN storage statements. Variables identified in CØMMØN statements are given absolute locations in the computer memory. If one then puts the same CØMMØN and DIMENSIØN statements in front of each subroutine, then for all the routines the variables will be located in the same portion of the memory space of the computer. If you then refer to the variable A, it makes no difference whether the instruction is in a subroutine or in the main program. So there is nc further need to identify the numbers and lists by means of arguments. This saves a lot of writing and machine time; but it has an important disadvantage which should be kept in mind. The subroutine loses generality when CØMMØN statements are used, because they are then tied to a particular program. If the subroutines are needed for a second program, they must be given a second CØMMØN statement and reassembled. Further, one must do careful bookkeeping on the names of variables in all subroutines for any given program, lest a given name be

used inconsistently by accident.

In general, if subroutines have few arguments, it is apt to turn out that explicit use of subroutine arguments is advantageous; while if subroutines have many arguments, CØMMØN statements have a great advantage. It is possible to put some variables in CØMMØN and others in arguments and to some extent gain the advantages of both systems; but in this program we use CØMMØN statements almost exclusively.

We conclude this section with a list of all the WALLSTREET variables in CØMMØN storage, as a useful reference for the programs of section 32.

Table I-31.1. Definition of Symbols Listed in CØMMØN Storage.

A	the half-width of the street.
AT	detailed table of total attenuation coefficient data.
ATB	input table of total attenuation coefficient data from which the longer table AT is generated.
ATNØRM	normalization constant to choose the units of the attenuation coefficient data. In the list ATB, units cm^2 per gram are used; we want AT in units of inverse feet. The conversion constant is .0367 for air and 71.6 for concrete.
B	wall thickness, in arbitrary units.
CCH	$\cos\Phi$, where Φ is the azimuthal deflection angle in a scattering.
CDPH	$\cos(\phi_{n+1}-\phi_n)$, where ϕ_n and ϕ_{n+1} are azimuthal coordinates indicating the direction of motion before and after the n'th scattering.
CIMAX	number of histories to be done (in floating form).
COM	$\cos\theta$, where θ is the polar deflection angle in a scattering.
CPH	$\cos\phi$, where ϕ is an azimuthal variable of the photon direction of motion.
CPHN	new value of CPH, after a scattering.

CTH	$\cos\theta$, where θ is the obliquity angle of the photon direction of motion.
CTHN	new value of CTH.
DNØRM	normalization constant to make the results for dose come out in desired units.
DOS	product of spectral energy E times energy absorption coefficient for air, at that energy. The units are determined by DNØRM.
DOSB	energy absorption coefficient table, for air, read into program as input data.
EB	basic list of energies for which all cross section data are read in.
EFS	energy list for which the fission spectrum is read in.
EMAX	largest photon energy in problem.
EMIN	smallest energy to which photons are followed by random sampling.
FL	output, listing of dose received by detector at various heights immediately behind the left wall for various thicknesses of the left wall.
FLSQ	sum over squares of individual contributions to FL.
FR	output, same as FL except that it is for the right wall.
FRSQ	sum over squares of individual contributions FR.
FS	fission source spectrum.
FSCUM	cumulative fission source spectrum, prepared in PRELIM from the data read into FS.
H	list of wall heights.
I	index labeling I'th history.
IMAX	number of histories to be done (in integer form).
INRAN	initial random number.
IRA	random number (octal), generated by the multiplier 5^{15}.
IRB	random number (octal), generated by the multiplier 5^{13}.
IRC	random number (octal), generated by the multiplier 5^{11}.

IREP	number of histories to be done before a comment appears on the on-line printer.
JAT	index for picking an attenuation coefficient from table.
JAZ	index for picking the cosine and sine of an angle distributed uniformly between 0 and 360 degrees.
JB	index labeling the thinnest wall (right or left) still to be crossed.
JBMAX	maximum number of wall thicknesses considered.
JGO	indicator variable used to aid in computing the index JAT.
KMAX	largest number of detector heights considered in the problem (minus one).
KMAX1	KMAX + 1.
MAT	total number of energies for which cross section data is to be read into the program.
MZ	parameter which indicates direction of travel of photon upon leaving source. Value 0: into ground, value 1: into air.
NC	index which has value unity if air-concrete interface has been crossed during step, is zero otherwise.
NLTAB	index to instruct subroutine QLØG whether or not to compute a table of logarithms. Value 1: subroutine computes table, Value 2: subroutine has already computed table and does not need to repeat this operation.
NMAT	index labeling the medium; 1=air, 2=concrete.
NRUN	number of computer run.
NSPEC	number of energies in the fission source list. If NSPEC=0, the program does not read in a fission spectrum but instead assumes that the source is monoenergetic with the source energy equal to EMAX.
P	survival weight factor.
RA	random number in floating form corresponding to IRA.
RB	random number in floating form corresponding to IRB.

RC — random number in floating form corresponding to IRC.

SCH — $\sin\Phi$, see CCH.

SDPH — $\sin(\phi_{n+1} - \phi_n)$, see CDPH.

SIGL — standard deviation of results for dose received by detector behind the left wall.

SIGR — standard deviation of results for dose received by detector behind the right wall.

SOM — $\sin\Theta$, see COM.

SPH — $\sin\phi$, see CPH.

SPHN — new value of SPH.

STH — $\sin\theta$, see CTH.

STHN — new value of STH.

SURV — probability that given an interaction for a photon of a certain energy, the interaction will be a Compton scattering.

SURVB — same as SURV except that this is the list read into the machine to be used in generating the more detailed list SURV.

UY — direction cosine $\sin\theta\sin\phi$.

UYA — absolute value of UY.

UYL — comparison constant for UYA. No UYA values smaller than UYL are accepted.

UZ — direction cosine, $\cos\theta$.

W — photon wavelength.

WALDEN — normalization factor to convert wall thickness to units needed to do calculation.

WB — list of wavelengths at which cross sections are tabluated (detailed list manufactured by program).

WMAX — wavelength corresponding to EMIN.

WMIN — wavelength corresponding to EMAX.

Y	the y-coordinate of the photon.
YC	the y-coordinate of the photon upon crossing an air-concrete interface.
YD	auxiliary variable.
YDN	auxiliary variable.
YN	the y-coordinate of the photon after a scattering.
Z	the z-coordinate of the photon.
ZC	the z-coordinate of the photon upon crossing an air-concrete interface.
ZN	the z-coordinate of the photon after scattering.
ZSC	height of photon above the ground (or below) when it emerges from an exterior boundary of the wall.

32. WALLSTREET: Computer Routines

In all subroutines the CØMMØN and DIMENSIØN statements are indicated, but not given. The control routine includes these statements explicitly.

a) SCATT and TURN

SCATT selects a new wavelength by sampling the Klein-Nishina distribution The first part of it appears complicated; but it follows the flow chart given in Figure I-28.5 faithfully, step by step. Note that W, the wavelength, is called λ_n in the flow chart; but when WØLD is equated to λ_n, W becomes λ_{n+1}.

```
C     *     *     *     *     *

      SUBRØUTINE SCATT
      DIMENSIØN
      CØMMØN
```

The DIMENSIØN and CØMMØN statements just indicated are those of the control routine; and the SUBRØUTINE statement has no arguments.

```
   10 CALL RANDA(IRA,RA)
```

Recall that IRA is a random number in octal integer form, while RA is the normalized floating point version of IRA. We first test RA against $(1+2/\lambda_n)/(9+2/\lambda_n)$.

```
      T=2./W
      IF(RA-(1.+T)/(9.+T)) 20,20,30
```

If ρ_1 is smaller, we take the left branch, calculate $R=1+\rho_2(2/\lambda_n)$ and test ρ_3.

```
   20 CALL RANDA(IRA,RA)
      R=1.+RA*T
      CALL RANDA(IRA,RA)
      IF(RA-4.*(R-1.)/R**2)) 40,40,10
```

If ρ_1 is larger, we take the right branch, calculate $R=(1+2/\lambda_n)/(1+\rho_2(2/\lambda_n))$ and test ρ_3.

```
      CALL RANDA(IRA,RA)
      R=(1.+T)/(1.+RA*T)
      CALL RANDA(IRA,RA)
      IF(RA-.5*((W-R*W+1.)**2+1./R)) 40,40,10
```

If the ρ_3 comparison is successful, we compute λ_{n+1} as well as the sine and cosine of the deflection angle.

```
   40 WØLD=W
      W=R*WØLD
      CØM=1.-W+WØLD
      SØM=SQRTF(1.-CØM**2)
```

Lastly, the survival weight is modified by a factor μ_{KN}/μ, determined by the wavelength W, as expressed by the pre-calculated index JAT.

```
      P=P*SURV(JAT,NMAT)
      RETURN
      END
C     *     *     *     *     *
```

The subroutine TURN calculates new direction coordinates, by using the deflection data (CØM,SØM) of SCATT, and by sampling azimuthal trigonometric functions randomly, using table look-up. Figure I-32.1 identifies the angular variables. The formulae are given in any treatise on spherical trigonometry, and will not be repeated here. The only point worth special comment is the case in which either θ_n or θ_{n+1} is very nearly zero. Then the product $\sin\theta_n \sin\theta_{n+1}$, which is a denominator, is very small, and one could

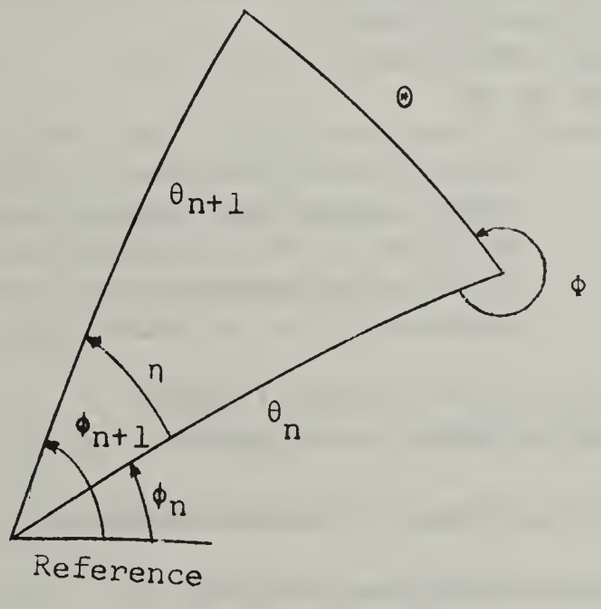

Fig. I-32.1. Spherical triangle for TURN.

have trouble. But it should be noted that if θ_n is small, η is nearly random, while if θ_{n+1} is small the value of η is essentially irrelevant.

```
C     *     *     *     *     *     *

      SUBRØUTINE TURN
      DIMENSIØN
      CØMMØN
```

The DIMENSIØN and CØMMØN statements just indicated are those of the control routine; and the SUBRØUTINE statement has no arguments.

```
      CALL RANDA(IRA,RA)
      JAZ=XFIXF(360.*RA)
```

JAZ is a random integer measure of Φ between zero to 360 , as discussed in section 28d. We next use table look-up on the azimuthal cosine table (CCH) to generate the new obliquity cosine and sine.

```
      CTHN=CTH*CØM+STH*SØM*CCH(JAZ+1)
      STHN=SQRTF(1.-CTHN**2)
      DENØM=STH*STHN
```

We now test DENØM to see if it is so small that special measures should be taken to avoid possible cancellation peculiarities.

```
      IF(ABSF(DENØM)-0.000001) 10,10,20
   10 CDPH=-CCH(JAZ+1)
      SDPH=SCH(JAZ+1)
      GØ TØ 30
```

Recall that CDPH=cosη, SDPH=sinη in Fig. I-32.1. These orders take care of the case of very small DENØM. The minus sign is obtained in the limiting case of vanishing θ_n. While it appears to be unnecessary, one should remember that JAT has been used previously to calculate θ_{n+1}.

```
   20 CDPH=(CØM-CTH*CTHN)/DENØM
      SDPH=SØM*SCH(JAZ+1)/STHN
```

We now calculate CPHN=cosϕ_{n+1} and SPHN=sinϕ_{n+1}.

```
   30 CPHN=CPH*CDPH-SPH*SDPH
      SPHN=SPH*CDPH+CPH*SDPH
```

Next, the new values of direction coordinates are inserted in the address recognized by the rest of WALLSTREET.

```
      CTH=CTHN
      STH=STHN
      CPH=CPHN
      SPH=SPHN
```

Finally, z and y direction cosines are identified.

```
      UZ=CTH
      UY=STH*SPH
      RETURN
      END
C     *     *     *     *     *     *
```

b) STEP and CRØSS.

CRØSS is a subroutine applied in conjunction with STEP to determine whether or not a boundary has been crossed. It is easier to interpret CRØSS if STEP has first been discussed.

The object of STEP is to determine the position of the next interaction. To accomplish this it is necessary first to determine the path length from the n'th interaction to the (n+1)st, then to determine whether or not a boundary has been crossed, and finally to locate the (n+1)st interaction, if need be, beyond the interface.

Determination of the path length is complicated by the fact that the table of cross sections is really 4 tables, with different mesh sizes, corresponding to different regions of the photon wavelength (W): $.1 \leq W \leq .5$, $.5 < W \leq 1.7$, $1.7 < W \leq 10.$, and $W > 10$. The index which is used in this table look-up is JAT.

If the path crosses a boundary from air to concrete, or vice versa, the position of the next interaction must be determined by special methods. In CRØSS the point of crossing is located, and in STEP the photon path is continued by sampling again, as if the point of crossing were an interaction, with use of the cross sections for the new material to determine actual distance in the material beyond the interface.

In determining whether an interface has been crossed, the important thing is to examine the various possibilities in the right order. The reason for this is the possibility of crossing two interfaces, in which case the first crossed should be the first examined. This is discussed in detail at appropriate points in the program.

```
C     *     *     *     *     *     *     *

      SUBRØUTINE STEP
      DIMENSIØN
      CØMMØN
```

The DIMENSIØN and CØMMØN statements just indicated are those of the control routine; and the SUBRØUTINE statement has no arguments

```
   10 GØ TØ (20,50,80,110),JGØ
```

This first order takes advantage of the JGØ value from the preceding occasion on which the subroutine was used. If W was then, say 6.3, corresponding to JGØ=3, the search for the new cross section value is started at order number 80; one does not bother to examine parts of the table appropriate to smaller W values.

```
   20 IF(W-.5) 30,30,40
   30 JAT=XFIXF(1000.*(W-.1))+1
      GØ TØ 120
```

Note that the first part of the table consists of 401 entries, the first three corresponding to W=.1000, .1010, .1020. The mesh size is thus .0010. Order number 30 generates the index of the desired cross-section value.

```
   40 JGØ=2
   50 IF(W-1.7) 60,60,70
   60 JAT=XFIXF(200.*(W-.5))+402
      GØ TØ 120
```

The second part of the table consists of 241 entries, the first three (i.e. entries 402, 403, and 404) corresponding to W=.500, .505, .510.

```
   70 JGØ=3
   80 IF(W-10.) 90,90,100
   90 JAT=XFIXF(50.*(W-1.7))+642
      GØ TØ 120
```

The third part of the table consists of 416 entries, the first

three (i.e., entries 642, 643, and 644) corresponding to W=1.7, 1.72, 1.74.

```
100 JGØ=4
110 JAT=XFIXF(10.*(W-10.))+1057
```

The fourth part of the table consists of an undetermined number of entries; but the first three (i.e., entries 1057, 1058, and 1059) correspond to W=10.0, 10.1, 10.2. If the final wavelength were 30, there would be 301 entries in this final portion.

Next we determine the path length in mean free paths, by sampling.

```
120 CALL RANDA(IRA,RA)
    CALL QLØG(RA,RAL,NLTAB)
```

The random number RA generates a path length of -RAL mean free paths. This must be translated into distance, according to the (pre-specified) medium of the last interaction, indicated by the existing value of NMAT.

```
    NMAT=NMAT
```

This strange order occurs because of a peculiarity of FORTRAN II which has been corrected in FORTRAN IV, and which may be corrected in future FORTRAN II compilers. It turns out that variables which are to be used as indices are not necessarily transmitted from one program to another by the CØMMØN statement. The dummy arithmetic statement guarantees such transmission of information; it is placed after all possible modifications by other routines.*

```
    S=-RAL/AT(JAT,NMAT)
    YN=Y+S*UY
    ZN=Z+S*UZ
```

The last two orders generate projections parallel to y and z axes. Now comes the problem of determining whether boundaries have been crossed. Recall that NC=0 if no crossing, while NC=1 if crossing, and that the argument of CRØSS identifies the boundary.

```
    NC=0
    IF(UY) 160,140,130
```

We first test the sign of the y-component of the path (see

---

*Note that the SAP, FAP, or MAP program gives a clear indication of what actually occurs. The whole problem can be sidestepped in FORTRAN II by putting all variables which are used as indices into argument lists rather than CØMMØN statements.

Fig. I-31.1) This tells whether the photon travels to the left or to the right.

```
  130 CALL CRØSS(-A)
      IF(NC) 140,140,120
```

If the photon travels to the right, we must sample boundaries beginning at the left, i.e. y=-A. In this and the following tests, NC=1 means that the boundary has been crossed, and the position coordinates Y and Z have been recalculated by CRØSS to give the point of crossing.

```
  140 CALL CRØSS(0.0)
      IF(NC) 150,150,120
```

Here we test the z=0 boundary, photon traveling to the right. If by accident the photon goes neither right nor left, this is the first test.

```
  150 CALL CRØSS(A)
      IF(NC) 190,190,120
```

Photon still traveling to the right, y=A boundary being tested. Note that should the test be positive (NC=1), all remaining tests are skipped. This completes tests for photons traveling to the right.

```
  160 CALL CRØSS(A)
      IF(NC) 170,170,120
```

Photon travels left, y=A boundary, i.e. the boundary farthest right.

```
  170 CALL CRØSS(0.)
      IF(NC) 180,180,120
  180 CALL CRØSS(-A)
      IF(NC) 190,190,120
```

After failure of all the tests, or after the last crossing has been determined, we exit from STEP.

```
  190 RETURN
      END
C     *     *     *     *     *     *     *
```

CRØSS is not a particularly clever program; it is a straightforward treatment of the different cases that can arise, with no special difficulties to be encountered.

```
C     *    *    *    *    *    *    *
      SUBRØUTINE CRØSS(C)
      DIMENSIØN
      CØMMØN
```

The DIMENSIØN and CØMMØN statements just indicated are those of the control routine; the subroutine argument is the identifying coordinate of the boundary to be tested for crossing.

```
      IF(C)  60,10,60
```

The z=0 boundary (i.e. C=0) is first taken care of in this program. Order number 60 corresponds both to y=+A and y=-A.

```
10    IF(Z)  20,140,30
```

If the Z value for the preceding interaction is zero, then it will not be because of random sampling, but because of a crossing detected in a previous application of CRØSS. But in that case the material has already been changed; hence the transfer to 140 rather than 110.

```
20    IF(ZN) 140,40,40
30    IF(ZN) 40,40,140
```

If the old Z is positive, and if the new (ZN) value is also positive, the z=0 boundary isn't crossed. Likewise, Z<0 and ZN<0 means no z=0 crossing.

```
40    YC=Y-Z*UY/UZ
      IF(ABSF(YC)-A) 50,140,140
```

YC is the new Y value assuming a crossing. But YC must lie between -A and +A. If so, we record the necessary items and exit from the subroutine. If not, no crossing has occurred.

```
50    Y=YC
      Z=0.
      NC=1
      GØ TØ 110
```

Now we are ready to treat the y=+A and y=-A interfaces in a similar way. The next two orders create parameters analogous to C and Z in the first two orders of the routine.

```
60    YD=Y-C
      YDN=YN-C
```

The next three orders are analogous to orders 10, 20, and 30.

```
      IF(YD) 70,140,80
```

```
   70 IF(YDN) 140,90,90
   80 IF(YDN) 90,90,140
```

If YD and YDN are both positive or both negative, no crossing. If YD=0, it will be because it was set equal to zero in a previous CRØSS application. If YD and YDN have opposite signs, a crossing of the interface plane has occurred, but perhaps not the interface.

```
   90 ZC=Z-YD*UZ/UY
      IF(ZC) 140,140,100
```

ZC must be positive; it is the z value of the interface crossing.

```
  100 Y=C
      Z=ZC
      NC=1
```

Having recorded coordinates and crossing, only the change of material is left to be done.

```
  110 IF(NMAT-1) 120,120,130
  120 NMAT=2
      RETURN
  130 NMAT=1
  140 RETURN
      END
C     *     *     *     *     *     *     *
```

c) START and SCØRE

The remaining routines called by HISTØR are START, which gives each case history its initial conditions, and SCØRE, which applies when a case history has penetrated a wall.

Photons are started at points equally distributed between -A and +A. Use is made in the START routine of a parameter MZ, which is unity if the photon initially travels up into the air and zero if the photon initially travels downward into the concrete. Since MZ is pre-specified, it is possible to perform calculations separately for the two types of starting conditions, and choose different sample sizes. It is advantageous to perform most calculations for upward-traveling photons, since they contribute

perhaps 80% or more of the dose beyond the wall. This is the only type of importance sampling in WALLSTREET.

```
C     *     *     *     *     *     *     *
      SUBRØUTINE START
      DIMENSIØN
      CØMMØN
```

The DIMENSIØN and CØMMØN statements just indicated are those of the control routine; and the SUBRØUTINE statement has no arguments.

```
      CALL RANDC(IRC,RC)
      IRB=IRC
      CALL RANDC(IRC,RC)
      IRA=IRC
```

We here use RANDC to generate initial random numbers IRB and IRA for the case history being started. This approach makes correlated Monte Carlo calculations easy to do.

```
      IF(NSPEC) 40,40,10
```

NSPEC=0 means that a monoenergetic source is being used. NSPEC>0 means that NSPEC is the number of energy boxes in the spectrum.

```
   10 CALL RANDB(IRB,RB)
      DØ 20 NS=1,NSPEC
      IF(RB-FSCUM(NS)) 30,20,20
   20 CØNTINUE
```

Recall that FSCUM is a cumulation over the probabilities that the photon represent different energy boxes. These four orders generate NS, the index of the energy box sleected by RB. The next (arithmetic) statement guarantees that the index has a proper address.*

```
   30 N=NS
      CALL RANDB(IRB,RB)
```

We are going to sample an energy within the energy box randomly. This random number is to be used for that purpose.

```
      IF(N-NSPEC) 32,34,34
   32 W=.510976/(EFS(N)+RB*(EFS(N+1)-EFS(N)))
```

---

*For more comments about this (possibly unnecessary) order see the footnote in the CRØSS writeup.

```
   GØ TØ 50
34 W=.510976/(EFS(N)+RB*(EMAX-EFS(N)))
   GØ TØ 50
```

The list of NSPEC EFS values doesn't include EMAX.

```
40 W=WMIN
```

For the monoenergetic case. The next 5 orders establish the initial obliquity angle θ relative to the vertical axis.

```
50 CALL RANDA(IRA,RA)
   CTH=RA
   STH=SQRTF(1.-CTH**2)
```

Note that for an isotropic source, different values of the obliquity cosine are equally probable. Next we determine whether the photon starts up or down, and fix the material index accordingly.

```
   IF(MZ) 60,60,70
60 CTH=-CTH
   NMAT=2
   GØ TØ 80
70 NMAT=1
```

Next we sample the azimuthal angle randomly, using table look-up. Recall that the 2nd order generates an integer between 0 and 89. Photons are started only towards the right wall. This permits an investigation of the relative contributions due to photons which start towards a wall and those which initially travel away from the wall and must scatter to strike the wall.

```
80 CALL RANDA(IRA,RA)
   JAZ=XFIXF(90.*RA)
   CPH=CCH(JAZ+1)
   SPH=SCH(JAZ+1)
```

The next three orders position the photon with equal likelihood in y between -A and +A, and at z=0.

```
   CALL RANDA(IRA,RA)
   Y=A*(1.-2.*RA)
   Z=0.
```

Lastly, we identify direction cosines (UZ,UY), survival probability (P), initial SCØRE wall index (JB) and energy table index (JGØ).

```
      UZ=CTH
      UY=STH*SPH
      P=1.
      JB=1
      JGØ=1
      RETURN
      END
C     *     *     *     *     *     *
```

In the SCØRE routine we permit scoring through either left or right walls. The photon must be classified into an appropriate height interval. Energy classification is already taken care of by the index JAT; but it is necessary to weight according to some kind of dose.

The old question of flux vs current must now be faced. If we simply count photons which cross the wall, we calculate the current through the wall. To calculate the flux as seen by an isotropic detector, it is necessary to introduce a cosine factor. This has unpleasant features, because the obliquity cosine divides the current. Since this factor can become arbitrarily small, fluctuations in the dose are increased relative to fluctuations in the current. To control these fluctuations to some extent, the cosine is not permitted to become smaller than an arbitrary limiting value.

The program calculates results for several wall thinknesses simultaneously. Since a photon is never permitted to SCØRE more than once at a given wall thickness, an index (JB) is necessary to keep track of the of the next wall thickness at which the photon can SCØRE.

```
C     *     *     *     *     *     *     *
      SUBRØUTINE SCØRE
      DIMENSIØN
      CØMMØN
```

The DIMENSIØN and CØMMØN statements just indicated are those of the control routine; and the SUBROØTINE statement has no arguments.

```
   IF(UY) 30,30,10
```

This tells whether the direction is right (UY>0) or left.

```
10 IF(YN-B(JB)) 100,100,20
20 ZSC=Z+(B(JB)-Y)*UZ/UY
   GØ TØ 50
```

If the new y value (YN) exceeds the next wall thickness (B(JB)) we calculate the height (ZSC) of the point of crossing, by use of direction cosines and the old height (Z). This applies to the right wall; we next perform the same calculation for the left wall.

```
30 IF(YN+B(JB)) 40,100,100
40 ZSC=Z-(B(JB)+Y)*UZ/UY
```

Note that failure to cross means exit from the routine after identifying Y,Z values (transfer to order 100). Next we must locate the correct height bin (KS).

```
50 DØ 60 KS=1,KMAX
   IF(ZSC-H(KS)) 70,60,60
60 CØNTINUE
70 K=KS
```

Order number 70, possibly unnecessary, guarantees that KS has a proper address. (See the footnote in the CRØSS writeup.) We next take into account survival weight, dose weight, and the cosine to determine flux contribution.

```
75 UYA=ABSF(UY)
   IF(UYA-UYL) 76,76,78
76 DØSE=DOS(JAT)*P/UYL
   PRINT 77,DØSE,UY,K,JB
77 FØRMAT(1P2E13.5,2I6)
   GØ TØ 79
```

If the cosine magnitude is below the limit, the various parameters are recorded for observation. The initial symbols in the FØRMAT, 1P, move the decimal point of the E format numbers 1 Place to the right.*

```
78 DØSE=DØS(JAT)*P/UYA
```

---

*This decimal shift will affect numbers in E and F formats to the right as far as, say, a 0P or other comparable decimal shift indication.

The usual case is not recorded. Next we add in this contribution and its square.

```
 79 IF(UY) 90,90,80
 80 FR(K,JB)=FR(K,JB)+DØSE
    FRSQ(K,JB)=FRSQ(K,JB)+DØSE**2
    JB=JB+1
    IF(JB-JBMAX) 10,10,110
```

If JB is not larger than JBMAX, the photon may cross another wall interface. Hence the transfer to order number 10. The next orders repeat for the left wall. Recall that by starting photons only towards the right wall, the two results are different.

```
 90 FL(K,JB)=FL(K,JB)+DØSE
    FLSQ(K,JB)=FLSQ(K,JB)+DØSE**2
    JB=JB+1
    IF(JB-JBMAX) 30,30,110
```

Lastly, we equate Y and Z to tne new values YN and ZN, when the photon fails to cross the next wall thickness tried.

```
100 Y=YN
    Z=ZN
110 RETURN
    END
C     *     *     *     *     *     *     *
```

d) HISTØR and PRELIM

HISTØR is the central routine of WALLSTREET. It initiates and carries along a photon until it has either penetrated through the thickest wall, or has exceeded the maximum wavelength (WMAX). Thus, HISTØR is used once for each case history.

```
C     *     *     *     *     *     *     *
      SUBRØUTINE HISTØR
      DIMENSIØN
      CØMMØN
```

The DIMENSIØN and CØMMØN statements just indicated are those of the control routine; the SUBRØUTINE statement has no arguments.

```
      CALL START
 10   CALL STEP
      CALL SCØRE
      IF(JB-JBMAX) 20,20,40
```

The photon starting point plays the role of the position of the preceding interaction.

```
   20 CALL SCATT
```

If the photon has not penetrated through the thickest wall, it scatters again.

```
      IF(W-WMAX) 30,30,40
   30 CALL TURN
      GØ TØ 10
```

If the photon has not exceeded the maximum wavelength, it is continued further. If the photon has either penetrated the thickest wall or exceeded the maximum wavelength, an exit from the subroutine occurs.

```
   40 RETURN
      END
C     *     *     *     *     *     *     *
```

PRELIM is a much longer subroutine, which establishes all the tables to be used in the computation; it also does a number of routine scaling computations which save work in the preparation of the data for INPUT.

The bulk of the computations in PRELIM are concerned with the sine and cosine tables (CCH,SCH), the list of energies at which the cross sections are tabluated (WB), the cross-section tables (EB, DØSB, ATB, SURVB), the wall thicknesses (B), and the cumulative probability function for the spectrum (FSCUM).

```
C     *     *     *     *     *     *     *
      SUBRØUTINE PRELIM
      DIMENSIØN
      CØMMØN
```

The DIMENSIØN and CØMMØN statements just indicated are those of the control routine; the SUBRØUTINE statement has no arguments. The first 6 orders generate parameters to be used in the calculation, all of which are in the CØMMØN list.

```
      KMAX1=KMAX+1
      CIMAX=IMAX
```

```
   IRC=INRAN
   NLTAB=1
   WMIN=.510976/EMAX
   WMAX=.510976/EMIN
```

Next we generate the table of sines and cosines.

```
   CH=-.5
   DØ 10 N=1,360
   CH=CH+1.
   CCH(N)=CØSDF(CH)
10 SCH(N)=SINDF(CH)
```

CØSDF is the cosine of the angle CH in degrees. We now set up the energy list for the cross sections. Recall that this is four lists with different mesh sizes.

```
   WB(1)=.1
   DØ 20 N=2,401
20 WB(N)=WB(N-1)+.001
   DØ 30 N=402,641
30 WB(N)=WB(N-1)+.005
```

The first 400 energies begin at .1 and are spaced .001 apart in wavelength. The next 240 wavelengths begin at .5 and are spaced .005 apart. The third part of the list begins at 1.7 and has spacing .02. The last part begins at 10. and has spacing .1.

```
   DØ 40 N=642,1056
40 WB(N)=WB(N-1)+.02
   DØ 50 N=1057,1256
50 WB(N)=WB(N-1)+.1
```

The cross section tables which were read into the machine must now be interpolated for the energies of the WB list. This interpolation is accomplished on a logarithmic basis -- the log of the cross section is interpolated against the log of the energy -- with tabulation of the anti-log (exponential) of the interpolated value. This type of interpolation is used because the cross sections are relatively smooth on a log-log plot.

```
   DØ 60 N=1,MAT
   EB(M)=LØGF(EB(M))
   DØSEB(M)=LØGF(DØSB(M))
   DØ 60 M=1,2
   ATB(M,K)=LØGF(ATB(M,K))
60 SURVB(M,K)=LØGF(SURVB(M,K))
```

These orders replace the input data by logarithms of the

numbers. Recall that EB is the energy, not the wavelength. We next calculate the logarithms of energies of "mid-point" wavelengths $E=-\log[\frac{1}{2}(\lambda_n+\lambda_{n+1})/.510976]$, and carry out both interpolations and anti-log calculations.

```
      DØ 70 N=1,1256
      E=.021714-LØGF(WB(N)+WB(N+1))
      CALL INTRP(MAT,EB,DØSB,3,E,DØS(N))
      DØS(N)=DNØRM*EXPF(DØS(N)+E)
```

The addition of E in the exponent provides an energy factor which changes the energy absorption coefficient to an appropriate dose weight. DNØRM is simply a factor to make units correct.

```
      DØ 70 K=1,2
      CALL INTRP(MAT,EB,ATB(1,K),3,E,AT(N,K))
      CALL INTRP(MAT,EB,SURVB(MAT,K),3,E,SURV(N,K))
      AT(N,K)=ATNØRM(K)*EXPF(AT(N,K))
      SURV(N,K)=EXPF(SURV(N,K))
   70 CØNTINUE
```

Next, we must clear all cells in which dose will be cumulated.

```
      DØ 80 K=1,KMAX1
      DØ 80 J=1,JBMAX
      FR(K,J)=0.
      FRSQ(K,J)=0.
      FL(K,J)=0.
   80 FLSQ(K,J)=0.
```

The arbitrary wall heights are now to be renormalized.

```
      DØ 90 J=1,JBMAX
   90 B(J)=A+B(J)/WALDEN
```

Lastly, the cumulative probability distribution for source energy is generated from the spectrum.

```
      FSCUM(1)=FS(1)
      DØ 100 NS=2,NSPEC
  100 FSCUM(NS)=FSCUM(NS-1)+FS(NS)
      DØ 110 NS=1,NSPEC
  110 FSCUM(NS)=FSCUM(NS)/FSCUM(NSPEC)
      RETURN
      END
C     *     *     *     *     *     *     *
```

e) The WALLSTREET Control Routine and Subroutines INPUT and ØUTPUT.

The only unusual feature of the WALLSTREET control routine is what might be called a "pacifier" for computer operators. Monte Carlo calculations tend to be fairly long. If half an hour or more goes by and nothing appears to be happening on the computer, the operator is apt to become worried that something is wrong with the program. Sometimes they get so worried and tense that they stop the calculation and start someone else's program, thus wasting all the time and money up to that point. The control routine therefore prints out every now and then the number of case histories completed and the total number to be done.

```
C     *     *     *     *     *     *     *
C     WALLSTREET
      DIMENSIØN AT(1256,2),STB(40,2),ATNØRM(2),B(10),CCH(360),DØS(1256),
     1 DØSB(40),EB(40),EFS(50),FL(100,10),FLSQ(100,10),FR(100,10),
     2 FRSQ(100,10),FS(50),FSCUM(50),H(99),SCH(360),SIGL(100,10),
     3 SIGR(100,10),SURV(1256,2),SURVB(40,2),WB(1256)
      CØMMØN A,AT,ATB,ATNØRM,B,CCH,CDPH,CIMAX,CØM,CPH,CPHN,CTH,CTHN,
     1 DNØRM,DØS,DØSB,EB,EFS,EMAX,EMIN,FL,FLSQ,FR,FRSQ,FS,FSCUM,H,I,
     2 IMAX,INRAN,IRA,IRB,IRC,IREP,JAT,JAZ,JB,JBMAX,JGØ,KMAX,KMAX1,MAT,
     3 MZ,NC,NLTAB,NMAT,NRUN,NSPEC,P,RA,RB,RC,SCH,SDPH,SIGL,SIGR,SØM,
     4 SPH,SPHN,STH,STHN,SURV,SURVB,UY,UYA,UYL,UZ,W,WALDEN,WB,WMAX,
     5 WMIN,Y,YC,YD,YDN,YN,Z,ZC,ZN,ZSC
```

These DIMENSIØN and CØMMØN statements are to be used with the subroutines, except for utility subroutines.

```
      CALL INPUT
      CALL PRELIM
      WRITE ØUTPUT TAPE 81,10
   10 FØRMAT(41H HISTØRIES TO BE DØNE                    DØNE)
```

This is the heading for the "operator pacifier". The order utilizes the online printer at the NBS installation.* This will probably not be true at other installations.

```
      ITALLY=0
      PRINT 15
   15 FØRMAT(24H SMALL DIRECTIØN CØSINES)
```

This is the heading for SCØRE cases in which the cosine in the denominator is unusally small. Oddly, this PRINT order is

*In the BELL system, the statements READ, PRINT, and PUNCH refer to offline input and output.

240-816 O-67—17

offline, so that it does not become confused with the "pacifier". Next comes the main loop of the program.

```
      DØ 40 I=1,IMAX
      CALL HISTØR
      ITALLY=ITALLY+1
      IF(ITALLY-IREP) 40,20,20
   20 WRITE ØUTPUT TAPE 81,30,IMAX,I
   30 FØRMAT(I12,I29)
```

Order 20 prints out the number of case histories to be calculated and the number done so far, i.e. it is the "pacifier".

```
      ITALLY=0
   40 CØNTINUE
```

ITALLY is the counter for each batch. I is the counter for the whole calculation.

```
      CALL ØUTPUT
      CALL ENDJØB
      END
C     *     *     *     *     *     *     *
```

The INPUT subroutine is straightforward, and requires very little comment. It is included here mainly for completeness; most programmers have their own favored INPUT formats. In this program there is evident the habit of printing out immediately the data which the machine has just read, using the same FØRMAT statement. This gives a record which is useful when and if the question arises about the data used for a given calculation, as well as a record which establishes whether or not the machine received and interpreted the data properly.

```
C     *     *     *     *     *     *     *
      SUBRØUTINE INPUT
      DIMENSIØN
      CØMMØN
```

The DIMENSIØN and CØMMØN statements are those of the WALLSTREET control routine; the SUBROUTINE statement has no arguments.

```
      PRINT 10
   10 FØRMAT(1HO)
```

This order is used throughout as a spacer, since it results in a two-line gap on the page. It is used here at the beginning to separate output from tabulations of run parameters, which usually precede the output.

```
   READ 20
   PRINT 20
   PUNCH 20
20 FØRMAT(72H
  1                                                    )
   PRINT 10
```

This is an arbitrary title card which is read, recorded, and eventually repunched at the beginning, hence at the beginning of output cards.

```
   PRINT 30
30 FØRMAT(71H  NRUN  IMAX  IREP NSPEC   MAT    MZ  KMAX JBMAX
  1 INRAN      UYL)
   READ  40,NRUN,IMAX,IREP,NSPEC,MAT,MZ,KMAX,JBMAX,INRAN,UYL
   PRINT 40,NRUN,IMAX,IREP,NSPEC,MAT,MZ,KMAX,JBMAX,INRAN,UYL
40 FØRMAT(8I6,Ø14,F9.5)
   PRINT 10
```

These are the control indices. Note that INRAN is the (octal) starting random number.

```
   PRINT 50
50 FØRMAT(51H  EMAX  EMIN    ATNØRM(1)     ATNØRM(2)       DNØRM)
   READ  60,EMAX,EMIN,ATNØRM(1),ATNØRM(2),DNØRM
   PRINT 60,EMAX,EMIN,ATNØRM(1),ATNØRM(2),DNØRM
60 FØRMAT(2F6.3,1P3E13.5)
   PRINT 10
```

These are control parameters. Note the use of 1P to shift the decimal one place to the right.

```
   IF(NSPEC) 100,100,70
```

Recall that NSPEC=0 means a monoenergetic source.

```
70 PRINT 80
80 FØRMAT(33H FISSIØN SPECTRUM AND ENERGY LIST)
   READ  90,(FS(NS),NS=1,NSPEC)
   PRINT 90,(FS(NS),NS=1,NSPEC)
90 FØRMAT(8F9.5)
   PRINT 10
   READ  90,(EFS(NS),NS=1,NSPEC)
   PRINT 90,(EFS(NS),NS=1,NSPEC)
   PRINT 10
```

```
      GØ TØ 120
  100 PRINT 110
  110 FØRMAT(21H MØNØENERGETIC SØURCE)
      PRINT 10
```

The cross section data is read next.

```
  120 PRINT 130
  130 FØRMAT(19H CRØSS SECTIØN DATA)
      READ  90,(EB(M),M=1,MAT)
      PRINT 90,(EB(M),M=1,MAT)
      PRINT 10
      READ  90,(DØSB(M),M=1,MAT)
      PRINT 90,(DØSB(M),M=1,MAT)
      PRINT 10
      DØ 140 K=1,2
      READ  90,(SURVB(M,K),M=1,MAT)
      PRINT 90,(SURVB(M,K),M=1,MAT)
      PRINT 10
      READ  90,(ATB(M,K),M=1,MAT)
      PRINT 90,(ATB(M,K),M=1,MAT)
  140 PRINT 10
```

Finally, we read in wall parameters, thicknesses, and heights.

```
      PRINT 150
  150 FØRMAT(28H FIELD SIZE,A    WALL DENSITY)
      READ  160,A,WALDEN
      PRINT 160,A,WALDEN
  160 FØRMAT(F9.2,F20.3)
      PRINT 10
      PRINT 170
  170 FØRMAT(17H WALL THICKNESSES)
      READ  90,(B(J),J=1,JBMAX)
      PRINT 90,(B(J),J=1,JBMAX)
      PRINT 10
      PRINT 180
  180 FØRMAT(8H HEIGHTS)
      READ  90,(H(K),K=1,KMAX)
      PRINT 90,(H(K),K=1,KMAX)
      PRINT 10
      RETURN
      END
C     *     *     *     *     *     *     *
```

The ØUTPUT subroutine is likewise uncomplicated. It is in two parts; through order number 50 the information is directly punched and printed.

After that comes a longer section of the code in which some attempt to normalize the data is made and formats for easy scanning are constructed. The normalization is accomplished simply by dividing the results by the number of case histories initiated. This is essentially meaningless, because it does not take account of the street width (2A) or the wall height intervals.

```
C     *     *     *     *     *     *     *
      SUBRØUTINE ØUTPUT
      DIMENSIØN
      CØMMØN
```

The DIMENSIØN and CØMMØN statements are those of the WALLSTREET control routine; the SUBRØUTINE statement has no arguments.

```
      PRINT 10
   10 FØRMAT(1HO)
```

As in the INPUT subroutine, PRINT 10 is a spacing order.

```
      PRINT 20
   20 FØRMAT(12H CARD ØUTPUT)
      PRINT 10
      PRINT 30
   30 FØRMAT(56H  NRUN  IMAX    MZ NSPEC     EMAX    EMIN         INRAN
     1)
      PRINT 40,NRUN,IMAX,MZ,NSPEC,EMAX,EMIN,INRAN
      PUNCH 40,NRUN,IMAX,MZ,NSPEC,EMAX,EMIN,INRAN
   40 FØRMAT(4I6,2F9.5,Ø14)
      PRINT 10
      PRINT 50,((FR(K,J),FRSQ(K,J),K=1,KMAX1),J=1,JBMAX)
      PUNCH 50,((FR(K,J),FRSQ(K,J),K=1,KMAX1),J=1,JBMAX)
      PRINT 10
      PRINT 50,((FL(K,J),FLSQ(K,J),K=1,KMAX1),J=1,JBMAX)
      PUNCH 50,((FL(K,J),FLSQ(K,J),K=1,KMAX1),J=1,JBMAX)
   50 FØRMAT(1P6E12.5)
```

This completes the main output. Notice that the 1P is again used to shift the decimal point to the right. Next we introduce the number of case histories as a preliminary normalization, and calculate standard deviations and variances.

```
      DØ 60 K=1,KMAX1
      DØ 60 J=1,JBMAX
      FR(K,J)=FR(K,J)/CIMAX
```

```
      FRSQ(K,J)=FRSQ(K,J)/CIMAX
      SIGR(K,J)=SQRTF((FRSQ(K,J)-FR(K,J)**2)/CIMAX)
      FL(K,J)=FL(K,J)/CIMAX
      FLSQ(K,J)=FLSQ(K,J)/CIMAX
   60 SIGL(K,J)=SQRTF((FLSQ(K,J)-FL(K,J)**2)/CIMAX)
```

The output is now to be arranged to take account of the possibility that there may be too many wall thicknesses to put side by side across the page. Provision is made to print out the first 5, and if there are more, to print other sets of results below.

```
      IF(JBMAX-5) 70,70,80
   70 JSTØP=JBMAX
      GØ TØ 90
   80 JSTØP=5
   90 JSTART=1
      JCHECK=5
  100 PRINT 110
  110 FØRMAT(1H1)
```

This is another spacing order.

```
      PRINT 120,(B(J),J=JSTART,JSTØP)
  120 FØRMAT(10H     J    B= F15.5,9F20.5)
      DØ 140 K=1,KMAX1
      PRINT 130,H(K),(FR(K,J),SIGR(K,J),J=JSTART,JSTØP)
  130 FØRMAT(F10.5,1P10E10.2)
  140 CØNTINUE
      PRINT 10
      DØ 150 K=1,KMAX1
  150 PRINT 130,H(K),(FL(K,J),SIGL(K,J),J=JSTART,JSTØP)
      If(JCHECK-JSTØP) 160,160,190
  160 IF(JBMAX-JSTØP) 190,190,170
  170 JSTART=JSTART+5
      JCHECK=JCHECK+5
      JSTØP=JSTØP+5
      IF(JBMAX-JSTØP) 180,100,100
  180 JSTØP=JBMAX
      GØ TØ 100
  190 RETURN
      END
C     *     *     *     *     *     *     *
```

G. APPENDIX ON NUMERICAL METHODS

33. Approximation of Functions by Points

The numerical methods given in these sections are quite familiar; and many treatises exist in which they are elaborated far beyond anything which will be attempted here. We include this material because it was presented in the lectures as basic reference material for the discussions of that part of the manuscript beginning with section 22. Even though the material is quite familiar, our approach is not always the usual one.

Many types of calculations involve a function $f(x)$, whose analytic form, even if known, is so complicated that we wish to replace it with a simpler function for analytic or numerical manipulations. Suppose, therefore, that by perseverance we manage to determine several values f_1, f_2, and f_3 of this function at points x_1, x_2, and x_3. We illustrate with three points only, because the generalization to a larger or smaller number of points will be obvious. Fig. I-33.1 is a sketch of the situation.

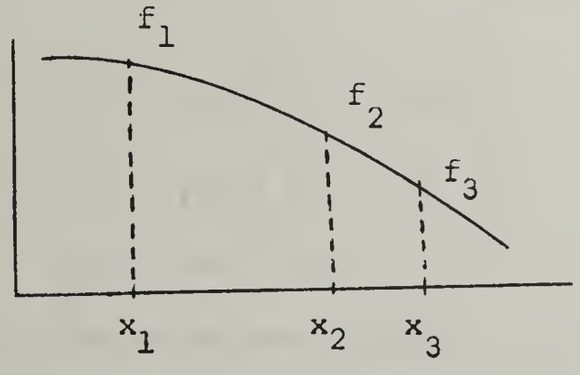

Fig. I-33.1. A function, with three points determined.

The simplest function of our acquaintance is a combination of the first few powers. Because of its simplicity we choose this form of representation--other forms could serve as well--and write

$$\hat{f}(x) = a + bx + cx^2, \qquad \text{(I-33.1)}$$

where $\hat{f}(x)$ will be made to resemble $f(x)$ to the extent that both functions pass through the three points (x_1,f_1), (x_2,f_2), and (x_3,f_3). Three constants are inserted in the expression for $\hat{f}(x)$ to correspond to the conditions imposed by requiring the curve to pass through these three points.

The conditions are easily written down:

$$\begin{aligned} f_1 &= a + bx_1 + cx_1^2, \\ f_2 &= a + bx_2 + cx_2^2, \\ f_3 &= a + bx_3 + cx_3^2. \end{aligned} \qquad \text{(I-33.2)}$$

Since both the x_i's and the f_i's are known, these represent three simultaneous, linear equations for the constants a, b, and c.

We solve these equations by a somewhat indirect procedure. In the first step, we lump the equation for f(x) with the three conditions to make a total of four equations, rewriting each to place all terms on the left side:

$$\begin{aligned} -\hat{f}(x) + a + bx + cx^2 &= 0, \\ -f_1 + a + bx_1 + cx_1^2 &= 0, \\ -f_2 + a + bx_2 + cx_2^2 &= 0, \\ -f_3 + a + bx_3 + cx_3^2 &= 0. \end{aligned}$$

We put this set of equations into matrix form,

$$\begin{bmatrix} \hat{f}(x) & 1 & x & x^2 \\ f_1 & 1 & x_1 & x_1^2 \\ f_2 & 1 & x_2 & x_2^2 \\ f_3 & 1 & x_3 & x_3^2 \end{bmatrix} \begin{bmatrix} -1 \\ a \\ b \\ c \end{bmatrix} = \begin{bmatrix} 0 \\ 0 \\ 0 \\ 0 \end{bmatrix} \qquad \text{(I-33.3)}$$

Next, we introduce an apparent complication, by expanding the column matrices into 4x4 matrices. The simplest way to do this is to fill nearly all the new spaces with zeros, while putting 1's down the diagonal. The column matrix then becomes

$$\begin{pmatrix} -1 & 0 & 0 & 0 \\ a & 1 & 0 & 0 \\ b & 0 & 1 & 0 \\ c & 0 & 0 & 1 \end{pmatrix},$$

where the values on the diagonal ensure that the determinant of this matrix is not zero. If this square matrix is inserted in place of the left column matrix, the ordinary rules of matrix multiplication tell us the square matrix which is an appropriate replacement for the right column matrix; and our modified equation has the form

$$\begin{pmatrix} \hat{f}(x) & 1 & x & x^2 \\ f_1 & 1 & x_1 & x_1^2 \\ f_2 & 1 & x_2 & x_2^2 \\ f_3 & 1 & x_3 & x_3^2 \end{pmatrix} \begin{pmatrix} -1 & 0 & 0 & 0 \\ a & 1 & 0 & 0 \\ b & 0 & 1 & 0 \\ c & 0 & 0 & 1 \end{pmatrix} = \begin{pmatrix} 0 & 1 & x & x^2 \\ 0 & 1 & x_1 & x_1^2 \\ 0 & 1 & x_2 & x_2^2 \\ 0 & 1 & x_3 & x_3^2 \end{pmatrix}. \qquad \text{(I-33.4)}$$

This expanded form contains no information other than that of the set of four simultaneous equations with which we began. The extra spaces have been so filled that all the extra equations are identities.

There is a theorem, given in any standard treatise on determinants and matrices, which states that for such an equation involving <u>square</u> matrices, a corresponding equation will hold if each matrix is replaced by its determinant. That is to say,

$$\begin{vmatrix} \hat{f}(x) & 1 & x & x^2 \\ f_1 & 1 & x_1 & x_1^2 \\ f_2 & 1 & x_2 & x_2^2 \\ f_3 & 1 & x_3 & x_3^2 \end{vmatrix} \begin{vmatrix} -1 & 0 & 0 & 0 \\ a & 1 & 0 & 0 \\ b & 0 & 1 & 0 \\ c & 0 & 0 & 1 \end{vmatrix} = \begin{vmatrix} 0 & 1 & x & x^2 \\ 0 & 1 & x_1 & x_1^2 \\ 0 & 1 & x_2 & x_2^2 \\ 0 & 1 & x_3 & x_3^2 \end{vmatrix}. \qquad \text{(I-33.5)}$$

But the determinant on the right is obviously zero, because the first column is filled with zeros. On the other hand, the second determinant on the left has the value -1, not zero. Therefore, because one of the factors on the left must be zero, we find that

$$\begin{vmatrix} \hat{f}(x) & 1 & x & x^2 \\ f_1 & 1 & x_1 & x_1^2 \\ f_2 & 1 & x_2 & x_2^2 \\ f_3 & 1 & x_3 & x_3^2 \end{vmatrix} = 0. \qquad \text{(I-33.6)}$$

We could have written this result much earlier, because it follows from the first matrix equation. This somewhat more long-winded procedure has been used so that we can refer to it in later, less obvious applications. Note that if in the top row $\underline{x}$ is assigned any of the three values x_1, x_2, or x_3, the top row of values will coincide with one of the other rows, making the whole determinant zero and satisfying the equation.

This determinant equation is useful in the discussion of standard numerical techniques. Suppose we expand the determinant by minors of the top row:

$$\hat{f}(x) \cdot \begin{vmatrix} 1 & x_1 & x_1^2 \\ 1 & x_2 & x_2^2 \\ 1 & x_3 & x_3^2 \end{vmatrix} - 1 \cdot \begin{vmatrix} f_1 & x_1 & x_1^2 \\ f_2 & x_2 & x_2^2 \\ f_3 & x_3 & x_3^2 \end{vmatrix} + x \cdot \begin{vmatrix} f_1 & 1 & x_1^2 \\ f_2 & 1 & x_2^2 \\ f_3 & 1 & x_3^2 \end{vmatrix} - x^2 \cdot \begin{vmatrix} f_1 & 1 & x_1 \\ f_2 & 1 & x_2 \\ f_3 & 1 & x_3 \end{vmatrix} = 0.$$

If we divide this equation by the factor multiplying f(x), we have Cramer's rule for the three constants a, b, and c. But the main thing to observe is the linearity of the equation in terms of the elements of the top row. From this it is quite clear that if a linear operation $\underline{T}$ is applied to the terms of this equation, the result can be put in the form

$$\begin{vmatrix} T\cdot\hat{f}(x) & T\cdot 1 & T\cdot x & T\cdot x^2 \\ f_1 & 1 & x_1 & x_1^2 \\ f_2 & 1 & x_2 & x_2^2 \\ f_3 & 1 & x_3 & x_3^2 \end{vmatrix} = 0. \qquad \text{(I-33.7)}$$

In the following sections we apply this rule to obtain "weights" for several numerical operations.

34. Interpolation*

The three operations of interpolation, differentiation, and integration are closely related and can be discussed together.

Let us consider Eq. (I-33.6), which is equivalent to Eq. (I-33.7) with $\underline{T}$ a simple multiplication by unity. We expand the determinant by the elements in the first column to get an equation in which $\hat{f}(x)$ and the f_i are factors. Designating the minor of $\hat{f}(x)$ by D, and the minors of the f_i by $m_i(x)$, the expansion gives

$$\hat{f}(x)D - f_1 m_1 + f_2 m_2 - f_3 m_3 = 0.$$

Dividing by D, and defining functions $w_i(x)$ by

$$w_i(x) = (-1)^{i+1} m_i(x)/D,$$

we write this equation in the simple form

$$\hat{f}(x) = \sum_{i=1}^{3} f_i w_i(x). \qquad \text{(I-34.1)}$$

The $w_i(x)$ are called "weights," and in this case they are <u>interpolation</u> weights. If we specify a particular value of $\underline{x}$, we can evaluate $w_i(x)$. The sum then gives a value for f, which approximates the value for f at this $\underline{x}$. This is precisely the interpolation procedure. Note that the weights <u>do not depend on the f_i values</u>. But they do depend on x_1, x_2, and x_3.

Before leaving the subject, we will point out some additional features of the interpolation weights. It is clear from Eq. (I-34.1) that $w_i(x_j) = 0$, $i \neq j$, and that $w_i(x_i) = 1$. From this it is possible to infer the analytic

*Of the many general treatments, Ref. 46 has been most useful here.

form of the weights without evaluating the determinants. Eq. (I-34.1) can be explicitly written

$$f(x) = \frac{(x - x_2)(x - x_3)}{(x_1-x_2)\ (x_1-x_3)} f_1 + \frac{(x - x_3)(x - x_1)}{(x_2-x_3)(x_2 - x_1)} f_2 + \frac{(x - x_1)(x - x_2)}{(x_3-x_1)(x_3-x_2)} f_3 \ . \quad \text{(I-34.2)}$$

This expression is widely known as the "Lagrange interpolation" formula.

If we consider the special case $f_1 = f_2 = f_3$, we immediately see that the weights have the general property

$$\sum_{i=1}^{3} w_i(x) = 1, \quad \text{(I-34.3)}$$

from which it follows that, for example,

$$w_3(x) = 1 - \sum_{i=1}^{2} w_i(x). \quad \text{(I-34.4)}$$

Lastly, we call attention to a well known procedure and terminology for simplifying the solution of the determinant equation (I-33.6).* Suppose, in this determinant, each row is subtracted from the row above. Then

$$\begin{vmatrix} \hat{f}(x) & 1 & x & x^2 \\ f_1 & 1 & x_1 & x_1^2 \\ f_2 & 1 & x_2 & x_2^2 \\ f_3 & 1 & x_3 & x_3^2 \end{vmatrix} = \begin{vmatrix} f(x) - f_1 & 0 & x-x_1 & x^2-x_1^2 \\ f_1 - f_2 & 0 & x_1-x_2 & x_1^2-x_2^2 \\ f_2 - f_3 & 0 & x_2-x_3 & x_2^2-x_3^2 \\ f_3 & 1 & x_3 & x_3^2 \end{vmatrix} = 0.$$

Next, we divide each member of the top three rows by the third element on the same row, to obtain

---

*See, for example, Ref. 46.

$$\begin{vmatrix} \dfrac{\hat{f}(x) - f_1}{x - x_1} & 0 & 1 & x + x_1 \\ \dfrac{f_1 - f_2}{x_1 - x_2} & 0 & 1 & x_1 + x_2 \\ \dfrac{f_2 - f_3}{x_2 - x_3} & 0 & 1 & x_2 + x_3 \\ f_3 & 1 & x_3 & x_3^2 \end{vmatrix} = 0.$$

At this point we introduce the notation

$$\frac{\hat{f}(x) - f_1}{x - x_1} = [x,x_i]; \qquad \frac{f_i - f_{i+1}}{x_i - x_{i+1}} = [x_i,x_{i+1}]. \qquad \text{(I-34.5)}$$

Because of the form of the second column, the determinant can be reduced to

$$\begin{vmatrix} [x,x_1] & 1 & x + x_1 \\ [x_1,x_2] & 1 & x_1 + x_2 \\ [x_2,x_3] & 1 & x_2 + x_3 \end{vmatrix} = 0.$$

Next, we again subtract each row from the row above and divide by the elements of the third row so obtained:

$$\begin{vmatrix} \dfrac{[x,x_1] - [x_1,x_2]}{x - x_2} & 0 & 1 \\ \dfrac{[x_1,x_2] - [x_2,x_3]}{x - x_3} & 0 & 1 \\ [x_2,x_3] & 1 & x_2 + x_3 \end{vmatrix} = 0.$$

We again collapse the determinant by the expansion which utilizes the second column. Extending the notation as follows,

$$\frac{[x,x_1] - [x_1,x_2]}{x - x_2} = [x,x_1,x_2],$$

$$\frac{[x_i,x_{i+1}] - [x_{i+1},x_{i+2}]}{x_i - x_{i+2}} = [x_i,x_{i+1},x_{i+2}], \qquad \text{(I-34.6)}$$

we write

$$\begin{vmatrix} [x,x_1,x_2] & 1 \\ [x_1,x_2,x_3] & 1 \end{vmatrix} = 0,$$

which is simply

$$[x,x_1,x_2] = [x_1,x_2,x_3]. \qquad \text{(I-34.7)}$$

The quantities defined by the ratios of (I-34.5) and I-34.6) are referred to as <u>divided differences</u>. They exemplify only the first and second order terms of a sequence. The definitions can obviously be extended to the third, $[x_i,x_{i+1},x_{i+2},x_{i+3}]$, and higher.

Recalling (I-34.6), we see that Eq. (I-34.7) can be written in the form

$$\frac{[x,x_1] - [x_1,x_2]}{x - x_2} = [x_1,x_2,x_3],$$

or,

$$[x,x_1] = [x_1,x_2] + [x_1,x_2,x_3](x - x_2).$$

Inserting the expression for $[x,x_1]$ and rearranging in a similar way, we obtain the simple expression called Newton's formula,

$$f(x) = f_1 + [x_1,x_2](x - x_1) + [x_1,x_2,x_3](x - x_1)(x - x_2). \quad \text{(I-34.8)}$$

There is a useful degree of freedom in Newton's formula which should be appreciated. Suppose one has a function f(x) tabulated at x values which increase monotonically,

$\underline{x}$	$\underline{f(x)}$
x_1	f_1
x_2	f_2
x_3	f_3
x_4	f_4 .

Application of Newton's formula proceeds in a routine way, from the top down. But suppose that without changing any of the numerical values, we re-label the points as follows:

$\underline{x}$	$\underline{f(x)}$
x_4	f_4
x_3	f_3
x_2	f_2
x_1	f_1 .

Application of Newton's formula proceeds as before, but from the bottom up. All terms are different from the corresponding terms in the preceding calculation.

Finally, suppose that we once more re-label the values of our list, as follows:

x	$f(x)$
x_4	f_4
x_2	f_2
x_1	f_1
x_3	f_3 .

Now the calculation proceeds from the middle outward in both directions alternately. A similar alternate progression is given by

x	$f(x)$
x_3	f_3
x_1	f_1
x_2	f_2
x_4	f_4 .

These last two arrangements give interpolation formulae to which the name of Gauss has been attached.

We illustrate the use of divided differences by interpolating a value of $f(x)$ at $x = .74$, where $f(x)$ is the polynomial

$$f(x) = 1 - 2x + 3x^2 - 4x^4. \qquad \text{(I-34.9)}$$

Choosing the arrangement due to Gauss, we construct the following table:

240-816 O-67—18

Table I-34.1. Data for sample interpolation.

i	x_i	f_i	$[x_{i-1},x_i]$	$[x_{i-2},x_{i-1},x_i]$	$[x_{i-3},x_{i-2},x_{i-1},x_i]$
1	.7	.1096			
2	.8	-.3184	-4.28		
3	.6	.3616	-3.40	- 8.8	
4	.9	-.9944	-4.52	-11.2	-12

Newton's formula (I-34.8) then gives

$$\hat{f}(.74) = .1096+(-4.28)(.74-.7)+(-8.8)(.74-.7)(.74-.8)$$
$$+(-12)(.74-.7)(.74-.8)(.74-.6)$$
$$= .1096 - .1712 + .02112 + .004032$$
$$= -.03645.$$

This is to be compared with the correct value, f(.74) = -.03666.

Note that the successive terms decrease, and that, by taking enough terms, the interpolation can be made arbitrarily accurate. But this feature is dependent on (a) the precision of the known values of f(x), and (b) the well-behaved nature of f(x).

If all the known points f_i are used to obtain an interpolated value, the result is independent of the arrangement.

We might close this discussion by observing that the asymmetry of the Gauss arrangement proved bothersome, with the result that new formulae were devised in which a mean was calculated for the results from the two alternative sequences. Formulae of this type are attributed to Stirling. Still other analogous formulae exist and are attributed to various people; many of these apply to the special case of equidistant values of x_i.

35. Roots of Equations, Differentiation and Integration Weights

a) Roots of equations. The numerical illustration at the close of the preceding section was chosen because the function (I-34.9) has a root for x between .7 and .8. Calculation of such a root is a standard algebraic problem, but it is not widely appreciated that such a calculation is essentially an interpolation.

Note the symmetry of the numerical data which we utilize. We refer to one (the x_i list) as the list of abscissas, and the other (the f_i list) as the list of ordinates. But we could as easily have interchanged the two, so that the resulting function is the inverse of (I-34.9). If this is done, it is immediately obvious that the value for x at which $f = 0$ can be estimated by a straightforward interpolation procedure.*

We illustrate this point by a calculation similar to that of the last section, again utilizing the Gauss arrangement:

Table I-35.1. Data for a sample root calculation.

i	f_i	x_i	$[f_{i-1},f_i]$	$[f_{i-2},f_{i-1},f_i]$	$[f_{i-3},f_{i-2},f_{i-1},f_i]$
1	.1096	.7			
2	-.3184	.8	-.23365		
3	.3616	.6	-.29412	-.23997	
4	-.9944	.9	-.22124	-.10781	-.11971

Application of Newton's formula gives

---

*If the f_i list is not monotonic, the procedure can be applied to monotonic subsections.

$$x_{root} = .7 + (-.23365)(0-.1096) + (-.23997)(0-.1096)(0+.3184)$$
$$+ (-.11971)(0-.1096)(0+.3184)(0-.3616)$$
$$= .7 + .02561 + .00837 - .00151$$
$$= .7325,$$

which is to be compared with the value .7307, obtained in a more detailed calculation.

Note that once again the successive terms in Newton's formula converge. Considering the wide separation between points used, both the convergence obtained and the accuracy of the final result are gratifying.

b) Numerical Differentiation. It turns out that for a discussion of numerical differentiation, it is more convenient to use Newton's formula than the determinant equation (I-33.7). If we differentiate Newton's formula, the result is

$$\frac{\hat{df}}{dx} = [x_1,x_2] + [x_1,x_2,x_3]\{(x-x_2) + (x-x_1)\}$$
$$+ [x_1,x_2,x_3,x_4]\{(x-x_2)(x-x_3)+(x-x_1)\frac{d}{dx}(x-x_2(x-x_3)\}$$
$$+ [x_1,x_2,x_3,x_4,x_5]\{(x-x_2)(x-x_3)(x-x_4)+(x-x_1)\frac{d}{dx}(x-x_2)(x-x_3)(x-x_4)$$
$$+ \ldots.$$

Evaluation of this expression at x_1 has the effect of making the last term zero in each of the curly brackets, since they all are proportional to $(x-x_1)$. The terms remaining have a very simple form, namely

$$\frac{\hat{df}}{dx} = [x_1,x_2] + [x_1,x_2,x_3](x_1-x_2) + [x_1,x_2,x_3,x_4](x_1-x_2)(x_1-x_3)$$
$$+ [x_1,x_2,x_3,x_4,x_5](x_1-x_2)(x_1-x_3)(x_1-x_4) + \ldots.$$

This is more general than it seems, because the designation of points is arbitrary here as in the case of interpolation.

Numerical differentiation by such formulae is not an entirely reliable procedure, even when the f_i are accurately known. As a general rule, it is safer to interpolate on a table of values of $\hat{f}'(x)$ than to use a formula such as (I-35.1).

c) Numerical integration. If $\underline{T}$ (I-33.7) is the integral operator $\int_{-\Delta}^{\Delta} dx$, and if the x_i are assigned the values

$$x_1 = \Delta,$$

$$x_2 = 0,$$

$$x_3 = \Delta,$$

evaluation of (I-33.7) gives

$$\int_{-\Delta}^{\Delta} dx \hat{f}(x) = \sum_{i=1}^{3} f_i w_i, \qquad \text{(I-35.1)}$$

where $w_1 = w_3 = \frac{\Delta}{3}$, and $w_2 = \frac{4\Delta}{3}$. This rule dates back to Kepler, and has gone by many names, among them "Kepler's barrel rule".

Extension of this rule to weights for an even number of equal intervals, bounded by an odd number of points, is straightforward. One applies the barrel rule many times and adds the weights which apply to the same point, as indicated in the diagram of Fig. I-35.1.

Fig. I-35.1. Multiple application of the barrel rule.

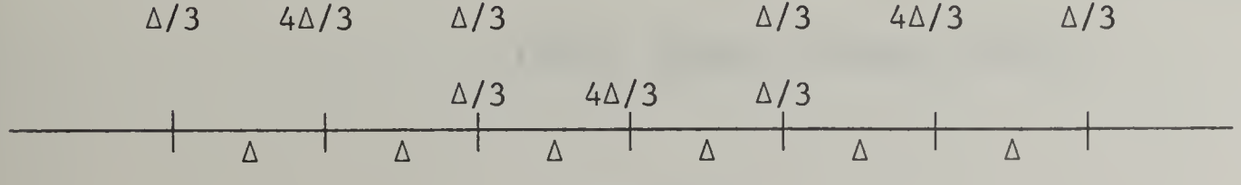

The resulting set of weights,

$$(\Delta/3,\ 4\Delta/3,\ 2\Delta/3,\ 4\Delta/3,\ 2\Delta/3,\ 4\Delta/3,\ \Delta/3)$$

is most commonly called Simpson's rule.

Simpson's rule has proved extremely useful in machine calculations, because it is both accurate and simple. Often in complicated calculations it is better to use such a simple method in preference to a more sophisticated procedure because of the advantage of stability.

Most of the gamma ray moment computations have used Simpson's rule. But in the evaluation of the scattering integral the number of points may be either even or odd. Simpson's rule, as usually presented, only applies to half the integrals; for the others it is necessary to make a modification. To preserve both the symmetry of the sequence of weights and the accuracy of Simpson's rule, the following device has been adopted: When the number of points is four or greater, and even, the middle four points are approximated by a cubic, which is then integrated over the middle interval only. The resulting weights can be ascertained from a four-point version of Eq. (I-33.7) by the assignments

$$T = \int_{-\Delta/2}^{\Delta/2} dx$$

$$x_4 = -x_1 = 3\Delta/2,$$

$$x_3 = -x_2 = \Delta/2.$$

The weights which are obtained by this calculation turn out to be

$$(-\Delta/24,\ 13\Delta/24,\ 13\Delta/24,\ -\Delta/24).$$

Our final set of modified weights is obtained by applying Simpson's rule symmetrically from both left and right. When the number of integration points is divisible by four, the correction weights are subtracted as shown in the diagram of Fig. I-35.2 below.

Fig. I-35.2. Modified Simpson rule, number of points divisible by four.

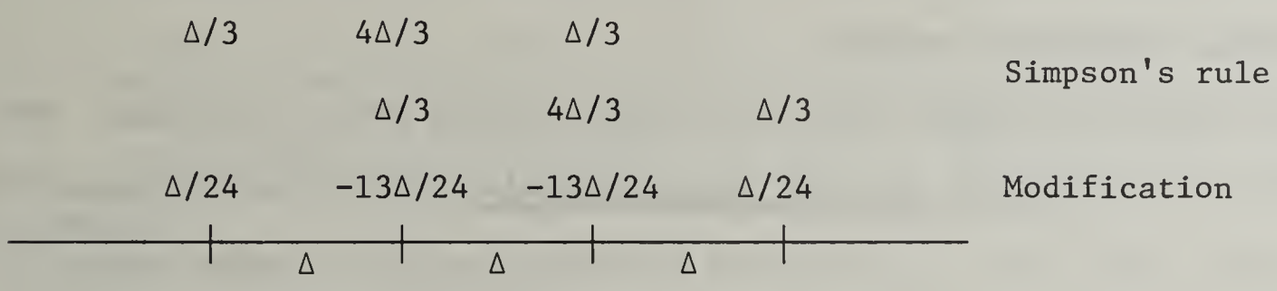

When the number of integration points is even, but is not divisible by four, the same procedure applies, but in this case the correction weights are added instead of subtracted, as shown in Fig. I-35.3.

Fig. I-35.3. Modified Simpson rule, number of points not divisible by four.

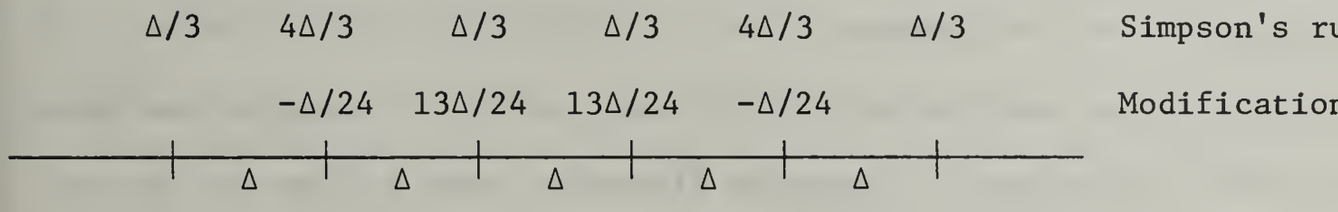

For desk calculations, alternative modifications of Simpson's rule exist which are more easily remembered. But for machine calculations, this leads to a fast, reliable subroutine for numerical integration.

36. Utility Subroutines.

As part of the Summer Institute, the participants constructed a number of elementary machine programs. One of these programs was a determinant evaluator, based on the method of pivotal condensation. Another program, written by Mr. V. Cain, was an interpolation routine. Still other programs required numerical integration; and a subroutine was made available for calculating integration weights.

The WALLSTREET program uses two utility subroutines in addition. One of these is a very quick, but not highly accurate, subroutine for logarithm computation. The other is a fast and extremely versatile random number generator. This last subroutine is the only one of the five which is not in FØRTRAN; it is in machine language.

In this section we present these subroutines, each accompanied by a discussion of the intent of the various orders.

a) Interpolation. The subroutine INTRP, written by Mr. Cain, can utilize an arbitrary number of points. It features the Gauss arrangement in which additional points are on alternate sides of the point of interpolation. If the interpolation is near one end of the table, after the endpoint has been used additional points are no longer on alternate sides but are all on the side of the point of interpolation away from the endpoint.

Approximation is by polynomials of degree appropriate to the number of points used. A check is made early to ensure that the interpolation calls for no more points than are available.

```
C     *     *     *     *     *     *     *     *
      SUBRØUTINE INTRP(IMAX,X,F,NPTS,VAR,SØM)
      DIMENSIØN X(50),F(50),XN(7),FN(7)
```

We assume at this point that all input numbers and lists are defined. IMAX is the length of the list on which interpolation is being made. X(I) is the abscissa list for interpolation and F(I) is the ordinate list. NPTS is the number of points in the list used for interpolation;

thus NPTS = 3 would refer to a 3-point interpolation. VAR is the entry value into the X list at which an interpolated F value is desired. SØM is the desired F value. According to the dimension statement lists up to 50 entries can be used, with up to 7 point interpolation.

```
894 IF (IMAX-1) 294,304,314
294 SØM=0.
    GØ TØ 324
304 SØM=F(1)
    GØ TØ 324
```

These introductory orders take care of lists containing either one entry or zero entries, i.e. eccentrically short. A list with zero entries gives a zero interpolated value, while a list with one entry gives an interpolated value equal to the sole entry. Note that order number 324 concludes subroutine control.

```
314 NPT=NPTS
    IF (NPTS - IMAX) 234,214,214
214 NPT = IMAX
```

If the interpolation list is shorter than the number of interpolation points intended, the latter is reduced to correspond exactly to the number of points available.

```
234 XØ=ABSF(VAR-X(1))
```

The important thing here is the necessity for starting XØ with a value as large as VAR-X(1) in magnitude. The next little loop selects the value of X(I) nearest to VAR. When |VAR-X(I)| starts to increase, we transfer out of the loop with IP and XØ referring to the smallest difference.

```
    IP=1
    DØ 84 I=2,IMAX
    A=ABSF(VAR-X(I))
    IF (A-XØ) 74,64,64
 74 IP=I
    XØ=A
 84 CØNTINUE
 64 IF(ABSF(X(IP)-X(IP+1))-ABSF(VAR-X(IP+1)))54,554,254
```

We must find out whether VAR is between X(IP) and X(IP+1) or between X(IP-1) and X(IP).

```
554 SØM=F(IP)
    GØ TØ 324
```

If VAR=X(IP) we are done.

```
 54 IN=-1
    GØ TØ 354
```

```
254 IN=1
354 DØ 164 I=1,NPT
```

The integer IN oscillates between +1 and -1. This loop is to order the points used for interpolation in the XN and FN lists. The Gauss ordering is used, with points taken alternately on each side of the entry, and increasingly far from the interpolation point. In the original version of the subroutine, convergence was examined and interpolation occurred with prespecified accuracy. In this version, the Gauss ordering is irrelevant because all points are used.

```
    XN(I)= X(IP)
    FN(I)= F(IP)
    IF(IN) 94,94,104
 94 IQ=IP-I
    GØ TØ 134
104 IQ=IP+I
```

This set of orders is designed to yield a new value for IP, which is the index of the next pair of values to be put into the XN and FN lists for use in the interpolation. A positive IN increases IP by I, while a negative I decreases IP by I, in the normal case. Note that IP will normally be equated to IQ.

```
114 IF (IMAX-IQ) 124,134,134
124 IP=IP-1
    GØ TØ 164
134 IF (IQ) 144,144,154
144 IP=IP+1
    GØ TØ 164
154 IP=IQ
    IN=-IN
164 CØNTINUE
```

In abnormal cases, when the interpolation is performed near the end of the list, the index values normally determined may be unacceptable. Hence orders 114 and 124 decrease IP by unity if IMAX would otherwise be exceeded, while 134, 144 increase IP by unity if IP-I would otherwise be zero or negative. Once the end of the list has been reached, all further IP values must be taken in the other direction. Note that 164 is the CØNTINUE statement which ends the loop, so that the sign of IN is unchanged after one end of the list has been encountered. Normally, 164 would be reached through 154.

```
    SØM=FN(1)
    FACT=1.
```

SØM is the cell in which the answer is to be cumulated. FACT is to be a product of (VAR-X(I)) factors multiplying the divided differences

```
    DØ 184 J=2,NPT
```

```
      DØ 174 I=J,NPT
      IQ=I-J+1
  174 FN(IQ)=(FN(IQ+1)-FN(IQ))/(XN(I)-XN(IQ))
```

This loop calculates the next set of divided differences and stores them in FN(1), FN(2), etc. Thus FN(1) always contains the divided difference next to contribute to SØM.

```
      FACT=FACT*(VAR-XN(J-1))
  184 SØM=SØM+FN(1)*FACT
  324 RETURN
      END
C     *     *     *     *     *     *     *     *
```

b) Integration (IWATE). The subroutine which we give here constructs a list of integration weights for two cases, equally spaced points and points whose logarithms are equally spaced. In the latter case, the points are obtained from one another by successive multiplications by a fixed factor.

The procedure is that of Simpson's rule, modified as discussed in the preceding section when the number of points is even. When integration weights for only two points are to be calculated, the trapezoidal rule is applied, while for one point integration the weight is made equal to zero.

The subroutine assumes that the computer rounds off numbers downward when an integer value is assigned to a floating point number.

```
C     *     *     *     *     *     *     *     *

      SUBRØUTINE IWATE(IWT,NWT,WTAB,WATES)
      DIMENSIØN WTAB(300),WATES(300)
```

WTAB is here the abscissa list for which integration weights are to be determined, while WATES is the list of integration weights to be determined. Both lists have NWT entries, where NWT may be any number up to 300. If IWT=1, the entries in the WTAB list are equally spaced, while if IWT=2, the entries in the WTAB list are in constant ratio with one another.

```
  819 WTA=NWT
```

This order constructs a floating point version of NWT.

```
      IF(NWT-2) 19,39,39
   19 WATES(1)=0.
      GØ TØ 259
```

These orders take care of the case in which the list consists of a single value only. Order number 259 concludes control by this subroutine.

```
 39 IF (IWT-2) 59,79,79
 59 WTDEL=(WTAB(1)-WTAB(NWT))/(WTA-1.)
    GØ TØ 99
```

The first order determines whether the list progression is linear or geometric. The second calculates the interval between points of the list for the linear case. (One could also difference successive values.)

```
 79 WTDEL=LØGF(WTAB(1)/WTAB(NWT))/(WTA-1.)
 99 IF(WTDEL) 119,990,990
119 WTDEL=-WTDEL
```

The first order calculates the logarithm of the factor between points if the interval changes geometrically. The last two orders make the interval size positive in all cases. This may or may not be advantageous; it has the effect of producing a list of weights which is always positive.

```
990 IF (NWT-2) 259,1190,139
1190 WATES(1)=.5*WTDEL
     WATES(2)=WATES(1)
     GØ TØ 199
```

This takes care of the case in which only two points are involved in the integration, which then is performed by the trapezoidal rule. The distinction between linear and geometric progression is made following order 199.

```
139 NWTA=(WTA/2.+.1)
    NWTB=(WTA/2.-.1)
    NWTC=(WTA/4.+.1)
    NWTD=(WTA/4.-.1)
```

These four orders generate parameters to be used in determining whether the number of weights is odd, divisible by 4, or even. WTA is numerically equal to NWT; and recall that we assume the integer obtained in these calculations to be always less than or equal to the floating point number. Then if NWT is divisible by 2, NWTA will be larger than NWTB by unity. Likewise, if NWT is divisible by 4, NWTC will be larger than NWTD by unity.

```
    WATES(1)=WTDEL/3.
    WTC=WATES(1)
    WATES(NWT)=WATES(1)
```

```
      DØ 159 I=1,NWTB
      WATES(I+1)=WTDEL+WTC
      INDX=NWT-I
      WATES(INDX)=WTDEL+WTC
  159 WTC=-WTC
```

This group of orders assigns the bulk of the weights their 1,4,2,4,... structure. Notice the symmetry between WATES(I+1) and WATES(NWT-I). NWTB will be either the middle value or the lower of two middle values. In the latter case, the middle interval has not been properly treated, and the middle weights need a correction. The middle two weights are then either 2.*WTDEL/3., when the number of points is <u>not</u> divisible by 4, or 4.*WTDEL/3., when NWT is divisible by 4.

```
      WTD=1./24.
      IF (NWTC-NWTD) 1790,1790,1590
 1590 WTD=-WTD
```

The first order establishes the divisor for the middle interval correction, and the other two orders determine the sign of the correction.

```
 1790 IF (NWTA-NWTB)  199,199,179
  179 WATES(NWTB)=WATES(NWTB)-WTD*WTDEL
      WATES(NWTB+1)=WATES(NWTB+1)+5.*WTD*WTDEL
      WATES(NWTB+3)=WATES(NWTB)
      WATES(NWTB+2)=WATES(NWTB+1)
```

Note that when NWTC=NWTD and NWTA=NWTB no correction is required. When the former is true but not the latter, the middle points are corrected by (Δ/24,-13Δ/24+Δ/3,-13Δ/24+Δ/3,Δ/24). When neither is true, the correction changes sign.

```
  199 IF (IWT-2) 259,219,219
  219 DØ 239 I=1,NWT
  239 WATES(1)=WATES(I)*WTAB(I)
```

These orders multiply the weights by the abscissa values, for the case in which the points are geometrically spaced.

```
  259 RETURN
C     *     *     *     *     *     *     *     *
```

Perhaps more frequently the integral, rather than the weights, is desired. The calculation of weights has two advantages here: In the evaluation of Volterra integral equations numerically, the final integration weight enters the expressions explicitly. Further, in the linked system of moment equations it is frequently desirable to perform many similar integrals with identical sets of weights.

c) Determinant Evaluation (DET). Participants in the Summer Institute were asked to construct a program for evaluation of a determinant, as an exercise in machine programming. The subroutine given here is typical of those which were devised by the participants.

The method used is pivotal condensation, using as a pivot element the corner with maximum indices.

```
C     *     *     *     *     *     *     *
      SUBRØUTINE DET(N,A,PRØD)
      DIMENSIØN A(14,14)
      K=N
      IF(N) 135,135,2
```

N is the number of rows and columns in the determinant. PRØD is the value of the determinant. The first order preserves the value of N, which can then record the reduced size of the determinant. We then guard against an accidental case in which N=0.

```
    2 PRØD=1.
    4 IF(A(N,N)) 60,140,60
```

The pivot element must not be zero. The following double loop is the main calculation, which reduces the order of the determinant by one, using pivotal condensation.

```
   60 DØ 100 I=1,N
      IF(A(I,N)) 70,100,70
   70 PRØD=PRØD*A(I,N)
      DØ 90 J=1,N
   90 A(I,J)=A(I,J)/A(I,N)-A(N,J)/A(N,N)
  100 CØNTINUE
      N=N-1
      IF(N-1) 125,150,4
```

Exit from the subroutine occurs when N=1, ordinarily. The next DØ loop interchanges rows when the pivot element is zero.

```
  140 DØ 130 I=1,N
      IF(A(I,N)) 145,130,145
  145 PRØD=PRØD*(-1.)**(N-I)
      DØ 148 J=1,N
      B=A(N,J)
      A(N,J)=A(I,J)
  148 A(I,J)=B
      GØ TØ 60
  130 CØNTINUE

          If all elements in the last column are zero, the value
          of the determinant is zero.

  135 PRØD=0.
      GØ TØ 125
  150 PRØD= PRØD*A(1,1)
  125 N=K
      RETURN
      END
C     *     *     *     *     *     *     *     *
```

d) RANDA, RANDB, RANDC, RANDD.

This simple, fast pseudo-random number generator has been used by Dr. M. J. Berger in many Monte Carlo programs. Several entries are provided to permit correlated sampling applications, and different multipliers are used for the four different calling identifications.

The most common procedure for use of this routine entails the generation of random numbers by RANDC, say, which initiate random number sequences obtained by calling RANDB or RANDA. Thus, RANDC may provide the first random number in

the sequence required for a given case history. Then, for a new case history, RANDC would provide a new initial random number.

Current information on the speed of this routine indicates that on the IBM 7094, it will produce approximately a million pseudo-random numbers per minute.

```
        FAP
```

The FAP and END statements are subroutine assembly orders, appropriate to FORTRAN II.

```
        REM  CALL RANDA(IR,R), CALL RANDB(IR,R), CALL RANDC(IR,R) CALL RANDD(IR,R)
```

This is a comment card, which doesn't do anything.

```
        ENTRY   RANDA
        ENTRY   RANDB
        ENTRY   RANDC
        ENTRY   RANDD
```

These orders apply to both FAP and MAP systems, and identify the first order of the subroutine.

```
RANDA   CLA     MULT
        TRA     *+6
```

Pick up the number in the cell MULT and transfer to the 6'th order beyond this TRA.

```
RANDB   CLA     MULT+1
        TRA     *+4
```

Pick up the number in the cell just beyond MULT, and transfer to the 4th order beyond this TRA.

```
RANDC   CLA     MULT+2
        TRA     *+2
RANDD   CLA     MULT+3
        STØ     TEMP
```

All these sets of orders have the purpose of putting the appropriate multiplier in TEMP.

```
        LDQ*    1,4
```

This locates the value of the octal integer IR, and loads it into the MQ register. (Indirect addressing is used, as indicated by the asterisk.)

```
      MPY     TEMP
      STQ*    1,4
```

Stores the product of IR and TEMP back in IR. The product is still in AC and MQ registers.

```
      PXD
```

This places zero in the sign bit and 35 accumulater bits, thus destroying the 35 most significant bits of the product.

```
      LLS     27
```

The remaining 36 bits in the MQ register are shifted left 27 places into the accumulater, so that they occupy positions 9-35 of the mantissa of a floating point number.

```
      ADD     *+4
```

Puts the octal number 200 in the characteristic (the exponent) of the floating point number; note that exponents are plus or minus relative to this number. (The Binary bits in positions 1-8 are now 01000000.)

```
      FAD     *+3
```

Note that this number is actually the floating point zero. This operation "normalizes" the number being constructed, introducing a one in bit position 9.

```
      STØ*    2,4
      TRA     3,4
```

These orders are correct for FAP. The MAP equivalents would be STØ* 4,4 and TRA 1,4. The floating point number just constructed is stored in the cell reserved for R, which lies just beyond the IR cell. The transfer order is to the appropriate location to send control back to the calling program.

```
      OCT     200000000000
MULT  OCT     343277244615
      OCT     011060471625
      OCT     000272207335
      OCT     000007346545
```

The last four numbers are 5^{15}, 5^{13}, 5^{11}, and 5^{9}, which are the multipliers for RANDA, RANDB, RANDC, and RANDD respectively. The next order reserves one cell for temporary storage.

```
TEMP  BSS     1
      END
```

e) "Quick" Logarithms (QLØG).

This subroutine is a Quick LOGarithm calculater, for determination of path lengths in Monte Carlo penetration calculations. It uses table look-up. Because accuracy is sacrificed for speed, this subroutine is not generally applicable to calculation of logarithms.

A table of logarithms is generated for arguments from 0.2 to 0.6. If the argument desired, presumably a random number ρ between zero and unity, falls between 0.2 and 0.6, the table look-up is straightforward. If the argument is greater than 0.6 the subroutine calculates

$$\log(.6\rho) - \log.6.$$

If the argument is less than 0.2, and a factor 3^N is sufficient to give $0.2 \leq 3^N\rho \leq .6$, the subroutine calculates

$$\log(3^N\rho) - N\log 3.$$

Over much of the range of arguments, the accuracy is a few tenths of a percent. The accuracy is better than this for very small ρ because N(log3) is quite accurate; and the accuracy is very poor for $\rho \lesssim 1$. Because this region of poor accuracy is associated with very small path lengths, it is of small concern usually. In any case, it would be simple to improve the accuracy of the whole routine by adding a linear interpolation; but this doesn't appear to be warranted for WALLSTREET.

```
C     *     *     *     *     *     *
      SUBRØUTINE QLØG(X,XL,NLTAB)
      DIMENSIØN XBL(400)
```

Our first concern is with the generation of the basic table.

This will occur when NLTAB=1. When NLTAB=2, the tabulation will be skipped, as is shown in the first order.

```
   GØ TØ (10,30),NLTAB
10 XB=.1995
   DØ 20 I=1,400
   XB=XB+.001
20 XBL(I)=LØGF(XB)
```

Having generated the table, we change NLTAB to 2, so that the additional calls upon QLØG will skip the preceding.

```
   NTAB=2
30 XB=X
   IF(XB-.6) 50,40,40
```

If XB (i.e.X) is greater than 0.6, we reduce the value by multiplying by 0.6, and prepare to add XL=-log .6=.51083.

```
40 XB=XB*.6
   XL=.51083
   GØ TØ 80
```

If XB < .6, we start XL at zero and then cycle to see how many factors of 3 are required to raise XB beyond .2. Note that 1.09861=log3.

```
50 XL=0.
60 IF(XB-.2) 70,70,80
70 XB=XB*3.
   XL=XL-1.09861
   GØ TØ 60
```

When XB is large enough, the table look-up is performed and the result modified by XL. The first order generates the index for the table look-up.

```
80 I=XFIXF(1000.*XB)
   XL=XL+XBL(I-199)
```

Note that the smallest value of 1000.*XB is 200, but that the index of the logarithm of .2005 is 1; hence subtraction of 199.

```
   RETURN
   END
C     *     *     *     *     *     *     *
```

37. Polynomial Approximation using Moments of a Function

In section 33 we discussed the approximation of a function from a set of numerical values. Here we discuss the analogous problem of approximation of a function from a different set of numerical parameters, the moments, by which we will mean integrals of a function f(z) of the form

$$f_n = \int_R dz\ z^n f(z), \qquad \text{(I-37.1)}$$

where R refers to the range of integration, which may be finite, semi-infinite, or infinite. Our discussion features moments, as just defined, but it is applicable to cases in which other types of numerical parameters are known.

Suppose that we do not know f(z), but that we have values for a finite number of the f_n. Our problem is to obtain an approximation $\hat{f}(z)$ which has the same moments, and which agrees with f(z) in all known characteristic features.

Our first step in obtaining an approximation is that of identifying a suitable "weight function", w(z), whose moments will be designated

$$w_n = \int_R dz\ z^n w(z). \qquad \text{(I-37.2)}$$

The characteristics of a good weight function should be the subject of more study than has taken place to date. Our point of view here is that a good weight function is a simple (uncomplicated) function which, on multiplication by a polynomial of low degree, can agree with f(x) in regards to a) singular features, such as discontinuities, b) trends such as the behavior of f(z) for large $|z|$ or for z near the limits of R, and c) maxima and minima.

We assume that f(z) can be approximated by a function $\hat{f}(z)$ of the form

$$\hat{f}(z) = (a + bz + cz^2)w(z). \qquad \text{(I-37.3)}$$

Three terms are employed here for the same reason as in section 33 : The equations can be quickly written, while the generalization to more or fewer terms is apparent.

If we multiply all terms of Eq. (I-37.3) by z^n and integrate over R, we obtain equations connecting the moments of $\hat{f}(z)$ with the moments of the weight function. We require that $\hat{f}(z)$ agree with f(z) in that three moments of both functions are identically the same, and so obtain the set of equations

$$f_n = aw_n + bw_{n+1} + cw_{n+2}, \; n = n_1, n_2, n_3. \qquad \text{(I-37.4)}$$

While we are at liberty to choose any three such equations to use in determining the constants a, b, and c, we would usually select the first three, n = 0, 1, 2. Rearranging, and adding Eq. (I-37.3), we obtain the set of equations

$$\begin{aligned}
&-\hat{f}(z) + aw(z) + bzw(z) + cz^2w(z) = 0 \\
&-f_0 \quad + aw_0 \quad + bw_1 \quad + cw_2 \quad = 0 \\
&-f_1 \quad + aw_1 \quad + bw_2 \quad + cw_3 \quad = 0 \\
&-f_2 \quad + aw_2 \quad + bw_3 \quad + cw_4 \quad = 0
\end{aligned} \qquad \text{(I-37.4)}$$

which are identical in form to the equation (I-37.3). Clearly, the solution to Eqs. (I-37.4) are given by

$$\begin{vmatrix}
\hat{f}(z) & w(z) & zw(z) & z^2w(z) \\
f_0 & w_0 & w_1 & w_2 \\
f_1 & w_1 & w_2 & w_3 \\
f_2 & w_2 & w_3 & w_4
\end{vmatrix} = 0. \qquad \text{(I-37.5)}$$

Expansion by minors of the top row will yield an equation for $\hat{f}(z)$ in terms of w(z) multiplied by a quadratic polynomial in $\underline{z}$, which is the representation we seek.

The calculation just described is closely similar to the earlier calculation in which a function was approximated by use of a simple form which agreed at three points. As a matter of fact, we have actually approximated a moment "curve" at three points and then made a type of inverse "Mellin" transformation to obtain $\hat{f}(z)$ from the approximate moment "curve".

The approximation just obtained is a best approximation in a least square error sense. To demonstrate this, we consider the following integral:

$$E = \int_R dz w(z) \left[f(z)/w(z) - (a_0 + a_1 z + a_2 z^2)\right]^2 = \int_R dz \frac{f^2(z)}{w(z)} - 2 \sum_{i=0}^{2} a_i f_i + \sum_{i=0}^{2} \sum_{j=0}^{2} a_i a_j w_{i+j} , \qquad \text{(I-37.6)}$$

where the constants are yet to be specified. If we minimize E with respect to variations in all three constants we obtain the equations

$$\frac{\partial E}{\partial a_n} = -2f_n + 2 \sum_{i=0}^{2} a_i w_{i+n} = 0, \quad n=0, 1, 2. \qquad \text{(I-37.7)}$$

If we write out these equations, and add to them the equation

$$\hat{f}(z) = (a_0 + a_1 z + a_2 z^2) w(z) , \qquad \text{(I-37.8)}$$

we obtain equations for the numerical coefficients which are precisely the same as Eqs. (I-37.4).

38. Generalized Approximations and Biorthogonal Functions

a) Generalized Approximations.

Before going into specific problems of distribution construction using moments, we will generalize the discussion of the preceding section; and in the process we hope to mention a few things not generally realized, particularly about biorthogonal functions.

Let us first introduce a standard terminology for the following integral over the range R of two functions of the real variable z:

$$(u,v) = \int_R dz\, u(z)\, \overline{v}(z). \tag{I-38.1}$$

The quantity (u,v) is referred to as the "inner product" of the two functions u(z) and v(z).* The functions u and v are said to be "orthogonal" if

$$(u,v) = 0. \tag{I-38.2}$$

Properties of the inner product are

$$\begin{aligned} (u, v_1 + v_2) &= (u,v_1) + (u,v_2), \\ (u_1 + u_2, v) &= (u_1,v) + (u_2,v), \\ (u,cv) &= (\overline{c}u,v) = \overline{c}(u,v). \end{aligned} \tag{I-38.3}$$

Next, suppose that the function F(z) is not known, but that we have values for a few integrals, (u_1,F), (u_2,F), etc. Further, we know enough about F(z) to determine that it should be representable with fair accuracy by a sum of terms,

*Note that all the functions which we will consider are real, so that $\overline{v} = v$, and, in Equation (I-38.3), $\overline{c} = c$.

$$\hat{F}(z) = a_0 v_0(z) + a_1 v_1(z) + a_2 v_2(z). \qquad \text{(I-38.4)}$$

Clearly,

$$(u_n, \hat{F}) = a_0(u_n, v_0) + a_1(u_n, v_1) + a_2(u_n, v_2). \qquad \text{(I-38.5)}$$

If we require that the approximate funtion, $\hat{F}(z)$, be such that

$$(u_n, \hat{F}) = (u_n, F), \; n = 0,1,2, \qquad \text{(I-38.6)}$$

we obtain three conditions, which, together with Eq. (I-38.4) form the system

$$\begin{aligned}
&-\hat{F}(z) + a_0 v_0 + a_1 v_1 + a_2 v_2 = 0, \\
&-(u_0, F) + a_0(u_0, v_0) + a_1(u_0, v_1) + a_2(u_0, v_2) = 0, \\
&-(u_1, F) + a_0(u_1, v_0) + a_1(u_1, v_1) + a_2(u_1, v_2) = 0, \\
&-(u_2, F) + a_0(u_2, v_0) + a_1(u_2, v_1) + a_2(u_2, v_2) = 0. \qquad \text{(I-38.7)}
\end{aligned}$$

This system has a solution which by now should be transparent, because of the special cases, (I-38.3) and (I-38.5), already considered:

$$\begin{vmatrix}
\hat{F} & v_0 & v_1 & v_2 \\
(u_0, F) & (u_0, v_0) & (u_0, v_1) & (u_0, v_2) \\
(u_1, F) & (u_1, v_0) & (u_1, v_1) & (u_1, v_2) \\
(u_2, F) & (u_2, v_0) & (u_2, v_1) & (u_2, v_2)
\end{vmatrix} = 0. \qquad \text{(I-38.8)}$$

b) Biorthogonal Functions*.

Up to this point we have been considering both the u_i's and the v_i's to be completely arbitrary; and the preceding result holds regardless of our choice

*General references on biorthogonal functions are scarce, as is the literature. Perhaps the most complete is Ref. 162.

of function types. But from this point on, we will regard both sets of these functions as elementary in the sense of a series of powers, z^i, and will refer to them as "base functions".

We now wish to consider two sets of functions, $p_n(z)$, $q_n(z)$, n=1,2,..., with the property of <u>biorthogonality</u>, namely,

$$(q_i,p_j) = 0, \quad i \neq j. \tag{I-38.9}$$

We will shortly consider very general methods for developing sets of functions with this property. At present, we assume that these functions are finite linear combinations of our base functions, so that there exist constants p_{ni}, q_{ni} such that

$$q_n = \sum_{i=0}^{n} q_{ni} u_i,$$

$$p_n = \sum_{i=0}^{n} p_{ni} v_i. \tag{I-38.10}$$

Note that these linear representations imply the existence of the inverse relationships, that is, the existence of constants u_{ni}, v_{ni} such that

$$u_n = \sum_{i=0}^{n} u_{ni} q_i,$$

$$v_n = \sum_{i=0}^{n} v_{ni} p_i. \tag{I-38.11}$$

These can be obtained, for example, by simultaneous solution of the first <u>n</u> equations from each set in (I-38.10), with the u_i's and v_i's as unknowns.

Next, consider two indices, <u>m</u> and <u>n</u>, with <u>m</u>≤<u>n</u>. The values of the two inner products, (q_n,v_m) and (u_m,p_n), are very useful to know and easily calculated

$$(q_n,v_m) = (q_n, \sum_{i=0}^{m} v_{mi} p_i) = \sum_{i=0}^{m} v_{mi} (q_n,p_i) = 0, \tag{I-38.12}$$

$$(u_m,p_n) = \left(\sum_{i=0}^{m} u_{mi}q_i,p_n\right) = \sum_{i=0}^{m} u_{mi}(q_i,p_n) = 0. \qquad \text{(I-38.12')}$$

In each case the result follows because $i \leq m < n$. This property can be used to construct biorthogonal sets of functions. For example, the first set of equations in (I-38.12) represents a set of n conditions on the function q_n, which has (n+1) constants. These conditions determine all ratios of these constants to one another. Only a normalization constant is not fixed.

The two biorthogonal sets will be referred to as "bi-ortho-normal" if, in addition to (I-38.9), we have

$$(q_n,p_n) = 1. \qquad \text{(I-38.13)}$$

Since two normalization constants are to be determined, one each for p_n and q_n, this last condition does not establish both. Thus, if (I-38.13) holds, so also does

$$(\xi_n q_n, \xi_n^{-1} p_n) = 1 . \qquad \text{(I-38.14)}$$

To close this discussion, let us refer back to (I-38.8) while recalling that this expression was written without restrictions on the nature of the functions. We may therefore apply it to the biorthogonal functions, as follows:

$$\begin{vmatrix} \hat{F} & p_0 & p_1 & p_2 \\ (q_0,F) & (q_0,p_0) & (q_0,p_1) & (q_0,p_1) \\ (q_1,F) & (q_1,p_0) & (q_1,p_1) & (q_1,p_2) \\ (q_2,F) & (q_2,p_0) & (q_2,p_1) & (q_2,p_2) \end{vmatrix} = \begin{vmatrix} \hat{F} & p_0 & p_1 & p_2 \\ (q_0,F) & (q_0,p_0) & 0 & 0 \\ (q_1,F) & 0 & (q_1,p_1) & 0 \\ (q_2,F) & 0 & 0 & (q_2,p_2) \end{vmatrix} = 0. \qquad \text{(I-38.15)}$$

Evaluation of the determinant equation gives the simple result,

$$\hat{F}(z) = \sum_{i=0}^{2} \frac{(q_i,F)}{(q_i,p_i)} p_i(z) \ . \qquad \text{(I-38.16)}$$

This is equivalent to the more complicated expression which would be obtained if (I-38.8) were evaluated using the base functions u_i and v_i for the p_n and q_n. One can start with either expression for $\hat{F}(z)$ and obtain the other by substitution using (I-38.10) or (I-38.11).

c) Adjoint Operators: Application to Deep Penetration Equations.

If, for arbitrary functions f and g whose inner product exists one can find two operators, $\emptyset$ and $\emptyset^\dagger$ which have the property

$$(g,\emptyset f) = (\emptyset^\dagger g, f) \ , \qquad \text{(I-38.17)}$$

we say that the operators $\emptyset, \emptyset^\dagger$ are adjoint. The eigenvalues of $\emptyset^\dagger$ are the complex conjugates of the eigenvalues of $\emptyset$, and if the eigenvalues of $\emptyset$ are real, they are equal to the eigenvalues of $\emptyset^\dagger$. The eigenfunctions of $\emptyset^\dagger$ and $\emptyset$ which correspond to the same eigenvalue (or eigenvalues which are complex conjugates) are said to be adjoint eigenfunctions.

These definitions have an elementary illustration using finite sets of biorthogonal functions. If we write

$$\emptyset f = \sum_{i=0}^{N} (q_i,f) p_i = \hat{f}_N \ ,$$

$$\emptyset^\dagger g = \sum_{i=0}^{N} (g,p_i) q_i \ , \qquad \text{(I-38.18)}$$

it is quite clear that $\emptyset$ and $\emptyset^\dagger$ satisfy the condition (I-38.17). The eigenfunctions of $\emptyset$ are clearly the p_i; the eigenfunctions of $\emptyset^\dagger$ are the

q_i; and the eigenvalues of both operators are (q_i, p_i).

In section 21 there is an illustration of this concept. Here the operator is

$$\emptyset = \{\dot{\mu}_0 \frac{s}{2} \frac{d}{ds} - \frac{\mu_0}{2} \frac{1}{s} \frac{d}{ds} s \frac{d}{ds} - Ce^{-s^2/2}\} \qquad \text{(I-38.19)}$$

Since the inner product is here the integral

$$(g, \emptyset f) = \int_0^\infty sds\, g\, \emptyset f \ ,$$

we obtain the adjoint operator by integration by parts. It turns out to be

$$\emptyset^\dagger = \{-\frac{\dot{\mu}_0}{2} \frac{1}{s} \frac{d}{ds} s^2 - \frac{\mu_0}{2} \frac{1}{s} \frac{d}{ds} s \frac{d}{ds} - Ce^{-s^2/2}\} \ . \qquad \text{(I-38.20)}$$

In this case it is a simple matter to modify the differential operator (I-38.19) to obtain a related "self-adjoint" operator with the same eigenvalues and closely related eigenfunctions. Calculations are then somewhat easier and more efficient than is the case with the two operators (I-38.19) and (I-38.20).[14/]

39. Construction of Biorthogonal Functions

There are many ways to generate biorthogonal functions. The best-known process, that due to Schmidt, will be given last here, simply because it is most available in the literature.* The most practical process, when it works, is by recursion; and one could view the Schmidt process as a general example of this. Simple recursion formulae exist only for particularly elementary systems; and we wish here to stress the more general procedures. Hence there will be no discussion of specialized recursion formulae.

a) General Formula.

It is possible to write down general expressions for functions with the biorthogonality property. Consider, for example,

$$p_2(z) = c \begin{vmatrix} v_0(z) & v_1(z) & v_2(z) \\ (u_0,v_0) & (u_0,v_1) & (u_0,v_2) \\ (u_1,v_0) & (u_1,v_1) & (u_1,v_2) \end{vmatrix}. \qquad \text{(I-39.1)}$$

Clearly, for i = 1,2 we may write

$$(u_i,p_2) = c \begin{vmatrix} (u_i,v_0) & (u_i,v_1) & (u_i,v_2) \\ (u_0,v_0) & (u_0,v_1) & (u_0,v_2) \\ (u_1,v_0) & (u_1,v_1) & (u_1,v_2) \end{vmatrix} = 0, \qquad \text{(I-39.2)}$$

since two rows of the determinant are identical. Since the function $p_2(z)$ is a linear combination of v_0, v_1, and v_2, it must be proportional to the corresponding member of the biorthogonal set p_n discussed in the preceding section. The normalization constant can be calculated directly, if the function $q_2(z)$ has already been determined. We have

*An informative reference on biorthogonal functions which includes this is Ref. 146.

$$(q_2,p_2) = 1 = c \begin{vmatrix} (q_2,v_0) & (q_2,v_1) & (q_2,v_2) \\ (u_0,v_0) & (u_0,v_1) & (u_0,v_2) \\ (u_1,v_0) & (u_1,v_1) & (u_1,v_2) \end{vmatrix} = c \begin{vmatrix} 0 & 0 & (q_2,v_2) \\ (u_0,v_0) & (u_0,v_1) & (u_0,v_2) \\ (u_1,v_0) & (u_1,v_1) & (u_1,v_2) \end{vmatrix},$$

so that

$$c = \frac{1}{(q_2,v_2)D^{(1)}}, \tag{I-39.3}$$

where we adopt the notation

$$D^{(i)} = \begin{vmatrix} (u_0,v_0) & (u_0,v_1) & \cdots & (u_0,v_i) \\ (u_1,v_0) & (u_1,v_1) & \cdots & (u_1,v_i) \\ \vdots & & & \vdots \\ (u_i,v_0) & (u_i,v_1) & \cdots & (u_i,v_i) \end{vmatrix}. \tag{I-39.4}$$

Since an analogous expression for $q_2(z)$ must hold,

$$q_2(z) = d \begin{vmatrix} u_0(z) & u_1(z) & u_2(z) \\ (u_0,v_0) & (u_1,v_0) & (u_2,v_0) \\ (u_0,v_1) & (u_1,v_1) & (u_2,v_1) \end{vmatrix}, \tag{I-39.5}$$

we have

$$(q_2,v_2) = d \begin{vmatrix} (u_0,v_2) & (u_1,v_2) & (u_2,v_2) \\ (u_0,v_0) & (u_1,v_0) & (u_2,v_0) \\ (u_0,v_1) & (u_1,v_1) & (u_2,v_1) \end{vmatrix} = d\, D^{(2)}, \tag{I-39.6}$$

by reason of two exchanges of rows which put the top row at the bottom.

Our final result is

$$cd = \frac{1}{D^{(1)}D^{(2)}} . \qquad \text{(I-39.7)}$$

The determinants which we label $D^{(i)}$ are known as "Gram" determinants; they play an important role in many calculations of this type, as well in the general theory of determinants.

This calculation enables us to write an expression for p_n or q_n for any value of n. We might observe that if n is odd, a minus sign must be added to the right side of (I-39.3). But the exchange of rows in (I-39.6) adds another minus sign, cancelling the first and leaving Eq. (I-39.7) unchanged.

b) Biorthogonal Functions by Differencing .

The next procedure which we discuss has implications which we can only begin to explore.

Consider two approximations to F(z). The first will be designated $\hat{F}_1(z)$ and will be such that

$$(u_n,\hat{F}_1) = (u_n,F), \; n = 0,1. \qquad \text{(I-39.8)}$$

Likewise, the second will be designated $\hat{F}_2(z)$, and will be determined by the two conditions (I-39.8), plus the added condition that $(u_2,\hat{F}_2)=(u_2,F)$. It is clear then that the function

$$P_2(z) = \hat{F}_2(z) - \hat{F}_1(z) \qquad \text{(I-39.9)}$$

has the property

$$(u_n,P_2) = 0, \; n = 0,1. \qquad \text{(I-39.10)}$$

Similarly, we may construct approximations $\hat{G}_1$ and $\hat{G}_2$ to an arbitrary function G(z), in such a way that $(\hat{G}_1,v_n)$ vanishes for n = 1,2, while $(\hat{G}_2,v_n)$ vanishes

for n = 1,2,3. The difference function, $Q_2 = \hat{G}_2 - \hat{G}_1$ is similarly orthogonal to v_0 and v_1.

Clearly, P_2 and Q_2 have orthogonality properties identical with the biorthogonal functions p_2, q_2 previously discussed. Further, one can proceed by this method to construct P_n and Q_n for arbitrary values of $\underline{n}$. The two sets of functions so obtained are biorthogonal.

In the case in which the approximate functions $\hat{F}_i, \hat{G}_i$ are linear combinations of the v_i's and u_i's, this method provides a more general expression than (I-39.1). Expressions for $\hat{F}_1$ and $\hat{F}_2$ are given by

$$\begin{vmatrix} \hat{F}_1(z) & v_0(z) & v_1(z) \\ (u_0,F) & (u_0,v_0) & (u_0,v_1) \\ (u_1,F) & (u_1,v_0) & (u_1,v_1) \end{vmatrix} = \hat{F}_1(z)D^{(1)} + \begin{vmatrix} 0 & v_0(z) & v_1(z) \\ (u_0,F) & (u_0,v_0) & (u_0,v_1) \\ (u_1,F) & (u_1,v_0) & (u_1,v_1) \end{vmatrix} = 0,$$

and

$$\begin{vmatrix} \hat{F}_2 & v_0(z) & v_1(z) & v_2(z) \\ (u_0,F) & (u_0,v_0) & (u_0,v_1) & (u_0,v_2) \\ (u_1,F) & (u_1,v_0) & (u_1,v_1) & (u_1,v_2) \\ (u_2,F) & (u_2,v_0) & (u_2,v_1) & (u_2,v_2) \end{vmatrix} = \hat{F}_2(z)D^{(2)} + \begin{vmatrix} 0 & v_0 & v_1 & v_2 \\ (u_0,F) & (u_0,v_0) & (u_0,v_1) & (u_0,v_2 \\ (u_1,F) & (u_1,v_0) & (u_1,v_1) & (u_1,v_2) \\ (u_2,F) & (u_2,v_0) & (u_2,v_1) & (u_2,v_2) \end{vmatrix} = 0.$$

From these it is clear that

$$P_2(z) = \frac{1}{D^{(1)}} \begin{vmatrix} 0 & v_0(z) & v_1(z) \\ (u_0,F) & (u_0,v_0) & (u_0,v_1) \\ (u_1,F) & (u_1,v_0) & (u_1,v_1) \end{vmatrix} - \frac{1}{D^{(2)}} \begin{vmatrix} 0 & v_0(z) & v_1(z) & v_2(z) \\ (u_0,F) & (u_0,v_0) & (u_0,v_1) & (u_0,v_2) \\ (u_1,F) & (u_1,v_0) & (u_1,v_1) & (u_1,v_2) \\ (u_2,F) & (u_2,v_0) & (u_2,v_1) & (u_2,v_2) \end{vmatrix} \quad \text{(I-39.11)}$$

Correspondingly, we have

$$Q_2(z) = \frac{1}{D^{(1)}} \begin{vmatrix} 0 & u_0(z) & u_1(z) \\ (G,v_0) & (u_0,v_0) & (u_1,v_0) \\ (G,v_1) & (u_0,v_1) & (u_1,v_1) \end{vmatrix} - \frac{1}{D^{(2)}} \begin{vmatrix} 0 & u_0(z) & u_1(z) & u_2(z) \\ (G,v_0) & (u_0,v_0) & (u_1,v_0) & (u_2,v_0) \\ (G,v_1) & (u_0,v_1) & (u_1,v_1) & (u_2,v_1) \\ (G,v_2) & (u_0,v_2) & (u_1,v_2) & (u_2,v_2) \end{vmatrix} \tag{I-39.12}$$

It is a nice exercise to work out the normalization constant, CD = $1/(Q_2,P_2)$. Clearly

$$(Q_2,P_2) = (Q_2,\hat{F}_2) - (Q_2,\hat{F}_1) = -\frac{1}{D^{(2)}} \begin{vmatrix} 0 & 0 & 0 & (Q_2,v_2) \\ (u_0,F) & (u_0,v_0) & (u_0,v_1) & (u_0,v_2) \\ (u_1,F) & (u_1,v_0) & (u_1,v_1) & (u_1,v_2) \\ (u_2,F) & (u_2,v_0) & (u_2,v_1) & (u_2,v_2) \end{vmatrix}$$

$$= \frac{(Q_2,v_2)}{D^{(2)}} \begin{vmatrix} (u_0,F) & (u_0,v_0) & (u_0,v_1) \\ (u_1,F) & (u_1,v_0) & (u_1,v_1) \\ (u_2,F) & (u_2,v_0) & (u_2,v_1) \end{vmatrix} .$$

The value of (Q_2,v_2) can be determined similarly:

$$(Q_2,v_2) = \frac{1}{D^{(1)}} \begin{vmatrix} 0 & (u_0,v_2) & (u_1,v_2) \\ (G,v_0) & (u_0,v_0) & (u_1,v_0) \\ (G,v_1) & (u_0,v_1) & (u_1,v_1) \end{vmatrix} - \frac{1}{D^{(2)}} \begin{vmatrix} 0 & (u_0,v_2) & (u_1,v_2) & (u_2,v_2) \\ (G,v_0) & (u_0,v_0) & (u_1,v_0) & (u_2,v_0) \\ (G,v_1) & (u_0,v_1) & (u_1,v_1) & (u_2,v_1) \\ (G,v_2) & (u_0,v_2) & (u_1,v_2) & (u_2,v_2) \end{vmatrix} .$$

In the second determinant on the right of this expression, we subtract the first row from the fourth row, and thus obtain the value $-(G,v_2)D^{(2)}$ for this determinant. Multiplying and dividing by $D^{(1)}$, we obtain

$$(Q_2,v_2) = \frac{1}{D^{(1)}}\left\{ \begin{vmatrix} 0 & (u_0,v_2) & (u_1,v_2) \\ (G,v_0) & (u_0,v_0) & (u_1,v_0) \\ (G,v_1) & (u_0,v_1) & (u_1,v_1) \end{vmatrix} + (G,v_2)D^{(1)} \right\}$$

$$= \frac{1}{D^{(1)}} \begin{vmatrix} (G,v_0) & (u_0,v_0) & (u_1,v_0) \\ (G,v_1) & (u_0,v_1) & (u_1,v_1) \\ (G,v_2) & (u_0,v_2) & (u_1,v_2) \end{vmatrix} .$$

Combining the expression for (Q_2,P_2) with the expression for (Q_2,v_2), we obtain

$$(Q_2,P_2) = \frac{1}{D^{(1)}D^{(2)}} \begin{vmatrix} (G,v_0) & (u_0,v_0) & (u_1,v_0) \\ (G,v_1) & (u_0,v_1) & (u_1,v_1) \\ (G,v_2) & (u_0,v_2) & (u_1,v_2) \end{vmatrix} \begin{vmatrix} (u_0,F) & (u_0,v_0) & (u_0,v_1) \\ (u_1,F) & (u_1,v_0) & (u_1,v_1) \\ (u_2,F) & (u_2,v_0) & (u_2,v_1) \end{vmatrix} . \quad \text{(I-39.13)}$$

The remarkable feature about this whole development is the fact that the functions F and G are quite arbitrary; therefore, so must the inner products involving these functions be arbitrary. Accordingly, we can take (G,v_i) and (u_i,F) to be zero for i = 0 , 1, and unity for i = 2. The expressions for P_2 , Q_2 then reduce to (I-39.1) and (I-39.5), while $(Q_2,P_2) = D^{(1)}/D^{(2)}$.

c) The Schmidt Method.

This method uses the previously constructed members of a set of biorthogonal functions to simplify the determination of p_n and q_n. Thus, the functions p_2 and q_2 can be written

$$p_2(z) = c'\begin{vmatrix} p_0(z) & p_1(z) & v_2(z) \\ (q_0,p_0) & (q_0,p_1) & (q_0,v_2) \\ (q_1,p_0) & (q_1,p_1) & (q_1,v_2) \end{vmatrix} = c'\begin{vmatrix} P_0(z) & P_1(z) & v_2(z) \\ 1 & 0 & (q_0,v_2) \\ 0 & 1 & (q_1,v_2) \end{vmatrix} = c'\{v_2(z) - \sum_{i=0}^{1} (q_i,v_2)p_i(z)\}. \quad \text{(I-39.14)}$$

and

$$q_2(z) = d'\begin{vmatrix} q_0(z) & q_1(z) & u_2(z) \\ (q_0,p_0) & (q_1,p_0) & (u_2,p_0) \\ (q_0,p_1) & (q_1,p_1) & (u_2,p_1) \end{vmatrix} = d'\begin{vmatrix} q_0(z) & q_1(z) & u_2(z) \\ 1 & 0 & (u_2,p_0) \\ 0 & 1 & (u_2,p_1) \end{vmatrix} = d'\{u_2(z) - \sum_{i=0}^{1} (u_2,p_i)q_i(z)\}. \quad \text{(I-39.15)}$$

These expressions give p_2 and q_2, which must now be normalized to assist the calculation of higher functions in the sequence. Calculation of the normalization constant proceeds very much as before. From (I-39.14) it is clear that

$$1 = (q_2,p_2) = c'(q_2,v_2). \quad \text{(I-39.16)}$$

Then, from (I-39.15) we obtain

$$(q_2,v_2) = d'\{(u_2,v_2) - \sum_{i=0}^{1} (u_2,p_i)(q_i,v_2)\}.$$

Inserting into (I-39.16), we obtain

$$c'd' = \frac{1}{(u_2,v_2) - \sum_{i=0}^{1} (u_2,p_i)(q_i,v_2)}. \quad \text{(I-39.17)}$$

40. Calculation of the Functions

We will make no attempt here to demonstrate most of the general properties of the U_n polynomials, but will rather approach them from the point of view of the preceding sections. For more complete information, see Ref. 15, section 17.

For our base functions we choose (for some constant ℓ)

$$u_i(r) = \frac{r^{\ell+2i}}{(\ell+2i)!}, \quad v_i(r) = r^i \ ; \tag{I-40.1}$$

and the inner products are given by

$$(u_i, v_j) = \int_0^\infty dr e^{-r} \frac{r^{\ell+2i+j}}{(\ell+2i)!} = \frac{(\ell+2i+j)!}{(\ell+2i)!} \ . \tag{I-40.2}$$

Construction of the two (biorthogonal) sets of functions can be by many of the methods of the preceding section. But for directness and simplicity we choose the first method and carry through illustrative calculations of $U_n^{\ell}(u)$ and $U_n^{\ell+}$ for $\ell = 0$, $n = 2$:

$$U_2^o(r) = C_2 \begin{vmatrix} 1 & r & r^2 \\ \frac{0!}{0!} & \frac{1!}{0!} & \frac{2!}{0!} \\ \frac{2!}{2!} & \frac{3!}{2!} & \frac{4!}{2!} \end{vmatrix} = C_2(6-10r+2r^2).$$

and

$$U_2^{o\dagger}(r) = d_2 \begin{vmatrix} 1 & \frac{r^2}{2!} & \frac{r^4}{4!} \\ \frac{0!}{0!} & \frac{2!}{2!} & \frac{4!}{4!} \\ \frac{1!}{0!} & \frac{3!}{2!} & \frac{5!}{4!} \end{vmatrix} = d_2\left(2-4\,\frac{r^2}{2!}+2\,\frac{r^4}{4!}\right).$$

The normalization constant is given by

$$\frac{1}{c_2 d_2} = D^{(1)}D^{(2)} = \begin{vmatrix} \frac{0!}{0!} & \frac{1!}{0!} \\ \frac{2!}{2!} & \frac{3!}{2!} \end{vmatrix} \begin{vmatrix} \frac{0!}{0!} & \frac{1!}{0!} & \frac{2!}{0!} \\ \frac{2!}{2!} & \frac{3!}{2!} & \frac{4!}{2!} \\ \frac{4!}{4!} & \frac{5!}{4!} & \frac{6!}{4!} \end{vmatrix} = 2 \cdot 16 = 32.$$

Any of the polynomials can be determined in this manner, which, though clumsy, is extremely direct.

For rapid and easy computation, the following recursion relation is most useful:[15/]

$$U_{n+1}^{\ell} = \frac{1}{2(n+1)}\left\{(2n+1+\ell) - x + x\frac{d}{dx}\right\} U_n^{\ell}(x). \qquad \text{(I-40.3)}$$

Of greater importance than this are recursion relations derivable from it that hold between coefficients u_{ni}^{ℓ} in the expression

$$U_n^{\ell}(r) = \sum_{i=0}^{n} u_{ni}^{\ell}\, r^i. \qquad \text{(I-40.4)}$$

Inserting (I-40.4) into (I-40.3), we obtain

$$\sum_{i=0}^{n+1} u^{\ell}_{n+1,i}\, r^i = \sum_{i=0}^{n} \frac{1}{2(n+1)}\, u^{\ell}_{ni} \left\{(2n+1+\ell)r^i - r^{i+1} + ir^i\right\}.$$

When like powers of r are separately equated to zero in this expression we obtain

$$u^{\ell}_{n+1,i} = \frac{2n+\ell+i+1}{2(n+1)}\, u^{\ell}_{ni} - \frac{1}{2(n+1)}\, u^{\ell}_{n,i-1}, \qquad \text{(I-40.5)}$$

with the special cases

$$u^{\ell}_{n+1,0} = \frac{2n+\ell+1}{2(n+1)}\, u^{\ell}_{n0}, \quad i = 0,$$

$$u^{\ell}_{n+1,n+1} = -\frac{1}{2(n+1)}\, u^{\ell}_{n,n}, \quad i = n+1, \qquad \text{(I-40.6)}$$

$$u^{\ell}_{00} = 1, \quad i = n = 0.$$

The value for $n = i = 0$ does not follow from the recursion system, but is consistent with the normalization of the $U^{\ell}_{n}(r)$ polynomials adopted in Ref. 15, section 17.

The structure of the linkage between different coefficients u_{ni} can be exhibited with the help of Fig. I-40.1. The arrows indicate that knowledge of the two preceding coefficients is sufficient to determine $u^{\ell}_{n+1,i}$. Evaluation of the coefficients therefore proceeds down and to the right. But it is clear from Eqs. (I-40.6) that both the first column and the diagonal can be determined by

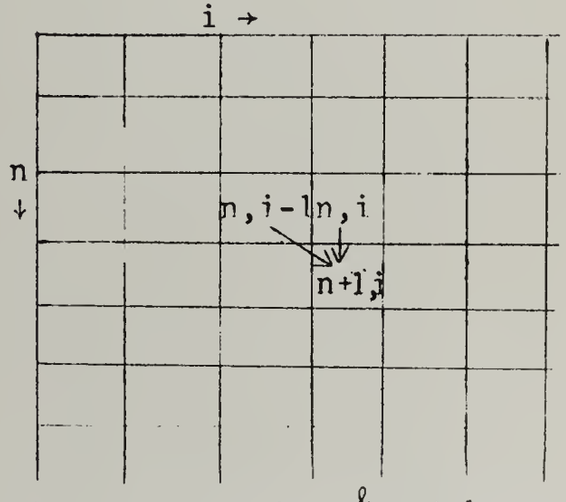

Fig. I-40.1 The u^{ℓ}_{ni} linkage structure.

application of the special cases of the recursion formula. One can therefore evaluate each column in turn, proceeding from left to right.

Note that calculations for each ℓ value are independent of the other ℓ values. No cross linkage exists.

Eqs. (I-40.5) and (I-40.6) greatly simplify both the calculation and tabulation of the polynomials. Lists of the low degree polynomials and their adjoints are given in Table I-40.1 for easy reference. Table I-40.2 gives brief corresponding tabulation due to Mr. R. E. Faw, whose machine program was based on Eqs. (I-40.5) and (I-40.6).

Table I-40.3 gives numerical values for the coefficients u_{ni}^{ℓ}, as calculated from the recursion system of Equations (I-40.5) and (I-40.6). In effect, this table extends Table I-40.1 to higher values of ℓ.

Table I-40.1. Expressions for some of the low degree U_n^{ℓ} and $U_n^{\ell\dagger}$ polynomials.

$U_0^{0\dagger} = 1$	$U_0^0 = 1$
$U_1^{0\dagger} = 1 - \frac{x^2}{2!}$	$U_1^0 = \frac{1}{2}(1 - x)$
$U_2^{0\dagger} = 1 - 2\frac{x^2}{2!} + \frac{x^4}{4!}$	$U_2^0 = \frac{1}{8}(3 - 5x + x^2)$
$U_3^{0\dagger} = 1 - 3\frac{x^2}{2!} + 3\frac{x^4}{4!} - \frac{x^6}{6!}$	$U_3^0 = \frac{1}{48}(15 - 33x + 12x^2 - x^3)$
$U_4^{0\dagger} = 1 - 4\frac{x^2}{2!} + 6\frac{x^4}{4!} - 4\frac{x^6}{6!} + \frac{x^8}{8!}$	$U_4^0 = \frac{1}{384}(105 - 279x + 141x^2 - 22x^3 + x^4)$
$U_0^{1\dagger} = 1$	$U_0^1 = 1$
$U_1^{1\dagger} = 1 - \frac{x^2}{3!}$	$U_1^1 = \frac{1}{2}(2 - x)$
$U_2^{1\dagger} = 1 - 2\frac{x^2}{3!} + \frac{x^4}{5!}$	$U_2^1 = \frac{1}{8}(8 - 7x + x^2)$
$U_3^{1\dagger} = 1 - 3\frac{x^2}{3!} + 3\frac{x^4}{5!} - \frac{x^6}{7!}$	$U_3^1 = \frac{1}{48}(48 - 57x + 15x^2 - x^3)$
$U_4^{1\dagger} = 1 - 4\frac{x^2}{3!} + 6\frac{x^4}{5!} - 4\frac{x^6}{7!} + \frac{x^8}{9!}$	$U_4^1 = \frac{1}{384}(384 - 561x + 207x^2 - 26x^3 + x^4)$

Table I-40.2. Values for some of the U_n^ℓ polynomials.

r	$U_0^0(r)$	$U_1^0(r)$	$U_2^0(r)$	$U_3^0(r)$	$U_4^0(r)$
.0	1.0	.5	.375	.31250	.27343
1.0	1.0	.0	-.125	-.14583	-.14062
2.0	1.0	-.5	-.375	-.22916	-.12760
3.0	1.0	-1.0	-.375	-.06249	.06250
4.0	1.0	-1.5	-.125	.22916	.24218
5.0	1.0	-2.0	.375	.52083	.28645
6.0	1.0	-2.5	1.125	.68750	.13281
7.0	1.0	-3.0	2.125	.60416	-.21874
8.0	1.0	-3.5	3.375	.14583	-.70572
9.0	1.0	-4.0	4.875	-.81249	-1.20312
10.0	1.0	-4.5	6.625	-2.39583	-1.52343
11.0	1.0	-5.0	8.625	-4.72916	-1.41666
12.0	1.0	-5.5	10.875	-7.93749	-.57031
13.0	1.0	-6.0	13.375	-12.14582	1.39061
14.0	1.0	-6.5	16.125	-17.47915	4.90363
15.0	1.0	-7.0	19.125	-24.06248	10.46873

r	$U_0^1(r)$	$U_1^1(r)$	$U_2^1(r)$	$U_3^1(r)$	$U_4^1(r)$
.0	1.0	1.0	1.0	1.0	1.0
1.0	1.0	.5	.25	.10416	.01302
2.0	1.0	.0	-.25	-.29166	-.26562
3.0	1.0	-.5	-.5	-.31249	-.14843
4.0	1.0	-1.0	-.5	-.08333	.11458
5.0	1.0	-1.5	-.25	.27083	.33594
6.0	1.0	-2.0	.25	.62500	.39063
7.0	1.0	-2.5	1.0	.85416	.21615
8.0	1.0	-3.0	2.0	.83333	-.18749
9.0	1.0	-3.5	3.25	.43750	-.75780
10.0	1.0	-4.0	4.75	-.45833	-1.36978
11.0	1.0	-4.5	6.50	-1.97916	-1.83592
12.0	1.0	-5.0	8.50	-4.24999	-1.90624
13.0	1.0	-5.5	10.75	-7.39582	-1.26821
14.0	1.0	-6.0	13.25	-11.54165	.45315
15.0	1.0	-6.5	16.0	-16.81248	3.69533

r	$U_0^2(r)$	$U_1^2(r)$	$U_2^2(r)$	$U_3^2(r)$	$U_4^2(r)$
.0	1.0	1.5	1.875	2.1875	2.46093
1.0	1.0	1.0	.875	.72916	.58854
2.0	1.0	.5	.125	-.10416	-.23177
3.0	1.0	.0	-.375	-.43749	-.37499
4.0	1.0	-.5	-.625	-.39583	-.15364
5.0	1.0	-1.0	-.625	-.10416	.18229
6.0	1.0	-1.5	-.375	.31250	.44531
7.0	1.0	-2.0	.125	.72916	.51042
8.0	1.0	-2.5	.875	1.02083	.31511
9.0	1.0	-3.0	1.875	1.0625	-.14061
10.0	1.0	-3.5	3.125	.72917	-.79426
11.0	1.0	-4.0	4.625	-.10416	-1.52082
12.0	1.0	-4.5	6.375	-1.56249	-2.13279
13.0	1.0	-5.0	8.375	-3.77082	-2.38018
14.0	1.0	-5.5	10.625	-6.85415	-1.95051
15.0	1.0	-6.0	13.125	-10.93748	-.46874

r	$U_0^3(r)$	$U_1^3(r)$	$U_2^3(r)$	$U_3^3(r)$	$U_4^3(r)$
.0	1.0	2.0	3.0	4.0	5.0
1.0	1.0	1.5	1.75	1.85416	1.86718
2.0	1.0	1.0	.75	.45833	.19270
3.0	1.0	.5	.0	-.31249	-.46093
4.0	1.0	.0	-.5	-.58333	-.46874
5.0	1.0	-.5	-.75	-.47916	-.14322
6.0	1.0	-1.0	-.75	-.12499	.26562
7.0	1.0	-1.5	-.50	.35416	.57031
8.0	1.0	-2.0	.0	.83333	.64583
9.0	1.0	-2.5	.75	1.18750	.42969
10.0	1.0	-3.0	1.75	1.29167	-.07812
11.0	1.0	-3.5	3.0	1.02083	-.81509
12.0	1.0	-4.0	4.5	.250	-1.65624
13.0	1.0	-4.5	6.25	-1.14582	-2.41406
14.0	1.0	-5.0	8.25	-3.29165	-2.83854
15.0	1.0	-5.5	10.50	-6.31248	-2.61719

r	$U_0^4(r)$	$U_1^4(r)$	$U_2^4(r)$	$U_3^4(r)$	$U_4^4(r)$
.0	1.0	2.5	4.375	6.56250	9.02343
1.0	1.0	2.0	2.875	3.60416	4.19270
2.0	1.0	1.5	1.625	1.52083	1.28906
3.0	1.0	1.0	.625	.18750	-.18749
4.0	1.0	.5	-.125	-.52083	-.67447
5.0	1.0	.0	-.625	-.72916	-.54687
6.0	1.0	-.5	-.875	-.56249	-.11718
7.0	1.0	-1.0	-.875	-.14583	.36458
88.0	1.0	-1.5	-.625	.39583	.71094
9.0	1.0	-2.0	-.125	.93750	.79688
10.0	1.0	-2.5	.625	1.35417	.55991
11.0	1.0	-3.0	1.625	1.52083	.00002
12.0	1.0	-3.5	2.875	1.31250	-.82029
13.0	1.0	-4.0	4.375	.60417	-1.77601
14.0	1.0	-4.5	6.125	-.72915	-2.67967
15.0	1.0	-5.0	8.125	-2.81248	-3.28123

r	$U_0^5(r)$	$U_1^5(r)$	$U_2^5(r)$	$U_3^5(r)$	$U_4^5(r)$
.0	1.0	3.0	6.0	10.0	15.0
1.0	1.0	2.5	4.25	6.10416	7.97135
2.0	1.0	2.0	2.75	3.20833	3.40104
3.0	1.0	1.5	1.50	1.18750	.72655
4.0	1.0	1.0	.5	-.08333	-.55208
5.0	1.0	.5	-.25	-.72916	-.87240
6.0	1.0	.0	-.75	-.87499	-.60938
7.0	1.0	-.5	-1.0	-.64583	-.07554
8.0	1.0	-1.0	-1.0	-.16666	.47914
9.0	1.0	-1.5	-.75	.43750	.86715
10.0	1.0	-2.0	-.25	1.04167	.96350
11.0	1.0	-2.5	.50	1.52083	.70568
12.0	1.0	-3.0	1.5	1.750	.09369
13.0	1.0	-3.5	2.75	1.60417	-.80996
14.0	1.0	-4.0	4.25	.95834	-1.88030
15.0	1.0	-4.5	6.0	-.31248	-2.92980

Table I-40.3. Coefficients u^{ℓ}_{ni} for the polynomials $U^{\ell}_{n}(r) = \sum_{i=0}^{n} u^{\ell}_{ni} r^{i}$.

$\ell = 0$

n \ i	0	1	2	3	4
0	1				
1	.500000	-.5000			
2	.375	-.625	.125		
3	.3125	-.6875	.250	-.0208333	
4	.273437	-.726563	.367188	-.0572916	.0026041

$\ell = 1$

n \ i	0	1	2	3	4
0	1				
1	1	-.50000			
2	1	-.875	.125		
3	1	-1.1875	.3125	-.0208333	
4	1	-1.460938	.539063	-.067708	.0026041

$\ell = 2$

n \ i	0	1	2	3	4
0	1				
1	1.5	-.5			
2	1.875	-1.125	.125		
3	2.1875	-1.8125	.375	-.0208333	
4	2.46094	-2.53906	.74219	-.078125	.0026041

$\ell = 3$

n \ i	0	1	2	3	4
0	1				
1	2	-.5			
2	3	-1.375	.125		
3	4	-2.5625	.4375	-.0208333	
4	5	-4.02344	.97656	-.088542	.0026041

$\ell = 4$

n \ i	0	1	2	3	4
0	1				
1	2.5	-.5			
2	4.375	-1.625	.125		
3	6.5625	-3.4375	.5	-.0208333	

41. Approximation of Distributions

We approximate a distribution $D_\ell(r)$ for which we have moments $D_{n\ell}$, $n = \ell, \ell+2, \ell+4, \ldots$, by the finite sum

$$\hat{D}_\ell(r) = e^{-r} \sum_{i=0}^{N} (U_i^{\ell\dagger}, D_\ell) U_i^\ell(r), \tag{I-41.1}$$

where

$$(U_m^{\ell\dagger}, D_\ell) = \sum_{j=0}^{m} (-)^j \binom{n}{j} \frac{D_{\ell+2j,\ell}}{(\ell+2j)!}, \quad m = \frac{1}{2}(n-\ell) . \tag{I-41.2}$$

As has been mentioned before, all the point isotropic gamma ray dose distributions have basically exponential trends; and if the sources are monoenergetic the exponential trends are known. If $\underline{r}$ measures distance from the source in units of the mean free path of the source gamma rays, the convergence of the terms in the sum on the right of (I-41.1) will normally be rapid and the representation accurate.

Strictly speaking we should at this point investigate problems of ultimate convergence for N indefinitely large, and the problem of completeness of the two biorthogonal sets. But we will bypass these questions. In fact the two sets are complete; and the practical convergence is ordinarily adequate for our purpose.

For machine calculations the representation in terms of U_n polynomials is less useful that the representation in terms of powers. The power series representation can be obtained formally from the equation

$$\begin{vmatrix} \hat{D}_\ell(r) & e^{-r} & re^{-r} & r^2e^{-r} \\ \left(\frac{r^\ell}{\ell!}, D_\ell\right) & \frac{\ell!}{\ell!} & \frac{(\ell+1)!}{\ell!} & \frac{(\ell+2)!}{\ell!} \\ \left(\frac{r^{\ell+2}}{(\ell+2)!}, D_\ell\right) & \frac{(\ell+2)!}{(\ell+2)!} & \frac{(\ell+3)!}{(\ell+2)!} & \frac{(\ell+4)!}{(\ell+2)!} \\ \left(\frac{r^{\ell+4}}{(\ell+4)!}, D_\ell\right) & \frac{(\ell+4)!}{(\ell+4)!} & \frac{(\ell+5)!}{(\ell+4)!} & \frac{(\ell+6)!}{(\ell+4)!} \end{vmatrix} = 0 \ . \qquad \text{(I-41.3)}$$

Although this determinant equation is advantageous for showing what is involved in the power series representation, it turns out that by far the most efficient calculation of this type relies on the U-polynomial expansion as an intermediate step. Using the results of the last section, let us write (I-41.3) as a sum of powers:

$$\hat{D}_\ell(r) = e^{-r} \sum_{n=0}^{N} \sum_{i=0}^{n} (U_n^{\ell\dagger}, D_\ell) u_{ni}^{\ell} r^i . \qquad \text{(I-41.4)}$$

To obtain expressions for the coefficients of the powers, we must invert the order of this double sum. Noting that the terms of the double sum correspond in Fig. I-41.1 to the points of intersection on and above the diagonal, we see that the inner sum (over i) runs parallel to the abscissa from zero to the diagonal. The outer sum (over n) is over rows up to row N. If the order of the sums is inverted, the inner sum (over n) must correspond to points of the i'th row from the diagonal to N, while the outer sum (over i) must be over columns up to the N'th. That is to say,

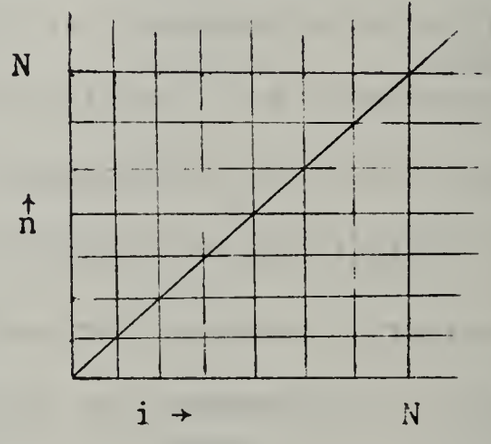

Fig. I-41.1

$$\hat{D}_\ell(r) = e^{-r\sum_{i=0}^{N} r^i \sum_{n=i}^{N} (U_n^{\ell\dagger}, D_\ell) u_{ni}^\ell}, \tag{I-41.5}$$

so that the coefficients of the $\underline{r}^i$, which we designate $a_{\ell i}$, are given by

$$a_{\ell i} = \sum_{n=i}^{N} (U_n^{\ell\dagger}, D_\ell)\, u_{ni}^\ell. \tag{I-41.6}$$

To put this in terms of the moments, we insert the expression (I-41.2) for the inner products. Again the order of summations can be inverted using a sketch much like Fig. I-41.1, with the result

$$\begin{aligned} a_{\ell i} &= \sum_{n=i}^{N} u_{ni}^\ell \sum_{j=0}^{n} (-)^j \binom{n}{j} D_{\ell+2j,\ell} \\ &= \sum_{j=0}^{N} D_{\ell+2j,\ell} (-)^j \sum_{n=n_{min}}^{N} \binom{n}{j} u_{ni}^\ell, \quad n_{min} = \begin{cases} i, & j<i, \\ j, & j\geq i. \end{cases} \end{aligned} \tag{I-41.7}$$

But this is simply the matrix multiplication

$$\begin{bmatrix} M_{00} & M_{01} \cdots M_{0N} \\ M_{10} & M_{11} \cdots M_{1N} \\ \vdots & \vdots \\ M_{N0} & M_{N1} \cdots M_{NN} \end{bmatrix} \begin{bmatrix} D_{\ell,\ell} \\ D_{\ell+2j,\ell} \\ \vdots \\ D_{\ell+2N,\ell} \end{bmatrix} = \begin{bmatrix} a_{\ell 0} \\ a_{\ell 1} \\ \vdots \\ a_{\ell N} \end{bmatrix}, \tag{I-41.8}$$

where the matrix elements are given by

$$\begin{aligned} M_{ij} &= (-)^j \sum_{n=i}^{N} \binom{n}{j} u_{ni}^\ell, \quad j<i, \\ &= (-)^j \sum_{n=j}^{N} \binom{n}{j} u_{ni}^\ell, \quad j\geq i. \end{aligned} \tag{I-41.9}$$

Therefore, we have the possibility of calculating the coefficients a in three stages: (1) First, the coefficients u_{ni}^{ℓ} are calculated using the recursion system described in the preceding section; (2) then the matrix elements M_{ij} appropriate to the number of moments to be used in the calculation are determined; and (3) finally the matrix multiplication (I-41.8) is performed.

This calculation can be viewed either as a device for inverting a special type of matrix or as a device for evaluating a special type of determinant.

Table I-41.1 lists matrix coefficients M_{ij} for several values of ℓ and for N = 4. These were computed by a simple machine program written by Mr. J. R. Fagan, based on the recursion system for the u_{ni}^{ℓ} and the equations (I-41.9).

Table I-41.1. Matrix coefficients M_{ij} for a 4-term power series approximation to $D_\ell(r)$, based on the moments $D_{\ell+2j,\ell}$, $j = 0, 1, 2, 3$.

$\ell = 0$

i \ j	0	1	2	3
0	2.1875	-2.1875	1.3125	-.3125
1	-1.8125	3.8125	-2.6875	.6875
2	.375	-1.	.875	-.2500
3	-.0208333	.0625	-.0625	.0208333

$\ell = 1$

i \ j	0	1	2	3
0	4.	-6.	4.	-1.
1	-2.5625	5.8125	-4.4375	1.1875
2	.4375	-1.1875	1.0625	-.3125
3	-.0208333	.0625	-.0625	.0208333

$\ell = 2$

i \ j	0	1	2	3
0	6.5625	-11.8125	8.4375	-2.1875
1	-3.4375	8.1875	-6.5625	1.8125
2	.5	-1.375	1.25	-.375
3	-.0208333	.0625	-.0625	.0208333

$\ell = 3$

i \ j	0	1	2	3
0	10.	-20.	15.	-4.
1	-4.4375	10.9375	-9.0625	2.5625
2	.5625	-1.5625	1.4375	-.4375
3	-.0208333	.0625	-.0625	.0208333

$\ell = 4$

i \ j	0	1	2	3
0	14.4375	-30.9375	24.0625	-6.5625
1	-5.5625	14.0625	-11.9375	3.4375
2	.625	-1.75	1.625	-.5
3	-.0208333	.0625	-.0625	.0208333

42. Discussion of Function Fitting Procedures*

For many configurations and radiation source types, one knows that the penetration is basically exponential, but it is not clear what the exponential coefficient is. Therefore, one does not know what weight function to use with a polynomial expansion. In this circumstance it might be natural to make exploratory calculations with several different weight functions to see if a pattern begins to emerge; but this is not very satisfactory. The fundamental problem is that with polynomial expansions it is necessary to incorporate in the weight function an approximation which differs from the distribution in such a way that the ratio between the two can be accurately characterized by a low-order polynomial. When the nature of the distribution is not known in many details, an arbitrary weight function guess is apt to be in error in such a way that the correction requires a high-order polynomial, i.e. many terms in the expansion.

This situation holds for plane monodirectional slant source distributions, for instance, and for nearly all peaked angular distributions. The approach which has been most useful in such cases begins with a "weight function" which contains an internal parameter, and which has three characteristics: the form expresses known information about the desired distribution; the value of the internal parameter determines the width of the function; and the functions are simple enough to be well-behaved in superposition.

To illustrate, we consider a distribution I(z) which is essentially exponential for $z \geq 0$, but for which it is impossible to identify a particular exponential coefficient known to be dominant at large penetrations. This is

*In addition to Ref. 15, section 18, see Refs. 25, 40.

the case for plane slant gamma ray sources, and it may occur for other source types if the source spectrum is not monochromatic. Because of the exponential nature of the distribution we write

$$I(z) \simeq \hat{I}(z) = \sum_i \frac{\alpha_i}{\beta_i} e^{-z/\beta_i}. \qquad \text{(I-42.1)}$$

Values of the parameters α_i, β_i must then be determined so that this approximation has the spatial moments which are known to characterize the unknown distribution.

In this way, the spatial moments can be used to specify "effective" exponential trends for the problem; and the troublesome problem of unusual peaking near $z = 0$ can be approximated satisfactorily at the same time.

a). Gauss Integration Point of View.

Before proceeding to outline the calculation of the parameters in greater detail, we consider more general aspects of this type of approximation. Thus, suppose that the unknown distribution $I(z)$ can be represented as follows:

$$I(z) = \int_0^\infty \frac{dx}{x} e^{-z/x} f(x). \qquad \text{(I-42.2)}$$

where $f(x)$ is to be determined. If we multiply this equation by z^n and integrate over z, we obtain, by changing the order of integrations,

$$\int_0^\infty dz z^n I(z) = \int_0^\infty dz z^n \int_0^\infty \frac{dx}{x} e^{-z/x} f(x)$$

$$= \int_0^\infty dx\, x^n f(x) \int_0^\infty d(z/x) \left(\frac{z}{x}\right)^n e^{-z/x}.$$

This is recognizable as a very simple relationship between moments of the three functions of Eq. (I-42.2),

$$I_n = n! f_n . \qquad \text{(I-42.3)}$$

Thus, it is possible to determine moments of f(x) without actually knowing the function I(z).

In principle, therefore, we can construct the function f(x) from its moments rather than the function I(z), providing this function exists. The distribution I(z) can then be determined by quadrature. The advantage to this approach is not difficult to appreciate. Integrations always tend to wash out irregularities in the integrand. Therefore, if an approximate calculation of f(x) is imperfect, and yields a function with irregularities, the resulting approximation to I(z) may be quite accurate notwithstanding.

This aspect of the representation (I-42.2) leads to another idea. Suppose we were to make what is in one sense the most extreme approximation to f(x) consistent with its moments, could we depend entirely on the integral to give us a smooth approximation to I(z)? That is to say, suppose we approximate f(x) by a sum of Dirac delta functions,

$$\hat{f}(x) = \sum_i \alpha_i \delta(x-\beta_i). \qquad \text{(I-42.4)}$$

The parameters in this approximation can be determined in principle so that moments $\hat{f}_n$ of this expression agree with f_n values determined using (I-42.3); and in a real sense this is the least smooth type of approximation which can be made to f(x) in this manner. The corresponding $\hat{I}(z)$ can be obtained by inserting this $\hat{f}(x)$ into Eq. (I-42.2),

$$\hat{I}(z) = \sum_i \alpha_i \int_0^\infty \frac{dx}{x} e^{-z/x} \delta(x-\beta_i) = \sum_i \frac{\alpha_i}{\beta_i} e^{-z/\beta_i} . \qquad \text{(I-42.5)}$$

That is to say, the resulting approximation is just that of Eq. (I-42.1), and can, in fact, be very accurate.

The thought that smoother approximations to f(x) might be intrinsically better has led to investigations of related approximations.[25] But it is not clear that the smoothness of f(x) determines the accuracy of the approximation.

An extremely well-known and useful integration procedure, called Gaussian integration, consists of the approximate evaluation of an integral in terms of a set of values of the integrand, as for example,

$$\int_R dx\, w(x)F(x) = \sum_i w_i F(x_i) , \qquad \text{(I-42.6)}$$

where w(x) is a weight function for the integration.[42] The weights w_i depend on this weight function but are <u>not</u> the values $w(x_i)$. The problem of Gaussian integration is the determination of the values x_i and the corresponding constants w_i so that the approximation is particularly accurate. It turns out that the x_i chosen are the zeros of one of the set of polynomials orthogonal with respect to w(x). It can be easily shown that this choice is equivalent to the construction of an approximate function of the type

$$\hat{w}(x) = \sum_i w_i \delta(x-x_i), \qquad \text{(I-42.7)}$$

in such a way than a set of moments $\int_R dx\, x^n \hat{w}(x)$ are equal in value to the

corresponding $\int_R dx\, x_n w(x)$. Insertion of $\hat{w}(x)$ in the place of $w(x)$ in the integral of (I-42.6) gives the approximation.

A comparison of Eqs. (I-42.6) and (I-42.7) with Eqs. (I-42.2) through (I-42.5) makes it clear that "function fitting" approximations such as (I-42.1) are essentially a Gaussian integration of an integral representation for I(z). Interestingly, the unknown function f(x) plays the role of weight function in the calculation.

b) Calculation of the coefficients.

We illustrate the calculation of the α_i, β_i in Eq. (I-42.1) by consideration of the case of a 2-term approximation in which moments I_n, n = 0,1,2,3 are used. As in the case of earlier illustrative calculations, the generalization to higher approximations will be quite clear.

The procedure which we use is not the simplest, but lends itself readily to a variety of related arguments and extensions.

If we calculate moments of f(x), as given by Eq. (I-42.4), and recall that $\hat{f}_n = f_n = \frac{I_n}{n!}$, for n = 0,1,2,3, we see that our problem is that of solving the equations

$$\alpha_1 \beta_1^n + \alpha_2 \beta_2^n = f_n \,, \quad n = 0,1,2,3. \tag{I-42.8}$$

We divide these four equations into 2 sets of 3 each, as follows:

$$\begin{aligned} \alpha_1 + \alpha_2 &= f_0, & \alpha_1\beta_1 + \alpha_2\beta_2 &= f_1, \\ \alpha_1\beta_1 + \alpha_2\beta_2 &= f_1, & \alpha_1\beta_1^2 + \alpha_2\beta_2^2 &= f_2, \\ \alpha_1\beta_1^2 + \alpha_2\beta_2^2 &= f_2, & \alpha_1\beta_1^3 + \alpha_2\beta_2^3 &= f_3. \end{aligned}$$

These two sets of equations can be summarized in matrix form very easily,

using

$$\begin{bmatrix} \alpha_1 & \alpha_2 \\ \alpha_1\beta_1 & \alpha_2\beta_2 \end{bmatrix} \begin{bmatrix} 1 & \beta_1 & \beta_1^2 \\ 1 & \beta_2 & \beta_2^2 \end{bmatrix} = \begin{bmatrix} f_0 & f_1 & f_2 \\ f_1 & f_2 & f_3 \end{bmatrix}.$$

Finally, we expand this matrix equation into an equation involving 4x4 matrices, by the use of identities, to obtain

$$\begin{bmatrix} 1 & 0 & 0 & 0 \\ 0 & \alpha_1 & \alpha_2 & 0 \\ 0 & \alpha_1\beta_1 & \alpha_2\beta_2 & 0 \\ 0 & 0 & 0 & 1 \end{bmatrix} \begin{bmatrix} F(x) & 1 & x & x^2 \\ 0 & 1 & \beta_1 & \beta_1^2 \\ 0 & 1 & \beta_2 & \beta_2^2 \\ 1 & f_2 & f_3 & f_4 \end{bmatrix} = \begin{bmatrix} F(x) & 1 & x & x^2 \\ 0 & f_0 & f_1 & f_2 \\ 0 & f_1 & f_2 & f_3 \\ 1 & f_2 & f_3 & f_4 \end{bmatrix}, \qquad \text{(I-42.9)}$$

where the function F(x) is arbitrary, and for our immediate purpose a knowledge of f_4 turns out to be unnecessary. Notice that all elements of the top and bottom rows must be identical in the last two matrices, but are otherwise arbitrary. We are stressing here the similarity with, for example, Eq. (I-37.5).

Now, we consider the determinant equation corresponding to (I-42.9). The middle determinant will vanish if F(x) = 0, when $\underline{x}$ takes on either of the values β_1 or β_2. Since the right determinant must vanish under the same circumstances, we find using expansion by minors of the first column that the polynomial

$$F(x) = \frac{1}{D^{(2)}} \begin{vmatrix} 1 & x & x^2 \\ f_0 & f_1 & f_2 \\ f_1 & f_2 & f_3 \end{vmatrix} \qquad \text{(I-42.10)}$$

must vanish for the two values β_1 and β_2. Note that the constant $D^{(2)}$, i.e. the minor of F(x) in (I-42.9), then factors out and thus has no influence on the result.

The polynomial F(x) is the 3rd in the series of polynomials which are orthogonal with respect to the weight function f(x), as can be seen by comparison with Eq. (I-39.1). Thus, we confirm the earlier comments to the effect that this procedure is essentially a Gaussian integration.

Determination of the two constants β_1 and β_2 makes it possible to evaluate the corresponding constants α_1 and α_2 by solution of any two of the four equations (I-42.8). But it is interesting to obtain a neat expression for these, even if it is not particularly useful. To this end we modify the matrix equation (I-42.9) and write

$$\begin{bmatrix} 1 & 0 & 0 & 0 \\ 0 & \alpha_1 & \alpha_2 & 0 \\ 0 & \alpha_1\beta_1 & \alpha_2\beta_2 & 0 \\ 0 & 0 & 0 & 1 \end{bmatrix} \begin{bmatrix} F(x) & 1 & x & x^2 \\ 1/\alpha_1 & 1 & \beta_1 & \beta_1^2 \\ 0 & 1 & \beta_2 & \beta_2^2 \\ \beta_1^2 & f_2 & f_3 & 0 \end{bmatrix} = \begin{bmatrix} F(x) & 1 & x & x^2 \\ 1 & f_0 & f_1 & f_2 \\ \beta_1 & f_1 & f_2 & f_3 \\ \beta_1^2 & f_2 & f_3 & 0 \end{bmatrix}. \qquad \text{(I-42.11)}$$

If we now assign $\underline{x}$ the value β_1, and $F(\beta_1)$ the value $1/\alpha_1$, the determinant of the middle matrix vanishes, as must the determinant of the right matrix, so that we obtain the equation

$$\begin{vmatrix} 1/\alpha_1 & 1 & \beta_1 & \beta_1^2 \\ 1 & f_0 & f_1 & f_2 \\ \beta_1 & f_1 & f_2 & f_3 \\ \beta_1^2 & f_2 & f_3 & 0 \end{vmatrix} = 0 , \qquad \text{(I-42.12)}$$

which gives $1/\alpha_1$, since all other entries are known. If α_1,β_1 are replaced by α_2,β_2, we obtain an equation for $1/\alpha_2$. Finally, we might observe that if in (I-42.11) we write $x = \beta_2$, and $F(\beta_2) = 0$, we obtain the pretty result that

$$\begin{vmatrix} 0 & 1 & \beta_2 & \beta_2^2 \\ 1 & f_0 & f_1 & f_2 \\ \beta_1 & f_1 & f_2 & f_3 \\ \beta_1^2 & f_2 & f_3 & 0 \end{vmatrix} = 0.$$

c) Function Fitting and Biorthogonal Systems.

We might designate the approximation just discussed as $\hat{I}_3(z)$, signifying that the moments 0 through 3 are correctly reproduced by the approximation. It is then clear that the function

$$p_n(z) = \hat{I}_n(z) - \hat{I}_{n-1}(z) \qquad \text{(I-42.13)}$$

has the property that its moments through the (n-1)'st are zero. Accordingly, this function can be considered the n'th in one set of a biorthogonal series. The adjoint set, $\{q_n(z)\}$ consists of polynomials. We may then write

$$\hat{I}_n(z) = \sum_{i=0}^{n} p_i(z). \qquad \text{(I-42.13)}$$

From this it is clear that the theory of biorthogonal functions can be applied to study function fitting approximations.

We have not indicated at this point how one might obtain $\hat{I}_n(z)$, n even, and we do not intend to pursue this line of thought further here, though it leads to some useful results.

43. Calculation of Spatial Distributions for Plane Monodirectional Sources

We give here some details of the calculation of results reported in Ref.36 for plane monodirectional sources.

The distribution desired will be designated I(z) as in the preceding section; and we wish to determine an approximate distribution of the form (I-42.1). For accuracy we wish the $\hat{I}(z)$ to reproduce 6 moments correctly; the nature of the configuration requires that these moments be, for example, I_0, I_2, ... , I_{10}. The reasons for use of these moments are more fully discussed in section 26.

Strictly speaking, we would expect these 6 moments to determine the parameters for 3 terms in the sum (I-42.1). But we know from previous experience that solution of the relevant determinant equation requires a precision in the values for I_{2n} great enough to make it largely a matter of chance whether the values for β_1, β_2, β_3 are all real or not. If these parameters are complex, the accuracy of the approximation is expected to be somewhat less, and the nature of the calculation is substantially changed.

Accordingly, we adopt a somewhat less sensitive procedure, and write

$$\hat{I}(z) = \sum_{i=1}^{4} \frac{\alpha_i}{\beta_i} e^{-z/\beta_i}, \qquad \text{(I-43.1)}$$

with the intention of determining the <u>eight</u> parameters α_i, β_i, i = 1,..4, so that <u>six</u> moments of $\hat{I}(z)$ are correctly given. We can assign values to two of the parameters in (I-43.1), and the parameters we choose to fix are β_1 and β_2. The first is given a value corresponding to the exponential trend of the unscattered gamma rays produced by the source, as discussed in section 26; and the second is given a value usually near .7.

The equations which determine the remaining coefficients are

$$\begin{aligned}
&\alpha_1 + \alpha_2 + \alpha_3 + \alpha_4 = I_0, \\
&\alpha_1\beta_1^2 + \alpha_2\beta_2^2 + \alpha_3\beta_3^2 + \alpha_4\beta_4^2 = I_2/2! \\
&\quad\vdots \qquad\quad \vdots \qquad\quad \vdots \qquad\quad \vdots \\
&\alpha_1\beta_1^{10} + \alpha_2\beta_2^{10} + \alpha_3\beta_3^{10} + \alpha_4\beta_4^{10} = I_{10}/10!.
\end{aligned} \tag{I-43.2}$$

We can simplify these relations by multiplying each equation by β_1^2 and subtracting from the following equation. When this is done, the first term cancels, and we are left with the five equations

$$\begin{aligned}
&\alpha_2(\beta_2^2-\beta_1^2) + \alpha_3(\beta_3^2-\beta_1^2) + \alpha_4(\beta_4^2-\beta_1^2) = \frac{I_2}{2!} - I_0, \\
&\alpha_2(\beta_2^2-\beta_1^2)\beta_2^2 + \alpha_3(\beta_3^2-\beta_1^2)\beta_3^2 + \alpha_4(\beta_4^2-\beta_1^2)\beta_4^2 = \frac{I_4}{4!} - \frac{I_2}{2!}, \\
&\quad\vdots \qquad\qquad\qquad \vdots \qquad\qquad\qquad \vdots \qquad\qquad \vdots \\
&\alpha_2(\beta_2^2-\beta_1^2)\beta_2^8 + \alpha_3(\beta_3^2-\beta_1^2)\beta_3^8 + \alpha_4(\beta_4^2-\beta_1^2)\beta_4^8 = \frac{I_{10}}{10!} - \frac{I_8}{8!}.
\end{aligned}$$

Because β_2 is also known, we can go through this procedure once more, to obtain the six equations

$$\begin{aligned}
\alpha_3(\beta_3^2-\beta_1^2)(\beta_3^2-\beta_2^2)\beta_3^{2i} + \alpha_4(\beta_4^2-\beta_1^2)(\beta_4^2-\beta_2^2)\beta_4^{2i} &= \left(\frac{I_{2i+4}}{(2i+4)!} - \frac{I_{2i+2}}{(2i+2)!}\beta_1^2\right) \\
&\quad - \left(\frac{I_{2i+2}}{(2i+2)!} - \frac{I_{2i}}{(2i)!}\beta_1^2\right)\beta_2^2, \quad i = 0,1,2,3.
\end{aligned}$$

Finally, we define new constants as follows:

$$\begin{aligned}
\alpha_3^* &= \alpha_3(\beta_3^2-\beta_1^2)(\beta_3^2-\beta_2^2), \\
\alpha_4^* &= \alpha_4(\beta_4^2-\beta_1^2)(\beta_4^2-\beta_2^2), \\
f_i^* &= \frac{I_{2i+4}}{(2i+4)!} - \frac{I_{2i+2}}{(2i+2)}(\beta_1^2+\beta_2^2) + \frac{I_{2i}}{(2i)!}\beta_2^2\beta_1^2,
\end{aligned} \tag{I-43.3}$$

and thus reduce the system to four equations in the standard form of (I-43.8),

$$\alpha_3^* \beta_3^{2i} + \alpha_4^* \beta_4^{2i} = f_i^* , \quad i = 0,1,2,3. \tag{I-43.4}$$

Solution of these equations by evaluation of the roots of the polynomial equation

$$\begin{vmatrix} 1 & \beta^2 & \beta^4 \\ f_0^* & f_2^* & f_4^* \\ f_2^* & f_4^* & f_6^* \end{vmatrix} = 0$$

gives first the constants β_3 and β_4. Next, α_3^* and α_4^* can be calculated from two of Eqs. (I-43.4). Then, α_3 and α_4 can be determined from Eqs (I-43.3), and finally α_1 and α_2 can be calculated from the first two Eqs. (I-43.2)

Since β_3 and β_4 are obtained as the roots of a quadratic equation, it may happen that they turn out to be complex. The terms of the representation (I-43.1) then have the form of exponentials multiplied by sines and cosines, so that they give damped oscillatory trends. These can be quite accurate; but they have usually be ruled out as unrealistic over large regions. Instead of accepting such solutions, they have been rejected in favor of new calculations with a change in the value of the prespecified parameter.

It is possible for a set of parameters α_i, β_i to occur which are real, but which give a distribution I(z) which is nonsense physically because of the occurrence of features for which there is no physical reason.

Such features are mostly frequently "bumps" or unreasonably large values of β_3 or β_4. This possibility has the effect of making it difficult to apply function fitting mechanically. Distributions obtained by this method require examination in regard to their acceptability on the basis of known trends and characteristics.

In general, the function fitting method has a go or no-go character. Either the distributions obtained in this way are quite accurate, or the calculation fails in one of the obvious ways just noted.

BIBLIOGRAPHY

1. Berger, M. J., "Penetration of Gamma Radiation from a Plane Monodirectional Oblique Source," *J. Res. Nat. Bur. Stand.* 56, 111(1956).

2. Berger, M. J., "Angular Distribution of Multiple Scattered Gamma Radiation from a Plane Isotropic Source," *J. Appl. Phys.* 26, 1504(1955).

3. Berger, R. T., "The X- or Gamma-Ray Energy Absorption or Transfer Coefficient: Tabulations and Discussion," *Rad. Research* 15, 1(1961).

4. Björnerstedt, R., "Health Hazards from Fission Products and Fallout II. Gamma Radiation from Nuclear Weapons Fallout," *Arkiv för Fysik* 16, 293(1959).

5. Bolles, R. C., and N. E. Ballou, "Calculated Activities and Abundances of U235 Fission Products," USNRDL-456(1956). See also *Nucl. Sci. Eng.* 5, 156(1959).

6. Chilton, A. B., *Nuc. Sci Eng.*, to be published.

7. Cook, C. S., "Energy Spectrum of Gamma Radiation from Fallout," USNRDL-TR-318(October 26, 1959).

8. Coveyou, R. R., "Serial Correlation in the Generation of Pseudo-Random Numbers," *J. Assoc. Comput. Mach.* 7, 72(1960).

9. Davisson, C. M., "Interaction of γ-Radiation with Matter," Alpha- Beta-, and Gamma-Ray Spectroscopy, edited by K. Siegbahn, 37ff and 827ff, North-Holland(1965).

10. Dolan, P. J., "Gamma Spectrum of Uranium-238 Fission Products at Various Times after Fission," DASA 526(May, 1959).

11. Fano, U., "Note on the Bragg-Gray Cavity Principle for Measuring Energy Dissipation," *Rad. Research* 1, 237(1954).

12. Fano. U., "Penetration of X- and Gamma-Rays to Extremely Great Depths," *J. Res. Nat. Bur. Stand.* 51, 95(1953).

13. Fano. U., and M. J. Berger, "Deep Penetration of Radiation," *Proc. of Symposia in Appl. Math.*, XI Nuclear Reactor Theory, 43(1961).

14. Fano, U., H. Hurwitz, Jr., and L. V. Spencer, "Penetration and Diffusion of X-Rays. V. Effect of Small Deflections upon the Asymptotic Behavior," *Phys. Rev.* 77, 425(1950).

15. Fano, U., L. V. Spencer, and M. J. Berger, "Penetration and Diffusion of X-Rays," *Handbuch der Physik*, B. 38, Neutrons and Related Gamma Ray Problems, 660, Springer-Verlag(1959).

16. Goldstein, H., and J. E. Wilkins, "Calculations of the Penetration of Gamma Rays," NYO-3075(1954).

17. Greenberger, M., "An A Priori Determination of Serial Correlation in Computer-Generated Random Numbers," *Math. Comput.* 15, 383(1961).

18. Greenberger, M., "Notes on a New Pseudo-Random Number Generator," *J. Assoc. Comput. Mach.* 8, 163(1961).

19. Grodstein, G. W., "X-Ray Attenuation Coefficients from 10 Mev to 100 Mev," NBS Circular 583(April 30, 1957).

20. Heitler, W., The Quantum Theory of Radiation, 3rd edition, Oxford(1954).

21. International Commission on Radiological Units and Measurements (ICRU), "Radiation Quantities and Units," NBS Handbook 84(November 14, 1962).

22. Kaczmarz-Steinhaus, Theorie der Orthogonal-Reihen, 261ff, Warsaw(1935).

23. Kahn, H., "Applications of Monte Carlo," USAEC R-1237(April 19, 1954).

24. Kendall, M. G., The Advanced Theory of Statistics, V. 1, Charles Griffin & Co., Ltd.(1947).

25. Langer, J. S., and S. Varga, "The Problem of Moments with Application to Neutron Flux Distributions," WAPD-TN-520(November, 1955).

26. Larson, K. H., "Adherence of Fallout to Trees and Shrubs," unpublished USNRDL Letter Report(January, 1959).

27. Lehmer, D. H., "Mathematical Methods in Large Scale Computing Units," *Annals Comput. Lab. Harvard U.* V. 26, Proceedings of a Second Symposium on Large-Scale Digital Calculating Machinery, 141(1951).

28. Mather, R. L., "Residual Gamma Radiation Fields from Induced Soil Activities," USNRDL-TR-240(April 9, 1958).

29. Mather, R. L., R. F. Johnson, and F. M. Tomnovec, "Gamma Radiation Field above Fallout-Contaminated Ground," *Health Physics* 8, 245(1962).

30. Meixner, J., "Specielle Funktionen der Mathematischen Physik," *Handbuch der Physik*, B. 1, Mathematische Methoden, 147ff, Springer-Verlag (1956).

31. Miller, C. F., "Gamma Decay of Fission Products from the Slow Neutron Fission of U-235," USNRDL-TR-187(1957).

32. Nelms, A., and J. W. Cooper, "U-235 Fission Product Decay Spectra at Various Times after Fission," *Health Physics* 1, 427(1959).

33. Pell, A., "Biorthogonal Systems of Functions," *Trans. Am. Math. Soc.* 12, 135(1911).

34. Rotenberg, A., "A New Pseudo-Random Number Generator," *J. Assoc. Comp. Mach.* 7, 75(1960).

35. Spencer, L. V., "Penetration and Diffusion of X-Rays: Calculation of Spatial Distributions by Semi-Asymptotic Methods," *Phys. Rev.* 88, 793(1952).

36. Spencer, L. V., "Structure Shielding against Fallout Radiation from Nuclear Weapons," NBS Monograph 42(June 1, 1962).

37. Spencer, L. V., and F. H. Attix, "A Theory of Cavity Ionization," *Rad. Research* 3, 349(1955).

38. Spencer, L. V., and U. Fano, "Calculation of Spatial Distributions by Polynomial Expansion," *J. Res. Nat. Bur. Stand.* 46, 446(1951).

39. Spencer, L. V., and J. Lamkin, "Slant Penetration of Gamma Rays in H_2O," unpublished NBS Report 5944(July 17, 1958).

40. Spencer, L. V., and J. C. Lamkin, "Slant Penetration of Gamma Rays, Mixed Radiation Sources," unpublished NBS Report 6322(February 27, 1959).

41. Spencer, L. V., and J. C. Lamkin, "Slant Penetration of Gamma Rays in Concrete," unpublished NBS Report 6591(November 10, 1959).

42. Szego, G., Orthogonal Polynomials, 346ff, American Mathematical Society(1959).

43. von Neumann, J., "Various Techniques Used in Connection with Random Digits," *Nat. Bur. Stand. Appl. Math. Ser.*, No. 12(1951).

44. Weinberg, A. M., and E. P. Wigner, The Physical Theory of Neutron Chain Reactors, Chapt. 5, University of Chicago(1958).

45. Wick, G. C., "On the Space Distribution of Slow Neutrons," *Phys. Rev.* 75, 738(1949).

46. Willers, F. A., Practical Analysis, translated by R. T. Beyer, Dover(1948).

47. Spencer, L. V. and F. Stinson, "Further Calculations of X-ray Diffusion in an Infinite Medium," *Phys. Rev.* 85, 662(1952).

48. Goldstein, H., Fundamental Aspects of Reactor Shielding, Addison-Wesley (1959).

49. Davison, B., Neutron Transport Theory, Oxford(1957).

50. Leimdorfer, M., "On the Transformation of the Transport Equation for Solving Deep Penetration Problems by the Monte Carlo Method," *Trans. of Chalmers Univ. of Tech.*, No. 286(1964). See also *Trans. Am. Nucl. Soc.* 6, 427(1963).

240-816 O-67—22

Vol. II

ENGINEERING ANALYSIS AND DESIGN

BASIS AND METHODS

J. C. LeDoux
CDR,CEC,USN

I N D E X

VOL. II

VOL. III

Foreword

This portion of the proceedings of the Kansas State University 1962-1963 Summer Institute on Radiation Shielding has been titled "Engineering Analysis and Design, Basis and Methods" as an attempt at a brief descriptive title. Actually, it is much more than engineering analysis and design, though the end objective of this effort is that the reader understand and be able to apply the latest practical methods of fallout radiation shielding analysis and design.

For a thorough understanding of these engineering methods the designer or analyzer must understand the basis of the method. This is especially true of the person who wishes to teach this engineering to others. Since these summer institutes were established to develop the capabilities of university faculty members in the relatively new science of radiation shielding, a great deal more emphasis has been given to the "fundamentals" than to the "practical" engineering.

This section of the institute has three distinct parts: (1) description of the methods and the data which have been generated as a result of research on the penetration of fallout radiation; (2) the technical assumptions underlying the conversion of this basic data into engineering methods; and (3) description of these engineering methods.

During the 1962 institute, all three parts were covered during the four-week period by a series of lectures given by the author. During the 1963 institute CDR LeDoux was unavailable for the entire institute. Part (1) was covered by Dr. R. E. Faw, Kansas State University; part (2) was given by C. Eisenhauer, National Bureau of Standards; and part (3) by CDR LeDoux. Since Charles Eisenhauer was mainly responsible for the actual development of the basic engineering method now in use, the institute was fortunate indeed in obtaining his services. His work in this has been published as NBS report 7810, dated February 1963.

This final report is then a synthesis of the 1962 proceedings, the lecture notes of Dr. Faw and Charles Eisenhauer during the 1963 institute, and the since published reports which bear directly on the subject matter of the institute. The valuable editorial comments and suggestions of Paul I. Richards of Technical Operations Inc., Burlington, Massachusetts are also acknowledged.

I - INTRODUCTION

A. Purpose.

This document, being a commentary on other documents, is not entirely self-contained. It is to be used in conjunction with detailed information in one or more of the following references:

1. "Structure Shielding Against Fallout Radiation from Nuclear Weapons", by L. V. Spencer, National Bureau of Standards Monograph 42, U.S. Gov't Printing Office, June 1962.

2. "Design and Review of Structures for Protection from Fallout Gamma Radiation", Department of Defense, Office of Civil Defense, OCD PM 100-1, 1964.

3. "Equivalent Building Method of Fallout Radiation Shielding Analysis and Design", TR 20(Vol 2), Sept 1963, Department of Defense, Office of Civil Defense.

The purpose of the present commentary is to introduce such information to readers whose professional experience has not prepared them for either the specialized technical discussions or the abbreviated summaries in these references. In particular, we attempt to bridge the gap between the training of civil engineer or architect and the sometimes complex techniques that are often required when calculating the protection factors of practical buildings which are used as shelters against fallout radiation.

Because radiation shielding is an inherently complicated subject, those who use its results should understand the underlying physical phenomena at least in a qualitative way. Such an understanding can forestall hasty application of standardized charts to special situations; it will allow the professional to be selective in his calculations and to judge the practical reliability of an answer that has been obtained "by the book." In short, the professional estimator should develop a "feel" for radiation shielding, and this document attempts to provide such an understanding.

B. Organization.

The ensuing discussion will start with a review of important qualitative features of fallout radiation - what it is and how it acts. The discussion then examines how a complex practical situation can be broken down into simpler partial problems that can be analyzed individually and later reassembled to provide practical answers.

The discussion then turns to information in the references already cited. The basic, highly accurate information in the first 53 pages of Spencer's monograph (Ref 1) is reviewed first. With a few exceptions, it is this information upon which all calculations of fallout shielding are ultimately based.

Next we explain the manner in which this basic information was adapted to practical calculations in the Engineering Manual (Ref 2). This is the step where the accurate but limited basic information is subjected to a number of engineering approximations, which, while justified in most practical cases, must be appreciated if the best use is to be made of the charts that result.

Finally, a shorter method of estimating protection factors (Ref 3) is also reviewed.

II - BASIC CONCEPTS

A. What is Fallout?

Fallout is essentially radioactive dust from a nuclear explosion. The highly dangerous type, which requires shelter for human survival, occurs when a bomb has been exploded close to the surface of the earth. The dust itself comes from dirt, sand, and other debris that is swept aloft into the nuclear "fireball" by the same winds that form the famous mushroom cloud.

The dust acquires its dangerous radioactivity while it is in this cloud. At that time, vaporized radioactive materials from the bomb itself condense on the dirt particles. When the updrafts from the explosion finally die down, the dust particles, with their radioactive burden, are then carried horizontally by prevailing winds as they settle back toward the earth.

In this way, much of the long-lived radioactivity generated by the nuclear explosion may be carried a hundred miles or more from the site of the explosion and deposited several hours later in areas that are otherwise unaffected. Fallout shielding is designed to protect human beings from this one danger, the radioactivity of the contaminated dust.

Fallout shielding is easily confused with blast shielding, because both must be massively constructed. Indeed the two types of shielding can often be combined advantageously. The distinction between the two types lies merely in the fact that blast shielding must possess strength as well as mass, whereas mass by itself suffices for fallout protection.

B. What is Fallout Radiation?

Fallout dust gives off several types of radiation, but as long as the dust is not ingested, only one type, called "gamma rays," is highly dangerous. These gamma rays are similar to X-rays: they can penetrate large thicknesses of matter, and when they finally do interact with matter, they damage the tiny volume in which the interaction occurs. In most materials, such damage is invisible at moderate dosage, but biological systems are quite sensitive to internal damage, and dosages that produce no visible effect in ordinary matter can easily be fatal to an animal or person. Again like X-Rays, gamma rays are invisible and cannot be detected by any human senses, at least, not sufficiently to serve as a practical warning of danger.

Both the penetrating power of a gamma ray and the damage it may do depend on its energy. Indeed, the only intrinsic distinction between a gamma ray and an X-ray is the energy of the individual "rays," technically called "quanta" or "photons." The energy, in fact, is nearly proportional to the damage that the photon can do, although there are discrepancies at the lower energies. For rough, qualitative estimates of the danger of fallout radiation, and of the effectiveness of fallout shielding, it suffices to consider the energy flux, the "gamma illumination," at various points inside the shelter.

A fallout shelter, then, requires massive walls to stop the highly penetrating gamma rays before they reach the interior of the structure. It might appear that such a shelter should have no openings, but this is seldom practical, and indeed, it is not even necessary, although simple open windows are best avoided. To see the governing principles behind these remarks, we must consider some additional properties of gamma rays.

C. How Radiation Travels.

Gamma rays are like X-Rays in their penetrating power, but they resemble ordinary light rays more in their ability to be scattered and "reflected." All thesereradiations travel in straight lines for the most part, and for all three types, a straight-line flight may be terminated by an absorption, a complete disappearance of the ray (accompanied by release of its energy in some other form).

Both light and gamma rays, however, can be scattered by matter, and thereby can be deflected into new straight-line paths, perhaps many times over. Gamma radiation shares the penetrating power of X-rays, however, its scattering mechanism, unlike that for light, is extremely simple. In effect, a gamma ray "sees" only

the individual electrons in matter, and it can be deflected only by bouncing off one of the atomic electrons, usually deep in the interior of even a "solid" block of dense material, like steel or concrete.

We might summarize these explanations by saying that gamma rays travel like light rays but to gamma rays, all materials are translucent; none are opaque, and none are fully transparent. Like most succinct statements, this must not be taken too literally, for it seems to suggest a limitation on attainable shielding factors. Whereas in principle no finite limit exists.

To develop qualifications such as this, we need one final property of gamma ray behavior. Namely when a gamma ray is scattered, it loses energy. (The "lost" energy, of course, is transferred to the electron that caused the scattering, and indeed, the major damage from gamma rays is performed by proxy, through the recoiling electrons.) This energy loss can be surprisingly great if the angle of scattering is large. For example, no matter how energetic the incoming gamma may be, the outgoing, scattered ray can contain no more than 0.51 Mev (million electron volts), if the scattering angle is 90^{o}; and no more than 0.26 Mev if the scattering is directly backwards.

These descriptions do not exhaust all possible behaviors of gamma rays, but they cover the main features of importance to fallout shielding: gamma rays have high degrees of penetration through all materials and straight-line paths of travel that are altered every now and then by a sudden change of direction, with an attendant loss of energy that is greatest when the change of direction is greatest.

It must be emphasized that, penetrating as they are, gamma rays scatter in air as well as in other materials. To be sure, air has fewer electrons per unit volume than denser matter, and the straight-line portions of a gamma ray path in air are correspondingly longer than in dense matter. But, except for this difference in scale-factor, the processes are identical. For fallout shielding, the implication of this is that not all dangerous gamma rays need to travel straight from the radioactive dust to a shelter. In many situations, they may travel upward and be scattered by the atmosphere into paths that can take them through a weak point in a shelter.

D. The Mechanisms of Shielding.

Before considering the usual massive shield we should mention one point that is sometimes overlooked. Clearly, one protection against fallout is to remove oneself to a sufficient distance from it. Even small distances can be helpful under some circumstanes: despite air scattering and the possible presence of contaminated dust on nearby roofs, the upper stories of a high-rise building may offer some protection merely because they are not close to dust that has fallen to street level. While such protection may often be inadequate by itself, yet under suitable circumstances, it may offer a valuable supplement to the more common massive shielding, and it should be examined carefully where circumstances suggest it.

Massive shielding, the only other form of protection, operates by interposing a blanket of electrons between the radioactive dust and the protected area. If sufficient numbers of electron are present, they will scatter the gamma rays and degrade their energy a sufficient number of times to render them relatively harmless (or allow them, finally, to be absorbed like X-Rays). Of course, this is a random process; a very few gamma rays will always penetrate the entire shield without scattering at all, and a somewhat greater number will manage to penetrate the electron blanket with only a few minor scatterings. But if the shield is made thick enough, the vast majority of incident gamma rays will be stopped or turned aside or rendered harmless in one way or another.

We have spoken both of mass and of electrons in the shield, and it may not be clear that these are nearly equivalent. From our discussion of gamma ray behavior, it is evident that electron-density is the only important property of fallout shielding, but electron density is closely correlated with mass density, because the atomic mass, A, of almost every chemical element is roughly equal to twice the total number of electrons, Z, in the atom (A = 2Z). The most important exception is the rather common element hydrogen (A = Z), which, accounts for only a small proportion of the mass density of common materials. For example, water (H_2O) has a mass density of 62.4 lb/ft^3, while its "effective density" is 69.2 lb/ft^3 if we express its true electron density on a scale appropriate to the relation, A = 2Z. Thus, the "effective" density of a shield against fallout radiation is very closely correlated with its mass density. This rule of thumb is extremely useful in searching for the weak points of a shelter, although corrected effective densities should be used for actual numerical calculation.

We mentioned earlier that openings in a shelter are allowable when they are properly designed. Of course, even a simple open window does not make a shelter entirely useless, but a window is far less desirable than another type of opening, the "maze." By this, we mean a duct or passageway with massive walls and a meandering path that will force the radiation to make several sharp turns in order to enter the shelter. Since gamma rays can execute a turn only by being fortuitously scattered at the right moment, and because they lose energy in the process, such a "maze" opening can offer considerable shielding without obstructing air flow at all.

In summary, the prime means of shielding is by massive protective walls (although sufficient distance from major areas of contamination is a valuable secondary factor, when available). Complete closure is not necessary, however. If open pathways contain several bends, they may be almost as effective as an unbroken wall. We shall discuss precise forms of these statements in later sections.

E. Finding a Likely Shelter,

Before turning to quantitative treatments, we discuss a few qualitative approaches to estimating the value of a proposed shelter. These considerations are helpful in searching for likely-looking spots in existing buildings and for judging what sorts of additional construction or remodeling would probably be most valuable and offer the greatest improvement at least cost.

Thus, we are speaking about the first, exploratory approaches to a shielding problem. These rough rules must be supplemented by careful calculations before any firm conclusions can be reached, but they are helpful in deciding what structures and locations would be most likely to repay more careful examination.

First, it is helpful to visualize what the radiation would look like if we could see all the individual gamma rays. Outdoors, in an open field uniformly contaminated with fallout, the first impression would be one of rays traveling in every conceivable direction, criss-crossing each other in all manners imaginable; the rays literally travel "every which way." Upon closer study, one would note that, at any point (less than about 100 ft above the ground), only some 10% of the energy flux is traveling generally downward. The total intensity of the flux falls off slowly with increasing height: at some 60 to 70 feet above the surface, the total illumination drops to about half its value at the surface. At this same height, one also notes a change from predominantly horizontal or

slightly upward rays to more predominantly vertical travel as the height increases.

The general picture of the gamma flux that will strike a shelter, then, is roughly similar to the illumination that would be observed in a tank of somewhat milky water, lighted from below by a bright, ground-glass screen. The shelter problem is analogous to constructing a darkened volume over a thin opaque floor-slab inside the tank, but using only translucent materials for the walls and roof.

When searching for potential shelter, then, one should first look for massive walls, preferably below grade where the surrounding earth will offer additional mass. If there are other buildings nearby, they may offer some additional attenuation. The next best location is perhaps on the higher floors of high-rise building, not closely surrounded by nearby roof areas that could hold fallout dust. The top floor, however, would usually be too close to the fallout on the roof of the same building.

It should be kept in mind that several heavy partitions can act like a single wall with roughly the same total mass per unit area. Thus the central area of a building that has heavy partitions may offer almost as much protection as a basement with massive walls. Thin partitions, however, seldom offer any significant additional protection.

Second only to massive walls in importance is a massive roof and, if the shelter is above grade, a massive floor. Again, the effective mass of several floors above or below the central location may be added to obtain an effective "roof" or floor thickness. The roof thickness is usually more important than the floor thickness, because even a sloping roof can collect fallout particles, and the gamma radiation from such a deposit on the roof can readily penetrate to the shelter unless the effective roof thickness is large. While even a single story building without a basement can offer some protection if the walls are reasonably thick, it will usually be inadequate unless the roof is also massive.

Windows, of course, are never desirable, but they may be unavoidable. If they do not allow a direct view of the surrounding flat areas where fallout may come to rest, they are less serious than if they do. If any case, the remaining portions of the wall will screen off much of the incoming radiation. As a rough rule of thumb, the effective mass

thickness of a wall with windows is about equal to its total mass divided by its total area, including window areas. This rule can be misleading in special cases, but it can give a rough indication of whether a given structure is worth further study.

Generally speaking, the structure should be examined for path-ways where gamma radiation can enter the proposed shelter without encountering very much mass and without having to turn very many corners. Thus, stair wells and elevator shafts may sometimes drastically reduce the effectiveness of an otherwise massive building. Again, windows set high under a massive overhanging roof can allow direct radiation from the surrounding ground to strike the ceiling and be scattered down into the interior of a shelter. As a final example, a building with a below-grade basement may be less effective than it first seems to be, because of a thin basement ceiling and just enough mass in the first-floor walls to scatter gamma rays down into the basement.

While more could be said about particular situations, these general principles are usually sufficient for initial judgements concerning the possible value of a given site. Rather than entering into further detail in a qualitative assessment, it is usually more profitable to make specific calculations. In the preliminary stages of such calculations, it is usually most profitable to concentrate at first on contributions from what appear to be the weakest features of the proposed shelter. If these results do not eliminate it, then a complete calculation would be indicated.

III - DETECTORS AND DETECTOR RESPONSE

A. Introduction.

"The analysis of structures for their protection against ionizing radiation represents a new field of engineering which has many similarities to illuminating engineering. Estimating radiation levels at different locations in a complex structure is comparable to the problem of determining the illumination levels in a similar structure on a cloudy day, but with all partitions and walls having varying degrees of transparency or translucense rather than being opaque. The complexity of the problems is such that, despite intensive research, significant gaps in our knowledge still remain."

This introductory statement by Dr. L. V. Spencer in NBS Monograph 42 (the basic treatise on fallout radiation shielding),

briefly describes the problem of analyzing structures as shields against fallout radiation. He says, in effect, that our knowledge is still far from complete, and thus any engineering technology based on this present knowledge must also be non-exact and approximate. Yet this is nothing new to engineers who candidly admit that their safety factors are in reality "factors of ignorance." Despite these gaps in our knowledge, the science or art of radiation shielding as applied to fallout sources is accurate enough for practical applications. Although it is possible to launch immediately into the present day methods of engineering analysis, a complete understanding of the state of the art would not be gained. In this report, the basic work of Dr. Spencer will be described in detail; next, the assumptions underlying the conversion of the basic data into an engineering method will be explored; and finally, the various popular engineering methods in use today will be explained and demonstrated.

We are concerned here only with fallout radiation fields. The engineering problems commences with the basic assumption that fallout will be distributed uniformly over all horizontal surfaces. We could, at this point, treat in detail what fallout is, how it is formed, its various characteristics in space and time. Since this has already been done in numerous other publications, we will omit a discussion of this subject here and refer the unitiated reader to the best reference on this subject, namely "The Effect of Nuclear Weapons-1962" available from the Government Printing Office, Washington, D. C. The pertinent chapters are I, II, VIII, and IX.

The following assumptions will hold throughout this text unless specifically retracted for a particular example or discussion:

(1) Fallout is uniformily distributed over all horizontal surfaces.

(2) The 1.12 Hr energy spectrum is assumed to be time invariant.

(3) Only gamma radiation is considered.

(4) Fallout decays according to the $t^{-1.2}$ approximation.

(5) Radiation is emitted from individual fallout particles isotropically.

None of these assumptions are so restrictive that they make any subsequent development only academic. We would not expect dry sand particles to stick to vertical surfaces in such quantities that they would materially affect the total contribution. The 1.12 hour spectrum is the most energetic early spectrum for fission products and subsequent spectra would tend to be less penetrating. Any actual differences within the first 10 days in energy spectrum and thus in penetration characteristics are so minor as to have no practical significance. Even the lightest of construction material screens out all but gamma radiation and thus only gamma radiation need be considered. The $t^{-1.2}$ "law" has been verified to be an extremely good approximation for fission product decay for times from roughly 1 hour to several months. Since it is only used to determine total dose over a period of shelter stay time, its use does not affect the shielding properties of a structure but only the total estimated dose to be expected under assumed fallout conditions. The final assumption is the only logical one to make since individual fallout particles range from 50 to 300 microns in size and their orientation on the ground must be a strictly random process. Thus any possible anisotropic properties which any particle may have would be cancelled out by other particles and the radiation field would be a plane, isotropic field.

Before we can proceed further with a discussion of radiation shielding, we must describe the device or instrument we will use to measure the quantity of radiation energy at various points of interest. The next section then, will describe radiation "detectors."

B. Detectors.

In structural engineering, a designer considers each component such as columns, beams, floor slabs, etc., separately. He designs this component to resist the loads and forces which are assumed will act upon it. The structural engineer does not have a simple device with which he can readily measure the true worth of the final product. The final test is the integrity and durability of the structure under load. In some dramatic cases (such as the Tacoma Narrows Bridge) the structure may fail after long use due to some error in design.

In radiation shielding, on the other hand, the design engineer has a measuring device which he can use to check the total effectiveness of his design under "load" conditions. In design work it is an entirely theoretical device but an extremely useful one. In experimental work, it is an actual,

though imperfect, instrument. These devices are called radiation detectors. In theory we can use an isotropic detector to measure radiation which comes from all directions to tell us the total "response" at any particular location. For certain applications, we make use of directional detectors to measure radiation coming only from certain specified directions or from certain limited sources. This is possible in practice although much more difficult.

No improvement can be made on the description of the type of detector which is considered hereafter than that of Dr. Spencer's in NBS-42, "Every detector is characterized by its 'response function' which is the 'efficiency' of gamma rays of photon energy E, incident on the detector from various directions, in producing the measured effect. It is frequently advantageous to have an 'isotropic' detector, i.e., one equally efficient regardless of the direction of incidence of the photons.

The most commonly used radiation detector consists of an enclosed air space containing a pair of oppositely charged electrodes. When exposed to radiation, the gamma rays interact with the material surrounding the air space, producing high-velocity recoil electrons, some of which traverse the cavity and ionize the air within. A measurable electron current is produced as the ions travel to the electrodes and deposit their charge. It is this current, divided by the volume of the air space, which constitutes the response of the instrument.

These so-called 'cavity ionization chambers' are usually constructed in such a way that their response is nearly isotropic. But the current per cm^3 measured by the instruments is not proportional to the total energy incident upon the detector. Instead it is nearly proportional to the energy deposited per gram of detector material, as a result of gamma ray interactions occurring within the detector. When such detectors have cavity walls of a material similar to air in its reaction to irradiation, the response can be measured in roentgens and referred to as 'dose', or more precisely as the 'exposure dose.' (i.e., the energy deposited in air)."

The use of the term "detector response" hereafter will always imply an isotropic detector of the air-equivalent type whose response in roentgens is called "exposure dose."

C. Standard Dose.

In order to measure or test the effectiveness of a particular shield design, we compare the detector response of

the protected location to a "standard." The standard dose is the response of our isotropic detector when it is placed 3 feet above a smooth, infinite plane which has been uniformly contaminated with fallout. The density of fallout particles on this smooth plane must be exactly the same as the density distribution surrounding the shielded position. In most cases, the detector position within the shielded space is also located 3 feet above some reference plane, usually the floor of the detector. This need not be the case however. The distance of 3 feet was chosen for the standard since this is roughly the distance to the vital organs of an adult standing erect.

The effectiveness of a protected location is described by either a "reduction factor" or a "protection factor." These are abbreviated as Rf and Pf respectively. If we allow the standard dose to be D_o and the dose within a protected location to be D, then

$$Rf = D/D_o$$

and

$$Pf = D_o/D$$

Thus a reduction factor is always a number less than 1, and a protection factor is always a number greater than 1.

Note that the concepts of reduction factor or protection factor and standard dose are completely independent of the fallout intensity, time after burst, location relative to ground zero and so forth. The standard is always measured relative to local conditions and can be thought of as normalized to unity. This procedure enables us to compare the shielding effectiveness of structures located at different points. A protection factor of 100 means that this particular building will reduce the amount of radiation received by a factor of 100 over what one would receive if exposed to an infinite, smooth plane of fallout contamination with the same particle density. Note that the Pf and Rf are not really ratios of inside to outside doses. Most real locations in open areas offer better protection than the smooth, infinite, idealized plane. It is possible for two buildings with the same Pf to provide different degrees of protection. Thus one building may be safe and the other unsafe depending on the radiation field outside, though the reduction factor for dose is the same.

This is an appropriate place to briefly discuss the "philosophy" of Pf numbers. A normal frame house will provide a Pf of about 2. An inner office of a large building perhaps a Pf of 10. A completely buried basement may provide a Pf of 500 or more. Obviously the higher the Pf the better, since any amount of radiation is harmful to a certain extent. A 1 roentgen dose has been likened to receiving 2-4 chest X-rays without benefit of seeing any pictures. A 100 r dose will not affect most healthy adults enough so that they would know

they had been irradiated. All will get sick and some will die with a dose of 250 r. At 450-500 r about 50% will die and a 600-700 r acute dose will kill up to 100% of those exposed. These figures apply to a large group of healthy, young adults.

What Pf do we need to insure that no one will die? That no one will be sick? These cannot be answered with exactness since there are so many variables involved, but statistical studies of fallout conditions from expected raids are used to determine minimum criteria. A Pf of 100 provides sufficient protection to insure that few people will become sick and none will die even in the most intense fallout fields. This is the minimum OCD Pf for new construction. In many areas a Pf of 40 will be sufficient for no deaths and few sick. This Pf 40 is allowed by OCD in those areas where the risk is less and where there are not sufficient Pf 100 shelters.

D. Coordinate System.

In order to orient a detector relative to radiation sources, some coordinate system must be selected. Figure 1 illustrates the coordinate system which will be used. This is a coordinate system oriented from the detector viewpoint. The polar coordinates θ and ϕ are measured relative to an arbitrary polar axis through the center of the detector and a reference half-plane terminating along the polar axis. Both θ and ϕ are determined from a line pointing in the opposite direction to photon travel. This line also originates at the detector center.

The coordinate system chosen above orients our thinking in terms of radiation sources. A detector inside a closed box structure "sees" radiation as it emerges from the walls and roof. For all practical purposes, these surfaces are in effect secondary sources. The primary sources (the fallout particles) are not observed by the detector, and are not then of direct importance to the detector. The coordinate system chosen also allows us to focus our attention on individual surfaces which is necessary if we wish to break down the problem into simple components. The detector response will be compared to the response of the same detector at the standard location.

E. Detector Description.

We will choose a detector in the form of a spherical probe, all parts of which are exposed to the same radiation flux. The probe is small enough that it does not appreciably disturb the flux. The response of this detector will be isotropic except in certain cases where a directionally dependent detector will be used. A directionally dependent detector allows us to limit

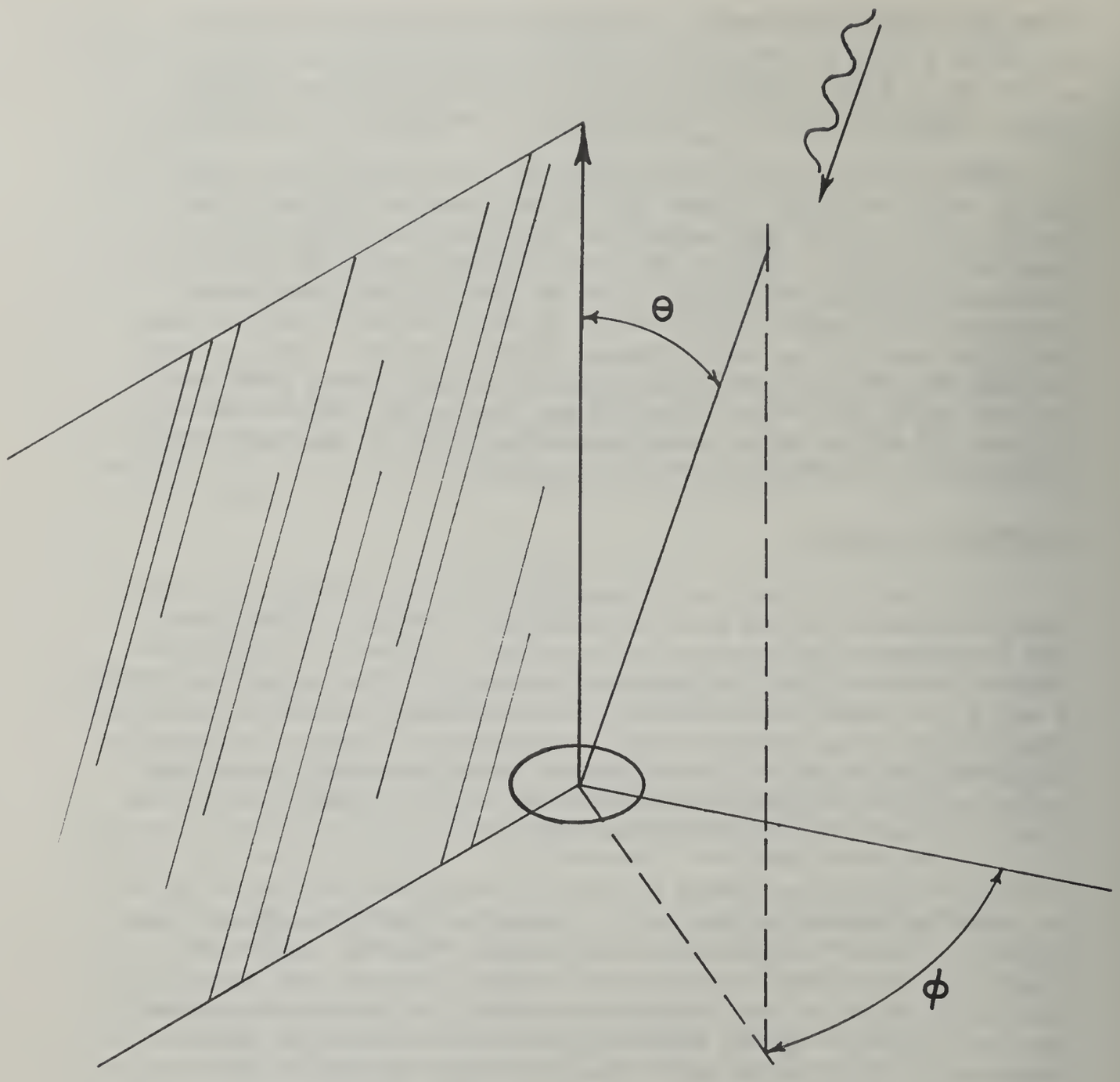

COORDINATE SYSTEM

Figure II-1

the response to a single surface source. The detector will be constructed of air-equivalent material whose response is measured in roentgens (exposure dose). For our purposes, "dose" can be considered as a measure of the energy transferred by fast electrons in the air-volume of detector space.

F. Detector Response .

Consider a small differential area dA on a unit sphere (the detector sphere). See Figure 2. Using the coordinates θ and ϕ, the differential area is $\sin\theta \cdot d\theta \cdot d\phi$. This is also the differential solid angle. $\sin\theta \cdot d\theta$ is also the differential of $\cos\theta$, i.e., $d(\cos\theta)$.

At this point we begin to introduce the mathematical notation used by Dr. Spencer in NBS Monograph 42. The integral equations for the various functions derived by Dr. Spencer will be presented even though we will not attempt to solve any of these equations. Their solution actually requires electronic computers. The solutions of these equations are presented in the forms of graphs and charts. They are used because they are the best shorthand notation available to present complex mathematical concepts of radiation source distributions and the dependent barrier and geometry functions. A casual inspection of the various functions used by Dr. Spencer seems to indicate that they are all almost the same. A careful study of the limits of integration and the various parts within the integrand will be profitable for the reader if he wishes to extract the maximum benefit from NBS-42. There is a wealth of basic information in this document which has wider application than the field of fallout radiation.

The detector response will consist of all contributions from all θ,ϕ. This detector response function will be labeled $D(\theta,\phi)$. This functional notation is used extensively in this paper and in other shielding documents. The notation $D(\theta,\phi)$ means that detector response D, for dose, is a function of the angles θ and ϕ, and is read "Dee of theta, phee." The detector response function depends not only on the detector physical construction but on the radiation source as well.

Thus the function $D(\theta,\phi) \cdot \sin\theta \cdot d\theta \cdot d\phi$ is the response of the detector to photons passing through the probe between θ and $\theta + d\theta$, and ϕ and $\phi + d\phi$. The total response over all directions would then be:

$$D = \int_0^{\pi} \sin\theta\, d\theta \int_0^{2\pi} d\phi\, D(\theta,\phi). \qquad (1)$$

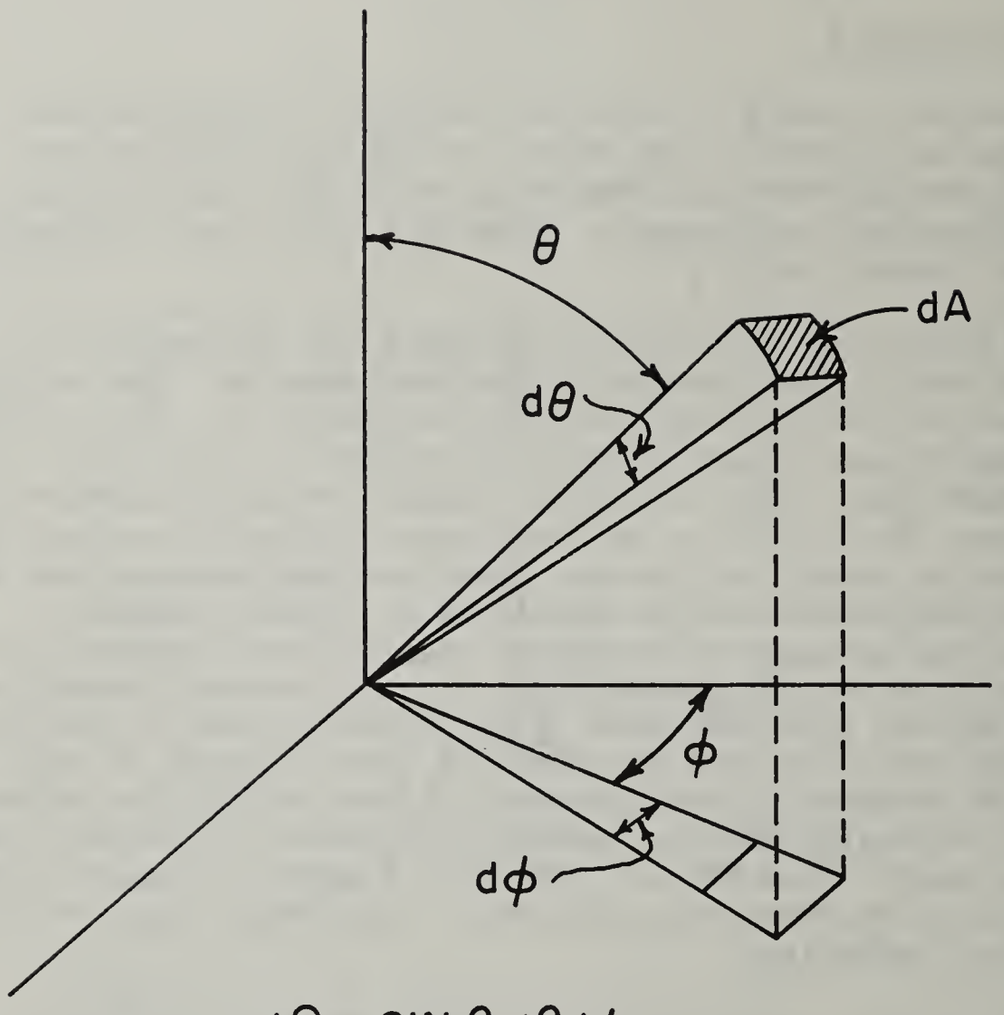

$$d\Omega = \text{SIN}\,\theta\, d\theta d\phi$$

UNIT SPHERE SOLID ANGLE

Figure II-2

$D(\theta,\phi)$ can also be called the dose angular (or directional) distribution. This quantity, dose angular distribution, sums up the contribution of the radiation flux by integrating over energy of the photons present weighted by the proper energy transfer coefficient.

The concept of dose angular distribution is very important and should be thoroughly understood. In order to measure the effectiveness of a shield we must not only know how much radiation penetrates the barrier, but the directional distribution of the radiation which emerges from the shield. A real detector does this automatically since it will "count" only those photons which interact within the detector cavity. Mathematically, our detector is only a point in space and we must know the distribution of radiation so that we can "count" the photons which would interact with our ideal detector if we had one at the point in question.

Suppose that we had a special detector which would only accept radiation coming in a very narrow beam the diameter of an ordinary pencil. This is called a collimated detector or a directional detector. If we then had some source of radiation and we wished to measure the dose angular distribution of radiation from that source at some point in space, we could use this pencil detector. By rotating this detector through planes and angles of interest and plotting the results, we would be able to graph the dose angular distribution at that point.

To illustrate an angular distribution encountered in every day life, let us suppose that we had a point source of light suspended in space. We will use the eye as the detector and graph the directional distribution of light photons which we see. With nothing between the source of light and our eye, we would see only a bright point of light. This would graph as a single straight line whose length represented the intensity of the light received. The line would be on the axis joining the source and the eye (detector). Now let us place a thin piece of frosted glass between the light and our eye. We would still be able to see the point of light, but the intensity would be less. In addition, we would see a less intense fringe of light surrounding the center point from light which has been scattered in the glass. This would graph as a sharp peak along the axis of our graph, but there would now be points on either side of less length. Finally, if we placed a heavy piece of frosted glass between the light and our eye, the point of light would no longer be visible and the light would be diffused over a much greater area. Such a distribution would plot something like an ellipse with the major axis pointed along the line between the eye and the light. Such "rose" diagrams will be used later to describe the angular distributions of concern in fallout radiation sources.

We will return now to our main discussion. There will be some cases where we will be interested in thinking of directional detectors similar to the pencil detector mentioned above. These can be constructed from an isotropic detector by placing a shield around the detector in those directions from which we wish to exclude response. Figure 3 is such a detector. This can be indicated by the integral:

$$D=\int_{1-\cos\theta_{max}}^{1} d(\cos\theta)\int_{0}^{2\pi} d\phi\, D(\theta,\phi). \qquad (2)$$

Note that we have used the differential cosine notation. This can also be written using a limiting response function:

$$D=\int_{-1}^{1} d(\cos\theta)\int_{0}^{2\pi} d\phi\, D(\theta,\phi)\, g(\cos\theta_{max}), \qquad (3)$$

where $g=1,\ \theta=\theta_{max}$

$=0,\ \theta>\theta_{max}.$

The use of such a function as $g(\theta)$ makes the equation either general or specific at our discretion and is more flexible than the change of integration limits.

For discussion purposes these equations are easy to write but in practice we will need to know specific information about the detector response function $D(\theta,\phi)$. The directional distribution and energy spectrum will depend on the source of radiation. We would expect considerable difference between a roof source and a wall source even though both were produced by essentially the same primary source field. Reverting again to the viewpoint of the detector, let us define a limiting response function g_s which defines the radiation surface of interest. The "s" stands for surface. This function will depend only on direction and not on energy. The dose angular distribution function $D(\theta,\phi)$ will include any dependence on energy. The surface limiting response function g_s will be equal to one when radiation can intercept both the detector and the surface; otherwise g_s

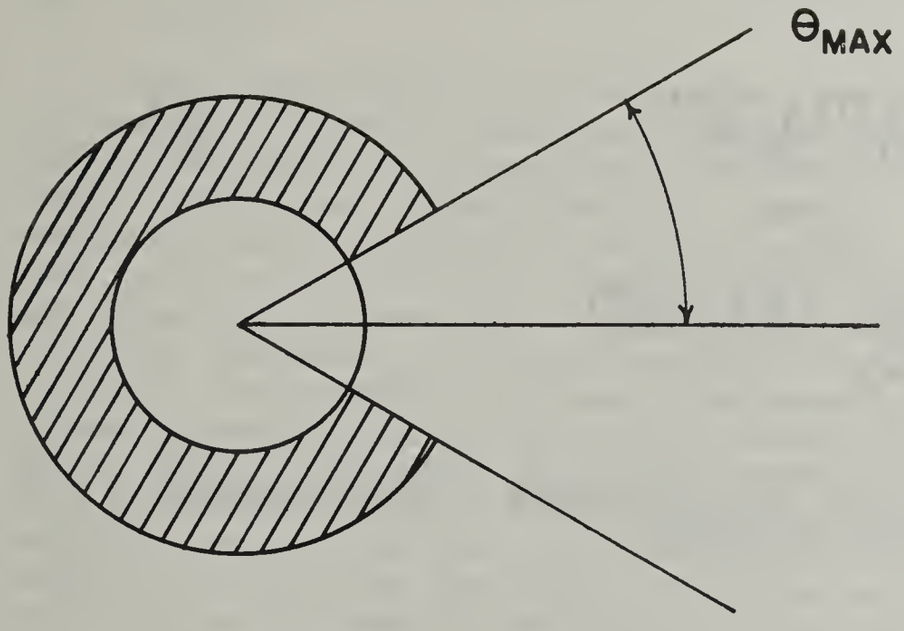

DIRECTIONAL DETECTOR

Figure II-3

will be zero. Using such a limiting response function will also make the detector response dependent on the surface being considered and we will label this detector response D_s.

$$D_s = \int_{-1}^{1} d(\cos\theta) \int_{0}^{2\pi} d\phi\, D(\theta,\phi)\, g_s(\theta,\phi) \qquad (4)$$

This is equation 16.2 from NBS Monograph 42. If the response is independent of ϕ, the equation reduces to 16.3:

$$D_s \int_{-1}^{1} d(\cos\theta)\, D(\theta)\, g_s(\theta) \qquad (5)$$

$$\text{where: } g_s(\theta) = \frac{1}{2\pi} \int_{0}^{2\pi} d\phi\, g_s(\theta,\phi)$$

Equations (4) and (5) are starting points in the development of the various functions in NBS-42.

IV - BASIC THEORY FOR STRUCTURE SHIELDING ANALYSIS

A. Introduction.

1. At this point the reader should have an understanding of the following terms: detector, standard dose, reduction factor, protection factor, and dose angular distribution. With these in mind and before we discuss the various functions used by Dr. Spencer, it would be instructive to discuss radiation shielding in a qualitative sense.

The radiation of primary interest in fallout radiation shielding in the so-called "gamma radiation," Gamma rays belong to the high energy, short wavelength portion of the electromagnetic spectrum. They are in the family of X-rays, radio-waves, and light. They therefore have many characteristics

common to these more familiar members of the electromagnetic family. They travel in straight lines at the maximum speed allowable in the universe, namely the speed of light, 3×10^{10} cm/sec. They interact with matter and are absorbed or scattered during this interaction. Because of their extremely short wavelength and high energy, they can penetrate matter quite easily and conversely and are rather difficult to stop. Gamma rays interact mainly with electrons. Quantum mechanics and extensive experimental evidence tells us that all matter has both a wave-like and a particle-like nature. Thus gamma rays are identifiable as "packets" of energy called photons. These individual photons then interact with individual electrons and in a scattering event, the collision is particle-like. The electron recoils with some of the photon's energy, and the photon careens off in a new direction with less energy than it had initially.

In any real radiation process, there are billions of photons and billions of electrons involved. Consequently, statistical laws can be employed to predict the results of these interactions. Thus, if we had a parallel beam of photons striking a given thickness of known material, we could predict what fraction of the incident photons would emerge which did not undergo any interaction. Linear absorption coefficients, μ, have been tabulated for various materials for ranges of photon energies. This coefficient times a thickness of material, dt, is the probability that a photon will have some sort of interaction while it traverses this small thickness, dt. If the slab is not too thick, we would expect that this probability would be constant for the entire thickness, t. In mathematical terms, if we let N be the number of photons striking one side of a slab, a differential thickness dt wide, then the loss of photons by interactions within dt would be:

$$\frac{dN}{dt} = -uN. \qquad (6)$$

The minus sign is necessary since there is a net loss of photons during the process. For the total thickness of the slab, this integrates out to:

$$N = N_0 e^{-ut}. \qquad (7)$$

The exponential nature of radiation attenuation in matter is the important result. Regardless of the source geometry this exponential behavior will be evident. One of the conclusions of such behavior is that some photons will penetrate a shield no matter how thick it is. The purpose of shielding is to reduce the fraction penetrating a shield to a limit that is tolerable.

Referring now to Figure 4, there are five contributing surface sources, the roof and the four walls. The sum of all responses to these sources could be noted as follows:

$$D = D_1 + D_2 + D_3 + D_4 + D_5 . \qquad (8)$$

or

$$D = \sum_{i=1}^{5} D_i . \qquad (9)$$

Observe for a moment one of the contributing walls, Figure 5. Using this sketch, we can define more exactly what we mean by "reduction factor" and "protection factor." We are primarily interested in detector position A. Consider first though, detector positions, B and C. Detector C would measure radiation entering the wall (neglecting any reflected radiation) and B would measure any radiation leaving the wall (neglecting any radiation scattered back from the other walls or roof). The ratio of these two detector responses would measure the "barrier" effect of the wall. We will lable this barrier factor B_1. It is essentially dependent only on the mass thickness of the wall. There is no geometry effect here. As previously discussed, we would find that the ratio of dose at B (D_B) to the dose at C (D_C) would have an exponential behavior as the wall mass thickness was varied, or:

$$D_B \cong K D_C e^{-ut} , \qquad (10)$$

where t is the thickness of the wall.

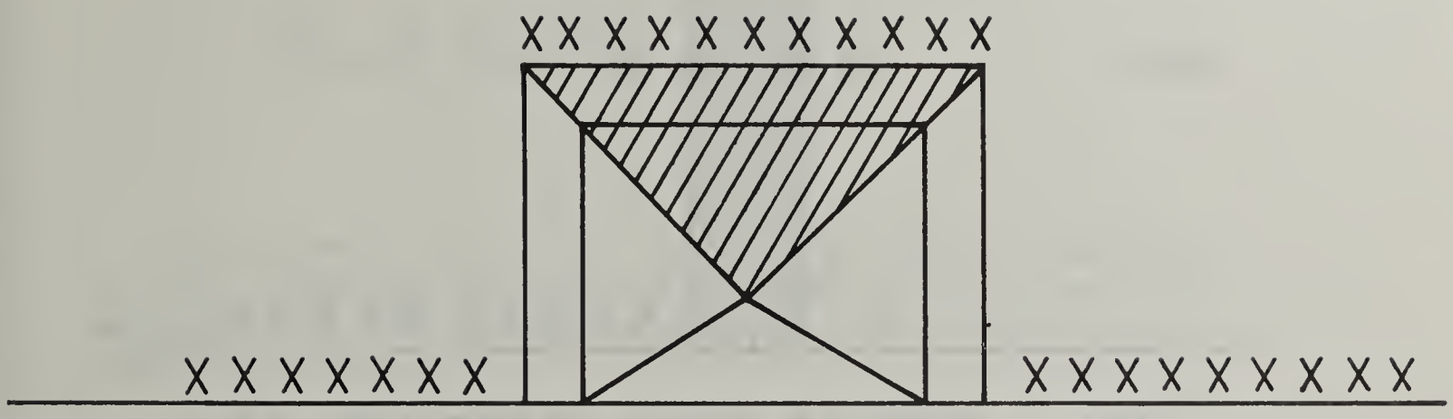

TYPICAL BLOCKHOUSE

Figure II-4

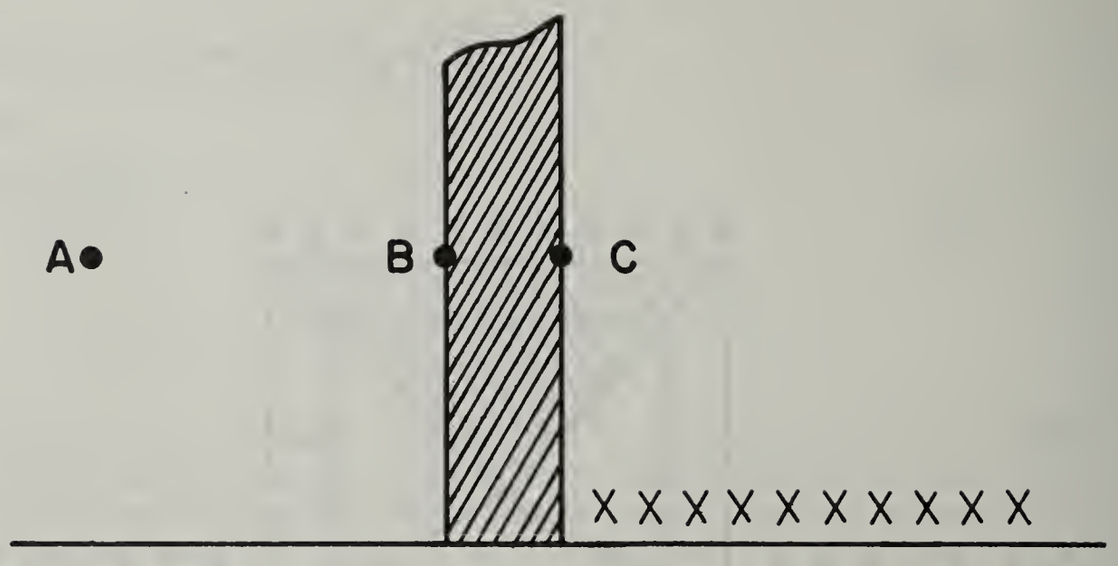

WALL BARRIER WITH DETECTORS AT POSITIONS A, B, AND C

Figure II-5

If we now moved to detector position A we would expect a further decrease in response and would find that this decrease was roughly proportional to $1/d^2$, where d is the distance from A to B. This is a geometry effect, or a "limited" source effect. The size of the contributing wall now becomes important.

The ratio of D_A/D_B is the geometry factor which we will label G_1. The dose at A would then be the product of B_1 times G_1 times the dose measured at C. However we wish to always refer our dose measurements to what we have called the "standard" dose and not to a dose like D_C which will depend on the local conditions. The standard dose is the dose measured 3 feet above a plane infinite radiation source. We label this standard dose D_o. The barrier factor will be modified slightly to include the ratio of the dose at C to this standard dose, and we will relabel the barrier factor to B_1':

$$B_1' = D_C/D_o \times B_1. \qquad (11)$$

The product then of B_1' times G_1 is called a reduction factor. This reduction factor is essentially a normalized partial dose. The protection factor is the inverse of the reduction factor.

Thus we can say that the barrier factor is the attenuation which would occur if the source were of a simple type and the medium everywhere uniform in density. The geometry factor accounts for all other features of the actual situation.

2. The <u>barrier factor</u> depends on the following variables:

   a. Weight per unit area of the barrier,

   b. Type of barrier material,

   c. Gamma ray spectrum, and

   d. Directional distribution of radiation striking barrier.

NBS Monograph 42 and the Engineering Manual assume the 1.12 hour prompt fission spectrum. Although the spectrum does change with time, the 1.12 hour spectrum is the hardest (most energetic)

early spectrum when shielding is most important. Using it tends to be conservative. The directional distributions vary widely depending on the particular barrier orientation with respect to source. The various distributions will be discussed at greater length later.

The weight per unit area and type of material will be discussed together. Almost all common construction materials have low atomic numbers so that attenuation is due primarily to scattering interactions. Thus the attenuation in a barrier is due almost entirely to how many electrons are in the path of the photon. This is the product of the number of electrons per unit volume times the thickness of the barrier. To measure the effectiveness of a barrier, a parameter is used called the "effective mass thickness" and is identified by "X." Thus:

$$X = 2\left[\frac{Z}{A}\right]\rho\Delta, \qquad (12)$$

where Z/A = atomic charge/atomic mass number.

The ratio of Z/A is close to 0.5 for most material, hence the factor of 2 to yield tabular values close to 1. Table I lists the ratio 2(Z/A) for various materials.

Table I. Values of 2(Z/A) and

Material	2(Z/A)	ρ, density in pcf
Water	1.11	62.4
Wood	1.06	34.0 (average)
Air	1.0	0.076
Brick	1.0	115
Concrete	1.0	144
Soil	1.0	100 (average, depends on water content)
Steel	0.931	480
Lead*	0.791	710

*Lead is included strictly for comparison. It should be remembered that the data from NBS-42 does not apply to lead because it absorbs rather than scatters the radiation.

The units of X are pounds per square foot (psf), but X is not density x thickness. This is only true for materials where the ratio 2(Z/A) is exactly equal to unity. A foot of water, for instance, has an effective mass thickness of 69.2 psf but a density x thickness value of 62.4. Layers of materials can be added together to obtain the proper total mass thickness::

$$X = X_1 + X_2 + \ldots + X_n \qquad (13)$$

and

$$X = \sum_i X_i \,. \qquad (14)$$

3. The geometry factor also depends on certain variables. They are:

a. Solid Angle Fraction. It is clear that the detector response will depend on the "apparent" size of the wall as seen from the detector. Since "apparent size" is conveniently measured in terms of solid angle or solid angle fraction, we say that the detector response will depend upon the solid angle fraction, ω , subtended at the detector by the radiation source.

To visualize the concept of solid angle, place a detector at the center of sphere of unit radius. To measure the solid angle subtended at the detector from a source area, draw radii from the corners of the surface to the center of the detector. The area determined by the intersection of these radii on the unit sphere is defined as the solid angle. The area is measured in steradians. There are 4π steradians on the unit sphere. In shielding, it is more convenient to use a hemisphere instead of the sphere, and the resulting solid angle is called "solid angle fraction."

b. Barrier Thickness. The thickness of the wall (X) will have an effect upon the detector response over and above the attenuation which we describe by a barrier factor. This is because the directional distribution of radiation emerging from the wall affects the detector response but is in turn affected by the wall thickness. In most cases

and up to a limit, thicker walls tend to produce directional distributions more and more concentrated along the perpendicular to the wall surface.

c. Wall Shape and Detector Position. The dependence on detector position is easy to demonstrate in the blockhouse illustration by the fact that one can find detector positions at the ceiling and floor in which the wall subtends the same solid angle fraction, but in which the detector response is expected to differ considerably. Shape effects can also be easily demonstrated; a detector 10 ft. out from the center of the wall will have one response if the wall is long and narrow and another if the wall is square, though subtending the same solid angle fraction.

d. Type of Source: The type of primary source, as in the case of barrier factors, varies widely enough so that we identify each with a special symbol.

e. Type of Wall Material. We treat, for the present only, the case of materials of atomic number 30 or below. This range includes the most important materials commonly employed in construction. As indicated previously, these low Z materials have a certain equivalence which we utilize.

The geometry factor is then a function of both X and ω. In functional notation, the geometry factor G_1 is represented as:

$$G_1 = G(X, \omega), \tag{15}$$

$$G(X, \omega) = \sum_i G(X, \omega_i), \tag{16}$$

and

$$\omega = \sum_i \omega_i. \tag{17}$$

In summary then, since $D = D_o G_1 B_1'$, the dose to a detector within a structure can be described by the following composite functional equation:

$$D = D_o \sum_i B(X_i) \left\{ \sum_{ij} G(X_i, \omega_{ij}) \right\}. \qquad (18)$$

B. Basic Functions.

1. Up to this point, we have discussed shielding in a qualitative sense and have defined the various words which make up the language of shielding. We will now turn our attention to the "basic" data upon which the shielding methodology has been built. This basic data and basic functions are from NBS Monograph 42 and the reasons for studying this aspect of the subject are best described by again quoting Dr. Spencer.

"First we give a description of the 'basic' data used to obtain the functions for applications, so that an appreciation of the limitations of the graphs of barrier and geometry factors is possible and also so that one can get an idea how additional information might be obtained.

Not all the factors which one might desire can be easily obtained theoretically, or even experimentally. In applications, the graphs of the various factors will no doubt be used in cases beyond their range of applicability. This makes it especially important to give a clear statement of their origin and interpretation. Because this type of background information is least ambiguous when stated mathematically, no attempt is made to avoid mathematical terminology.

To produce varied types of basic data, digital computers have proved essential. They are used to generate solutions of the integral equations describing the transport, diffusion, and energy loss of gamma radiation. These 'transport equations' have been solved by 'moment methods' and by 'Monte Carlo methods.' The former yield solutions for a source in a medium without boundaries, while the latter permit calculations of boundary effects.

All tables and graphs presented here (NBS Monograph 42) have been obtained from four types of basic data: (1) plane isotropic source case; (2) point isotropic source case; (3) plane oblique source case; and (4) albedo results."

2. Plane Isotropic Source Case. The plane isotropic source case consists of infinite plane source of fallout radiation embedded in an infinite homogeneous medium. The distance from the plane source to the detector is d, (ft of air), or X, which is the effective mass thickness, psf. A conversion factor

between these two quantities is d = 13.3 X. The radiation from a plane infinite source of radiation produces a dose angular distribution which Spencer identifies as $\ell(d,\cos\theta)$. The scale of this function is fixed so that an isotropic detector will register the standard dose, D_o, 3 ft above the source plane. At d ft the differential dose would then be equal to $D_o\,\ell(d,\cos\theta)\cdot\sin\theta\cdot d\theta$ due to gamma rays striking the detector between θ and $\theta + d\theta$. This implies that:

$$\int_{-1}^{1} d(\cos\theta)\,\ell(3\text{ft},\cos\theta) \equiv 1. \tag{19}$$

For heights other than 3 ft, the total dose D, would be:

$$D = D_o \int_{-1}^{1} d(\cos\theta)\,\ell(d,\cos\theta)\,. \tag{20}$$

Dividing both sides of the equation by D_o we would obtain the reduction factor for this situation. Since the detector is also embedded in the infinite medium, there is no geometry factor (or G=1.0), hence the result is a barrier factor alone. Dr. Spencer identifies this barrier factor by L(d) or L(X) depending on the argument used for the barrier material. L(d) is then:

$$L(d) = \int_{-1}^{1} d(\cos\theta)\,\ell(d,\cos\theta). \tag{21}$$

Figure 6 is a plot of the dose angular distribution function, $\ell(d,\cos\theta)$, for an infinite plane source of fallout radiation. This is Figure 26.1 from NBS Monograph 42. The characteristics of this set of curves will be discussed after the following derivation.

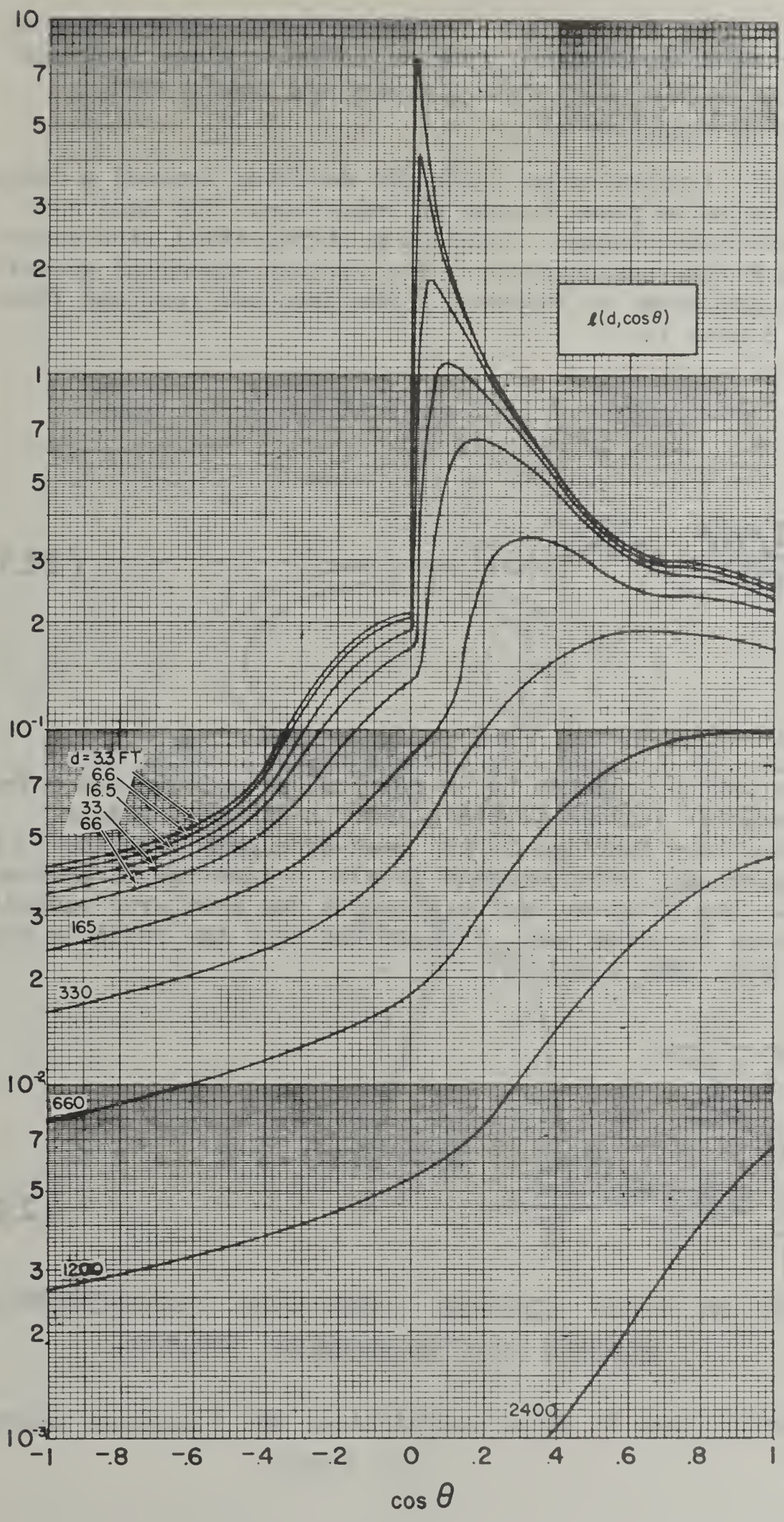

Figure 6. Dose angular distributions (d,cosΘ) for an idealized plane fallout source at different heights in air (d) above the source. (H_2O, 1.12 hr fission) NBS-42 Figure 26.1

It is interesting and instructive to derive an expression for the dose rate or total dose from an infinite plane isotropic source of radiation and then to compare the result with Dr. Spencer's L(d) function.

Figure 7 illustrates an isotropic detector located a distance d from an infinite plane source of radiation. The medium is infinite and homogeneous. Consider a differential ring source a distance R from the detector. The various essential geometry parameters are shown on Figure 7. The detector response from this ring source is:

$$dD = \frac{S \cdot 2\pi\rho d\rho}{4\pi R^2} e^{-uR} B(uR). \qquad (22)$$

The source term S is taken to be $r/hr/cm^2$ at unit distance from one of the point sources in the plane. B is the build-up factor which is a function of the mean-free path distance (μR) between source and detector, and is also a function of photon energy, E. The build-up factor accounts for scattered radiation which reaches the detector. Integrating over the infinite plane, the total dose rate would be:

$$D = \tfrac{1}{2} \int_d^\infty SB e^{-uR} \frac{dR}{R} . \qquad (23)$$

Converting this to polar coordinates, the following expression results:

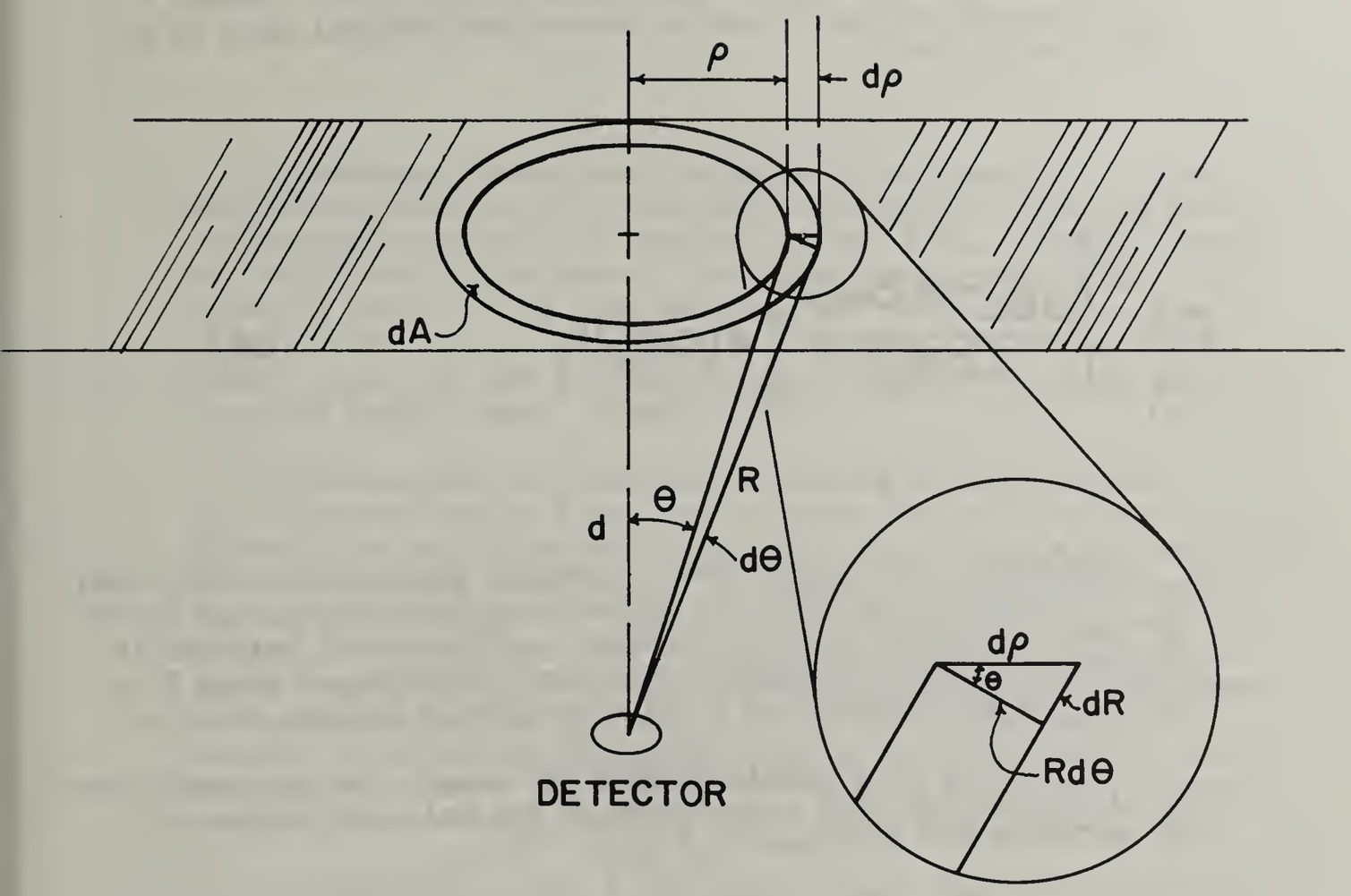

DIFFERENTIAL ISOTROPIC SOURCE AREA IN AN INFINITE HOMOGENEOUS MEDIUM

Figure II-7

$$D = \int_{\theta=0}^{\pi/2} \frac{SB}{2} e^{-ud \sec\theta} \tan\theta \, d\theta. \qquad (24)$$

In order that we may compare this function with Spencer's L(d) function, we must finally convert the integral part to a function of cosθ.

$$D = \int_{-1}^{1} \left[\frac{SBe^{-ud/\cos\theta}}{2\cos\theta} \right] d(\cos\theta). \qquad (25)$$

The expression in brackets is roughly equivalent to $\ell(d,\cos\theta)$. The difference is mainly in B since the build-up factor is based on total scattered radiation whereas a differential build-up is needed for angles of interest. However for distances where B is small, the two expressions yield surprisingly similar results.

Let us compute a simple example to compare the two expressions. We will normalize both expressions at the value of cosθ = 1.0, by replacing the SB/2 quantity by K. Thus:

$$\frac{Ke^{-ud/\cos\theta}}{\cos\theta} \cong \ell(d, \cos\theta). \qquad (26)$$

Example: For d=66' and cosθ = .2, what is (d,cosθ)?

From Figure 6, $\ell(d,\cos\theta)$, for $\ell(66', 0.2) = .65$. Fallout radiation has an average energy of about 1.25 Mev. The linear attenuation coefficient, μ, for E=1.25 Mev, is 7.38×10^{-5} cm^{-1}, and K=0.23 for d=66'. 66' converted to cm is 2010 cm. Using these values, and $\cos\theta = .2$ we obtain:

$$\frac{K\bar{e}^{ud/\cos\theta}}{\cos\theta} = \frac{(.23)(\bar{e}^{.58})}{(.2)} \qquad (26a)$$

$$= 645 \quad vs \quad .65$$

To obtain a better understanding of the meaning of "dose angular distribution," refer again to Figure 6. The top curve is the dose angular distribution for d=3.3 ft. Greater depths are the curves below the top one. For the direction pointing directly down (or up) from the detector to the infinite source plane, $\cos\theta = 1.0$. For the direction parallel to the source plane, $\cos\theta = 0$, and for the direction pointed directly away from the source plane, $\cos\theta = -1.0$.

To pictorially illustrate the meaning of dose angular distribution, Figure 8 has been plotted for the case of d=3.3 ft. Figure 9 is the distribution for d=330 ft. For small d distances, the dose angular distribution is peaked in a direction toward the horizon whereas for large d, the distribution is peaked in a vertical direction. This simply means that radiation tends to be collimated in a direction perpendicular to a source plane as the distance from the source increases. This change in angular distribution with height has an important effect on the wall barrier factor and this effect will be discussed in more detail in the section dealing with engineering applications.

3. Point Isotropic Source Case. Next the point isotropic source case will be discussed. This is a source of radiation concentrated in a very small volume. The source emits radiation equally (isotropically) in all directions. At a distance d from this point source, the dose angular distribution is denoted by the following function:

$$D(\theta,\phi)pt = p(d,\cos\theta). \qquad (27)$$

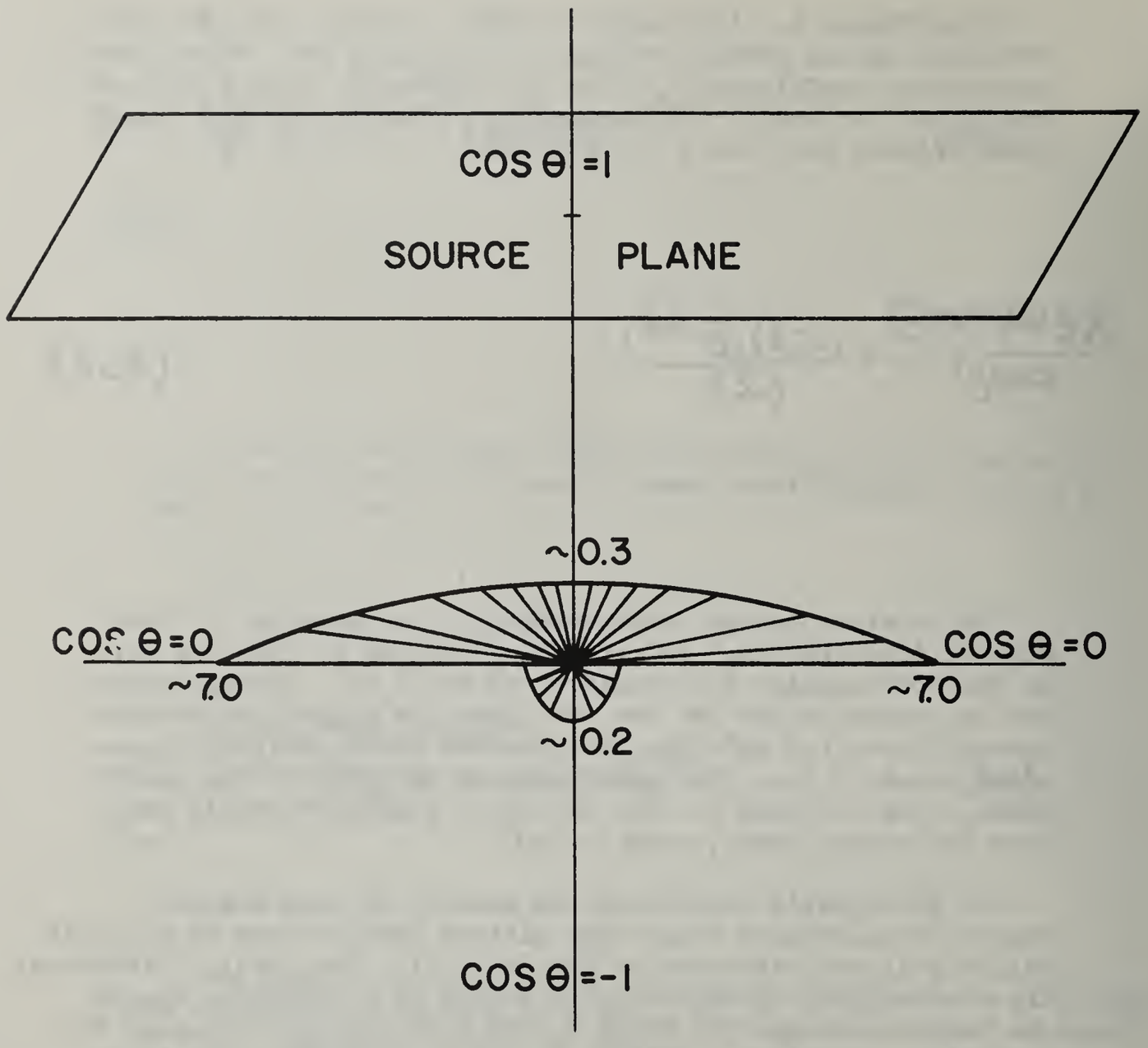

DOSE ANGULAR DISTRIBUTION, $\ell(d,\cos\theta)$, FROM AN INFINITE, ISOTROPIC, PLANE SOURCE WHERE d=3 FEET

Figure II-8

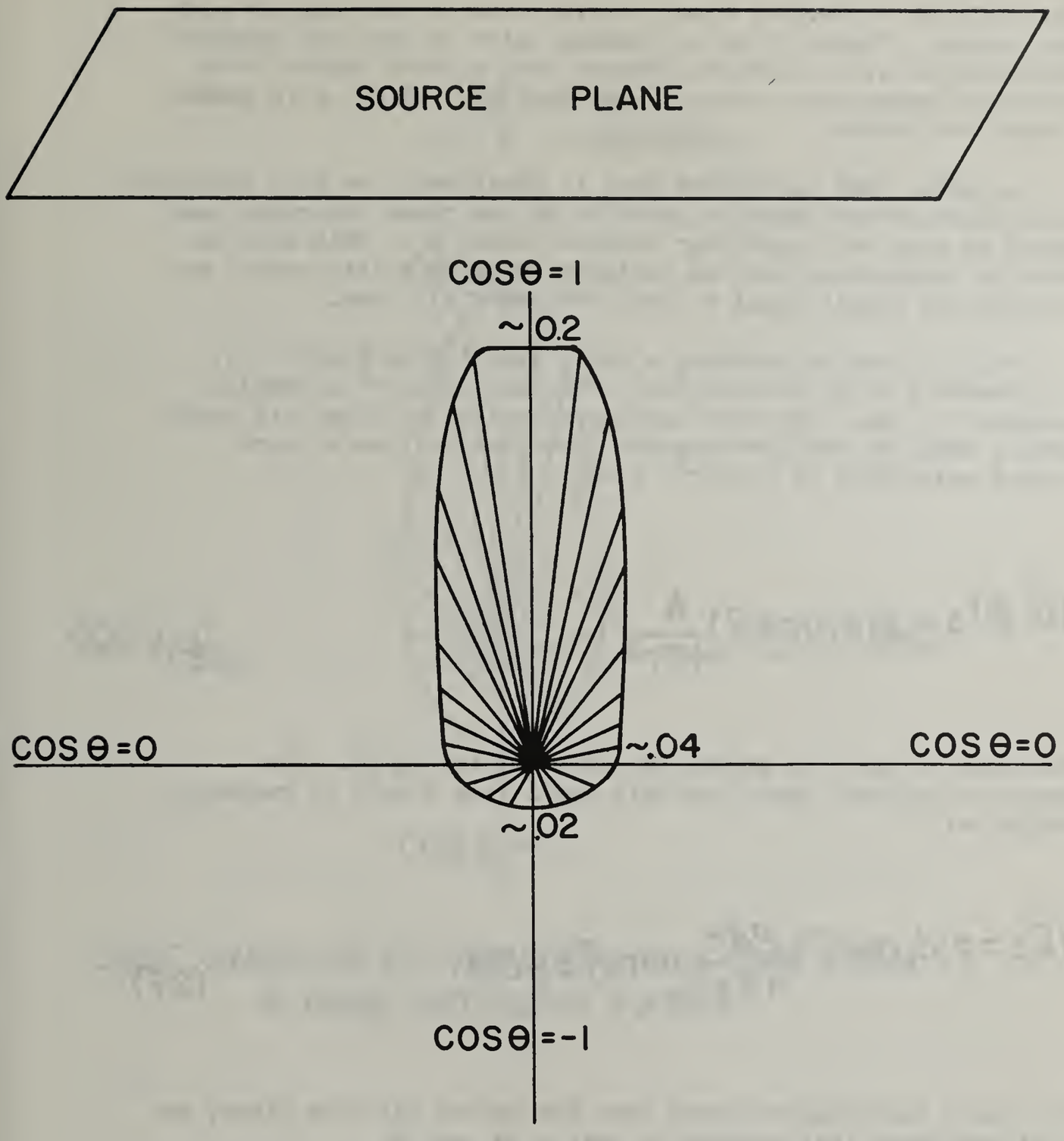

DOSE ANGULAR DISTRIBUTION, $f(d, \cos\theta)$, FROM AN INFINITE, ISOTROPIC, PLANE SOURCE WHERE d = 330 FEET

Figure II-9

The angle θ is measured from the axis between the detector and the source. Figure 10 is a schematic plot of the dose angular distribution at a detector distance from a point source in an infinite homogeneous medium. Note that the radiation is peaked toward the source.

In order that our source data is consistent, we must normalize this point source function relative to the plane isotropic case which is used to compute our standard dose, D_o. This will be done by integrating over an infinite field of point sources and setting the result equal to the infinite field case.

This is done by assuming a small area A (See Figure 11), a distance r from the detector. The ratio of A/r^2 is small compared to one. The dose angular distribution from this small area A would be the dose angular distribution from a point source multiplied by $A/4\pi r^2$, i.e.,

$$D(\theta,\phi)_A = p(d,\cos\theta)\frac{A}{4\pi r^2}. \qquad (28)$$

The area of the ring source of radiation is $\rho\, d\rho\, d\theta$. The detector response then from this small ring source of radiation would be:

$$dD_A = p(d,\cos\theta)\frac{\rho d\rho}{4\pi r^2}\sin\theta\, d\theta\, d\phi. \qquad (29)$$

To obtain the total response over the entire infinite plane, we must integrate this expression over ρ, θ, and ϕ.

$$D_A = \int_{-1}^{1} d(\cos\theta) \int_{0}^{2\pi} d\phi\, p(d,\cos\theta) \int_{r'}^{\infty} \frac{\rho d\rho}{4\pi r^2}. \qquad (30)$$

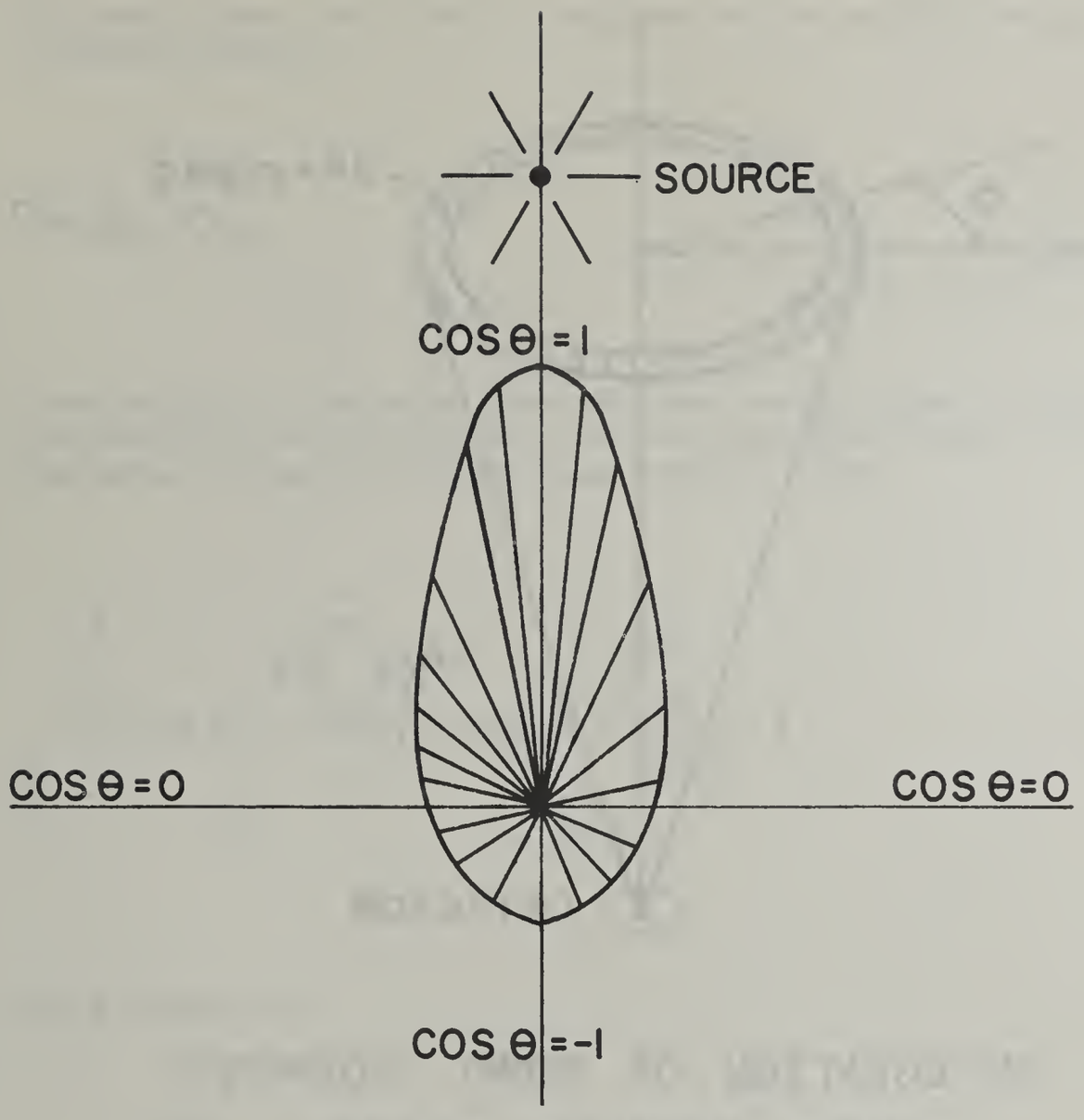

DOSE ANGULAR DISTRIBUTION, p(d, COS Θ), FROM A POINT ISOTROPIC SOURCE

Figure II-10

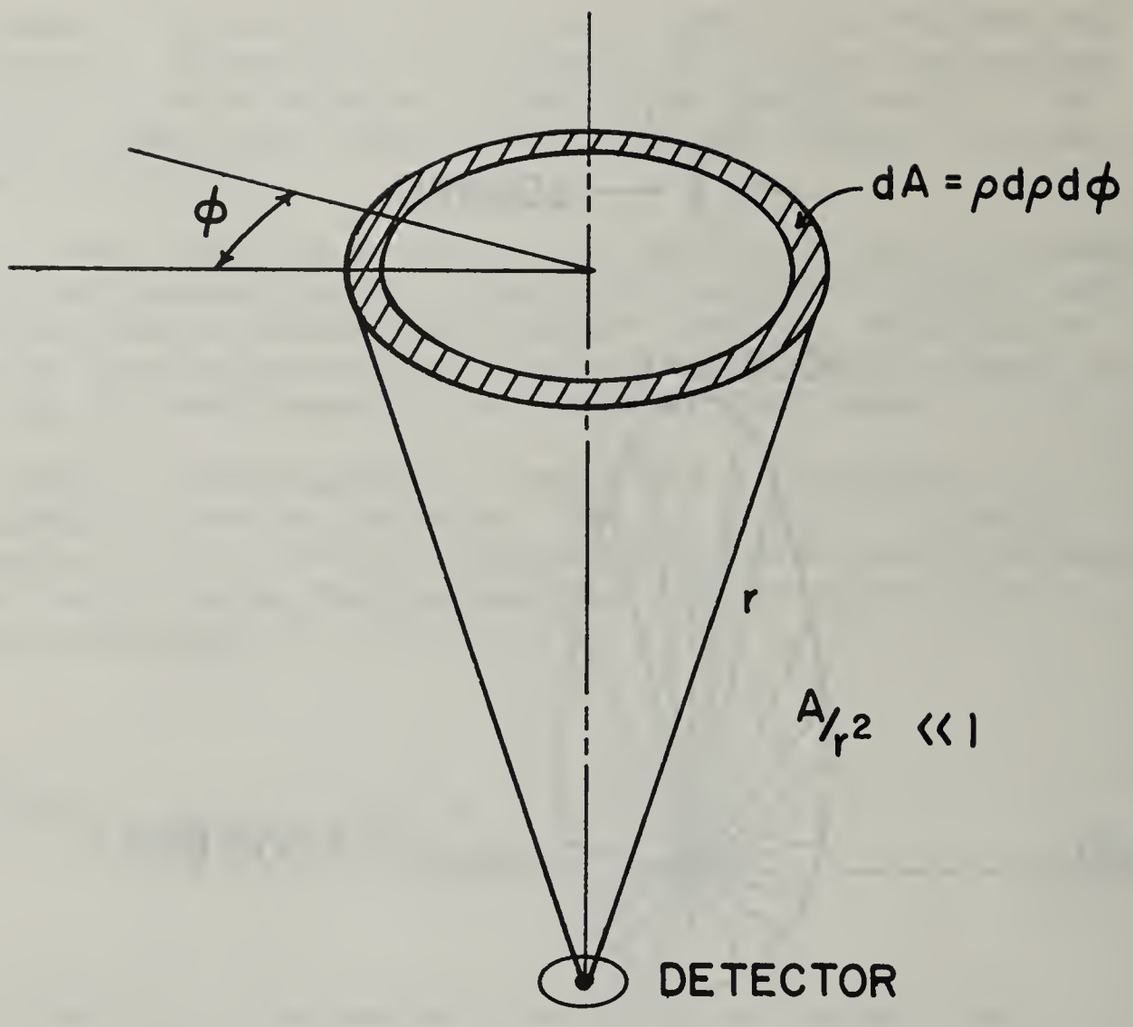

INTEGRATION OF POINT SOURCES
OVER INFINITE PLANE

Figure II-11

To obtain dose, the detector response must be multiplied by the standard dose D_o:

$$D = D_o \cdot D_A . \tag{31}$$

Physically, the infinite plane of point sources must be identical to the infinite plane source. We know that $D_o=1$, when d or r=3 ft. Therefore, equation 30 must equal 1 when r=3 ft:

$$\int_{-1}^{1} d(\cos\theta) \int_{0}^{2\pi} d\phi\, p(r,\cos\theta) \int_{3\text{ft.}}^{\infty} \frac{dr}{4\pi r} = 1. \tag{32}$$

This reduces to:

$$1/2 \int_{3\text{ft.}}^{\infty} \frac{dr}{r} \int_{-1}^{1} d(\cos\theta)\, p(r,\cos\theta) = 1. \tag{33}$$

If we let

$$P(r) = \int_{-1}^{1} d(\cos\theta)\, p(r,\cos\theta) , \tag{34}$$

we finally have:

$$\frac{1}{2}\int_{3}^{\infty}\frac{dr}{r}P(r)=1, \qquad (35)$$

or in general terms:

$$\frac{1}{2}\int_{X}^{\infty}\frac{dX'}{X'}P(X')=L(X), \qquad (36)$$

where

$$L(X)=\int_{-1}^{1}d(\cos\theta)\,\ell(X,\cos\theta). \qquad (37)$$

The charts from NBS-42 most useful in practical application for fallout radiation problems are attached at the end of this section. In order that we may verify the above normalization, an example problem will be worked using both the L(X) and P(X) charts.

Example: What is the detector response (or reduction factor) from an infinite plane isotropic source when there is 300 psf of mass between the detector and source plane?

From Figure 19, L(X); $L(300) = 1.85 \times 10^{-4}$.

From the normalizing process, equation 36 tells us that:

$$L(X) = \tfrac{1}{2} \int_{X}^{\infty} \frac{dX'}{X'} P(X') . \qquad (36)$$

Turning to Figure 30, P(X), we can see that at X=300, the curve is a straight line on log paper, therefore, we can approximate the P(X) function by the following:

$$P(X) \cong K e^{-mX} . \qquad (38)$$

Using two points, the two constants, K and m, can be determined. They are: K= .655, and m=.0186. Therefore:

$$L(X) = \tfrac{1}{2} \int_{X'}^{\infty} \frac{dX}{X} (.655) e^{-.0186X} .$$

For X=300 psf;

$$L(X) = \tfrac{1}{2} (.655)\, E_1(5.58)$$

$$= 1.91 \times 10^{-4} \text{ compared to } 1.85 \times 10^{-4} .$$

This verifies the normalizing process.

4. Plane Oblique Source Case. Though radiation from a plane source goes in all directions, it is often advantageous to break it up and consider at one time only those rays which initially go at an obliquity θ_o relative to the plane source. In Dr. Spencer's Monograph, this particular type of partial source is designated $s(X,\cos\theta)$.

This function must also be normalized. The normalizing function which is used, is:

$$\cos\theta_o \, s^{(0)}(0,\cos\theta_o) = 1, \qquad (39)$$

where $S^{(0)}$ is the detector response to the unscattered component.

Figure 12 gives the above function for different values of $\cos\theta_o$. This curve is for the 1.12 hour fission spectrum of fallout radiation. The general features of this curve can be interpreted as follows: for $\cos\theta_o=1$, the photons initially are going directly away from the source plane. On the average, such photons will penetrate deeply before interacting. Thus attenuation vs. mass thickness (X) is small relative to angles which are oblique to the plane. For $\cos\theta$ near zero, the photons are initially traveling nearly parallel to the source plane, hence penetration away from the plane is small. Figure 13 is the same function plotted for negative values of θ_o and are a measure then of backscattered penetration.

5. Albedo. The gamma ray albedo (backscattered) function is shown on Figure 14. The albedo is a ratio of gamma dose rate striking a surface at an angle θ_o to the dose rate which is reflected from that surface. The following equation is the albedo function:

$$a = \frac{\int_{-1}^{0} d(\cos\theta)\cos\theta D(\cos\theta)}{\int_{0}^{1} d(\cos\theta)\cos\theta D(\cos\theta)} . \qquad (40)$$

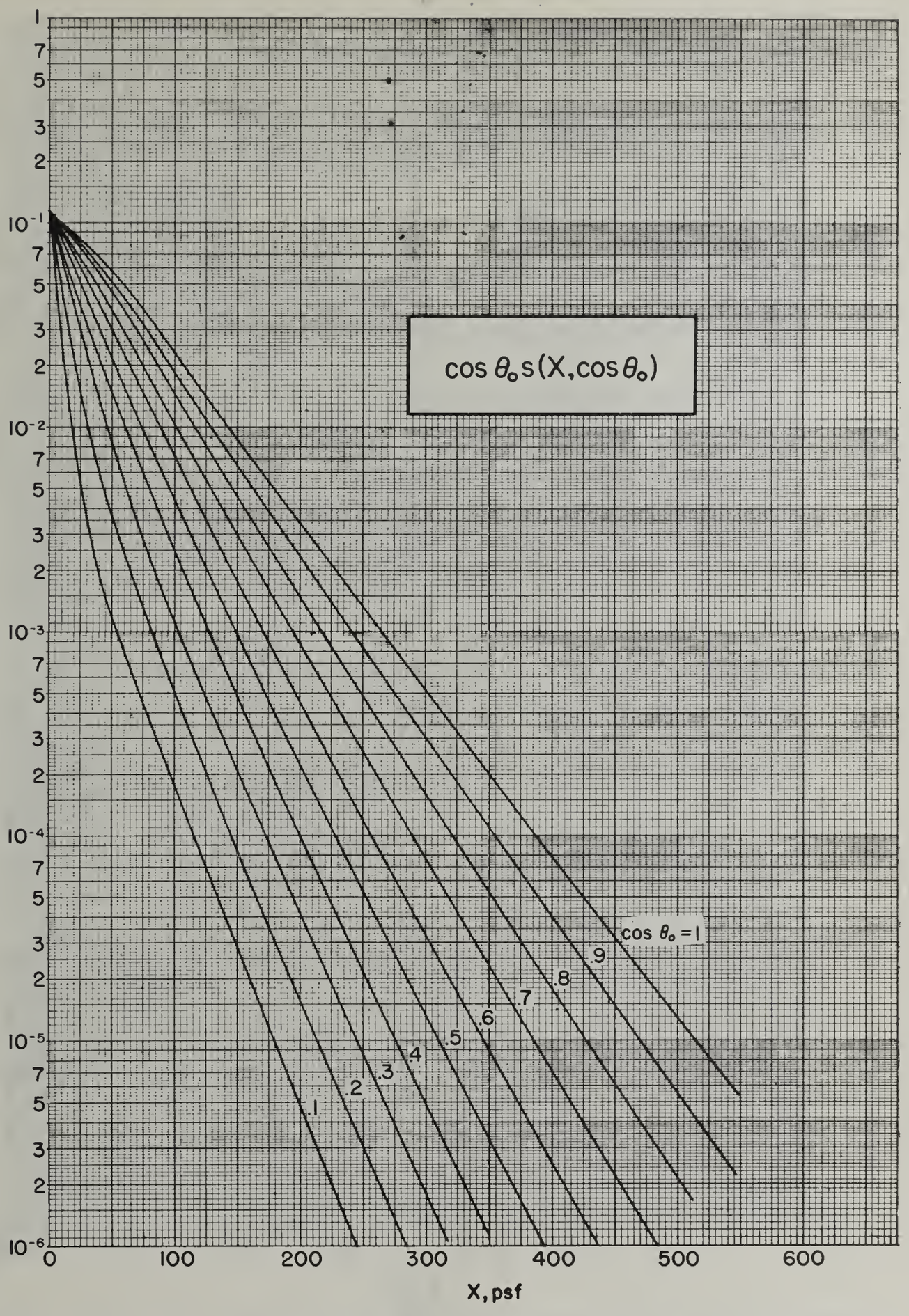

Figure 12. Gamma ray attenuation curves for monodirectional gamma rays from a plane source for incident obliquities Θ_o 90° relative to the normal to the source plane. (H_2O, 1.12 hr fission. NBS-42 Figure 26.4)

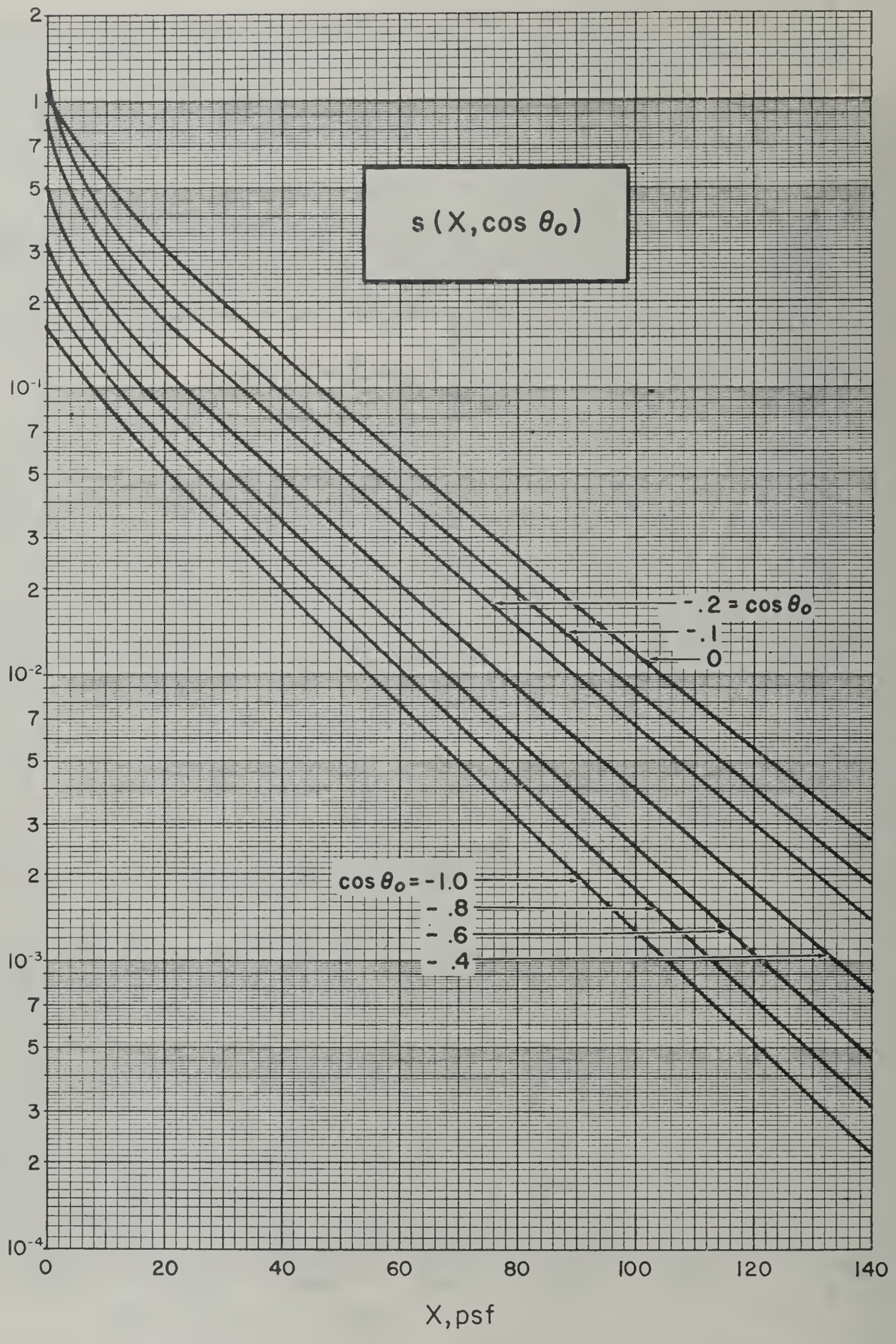

Figure 13. Gamma ray attenuation curves for monodirectional gamma rays from a plane source, for incident obliquities Θ_o 90° relative to the normal to the source plane. (H_2O, 1.12 hr fission, NBS-42 Figure 26.5)

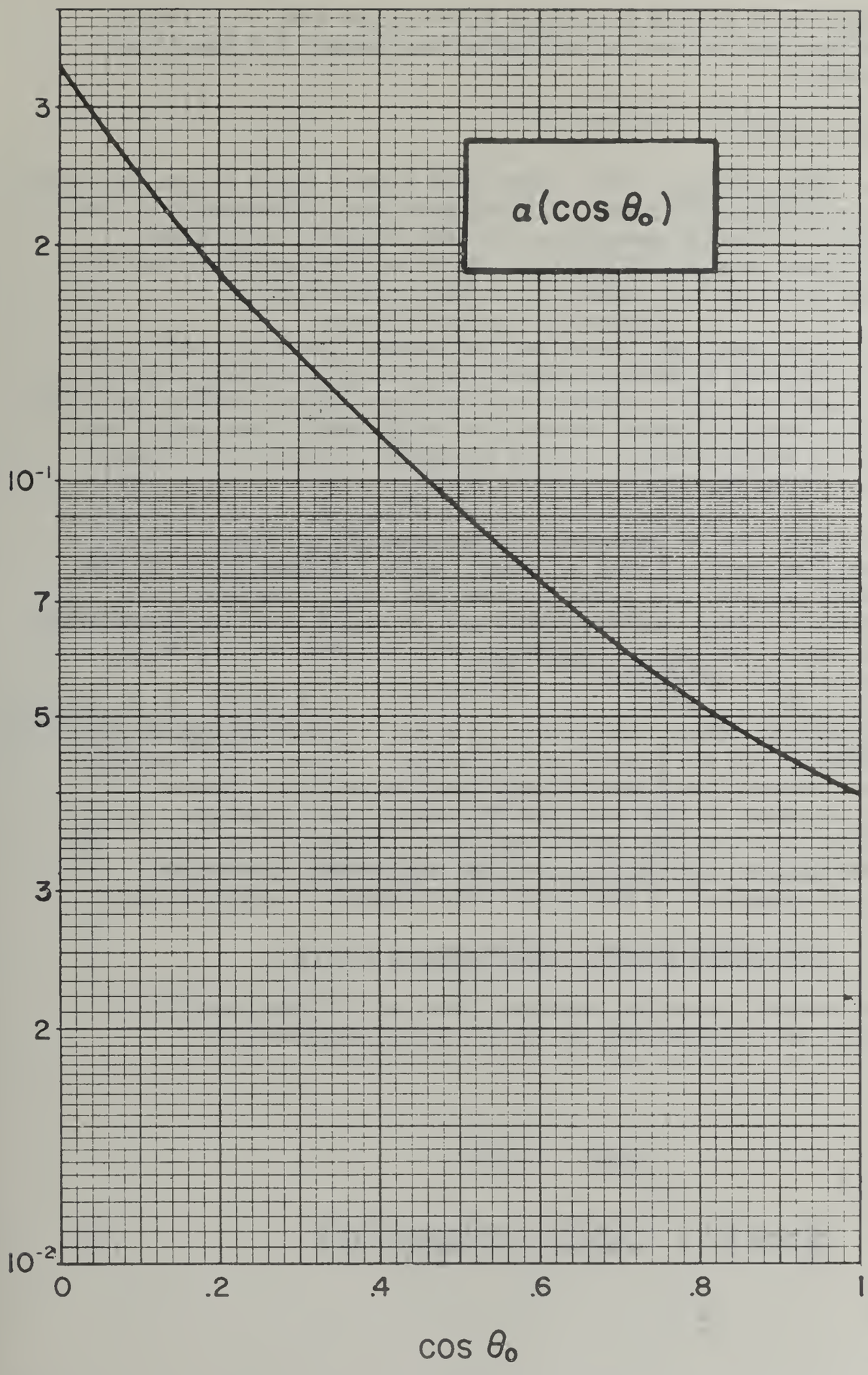

Figure 14. Dose albedo for monodirectional gamma rays incident on concrete, as a function of the cosine of the incident obliquity. (1.12 hr fission. NBS-42 Figure 26.8)

These basic source functions will now be used to develop the various barrier and geometry factors needed for practical applications.

C. Barrier and Geometry Functions.

1. Introduction. The three main source types (plane isotropic, point isotropic, and plane oblique) have been discussed. To see what sorts of useful quantities we can construct from these source types consider Figure 15. This is a schematized building of three stories: one basement and two upper floors.

Detector position A receives radiation from roof, walls, and floor. Detector B receives radiation through two floor layers and through the walls. Detector C receives ground source radiation which has been reflected from air or walls and subsequently has penetrated the basement ceiling. Detector C would also receive radiation from the roof source.

In order that we may predict the response of these three detectors we need information about radiation from (1) a finite portion of an infinite plane source (for roof contribution); (2) radiation which scatters from air or walls into the detectors; and (3) radiation which penetrates vertical barrier (or wall) and reaches the detectors.

In each of these cases there is a barrier interposed between the detector and the source of radiation. In addition there is distance between the detector and the source. Dr. Spencer in NBS-42 has used the source types to derive and catalogue various functions into "barrier functions" and "geometry functions." We will now discuss the various barrier and geometry functions which are generated by the three basic angular distributions.

2. Barrier and Geometry Equations.

The general detector response from an arbitrary source of radiation was represented by the following expression:

$$D_s = \int_{-1}^{1} d(\cos\theta) \int_{0}^{2\pi} d\phi\, D(\theta,\phi)\, g_s(\theta,\phi). \qquad (4)$$

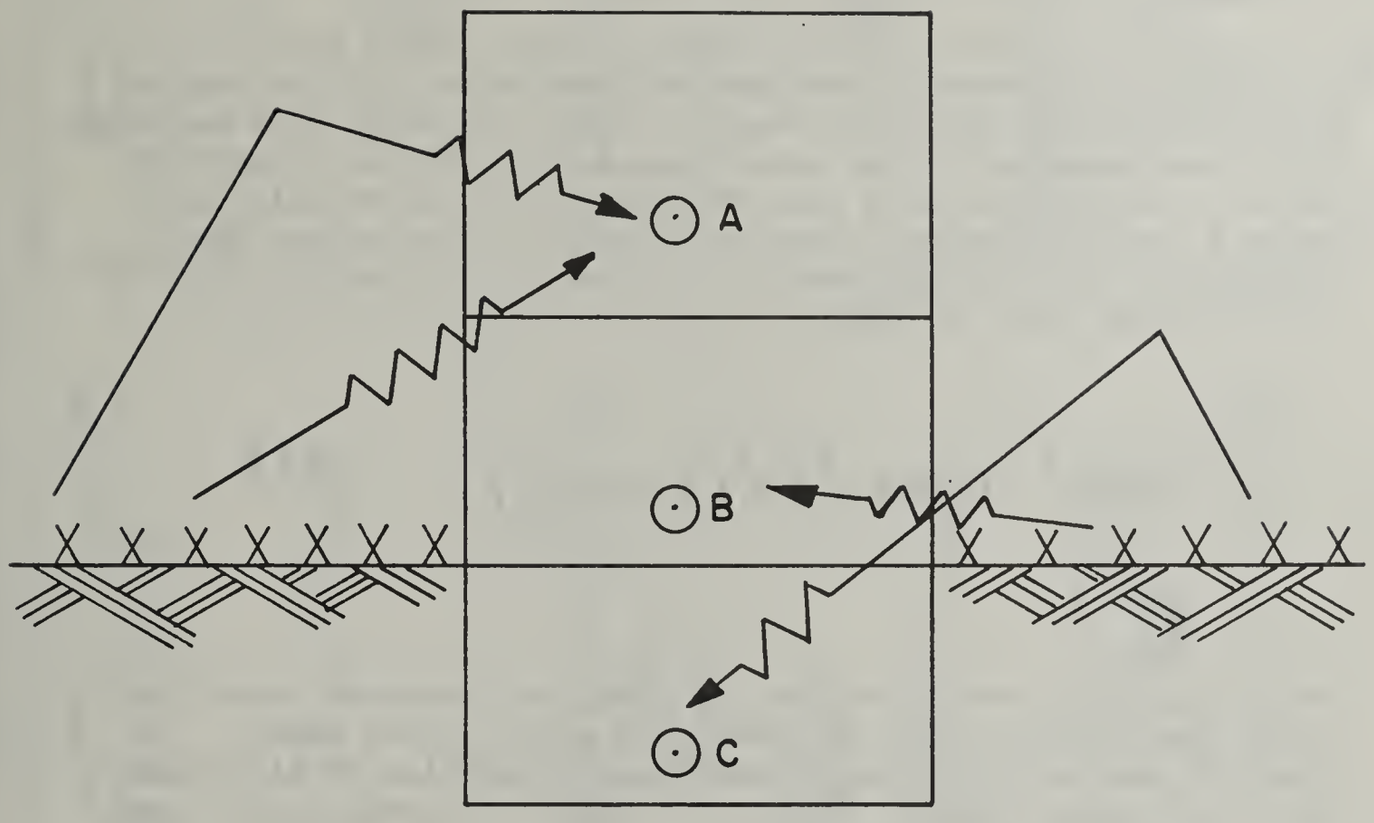

SCHEMATIZED BUILDING

Figure II-15

Both barrier and geometry functions are developed by the use of integrals of the above type using appropriate angular distributions for $D(\theta,\phi)$. The geometry functions are derived by developing an expression for total response and then dividing by the appropriate barrier function. The functions derived from the infinite plane isotropic source case will be discussed first.

3. Infinite Plane Isotropic Functions. Figure 16a illustrates the angular distribution, the barrier functions, and the geometry functions that have been generated from the infinite plane isotropic source case.

The first barrier function that depends on the plane isotropic source case is obtained by integration of this angular distribution over all solid angle. Since the angle ϕ is measured in a plane parallel to the source plane, this barrier function would be independent of ϕ and would be a function of only the angle θ and the distance from the detector to the source plane. Integration of $\ell(d,\cos\theta)$ over all θ produces the barrier function identified by $L(d)$ or $L(X)$:

$$L(X)=\int_{-1}^{1} d(\cos\theta)\,\ell(X,\cos\theta). \qquad (37)$$

We have already noted that the standard dose measured three feet above the infinite plane is identified as D_o. This means that for our calculational schemes the integration of $L(d)$ when $d=3ft$ must equal unity. This is the basis of normalization used for other source types as well.

The second useful barrier function is obtained by the integration of the plane isotropic source over angles from $\cos\theta = 0$ to $\cos\theta = -1$, identified as the function $S(d)$ or $S(X)$. It can be seen from Figure 16a that the detector receives or accepts only radiation which is scattered and therefore this function is called the "skyshine" function:

$$S(d)=\int_{-1}^{0} d(\cos\theta)\,\ell(d,\cos\theta). \qquad (41)$$

BARRIER AND GEOMETRY FUNCTIONS FROM INFINITE PLANE SOURCE

Fig 16-a

ANGULAR DISTRIBUTION

INFINITE PLANE, ISOTROPIC SOURSE

$$D(\theta,\phi)_{PL} = \ell(d, \cos\theta)$$

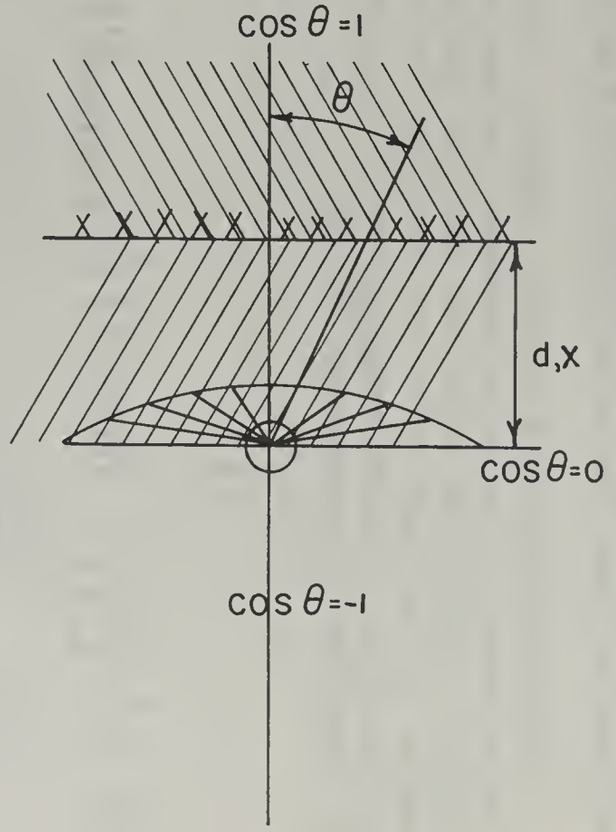

BARRIER FUNCTION

1. SUM OVER ALL θ

$$L(X) = \int_{-1}^{1} d(\cos\theta)\,\ell(X, \cos\theta)$$

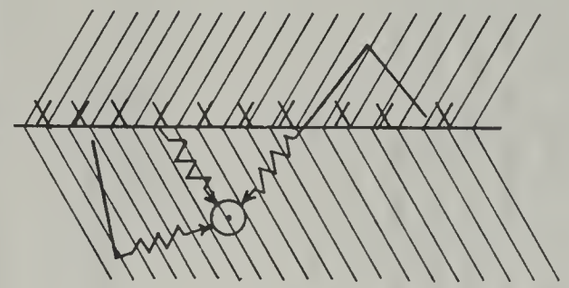

2. SKYSHINE

$$S(X) = \int_{-1}^{0} d(\cos\theta)\,\ell(X, \cos\theta)$$

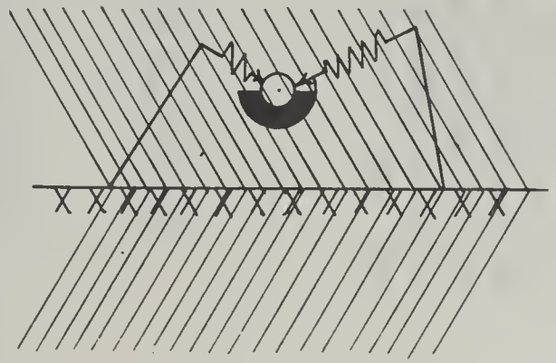

GEOMETRY FUNCTION

1. FINITE PLANE

$$L_c(X,\omega) = \frac{1}{L(X)}\left[L(X) - L\left(\frac{X}{1-\omega}\right)\right]$$

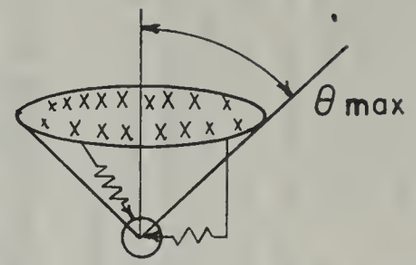

2. LIMITED DETECTOR RESPONSE

$$L_a(X,\omega) = \frac{1}{L(X)} \int_{1-\omega}^{1} d(\cos\theta)\,\ell(X, \cos\theta)$$

3. LIMITED SKYSHINE

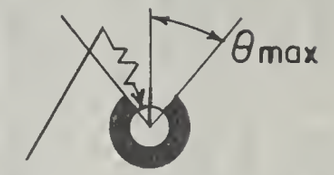

$$S_a(d,\omega) = \frac{1}{S(d)} \int_{-1}^{-1+\omega} d(\cos\theta)\,\ell(d, \cos\theta)$$

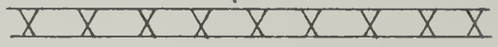

Geometry functions, as noted earlier, really refer to what might be called limited source or limited field of view functions. The function L(X) is the detector response from an infinite plane source of radiation when the detector is a distance 'X' measured in pounds per square foot from the source plane. If we wish to measure the response from a circular portion of this infinite plane, when the detector is located on a line through the center of the circle and perpendicular to the source plane, we would measure the response from the infinite plane first. From this value we would subtract out the response from the source plane outside of the circle of interest.

If L(X) is the response from the total infinite plane, then $L(X\sec\theta)$ would be the response from that portion of the infinite plane beyond the circle of interest. The solid angle fraction, ω, which defines the circle from the detector point of view is $1-\cos\theta$. Therefore $L(X\sec\theta)$ can also be represented by $L(X/1-\omega)$. The total response from the limited circular area would then be $L(X) - L(X/1-\omega)$. Since we have defined the total response of the detector as the product of barrier factor times geometry factor $(B_1' \cdot G_1)$, we can obtain the geometry factor by dividing by the barrier factor appropriate to this case, i.e., L(X). The geometry function which describes the response of a detector from a limited circular area is identified as $L_c(X, \omega)$ and is:

$$L_c(X,\omega) = \frac{1}{L(X)}\left[L(X) - L\left(\frac{X}{1-\omega}\right)\right]. \qquad (42)$$

Similar procedures are used for all geometry functions, i.e., the total response is obtained for a limited source or field of view and then the proper barrier factor is factored out.

The second useful function based on the plane infinite source case is a detector shielded through certain specified angles. Figure 16a shows the detector shielded through certain angles so that radiation comes through the solid angle from $\theta=0$ to θ_{max}. The following geometry function, identified as L_a describes this geometry factor:

$$L_a(X,\omega) = \frac{1}{L(X)} \int_{1-\omega}^{1} d(\cos\theta)\, \ell(X, \cos\theta). \qquad (43)$$

In certain instances we are interested in shyshine which reaches the detector only through a limited cone of oblique angles pointed away from the source plane. This is noted by the following function:

$$Sa(d,\omega) = \frac{1}{S(d)} \int_{-1}^{-1+\omega} d(\cos\theta)\, \ell(d,\cos\theta). \qquad (44)$$

4. Plane Oblique Source. Next, consider the plane oblique partial source distribution (Figure 16b). There is onlv one barrier function termed "barrier to skyshine" that can be derived from the oblique source distribution. This is the case where photons leave the source plane at a certain angle θ_o moving away from the detector and are then reflected back toward the detector and through a barrier distance X before reaching the detector. This is described by the following:

$$S'(X) = \frac{\int_{-1}^{0} d(\cos\theta_o)\, s(X,\cos\theta_o)}{\int_{-1}^{0} d(\cos\theta_o)\, s(0,\cos\theta_o)} . \qquad (45)$$

Note: when X = 0, S'(X) = 1.

The geometry function which is related to this oblique case is the case where the angles of the initial radiation from the source plane are limited to certain prescribed directions. This situation is described by the following function:

$$Lb(X,\omega) = \frac{\gamma}{L(X)} \int_{1-\omega}^{1} d(\cos\theta_o)\, s(X,\cos\theta_o). \qquad (46)$$

BARRIER AND GEOMETRY FUNCTIONS FROM PLANE OBLIQUE SOURCE

DOSE ANGULAR DISTRIBUTION

OBUQUE SOURCE

$$D(\theta_0) = s(X, \cos\theta_0)$$

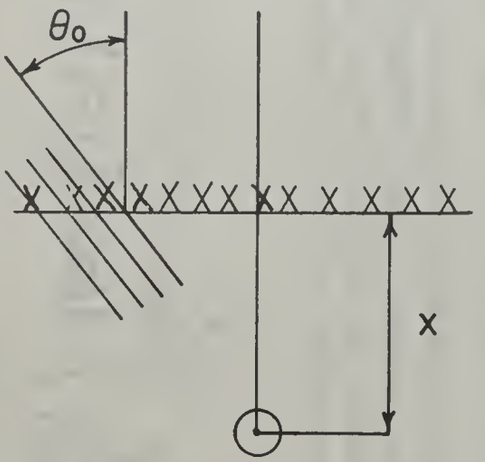

BARRIER FUNCTION

I. BARRIER TO SKYSHINE

$$S'(X) = \frac{\int_{-1}^{0} d(\cos\theta_0)\, S(X, \cos\theta_0)}{\int_{-1}^{0} d(\cos\theta_0)\, S(0, \cos\theta_0)}$$

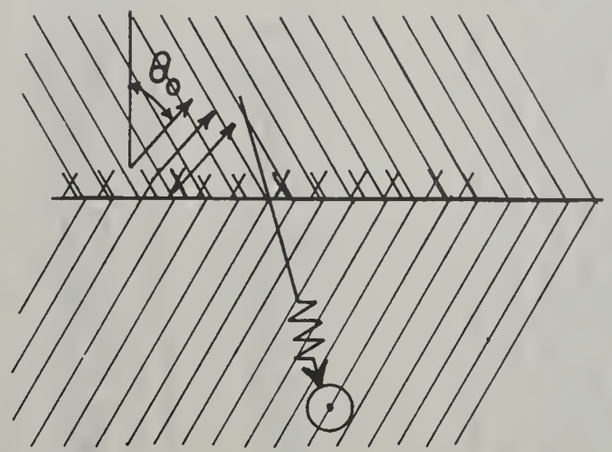

GEOMETRY FUNCTION

I. LIMITED SOURCE OBLIQUITIES

$$L_c(X, \omega) = \frac{\nu}{L(X)} \int_{1-\omega}^{1} d(\cos\theta_0)\, S(X, \cos\theta_0)$$

$$\nu = \frac{1}{2} P(0)$$

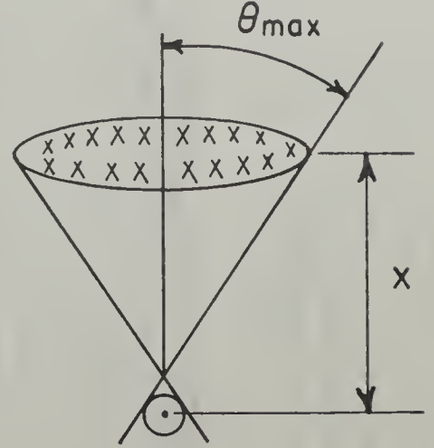

Figure II-16b

This function, L_b, is normalized by letting $L_b(X,2) = 1$. The normalizing constant insures that the integral of the function L_b over all angles equals 1. The "all angles" feature means that we must use $\omega = 2$ to insure that both hemispheres are included. The derivation of the constant will be discussed later after the point source functions have been discussed.

5. Plane Source and Oblique Source. The derivation of wall barrier factor combines the infinite plane source and the oblique source distributions. The infinite plane isotropic source distribution is employed to define the angular distribution. The oblique data is used to properly weight the attenuation of photons for the different angles of incidence on the vertical wall. In deriving wall barrier factors the detector axis is oriented parallel to the source plane. This is done to maintain the axis perpendicular to the barrier. The shift in axis now makes the infinite plane angular source distribution a function of the angle ϕ as well as θ. The function $\ell(d,\cos\theta)$ now becomes $\ell(d,\sin\theta\cos\phi)$, when we rotate the axis 90°. The reader can easily verify this by applying the usual analytical geometry methods in shifting an axis in spherical coordinates.

The infinite plane source function $\ell(d,\sin\theta\cos\phi)$ is used to describe the source field. The distance d is the distance above the source plane. This angular source distribution is then weighted for each angular component by the oblique barrier function $\cos\theta \cdot s(X,\cos\theta)$. The distance X is now the horizontal thickness of the wall, psf. To obtain the total response over the hemisphere of interest, i.e., over all ϕ and θ, we use the wall barrier factor $W(X,d)$:

$$W(X,d) = \int_0^1 d(\cos\theta)\cos\theta\, s(X,\cos\theta) \frac{1}{2\pi} \int_0^{2\pi} d\phi\, \ell(d,\sin\theta\cos\phi) . \quad (47)$$

The first geometry function which derives in turn from this wall barrier factor is a circular wall area which is obtained by limiting the angle θ to θ_{max}. A geometry factor is theoretically independent of wall thickness, which means that $X = 0$. When $X = 0$, $\cos\theta \cdot s(X,\cos\theta) = 1$. The barrier factor $W(X,d)$ for $X=0$ is factored out and we obtain the wall geometry factor $W_a(d, \omega)$:

$$W_a(d,\omega) = \frac{1}{W(0,d)} \int_{1-\omega}^{1} d(\cos\theta \frac{1}{2\pi} \int_{0}^{2\pi} d\phi \ell(d, \sin\theta\cos\phi) . \quad (48)$$

The second useful geometry function called "Vertical Aperture" that we can derive from the vertical wall orientation is obtained by limiting the detector response to directions above the detector plane. This is very similar to the previous function W_a except that it is normalized to the total skyshine factor $S(d)$. Since θ is limited to the angles from $\theta = 0$ to $\theta = \pi/2$, we divide the skyshine by $\frac{1}{2}$ and thus the factor 2 enters the equation. Also the limits of integration on the angle ϕ are those above the horizontal plane.

$$W_b(d,\omega) = \frac{2}{S(d)} \int_{1-\omega}^{1} d(\cos\theta) \frac{1}{2\pi} \int_{-\pi/2}^{\pi/2} d\phi \ell(d, \sin\theta\cos\phi . \quad (49)$$

Figure 16c applies to the above functions.

6. Point Isotropic Source. Finally the barrier and geometry functions associated with the point isotropic source distribution are considered. The first function, P(d) or P(X) is the response of an isotropic detector at a distance d (or X) from a point isotropic source. The integration is over all solid angle, where $\theta = 0$ along the axis from the source to detector. See Figure 16d.

$$P(d) = \int_{-1}^{1} d(\cos\theta) p(d, \cos\theta) . \quad (50)$$

BARRIER AND GEOMETRY FUNCTIONS FROM INFINITE PLANE @ OBLIQUE θ

DOSE ANGULAR DISTRIBUTION

$$D(\theta,\phi)=\begin{cases}\ell(d,\sin\theta\cos\phi)\\ s(x,\cos\theta)\end{cases}$$

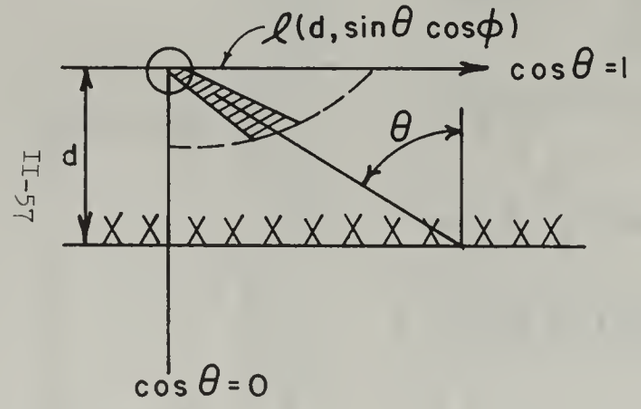

BARRIER FUNCTION

1. WALL BARRIER

$$W(x,d)=\int_0^1 d(\cos\theta)\cos\theta_0\, s(x,\cos\theta_0)\times\frac{1}{2\pi}\int_0^{2\pi}d\phi\,\ell(d,\sin\theta\cos\phi)$$

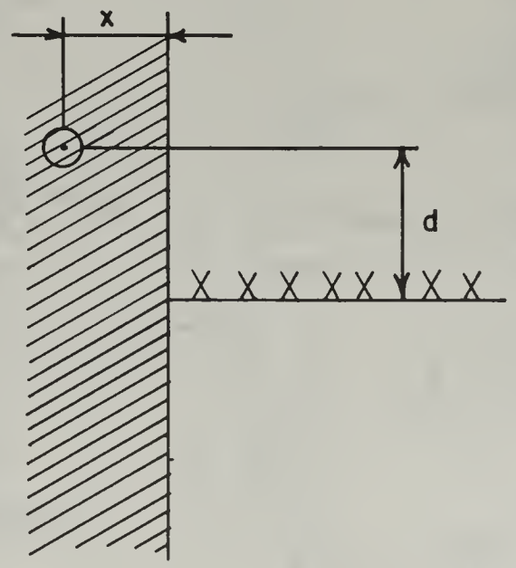

Figure II-16c

GEOMETRY FUNCTIONS

1. LIMITED WALL

$$W_a(d,\omega)=\frac{1}{W(o,d)}\int_{1-\omega}^{1}d(\cos\theta)\frac{1}{2\pi}\int_0^{2\pi}d\phi\,\ell(\sin\theta\cos\phi)$$

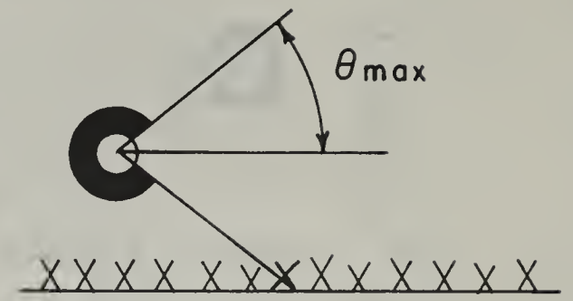

2. VERTICAL APERTURE

$$W_b(d,\omega)=\frac{2}{S(d)}\int_{1-\omega}^{1}d(\cos\theta)\times\frac{1}{2\pi}\int_{-\pi/2}^{\pi/2}d\phi\,\ell(d,\sin\theta\cos\phi)$$

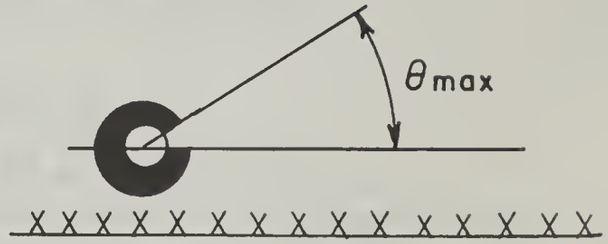

BARRIER AND GEOMETRY FUNCTIONS FROM POINT ISOTROPIC SOURCE

DOSE ANGULAR DIST.

$$D(\theta)_{PT} = p(d, \cos\theta)$$

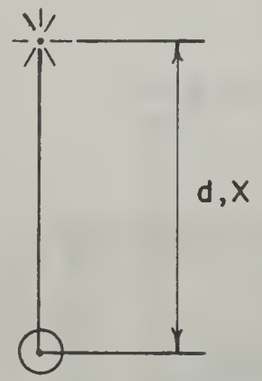

BARRIER FUNCTION

1. DIRECT + SCATTERED

$$P(d) = \int_{-1}^{1} d(\cos\theta)\, p(d, \cos\theta)$$

2. SCATTERED

$$P^{(S)}(d) = \int_{-1}^{1} d(\cos\theta)\, p^{(S)}(d, \cos\theta)$$

$$P^{(S)}(d) = P(d)\, g(\theta)$$

$$g(\theta) = \theta, \quad \theta = 0$$

$$= 1, \quad 0 < \theta \leq \pi$$

GEOMETRY FUNCTION

1. LIMITED DETECTOR

$$P_a(d, \omega) = \frac{1}{P(d)} \int_{1-w}^{1} d(\cos\theta)\, p(d, \cos\theta)$$

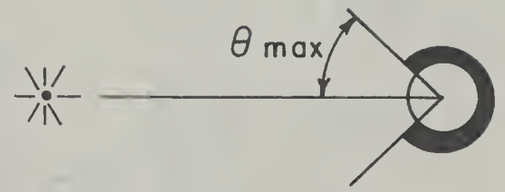

2. LIMITED DETECTOR, SCATTERED

$$P_a^{(S)}(d, \omega) = \frac{1}{P^{(S)}(d)} \int_{1-\omega}^{1} d(\cos\theta)\, p^{(S)}(d, \cos\theta)$$

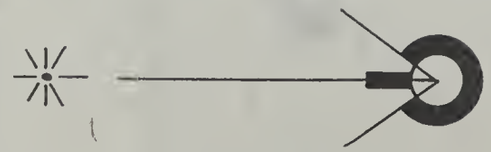

3. LIMITED DETECTOR, ROTATED AXIS

$$P_b^{(S)}(d, \omega) = \frac{2}{P^{(S)}(d)} \int_{1-\omega}^{1} d(\cos\theta) \frac{1}{2\pi} \int_{0}^{2\pi} d\phi\, p(d, \sin\theta\cos\phi)$$

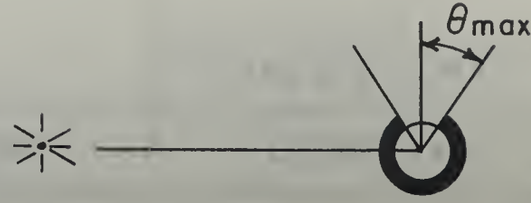

Figure II-16d

In certain cases only scattered radiation from the point source is desired. This can be described by the equation below where $P^{(s)}(d,\cos\Theta)$ includes only scattered radiation:

$$P^{(s)}(d) = \int_{-1}^{1} d(\cos\Theta)\, p^{(s)}(d,\cos\Theta). \tag{51}$$

The associated geometry functions which go with these barrier functions are those which limit the detector response to a specified cone of obliquities:

$$P_a(d,\omega) = \frac{1}{P(d)} \int_{1-\omega}^{1} d(\cos\Theta)\, p(d,\cos\Theta). \tag{52}$$

Finally, to complete the picture, we measure the response through a limited cone whose axis has been rotated 90° to the previous orientation. This is similar to the wall case. Note that only scattered radiation can reach such a detector.

$$P_b^{(s)}(d,\omega) = \frac{2}{P^{(s)}(d)} \int_{1-\omega}^{1} d(\cos\Theta) \frac{1}{2\pi} \int_{0}^{2\pi} d\phi\, p(d,\sin\Theta\cos\phi). \tag{53}$$

Again note that the total response from the barrier factor for scattered radiation has been used and divided by 2 since we are only concerned with $\frac{1}{2}$ of the radiation. Also note that the angular distribution from the point source notation has changed to account for the rotation of axis.

7. Normalizing Constant for L_b. We can now go back and evaluate the normalizing factor which was used for the geometry factor L_b. This constant was derived from setting $L_b(X,2) = 1$.

The L_b function is

$$L_b(X,\omega) = \frac{\gamma}{L(X)} \int_{1-\omega}^{1} d(\cos\theta_o)\, s(X, \cos\theta_o). \qquad (46)$$

Transposing L(X) and setting $L_b(X,2) = 1$, we now have

$$L(X) = \gamma \int_{-1}^{1} d(\cos\theta)\, s(X, \cos\theta). \qquad (54)$$

Note that the limits of integration in equation (54) have been changed to include integration over all solid angle, i.e., $\omega = 2$.

From the point source normalization process, we had

$$\frac{1}{2} \int_{X}^{\infty} \frac{dX'}{X'} P(X') = L(X). \qquad (36)$$

Since both are equal to L(X), they are equal to each other, or

$$\frac{1}{2} \int_{X}^{\infty} \frac{dX'}{X'} P(X') = \gamma \int_{-1}^{1} d(\cos\theta) s(X, \cos\theta). \qquad (55)$$

For monoenergetic sources and for the unscattered component,

$$\left.\begin{aligned} P^{(0)}(X) &= P(0)e^{-\mu X}, \quad \text{and} \\ S^{(0)}(X, \cos\theta) &= (\cos\theta)^{-1} e^{-\mu X/\cos\theta} \end{aligned}\right\}$$

Inserting these results into equation (55) and remembering that the unscattered component is completely dominant when $X \to 0$, the equation reduces tc

$$\frac{P(0)}{2}\int_{X}^{\infty}\frac{dx'}{x'}e^{-\mu x'} = \beta\int_{-1}^{1}\frac{d(\cos\theta)\,e^{-\mu X/\cos\theta}}{\cos\theta} \qquad (56)$$

Since the integrands are identical, $\beta = \frac{1}{2}P(0)$. Equation (55) holds for all X and for scattered as well as unscattered radiation, since both integrals represent the plane isotropic dose rigorously. Extension of the argument to include polychromatic sources is therefore straightforward.

Figure 17 is a summation of the relation between the angular source distributions, the barrier functions, and the geometry functions, and the corresponding graphs in the Spencer Monograph. The function for total detector response for a limited cone $P_a(X, \omega)$ is not shown but is defined by the following simple relation:

$$P_a(X,\omega) = \frac{1}{P(X)}\left[P^{(0)}(X) + P^{(S)}(X)\cdot P_a^{(S)}(X,\omega)\right]. \qquad (57)$$

SUMMARY: BARRIER AND GEOMETRY FUNCTIONS

DOSE ANGULAR DISTRIBUTION $D(\theta,\phi)$	BARRIER FUNCTION $B=\int d(\cos\theta)D(\theta,\phi)$	GEOMETRY FUNCTION $G=\frac{\int d(\cos\theta)D(\theta,\phi)\ g}{\int d(\cos\theta)D(\theta,\phi)}$
Infinite Plane Isotropic	Integration over all plane	Finite plane
$\ell(d,\cos\theta)$ 26.1	L(d) or L(X) 28.2	$L_c(X,\omega)$ 28.9
	Skyshine	Limited Detector Response
	S(d) 28.3	$L_a(X,\omega)$ 28.10
		Limited Skyshine
		$S_a(d,\omega)$ 28.15
Oblique	Barrier to Skyshine	Limited Source Obliquities
$s(X,\cos\theta)$ 26.4 26.5	S'(X) 28.4	$L_b(X,\omega)$ 28.11
Infinite Plane Weighted by Oblique Directions	Wall Barrier	Limited Wall, X = 0
$\ell(d,\sin\theta\cos\phi)$ and $s(X,\cos\theta)$	W(X,d) 28.7	$W_a(d,\omega)$ 28.12
		Vertical Aperture-Skyshine
		$W_b(d,\omega)$ 28.14
Point Isotropic	Integration over all θ,ϕ	Limited Detector
$p(d,\cos\theta)$ 26.3	P(d) or P(X) 28.5	$P_a(d,\omega)$
	Scattering Only	Limited Scatter
	$P^{(s)}(d)$ 28.6	$P_a^{(s)}(d,\omega)$ 28.16
		Limited Scatter, Rotated Axis
		$P_b^{(s)}(d,\omega)$ 28.17

Note: $P_a(X,\omega) = \left[P^{(o)}(X) + P^{(s)}(X)\cdot P_a^{(s)}(X,\omega)\right] / P(X)$

Figure 17

8. Monograph 42 Charts. Some of the charts from NBS Monograph 42 are included here for convenience. Only those dealing with the fallout radiation spectrum have been included. Experimentalists will find that the charts for Cobalt-60 and Cesium-137 are very useful. Spencer has combined the barrier and geometry functions for the limited overhead source cases, such as $L(X)L_c(X, \omega)$ since they are used quite frequently. The charts have been grouped somewhat differently than in the Monograph for convenience in use. The following table lists the figure number, the identifying symbol, NBS figure number, and a brief description of the function.

TABLE I Barrier and Geometry Charts from NBS Monograph 42

Fig #	Symbol	NBS-42 #	Description
18	$L(d)$	28.2a	Barrier factor for plane source, mass in ft of air.
19	$L(X)$	28.2b	Barrier factor for plane source, mass in psf.
20	$L(X)L_c(X, \omega)$	28.18	Reduction factor for plane source, limited area (smeared barrier).
21	$L(X)L_a(X, \omega)$	28.19	Reduction factor for plane source, limited detector (mass concentrated at source).
22	$L(X)L_b(X, \omega)$	28.20	Reduction factor for plane source, limited obliquities (mass concentrated at detector).
23	$W(X,d)$	28.7	Wall barrier factor.
24	$W_a(d, \omega)$	28.12	Geometry factor for limited circular wall area.
25	$W_b(d, \omega)$	28.14	Geometry factor for vertical opening subject to skyshine only.
26	$S'(X)$	28.4	Barrier to reflected radiation, barrier to skyshine.
27	$S(d)$	28.3	Response to skyshine as a function of height in ft above plane.
28	$S_a(d, \omega)$	28.15	Limited skyshine, axis vertical.
29	$P(d)$	28.5a	Barrier factor for point source, mass in ft of air.
30	$P(X)$	28.5b	Barrier factor for point source, mass in psf.
31	$P_a^{(s)}(d, \omega)$	28.16	Geometry factor for scattered radiation from point source, limited detector, axis toward source.
32	$P_b(d, \omega)$	28.17	Geometry factor for scattered radiation from point source, limited detector, axis at 90° from source.
33	$P^{(o)}(X), P^{(s)}(X)$	28.6	Scattered and unscattered components of $P(X)$.

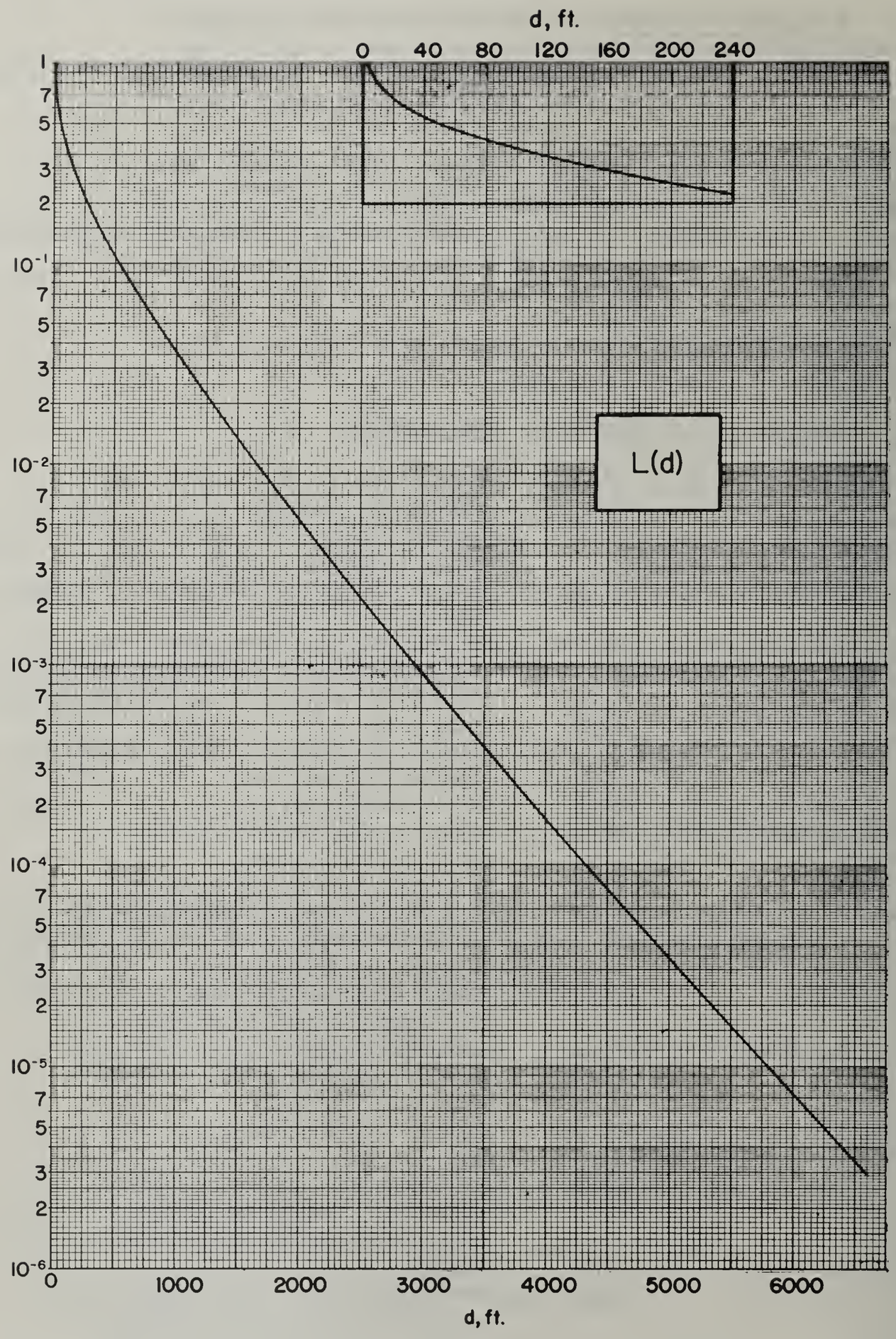

Figure 18. Plane source of fallout radiation: the (isotropic) detector response ratio D/D_o as a function of height d in air above the source plane. (H_2O, 1.12 hr fission. NBS-42 Figure 28.2a)

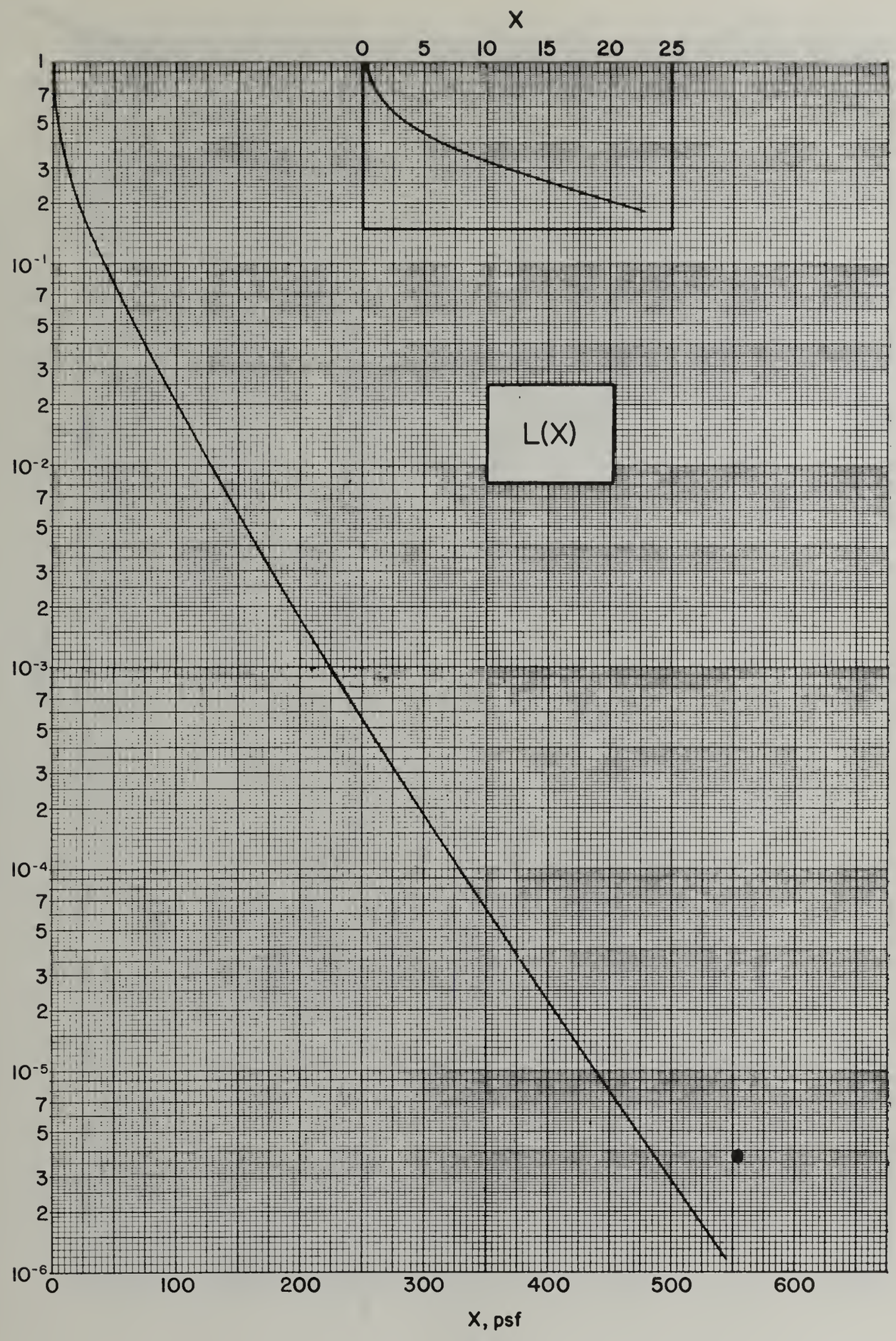

Figure 19. Plane source of fallout radiation: the (isotropic) detector response ratio D/D_o as a function of effective mass thickness separating the detector and the source plane. (H_2O, 1.12 hr fission. NBS-42 Figure 28.2b)

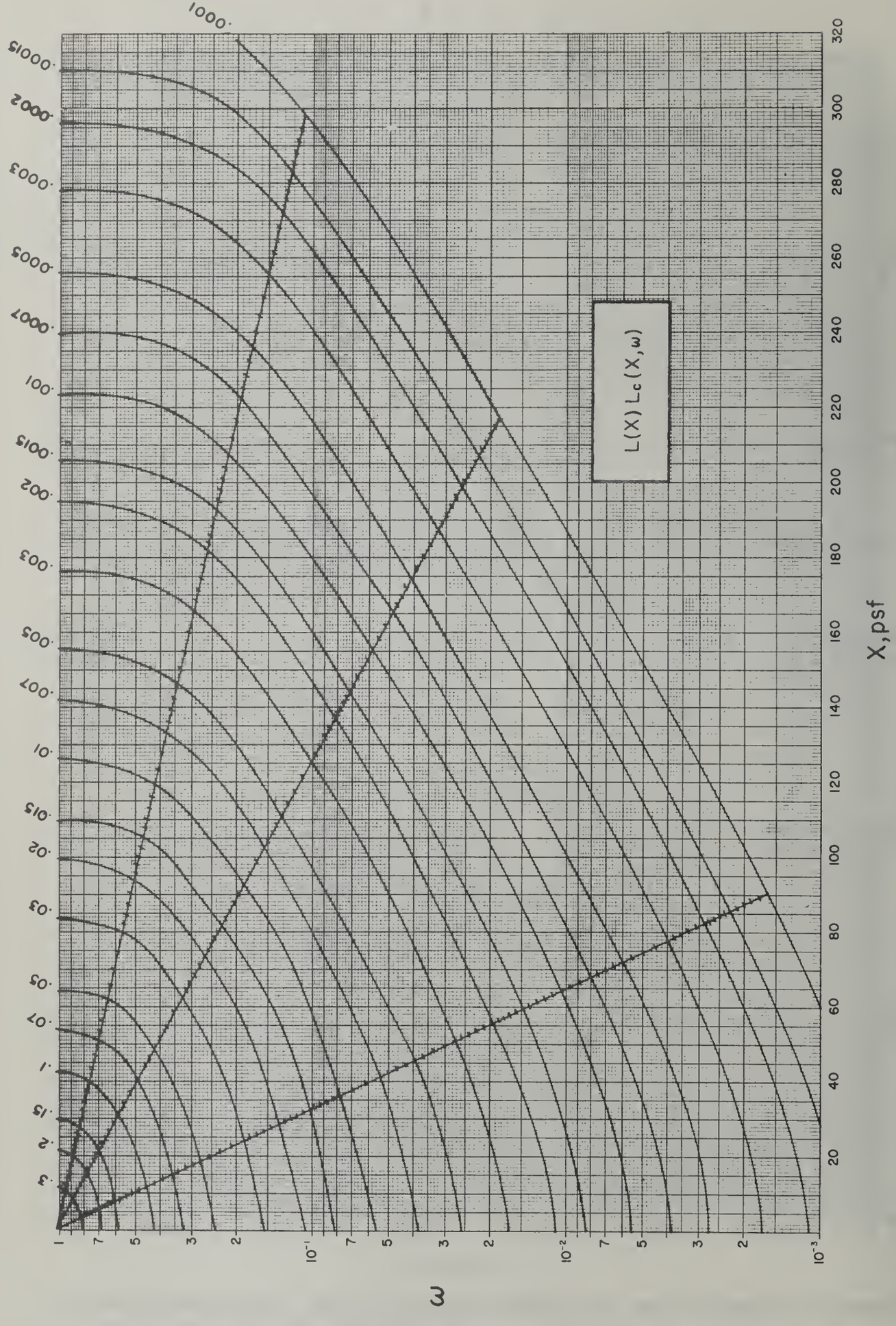

3

Figure 20. Contours of constant $L(X)L_c(X, \quad)$. (H_2O, 1.12 hr fission NBS-42 Figure 28.18)

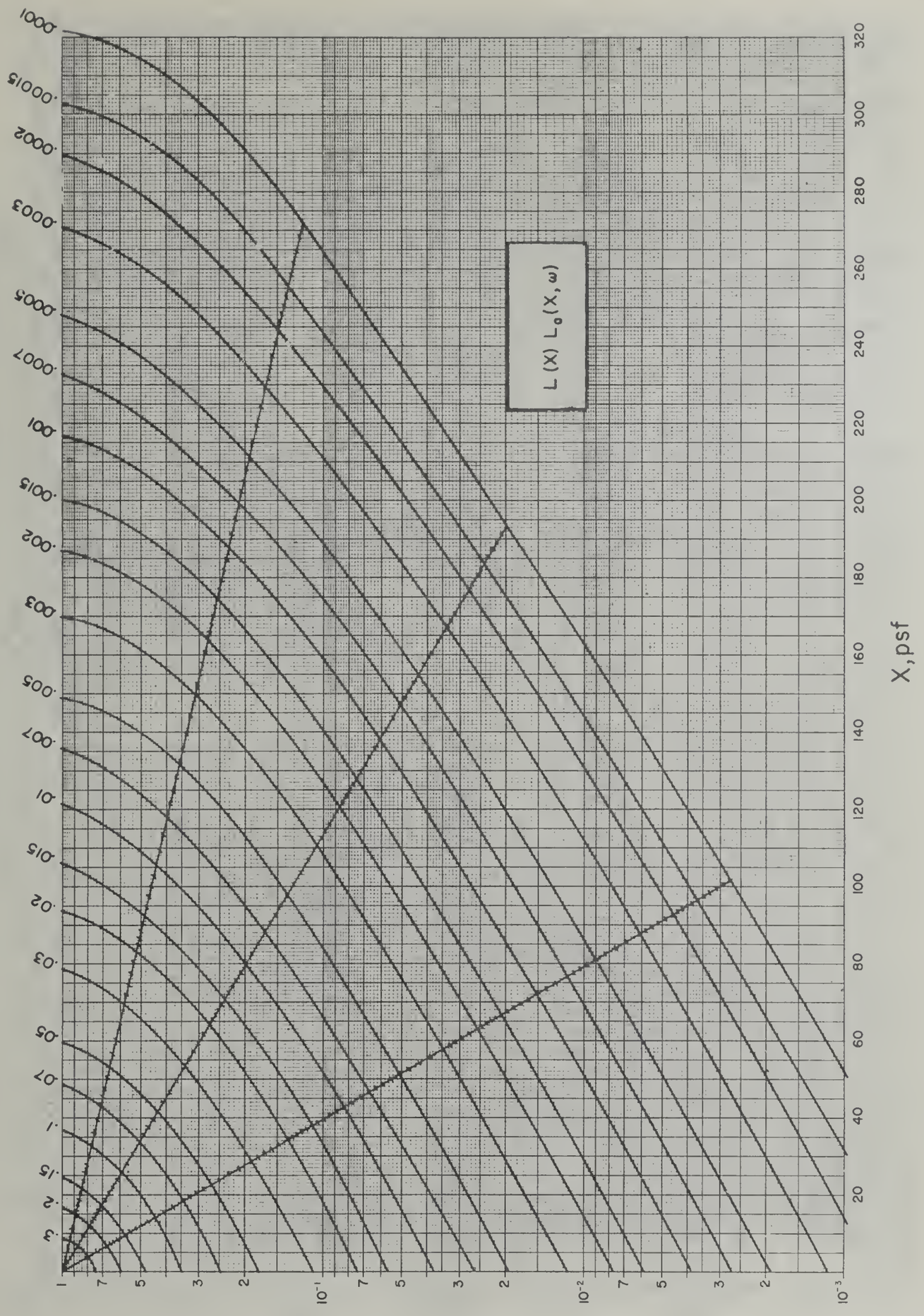

Figure 21. Contours of constant $L(X)L_a(X,\omega)$. (H_2O, 1.12 hr fission NBS-42 Figure 28.19)

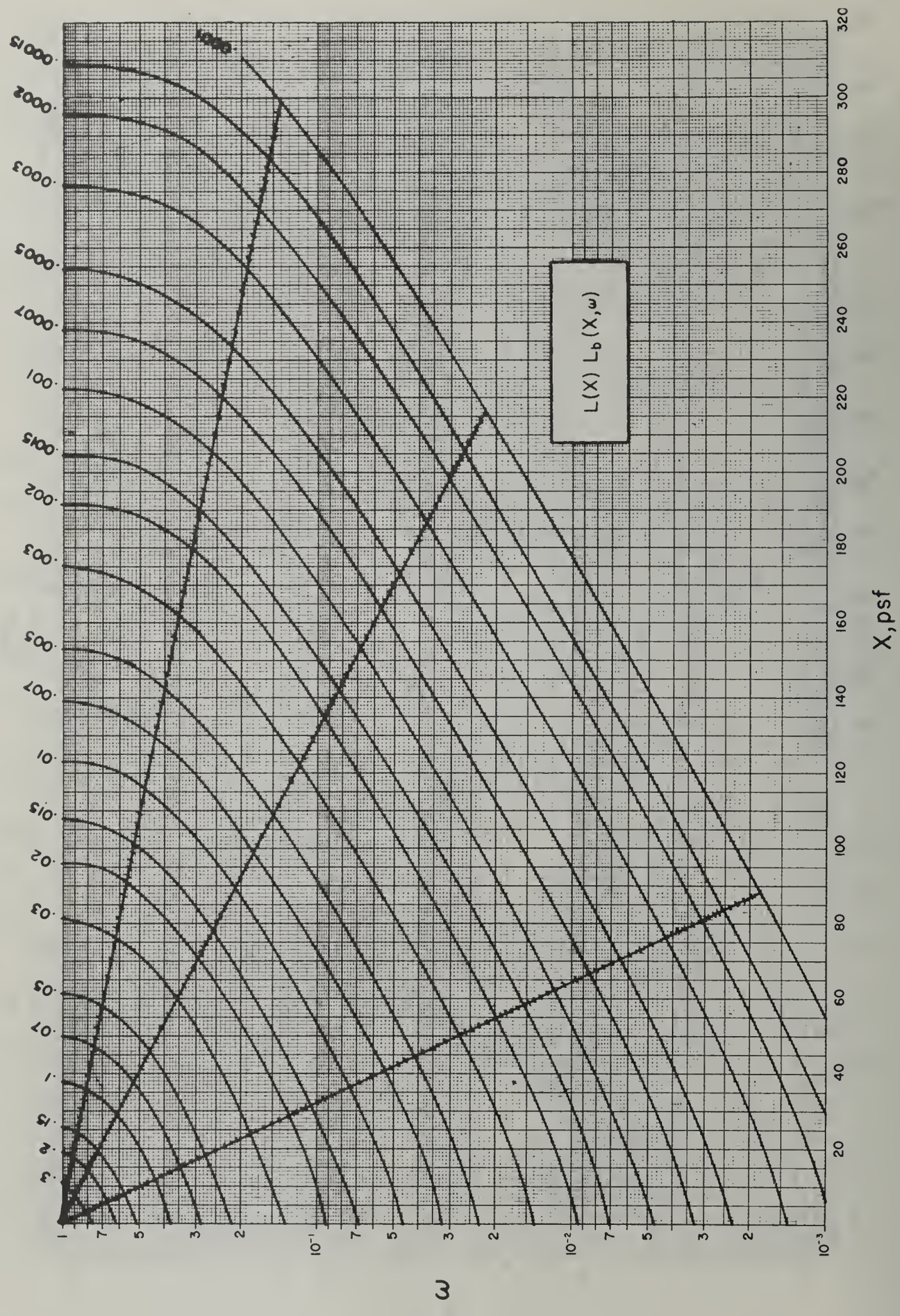

Figure 22. Contours of constant $L(X)L_b(X,\omega)$. (H_2O, 1.12 hr fission NBS-42 Figure 28.20)

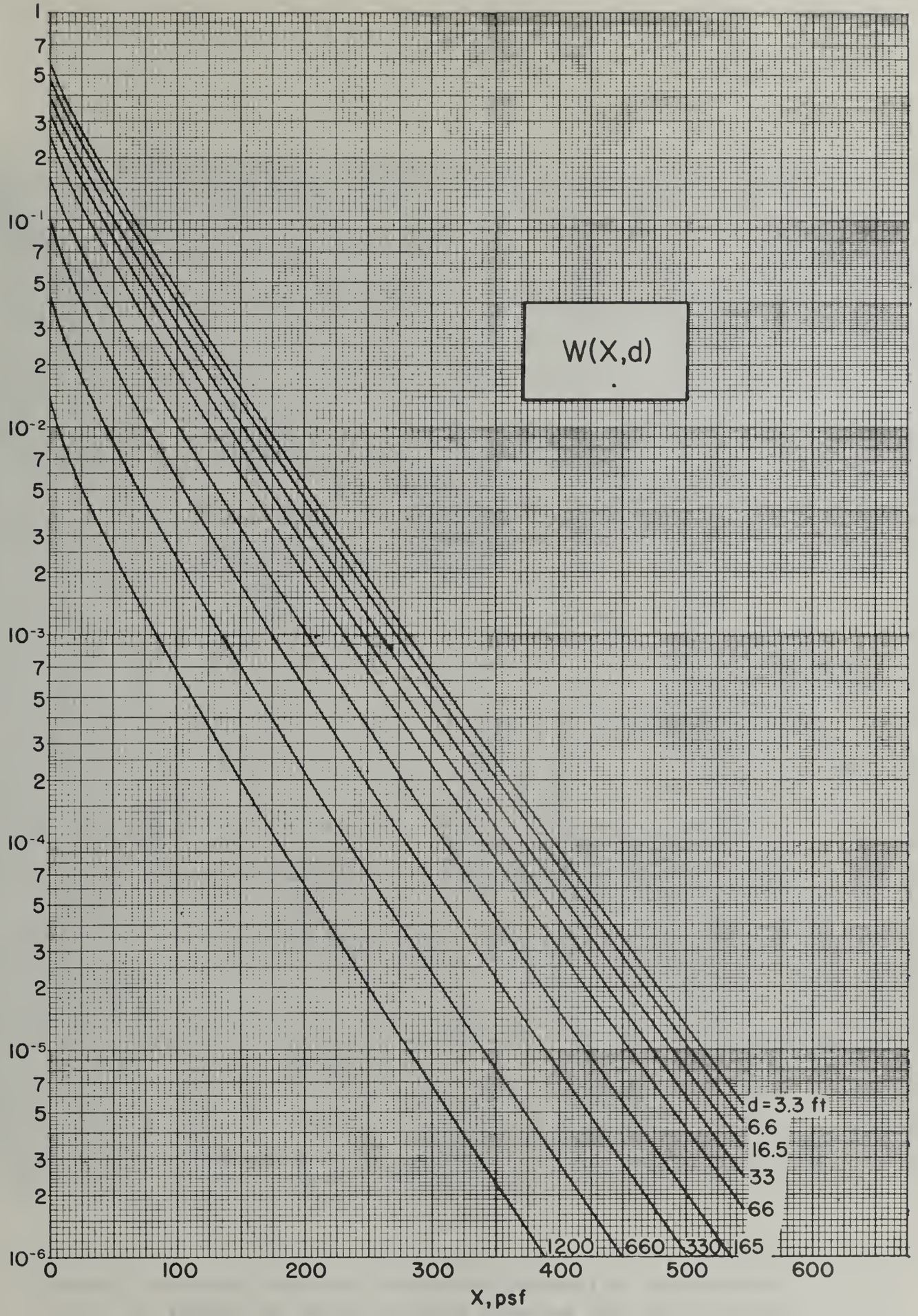

Figure 23. Detector response ratio for effective mass thickness X separating the detector from a plane fallout source. (H_2O, 1.12 hr fission - NBS-42 Figure 28.7).

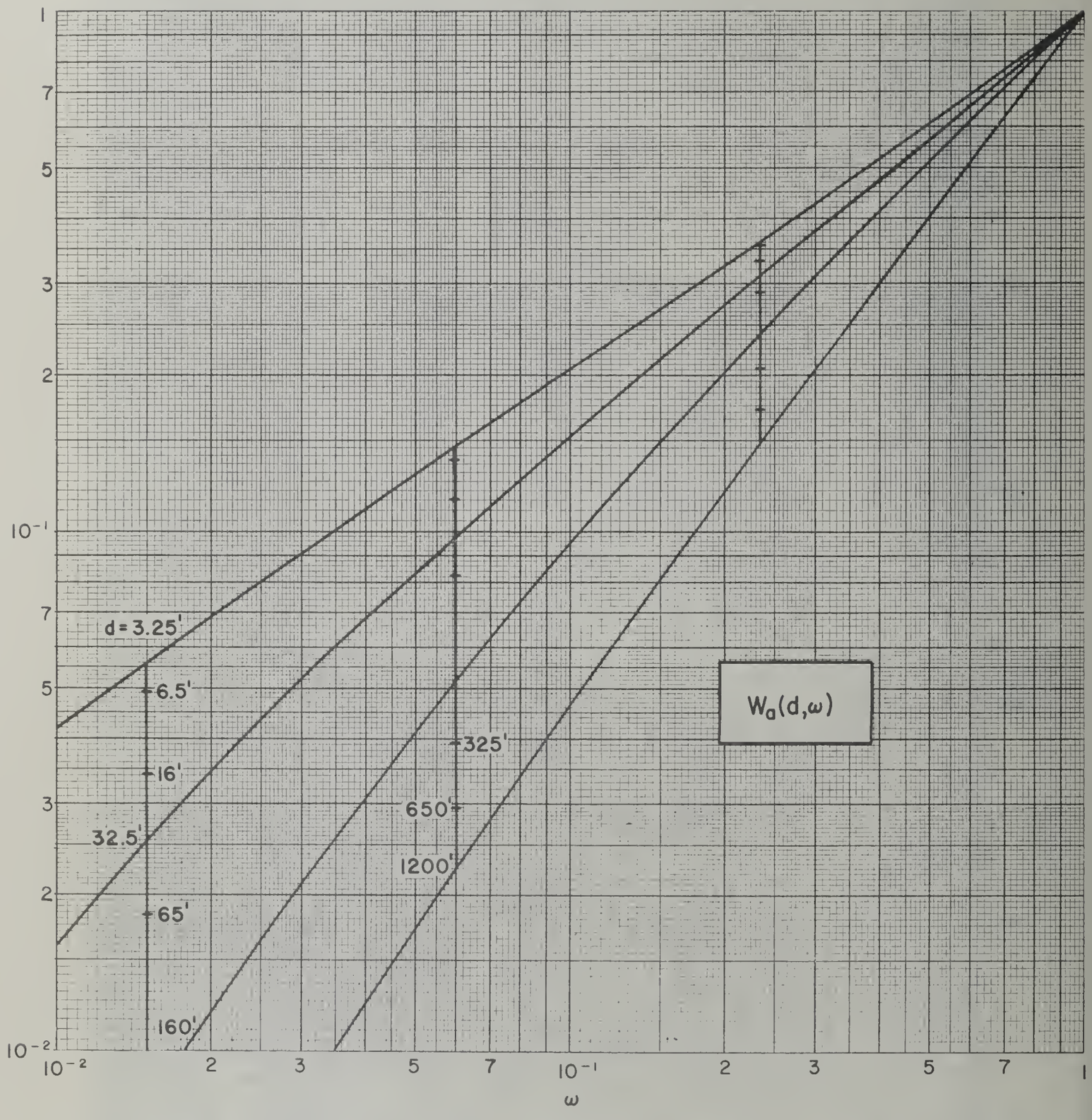

Figure 24. Geometry factor describing detector response to radiation incident in a limited cone of directions about an axis parallel to the primary source plane, at height d, (H_2O, 1.12 hr fission - NBS-42 Figure 28.12).

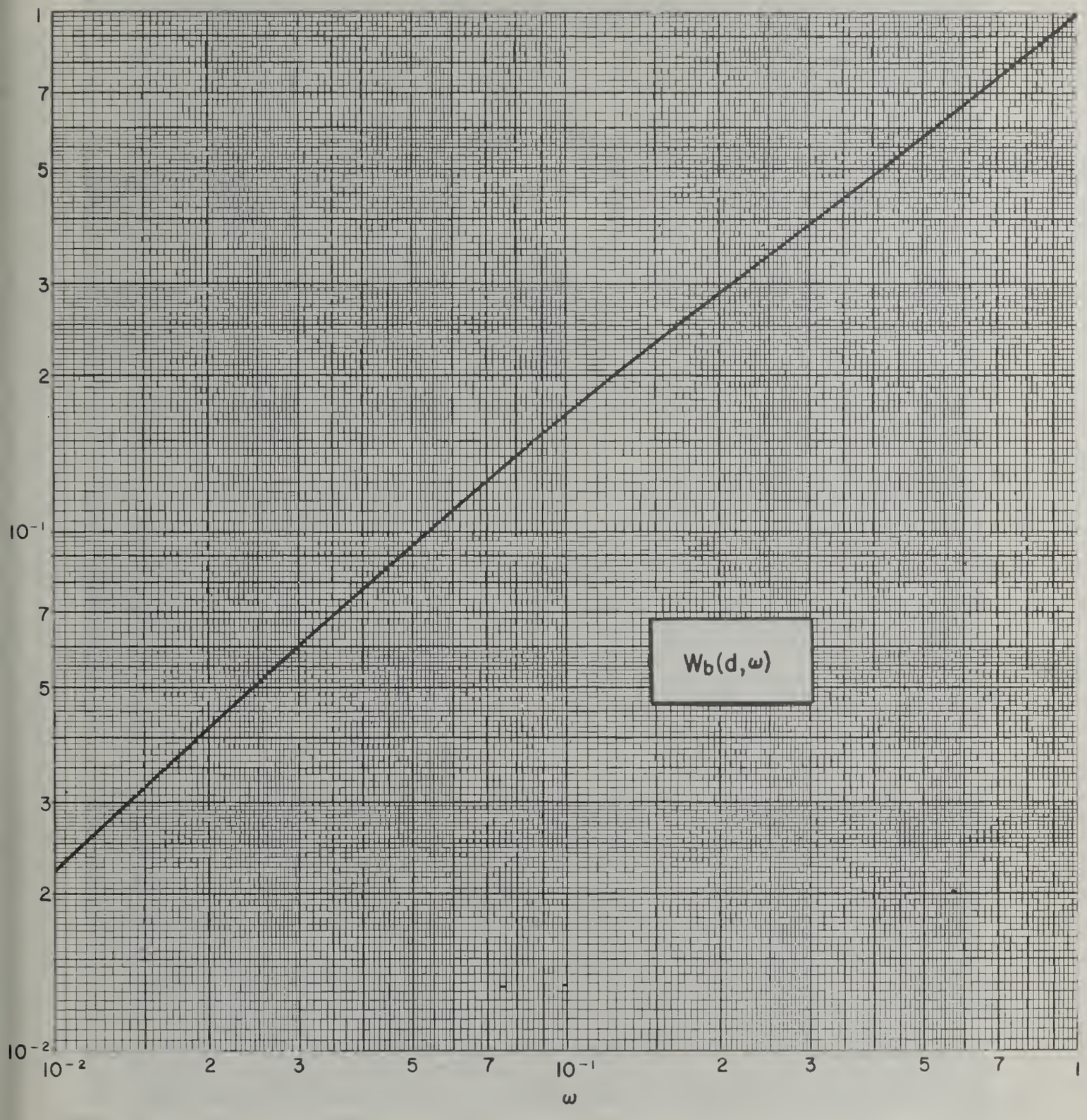

Figure 25. Geometry factor describing detector response to skyshine radiation incident in a limited cone of directions about as axis parallel to the primary source plane. (H_2O, 1.12 fission - NBS-42 Figure 28.14).

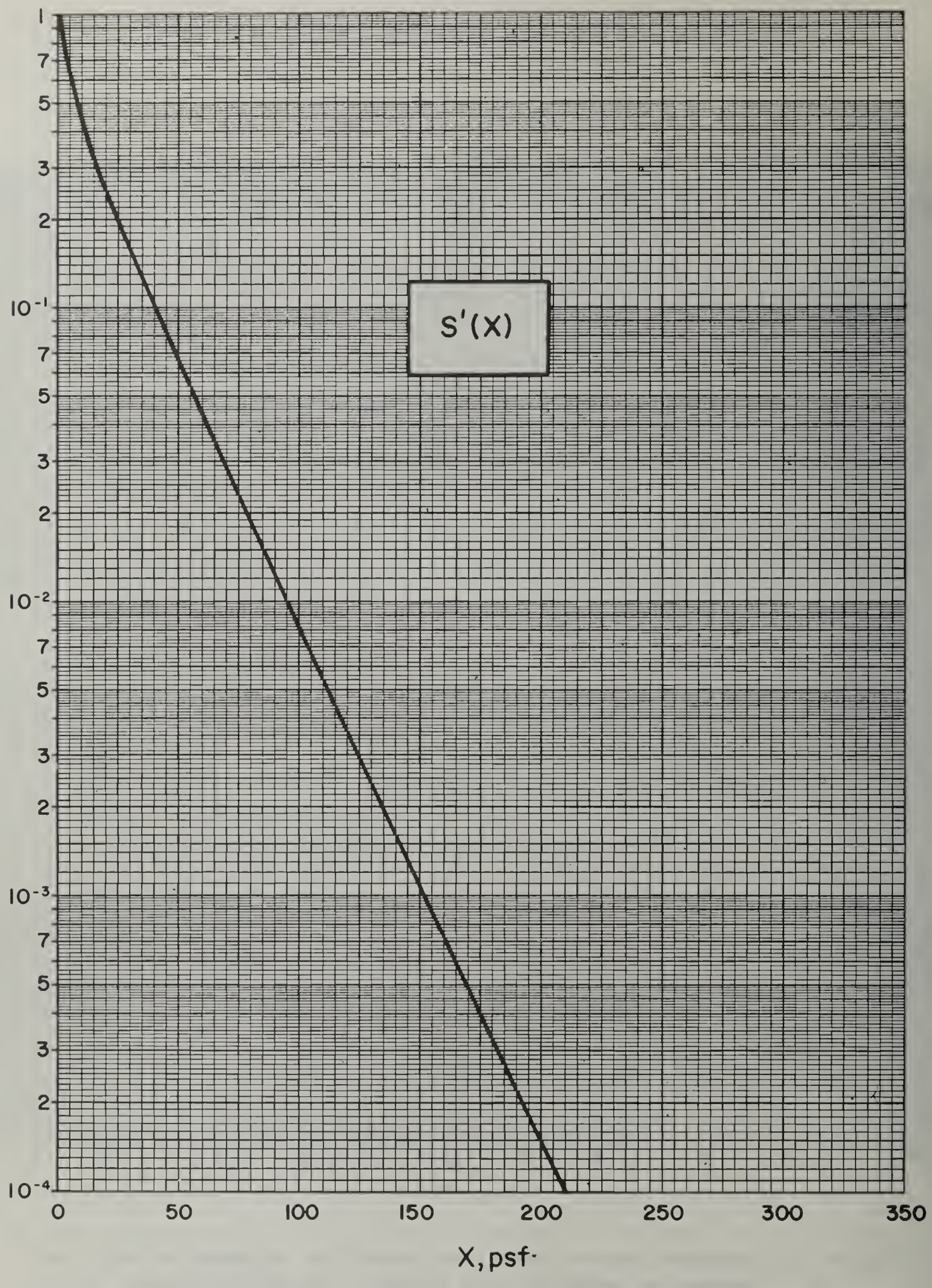

Figure 26. Attenuation curve for radiation backscattered from a plane source isotropic over one hemisphere only, corresponding to skyshine radiation incident on the ground. (H_2O, 1.12 hr fission - NBS-42 Figure 28.4).

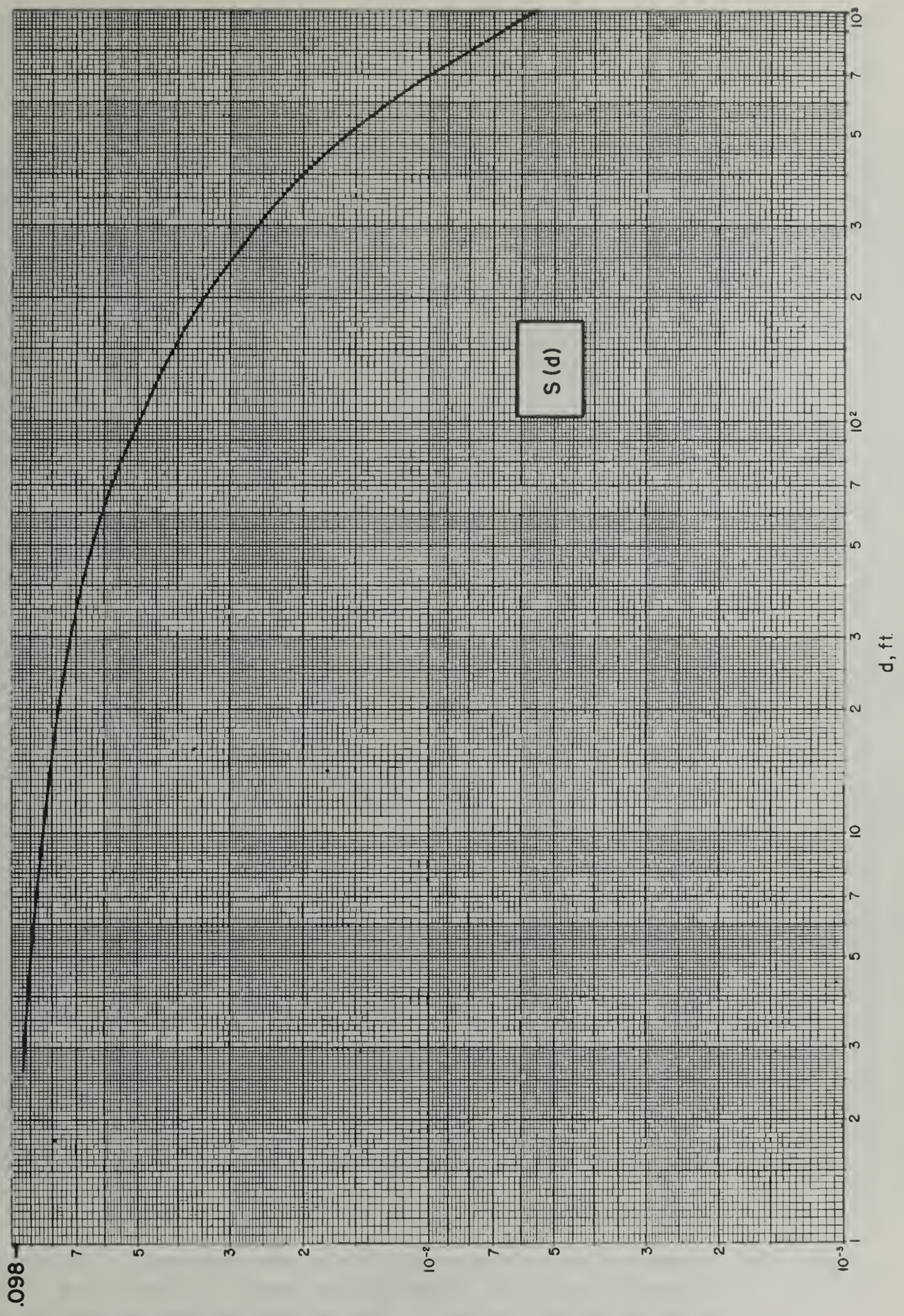

Figure 27. The detector response ratio D/D_o due to skyshine, as a function of height above a plane source of fallout radiation. (H_2O, 1.12 hr fission: NBS-42 Figure 28.3).

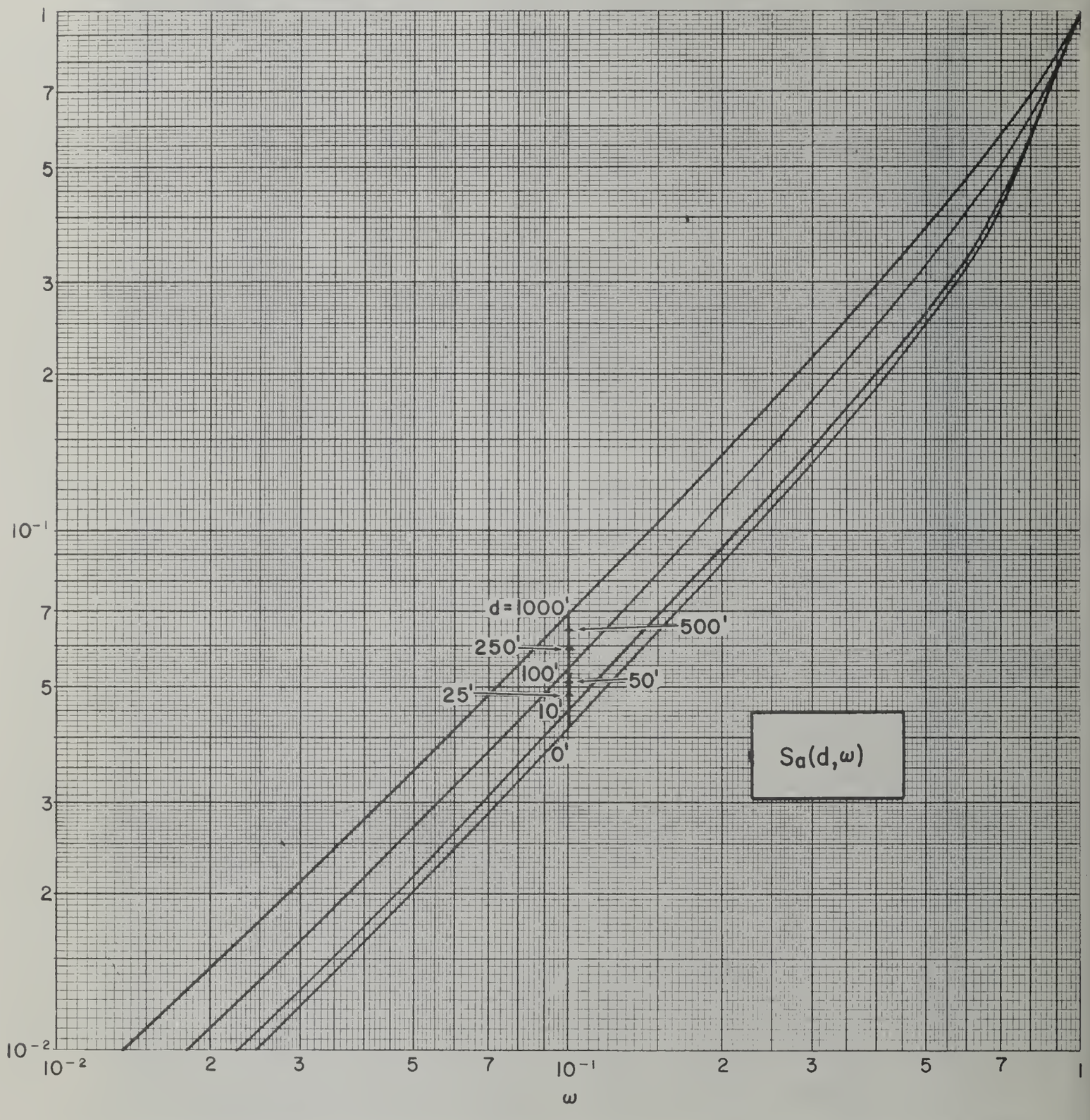

Figure 28. Geometry factor describing detector response to skyshine radiation incident in a limited cone of directions about an axis perpendicular to the primary plane, at height d above the ground. (H_2O, 1.12 hr fission: NBS-42 Figure 28.15).

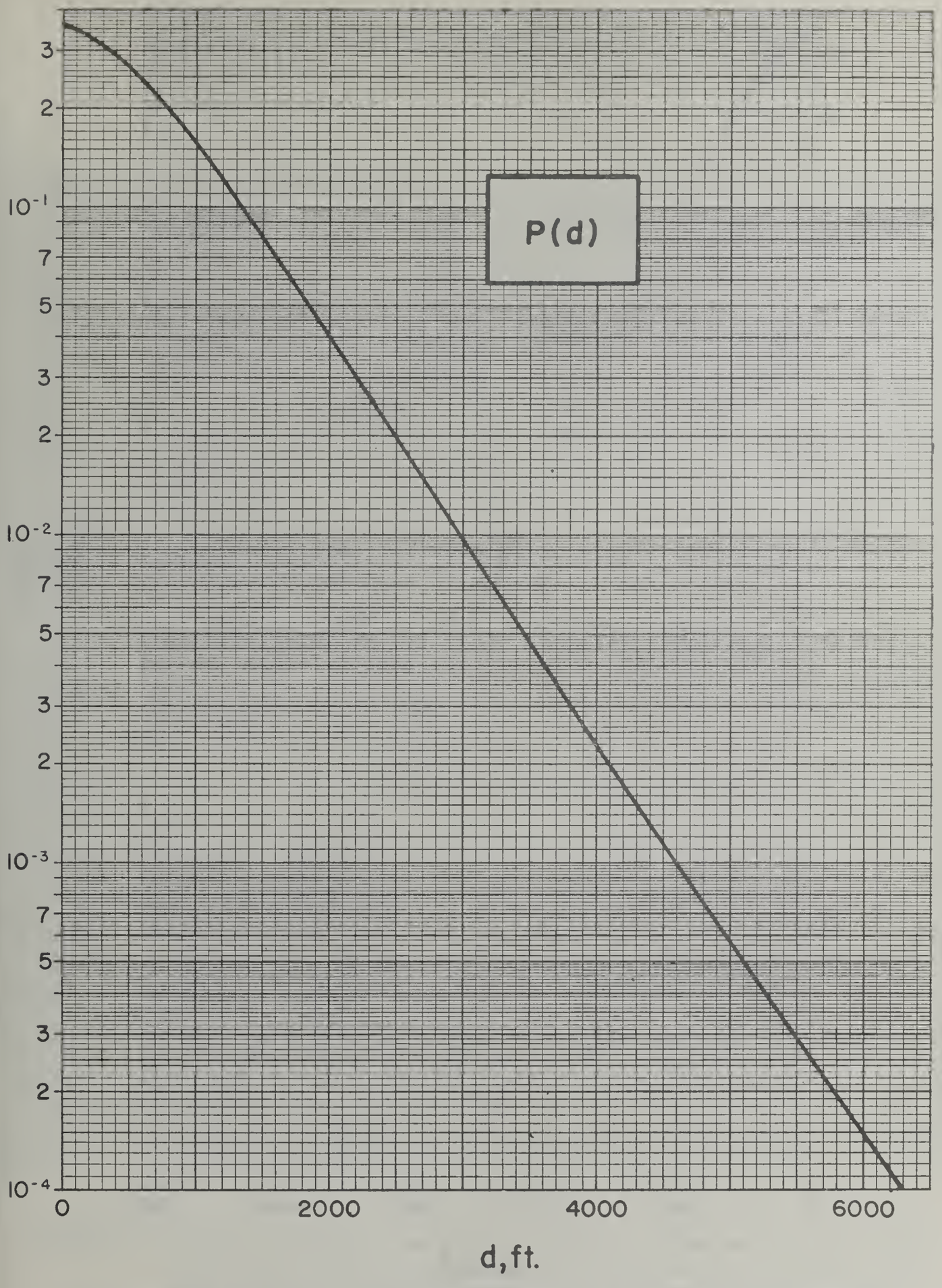

Figure 29. Point source of fallout radiation: P(d) as a function of distance d in air between detector and source. (H_2O, 1.12 hr fission: NBS-42 Figure 28.5a).

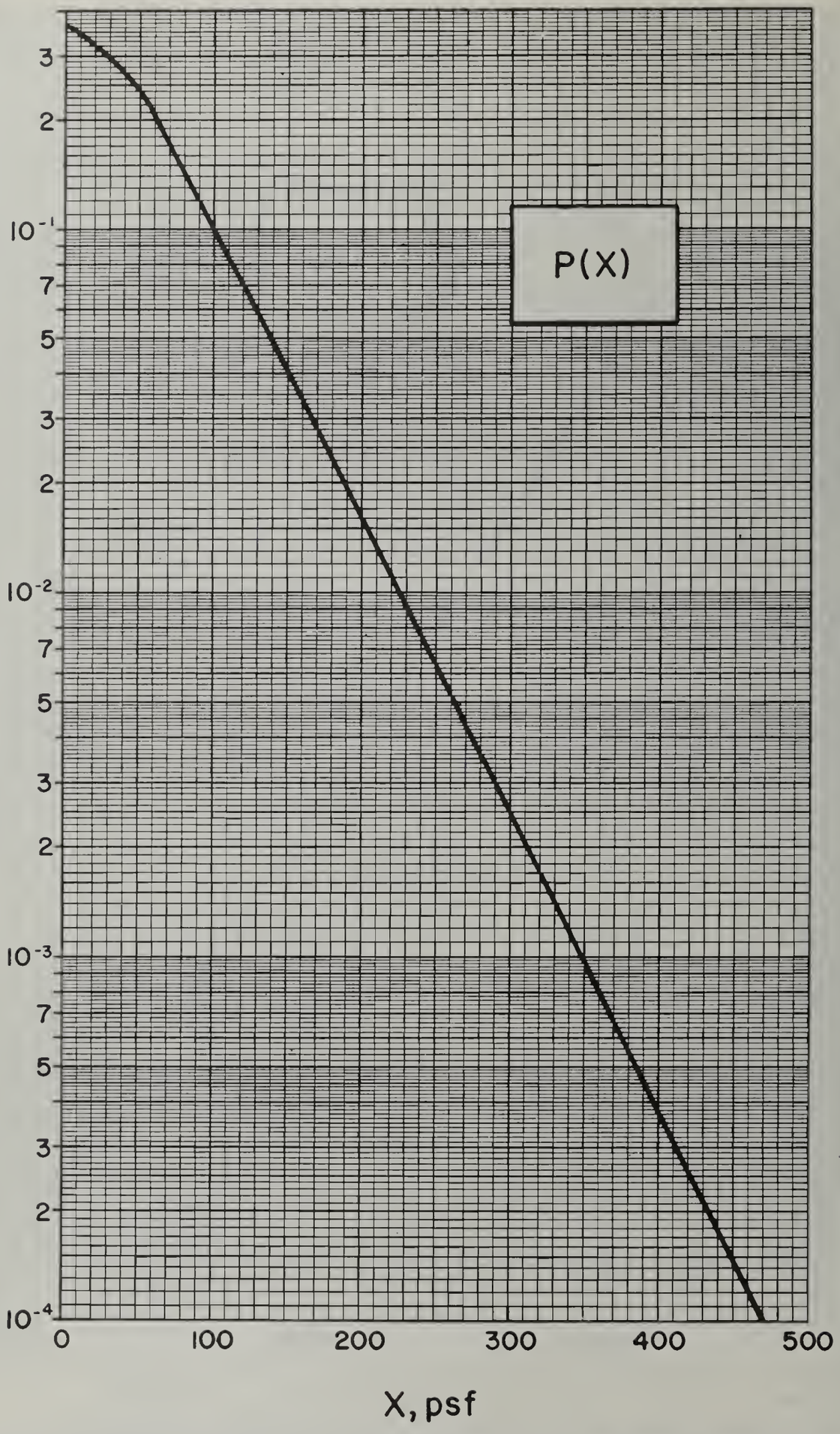

Figure 30. Point source of fallout radiation: (P(X) as a function of effective mass thickness between source and detector. (H_2O, 1.12 hr fission: NBS Figure 28.5b).

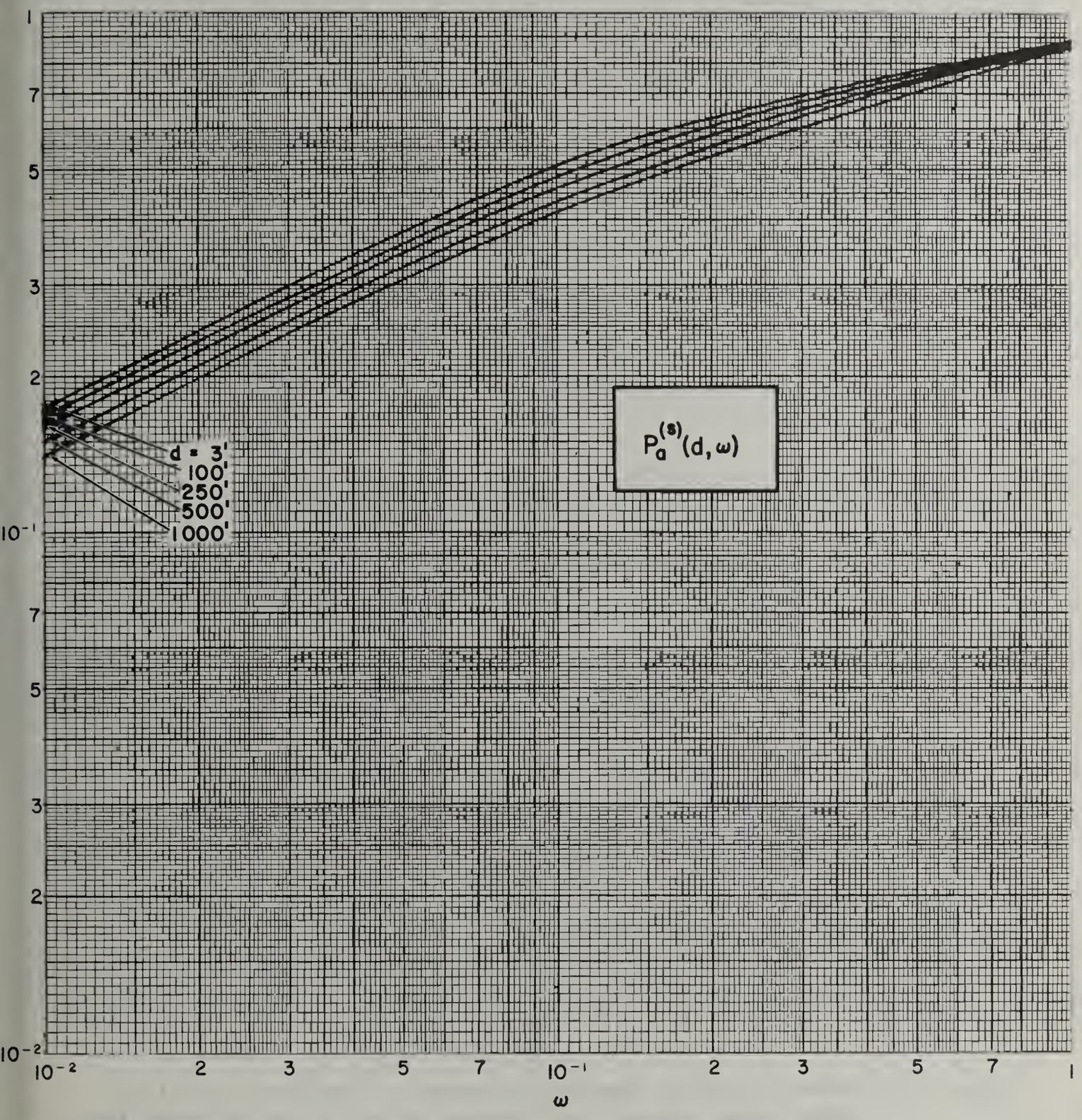

Figure 31. Geometry factor describing detector response to scattered gamma rays from a point source of radiation, striking the detector in a limited cone of directions about the line from source to detector. (H_2O, 1.12 hr fission: NBS-42 Figure 28.16).

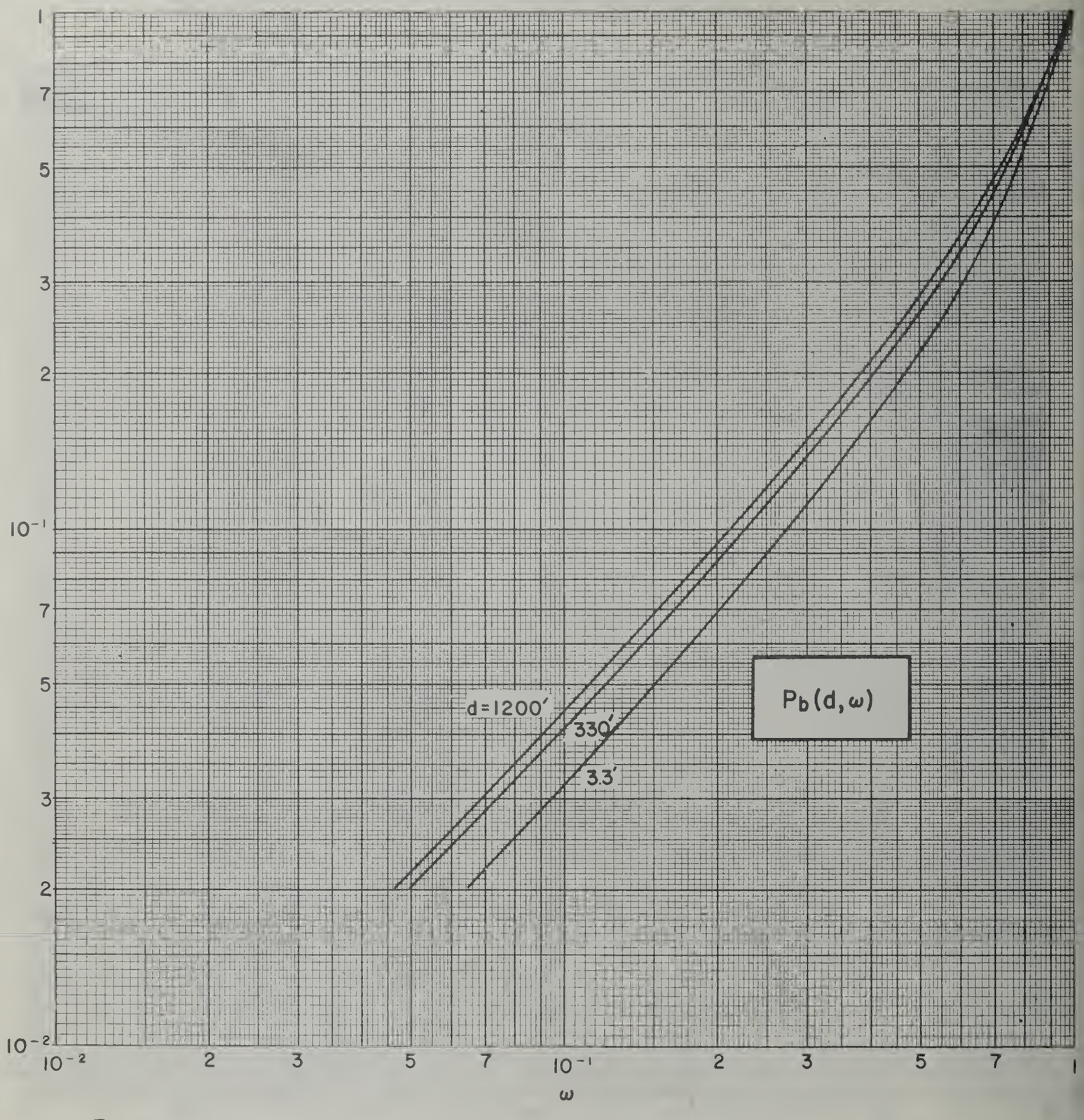

Figure 32. Geometry factor describing detector response to fallout gamma rays from a point source, striking the detector in a limited cone of directions about an axis perpendicular to the line from source to detector. (H_2O, 1.12 hr fission: NBS-42 Figure 28.17).

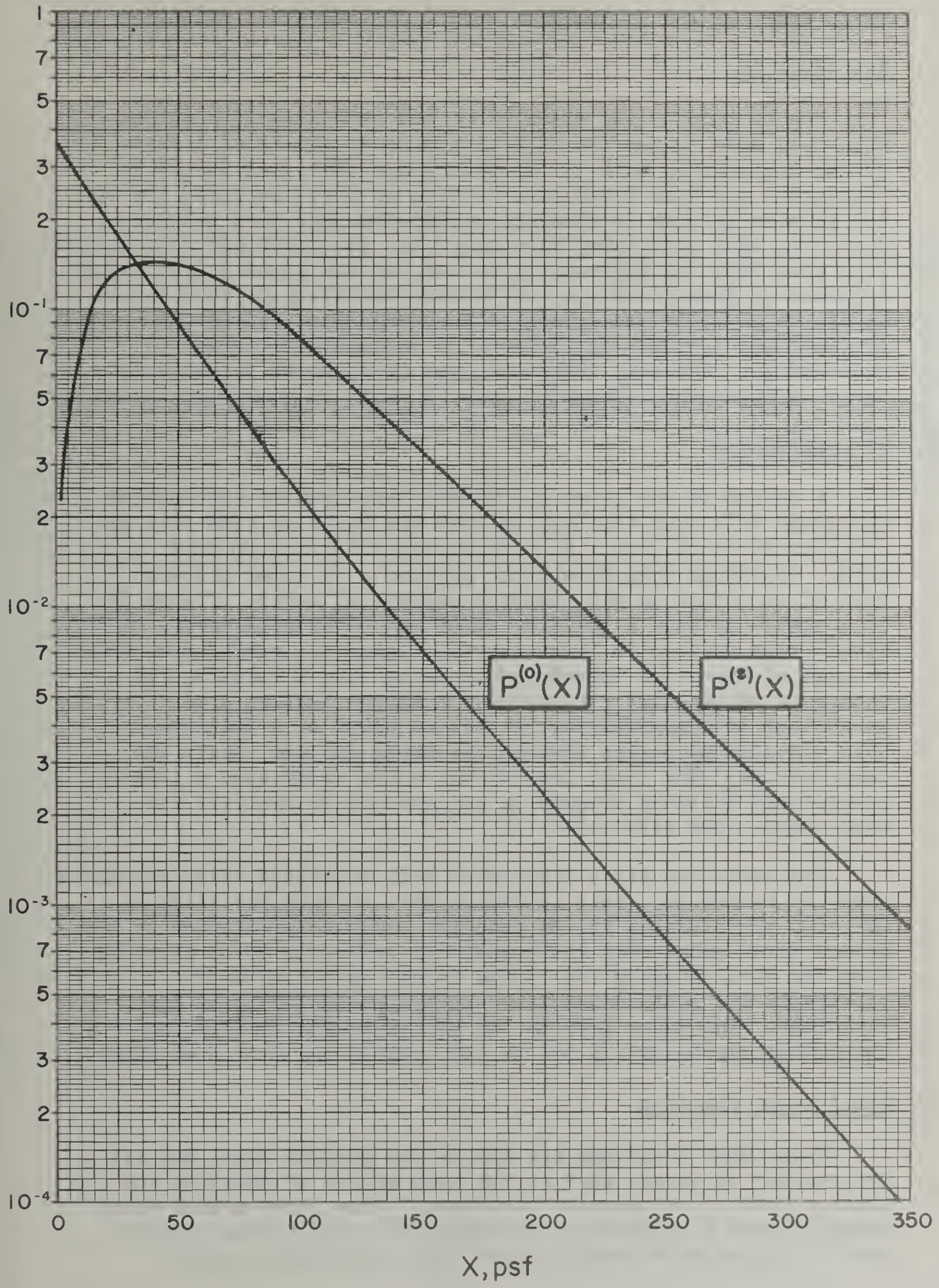

Figure 33. Unscattered and scattered components of P(X), (H_2O, 1.12 hr fission: NBS-42 Figure 28.6).

V - DEVELOPMENT OF THE ENGINEERING METHOD FOR STRUCTURE SHIELDING

A. Introduction.

Now we turn to the assumptions and approximations which have been made to use the data available in NBS-42 as a basis for an engineering method. C. Eisenhauer (National Bureau of Standards) and Neal FitzSimons (Office of Civil Defense) are the two primary authors to whom the credit for this task belongs. Since the 1962 institute, Eisenhauer has published NBS report 7810 (Feb '63) "An Engineering Method for Calculating Protection Afforded by Structures Against Fallout Radiation." This report covers essentially the same ground as this part (V) of the proceedings; i.e., the development of the engineering method from NBS-42. However, there are some differences in interpretation and presentation which makes a study of both worthwhile.

B. Schematization.

A review of the geometry factors developed in the Spencer Monograph will show that all of them are based on some sort of circular field of view. As a first approximation to most actual buildings then, Eisenhauer assumed a circular pillbox type of structure as his standard analytical model. Figure 34 is a sketch of such a building which has horizontal layers or floors with windows in these layers. Later on, comparisons will be made of the error introduced by using such a building for square or rectangular structures. Although factors are introduced to compensate for the actual shape of a building, this circular structure remains the basis for all charts and computations. The final justification for using such a simple schematized building depends on the results it predicts for more complicated structures.

The radiation field associated with shielding calculations is shown in Figure 35. This indicates that we have radiation on the roof contributing to the detector response, radiation on the ground which penetrates the walls, and radiation which scatters from the air. Roughly 75% of the direct radiation which penetrates the walls comes from approximately 100 ft of the structure. The major part of the air scattered contribution comes from approximately 500 ft (or roughly one mean free path).

C. Solid Angle Fraction.

Since most buildings are not of the pillbox type, but are rectangular in shape, what is the best method of relating the pillbox data to rectangular structures? The first method which comes to mind is equating the rectangular area to the circular area; in other words making equal areas contribute equally.

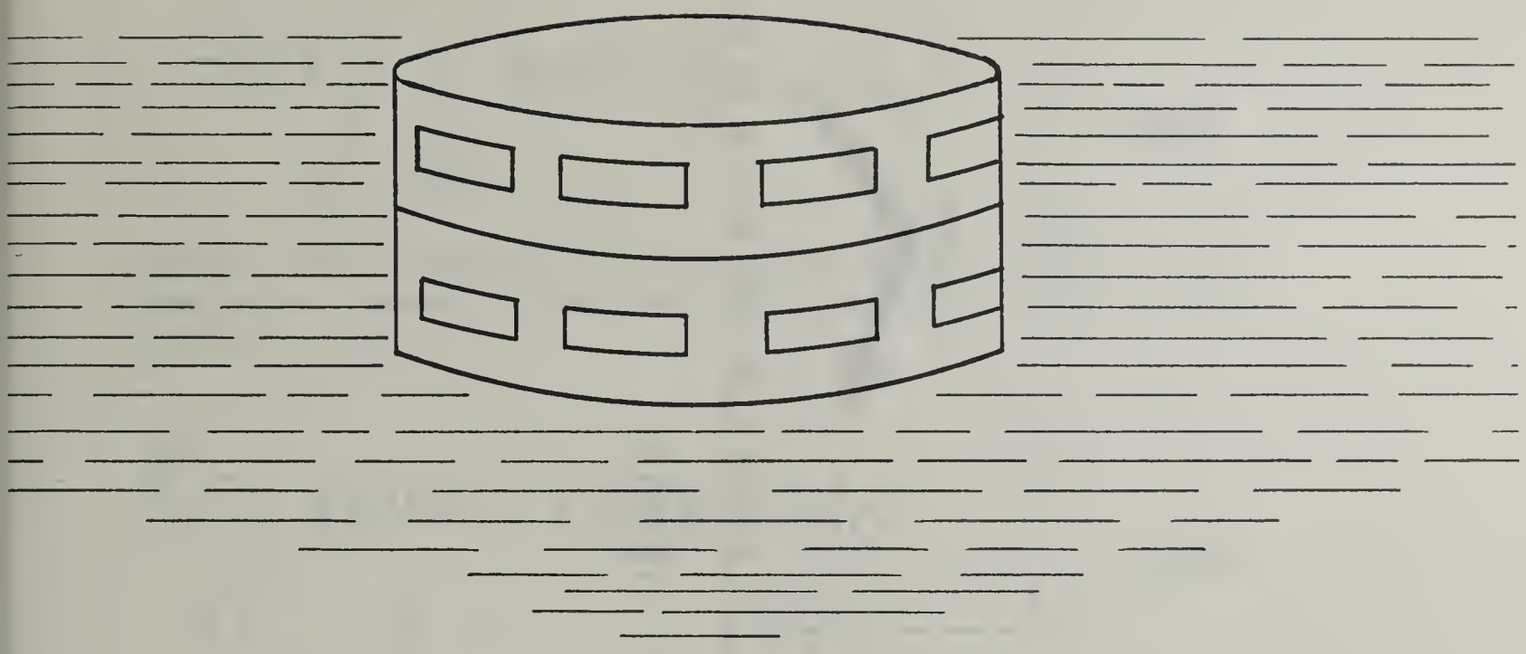

SCHEMATIZED PILLBOX BUILDING

Figure II-34

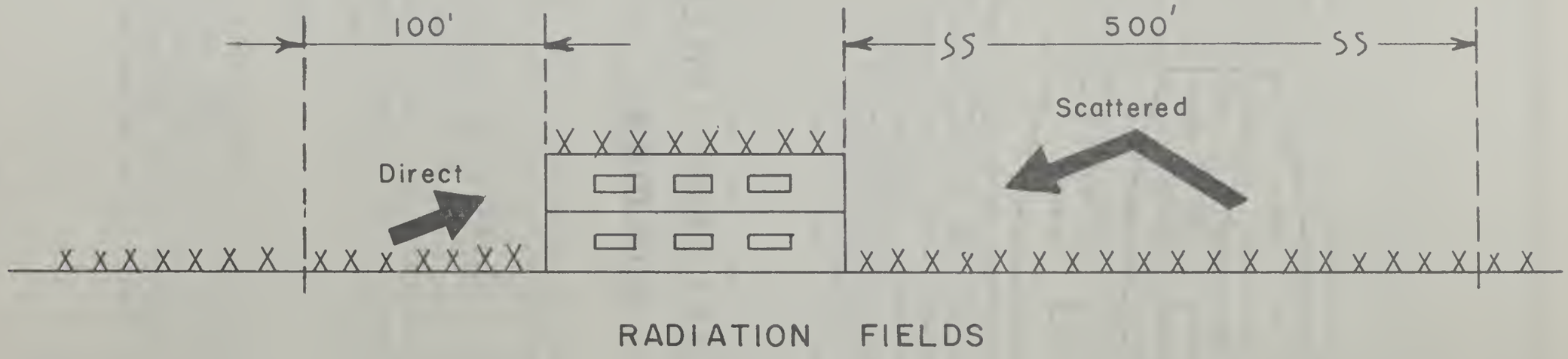

Figure II-35

This is normally a poor procedure when applied to gamma rays, since this weights the areas which are far from the detector too heavily. This can be shown by comparing the expression for an arbitrary area and the response of a detector to a uniform distribution of point isotropic sources within that area. The expression for the area of an arbitrary shape is:

$$A = h^2 \int_0^{2\pi} \int_{F(\theta)}^{1} \sec^3\theta \, d(\cos\theta) \, d\phi. \qquad (58)$$

Compare this result with the response of a detector to this same area, assuming a uniform distribution of point sources within the area :

$$R = \int_{\Omega} g(\cos\theta, \phi) \, d(\cos\theta) \, d\phi. \qquad (59)$$

The function $g(\cos\theta,\phi)$ is the angular distribution of radiation at the detector. Referring now to the above equation for the area, if the angular distribution of radiation at the detector varied as $\sec^3\theta$, then the responses from a rectangle and a circle of the same area would be equal. But the angular distribution of radiation at a detector is more nearly isotropic and usually never exceeds the first power of $\sec\theta$.

A better scheme is to equate surfaces on the basis of the solid angle subtended at the detector by the surface. If a rectangular area and a circular area subtend the same solid angle, and if the radiation is isotropic, then the rectangle and circle would give the same detector response. The solid angle used here, as in the Spencer Monograph, is actually the total solid angle Ω divided by 2π and is termed the solid angle fraction (ω).

Refer back to Figure 6. This is the dose angular distribution for an infinite plane fallout source (Figure 26.1 NBS-42). Radiation at the detector from a plane isotropic source actually varies from a sec θ distribution which peaks from the horizon, to a cot θ distribution which peaks from the source plane itself. Most distributions will vary between these two extremes but will tend to be more nearly isotropic than anything else. This is the basis of justification for the use of the solid angle fraction concept.

The solid angle fraction is easy to calculate, for both circular and rectangular shapes. Solid angle fraction for a circle is:

$$\omega = 1 - \cos\theta_0 \quad (60)$$

The solid angle fraction for a rectangle is:

$$\omega = \frac{2}{\pi} \tan^{-1} \frac{\epsilon}{n\sqrt{n^2+\epsilon^2+1}} \qquad \epsilon = \frac{W}{L} \qquad n = \frac{2Z}{L} \quad (61)$$

See Section X for derivation.

D. Roof Contribution Approximations.

Figure 36 illustrates a roof contaminated with radiation in a schematized building with several floors, and a detector below the first floor. Spencer has calculated three cases relevant to roof radiations: 1) a circular source with a uniform barrier between the source and detector; 2) a circular source with the barrier concentrated at the source, and 3) a circular source with a barrier concentrated at the detector. None of these cases fit the real situation exactly, but the "smeared barrier" of case 1 is the one which was chosen for the Engineering Manual. This best describes the situation shown in the sketch; i.e., several floors between the source and the detector. It should be noted, however, that the other two cases have application in other practical situations. Case 2, for instance, with the barrier concentrated at the source, would apply to a massive roof, and a detector at some distance with only very light floors intervening. The third case would apply to the opposite extreme, with intervening floors of very light material and the detector located in a basement with a very massive basement ceiling.

In order to determine the relative error in using the smeared barrier concept for the Engineer Manual, Eisenhauer has made a calculation which is shown in Table I. The calculations were made for several mass thicknesses, (X = 0, X = 50 and X = 100 psf) and for several solid angle fraction (ω = .05, .1 and .5). Comparing the three types of configurations we see that the uniformly distributed barrier is not conservative when X is small; it tends to be conservative for X = 50 and X = 100. The difference between the three cases

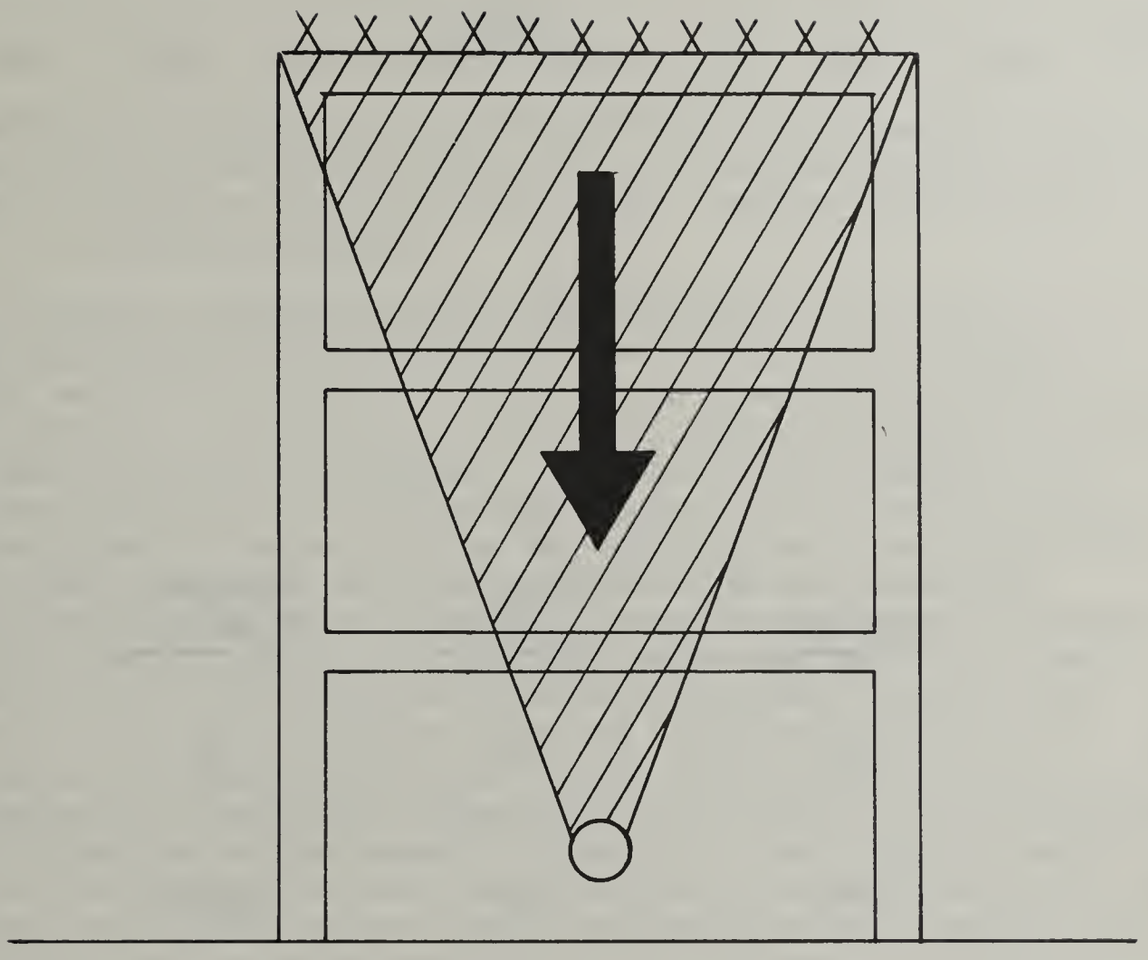

Figure II-36

Table I

ω =	X=0			X=50			X=100		
	.05	.1	.5	.05	.1	.5	.05	.1	.5
Uniformly distributed barrier	.009	.019	.125	.0058	.011	.058	.0026	.0048	.017
Barrier at source	.013	.027	.16	.005	.010	.045	.0018	.0036	.0125
Barrier at detector	.011	.022	.15	.0055	.0105	.050	.0022	.0040	.015

Table II

	Circle	Circle + 2 Sectors	Circle + 4 Sectors
$\eta = 0.2$ $D = \sec\theta$	.669	.824	.791
$\eta = 0.2$ $D = \cot\theta$	.859	.934	.939
$\eta = 1.0$ $D = \sec\theta$	.0928	.1038	.1016
$\eta = 1.0$ $D = \cot\theta$	.411	.329	.340

From work of C. Eisenhauer, NBS 7810, February 28, 1963.
For see equation (61).

can be as much as 40%. We would expect practical applications to be closer to the smeared barrier case. Any error, then, would be much less than the 40% maximum.

The approximation of a rectangular source area by a circular disk also introduces error. The approximation is equivalent to:

$$\int_R D(\cos\theta)\, d(\cos\theta)\frac{d\phi}{2\pi} \simeq \int_{\cos\theta_0}^{1} D(\cos\theta)\, d(\cos\theta) . \qquad (62)$$

R indicates integration over the domain of the rectangle. The value of cosine θ_0 on the right side of the equation is determined from the condition that the solid angle fraction subtended by the two surfaces be equal.

The error involved in treating rectangles as circles of equal solid angle depends then on the form of $D(\cos\theta)$ which is the angular distribution of radiation reaching the detector. Again if the distribution is isotropic, that is $D(\cos\theta) = 1$, then the two schemes are equivalent. Eisenhauer has examined two extreme distributions of $D(\cos\theta)$; distribution proportional to sec θ, (that is radiation from the horizon), and one proportional to cot θ, (radiation from the vertical). He then examines these cases for a rectangle with a large eccentricity, (a length to width ratio equal to 5), with two subcategories: The detector close to the surface and the detector relatively far from the surface. Sec θ is the horizon peaked distribution and cot θ is the zenith peaked distribution. To obtain more accurate estimates as a basis for comparison, the rectangles are approximated by circular sectors as shown in Figure 37 . In the approximation we are evaluating, the rectangle is replaced by one circle; for a first refinement, by one circle and two circular segments, and in the most accurate estimate, by one circle and four circular segments.

Table II indicates the results of these comparisons. The values in the final column should be close to the correct values. The errors then, in approximating a 5-to-1 rectangle by a single circular disk are at most 25%. This is an acceptable error since such large eccentricities would be the exception. When the detector is further out, the relative error is greatest for the peaked distribution, (cot θ). Most practical cases, however, will have more nearly isotropic distributions and less extreme eccentricity ratios.

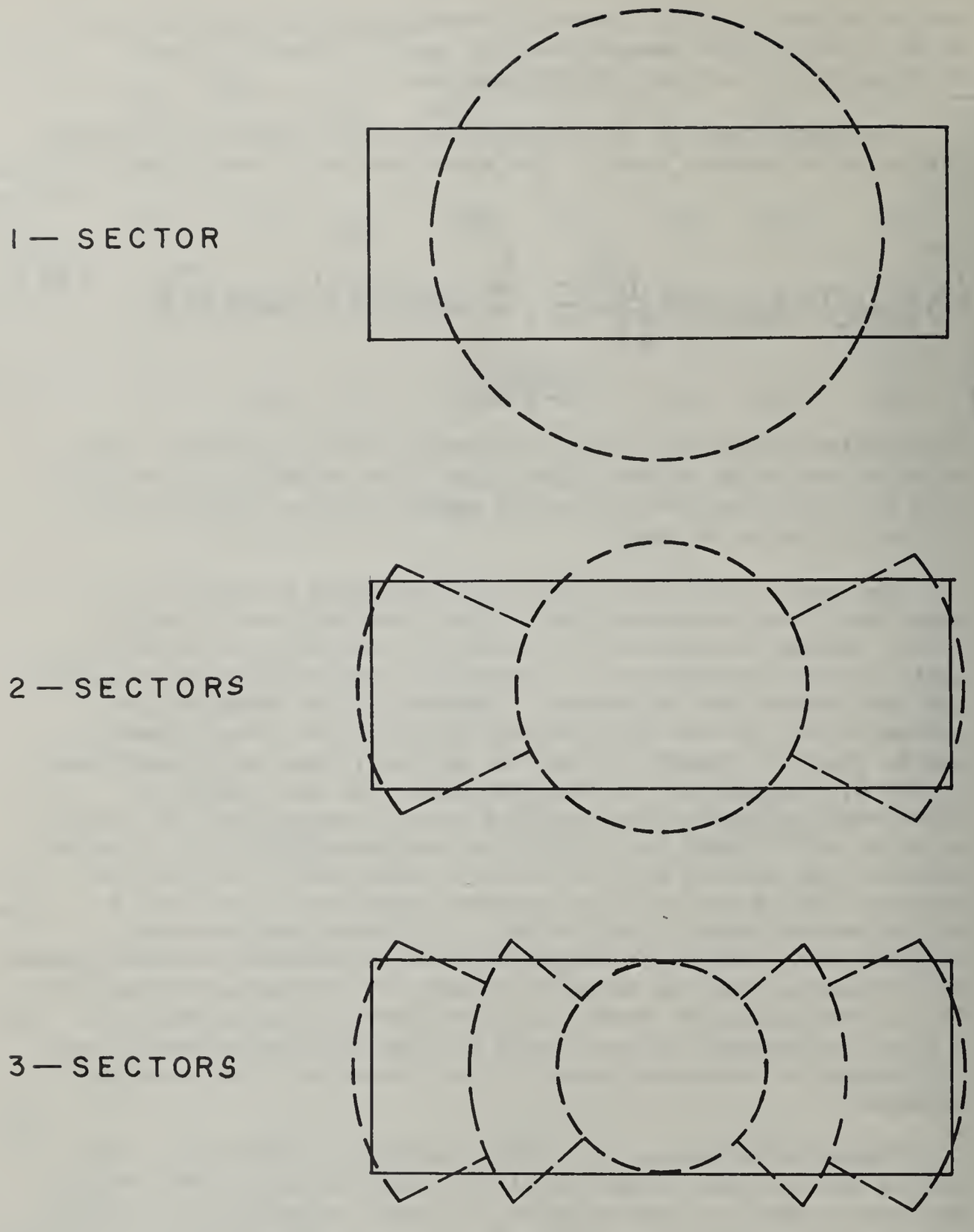

REPLACEMENT OF RECTANGLE BY CIRCULAR SECTIONS

Figure II-37

The angular distribution assumed for the roof case is that for the plane isotropic case, that is $\ell(d, \text{Cos } \Theta)$, shown on Figure 6. For small d, this source is peaked toward the horizon. For large d, the distribution of radiation is peaked from the source plane. The integration of this source for various depths is given by Spencer in the curves L(X) or L(d), Figures 18 and 19.

E. Ground Sources.

Next the radiation which comes to the detector from the ground will be discussed. This is a much more complex procedure than the roof case. There is a vertical wall perpendicular to the source plane and we must choose an axis either relative to the source plane or relative to the wall. Spencer has rotated his axis for this case 90° so that his polar axis is perpendicular to the wall. The Engineer Manual keeps the axis perpendicular to the source plane.

1. Thin Wall Case.

First, the thin wall case ($X \tilde{=} 0$) will be considered. This is shown in Figure 38. To isolate the part of the radiation that comes through the wall, we may think of a detector located between an infinitely thick ceiling and an infinitely thick floor. By infinite, we mean a thickness great enough so that any contribution through these areas is negligible. The detector plane is the horizontal plane which passes through the center of the detector. The upward normal is associated with the angle Θ which is labeled Θ_u or Θ upper. The downward normal is associated with the angle Θ_ℓ or Θ lower. Solid angle fractions associated with these angles are similarly labeled.

The detector will receive radiation from below the detector plane and from above the detector plane. Eisenhauer has developed what he calls "directional responses" which are the detector geometry responses. The contribution from below the detector plane will be primarily the direct radiation since the thin wall case will not involve any wall scattering. The direct radiation from the source plane will far exceed any air scatter from below the detector plane and therefore air-scattered radiation from below the detector plane is neglected. Consider now the contribution to the detector from above the detector plane. This must be all air-scattered radiation. Again there is no wall; therefore, the response of the detector will be due to air-scattered radiation.

The direct detector response, G_d, is the integration from 0 to cos Θ, of the infinite plane distribution, (Figure 6). Thus, G_d equals:

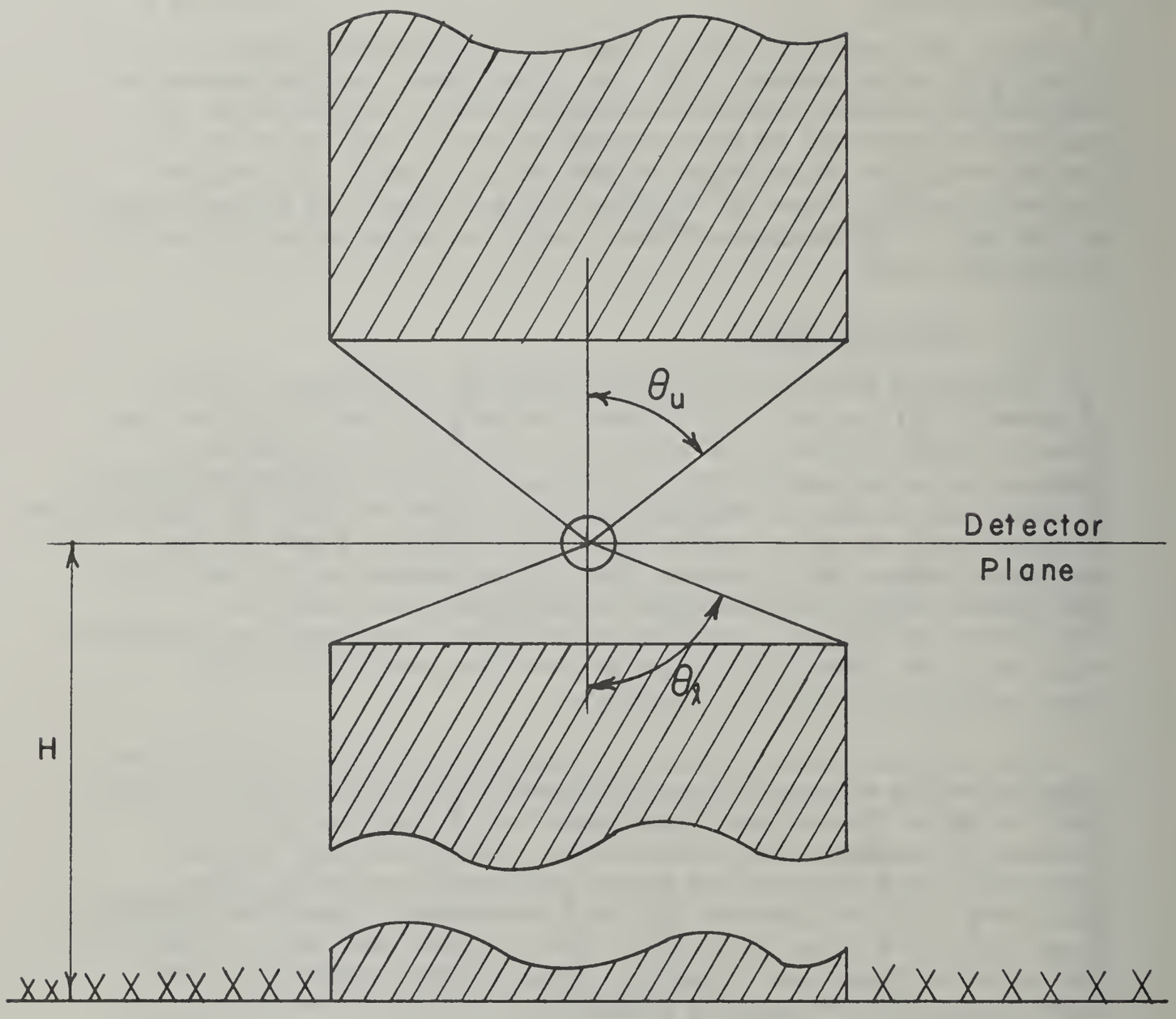

THIN-WALL CASE

Figure II-38

$$G_d(H,\omega_\ell) = \frac{\int_0^{\cos\theta_\ell} \ell(d,\cos\theta)\, d(\cos\theta)}{\int_{-1}^{1} \ell(d,\cos\theta)\, d(\cos\theta)} \quad . \qquad (63)$$

Note that G_d depends on detector height, H, and the lower solid angle fraction.

Consider now the air scattered radiation. This will consist of radiation which is reflected into the detector from the air. Also, it will have a component of radiation reflected from the ceiling. These two components are called "skyshine" and "ceiling-shine" respectively. The skyshine contribution can be noted by a symbol G_a and is as follows:

$$G_a(3',\omega_u) = \int_{-\cos\theta_0}^{1} d(\cos\theta)\, \ell(3',\cos\theta) \quad . \qquad (64)$$

This can also be shown to be related to Spencer's function as:

$$G_a(3',\omega_u) = S(d)\left[1 - S_a(3',\omega_u)\right] \quad . \qquad (65)$$

The skyshine and ceiling-shine function is:

$$G_a(\omega_u) = 0.1\left[1 - S_a(3',\omega)\right]\left[1 + 0.5\, S_a(3',\omega)\right] \quad . \qquad (66)$$

Term in 2nd brackets is the ceiling-shine factor. The Engineering Manual assumes that this function, G_a, is invariant with height.

Since the 1963 summer institute, some work has been done on the ceiling-shine problem. Although this is not usually an important source of contribution, it is an interesting problem and one of the "loose" ends which needs to be tied up. Under the section "Miscellaneous Topics" I have included an estimate which I made to provide a more logical solution to the ceiling-shine contribution. Kansas State University has both a theoretical and experimental program in progress and Technical Operations Report TO-B-63-25 by Jack Batter was on this problem.

2. Thick Wall Structures.

Now consider the opposite extreme of a very thick-walled structure. Here the direct radiation and the air-scattered radiation are assumed to be negligible compared with the radiation which scatters in the wall itself. Some assumption must be made about the angular distribution and the absolute magnitude of this radiation since neither has been calculated precisely. The Engineering Manual assumes that the angular distribution above the detector plane is the same as air-scattered radiation at a structure with zero wall thickness. This is equivalent to assuming that the thick wall produces the same effect as an equal mass of air. Excluding direct radiation and air-scattered radiation, all radiation reaching the detector through thick walls would have been scattered at least once, and would have approximately the same angular distribution which is observed from air-scattered radiation. The ultimate justification for this assumption is based on the fact that this distribution is peaked toward the horizon and this is the type of distribution which is needed. There is as yet no information available on the actual distribution. The response function to scattered radiation is divided into two parts: above and below the detector plane. The manual assumes that the angular distribution of radiation above and below the detector plane is the same. This assumes that any asymmetry which actually exists as the radiation strikes the wall is washed out by the multiple scatterings which takes place in the wall. With equal solid angles, then, both above and below the detector plane, we would expect the response to be the same. Integrating over the entire detector, we would expect to get a response function equal to one. However, the integration of the scattered radiation from the infinite plane source at 3 ft is equal to approximately 0.1. We wish to normalize our response function from either above or below the detector plane to 0.5; that is, they both contribute equally and must, therefore, both contribute 1/2 of the response function. Therefore, the following response function, G_s, has been used to obtain the curve for wall scattered radiation:

$$G_s(w) = 5 \int_{-1+w}^{0} \ell(3', \cos\theta)\, d(\cos\theta) \quad . \qquad (67)$$

We now have a geometry factor for scattered radiation. In order to compute "dose" then from scattered radiation, a barrier factor for vertical walls is also needed. The only barrier factor which we have is the Spencer Monograph function W(X), Figure 23, and this is for a wall which is infinite in extent and therefore, gets contributions from 1/2 an infinite plane source. What is needed is some factor which relates this geometry to actual four-wall geometry. Let us compare, then, the response from two infinitely high buildings with two walls and one with four walls.

The distribution of radiation emerging from these thick walls must be estimated. Radiation will tend to be collimated as it passes through thick walls and will emerge perpendicular to the wall. Eisenhauer assumed the following distribution of radiation:

$$p(\phi)\,d\phi = A\cos\phi\,d\phi. \qquad (68)$$

This distribution will now be used to derive a "shape-factor" to compensate the wall barrier factor when used in four wall geometry. The Engineering Manual identifies this shape-factor by the letter E. (A tribute to its author, Eisenhauer.)

The function W(X) is based on two semi-infinite parallel walls with a detector between the walls. The shape-factor for this case is defined as unity. Using the assumed distribution (cos ϕ), the integral which describes the shape-factor for this case is:

$$E = 4A\int_0^{\pi/2} \cos\phi\,d\phi. \qquad (69)$$

The 4 results from 4 symmetrical quadrants. The A is a normalizing constant to be determined.

Integrating:

$$E = 4A. \qquad (70)$$

But for the two-wall case,

$$E = 1. \qquad (71)$$

Therefore,

$$A = \frac{1}{4}.$$

Figure 39 illustrates the geometry for the four-walled shape factor. Since the geometry here varies for each wall considered, we must sum over the four walls, thus:

$$E = \sum_{i=1}^{8} \int_{2\pi} A \cos\phi \, d\phi, \qquad (72)$$

or

$$E = \sum_{i=1}^{8} A \sin\phi_i. \qquad (73)$$

The 8 results from 8 separate ϕ_i which must be considered. Summing over 360° we get:

$$E = 4A\left[\frac{W}{\sqrt{W^2+L^2}} + \frac{L}{\sqrt{W^2+L^2}}\right]. \qquad (74)$$

But $e = W/L$ (Eccentricity Ratio), and $A = \frac{1}{4}$, therefore:

$$E = \frac{e+1}{\sqrt{e^2+1}}. \qquad (75)$$

For long-narrow building where e=0, E = 1. For a square building where e = 1, $E = \sqrt{2}$. For a circular building, a simple integration shows that $E = \pi/2$.

Most buildings have neither thin walls nor extremely thick walls, but walls of intermediate thickness. We must therefore have a method of calculating the response of the detector to contributions from walls of intermediate thickness.

The Engineering Manual assumes that the intermediate case can be handled by averaging the extreme cases with a weighting factor, $S_w(X)$ which is a function of wall thickness. Our geometry factor then would be as follows:

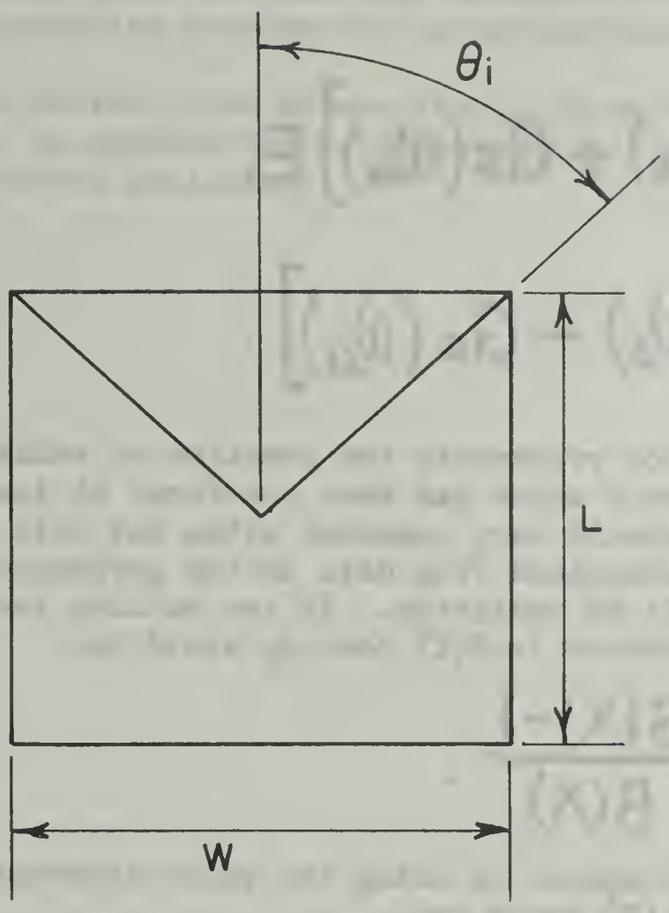

SHAPE FACTOR PARAMETERS
FOR FOUR—WALLED BUILDING

Figure II-39

$$G(X,\omega) = S_W(X)\, G_{THICK} + (1-S_W)\, G_{THIN}. \qquad (76)$$

where

$$G_{THICK} = \left[G_s(\omega_\ell) + G_s(\omega_u)\right] E, \qquad (77)$$

$$G_{THIN} = \left[G_d(\omega_\ell) + G_a(\omega_u)\right], \qquad (78)$$

The weighting factor represents the fraction of radiation reaching the detector which has been scattered at least once in the wall. It should vary somewhat with ω but this is also ignored. S_w is determined from data on the perpendicular incidence of Cobalt 60 radiation. If the buildup factor for perpendicular incidence is B(X) then S_w would be:

$$S_W(X) = \frac{B(X)-1}{B(X)}. \qquad (79)$$

This can also be computed by using the point isotropic source case Figure 33; $S_w(X)$ would be:

$$S_W(X) = \frac{P^{(S)}(X)}{P^{(S)}(X) + P^{(0)}(X)}. \qquad (80)$$

The direct geometry factor G_d should also be multiplied by a shape factor but no attempt has been made to derive an expression for it. This factor would be unity for a circular structure and approximately unity for a square structure. The factor would decrease as does the eccentricity factor for scattered radiation for more elongated buildings whose floors subtend the same solid angle. It was not calculated because it was thought that it would only be important in areas with low protection factors since the direct geometry factor is important only for thin walls. There are some situations where this is not true however. For example, in buildings with very thick walls, small

apertures may be the dominant contribution in an otherwise well-protected location. The shape-factor for direct radiation should probably be included in those cases. This again is one of those areas that would be nice to have a factor for. The fact that it probably is not important for practical buildings is the reason that no effort has been expanded on it. It would be an interesting problem for an enterprising student.

In the next section, the schematization developed by Eisenhauer will be applied to the development of an engineering method for shielding analysis.

VI - ENGINEERING MANUAL METHOD (DETAILED PROCEDURE)

A. Introduction.

The charts and data in the Spencer Monograph can not be readily adapted for practical application. This is the reason that Eisenhouer and FitzSimons converted this information into a more useable form. The result of this transformation has been identified as the Engineering Manual (OCD PM-100-1)*. Since October 1961, the Engineering Manual, in draft form, has been the basis of postgraduate-type courses for architects and engineers in fallout shelter analysis. As of this writing, the final draft version of the Engineering Manual is being reviewed prior to official issuance by the Office of Civil Defense. The explanation which follows is an abbreviated version of PM-100-1 taken from lecture notes used to teach the Engineering Manual method. For a more detailed discussion of this method and for more example problems, the reader is advised to obtain a copy of OCD PM-100-1 when it is available.

B. Engineering Manual Charts.

In the last section, we have described how the Spencer data was converted into engineering-type charts. Before discussing the methodology which is based on these charts, it would be well to summarize what these charts are and how they are related to the Spencer data and notation. Figure 40 has been provided to briefly correlate this information. In the first column is listed the Engineering Manual chart number and the corresponding Engineering Manual notation. The second column lists the source of this chart in the Spencer Monograph and the Spencer notation. The third column is a sketch depicting the physical representation of each chart, if such a representation is possible. The Engineering Manual charts are located immediately following this discussion.

Chart 1. Four barrier factors are plotted on Chart 1, as follows:

- $B_i(X_i)$ - Barrier factor for interior partitions for ground contribution.
- $B_i'(X_i')$ - Barrier factor for interior partitions from roof contribution.
- $B_f(X_f)$ - Barrier factor for ground contribution through the floor below.
- $B_o'(X_o')$ - Barrier factor for ground contribution through ceiling above.

This chart includes a representative sketch of where each of these barrier factors is applied.

---

*Design and Review of Structures for Protection From Fallout Gamma Radiation, OCD PM-100-1, Dec 1963.

Figure 40. BASIS OF ENGINEER MANUAL CHARTS

Engineer Manual	NBS - 42	Physical Interpretation
CHART 1.		
$B_i(X_i)$	2W(X_i3') less backscatter	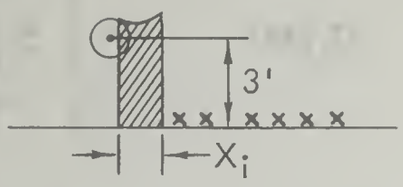
$B_i'(X_i)$	Derived Function	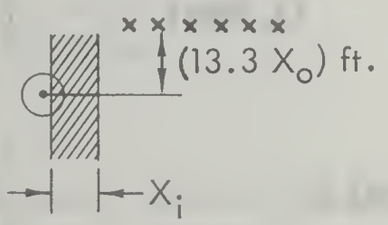
Bf (X_f)	L(X)	
Bo'(X_o')	S'(X)	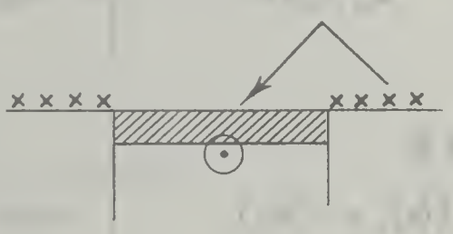
Chart 2.		
$B_e(X_e, H)$	2W (X, d) less backscatter for H ≥ 3'	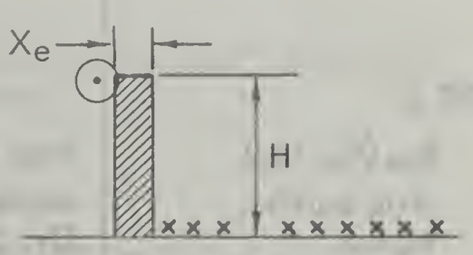
Chart 3.		
ω, (e, n)	ω	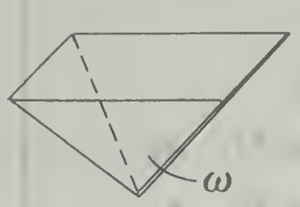
Chart 4.		
$C_o(X, \omega)$	L(X) $L_c(X, \omega)$	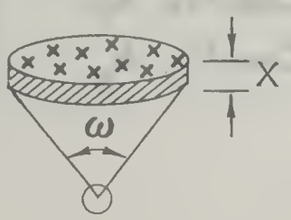

Chart 5.		
$G_s(\omega)$	$G_s = 5 \int_{-(1-\omega)}^{0} \ell\,(3', \cos\theta)\,d(\cos\theta)$	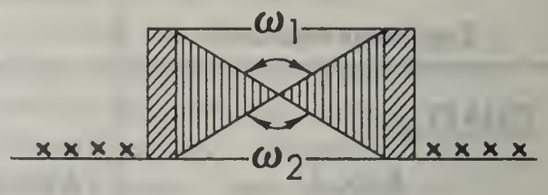
$G_a(\omega_1)$	$G_a = 0.1(1-S_a)\,(1 + 0.5S_a)$	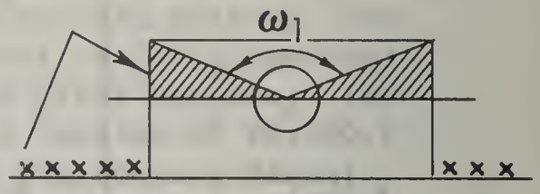
Chart 6.		
$G_d(H, \omega)$	$G_d = \dfrac{\int_0^{\cos\theta} \ell(d, \cos\theta)\,d(\cos\theta)}{\int_0^{1} \ell(d, \cos\theta)\,d(\cos\theta)}$	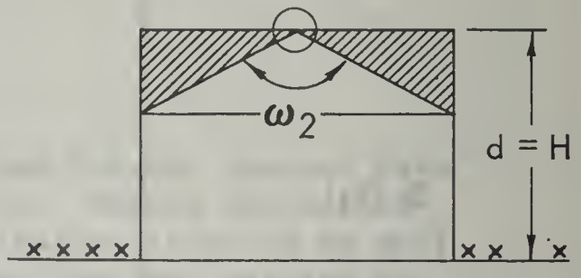
Chart 7.		
$S_w(X_e)$	$S_w = p^{(s)}(X)/p(X)$	
Chart 8.		
E(e), e = W/L	Not from Monograph	$E = (1 + e)/(1 + e^2)^{1/2}$
Chart 9.		
$B_{ws}(X_e, \omega_s)$ strip barrier factor	Not from Monograph, separate calculation by Dr. Spencer	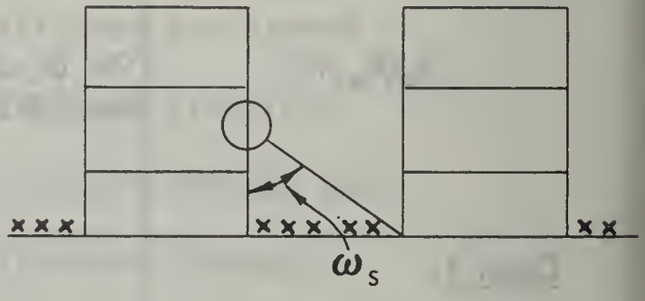
Chart 10.		
Case #1. A_h	$L(X)\,L_c(X, \omega)$ for X=0	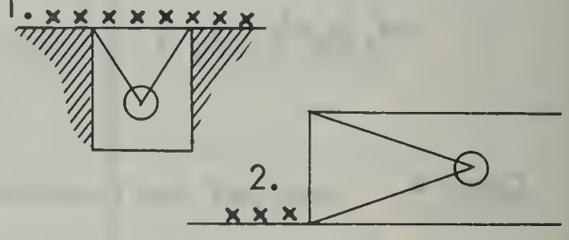
Case #2. A_v	$1/2\ W_a(3', \omega)$	
Case #3. A_a	$S_a\,(d, \omega)$ for d=0	

Chart 2.

$B_e(X_e,H)$ - Barrier factor for exterior wall for ground contribution. This barrier factor includes all the height effect and for H=3' is the same as $B_i(X_i)$.

Chart 3.

ω (e,n) - Solid angle fraction contours.

Chart 4.

$C_o(X_o,\omega)$- Reduction factor for roof contribution. This is a combined barrier and geometry factor function.

Chart 5.

$G_s(\omega),G_a(\omega)$ - Directional response functions for wall scattered and air-scattered responses for ground contribution.

Chart 6.

$G_d(\omega,H)$ - Directional response function for direct radiation.

Chart 7.

$S_w(X_w)$ - Fraction of Emergent Radiation Scattered in Wall Barrier.

Chart 8.

E(e) - Shape factor for wall scattered radiation.

Chart 9.

$B_{ws}(X_e, \omega s)$- Barrier reduction factor for wall scattered radiation for limited planes of contamination.

Chart 10.

Reduction factors for passageways and shafts for vertical and horizontal orientations.

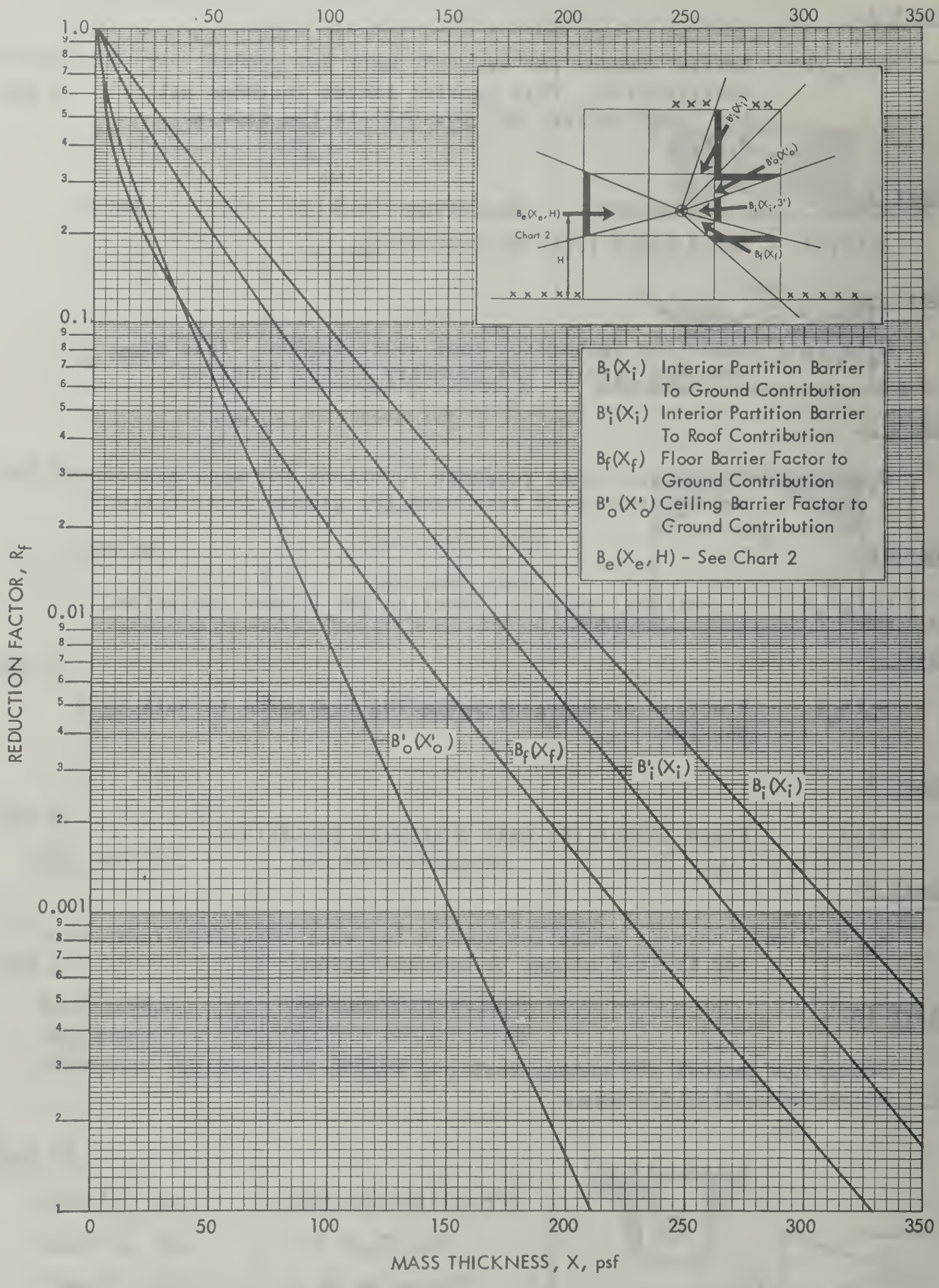

Chart 1. BARRIER SHIELDING EFFECTS, PLANE ISOTROPIC SOURCES, B_0, B'_0, B_i

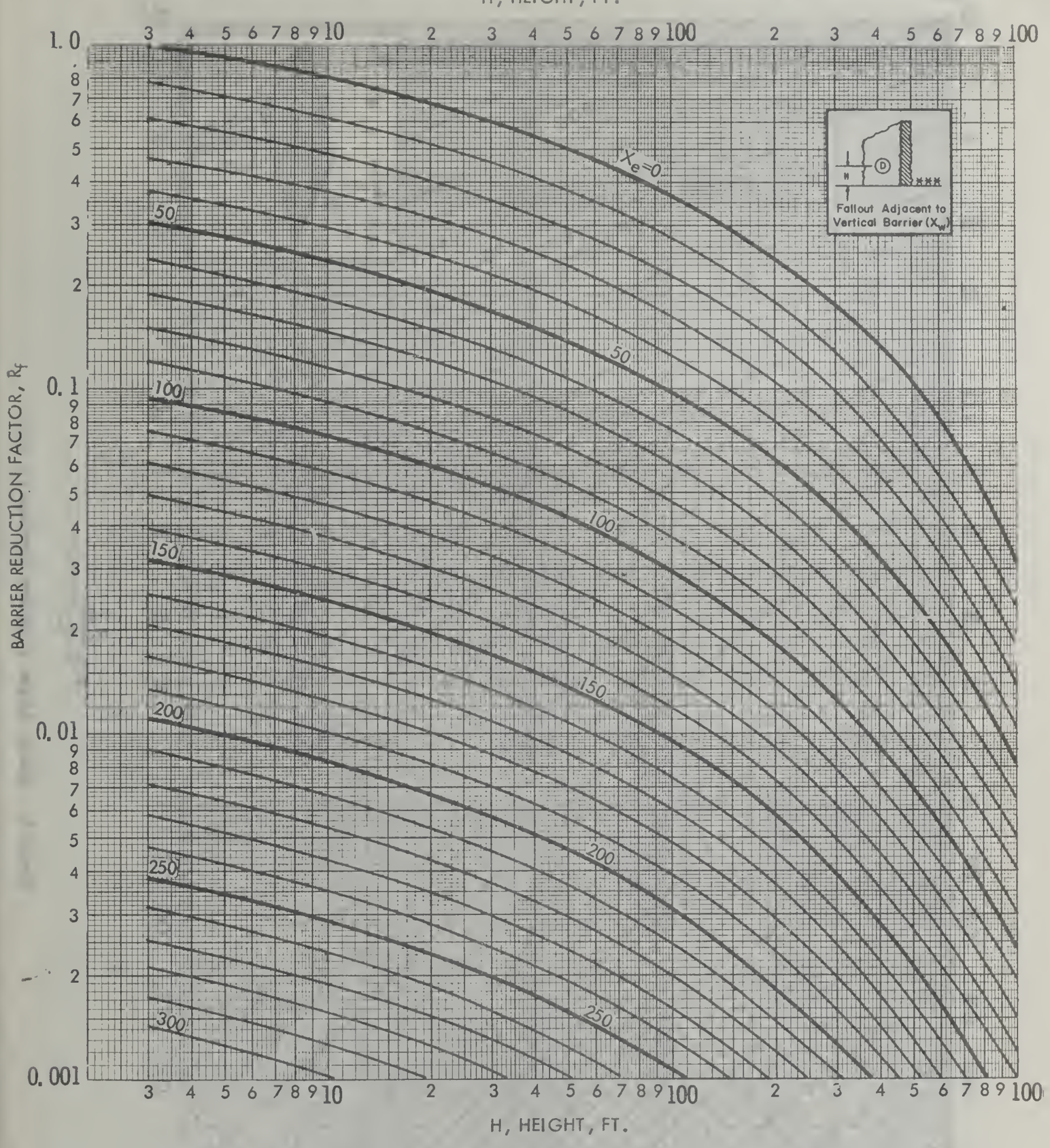

Chart 2. WALL BARRIER SHIELDING EFFECTS $B_e(X_e)$ FOR VARIOUS HEIGHTS

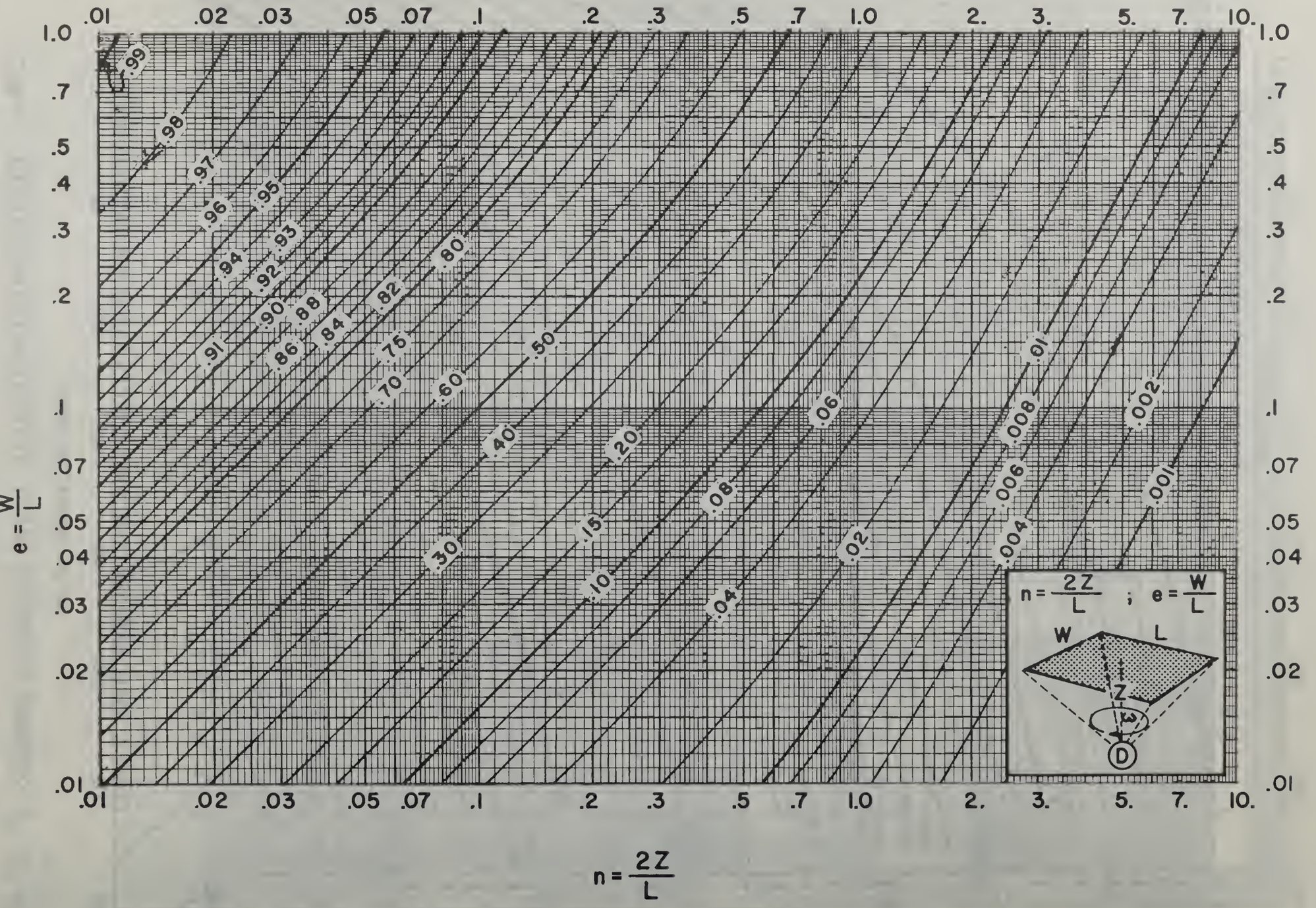

Chart 3 . Solid Angle Fraction Contours, ω.

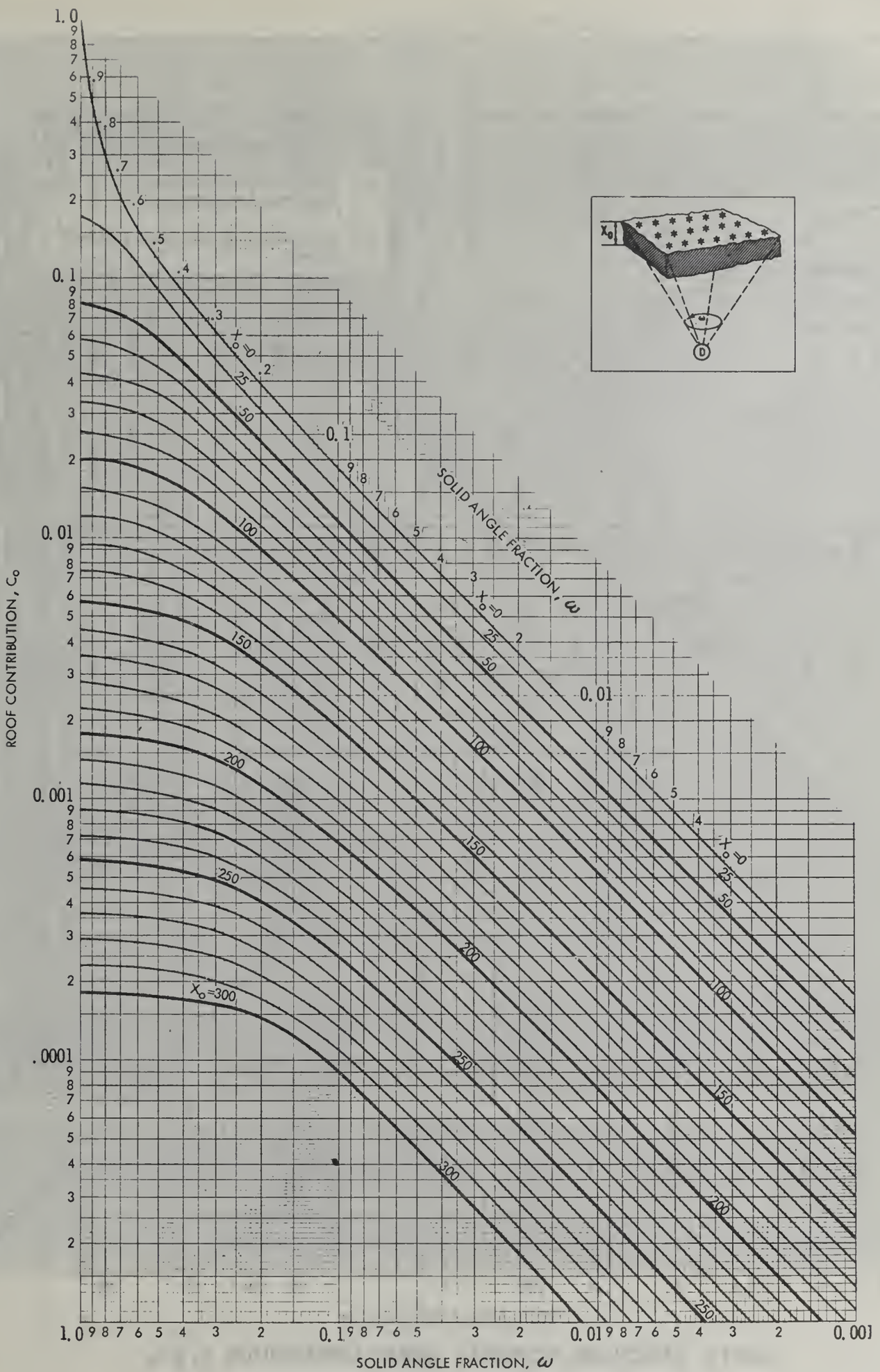

Chart 4. REDUCTION FACTOR FOR ROOF CONTRIBUTION, C_o

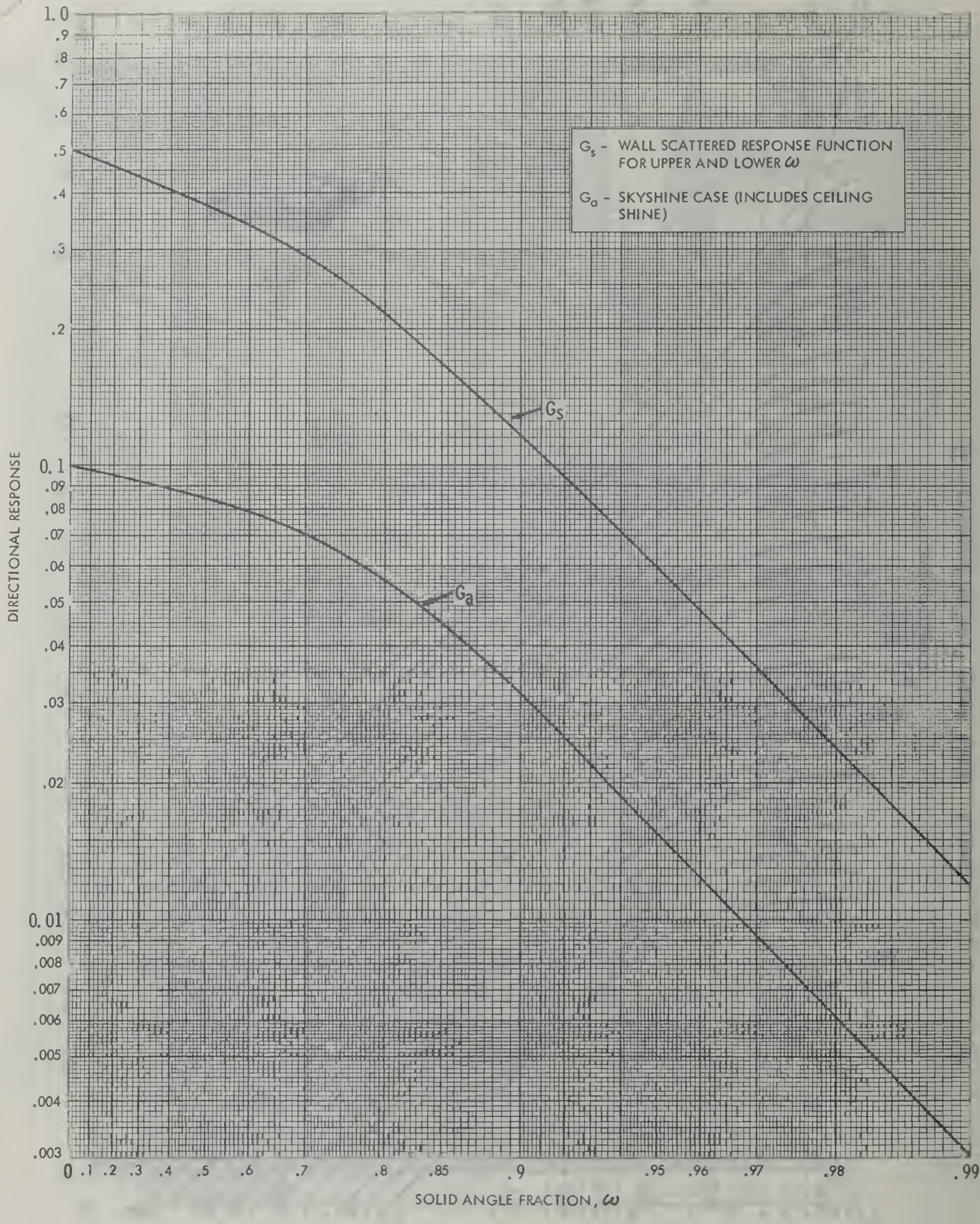

Chart 5. DIRECTIONAL RESPONSES, GROUND CONTRIBUTION, G_S & G_a

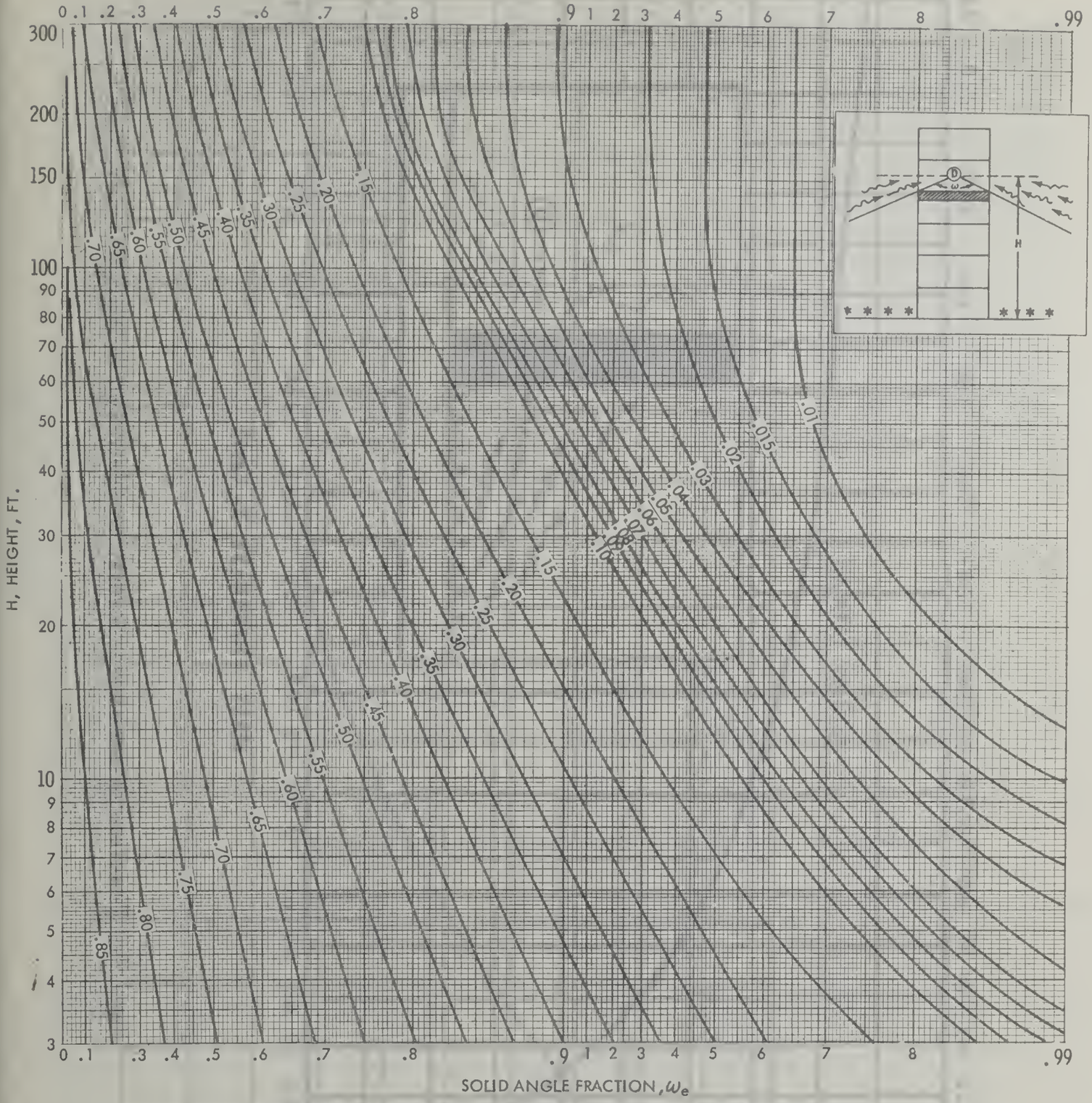

Chart 6. DIRECTIONAL RESPONSE FOR DIRECT RADIATION, G_d, FOR VARIOUS HEIGHTS

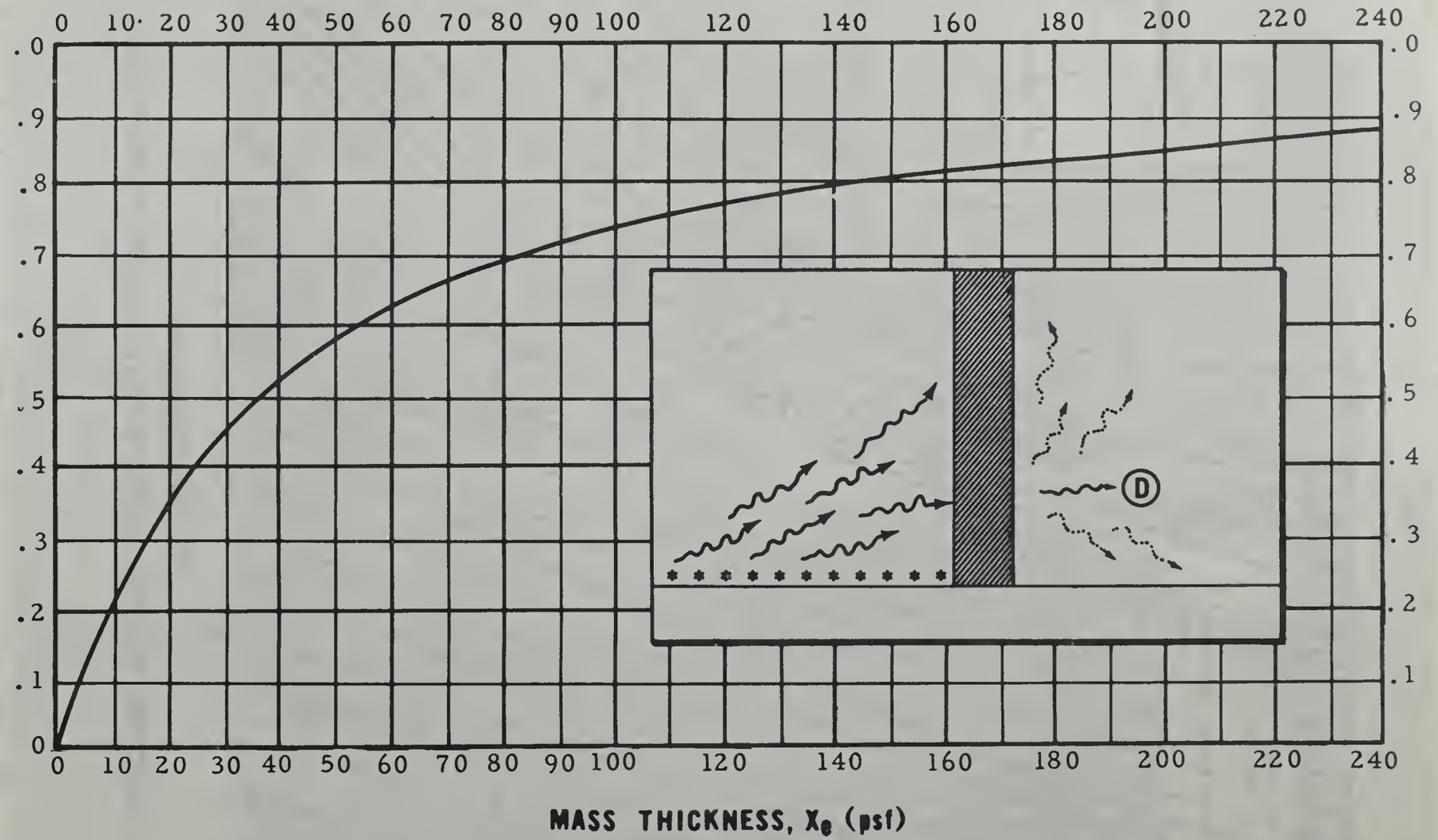

Chart 7. Fraction of Emergent Radiation Scattered in Wall Barrier, S_w

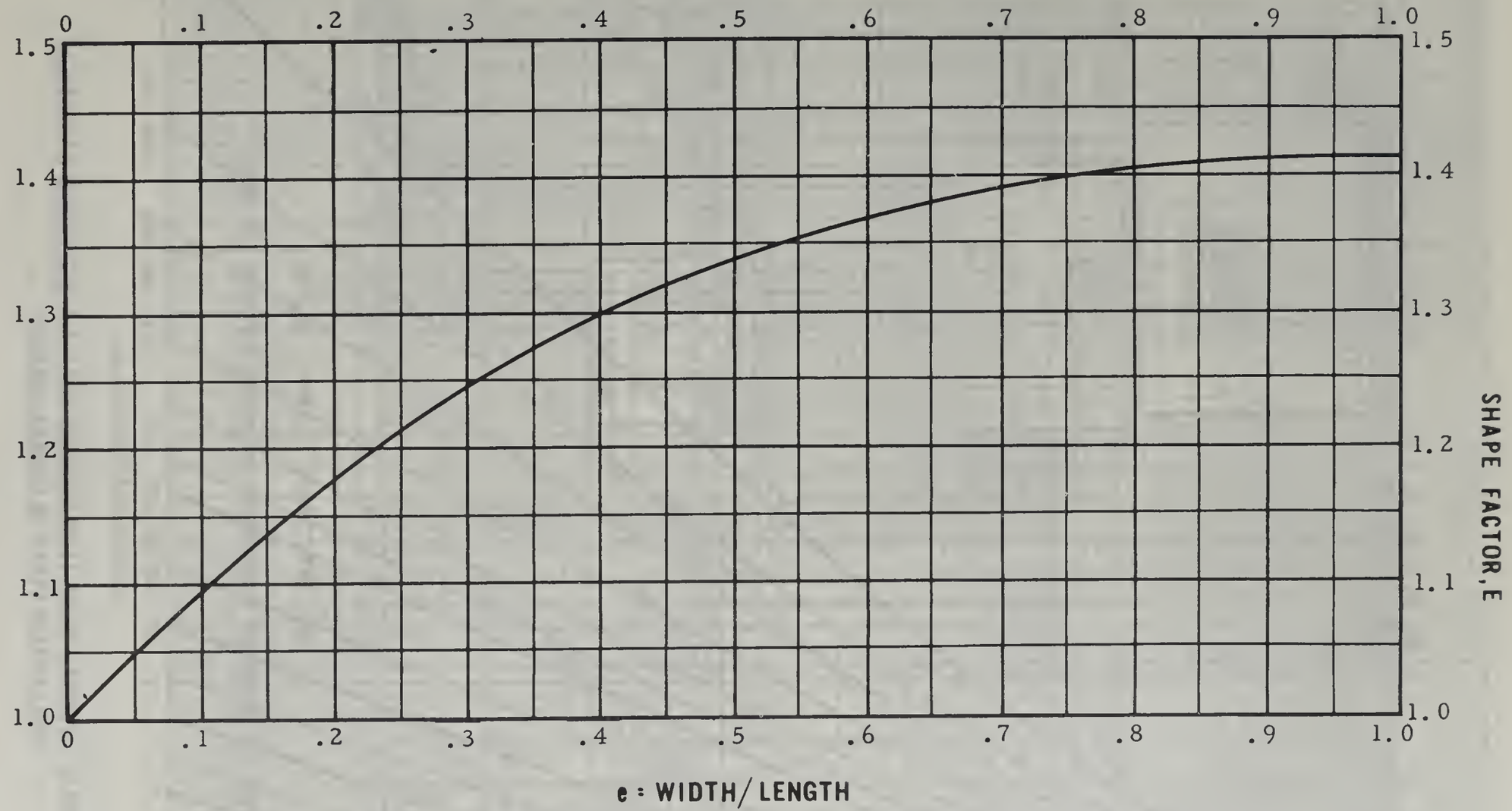

Chart 8. Shape Factor for Wall-scattered Radiation, E

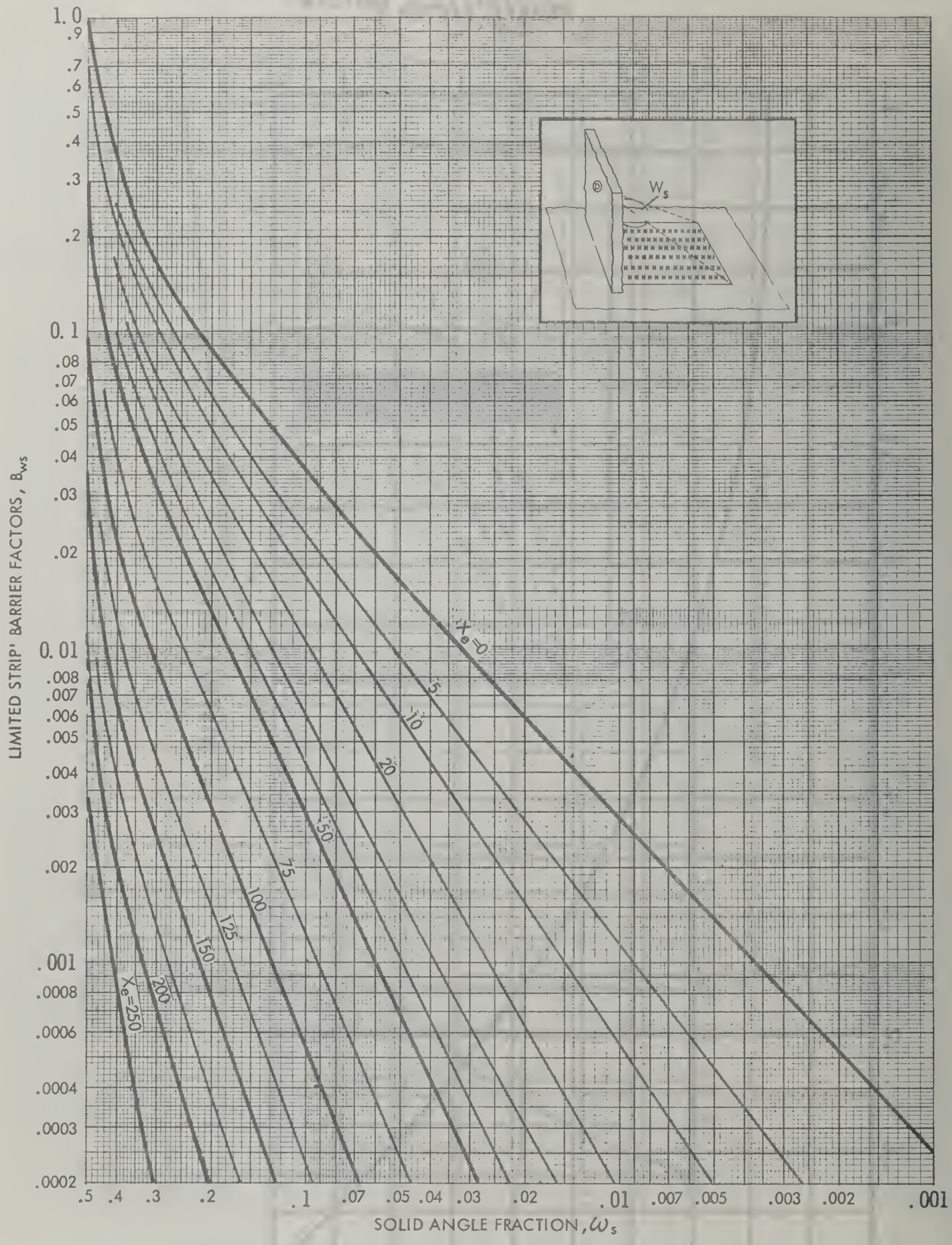

Chart 9. BARRIER REDUCTION FACTORS FOR WALL-SCATTERED RADIATION FOR LIMITED STRIP OF CONTAMINATION

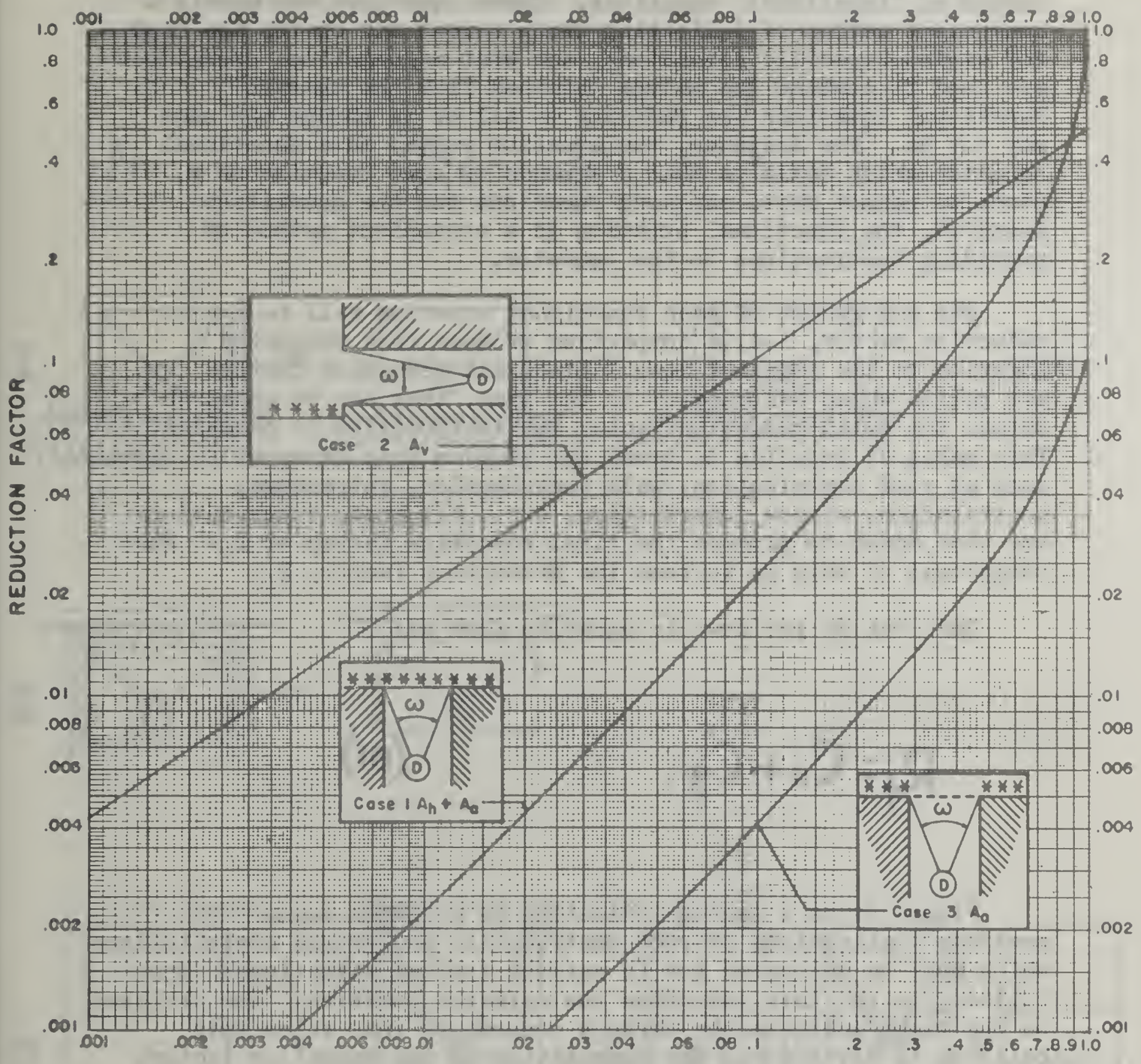

Chart 10. Reduction factors for passageways and shafts, A_v, $A_h + A_a$ & A_c

C. Engineering Manual Functional Equations.

1. Introduction. The Engineering Manual method is based on a series of "functional" equations. These equations are merely a convenient method of indicating which curves and charts are used for various specific situations, and what mathematical operations are used to combine the values obtained from the charts. Functional equations are familiar to all of us though the name may not be. For instance, the equation $y=f(x)$ is a functional equation which tells us that y depends on some function of x. Since we cannot write explicit functions for the quantities involved, the functional notation is a convenient method of providing instructions to the operator.

The end result of each functional equation will be a reduction factor, i.e.,a comparison of dose in a protected location to the standard dose. Since all reduction factors are ratios whose denominator is the same, they can be added to obtain the total reduction factor for the position in question. This makes it possible to break our problem into manageable components, such as roof contribution, wall contribution, entranceway contribution, window contribution, etc. All these contributions are then added to produce the final reduction factor or R_f. The reciprocal of this R_f is then the protection factor, P_f.

This can be put down in equation form as:

$$R_f = C_o + C_g . \qquad (81)$$

Figure 41 is a sketch indicating in a simple manner the possible combinations of roof contribution and ground contributions which must be accounted for in various typical situations. The building on the left indicates the detector position. The sketches on the right indicate the various components into which this building is divided for the computation of the reduction factor. The third case, III, illustrates a building of the most general type. The roof contribution has several floors between detector and roof. The ground contribution has three components; (1) the floor of the detector, (2) the floor above the detector floor, and (3) the floor below the detector floor. With this figure in mind, we will develop functional equations for each of the various components needed for a full solution.

2. Solid Angle Fraction. Since solid angle fraction is used in every computation as a measure of the geometry effect, an example problem of computing ω will be demonstrated. See example VI - 1.

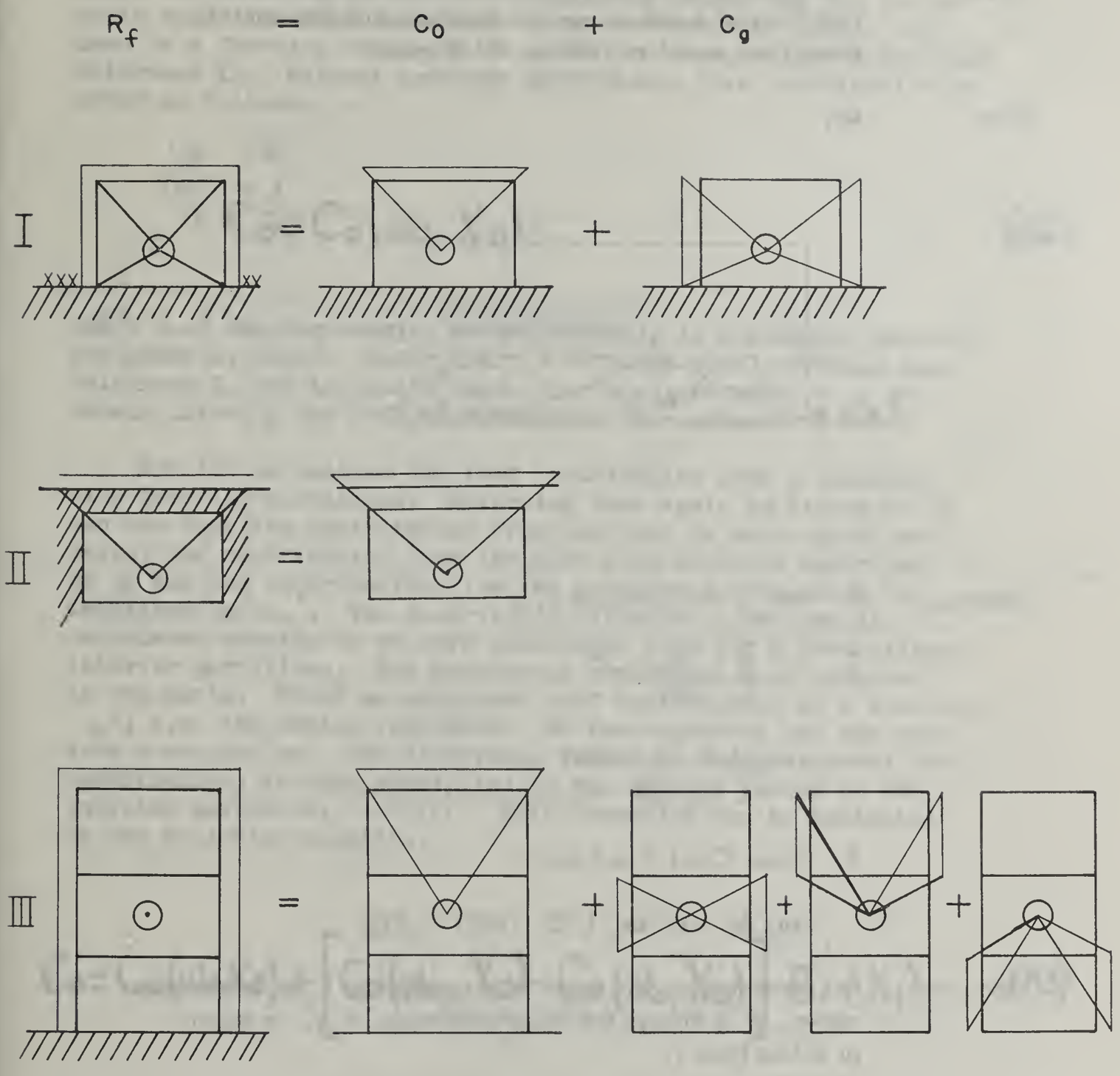

SYMBOLIZED FUNCTIONAL EQUATIONS

Figure II-41

Example VI-1 - SOLID ANGLE FRACTION

Given: The detector is centrally located three feet above the first floor of a slab-on-grade structure with horizontal dimensions equal to 180' by 45' (Figure).

Find: ω_1

W = 45'
L = 180'
Z = 3'

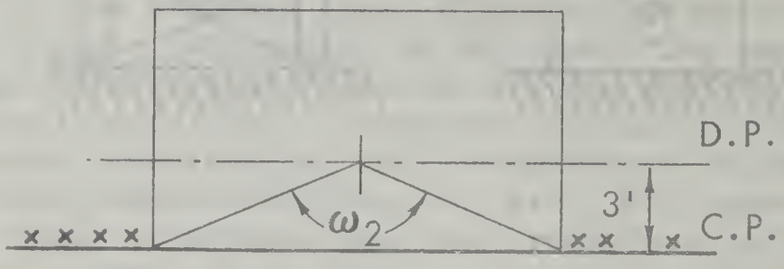

Solution:

1. ω_2 is a function of e, n

2. $e = \frac{W}{L} = \frac{45}{180} = .25$

$n = \frac{2A}{L} = \frac{6}{180} = .033$

3. Enter Chart 3 and read

$\omega_2 (e, n) = \omega_2 (.25, .033) = \underline{.915}$

Discussion: For computation of e when W is unequal to L, as in the case above, W is always the lesser dimension, e.g., e equals or is less than 1.

3. Roof Contribution. Now let us consider the contribution from the roof of a building. Figure 42 illustrates the various parameters which may be involved. Let us consider first a simple building which has no interior partitions. Here the solid angle fraction which describes the geometry of the roof is labeled, ω_o. The thickness of the roof above the detector is X_o. X_o consists of the summation of all the roof mass thickness immediately above the detector up to the contaminated roof. The ω_o is the solid angle fraction subtended by the contaminated plane. C_o then is a function of the solid angle fraction, ω_o, and the roof thickness X_o. Without interior partitions, this contribution is noted as follows:

$$C_o = C_o(\omega_o, X_o). \tag{82}$$

Chart 4 of the Engineering Manual actually is a combined barrier and geometry chart. Enter Chart 4 with the total overhead mass thickness X_o and the solid angle fraction subtended, ω_o, and obtain directly the roof contribution. See example VI - 2.

Now let us analyze the roof contribution from a building with interior partitions. Referring back again to Figure 42 we can see that the contribution from the roof is made up of two parts; the contribution from the core area which is described by ω_o and the contribution from the peripheral area which is described by ω_o'. The contribution from the core area is calculated exactly as we have previously done for a roof without interior partitions. The peripheral contribution is computed in two parts. First we calculate roof contribution as a function ω_o'; i.e. the entire roof area. We then subtract out the core area contribution. The difference (which is the peripheral roof contribution) is then multiplied by the barrier factor of the interior partition, $B_i'(X_i)$. This operation can be indicated by the following equation:

$$C_o = C_o(\omega_o, X_o) + \left[C_o(\omega_o', X_o) - C_o(\omega_o, X_o)\right] B_i'(X_1). \tag{83}$$

The first term is the core contribution. The second term is the peripheral roof contribution. Similar techniques of differencing contributions can be used for more complicated problems. Example VI - 5 is a core type problem which employs equation 83 for the roof contribution.

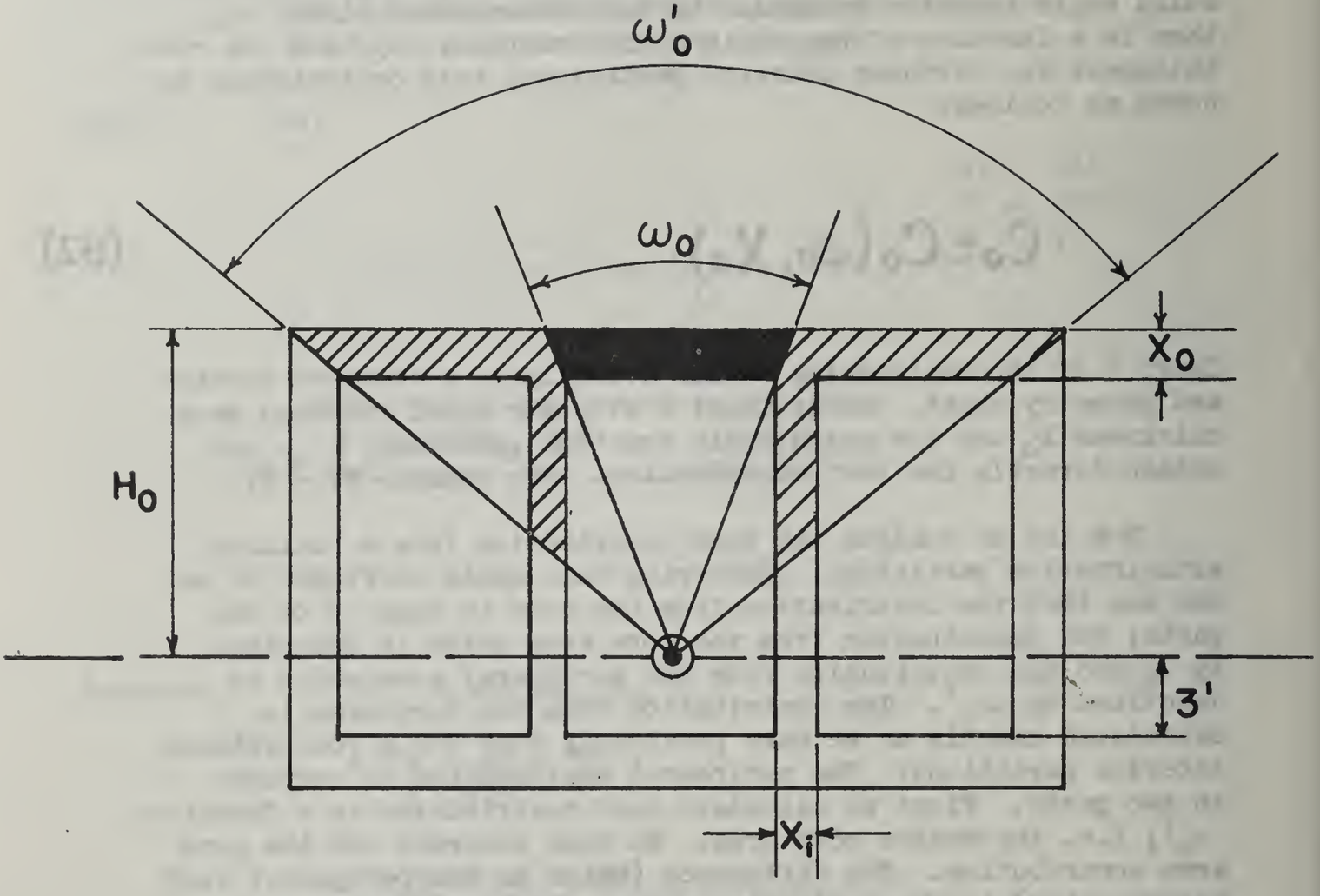

ROOF CONTRIBUTION

Figure II-42

Example VI-2 - ROOF CONTRIBUTION

Given: A detector is located centrally 3' above the floor of a slab-on-grade structure with horizontal dimensions of:

W = 42' L = 175'; and height = 10'

Both roof and ground are contaminated.

Overhead mass thickness (X_o) = 100 psf.

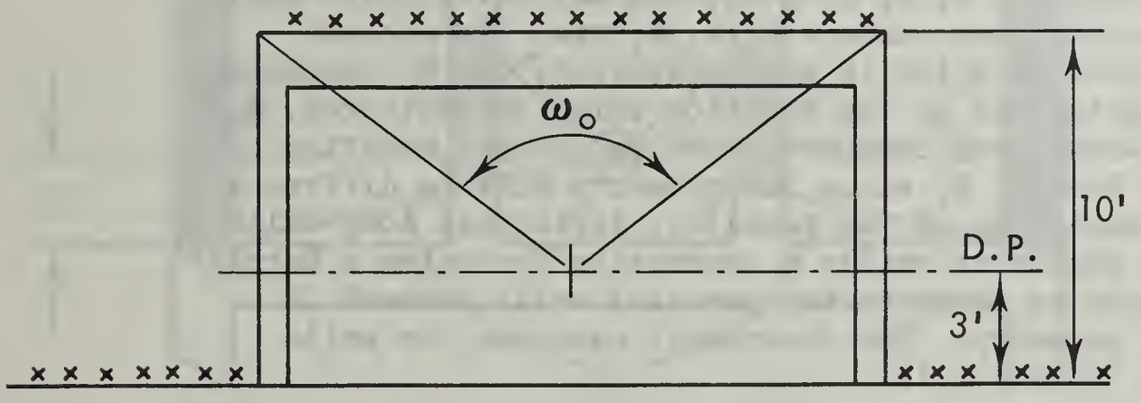

Find: Roof contribution

Solution:

1. Compute ω_o (e, n)

   a. $e = \frac{W}{L} = \frac{42}{175} = .24$; $n = \frac{2Z}{L} = \frac{2\,[10-3]}{175} = .08$

   b. $\omega_o(e, n) = \omega_o(.24, .08) = .80$ Chart 3

2. $C_o\ (X_o, \omega_o) = C_o\ (100, .80) = .02$ Answer Chart 4

4. Ground Contribution.

a. Ground Contribution Through Adjacent Walls. Let us now analyze the ground contribution through the walls of the detector floor. Figure 43 illustrates the geometry involved with a building with interior partitions. The exterior walls are noted by X_e; interior walls by X_i. The upper solid angle fraction is ω_1 and the lower solid angle fraction is ω_2. The height of the detector from the contaminated plane is the distance H.

The ground contribution through any particular floor is a summation of radiation which goes from the contaminated plane directly to the detector, plus radiation scattered in air, and radiation scattered in the walls.

The wall-scattered radiation geometry factor is a sum of G_s for the upper and lower solid angle fractions. For convenience, all upper solid angle fractions will be labeled with odd numbers, 1, 3, 5, etc., and all lower solid angle fractions with even numbers 2, 4, 6, etc. To account for that portion which is wall-scattered, the G_s responses must be multiplied by the fraction which is scattered, S_w. This wall-scattered component must be further modified by the Shape Factor, E, since the geometry will be different from the basic one of two parallel, infinitely long walls. The Shape Factor is really a correction for using a barrier factor which is based on two parallel walls instead of four-wall geometry. The functional equation for wall-scattered radiation is:

$$\left[G_s(\omega_1) + G_s(\omega_2)\right] S_w(X_e) E(e). \qquad (84)$$

For convenience when we combine functional equations, the term in brackets will be shortened to:

$$\sum_1^2 G_s = \left[G_s(\omega_1) + G_s(\omega_2)\right]. \qquad (85)$$

G_s is obtained from Chart 5.

Figure 43. GROUND CONTRIBUTION (DETECTOR FLOOR) - NO WINDOWS

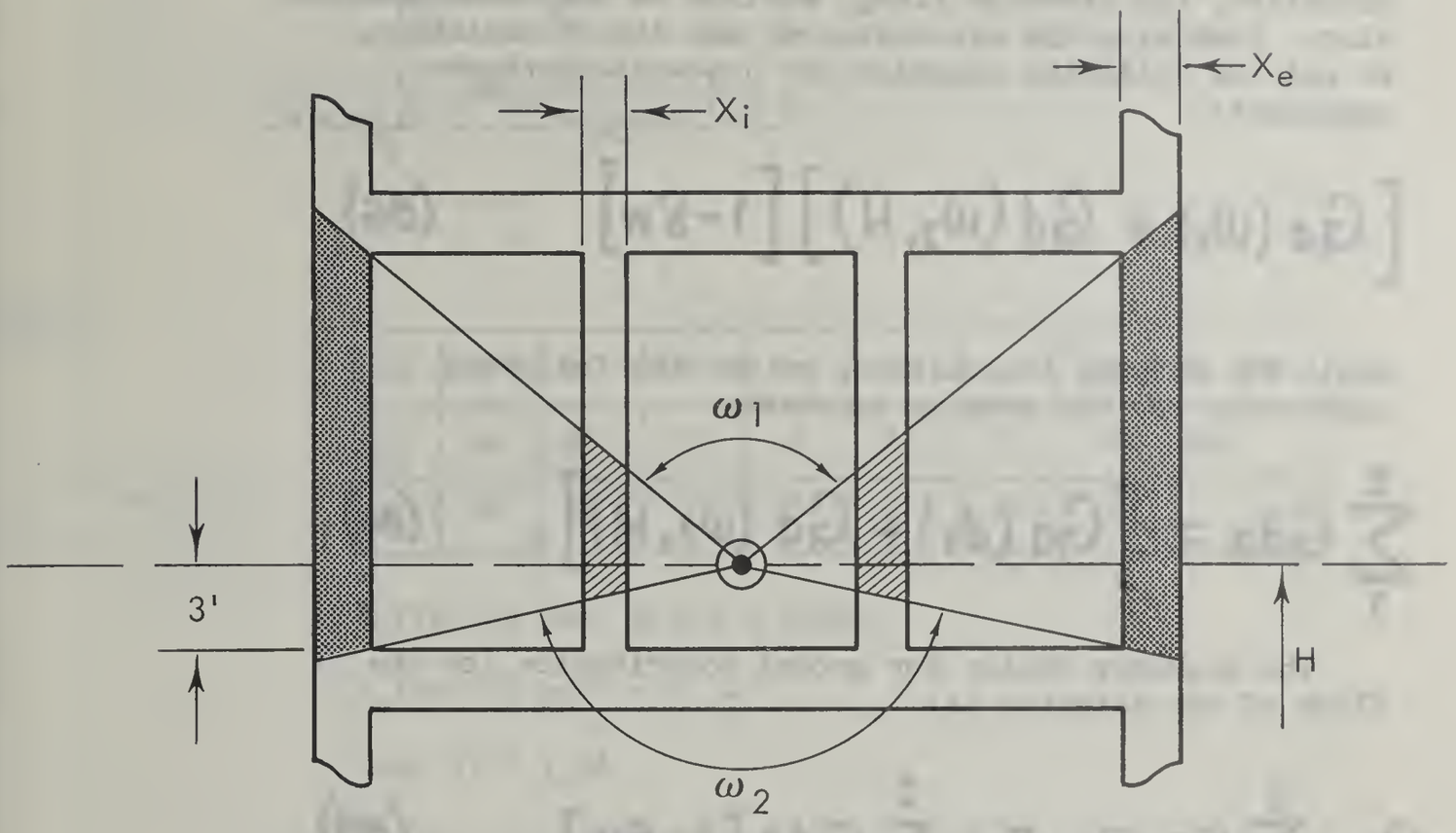

GROUND CONTRIBUTION (DETECTOR FLOOR)
-NO WINDOWS

The air-scattered radiation is a function of the upper solid fraction only. Enter Chart 5 with ω_1 and obtain the value of G_a. This must be multiplied by the fraction which is not wall-scattered, or $(1-S_w)$.

Finally, the direct radiation is a function of the lower solid angle fraction only. Chart 6 is used to obtain the value of G_d. Since this is also non-wall-scattered radiation, the fraction $(1-S_w)$ applies to this contribution also. Combining the air-scattered and direct radiation, we get the following equation for non-wall-scattered component:

$$\left[G_a(\omega_1) + G_d(\omega_2, H)\right]\left[1-S_w\right]. \qquad (86)$$

Again for economy in notation, we use the following expression for the term in brackets:

$$\sum_1^2 G_{da} = \left[G_a(\omega_1) + G_d(\omega_2, H)\right]. \qquad (87)$$

The geometry factor for ground contribution for the floor of the detector is:

$$G_g = \sum_1^2 G_s \cdot S_w \cdot E + \sum_1^2 G_{da}\left[1-S_w\right]. \qquad (88)$$

To obtain the total ground contribution, which is a reduction factor, we must multiply by the proper barrier factors. These are the barrier factor for the exterior walls, and the barrier factor for the interior walls. The barrier factor for the exterior wall includes the effect of detector height. These barrier factors are obtained from Chart 2 and Chart 1, respectively. The final expression for ground contribution for the floor of the detector is:

$$C_g = B_w(X_e, H)\, B_w(X_i)\, G_g. \qquad (89)$$

Example VI-3 illustrates the use of equation (89).

Example VI-3 - ONE STORY BUILDING ABOVE GRADE

Find Pf at center of building

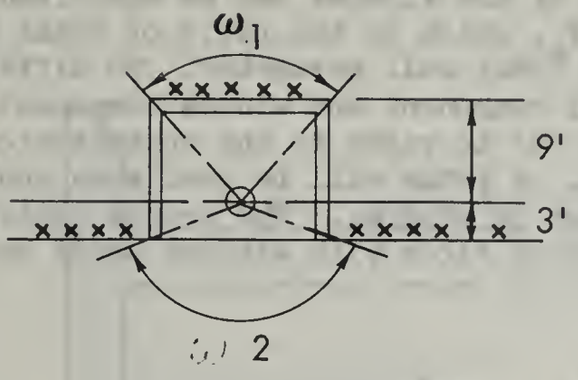

ω	W	L	z	e	n	ω	Gs	Ga	Gd
ω_1	40	80	9'	.5	.225	.70	.28	.069	
ω_2	40	80	3'	.5	.075	.895	.12	-	.42

B_e(Xe=100 psf, H=6') = 0.082

S_w(Xe=100 psf) = 0.74

E(e=.5) = 1.34

ROOF CONTRIBUTION

Co = Co(ωu, Xo) = Co(.70, 60) = <u>0.055</u>

GROUND CONTRIBUTION

$$Cg = \{[Gd(\omega_2, Hd) + Ga(\omega_1)]\ [1 - Sw(Xe)] + [Gs(\omega_2) + Gs(\omega_1)]\ [Sw(Xe)E(e)]\}\ Be(Xe, H)$$

$$Cg = \{[.42 + .069]\ [1 - .74] + [.12 + .28]\ (.74)(1.34)\}\ (0.082)$$

Cg = <u>0.043</u>

Rf = Co + Cg = 0.055 + 0.043 = <u>0.098</u>

$$Pf = \frac{1}{Rf} = \frac{1}{0.098} = \underline{\underline{10.2}}$$

b. Detector Floor-With Windows. Consider the same case as above but now with windows in the exterior walls. Assume that the lower window sill is at the height of the detector. The extent of the windows in the vertical direction can be described by a solid angle fraction, ω_a. The horizontal extent of the windows can be described by a perimeter ratio, P_a, which is the ratio of total window widths divided by total wall perimeter. To differentiate between solid wall component and window component, we will use the subscript 'a' to refer to the contribution through the aperture area. A prime will be used when contribution includes the effect of windows. The ground contribution then for the detector floor with windows would be:

$$C_g' = C_g - C_a + C_a' \quad (90)$$

In words, this equation means: the ground contribution through the floor of the detector with windows (C_g') equals the contribution as if the wall was all solid (C_g) (equation 89) minus the contribution through the window area assuming solid wall conditions (C_a) plus the contribution through window area with Xe=0 (C_a').

The equation for C_a and C_a' are:

$$C_a = B_w(X_e, H)\, B_w(X_i) \left[G_s(w_a)\, S_w \cdot E + G_a(w_a)(1-S_w) \right] P_a \quad (91)$$

$$C_a' = B_w(0, H)\, B_w(X_i)\, G_a(w_a)\, P_a \quad (92)$$

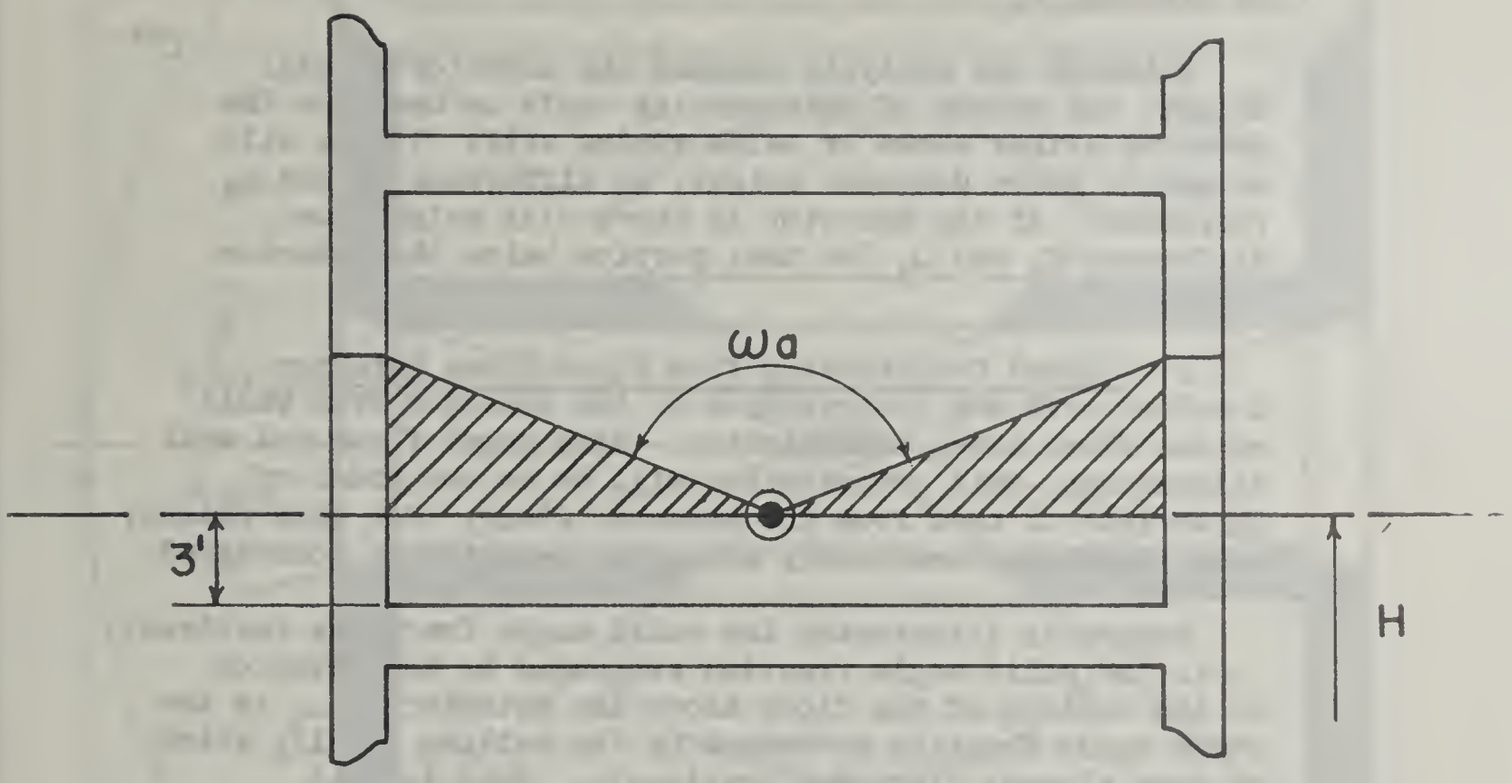

GROUND CONTRIBUTION (DETECTOR FLOOR)
-WINDOWS

Figure II-44

Note that C_a is concerned only with scattered radiation since we have assumed that the window sill is at detector height. This is usually the normal case. Thus no direct radiation can reach the detector through the window solid angle fraction, ω_a. The exterior wall barrier factor for both C_a and C_a' MUST include a height effect. Each of these two quantities are also multiplied by the perimeter ratio of windows, P_a.

Although the analysis assumed the detector at sill height, the method of differencing could be used for the detector either above or below window sill. If the sill height is above detector height, we difference G_s and G_a responses. If the detector is above sill height, we difference G_s and G_d for that portion below the detector plane.

c. Ground Contribution from Floor Above Detector. Consider next the contribution to the detector from walls of the floor above the detector. With usual floor and wall thicknesses, this contribution will be on the order of 5% or less of that from the detector floor. For this reason, only the floor immediately above the detector is considered.

Figure 45 illustrates the solid angle fractions involved. ω is the solid angle fraction subtended by the detector at the ceiling of the floor above the detector. ω_1 is the solid angle fraction subtended by the ceiling itself, which we have already discussed previously. Note in this particular case that we are concerned only with radiation above the detector plane. There will be no direct contribution from the floor above the detector. The equation for this contribution is:

$$Cgu = B\left[\Delta Gsu\, Sw\, E + \Delta Ga\,(1-Sw)\right], \tag{93}$$

$$B = Bw\,(Xe, H)\; Bo'\,(X_o')\; Bw\,(Xi), \tag{94}$$

$$\Delta Gsu = Gs(\omega_3) - Gs(\omega_1), \tag{95}$$

and

$$\Delta Ga = Ga(\omega_3) - Ga(\omega_1). \tag{96}$$

Figure 45. CEILING AND FLOOR CONTRIBUTIONS

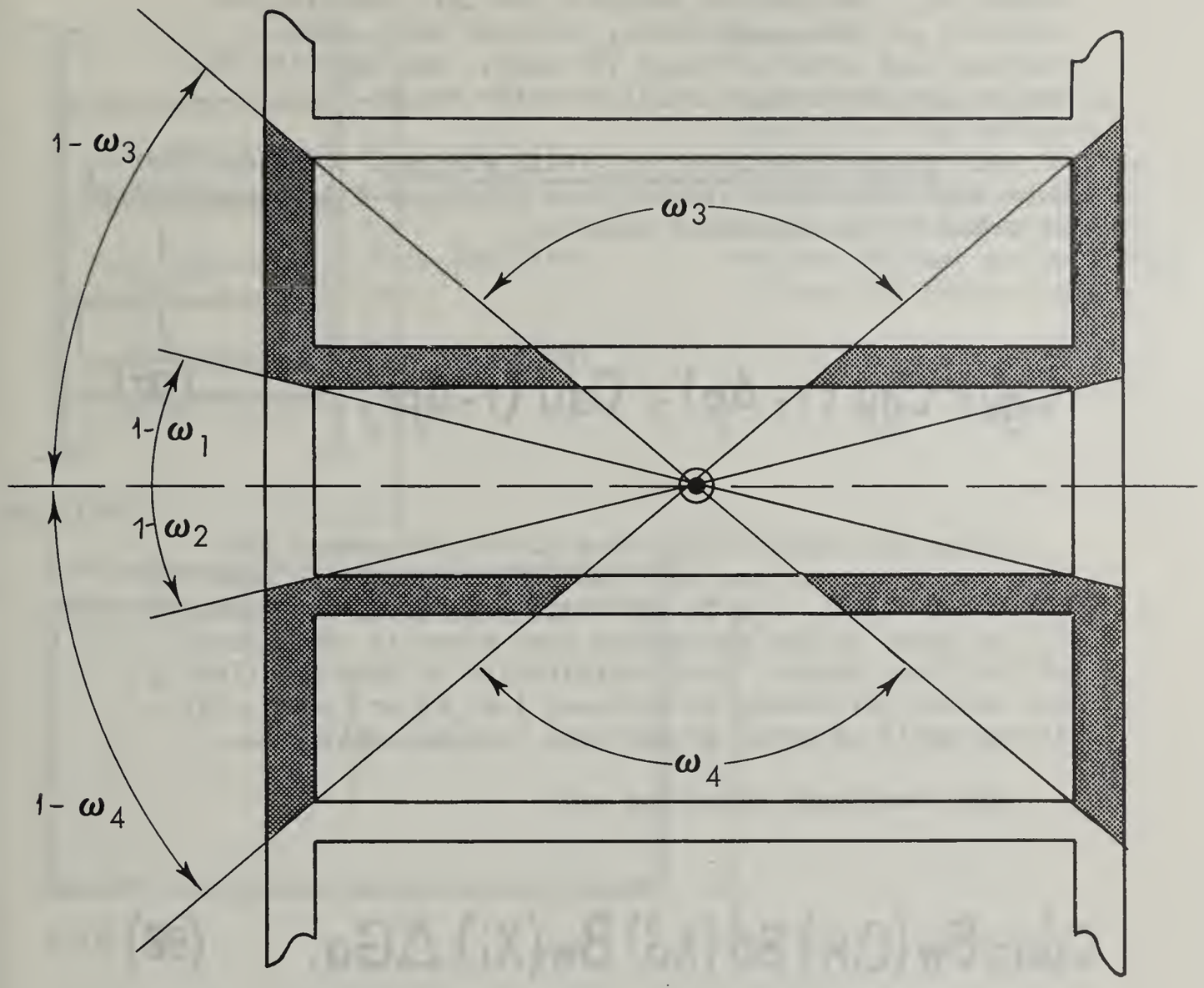

CEILING AND FLOOR CONTRIBUTIONS

Note in both the G_s and the G_a functions that we are now taking a difference of response functions similar to the roof core problem. Again we multiply by the scattered fraction and the shape factor for the wall-scattered radiation. The barrier factor B for this contribution consists of three components; exterior wall, floor barrier, and interior walls (if any). See equation 94. The height factor, H, is still detector height.

d. Floor Above Detector - With Windows. Consider the case where the upper stories have windows. This contribution is noted by the following equation:

$$C'_{gu} = C_{gu}(1-Ap) + C'_{au}(1-Ap). \qquad (97)$$

Since the contribution from floors other than the detector floor are small, a smearing technique is used for the window case. C_{gu} is the solid wall case, equation 93. C'_{au} is based on the assumption that there is 100% glass in the floor above. Each contribution is then modified by the actual percentage of windows, i.e. Ap or (1-Ap). Ap is the ratio of total window area to total wall area.

The functional equations are:

$$C'_{au} = Bw(0,H)\, B'_o(X'_o)\, Bw(Xi)\, \Delta Ga. \qquad (98)$$

ΔG_a is taken from equation 96. See example VI-4.

e. Ground Contribution From Floor Below Detector. Next consider the contribution to the detector from the walls of the floor below the detector. Figure 45 illustrates the various factors involved here. Note that we now have no G_a response since only contributions below the detector plane are being considered. Only G_s and G_d are contributing.

The ground contribution from the floor below, C_{gb} is:

EXAMPLE VI-4 MULTISTORY BUILDING WITH APERTURES

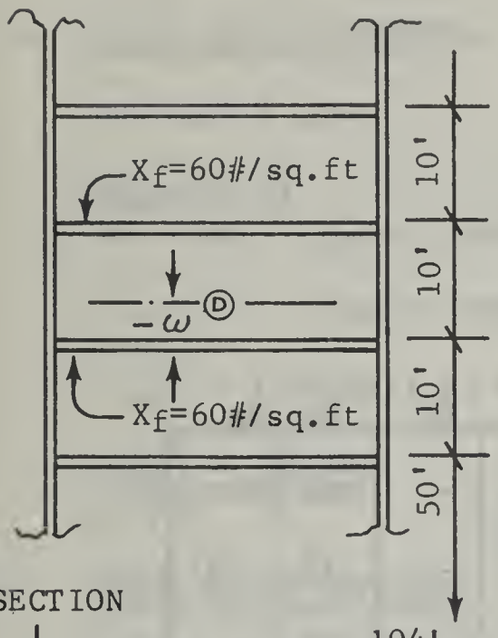

SECTION

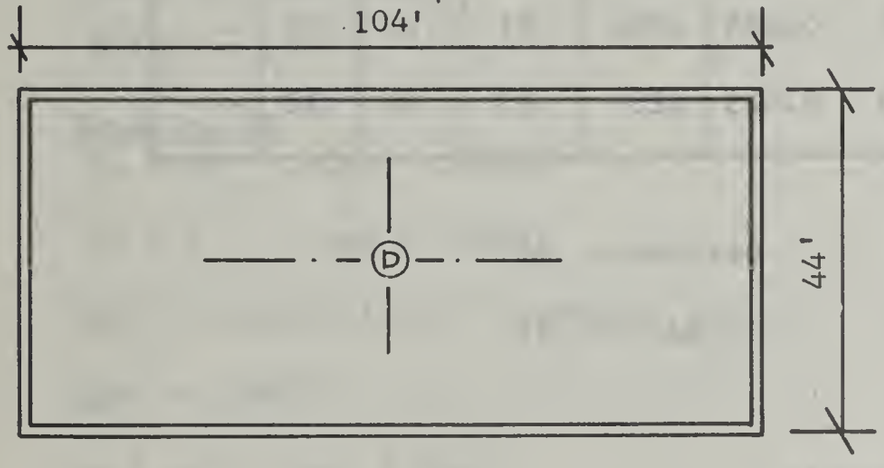

PLAN

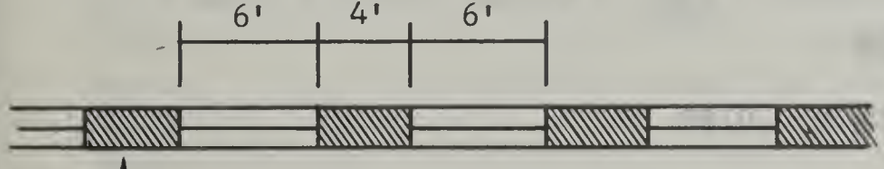

Brick Xe=80#/sq.ft.
Glass Xe=0

Typical Wall Plan

Problem:

Determine the protection factor for the detector positioned as shown on the 7th floor of the multistory building. Consider contributions through walls of 6th, 7th and 8th floors only.

Typical wall detail in plan repeats continuously around full perimeter of building brick and glass run continuously vertically for full height of building.

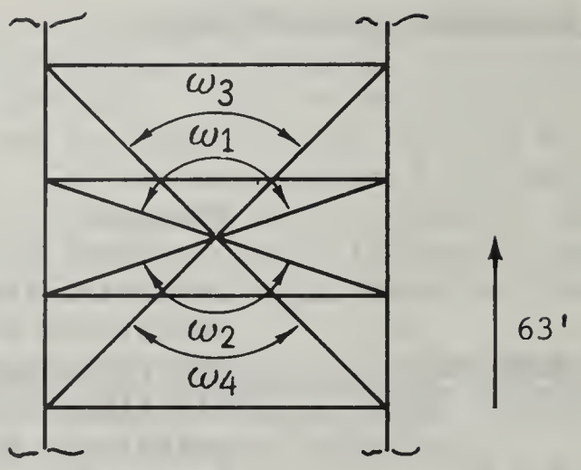

ω	W	L	Z	e	n	ω	Gd	Gs	Ga
ω_3	44	104	17	0.423	.327	.54	--	.36	--
ω_1	44	104	7	0.423	.135	.78	--	.23	.057
ω_2	44	104	3	0.423	.058	.91	.05	.10	--
ω_4	44	104	13	0.423	.25	.63	.40	.32	--

Be(80,63) = 0.06 Be(0.63 = .45

Sw(80) = 0.69 (1-Sw) = .31

E (.423) = 1.31

Assume Co is negligible

a) FLOOR OF DETECTOR:

Equation 89 Cg = .0199
for Xe = 80

for Xe = 0 Cg = .0483

for each 10' of wall 4' is solid, 6' is wall

Cg' = (0199)(.4) + (.0483)(.6)

Cg' = .0370

b) FLOOR ABOVE DETECTOR:

Bo'(60) = .044

Equation 93

Xe = 80 Cgu = .00036

Xe = 0 Cgu = .000495

Cgu' = (.00036)(.4) + (.000495)(.6)

Cgu' = .00044

c) FLOOR BELOW DETECTOR:

Bf(Xf) = .06

Equation 99

Xe = 80 Cgb = .00101

Xe = 0 Cgb = .00945

Cgb' = (.00101)(.4) + (.00945)(.6)

Cgb' = .00607

Cg = Cg' + Cgu' + Cgb'

= .037 + .0004 + .0061 = .043 (rounded off)

$$Cgb = B[\Delta GsbSw E + \Delta Gd(1Sw)]. \quad (99)$$

where

$$B = Bw(Xe, H)\, B_f(Xf)\, Bw(Xi). \quad (100)$$

$$\Delta Gsb = Gs(\omega_4) - Gs(\omega_2). \quad (101)$$

and

$$\Delta Gd = Gd(\omega_4, H) - Gd(\omega_2, H). \quad (102)$$

Note again that we are differencing response functions for both G_s and G_d. G_d is still a function of detector height. The barrier factors are the barrier factor for external walls (with height factor), the barrier factor for internal walls, and a barrier factor for the floor below the detector. This last barrier factor $B_f(X_f)$ is the "roof" barrier factor from Chart 1. It is obvious that the orientation of radiation from the ground through this barrier is identical with radiation from the roof which makes the use of this barrier factor logical. The contribution from the floor below the detector will be on the order of 10% of the detector floor contribution.

f. Floor Below-With Windows. The window case for the floor below is handled in the same manner as the floor above the detector. The only difference is that we now have G_d instead of G_a. The functional equations are:

$$Cgb' = Cgb(1 - Ap) + Ca'b \cdot Ap. \quad (103)$$

$$C'ab = Bw(0, H)\, Bo(Xf)\, Bw(Xi)\, \Delta Gd \quad (104)$$

5. Methods of Analysis.

a. Fictitious Buildings. The above functional equations can be used to calculate the protection factor for various types of practical buildings. However, we have always assumed that the detector was in the center of the building. In many actual cases, the rooms which will be used for shelters will be off center or in one corner of the building. To compute the detector response then from a detector which is off center, we make use of the fictitious building concept. In order to examine the fictitious building concept, let us compute the contribution from sector number one of the building shown in Figure 46. All we do is construct a building such that the detector is in the center of this building, as shown.

We compute the contribution from segment number one of this building in a normal fashion, but since only one-fourth of the building is actually in existance the contribution will be one-fourth of the total that we initially compute. In like fashion we compute contributions from the other three sectors by constructing fictitious buildings. Finally, we add up all these separate contributions. This method can also be used where we have parallel partitions in the building by assuming a fictitious building which has uniform conditions in any particular direction. We then compute the contribution through the walls or wall of the building which is actually in existence by the use of a perimeter ratio, that is the length of the wall contributing to the total fictitious building, and then we circle the detector until we have gone around 360 degrees computing the various fictitious buildings which contribute to the detector.

b. Azimuth Sectors. Another method of computing partial contributions to detectors is by use of azimuth sectors. Here we divide the building up with radial lines from the detector as center through uniform sections of the building again. Figure 47 illustrates this technique. In this case we merely take a ratio of the angle contributing to 360 degrees and then sum up all the angular sectors to give us our total detector response. This technique is particularly useful in analyzing contributions from narrow corridors or from windows which are not uniformly spaced around the building. See example VI-5.

c. Non-Smooth Finite Plane. We have assumed up to this point that the building is situated in an infinite plane of contamination which is smooth. In actual practice this seldom exists. There may also be other buildings in the area which will tend to produce shields for the building in question.

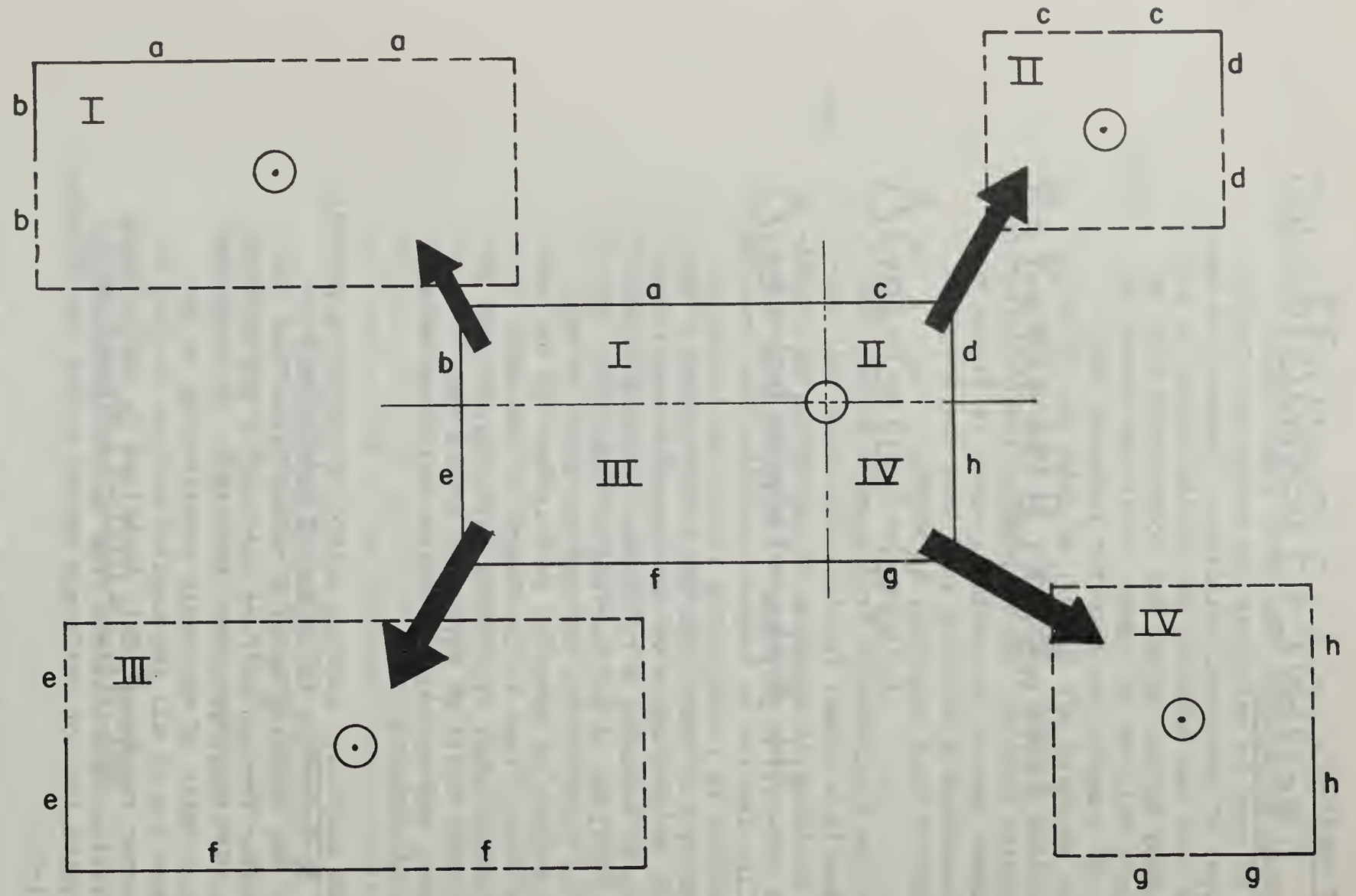

FICTITIOUS BUILDING CONCEPT

Figure II-46

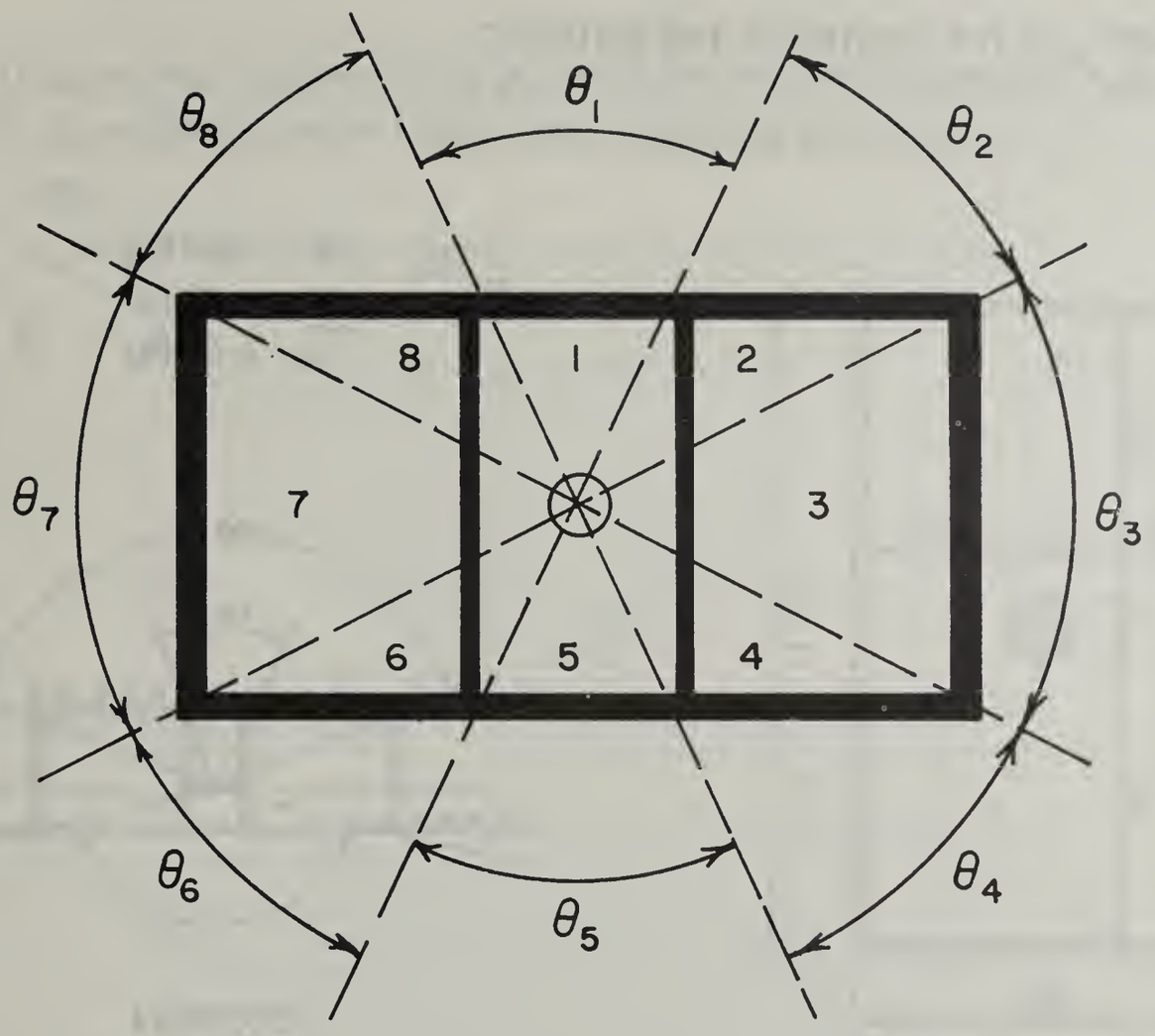

AZIMUTH SECTORS

Figure II-47

Example VI-5 - ONE STORY BUILDING, PARTITIONS

FIND P_f AT THE CENTER OF THE BUILDING

X_r = 60 PSF
X_e = 80 PSF
X_i = 50 PSF

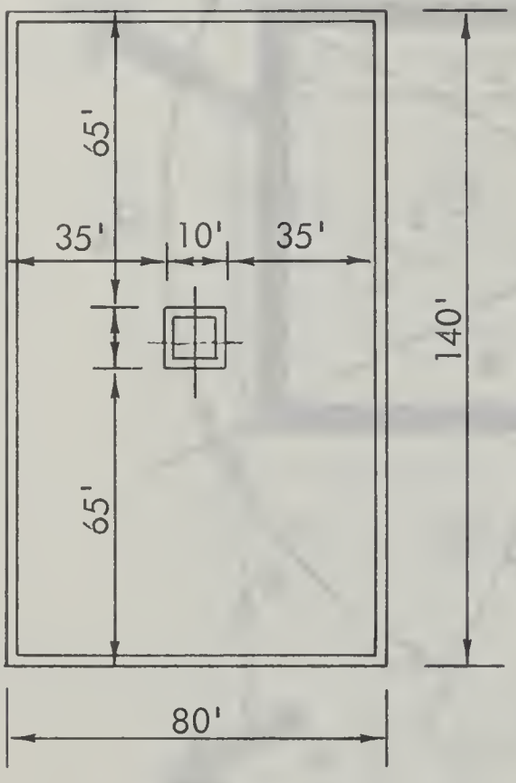

PLAN

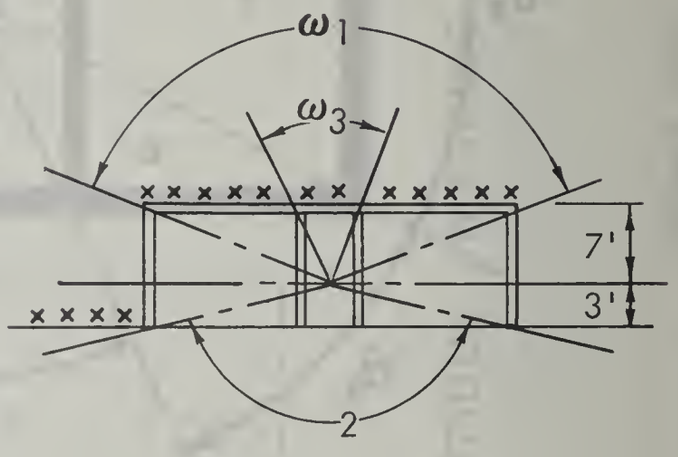

SECTION

ω	W	L	Z	e	n	ω	Gs	Ga	Gd
ω_1	80	140	7	.57	.10	.87	.145	.039	-
ω_2	10	10	7	1.0	1.4	.22			
ω_3	80	140	3	.57	.04	.945	.069	-	.275

$B_e(X_e=80,\ H = 3') = .15$
$B_i(X_i=50,\ H = 3') = .3$
$S_w(X_e=80) = .69$
$E(e = .57) = 1.36$
$B_i(X_i = 50) = .2$

ROOF CONTRIBUTION

$$C_o = C_o(\omega_3, X_o) + [C_o(\omega_1, X_o) - C_o(\omega_3, X_o)]\ B'_i(X_i)$$
$$= C_o(.22, 60) + [C_o(.87, 60) - C_o(.22, 60)]\ .2$$
$$= .022 + [.057 - .022]\ .2 = \underline{.029}$$

GROUND CONTRIBUTION

$$C_g = \left\{[G_d(\omega_2, H_d) + G_a(\omega_1)]\,[1-S_w(X_e)] + [G_s(\omega_2) + G_s(\omega_1)]\,S_w(X_e)E(e)\right\} B_e(X_e, 5')\,B_i(X_i, H)$$

$$= \left\{[.275 + .039]\,[1-.69] + [.069 +, 145]\,(.69)(.1.36)\right\}\,(.15 \times .3)$$

$$= \underline{.0134}$$

$$R_f = C_o + C_g = .029 + .013 = \underline{.042}$$

$$P_f = \frac{1}{R_f} = \frac{1}{.042} = \underline{\underline{24}} \longleftarrow \text{ANSWER}$$

We take account of the roughness of the ground or non-uniformity of the ground by a roughness factor. This is merely a fictitious height which we add to the actual height of the detector. The table below gives various fictitious heights which are used for various conditions. We merely use these fictitious heights and calculate as before but assume the height of the detector is at the fictitious height plus 3 feet.

FICTITIOUS HEIGHTS FOR VARIOUS GROUND ROUGHNESS CONDITIONS

Description	Fictitious Height* (Feet)
Smooth Plane	- 0
Paved Areas	0 - 5
Lawns	5 - 10
Graveled Areas	10 - 20
Ordinary Plowed Field	20 - 40
Deeply Plowed Field	40 - 60

*To add to actual detector height for use with wall-barrier curves, Chart 2.

d. Limited Strips. In many cases the building which we are analyzing will be protected or screened by other buildings. This sets up a limited contaminated strip of radiation sources instead of the "standard" semi-infinite plane. Such buildings are also called "mutual shields." Limited strip information is also required when areas are decontaminated thus reducing the concentration of radiation sources.

The method of handling limited strips of radiation is different for each of the three response functions. For the direct radiation, a differencing method is used. The upper and lower solid angle fractions are determined by the geometry of the situation. Figure 48 illustrates the parameters involved. The lower solid angle fraction, ω_2, is the same as before. A line drawn from the detector to the base of the mutual shield determines the second solid angle fraction needed, and is labeled ω_6 on Figure 48. The direct radiation component is:

$$C_g(D) = B\left[G_d(\omega_2, H) - G_d(\omega_6, H)\right]\left[1 - S_w\right] \qquad (105)$$

Figure 48. MUTUAL SHIELDING

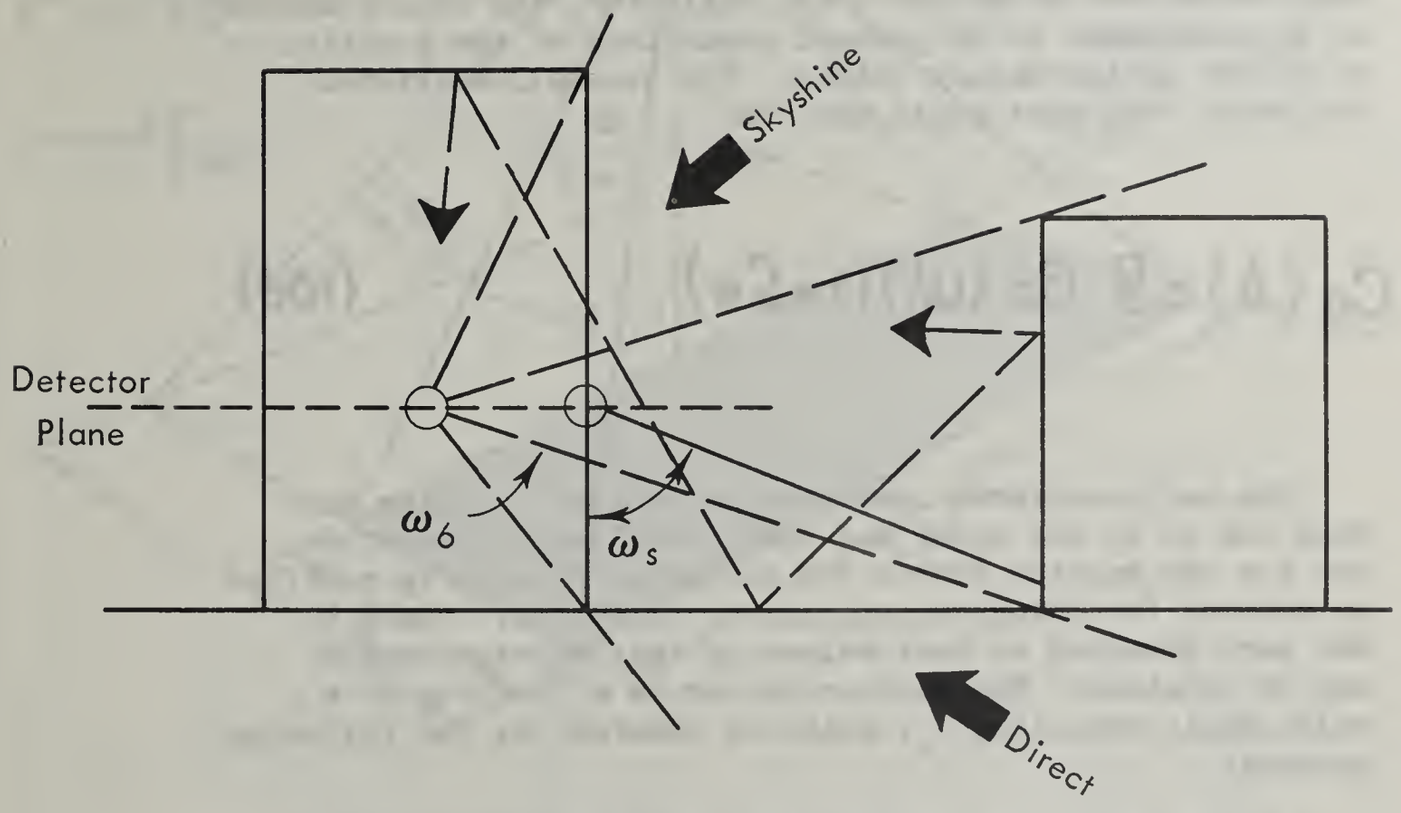

MUTUAL SHIELDING

If the detector is located at a height where ω_2 intercepts the mutual shield, the direct contribution for the floor of the detector will be zero. A similar technique of differencing is used for the floor below the detector. Again, if ω_4 intercepts the mutual shield, the direct radiation contribution will be zero.

The air-scattered component includes not only skyshine but also all other reflected radiation. This includes ceiling shine and radiation reflected from the adjacent building. Reflected radiation is normally a small fraction (10%) of the total ground contribution. Computing each of these components separately would be quite tedious and would not materially affect the final result. To insure that reflected radiation is not neglected, the full component of G_a is assumed to be present regardless of the position or height of the mutual shield. The non-wall-scattered reflected component would then be:

$$C_g(A) = B\, G_a(\omega_1)(1-S_w). \qquad (106)$$

The wall-scattered component is handled by using the same sum of G_s for upper and lower solid angle fractions but now the barrier factor for the exterior wall is modified to account for change in angular distribution. Chart 9 has been provided so that values of this barrier factor may be obtained. The barrier factor is a function of a solid angle fraction, ω_s, which is obtained by the following process:

For the floor of the detector, the Z distance used to compute n for ω_s is taken as the detector height. The rectangle used to compute e is equal to twice the strip width, W_c, and the length of the building plus $2W_c$. Figure 49 illustrates this geometry. After ω_s is computed, Chart 9 is entered with ω_s amd Xe and the barrier factor $B(\omega_s)$ is determined. The contribution then from wall-scattered radiation is:

$$C_g(S) = B(\omega_s, Xe) \sum_1^2 G_s\, S_w \cdot E. \qquad (107)$$

Figure 49. SOLID ANGLE FRACTION FOR LIMITED FIELD

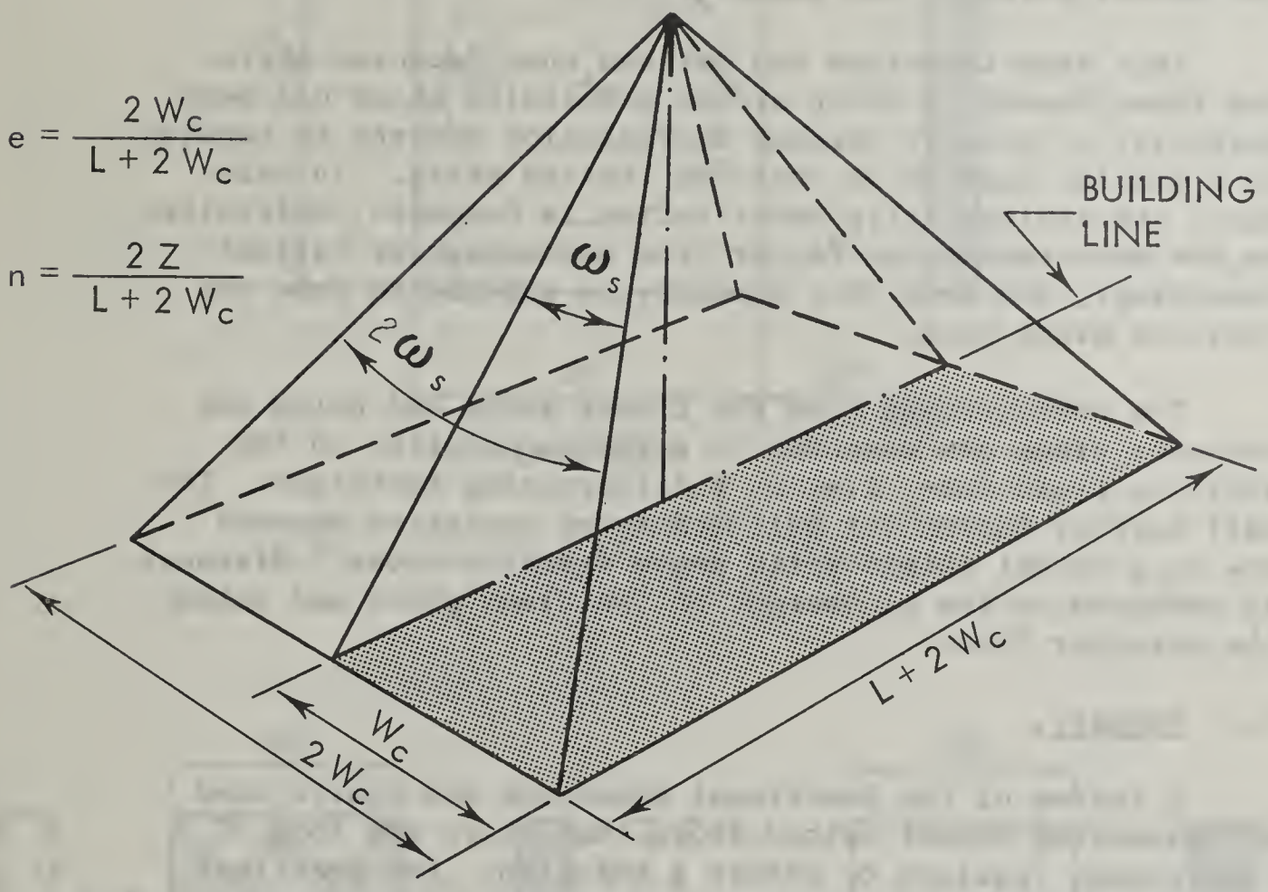

The total contribution from the sector with a mutual shield would then be:

$$C_g = [C_g(D) + C_g(A) + C_g(s)] Az. \quad (108)$$

where Az is the azimuth sector which defines the limits of the mutual shield. See example VI-6.

This same technique can be used when decontamination has taken place. A strip around a building which has been partially or totally cleared of radiation sources is handled in a similar fashion as that for limited strip. In this case, the limited strip contribution is computed, multiplied by the decontamination factor (the percentage of fallout remaining), and then this quantity is subtracted from the infinite plane case.

The contribution from the floors above and below the detector plane are computed in a fashion similar to the infinite field case, i.e. by a differencing technique. The wall barrier factor for wall-scattered radiation depends now on a mutual shield solid angle fraction whose Z distance is measured to the mid-height of the floor above and below the detector floor.

6. Summary.

A review of the functional equations and charts used in the Engineering Manual method shows that there are some 50 to 60 operations required to effect a solution. For practical engineering applications the method leaves much to be desired. In view of the fact that fallout shielding is not an exact science (see Section VIII), but is in fact based on a series of assumptions yet to be fully measured or justified, the question always arises as to the justification of teaching or learning this method. The major justification is the fact that it provides a logical sequence of steps in accounting for the major contributions from a fallout source field. Once an engineer fully understands the strengths and weaknesses inherent in shielding analysis, he can use simpler and more direct methods of computing the protection factors of buildings. Such a method is presented in the next section. It is called "The Equivalent Building Method of Fallout Shielding Analysis." It was developed by Commander LeDoux to more fully meet the needs of the designer.

Example VI-6 - MUTUAL SHIELDING

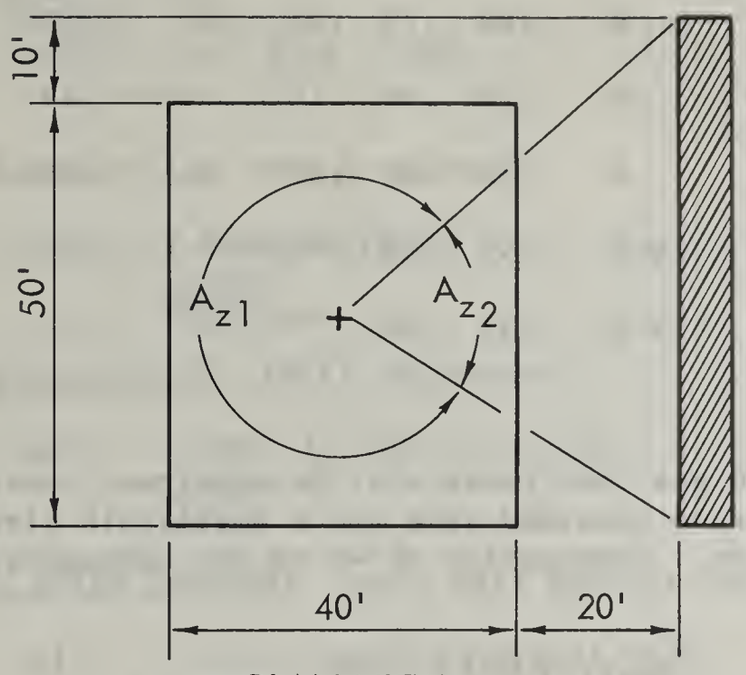

PLAN VIEW

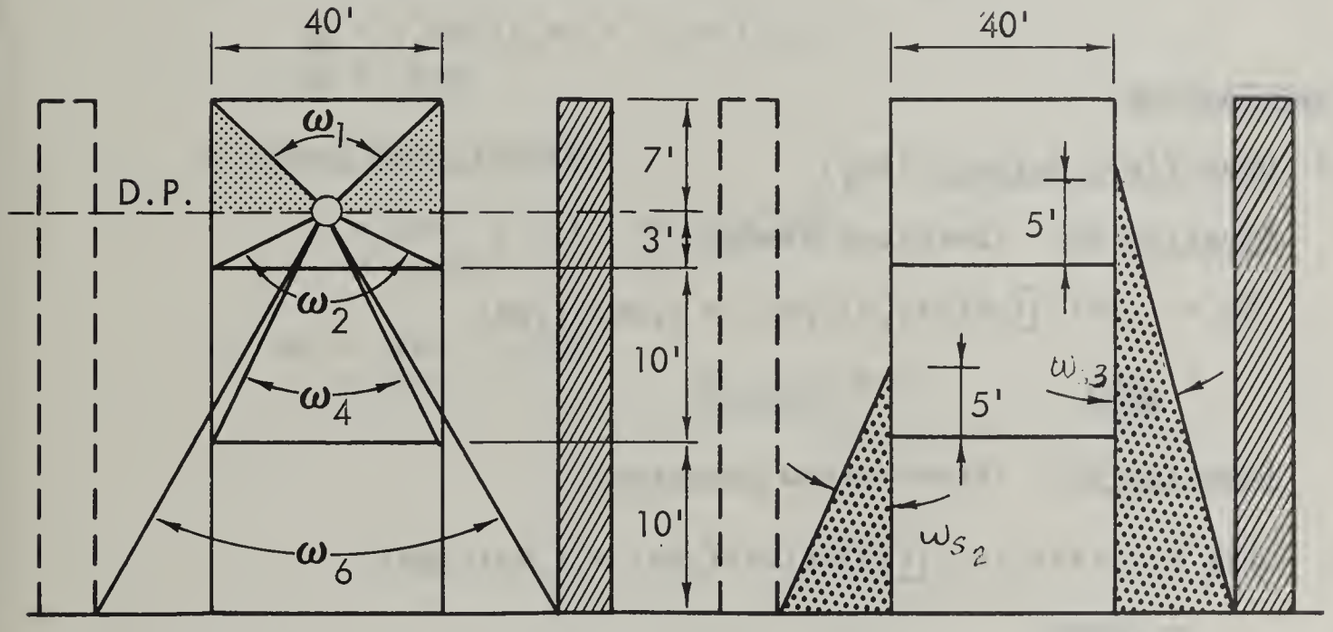

NON-WALL SCATTERED GEOMETRY

WALL-SCATTERED GEOMETRY

ELEVATIONS

1. Shielding Parameters

ω	W	L	Z	e	n	ω	Gs	Ga	Gd (H=23'
ω_1	40	50	7	.8	.28	.73	.27	067	---
ω_2	40	50	3	.8	.12	.88	.14	---	.19
ω_4	40	50	13	.8	.52	.52	.37	---	.61
$2\omega_{s_3}$	40	90	25	.445	.55	.38	ω_{s_3} = .19	---	---
$2\omega_{s_2}$	40	90	15	.445	.33	.54	ω_{s_2} = .27	---	---

From sketch we can see that there will be no direct contribution (Gd) to the third floor on shielded side and a negligible direct contribution from second floor. Computation of ω_6 is not necessary.

Sw(60) = .62

E(.80) = 1.4

Be(60,23') = .14

Bf(40) = .11

Bws(.19,60) = .009

Bws(.27,60) = .020

A_{Z_1} = 287/360 = .80

A_{Z_2} = .20

2. Computations

a) Open-Field Azimuth (AZ_1)

Equation 89: (Detector Floor)

$Cg = (.14)\left[(.41)(1.4)(.62) + (.257)(.38)\right.$

$= \underline{.063}$

Equation 99: (Floor below detector)

$Cg_b = (.14)(.11)\left[(.23)(1.4)(.62) + (.42)(.38)\right.$

$= \underline{.0056}$

$\underline{Cg(TOT) = .069}$

b) Shielded Azimuth (A_{Z2})

Detector Floor

Equation 105

Direct

$Cg(D) = (.14)\boxed{0}\ (.38) -$

$= 0$

Equation 106 (air scattered)

$Cg(A) = (.14)(.067)(.38)$

$= \underline{.0035}$

Equation 107 (Wall scattered)

$Cg(S) = (.009)\ \boxed{(.41)(1.4)(.62)}$

$= \underline{.0032}$

Floor Below Detector (only wall scatter contrit

$Cg(S) = (.020)(.11)\ \boxed{(.23)(1.4)(.62)}$

$= \underline{.0004}$

$Cg(TOT) = .0035 + .0032 + .0004$

$= \underline{.0071}$

c) Apply Azimuth Fractions

$Cg = (.069)(.8) + (.0071)(.2)$

$Cg = .056$

d) Roof Contribution

$Co = CO(\ _1\ Xo) = Co(.73,100)$

$= .020$

e) $Rf = .020 + .056$

$= .076$ $\underline{Pf = 13}$ Ans

VII EQUIVALENT BUILDING METHOD

This section consists of a reprint of the September 1963 printing of OCD-TR-20 (Vol 2) - Shelter Design and Analysis, Equivalent Building Method, and Revision #1 dated April 1964. Revision #1 replaces Section V - Computing the Equivalent Overhead Mass Thickness.

The Equivalent Building Method was developed primarily as a preliminary design aid and as such complements the more exact Detailed Procedure discussed in the previous section. A simplified version of the Equivalent Building Method called the Protection Factor Estimator - TM-64-1, May 1964, has been published in pocket edition size. TM-64-1 can be obtained from the Office of Civil Defense.

SHELTER DESIGN AND ANALYSIS

Volume 2 –Equivalent Building Method of Fallout Radiation Shielding Analysis and Design

Supersedes Shelter Design and Analysis, Volume 2,
dated February 1963

DEPARTMENT OF DEFENSE • OFFICE OF CIVIL DEFENSE

SEPTEMBER 1963

FOREWORD

This publication is a simplified approach to fallout radiation shielding analysis and design. It has been distributed by the Architectural and Engineering Development Division, Technical Operations Directorate, Office of Civil Defense in the interest of providing to the engineering and architectural professions new technical data and methods which are more easily manipulated in the preliminary design stages.

This report is based on the Engineering Manual (OCD PM 100–1) and should provide results within a few percent of this approved method of analysis and design. The Equivalent Building Method presented here is designed to provide a rapid method of analysis of structures, a means of investigating the effect of the various shielding parameters and a procedure for the economic design of shelter shielding.

This report does not explain the basic physics of structure shielding against fallout radiation. Readers who are not familiar with the basic aspects of fallout radiation and fallout radiation shielding are advised to consult the OCD Engineering Manual,[1] NBS Monograph 42,[2] and the Effects of Nuclear Weapons.[3] This report will be of most value to those engineers and architects who have completed the OCD sponsored courses in Fallout Shelter Analysis or their equivalent.

NOTE: These superior figures refer to numbered references on page 13.

ABSTRACT

The Equivalent Building Method of Fallout Shielding Analysis and Design is a simplified approach to fallout shielding based on replacing a complicated actual situation by a simple, single-story, solid wall "equivalent" building of the same floor area. This is done by computing "equivalent" roof and wall mass thicknesses to replace the actual mass thicknesses and other shielding parameters. These equivalent mass thicknesses are used with a protection factor chart from which the proper protection factor is directly obtained. Two basic functional equations are used:

$$Xo' = Xo(A,z,Xi) \quad \text{for Equivalent Roof,}$$
$$Xw' = Xe'(Xe,Ap) + Xi \pm \Delta Xw \quad \text{for Equivalent Wall.}$$

Although the method is simple and quick, it is based on the OCD Engineering Manual and NBS Monograph 42 and solutions obtained with it will yield comparable results. In addition, the Equivalent Building Method offers a rapid means of obtaining the most economic shield for a required protection factor.

SYMBOLS

Note: Wherever possible the Symbols used in the Equivalent Building Method are the same as those used in the Engineering Manual.

Mass Thickness Symbols, psf (pounds per square foot)

Xe —Exterior Wall
Xf —Floor
Xi —Interior Wall
Xo —Total Overhead
Xr —Roof
Xw —Total Wall
Xop—Equivalent Peripheral Roof
Xe′ —Equivalent Exterior Wall
Xo′ —Equivalent Total Roof
Xw′—Equivalent Total Wall

Mass Thickness Correction Factors, psf

ΔXo(Xi) —Interior Partition to Overhead
ΔXw —Total Wall
ΔXw(A,H)—Height
ΔXw(Ms) —Mutual Shield
ΔXw(Xf) —Floor Barrier
ΔXw(Ex) —Exposed Basement Wall
ΔXw(FC) —Floor Above and Below Detector Floor

Area Symbols

A —Total Area of Building
Ab —Equivalent Basement
Ac —Core
Ar —Roof
Aw—Wall
A′ —Adjusted Total Building
Ac′—Adjusted Core

Protection Factors

Pf —Protection Factor for Detector Location
Pfo—For Contribution From Detector Floor Only
Pfu—For Contribution From Floor Above Only
Pfb—For Contribution From Floor Below Only

Miscellaneous

Ap —Percentage of Apertures in Wall
Co —Contribution from Overhead (Roof)
Cg —Contribution from Ground
Cr —Cost of Roof ($/pound)
Cw —Cost of Wall ($/pound)
Bo —Barrier Factor for Roof Barrier
Bo′ —Barrier Factor for Floor Barrier
Bw —Barrier Factor for Wall
EM —Engineering Manual
EBM—Equivalent Building Method
Ex —Exposed Basement Wall Fraction
FC —Floor Above and Below Contribution Factor
H —Height of Detector Above Ground
psf —Pounds per square foot
Rf —Reduction Factor (Reciprocal of Pf)
z —Distance of Detector from Roof Contamination

VOLUME 2 -EQUIVALENT BUILDING METHOD OF FALLOUT RADIATION SHIELDING ANALYSIS AND DESIGN

I. Introduction and Background

During the late summer and fall of 1961, a number of fallout shielding courses were given throughout the United States to architects and engineers in support of the National Shelter Survey Program. The main text used and method taught at all the participating schools was the "Engineering Manual," and its method.[1] This publication was issued in draft form and the final edition is scheduled for printing in 1963. The Engineering Manual is based on the work of Dr. L. V. Spencer, NBS Monograph 42 [2] which was issued in June 1962.

The Engineering Manual offers a complete method of analyzing fallout shielding problems, even for the most complex situations. The method is based on a series of functional equations which can be used for almost any conceivable shielding problem. It is a significant contribution to the engineering literature.

Solving for the protection factor at one detector location by the Engineering Manual method may take a number of pages of tedious calculations. The method requires numerous numerical calculations and the probability of a calculational error is therefore quite high. Furthermore, the solution of the protection factor for one building or for one location within a building, does not readily lend itself to a change of parameters for comparison purposes.

For these reasons, the author (CDR J. C. LeDoux), and a colleague (LCDR R. C. Vance, CEC, USN) began to investigate various other approaches to the fallout shielding problem. The objective was to provide a means of analyzing shielding problems which would give engineers and architects a better "feel" for the interplay of the various parameters involved and still provide answers comparable to those provided by the Engineering Manual. At first only a few simple protection factor charts were developed and used. These were inspired by the Canadian A&E Guide.[4]

The protection factor chart provided a quick means of analyzing the interaction of wall and roof thicknesses for a simple, single-story, solid wall structure, for a given floor area. These simple charts are the cornerstone of the Equivalent Building Method. The relative simplicity of the Equivalent Building Method rests on the fact that large changes in magnitude of building area produce only small changes in the protection factor. The difference in protection factor for a building with an area of 100 sq ft and one with an area of 100,000 sq ft is, in most cases, less than a factor or two. For the simple, solid wall single-story structure, then, only a few protection factor charts are needed to obtain the same answer as the Engineering Manual for the same type of simple structure.

Without further refinements, these protection factor charts are useful and instructive. With a little engineering judgment, they can be used to provide quickly maximum and minimum values of protection factors for structures with complicated geometry. Further investigation revealed that the other parameters, such as height, windows, mutual shielding, etc., also produced regular and slow variations to the protection factor. Instead of modifying the barrier factor or geometry factor directly, it is possible to substitute an "equivalent" wall or roof mass thickness which will yield the same answer.

II. Basis of the Equivalent Building Method

The Equivalent Building Method is based on the assumption that any complex shielding situation can be reduced to an equivalent simple, solid-wall, single-story structure problem. An analogy for engineers is the beam curves from the AISC Steel Handbook, where moment and span are used to find the correct beam to carry the load.

NOTE: Superior figures refer to numbered references on page 13.

No computation of section modulus, moment of inertia, etc., is needed since the beam curves are based on these parameters. Similarly, the Equivalent Building Method is based on thousands of shielding problems worked by the Engineering Manual or Spencer Monograph. The solutions of these problems have been translated into various charts and tables from which equivalent wall and roof mass thicknesses can be selected.

The Equivalent Building Method is based on the Protection Factor (Pf) chart. The wall mass thickness is plotted along the abscissa; the protection factor along the ordinate; there are a series of overhead mass thickness curves from 0 psf to 300 psf (every 4″ of concrete). The overhead curves are bounded by an envelope based on an infinite roof mass thickness curve. This infinite roof curve is actually the ground contribution line since only ground contribution is included.

There are four aboveground charts for areas of 100, 1,000, 10,000, and 100,000, sq ft (figs. 1–4). There are five basement charts for areas of 100, 1,000, 4,000, 10,000, and 100,000 sq ft (figs. 5–9). The 4,000 sq ft chart is needed for the basement case since this area is a maximum point for ground contribution.

For aboveground, the basic structure assumed for these charts is a single-story, solid wall, square building. The wall height is 13 ft with the detector 3 ft above the floor. The sill height of any windows is assumed to be at detector height, 3 ft. Figure II–1 is a sketch of this equivalent building.

For the basement case, the basic structure is a 2-story, solid wall, square building with the lower story completely below grade. The story height assumed here was 10 feet with the detector 7 feet below grade. The floor above the detector was assumed to have zero mass thickness. A correction must be made for this added barrier. This was done so that the correction would always be positive. Section IV–7 describes this correction. Figure II–1 is a sketch of the belowground equivalent building.

The assumption of a square building will not cause much error since an eccentricity ratio of 5 to 1 will cause only a reduction in shape factor of about 20%. The shape factor applies only to wall-scattered radiation, and thus the total error will be less than 20%. Furthermore, using a square building is conservative when applied to an eccentric building.

Figure II - 1.

EQUIVALENT BUILDINGS

ABOVEGROUND AND BASEMENT

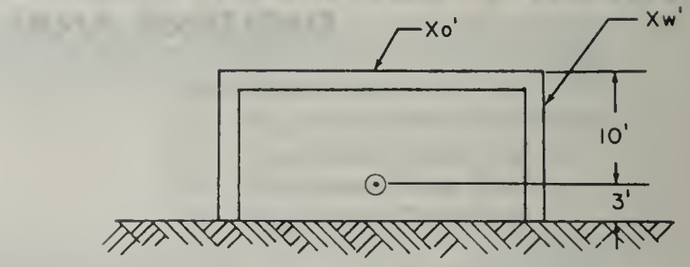

ABOVEGROUND

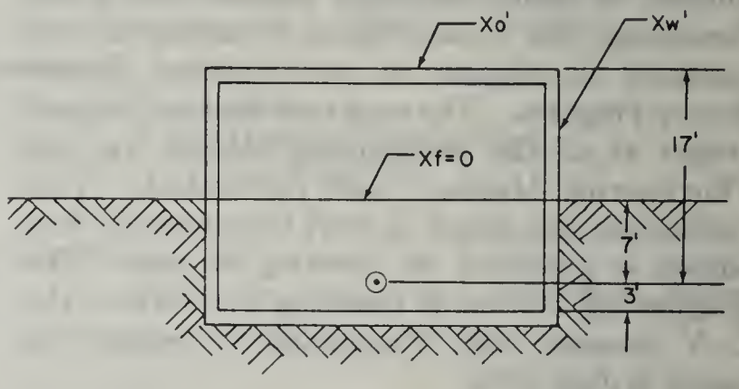

BASEMENT

If the actual structure happens to be of the simple type assumed in the construction of the protection factor charts, the solution is immediately available. Most buildings are not very simple. There may be windows; the detector may not be at the standard height of 3 ft; the distance to the roof may be other than the standard distance; adjacent buildings may provide mutual shielding, and so forth. Each of these variations from the simple geometry can be handled by modifying either the roof mass thickness, the wall mass thickness, or both so that a "substitute" building can be derived that will have the same protection factor as the actual building. The two structures are thus "equivalent" in the degree of protection provided.

In addition to the basic protection factor charts (four above-ground, five basement), there are eight auxiliary charts and three tables which are used to determine the equivalent mass thicknesses of roof and wall. Each of these charts and tables have been derived empirically since they were developed by solving shielding problems using the Engineering Manual. Once the true protection factor was known, the previously developed protection factor charts were used to determine the equivalent roof

or wall mass thickness which would yield the same value. Thus, points on the auxiliary charts or tables were determined.

III. Equivalent Building Method Functional Equations

A functional equation describes in symbols what parameters are involved in determining a particular quantity. Thus, when we write $y=f(x)$, we mean that y depends on some function of x. It is often possible to write an explicit equation for x. In some cases, only the curve representing x may be available. In The Equivalent Building Method and in the Engineering Manual, the functional equation is used to indicate the dependent parameters and tables or curves are provided to determine the desired value of the function.

There are two basic functional equations for the Equivalent Building Method, one for the roof and one for the wall.

1. Equivalent Overhead Mass Thickness.

The equivalent overhead mass thickness, Xo′, depends on the actual overhead mass thickness, Xo, the area of the contributing roof, A, and the distance from the detector to the roof, z. In certain problems, Xo′ also depends on the additional barrier effect of interior partitions.

In functional equation form, this relationship is written:

$$Xo'=Xo(A, z, Xi) \quad \text{---------- (1).}$$

Figures 16 and 17 are used to determine Xo′ as explained in Section V.

2. Equivalent Wall Mass Thickness.

The equivalent wall mass thickness depends on the exterior wall mass thickness, the window area, the interior wall mass thickness, the height of the detector, any mutual shielding, contributions from the floor above and below the detector floor, and the percentage of wall exposed for semiburied cases. The functional equation is:

$$Xw'=Xe'(Xe, Ap)+Xi\pm\Delta Xw \quad \text{------ (2).}$$

The Δ symbol stands for an additional quantity of mass thickness added or subtracted to the wall mass thickness. For the floor of the detector, ΔXw has the following components:

a. *Floor of detector*

ΔXw(A, H)—Correction for height of detector above contaminated plane (fig. 12).

ΔXw(Ms) —Correction for mutual shielding (fig. 13).

ΔXw(Ex) —Correction for exposed basement walls (fig. 15).

b. *Floor above or below detector floor*

ΔXw(A, H)—Correction for height (fig. 12).

ΔXw(Ms) —Correction for mutual shield (fig. 13).

ΔXw(FC) —Correction for floor above or floor below detector floor (tables II and III).

ΔXw(Xf) —Correction for barrier effect of floors (fig. 14).

IV. Explanation of Wall Factors

1. Effect of Apertures—Xe′(Xe, Ap).

The first term of equation 2 adjusts the exterior wall mass thickness, Xe, for the effect of windows. Figures 10a–10d are used to obtain the equivalent exterior wall mass thickness, Xe′, for aboveground locations. Figures 11a–11e are used to obtain the equivalent exterior wall mass thickness for the basement case. The wall considered for the basement case is the exposed first story wall and not the buried wall. These charts plot Xe along the abscissa and Xe′ along the ordinate. There are a series of aperture percentage (Ap) curves on each chart. Enter with Xe, go vertically to the proper Ap curve and read out Xe′. The aperture percentage is the ratio of window area to total wall area×100. The detector is assumed to be at sill height.

The aperture curves give a pictorial view of the effect of windows on wall mass thickness. The curves flatten out when the amount of radiation streaming in the windows is the predominant effect. Adding more weight to exterior walls at this point will not produce any added shielding. These curves can be used in design problems to determine the best exterior wall weight (from a shielding viewpoint). If the slope of the curves is at or near 45°, every pound of wall produces an effective pound for shielding. As the slope decreases, adding weight to the walls does not produce the same weight in shielding.

For detectors above sill height, an approximate solution is to assume Xe=0 for the entire wall where windows are present. Protection factors from the window area and from solid wall are weighted in accordance with the fraction of each.

2. Interior Partitions—Xi.

In this method the interior wall mass thickness, Xi, is added to Xe′. This is equivalent to using a

barrier factor which is a function of the sum of the exterior and interior wall mass thicknesses, or Bw (Xe′+Xi). The Engineering Manual uses Bw (Xe)Bw(Xi); i.e., the product of barrier factors. Recent experimental work [5] indicates that the product method predicts too low. The sum method will always yield a higher contribution than the product and thus brings theory closer to experiment.

3. Detector height—ΔXw(A,H).

Figure 12 is used to obtain a correction to equivalent wall mass thickness when the detector is elevated above the standard height of 3 feet. The curves include two effects: the change in wall barrier effectiveness with height; and the screening effect of the floor below the detector. This second effect is dependent on the area of the building. Calculations show that for exterior walls equal to or greater than 50 psf, the combined correction remains constant for a particular height. For weights below 50 psf, there is a noticeable change in the positive direction. Two supplementary tables for Xw=0 and Xw=25 have been placed above the curves. These tables provide additive corrections to the basic curves for walls less than 50 psf.

The fact that ligher walls require heavier equivalent weights requires further explanation. For heavy walls, radiation absorption is greater than radiation scatter. For very thin walls (Xw=0), the radiation is neither absorbed nor scattered but is transmitted. For detectors in upper floors, the detector is screened from much of the direct radiation by the floor below. Since radiation is not scattered by the thin walls into the detector, very little except skyshine and ceiling shine reaches the detector and thus walls appear to be relatively thick which requires an added equivalent wall weight. For medium thick walls (Xw=25) a considerable portion of the incident radiation is scattered by the walls into the detector. The 25 psf corrections are thus lower than the 0 psf correction.

4. Mutual Shield—ΔXw(Ms).

A mutual shield improves the protection factor of a building. This effect can be simulated by changing the actual wall mass thickness by the proper amount to obtain the same effect. Figure 13, ΔXw(Ms), is an incremental increase to Xw due to the effect of a limited strip of contamination. For a strip 100 ft wide, the wall is increased by 40 psf. (See example problem No. 10.)

5. Exposed Basement Walls—ΔXw(Ex).

When basement walls are partially exposed, the protection factor of the basement location decreases. Such a problem could be handled in two ways; the basement protection factor curves could be used by providing a negative correction to the belowground charts or an additive correction could be used with the aboveground charts. The latter proved to be more feasible, since exposing even a small portion of a basement wall drastically reduces the protection factor and more nearly approaches the aboveground case.

Figure 15, ΔXw(Ex), is used with the *aboveground charts*, though a correction for a semibasement case. We simply consider all such cases as partially buried instead of partially exposed. The belowground curves do not provide low enough protection factor values and thus the aboveground curves were easier to use. The exposed wall fraction (EX) is the ratio of wall exposed to total walls.

6. Contributions from Floor Above and Below the Detector Floor—ΔXw(FC).

In addition to the ground contribution through the walls of the detector floor, significant amounts of radiation may reach the detector from the floors above and below the detector floor. For nominal floor and wall thicknesses, this usually amounts to approximately 10%. Table I has been provided as an approximate correction for this additional contribution. The values in table I are subtracted from Xw.

Tables II and III and figure 14 are provided so that a more accurate computation of this effect can be made. The method used is to obtain the protection factor for the floor of the detector (Pfo), the protection factor for the floor above (Pfu), and the protection factor for the floor below (Pfb). These three protection factors are then directly combined to obtain the Pf of the detector, as follows:

$$Pf = Pfo \times \frac{Pfu}{(Pfo+Pfu)} \times \frac{Pfb}{(Pfo+Pfb)}$$

(See Example, p. 5.)

a. *For Floor Above Detector.* Since the protection factor for the floor of the detector included the roof contribution, the protection factor for the floor above should be determined by excluding any roof contribution. This is easily

EQUIVALENT BUILDING METHOD SOLUTION FORM

PARAMETERS

W= 100 L= 100 A= 10,000
Wc= — Lc= — Ac= —
Z= 17 A'= 3460
H= 23 Ac'=
Ap= Xo= 100
Ms= Xe= 100
Xi=
X_f = 50

SKETCH

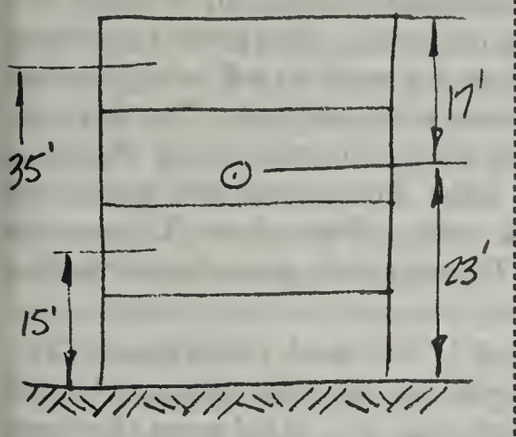

ACCURATE METHOD USING TABLES II + III (SECTORS #1, 2, 3)

$P_f = 31 \times \frac{3300}{3331} \times \frac{740}{771}$

P_f = 29.5 ANS.

APPROXIMATE METHOD USING TABLE I (SECTOR #4)

P_f = 28 ANS

EQUATIONS

$Xw' = Xe'(Ap) + Xi + \sum \Delta Xw$

$Xo' = Xo(A,Z) + \Delta Xo(Xi)$

EQUIVALENT WALL MASS THICKNESS Xw'

Factor	Fig.	Sector #1 (P_{fo})	Sector #2 (P_{fu})	Sector #3 (P_{fG})	Sector #4 (P_f TABLE I)
Xe'(Ap)	10, 11	100	100	100	100
Xi	--	0	0	0	0
ΔXw(A,H)	12	32	41	24	32
ΔXw(Ms)	13	0	0	0	0
ΔXw(FC)	1	0	45	-3	-7.5
*ΔXw(Xf)	14	0	125	117	0
*ΔXw(Ex)	15	0	0	0	0
Xw'		132	311	238	124.5

EQUIVALENT ROOF MASS THICKNESS Xw'

Co(A', Xo+ΔXo)				
-Co(Ac', Xo+ΔXo)				
Co(Periphery)				
+Co(Ac', Xo)(Core)				
Co(Total Roof)				
Area=				
Xo'=	100	∞	∞	100
P_f =	31	3300	740	28

* For Basement Case

accomplished by assuming a roof with infinite mass thickness. The upper curve of the protection factor charts is the infinite roof case or simply the ground contribution curve. Table II provides the $\Delta Xw(FC)$ correction of the floor above. In addition, figure 14 (upper curves) must be used to correct for the barrier effect of the floor above the detector. All other corrections which apply must be made.

For the height correction $\Delta Xw(A,H)$, the mid-height of the floor above the detector is used for H. If there is no floor below the detector, the final Pf is:

$$Pf=(Pfo\times Pfu)/(Pfo+Pfu).$$

b. *Basement Problems.* In addition to charts 5–9, the above procedure can be used to solve basement problems since the only ground contribution in a basement is from the floor above the detector. For basement problems, however, the equivalent roof mass thickness, Xo′, must be used so that roof contribution will be included.

c. *For Floor Below Detector.* The same procedure is used for this case as for the floor above the detector. Table III is used to provide the $\Delta Xw(FC)$ correction. Figure 14 (lower curves) provides the correction for the floor barrier effect, in this case, the floor below the detector. The height used for the $\Delta Xw(A,H)$ correction is the mid-floor height of the floor below the detector. Again an infinite roof mass thickness is used to insure that only ground contribution is added. If there is no floor above the detector, the final Pf is:

$$Pf=(Pfo\times Pfb)/(Pfo+Pfb).$$

7. Floor Barrier Factor Correction—$\Delta Xw(Xf)$.

In the Engineering Manual method, floor barrier factors Bo and Bo′ are included as multipliers in the ground contribution equations. The previous section explained how figure 14 was used to include this factor in the contribution from the floors above and below the detector floor. Figure II–1 indicates that the basement Pf charts (fig. 5–9) are based on a floor barrier factor of 1.0 or a mass thickness of zero for the floor above the detector. This was done so that any correction made would be additive. When using figures 5–9 to compute a Pf for a basement location, figure 14 (upper curves) must be used to correct for the barrier effect of the floor above the detector. The curves of figure 14 were derived by simply converting the Bo and Bo′ curves from chart 1 of the Engineering Manual to equivalent weights of wall barrier factor, Bw, from the same chart.

V. Computing Equivalent Overhead Mass Thickness

The equivalent overhead mass thickness, Xo′, depends on the contributing roof area, the distance of the detector from this roof area, and for certain problems, the interior screening partitions. The functional equation for Xo′ is:

$$Xo'=Xo(A,z,Xi)\text{----------}(1)$$

The basic value of roof mass thickness, Xo, is the total mass overhead between the detector and the contributing roof area. The protection factor charts have curves for each 50 psf of equivalent roof mass thickness up to 300 psf. The final upper curve is for an infinite roof mass thickness for those cases when Xo′ exceeds 300 psf or for decontaminated roofs. This infinite Xo′ curve is also the plot of Cg since only ground contribution is included.

Figures 16 and 17 are used to determine Xo′. Figure 16 is a plot of roof contribution, Co, vs the adjusted roof area, A′. Roof mass thickness is plotted for each 10 psf from 0 to 300 psf. Figure 16 is based on a distance from roof to detector of 10 feet (z=10′). This is the standard distance for the aboveground equivalent building. See figure II–1. Determining Xo′ is easy if we keep in mind that every point on figure 16 is the intersection of three values: Roof contribution, Co, adjusted roof area, A′, and roof mass thickness, Xo.

Figure 16 has several characteristics which should be noted. The terminal value line means that all Xo curves above this line are vertical and thus each Xo curve has reached a maximum and constant value of Co at this terminal line. The chart is actually a 6 cycle log chart which has been split at the 1,000 sq ft area line. Areas greater than 1,000 sq ft have been plotted in the lower righthand corner. This was done to keep the chart as compact as possible. Use the left hand ordinate for curves above and to the left (areas from 1–1,000); use the right hand ordinate for curves below and to the right (areas from 1,000 to 1 million sq ft). Since these two sections are parts of the same chart, you may proceed vertically from one set of curves to the other as necessary.

The abscissa is the roof contribution reduction factor, Co, and should provide the same value as chart No. 4 in the Engineering Manual for square roofs. Figure 16 is used to determine the Reduction Factor (Rf) for completely buried shelters where Co is the only contribution.

There is only one rule to remember in solving for Xo′. *Find the actual roof contribution*, Co; *with* Co *and the total actual roof area, enter figure 16 and determine the corresponding value of* Xo. *This is the equivalent roof mass thickness*, Xo′.

This rule will now be applied to the various circumstances that occur.

1. Variation in Distance of Detector from Roof.

Figure 16 is based on a standard "z" distance of 10 feet. If the detector distance is other than 10 feet, Xo′ will be different than Xo. To determine Co, we enter figure 16 with an adjusted roof area (A′) and with Xo. This adjusted roof area corrects for the change in solid angle fraction subtended by the roof from the solid angle subtended at the standard distance. The solid angle varies inversely as the distance squared, therefore:

$$A' = A\,(10/z)^2 \qquad (3).$$

In this case the actual value of Co is not needed. With A′ and Xo, we locate a point on figure 16. To maintain the proper value of Co, we *stay on the vertical* Co *line of the point determined.* On this vertical Co line, proceed either up or down to the *actual total building area* and read out the equivalent roof mass thickness, Xo′. We use the total building area, since we use this area with the protection factor chart.

Example: If A=7,500 sq ft
z=53′
Xo=150 psf, find Xo′.

Compute A′: $A' = A(10/z)^2$
$= 7{,}500(10/53)^2$
$= 267$ sq ft.

With A′=267, and Xo=150, enter figure 16. (This particular example is shown on figure 16 in dotted lines.) At the intersection of 267, and 150 psf (Co=0.0037), proceed vertically down to 7,500 sq ft. In this case the terminal value line lies below 7,500 and so we must keep going down until we intersect this terminal value line. This intersection occurs at Xo=172 psf; this is the proper value of Xo′ for this problem.

2. Variation in Roof Area.

There are many cases when the contributing roof area is different than the total building area at ground level. A stepped building, or a building with a central core area are two examples. In this case use the contributing roof area under consideration and Xo to determine Co and then proceed vertically to the total building area to determine Xo′. If there is a change in height and a different roof area, compute the proper adjusted area and enter figure 16 with this area and Xo to determine Co.

Example: If A=1,000 with a central core area, Ac=200
z=20′
Xo=100 psf, find Xo′.

First compute the adjusted core area, Ac′

$Ac' = Ac(10/z)^2$
$= 200(10/20)^2$
$= 50$ sq ft.

With Ac′=50 and Xo=100, find Co. At this point, go vertically up to 1,000 sq ft and read out Xo′=165 psf.

Note that in both of these examples, the actual value of Co was not needed or used to determine Xo′.

3. Core Type Problems.

In many practical shielding problems, the shielded space is protected by interior partitions. These interior partitions not only provide a barrier to ground contributions but also act as a barrier to portions of the roof contribution. In these cases, the standard procedure is to compute the roof contribution in two parts. The area of the roof not screened by interior partitions is called the "Core Area," and the portion of the roof screened by interior partitions is called the "Peripheral Area."

The general principle of solving for Xo′ applies for this type of problem. The total roof contribution, Co, is determined and is used with total building area to determine Xo′. In this case, however, Co is determined by adding the peripheral roof contribution to the core roof contribution. In determining the roof contribution to the periphery, figure 17 is used to include the barrier effect of interior partitions. For the periphery then, the value of mass thickness which is used to determine the periphery roof contribution is:

$$Xop = Xo + \Delta Xo(Xi)$$

Where Xop is the equivalent periphery roof mass thickness. $\Delta Xo(Xi)$ is the additional mass thickness required to account for the interior partition barrier.

To solve for Xo′, use the following steps, using figures 16 and 17:

(1) Solve for Co for the core area (fig. 16, with Ac′, Xo).

(2) Solve for Co for the total roof area. Include the interior partition effect (fig. 16 with A′, Xop).

(3) Solve for Co for the core area as if it was affected by interior partitions (fig. 16 with Ac′, Xop).

(4) The difference between steps (2) and (3) is the contribution from the periphery.

(5) Solve for total Co (add step 4 to step 1).

(6) Determine Xo′ from figure 16 by using Co and total area of building, A.

Example:

Let A=1,000 sq ft
Ac=200 sq ft
Xi=50 psf
Xo=100 psf
z=20 ft, find Xo .

This is the same example we had before, but now we will include the effect of the periphery. The numbers refer to the steps above.

(1) Solve for Co for the core area.

a. The adjusted core area Ac′ is:

$$Ac' = 200(10/20)^2$$
$$= 50 \text{ sq ft.}$$

b. Enter figure 16 with 50 sq ft and Xo=100. At this intersection, read out Co=0.0040

(2) Solve for total area including effect of interior partitions.

a. The adjusted area is:

$$A' = 1{,}000(10/20)^2$$
$$= 250 \text{ sq ft.}$$

b. Determine the equivalent periphery roof mass thickness, Xop:

$$Xop = Xo + \Delta Xo(Xi)$$

From figure 17, for Xi=50 and Xo=100, ΔXo(Xi)=60 psf

$$Xop = 100 + 60 = 160$$

c. Enter figure 16 with A′=250, and Xop=160, and read out Co=0.0030

(3) Solve for Co for core area with interior partition effect.

Ac′=50, Xop=160; from figure 16 read out Co=0.0011

(4) Solve for the peripheral contribution:

Co(P)=0.0030−0.0011=0.0019

(5) Solve for total roof contribution:

Co=0.0040+0.0019=0.0059

(6) Solve for Xo′:

Enter figure 16 with Co=0.0059 and A=1,000; Xo′=145 psf

The example on page ? is solved using the suggested solution form, from section IX. Note that the periphery contribution is determined first. Then the core area contribution is added.

4. Basement Roof Problems

The basement protection factor charts (figs. 5–9) are based on a detector to roof distance of 17′ as shown on figure II–1. Two methods can be used to solve for basement protection factors. The first method uses the aboveground charts and table II to correct for the basement location (the floor above the detector). In this case, the equivalent roof mass thickness is determined as described above.

If we wish to use the belowground charts (figs. 5–9) chart 16 must be corrected to allow for the basement standard distance of 17′. This is done by computing an equivalent roof area for the basement, Ab.

$$Ab = A(10/17)^2$$
$$= 0.346A$$

With this value of Ab and the true roof contribution, Co, enter figure 16 and determine Xo′ (see Example p. 9).

VI. Complex Applications

The Equivalent Building Method was originally developed to provide "ball park" estimates. With engineering judgment, the protection factor charts can still be used for estimating purposes. Problem 14, for example, required a twelve page Engineering Manual solution for a value of 47; a quick estimate yielded a Pf of 47; the Equivalent Building "wall by wall" analysis gives a value of 50.

Complex applications are best solved by using a "wall by wall" analysis with appropriate fictitious buildings similar to the Engineering Manual method. One must remember, however, that the Equivalent Building Method yields an answer which has both an overhead contribution and a ground contribution. When the protection factors are modified by an azimuth sector, the overhead contribution is also affected by the same azimuth fraction. It is important to make certain

EQUIVALENT BUILDING METHOD SOLUTION FORM

PARAMETERS

W= 50 L= 100 A= 5000
Wc= 20 Lc= 50 Ac= 1000
Z= 17 A'= 1730
H= 3 Ac'= 346
Ap= Xo= 100
Ms= Xe= —
Xi= 50

EQUATIONS

$Xw' = Xe' (Ap) + Xi + \sum \Delta Xw$

$Xo' = Xo(A,Z) + \Delta Xo(Xi)$

SKETCH

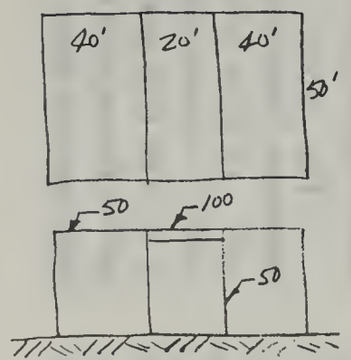

$\Delta Xo(Xi) = 57$ psf (Fig 11)

$Xop = Xo + \Delta Xo(Xi)$
$= 50 + 57 = 107$

$Xo' = 101$ psf

EQUIVALENT WALL MASS THICKNESS Xw'

Factor	Fig.	Sector #1	Sector #2	Sector #3	Sector #4
Xe'(Ap)	10 11				
Xi	--				
ΔXw(A,H)	12				
ΔXw(Ms)	13				
ΔXw(FC)	1				
* ΔXw(Xf)	14				
* ΔXw(Ex)	15				
Xw'					

EQUIVALENT ROOF MASS THICKNESS Xw'

Co(A', Xo+ΔXo) [1730, 107]	.0160			
-Co(Ac', Xo+ΔXo) [346, 107]	.0103			
Co(Periphery)	.0057			
+Co(Ac', Xo)(Core) [346, 100]	.0135			
Co(Totol Roof)	.0192			
Areo=	5000			
Xo'=	101			

* For Basement Case

EQUIVALENT BUILDING METHOD SOLUTION FORM

PARAMETERS

W= L= A= 1000
Wc= Lc= Ac=
Z= 40 A'= 62.5
H= Ac'=
Ap= Xo= 100
Ms= Xe=
Xi=

EQUATIONS

$Xw' = Xe' (Ap) + Xi + \sum \Delta Xw$

$Xo' = Xo(A,Z) + \Delta Xo(Xi)$

SKETCH

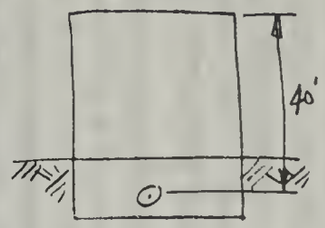

$A = 1000$

$A' = 1000\left(\frac{10}{40}\right)^2$

$= 62.5$

$A_B = .346 \times 1000$

$= 346$

$Xo' = 147$ psf

EQUIVALENT WALL MASS THICKNESS Xw'

Factor	Fig.	Sector #1	Sector #2	Sector #3	Sector #4
Xe'(Ap)	10 11				
Xi	--				
ΔXw(A,H)	12				
ΔXw(Ms)	13				
ΔXw(FC)	1				
* ΔXw(Xf)	14				
* ΔXw(Ex)	15				
Xw'					

EQUIVALENT ROOF MASS THICKNESS Xw'

Co(A', Xo+ΔXo)	—			
-Co(Ac', Xo+ΔXo)	—			
Co(Periphery)	—			
+Co(Ac' [62.5, 100], Xo)(Core)	.0046			
Co(Totol Roof)	.0046			
Area= A_B=346	346			
Xo'=	147			

* For Basement Case

that important parts of the roof contribution are not omitted. Problem 14 is a good example of the correct procedure. In this problem, certain sectors had a negligible Cg because of many intervening partitions, however, the contributions from the roof over these azimuth sectors could not be ignored. This was easily handled by assuming that the walls for these sectors were infinitely thick. The protection factors obtained for each contributing sector are combined by inverting (or changing to reduction factors), multiplying by the azimuth fraction, and then adding. The azimuth fractions can be divided by the Pf to obtain the same result. Once the total reduction factor is known, this is inverted to obtain the protection factor.

In complex applications it is not uncommon to have 15 or 20 separate azimuth fractions since an azimuth fraction is used whenever the conditions within a structure change. Changes are caused by doorways and interior partitions. The protection factor charts are helpful in combining sectors. For example, if the overhead mass thickness for a particular building is 100 psf, and the gross area of the building is 10,000 sq ft., Figure 3 tells us that all sectors with wall weights equal or greater than 250 psf can be combined because the resulting Pf will be the same.

VII. Design Procedure.

The Equivalent Building Method lends itself to preliminary design of fallout shelter since it provides the architect or engineer with a quick method of determining the effect of changing the various parameters concerned. We are concerned here only with the design of the shielding required and not with structural design methods. A designer is concerned with obtaining the most protection for the least money. Since the protection factor is a complex function of radiation contributions from various sources, determining the economic shield for a particular application can be a most complex process. To indicate how the Equivalent Building Method can be used to solve such problems, an example will be demonstrated.

Figure VII–1 is a simplified sketch of a two story school building with 24 classrooms. The classrooms surround a central area which houses the administration and service areas. In the center of this area on the first floor is the cafeteria. The second floor has a clerestory section over a

Figure VIII - 1

ECONOMIC DESIGN PROBLEM

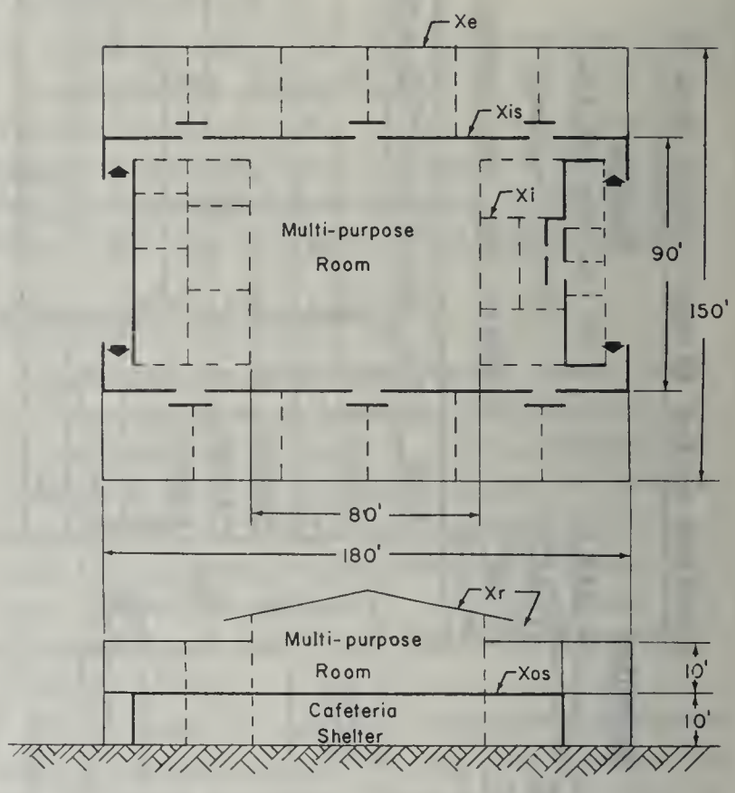

multi-purpose area. The service area includes office space, lavatories, machinery spaces, etc. If we use the cafeteria area for shelter, what wall and roof thicknesses should be used to obtain the most economic shield?

The following assumptions will be used for this problem:

1. Reinforced concrete will be used as shielding material. Inplace costs are: walls, $50/cu yd; ceiling, $80/cu yd.

2. The following material would normally be used if no shelter was included:

   a. North-South exterior walls (classroom walls) would be 8″ concrete faced with 4″ brick. Xe=140 psf. 60% of these walls will be window area, with sill height at 3 ft.

   b. East-West walls would be 12″ concrete block with no windows. The clerestory will have windows all around. Xe=85 psf.

   c. The interior partitions supporting the clerestory will be 12″ concrete block, Xi=85 psf. All other interior partitions will be lightweight concrete block, Xi=22 psf.

   d. The East entrance to the school contains office space with exterior walls light metal framing and glass, Xe=0.

3. The dotted lines indicate interior partitions. The heavy lines indicate the position of shelter shield. The shelter ceiling covers the service area. The following data has been taken off the sketch:

a. Area of school=27,000 sq ft.

b. Area of shelter=13,500 sq ft.

c. North and South wall area including baffles=4,500 sq ft.

d. Area of baffles, North and South=900 sq ft.

e. East and West wall area=2,640 sq ft.

Problem: Determine wall and ceiling weights for shelter area which can be placed at least cost. Determine cost per sq ft of shelter space over and above cost without shelter and compare to $2.50/sq ft shelter incentive allowance. Pf=100 required.

Assuming that concrete weighs 4,000 lbs/cu yd, we can write the following cost equation:

Cost = Cost of interior walls (NS)+ Cost of exterior walls (EW)+ Cost of Shelter Ceiling.

For a first cut at the problem, we will assume that the contribution from the floor above will be negligible. Since the area of the shelter is quite large, we will assume that the "z" distance of 22′ will not materially affect Xo′. There is no mutual shielding or height correction to make.

The cost of interior walls (NS) depends on the area of the NS walls, the required weights (Xi), and the unit cost of material, or

$$\text{Cost (NS-walls)} = \text{Xi Aw(NS) Cw},$$

For exterior walls (EW), assuming the walls inside the exterior office space are exterior walls, the equation would be:

$$\text{Cost (EW-walls)} = \text{Xe Aw(EW) Cw}$$

For the ceiling:

$$\text{Cost (ceiling)} = \text{Xf Ar Cr}.$$

If the costs (Cw, Cr) are costs in $/lb, these can be obtained by dividing the cost per cu yd by the 4,000 lbs/cu yd. The product of mass thickness and area is lbs of material and our equation gives us costs in dollars.

The wall functional equation which applies to this problem is:

$$Xw' = Xe'(Ap, Xe) + Xi.$$

Thus for the North-South walls, $Xi = Xw' - Xe'$. For the East-West walls, $Xe = Xw' - Xi$. For the ceiling, $Xf = Xo' - Xr$. Substituting these quantities into our cost equations, we have the following:

$$\text{Cost} = (Xw' - Xe')Aw(NS)Cw + (Xw' - Xi)\, Aw(EW)Cw + (Xo' - Xr)ArCr.$$

For $ costs, this equation must be divided by 4,000 lbs/cu yd.

Substituting areas and weights from the data of the building and dividing by 4,000 yields:

$$\text{Cost} = 56.3(Xw' - Xe') + 33(Xw' - Xi) + 270\,(Xo' - Xr).$$

From Figure 10c, for Xe=140 and Ap=60%, we obtain Xe′=77. For Xi, we have 85+22 or 107. For Xr, we have 50. Substituting and adding we have:

$$\text{Cost} = 89.3\ Xw' + 270\ Xo' - 21{,}260$$

The only unknowns in this equation are Xw′ and Xo′. These are directly obtained from the Pf charts. Referring to figures 3 and 4 we obtain the following set of combinations of Xw′ and Xo′ which will produce a Pf of 100.

For Pf=100, A=10,000

Xw′=145 155 165 173 185 210 233 297,
Xo′=250 200 175 160 150 140 135 130.

For Pf=100, A=100,000

Xw′=	97	103	113	145	153	200	350,
Xo′=	250	200	175	150	140	130	127,

using the cost equation, we can now construct a cost table (not shown) for both areas. We will interpolate linearly between the two sets of values for our area of 27,000 sq ft. The cost table indicates a minimum cost value for Xo′=140 for both tables. Listing the values from both tables to obtain the required wall thickness, we have:

A= 10,000	Xo′=140	Xw′=210
A=100,000	Xo′=140	Xw′=153
A= 27,000	Xo′=140	Xw′=199. (use 200)

For the North-South walls then, the interior mass thickness required would be 200–77 or 123 psf. For East–West walls, the exterior mass thickness required would be 200–107 or 93 psf. The shelter ceiling would have to be 140–50 or 90 psf, or 40 psf more than normal construction.

Since the exterior East–West walls would normally be 85 psf, these walls are almost sufficient as is. By filling the hollow blocks with sand or grout, the additional mass thickness would exceed the required 8 psf. The cost would be very small but for purposes of this problem we will compute this cost at $50/cu yd. The North–South walls

would have to be 11″ of concrete for the 123 psf required or 101 psf more than normal construction. The added cost of shelter would be:

Cost ceiling =
$(140-100)\times 270 = \$10,800$

Cost NS walls =
$(101)(50)(3{,}600/4{,}000) = 4,550$

Cost NS baffles =
$(123)(50)(900/4{,}000) = 1,400$

Cost EW walls =
$(8)(50)(2{,}640/4{,}000) = 264$

Total additional cost = 17,014

Cost per sq ft = \$17,014/13,500 sq ft = \$1.26 per sq ft.

Using the values of Xo′=140 and Xw′=200, we should check the Pf of this structure. This should be done by the Engineering Manual method. Using the EBM, for A=10,000 the Pf =95. For A=100,000, the Pf is 125. For 27,000, the Pf is 101. A check of the contribution from floor above indicates negligible contribution. Xo′ does change from 140 to 142 for a change in Z from 10′ to 22′, but this increases the Pf slightly. Thus the two assumptions used for simplicity do not materially change the economic analysis.

VIII. Engineering Estimate Procedure

The ability to make good engineering approximations is usually directly proportional to the experience in a given field. For estimating protection factors of buildings, the Pf charts plus a few rules of thumb should aid in obtaining good estimates.

If possible, try to bracket the Pf by obtaining maximum and minimum values. If the maximum and minimum are within a factor of two, you have accomplished the purpose of estimating the Pf of a building; i.e., getting within a factor of two. An average of these two values could be used if a single number is desired.

For most problems, using the actual roof mass thickness will give good results. If the "z" distance is large or if the core is small, use Xo. The Pf obtained will be lower than the actual Pf. A check of the Pf chart will indicate the degree of conservativeness that may be involved, and how sensitive the Pf is to the Xo′ in this particular configuration.

For example, suppose that a building has an area of 1000 sq ft with Xo=100 and z=40 ft. The walls are 100 psf. Chart 3 tells us that the Pf must be at least 14 (using Xw′=100, and Xo′ =100). With an infinitely thick roof, the Pf would only be 19. Thus a change in z for this example is not very important. However, if Xw=200, the minimum Pf would be 40 and the maximum would be 160 (for an infinite Xo′). The following rule of thumb works fairly well for a change in z.

Rule for Change in "z": For small areas (A≅1,000), add 1 psf for each foot over standard distance (10′). For large areas (A≅10,000) add 1 psf for each 4 feet over the standard distance.

For the example above, add 30 psf (40–10) to Xo for a total of 130. The estimated Pf would then be 65.

The following additional rules of thumb are useful.

Rule for Windows: Xe′=Xe(1–Ap).

Rule for Height: Up to 50′, add 1 psf for each foot of height over the standard 3′. For heights over 50′, add 1 psf for each 4 ft over 50 ft. (For 100 ft height, correction =50 +50/4=62 psf.)

Rule for floor above and floor below correction: Decrease Pf by 10%.

For Minimum Pf: Assume ground floor conditions. Correct for windows.

For Maximum Pf: Follow Xo line to right ordinate. Correct for any large z changes or for small cores.

To correct for core changes, convert the core area into a z change and apply z rule. A 400 sq ft core in a 10,000 sq ft building is the same as a z change of 50 ft. The Xo correction would be 10 psf.

Example: Suppose we have a building with a gross area of 5,000 sq ft. We wish to estimate the Pf on the 7th floor of a nine story building. If Xe=200, Ap=60%, Xf=50 (all floors), z=27′, and H=63′, what is the Pf?

Minimum Pf: Assume ground floor conditions. Xw′=200×0.4=80, Xo′=3×50=150 psf (3 floors). Average Pfs from figures 2 and 3:

$$Pf(min) = (11+21)/2 = 16.$$

Maximum Pf: Average Pfs from figures 2 and 3 for Xo=150 at right ordinate:

$$Pf(max) = (180+160)/2 = 170.$$

Since the min and max are not close, we should make a closer estimate by applying rules of thumb.

Height correction=50+13/4=53 psf Xw′= 80+53=133 psf "z" correction=(27–10)/4=4; Xo′=150+4=154 psf.

Use average of Figures 2 and 3.

$$Pf(est) = (35+65)/2 = 50 .$$

Reduce by 10% for floor and ceiling correction:

$$Pf(est) = 45 \ ANS \quad (\text{EBM Sol} = 43) .$$

IX. Summary

The Equivalent Building Method is not presented as a cure-all for all fallout shelter shielding problems. Rather it has been developed to explore the problem of fallout shielding from a different viewpoint. The state of the art at present can only furnish answers that are within, roughly, a factor of two. This method is within this range.

There are many complex shielding situations which require a tremendous amount of arithmetic to compute the protection factor using the Engineering Manual Method. The complexity does not lend itself to analyzing or obtaining a "feel" for how various changes in the parameters would affect the final answer. The Equivalent Building Method does give a quick method of "seeing" how changes affect the result; how the various parameters influence each other. This Equivalent Method then lends itself to preliminary design as well as analysis since changes can be made easily or a number of possible solutions can be done. The Engineering Manual Method should be used as a final check of any preliminary design. The method also lends itself to the quick bracketing of maximum and minimum answers which may, in many cases, be sufficient for the purposes at hand.

The Equivalent Building Method is based on empirical corrections to the overhead and wall mass thicknesses of a building. These empirical vaues have been derived by solutions to many problems by using either the Engineering Manual or the Spencer Monograph. Correct use of this method should yield results within 10% of the Engineering Manual Method.

A suggested solution form for the EBM method is shown on page 5.

REFERENCES

1. OCD-Engineering Manual. Office of Civil Defense. Washington, D.C., Draft Version—October 1961.
2. Spencer, L. V., Structure Shielding Against Fallout Radiation from Nuclear Weapons. NBS Monograph 42. National Bureau of Standards, Washington, D.C., June 1962.
3. Effects of Nuclear Weapons—1962. U.S. Atomic Energy Commission-U.S. Department of Defense, April 1962.
4. An Engineer Looks at Fallout Shelter, EMO Manual No. 1, Privy Council Office, Ottawa, Canada.
5. Starbird, Albert W., et al., The Effect of Interior Partitions on the Dose Rate in A Multistory Windowless Building. TO–B 63–6. Technical Operations, Incorporated. Burlington, Mass., January 1963.

TABLE I CORRECTION TO Xw FOR FLOOR AND CEILING CONTRIBUTIONS
(Tabular values are subtracted from Xw)

Area	Xf=20	40	60	80
1,000	5	2½	--	--
10,000	12½	10	5	2½
100,000	10	7½	5	2½

TABLE II CORRECTION TO Xw FOR CONTRIBUTION
FROM FLOOR ABOVE DETECTOR (BASEMENT)

AREA =	100	1,000	5,000	10,000	100,000
Xw=0	255	150	105	107	70
25	190	95	52	60	45
50	180	80	45	50	35
100	170	80	43	45	25
150	170	80	38	40	20

TABLE III CORRECTION TO Xw FOR CONTRIBUTION
FROM FLOOR BELOW DETECTOR

AREA =	100	1,000	10,000	100,000
Xw=0	55	15	-20	-45
50	70	20	- 7	-30
100	82	22	- 3	-18
150	85	30	3	-15
200	90	32	7	-12
250	90	35	8	- 7
300	90	35	10	- 3

Change #1 to TR-20, Shelter Design and Analysis Volume 2, Equivalent Building Method
(This change replaces Figures 16 and 17)

V. Computing Equivalent Overhead Mass Thickness

The equivalent overhead mass thickness, Xo', depends on the contributing roof area, the distance of the detector from this roof area, and for certain problems, the interior screening partitions. The functional equation for Xo' is:

$$Xo' = Xo(A,z,Xi) \text{ - - - - - - - - - - - (1)}$$

The basic value of roof mass thickness, Xo, is the total mass overhead between the detector and the contributing roof area. The protection factor charts have curves for each 50 psf of equivalent roof mass thickness up to 300 psf. The final upper curve is for an infinite roof mass thickness for those cases when Xo' exceeds 300 psf. This infinite roof curve is also the plot of Cg since only ground contribution is included.

Figure 16 with subsections a, b, c, and d is used to determine Xo'. Figure 16 is a plot of roof contribution, Co, vs the adjusted roof area, A'. Figure 16 is based on a Z distance of 10 ft. The adjusted area depends on the actual Z distance which may be different than 10 ft. The roof mass thickness is plotted for each 10 psf from 0 to 300 psf. Every point on Figure 16 is the intersection of three parameters; roof weight, Xo, roof contribution, Co, and the adjusted roof area, A'.

1. Detector to Roof Distance Variation.

Part a) of Figure 16 is a nomogram for computing A'. Since the solid angle fraction varies inversely with the square of the distance, the adjusted area can be found by the following equation:

$$A' = A\ (10/Z)^2 .$$

To find A' using the nomogram, draw a line from the total roof area A (left hand line) through the Z distance (middle line) to the left hand ordinate of part b) of Figure 16. This is the adjusted area A'.

Part b)of Figure 16 is the plot of Xo vs A' for the determination of roof contribution Co and the equivalent roof mass thickness, Xo'.

Once A' is determined, go horizontally in Part b) until the total overhead mass thickness line is reached. This point is the roof contribution Co line. If we remain on this vertical line, the true value

of Co will be maintained in the problem. To determine the value of equivalent roof thickness, Xo', go vertically to the area of the building. The area of the building is the area used with the Pf charts and is that area from which ground contamination is excluded.

Example: A = 1500 sq ft Z=30'
Xo = 150 psf
Xw = 200 psf

From 1500 on Part a), a line is drawn through 30', intersecting the left hand ordinate of Part b) at 170. Go horizontally until the Xo=150 line is reached. Note that the Co value is .0031.

Go vertically to A=1500, and read out Xo'=172 psf. From Figure 2 with Xw'=200 and Xo'=172, the Pf=100.

Note that in this problem, the actual value of Co was not needed nor used. The value was extracted only for instructional purposes. The procedure used in this simple problem can be applied to more complicated ones. There is only one rule to remember when solving for Xo' and that is: FIND THE ACTUAL ROOF CONTRIBUTION, Co. WITH Co AND BUILDING AREA TO BE USED IN THE PROBLEM, FIND THE VALUE OF Xo. THIS IS THE EQUIVALENT ROOF MASS THICKNESS Xo'.

2. Intermediate Area Problems.

For adjusted roof areas less than 1000 sq ft, the roof lines slope sharply to the left. For accuracy, we should interpolate for roof areas as well as ground areas. The following problems illustrate this.

Example: A = 400 Z=10'
Xo = 100
Xw = 200

From Figure 16, the following values of Xo' are obtained:

Xo' (100) = 55 psf
Xo' (1000) = 110 psf

The corresponding Pf values from Figure 1 and 2 are:

Pf (100) = 43
Pf (1000) = 47
Pf (400) = 45 (linear interpolation)

(Note: The method of section 1 for solving this problem, i.e. using a value of Xo' = 100 for both A = 100 and A = 1000 and then interpolating,

yields a value of 55. Such large differences will only result for small areas between 100 and 1000 sq ft. Above 1000 sq ft, the value of Xo' will be essentially constant, and only one value of Xo' is needed for interpolation).

3. Core Type Problems.

In many practical shielding problems, the shielded space is protected by interior partitions. These interior partitions not only provide a barrier to ground contributions but also act as a barrier to portions of the roof contribution. In these cases, the standard procedure is to compute the roof contribution in two parts. The area of the roof not screened by interior partitions is called the "Core Area," and the portion of the roof screened by interior partitions is called the "Peripheral Area."

The general principle of solving for Xo' applies for this type of problem. The total roof contribution, Co, is determined and is used with total building area to determine Xo'. In this case, however, Co is determined by adding the peripheral roof contribution to the core roof contribution. In determining the roof contribution from the periphery, Part c) is used to include the barrier effect of interior partitions. For the periphery then, the value of roof mass thickness which is used to determine the periphery roof contribution is:

$$Xop = Xo + \triangle Xo(Xi)$$

Where Xop is the equivalent periphery roof mass thickness.

$\triangle$ Xo(Xi) is the additional mass thickness required to account for the interior partition barrier. (Part c).

To solve for Xo', use the following steps:

(1) Solve for Co for the core area (Ac', Xo).
(2) Solve for Co for the total roof area. Include the interior partition effect (A', Xop).
(3) Solve for Co for the core area as if it was effected by interior partitions (Ac', Xop).
(4) The difference between steps (2) and (3) is the contribution from the periphery.
(5) Solve for total Co (add step 4 to step 1).
(6) Determine Xo' from figure 16 by using Co and total area of building A.

Example:

Let A = 1,000 sq ft
Ac = 200 sq ft
Xi = 20 psf
Xo = 100 psf
z = 20 ft, find Xo'

Figure V-1 indicates schematically the solution to this problem. Each step is labeled to correspond with the following steps:

(1) Solve for Co for the core:

a. Using nomogram: A = 200; Z = 20'; Xo = 100: Co = .0035,

(2) Solve for Co from the entire roof but include the effect of interior partition barrier:

a. From part c) obtain Δ Xo = 25 psf,
b. Using nomogram: A = 1000; Z = 20'; Xop = 125: Co = .0063.

(3) Solve for Co from core area but with interior partition effect:

a. Using nomogram: A = 200; Z = 20'; Xop = 125: Co = .0022.

An alternate procedure is to move along the Xo = 125 line until you intersect the Ac' line.

(4) Obtain Δ Co: Δ Co = (2)-(3) = .0063 - .0022 = .0041.

(5) Add this peripheral contribution (Δ Co) to the core contribution to get Co.

a. Co = (1) + Δ Co = .0035 + .0041 Co = .0076.

(6) Determine Xo' by going vertically to A

a. With Co = .0076; A = 1000; Xo' = 135 Xo' = 135 psf ANS.

As a general rule of thumb, if the adjusted core area exceeds 1000 sq ft or if the interior partition mass thickness exceeds 100 psf, the peripheral roof contribution will be negligible.

4. Eccentric Roof Areas.

For many practical problems, the best shelter area is located in the central corridor of a building. This corridor will likely be quite

eccentric and using the total area of the CORRIDOR AS IF IT WERE SQUARE could lead to serious error. The areas far from the detector will not contribute very much to the total roof contribution.

Part d) of Figure 16 has been included to correct for eccentric roof areas. The abcissa of this chart is the eccentricity ratio, e, or simply the ratio of width to length, W/L. The ordinate is a multiplying factor which is applied to the actual roof area to obtain an "effective contributing" area. This effective area is always smaller than the actual area.

The correction factor F(A) is limited to eccentricities of 10 to 1 (e = 0.1). If the roof has an eccentricity ratio of less than 0.1 use only that portion of the corridor or roof area which will yield an eccentricity ratio of 0.1.

For example: suppose that we are analyzing a corridor 10' wide and 150' long. The eccentricity ratio for this corridor is .067. To increase the e ratio to 0.1, we simple reduce the effective corridor length to 100'. In effect we are neglecting roof contribution from the corridor roof beyond 50' from the detector for this problem. Even for thin roofs, (Xo = 25 psf) such contribution is negligible.

Using an e = 0.1 then, and an area of 1000 sq ft, we would obtain F(A) = .34 from Part d). Applying this to the 1000 sq ft, we obtain an effective contributing area of 340 sq ft for the core part of the roof problem. From this point, proceed as in the core type problem demonstrated in the previous section. In section VI (Complex Applications), a corridor type problem will be worked out in detail in conjunction with an azimuth problem.

5. Basement Roof Problems.

The basement protection factor charts (figs. 5-9) are based on a detector to roof distance of 17' as shown on figure II-1. Two methods can be used to solve for basement protection factors. The first method uses the aboveground charts and table II to correct for the basement location (the floor above the detector). In this case, the equivalent roof mass thickness is determined as described above.

If we wish to use the belowground charts (figs 5-9) chart 16 must be corrected to allow for the basement standard distance of 17'. This is done by computing an equivalent roof area for the basement, Ab.

$$Ab = A\ (10/17)^2$$
$$= 0.346A$$

This can be accomplished easily with the nomogram, part a). Area Ab is determined by drawing a line through A and Z = 17'. For basement cases, exit on Ab instead of A.

With this value of Ab and the true roof contribution, Co, enter figure 16 and determine Xo' (see Example p.9).

Figure V-1 SAMPLE ROOF CORE PROBLEM

240-816 O-67—33

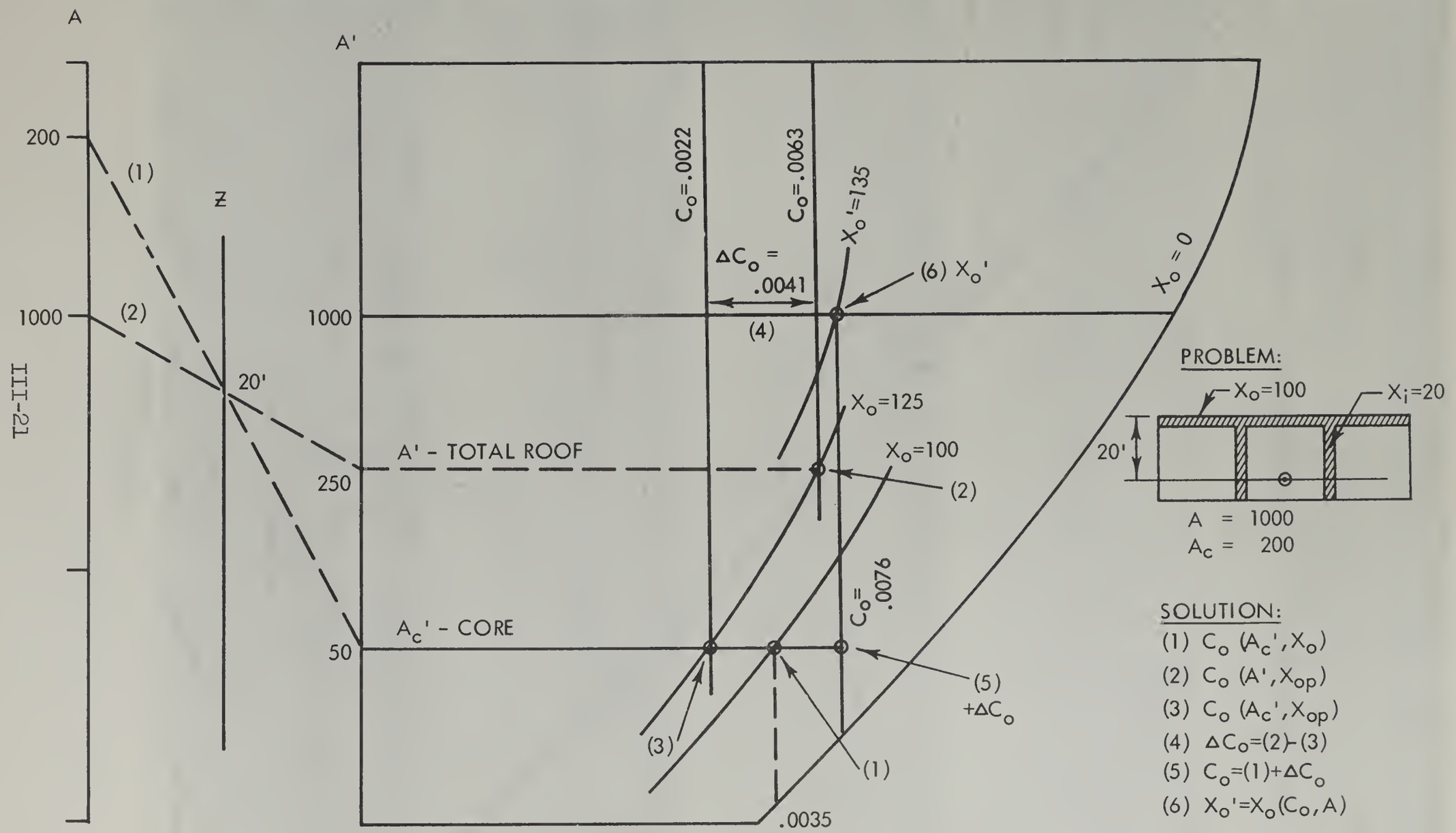

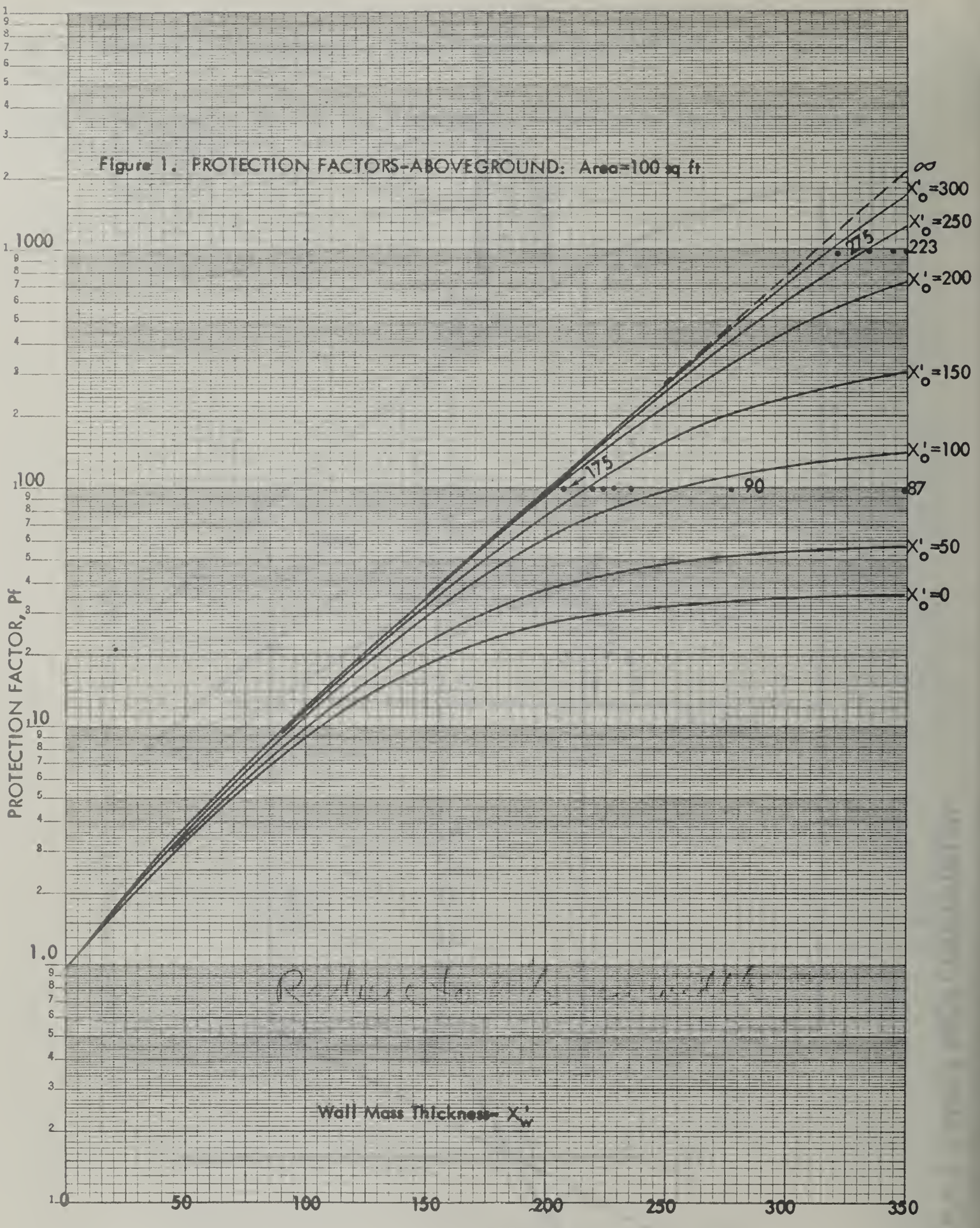
Figure 1. PROTECTION FACTORS-ABOVEGROUND: Area=100 sq ft
PROTECTION FACTOR, Pf
Wall Mass Thickness- X'_w
$X'_o=\infty$
$X'_o=300$
$X'_o=250$
$X'_o=200$
$X'_o=150$
$X'_o=100$
$X'_o=50$
$X'_o=0$
215
223
175
90
87
1000
100
10
1.0
0
50
100
150
200
250
300
350

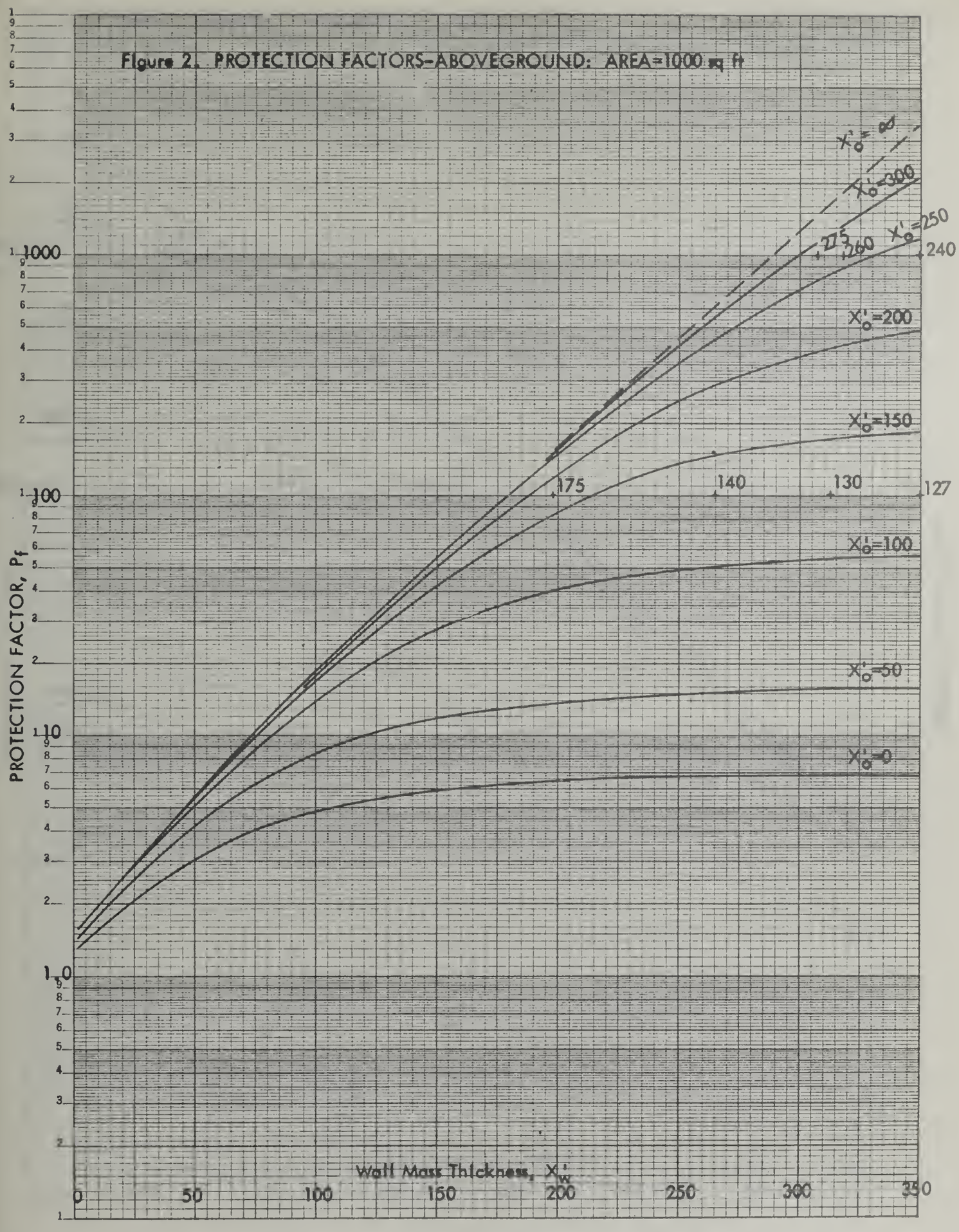
Figure 2. PROTECTION FACTORS-ABOVEGROUND: AREA=1000 sq ft
PROTECTION FACTOR, P_f
Wall Mass Thickness, X'_w
0
50
100
150
200
250
300
350
1000
100
10
1.0
$X'_o = \infty$
X'_o=300
X'_o=250
X'_o=200
X'_o=150
X'_o=100
X'_o=50
X'_o=0
275
260
240
175
140
130
127

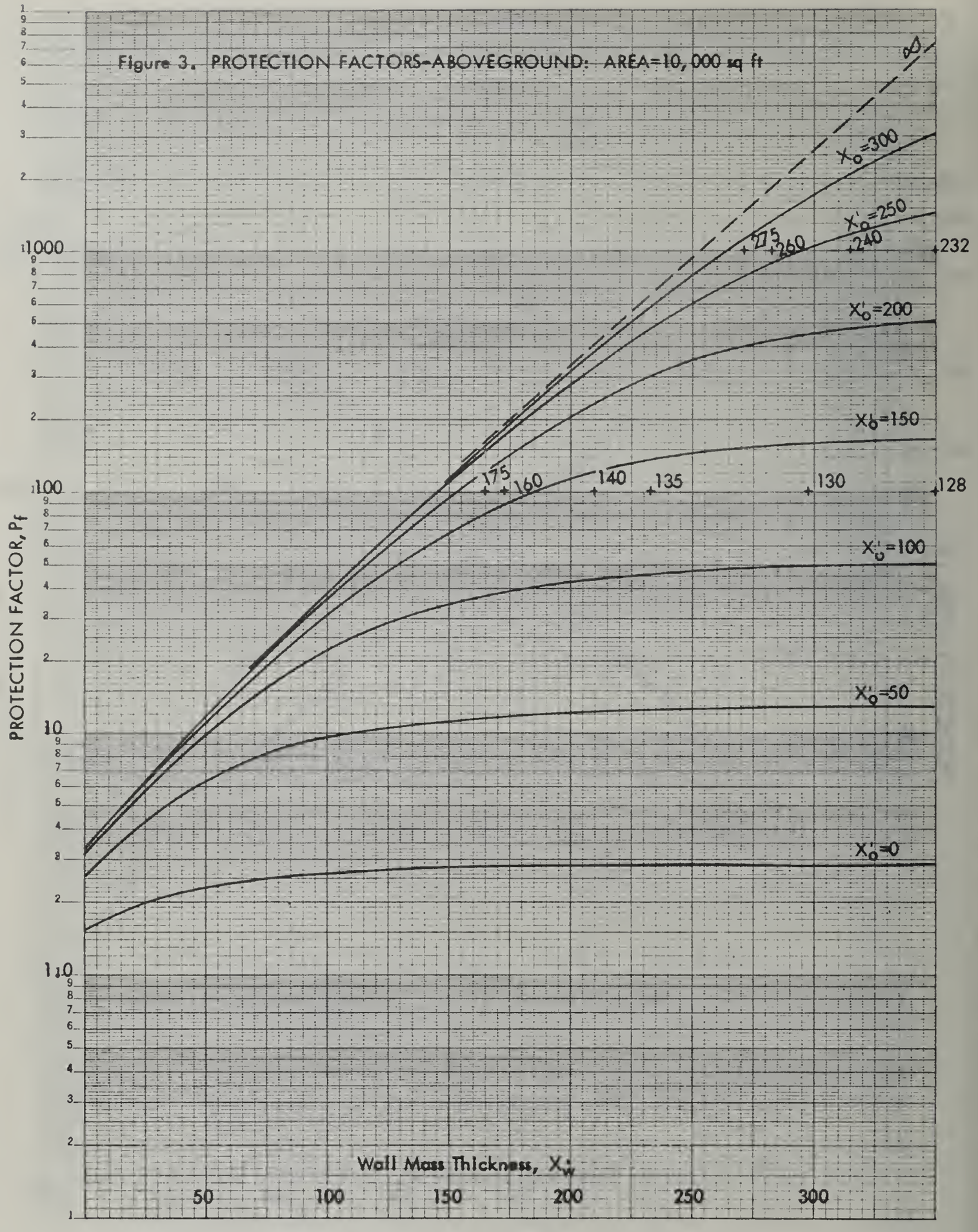
Figure 3. PROTECTION FACTORS-ABOVEGROUND: AREA=10,000 sq ft
PROTECTION FACTOR, P_f
Wall Mass Thickness, X_w
50
100
150
200
250
300
1000
100
10
1.0
$X'_o=\infty$
$X'_o=300$
$X'_o=250$
$X'_o=200$
$X'_o=150$
$X'_o=100$
$X'_o=50$
$X'_o=0$
275
260
240
232
175
160
140
135
130
128

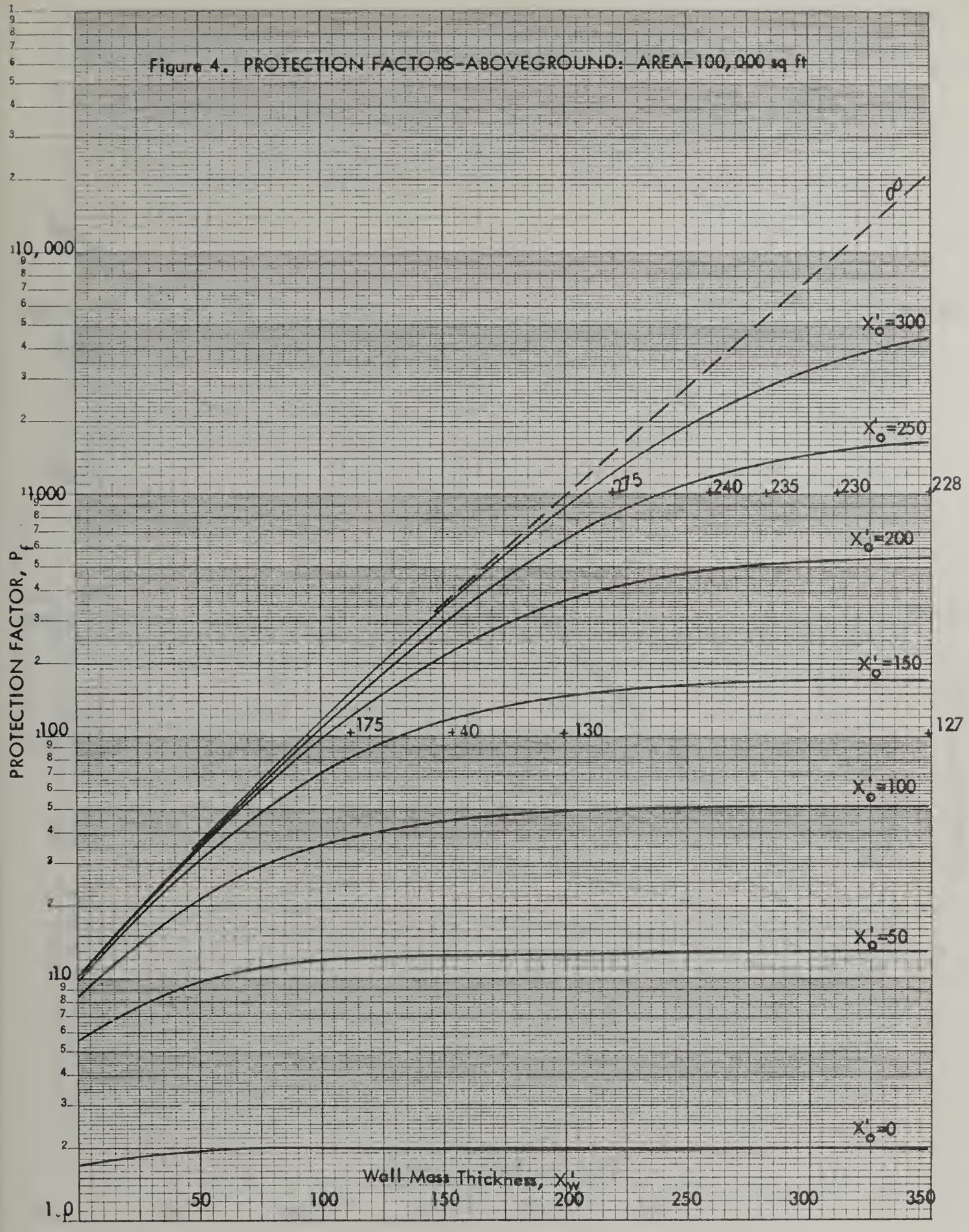
Figure 4. PROTECTION FACTORS-ABOVEGROUND: AREA-100,000 sq ft
PROTECTION FACTOR, P_f
10,000
1,000
100
10
1.0
∞
X'_o=300
X'_o=250
X'_o=200
X'_o=150
X'_o=100
X'_o=50
X'_o=0
275
240
235
230
228
175
40
130
127
Wall Mass Thickness, X'_w
50
100
150
200
250
300
350

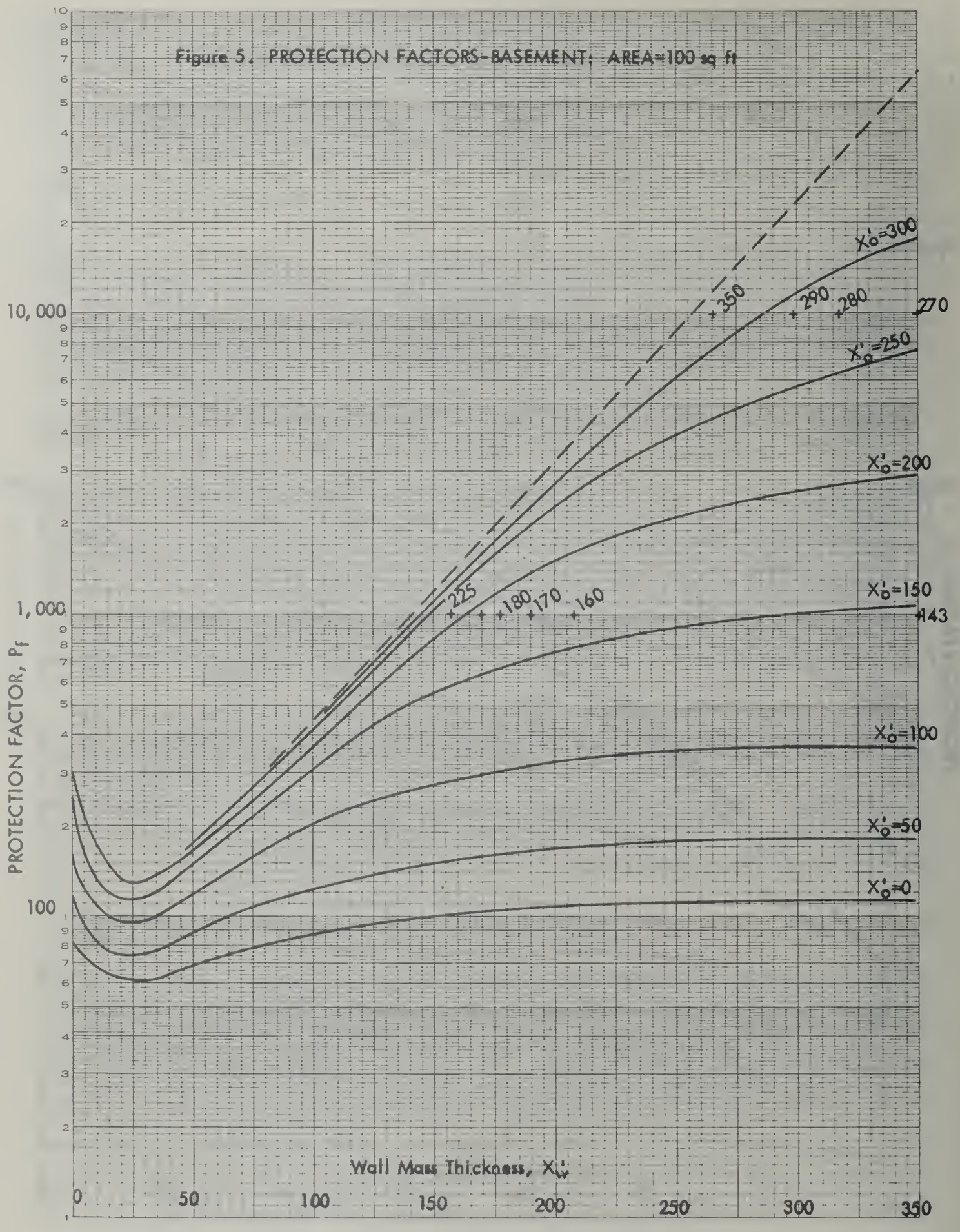
Figure 5. PROTECTION FACTORS-BASEMENT; AREA=100 sq ft
PROTECTION FACTOR, P_f
10,000
1,000
100
Wall Mass Thickness, X'_w
0
50
100
150
200
250
300
350
X'_o=300
X'_o=250
X'_o=200
X'_o=150
X'_o=100
X'_o=50
X'_o=0
350
290
280
270
225
180
170
160
143

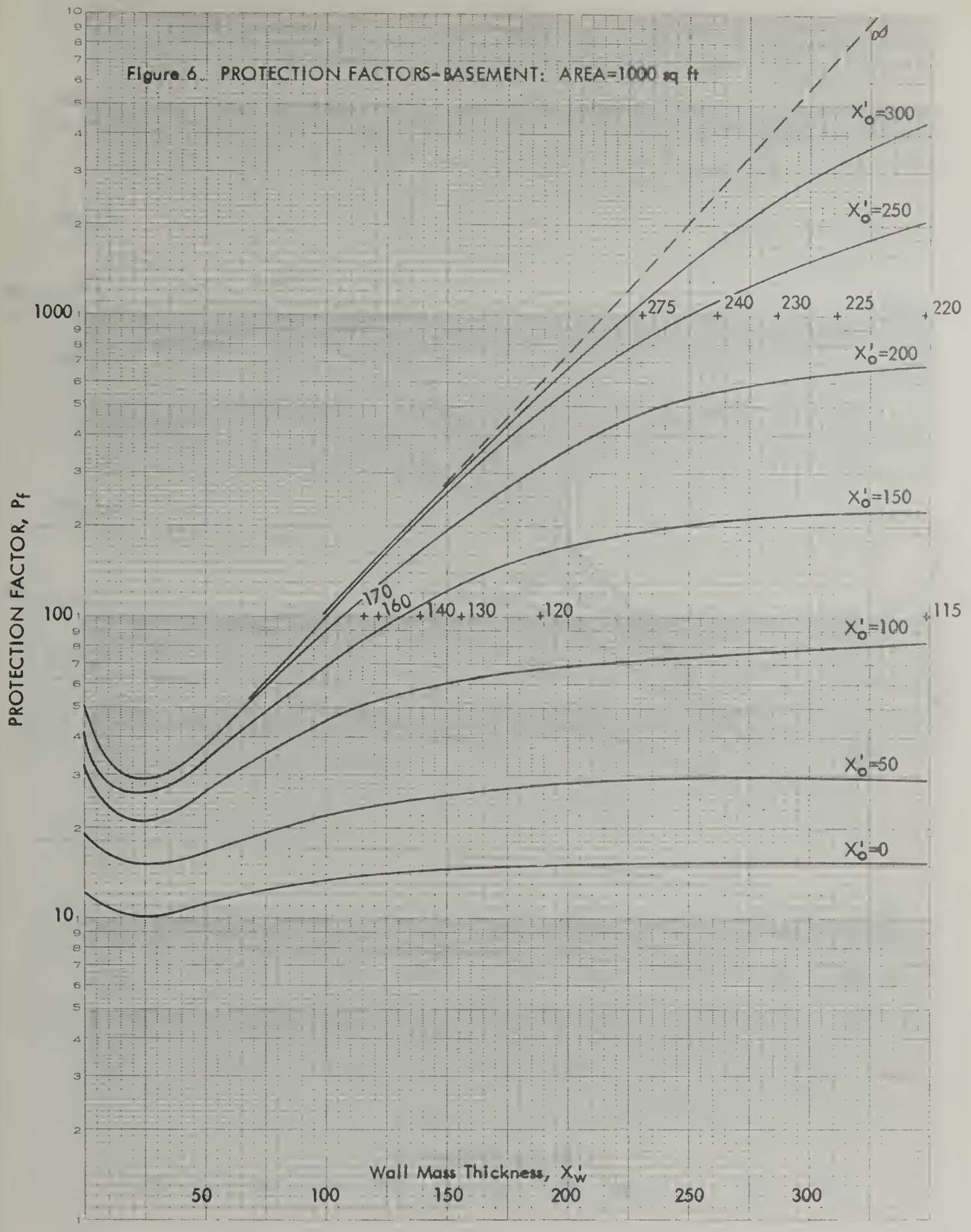
Figure 6. PROTECTION FACTORS-BASEMENT: AREA=1000 sq ft
PROTECTION FACTOR, P_f
Wall Mass Thickness, X'_w
50
100
150
200
250
300
1000
100
10
X'_o=∞
X'_o=300
X'_o=250
X'_o=200
X'_o=150
X'_o=100
X'_o=50
X'_o=0
275
240
230
225
220
170
160
140
130
120
115

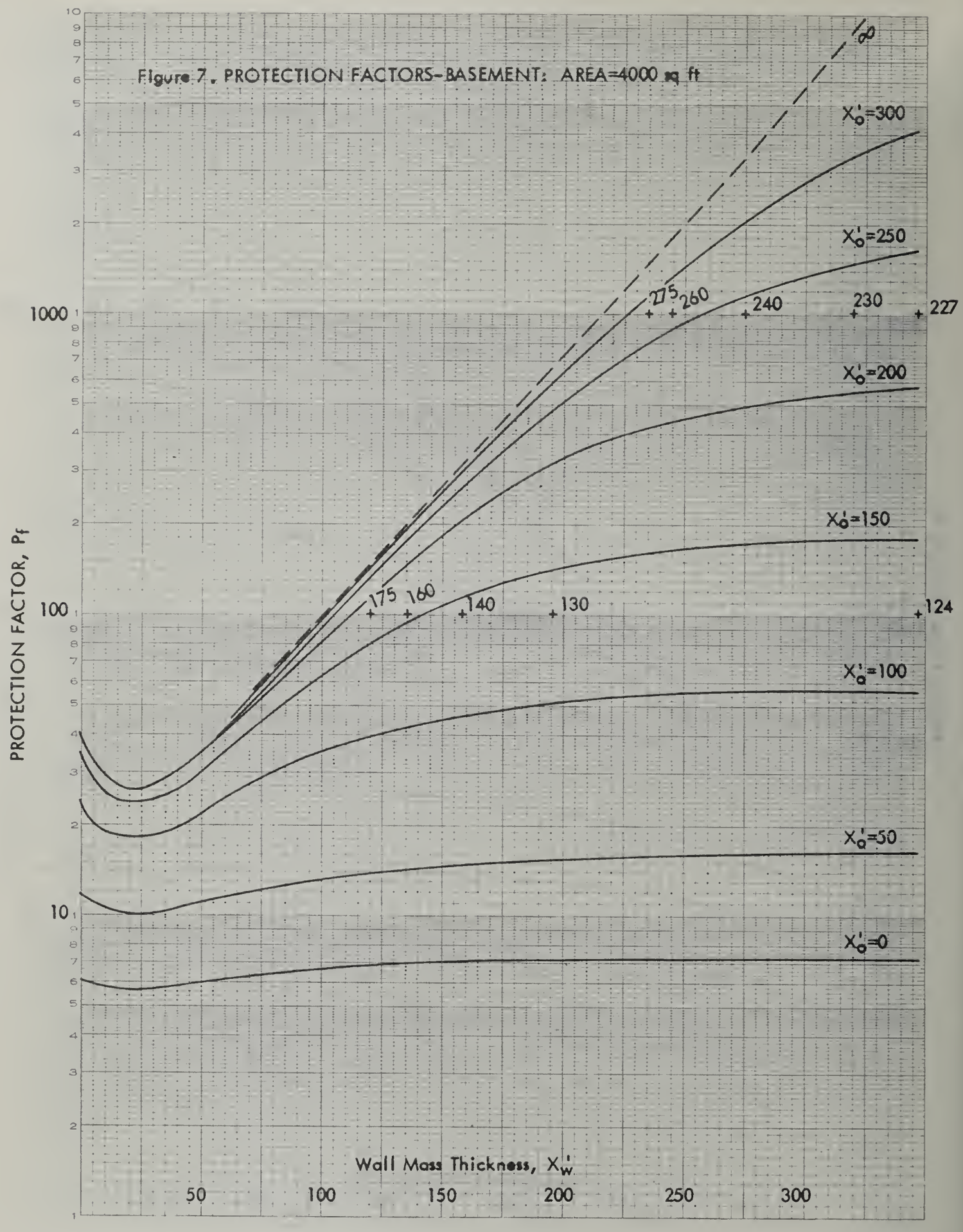
Figure 7. PROTECTION FACTORS-BASEMENT: AREA=4000 sq ft
PROTECTION FACTOR, P_f
Wall Mass Thickness, X'_w
X'_o=300
X'_o=250
X'_o=200
X'_o=150
X'_o=100
X'_o=50
X'_o=0
275
260
240
230
227
175
160
140
130
124
1000
100
10
50
100
150
200
250
300

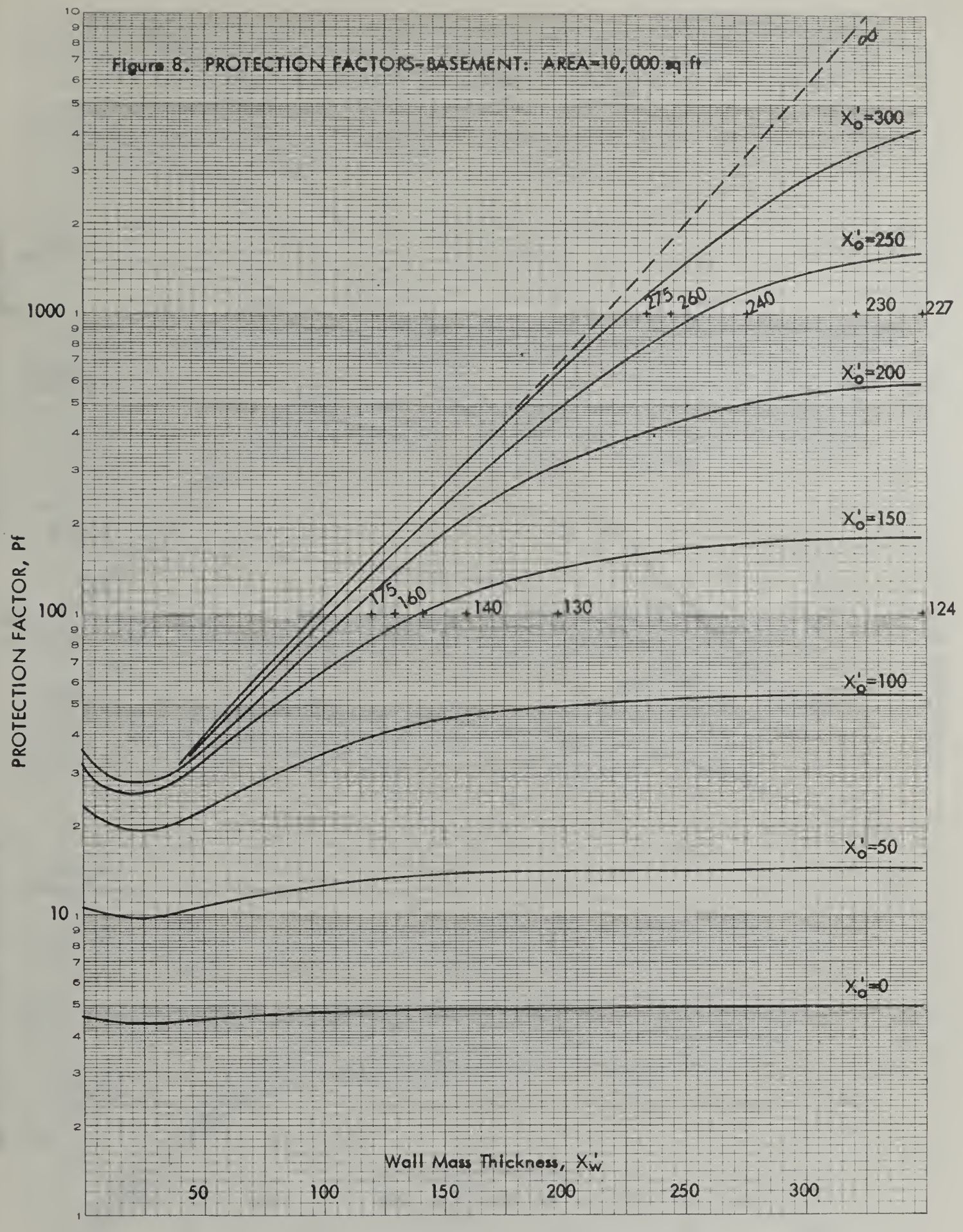
Figure 8. PROTECTION FACTORS-BASEMENT: AREA=10,000 sq ft
PROTECTION FACTOR, Pf
1000
100
10
∞
X'_o=300
X'_o=250
X'_o=200
X'_o=150
X'_o=100
X'_o=50
X'_o=0
275
260
240
230
227
175
160
140
130
124
Wall Mass Thickness, X'_w
50
100
150
200
250
300

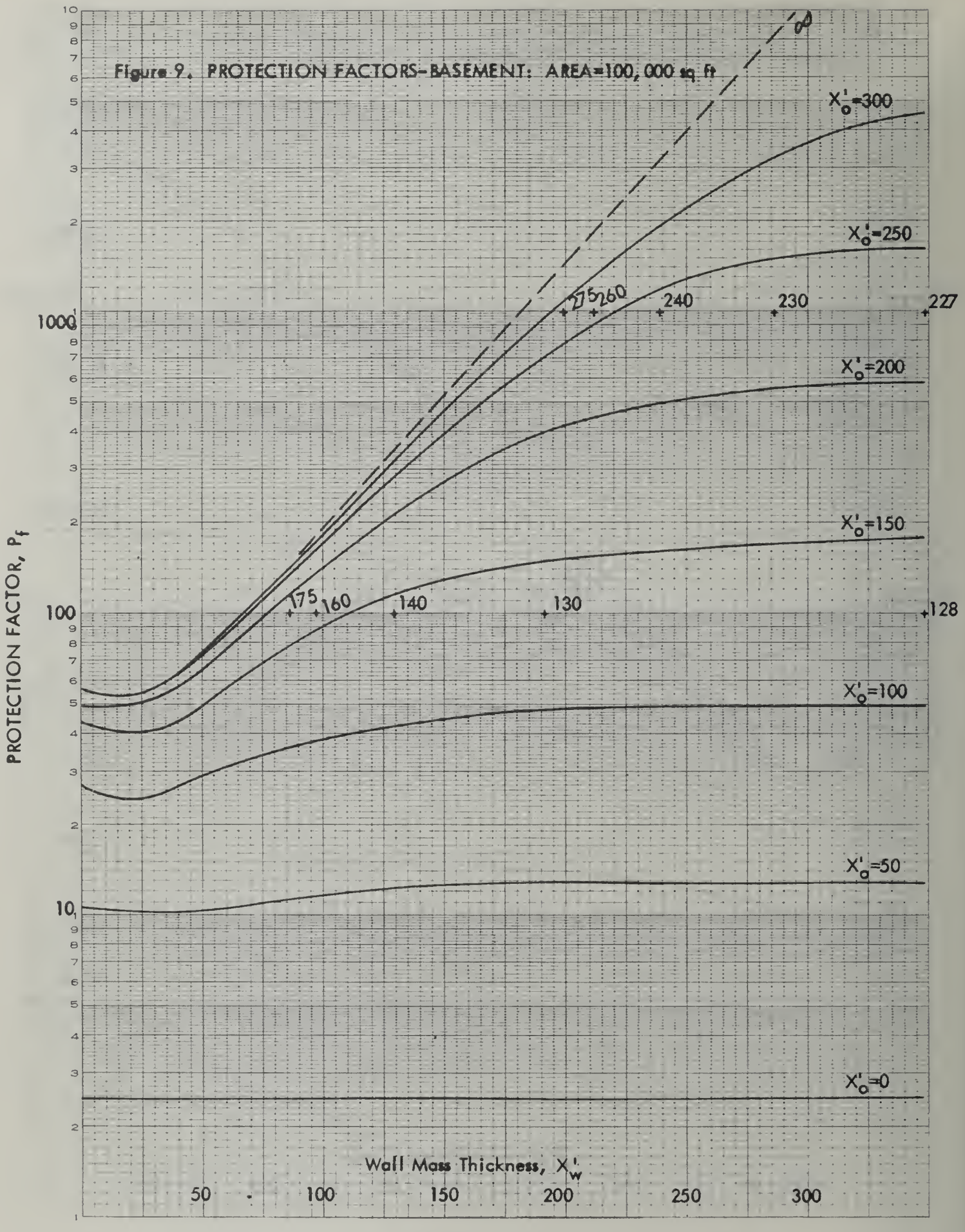
Figure 9. PROTECTION FACTORS-BASEMENT: AREA=100,000 sq ft
PROTECTION FACTOR, P_f
Wall Mass Thickness, X'_w
50
100
150
200
250
300
1000
100
10
X'_o=300
X'_o=250
X'_o=200
X'_o=150
X'_o=100
X'_o=50
X'_o=0
175
160
140
130
128
275
260
240
230
227

Figure 10. CORRECTION TO X_e FOR WALL APERTURES–ABOVEGROUND

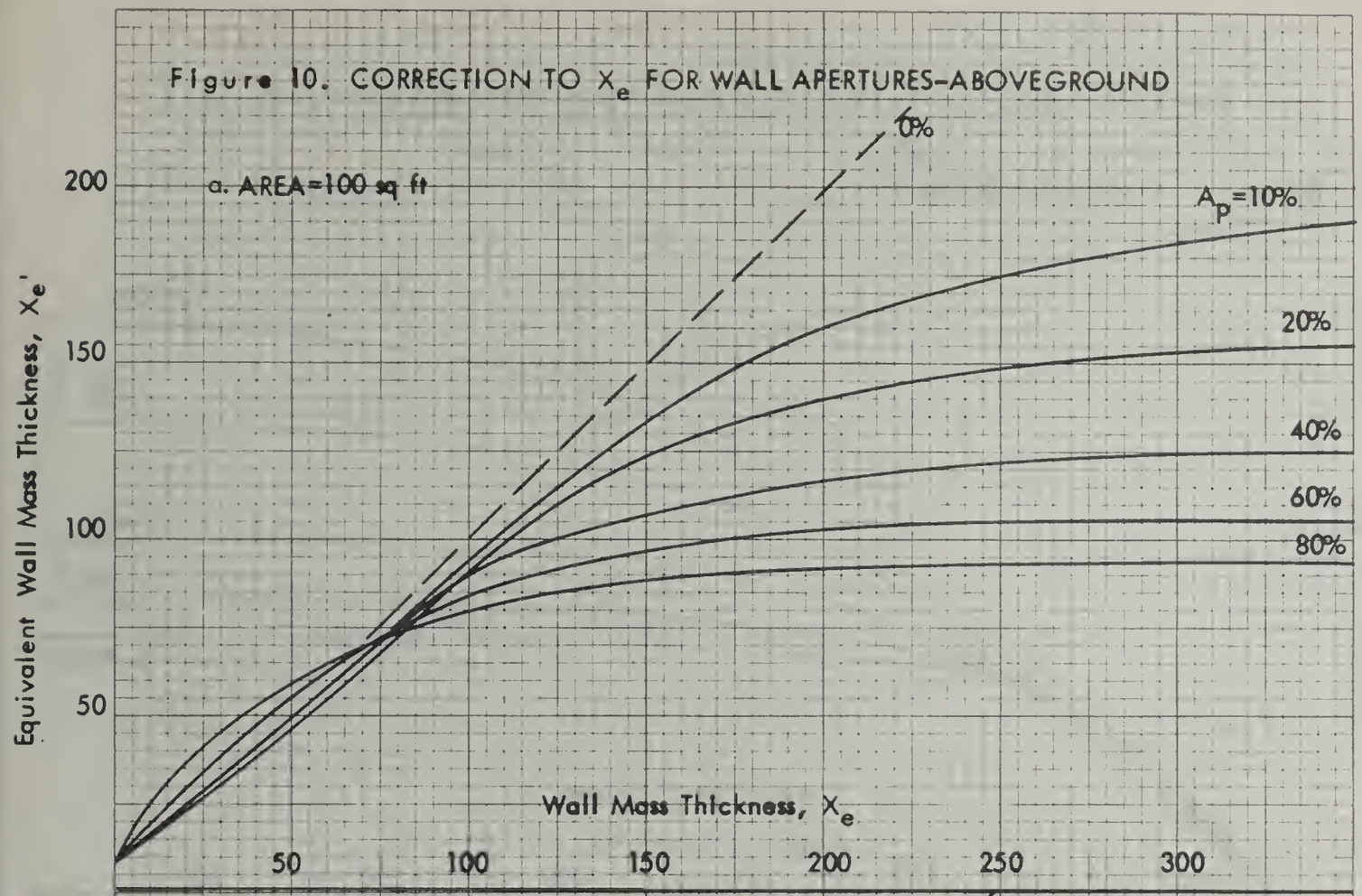

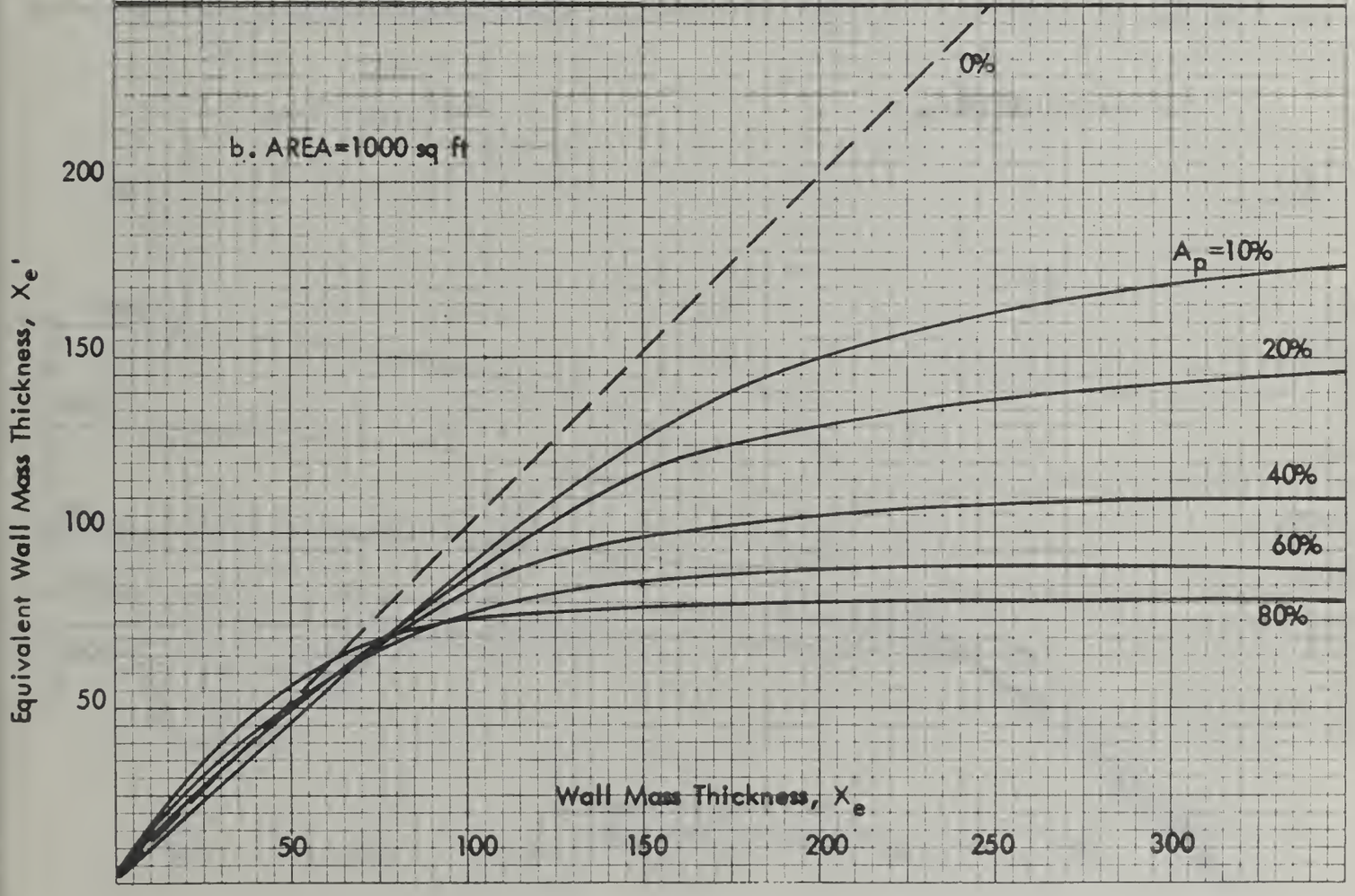

Figure 10. CORRECTION TO X_e FOR WALL APERTURES-ABOVEGROUND

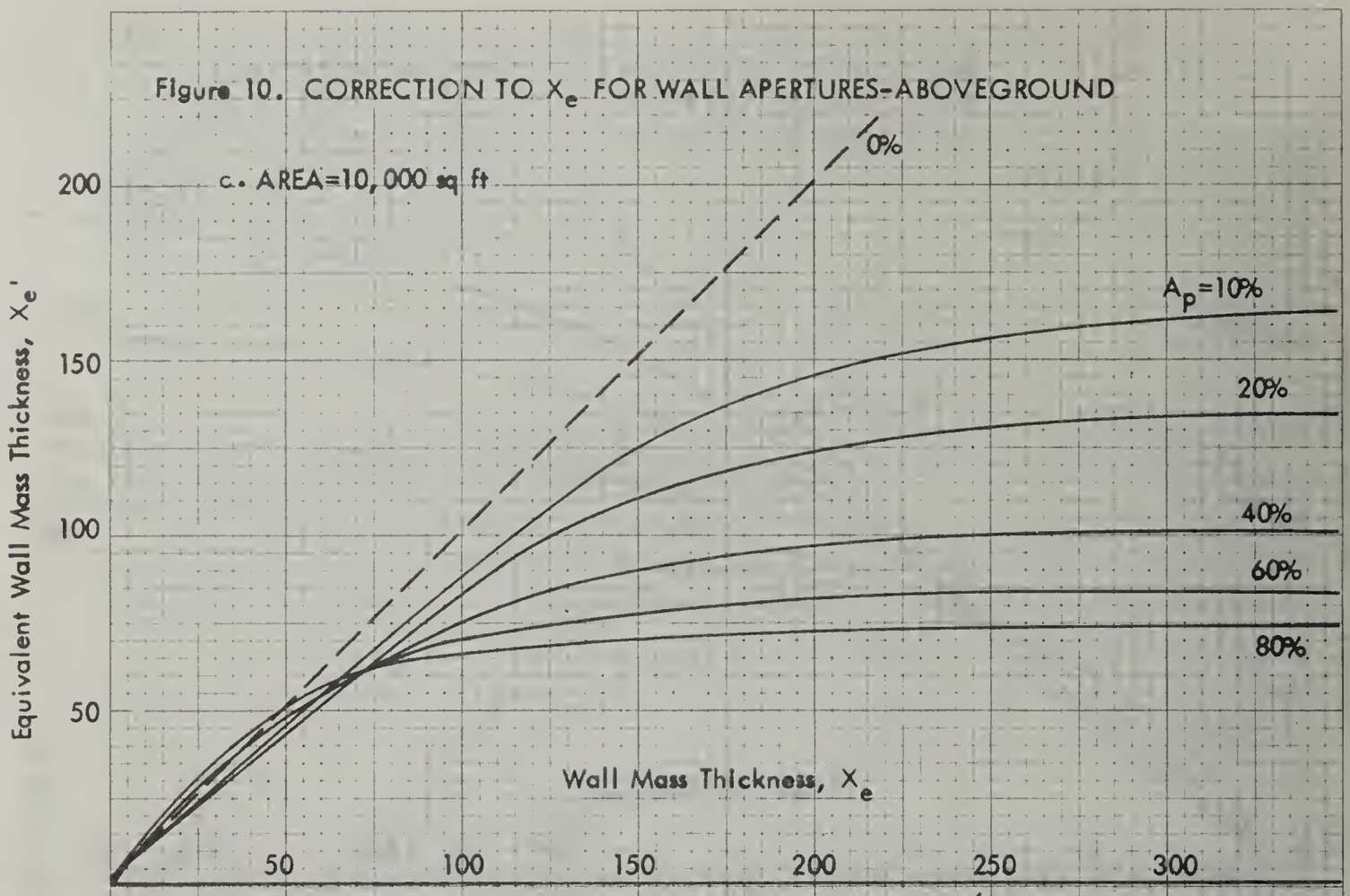

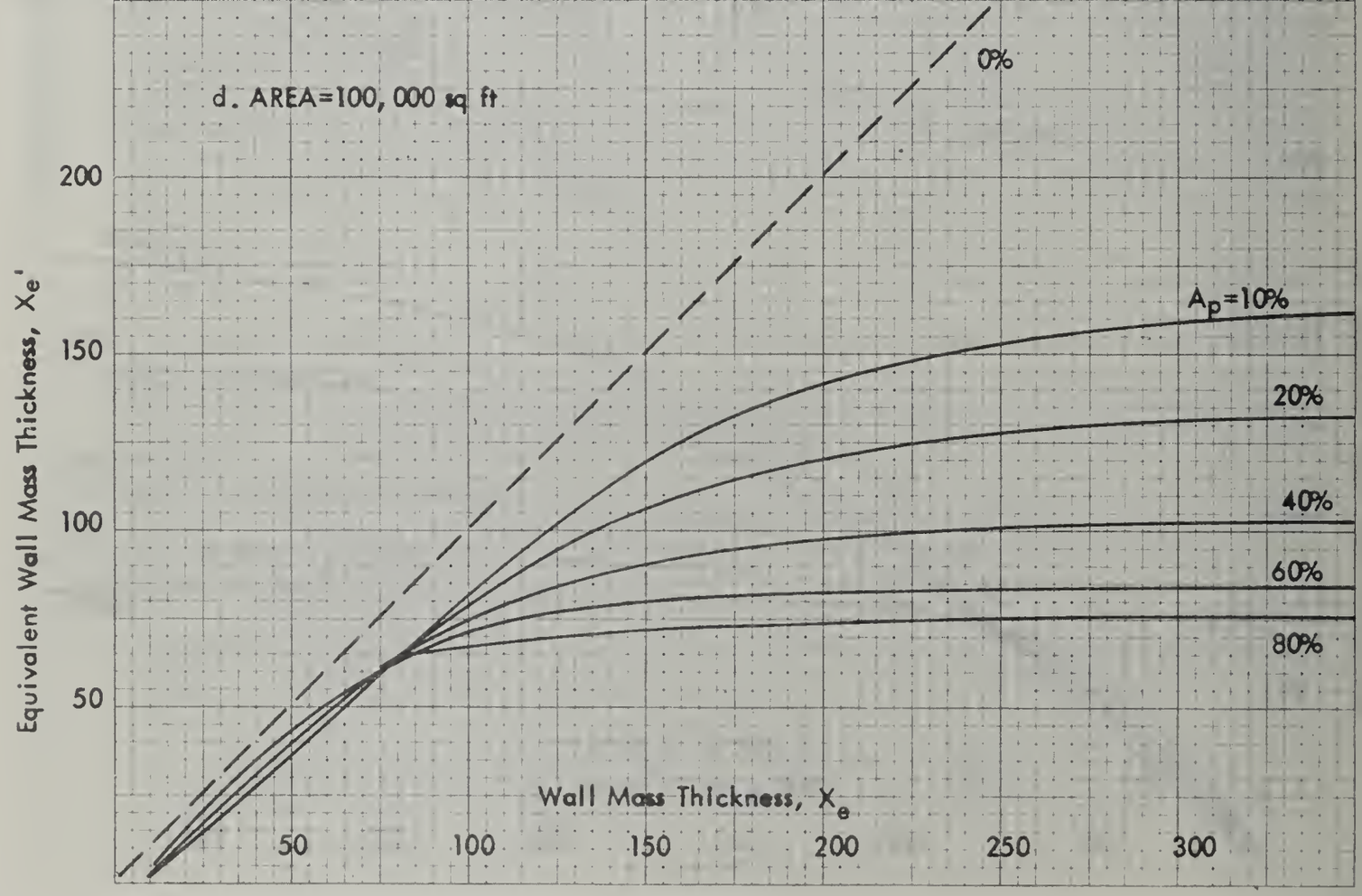

Figure 11. CORRECTION TO X_e FOR WALL APERTURES-BASEMENT

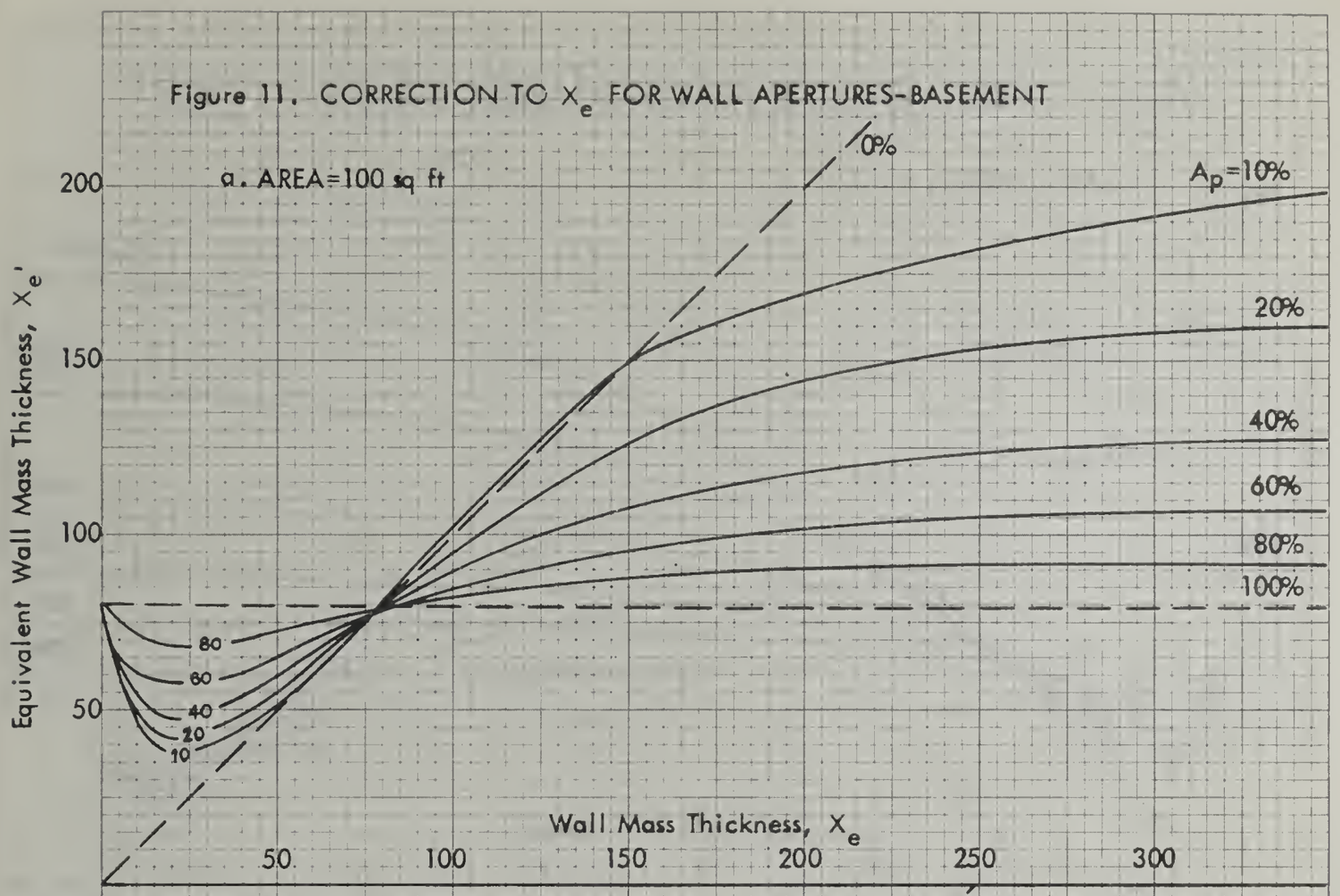

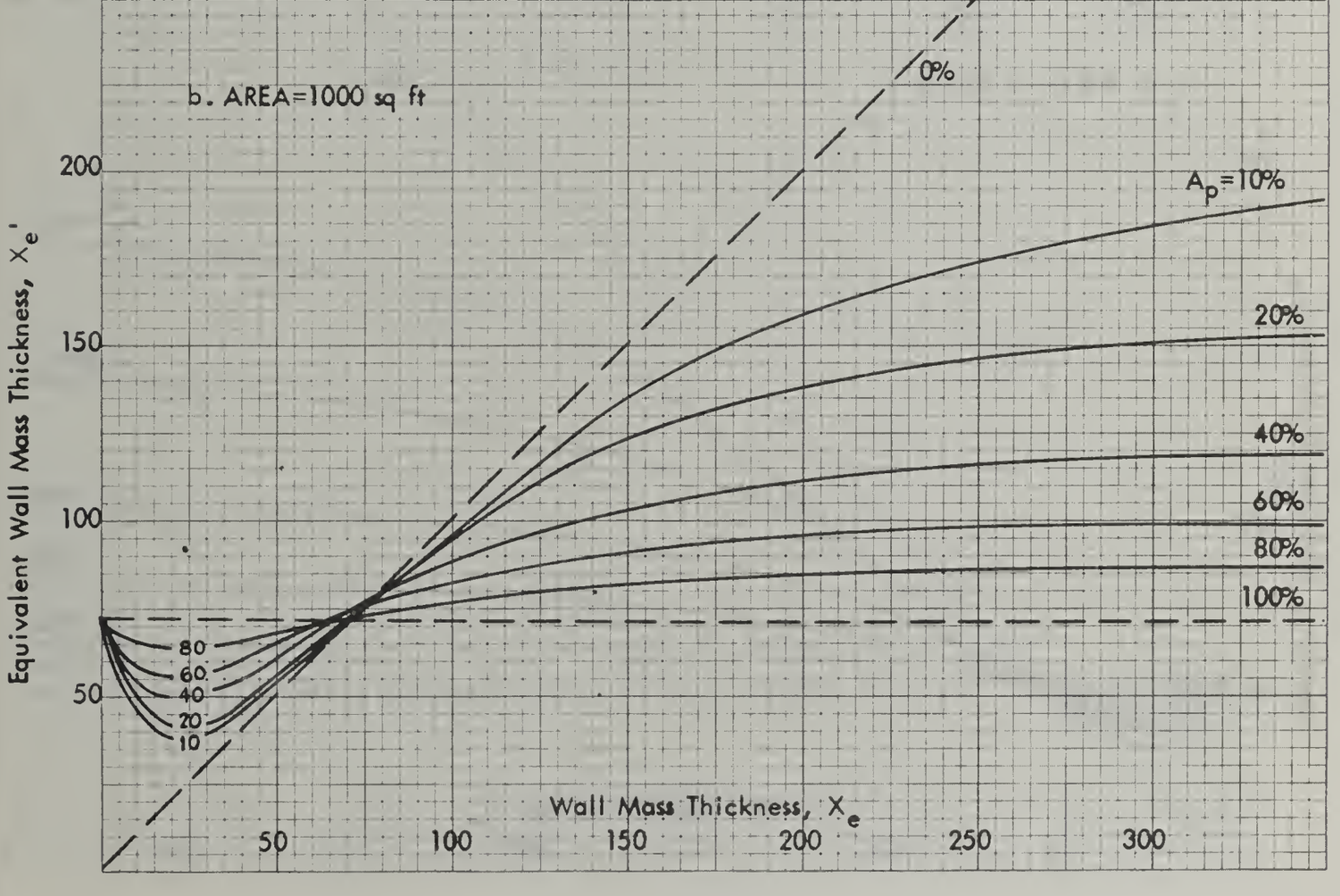

Figure 11. CORRECTION TO X_e FOR WALL APERTURES-BASEMENT

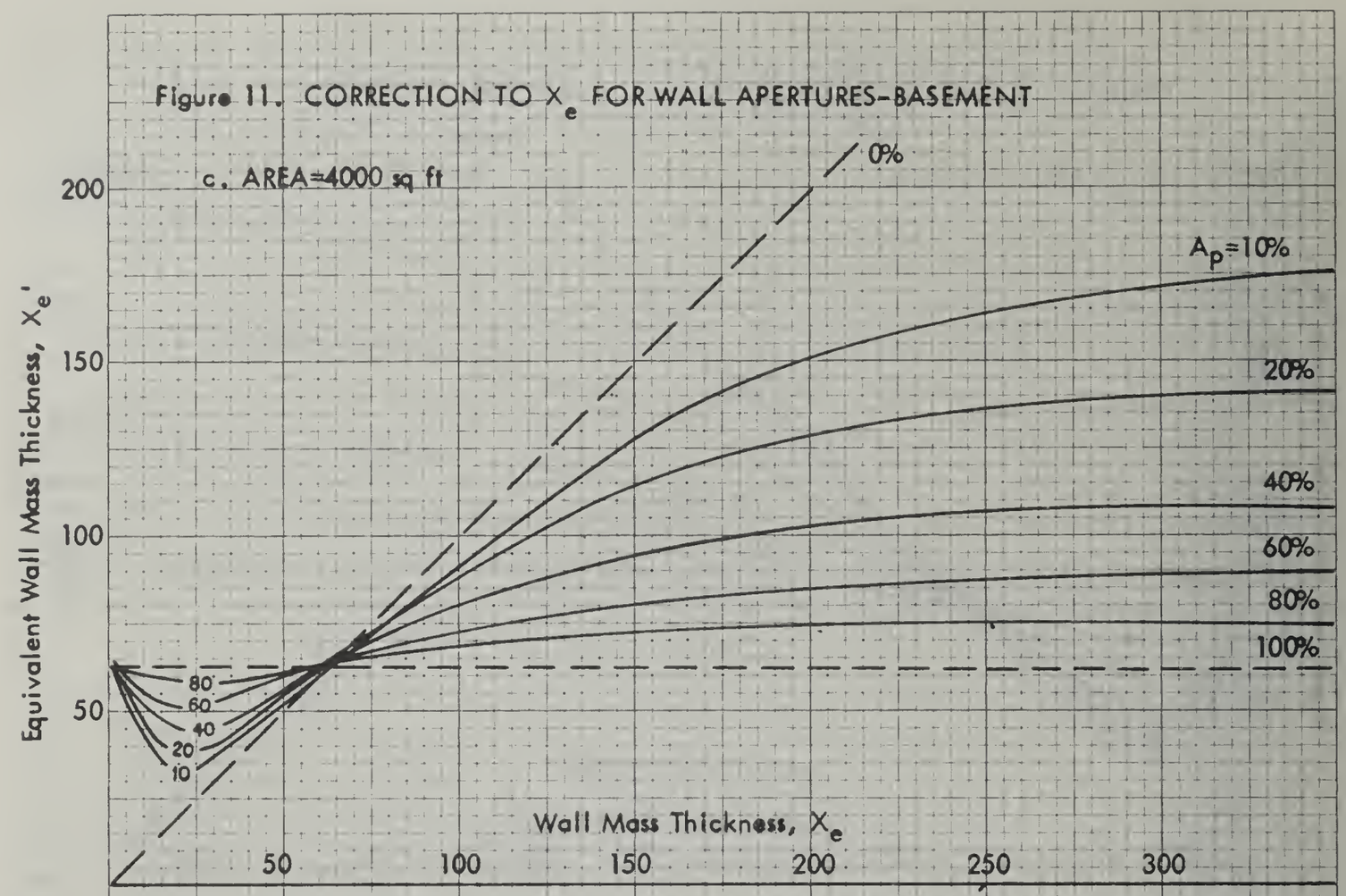

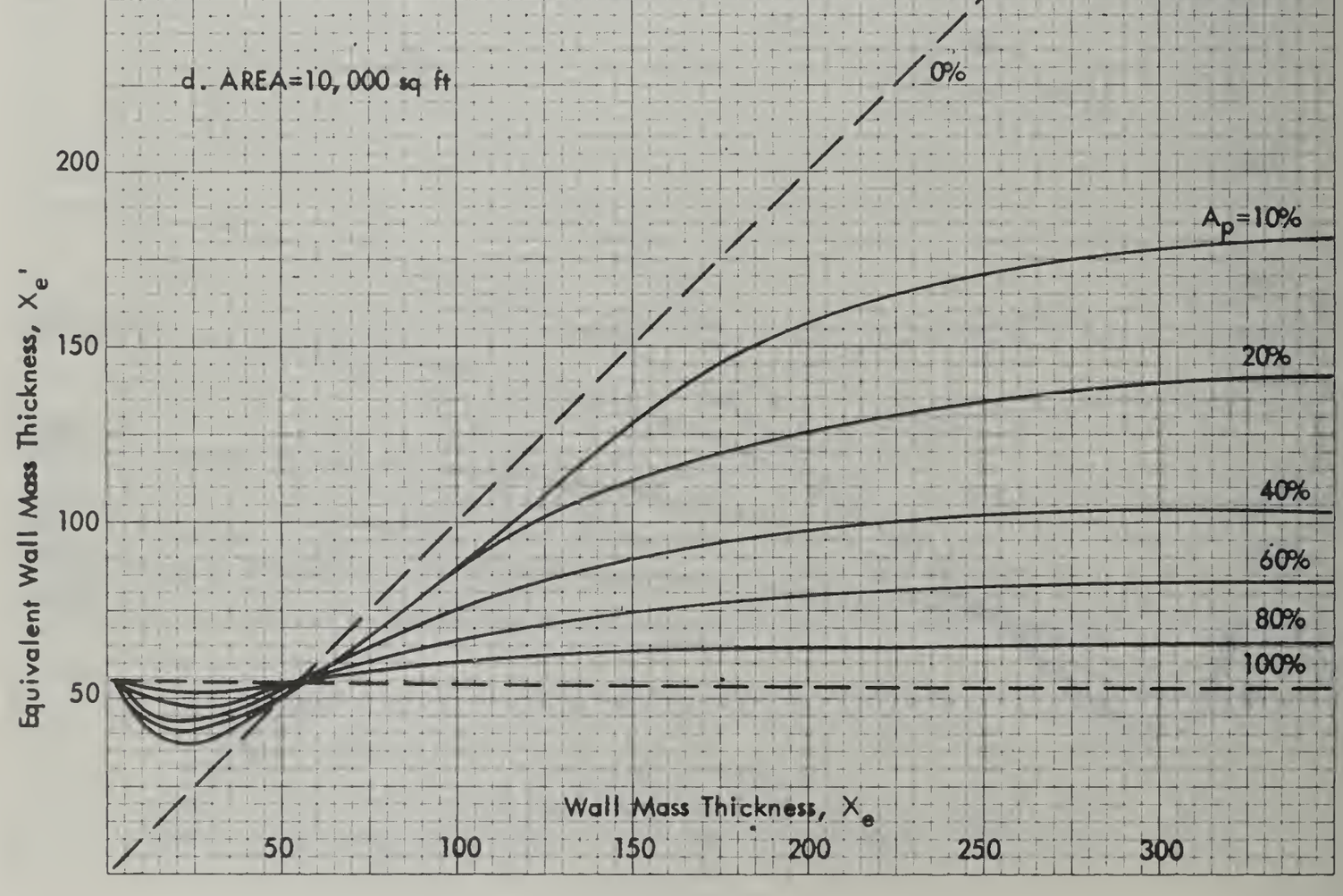

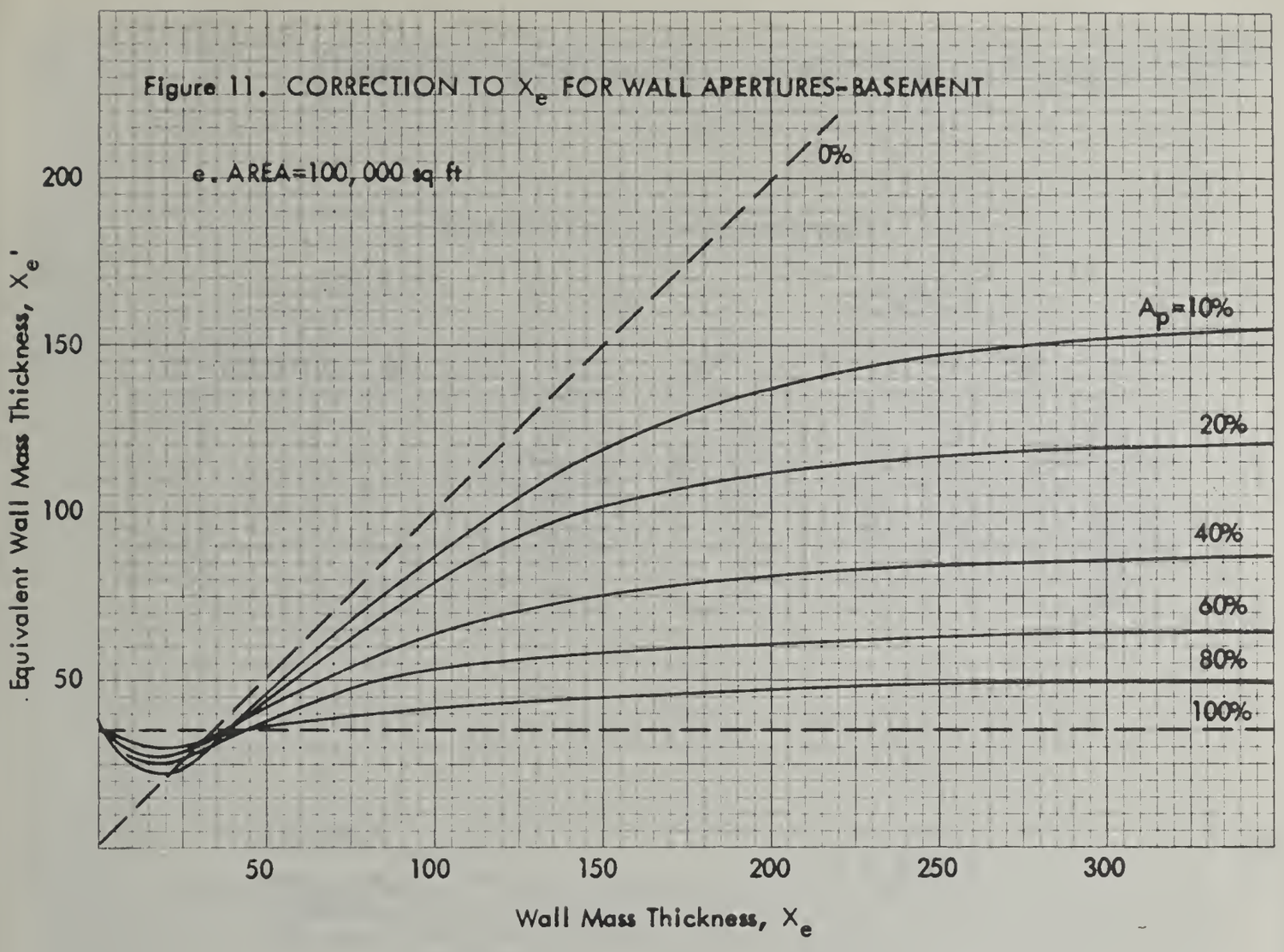
Figure 11. CORRECTION TO X_e FOR WALL APERTURES-BASEMENT
e. AREA=100,000 sq ft
0%
A_p=10%
20%
40%
60%
80%
100%
200
150
100
50
50
100
150
200
250
300
Equivalent Wall Mass Thickness, X_e'
Wall Mass Thickness, X_e

Figure 12. CORRECTION TO X_w FOR HEIGHT OF DETECTOR, H

ADD VALUES TO CURVES BELOW

For X_e=0

HEIGHT	A=	100	1000	10,000	100,000
	20	6	14	28	53
	40	10	21	38	51
	60	11	29	42	49
	80	10	33	43	47
	100	10	36	45	47
	150	10	42	46	47
	200	9	45	49	47

For X_e=25

HEIGHT	A=	100	1000	10,000	100,000
	20	0	3	5	10
	40	5	5	6	11
	60	6	8	6	12
	80	7	9	6	11
	100	5	9	6	12
	150	4	8	6	10
	200	0	5	6	10

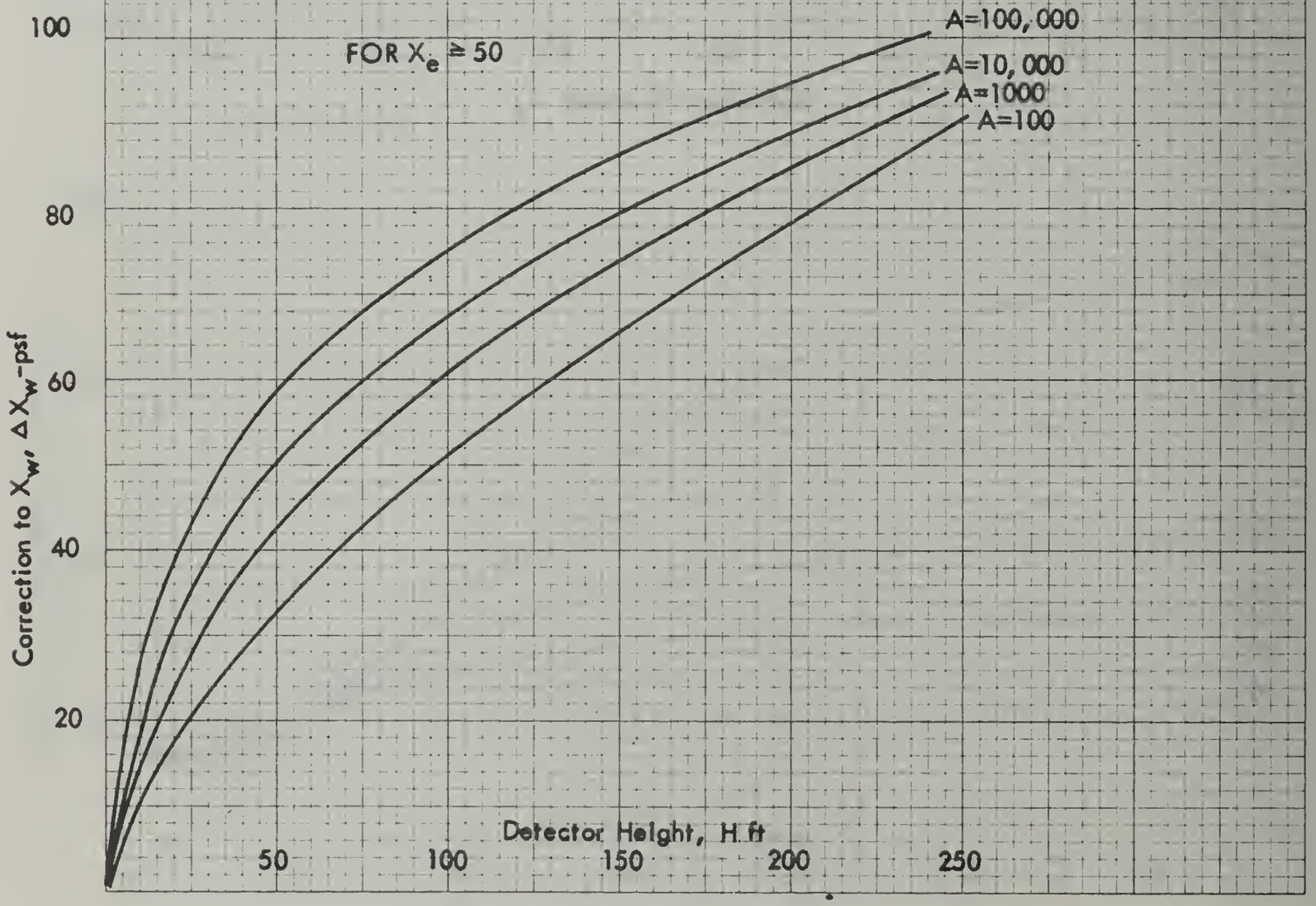

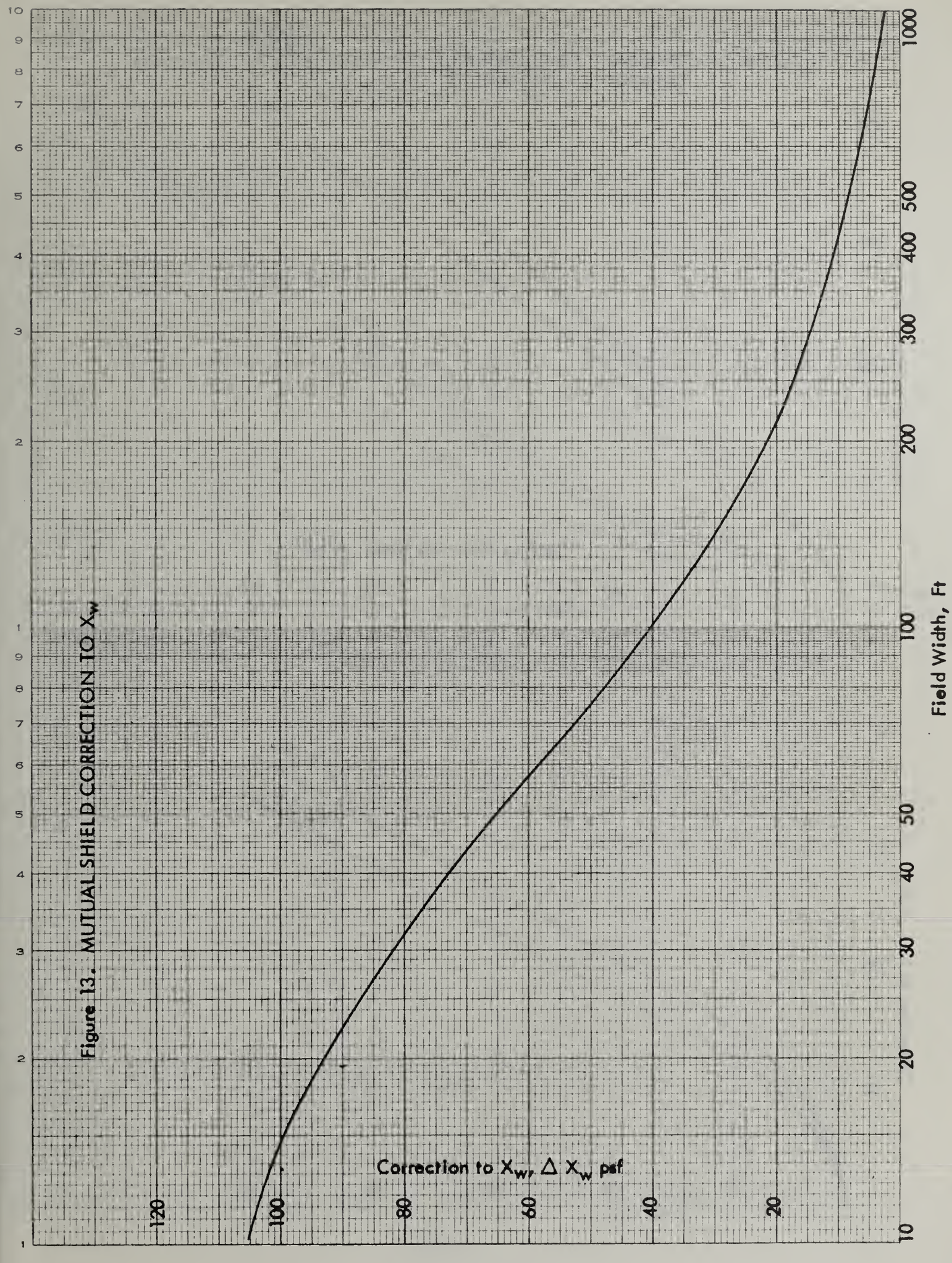

Figure 13. MUTUAL SHIELD CORRECTION TO X_w

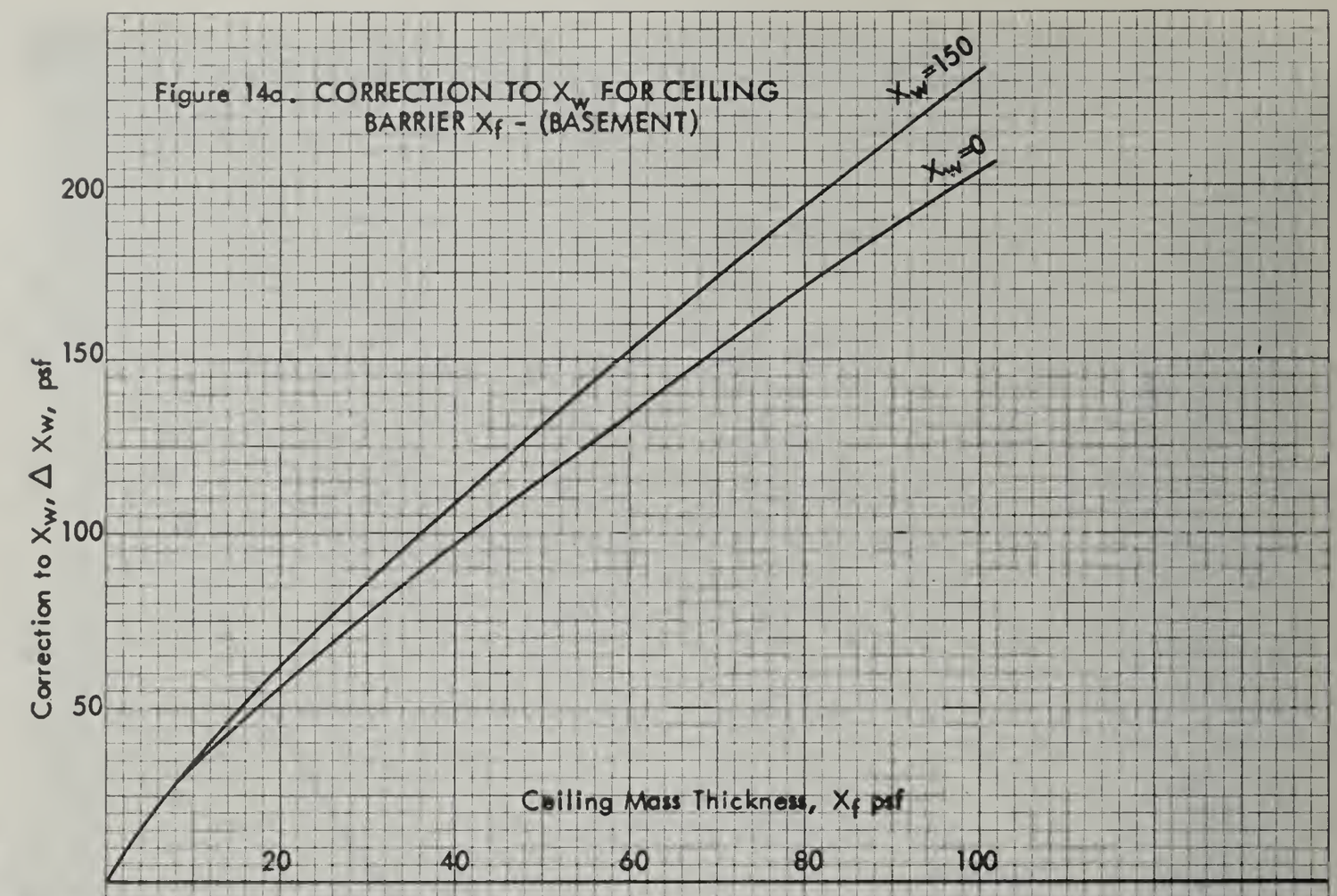

Figure 14a. CORRECTION TO X_w FOR CEILING BARRIER X_f - (BASEMENT)

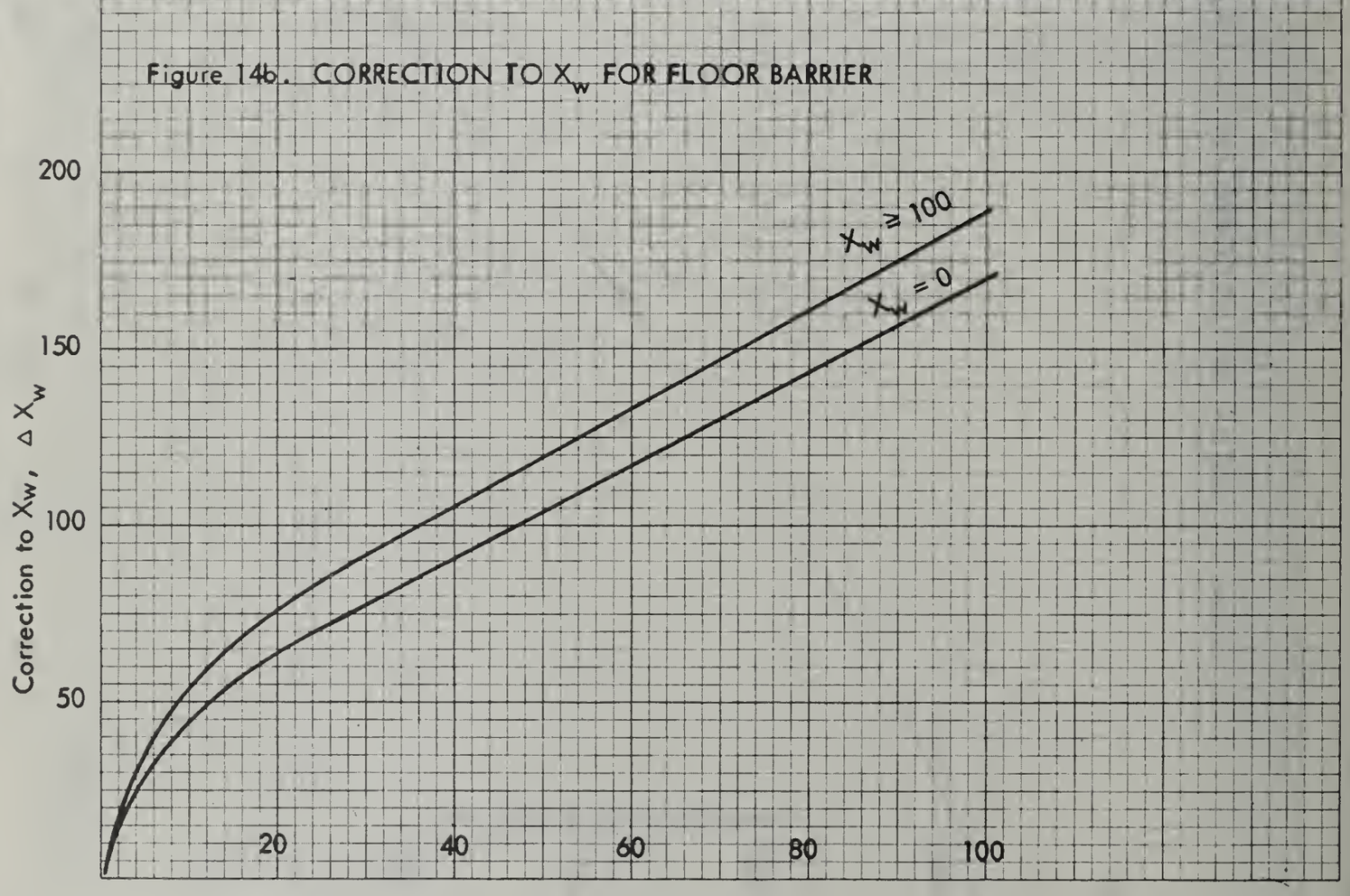

Figure 14b. CORRECTION TO X_w FOR FLOOR BARRIER

Figure 15. CORRECTION TO X_w FOR EXPOSED BASEMENT WALLS - USE WITH ABOVEGROUND PF CHARTS

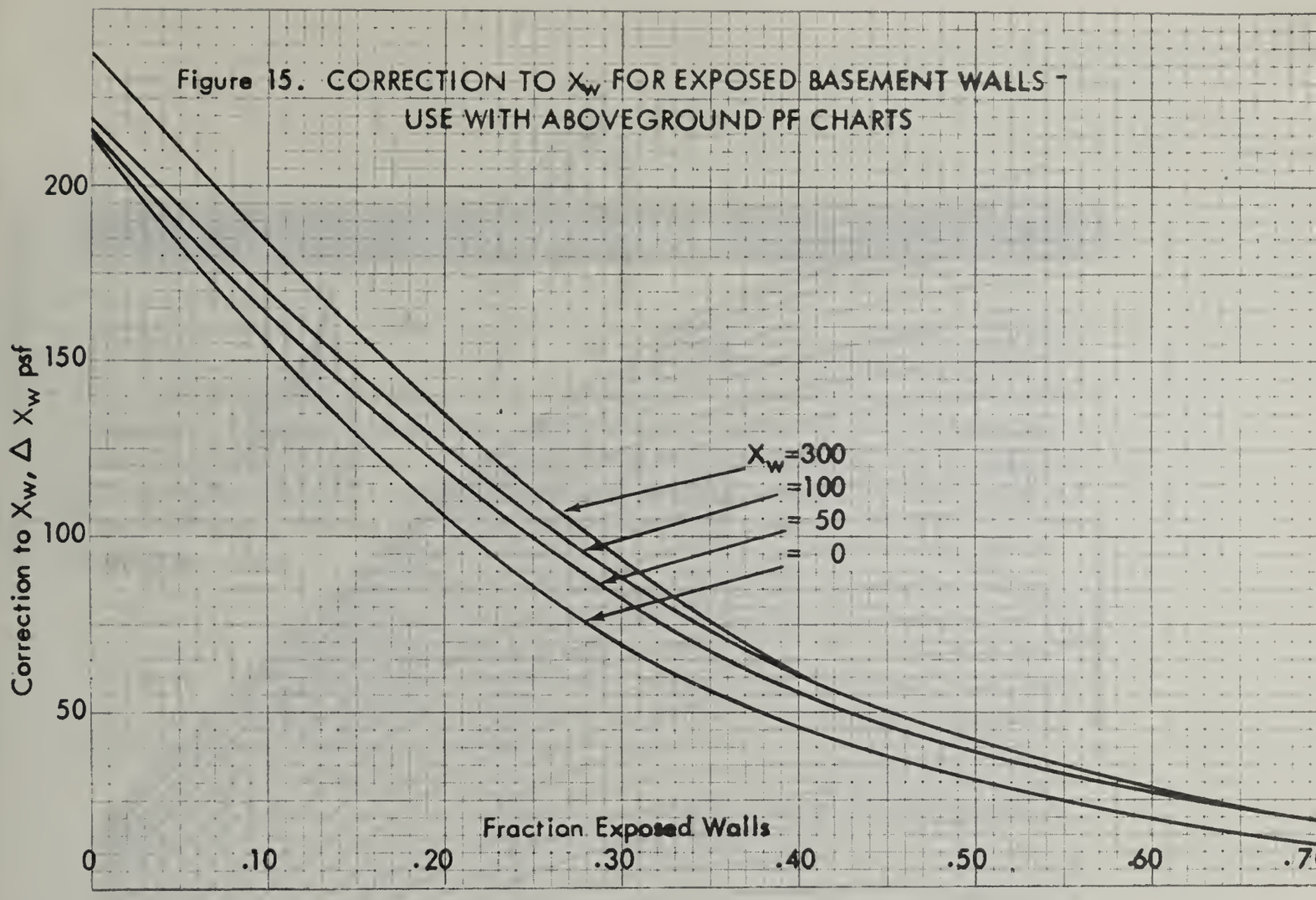

Figure 16

Chart 1. EQUIVALENT ROOF MASS THICKNESS (Revision #1 Feb 1964)

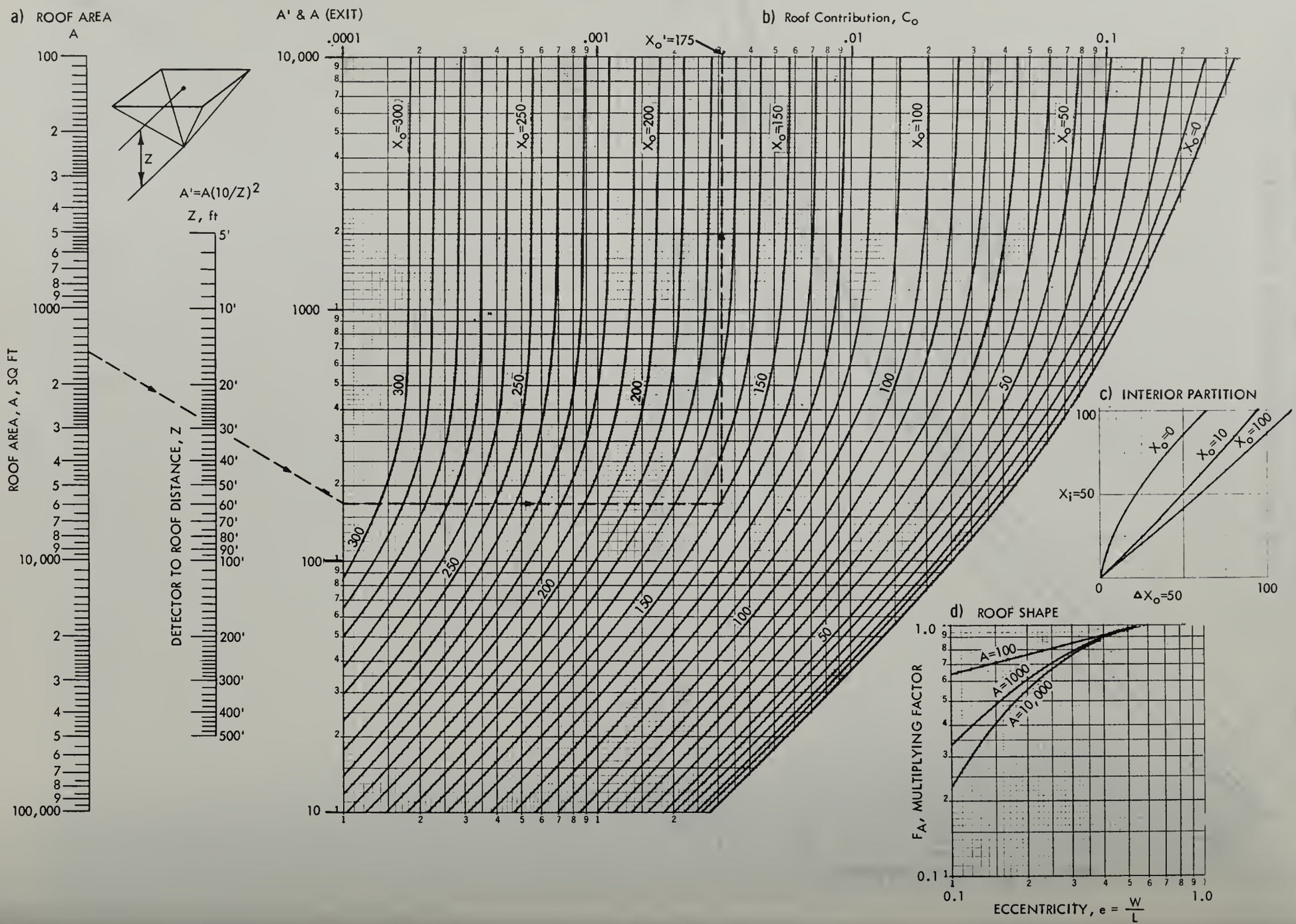

SAMPLE PROBLEMS

The Equivalent Building Method will be demonstrated by a number of typical examples. Most of these problems have been worked out in other publications by the Engineering Manual. Where this is the case, the answers will be compared. The notation (EM=25) means: Engineering Manual method protection factor is 25. Several design problems are worked out indicating the use of this method for such problems.

These sample problems are organized as follows: (1) Descriptions of the 14 problems, (2) solution of problems 1–8, (3) quick estimates for the complex problems 9–14, and (4) complete solutions for problems 9–14.

When possible for short problems, one solution form has been used for more than one problem to conserve space. All problems are worked out "long hand" to differentiate solution form from solution.

Sample Problems

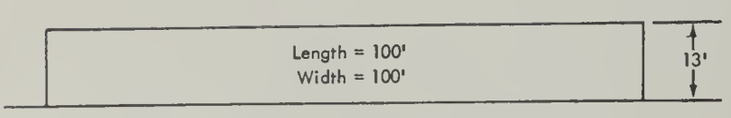

Sketch for examples 1–4

1. *Aboveground Windowless:* Xw=100 psf,
   Xo=150 psf,
   Pf=?

2. *Required Wall Thickness:* With Xo=150 psf, what Xw is required for a protection factor of 100?

3. *Economic Design Analysis:* What is the most economical roof and wall thickness assuming that roof concrete cost $100/cu yd and wall concrete $75/cu yd? Assume concrete weighs 4,000 lbs per cu yd. Find the best combination for a Pf of 100 and a Pf of 1,000. (Use a wall height of 10 ft for this problem.)

4. *Aboveground With Windows:* With windows as sketched below, what is the protection factor when Xw=210 psf and Xo=140 psf?

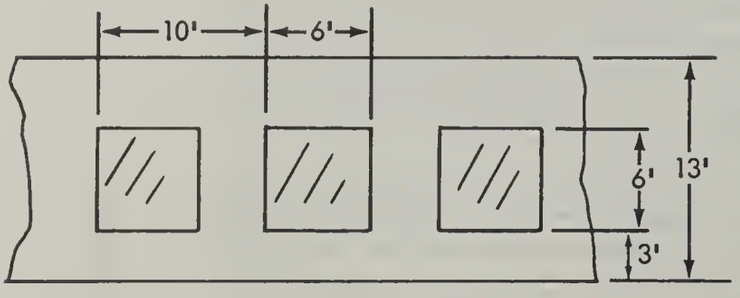

Sketch for problem 4

5. *Aboveground-Intermediate Area:* Same sketch as above except Width=60′. What is protection factor when Xw=200 psf and Xo=150 psf?

6. *Basement-Windowless Ground Floor:* What is the protection factor for the following building?
   Length=110′ Width=90′
   Xw=70 psf Xr=100 psf Xf=50 psf

7. *Basement With Exposed Walls:* What is the protection factor for the following building?
   Length=100′ Width=50′
   Xw=100 psf Xr=100 psf Xf=60 psf

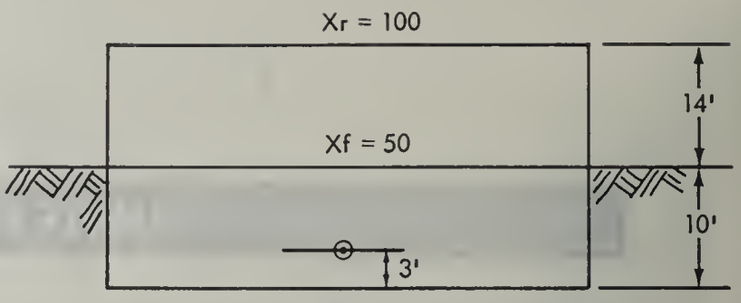

Sketch for problem 6

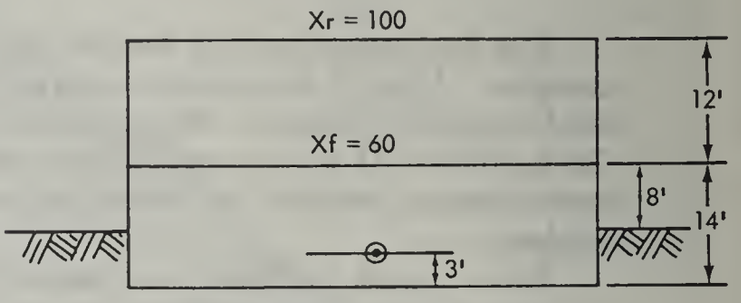

Sketch for problem 7

8. *Basement With Windows on Ground Floor:* Same building as Problem 6 but with windows on the ground floor. The aperture fraction is 0.80. What is the protection factor for the basement?

9. *Building With Core:* What is the protection factor at the center of the core?
   Xe=100 psf Xi=40 psf Xo=80 psf

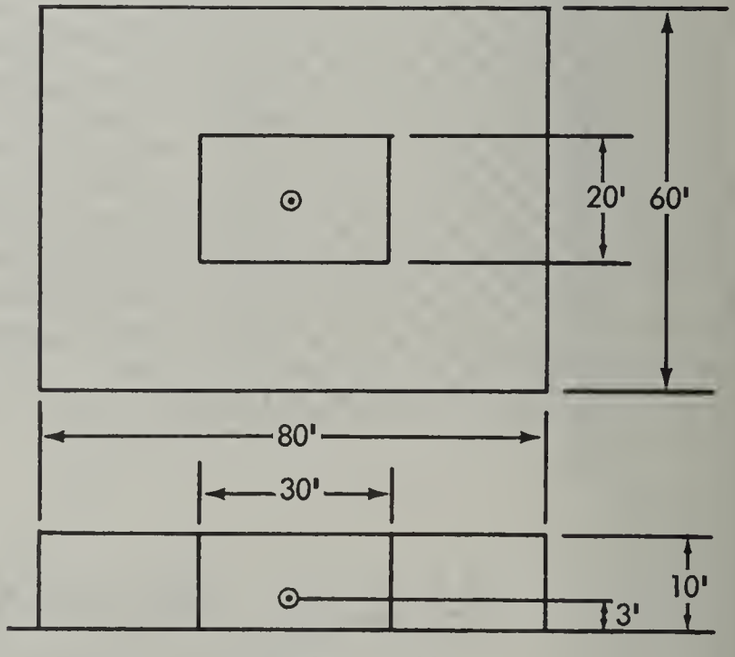

Sketch for problem 9

10. *Mutual Shield:* What is the Pf on the upper floor?

Xe=60 psf Xo=100 psf Xf=40 psf

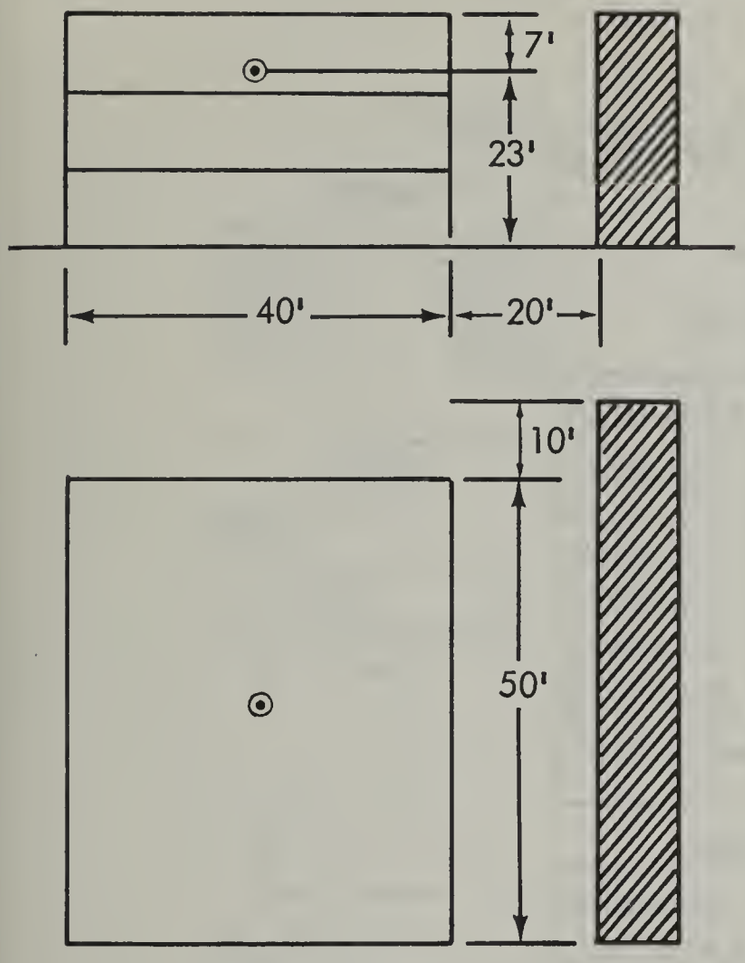

Sketch for problem 10

11. *Upper Story-Windowless:* What is protection factor at location indicated?

Length=100′ Width=75′

Xe=80 psf Xr=90 psf Xf=60 psf

(all floors)

12. *Upper Story With Windows:* Same as Problem 11 except Aperture fraction is 0.40. What is protection factor at same location?

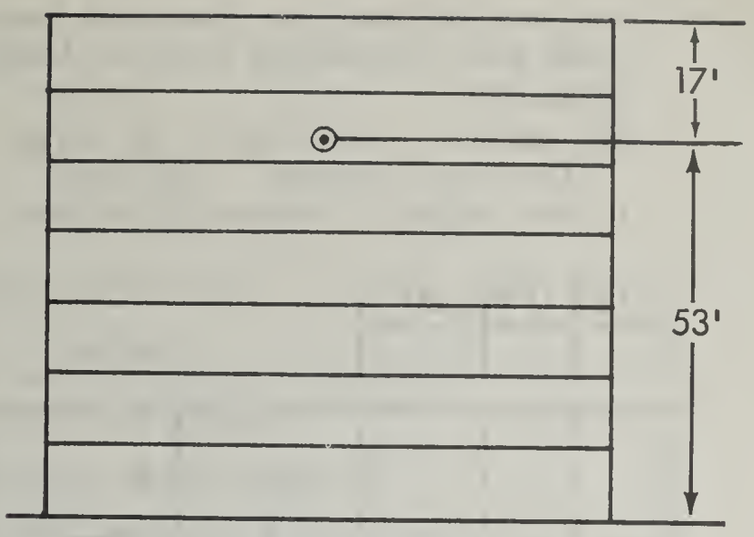

Sketch for problem 11

13. *Complex Building With L-Wing:* What is protection factor for location indicated?

Xe=55 psf Xr=60 psf

Xf=75 psf Xd=0 psf Ap=0.15

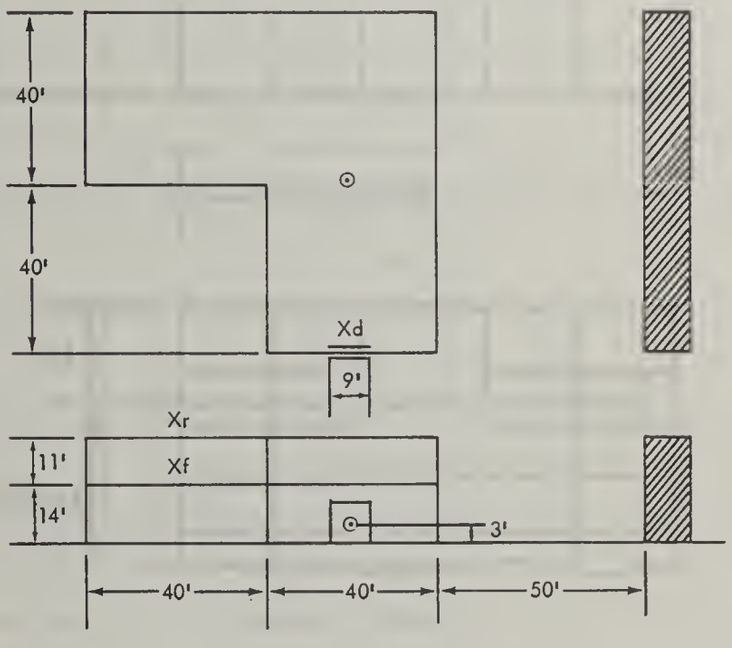

Sketch for problem 13

14. *Complex Building-Upper Story With Interior Well:* What is protection factor for location indicated?

Xe=100 psf Xi=50 psf Xr=50 psf
Xf=75 psf (all floors) Ap=0.36
10′ floor heights Detector 3′ from floor

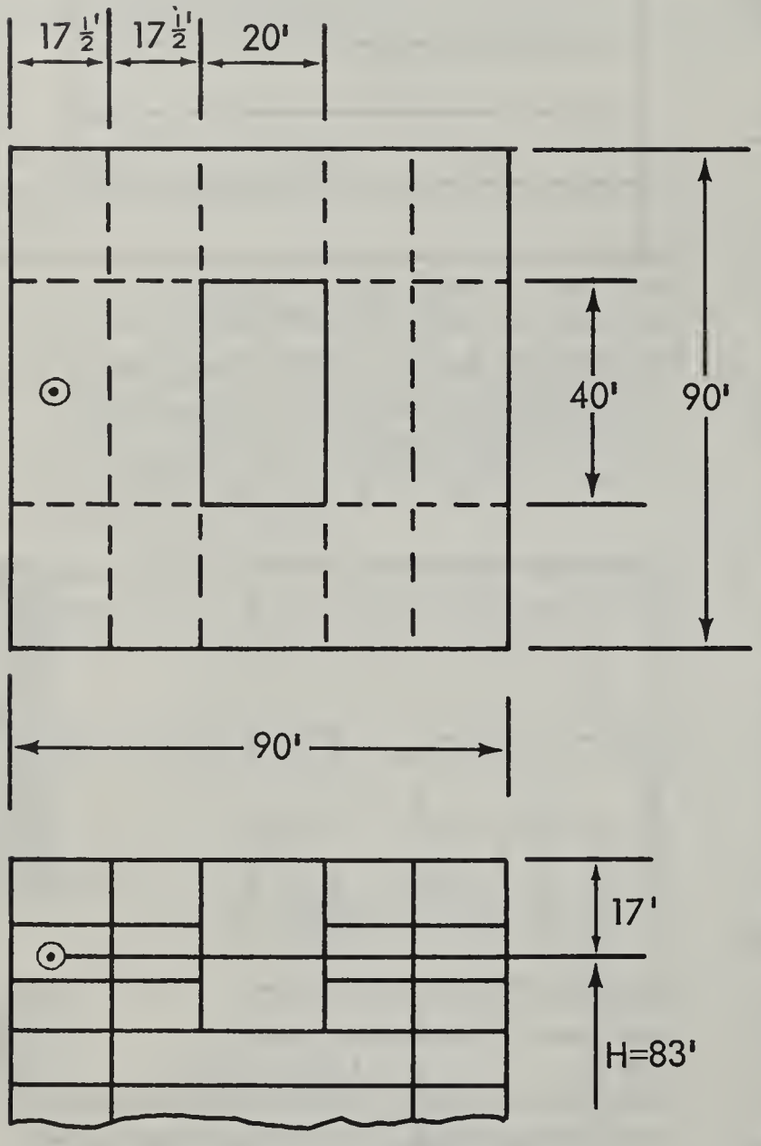

Sketch for problem 14

PROBLEMS #1 & 2

EQUIVALENT BUILDING METHOD SOLUTION FORM

PROBLEMS #1 + 2

PARAMETERS

W= 100	L= 100	A= 10,000
Wc= —	Lc= —	Ac= —
Z= 10		A'= 10,000
H= 3		Ac'= —
Ap= 0		Xo= 150
Ms= —		Xe= 100
		Xi= —

EQUATIONS

$$Xw' = Xe'(Ap) + Xi + \sum \Delta Xw$$

$$Xo' = Xo(A,Z) + \Delta Xo(Xi)$$

SKETCH

Prob #1.

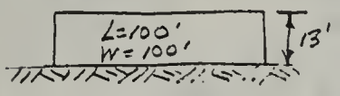

A = 10,000

A' = 10,000

X_W = 100 psf

X_o = 150 psf

P_f = 31 ANS

Prob #2.

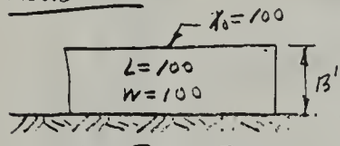

X_W = ? for P_f = 100

X_W = 185 psf ANS

EQUIVALENT WALL MASS THICKNESS Xw'

Foctor	Fig.	Sector #1 (Prob #1)	Sector #2	Sector #3 (Prob #2)	Sector #4
Xe'(Ap)	10, 11	100		?	
Xi	--	—			
ΔXw(A,H)	12	—			
ΔXw(Ms)	13	—			
ΔXw(FC)	1	—			
* ΔXw(Xf)	14	—			
* ΔXw(Ex)	15	—			
Xw'		100		?	

EQUIVALENT ROOF MASS THICKNESS Xw'

Co(A', Xo+ΔXo)				
-Co(Ac', Xo+ΔXo)				
Co(Periphery)				
+Co(Ac', Xo)(Core)				
Co(Totol Roof)				
Area=				
Xo'=	150		150	
P_f =	31		100	

* For Basement Cose

Problem No. 3 Solution:

This problem asks that we obtain the most economical combination of roof and wall mass thickness. First we write a cost equation.

$$\text{Cost} = (\$75\ \text{AwXw} + \$100\ \text{ArXo})/4{,}000$$
$$= \$75\ \text{Xw} + \$250\ \text{Xo}.$$

Since the building area is 10,000 sq ft we can use figure 3. For intermediate areas, simple interpolation is possible. At the horizontal line for Pf 100 and Pf 1,000, list the combinations of Xw and Xo which are possible. Then construct a cost table to determine the minimum cost.

Xw	*Xo*	*Cw*	*Cr*	*Ctot*
145	250	10, 900	62, 500	73, 400
153	200	11, 500	50, 200	61, 500
165	175	12, 400	43, 700	58, 100
173	160	13, 000	40, 000	53, 000
185	150	13, 900	37, 500	51, 400
210	140	15, 800	35, 000	50, 800*
232	135	17, 400	33, 700	51, 100
297	130	22, 300	32, 500	54, 800

*Minimum.

For part (a) then, the answer would be: *Xw=210, Xo=140*.

The same procedure is used for the Pf 1,000 case:

Xw	*Xo*	*Cw*	*Cr*	*Ctot*
265	300	19, 900	75, 000	94, 900
272	275	20, 400	68, 700	89, 100
283	260	21, 200	65, 000	86, 200
295	250	22, 100	62, 500	84, 600
315	240	23, 600	59, 000	82, 600*
350	232	26, 200	58, 000	84, 200

*Minimum.

For part (b), the answer would be: *Xw=315, Xo=240*.

PROBLEMS #4 & 5

EQUIVALENT BUILDING METHOD SOLUTION FORM

PROBLEMS #4 & 5

PARAMETERS

W= ____ L= ____ A= ____
Wc= ____ Lc= ____ Ac= ____
Z= ____ A'= ____
H= ____ Ac'= ____
Ap= ____ Xo= ____
Ms= ____ Xe= ____
Xi= ____

EQUATIONS

$Xw' = Xe'(Ap) + Xi + \sum \Delta Xw$

$Xo' = Xo(A,Z) + \Delta Xo(Xi)$

SKETCH

PROB #4

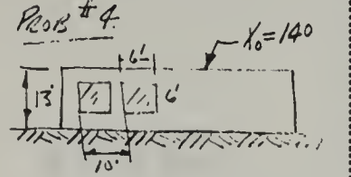

$A = 100 \times 100 = 10{,}000$

$Ap = \frac{6 \times 6}{10 \times 13} \times 100 = 28\%$

$Xc = 210$

$Pf = 34$ ANS

PROB #5:

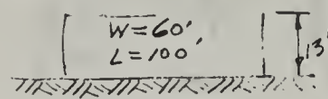

$Xw = 200$,
$Xo = 150$

$Pf = 100$ ANS

EQUIVALENT WALL MASS THICKNESS Xw'

PROB #4 PROB #5

Factor	Fig.	Sector #1	Sector #2	Sector #3	Sector #4
Xe'(Ap)	10, 11	112		200	
Xi	--				
ΔXw(A,H)	12				
ΔXw(Ms)	13				
ΔXw(FC)	1				
*ΔXw(Xf)	14				
*ΔXw(Ex)	15				
Xw'		112		200	

EQUIVALENT ROOF MASS THICKNESS Xw'

Co(A', Xo+ΔXo)				
-Co(Ac', Xo+ΔXo)				
Co(Periphery)				
+Co(Ac', Xo)(Core)				
Co(Total Roof)				
Area=				
Xo'=	140		150	

Pf = 34 Pf = 86 A = 1000
Pf = 112 A = 10,000
Pf = 100 A = 6,000

* For Basement Case

PROBLEM #6

EQUIVALENT BUILDING METHOD SOLUTION FORM

PROBLEM #6

PARAMETERS

W= 90 L= 110 A= 9900
Wc= ____ Lc= ____ Ac= ____
Z= 21 A'= 2250
H= ____ Ac'= ____
Ap= ____ Xo= 150
Ms= ____ Xe= 70
Xi= ____

EQUATIONS

$Xw' = Xe'(Ap) + Xi + \sum \Delta Xw$

$Xo' = Xo(A,Z) + \Delta Xo(Xi)$

SKETCH

PROB. #6. (USING RECONTROL)

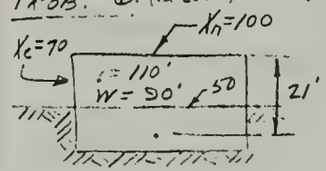

$A = 110 \times 90 = 9900$

$A' = 9900\left(\frac{10}{21}\right)^2 = 2250$

$A_B = 9900\left(\frac{10}{11}\right)^2 = 3400$

$Pf = 138$ ANS (Fig 5)

PROB. #6 (USING ABOVE GROUND)

NOTE WE NOW CORRECT FOR FC FROM TABLE II AND USE ACTUAL AREA FOR ROOF Xo'

$Pf = 140$ ANS (Fig 3)

EQUIVALENT WALL MASS THICKNESS Xw'

PROB #6 PROB #6

Factor	Fig.	Sector #1	Sector #2	Sector #3	Sector #4
Xe'(Ap)	10, 11	70		70	
Xi	--	—		—	
ΔXw(A,H)	12	--		—	
ΔXw(Ms)	13	--		--	
ΔXw(FC)	I, II	--		47	
*ΔXw(Xf)	14	125		125	
*ΔXw(Ex)	15	—			
Xw'		195		242	

EQUIVALENT ROOF MASS THICKNESS Xw'

Co(A', Xo+ΔXo)	—		—	
-Co(Ac', Xo+ΔXo)	—		—	
Co(Periphery)	—		—	
+Co(Ac', Xo)(Core)	.0058		0058	
Co(Total Roof)	.0058		.0058	
Area= Ab =	3400		9900	
Xo'=	150		150	

Pf = 135 Pf = 140

* For Basement Case

III-47

PROBLEM #7

EQUIVALENT BUILDING METHOD SOLUTION FORM

PROBLEM #7

PARAMETERS

W= 50 L= 100 A= 5000
Wc= ____ Lc= ____ Ac= ____
Z= 23 A'= 946
H= ____ Ac'= ____
Ap= ____ Xo= 160
Ms= ____ Xe= 100
Xi= ____

EQUATIONS

$Xw' = Xe'(Ap) + Xi + \sum \Delta Xw$

$Xo' = Xo(A,Z) + \Delta Xo(Xi)$

SKETCH

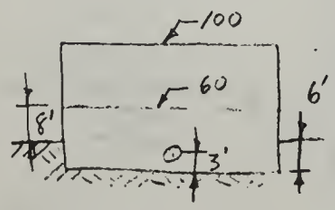

$Ex = 8/14 = .57$

$P_f = 44 \times \frac{1420}{1464}$

$P_f = 43$ ANS

EQUIVALENT WALL MASS THICKNESS Xw'

Pfo Pfu

Factor	Fig.	Sector #1	Sector #2	Sector #3	Sector #4
Xe'(Ap)	10 11	100	100		
Xi	--	—	—		
ΔXw(A,H)	12	—	—		
ΔXw(Ms)	13	—	—		
ΔXw(FC)	II		43		
* ΔXw(Xf)	14 a	—	145		
* ΔXw(Ex)	15	33			
Xw'		133	288		

EQUIVALENT ROOF MASS THICKNESS Xw'

Co(A', Xo+ΔXo)				
- Co(Ac', Xo+ΔXo)				
Co(Periphery)				
+ Co(Ac', Xo)(Core)				
Co(Total Roof)	.0043			
Area=	5000			
Xo'=	165	0		

A=1000 33 950
A=14000 57 2000

* For Basement Case
A= 5000 44 1420

III-48

PROBLEM #8

EQUIVALENT BUILDING METHOD SOLUTION FORM

PROB. #8

PARAMETERS

W= 90 L= 110 A= 9900
Wc= — Lc= — Ac= —
Z= 21 A'= 2250
H= — Ac'= —
Ap= 0.8 Xo= 150
Ms= — Xe= 70
Xi= —

EQUATIONS

$Xw' = Xe'(Ap) + Xi + \sum \Delta Xw$

$Xo' = Xo(A,Z) + \Delta Xo(Xi)$

SKETCH

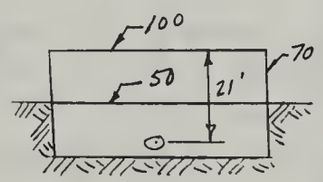

BELOWGROUND CHART
SECTOR #1 - COLUMN

$P_f = 130$ ANS (Fig. 8)

ABOVEGROUND CHART
SECTOR #2 - COLUMN

$P_f = 132$ ANS (Fig. 5)

EQUIVALENT WALL MASS THICKNESS Xw'

Pfo Pfu

Factor	Fig.	Sector #1	Sector #2	Sector #3	Sector #4
Xe'(Ap)	10 11	57	57		
Xi	--	—	—		
ΔXw(A,H)	12	—	—		
ΔXw(Ms)	13	—	—		
ΔXw(FC)	1	—	49		
* ΔXw(Xf)	14	125	125		
* ΔXw(Ex)	15	—	—		
Xw'		182	231		

EQUIVALENT ROOF MASS THICKNESS Xw'

Co(A', Xo+ΔXo)				
- Co(Ac', Xo+ΔXo)				
Co(Periphery)				
+ Co(Ac', Xo)(Core)				
Co(Total Roof)	.0058	0058		
Area= As	3400	[illegible]		
Xo'=	150	150		

P_f= 130 132

* For Basement Case

QUICK APPROXIMATE SOLUTIONS FOR PROBLEMS 9-14

Problem No. 9. Core Building

1. Use approximate area of 5,000 vs actual 4,800.
2. Use actual roof and wall thicknesses with no corrections.
3. Use Pf halfway between 1,000 and 10,000 sq ft charts.

Xw=140; Xo=80; For A=1,000 Pf=20
For A=10,000 Pf=25
For A=5,000 Pf=22 ANS (EM=22)

Problem No. 10. Mutual Shield.

1. Use A=1,000 in lieu of actual A=2,000.
2. Neglect effect of mutual shield since it affects only part of one wall.
3. For min Pf assume ground floor conditions:

Xw=60; Xo=100; Pf(min)=6.5

4. For max Pf assume infinite wall thickness:

Pf(max)=55

5. For estimate between min and max correct for height: H=23′, add 20 psf for Xw′=80

Pf(est)=10 (EM=12)

Problem No. 11. Upper Story Building-Windowless

1. Use approximate area of 10,000 vs actual 7,500.
2. For min Pf assume ground floor conditions:

Xw=80; Xo=150; Pf(min)=21

3. For max Pf assume infinite wall thickness:

Pf(max)=165

4. Correct for height. Add 50 pf for H=53′; Xw′=130

Pf(est)=50 (EM=43)

Problem No. 12. Upper Story Building-Windows

1. Use approximate area of 10,000 vs actual 7,500.
2. For minimum Pf assume ground floor conditions and correct for windows.

Xw′=80×0.6=48; Xo=150; Pf(min)=11

3. Max Pf: Pf(max)=165
4. Correct for height; H=53′, Xw′=48+50=98

Pf(est)=31 (EM=35)

Problem No. 13. Complex Building with L-Wing.

1. Neglect contribution from west wing.
2. Use area of remaining building for base, 3,200 sq ft.
3. Use actual wall and roof weights.
4. Neglect effect of door and mutual shield; they tend to compensate for each other.

Xw=55; Xo=135; For A=1,000; Pf= 6
For A=10,000; Pf=11
For A= 3,200; Pf= 8 (EM=7)

Problem No. 14. Complex Building with Interior Well;

1. Estimate minimum and maximum Pfs.
2. For min Pf assume ground floor conditions and include effect of windows:

Xw=100×0.54= 54; Xo′=125; Pf(min)=11

3. Max Pf: Pf(max)=95
4. Correct for height, H=83; 50+(8−50)/4=57
5. For wall without interior partitions, Xw′=54+57=111

For A=10,000; Pf=31

6. For walls with interior partitions, Xw′=111+50=161 Pf=52
7. Approximately 1/4 of walls have Pf=31 and 3/4 have Pf=52: combine, Pf=31/4+52(3/4)=47 (EM=47)

PROBLEM #9

EQUIVALENT BUILDING METHOD SOLUTION FORM

PROBLEM #9

PARAMETERS

W= 60 L= 80 A= 4800
Wc= 20 Lc= 30 Ac= 600
Z= 7' A'= 9800
H= 3' Ac'= 1220
Ap= 0 Xo= 80
Ms= — Xe= 100
Xi= 40

EQUATIONS

$Xw' = Xe'(Ap) + Xi + \sum \Delta Xw$

$Xo' = Xo(A,Z) + \Delta Xo(Xi)$

EQUIVALENT WALL MASS THICKNESS Xw'

Foctor	Fig.	Sector #1	Sector #2	Sector #3	Sector #4
Xe'(Ap)	10 11	100			
Xi	--	40			
ΔXw(A,H)	12	—			
ΔXw(Ms)	13	—			
ΔXw(FC)	1	—			
* ΔXw(Xf)	14	—			
* ΔXw(Ex)	15	—			
Xw'		140			

SKETCH

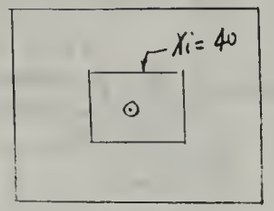

$Xop = Xo + \Delta Xo(Xi)$
$= 80 + 47 = 127$

A=1000, P_f = 20

A=10,000, P_f = 25

$P_f = 20 + 5\left(\frac{3800}{9000}\right)$

P_f = 22 ANS (EM=22)

EQUIVALENT ROOF MASS THICKNESS Xw'

Co(A', Xo+ΔXo) (9800, 127)	.0105				
-Co(Ac', Xo+ΔXo) (1220, 127)	.0100				
Co(Periphery)	.0005				
+Co(Ac', Xo)(Core) (1220, 80)	.031				
Co(Total Roof)	.0315				
Areo=	4800				
Xo'=	85				

* For Bosement Cose

PROBLEM #10

EQUIVALENT BUILDING METHOD SOLUTION FORM

PROBLEM #10

PARAMETERS

W= 40 L= 50 A= 2000
Wc= — Lc= — Ac= —
Z= 7' A'= 4100
H= 23' Ac'= —
Ap= — Xo= 100
Ms= 20' Xe= 60
Xi= 40

EQUATIONS

$Xw' = Xe'(Ap) + Xi + \sum \Delta Xw$

$Xo' = Xo(A,Z) + \Delta Xo(Xi)$

EQUIVALENT WALL MASS THICKNESS Xw'

Foctor	Fig.	P_{f_0} a=.203 Sector #1	P_{f_6} a=.203 Sector #2	P_{f_0} a=.797 Sector #3	P_{f_6} a=.797 Sector #4
Xe'(Ap)	10 11	60	60	60	60
Xi	--	—	—	—	—
ΔXw(A,H)	12	27	20	27	20
ΔXw(Ms)	13	93	93	0	0
ΔXw(FC)	1	—	17	—	17
* ΔXw(Xf)	14	—	97	—	97
* ΔXw(Ex)	15	—	—	—	—
Xw'		180	287	87	194

SKETCH

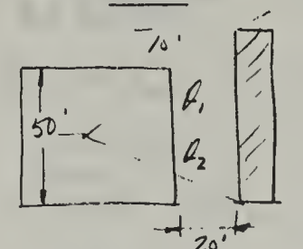

$\tan a_1 = \frac{35}{40} = .875$, $a_1 = 41°$

$\tan a_2 = \frac{25}{40} = .625$, $a_2 = 32°$

$a_1 = 73/360 = .203$

$P_f = \frac{.203}{35} + \frac{.797}{10.3}$

$= \frac{35 \times 10.3}{2.09 + 27.9}$

P_f = 12 ANS. (EM=12)

EQUIVALENT ROOF MASS THICKNESS Xw'

Co(A', Xo+ΔXo)				
-Co(Ac', Xo+ΔXo)				
Co(Periphery)				
+Co(Ac', Xo)(Core)				
Co(Totol Roof)				
Areo=				
Xo'=	100	∞	100	∞
Hic A=1000 P_f =	36	995	11	135

* For Bosement Case

35 10,3

PROBLEM #11

EQUIVALENT BUILDING METHOD SOLUTION FORM

PROBLEM #11

PARAMETERS

W= 75' L= 100 A= 7500
Wc= — Lc= — Ac= —
Z= 17' A'= 2600
H= 53' Ac'= —
Ap= — Xo= 150
Ms= — Xe= 80
Xi= —
Xf= 60

EQUATIONS

$Xw' = Xe'(Ap) + Xi + \sum \Delta Xw$

$Xo' = Xo(A,Z) + \Delta Xo(Xi)$

SKETCH

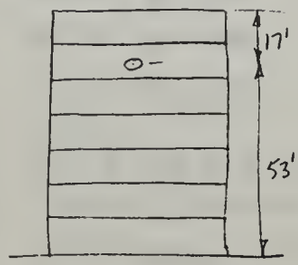

EQUIVALENT WALL MASS THICKNESS Xw'

Foctor	Fig.	Sector #1 Pfo	Sector #2 Pfa	Sector #3 Pfr	Sector #4 Pf (TAB I)
Xe'(Ap)	10 11	80	80	80	80
Xi	--	—	—	—	—
ΔXw(A,H)	12	49	53	45	49
ΔXw(Ms)	13	—	—	—	—
ΔXw(FC)	I, II, III	—	46	2	-5
*ΔXw(Xf)	14		142	127	—
*ΔXw(Ex)	15	—	—	—	—
Xw'		129	321	254	124

EQUIVALENT ROOF MASS THICKNESS Xw'

Co(A', Xo+ΔXo)				
-Co(Ac', Xo+ΔXo)				
Co(Periphery)				
+Co(Ac', Xo)(Core)				
Co(Totol Roof)				
Areo=				
Xo'=	150	∞	∞	150
A=1000	30	1900	480	27
A=10,000	51	4000	1000	47
* For Bosement Case				
A=7500	45	3400	860	41

1. SOLUTION USING TABLES II + III (SECTORS, 1, 2, 3).

$P_f = 45 \times \frac{3400}{3445} - X \frac{860}{905}$

$P_f = 41.5$ ANS.

2. SOLUTION USING TABLE I FOR FC. (SECTOR #4).

$P_f = 41$ ANS.

(EM=43)

PROBLEM #12

EQUIVALENT BUILDING METHOD SOLUTION FORM

PROBLEM #12

PARAMETERS

W= 75' L= 100' A= 7500
Wc= — Lc= — Ac= —
Z= 17' A'= 2600
H= 53' Ac'= —
Ap= — Xo= 150
Ms= — Xe= 80
Xi= —
Xf= 60

EQUATIONS

$Xw' = Xe'(Ap) + Xi + \sum \Delta Xw$

$Xo' = Xo(A,Z) + \Delta Xo(Xi)$

SKETCH

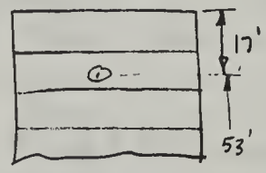

Ap = 40%

EQUIVALENT WALL MASS THICKNESS Xw'

Foctor	Fig.	Sector #1 Pfo	Sector #2 Pfa	Sector #3 Pfr	Sector #4 Pf (TAB I)
Xe'(Ap)	10 11	68	68	68	68
Xi	--	—	—	—	—
ΔXw(A,H)	12	49	53	45	49
ΔXw(Ms)	13	—	—	—	—
ΔXw(FC)	I		46	2	-5
*ΔXw(Xf)	14		142	127	—
*ΔXw(Ex)	15		—	—	—
Xw'		117	309	242	112

EQUIVALENT ROOF MASS THICKNESS Xw'

Co(A', Xo+ΔXo)				
-Co(Ac', Xo+ΔXo)				
Co(Periphery)				
+Co(Ac', Xo)(Core)				
Co(Totol Roof)				
Areo=				
Xo'=	150	∞	∞	150
A=1000	24	1500	380	21
A=10,000	41	3200	800	37
* For Bosement Case				
A=7500	36	2700	680	33

1. SOLUTION USING TABLES II + III, (SECTOR 1, 2, 3).

$P_f = 36 \times \frac{2700}{2736} \times \frac{680}{716}$

$P_f = 34$ ANS

2. SOLUTION USING TABLE I FOR FC (SECTOR 4)

$P_f = 33$ ANS

(EM=35)

PROBLEM #13

EQUIVALENT BUILDING METHOD SOLUTION FORM

Problem #13

PARAMETERS

W=≈80 L=≈80 A=≈4800
Wc=— Lc=— Ac=—
Z=22' A'=
H= Ac'=
Ap=.15 Xo=135
Ms= Xe=55
Xi=

EQUATIONS

$Xw' = Xe'(Ap) + Xi + \sum \Delta Xw$

$Xo' = Xo(A,Z) + \Delta Xo(Xi)$

EQUIVALENT WALL MASS THICKNESS Xw'

q= .167 .036 .176 .620

Foctor	Fig.	Sector #1	Sector #2	Sector #3	Sector #4
Xe'(Ap)	10 11	50	0	50	50
Xi	--	—	—	—	—
ΔXw(A,H)	12	—	—	—	—
ΔXw(Ms)	13	64	0	0	0
ΔXw(FC)	I	neg	neg	neg	neg
*ΔXw(Xf)	14	—	—	—	—
*ΔXw(Ex)	15	—			
Xw'		114	0	50	50

SKETCH

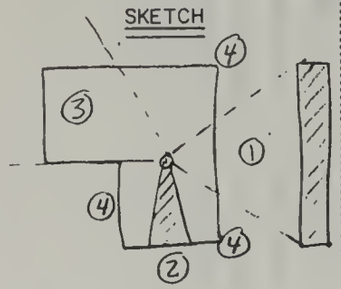

FOR SECTORS ①, ②, ④

A=40x80 =3200
A'= 661

FOR SECTOR ③

A=120x80 =9600
A'=1980

EQUIVALENT ROOF MASS THICKNESS Xw'

Co(A', Xo+ΔXo)				
-Co(Ac', Xo+ΔXo)				
Co(Periphery)				
+Co(Ac', Xo)(Core)				
Co(Totol Roof)	.0075	.0075	.0083	.0075
Areo=	3200	3200	6400	3200
Xo'=	140	140	137	140

A=1000 21 1.5 5.4 5.4
A=10,000 36 3.0 10.5 10.5
* For Basement Case
A= 3200/6400 25 1.9 10.3 6.6

$P_f^{-1} = \frac{.167}{25} + \frac{.036}{1.9} + \frac{.176}{10.3} + \frac{.620}{6.6}$

$P_f = .141$

$P_f = 7.1$ A.N.S (EM=7)

PROBLEM #14

EQUIVALENT BUILDING METHOD SOLUTION FORM

PARAMETERS

W=90 L=90 A=8100
Wc=17.5 Lc=40 Ac=700
Z=17' A'=7800
H=83' Ac'=240
Ap=36% Xo=125
Ms=20' Xe=100
Xi=50
Xf=75

EQUATIONS

$Xw' = Xe'(Ap) + Xi + \sum \Delta Xw$

$Xo' = Xo(A,Z) + \Delta Xo(Xi)$

EQUIVALENT WALL MASS THICKNESS Xw'

q= .369 .205 .207 .229

Foctor	Fig.	Sector #1	Sector #2	Sector #3	Sector #4
Xe'(Ap)	10 11	85	83	80	77
Xi	--	0	50	50	
ΔXw(A,H)	12	51	54	19	
ΔXw(Ms)	13	0	0	92	
ΔXw(FC)	1	0	0	0	
*ΔXw(Xf)	14	0	0	0	
*ΔXw(Ex)	15	0	0	0	
Xw'		136	187	241	∞

SKETCH

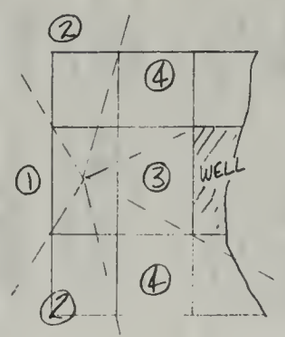

SECTOR #1

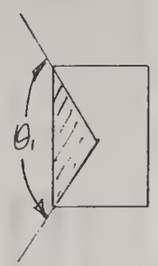

$\theta_1 = 133°$
$q_1 = .369$
A=700
A'=240
H=83'

EQUIVALENT ROOF MASS THICKNESS Xw'

Co(A', Xo+ΔXo)		.0023	.0027	.0027
-Co(Ac', Xo+ΔXo)		.0017	.0017	.0017
Co(Periphery)		.0006	.0010	.0010
+Co(Ac', Xo)(Core)		.0067	.0067	.0067
Co(Totol Roof)	.0067	.0073	.0077	.0077
Areo=	700	1570	4740	8100
Xo'=	142	140	140	140

* For Basement Case

SKETCH

SECTOR #2

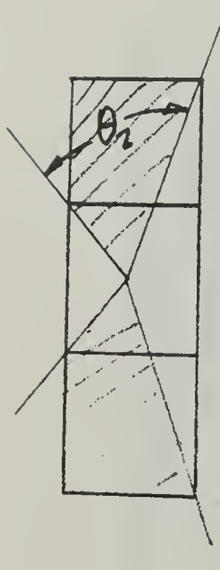

$2\theta_2 = 74°$

$a_2 = .205$

$A = 1570$

$A' = 540$

$A_c' = 240$

$H = 83'$

$X_{op} = 185$

SECTOR #3

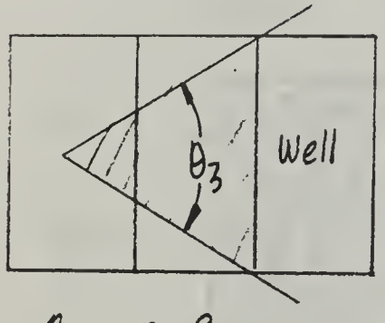

$\theta_3 = 75°$

$a_3 = .207$

$A = 4730$

$A' = 1640$

$A_c' = 240$

$H = 13'$

$X_{op} = 185$

CALCULATIONS

SECTOR #1, $a_1 = .369$

AREA	Pf
100	24
1000	30
700	28

$R_f = \frac{.369}{28} = .0132$

SECTOR #2, $a_2 = .205$

AREA	Pf
1000	64
10,000	85
1570	65

$R_f = \frac{.205}{65} = .0032$

SECTOR #3, $a_3 = .207$

AREA	Pf
1000	90
10,000	120
4730	104

$R_f = \frac{.207}{104} = .0020$

SECTOR #4, $a_4 = .229$

AREA	Pf
1000	150
10,000	130
8,100	135

$R_f = \frac{.229}{135} = .0017$

R_f (TOTAL) $= .0201$

$P_f = 50$ ANS (EM=47)

VIII - VARIOUS SOURCES OF UNCERTAINTIES IN FALLOUT SHIELDING METHODS OF ANALYSIS

A. Introduction

Discussions with various administrative and technical personnel have indicated that there is a general lack of knowledge concerning the accuracy of the present method used for fallout shielding analysis. Engineering methods in general are usually based on a number of assumptions to decrease the complexity of analysis and design. We usually compensate by introducing "safety factors" which are in essence "factors of ignorance." Nuclear radiation shielding, at the present time, is more an art than a science, and is also based on a number of simplifying assumptions. Such assumptions had to be made in order to develop a method at all. The fact that a method is long and tedious does not insure accuracy nor does writing a computer code improve the accuracy if the input data itself has limitations. It is well then to attempt to set forth the various sources of errors in the present method of fallout shielding analysis and design so that our technical personnel can appreciate the strengths and weaknesses of the present method. The method under discussion is the Engineering Manual method. Whenever possible, the range of possible error is listed. There are a certain number of assumptions, however, whose effect upon the accuracy is unknown. We merely know that the assumption is not based solidly on known facts.

The sources of error can be classified into five categories: (1) Those dealing with the physical measurements of the structure being analyzed; (2) the basic assumptions relative to fallout; (3) the basic input data and theory; (4) the basic methodology; and (5) computational errors.

1. Errors involved in physical measurements of structure being analyzed.

a. Measurements of mass thickness

b. Irregularities in walls and roofs

c. Mutual shield effect

d. Building and room dimensions

All of the above are subject to slight errors in either the analysis or design situation. It is very difficult to measure exactly the mass thickness of walls or roof unless wall borings are made. An error of about 7 per cent in wall and roof mass thickness in 12" concrete will produce a

possible ± 25 per cent difference in protection factors calculated. In addition most walls and roofs have irregularities such as beams and columns which make measurement even more difficult. The accuracy of measuring buildings providing mutual shields also will produce uncertainties.

2. Errors involved in the basic assumptions relative to fallout:

a. Spectrum. The 1.12 hr. fission spectrum is assumed for all methods of analysis. Generally, any error here will be in the conservative direction, although somewhat minor in nature. In certain cases, fractionation of the fission products could produce a harder spectrum than the 1.12 hr. spectrum; again, this is probably negligible.

b. Uniform distribution. For planning purposes, this is the only logical assumption to make. Under actual conditions it is almost certain not to be the case because of ground roughness and micrometeorological effects. Fallout will tend to drift like snow or dust and collect in valleys, gutters, etc. This may or may not improve the Pf of a shielded location.

c. Flat roof. We normally replace all roof structures by a flat roof. Fallout which is blown or falls from an eaved roof would collect on the ground next to the building or in gutters. Radiation penetrates vertical barriers easier than horizontal barriers and this assumption could be unconservative.

d. Horizontal surfaces. We assume that fallout will settle only on horizontal surfaces. We nelgect any fallout which may settle on window sills and which could, under certain conditions, cling or stick to vertical surfaces. (A water burst could produce a sticky type of fallout--Pacific tests and Japanese fishing boat experience.) Under these conditions, the protection factor for a location within a building would decrease by a factor roughly equivalent to another roof contribution (assuming one side of a building is contaminated.)

No ± figures are given here, although it would be possible to compute some for typical cases. Some are usually always conservative, such as the 1.12 hr. spectrum and the ground roughness. Others could go either way depending on the particular building involved.

3. Errors of basic input data and theory:

Here we must go back to the Spencer Monograph and investigate the input data which Dr. Spencer used. He discusses possible errors on page 81 of the monograph, but for our purposes we can summarize his discussion as follows:

a. Input data. The basic cross sectional information (i.e. the gamma ray interaction probabilities) are known to within a factor of 1 per cent. Nevertheless at deep penetrations, this could lead to errors of 10 per cent in barrier factors for good geometry conditions: i.e. an infinite, homogeneous medium. Variations from this ideal will produce further uncertainties. The following are Dr. Spencer's estimate of possible errors for various basic curves:

Roof barrier L(x)	8%	Wall barrier W(X,d)	10 to 50%
Skyshine S(d)	15%	Geometry factors	20 to 25%
Barrier to skyshine	100%		

b. Homogeneous medium. Most basic data is derived assuming an infinite homogeneous medium. Although basic interactions for air, water, concrete, and earth are somewhat the same on a mean free path basis, there are differences. The Monograph curves are based on water. Most practical situations are far from homogeneous. Error here is somewhere in the range of 10 per cent (guess).

c. Interface problem. Theory based on air-air interface. In practice, we have air to ground, air to concrete, etc. Range here also about 10 per cent (guess).

d. Vertical wall data: The available source data for vertical walls produces uncertainties in wall penetration. These uncertainties are due to inaccuracies in the angular distribution, changes in spectrum with depth of penetration, incorrect correlation of spectrum with direction. The uncertainties increase as height above the contaminated plane increase.

4. Errors involved in basic methodology: The following discussion relates to the Engineering Manual assumptions:

a. Solid angle fraction. Solid angle fraction is used throughout the Manual as the best parameter for representing the geometry. It doesn't measure or indicate the geometry factor directly, but is a basic parameter like mass thickness is a measure of barrier factor. The use of solid angle fraction

will introduce no error ONLY when the radiation is isotropic at the detector, i.e. coming equally from all directions. Though individual fallout parricles may be assumed to be isotropic, a fallout field will produce an isotropic response at the detector only under a few limited conditions.

b. Distribution of radiation. The angular distribution of radiation is known fairly well only for a few cases; through the roof; at the outside of the wall for small heights. For thick walls, or for great heights, the distribution is not known.

c. Pillbox building. The Engineering Manual is based on a pillbox (cylindrical) building. Buildings which vary from this round shape will be approximations to the basis of calculations.

d. Roof contributions. Spencer computed three separate cases for roof contributions. The Engineering Manual selected one of these for universal use, the so-called smeared barrier case. Here the total mass thickness between source and detector is assumed to be uniformly distributed between source and detector. Depending on the actual situation, using this smeared barrier curve could produce results $\pm$ 40 per cent from the other two Spencer curves. In addition, the use of a circle to represent a rectangular roof introduces an additional error which depends on the actual angular distribution of radiation. For rectangles with eccentricities of 5 to 1, the error could be as much as $\pm$ 25 per cent.

e. Wall scattered radiation. The wall scattered directional response function is based on the ASSUMPTION that radiation scattered within a wall has the same angular distribution as air scattered radiation both above and below the detector plane. We do not now have information of the actual distribution of wall scattered radiation. Range of uncertainty here now known. It appears, however, that G_s(upper) would be less than G_s(lower) since radiation tends to scatter in forward directions.

f. Ceiling-shine. The air scattered directional response function has a ceiling-shine factor incorporated in it. This is the radiation which reflects from the ceiling into the detector. This contribution is based on a series of assumptions which so far have not been tested or evaluated. The effect appears to be small, so that a large error will not normally be significant. However,

certain situations could neglect this effect when it was significant; for instance a high band of windows with a roof overhang would appear to cut out skyshine (which it would) but it would tend to increase ceiling-shine. Since ceiling-shine is part of skyshine in the present method, neglecting the skyshine effect also neglects ceiling-shine. (See Section X for ceiling-shine analysis.)

g. Shape Factor. Shape factor is based on the assumption that for very thick walls, radiation emerges with a cosine distribution. The factor is applied only to the scattered component. The wall scattered component is weighted further by the scattering fraction. For walls of nominal thickness, we know that the scattered radiation does not have a true cosine distribution. How good is the shape factor under these conditions? The factor varies from 1 to 1.4, thus the maximum error would be 40 per cent for the wall scattered component.

h. Scattered fraction. The scattered fraction is based on the data of perpendicular incidence of Co-60 radiation. First floor wall radiation is essentially peaked from the horizon and thus the perpendicular incidence should introduce little error. The use of Co-60 in lieu of the fission spectrum will produce perhaps a maximum error of 10 per cent. The procedure used in the Manual, however, applies this factor only to the exterior wall regardless of the interior wall thickness. Radiation will also scatter in the interior walls, but the distribution in energy and angle have changed because of exterior wall scatter. We have no information of the distribution at the interior walls and scattering here is neglected. As a matter of procedure, it seems that the scattering fraction should be based on the combined mass thickness of both interior and exterior walls. The possible error here could be as much as 100 per cent. In buildings with windows (see Section X for interior wall scatter analysis)

i. Azimuth sectors. Present procedure calls for the use of either azimuth sectors or perimeter ratios when computing contributions from portions of walls. No error is introduced when the total wall is used, as for example, when one wall of a building is thicker than the other three . When portions of walls are used, a large error is possible, because this method says, if effect, we receive equal contributions from equal angles (or equal perimeters).

This is not true. We receive the greatest radiation from the wall closest to the detector. As a rough rule, we receive about 90 per cent of the total contribution within an arc of 60° (30° on either side of the perpendicular to the wall) for an infinitely long wall. Any error here would depend on the actual situation and could be ±.

j. Entranceways and Ducts. Present method only accurate within a factor of 2 (200%) for simple, single 90° bend.

k. Detector location. We normally only analyze the center of a shelter. Other locations within shelter can be different by a factor of 2 to 4 depending on the situation. Normally, the center of the shelter would give the best protection.

5. Computational errors.

Because of the complexity of the method, hand computations have a large probability of error for any one computation. Machine computation will normally be errorless for the data fed into the program but machine programs normally have to be simplified from the Engineering Manual for reasonable workability. The program used for the survey was better than the A&E Guide, but less rigorous than the Engineering Manual.

Summary. It is very difficult to asses the total uncertainty in the present method of analysis. It appears that under certain conditions (complex situations, maximum errors applying, etc.), the degree of uncertainty could be in the range of 1.5 to 2. Thus a protection factor of 100 would lie in the range of 50 to 200. On the other hand, the degree of uncertainty of the source itself, (i.e. the intensity of fallout for any particular location) would probably be in the range 10-20. Since we can design for the worst conditions of high radiation intensity (a Pf of 100 seems to insure survival under these conditions), the degree of uncertainty on the actual protection factor may not be significant. Under actual conditions, the shelterees can also take corrective actions for actual conditions which exist.

IX - ENTRANCEWAYS AND DUCTS

The subject of entranceways and ducts is a complex one and has been given extensive coverage in the literature. Three of these reports have been selected to give a good overall picture of the state of the art for gamma rays streaming down ducts.

The first report is a summary of the field for both theory and experiment. It is:

> Huddleston, C. M. and W. L. Wilcoxin, "Gamma Rays Streaming Through Ducts." NCEL R 289, Naval Civil Engineering Laboratory, Port Hueneme, Calif., 6 Feb 1964 (Y-F008-08-05-201, DASA 11.026).

The second report has been the basic theoretical treatise for this field. It has been used as the starting point for further work. It is:

> LeDoux, J. C. and A. B. Chilton, "Gamma Rays Streaming Through Two-Legged Rectangular Ducts." Nuclear Science and Engineering: 11; 362-368 (1959).

The third report provides a method of computing differential dose albedo based on monte carlo computations. This differential dose albedo should be used in using the LeDoux-Chilton Theory in lieu of the assumed isotropic dose albedo assumed in their original work (second report above). The third report is:

> Chilton, A. B. and C. M. Huddleston, "A Semiempirical Formula for Differential Dose Albedo for Gamma Rays on Concrete." NCEL R-228, Nov 1962 (Y-F011-05-329(b)).

The Detailed Procedure, Section VI, also presents a method of computing the reduction factor in right angled ducts and entranceways. The method is quite simple and produces fairly good results for square ducts when the L/W ratio is equal to or greater than 3.

Chart 10 (Section VI) is used to determine the reduction factor for the first leg of the duct. The second leg attenuation is:

$$RF_2 = 0.2\ \omega_2$$

where ω_2 is the solid angle fraction measured from the point of interest (on the centerline of the duct exit) to the nearest edge of the duct. The Z distance is then L_2 minus W/2.

For subsequent legs, the multiplying factor is taken as 0.5.

GAMMA-RAY STREAMING THROUGH DUCTS

Y-F008-08-05-201, DASA 11.026

Type C

by

C. M. Huddleston and W. L. Wilcoxson

ABSTRACT

A survey is presented of the current status of experimental and theoretical investigations of the problem of gamma-ray streaming through air ducts in concrete. Data are tabulated and plotted for a variety of experiments. Comparisons are made between theory and experiment, inconsistencies are pointed out, and areas needing further investigation are indicated.

This work sponsored by the Defense Atomic Support Agency.

INTRODUCTION

In the shielding of personnel against gamma radiation from nuclear weapons, an important aspect of the problem is consideration of the hazard caused by radiation which is scattered off interior surfaces of entranceways and air ducts into the shelter area. The duct streaming problem has been investigated both experimentally and theoretically at several laboratories. Current understanding of the problem has progressed to the stage where a review of progress to date is indicated. This report purposes to survey this information.

Section I will describe some experimental determinations of the attenuation of gamma-ray dose within concrete ducts as a function of distance from the radioactive source. Section II will be concerned with albedo, which is an important concept in gamma-ray scattering. Section III will describe theoretical approaches to the duct streaming problem. The figures, presenting plotted and tabulated data, follow the text.

I. EXPERIMENTAL INVESTIGATIONS

Several investigators have conducted experiments giving information on the distribution of radiation along the axis of air ducts in concrete with square, rectangular, and round cross sections. Some of the ducts have one right-angle bend, and some have two right-angle bends. In every case treated here the measurements were made with a gamma-ray point source.

The significant results of these investigations will be discussed and compared with each other and with theory. A systematic effort will be made to give as much information as is available on actual experimental results so that the data may be convenient to other investigators.

Definition of Terms

A uniform terminology is used for the various sources of data:

D = measured dose rate in mr/hr at some distance along the axis of the duct

D_o = dose rate in mr/hr at 1 foot from source in air

L = total length of the duct in feet as measured along the axis; i.e., $L = L_1 + L_2$ for a two-legged duct, and $L = L_1 + L_2 + L_3$ for a three-legged duct

L_1 = length of first leg in feet, measured from the point source on the axis to the center of the first corner

L_2 = length of second leg in feet, measured from the center of the first corner to the end of the duct in the case of a two-legged duct, or from the center of the first corner to the center of the second corner in the case of a three-legged duct

T = the distance in feet from the source to a point on the axis measured along the axis of the duct

$W/2$ = half-width of duct in feet: for a square, $W/2$ is half of the width of a side of the cross section of the duct; for a rectangle, $W/2$ is the geometric mean of the half-height and half-width of the duct (i.e., W^2 is the area of the cross section of the duct); for a round cross section with radius R, $W/2$ is given by $W/2 = \sqrt{\pi}R/2$ (i.e., W^2 is the area of the cross section of the duct)

L-shape refers to a duct with a single right-angle bend.

U-shape refers to a duct with two right-angle bends of the same sense, so that radiation reaching the detector streams in the opposite direction to radiation streaming from the source down the first leg.

Z-shape refers to a duct with two right-angle bends of opposite sense, such as a tunnel with an offset.

Experimental Findings

Eisenhauer. The scattering of Co^{60} gamma radiation in square and rectangular air ducts in concrete was investigated experimentally by Eisenhauer.[1] He measured dose rates along the axis of the second leg of a two-legged duct, and along the axis of the third leg of a three-legged duct. Results are plotted and tabulated in Figures 1 through 5.

Eisenhauer found that the dose rate along the axis of the second leg of a two-legged duct varied as the inverse cube of the distance along the second leg. Also, he demonstrated the importance of scattering from the inside corner of the first right-angle junction. He made some "trapping" experiments by setting back one of the walls in a corner junction.

Terrell. Extensive experimental investigations of gamma-ray streaming through air ducts in concrete have been carried out by Terrell and his co-workers at the Armour Research Foundation.[2, 3, 4] Results are shown in Figures 6 through 23. This series of studies included Co^{60}, Cs^{137}, Na^{24}, and Au^{198}. All ducts had square cross sections, some 6 x 6 feet and some 1 x 1 foot. Some of the ducts had one right-angle bend, and some had two right-angle bends.

Terrell[3] investigated the relative importance of scattering from the walls and ceiling at a corner, both by covering surface areas with lead (which has a much lower gamma-ray albedo than does concrete) and by removing walls.

Experiments with U-shaped and Z-shaped ducts[4] showed that the sense of the second right-angle bend is not a significant factor, at least as long as the axes of all three legs of a duct lie in the same plane.

Green. An experimental study of the streaming of the gamma radiation of Co^{60} in an 11-inch square duct with one right-angle bend led Green[5] to three principal conclusions:

1. Trapping the corner surfaces of a duct is not generally an economically feasible means for improving attenuation factors.

2. Dose-rate contributions due to multiple scatter represent a significant contribution to total dose rate at the detector.

3. Dose rate falls off as the inverse square of axial distance along the first leg of a duct and almost as the inverse cube along the axis of the second leg.

Results of Green's measurements are shown in Figures 24 and 25.

Chapman. Dose-rate measurements and gamma-ray spectrum measurements were made inside a square concrete duct with a 3 x 3-foot cross section.[6] By measuring the energy spectra of gamma rays scattered from particular surface elements, Chapman was able to demonstrate the importance of multiple scatter. He showed that, at some places within a duct, dose contributions due to multiple scatter can be of the same magnitude as the dose contribution due to single scatter. Results of Chapman's duct-streaming measurements are presented in Figures 26 and 27.

Fowler and Dorn. Measurements were made of dose attenuation along the axis of a three-legged duct having a circular cross section.[7] Results are presented in Figures 28 and 29. It was shown that, except for minor differences, a round duct attenuates gamma radiation in much the same way as a square duct of the same cross-sectional area.

Jacovitch and Chapman. J. M. Chapman of NCEL is working on an experimental study initiated by J. Jacovitch of the possibility of a gamma-ray polarization effect which may improve the protection afforded by a three-legged duct if one of the legs is noncoplanar with the other two. The problem was suggested by L. V. Spencer, who pointed out that a gamma-ray photon is unlikely to scatter out of its plane of polarization. It is not clear whether gamma-ray polarization will be important in the crude geometry of a concrete duct. Experimental results are not yet available.

Review of Experimental Findings

Figures 30 and 31 are composite plots of all the data of Figures 1 through 29. There are several reasons why one would expect wide dispersion in the data:

1. Several different initial energies were used.

2. Some ducts had two legs and some had three.

3. Several different widths were used.

4. Several different lengths were used.

Despite all the reasons given above, it can be seen from Figures 30 and 31 that dose tends generally to fall off exponentially with T/L. Clearly, such an exponential decay cannot be true for both very short ($L \approx W$) and very long ($L \gg W$) ducts. The reason for the apparent $e^{-T/L}$ behavior is presumably that most experimenters chose leg lengths equal to a few (~ 3) duct diameters.

Efforts have been made at NCEL to find an empirical expression relating dose to such factors as number of legs, lengths of legs, initial energy, and duct width. No reasonable expression with acceptable accuracy has yet been found. A relatively simple formula needs to be found before useful criteria can be specified for designers.

II. ALBEDO

Theory

An important concept in gamma-ray scattering is "albedo," or reflection. The term "differential dose albedo" is discussed by Rockwell[8] and by Chilton and Huddleston.[9] The definition of differential dose albedo will be reproduced here since it will be important to theoretical arguments which will follow. The scattering of radiation from a point source incident on a slab is diagramed as follows.

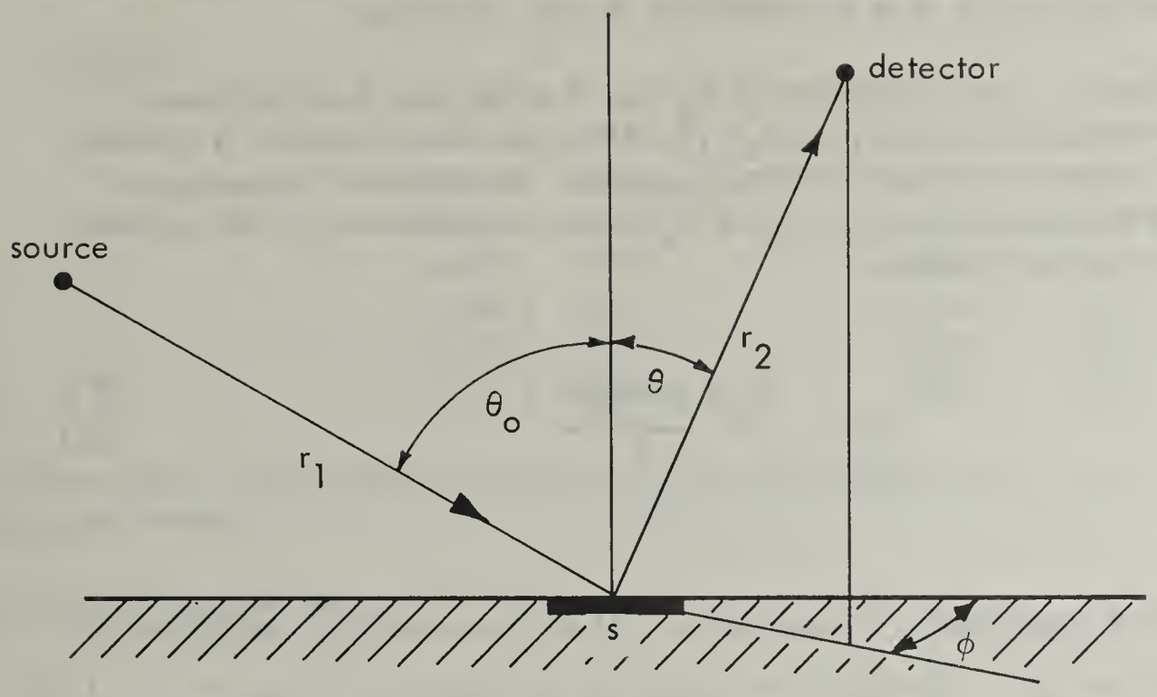

For such a case the differential dose albedo α is defined by the equation

$$dD = \frac{D_1 \alpha (E_o, \theta_o, \theta, \varphi) \cos\theta_o dA}{r_1^2 r_2^2}, \qquad (1)$$

where dD = differential dose at point of measurement

D_1 = dose in air at unit distance from source

E_o = energy of incident radiation

θ_o = polar angle of incidence of radiation

θ = polar angle of backscattered radiation

φ = azimuthal angle of backscattered radiation

dA = differential area of scattering surface

r_1 = distance from source to dA

r_2 = distance from dA to detector.

It is seen that α may be a function of E_o and of the three angles: θ_o, θ, and φ, where α can be thought of as a coefficient of dose reflection.

From Equation 1 and the diagram it is clear that the dose from the source incident per unit area at dA is $D_1 \cos\theta_o / r_1^2$. If the incident radiation is a broad parallel beam incident on a semi-infinite plane slab, the radiation intensity per unit area at dA becomes $D_o \cos\theta_o$, where D_o is the dose measured in the incident beam. Equation 1 then becomes

$$dD = \frac{D_o \alpha \cos\theta_o \, dA}{r_2^2} \tag{2}$$

Differential dose albedo, as used here, will be the quantity α as defined by Equation 2.

Attempts have been made to determine α as a function of angles and incident energy. Monte Carlo techniques,[10, 11, 12, 13] analytical approaches,[14] and experimental measurements[15, 16] have all been used to determine α.

Raso[11] performed Monte Carlo calculations for a broad, parallel monoenergetic beam of gamma rays incident on a semi-infinite slab of concrete. From backscattering histories, differential dose albedo was computed as a function of initial energy, polar angle of incidence, and polar and azimuthal angles of reflection. Using Raso's data, Chilton and Huddleston[9] developed a semiempirical formula for the differential dose albedo of gamma rays on concrete. The formula can be expressed as

$$\alpha = \frac{CK(\theta_s)\, 10^{26} + C'}{1 + \dfrac{\cos\theta_o}{\cos\theta}} \tag{3}$$

where $K(\theta_s)$ is the Klein-Nishina differential energy-scattering cross section; C and C' are parameters dependent on the initial energy, E_o; and α, θ_o, and θ are as previously defined. θ_s is the spacial angle of gamma-ray scatter.

The parameters for the energies considered by Raso are shown below:

E_o (Mev)	C	C'
.2	.0221 ± .0018	.0356 ± .0033
.5	.0336 ± .0016	.0220 ± .0012
1	.0547 ± .0020	.0111 ± .0007
2	.0869 ± .0027	.0077 ± .0004
4	.1238 ± .0046	.0076 ± .0003
6	.1490 ± .0065	.0075 ± .0003
10	.1660 ± .0084	.0070 ± .0002

The values were obtained by fitting the data of Raso to Equation 3 by a least-squares method.

Experimental Investigation

The U. S. Naval Radiological Defense Laboratory has made experimental measurements of the differential angular backscatter of gamma-ray doses from thick slabs of steel, aluminum, and concrete, using radioactive sources of Co^{60} and Cs^{137}. Although final results of the NRDL study are not yet available, preliminary results reported to NCEL indicate fair agreement with the results of Raso.

Uses of the Theory

The semiempirical formula of Equation 3 has been used by Chilton[17] to calculate the backscatter by an infinite concrete slab of the radiation from isotropic point sources of Na^{24}, Co^{60}, Cs^{137}, and Au^{198}. Agreement was found with the experimental results of Clarke and Batter[18] within the limits of experimental error.

Another test and use of Equation 3 is in the calculation of gamma-ray dose attenuation along the axis of a two-legged rectangular duct. Chapman[19] has found that the semiempirical formula can be used to calculate dose attenuation in a concrete duct. Chapman compares his calculated results with the experimental results tabulated in Figures 1 through 29. He finds agreement within 30 percent in all cases except for the Au^{198} data, where the calculated results are about a factor of 2 higher than the experimental results.

The theory indicates that protection factors (which are the reciprocals of the D/D_o attenuation factors) should decrease as the energy of the gamma-ray source decreases. Therefore, among the various sources experimentally investigated, the greatest protection factor should obtain for Na^{24}, while the protection factor for

Au^{198} should be the smallest, provided the duct geometry is the same in all cases. However, experimental results[3] indicate a larger protection factor for Au^{198} radiation than for Cs^{137} radiation. Further experimental study of the streaming of Au^{198} gamma radiation through concrete ducts should be undertaken to resolve the "gold anomaly."

A Simplification of the Albedo Problem

It has been shown by Shoemaker and Huddleston[20] that variations in the azimuthal angle φ are redundant in experimental measurements of differential dose albedo provided that Equation 3 or a generalization of Equation 3 is valid. Once differential dose albedo has been determined for a complete set of incident and reflected polar angles with zero azimuth, albedo at any azimuth is shown to be calculable by a suitable mathematical transformation.

III. THEORY OF DUCT STREAMING

Most treatments of the streaming of gamma radiation through air ducts in concrete are based on the method of LeDoux and Chilton.[21] They considered backscattered radiation from those areas within a two-legged duct which could be "seen" by both the source and the detector. They also considered in-scatter by the inside corner lip at the intersection of the two legs. Results generally gave good qualitative agreement with experiment, but theoretical predictions were low because of neglect of multiple-scatter contributions.

Green[5] demonstrated the importance of multiple scatter. Silverman[22] indicated how second scatter could be computed, although he did not actually carry out the calculations. Ingold[23] computed second-scatter contributions within a straight cylindrical duct. Chapman,[19] using the albedo concept and an extension of the LeDoux-Chilton method, calculated dose attenuations for gamma rays of various energies in two-legged concrete ducts of various sizes.

With the geometry of rectangular ducts it should be possible to use the ADONIS[24] computer code for calculating gamma-ray dose attenuation. Efforts are currently underway at NCEL to perform such calculations. ADONIS is an IBM-7090 Monte Carlo computer code which can compute the neutron or gamma-ray dose anywhere within a configuration composed of rectangular parallelepipeds. Such a code is expected to be useful for calculations of dose rates within ducts.

CONCLUSION

The status of the gamma-ray streaming problem is such that current theory accounts for almost all observed results. Although the problem is by no means solved, important advances of recent years have greatly added to our understanding.

The corresponding problem for neutrons is not nearly so well understood. Increased emphasis should be placed on neutron work in the future.

REFERENCES

1. C. Eisenhauer. National Bureau of Standards Technical Note 74, Scattering of Cobalt-60 Gamma Radiation in Air Ducts. Washington, D. C., 1960.

2. C. W. Terrell, A. J. Jerri, R. O. Lyday, and D. Sperber. Armour Research Foundation Report ARF 1158-12, Radiation Streaming in Shelter Entranceways. Chicago, Illinois, 1960.

3. C. W. Terrell and A. J. Jerri. Armour Research Foundation Report ARF-1158-A01-5, Radiation Streaming in Shelter Entranceways. Chicago, Illinois, 1961.

4. C. W. Terrell, A. J. Jerri, and R. O. Lyday. Armour Research Foundation Report ARF 1158-A02-7, Radiation Streaming in Ducts and Shelter Entranceways. Chicago, Illinois, 1962.

5. D. W. Green. U. S. Naval Civil Engineering Laboratory Technical Report R-195, Attenuation of Gamma Radiation in a Two-Legged 11-Inch Rectangular Duct. Port Hueneme, California, May 1962.

6. J. M. Chapman. U. S. Naval Civil Engineering Laboratory Technical Note N-443, Gamma Dose Rates and Energy Spectra in a 3-Foot Square Duct. Port Hueneme, California, June 1962.

7. T. R. Fowler and C. H. Dorn. U. S. Naval Civil Engineering Laboratory Technical Note N-465, Gamma-Ray Attenuation in a 12-Inch-Diameter Round Concrete Duct. Port Hueneme, California, November 1962.

8. T. Rockwell, III, editor. U. S. Atomic Energy Commission Report TID-7004, Reactor Shielding Design Manual. Washington, D. C., 1956.

9. A. B. Chilton and C. M. Huddleston. U. S. Naval Civil Engineering Laboratory Technical Report R-228, A Semiempirical Formula for Differential Dose Albedo for Gamma Rays on Concrete. Port Hueneme, California, November 1962.

10. M. Leimdörfer. AB Atomenergi Report AE-92, The Backscattering of Gamma Radiation from Plane Concrete Walls. Aktiebolaget Atomenergi, Stockholm, Sweden, December 1962.

11. D. J. Raso. Technical Operations, Inc., Report TO-B 61-39 (revised), Monte Carlo Calculations on the Reflection and Transmission of Scattered Gamma Radiation. Burlington, Massachusetts, 1961.

12. M. Leimdörfer. AB Atomenergi Report AE-93, The Backscattering of Gamma Radiation from Spherical Concrete Walls. Aktiebolaget Atomenergi, Stockholm, Sweden, January 1963.

13. M. J. Berger and J. Doggett. Research Paper 2653, "Reflection and Transmission of Gamma Radiation by Barriers: Semianalytic Monte Carlo Calculation," Journal of Research of the National Bureau of Standards, Vol. 56 (1956), p. 89.

14. J. Corner and R. H. A. Liston. "The Scattering of Gamma Rays in Extended Media," Proclamation of the Royal Society, Ser. A, Vol. 204 (1950), p. 323.

15. E. Hayward and J. H. Hubbell. National Bureau of Standards Report 2264, An Experiment on Gamma-Ray Backscattering. Washington, D. C., 1953.

16. E. Hayward and J. H. Hubbell. "The Backscattering of the Co^{60} Gamma Rays From Infinite Media," Journal of Applied Physics, Vol. 25, No. 4 (1954), pp. 506-509.

17. A. B. Chilton. "Backscattering by an Infinite Concrete Plane of Gamma Radiation from a Point Isotropic Source," Transactions of the American Nuclear Society, Vol. 6, No. 1 (1963), p. 200.

18. E. T. Clarke and J. Batter. "Gamma-Ray Scattering by Nearby Surfaces," Transactions of the American Nuclear Society, Vol. 5, No. 1 (1962), p. 223.

19. J. M. Chapman. U. S. Naval Civil Engineering Laboratory Technical Report R-264, Computer Calculations of Dose Rates in Two-Legged Ducts Using the Albedo Concept. Port Hueneme, California, October 1963.

20. N. F. Shoemaker and C. M. Huddleston. "A Mathematical Simplification of the Gamma-Ray Albedo Problem," Transactions of the American Nuclear Society, Vol. 6, No. 1 (1963), p. 198. Also see: Shoemaker and Huddleston, A Mathematical Approach to Economy of Experiment in Determinations of the Differential Dose Albedo of Gamma Rays, U. S. Naval Civil Engineering Laboratory Technical Note N-478, December 1962.

21. J. C. LeDoux and A. B. Chilton. U. S. Naval Civil Engineering Laboratory Technical Note N-383, Attenuation of Gamma Radiation Through Two-Legged Rectangular Ducts and Shelter Entranceways. Port Hueneme, California, January 1961.

22. C. M. Park, C. B. Agnihotri, and J. Silverman. Department of Chemical Engineering, University of Maryland, Report UMNE-2, Interim Report on Scattering of Gammas Through Ducts. College Park, Maryland, 1962.

23. W. C. Ingold. U. S. Naval Civil Engineering Laboratory Technical Note N-469, Some Applications of a Semiempirical Formula for Differential Dose Albedo for Gamma Rays on Concrete. Port Hueneme, California, December 1962.

24. B. Eisenman and E. Hennessy. United Nuclear Corporation, UNUCOR-635, ADONIS — an IBM-7090 Monte Carlo Shielding Code Which Solves for the Transport of Neutrons or Gamma Rays in Three-Dimensional Rectangular Geometry. White Plains, New York, 1963.

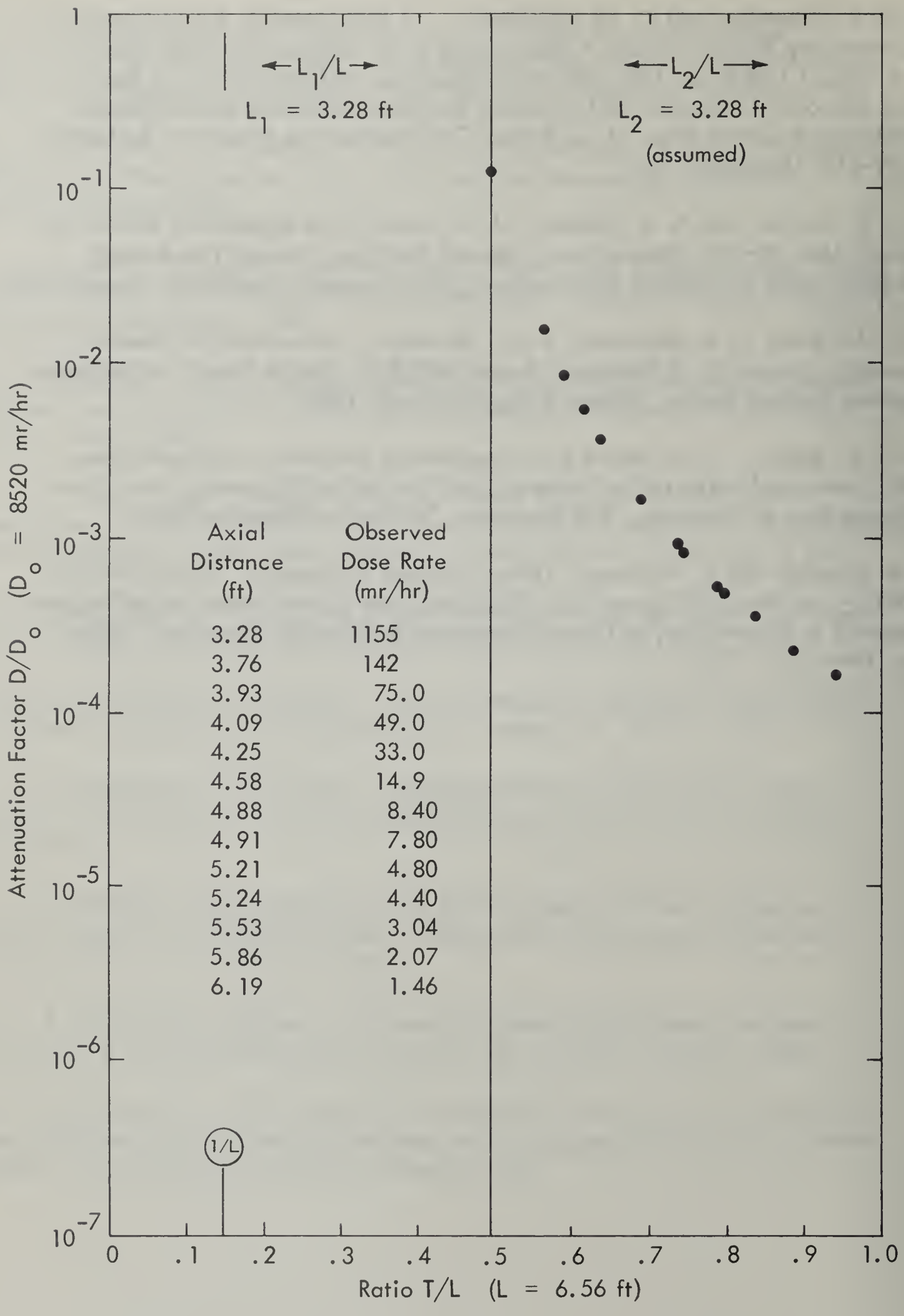

Figure 1. L-shaped 0.630 x 0.952-foot rectangular concrete duct with W/2 = 0.3815 foot; 0.6-curie Co^{60} point source. (From Reference 1, supplemented by correspondence.)

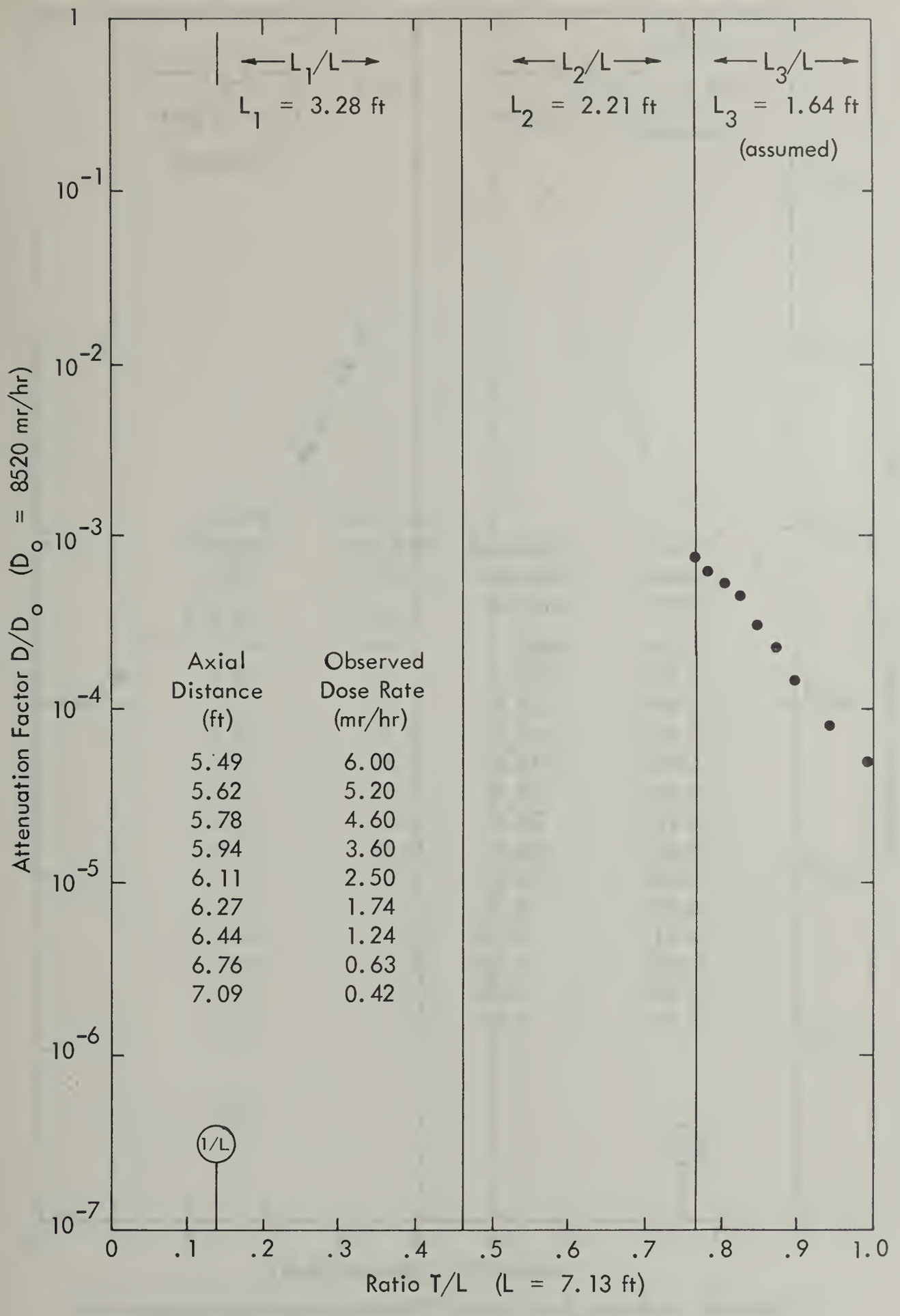

Figure 2. U-shaped 0.925 x 0.925-foot square concrete duct with W/2 = 0.4625 foot; 0.6-curie Co^{60} point source. (From Reference 1, supplemented by correspondence.)

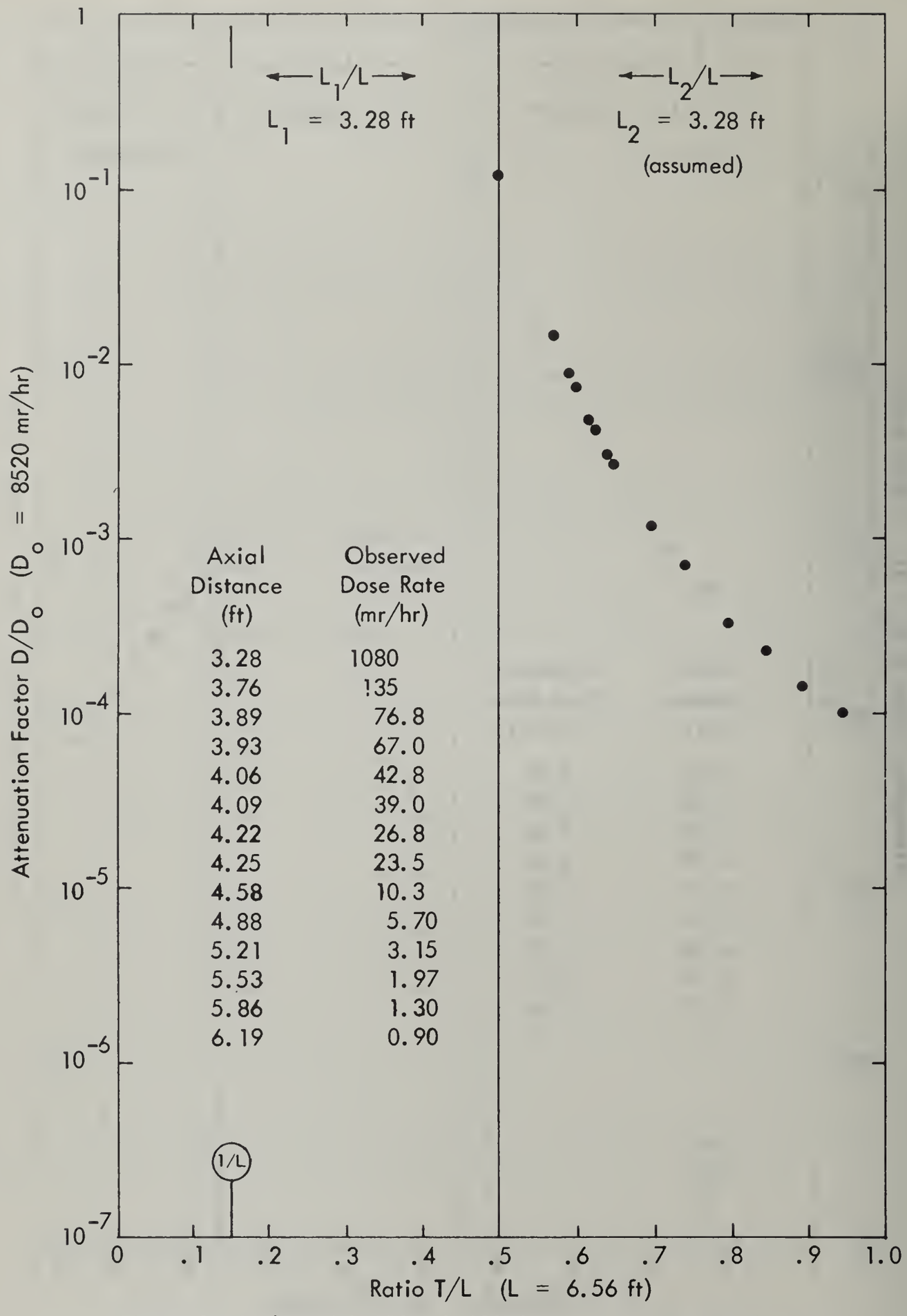

Figure 3. L-shaped 0.630 x 0.630-foot square concrete duct with W/2 = 0.3149 foot; 0.6-curie Co^{60} point source. (From Reference 1, supplemented by correspondence.)

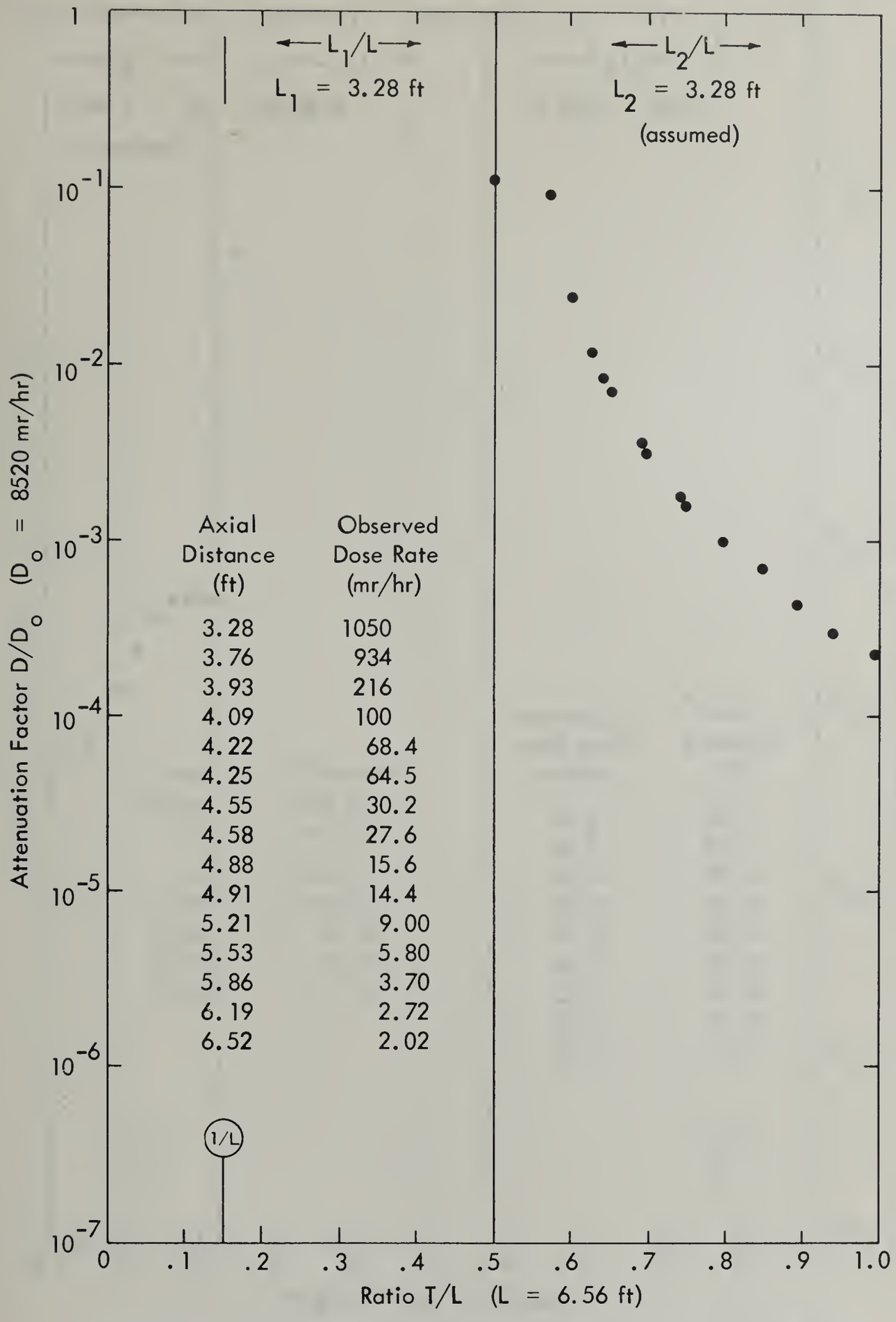

Figure 4. L-shaped 0.925 x 0.925-foot square concrete duct with W/2 = 0.4625 foot; 0.6-curie Co^{60} point source. (From Reference 1, supplemented by correspondence.)

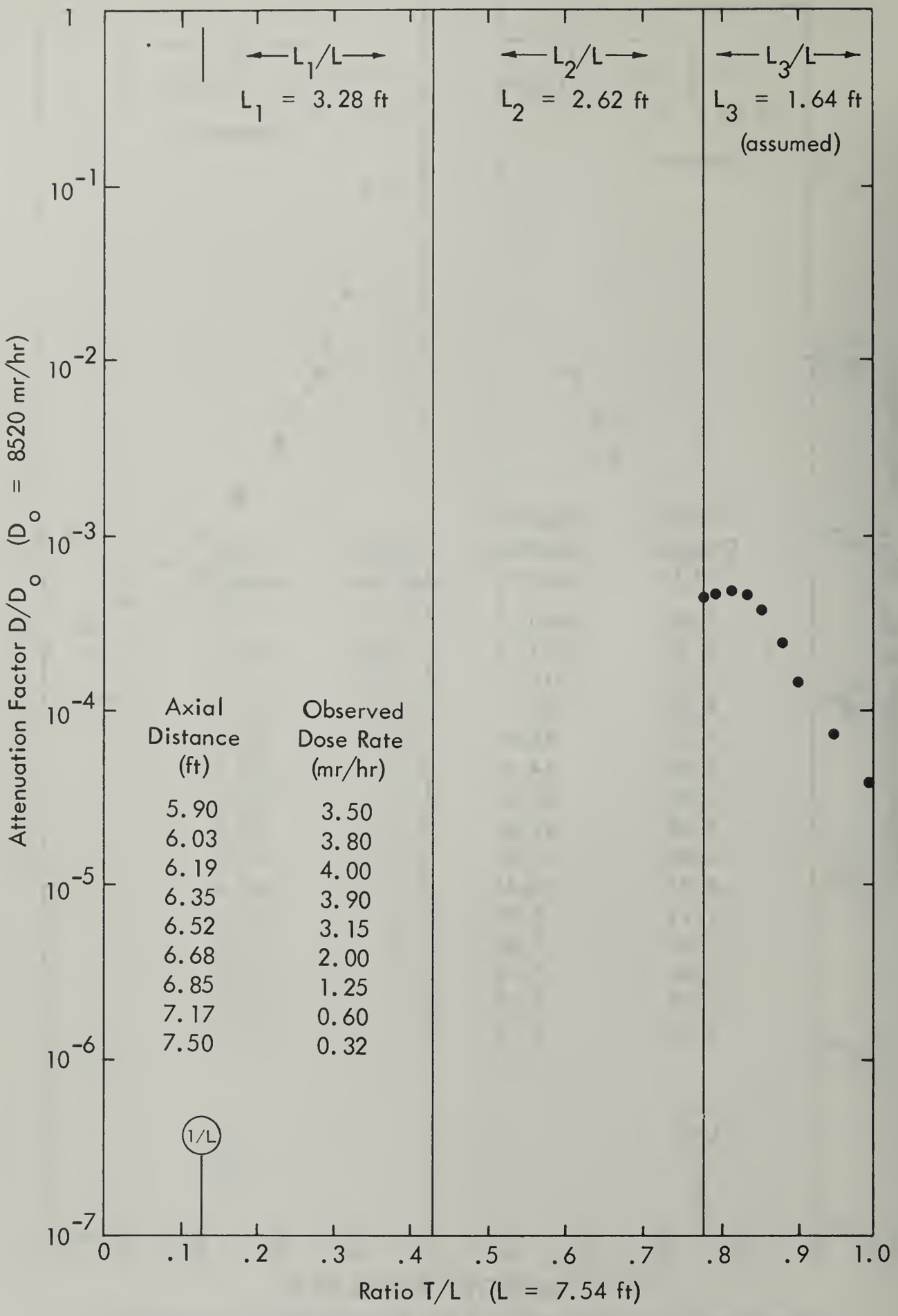

Figure 5. Z-shaped 0.925 x 0.925-foot square concrete duct with W/2 = 0.4625 foot; 0.6-curie Co^{60} point source. (From Reference 1, supplemented by correspondence.)

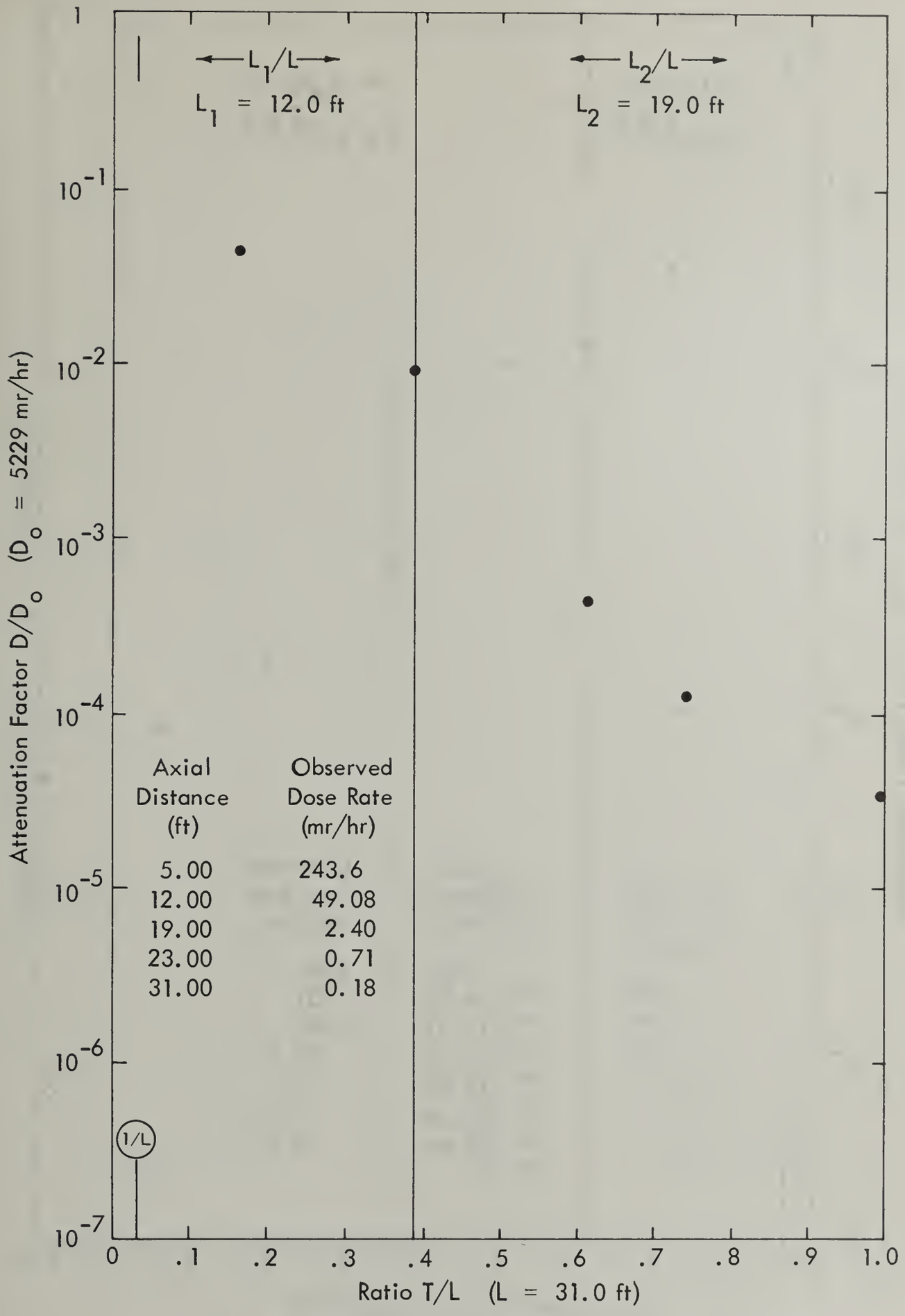

Figure 6. L-shaped 6 x 6-foot concrete entranceway with W/2 = 3.0 feet; 1.52-curie Cs^{137} point source. (From Reference 2, Table 4.)

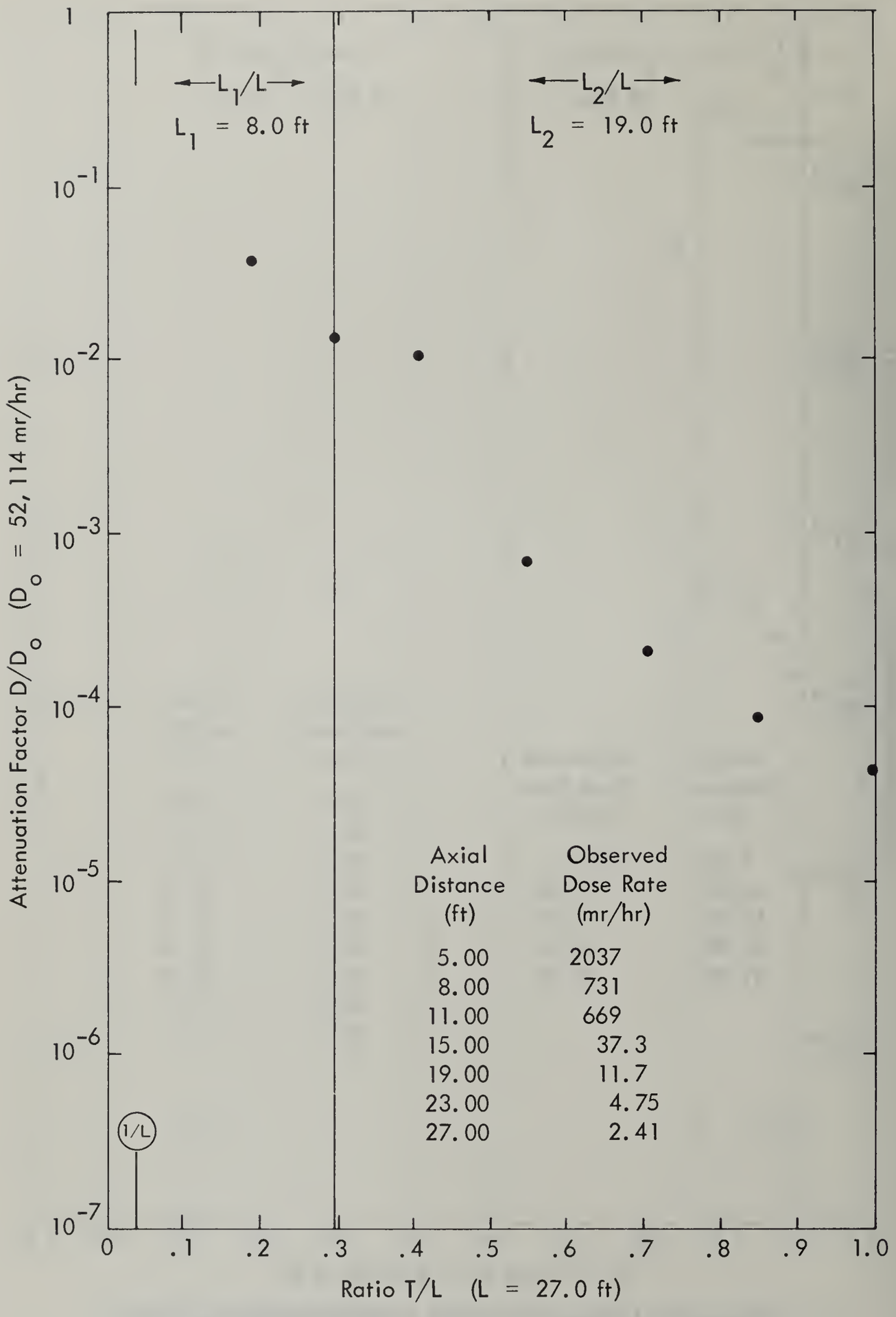

Figure 7. L-shaped 6 x 6-foot concrete entranceway with W/2 = 3.0 feet; 3.67-curie Co^{60} point source. (From Reference 2, Table 5A.)

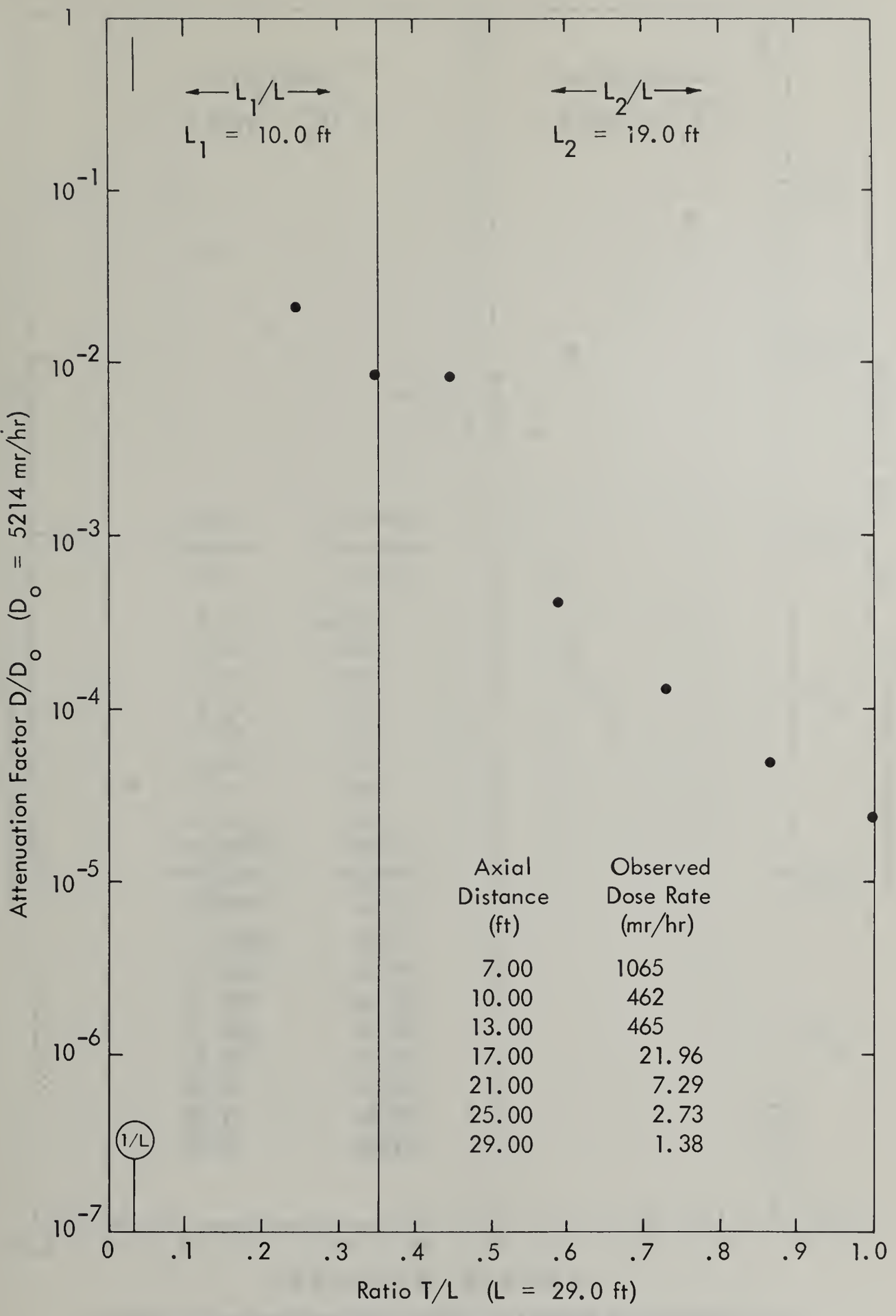

Figure 8. L-shaped 6 x 6-foot concrete entranceway with W/2 = 3.0 feet; 3.67-curie Co^{60} point source. (From Reference 2, Table 5B.)

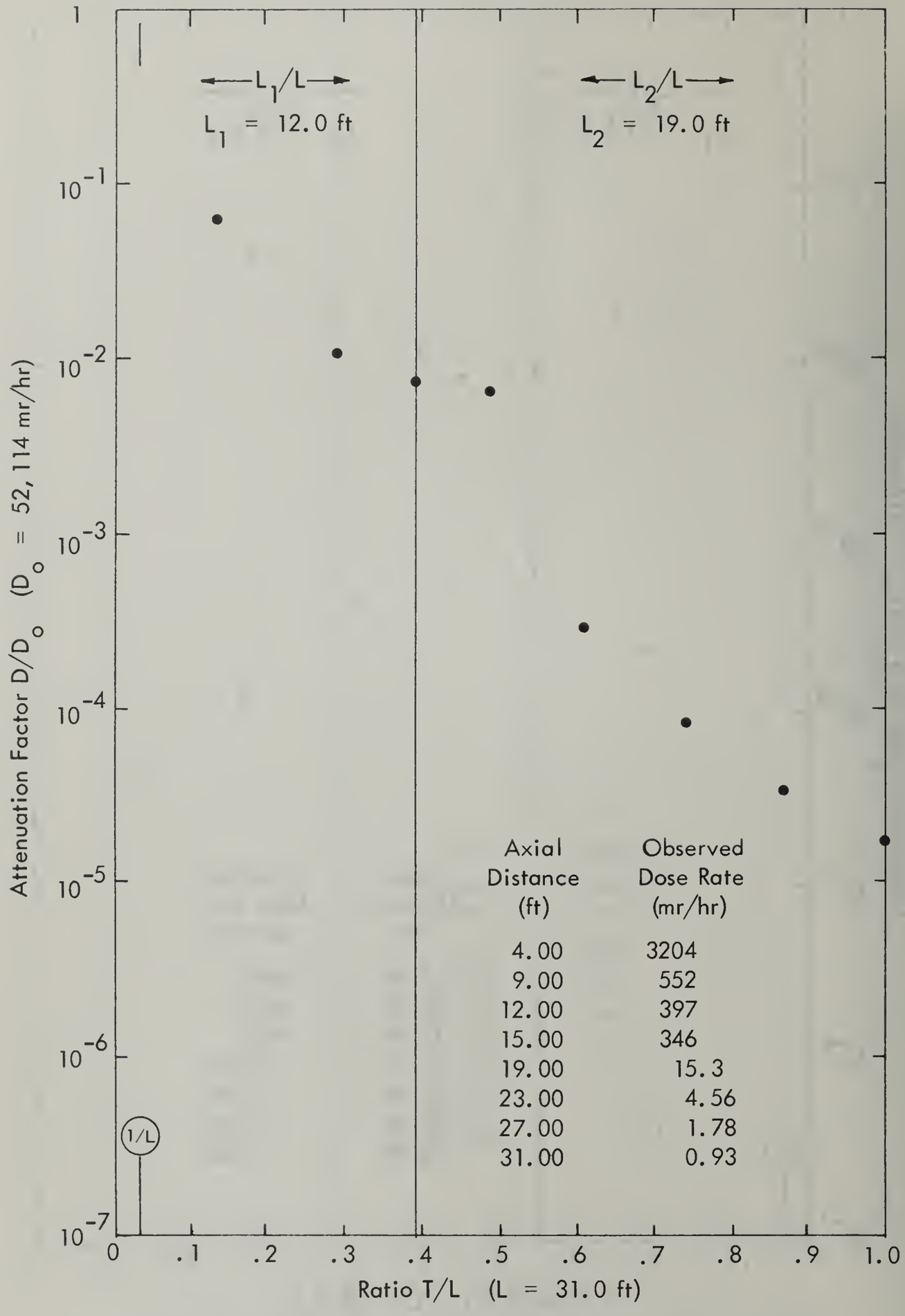

Figure 9. L-shaped 6 x 6-foot concrete entranceway with W/2 = 3.0 feet; 3.67-curie Co^{60} point source. (From Reference 2, Table 5C.)

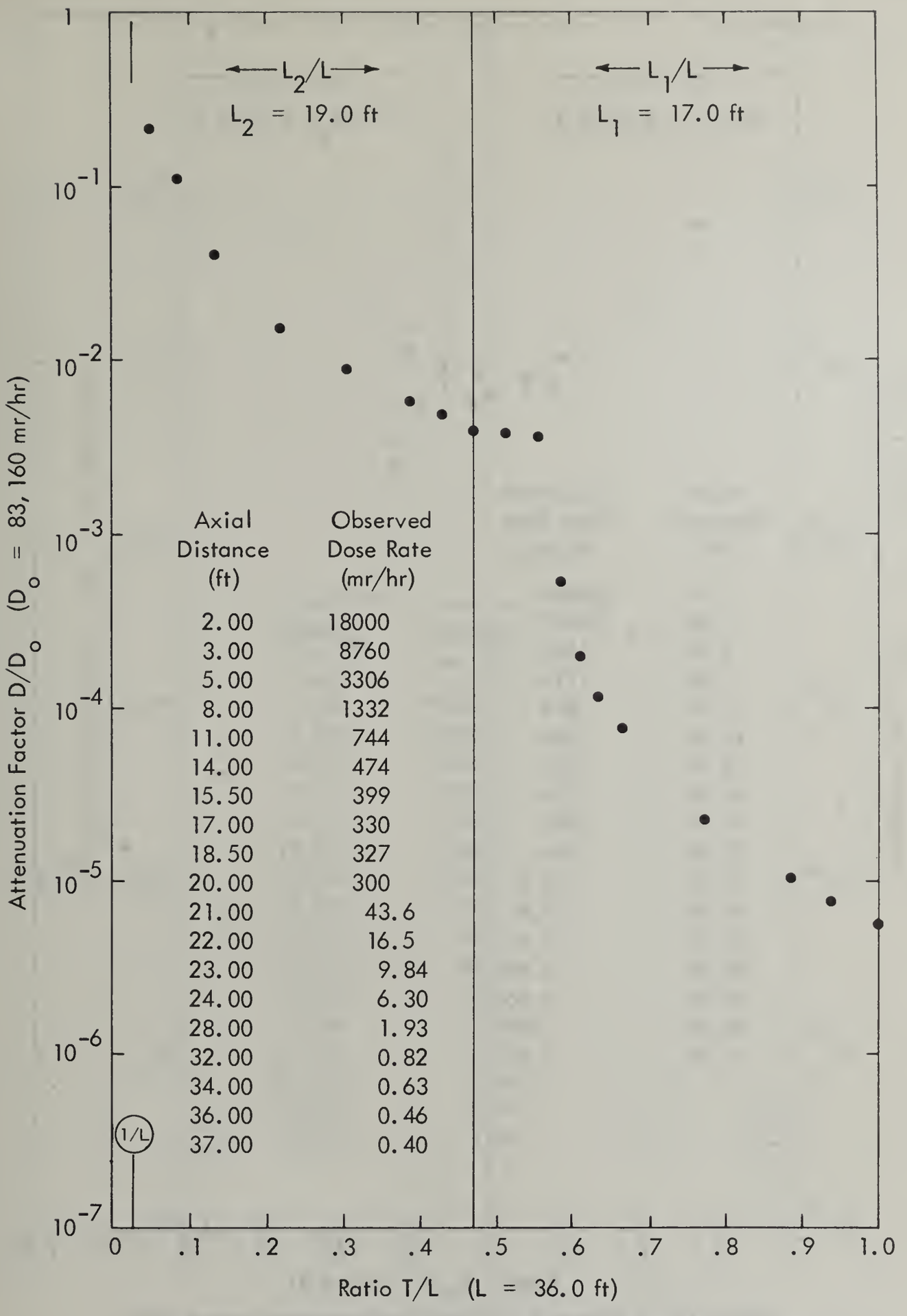

Figure 10. L-shaped 6 x 6-foot concrete entranceway with W/2 = 3.0 feet; 4.2-curie Na^{24} point source. (From Reference 3, Table 1.)

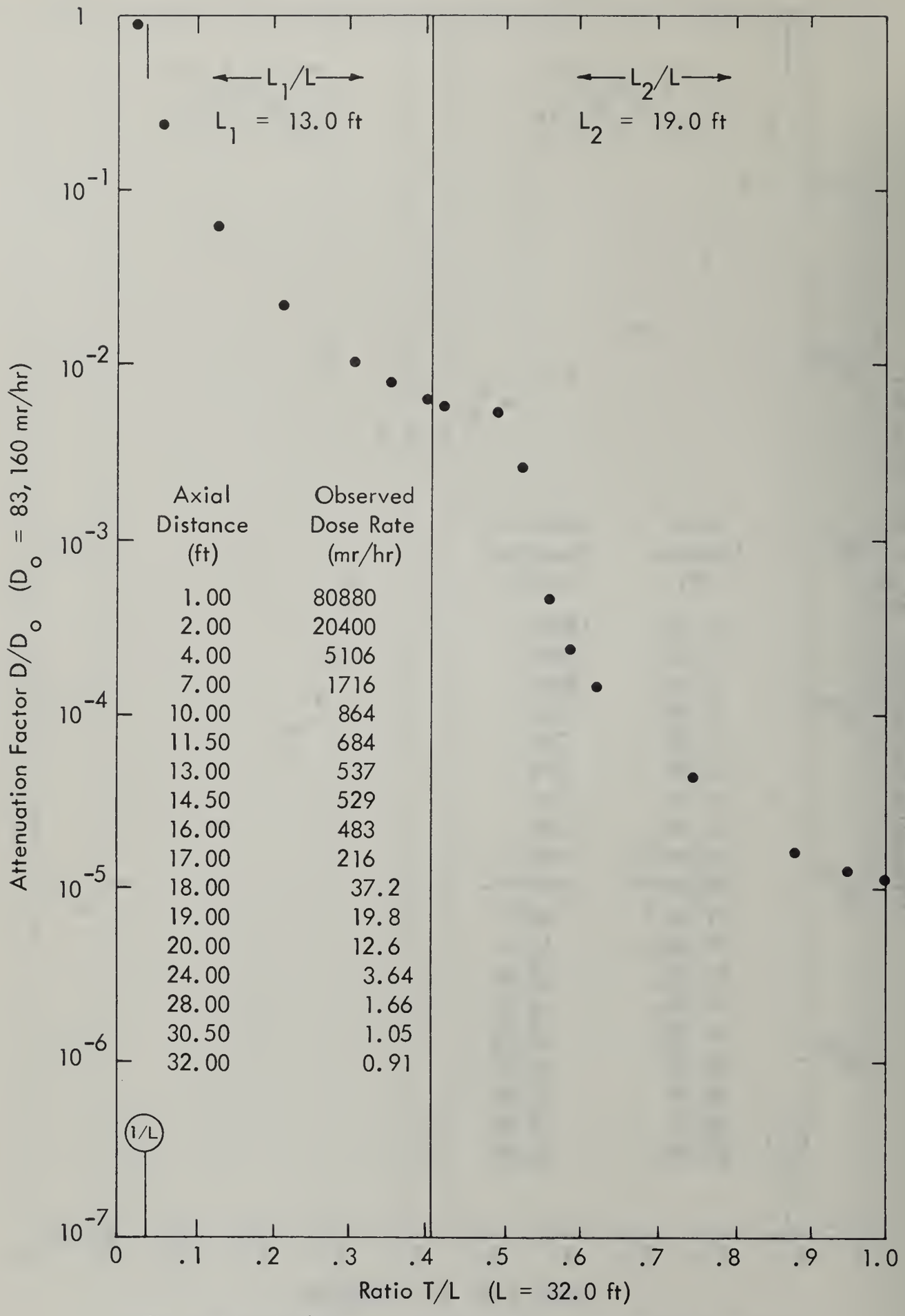

Axial Distance (ft)	Observed Dose Rate (mr/hr)
1.00	80880
2.00	20400
4.00	5106
7.00	1716
10.00	864
11.50	684
13.00	537
14.50	529
16.00	483
17.00	216
18.00	37.2
19.00	19.8
20.00	12.6
24.00	3.64
28.00	1.66
30.50	1.05
32.00	0.91

Figure 11. L-shaped 6 x 6-foot concrete entranceway with W/2 = 3.0 feet; 4.2-curie Na^{24} point source. (From Reference 3, Table 2.)

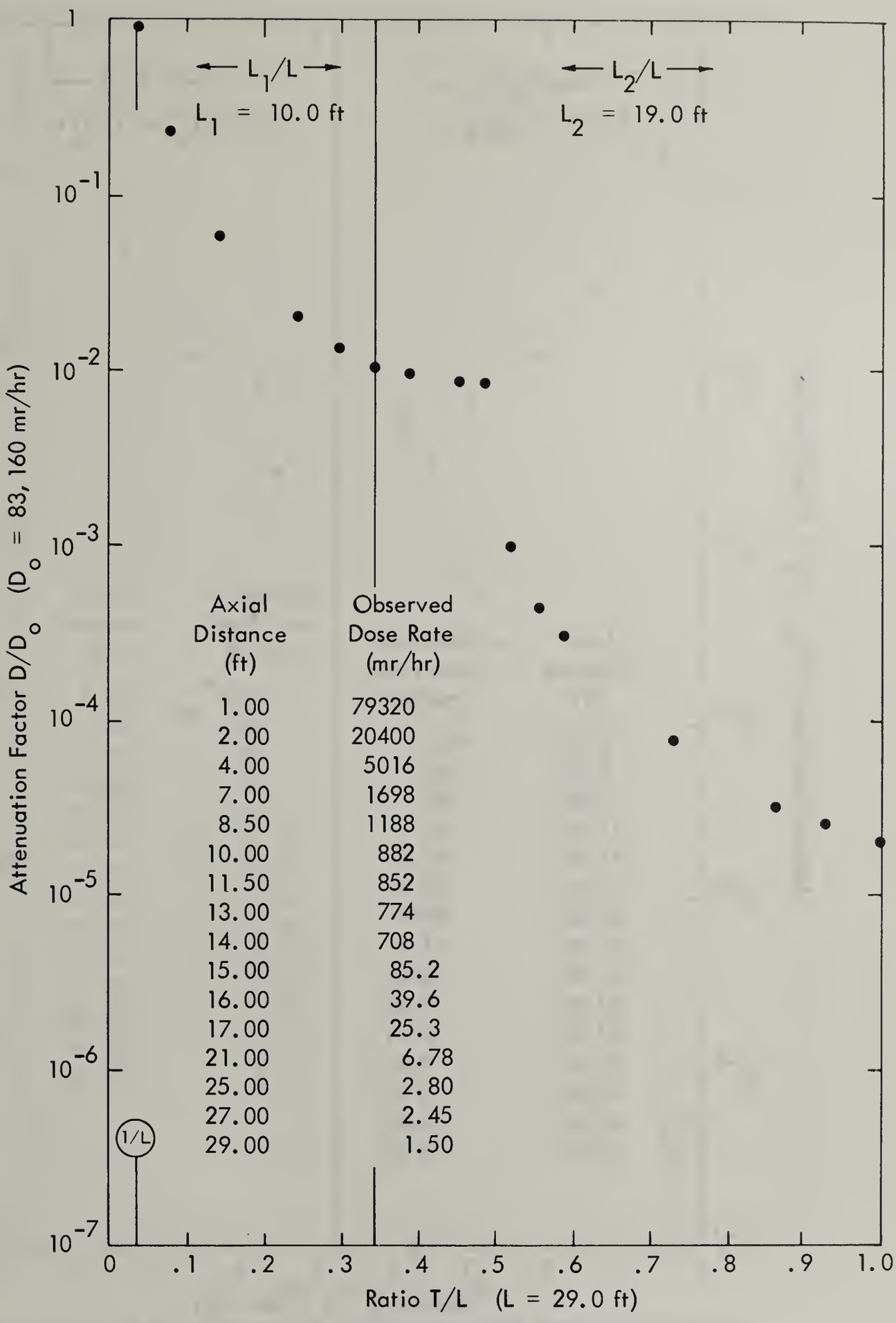

Axial Distance (ft)	Observed Dose Rate (mr/hr)
1.00	79320
2.00	20400
4.00	5016
7.00	1698
8.50	1188
10.00	882
11.50	852
13.00	774
14.00	708
15.00	85.2
16.00	39.6
17.00	25.3
21.00	6.78
25.00	2.80
27.00	2.45
29.00	1.50

Figure 12. L-shaped 6 x 6-foot concrete entranceway with W/2 = 3.0 feet; 4.2-curie Na^{24} point source. (From Reference 3, Table 3.)

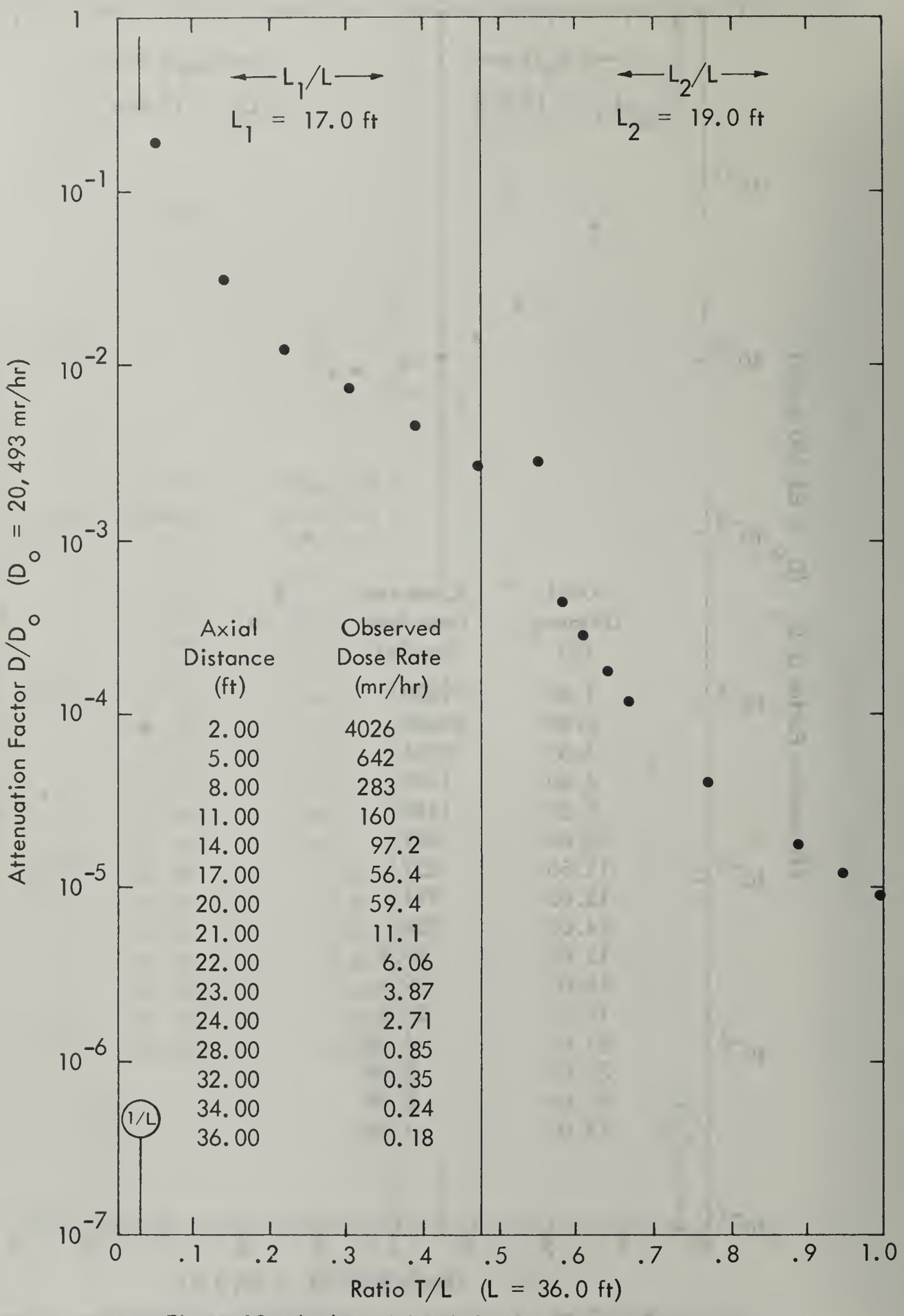

Axial Distance (ft)	Observed Dose Rate (mr/hr)
2.00	4026
5.00	642
8.00	283
11.00	160
14.00	97.2
17.00	56.4
20.00	59.4
21.00	11.1
22.00	6.06
23.00	3.87
24.00	2.71
28.00	0.85
32.00	0.35
34.00	0.24
36.00	0.18

Figure 13. L-shaped 6 x 6-foot concrete entranceway with W/2 = 3.0 feet; 8.1-curie Au^{198} point source. (From Reference 3, Table 4.)

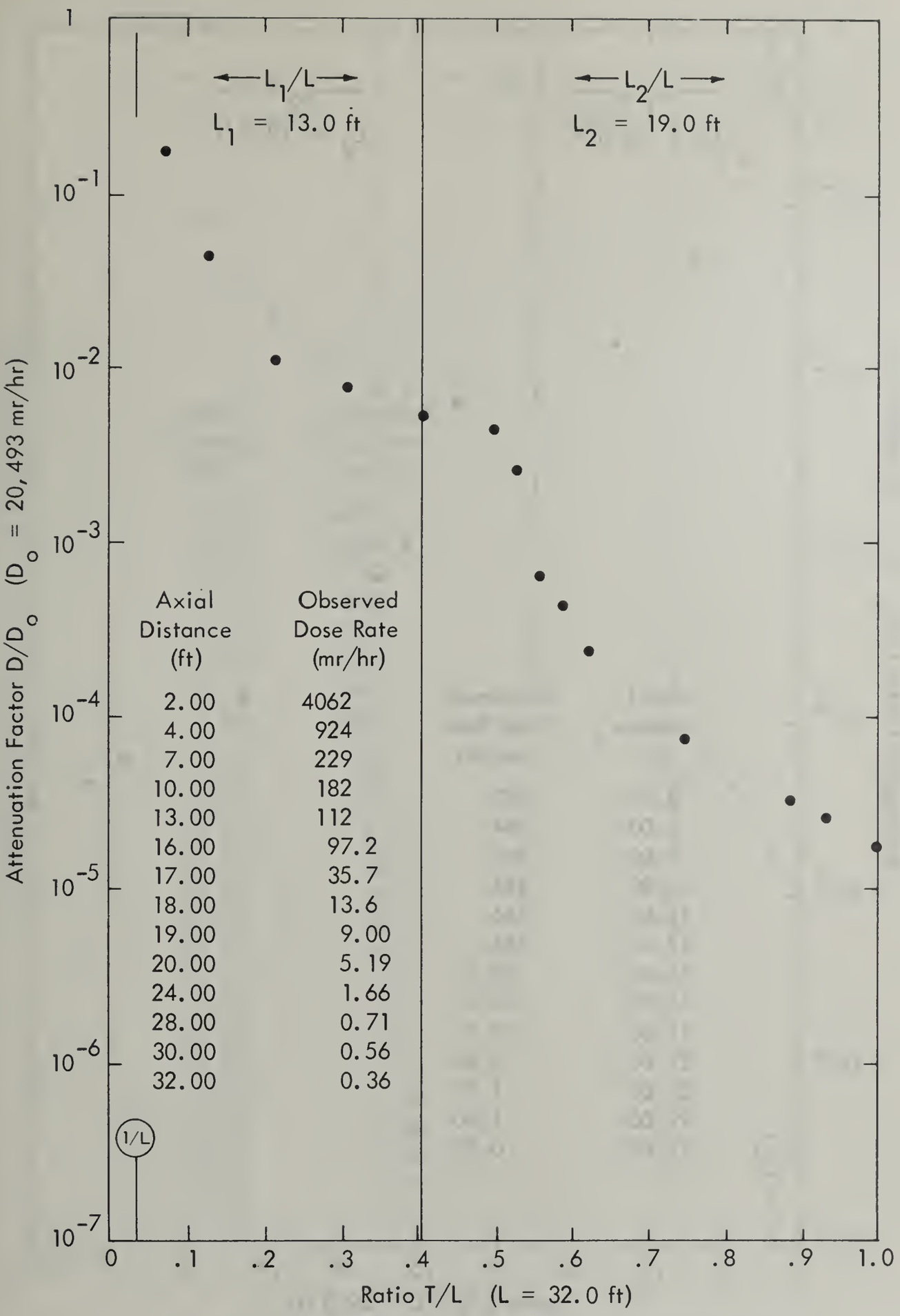

Figure 14. L-shaped 6 x 6-foot concrete entranceway with W/2 = 3.0 feet; 8.1-curie Au^{198} point source. (From Reference 3, Table 5.)

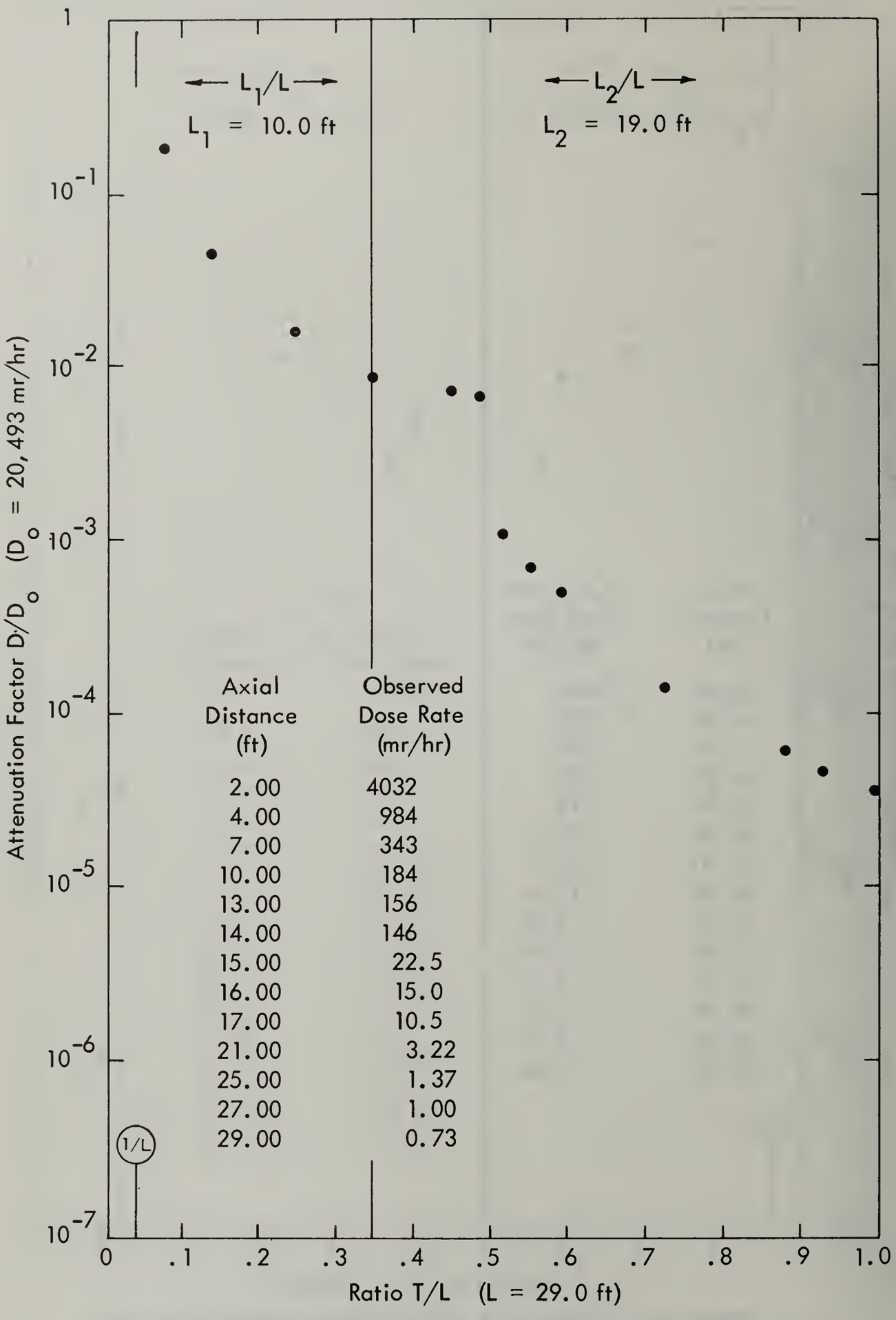

Axial Distance (ft)	Observed Dose Rate (mr/hr)
2.00	4032
4.00	984
7.00	343
10.00	184
13.00	156
14.00	146
15.00	22.5
16.00	15.0
17.00	10.5
21.00	3.22
25.00	1.37
27.00	1.00
29.00	0.73

Figure 15. L-shaped 6 x 6-foot concrete entranceway with W/2 = 3.0 feet; 8.1-curie Au^{198} point source. (From Reference 3, Table 6.)

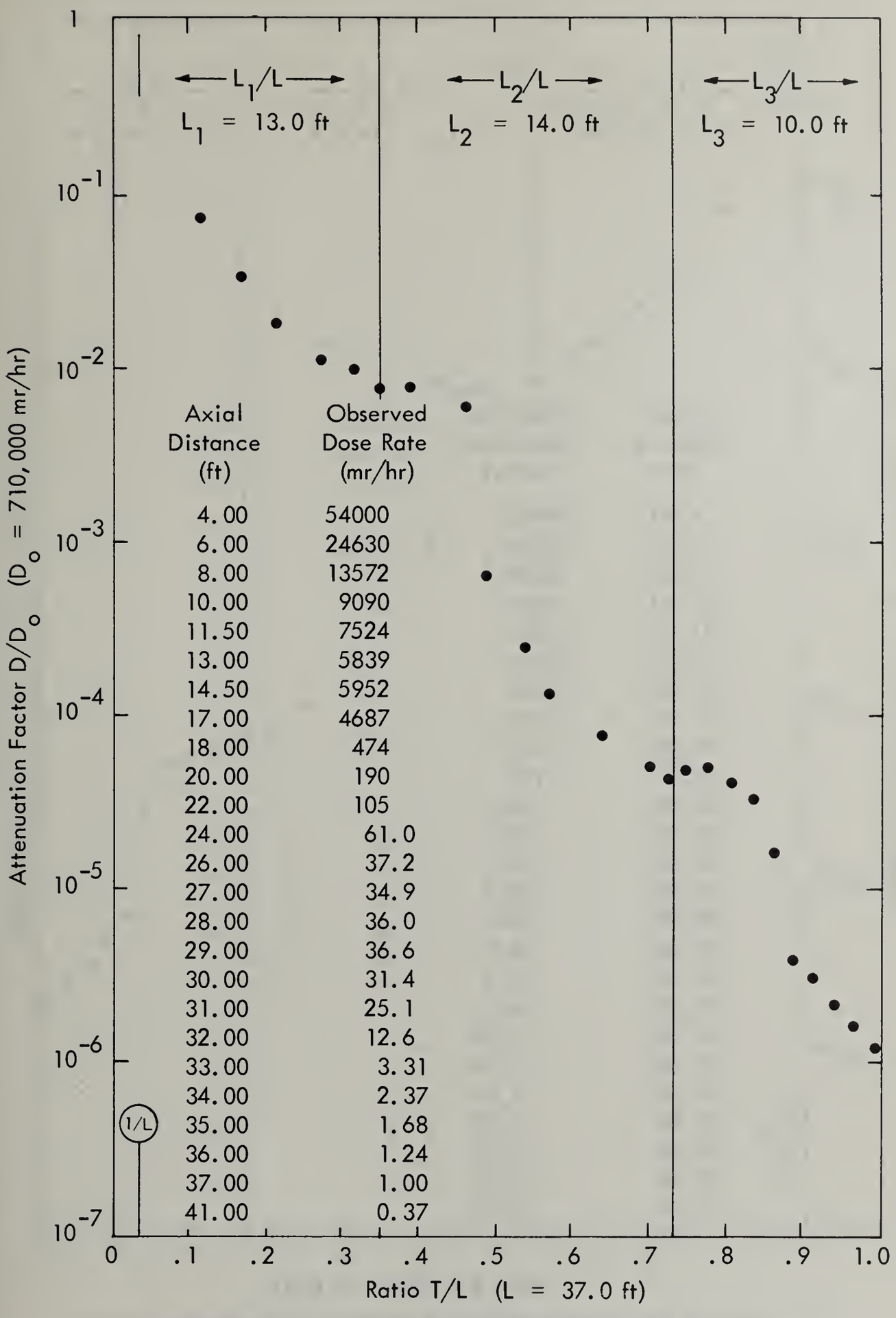

Figure 16. Z-shaped 6 x 6-foot concrete entranceway with W/2 = 3.0 feet; 50-curie Co^{60} point source. (From Reference 4, Table 1.)

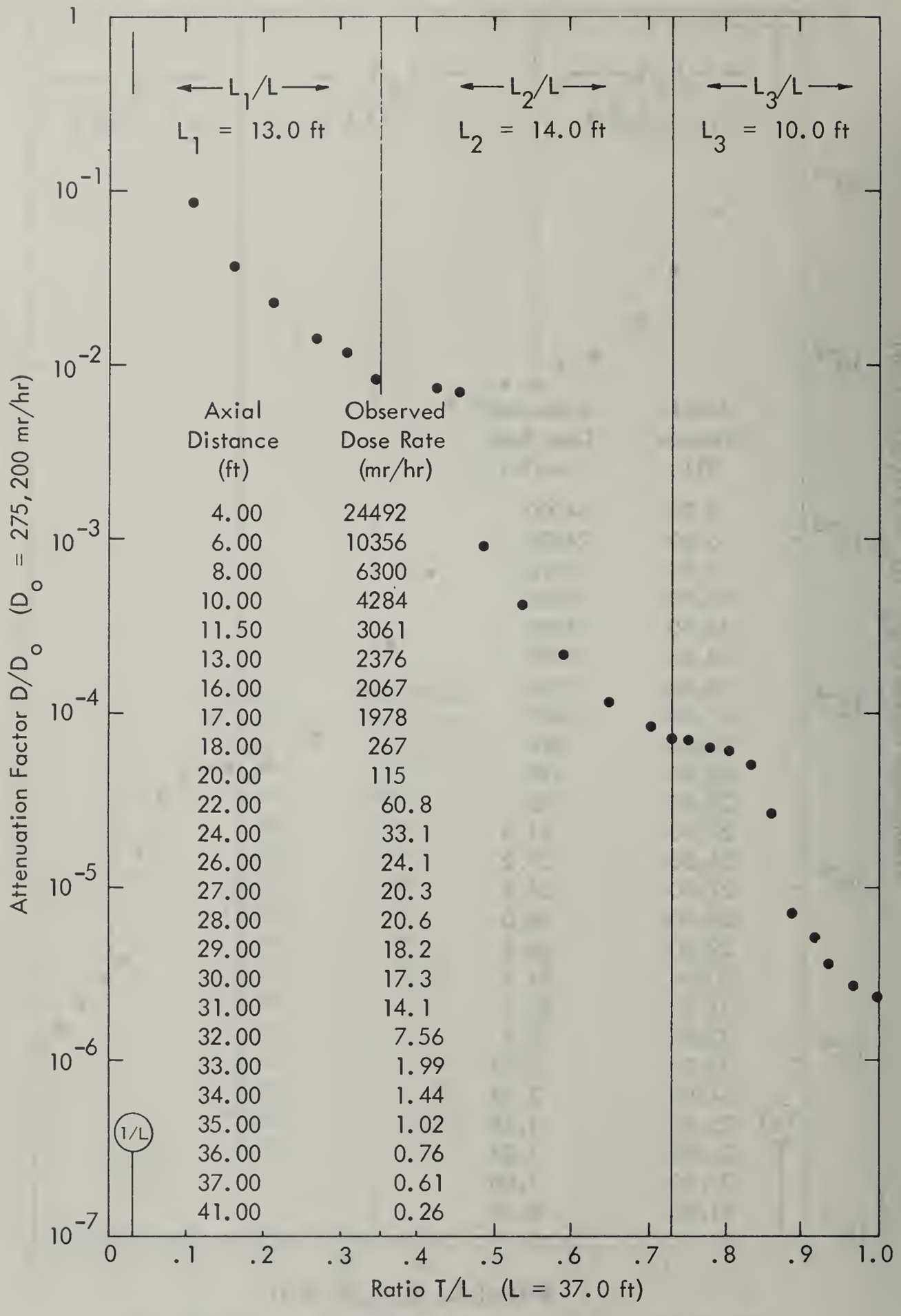

Axial Distance (ft)	Observed Dose Rate (mr/hr)
4.00	24492
6.00	10356
8.00	6300
10.00	4284
11.50	3061
13.00	2376
16.00	2067
17.00	1978
18.00	267
20.00	115
22.00	60.8
24.00	33.1
26.00	24.1
27.00	20.3
28.00	20.6
29.00	18.2
30.00	17.3
31.00	14.1
32.00	7.56
33.00	1.99
34.00	1.44
35.00	1.02
36.00	0.76
37.00	0.61
41.00	0.26

Figure 17. Z-shaped 6 x 6-foot concrete entranceway with W/2 = 3.0 feet; 80-curie Cs^{137} point source. (From Reference 4, Table 2.)

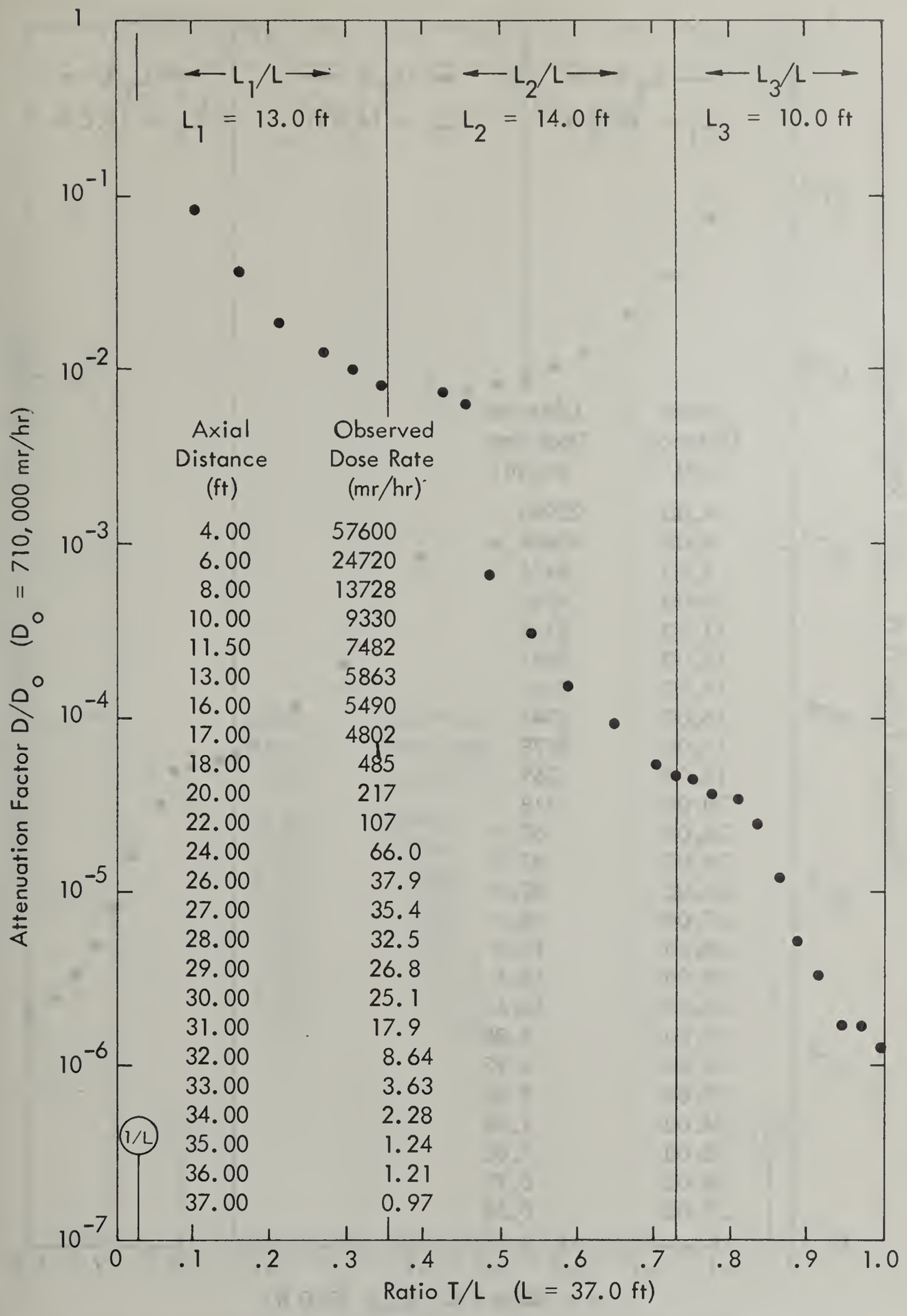

Axial Distance (ft)	Observed Dose Rate (mr/hr)
4.00	57600
6.00	24720
8.00	13728
10.00	9330
11.50	7482
13.00	5863
16.00	5490
17.00	4802
18.00	485
20.00	217
22.00	107
24.00	66.0
26.00	37.9
27.00	35.4
28.00	32.5
29.00	26.8
30.00	25.1
31.00	17.9
32.00	8.64
33.00	3.63
34.00	2.28
35.00	1.24
36.00	1.21
37.00	0.97

Figure 18. U-shaped 6 x 6-foot concrete entranceway with W/2 = 3.0 feet; 50-curie Co^{60} point source. (From Reference 4, Table 3.)

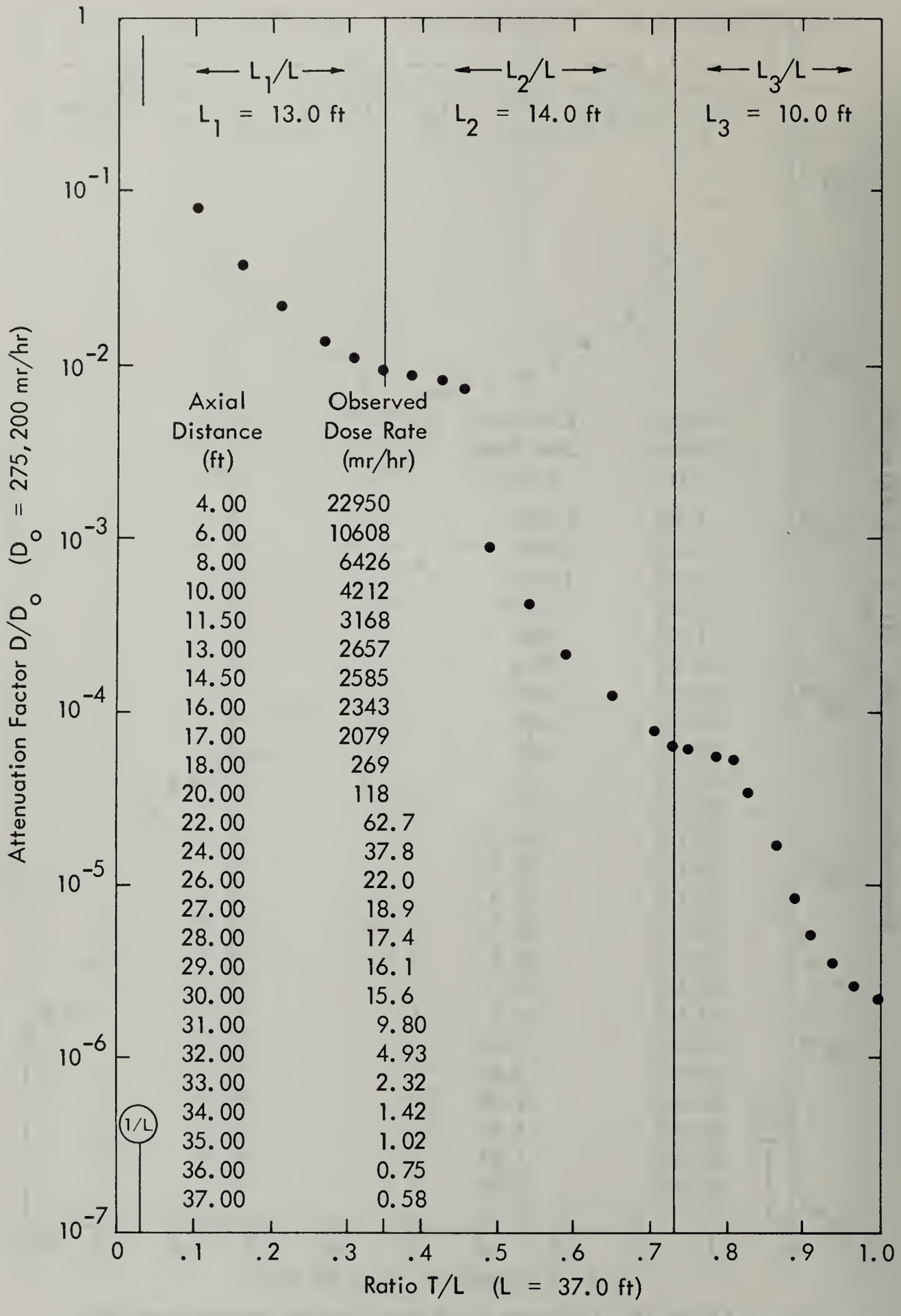

Axial Distance (ft)	Observed Dose Rate (mr/hr)
4.00	22950
6.00	10608
8.00	6426
10.00	4212
11.50	3168
13.00	2657
14.50	2585
16.00	2343
17.00	2079
18.00	269
20.00	118
22.00	62.7
24.00	37.8
26.00	22.0
27.00	18.9
28.00	17.4
29.00	16.1
30.00	15.6
31.00	9.80
32.00	4.93
33.00	2.32
34.00	1.42
35.00	1.02
36.00	0.75
37.00	0.58

Figure 19. U-shaped 6 x 6-foot concrete entranceway with W/2 = 3.0 feet; 80-curie Cs^{137} point source. (From Reference 4, Table 4.)

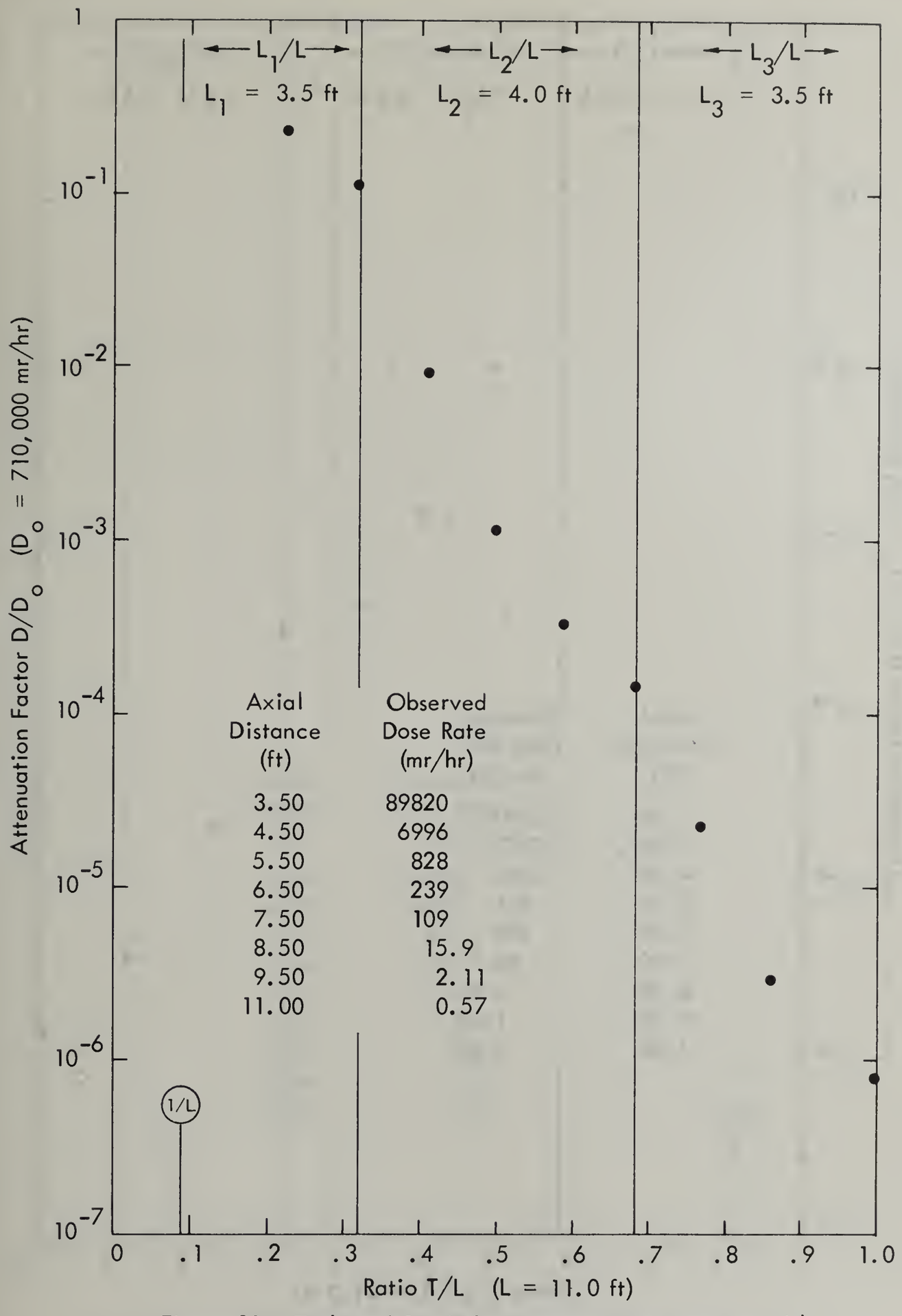

Figure 20. Z-shaped 1 x 1-foot concrete entranceway with W/2 = 0.5 foot; 50-curie Co^{60} point source. (From Reference 4, Table 6.)

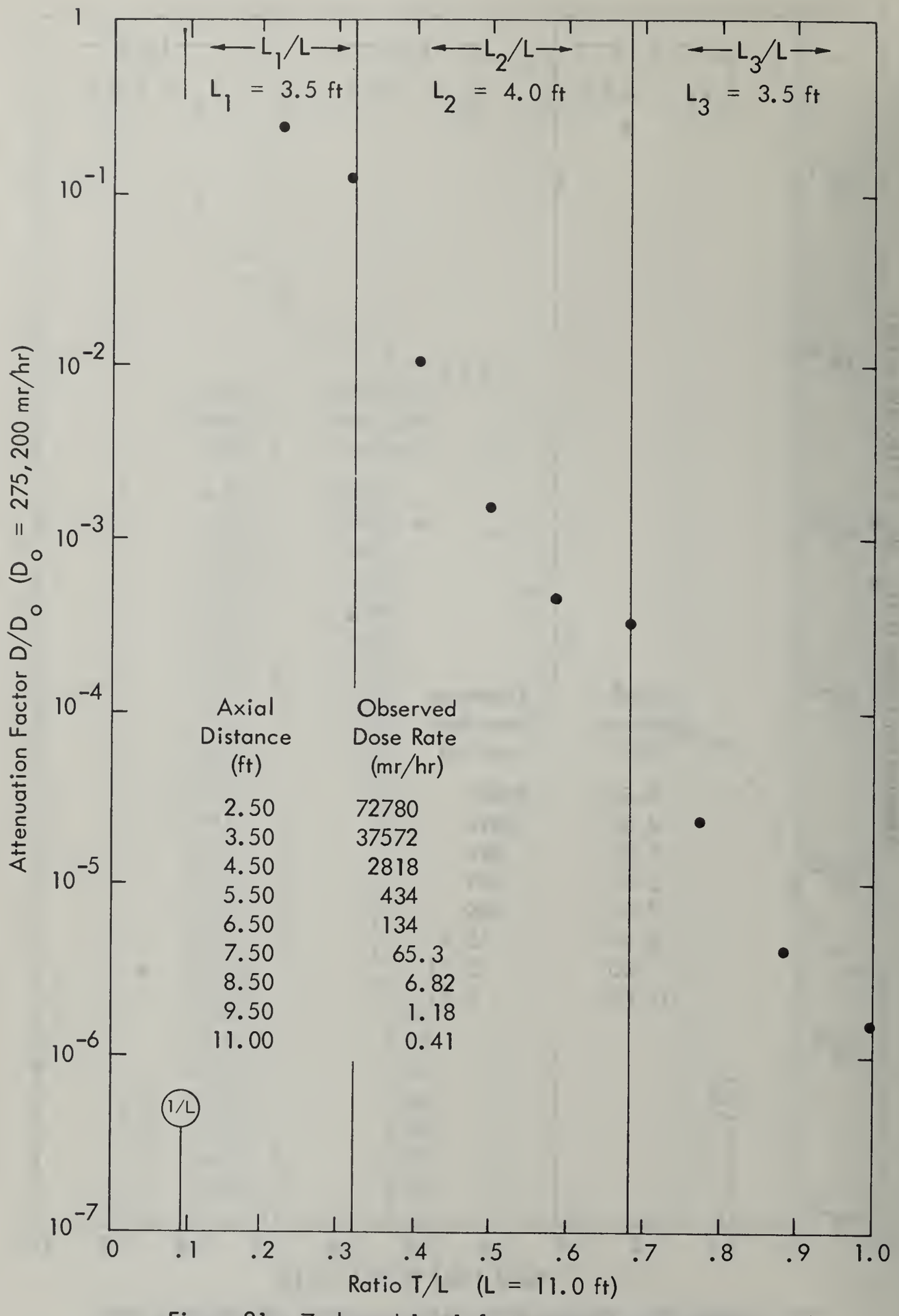

Figure 21. Z-shaped 1 x 1-foot concrete entranceway with W/2 = 0.5 foot; 80-curie Cs^{137} point source. (From Reference 4, Table 7.)

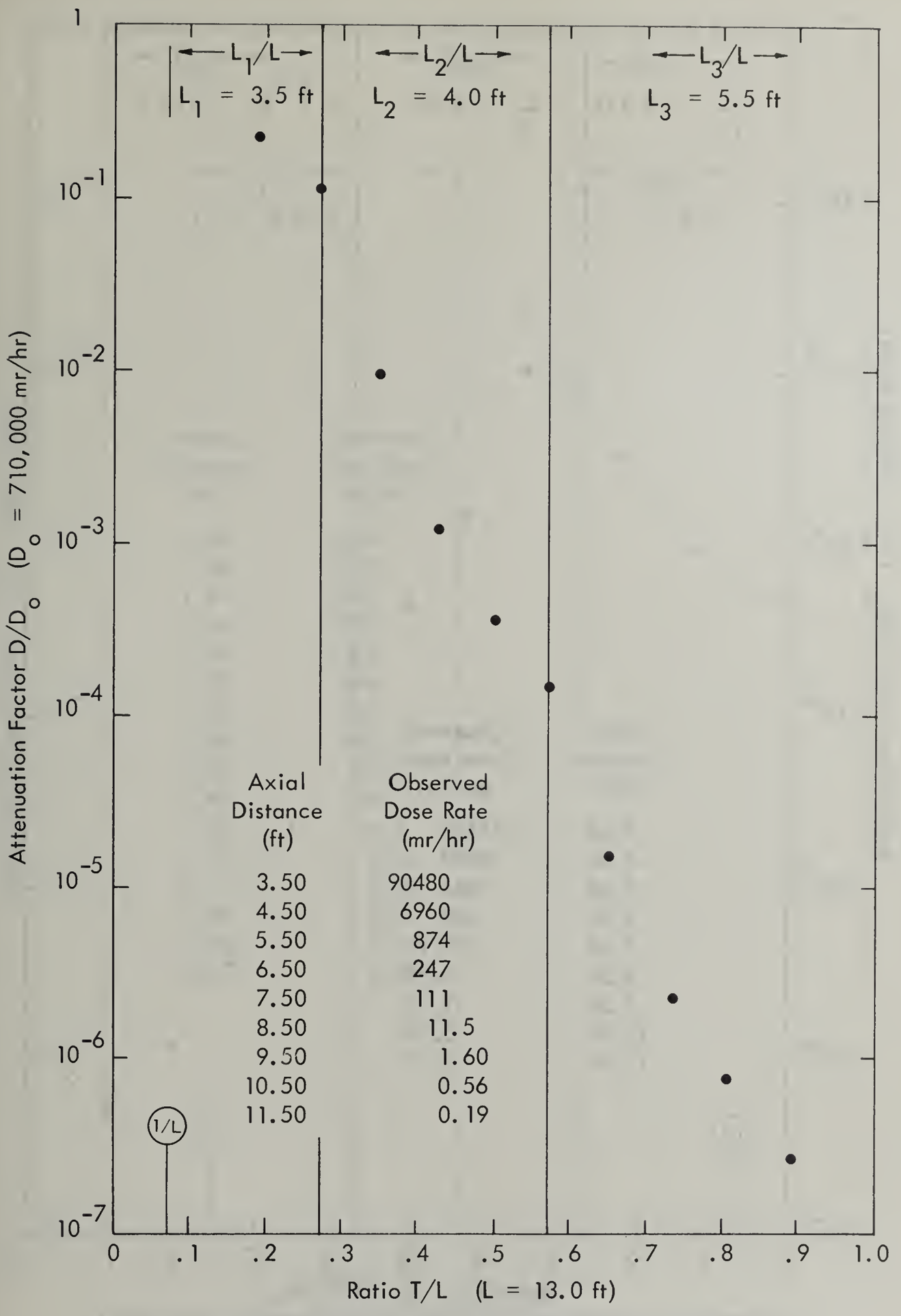

Figure 22. U-shaped 1 x 1-foot concrete entranceway with W/2 = 0.5 foot; 50-curie Co^{60} point source. (From Reference 4, Table 8.)

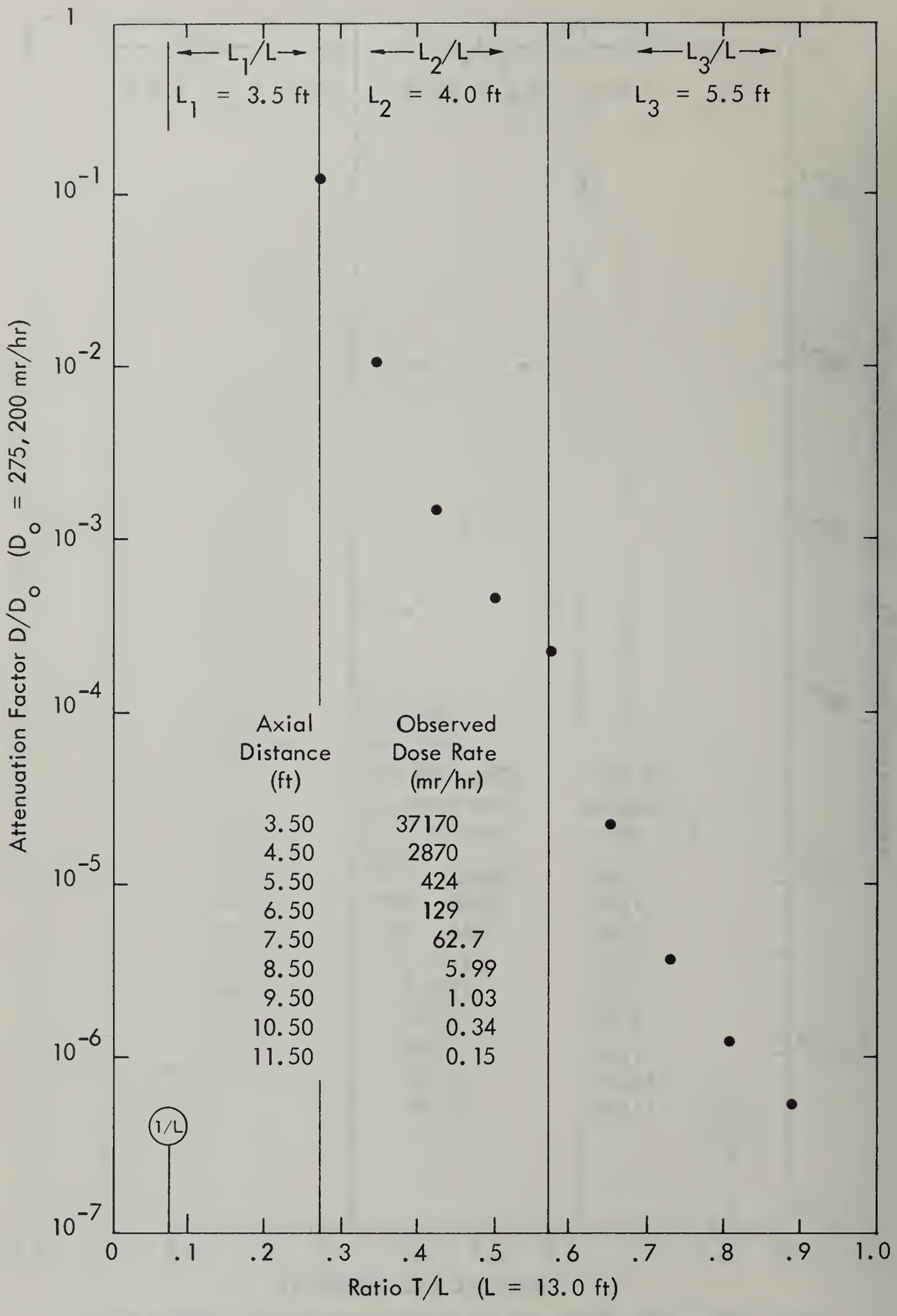

Figure 23. U-shaped 1 x 1-foot concrete entranceway with W/2 = 0.5 foot; 80-curie Cs^{137} point source. (From Reference 4, Table 9.)

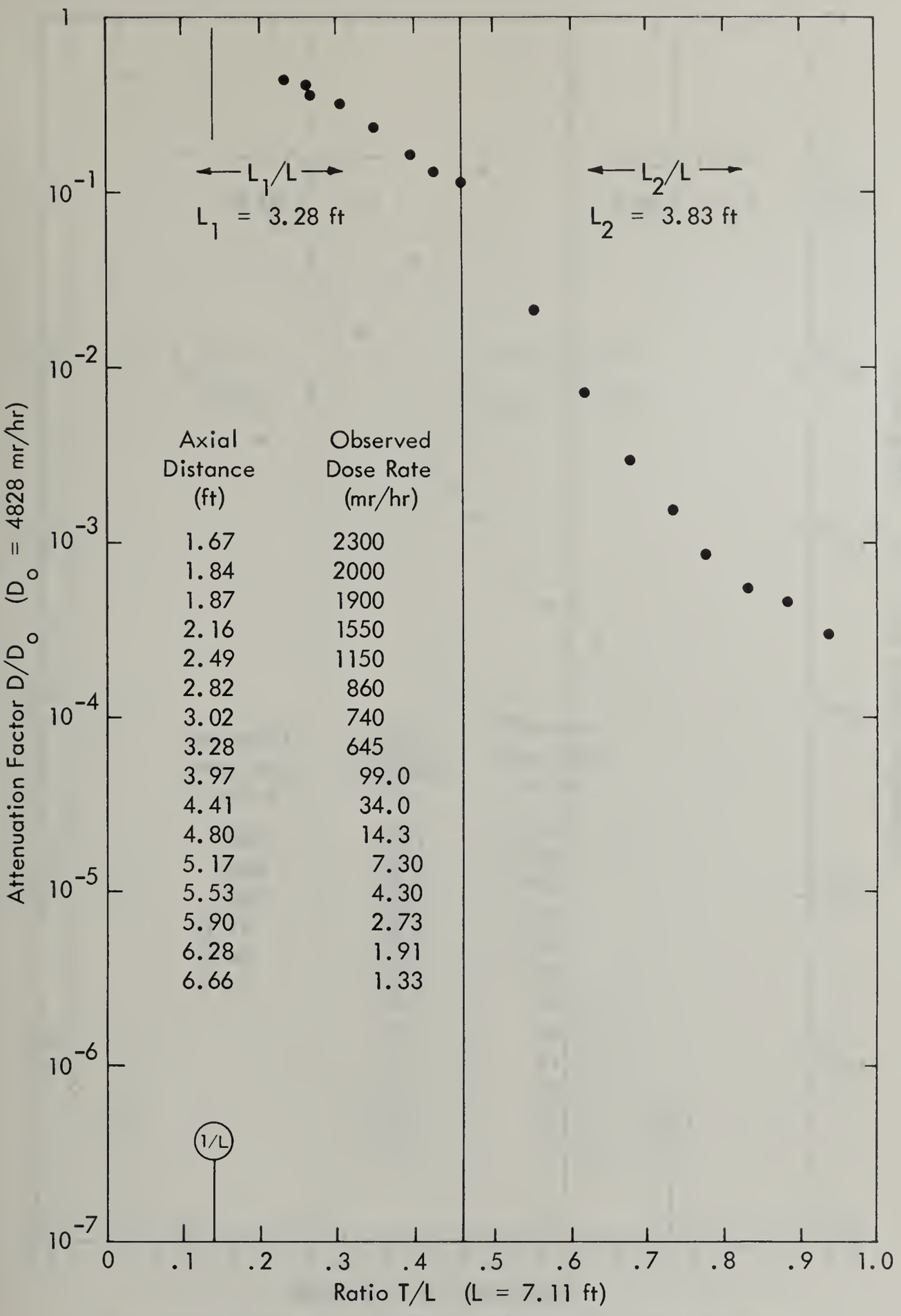

Figure 24. L-shaped 0.9167 x 0.9167-foot square concrete duct with W/2 = 0.4583 foot; 0.34-curie Co^{60} point source. Source in corner for L_1 measurements. (From Reference 5, Figure 12 and Table 8C-C.)

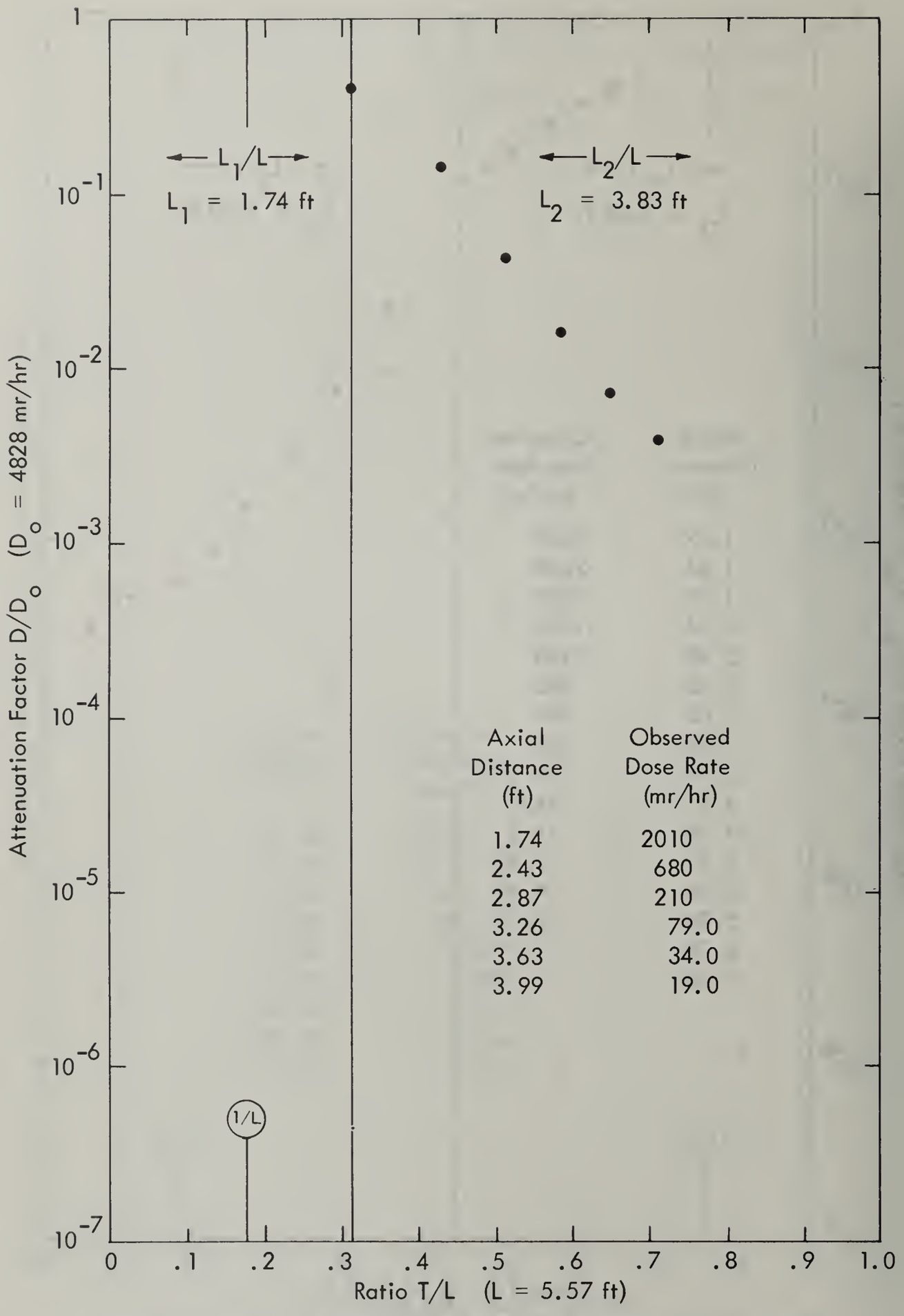

Figure 25. L-shaped 0.9167 x 0.9167-foot square concrete duct with W/2 = 0.4583 foot; 0.34-curie Co^{60} point source. (From Reference 5, Table 10C-C.)

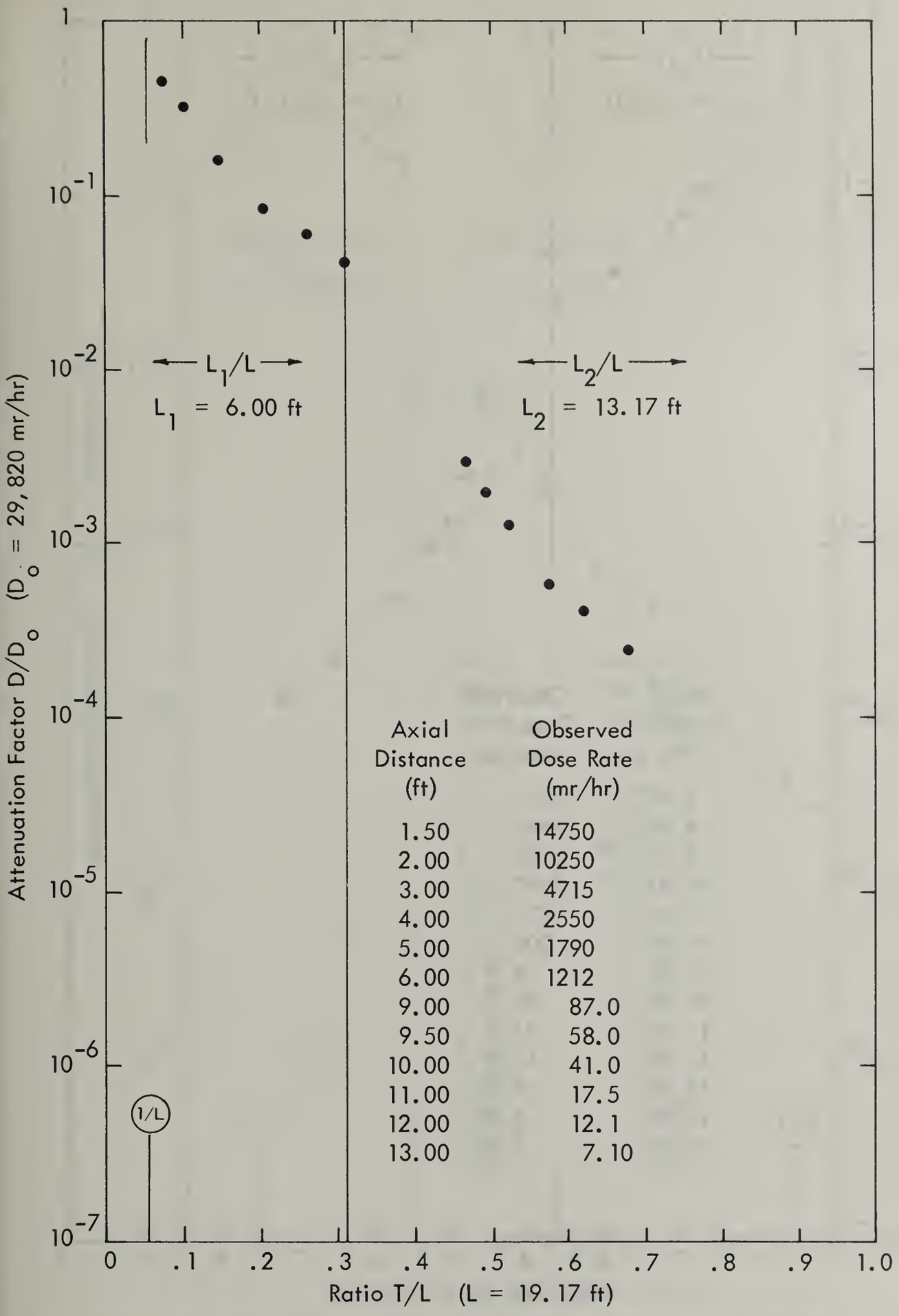

Axial Distance (ft)	Observed Dose Rate (mr/hr)
1.50	14750
2.00	10250
3.00	4715
4.00	2550
5.00	1790
6.00	1212
9.00	87.0
9.50	58.0
10.00	41.0
11.00	17.5
12.00	12.1
13.00	7.10

Figure 26. L-shaped 3 x 3-foot square concrete entranceway with W/2 = 1.5 feet; 2.1-curie Co^{60} point source. (From Reference 6, Table IA.)

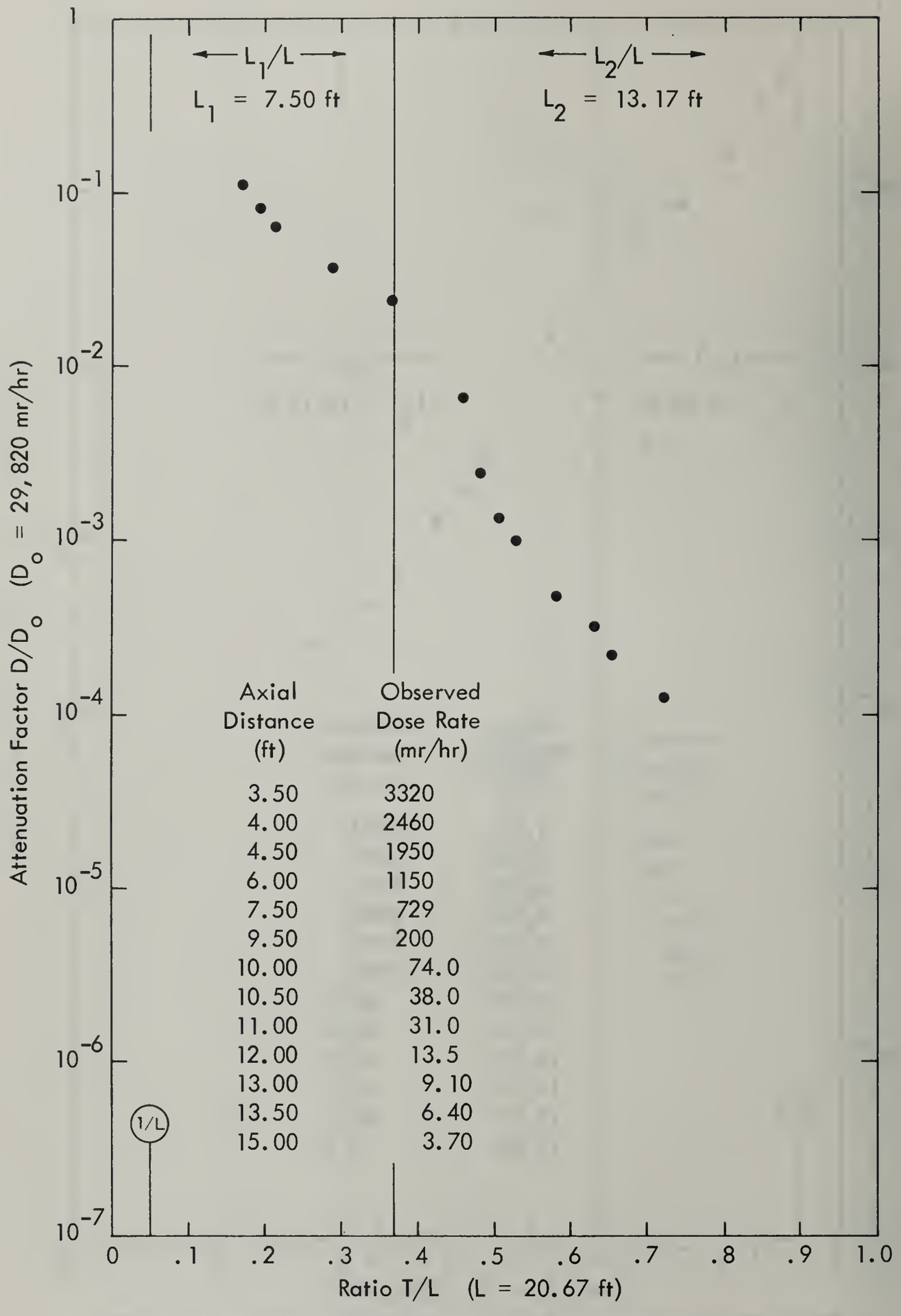

Axial Distance (ft)	Observed Dose Rate (mr/hr)
3.50	3320
4.00	2460
4.50	1950
6.00	1150
7.50	729
9.50	200
10.00	74.0
10.50	38.0
11.00	31.0
12.00	13.5
13.00	9.10
13.50	6.40
15.00	3.70

Figure 27. L-shaped 3 x 3-foot square concrete entranceway with W/2 = 1.5 feet; 2.1-curie Co^{60} point source. (From Reference 6, Table IB.)

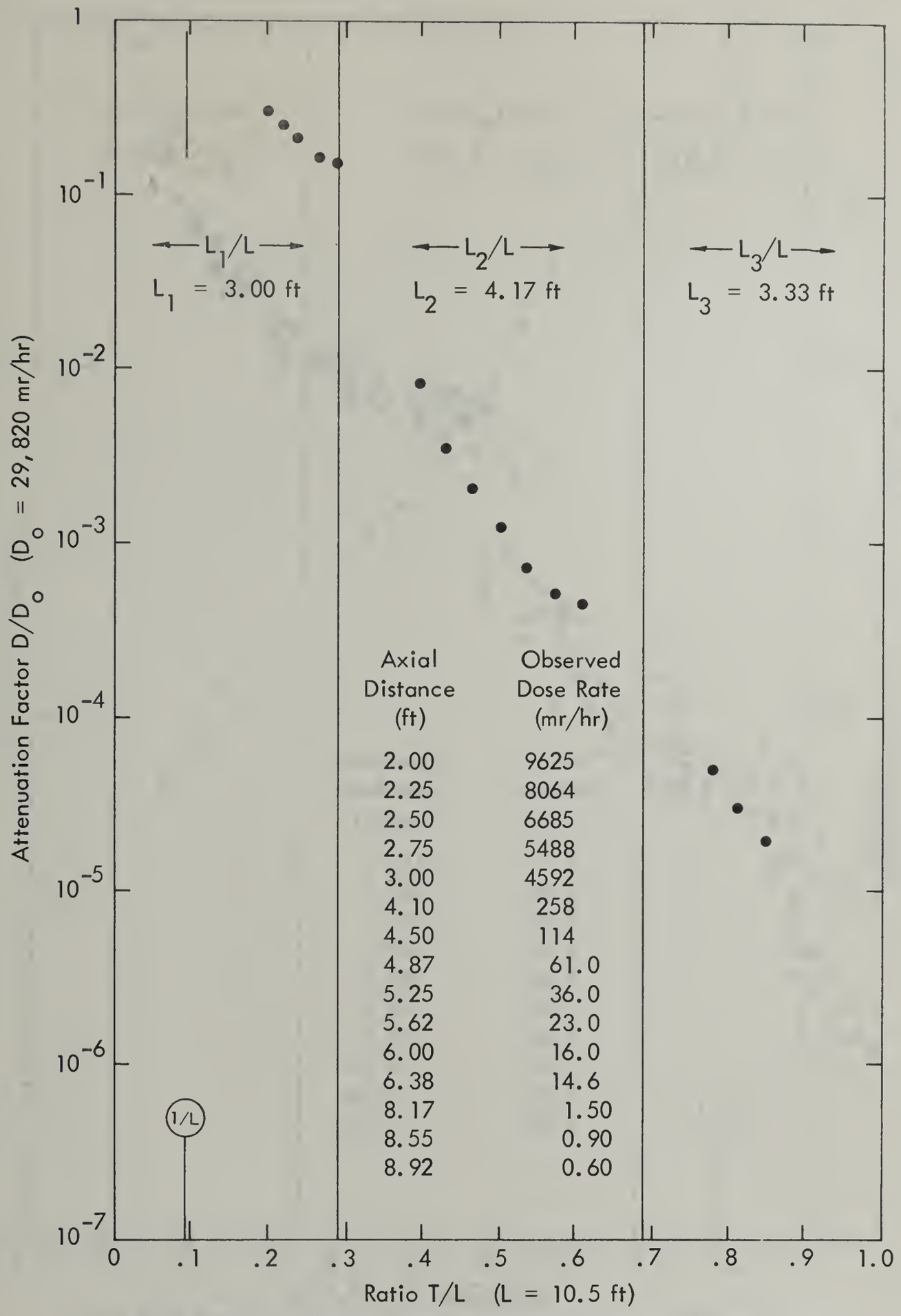

Axial Distance (ft)	Observed Dose Rate (mr/hr)
2.00	9625
2.25	8064
2.50	6685
2.75	5488
3.00	4592
4.10	258
4.50	114
4.87	61.0
5.25	36.0
5.62	23.0
6.00	16.0
6.38	14.6
8.17	1.50
8.55	0.90
8.92	0.60

Figure 28. Z-shaped 1-foot-diameter round concrete duct with W/2 = 0.443 foot; 2.1-curie Co^{60} point source; 0.3-curie source used for L_1 (D/7 = actual dose). (From Reference 7, Tables I, III, IV.)

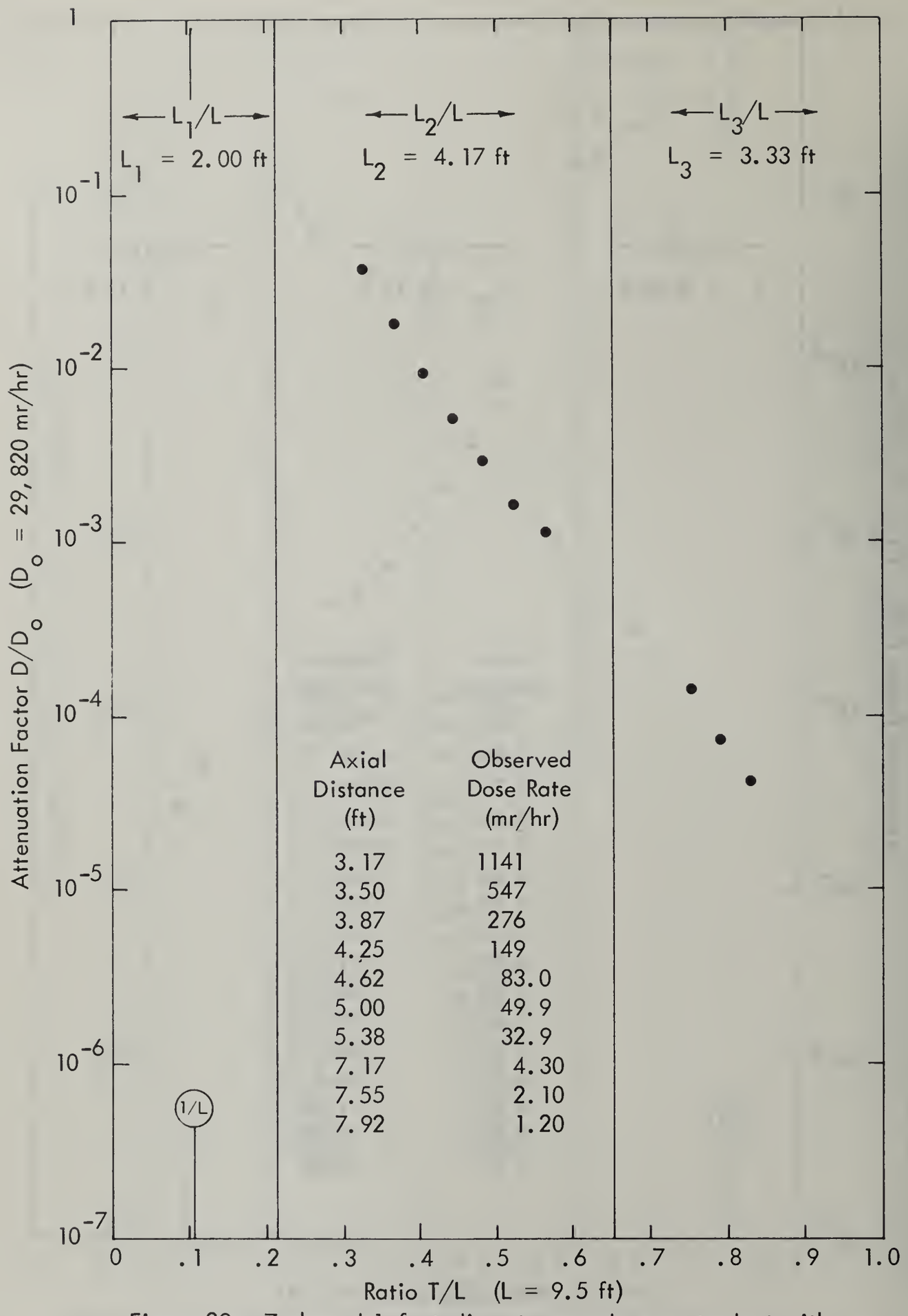

Figure 29. Z-shaped 1-foot-diameter round concrete duct with W/2 = 0.443 foot; 2.1-curie Co^{60} point source. (From Reference 7, Tables III, IV.)

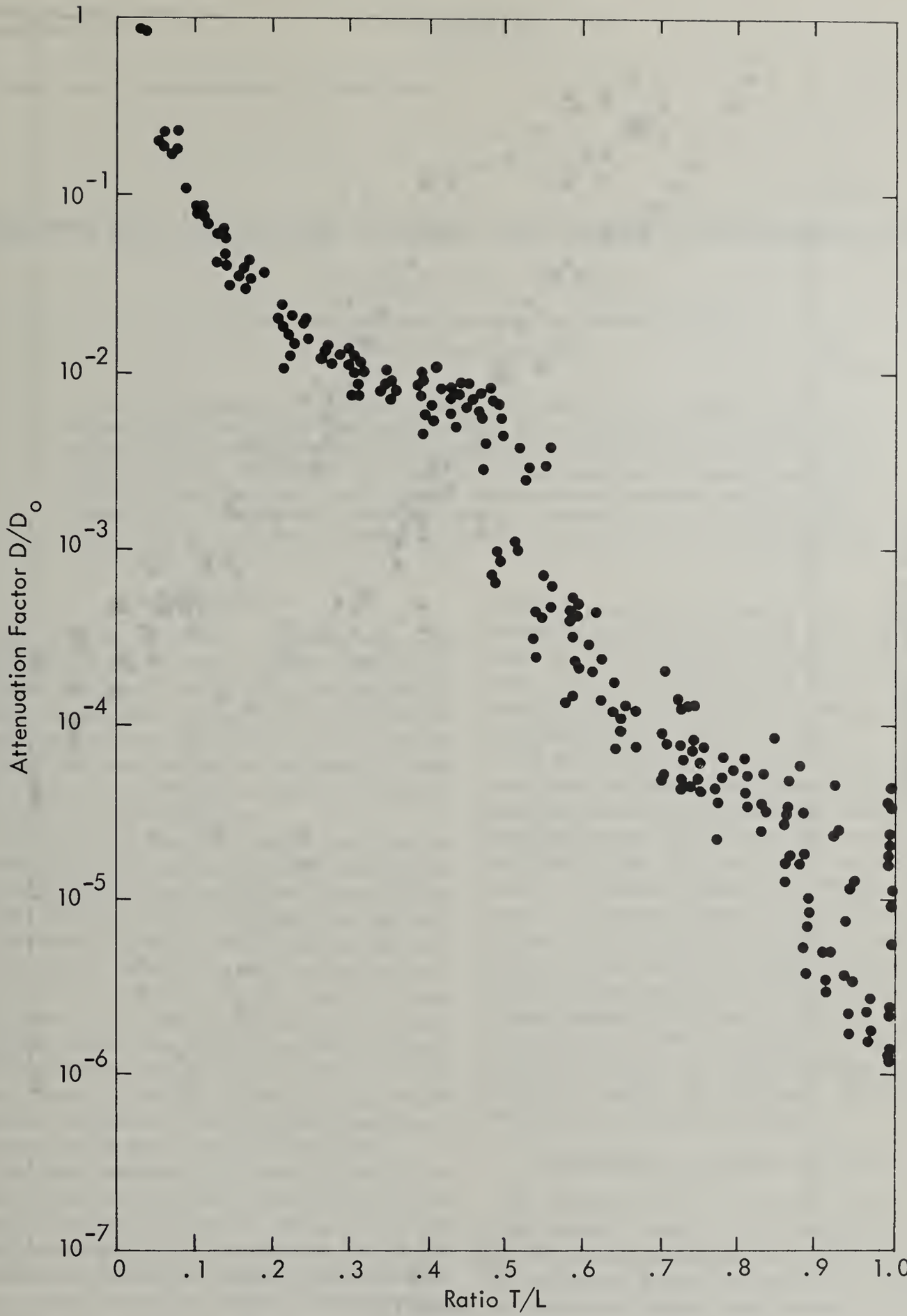

Figure 30. Attenuation factor vs ratio T/L for 6 x 6-foot ducts.

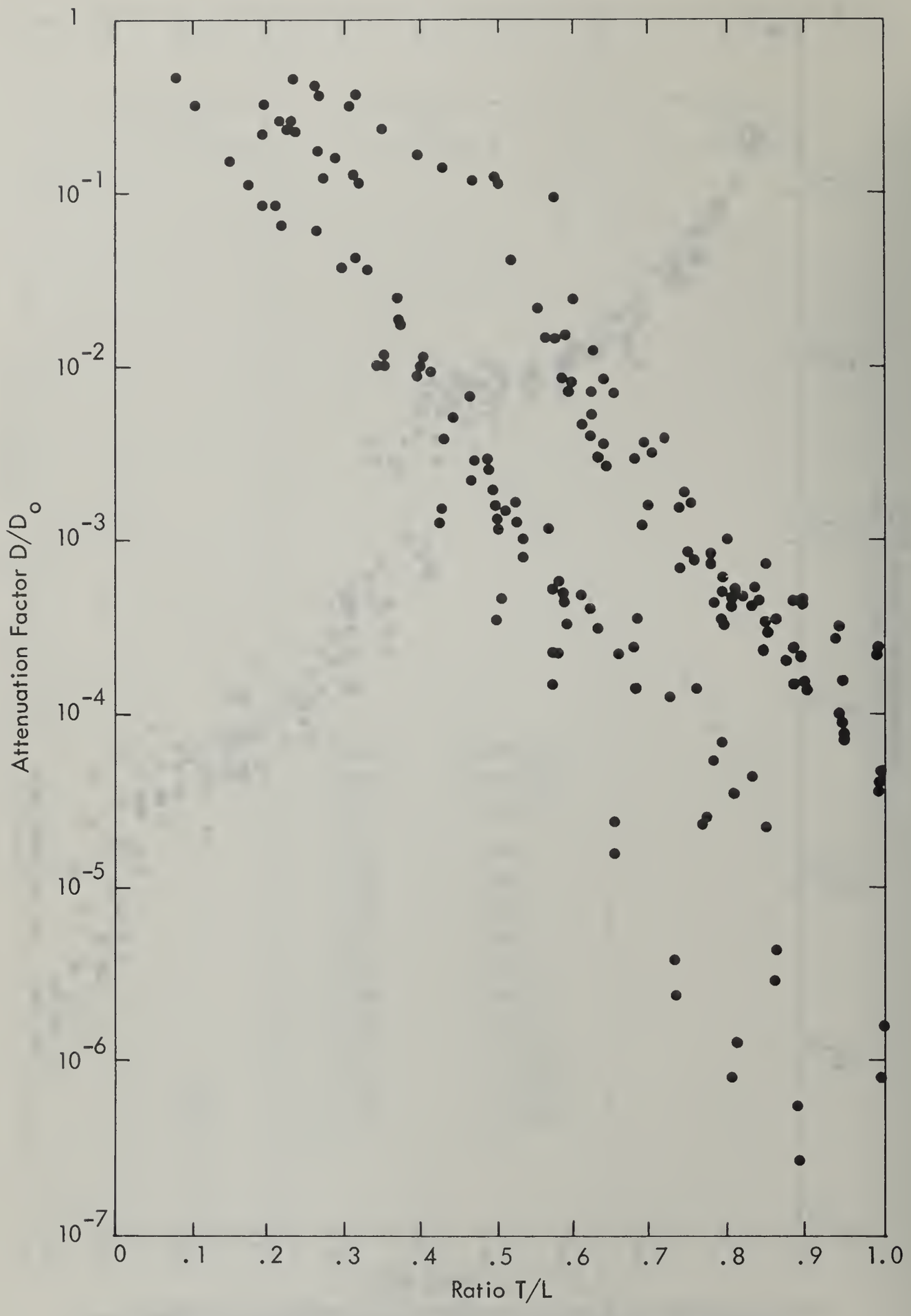

Figure 31. Attenuation factor vs ratio T/L for other than 6 x 6-foot ducts.

Reprinted from NUCLEAR SCIENCE AND ENGINEERING, Volume 11, No. 4, December 1961
Academic Press Inc. *Printed in U.S.A.*

NUCLEAR SCIENCE AND ENGINEERING: **11**, 362–368 (1959)

Gamma Ray Streaming Through Two-Legged Rectangular Ducts

J. C. LEDOUX* AND A. B. CHILTON

U. S. Naval Civil Engineering Laboratory, Port Hueneme, California

Received February 27, 1961

An analytical approach is developed to permit determination of gamma radiation attenuation as it passes through two-legged rectangular ducts and shelter entranceways. The approach used employs the albedo concept for wall scattering and includes correction terms neccssary to account for the "corner lip effects." With appropriate simplifying assumptions, moderately simple engineering formulas are obtained. Actual use of the formulas requires better knowledge of differential angular albedo than is presently available; however, by assuming isotropic distribution of the albedo function, a very good comparison of experimental information with results calculated by this technique is obtained.

INTRODUCTION

The analysis of nuclear radiation streaming through ducts has received insufficient attention in the past. For small diameter ducts through reactor shields, the provision of one or two 90° bends has usually proved more than adequate. More accurate methods are now needed for the design of large ducts and entranceways for irradiation facilities, hot cells, and civil defense shelters.

Previous work has dealt mainly with neutron streaming through straight, cylindrical ducts. Simon and Clifford (*1*) have studied this, using both an albedo approach and a single-scattering approach to determine the effect of the walls. Isotropic scattering was assumed, and a duct radius to length ratio $\ll 1$ was specified. For the case of a bend, equivalent to two straight ducts joined at an angle, the basic formula was modified in a rather approximate fashion by a simple function of the sine of the angle. Roe (*2*) had previously analyzed similar problems, using a one-group diffusion approach and assuming also a small radius to length ratio.

Analytical approaches for gamma rays or particles with nonisotropic scattering behavior seem to be lacking. Previously published techniques are not readily applied in such a case with any hope of getting accurate results. In particular, the two-legged duct problem seems to require additional study. There have been some recent experimental results published dealing with gamma rays streaming through square ducts having one 90° bend. Eisenhauer (*3*) has performed experiments on small ducts, using a point source of Co^{60}. The work of Terrell (*4*) deals with ducts up to 6 ft in width, employing both Co^{60} and Cs^{137} sources.

It is the purpose of this paper to analyze the transmission of gamma rays through rectangular ducts from basic scattering principles, using largely the albedo concept. In so doing, there are two primary ends in view. The first is to lay down a set of tentative analytical techniques to be used by nuclear shield designers concerned with this problem, pending further refinement of the art; the second is to provide some theory to tie together experimental data now being accumulated. It will also be possible to make comments as to how the radiation attenuation factors vary with the geometric scale of the physical layout. Such a knowledge may be useful in permitting analysis of large-scale entranceways through the use of model experiments.

ASSUMPTIONS AND BASIC APPROACH

The approach used in this paper employs the albedo concept, which we will review briefly in order to establish the notation to be used (see Fig. 1).

If appropriate means are provided to eliminate any passage of radiation from source to detector except by scattering off A, and if there is no attenuation by media in the path from-source-to-area-to-detector, the detector reading is (*5*):

* Now at the U. S. Naval School, Civil Engineer Corps Officers, Port Hueneme, California.

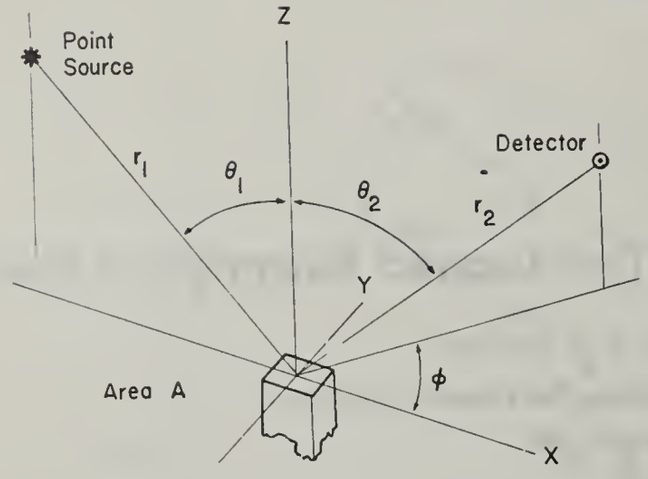

FIG. 1. Reflection of gamma rays from surface

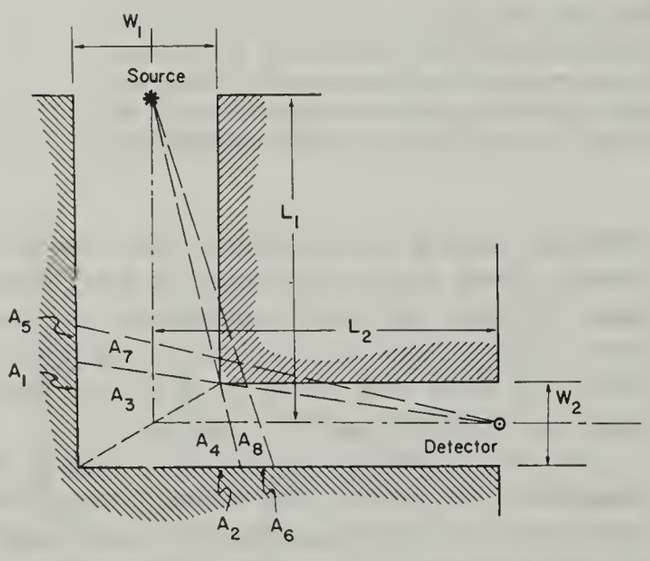

FIG. 2. Duct configuration, indicating reflecting areas

$$D = \frac{D_0 A \bar{a} \cos \theta_1}{r_1^2 r_2^2} \tag{1}$$

where D_0 is a detector response in the direct beam, at one unit of distance from the source; and $\bar{a} \equiv \bar{a}(\theta_1, \theta_2, \phi)$ is the differential directional albedo (hereinafter referred to as the "differential albedo"). All detectors are assumed to have isotropic response.

If D and D_0 are numbers of particles (or photons), $\bar{a}$ must be a "number albedo"; if, on the other hand, the detector measures radiation energy flux, D and D_0 represent energy and $\bar{a}$ is an "energy albedo"; finally, if D and D_0 indicate "dose," $\bar{a}$ is a "dose albedo."

There is available at present considerably more information on *total* albedo, than on the *differential* albedo. In such a case one must make some assumptions as to the actual distribution with emergent angles θ_2 and ϕ. For example, if an isotropic assumption is made, Eq. (1) becomes:

$$D = \frac{D_0 A a_T \cos \theta_1}{2\pi r_1^2 r_2^2} \tag{2a}$$

where $a_T \equiv a_T(\theta_1)$ is the total albedo factor for the radiation energy and reflecting material considered, and

$$a_T(\theta_1) = \int_{\text{upper hemisphere}} a(\theta_1, \theta_2, \phi) \sin \theta_2 \, d\theta_2 \, d\phi \tag{2b}$$

If a number of scattering areas of different orientation are involved, the detector dose becomes:

$$D = D_0 \sum_i \frac{\bar{a}(\theta_{i1}, \theta_{i2}, \phi_i) A_i \cos \theta_{i1}}{r_{i1}^2 \, r_{i2}^2} \tag{2c}$$

The basic problem to be solved is depicted in Fig. 2. This shows a two-legged duct, with legs intersecting perpendicularly, having a rectangular cross section. The height of the rectangle, H, is the dimension perpendicular to the plane of the paper in the figure; it is taken to be the same for both legs—a usual situation. The transmission of radiation through the duct will be calculated first with the assumption that only those areas which can be seen by both the source and the detector are important. The case is considered to be the "basic" case; its solution is the first approximation to the total solution; the scattering areas involved are called "prime" scattering areas and are shown as areas A_1 through A_4, inclusive, in Fig. 2. Areas 1 and 2 are wall areas; areas 3 and 4 each include both roof and floor.

It is assumed that the leg lengths are appreciably greater than the widths and the height. Also, to minimize direct transmission of radiation from source to detector, both legs should not be less than several feet in length. To establish an upper limit, we assume that the leg dimensions are much less than a mean free path of the radiation in air, so that interaction with the air may be considered negligible. All the linear dimensions of the duct, such as width and height, are on the order of or greater than a mean free path of the radiation in the material of which the walls are composed.

The wall materials are assumed uniform in composition and density, especially at the corner. If the wall is made of a liner of some material imbedded in another material, the liner has a thickness on the order of or greater than a mean free path of the radiation in the liner material.

The radiation source is assumed to be located at or near the center of the duct entrance; the detector is located at or near the center of the duct exit. A source distributed over the mouth of the duct

entrance may be considered as concentrated in the center without severe inaccuracy, provided D_0 is appropriately calculated for such a case.

The areas considered for significant contribution to the detector response are those providing a single reflecting path from source to detector. The most important areas are those labeled A_1 through A_4, inclusive, the values of which are readily obtained from geometrical considerations. We shall group the contributions from these four areas and consider the result as the basic calculation.

A very precise analysis would require that differential portions of each reflecting area be considered separately and the resulting expressions integrated over the whole reflecting surface. We have chosen a more simple procedure, although less elegant, in the belief that the lack of availability of accurate albedo data, in conjunction with the use of certain necessary analytical simplifications, makes such a procedure adequate for the purposes of this paper. In general, the procedure followed for each numbered area is as follows: The area is considered sufficiently small in linear dimensions to permit the use of a single representative value each of r_1 and r_2 in Eq. (1). The distances are generally taken to a convenient point at or near the centroid of the area, permitting use of simple mathematical expressions. The values of the incident and emergent angles are taken at this point, and the albedo value determined (or assumed) accordingly. The details and data used in this approach have been provided by the authors in a separate publication (*6*).

By this means, the doses resulting from the various areas are readily arrived at and are listed in Table I. The sum of the contributions from the four prime areas is given as follows:

$$D_{\text{basic}} = D_1(4\beta_1\,\beta_2\,\beta_3)(G_b) \tag{3a}$$

where

$$D_1 = \frac{D_0}{L_1^2} \tag{3b}$$

$$\beta_1 = \frac{W_1}{2L_2} \qquad \beta_2 = \frac{W_2}{2L_1} \qquad \beta_3 = \frac{H}{2L_2} \tag{3c}$$

$$G_b = \frac{a_1}{1+\beta_1} + \frac{a_2}{\beta_2(1+\beta_2)} + \frac{a_3}{1-\beta_1} + \frac{a_4}{1-\beta_2} \tag{3d}$$

a_1, a_2, a_3, and a_4 are the differential dose albedos from prime areas 1, 2, 3, and 4, respectively.

It is to be noted that D_1 is the theoretical dose expected (without wall scattering effects) at the corner, that is, where the mid-lines of the two legs intersect. It is useful to separate out this particular factor, since certain effects can be approximated by appropriate modifications to this term. This is discussed below.

TABLE I

DOSE CONTRIBUTIONS FROM AREAS INVOLVED IN BASIC ANALYSIS AND LIP TRANSMISSION EFFECT

Area designation	Dose contribution
1	$\dfrac{D_0W_2Ha_1W_1}{2L_1^3L_2^2(1+\beta_1)}$
2	$\dfrac{D_0W_1Ha_2}{L_1^2L_2^2(1+\beta_2)}$
3	$\dfrac{D_0W_1W_2a_3H}{2L_1^3L_2^2(1-\beta_1)}$
4	$\dfrac{D_0W_1W_2a_4H}{2L_1^3L_2^2(1-\beta_2)}$
5	$\dfrac{D_0W_2HW_1a_5}{4\mu_a'L_2^3L_1^3(1-\beta_2)^3(1-\beta_1)}$
6	$\dfrac{D_0W_1Ha_6}{2\mu_aL_1^3L_2^2(1-\beta_1)^2(1-\beta_2)}$
7	$\dfrac{D_0W_1W_2Ha_7}{2\mu_a'L_2^3L_1^3(1-\beta_2)^3(1-\beta_1)^2}$
8	$\dfrac{D_0W_1W_2Ha_8}{2\mu_aL_1^4L_2^2(1-\beta_1)^2(1-\beta_2)^2}$

CORNER LIP EFFECTS

It is desirable to consider certain other important contributions, for in some cases they are almost comparable to results of the basic computation. These effects are related to the existence of the so-called corner "lip," and their inclusion in the analysis constitutes an improvement to the accuracy of the basic solution.

There are two important corner lip effects. The first of these might be called "the corner lip transmission effect." In the basic calculation it has been assumed that the corner lip (the inner edge of the intersection of the two legs) is completely opaque to the radiation. This can never be precisely true, and in some cases radiation penetration of the lip can be quite significant.

If it is assumed that radiation absorption of a ray passing through the lip is exponential in character, one can show on an elementary basis that the amount of radiation passing through the lip is the

same as if all the radiation within a certain cutoff point were transmitted and all beyond it were absorbed. Furthermore, the distance of travel within the lip material of that particular ray passing exactly through the cutoff point can be shown to be the reciprocal of the effective attenuation coefficient for the radiation passing through it, assuming the use of an "effective attenuation coefficient" for dose absorption is valid (*6*).

The simplest assumption for an effective absorption coefficient is that which accounts for all energy-absorbing processes and assumes that all energy scattered but not absorbed is scattered through a negligibly small angle. The use of the "energy absorption coefficient" thus gives a reasonable value to use in this regard. It is fortuitous in application that this coefficient is a very slowly varying function of energy over the part of the gamma ray energy spectrum of practical interest.

On this basis, then, the effect of corner-lip penetration can be readily approximated by an increase in the scattering area beyond the primary scattering areas. The areas on Fig. 2 which are designated A_5 through A_8, inclusive, show the new scattering surfaces which contribute to detector response, through the albedo process. The calculation of the values of these areas and other variables required to determine their effect, according to Eq. (1), is straightforward. Table I lists the dose contribution from these areas also.

It is convenient to break up this lip transmission effect contribution into two parts: one in which wall scattering occurs before lip transmission, and the other in which lip transmission occurs before wall scattering. We find then that:

$$D_{tr} = D_{tr1} + D_{tr2} \tag{4a}$$

where $$D_{tr1} = D_1(4\beta_1\,\beta_2\,\beta_3)G_{t1} \tag{4b}$$

$$G_{t1} = \frac{(1-\beta_1)a_5 + 2a_7}{2\mu_a' L_2(1-\beta_1)^2(1-\beta_2)^3} \tag{4c}$$

and $$D_{tr2} = D_1(4\beta_1\,\beta_2\,\beta_3)G_{t2} \tag{5a}$$

$$G_{t2} = \frac{(1-\beta_2)a_6 + 2\beta_2\,a_8}{2\mu_a L_1\,\beta_2(1-\beta_1)^2(1-\beta_2)^2} \tag{5b}$$

D_1 has been previously defined by Eq. (3b). μ_a is the energy absorption coefficient of the primary radiation; μ_a' is the coefficient of the radiation reflected from the surfaces.

D_{tr1} and D_{tr2} can be added to give:

$$D_{tr} = D_1(4\beta_1\,\beta_2\,\beta_3)G_t \tag{6a}$$

where

$$G_t = G_{t1} + G_{t2} \tag{6b}$$

The other corner lip effect may be called the "corner lip in-scattering effect." Not only may the corner lip transmit some of the photons completely, but it may also serve to scatter some of them one or more times in the passage. Such scattering will in part redirect radiation toward the detector. Thus the detector not only "sees" the prime and additional scattering areas on the outer walls by means of their radiation scatter, but also "sees" the corner lip as a "bright" source—almost a line source.

In analyzing the contribution of this effect we make certain simplifications. In similar spirit to that used in the preceding section we utilize an "effective attenuation coefficient" for radiation passing to and from each scattering center, thus again using what might be considered a "straight-ahead approximation." The previous approach is modified to the extent that we recognize a small but definite probability of scattering into the direction which will cause the radiation to hit the detector. Thus we have a single-scatter approximation for the most part, but the approach does not eliminate multiple scattering provided all the scattering processes but one are considered of a small angle nature. Scattering through two or more large angles is considered of negligible proportion.

The computation of the effect for gamma ray photons is based on the Klein-Nishina scattering formula (*7*). Its use in this particular case has been explained in detail previously by the authors (*6*). The results of the detailed analysis are as follows:

$$D_s = \frac{D_0\,W_1\,W_2\,HZNK}{4L_1^3L_2^3\mu_a^2(1-\beta_1)^3(1-\beta_2)^3} \tag{7a}$$

$$= D_1(4\beta_1\,\beta_2\,\beta_3)G_s \tag{7b}$$

where

$$G_s = \frac{ZNK}{2\mu_a^2 L_2(1-\beta_1)^3(1-\beta_2)^3} \tag{7c}$$

and where

Z = number of electrons per atom of the scattering material

N = number of atoms per unit volume of the scattering material

K = $K(\theta_s, E_0)$ is the Klein-Nishina coefficient for scattering probability per electron.

$$\theta_s = 90° - \alpha_1 - \alpha_2 \tag{7d}$$

$$\alpha_1 = \tan^{-1}\frac{W_1}{2L_1(1-\beta_2)} \tag{7e}$$

$$\alpha_2 = \tan^{-1} \frac{W_2}{2L_2(1 - \beta_1)} \tag{7f}$$

COMPUTATION OF ATTENUATION FACTORS

Adding Eqs. (3a), (6a), and (7b) we get the total dose at the end of the second leg:

$$D_T = D_1(4\beta_1 \beta_2 \beta_3)G_{Tot} \tag{8a}$$

where

$$G_{Tot} = G_b + G_t + G_s \tag{8b}$$

We are now at the point where we can introduce the attenuation factor and solve for it. For the purpose of this paper, we will use the following definitions:

$F_T = D_T/D_0$, being the ratio of dose at the end of the second leg to that at the reference point, one foot from the source in a nonabsorptive, nonscattering medium

$F_1 = D_1/D_0$, being the ratio of the dose at the intersection of the leg center lines to that at the reference point, one foot from the source in a nonabsorptive, nonscattering medium

$F_2 = D_T/D_1$, being the ratio of the dose at the end of the second leg to that at the intersection of the leg center lines

We will commonly call F_1 the attenuation factor for the first leg, and F_2 the attenuation factor for the second leg. Obviously, $F_T = F_1F_2$.

We now find it possible to consider the attenuation factors for the two legs separately. We readily see that:

$$F_1 = \frac{1}{L_1^2} \tag{9}$$

and that

$$F_2 = 4\beta_1 \beta_2 \beta_3 G_{Tot} \tag{10}$$

By separating the factors in this way, one is permitted, if he wishes, to use a different reference point for over-all attenuation (rather than the point at which D_0 is measured) without affecting the analysis for F_2. For example, in case of a distributed source over the entrance to the duct, the equation for F_2 should still be approximately valid. The equation for F_1 would depend upon the nature of the source emission. It can be readily shown (*8*) that for the so-called isotropic source emission case

$$F_1' \doteq \frac{W_1 H}{\pi L_1^2 \ln [1 + (W_1 H/\pi)]} \tag{11}$$

if the reference point is taken as one unit of distance away from the center face of the duct; and for a cosine emission case the attenuation factor in the first leg, based upon a reference value at the entrance to the duct, is

$$F_1'' \doteq \frac{W_1 H}{2\pi L_1^2} \tag{12}$$

provided the first leg width and height are of the same order of magnitude.

SCALING RELATIONSHIPS

It is obvious from a glance at Eq. (3a) that the last two factors are nondimensional, and that for a given geometrical configuration, their product is independent of any scale selection. Under circumstances which allow this basic analysis to be an adequate approximation, the scaling-independence of this part of the expression permits ready adaptation of experimental solutions on a small model scale for solution of large-scale problems of this nature.

It is to be noted that in Eqs. (4b), (5a), and

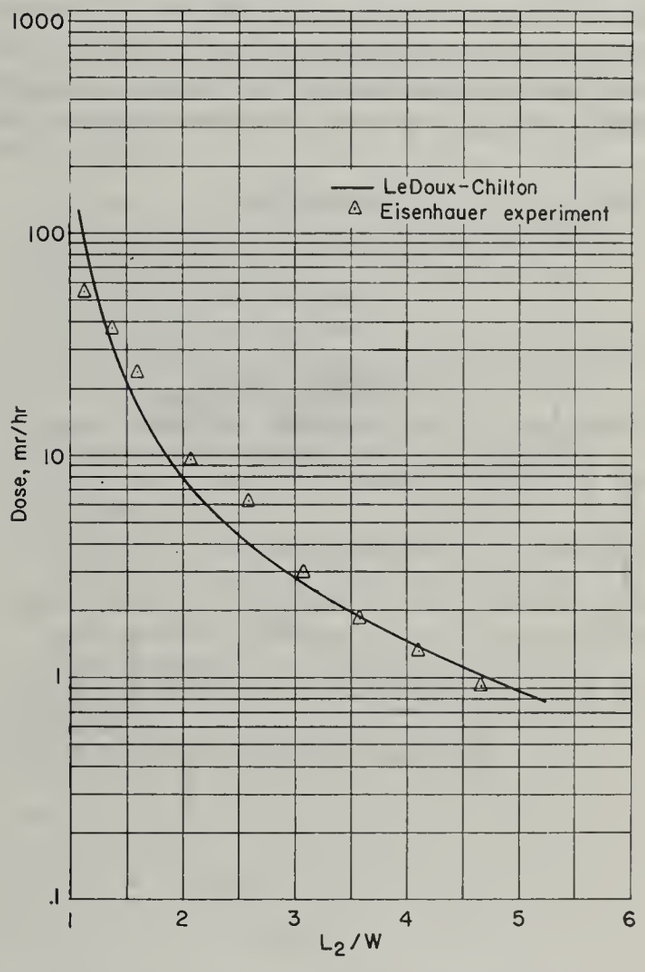

FIG. 3. Comparison of LeDoux-Chilton analysis with NBS experiment using Co^{60} source and a concrete duct 19.2-cm square.

(7b) the two latter terms of each equation are nondimensional; however, the product of these two terms is not independent of the geometric scale selection but is inversely proportional to the scale size. We note that the attenuation coefficients are fixed and do not change value with a change in geometric scale. Since the scaling relationships for similar factors in the basic problem and the corner lip correction are not the same, the problem of scaling up from model experiments to larger-scale prototypes is seen to be impossible unless means are found to separate experimental data into the basic part and the corner lip effect terms, or unless the corner lip effect terms can be shown to be negligible at all scales considered.

This comment of course relates to the second-leg attenuation only, since the factors involving first-leg attenuation are eliminated from consideration.

COMPARISON WITH EXPERIMENT

The experiments performed by Eisenhauer (*3*) were on concrete ducts, having two legs at right angles. In cross-section they were square, being 19.2 cm. on a side in one case and 28.2 cm. in another. The length of the first leg was fixed at 100 cm. With a Co^{60} source at the center of the entrance, measurements were made of dose at various points on the center line of the second leg, which was at right angles to the first.

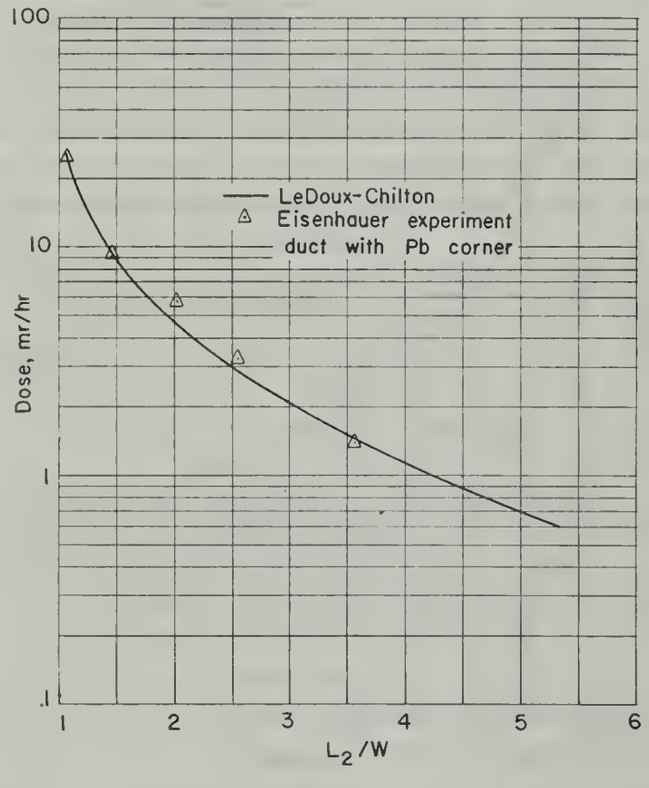

FIG. 4. Comparison of LeDoux-Chilton analysis with NBS experiment using Co^{60} source and a concrete duct 19.2-cm square and having a lead cornerlip.

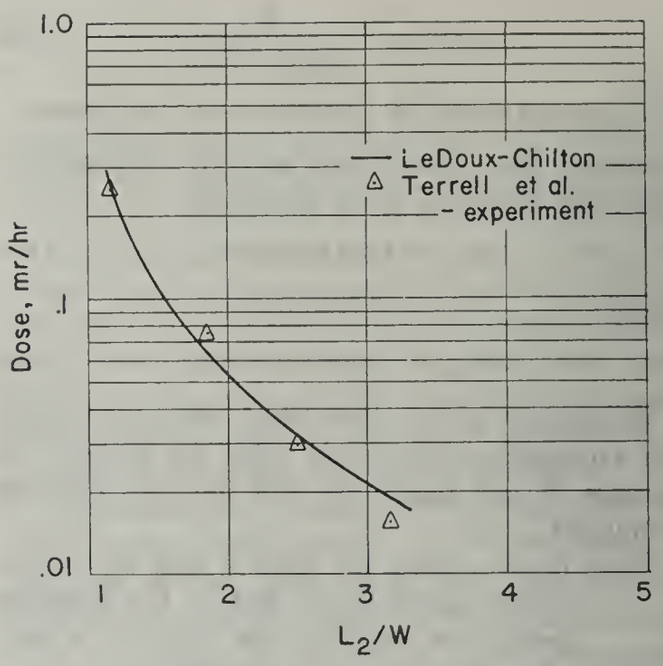

FIG. 5. Comparison of the LeDoux-Chilton analysis with ARF experiment using Co^{60} source and a concrete duct 6-ft square.

Figure 3 shows a comparison between Eisenhauer's experimental results for the 19.2 cm. duct and computations based on our present analysis. In making our analysis, the dose albedo data of Berger and Raso (*9*) were used, with an assumption of isotropicity of the differential dose albedo. Such an assumption for differential albedo, taken as total albedo divided by 2π, seems to give reasonably good agreement. A cosine distribution for differential albedo was also tried but compared less favorably with experimental results, giving answers greater than experimental results for small values of L_2/W and smaller than experimental results for larger values of L_2/W.

In order to determine the magnitude of the corner lip contributions Eisenhauer placed a lead block in the corner of the 19.2 cm. duct to reduce the effect to a small amount. Figure 4 shows the comparison of our analysis with the experimental results in such case. The corner lip contributions in the analysis were substantially lessened by considering lead rather than concrete as the corner material. It is only fair to state here that Eisenhauer does not consider his data highly accurate in this case, and the rather good agreement indicated might be somewhat fortuitous.

The experiments of Terrell *et al.* (*4*) were of a similar nature, but the ducts were large, being 6 feet by 6 feet. Figure 5 gives a comparison between

his data and our analysis, using isotropic albedo assumption. Again agreement is considered good.

DISCUSSION

We have provided herein a fairly simple analytical technique for predicting the attenuation of gamma radiation down two-legged rectangular ducts, with right-angle corner, under somewhat idealized conditions. Adequacy of the formulas developed seems to be confirmed by experiment. Nevertheless, it is only proper to emphasize some of the factors which make the present state of knowledge in the matter incomplete and subject to future study.

The elimination of multiple reflections is a factor which undoubtedly reduces the computed doses and thus abnormally improves the computed attenuation factors. The magnitude of such contribution can only be approximately guessed at except where specific measurements can be made. Measurements made by Terrell *et al.* (*4*) indicate that, because of wall scattering, radiation reaching the corner might be under some circumstances as much as 25% higher than would arrive directly from the source. Further wall scattering in the second leg undoubtedly occurs also.

The use of an assumed isotropic distribution for the differential albedo function, as derived from the data of Berger and Raso, can only be justified on the very pragmatic grounds that it seems to give good results when used in the analytical technique described in this paper. Aside from the theoretical dubiousness of the isotropic assumption, there is the fact, recently called to the attention of the authors (*10*), that the Berger-Raso dose albedo data are based on reflected photon current rather than flux and are thus not realistic. As we have used the data, there has undoubtedly been an exaggeration of the contribution from some of the reflecting areas and a corresponding slighting of the contribution from others. The overall effect of using accurate data for directional differential albedo, as well as the magnitude of the individual contributions of the various reflecting surfaces, awaits the publication of better data.

It should also be pointed out that the formulas derived are more accurate for conditions in which the legs are long compared to their width. In this respect, our analysis is similar to those previously referred to (*1*, *2*). Nevertheless, the results appear surprisingly good at rather short lengths of the second leg (see Figures 3, 4, and 5).

Further experimental confirmation is considered desirable. The present range in scale seems to be adequate, but there are other parameters to be varied. For example, experiments on non-square ducts should be carried out.

One further aspect of the results is worth mention here. A comparison between the results in Figure 3 and Figure 4 indicates that the overall effect of the corner is on the order of 35% of the total attenuated dose in the second leg in the case given. This indicates a degree of significance that cannot be ignored. However, the scaling relationship derived in this paper indicates that for an entranceway on the order of ten times the linear dimensions of such an experimental situation the corner effects will be reduced to only a few percent, and thus they may all be safely ignored under such circumstances.

Acknowledgment

This work was originally stimulated by C. M. Eisenhauer's experimental work. Discussions with him, with C. W. Terrell, and with their associates are appreciatively acknowledged.

REFERENCES

1. A. Simon and C. E. Clifford, *Nuclear Sci. and Eng.* **1**, 156–166 (1956).
2. G. M. Roe, KAPL-712 (1952).
3. C. M. Eisenhauer, NBS Tech. Note 74 (1960).
4. C. W. Terrell, A. J. Jerri, R. O. Lyday, and D. Sperber, ARF Rpt. 1158-12 (1960).
5. Reactor Shielding Design Manual, T. Rockwell III, editor, AEC, TID-7004.
6. J. C. LeDoux and A. B. Chilton, NCEL Tech. Note TN-383 (1961).
7. W. Heitler, "The Quantum Theory of Radiation," 2nd Ed., Oxford Univ. Press, London (1944).
8. B. T. Price, C. C. Horton, and K. T. Spinney, Radiation Shielding," Pergamon Press, London and New York (1957).
9. M. J. Berger and D. J. Raso, *Radiation Res.* **12**, 20–37 (1960).
10. E. C. Clarke, personal communication.

A SEMIEMPIRICAL FORMULA FOR DIFFERENTIAL DOSE ALBEDO FOR GAMMA RAYS ON CONCRETE

Y-F011-05-329(b)

Type C

by

A. B. Chilton* and C. M. Huddleston

*Presently, Associate Professor of Civil and Nuclear Engineering, University of Illinois, Urbana, Illinois

ABSTRACT

A semiempirical formula is developed which yields values for the differential dose albedo of gamma rays on concrete. Gamma rays of incident energies 0.2, 0.5, 1.0, 2.0, 4.0, 6.0, and 10.0 Mev are considered. Results of the formula are compared with values derived from Monte Carlo calculations for the backscattering of gamma rays from a semi-infinite slab of concrete.

Results show that a two-parameter formula gives satisfactory agreement with the Monte Carlo calculations.

The principal assumption involved in the theoretical analysis is that the actual reflection process can be approximated by two terms, one involving a single Compton scattering event, and the other involving isotropic scattering.

This work was supported by the Defense Atomic Support Agency.

INTRODUCTION

In problems involving the scattering of gamma rays by structural elements, it is often useful to employ the albedo concept. Such an approach has been used at the Naval Civil Engineering Laboratory and elsewhere in the study of gamma radiation streaming through ducts.[1,2,3]

Accurate analysis in this problem requires the use of differential dose albedo, rather than total albedo. Practical shielding technology generally uses concrete as the structural material involved in the shielding. Raso has given results of Monte Carlo studies in the determination of gamma-ray differential dose albedo for concrete.[4,5] The calculations involved the assumption of broad, parallel-beam monoenergetic radiation incident at various angles to the normal. The initial energy and incident angle were varied, and the results were tabulated as a function of exit polar and azimuthal angles. Because of the necessarily limited number of photon histories (5000) accumulated for each case, the data are subject to statistical fluctuations.

It would obviously be useful to find a simple formula which expresses differential dose albedo. Such a formula would provide assistance in smoothing and interpolating between the tabulated values in Raso's tables. Further, it would provide a simple analytical means for obtaining differential albedo under circumstances when use of tabulated data is inconvenient; e.g., in machine computations. Even if the formula provided were somewhat approximate, the usefulness of a simple formula might outweigh its lack of a high degree of accuracy.

This study undertakes to develop such a formula.

PRELIMINARY DISCUSSION

Differential dose albedo, as used herein and designated as $\bar{a}$, is the same as R in Rockwell's formula on page 335 of his manual:[6]

$$D = \frac{D_1 \bar{a} \cos\theta_o S}{r_1^2 r_2^2} \qquad (1)$$

where (see Figure 1) D = dose at point of measurement

D_1 = dose at reference point 1 unit distance from point source

θ_o = polar angle of incidence

S = area of scattering surface

r_1 = distance from source to S

r_2 = distance from S to detector.

Note that D_1/r_1^2 is the dose at area S due solely to the incident beam. If the beam has broad, parallel-ray geometry, one cannot, strictly speaking, assume a point source, and D_1/r_1^2 can be replaced by the dose measured in the incident beam, called, say, D_o.

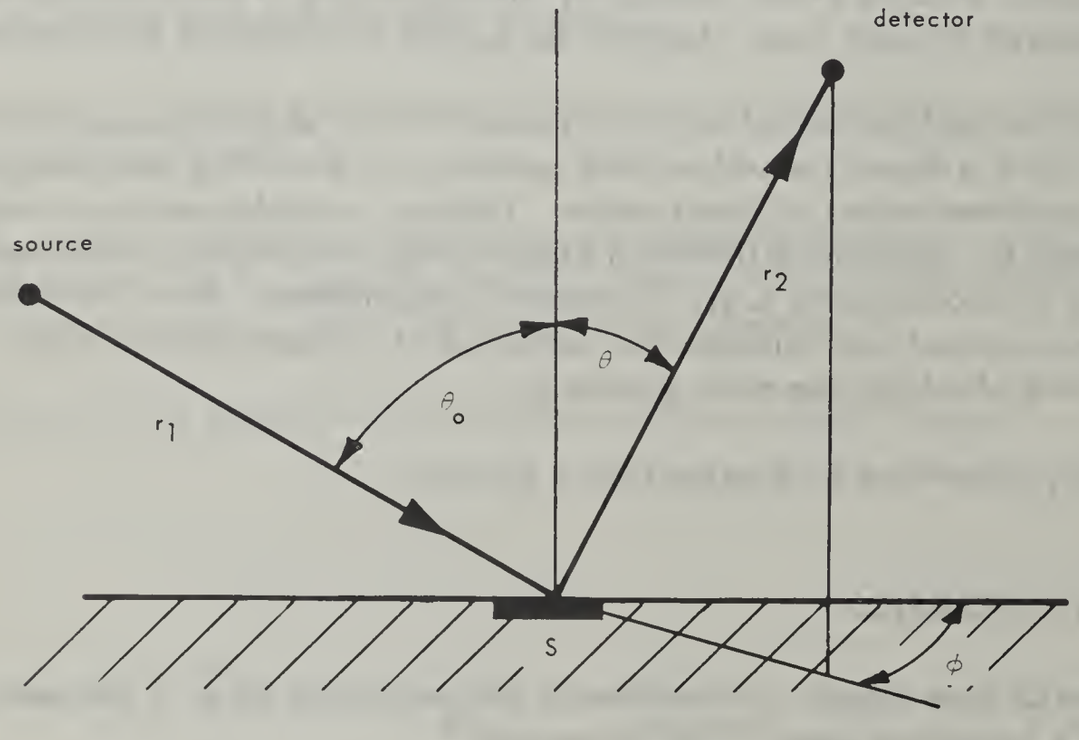

Figure 1. Scattering of radiation from a slab.

Thus, one has in this case:

$$D = \frac{D_o \bar{a} \cos\theta_o S}{r_2^2} .$$

Let us consider a case in which $S = \sec\theta_o$. This is the case if the pencil of rays striking the area is of unit cross-sectional area as measured in a plane normal to the incident direction. In such a case, one finds that

$$\bar{a} = \frac{Dr_2^2}{D_o} .$$

and by analyzing this case, one can approach the problem of determining $\bar{a}$.

One should particularly note that Dr_2^2 is representative of the reflected radiation per steradian, converted into dose, if D_o represents the radiation dose in the incident pencil of rays of unit cross-sectional area. This can be explained as follows: Consider that the detector has unit cross-sectional area. It intercepts all the incoming radiation when measuring the incident beam; it will subtend a unit solid angle if placed at a distance of 1 unit from the area S. At the distance r_2, the unit cross-section detector will detect $1/r_2^2$ of the radiation measured at 1 unit distance, and thus Dr_2^2 is equivalent to the interception of radiation scattered per steradian from the material.

DERIVATION OF FORMULA

Consider a beam of radiation, 1 unit in cross-sectional area, incident on a slab of material. See Figure 2.

Assume that the scattered radiation can be divided into two parts: that part which "remembers" the original direction of incidence, and that part which has "forgotton" the original direction of incidence. The former part is to a great extent singly scattered radiation, or radiation where only one of its scatterings is through a significantly large angle. The latter part is composed either of radiation scattered many times or of positron-annihilation radiation (under circumstances leading to such a contribution). Consider each part in turn.

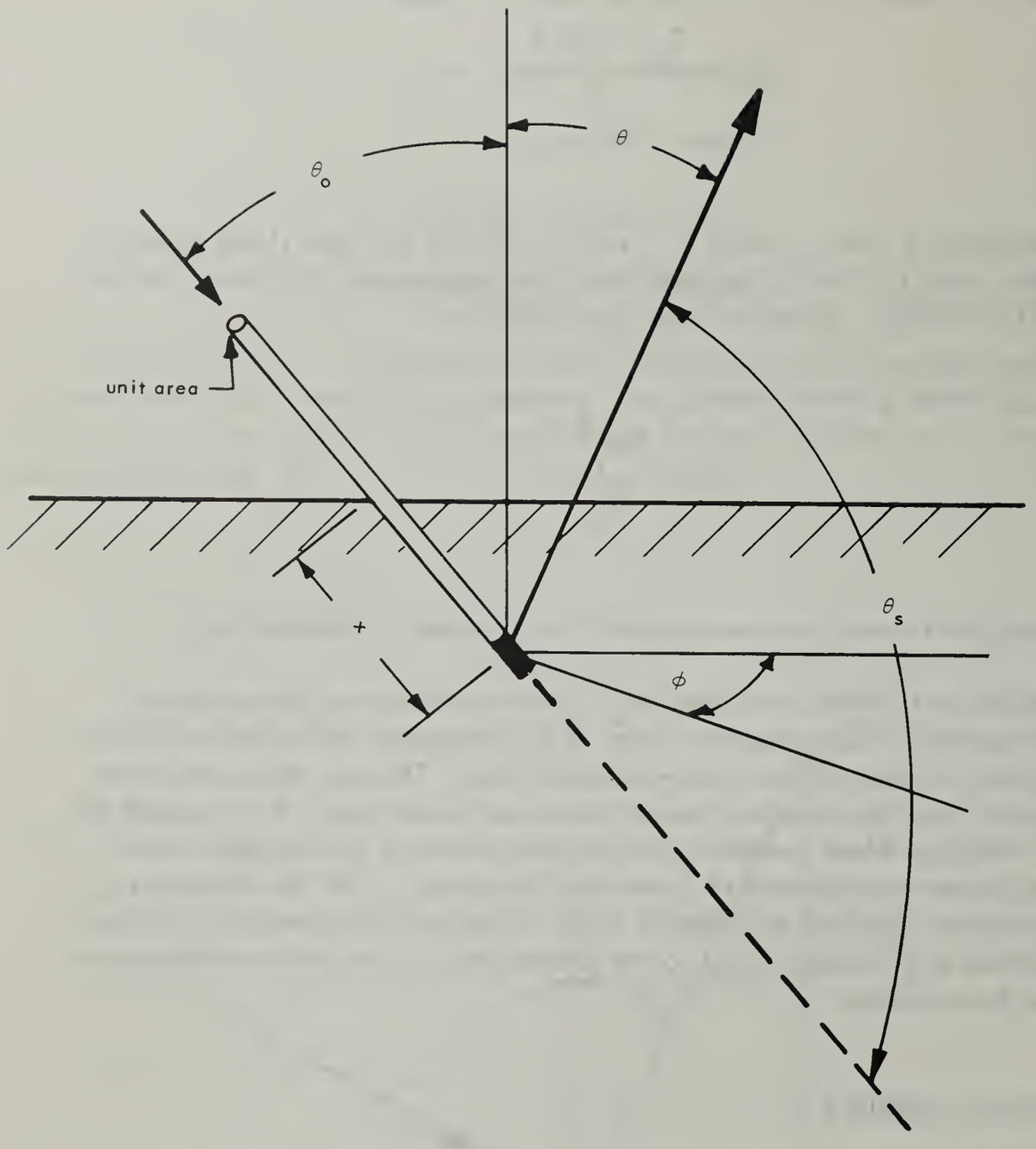

Figure 2. Radiation incident on a slab.

Since the first part is to a great extent single-scattered radiation, or nearly the same as single-scattered radiation, we will examine the single Compton scattering aspect, and assume that this scattered-radiation component is proportional to it.

Consider scattering from a volume dV, of unit cross-sectional area and thickness dx at slant depth x. The probability of energy scatter by a single electron through the angle θ_s is given by $K(\theta_s, E_o)$.[7]

The number of electrons in the differential volume dx is given by $ZM\rho dx$, where

Z = number of electrons per atom of the scattering material

M = number of atoms per unit mass of the scattering material

ρ = density of the scattering material

The probability of a unit of gamma-ray energy traversing the distance inward from the surface to the differential volume can be closely approximated by a function of the form

$$e^{-\bar{\mu}_1 \rho x}$$

where $\bar{\mu}_1$ = an effective mass attenuation coefficient for the gamma ray of initial energy E_o.

After scatter, the probability of a unit of gamma-ray energy traversing the distance from the scatterer to the outer surface is

$$e^{-\bar{\mu}_2 \rho x \cos\theta_o \sec\theta}$$

where $\bar{\mu}_2$ = an effective mass attenuation coefficient for the gamma-ray energy after scatter.

240-816 O-67--39

Thus, the proportion of initial energy scattering from this first type of effect into a direction (θ, ω) per unit solid angle from the layer of thickness dx equals:

$$AZM\rho K(\theta_s) \int_o^\infty e^{-\rho x (\bar{\mu}_1 + \bar{\mu}_2 \cos\theta_o \sec\theta)} dx$$

$$= \frac{AZM\rho K(\theta_s)}{\rho(\bar{\mu}_1 + \bar{\mu}_2 \cos\theta_o \sec\theta)}$$

$$= \frac{AZMK(\theta_s)}{\bar{\mu}_1 + \bar{\mu}_2 \cos\theta_o \sec\theta}$$

where A is an undetermined proportionality factor.

To get the proportion of dose scatter, it is necessary to multiply the above result by the ratio of air energy absorption coefficients $\bar{\mu}_{a1}$ and $\bar{\mu}_{a2}$, to obtain:

$$\frac{AZM\bar{\mu}_{a2}K(\theta_s)}{\bar{\mu}_{a1}(\bar{\mu}_1 + \bar{\mu}_2 \cos\theta_o \sec\theta)} .$$

By a similar reasoning, we may find the portion of the scattered radiation due (or proportional) to production and multiple scattering of an isotropic nature. This part, per differential volume dx, is expressed on an energy basis by:

$$B\rho e^{-\rho x (\bar{\mu}_1 + \bar{\mu}_3 \cos\theta_o \sec\theta)} dx$$

where $\bar{\mu}_3$ = an effective attenuation coefficient for the isotropically scattered gamma-ray energy. After integrating and converting to dose, we obtain:

$$\frac{B\{\bar{\mu}_{a2}\}_{Av}}{\bar{\mu}_{a1}(\bar{\mu}_1 + \{\bar{\mu}_3\}_{Av} \cos\theta_o \sec\theta)}$$

where B is an undetermined proportionality factor, $\{\bar{\mu}_{a2}\}_{Av}$ is an average value for the air energy absorption coefficient for outgoing radiation from dV, and $\{\bar{\mu}_3\}_{Av}$ is the average value of the effective energy attenuation coefficient for the outgoing radiation from dV.

For a given material, and a given initial energy, one may lump all parameters depending on such factors into parametric multipliers, and leave separate those parameters depending on angles; and then one gets for differential albedo the expression:

$$\bar{a}(\theta_o, \theta, \varphi) = \frac{A' K(\theta_s)}{\bar{\mu}_1 + \bar{\mu}_2 \cos\theta_o \sec\theta} + \frac{B'}{\bar{\mu}_1 + \{\bar{\mu}_3\}_{Av} \cos\theta_o \sec\theta} .$$

On the assumption that $\bar{\mu}$, the effective attenuation coefficient, is not greatly energy dependent for light material in the photon energy range of interest (a few hundred kev to several Mev), we can simplify the form still further by making it:

$$\bar{a}(\theta_1, \theta_2, \varphi) = \frac{CK(\theta_s)\, 10^{26} + C'}{1 + \cos\theta_o \sec\theta} \qquad (2)$$

where the factor 10^{26} is entered arbitrarily to make the empirical parameters C and C' of the same order of magnitude. C is a measure of that part of the scattered radiation which "remembers" the original direction of incidence, as mentioned under "Derivation of Formula," and C' is a measure of that part which has "forgotten" the original direction of incidence.

The approximation that $\bar{\mu}$ does not vary much with energy during a scattering history is surely the weakest part of the development. The results will show, however, that this simplifying assumption is good enough to give generally satisfactory agreement between the Monte Carlo results and the results of the two-parameter formula.

THE KLEIN-NISHINA FORMULA

In Equation 2, $K(\theta_s)$ is the Klein-Nishina differential energy scattering cross section for angle θ_s. $K(\theta_s)$ is also a function of the energy of the incident photon E_o.

For purposes of computation, a convenient way to write $K(\theta_s)$ is

$$K(\theta_s) = \frac{R_o^2}{2} P^2 [1 + P^2 - P(1 - \cos^2 \theta_s)]$$

where R_o is the electron radius (2.818×10^{-13} cm) and $P = E/E_o$.

The energy of a photon after a Compton scatter is given by:

$$E = \frac{E_o}{1 + \frac{E_o}{.511}(1 - \cos\theta_s)} .$$

A convenient way of defining θ_s, the angle of scatter, in terms of θ_o, θ, and φ (see Figure 2) is by the spherical trigonometric relationship:

$$\cos\theta_s = \sin\theta_o \cos\varphi \sin\theta - \cos\theta_o \cos\theta .$$

THE CONCEPT OF DIFFERENTIAL DOSE ALBEDO

Differential dose albedo, $\bar{a}$, as it is used in this paper, was defined in the "Preliminary Discussion." Since the tabulated values, TV, of Raso's study[4] are not the same as $\bar{a}$, the relationship between $\bar{a}$ and TV is expressed in Equation 3, as given by Raso:

$$\bar{a} = \frac{TV \frac{\cos\theta_k - \cos\theta_{k+1}}{2}}{1000 E_o \mu_a(E_o) [2\Delta\varphi(\cos\theta_k - \cos\theta_{k+1})]} \qquad (3)$$

where $\mu_a(E_o)$ is the mass absorption coefficient for a gamma ray of energy E_o, and E_o is expressed in Mev.

LEAST-SQUARES ANALYSIS

The Monte Carlo tabulated results are first converted to differential dose albedo by Equation 3. Best values for $\{C,\ C'\}$ for Equation 2 are then sought by a least-squares computer analysis.

For each of the 7 values of E_o considered, there are 480 tabulated values for backscattering, corresponding to 5 values for θ_o, 8 values for θ, and 12 values for φ.

To solve for the parameters $\{C,\ C'\}$, let

$$x = \frac{1}{1 + \dfrac{\cos\theta_o}{\cos\theta}}$$

$$y = xK(\theta_s)$$

$$z = \frac{TV}{E_o \mu_a(E_o)}\zeta$$

$$\zeta = \frac{\cos\theta_n + \cos\theta_{n+1}}{4000\Delta\varphi(\cos\theta_n - \cos\theta_{n+1})}$$

Now define:

$$Z_{ijk} = C'x_{ijk} + Cy_{ijk} + e_{ijk}$$

where $B = 10^{26}C$, and e_{ijk} is the (i, j, k)th deviation of the data from the fitted equation. The subscripts i, j, and k refer to θ_o, φ, and θ, respectively.

The sum of the squares of the errors is given by:

$$\sum_{i=1}^{n_{\theta_o}} \sum_{j=1}^{n_\varphi} \sum_{k=1}^{n_\theta} e_{ijk}^2 = \sum_{i=1}^{n_{\theta_o}} \sum_{j=1}^{n_\varphi} \sum_{k=1}^{n_\theta} (Z_{ijk} - C'x_{ijk} - By_{ijk})^2 \qquad (4)$$

The parameters $\{C,\ C'\}$ are obtained by differentiation of Equation 4 with respect to C and C'.

One then obtains:

$$C' = \frac{S_{yy}S_{xz} - S_{xy}S_{yz}}{D} \tag{5a}$$

$$B = \frac{S_{xx}S_{yz} - S_{xy}S_{xz}}{D} \tag{5b}$$

where $S_{xx} = \sum\sum\sum x_{ijk}^2$

$S_{yy} = \sum\sum\sum y_{ijk}^2$

$S_{xy} = \sum\sum\sum x_{ijk}y_{ijk}$

$S_{xz} = \sum\sum\sum x_{ijk}z_{ijk}$

$S_{yz} = \sum\sum\sum y_{ijk}z_{ijk}$

$D = S_{xx}S_{yy} - S_{xy}^2$.

A straightforward least-squares analysis, however, is not what is actually needed. A fit more useful in practice is obtained if Equation 4 is modified to include a weighting factor which will give greater weight to small values that to large. (It is hoped that this will improve the ratio of computed to tabulated values.) Thus:

$$\sum\sum\sum e_{ijk}^2 = \sum\sum\sum w_{ijk}(Z_{ijk} - C'x_{ijk} - By_{ijk})^2. \tag{6}$$

The procedure actually adopted was to solve Equations 5a and 5b for B and C'. Those values {B, C'} were then used to generate first guesses for Z. Weighting factors $w_{ijk} = 1/Z_{ijk}$ were then used in Equation 6. In this way new values were generated for {B, C'}. These new values for the parameters were used as a second guess to generate still another set of parameters {B, C'}. This iteration process was continued until the results {B, C'} converged.

Two points should be made concerning this iteration process:

1. Varying the values of the initial guess {B, C'} over a range of a factor of 2 does not change the values to which {B, C'} converge upon iteration.

2. The {B, C'} values converge very rapidly, with no more than 2 to 4 iterations being required before they change only in the 4th or 5th significant figure.

RESULTS

Some typical results of the computer program are compared with the Monte Carlo values in Figures 3 through 7. In Figure 3, the Monte Carlo results are indicated by the solid circles. In this case, the albedo must be independent of azimuthal angle since the gamma rays are normally incident on the concrete slab. In Figure 4, for non-normal incidence, it is seen that the two-parameter curve gives rather good agreement with the Monte Carlo results. In Figure 5, the radiation is again normally incident. Here it is seen that the Monte Carlo results vary by more than a factor of 10 because of statistical fluctuations. Figure 6 shows good agreement for near-grazing incidence. Figure 7 shows a case where agreement is not very good. This case is, in fact, one of the worst cases, the two-parameter formula generally giving values too low by a factor of about 1.5 for large polar angles of incidence and small azimuthal angles of the exiting ray.

Figure 8 shows how the parameters {C, C'} vary with energy. Table I gives the computed values for {C, C'} for the energies investigated.

It must be pointed out that what has been shown is generally good agreement between the results of Monte Carlo calculations and a semiempirical formula. Experimental data over a wide range of energies and angles are not yet available.

Definitive statements regarding differential dose albedo must await experimental study. Such an experimental investigation is being undertaken by the U. S. Naval Radiological Defense Laboratory.

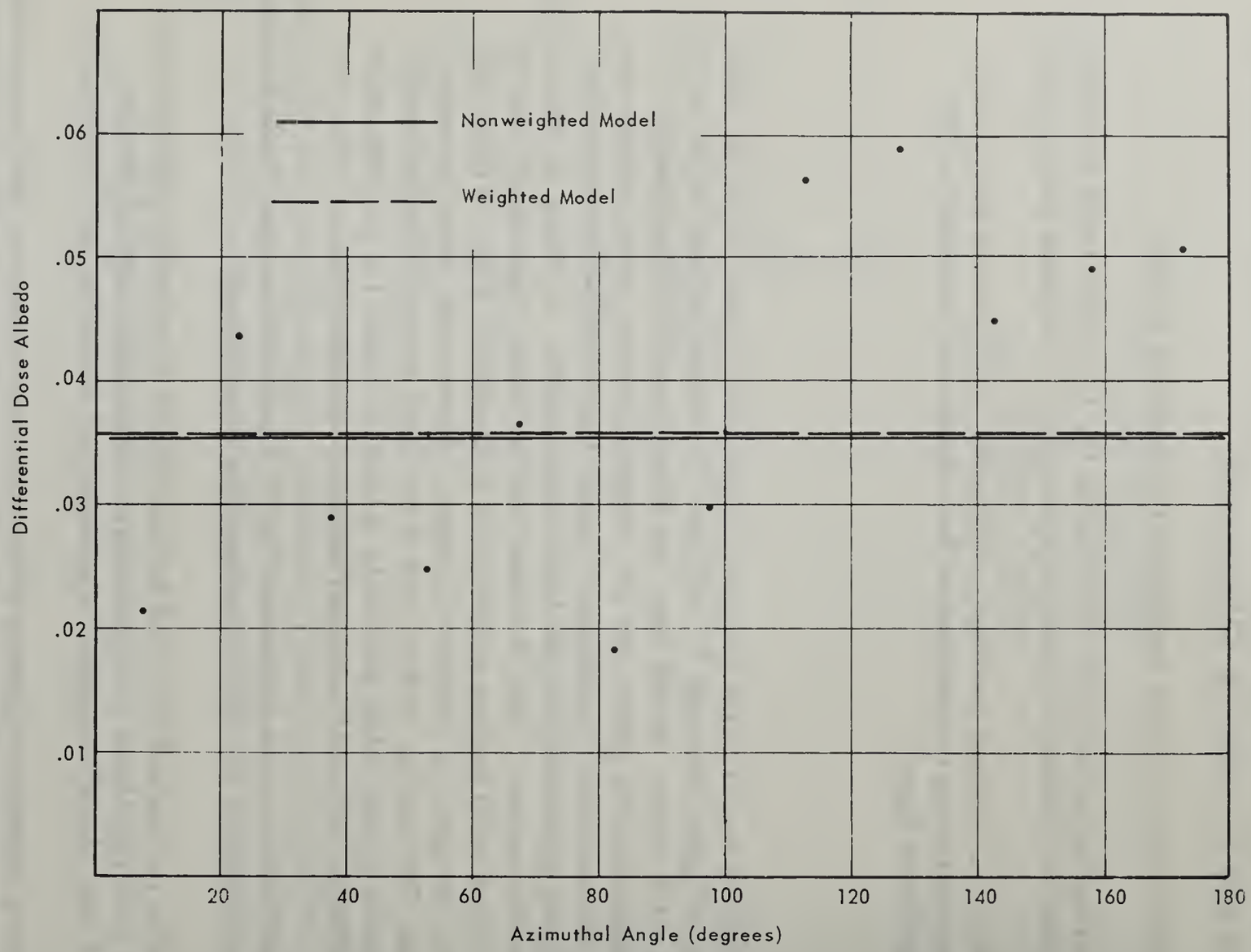

Figure 3. Differential dose albedo for E_o = 0.2 Mev, $\cos\theta_o$ = 1.00, θ = 8.12°.

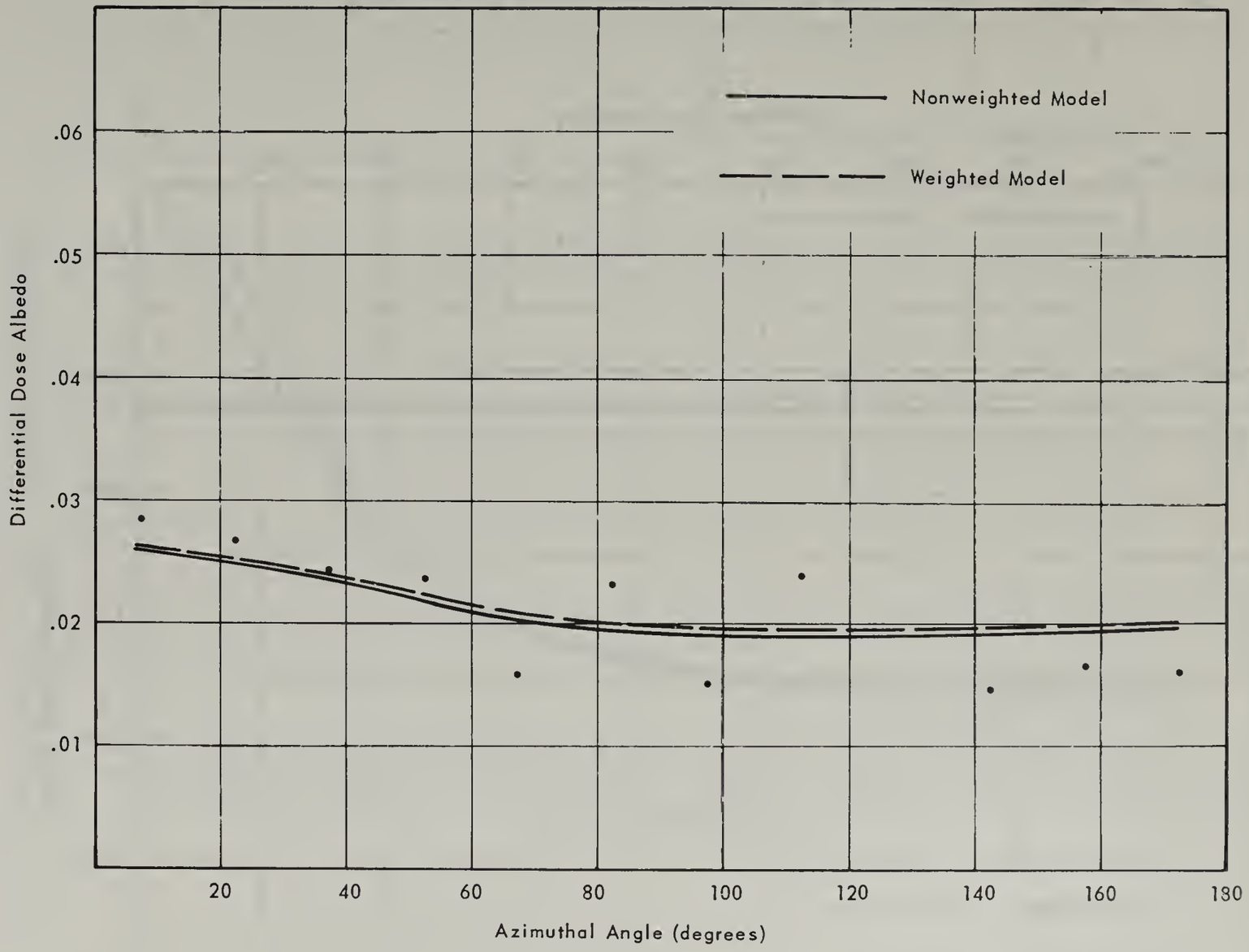

Figure 4. Differential dose albedo for E_o = 0.2 Mev, $\cos\theta_o$ = 0.75, θ = 72°.

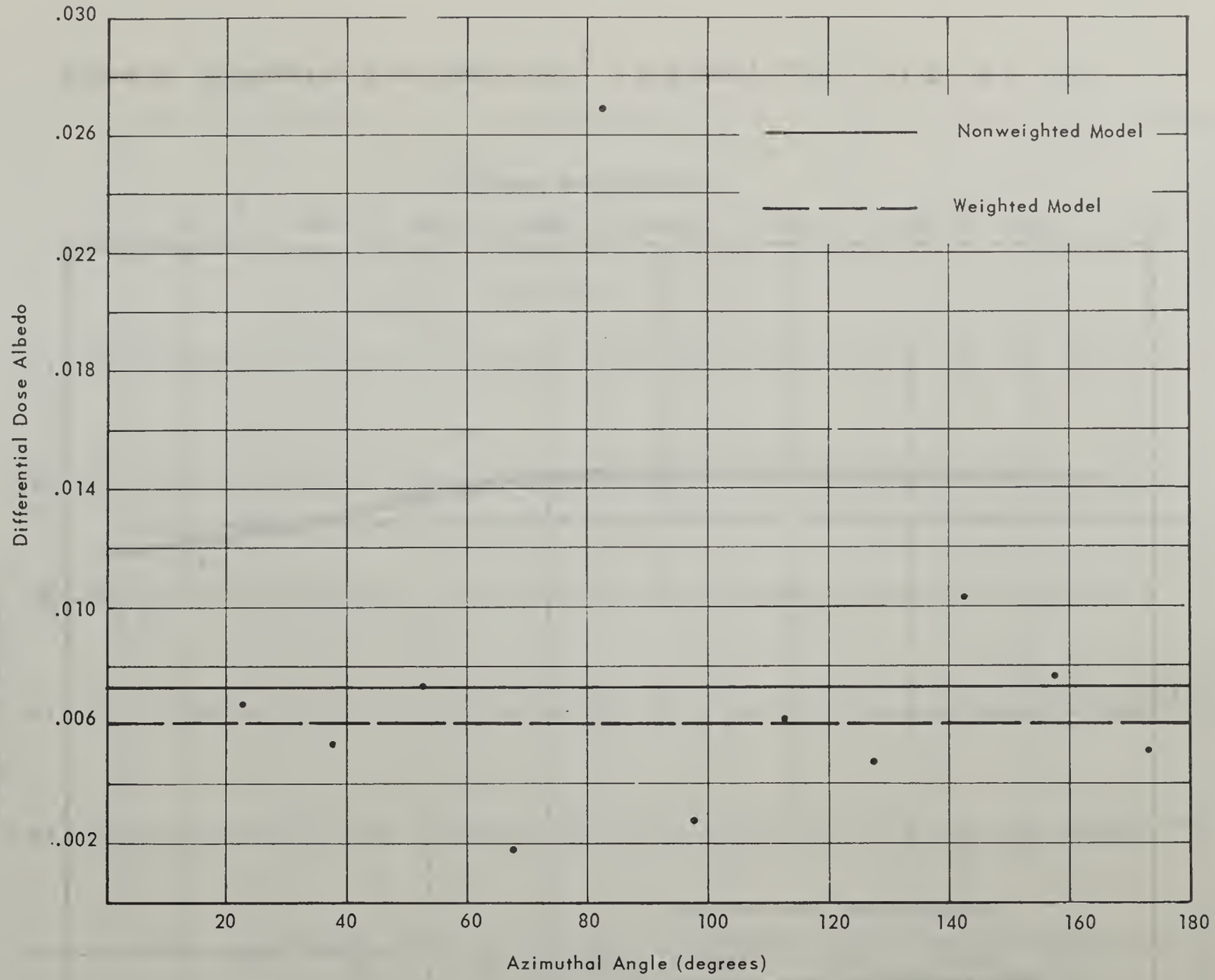

Figure 5. Differential dose albedo for E_o = 2 Mev, $\cos\theta_o$ = 1.00, θ = 8°.

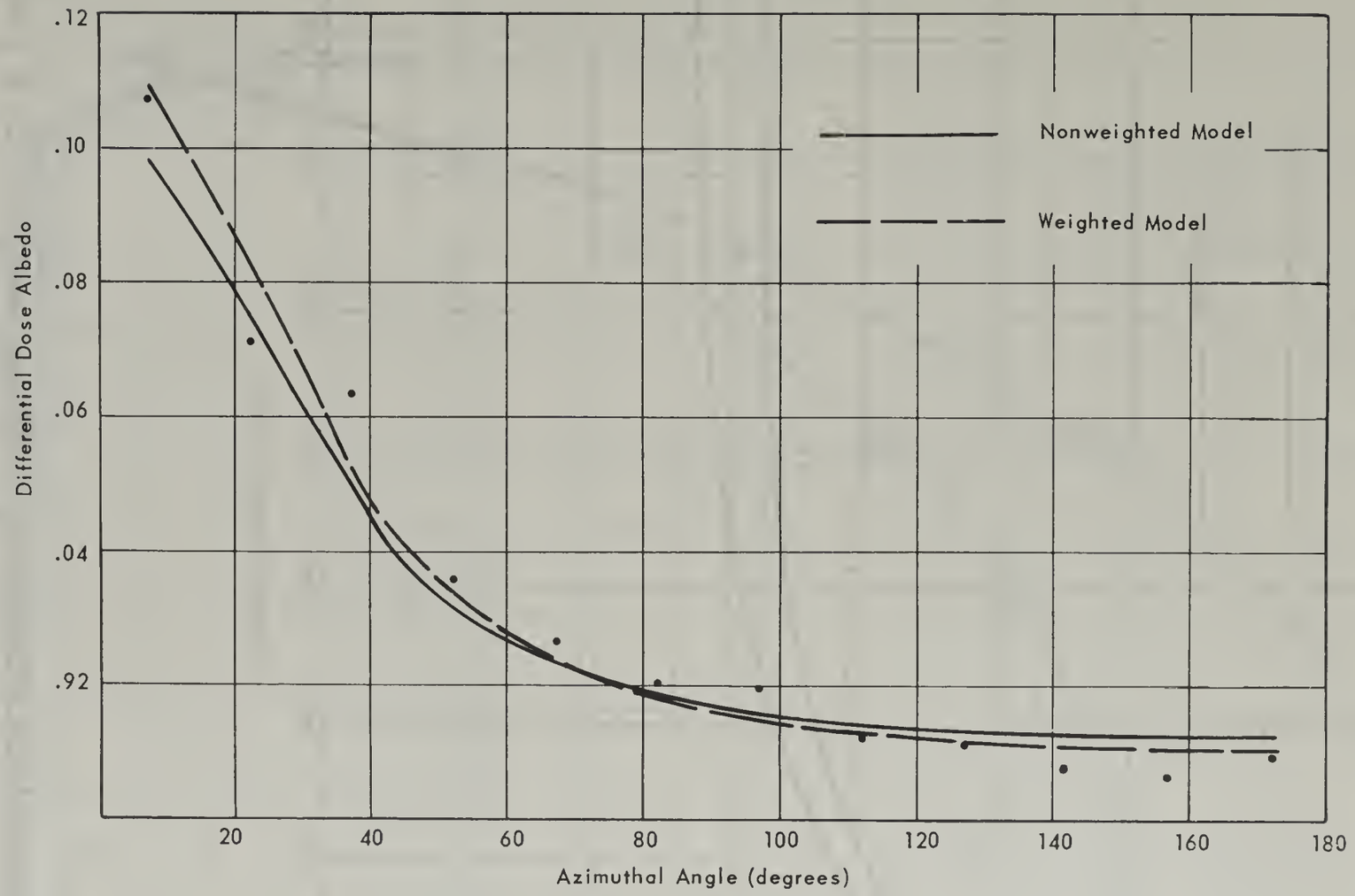

Figure 6. Differential dose albedo for E_o = 2 Mev, $\cos\theta_o$ = 0.10, θ = 64°.

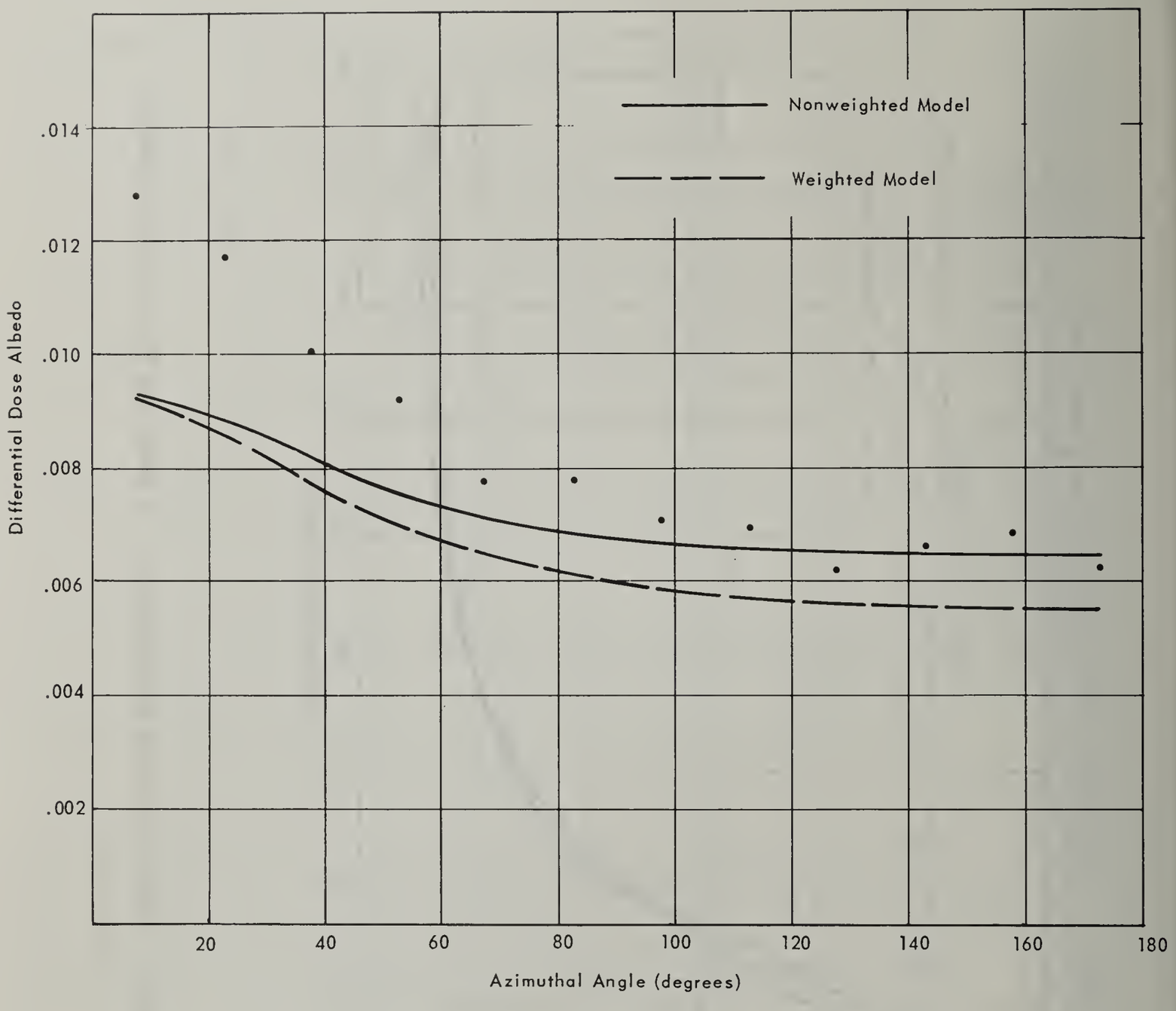

Figure 7. Differential dose albedo for E_o = 10 Mev, $\cos\theta_o$ = 0.25, θ = 45°.

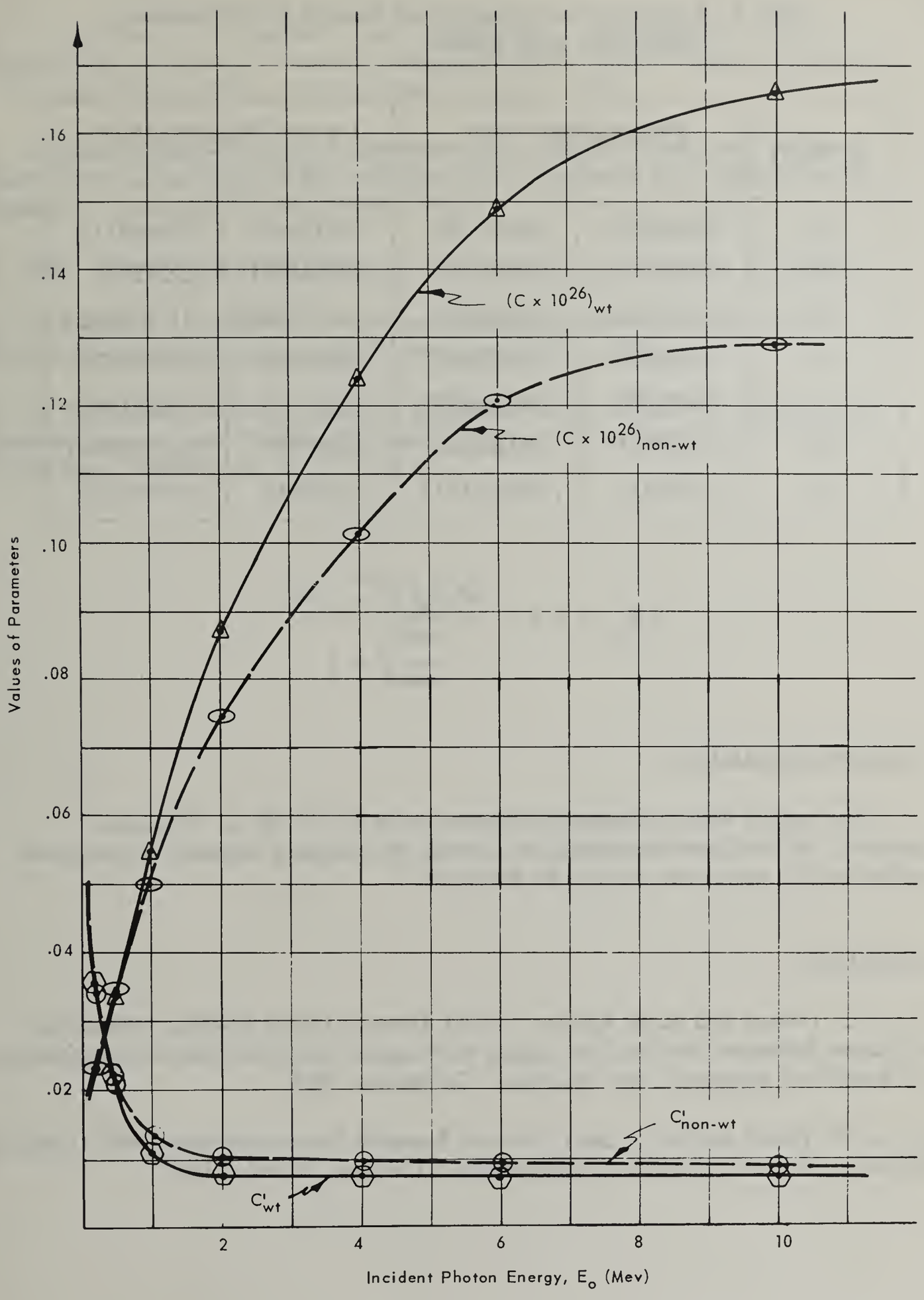

Figure 8. Variation of backscattering parameters with gamma-ray energy for weighted and nonweighted models.

Table I. Parameters for Semiempirical Formula for Differential Gamma-Ray Dose Albedo

E_o (Mev)	Nonweighted Model		Iterated Weighted Model	
	C	C'	C	C'
.2	.022437032	.034817388	.022126134	.035648111
.5	.034099514	.021695918	.033556571	.02215299
1	.050097528	.013696993	.054677888	.011132052
2	.074664107	.010657877	.086899748	.0077462231
4	.10184950	.0099281972	.12381103	.0075919821
6	.12089736	.0093307047	.14897540	.0074920140
10	.12836012	.0083441443	.16600843	.0070037501

$$\alpha(\theta_o, \theta, \omega) = \frac{CK(\theta_s)10^{26} + C'}{\frac{\cos\theta_o}{\cos\theta} + 1}.$$

ACKNOWLEDGMENTS

The authors wish to express their appreciation to Mr. W. L. Wilcoxson (presently at Iowa State University) for writing the necessary computer programs and performing the numerical analysis for this work.

REFERENCES

1. J. C. LeDoux and A. B. Chilton. NCEL Technical Note N-383, Attenuation of Gamma Radiation Through Two-Legged Rectangular Ducts and Shelter Entranceways — An Analytical Approach. Port Hueneme, California, 1961.

2. C. W. Terrell and A. J. Jerri. Armour Research Foundation Report ARF 115801-5, Radiation Streaming in Shelter Entranceways. Chicago, Illinois, 1961.

3. C. M. Park, C. B. Agnihotri, and J. Silverman. Department of Chemical Engineering, University of Maryland, Report UMNE-2, Interim Report on Scattering of Gammas Through Ducts. College Park, Maryland, 1962.

4. Dominic J. Raso. Technical Operations, Inc., Report TO-B 61-39 (revised), Monte Carlo Calculations on the Reflection and Transmission of Scattered Gamma Radiation. Burlington, Massachusetts, 1961.

5. Ibid. Transactions of the American Nuclear Society, Vol. 5, p. 218 (1962).

6. T. Rockwell III, editor. U. S. Atomic Energy Commission Report TID-7004, Reactor Shielding Design Manual. Washington, D. C., 1956.

7. A. T. Nelms. National Bureau of Standards NBS Circular 542, Graphs of the Compton Energy-Angle Relationship and the Klein-Nishina Formula from 100 kev to 500 Mev. Washington, D. C., 1953.

X - MISCELLANEOUS TOPICS

A. Ceiling Shine Analysis.

This is a copy of NCDL Technical Study #30. The basis of the ceiling shine component as derived in section V does not adequately account for all the parameters involved. This analysis is one attempt to do so. Both experimental and theoretical work is now in progress on this problem since it can be an important component under certain conditions.

B. Derivation of Solid Angle Fraction for Rectangles.

The solid angle fraction for rectangles is an important parameter for the detailed procedure. The derivation of ω for this case is easy if one happens to find or know a particular integral. This solution is presented merely to complete the notes of the student or instructor.

TECHNICAL STUDY #30 IN ATOMIC DEFENSE ENGINEERING

CEILING-SHINE CONTRIBUTION WITHIN BUILDINGS FROM FALLOUT RADIATION FIELD

By

J. C. LEDOUX
Commander, CEC, USN

February 1963

U. S. NAVAL CIVIL ENGINEERING LABORATORY

Port Hueneme, California

240-816 O-67—40

ABSTRACT

Ceiling-shine is that radiation which enters through the wall of a structure, reflects from the ceiling and increases the radiation within a shielded space. In most cases the ceiling-shine contribution is small when compared to direct and wall-scattered radiation. In some cases it can be an important contribution. The present method of analyzing buildings, the Engineering Manual, OCD PM 100-1, includes the ceiling-shine effect in the air scattered contribution, but does not provide a separate method of analysis. This report discusses the theory and application of ceiling-shine and proposes a method of computing its contribution.

Ceiling-Shine Contribution

BACKGROUND

The Engineering Manual[1] includes the ceiling-shine effect in the air-scattered (skyshine) directional response function, G_a. Since ceiling-shine is assumed to be small compared to skyshine, it was added as a corrective factor to skyshine. There are certain cases, however, where ceiling-shine could be a predominant effect in an otherwise well shielded structure. A building with a high narrow band of windows protected by a large roof overhang would appear to be a very good shelter if the roof and wall thicknesses were in the 200 to 250 psf range. Present methods of analysis would indicate excellent shielding against direct, wall-scattered, and air-scattered radiation. Calculations based on the method presented here, reduce the protection factor for such a building from 300 to 150 when ceiling-shine contribution is considered. Perhaps a more likely example would be a mutual shield which blocks out skyshine. Ceiling-shine would still be present and in the present method would be neglected. In view of this, it is evident that a method of computing ceiling-shine is needed to insure that its effect will not be overlooked.

THEORY

Figure 1 illustrates a simple building with windows and the two contributions--skyshine and ceiling-shine. Since there is little theoretical or experimental data available upon which to base a calculational procedure, we must use those functions which are now available in the Engineering Manual and the Spencer Monograph.[2]

Figure 2 is a sketch indicating that ceiling-shine must be some function of the radiation which is incident on the ceiling. The direct radiation directional response function, G_d, measures the radiation which comes from an infinite plane source of radiation, through the complement of the solid angle fraction which is below the detector plane. If we place a detector on the ceiling directly above the room detector position and measure the radiation which enters this detector through the complement of the solid angle fraction, we would have some measure of the radiation incident on the ceiling. The ceiling-shine response function, G_c, must then be proportional to G_d.

Scattering does not take place at the surface of the ceiling but within the interior of the slab. First floor ceiling height would be about 10 feet and we might be tempted to use G_d for H=10'. Within the first mean free path (about 2.5 inches of concrete for 1 mev gamma photons), 50% of the incident photons would suffer some interaction with the electrons. Only a smaller fraction of these would be back-scattered out of the slab to contribute to the ceiling-shine. The deeper the penetration into the slab before an interaction, the less is the probability that the photon will emerge again. Consequently, most of the gamma radiation contributing to ceiling-shine will be back-scattered within the first mean free path (32 psf). Fifty percent of the radiation which is back-scattered comes from the first 6 psf of a reflecting slab.[3]

Charts 5 and 6 of the Engineering Manual plot G_d as a function of solid angle fraction and height of the detector. In order to use this information to correspond to radiation incident on and then reflected from the ceiling, the slab was divided into a number of small horizontal slabs each at 1 psf. The thickness of the mid-point of each differential slab was converted to equivalent height of air. To this was added a nominal first floor ceiling height of 10'. The proper value of G_d was then obtained from Chart 6. This value was multiplied by the fraction of the radiation reflected from this incremental slab.[3] A response function was then constructed which "accounts" for the radiation incident on the ceiling and then reflected back toward the floor detector. Figure 5 has two G_r curves: one for a ceiling height, H_c, of 10 feet; one for a ceiling height of 100 feet. These curves have been normalized so that the 10' curve has a value of 1.0 for $\omega_c = 0$.

Since radiation which emerges from the ceiling and strikes the lower detector is all scattered radiation, it must be similar to air-scattered radiation. The 'S_a' function from the Spencer Monograph[2] (Figure 28.15) is the geometry factor for air-scattered radiation incident in a limited cone of directions about a perpendicular axis through the detector. S_a is a function of the solid angle fraction, ω_o, which measures the overhead contributing ceiling. The ceiling-shine function must then be proportional to S_a.

Finally the ceiling-shine will depend on the thickness of the reflecting slab. A thin slab will reflect some radiation, but will also transmit some. The G_r curves of Figure 5 have assumed an infinitely thick ceiling slab to produce maximum reflection. Actually a 4" concrete slab will reflect this same maximum amount. Any additional thickness does not materially increase the amount reflected out. Since 4" of concrete is a common thickness found in most floor slabs and would be a minimum thickness for shelters, maximum reflection is a good assumption.

The ceiling-shine equation must have a normalizing factor to make the function agree with some known conditions. The ceiling-shine equation would then be of the following form;

$$G_c = KG_r(\omega_c, H_c)\, S_a(\omega_o).$$

This equation has the proper characteristics. As the area of the reflecting surface increases, ceiling-shine increases. As the cleared area around the detector increases, ceiling-shine decreases. When either $\omega_o = 0$, or $\omega_c = 1$, ceiling-shine must be zero.

In order to determine our normalizing factor 'K', assume an infinite plane of contamination. Over this plane, place an infinitely thick roof slab of infinite extent at normal first floor ceiling height, 10'. Under these conditions, $\omega_o = 1$, and $\omega_c = 0$. From Figure 5, $G_r = 1.0$, and $S_a = 1.0$. Then:

$$G_c = K.$$

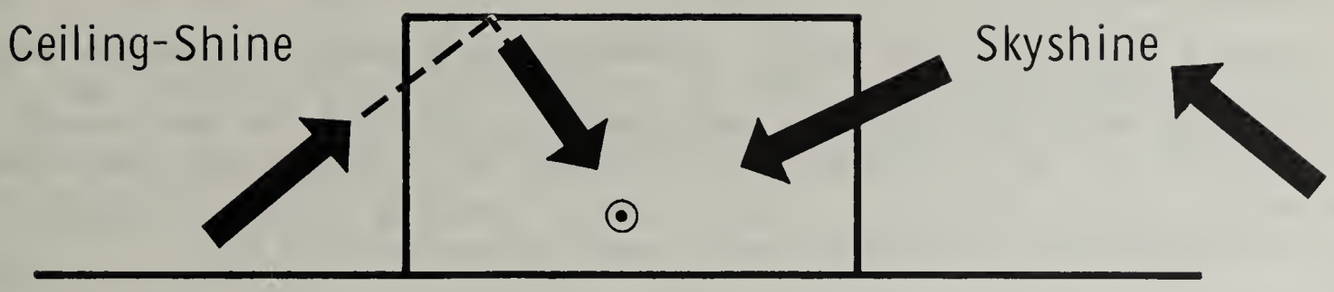

Figure 1. Concept of Ceiling-shine and Skyshine

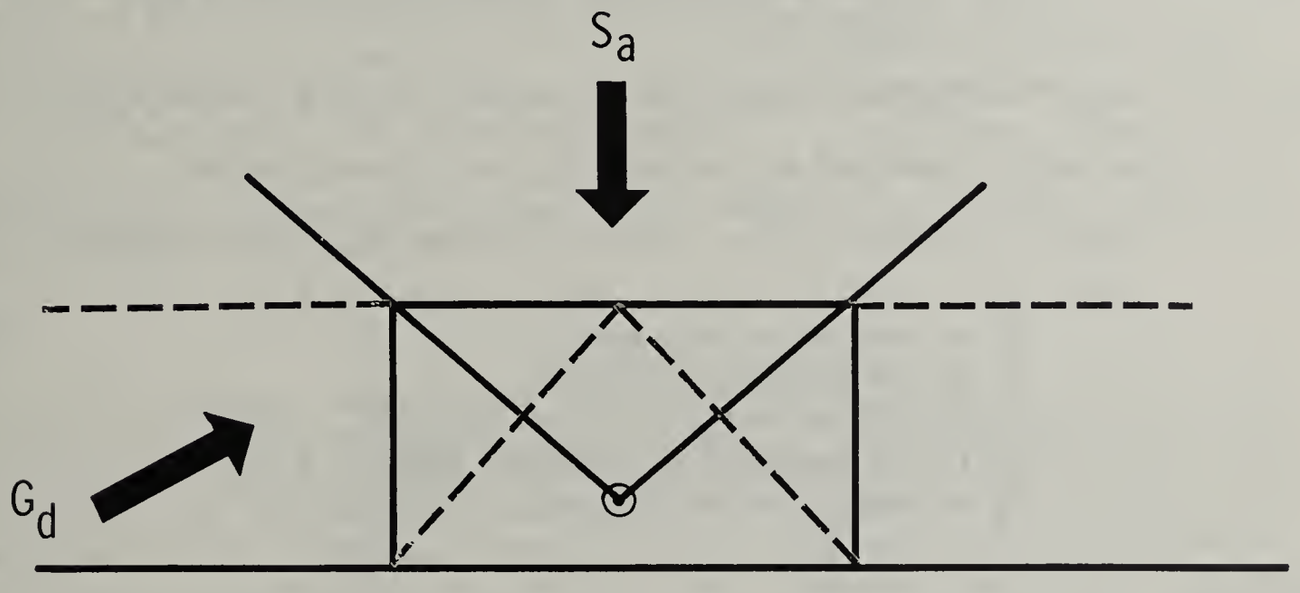

Figure 2. Dependence of Ceiling-Shine on functions G_d and S_a

Since we have assumed maximum reflection, ceiling-shine for this case must equal maximum skyshine which is 0.10. Therefore, K must equal 0.10. Figure 5 also plots S_a from the Spencer Monograph for two values of detector height, H. As detector height increases from 3', K must be modified by an additional height correction factor. Figure 5 has a chart of this correction.

GENERAL SOLUTION

Figure 3 illustrates the various parameters for a completely general case. This is a building with windows which do not extend to ceiling height. ω_c is the ceiling solid angle fraction which measures the extent of the cleared area. ω_g and ω_g' are the solid angle fractions which measure the lower and upper window sills respectively. Similar angles could be used if a limited plane of contamination existed and would apply to the value of G_r.

The total ceiling-shine contribution, C_c, would then be:

$$C_c = C_{cg} + C_{cw} - C_{cgw}$$

where C_{cg} is the ceiling-shine through windows

C_{cw} is the ceiling-shine through total solid wall
C_{cgw} is the ceiling-shine through window area with solid walls.

$$C_{cg} = 0.1\, B_w(0,H)\, [G_r(\omega_g, H_c) - G_r(\omega_g', H_c)]\, S_a(\omega_o) P_a F_h(H)$$

$$C_{cw} = 0.1\, B_w(X_e,H)\, G_r(\omega_c, H_c)\, S_a(\omega_o)\, [1-S_w]\, F_h(H)$$

$$C_{cgw} = 0.1\, B_w(X_e,H)\, [G_r(\omega_g, H_c) - G_r(\omega_g', H_c)]\, S_a(\omega_o) P_a\, [1-S_w]\, F_h(H)$$

where B_w is the wall barrier factor, Chart 2 E.M.
H is the detector height
H_c is the height of ceiling
P_r is the perimeter ratio of windows
S_w is the scattering fraction, Chart 7 E.M.
F_h is height correction factor, Figure 5.

APPLICATION

Normally, ceiling-shine, like skyshine, is small when compared with direct and wall-scattered radiation. Since it is small, some simplifying assumptions can be made for most building types.

Figure 4 illustrates the solid angle fractions which can be used for most buildings with little error. Three assumptions are made: (1) the lower sill height is at detector height, 3 feet; (2) windows extend to the ceiling; and (3) the ceiling-shine contribution from below the sill or through the solid wall is negligible. Using these assumptions, $\omega_o = \omega_c$ and composite curves

of skyshine + ceiling-shine can be plotted as a function of a single solid angle fraction. Figure 6 is a replacement for Chart 5 of the Engineering Manual. Two air-scattered curves are shown: G_a which is still skyshine + ceiling-shine, and G_a' which is skyshine only.

Buildings which meet the conditions of these three assumptions are handled in the usual manner using G_a. Slight variations from this idealized building will not introduce serious errors. For other applications, G_a' is used in place of G_a' is used in place of G_a, and the ceiling-shine contribution, C_c, is computed and added to C_o and C_g.[1] Figure 5 is used to compute C_c and has two curves for G_r and S_a; one for first floor applications and one for a height of 100 feet.

EFFECT OF HEIGHT

As the ceiling or reflecting surface height increases, ceiling-shine will decrease. The directional distribution of radiation changes from a horizon oriented distribution at the 3' level to a more and more vertical orientation as the height increases. This change in distribution is reflected in the G_d function as used in the Engineering Manual and in the G_r function used in this paper. Figure 5 has a plot of two G_r curves, one for a ceiling height of 10 feet and one for a ceiling height of 100 feet. Linear interpolation between these two curves for other heights should be accurate enough for ceiling-shine problem. The amount of radiation available for contribution to ceiling-shine decreases also due to absorption and scattering which take place before the ceiling is reached. This effect is reflected in the S_a curves and the Height Correction chart on Figure 5. The Height Correction (F_h) is a simple multiplying factor applied to the basic equations. H is the height of the room detector.

EXAMPLE

There are certain cases where ceiling-shine could be an important contribution to the total radiation. For example, a building with a roof overhang and a high band of windows could have an important contribution from ceiling-shine. If the roof and wall mass thicknesses are in the 200 to 300 psf range and if the overhang shields out air-scattered radiation from the window areas, ceiling-shine could be the most important contribution. Another and perhaps more likely example, is the case where a mutual shield apparently blocks out all skyshine. Ceiling-shine will still be present. In fact, the major source of ceiling-shine is fallout particles which are close to the structure.

The following example illustrates this point. Two solutions are shown: one with the usual Engineering Manual solution using the new value of G_a, and the second solution using G_a' and computing the ceiling-shine separately. The ceiling-shine contribution through the solid wall is computed but it is negligible.

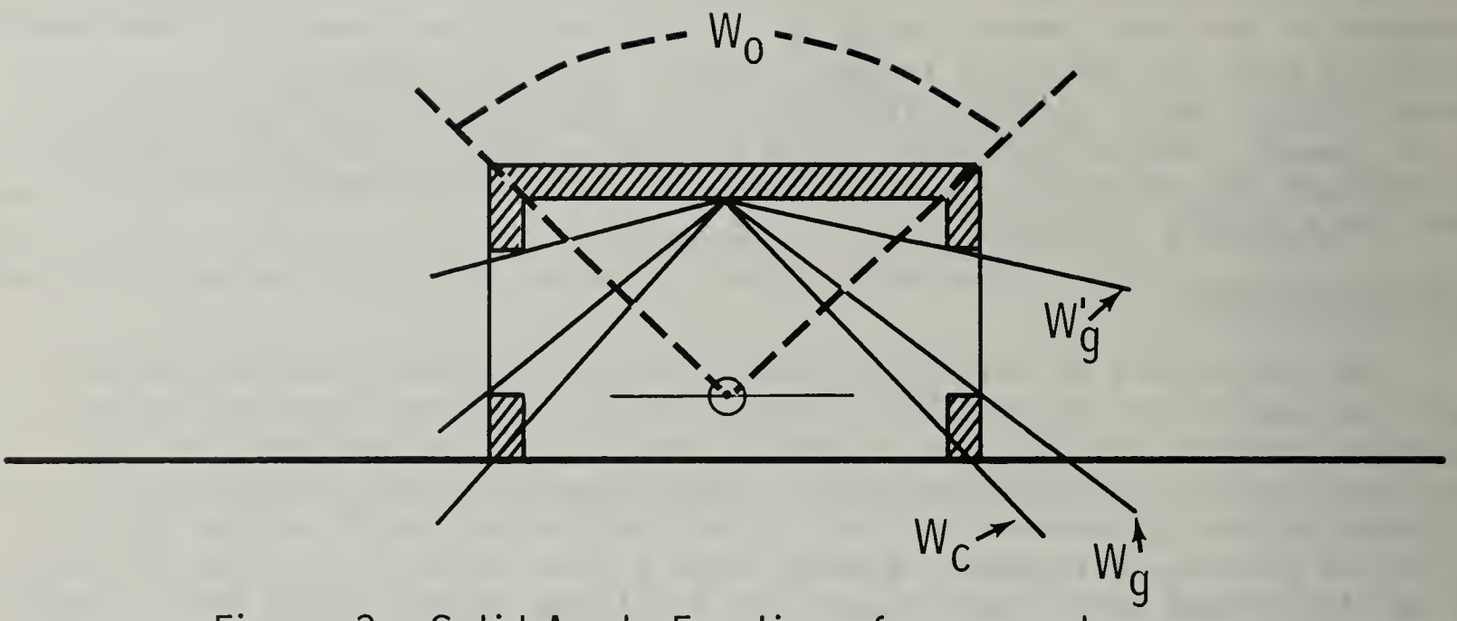

Figure 3. Solid Angle Fractions for general case.

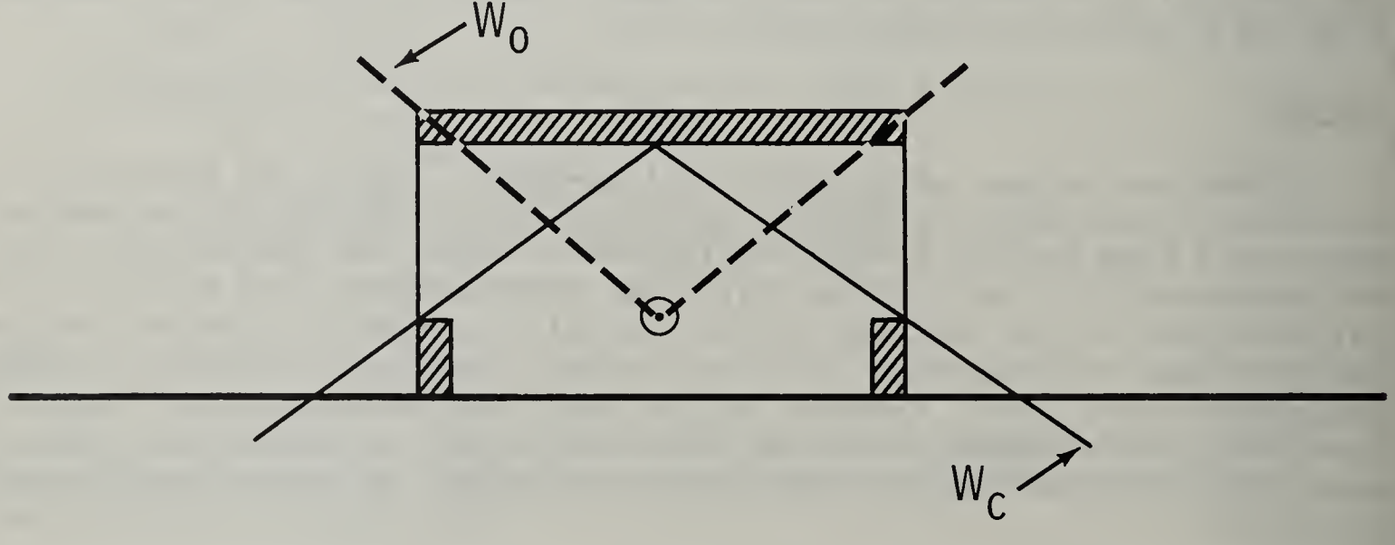

Figure 4. Solid Angle Fractions for simplified case.

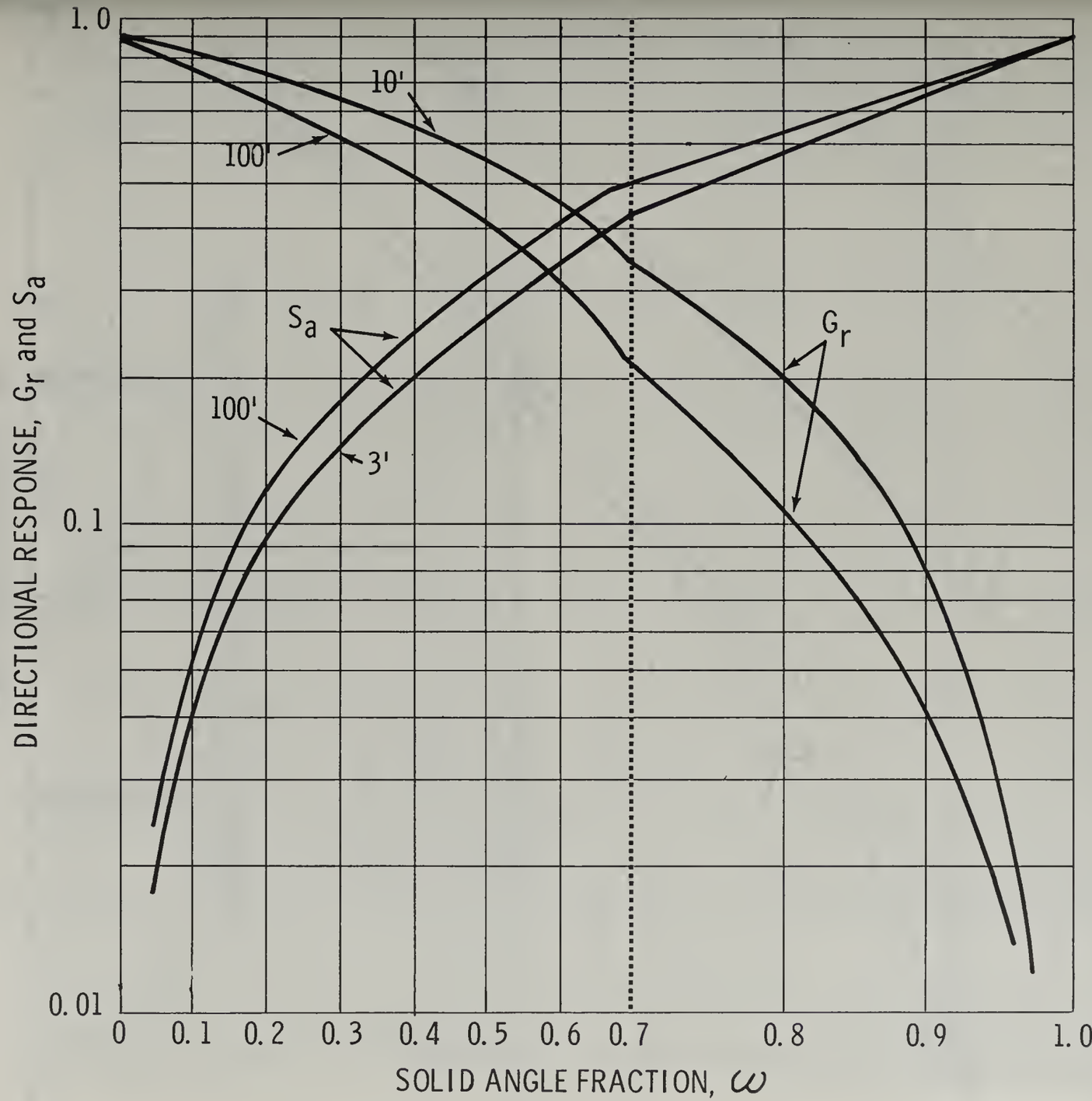

	G_r	
	H=10'	100'
.90	.083	.040
.91	.071	.035
.92	.060	.030
.93	.049	.025
.94	.038	.021
.95	.028	.017
.96	.020	.012
.97	.013	.007
.98	.006	.004
.99	.001	.001

Added Height Correction

H	Correction
10'	.84
20	.77
30	.72
40	.68
50	.64
60	.60
70	.57
80	.55
90	.52
100	.50

Figure 5. Plot of G_r and S_a vs solid angle fraction and height.

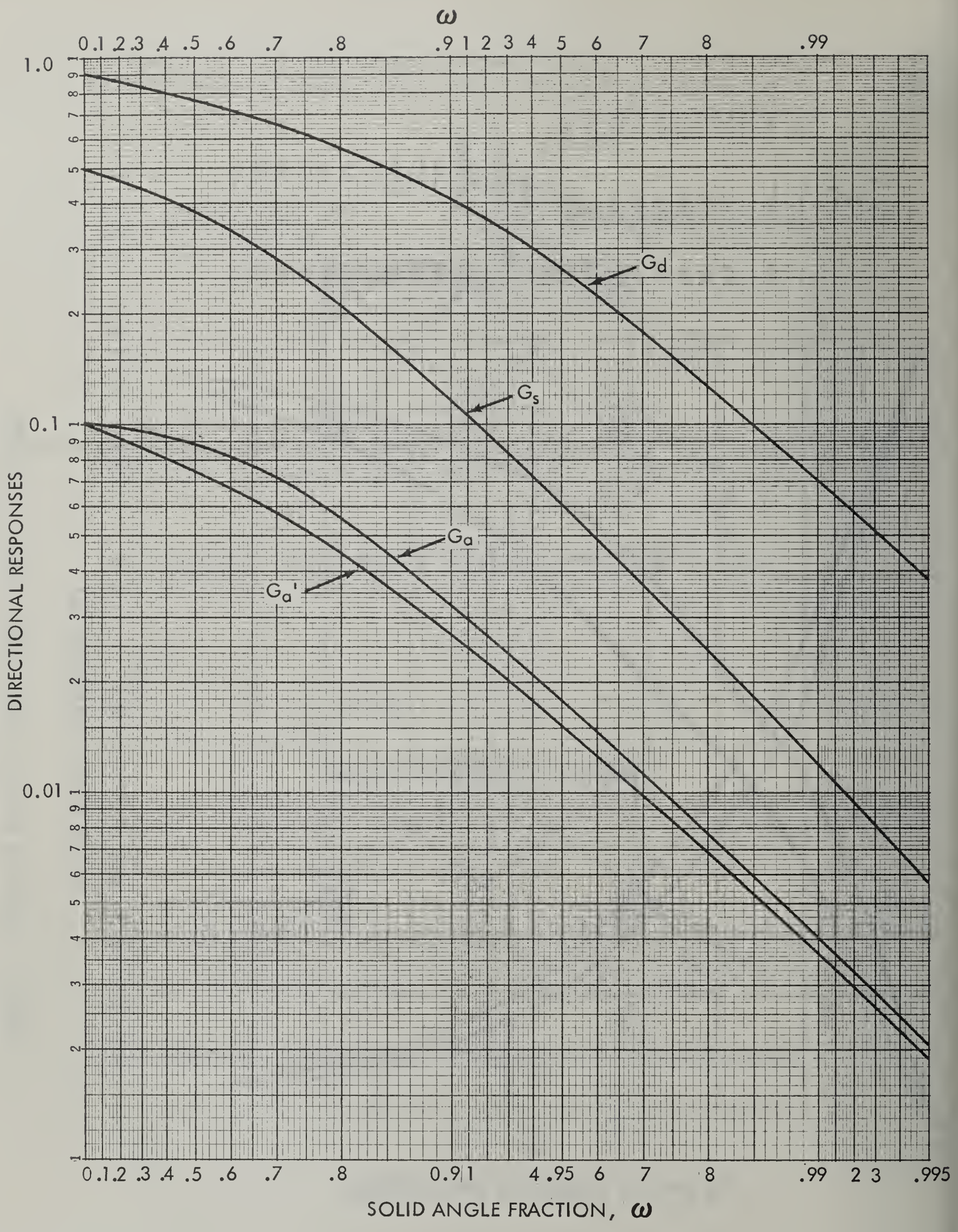

Figure 6. DIRECTIONAL RESPONSES, GROUND CONTRIBUTION

Example: Building with roof overhang.

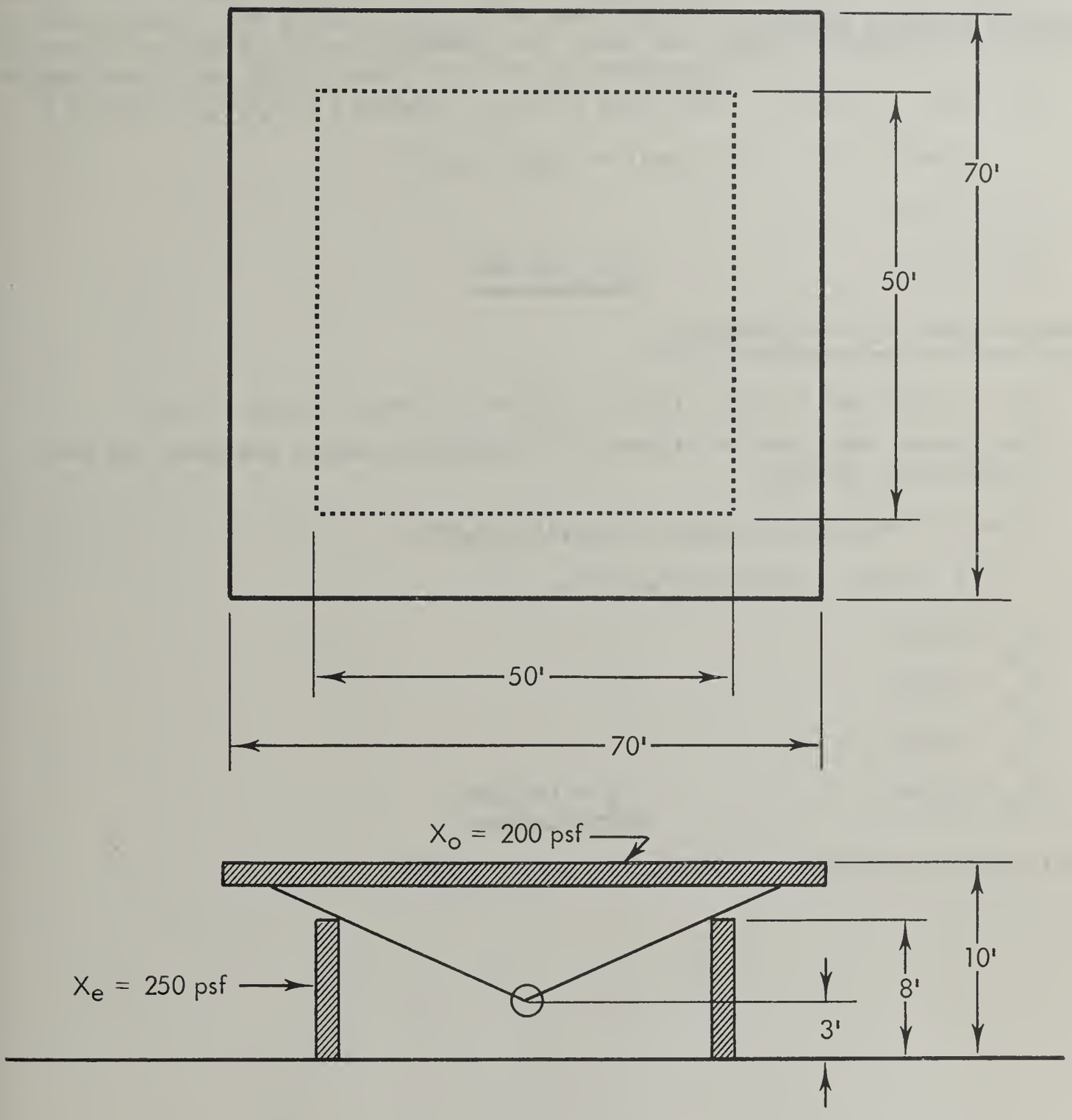

	z	e	n	ω	G_d	G_r	G_s	G_a	G_a'	S_a	
ω_o	7'	1.0	0.2	0.82	XX	XX	0.20	.051	.042	.58	$B_w(0,H)=1.0$
ω_ℓ	3'	1.0	0.12	0.89	.43	XX	0.13	XX	XX	XX	$B_x(X_e,H)=.0032$
ω_c	10'	1.0	0.4	0.66	XX	.39	XX	XX	XX	XX	$P_r=1.0$
ω_g	2'	1.0	0.08	0.92	XX	.06	XX	XX	XX	XX	$E=1.41$
											$S_w=0.88$

STANDARD SOLUTION USING G_a

$$C_g = B_w \left\{ [G_s(\omega_\ell) + G_s(\omega_o)] \; E \; S_w + [G_d(\omega_\ell) + G_a(\omega_o)] \; (1-S_w) \right\}$$

$$= .0032 \; (.33 \times 1.41 \times .88) + (.481 \times .12)$$

$C_o = .0018$

$R_f = .0033$ $\qquad P_f = 303$ ANS

SOLUTION USING G_a' AND ADDING C_c

G_a' is .042 and is only slightly different than G_a which is .051

The ground contribution without ceiling-shine remains the same, to two significant figures.

$$C_c = 0.1 \; Bw(0,H) \; G_r(\omega_c H_c) \; S_a(\omega_o, H) \; P_r F_h(H)$$

$$= 0.1 \times 1.0 \times .06 \times .58 \times 1.0 \times 1.0$$

$C_c = .0035$

$C_g = .0015$

$C_o = .0018$

$R_f = .0068$ $\qquad P_f = 147$ ANS

Ceiling-shine through solid wall is only 0.000007.

A recent report[4] derived a ceiling-shine solution in a similar but independent effort. Circular ring sources and reflecting areas using albedo theory were used to develop functions describing the source plane and reflecting surface. These two functions are basically the same as the G_r and S_a curves used in this paper. The correction for height is handled in a slightly different manner. This report[4] has some experimental results which verify the method. Both methods predict within a few percent the same total ceiling-shine. The method proposed in this paper is developed within the framework of the Engineering Manual and those familiar with the Engineering Manual should be able to apply it with no difficulty.

REFERENCES

1. The Engineering Manual, OCD PM 100-1. Office of Civil Defense, Washington, D. C., Draft October 1961.

2. Spencer, L. V., Structure Shielding Against Fallout Radiation from Nuclear Weapons. NBS Monograph 42. National Bureau of Standards, Washington, D.C., June 1962.

3. Private Communication from J. Batter, Technical Operations, Inc., Burlington, Massachusetts.

4. Batter, John F. and Joseph D. Velletri, The Effect of Radiation Reflected from the Ceiling of the Dose Rate Within Structures. TO-B-63-25. Technical Operations, Inc., Burlington, Massachusetts. April 1963.

A SOLUTION FOR ω FOR RECTANGLES

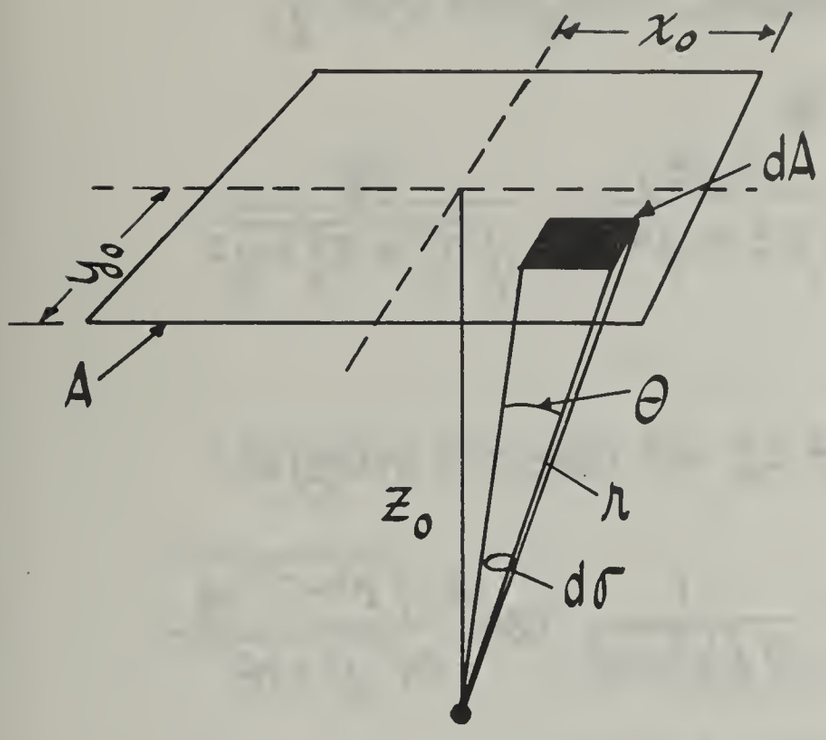

$$d\sigma \equiv \frac{dA \cos\theta}{r^2}$$

$$d\sigma = \frac{dA \cdot z_0}{r^3}$$

$$\therefore \Omega = \int_A \frac{z\, dA}{r^3}$$

$$r = \sqrt{x^2 + y^2 + z^2}$$

$$dA = dy\,dx$$

$$\omega \equiv \frac{\Omega}{2\pi}$$

$$\therefore \omega = 4 \cdot \frac{1}{2\pi} \int_0^{y_0} dy \int_0^{x_0} \frac{z\, dx}{\left(\sqrt{x^2+y^2+z^2}\right)^3}$$

Since z is constant, hold y constant by letting $a^2 = y^2 + z^2$ and integrate over x:

$$\therefore \omega = \frac{2}{\pi} \int_0^{y_0} dy \left[\frac{z}{a^2} \cdot \frac{x}{\sqrt{a^2+x^2}} \right]_0^{x_0}$$

z_o and x_o are now constant. Integrate over y.

$$\omega = \frac{2}{\pi} \int_0^{y_o} \frac{x_o z_o}{(z_o^2 + y^2)} \cdot \frac{dy}{\sqrt{x_o^2 + z_o^2 + y^2}}$$

If $a^2 = z_o^2$ and $b^2 = x_o^2 + z_o^2$ we have the integral:

$$\int \frac{dy}{(a^2+y^2)\sqrt{b^2+y^2}} = \frac{1}{a\sqrt{b^2-a^2}} \tan^{-1} \frac{\sqrt{b^2-a^2}\cdot y}{a\sqrt{y^2+b^2}}$$

or $$\omega = \frac{2x_o z}{\pi} \left[\frac{1}{z\sqrt{x^2+z^2-z^2}} \tan^{-1} \frac{y\sqrt{x^2+z^2-z^2}}{z\sqrt{x^2+y^2+z^2}} \right]$$

$$\omega = \frac{2}{\pi} \tan^{-1} \frac{x_o y_o}{z\sqrt{x_o^2+y_o^2+z_o^2}}$$

if $\epsilon = y/x$ and $\eta = z/x$

then: $$\boxed{\omega = \frac{2}{\pi} \tan^{-1} \frac{\epsilon}{\eta\sqrt{\epsilon^2+\eta^2+1}}}$$

Vol. IV

EXPERIMENTAL PROGRAM

Arthur B. Chilton

and

Participants of the 1962 and 1963

Shielding Institutes

240-816 O-67—41

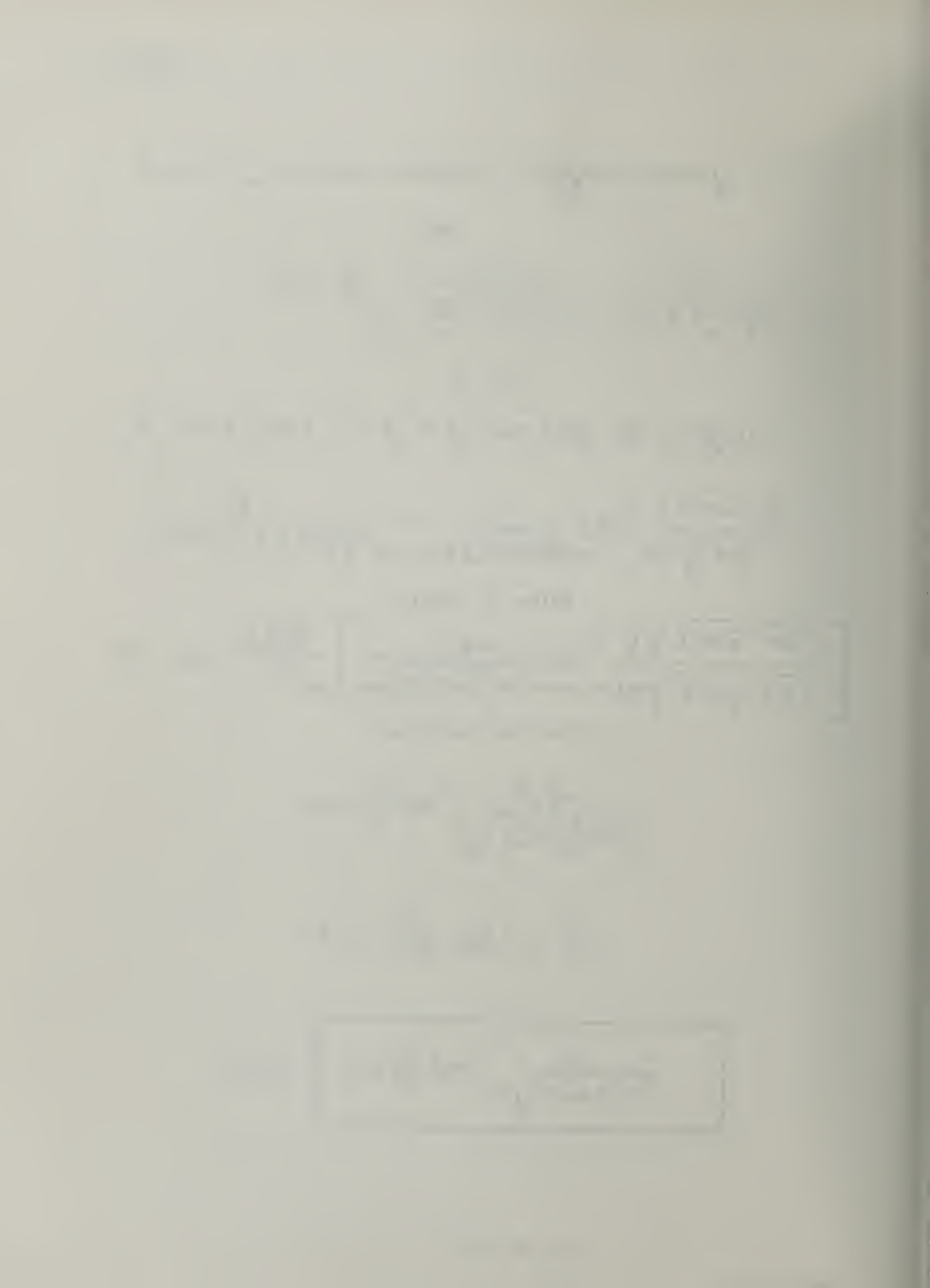

A. General Preliminaries

1. Introduction

In a sense, the experimental part of each summer's Shielding Institute was begun long before the official opening date, because of the many advance preparations required to assemble the equipment and facilities and check out their adequacy. This was particularly true of the first Institute, for which a great amount of preliminary effort was needed for planning the experiments, determining the budget estimates, negotiating the contract with OCD, obtaining the AEC license, obtaining a suitable site, procuring equipment and materials, calibration checking of sources and detectors, and taking care of a host of miscellaneous details.

The layout of the facilities constructed is shown in Figure III-0-1. These facilities were placed on a rather flat-topped hill, within a tract of land sufficiently large that there was no hazard outside the property to any member of the general public. The property was surrounded with a barbed wire fence, and a locked gate provided for entry. A gravel road was constructed from the gate to the experimental facilities.

When the detection instruments arrived, they were calibrated by the Institute staff, with the use of radium and cobalt-60 calibrated sources available in the Nuclear Engineering Department of Kansas State University. The self-reading instruments in general appeared to read correctly within a few percent. Some special effort was required in connection with the non-self-reading dosimeter chambers. Two different designs of readers were obtained for them, and calibration had to be performed for each combination of instrument type and reader.

The sources arrived at a time so close to the beginning of the 1962 Institute that careful checking of their calibration was not possible, but a brief preliminary checking seemed to indicate that the values given by the vendors were consistent with the instrument calibration data, within the limits of error considered acceptable for the purposes of the Institute, that is, within 10%. Subsequent experience in using the sources has increased confidence in their stated strengths, and it is now believed that one can accept the vendors' original claim within 5% limits of error.

The 1962 experimental program was so successful that no significant changes were made in the original experimental plan during the 1963 Institute. Certain minor improvements were made in the facilities; and some slight differences in techniques were tried, which did not necessarily turn out to give better results.

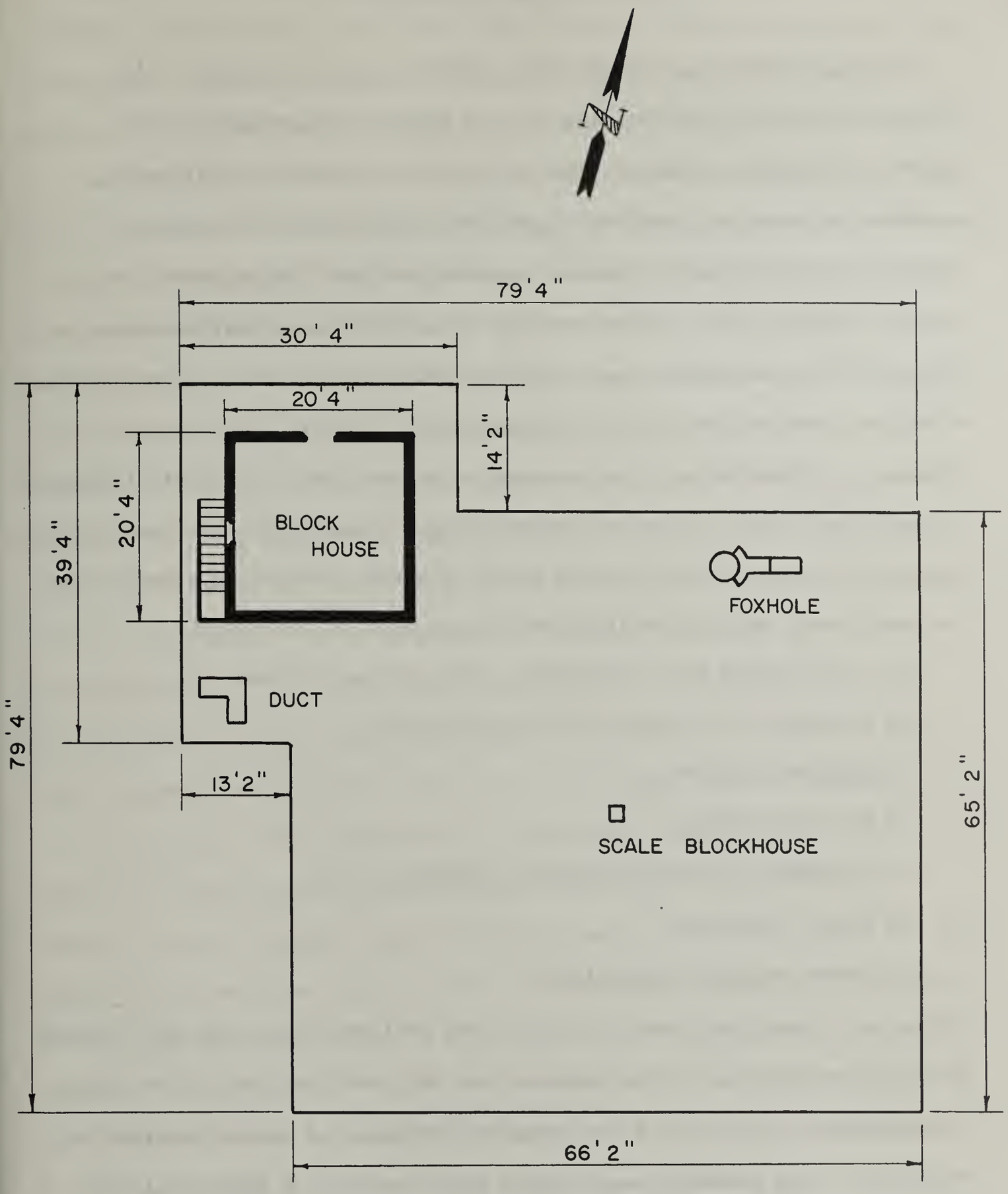

PLAN OF SHIELDING FACILITIES .

FIGURE III-O-1

2. Nature of the Experiments

The experiments undertaken were selected and planned with full recognition of the fact that their prime purpose was pedagogical in nature. It was not expected that the experiments would reveal much new and startling information; it was not expected that the results achieved would be highly accurate; most of the experiments themselves are not original. The effort was made to provide to the participants within the time available some knowledge and appreciation of experimental work being done in the field of radiation shielding for civil defense purposes, to learn to use the standard techniques and instruments involved in such work, and to obtain an appreciation of the difficulties and likely sources of error inherent in such work. Any new information arising from the experiments must be regarded as a by-product of the effort.

Six experiments were undertaken. They are as follows:

1) Blockhouse Experiment--Roof Contamination

2) Foxhole Experiment

3) Duct Experiment

4) Blockhouse Experiment--Ground Contamination

5) Model Experiment

6) Compartmentation Experiment

Others were considered, and facilities and equipment were provided in case they were undertaken. Time, however, has not permitted their study, but the capability still exists for possible inclusion in future programs of this sort. Such potential experiments might include: a study of light frame structure attenuation; gamma ray and neutron albedo experiments; simple attenuation experiments; more extended calibration experiments; and others.

Each experiment required its own particular set of instruments and equipment, and these are indicated in the sections devoted to the individual experiments. However, a general description of the facilities and the supporting items and services might be appropriate at this point.

The principle facilities are as indicated on the layout drawing, Figure III-0-1. The major facility item is a simple blockhouse, about 20' square and 8' high, with basement. This blockhouse is made of lightweight concrete, averaging about 103 pounds per cubic foot in density. The roof and floor were made of pre-cast, pre-stressed slabs, of nominal thickness 6", and with a more precise thickness value, based on pounds per square foot of material, of 55 psf. The sides were made of solid concrete block, which had been cast in a somewhat irregular shape so that when they were laid up the cracks between the blocks would not run straight through the wall but would be zig-zagged. These sides were of nominal thickness of 8", and were determined to have a thickness by weight of about 69 psf. The roof was tied down by cables to ground anchors, to provide resistance to high winds, inasmuch as the walls were laid up dry rather than with mortar.

In addition to the blockhouse, a cylindrical foxhole, lined with concrete of normal density was provided, measuring 4' deep and 4' in diameter. Also a concrete duct system was built in sections, so as to permit portability. The first one built was of lightweight concrete; but between the 1962 and 1963 Institutes, it was replaced with one of normal density concrete. Provisions for a model structure were provided, by having a hole representing the blockhouse basement, on a 1 to 12 model basis, put in the concrete pad. Over this hole a steel model representation of the blockhouse could be placed.

Auxiliary facilities included a small, portable, wooden building, about 10' by 20', which was built for storage and use as an instrument shelter. A truck was provided for transportation of the heavy storage pigs used to house the radioisotopes. Hoists and fork-lift trucks were provided to assist in the handling. Miscellaneous equipment included: spotting telescope, 20-power, for distant observations of the radiation sources; pumping apparatus and polyethylene tubing for movement of the sources to simulate fallout; sandbags; bags of lead shot; health physics monitoring equipment; and many kits of repair tools and spare parts.

Help and cooperation were rendered and received most appreciatively, from the University Physical Plant Department, the Student Health Center, and to a lesser extent from many other groups and individuals too numerous to mention.

3. Preliminary Analysis

Certain analyses are basic to all the experiments and are indicated at this point rather than being made a part of each experimental write-up.

a. Exclusion radius.

Average conditions at the site are taken to be the following:

Temperature--90° F. (32°C.)

Pressure--28.79" Hg. (731mm.)

Relative Humidity--50%

For these conditions, air density equals 1.1034×10^{-3} g./cm.^{3}

Following data apply:

At 1 m., 1 curie of Co-60 provides a dose-rate of 1.3r./hr. (NBS Handbook 73). This is equivalent to 14,000 mr./hr. per curie at 1 foot.

For air under site conditions:

$$\frac{\mu_o}{\rho} = 0.0567 \text{ cm.}^2\text{/g. at 1.25 Mev.}$$

$$\mu_o = 6.256 \times 10^{-5} \text{ cm.}^{-1}$$

$$1 \text{ mean-free-path} = \frac{1}{\mu_o} = 15{,}980 \text{ cm.} = 525 \text{ ft.}$$

Let D(r) = dose-rate 3' above ground, with source of Co-60 on ground at distance r.

$$D(r) = \frac{14{,}000 \; B \cdot K \; e^{-\mu r} \; C}{r^2} \qquad \text{(mr/hr.)}$$

where B = build-up factor for point isotropic source of Co-60 in infinite, homogeneous air-like medium (use of aluminum

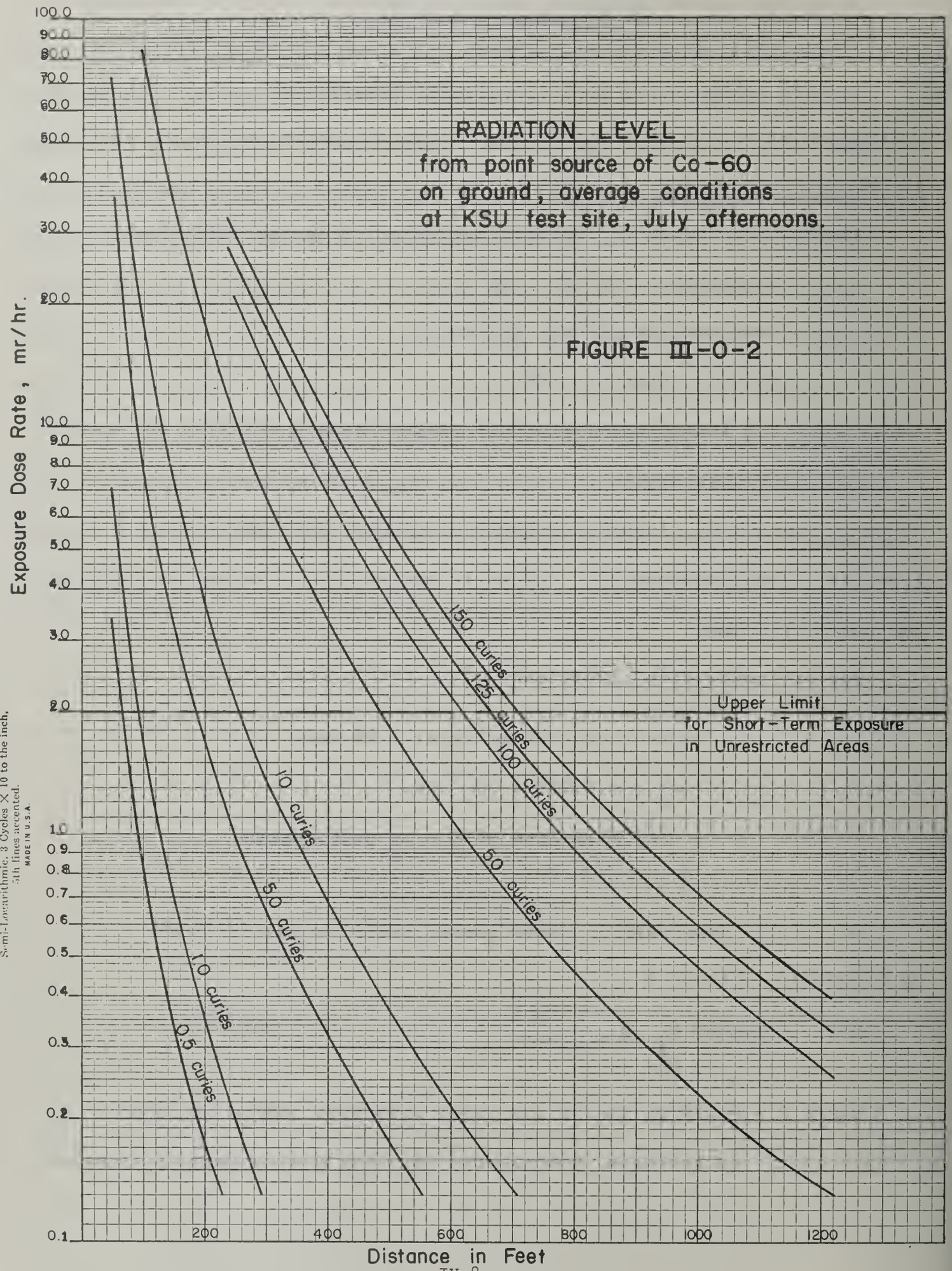
RADIATION LEVEL
from point source of Co-60
on ground, average conditions
at KSU test site, July afternoons.
FIGURE III-O-2
Exposure Dose Rate, mr/hr.
100.0
90.0
80.0
70.0
60.0
50.0
40.0
30.0
20.0
10.0
9.0
8.0
7.0
6.0
5.0
4.0
3.0
2.0
1.0
0.9
0.8
0.7
0.6
0.5
0.4
0.3
0.2
0.1
150 curies
125 curies
100 curies
50 curies
10 curies
5.0 curies
1.0 curies
0.5 curies
Upper Limit
for Short-Term Exposure
in Unrestricted Areas
200
400
600
800
1000
1200
Distance in Feet
358-71
KEUFFEL & ESSER CO.
Semi-Logarithmic, 3 Cycles X 10 to the inch,
5th lines accented.
MADE IN U.S.A.

is adequate). (See NYO-3075, Goldstein and Wilkins.)

K = correction factor for earth-air interface effect.

(M. J. Berger, Journal of Appl. Physics 28, No. 12, 1502-8 (1957).)

C = Number of curies.

As a sample calculation, the dose-rate from a 125 curie source at 525 feet (one mean-free-path)is indicated:

$$D\ (525) = \frac{14{,}000 \times 2.01 \times 0.835 \times e^{-1} \times 125}{(525)^2}$$

$$= 3.91 \text{ mr/hr.}$$

A plot of dose-rate at 3' height versus distance for Co-60 on the ground is given in Figure III-0-2. This figure was used as the basis for the preliminary estimate of the exclusion area at the site, being the area enclosed in the 2 mr./hr. perimeter. The final perimeter, determined by actual measurement with the 123 curie source exposed, extended as far as 660' from the exposure area, but in some directions was reduced by the topographic aspects of the area.

b. Reference Dosage.

For most shielding calculations relating to nuclear weapon fallout, the reference dose-rate, to which all others are compared, is usually taken as the dose-rate 3 feet (sometimes taken as one meter) above a smooth, infinite plane with fallout evenly distributed on it.

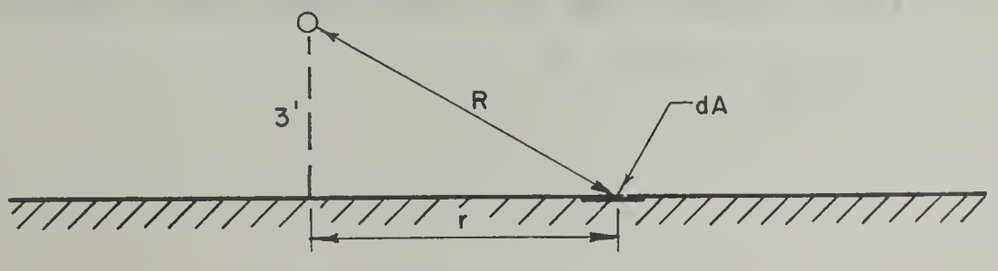

Figure III-0-3

Consider a source density of one curie per square foot over the infinite plane. A differential area in this plane will provide a differential dose-rate at the reference point, in r./hr.

$$dD = \frac{(14.0)\quad (dA)\quad B(\mu_o R)\quad e^{-\mu_o R}}{R^2}$$

where $B(R)$ = the build-up factor.

$$= 1.11 + 0.529\ \mu_o R$$

for source on ground and detector three feet above ground (see NDL Report NDL-TR-2).

$$dA = rdrd\varphi$$

$$D = 14.0 \int_0^{\pi} d\varphi \int_0^{\infty} \frac{r\quad B(\mu_o R)\quad e^{-\mu_o R}}{R^2}\ dr$$

Since $rdr = RdR$,

$$D = 2\pi \cdot 14.0 \int_{R=3'}^{\infty} \frac{B(\mu_o R)\quad e^{-\mu_o R}}{R}\ dR$$

$$= 87.8 \left[1.11\ E_1(3/525) + 0.529 e^{-(3/525)}\right]$$

$$= 494 \text{ r/hr., for 1 curie/ft.}^2$$

There is a theorem, given elsewhere in this report, which indicates that one could have used a build-up factor for infinite, homogeneous atmosphere, regardless of the air-ground interface, if one assumes the ground to act like condensed air in its radiation attenuation and scattering properties. Thus we could substitute in the above derivation an empirical expression for build-up factor assuming an infinite, homogeneous atmosphere (Chilton, Donovan, and Holoviak, NCEL Report N-389, 1960).

$$B = 1 + 0.92\ \mu_o R\ e^{+0.06 \mu_o R}$$

This gives:

$$D = 87.8 \left[E_1(3/525) + 0.979\, e^{+0.94 \times 3/525} \right]$$

$$= 490 \text{ r/hr., for 1 curie/ft.}^2$$

The latter figure is used herein for the experimental calculations.

c. Normalization of data. For the sake of consistent treatment of data, it is often necessary to normalize to a standard set of conditions. Usually, where this is necessary, the data in this report have been normalized to a dose-rate in milliroentgen (or roentgen) per hour, obtained from a fallout (or simulant) field of one curie per square foot. In case integrating dosimeters are used, the experiment is normalized on the assumption that the accumulation of dose occurred for a period of one hour.

In some experiments the infinite field is approximated by a pumped source of C curies moving with constant speed through a tube laid out so as to provide approximately uniform distribution over an area, A, (sq. ft.). If the source spends T hours in moving through the tube and $R(\bar{r})$ is the dose-rate per hour at any position, $\bar{r}$, due to a source of one curie per square foot, then the measured dose, $D(\bar{r})$ is:

$$D(\bar{r}) = \frac{C \; R(\bar{r}) \; T}{A}$$

Conversely, data taken can be normalized to 1 curie/ft.^{2}-hr. by an inverse calculation:

$$R(\bar{r}) = \frac{A}{C \; T} \qquad D(\bar{r})$$

B. Experimental Reports

1. Blockhouse Experiment-Roof Contamination

a) Purpose. Primarily, to determine the fallout protection capability of an idealized structure against simulated fallout roof contamination, and to compare experimental results with theoretical predictions. Secondarily, to provide experience in the calibration of field type dose-rate meters.

b) References and bibliography.

1) L. V. Spencer, "Structure Shielding against Fallout Radiation from Nuclear Weapons," National Bureau of Standards Monograph 42 (1962).

2) "Shelter Design and Analysis, Vol.1, Fallout Protection," Office of Civil Defense Compilation (Revised ed., 1962). (This is a revision of an OCD draft document commonly referred to as the "Engineering Manual.")

3) "Fallout Shelter Surveys: Guide for Architects and Engineers," Office of Civil Defense Document NP-10-2 (1960). (This is commonly referred to as the "Architect Engineers' Guide.")

4) C. Eisenhauer, "An Engineering Method for Calculation Protection Afforded by Structures against Fallout Radiation," National Bureau of Standards Report 7810 (1963).

5) R. E. Rexroad and M. A. Schmoke, "Scattered Radiation and Free Field Dose-Rates from Distributed Cobalt-60 and Cesium-137 Sources," Nuclear Defense Laboratory Report NDL-TR-2 (1960).

6) J. Batter, "Cobalt and Iridium Buildup Factors Near the Ground/Air Interface," Trans. Am. Nucl. Soc. 6, No. 1, 198 (1963).

c) Facilities and apparatus used.

1) Concrete blockhouse (see Figure III-1-1) with roof access ladder.

2) Five cobalt-60 sources of approximately equal strength, 4.60 millicuries each (± 10%). (As long as they are equal, the exact value of each source is not important, since results, obtained as ratios of dose-rates, are independent of source strength).

3) Four dose-rate survey meters, with scales permitting readings from background up to 50 mr./hr.

4) One pair radioactive source handling tongs, about 40" in length.

5) Miscellaneous equipment--flashlights, meter sticks, tape measure.

d) Background. The most basic type of penetration analysis of fallout gamma radiation is that required for the slab roof covered with fallout, uniformly distributed. This can be simulated by the use of a finite number of concentrated sources of equal strength, distributed in a pattern on the roof of a structure at equal intervals. Cobalt-60 makes a useful simulant for this purpose, especially since calculations have been published (Reference 1) for penetration of cobalt-60 radiation through slabs on which the radioactive material is considered to be spread.

The use of a full-scale structure, of a simplified and idealized type, is desirable to test theoretical predictions carefully, and thus bridge the gap between the analysis of simple elements and the complete analysis of practical structures.

e) Procedure.

1) Calibration of the dose-rate meters was carried out on a laid out calibration range, by using the five individual sources grouped

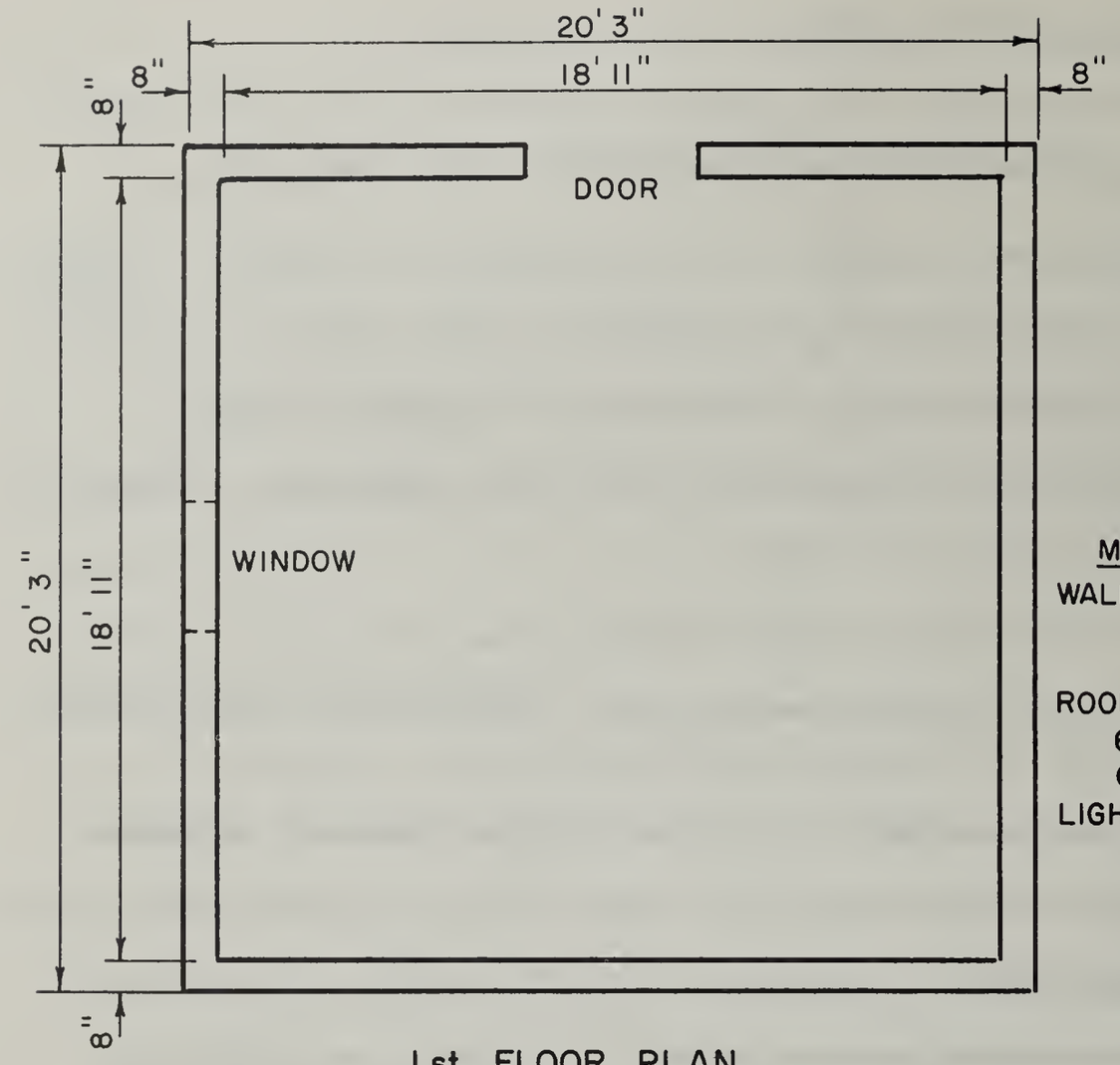

MATERIAL
WALLS - 8" SOLID CONCRETE BLOCK
ROOF & 1st FLOOR 6" PRESTRESSED CONCRETE SLABS
LIGHTWEIGHT CONC. THROUGHOUT

1st FLOOR PLAN

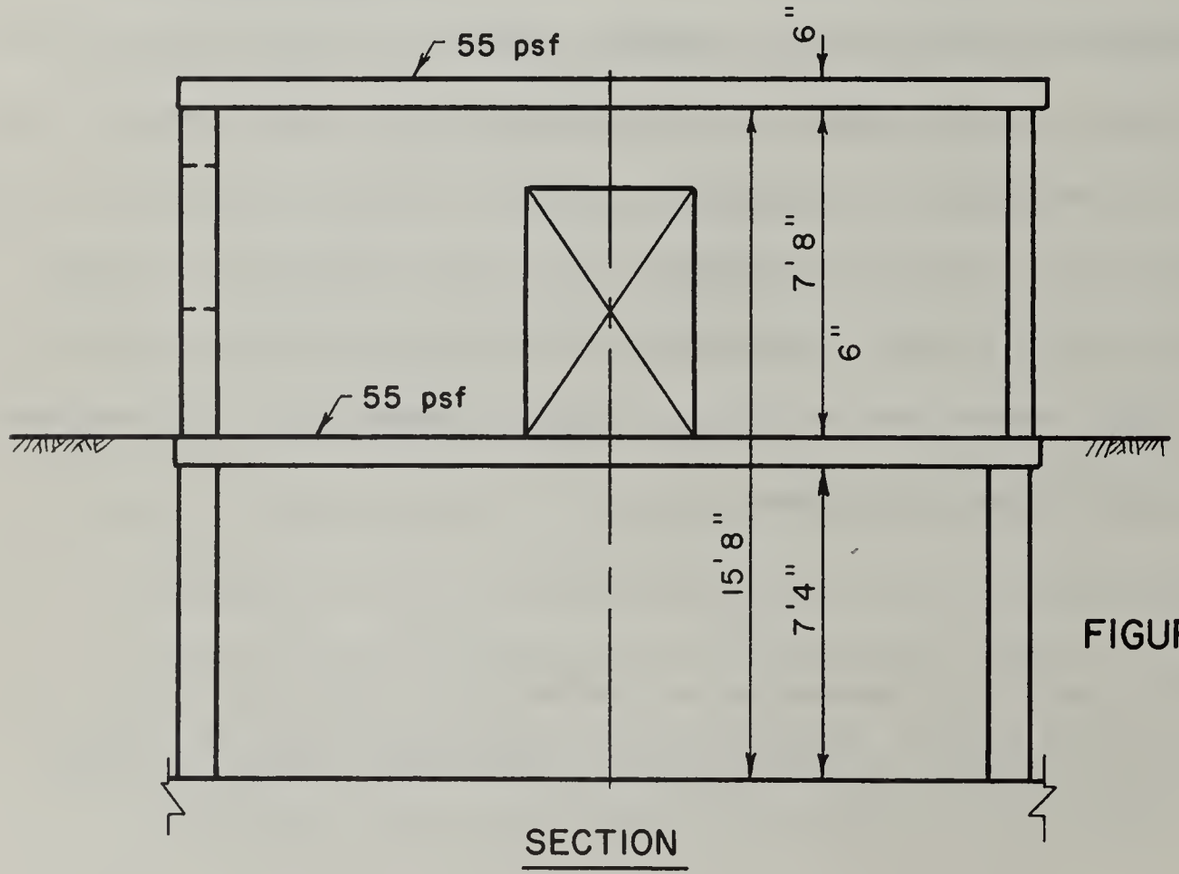

SECTION

FIGURE III-1-1

240-816 O-67—42

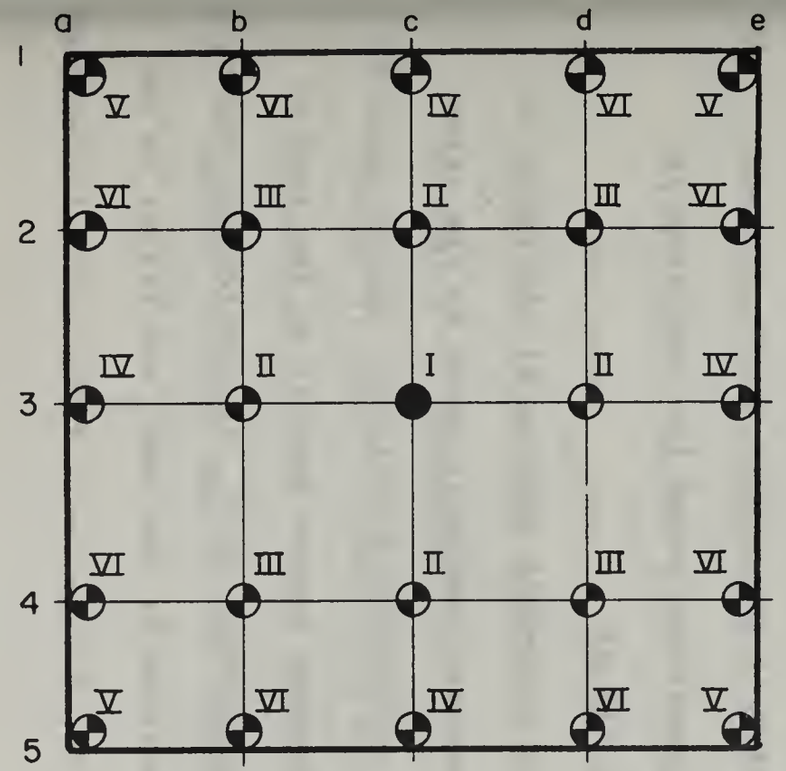

PLAN

DETECTOR LOCATIONS IN
BASEMENT & 1st FLOOR

HEIGHT OF DETECTOR
⊕ 3' ABOVE FLOOR
● 3' & 7' ABOVE FLOOR

NOTE: TOTAL DOSE RATE ARRIVED AT BY SUMMING ALL DETECTORS OF SAME ROMAN NUMERAL, EXCEPT AT I, TOTAL DOSE RATE = 4 x I; AND AT VI TOT. D.R. = Σ VI ÷ 2.

FIGURE III-1-2

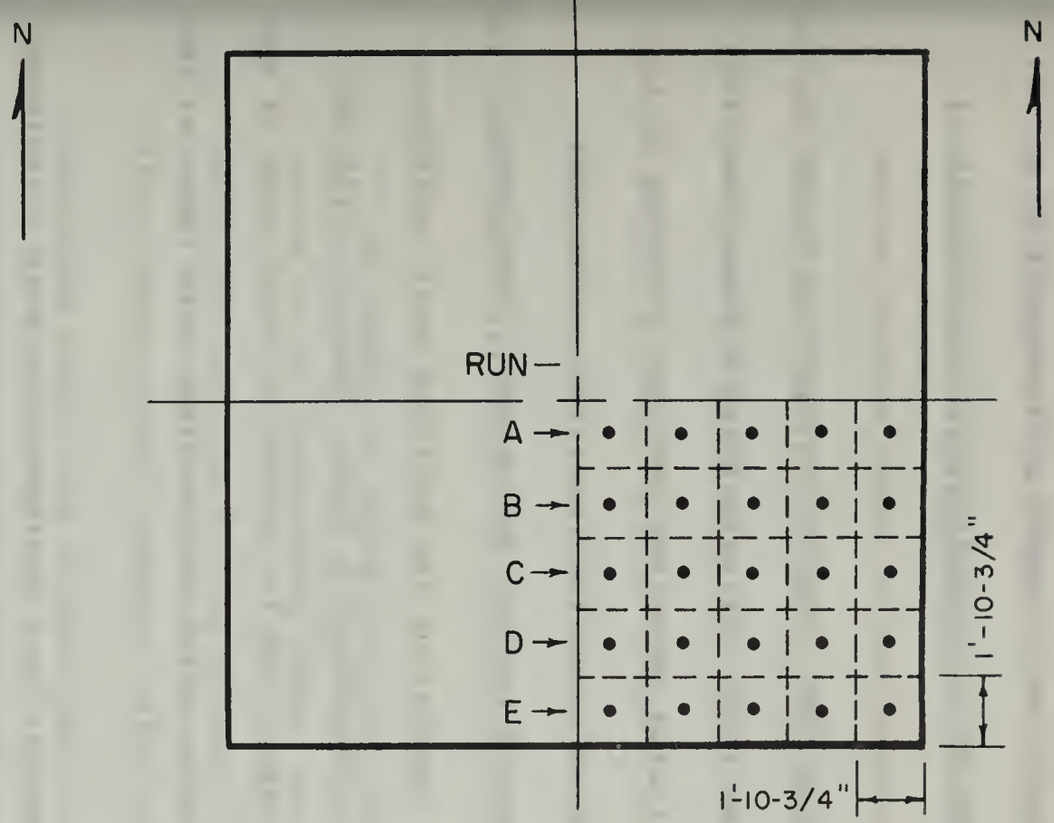

PLAN

RADIATION SOURCE LOCATIONS

ONE QUARTER ONLY OF ROOF TO RECEIVE RADIATION SOURCES.
5 SOURCES EACH RUN.

FIGURE III-1-3

together to form essentially a point source of (assumed) 23.0 millicuries strength. Section k, Appendix, gives the details of this calibration.

2) A uniformly distributed source was simulated by placing point sources at specific locations on the roof. (Figure III-I-1 shows the block house in general; Figure III-1-2 shows the detector stations in the blockhouse; and Figure III-1-3 shows the locations on the roof where individual sources were placed.) In actuality, since there were twenty-five locations in a quarter of the building roof, only one-fifth of the spots could be covered at a time. However, with one row covered readings were taken; and in successive runs, each of the other rows were covered, during which new readings were taken at the same reading stations.

3) Results for the case of complete roof contamination were calculated; and comparisons were made with theoretical predictions.

f) Theory.

1) The reduction factor for a point in the middle of the blockhouse can be obtained by the following equation, using the functions in Spencer's Monograph: $R_f = L(X)\ L(X,\omega)$.

R_f represents the ratio of the dose-rate reading at the point in question to the reference dose-rate, which is given as the value three feet above a uniformly contaminated, infinite, smooth plane of source density equal to the average source density on the roof of the blockhouse. (R_f is the reciprocal of P_f, the protection factor.) $L(X)$ is the barrier factor provided by the roof; and $L(X,\omega)$ is the geometry factor to allow for the finite area of the contaminated roof.

In the Engineering Manual, the reduction factor is given by a single factor, $C_o(X_o,\omega)$, which is equivalent to the product of the two factors given in the formula above. The value of this factor is found in a chart. The Architect-Engineers' Guide also handles this problem by use of a chart. The values are given for a detector ten feet below the roof, as a function of roof area and thickness; and a correction factor is provided for adjusting the roof area, should the detector distance be different from ten feet.

It should be noted that the predictions obtained from the curves of the Engineering Manual and the Architect-Engineers' Guide are based on fission product energy spectra at 1.12 hours after weapon burst, whereas calculations made for a distributed cobalt-60 source can be made most accurately by using curves from Spencer's Monograph for cobalt-60 gamma ray energies. Therefore, the experimental results are more properly comparable to calculations based on the Monograph than to predictions using either of the referenced OCD publications; and we compare results only with calculations from the former document.

The term L_c used in the above mentioned formula is one of three closely related terms provided in the Monograph, L_c, L_a, and L_b. According to Eisenhauer (Ref. 4), these three terms are used, respectively, in case the absorbing medium is uniformly distributed between source and detector, when the barrier material is concentrated at the source, or when the barrier material is concentrated at the detector.

Either of the three situations is an idealized extreme, and in an actual situation the proper answer is undoubtedly somewhere between extremes of the answers provided by these three factors. Since in a practical situation, the absorbing floors represent a somewhat distributed absorbing medium, the OCD publications follow Eisenhauer's suggestion that L_c be used for this type of calcuation. (It is to be noted that Spencer uses L_a for this type of problem; however, we follow Eisenhauer's suggestion, with the knowledge of the fact that for floor thicknesses of the order of those in the blockhouse under investigation the theoretical answers provided are an upper limit. See Table I, Ref. 4.)

2) For detector positions not in the center of the building, theoretical reduction factors can be calculated using the method of "fictitious structures" contained in the older draft of the Engineering Manual. The method is illustrated in the calculations.

3) In reducing the experimental data provided, the calibration curves obtained (see Figures III-1-4, -5, and -6 in Section k) are used to give corrected values. The results for each run are then added to give the total effect of covering one-quarter of the roof. Because of the symmetry of the situation, experimental values for a completely contaminated roof can be obtained by adding the readings for equivalent stations in the four quarters of the building.

The final value of the experimental reduction factor for each specific location is then determined by dividing the dose-rate obtained by the value of the reference dose-rate calculated on the

basis of a value of 490 r./hr. for a smooth infinite plane source density of one curie per square foot.

g) Preliminary Calculations.

1) Theoretical roof contamination reduction factors, based on Figure B-43 of Reference 1). All detector heights are 3' above the floor, unless otherwise noted. Detector positions are indicated on Figure III-1-2.

Equiv. Bldg. No.	W	L	ϵ	Z	η	ω	X_o	$L \cdot L_c$	Factor	R_f
Detector Location I, Center of Blockhouse, First Floor										
Det.=3'	19.0	19.0	1.0	5.17	.545	.56	55	.050	1.0	.050
" 7'	19.0	19.0	1.0	1.17	.123	.89	55	.062	1.0	.062
					Basement					
Det.=3'	19.0	19.0	1.0	13.0	1.37	.23	110	.0073	1.0	.0073
" 7'	19.0	19.0	1.0	9.0	.95	.36	110	.0098	1.0	.0098
Detector Location II, First Floor										
1	9.5	19.0	0.5	5.17	.545	.40	55	.036	0.5	.018
2	19.0	28.5	.667	5.17	.363	.62	55	.052	0.5	.026
										.044
		Basement								
1	9.5	19.0	0.5	13.0	1.37	.13	110	.0050	0.5	.0025
2	19.0	28.5	.667	13.0	.912	.29	110	.0088	0.5	.0044
										.0069

Equiv. Bldg. No.	W	L	ϵ	Z	η	ω	X_o	$L'L_c$	Factor	R_f
Detector Location III, First Floor										
1	9.5	9.5	1.0	5.17	1.09	.30	55	.029	0.25	.007
2	9.5	28.5	.333	5.17	.363	.45	55	.042	0.5	.021
3	28.5	28.5	1.0	5.17	.363	.69	55	.057	0.25	.014
										.042
		Basement								
1	9.5	9.5	1.0	13.0	2.74	.076	110	.0028	0.25	.0007
2	9.5	28.5	.333	13.0	.913	.17	110	.0060	0.5	.0030
3	28.5	28.5	1.0	13.0	.913	.37	110	.010	0.25	.0025
										.0062
Detector Location IV, First Floor										
1	19.0	38.0	0.5	5.17	.272	.64	55	.052	0.5	.026
		Basement								
1	19.0	38.0	0.5	13.0	.684	.32	110	.009	0.5	.0045
Detector Location V, First Floor										
1	38.0	38.0	1.0	5.17	.272	.77	55	.060	0.25	.015
		Basement								
1	38.0	38.0	1.0	13.0	.684	.48	110	.0116	0.25	.0029
Detector Location VI, First Floor										
1	28.5	38.0	.75	5.17	.272	.725	55	.062	0.25	.015
2	9.5	38.0	.25	5.17	.272	.46	55	.044	0.25	.011
										.026

Equiv. Bldg. No.	W	L	c	Z	η	ω	X_o	$L \cdot L_c$	Factor	R_f
		Basement								
1	28.5	38.0	.75	13.0	.684	.42	110	.0108	0.25	.0027
2	9.5	38.0	.25	13.0	.684	.18	110	.0063	0.25	.0016
										.0043

2) Normalization factor for experimental data.

A source strength of 4.60 millicuries placed in each square of dimension 1'10-3/4" is equivalent to 1.280×10^{-3} curies/ft.^{2} Since one curie per square foot provides a reference dose rate 3' above an infinitely contaminated smooth plane of 490 r./hr., a source strength of 1.280×10^{-3} curies/sq. ft. provides a reference point dose-rate of 627 mr./hr. Then for each point in the blockhouse, the value of R_f ($= D/D_o$) is given if the appropriate value from the experiment in mr./hr. is divided by 627, or is multiplied by 1.595×10^{-3}.

h) Data and data reduction.

Detector Readings, mr./hr.

Floor: First

Dose-rate meter: Victoreen #526 (3-scale unless noted)

Detector Location	Run A		Run B		Run C		Run D		Run E		Sum of Corrected Values
	Raw	Corr.*	Raw	Corr.	Raw	Corr.	Raw	Corr.	Raw	Corr.	
(1,A)	.05	.16	.05	.16	-	0	.02	.12	-	0	.44
B	.10	.21	.13	.24	.05	.16	.06	.17	.05	.16	.94
C	.25	.36	.12	.23	.06	.17	.08	.19	.05	.16	1.11
D	.40	.51	.24	.35	.13	.24	.10	.21	.05	.16	1.47
E	.35	.46	.20	.31	.10	.21	.10	.21	.05	.16	1.35
(2,A)	.15	.26	.10	.21	.05	.16	.08	.19	.03	.14	.96
B	.40	.51	.22	.33	.16	.27	.15	.26	.06	.17	1.54
C	1.00	1.12	.60	.71	.33	.44	.25	.36	.10	.21	2.84
D	1.45	1.55	.72	.83	.40	.51	.20	.31	.13	.24	3.44
E	.95	1.07	.55	.66	.35	.46	.20	.31	.12	.23	2.73
(3,A)	.25	.36	.20	.31	.15	.26	.10	.21	.08	.19	1.33
B	.55	.66	.50	.61	.37	.48	.23	.34	.15	.26	2.35
C 3'	2.35	2.45	2.10	2.22	1.20	1.31	.62	.73	.36*	.47	7.18
C 7'	6.80#	6.80	2.05	2.17	.50	.61	.25	.36	.12	.23	10.17
D	4.15#	4.23	2.67	2.80	1.80	1.91	.90	1.02	.50	.61	10.57
E	2.50#	2.50	2.40	2.52	1.65	1.76	.85	.97	.50	.61	8.36

*Corrected values are obtained by use of the calibration curves (see Figures III-1-4 and -5 in Section k Appendix).

#10 scale

Detector Location	Run A		Run B		Run C		Run D		Run E		Sum of Corrected Values
	Raw	Corr.	Raw	Corr	Raw	Corr	Raw	Corr.	Raw	Corr.	
(4,A)	.20	.31	.30	.41	.20	.31	.25	.36	.20	.31	1.70
B	.60	.71	.80	.91	.60	.71	.60	.71	.60	.71	3.75
C	1.70	1.82	2.20#	2.20	2.20#	2.20	2.60#	2.60	1.75	1.87	10.69
D	2.20	2.33	3.60#	3.65	4.00#	4.08	3.80#	3.87	2.60	2.72	16.65
E	1.65	1.77	2.50	2.62	3.10#	3.13	2.35	2.47	1.45	2.07	12.06
(5,A)	.10	.21	.10	.21	.15	.26	.23	.34	.17	.28	1.30
B	.20	.31	.30	.41	.40	.51	.60	.71	.59	.70	2.64
C	.45	.56	.85	.96	1.40	1.51	2.37	2.49	2.50	2.62	8.14
D	.45	.56	1.10	1.20	2.20	2.32	3.80#	3.87	4.10#	4.18	12.13
E	.60	.71	1.10	1.20	1.80	1.92	2.90#	2.93	3.00#	3.03	9.79

Floor: First

Dose rate meter: Victoreen #527 (3-scale unless noted)

Detector Location	Run A		Run B		Run C		Run D		Run E		Sum of Corrected Values
	Raw	Corr.*	Raw	Corr.	Raw	Corr.	Raw	Corr.	Raw	Corr.	
(1,A)	-	0	.10	0	.10	0	-	0	-	0	0
B	.20	.15	.15	.05	.15	.05	.05	0	-	0	.25
C	.25	.22	.20	.15	.10	0	.03	0	-	0	.37
D	.60	.56	.10	0	.10	0	.02	0	-	0	.56
E	.40	.39	.30	.29	.10	0	.08	.01	-	0	.68
(2,A)	.10	0	.10	-	.10	0	-	0	-	0	0
B	.30	.29	.30	.29	.10	0	.10	.03	-	0	.58
C	.90	.83	.70	.65	.40	.39	.30	.22	.05	0	2.16
D	1.15	1.04	1.10	1.00	.40	.39	.40	.32	.10	0	2.82
E	1.00	.91	.70	.65	.70	.65	.20	.13	.10	0	2.36
(3,A)	.25	.22	.20	.15	.10	0	.10	.03	.10	0	.37
B	.70	.65	.60	.56	.30	.29	.20	.13	.10	0	1.65
C 3'	2.35	2.45	2.10	2.22	1.20	1.31	.62	.73	.36*	.47	7.18
C 7'	6.80#	6.80	2.05	2.17	.50	.61	.25	.36	.12	.23	10.17
D	4.15#	4.23	2.67	2.80	1.80	1.91	.90	1.02	.50	.61	10.57
E	2.50#	2.50	2.40	2.52	1.65	1.76	.85	.97	.50	.61	8.36

*Corrected values are obtained by use of the calibration curves (see Figures III-1-4 and -5 in Section k, Appendix).

#10-scale

Detector Location	Run A		Run B		Run C		Run D		Run E		Sum of Corrected Values
	Raw	Corr.	Raw	Corr.	Raw	Corr.	Raw	Corr.	Raw	Corr.	
(4,A)	.30	.22	.40	.39	.40	.39	.30	.29	.20	.15	1.51
B	.80	.69	.40	.39	.70	.65	1.00	.91	.60	.56	3.25
C	2.00	1.81	3.40#	3.05	2.80#	2.52	2.80	2.56	1.90	1.72	11.66
D	2.80	2.56	4.70#	4.25	4.00#	3.60	3.80#	3.42	2.50	2.25	16.08
E	2.00#	1.78	3.60#	3.25	3.00#	2.68	2.65	2.38	1.80	1.62	11.71
(5,A)	.10	0	.30	.29	.20	.15	.30	.29	.20	.15	.87
B	.30	.29	.70	.65	.40	.39	.70	.65	.70	.65	2.63
C	.60	.56	1.00	.91	1.80	1.62	3.10#	2.78	3.60#	3.25	9.12
D	.80	.74	1.40	1.25	2.50	2.28	3.40#	3.05	4.20#	3.80	11.12
E	.90	.83	1.40	1.25	2.30	2.09	2.80#	2.52	3.00#	2.70	9.39

#10-scale

Detector Readings, mr./hr.

Floor: Basement

Dose-rate meter: Bendix #71 (X1-scale unless noted)

Detector Location	Run A		Run B		Run C		Run D		Run E		Sum of Corrected Values
	Raw	Corr.*	Raw	Corr.	Raw	Corr.	Raw	Corr.	Raw	Corr.	
(1,A)	.04	.020	.045	.025	.015	0	.015	0	.005	0	.045
B	.095	.075	.055	.075	.055	.055	.035	.015	.025	.005	.205
C	.135	.120	.095	.075	.065	.045	.045	.025	.025	.005	.270
D	.125	.110	.075	.055	.055	.035	.045	.025	.035	.015	.240
E	.095	.075	.045	.025	.075	.055	.025	.005	.045	.025	.185
(2,A)	.035	.015	.085	.065	.065	.045	.025	.005	.005	0	.130
B	.135	.120	.095	.075	.105	.090	.045	.025	.035	.015	.325
C	.165	.150	.145	.130	.085	.065	.065	.045	.055	.035	.425
D	.245	.235	.135	.120	.065	.045	.065	.045	.055	.035	.480
E	.145	.130	.095	.075	.095	.075	.015	0	.065	.045	.325
(3,A)	.055	.035	.065	.045	.035	.015	.045	.025	.025	.005	.125
B	.185	.170	.175	.160	.125	.110	.125	.110	.075	.055	.605
C 3'	.205	.195	.275	.265	.275	.265	.185	.175	.135	.120	1.015
C 7'	.375	.370	.375	.370	.425	.425	.215	.205	.095	.075	1.445
D	.275	.265	.275	.265	.175	.160	.255	.245	.125	.110	1.045
E	.225	.215	.155	.140	.185	.170	.205	.195	.095	.075	.795

*Corrected values are obtained by use of the calibration curves (see Figure III-1-6 in Section k, Appendix).

Detector Location	Run A		Run B		Run C		Run D		Run E		Sum of Corrected Values
	Raw	Corr.	Raw	Corr.	Raw	Corr.	Raw	Corr.	Raw	Corr.	
(4,A)	.065	.045	.105	.090	.025	.005	.125	.110	.025	.005	.255
B	.105	.090	.115	.100	.125	.110	.185	.170	.085	.065	.535
C	.225	.215	.275	.265	.365	.360	.245	.235	.175	.160	1.235
D	.245	.235	.335	.330	.325	.320	.335	.330	.215	.205	1.420
E	.195	.180	.175	.160	.195	.180	.235	.225	.135	.120	.865
(5,A)	.025	.005	.035	.015	.025	.005	.085	.065	.035	.015	.105
B	.025	.005	.095	.075	.115	.100	.145	.130	.095	.075	.385
C	.125	.110	.165	.150	.195	.180	.255	.245	.225	.215	.900
D	.195	.180	.255	.245	.235	.225	.335	.330	.215	.205	1.185
E	.175	.160	.125	.110	.195	.180	.225	.215	.195	.180	.845

Detector Readings, mr./hr.

Floor: Basement

Dose-rate meter: Bendix #72 (X1-scale unless noted)

Detector Location	Run A		Run B		Run C		Run D		Run E		Sum of Corrected Values
	Raw	Corr.*	Raw	Corr.	Raw	Corr.	Raw	Corr.	Raw	Corr.	
(1,A)	.06	.02	.06	.02	.01	0	.04	0	.03	0	.04
B	.08	.03	.06	.02	.02	0	.04	0	.04	0	.05
C	.24	.14	.11	.05	.03	0	.05	.01	.06	.02	.22
D	.24	.14	.16	.09	.06	.02	.09	.04	.06	.02	.31
E	.14	.075	.11	.05	.04	0	.03	0	.06	.02	.145
(2,A)	.06	.02	.16	.09	.02	0	.06	.02	.06	.02	.15
B	.21	.12	.11	.05	.06	.02	.09	.04	.02	0	.23
C	.36	.21	.26	.15	.21	.12	.14	.075	.12	.06	.615
D	.48	.28	.46	.27	.16	.09	.13	.065	.16	.09	.795
E	.26	.15	.21	.12	.11	.05	.11	.05	.06	.02	.39
(3,A)	.04	0	.14	.075	.01	0	.07	.025	.06	.02	.120
B	.26	.15	.21	.12	.06	.02	.14	.075	.11	.05	.415
C 3'	.41	.24	.36	.21	.36#	.21	.44#	.255	.16	.09	1.005
C 7'	.66	.385	.66	.385	.36#	.21	.46#	.21	.21	.12	1.370
D	.51	.30	.56	.325	.31#	.185	.46#	.27	.36	.21	1.290
E	.36	.21	.31	.185	.26#	.15	.26#	.15	.26	.15	.845

*Corrected values are obtained by use of the calibration curves (see Figure III-1-6 in Section k, Appendix).

#X10-scale

Detector Location	Run A		Run B		Run C		Run D		Run E		Sum of Corrected Values
	Raw	Corr.	Raw	Corr.	Raw	Corr.	Raw	Corr.	Raw	Corr.	
(4,A)	.12	.06	___	0	.11	.05	.06#	.02	.05	.01	.14
B	.13	.065	___	0	.16	.09	.16#	.09	.16	.09	.335
C	.36	.21	.29	.17	.26#	.15	.51#	.30	.36	.21	1.04
D	.36	.21	.51	.30	.36#	.21	.66#	.385	.34	.20	1.305
E	.33	.195	.31	.185	.36#	.21	.56#	.325	.31	.185	1.100
(5,A)	.07	.025	.06	.02	.11	.05	.06#	.02	.05	.01	.125
B	.14	.075	.20	.115	.16	.09	.21#	.12	.11	.05	.450
C	.26	.15	.31	.185	.36#	.21	.31#	.185	.46	.27	1.000
D	.26	.15	.35	.205	.36#	.21	.46#	.27	.41	.24	1.075
E	.14	.075	.22	.13	.36#	.21	.46#	.27	.36	.21	.895

i) Results. Experimental reduction factors.

1) First floor

Location	Quarter	Corrected Instr. Reading, mr./hr.			$R_f = 1.595 \times 10^{-3} \times$ Av. Rdg.
		Vict.#526	Vict.#527	Average	
Center, 3'Ht.	Each	7.18 x 4 =28.72	6.56 x 4 =26.16	27.44	.044
Center, 7'Ht.	Each	10.17 x 4 =40.68	7.66 x 4 =30.64	35.66	.057
Halfway to Side (II)	1	10.69	11.66		
	2	10.57	9.16		
	3	2.35	1.65		
	4	2.84	2.16		
	Total	26.45	24.63	25.54	.041
Halfway to Corner (III)	1	16.65	16.08		
	2	3.75	3.25		
	3	3.44	2.82		
	4	1.54	.58		
	Total	25.38	22.73	24.06	.038
Middle of Side (IV)	1	8.14	9.12		
	2	8.36	8.33		
	3	1.33	.37		
	4	1.11	.37		
	Total	18.94	18.19	18.56	.030

Location	Quarter	Corrected Instr. Reading, mr./hr.			$R_f = 1.595 \times 10^{-3} \times$ Av. Rdg.
		Vict.#526	Vict.#527	Average	
Corner	1	9.79	9.39		
(V)	2	1.30	.87		
	3	1.35	.68		
	4	.44	.00		
	Total	12.88	10.94	11.91	.019
Halfway	(	12.13	11.12		
	1 (				
between	(	12.06	11.71		
Corner	(	2.64	2.63		
	2 (				
and	(	1.70	1.51		
Middle	(	2.73	2.36		
	3 (				
of Side	(	1.47	.56		
(VI)	(	.96	.00		
	4 (				
	(	.94	.25		
	Total	34.63	30.14	16.20	.026
	½ Total	17.32	15.07		

2) Basement.

Location	Quarter	Corrected Instr. Reading, mr./hr.			R_f = 1.595 x 10^{-3} x Av. Rdg.
		Bend.#71	Bend.#72	Average	
Center, 3' Ht.	Each	1.015 x 4 =4.06	1.005 x 4 =4.02	4.04	.0064
Center 7' Ht.	Each	1.445 x 4 =5.78	1.370 x 4 =5.48	5.63	.0090
Halfway to Side (II)	1	1.235	1.040		
	2	1.045	1.290		
	3	.605	.415		
	4	.425	.615		
	Total	3.310	3.360	3.335	.0053
Halfway to Corner (III)	1	1.420	1.305		
	2	.535	.335		
	3	.480	.795		
	4	.325	.230		
	Total	2.760	2.665	2.712	.0043
Middle of Side (IV)	1	.900	1.000		
	2	.795	.845		
	3	.125	.120		
	4	.270	.220		
	Total	2.090	2.185	2.138	.0034

Location	Quarter	Corrected Instr. Reading, mr./hr.			$R_f = 1.595 \times 10^{-3} \times$ Av. Rdg.
		Bend.#71	Bend.#72	Average	
	1	.845	.895		
Corner	2	.105	.125		
(V)	3	.185	.145		
	4	.045	.040		
	Total	1.180	1.205	1.192	.0019
Halfway	(	1.185	1.075		
	1 (				
between	(	.865	1.100		
Corner	(	.385	.450		
	2 (				
and	(	.255	.140		
Middle	(	.325	.390		
	3 (				
of Side	(	.240	.310		
(VI)	(	.130	.150		
	4 (				
	(	.205	.050		
	Total	3.590	3.665		
	½ Tot.	1.795	1.832	1.814	.0029

j) Summary, discussion, and conclusions. The comparison between theory and experimental is provided in the following tabulation of reduction factors.

Location (first floor)		Theory	Experiment
I (3')	Building center	.050	.044
I (7')	" "	.062	.057
II	Halfway, center to midpoint wall	.044	.041
III	Halfway, center to corner	.042	.038
IV	Midpoint of wall	.026	.030
V	Corner	.015	.019
VI	Halfway, corner to midpoint wall	.026	.026

Location (basement)		Theory	Experiment
I (3')	Building center	.0073	.0064
1 (7')	" "	.0098	.0090
II	Halfway, center to midpoint wall	.0069	.0053
III	Halfway, center to corner	.0062	.0043
IV	Midpoint of wall	.0045	.0034
V	Corner	.0029	.0019
VI	Halfway, corner to midpoint wall	.0043	.0029

It is seen that experimental results are in rather good agreement with theoretical predictions for the first floor, but for the basement there is a consistent pattern in which the experimental are lower than theoretical by amounts from 10 to 30% of the latter.

The basis for this rather consistent picture cannot be ascribed to random statistical variations with any degree of likelihood. It is

recognized that, as explained in Section f, Theory, the theoretical values are expected to be an upper limit to the true values; however, the basic assumption behind the theoretical formula(uniform distribution of attenuating material between source and detector) is less true for the first floor case than for the basement case. Therefore, such an explanation of results is inadequate.

It may be noted that the percentage of disagreement tends to be greater for the locations having the lowest readings.* This may provide some basis for guessing the greatest source of variation. At these locations, the individual readings were hardly greater than background--in some cases smaller than background. The Bendix instruments provided were able to respond at this range; but because of the short time constant of this type of instrument, the pointers varied wildly in position for values near background, thus rendering accuate reading extremely difficult. This condition also prevailed for low values of the radiation field during calibration, and a look at the calibration data (Section k) for the Bendix dose-rate meters shows the wide percentage variability at low ranges.

For any future repetition of this experiment, it would be desirable either to use stronger sources, or to use instruments able to read more accurately at dose-rate levels near background, or both.

Considering the conditions under which the experiment was made, adequacy of the theory to predict experimental results is a tenable hypothesis. Further more careful experimentation would be needed to rule out the possibility that the lessened agreement for the basement is a real effect.

---

*Editorial comment: This experimental report is based upon the 1963 work. It should be pointed out that the same experiment conducted in 1962 gave results which were higher at these particular points and more consistent with present theory.

k) Appendix. This section covers the details of calibration of the dose-rate meters used in this experiment.

In the calibration exercise, undertaken just before the experiment proper, the five individual sources were grouped together on the ground (concrete pad) essentially as a point source. From this point, a calibration line was marked off so that the instruments could be held at various horizontal distances from the source and read. For each reading, the instruments were held three feet off the ground. The value of true dose-rate in mr./hr. is given by the following formula:

$$D = \frac{14.0\ S\ e^{-\mu R} B(\mu R)}{R^2}$$

where

S = source strength in millicuries.

R = distance, source to detector, $(H^2 + 3'^2)^{\frac{1}{2}}$

H = horizontal distance, source to detector, feet.

μ = total linear attenuation coefficient for cobalt-60 radiation, (1/525) $ft.^{-1}$

B is the build-up factor, = 1.11 x .529 μR for distances greater than 50 feet (Reference 5). For distances less than 50', data from Reference 6 are used, slightly smoothed out.

For correspondence between calculated true dose-rate values and those read during the calibration run for each instrument the table below provides the information. These data are used to plot calibration curves, included herein as Figures III-1-4, III-1-5, and III-1-6.

It might be noted that no specific correction is made for background in these calibrations. Likewise, no account is taken for background in the actual blockhouse measurements; and on the assumption that background is

constant for the whole period of the operation no error is introduced by disregarding it entirely.

H	Calculated Dose-rate	Observed Readings						
		Vict.#526		Vict.#527		Bendix#71		Bendix#72
		10-scale	3-scale	10-scale	3-scale	X10	XI	-
6'	8.21	8.8		9.0				
7	6.44	6.6		7.0				
8	5.11	5.2		5.6				
9	4.17	4.1		4.7				
10	3.45	3.4	2.8	3.8		3.6		7.9
15	1.61	1.6	1.5	1.8	1.8	1.3		3.7
20	.918	.8	.8		1.0	.9		1.5
30	.412	.3	.3		.40	.45	.4	.70
40	.233	.1	.1		.30	.30	.25	.40
50	.149	.1	.1		.22	.20	.17	.26
60	.103				.22	.15	.16	.19
80	.0588				.13		.09	.11
100	.0382				.13		.04	.10
125	.0249				.12		.055	.08
150	.0175				.13		.05	.06
175	.0131				.20		.03	.05
200	.0101				.22		.03	.08

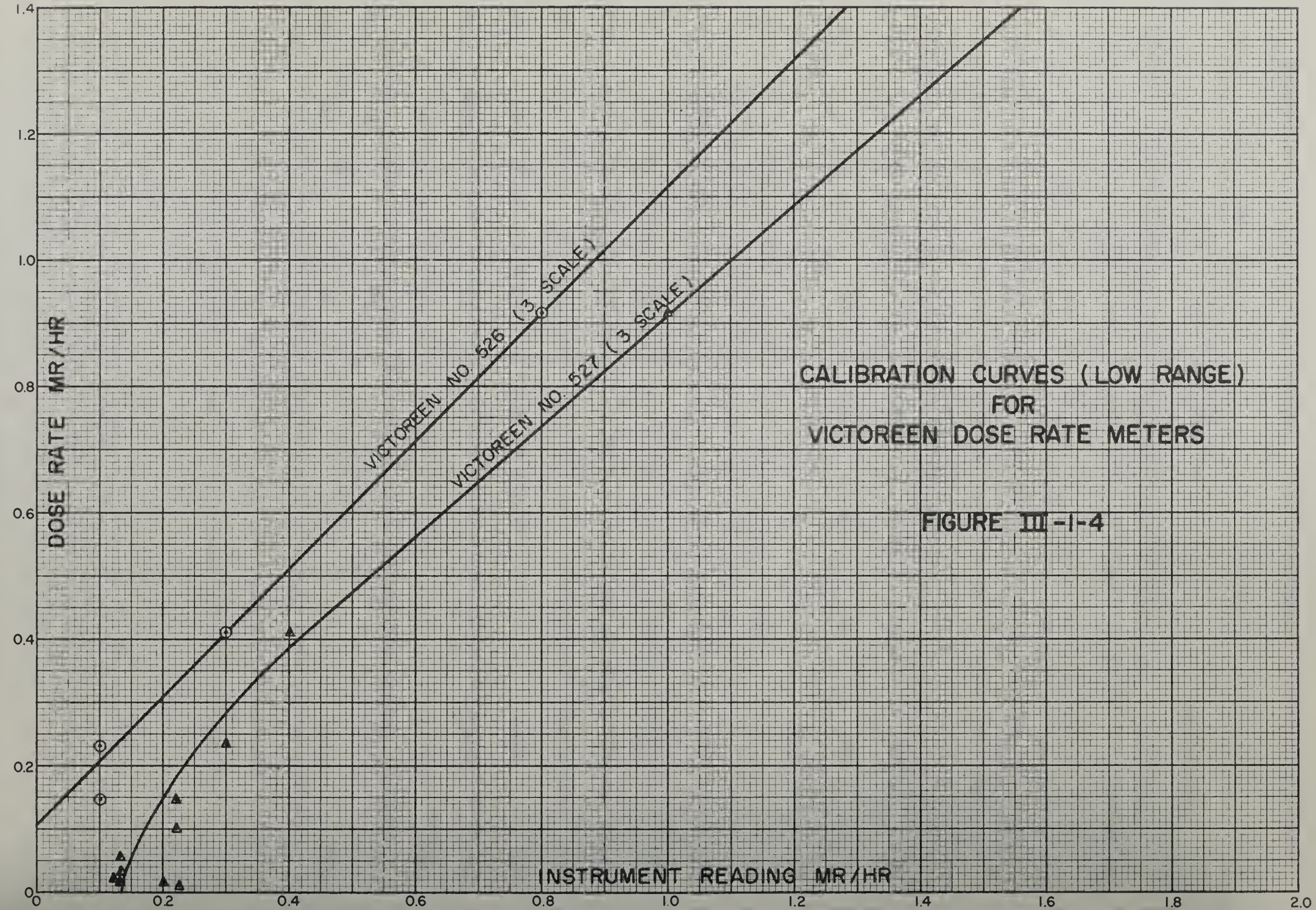

CALIBRATION CURVES (LOW RANGE)
FOR
VICTOREEN DOSE RATE METERS

FIGURE III-1-4

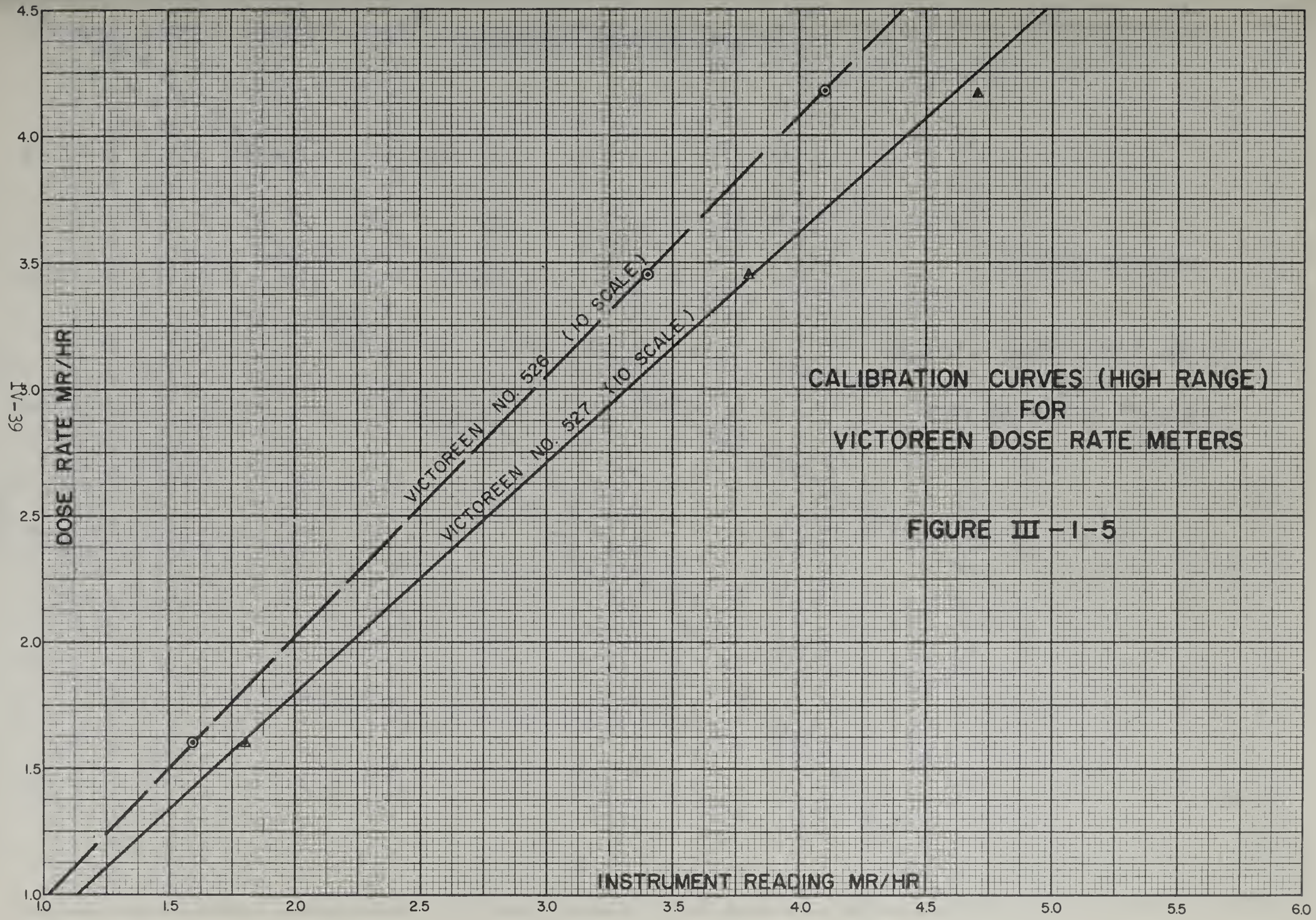

CALIBRATION CURVES (HIGH RANGE)
FOR
VICTOREEN DOSE RATE METERS

FIGURE III-1-5

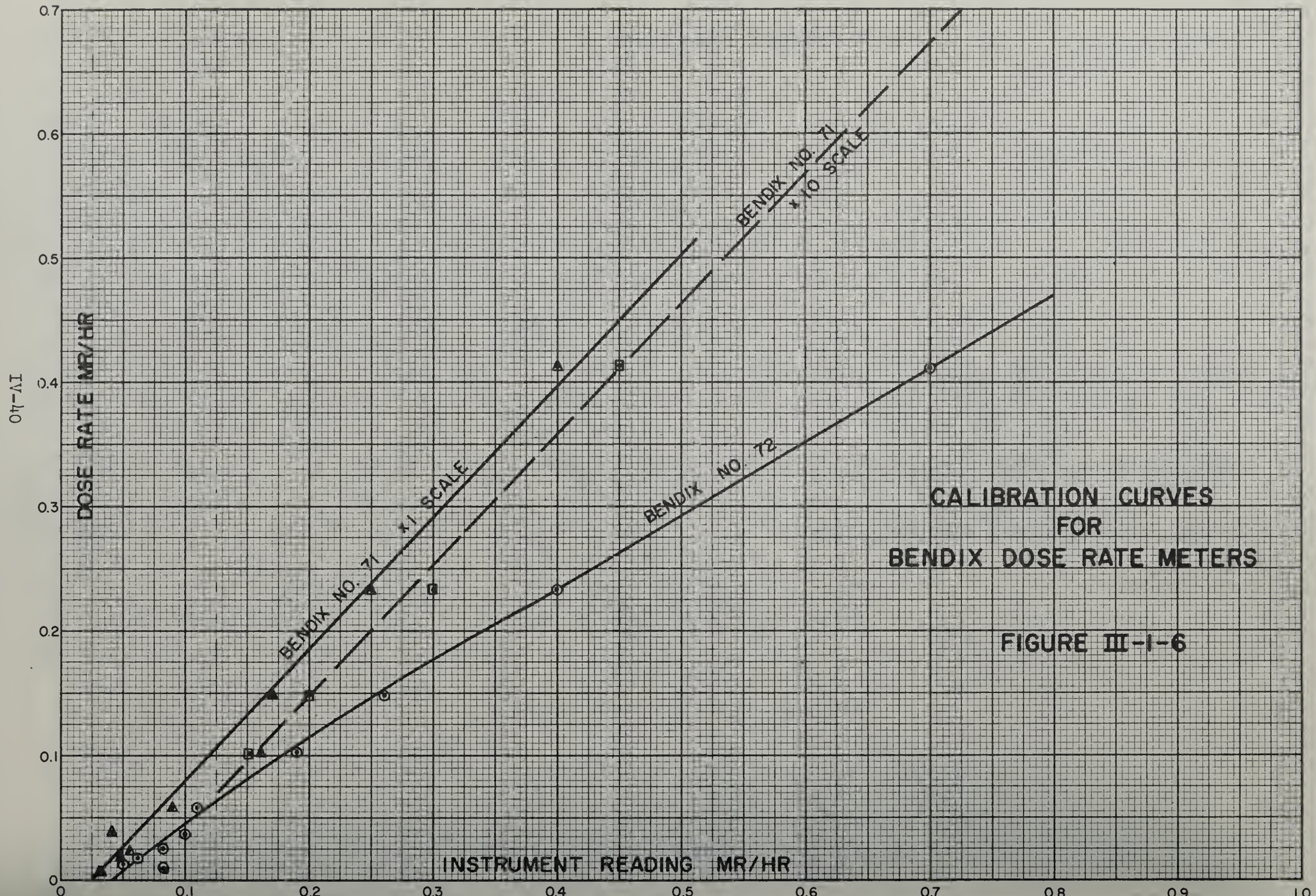

CALIBRATION CURVES
FOR
BENDIX DOSE RATE METERS

FIGURE III-1-6

2. Foxhole Experiment

a) Purpose. To determine the shielding potential of an idealized foxhole in the middle of a uniformly contaminated plane and to compare experimental results with predictions.

b) References and bibliography.

1) L. V. Spencer, "Structure Shielding against Fallout Radiation from Nuclear Weapons," National Bureau of Standards Monograph 42 (1962).

2) C. E. Clifford, "Gamma Dose in a Hole in a Uniformly Contaminated Plane: Contribution by Ground Penetration," Can. Jour. of Physics 39, 604 (1961). Also published as Defence Research Chemical Laboratories Report No. 310A.

3) H. Goldstein and J. E. Wilkins, Jr., "Calculations of the Penetration of Gamma Rays," U. S. Atomic Energy Commission Report NYO-3075 (1954).

4) M. J. Berger and L. V. Spencer, "Penetration of Gamma Rays from Isotropic Sources through Aluminum and Concrete," National Bureau of Standards Technical Note 11 (1959).

5) A. B. Chilton, D. Holoviak, and L. K. Donovan, "Determination of Parameters in an Empirical Function for Build-up Factors for Various Photon Energies," U. S. Naval Civil Engineering Laboratory Technical Note N-389 (1960).

6) M. J. Schumchyk and H. J. Tiller, "Ground Penetrating Radiation (Lip Contribution) in a Foxhole from a Fallout Field Simulated by Cobalt-60," Nuclear Defense Laboratory Report NDL-TR-3 (1960).

c) Facilities and apparatus used.

1) Concrete-lined cylindrical hole 4' diameter and 4' deep, in middle of concrete slab, with one radial line from it providing extensive lead shielding. (See Figure III-2-1.)

2) Cobalt-60 sources, of nominal strengths 0.5 and 5 curies, with appropriate container and projector.

3) Dosimeter chambers, 1-mr., 10-mr., and 200-mr., seven of each.

4) Charger-reader for dosimeters.

5) Thin lead blocks, bags of lead shot.

d) Background. The solution to this problem is important for the soldier in a foxhole, in order to determine the contribution of the radiation incident on him which penetrates the foxhole lip directly from the fallout near the lip edge. Similar considerations are also important in cases such as lip penetration for a basement. (See Reference 1, Sections 31 and 34.)

Two theoretical approaches to this subject have been suggested. One, given by Spencer (Ref. 1), provides a formula and graphed values of an appropriate integral used in the formula which can estimate directly the lip penetration dose for a uniformly distributed fallout field over the ground outside the foxhole. The other method involves a point-source-to-point-detector calculation for each incremental contaminated area, followed by an integration over all the contaminated plane. This approach is followed by Clifford, who suggests a semi-empirical approach for estimating the "build-up factor" which is part of the point-to-point kernel. (Reference 2).

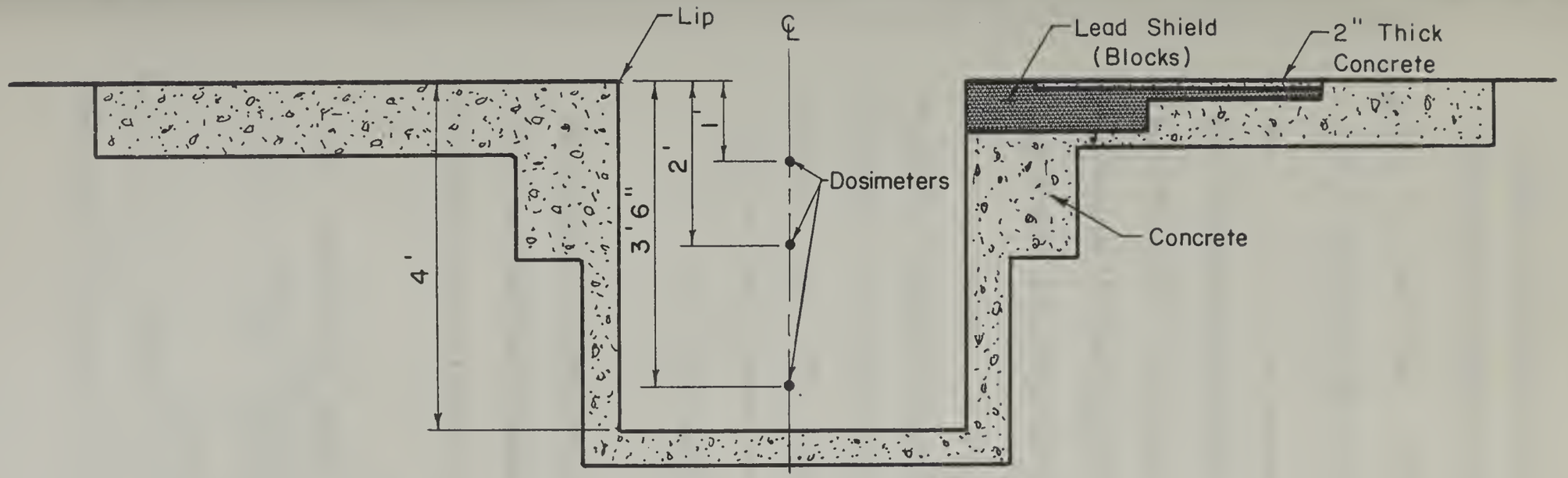

SCHEMATIC VIEWS
OF FOXHOLE

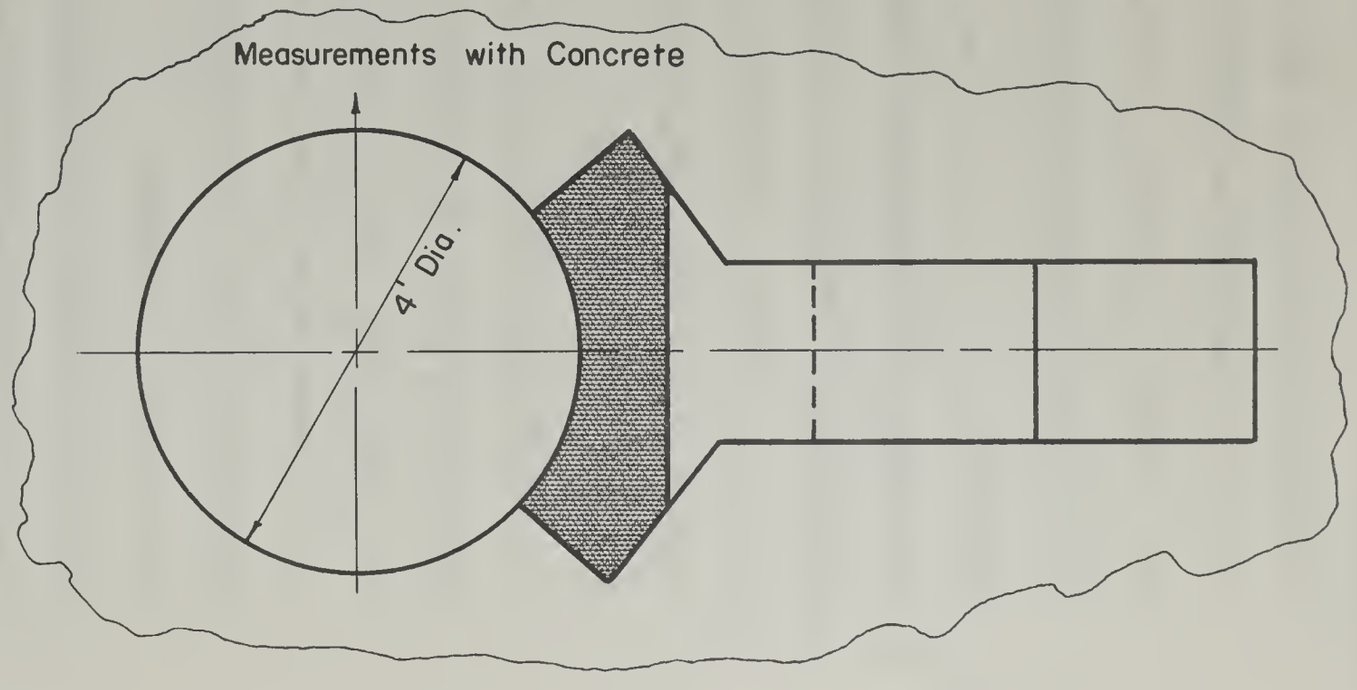

FIGURE III-2-1

e) Procedure.

1) Points were marked out on the ground, indicating locations of source at predetermined distances from the center of the foxhole. These were laid out in two radial lines--one over plain concrete and one over the line of lead bricks emplaced in the concrete.

2) Dosimeters were charged and placed in locations at or near the centerline of the hole at distances 1, 2, and 3.5 feet below the top of the foxhole. (Dosimeters were also placed at intermediate intervals, for some runs, but these results are not reported herein.)

3) As expeditiously as possible, the source was projected from the shielded container and placed on the spot nearest the foxhole on the radial line across the plain concrete. The source was left for a predetermined time; the source was removed back to its shielded container; the dosimeters removed and read. Times were recorded throughout.

4) The above procedure was repeated for each location designated from the edge of the lip out to a distance of 8' from the foxhole center. The designated distances from the center were: 2', 2'2", 2'4", 2'6", 3', 3'6", 4', and 6'.

5) The procedure was repeated over the line of lead bricks. The distances used for the source were 2'2", 2'4", 2'6", 3' and 4' from the center.

6) Dose readings were converted as necessary; skyshine was estimated and subtracted. Total dose from infinite contaminated plane was

calculated and compared with Spencer's theoretical prediction formula. Build-up factors for point-to-point kernals were calculated and compared with Clifford's "recipe".

f) Theory.

1) The following proof of Spencer's equation for lip penetration (Ref. 1, p. 57) is presented. Use is made of the function $\mathcal{L}(X, \cos\theta)$ which represents the dose angular distribution at a depth X below an infinitely contaminated plane as a function of this depth and the cosine of the angle between the normal and the direction from which the radiation is indent upon the detector. If we assume that the presence of the foxhole has little perturbing effect upon the radiation arriving at a point on the surface of the foxhole, it can be readily seen that at the point on the foxhole axis at depth y, the dose will be as given in the following equation:

$$D = \int_{-1}^{\cos\theta_1} d(\cos\theta) \; \mathcal{L}\left[X(\theta), \cos\theta\right] \quad .$$

The lower limit on the equation is based on the assumption that for all practical purposes the calculation is affected very little by assuming the foxhole to be bottomless.

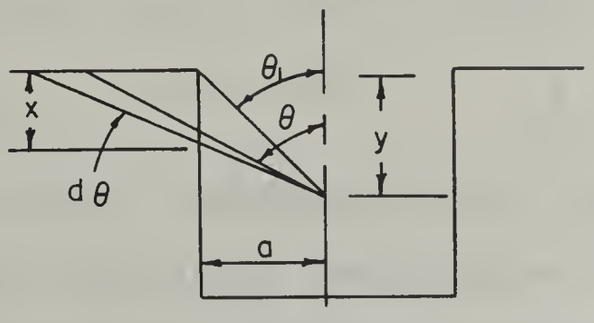

Figure III-2-2

From the figure it is clearly seen that

$$x = y - a \cot$$

$$dx = a \csc^2 \theta \; d\theta$$

The depth X is given in weight per unit area and obviously $X = \rho x$, where ρ is the material density. Thus,

$$dX = \rho \, dx = \frac{\rho a}{\sin^2 \theta} \; d\theta$$

$$a = y \; \frac{\sin \theta_1}{\cos \theta_1}$$

$$d(\cos \theta) = -\sin \theta \, d\theta$$

Therefore

$$dX = y \rho \frac{\sin \theta_1}{\cos \theta_1} \cdot \frac{d(\cos \theta)}{\sin^3 \theta}$$

Since important contributions arise only from directions near θ_1, to a fairly good approximation one can consider $\theta \approx \theta_1$ and therefore $\sin \theta_1 \approx \sin \theta$. With these approximations dX becomes

$$dX = - \rho y \; \frac{d(\cos \theta)}{\cos \theta_1 \sin^2 \theta_1}$$

$$\frac{d(\cos \theta)}{dX} = \frac{-1}{\rho y} \cos \theta_1 \sin^2 \theta_1$$

We thus get that

$$D = \int_{\infty}^{o} \frac{d(\cos \theta)}{dX} \; dX \cdot \ell\left[X(\theta), \cos \theta\right]$$

$$\approx \frac{(1 - \omega)(2 - \omega)}{\rho y} \cdot \int_{o}^{\infty} dX \cdot \ell(X, 1 - \omega),$$

where ω is equal to $1 - \cos \theta_1$. In the integrand of the last expression, it should be noted that $\cos \theta$ is not allowed to vary but is kept at the value $\cos \theta_1$ $(= 1 - \omega)$, since the greatest contributions to the value of the integral occur only for values of $\cos \theta$ near this limit.

2) Clifford's approach involves the determination of an equivalent build-up factor for the foxhole situation which can then be used in calculations. He theorizes as follows (Reference 2): Radiation penetrating the lip can be divided into that part which is uncollided and that part which is the scattered component. One might compare the lip penetration radiation to that which one would receive if an infinite attenuating medium were present through all space. In the latter case, the scattered contribution is evidently $B_\infty - 1$, expressed as a ratio to the uncollided contribution. Clifford then says that one should expect only about half the scattered contribution in case of the foxhole penetration as compared to the infinite medium case. Thus, the scattered contribution should be about in the proportion of $(B_\infty - 1)/2$ to the uncollided contribution; and if one adds 1 to this, one should get approximately the total dose measured, in terms of the uncollided contribution. This then, gives us a new build-up factor, $(B_\infty - 1)/2 + \frac{1}{2}$, or $(B_\infty + 1)/2$.

One can readily compute the uncollided contribution for any given situation, and one can determine experimentally the true total dose for said situation. A ratio of the latter to the former gives what might be called B_{exp}. The question which arises is: to what extent does B_{exp} deviate from the approximation computed above, to wit, $(B_\infty + 1)/2$. Clifford's experiments using cesium-137 provide a number, $\mathcal{R}$, where

$$\mathcal{R} = \frac{B_{exp}}{(B_\infty + 1)/2}$$

(B_∞ is readily available from Reference 3 or Reference 4, and may be approximated by a formula given in Reference 5.) The results of his experiments are given in Figure III-2-3, below.

240-816 O-67--44

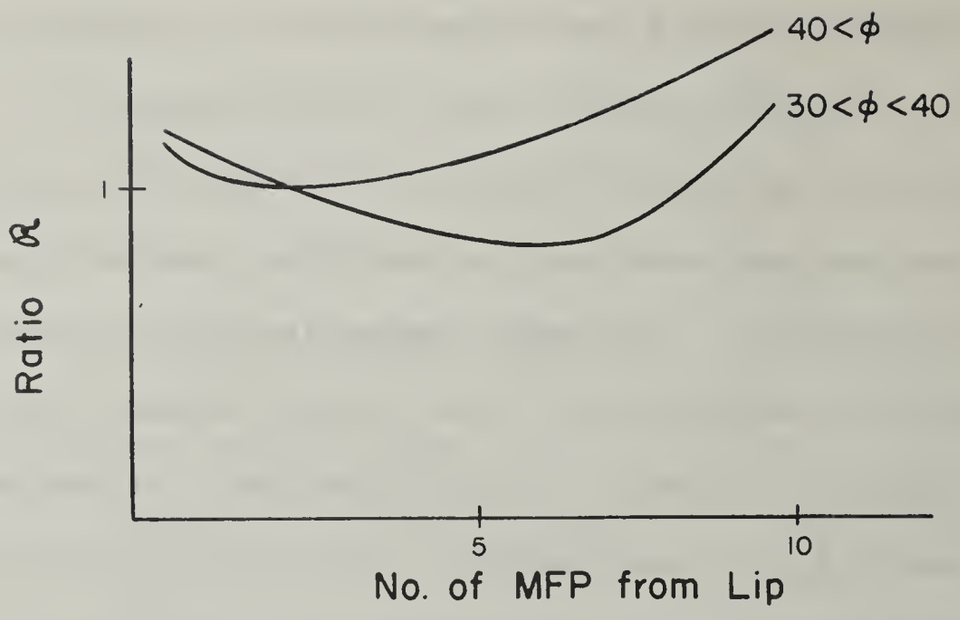

Figure III-2-3

In this figure, ϕ is the angle with the horizontal of the line between source and detector. It is thus $90^{\circ} - \theta$, where θ is as indicated in Figure III-2-2. (Clifford uses θ instead of ϕ, but in this report the nomenclature is modified to avoid confusion.)

As far as is known, neither Clifford nor anyone else has previously made such an analysis using cobalt-60.

3) The method for obtaining the dose from an infinite contaminated plane on the basis of point source measurements is readily shown.

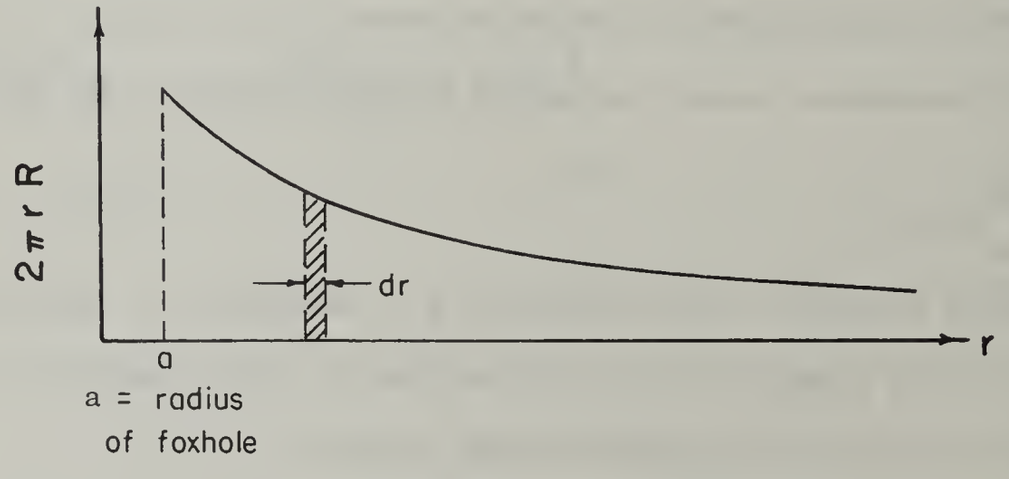

Figure III-2-4

Suppose that dose measurements at a certain point in the foxhole have been made with a one-curie source at various distances, r, from the axis of the foxhole, exposed for a certain period of time, say one hour. These measurements, R(r), are then multiplied by $2\pi r$; and the results are plotted to form a graph as shown in Figure III-2-4.

The hatched strip has the area $2\pi R(r)\ rdr$, which also can be seen to correspond to the differential dose from an annulus strip of the plane at radius r and of width dr, when the plane is contaminated uniformly to a source density of one curie per unit area.

Thus the dose from the whole infinite plane may be obtained by integrating the curve between the limits a and infinity. In practice, this integration may have to be done numerically; although if the curve can be expressed by a simple mathematical expression, an analytical integration may be possible.

4) There are several methods available for estimating the effect of skyshine, or air scattering into the foxhole. This must be done so that it may be subtracted from the measurements which include both skyshine and lip penetration. One method is to perform the experiment over a radial path with extensive lead inserted into the lip, to minimize the lip penetration and thereby lead to a close estimate of pure skyshine effect. (This method was tried in the present experiment, but results were dubious. The technique involves very low measurements, and results are easily influenced by minor variations in source position, cracks in lead bricks, and other non-ideal aspects which are difficult to eliminate.)

Another method is based upon the analysis of the originally plotted curve, which included both skyshine and lip penetration. Lip penetration,

as is fairly obvious, will fall off with distance from the lip in a very rapid fashion-- becoming negligible at a distance of half a dozen feet. The skyshine does not do so, but falls off very slowly-- in fact, over a distance of a few dozen feet, the plot of skyshine contribution multiplied by $2 \pi r$ should be almost constant, as one can see from previous experiments (see Ref. 6). One can also make this fact plausible through the following rationale:

It is reasonable to assume that the skyshine, being caused by atmospheric scattering, is proportional to the degree of scattering one would detect at the surface of the foxhole, which in turn should be roughly proportional to the scattering in an infinite, homogenous atmosphere with the same separation distance between source and detector. Thus, the skyshine from a point source at radial distance r should be given by

$$D_s = k\, e^{-\mu r} \left[B\,(\mu\, r) - 1 \right] / r^2$$

A simple empirical approximation to B is given in Reference 5 as

$$B = 1 + A \mu r\, e^{C \mu r}$$

in which, for average gamma ray energies, A is close to unity and C is very small. If D_s is multiplied by $2 \pi r$, the result will thus show

$$2 \pi r D_s = (k A \mu) \cdot \exp \left\{ (C - 1) \mu r \right\} .$$

Since μ is on the order of .002 $ft.^{-1}$ for cobalt-60, it can be seen that this expression changes very little over distances of many dozens of feet.

Thus the method involves carrying measurements out far enough that the curve becomes almost flat. In fact, if the plot is made on semilogarithmic paper, the equation above shows that the curve should,

after half a dozen feet more or less, become a straight line with a very slight negative slope. It is possible to extrapolate this straight portion back toward the origin (at least as far as the lip radius) and thereby estimate the skyshine for all distances. This gives what is called the "extrapolated skyshine" (Ref. 6).

A third method of eliminating skyshine is to perform the experiment in the first place in such a manner as to do so. That is to say, it is in principle possible to cover the source, as it is exposed at the appropriate distances, with a lead cover of sufficient thickness to prevent any appreciable amount of radiation from going upward into the atmosphere. There are certain practical difficulties inherent in this technique, but as it is not used in this experiment, no further discussion is warranted.

g) Preliminary calculations.

1) Theoretical predictions by Spencer's Monograph (Ref. 1, pp. 57 and 132).

Concrete density, ρ , given as 143 lb./cu. ft.

Depth:	1'	2'	3'6"
$\cos\theta_1 = 1 - \omega$	.447	.707	.868
ω	.553	.293	.132
$2 - \omega$	1.447	1.707	1.868
$\frac{\omega(1-\omega)(2-\omega)}{\rho y}$	.00250	.00131	.000428
$\int_0^{\infty} dX \; \ell(X, 1-\omega)$	12.3 x .94 = 11.56	12.3 x .98 = 12.05	12.3 x .99 = 12.17
D/D_o	.0289	.0158	.0052

2) Calculation of B_{exp} according to Clifford's analysis (Ref. 2).

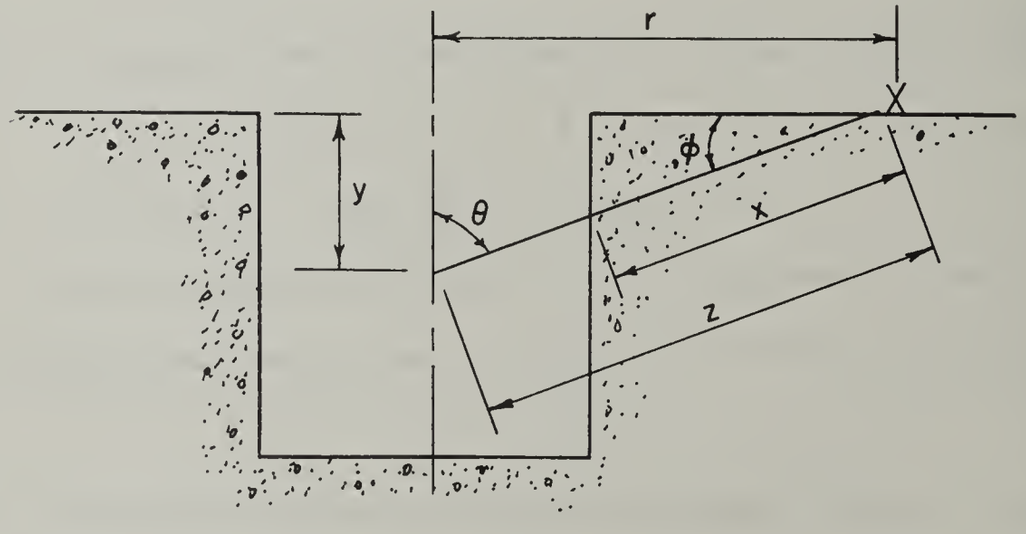

Figure III-2-5

As has been stated previously B_{exp} is that value which makes the following formula valid for a source strength of 1 curie:

$$D(1) \frac{14.0\ e^{-\mu x}\ B_{exp}}{z^2}$$, where distances are in feet, and where the variables are as given in Figure III-2-5. Then after experimental determination of D, for specific values of y and r, one can calculate B_{exp} by means of the expression:

$$B_{exp} = D(1) \cdot (z^2\ e^{\mu x}/14.0) \quad .$$

We may also calculate readily the denominator to Clifford's expression for R. B_{∞} can be readily obtained, for example, by use of the approximate formula provided in Reference 5:

$$B_{\infty}\ (1.25\ MeV) = 1 + .92\ \mu\ x\ e^{0.06\ \mu x} \quad .$$

From this, $(B_{\infty} + 1)/2$ is readily obtained. It is possible, then, to establish, for every value of y and r, a factor $F = (z^2\ e^{\mu x}/14.0)/((B_{\infty} + 1)/2)$, which when multiplied by the value of the appropriate normalized dose value at the detector point in r./hr. will give the value of R. The pertinent values of the variables and this factor are readily derived and summarized in the table below.

ρ = 143 lb./ft.^{3} = 2.29 g./cm.^{3}

μ = 2.29 x .0567 = .130 cm.$^{-1}$ = 3.96 ft.$^{-1}$

y	r	ϕ	x	z^2	$e^{\mu x}$	B_∞	$(B_\infty + 1)/2$	$(z^2 e^{\mu x}/14)$	Factor, F
2.0	2.333	49.4°	.439	9.443	5.69	2.775	1.888	3.84	2.03
	2.5	51.3	.640	10.25	12.55	3.71	2.36	9.19	3.89
	3.0	56.4	1.202	13.0	116.7	6.83	3.92	108.4	27.7
	4.0	63.4	2.24	20.0	7172.	14.89	7.94	10,170.	12,80.
3.5	2.333	33.6	.601	17.69	10.80	3.54	2.27	13.65	6.01
	2.5	35.5	.860	18.50	30.3	4.86	2.93	40.1	13.7
	3.0	40.5	1.537	21.25	441.	9.07	5.04	669.	133.
	4.0	48.8	2.66	28.25	37400	19.23	10.12	40,400.	3,990.

The computation is not carried out for y equal to 1.0, since measurements at this point are subject to great error with minor variations in location of source or detector; and it is not believed that this experiment should expect a sufficient degree of accuracy to permit a Clifford type analysis for this point.

h) Data and data reduction.*

1) Raw field data. Lip penetration plus skyshine.

Detector depth: 2.0 feet Estimate of background: .04 mr./hr.

Dist. from axis	Detector readings, mr.			Time, min.	Instr. type & no.	Charger-reader	Source stren. curies
	After	Before	Net				
2'	80	10	70	5.00	200mr. #083	Self-reading	0.47
2'2"	90	3	87	9.50	"	"	"
2'4"	52	12	40	10.00	"	"	"
2'6"	23	2	21	10.00	"	"	"
3'	5	0	5	10.00	"	"	"
3'	48	-		10.00	10-mr. #05	Tech/ Ops	"
4'	8	-		5.00	"	"	"
4'	14	-		5.00	1-mr. #36	"	"
6'	8.5	-		10.00	"	"	"
8'	10	-		15.00	1-mr. #32	"	"
8'	16	-		15.00	1-mr. #41	"	"

*Editorial comment: This was perhaps the least satisfactory of all experiments performed, for several reasons. The apparatus used was not highly suitable for this particular type of experiment. The experiment itself requires a great deal of care. There are many sources of substantial error. For these reasons, it is not desirable to pass on to posterity the dubious results obtained. As illustrations of the approximate magnitude of the data, the format of the tabulations, and the method of anlaysis, we are however including information for the

2) Reduced and corrected data. This is obtained by use of calibration curves previously obtained and provided for each combination of reader and detector type.

Dist. from axis, r	Time, min.	Corrected readings, R, mr.	Normalized values, (mr./hr.)/(c./ft.)*
2'	5.0	70	22,500
2'2"	9.5	87	16,000
2'4"	10.0	40	7,500
2'6"	10.0	21	4,220
3'	10.0	5	1,210
3'	10.0	4.2	1,010
4'	5.0	3.3 (?)	1,610
4'	5.0	0.4	694
6'	10.0	0.22	68
8'	15.0	0.14	69
8'	15.0	0.16	108

*This is obtained by the formula: 2π r(ft.) x R(mr.) x $\frac{60}{t(min.)}$ x $\frac{1}{0.47(c.)}$

(continued from previous page) readings of lip penetration plus skyshine at 2.0' depth in the foxhole, taken from the experiment conducted during the 1962 Institute. This particular set of data appear more reasonable and self-consistent than most of the other, but should still not be regarded as satisfying the minimum conditions of reportable experimentation.

i) Results. The reduced and normalized data are plotted in Figure III-2-6, and a smooth curve is drawn through the points. The extrapolated skyshine is estimated from what appears to be the asymptotic trend of the curve at large values of r. Subtraction of the values on the extrapolated skyshine curve from the main curve gives values for lip penetration only. Integration of this data provides the experimental value of lip penetration. This is accomplished in the following table, by use of Simpson's rule for numerical integration.

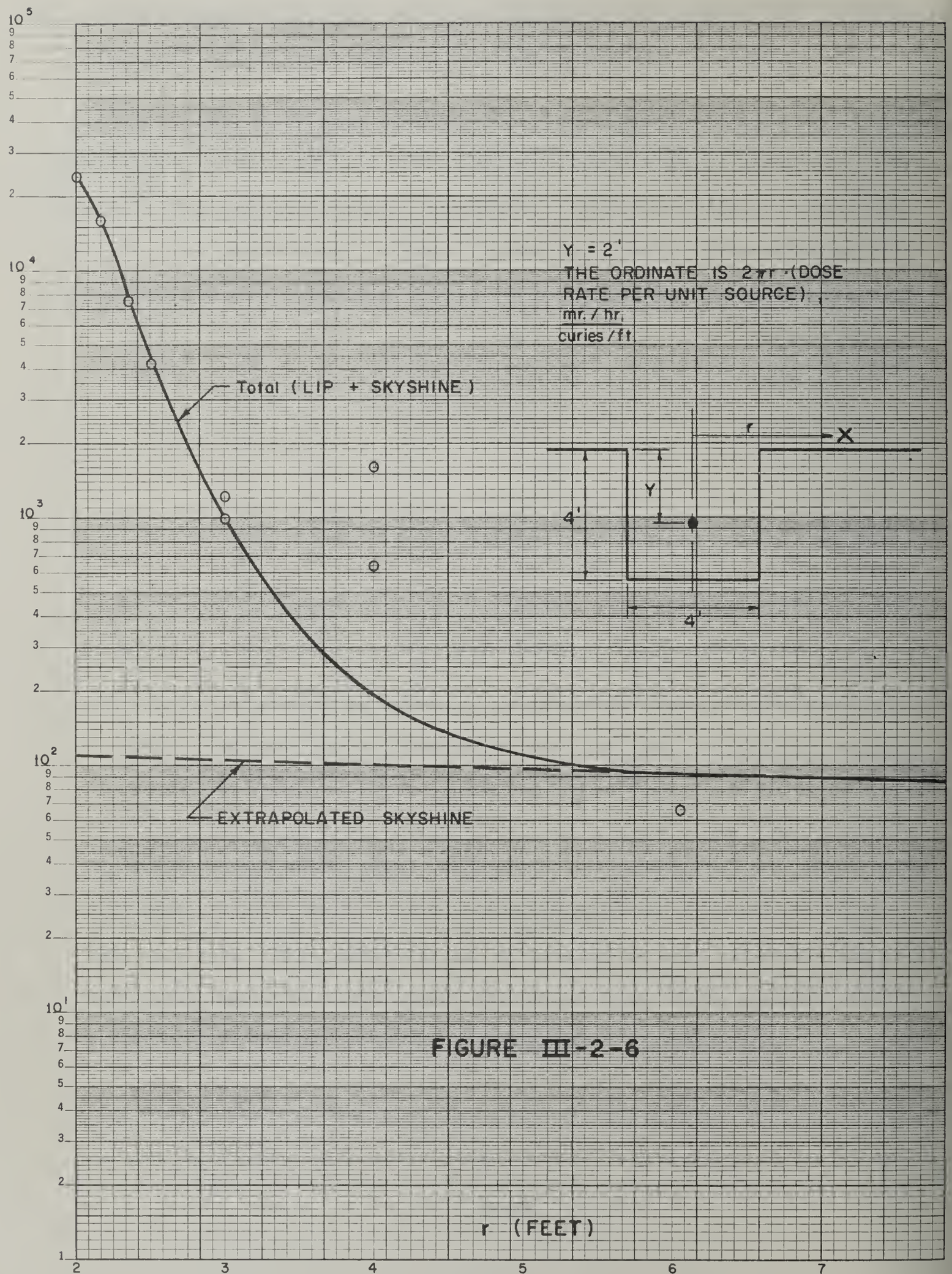

FIGURE III-2-6

Dist. from axis, r	Normalized values from smooth graph (skyshine subtracted)	Simpson's rule multiplier	Product
2'	22,400	1	22,400
2'2"	15,900	4	63,600
2'4"	7,400	2	14,800
2'6"	4,100	4	16,400
2'8"	2,500	2	5,000
2'10"	1,500	4	6,100
3'	950	2	1,900
3'2"	610	4	2,440
3'4"	400	2	800
3'6"	270	4	1,080
3'8"	180	2	360
3'10"	125	4	500
4'	90	2	180
4'2"	60	4	240
4'4"	40	2	80
4'6"	30	4	120
4'8"	20	2	40
4'10"	15	4	60
5'	10	2	20
5'2"	8	4	32
5'4"	6	2	12
5'6"	4	4	16
5'8"	3	1	3
		Total	136,183

The normalized dose at the 2' depth is then:

$D(2') = (1/3 \times (2/12) \times 136{,}183 = 7{,}560$ mr.

Since the normalized reference dose 3' above the contaminated plane is 490,000 mr. received in an exposure of 1 hour, the attenuation factor, with respect to lip penetration, is given by 7,560/490,000, or .0154. This is to be compared to the theoretical value, as calculated in Section g , of 0.0158.

A Clifford type analysis can be made at the 2' dosimeter depth for the radial values of r of 2'4", 2'6", and 3'. (It is not very likely that good answers should be obtained for values of r as small as 2'2" or as large as 4'. In the former case, the results are too sensitive to source position errors; in the latter case, the dose readings are so low that accurate values cannot be expected to be achieved in a hasty experiment such as this.) The results obtainable are as given in the following table:

y	r	No. of M.F.P.'s (μ x)	ϕ	D(1), r./hr.	Factor	R
2'	2'4"	1.74	49.4^{o}	.505	2.03	1.03
	2'6"	2.53	51.3	.280	3.89	1.09
	3'	4.76	56.4	.0504	27.7	1.40

In the above table, $D(1) = \frac{\text{(Experimental Lip Penetration Dose, roentgens)}}{\text{(Source strength, curies) x (Time, hours)}}$

These results are comparable to those of Clifford, noted in Section f.

j) Summary, discussion, conclusions. On the basis of the results analyzed in this report, it is obvious that an excellent agreement is found between Spencer's theory and the experimental facts. This fact is probably true, regardless of the difficulties encountered in this experiment; for the values of dose-rates are obtained by integrating over the whole contaminated plane and are largely governed by the experimental results with the source within a few inches of the lip, and the experimental results seemed more self-consistent in this region.

The results of the Clifford type analysis are inadequate to provide more than a qualitative conclusion. The results for a small number of mean-free-paths are fairly consistent with those of Clifford; and for greater than 40^{o}, a rising trend for higher values of the number of mean-free-paths is evident, again similar to Clifford's results. However the trend seems more marked than in the case of Clifford's results; and whether the effect is a true effect, because of the different gamma ray energies involved (one remembers that Clifford used cesium-137), or whether it is a result of poor data in the present experiment, there is no way of saying definitely.*

---

*Editorial comment: This experiment is being written up on the basis of the 1962 Institute results. However, it might be noted that the 1963 Institute obtained values in this experiment which were somewhat lower, especially at higher values of r (larger number of mean-free-paths in concrete). Even though the 1963 Institute results showed a rather unsatisfactory amount of individual scatter, results appeared on the whole to confirm the general shape of Clifford's curves for R as a function of φ and number of mean-free- paths.

It is felt desirable to conclude this report with a list of recommendations and precautions which should be observed in future conduct of this experiment.

1) The source used should be as small as possible, consistent with the requirements for safe and easy handling. It should be able to be exposed bare, and should be placed as close to the surface as possible. In fact, if the emphasis in the experiment is on lip penetration, it might be desirable to embed the source halfway into the concrete, by providing a slight recess in the concrete, with shape and size to accomodate the source snugly (personal comment from C. E. Clifford to A. B. Chilton). On the other hand, if the emphasis is on the skyshine component, it might be better to lay the source on the top of the concrete plane, without embedment (personal observation by John Batter to A. B. Chilton). In either case it is desirable to lay a sheet of lead between the source and the lip, of a thickness equal to the height that the source protrudes above the plane, so as to minimize the possible backscatter from the lip on the farther side of the foxhole.

2) Because there is a severe dose-rate gradient as one passes into the foxhole from a point above the foxhole, there is danger of not having electronic equilibrium in the dosimeters used in the measurement, if they are of usual commercial type. In such case, it is important to enclose the chambers in air-equivalent (such as plastic) sleeves of not less than 1/8" thickness. The dosimeters should be calibrated with sleeves on.

3) If small chambers are used, such as pocket chambers, it is probably all right to place a number of them in the foxhole for a single run at close intervals down the axis, say every six inches. However, for larger chambers, especially with sleeves on them, it is likely that too many chambers cause problems with respect to shielding of the lower ones by the upper ones. In such case, intervals closer than one foot apart are not recommended.

4) It is necessary that the dosimeters and sources used be calibrated so as to be consistent with one another. If possible, the source should be used to check the chambers' calibrations.

5) Any of the methods used to eliminate skyshine discussed earlier in this report can probably be made effective for this experiment; however, it is not believed that the skyshine component can be adequately studied for its own sake within the bounds of time and effort prescribed for an Institute of this sort. This is mainly because appreciable skyshine contribution is caused by sources many hundreds of feet away from the foxhole; and to study the effect at such distances, very strong sources and/or long periods of time must be involved.

240-816 O-67—45

3. Duct Experiment

a) Purpose. To study the streaming of gamma radiation through ducts and to compare the theoretical and engineering method results with the experimental values.

b) References and bibliography.

1) J. C. LeDoux and A. B. Chilton, "Gamma Ray Streaming through Two-legged Rectangular Ducts," Nucl. Sci. and Eng. 11, No. 4, 362 (1961). Also published under the title, "Attenuation of Gamma Radiation through Two-legged Rectangular Ducts and Shelter Entranceways--An Analytical Approach," U. S. Naval Civil Engineering Laboratory Note TN-383 (1961).

2) D. W. Green, "Attenuation of Gamma Radiation in a Two-legged Ducts Using the Albedo Concept," U. S. Naval Civil Engineering Laboratory Report R-195 (1962).

3) J. M. Chapman, "Computer Calculation of Dose Rates in Two-legged Ducts Using the Albedo Concept," U. S. Naval Civil Engineering Laboratory Report R-264 (1963).

4) C. W. Terrell, A. J. Jerri, R. O. Lyday, and D. Sperber, "Radiation Streaming in Shelter Entranceways," Armour Research Foundation Report ARF 1158-12 (1960).

5) D. J. Raso, "Monte Carlo Calculations on the Reflection and Transmission of Scattered Gamma Radiations," Technical Operations, Inc., Report TO-B 61-39 (1961, revised 1962).

6) A. B. Chilton and C. M. Huddleston, "A Semiempirical Formula for Differential Dose Albedo for Gamma Rays on Concrete," Nuclear Sci.

and Eng. 17, No. 3, 419 (1963). Also published as U. S. Naval Civil Engineering Laboratory Report R-228 (1962).

7) "Shelter Design and Analysis, Vol. 1, Fallout Protection," Office of Civil Defense Compilation (Revised ed., 1962). (This is a revision of an OCD draft document commonly referred to as the "Engineering Manual.")

8) C. W. Terrell, A. J. Jerri, and R. O. Lyday, "Radiation Streaming in Ducts and Shelter Entranceways," Armour Research Foundation Report ARF 1158A02-7 (1962).

9) A. B. Chilton, "Further Analysis of Gamma Ray Attenuation in Two-legged Rectangular Ducts," U. S. Naval Civil Engineering Laboratory Note TN-412 (1961).

c) Facilities and apparatus used.

1) Cast concrete structural segments, which, when put together, make up a concrete lined duct, with cross-section 11" x 11", with first leg of length 4' and with second leg of variable length from 2' to 4'. (See Figure III-3-1.)

2) Cobalt-60, of nominal strength 0.5 curies, with associated projection apparatus for storage and remote handling.

3) 6 pocket type dosimeters, 200-mr.

4) 1 low-level dose-rate meter (previously calibrated with respect to the source).

5) Several dosimeter chambers of 1-mr. and 10-mr. size, with associated charger-reader.

6) Lead block for corner lip replacement.

7) Several dozen lead brick, sandbags, bags of lead shot.

8) Stand and clamp for holding source in place.

d) Background. Knowledge of shield design is more advanced than knowledge of the transmission of radiation through ducts, although the latter has lately become the subject of intensive studies. Ducts of practical interest include radiation shelter entrances and ventilation and utility conduits piercing shelter walls. In the design of a shelter one must insure that necessary ducts and entrances do not compromise the specified protection factor. The otherwise satisfactory systems of shelter analysis and design require further refinement with respect to ducts.

Efficient ducts have two or more legs to eliminate unscattered radiation and induce a maximum of scattering and absorption. Two factors, therefore, complicate the analysis of ducts. The first is intractable

geometry. The second is the necessity of accounting for multiple scattering. The geometric difficulties preclude use of the elegant analytic approximation methods that have proved so successful in other aspects of shelter analysis. Experimentation and Monte Carlo calculations are useful and necessary, but cannot serve national shelter programs until simple and accurate methods of analysis are evolved. Two current methods of analysis are available which permit a straight-forward analytical approach to the problem.

Many variables appear in even the simplest duct problem. However, experimentation and analysis of idealized cases are desirable to give insight into duct phenomena so that more complex cases can be understood.

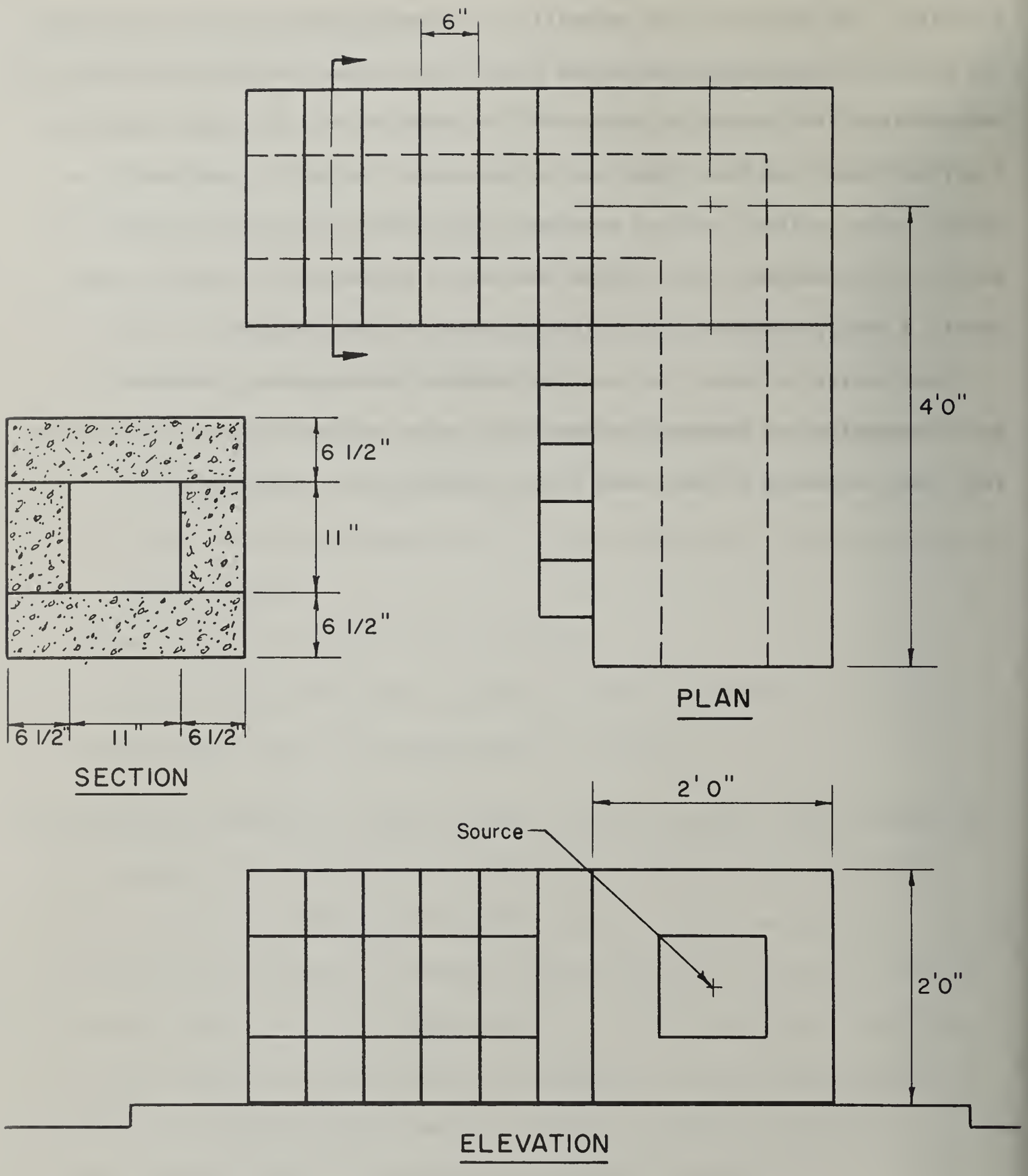

FIGURE III-3-1

e) Procedure.

1) 200-mr. chambers were placed at the middle of the corner position.

2) As expeditiously as possible, the source was brought into position in the middle of the duct entrance. The source was left exposed for a predetermined length of time; then it was withdrawn expeditiously into the shielded container.

3) The second leg was built to a length of 4'. The radiation field at the middle, sides, and bottom of the second leg was determined by means of the dose-rate meter and by a timed exposure of low level dosimeters.

4) The second leg length was reduced to 3'; and step 3 was repeated, using the dose-rate meter.

5) Step 4 was repeated, after the concrete corner had been removed and replaced with a lead block.

6) The concrete corner block was replaced, the second leg was shortened to 2', and step 4 was repeated.

f) Theory.

1) A somewhat tedious, but basically simple approach to radiation streaming through two-legged, rectangular ducts is provided by the LeDoux-Chilton technique (Reference 1), which essentially uses differential albedo to determine wall reflection by those areas which are in view both from the source end and the detector end of the duct system. The in-scattering contribution of the duct corner is added also.

The originally prescribed method ignores the possibility of multiple reflection contributions, although these effects have been recently proved to be not unimportant (References 2 and 3). If considerations

of multiple reflections are given the same type of treatment as the single reflections, the tediousness of the procedure is greatly compounded, and a programmed computer is needed to handle the problem (see Reference 3). An approximate way of doing the same thing is to multiply the results of a simpler type computation by factors to take account of multiple reflections. It is known, for example, that the attenuation factor at the end of the first leg is about 30% higher than that given by a simple inverse square relationship in the open (References 2 and 4); and the multiple reflection effect is such as to make the attenuation factor for the second leg about double the value given by considering only single reflections (Reference 3).

The previous use of the single reflection approach by LeDoux and Chilton had been successful in matching experimental values because of the use by them of an assumption of istropicity of the albedo function, which provided values of albedo for insertion in the attenuation formulas that were too high. This procedure is outmoded by the more recent publication of good albedo data (References 5 and 6), but it can still be used if desired (see Reference 1).

No detailed derivation of the LeDoux-Chilton formulas is considered warranted, since they are somewhat lengthy and the report given as Reference 1 developsthem in detail.* Section g illustrates

*Editorial comment: The LeDoux-Chilton theory is discussed and developed more fully elsewhere in the present document.

the method by presenting a sample solution in detail.

2) The method of handling ducts and entranceways given in the Engineering Manual (Reference 7) is quite simple in application, but rests upon rather crude theoretical considerations. Radiation coming down the first leg is simply computed as the direct contribution, subject to the inverse square relationship. This may be handled alternately by considering it proportional to the solid angle fraction of the entrance aperture. Since the corner acts as a new source for radiation down the second leg, the attenuation factor for this (and subsequent) legs is considered proportional to the solid angle subtended by the corner and with vertex at the end of the leg in question. The constant of proportionality is obtained empirically. It is said to be 0.1 for the second leg (including the first corner), and 0.5 for subsequent legs. There is some reason to suspect that the value of 0.1 may be low in some cases (personal observation by J. C. LeDoux), and there is experimental evidence (Reference 8) to suggest that a proportionality of 0.5 for the third leg is too high. LeDoux has made a suggestion that a value for the second leg of 0.2 would be safer.

3) Based upon the original premises of the LeDoux-Chilton approach, Chilton (Reference 9) has developed an analytical method of obtaining the attenuation factor when the detector is off-center to one side or the other, that is, near either wall. Although this development suffers from the same inadequacy as the basic LeDoux-Chilton formulation, in that it only considers single reflections, the

relative values of the computed attenuation factors at the walls with respect to the LeDoux-Chilton computed value at the center may have some significance. If the multiple-reflected radiation varies from one side of the duct to the other in the same way that the singly reflected radiation does, these computed relative values should be valid for the experimental situation. On the other hand, one would expect the multiple-reflected radiation to be more divergent in direction than the singly reflected radiation and thus to be less likely to show a change with respect to a side-to-side variation in detector position. Therefore, we have a possible hypothesis at the opposite extreme which would predict no change in multiple reflection contribution with respect to sidewise change in detector position. Under the latter hypothesis, if the multiple-reflected radiation is approximately half of the total radiation the detector sees, for example, then one would predict that the experimental dose rate variation with respect to change in detector position should be about half that predicte by Chilton's method of analysis. In actuality, one would expect the situation to be somewhere between these two extremes, so that at least there is a means of predicting an upper and a lower bound on the variation.

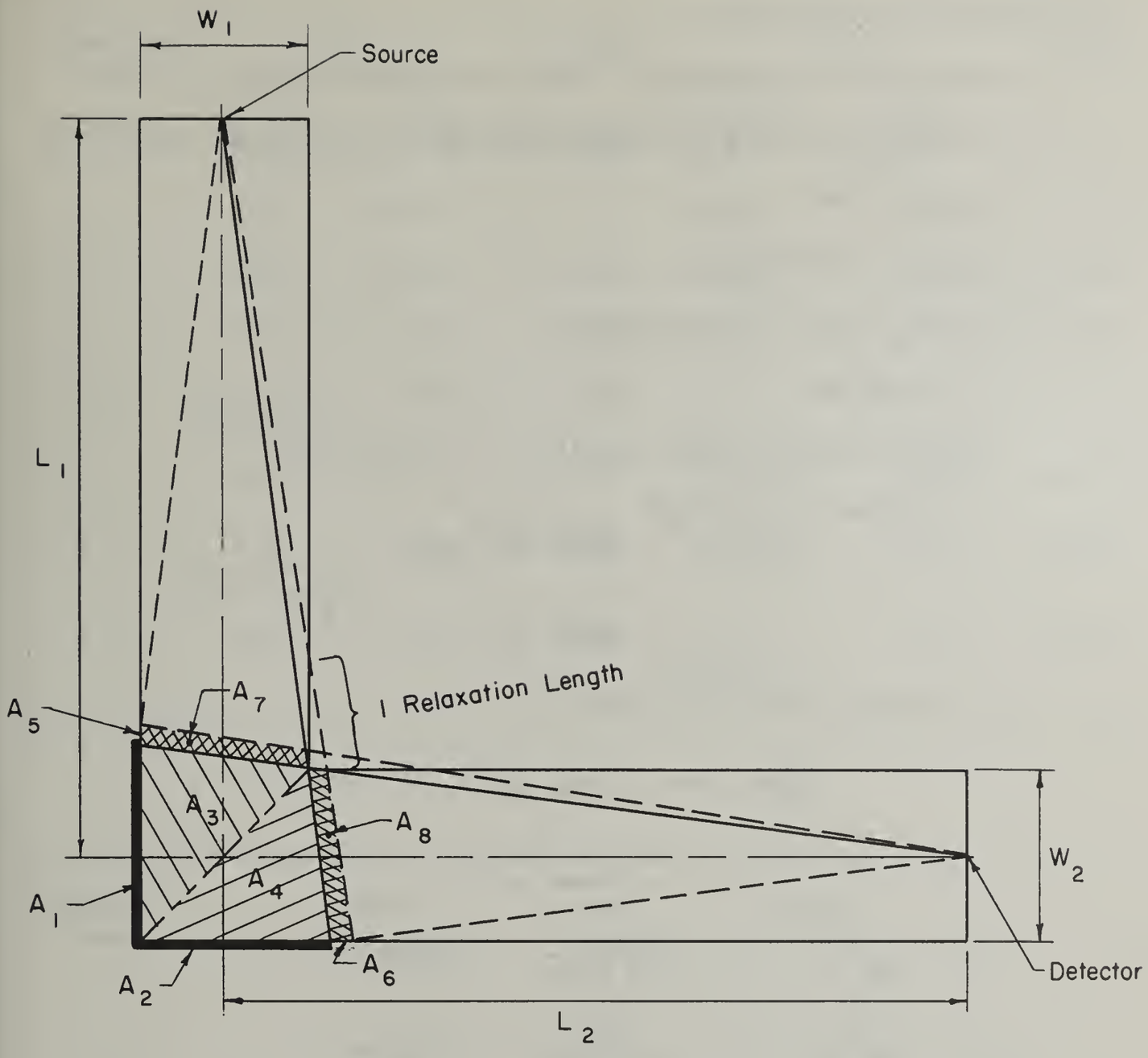

AREAS 1, 2, 5 & 6 ARE WALL AREAS,
AREAS 3, 4, 7 & 8 INCLUDE THE TOP
& BOTTOM AREAS OF THE
INSIDE OF THE DUCT.

DUCT GEOMETRY

FIGURE III-3-2

g) Preliminary calculations.

1) LeDoux-Chilton analysis. Sample calculation for L_2 = 4'0".

See Figure III-3-2 for description of the geometric parameters.

L_1 = 4' = 48"

L_2 = 4' = 121.92 cm.

$W_1 = W_2 = H$ = 11" = 27.94 cm.

E_o = 1.25 Mev .

Concrete (lightweight) density, = 1.65 g./cm.^{3}

At 1.25 Mev, $\frac{\mu_a}{\rho}$ = .0272 cm.^{2}/g.

μ_a = .0449 cm.$^{-1}$

At single scattering energy (~.35 Mev),

$\frac{\mu'_a}{\rho}$ = .0296 cm.^{2}/g.

μ'_a = .0488 cm.$^{-1}$

$\beta_1 = \frac{W}{2L_2} = \frac{11}{2 \times 48} = 0.1146$

$\beta_2 = \frac{W}{2L_1} = \frac{11}{2 \times 48} = 0.1146$

$\beta_3 = \frac{H}{2L_2} = \frac{11}{2 \times 48} = 0.1146$

	$1 + \beta$	$1 - \beta$	$(1 - \beta)^2$	$(1 - \beta)^3$
β_1	1.1146	.8854	.784	.694
β_2	1.1146	.8854	.784	.694

Scatter Area	$\cos\theta_1$ Formula	$\cos\theta_1$ Value	$\sin\theta_1$	$\cos\theta_2$ Formula	$\cos\theta_2$ Value	$\sin\theta_2$
A_1	$W/24L_1$	.1146	.993	1.00	1.00	0
A_2	1.00	1.00	0	$W/2L_2$	.1146	.993
A_3	$H/2L_1$	.1146	.993	$H/2L_2$	.1146	.993
A_4	$H/2L_1$	.1146	.993	$H/2L_2$	.1146	.993
A_5	$\frac{W}{2L_1(1-\beta_2)}$	.1294	.992	1.00	1.00	0
A_6	1.00	1.00	0	$\frac{W}{2L_2(1-\beta_1)}$	.1294	.992
A_7	$\frac{H}{2L_1(1-\beta_2)}$	.1294	.992	$H/2L_2$	.1146	.993
A_8	$H/2L_1$	.1146	.993	$\frac{H}{2L_2(1-\beta_1)}$	.1294	.992

$$\cos\theta_s = \sin\theta_1 \sin\theta_2 \cos\varphi - \cos\theta_1 \cos\theta_2$$

Scatter Area	φ	$\cos\theta_1 \cos\theta_2$	$\sin\theta_1 \sin\theta_2 \cos\varphi$	$\cos\theta_s$	θ_s
A_1	0	.1146	0	- .1146	96.6°
A_2	0	.1146	0	- .1146	96.6°
A_3	90°	.0131	0	- .0131	90.8°
A_4	90°	.0131	0	- .0131	90.8°
A_5	0	.1294	0	- .1294	97.4°
A_6	0	.1294	0	- .1294	97.4°
A_7	90°	.0148	0	- .0148	90.8°
A_8	90°	.0148	0	- .0148	90.8°

Klein-Nishina Energy Scattering Coef. for 1.25 MeV.

θ_s	$K_e(\theta_s)$
60^o	0.705×10^{-26}
65	0.573
70	0.478
75	0.400
80	0.344
85	0.300
90	0.266
95	0.239
100	0.217
105	0.199
110	0.184

Albedo Computation (Reference 6):

$$a = \frac{C\,K_e(\theta_s)\cdot 10^{26} + C'}{1 + \frac{\cos\theta_1}{\cos\theta_2}}$$

$C = 0.064$

$C' = 0.0090$

Area	$K_e(\theta_s) \times 10^{26}$	$C\,K_e(\theta_s) \times 10^{26}$	$C \cdot K \cdot 10^{26} + C'$	$\frac{\cos\theta_1}{\cos\theta_2}$	$1 + \frac{\cos\theta_1}{\cos\theta_2}$	a
1	0.232	.0148	.0238	.1146	1.1146	.0214
2	0.232	.0148	.0238	8.726	9.726	.00245
3	0.262	.0168	.0258	1.000	2.000	.0129
4	0.262	.0168	.0258	1.000	2.000	.0129
5	0.228	.0146	.0236	.1294	1.1294	.0209
6	0.228	.0146	.0236	7.298	8.728	.00270
7	0.262	.0168	.0258	1.129	2.129	.0121
8	0.262	.0168	.0258	.886	1.886	.0137

$$G_b = \frac{.0214}{1.1146} + \frac{.00245}{.1146 \times 1.1146} + \frac{.0129}{.8854} + \frac{.0129}{.8854}$$

$$= .0192 + .0192 + .0146 + .0146$$

$$= .0676$$

$$G_{t1} = \frac{.8854 \times .0209 + 2 \times 0.0121}{2 \times .0488 \times 121.92 \times .784 \times 0.694}$$

$$= \frac{.0185}{6.47} + \frac{.0242}{6.47} = .00286 + .00374$$

$$= .00660$$

$$G_{t2} = \frac{.8854 \times .00270 + 2 \times .1146 \times .0137}{2 \times .00449 \times 121.92 \times .784 \times .784 \times .1146}$$

$$= \frac{.00239}{.771} + \frac{.00314}{.771} = .00310 + .00407$$

$$= .00717$$

$$G_s = \frac{ZN}{\mu_a^2} \cdot \frac{K_e(\theta_s)}{2L_2 (1-\beta_1)^3 (1-\beta_2)^3}$$

ZN = No. of electrons/cm.^{3} = 4.97×10^{23}

$\mu_a = 0.0449$ cm.$^{-1}$

$\frac{ZN}{\mu_a^2} = 2.465 \times 10^{26}$

$$\alpha_1 = \tan^{-1} \frac{W_1}{2L_1 (1-\beta_2)} = \tan^{-1} \frac{11}{2 \times 48 (.8854)} = \tan^{-1} 0.1294$$

$$= 7.4^o$$

$$\alpha_2 = \tan^{-1} \frac{W_2}{2L_2 (1-\beta_1)} = \tan^{-1} \frac{11}{2 \times 48 \times .8854} = \tan^{-1} 0.1294$$

$$= 7.4^o$$

$$\theta_s = 90^o - (\alpha_1 + \alpha_2) = 75.2^o$$

$K_e (\theta_s) = .398 \times 10^{-26}$

$$G_s = \frac{2.465 \times .398}{2 \times 121.92 \times .694 \times .694} = \frac{.981}{117.4}$$

$$= .00836$$

$$G_{tot} = .0676 + .00660 + .00717 + .00836$$

$$= .0898$$

Attenuation factor for second leg is given by

$$F_2 = 4\beta_1\beta_2\beta_3 G_{tot}$$

$$= 4 \times .1146 \times .1146 \times .1146 \times .0898$$

$$= .000541$$

To account for multiple reflection, multiply this value by 2.

$$F_2' = 2 \times .000541 = .00108$$

The value of attenuation factor for first leg, based on direct dose, is:

$$F_1 = \frac{1}{L_1^2} = \frac{1}{4^2} = .0625$$

If wall reflections are included, multiply this value by 1.3.

$$F_1' = .0625 \times 1.3 = .08125$$

Similar calculations for L_2 = 2' and 3' give the following results:

$$F_2'(2') = 2 \times .00386 = .00772$$

$$F_2'(3') = 2 \times .00120 = .00240$$

Attenuation factor for L_2 = 3', with lead corner lip, involves only G_b, since it is assumed no radiation penetrates the lip. It can be readily found that

$$G_b = .0784 \text{ , for } L_2 = 3$$

$$F_2 = 4\beta_1\beta_2\beta_3 G_b \times 2 \quad \text{(including multiple reflection factor)}$$

$$= .00168$$

This value is $\frac{.00168}{.00240}$, or 70% of the value with regular concrete lip.

---

2) Attenuation calculation according to the Engineering Manual (Reference 7).

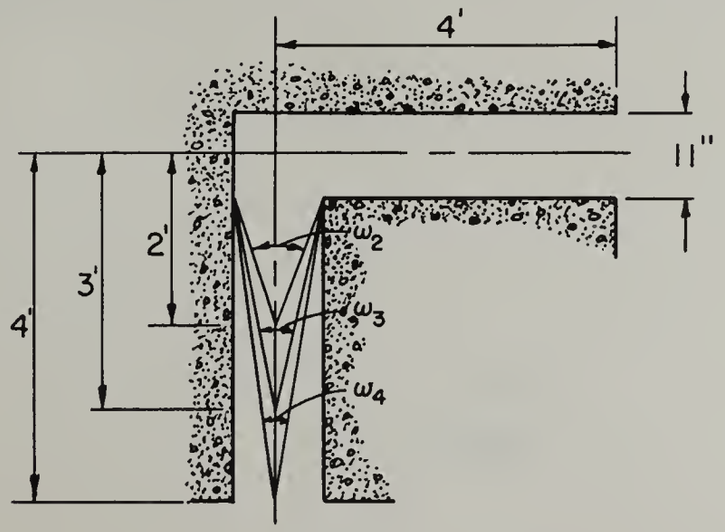

240-816 O-67—46

$$F_1 = \frac{1}{L_1^2} = 0.0625$$

L_2	ϵ	η	ω	$F_2 = 0.1$	$R_f = F_1 F_2$	$F_2' = 0.2$	$R_f' = F_1 F_2'$
2'	1.0	3.27	.055	.0055	.000344	.011	.000688
3'	1.0	5.45	.020	.0020	.000125	.004	.000250
4'	1.0	7.64	.0085	.00085	.000053	.0017	.000106

3) Effect of moving detector to walls, at $L_2 = 4'$: according to Reference 9, this is best accomplished by means of a table of comparative ratios with the individual area contributions in the original case. The original case is called the "C-C" case; the situation in which the detector is moved to the wall farthest from the first leg is called the "C-F" case; the detector at the nearer wall gives the "C-N" case.

There is no G_s contribution for the C-N case; for the C-F case,

$\alpha_1 = 7.4^\circ$

$\alpha_2 = \tan^{-1} .258 = 14.5^\circ$

$\theta_s = 68.1^\circ$

$K_e(\theta_s) = .514$

$G_s = .0216$

The Table of Individual Contributions Follows:

	Area	C-C Case	Multipliers for C-F	C-F Case	Multipliers for C-N	C-N
	1	.0192	1.115	.0214	.885	.0170
G_b	2	.0192	1	.0192	1	.0192
	3	.0146	1.115	.0163	.885	.0129
	4	.0146	1	.0146	1	.0146
G_{t1}	5	.00286	2	.00572	0	0
G_{t2}	6	.00310	1	.00310	1	.00310
G_{t1}	7	.00374	2	.00748	0	0
G_{t2}	8	.00407	1	.00407	1	.00407
G_s	Lip	.00836	-	.0216	-	0
G		.0898		.1135		.0709

It is seen that the C-F case gives a result of about 26% higher than the C-C case, whereas the C-N case gives a result of about 21% lower.

h) Data and data reduction.

All runs were made with the 0.47 curie cobalt-60 source. The locations of the instruments are as indicated in Figure III-3-4.

Measurements with 200-mr. dosimeters.

(All exposure times are 10-minutes.)

Detector Position	Detector No.	Reading, mr.			Dose-rate, mr./hr.	Position Average
		After	Before	Net		
1	095	93	0	93	558	540
1	091	88	6	82	492	
1	074	96	1	95	570	
2	086	91	1	90	540	540
2	095	92	2	90	540	
3	076	92	7	85	510	540
3	082	98	3	95	570	
4	075	92	3	89	534	534

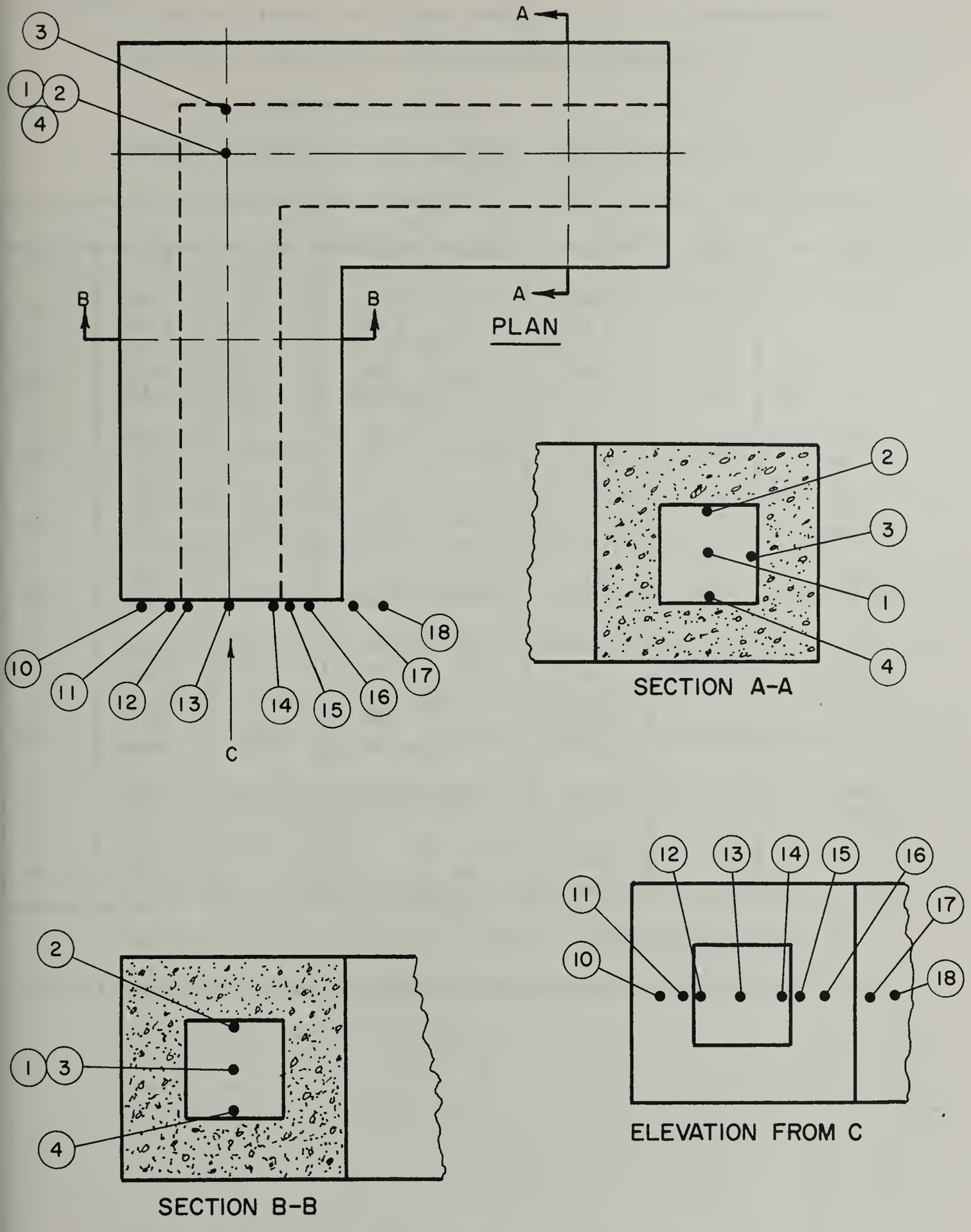

FIGURE III-3-4

Measurements (mr./hr.) with Dose-rate meter (Bendix No. 69)

Correction factors: 1.35 for 10-scale

1.05 for 100-scale

Unless stated, readings are with concrete corner lip.

Position	L_2 = 2'		L_2 = 3'		L_2 = 3'*		L_2 = 4'	
	Raw	Corr.	Raw	Corr.	Raw	Corr.	Raw	Corr.
10	205 x 10	2.77	.045 x 10	.61	.04 x 10	.54	.035 x 10	.47
11	.45 x 10 .05 x 100	6.10 5.25	.095 x 10	1.28	.055 x 10	.74	.05 x 10	.675
12	.062 x 100	8.40	.165 x 10	2.23	.12 x 10	1.62	.08 x 10	1.08
13	.056 x 100	7.60	.15 x 10	2.02	.135 x 10	1.82	.08 x 10	1.08
14	.40 x 10	5.40	.11 x 10	1.50	.12 x 10	1.62	.08 x 10	1.08
15	.26 x 10	3.50	.065 x 10	.88	.09 x 10	1.21	.059 x 10	.77
16	.15 x 10	2.00	.035 x 10	.47	.045 x 10	0.61	.05 x 10	.675
17	.40 x 10	5.40	.05 x 10	.675	.065 x 10	0.88	.055 x 10	.74
18			.04 x 10	.54			.08 x 10	1.08

*With lead corner.

The corrected values from this table are plotted in Figure III-3-5.

i) Results.

1) Measurements at corner. The resulting values at the corner, are all seen to be essentially 540 mr./hr., regardless of where the detector is placed in the corner. Assuming that this is the correct value, the resulting experimental reduction factor for the first leg is taken to be .540/(14.0 x .470) , or .0821. This is to be compared with the theoretical values of F_1 (without consideration of wall reflection) of .0625, or with the theoretical value of F_1' (including wall reflections) of .08125.

2) Measurements at end of second leg. The measurements which are displayed in Figure III-3-5 are subject to an appreciable background of radiation which either comes somewhat directly from the source through the sides of the duct or results from air and ground scatter contributions outside the duct system. The most practical way of determining this background in the present series of experiments seems to be to draw tangent lines underneath the individual curves and consider that it represents the background. This assumes that just to either side of the opening at the duct exit, the radiation level is all due to background. One may then obtain net readings which represent only duct streaming by direct reading of the differences from the graph. This gives the results displayed in the following table. Values are in mr./hr.

Length, second leg	2'	3'	3' (lead lip)	4'
Far (left) side	6.4	1.7	1.1	0.6
Center	5.6	1.5	1.2	0.55
Near (right) side	3.4	1.0	1.0	0.5

These results may be readily converted into second-leg attenuation factors, by dividing by 540 mr./hr. This gives a similar table.

Length, second leg	2'	3'	3' (lead lip)	4'
Far (left) side	.0119	.0031	.0020	.0011
Center	.0104	.0028	.0022	.0010
Near (right) side	.0063	.00185	.00185	.0009

It is possible to compare these attenuation factors with those previously computed from theory or by engineering formulas. It is also possible to compute the dose-rates at the end of the second leg by applying the theoretical values of attenuation to the reference dose-rate and comparing the results to the dose-rate experimental values given in the prior table. Figure III-3-6 presents the results of this type of comparison.

The experimental values of dose-rate are also presented in Figure III-3-7 as a function of ω, the solid angle fraction of the duct corner as seen from the end of the second leg. This figure also provides two theoretically determined values of dose-rate, according to the Engineering Manual approach, with the two suggested values of the proportionality constant, 0.1 and 0.2, for the sake of comparison. The reference dose at the corner is taken as 540 mr./hr.

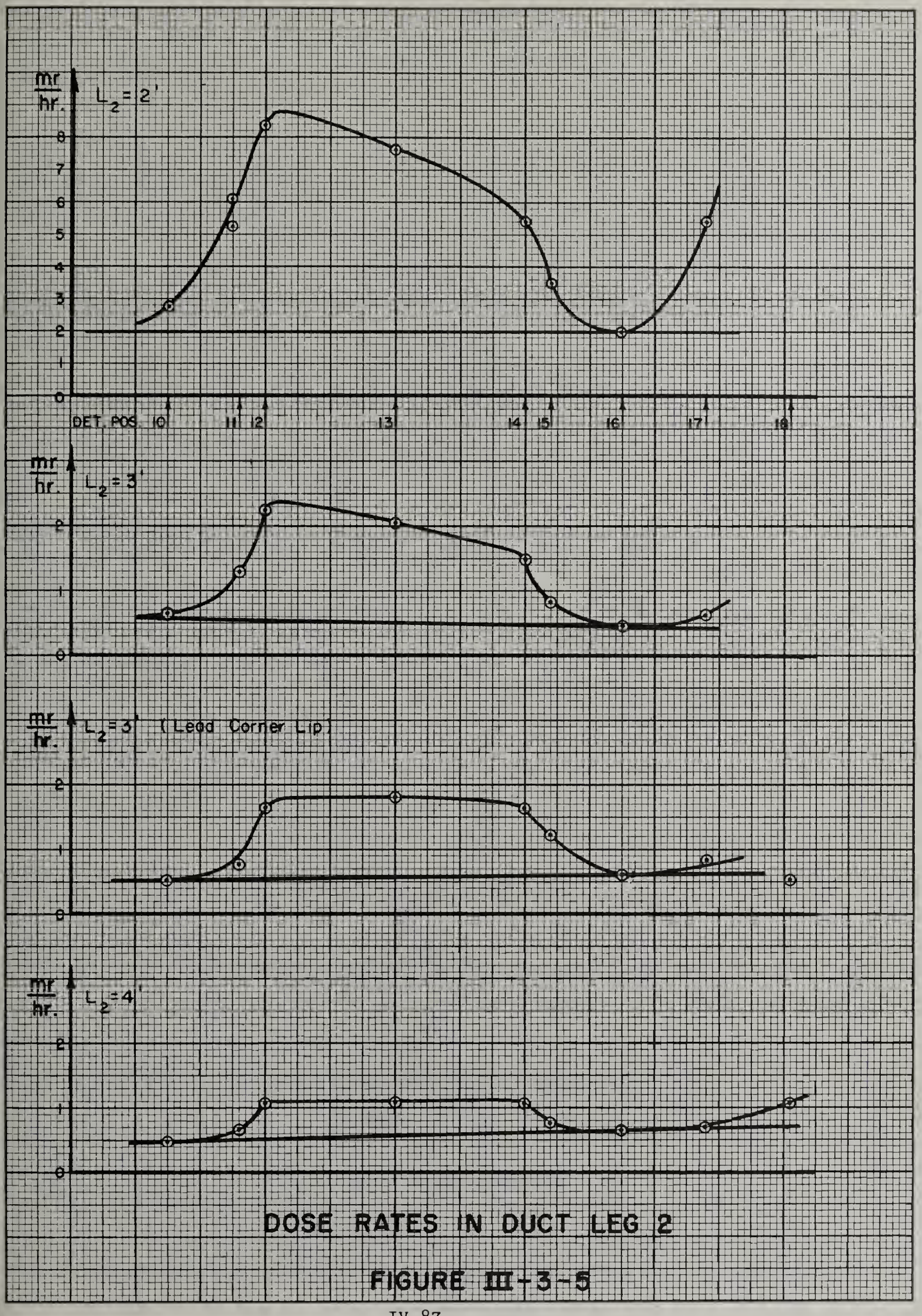

DOSE RATES IN DUCT LEG 2

FIGURE III-3-5

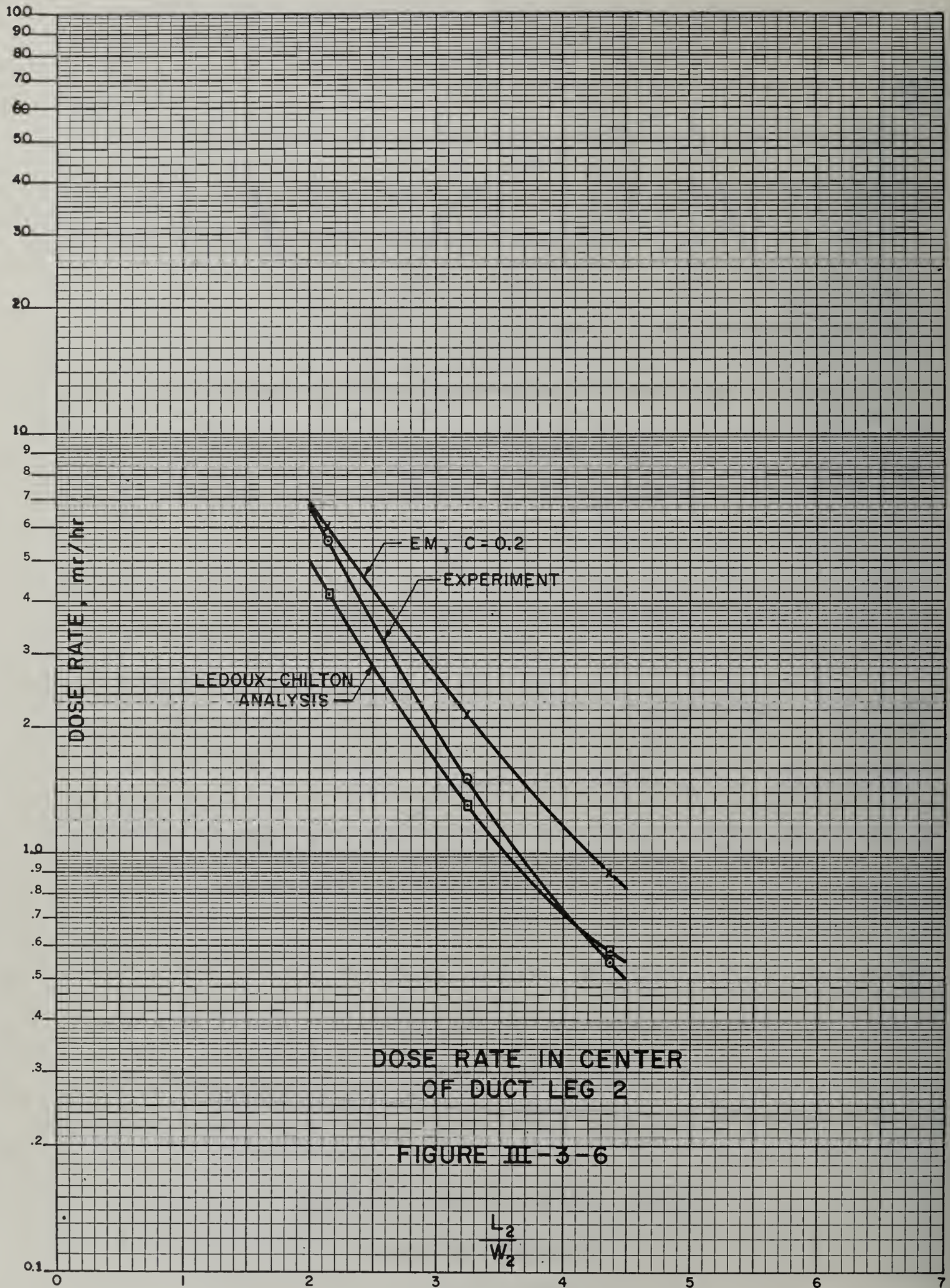

DOSE RATE IN CENTER OF DUCT LEG 2

FIGURE III-3-6

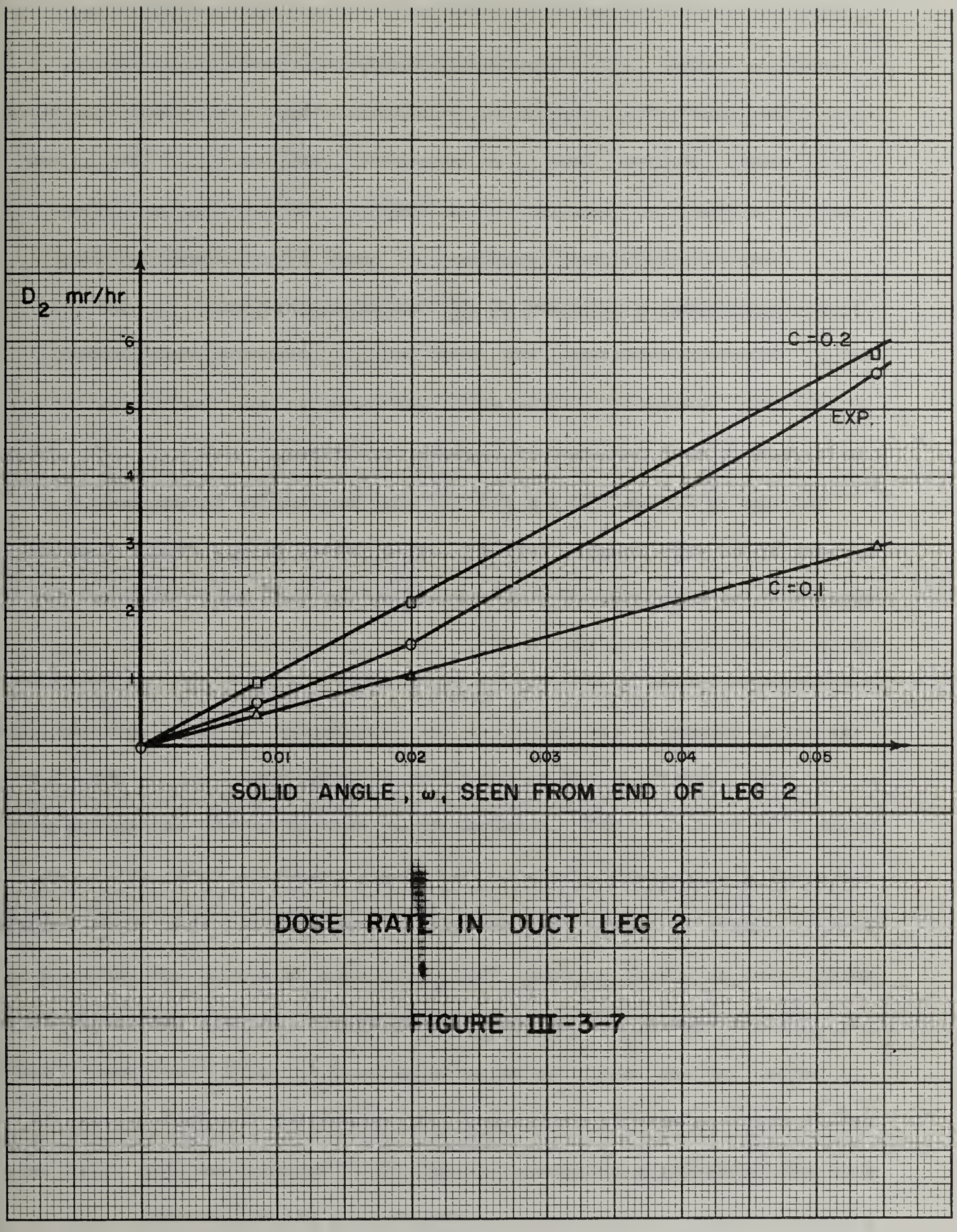

FIGURE III-3-7

j) Summary, discussion, and conclusions. Reasonably good agreement appears to exist between LeDoux-Chilton calculations and experiment, as shown in Figure III-3-6, provided appropriate means are taken to account for the multiple reflection process in the theoretical analysis. The agreement is better for large values of L_2/W , which is consistent with the assumptions inherent in the theory. Considering the appreciable amount of background present, the rough means of determining it, the questionable accuracy of the detection instrument for low energy scattered radiation, the approximation inherent in estimating the multiple-scattering factor and other possible sources of error--the agreement must be considered quite fortuitous.*

As seen in Figure III-3-6 and -7, the Engineering Manual method appears to be very roughly correct, but a factor of 0.2 rather than 0.1 appears to be necessary to give results on the safe side--at least for ducts of this general size.

---

*Editorial comment: The report of this experiment is based upon the work of the 1962 Institute. It is only fair to state that, during both the summers of 1962 and 1963, measurements at the end of the second leg with integrating dosimeters of the 1- and 10-mr. size were made, which gave results generally higher, and definitely more erratic, than those reported herein with dose-rate meters. These dosimeter data were not included in this present report, not so much because they do not fit the theory so well, but rather because the interfering background for such measurements could not be quite so readily estimated. The reason for the dubious results with the integrating chambers is a matter of speculation, but it is very probably related to the ornery nature of such instruments when used in the hot, humid, and dusty environment of a Kansas hilltop in July.

The reduction in dose at the end of the second leg when the lead corner lip was inserted, thus cutting out essentially all the corner lip transmission and scattering effects, is noted as expected in the experimental results, although the amount of the reduction (on the order of 20% for measurements on the axis 3' down the second leg) is somewhat lower than that expected from theoretical considerations (a reduction of 30% on the basis of single-reflection LeDoux-Chilton analysis). The reason for this is believed to be the fact that the lead corner blocks did not fit well, and there were substantial cracks in the lead lip, inadequately filled with small irregular bits of lead. This probably allowed some radiation leakage.

4. Blockhouse Experiment-- Ground Contamination

a) Purpose. To measure the protection afforded by an idealized structure against the radiation from simulated ground fallout contamination, to compare experimental results with theoretical predictions, and to obtain a knowledge of how protection from ground contamination varies within a structure.

b) References and bibliography.

1) "Operation of Tech/Ops Model 539 Duplex Hydraulic Source Circulation System," Technical Operations, Inc., Manual No. TO-B 62-38 (1962).

2) J. F. Batter, et al., "An Experimental Evaluation of Radiation Protection Afforded by a Large Modern Concrete Office Building," Technical Operations, Inc., Report TO-B 56-5 (1959). Also published as Atomic Energy Commission Report CEX-59.1 (1959).

3) J. F. Batter, et al., "Attenuation of Cobalt-60 Radiation Distributed about a Concrete Blockhouse," Technical Operations, Inc., Report TO-B 61-34 (1961).

4) J. F. Batter and A. W. Starbird, "Attenuation of Cobalt-60 Radiation by a Simple Structure with a Basement," Technical Operations, Inc., Report TO-B 61-38 (1961).

5) L. V. Spencer, "Structure Shielding against Fallout Radiation from Nuclear Weapons," National Bureau of Standards Monograph 42 (1962).

6) "Shelter Design and Analysis, Vol. 1, Fallout Protection," Office of Civil Defense Compilation (Revised ed., 1962). (This is a revision of an OCD draft document commonly referred to as the "Engineering Manual.")

7) Fallout Shelter Surveys: "Guide for Architects and Engineers," Office of Civil Defense Document NP-10-2 (1960). (This is commonly referred to as the "Architect-Engineers' Guide.")

8) C. Eisenhauer, "An Engineering Method for Calculating Protection afforded by Structures against Fallout Radiation," National Bureau of Standards Report 7810 (1963).

c) Facilities and apparatus used.

1) Concrete blockhouse, surrounded by level plain, at least out to 160' for one quarter of the perimeter. (See Fig. III-4-1.)

2) 1 cobalt-60 source, about 100 curies in strength, suitable for being pumped through polyethylene tubing.

3) Apparatus associated with the hydraulic pumping system, such as pump and valving assembly, water reservoir tank, lead "pig" for safe storage of source. (See Reference 1.)

4) About 5000 feet of polyetheylene tubing.

5) About 20 each of various sized dosimeter chambers, such as 1-mr., 10-mr., 200-mr., and 2-r.

6) Spotting telescope, 20-power.

d) Background. Analysis of idealized structures is required to bridge the gap between theoretical analysis of simple shielding elements and the analysis of practical structures.

Cobalt-60 is a practical simulant for fallout, especially as used in the pumped source technique (see References 1-4). Theoretical curves are available for cobalt-60, as well as for mixed fission products (see Reference 5). Procedures are available for analysis of structures in the OCD Engineering Manual (Reference 6). These procedures involve certain approximations, idealizations, and simplifications, and experimental confirmation is very desirable.

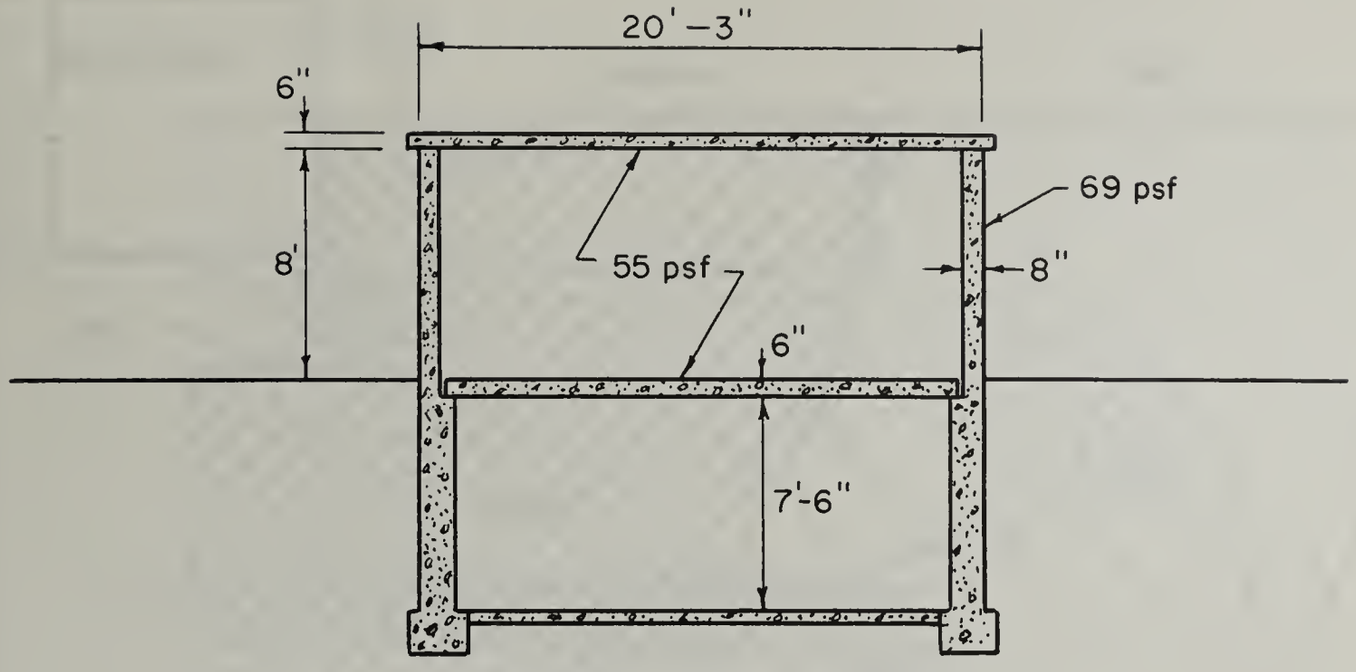

BLOCKHOUSE ELEVATION

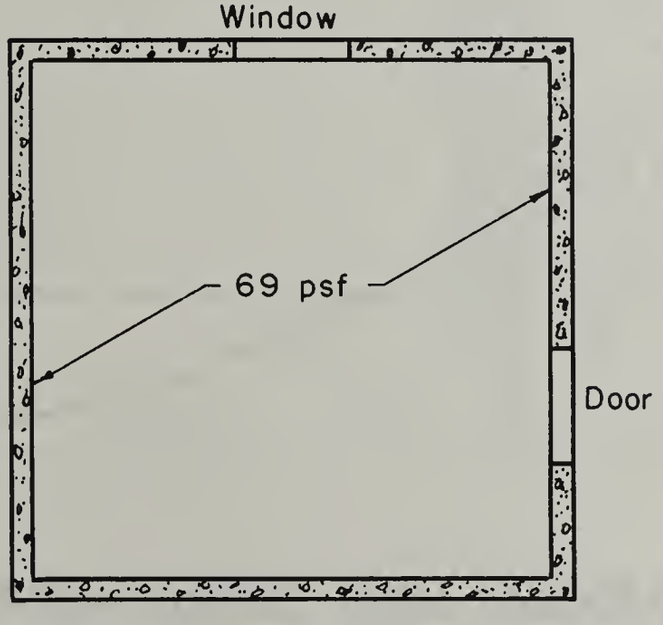

BLOCKHOUSE PLAN

FIGURE III-4-1

240-816 O-67—47

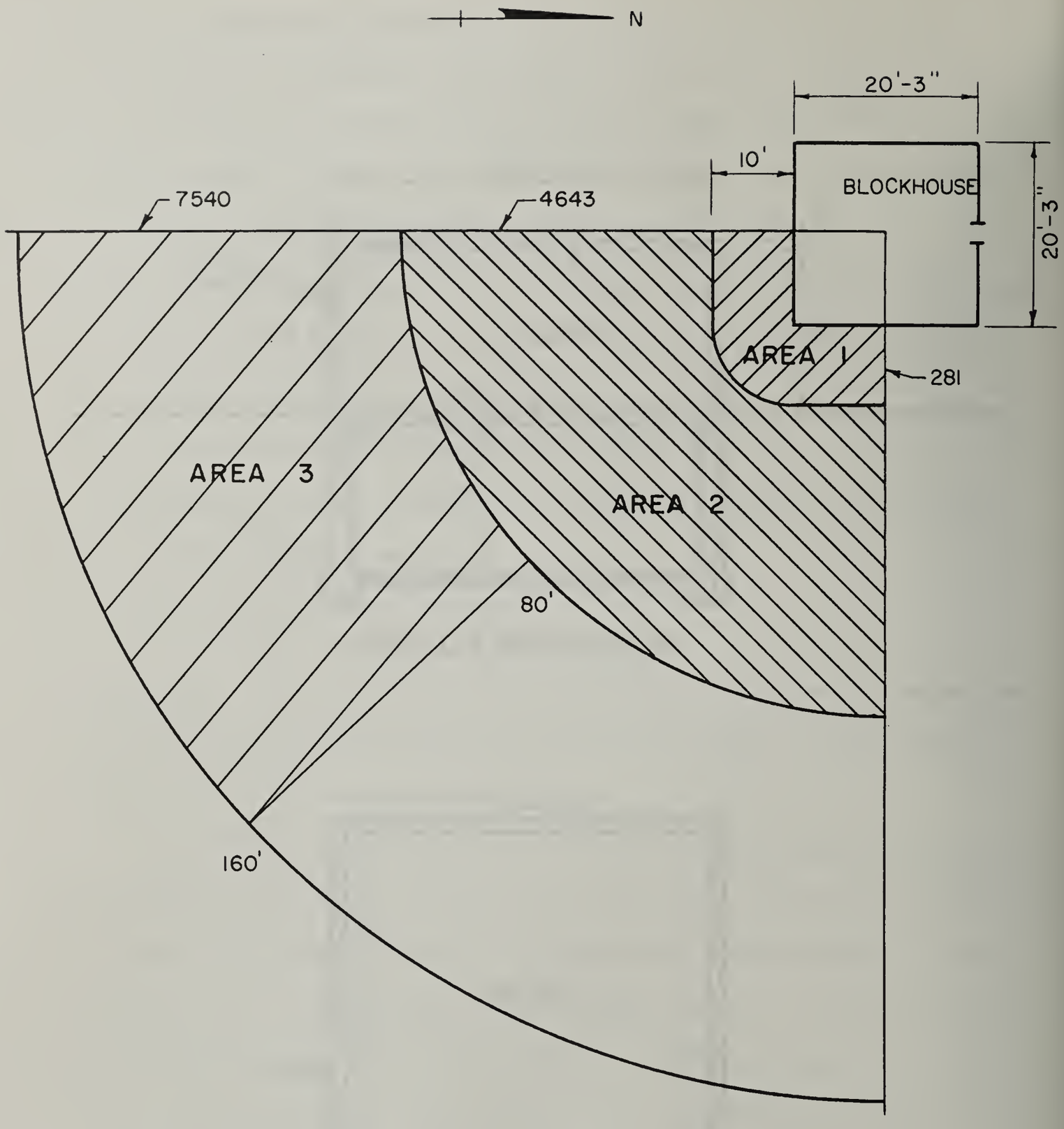

SKETCH OF OVERALL AREA LAYOUT FOR TUBING

FIGURE III-4-2

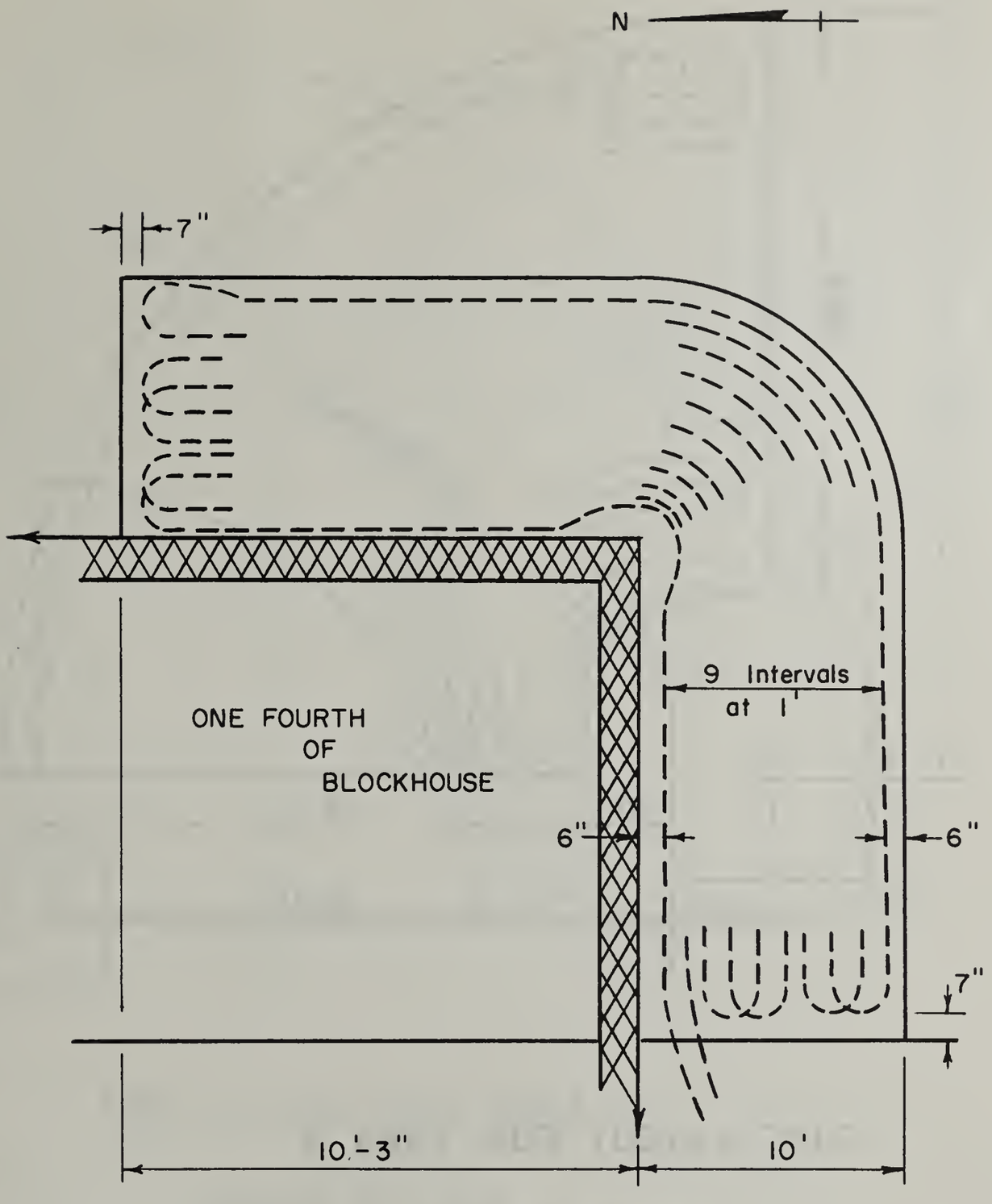

TUBE LAYOUT FOR AREA I

FIGURE III-4-3

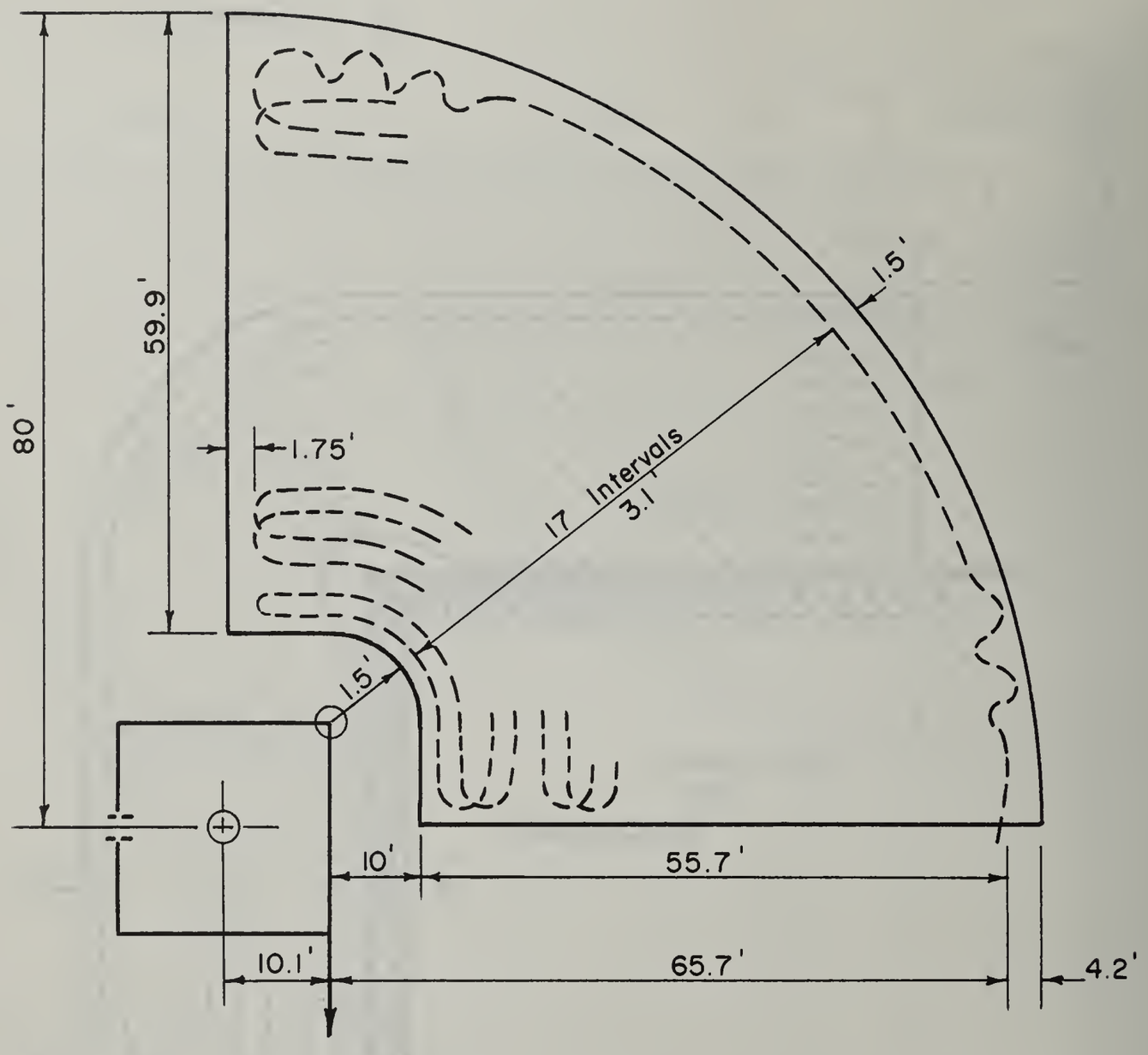

TUBE LAYOUT FOR AREA 2

FIGURE III-4-4

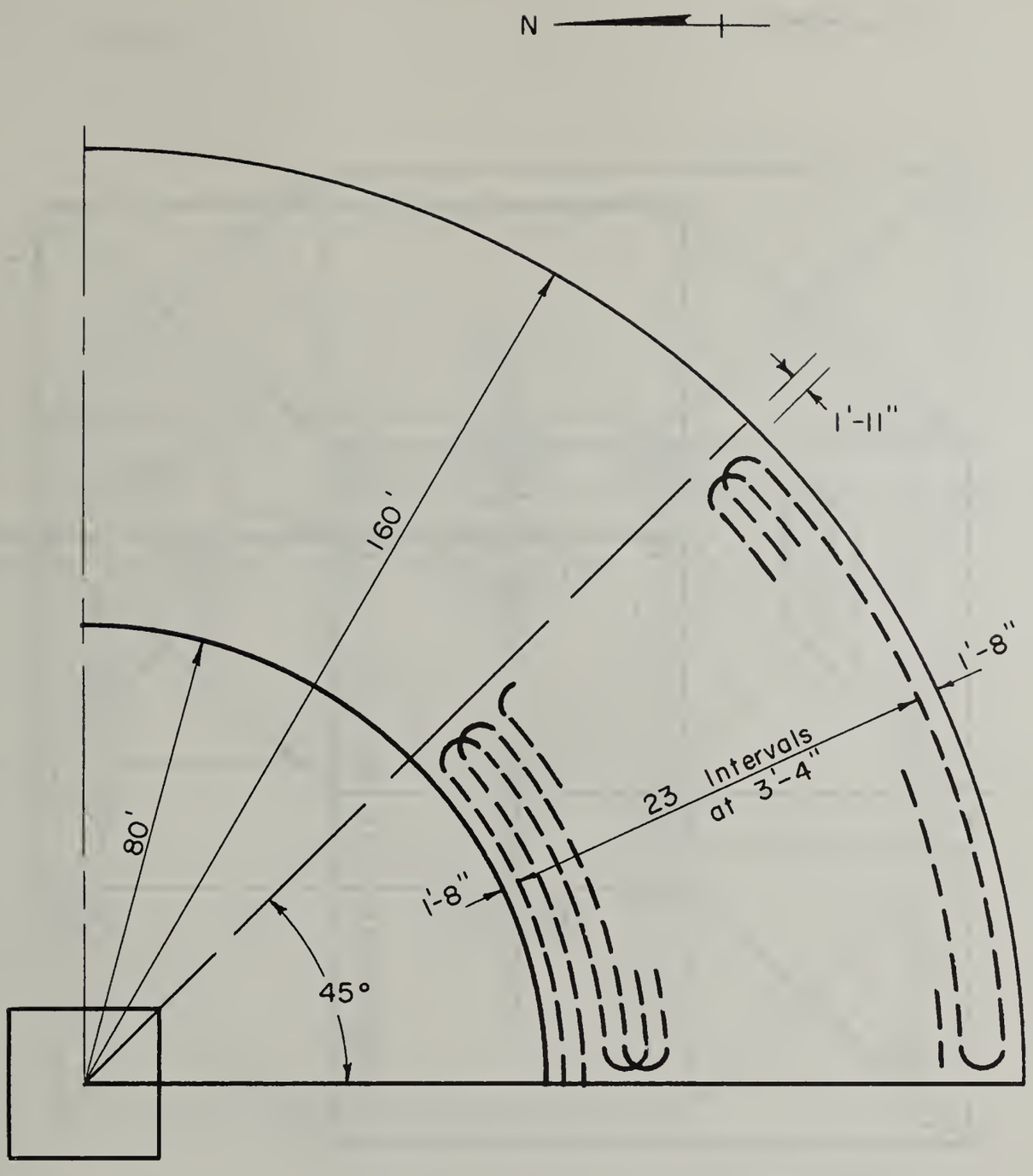

TUBE LAYOUT FOR AREA 3

FIGURE III-4-5

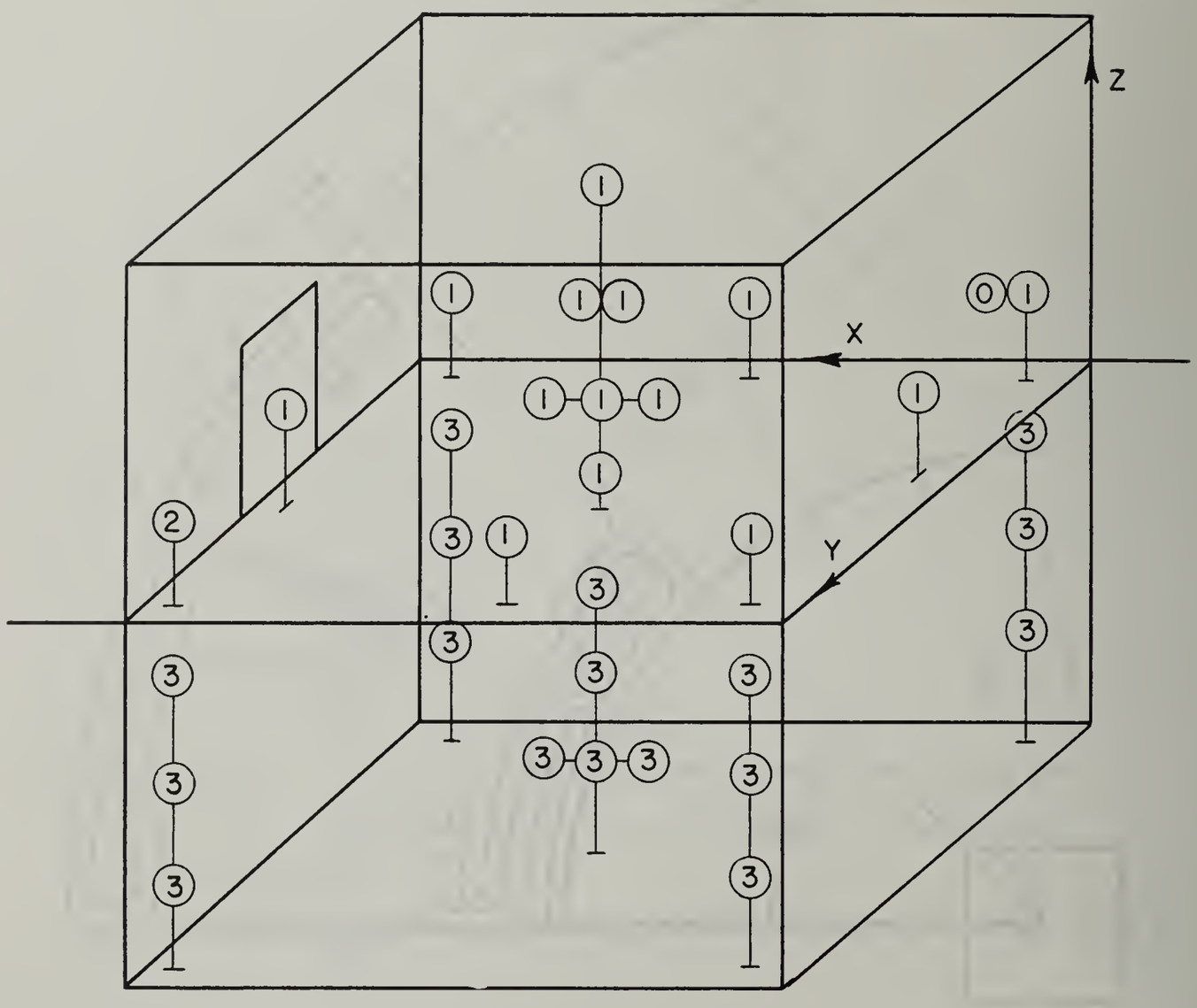

⓪ = 20r

① = 2 r

② = 200 mr

③ = 10 mr

④ = 1 mr

DETECTOR LOCATION FOR AREA 1.

FIGURE III-4-6

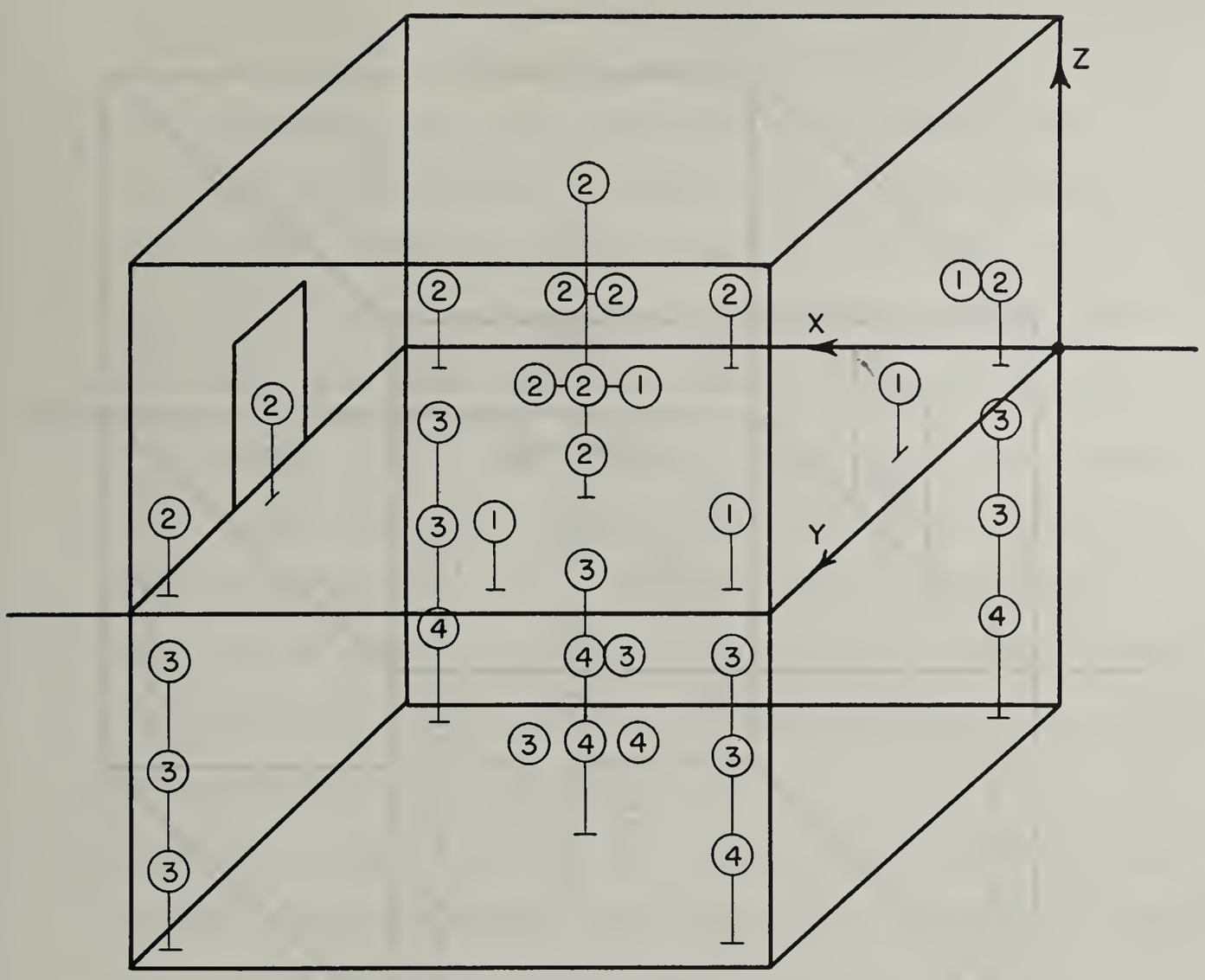

① = 2 r

② = 200 mr

③ = 10 mr

④ = 1 mr

DETECTOR LOCATION FOR AREA 2.

FIGURE III-4-7

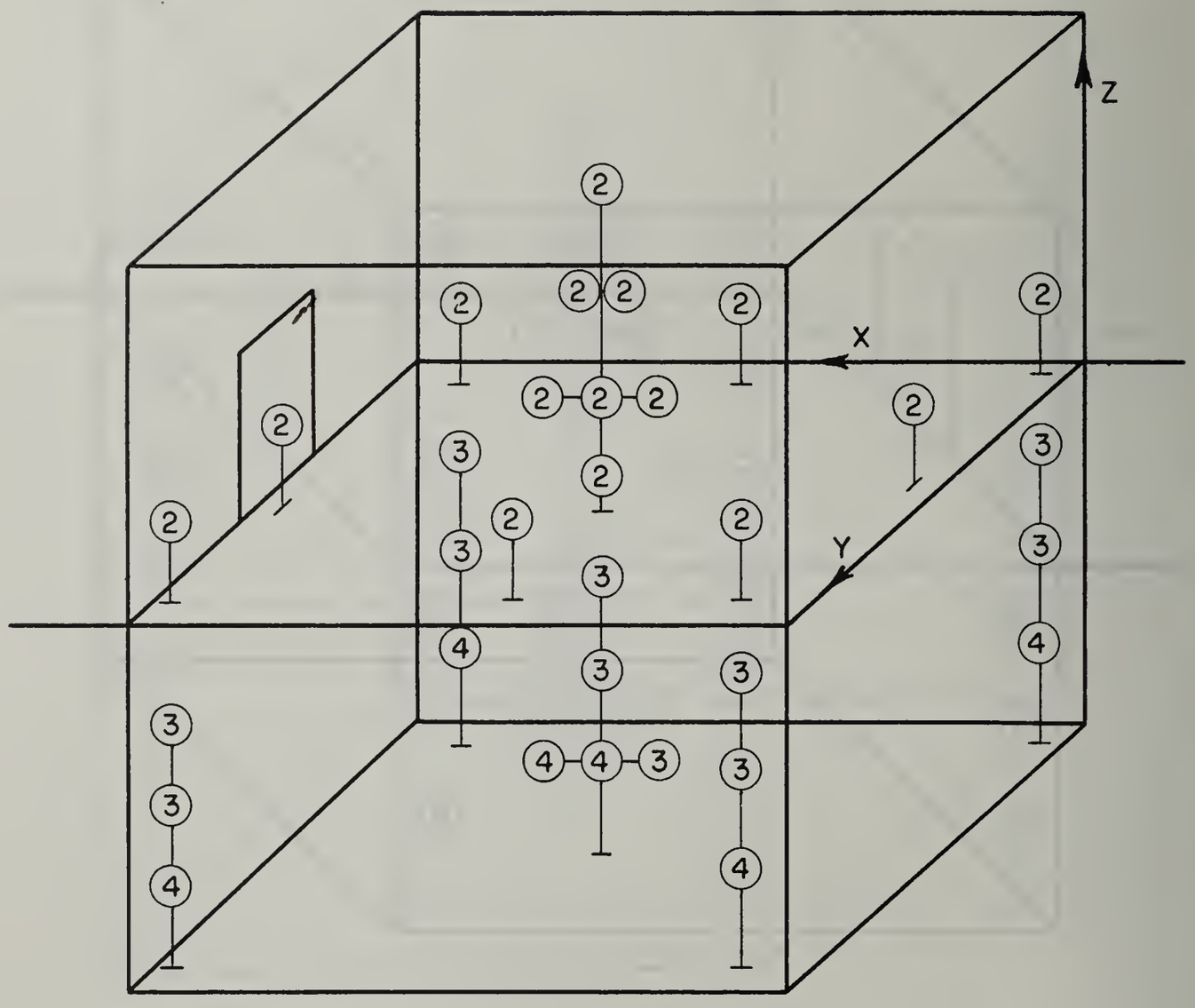

① = 2 r

② = 200 mr

③ = 10 mr

④ = 1 mr

DETECTOR LOCATION FOR AREA 3.

FIGURE III-4-8

e) Procedure.

1) The polyethylene tubing for the pumped source was laid out in each of three areas as shown in Figures III-4-2, III-4-3, III-4-4, and III-4-5, for three runs, made in successive periods.

2) For each of the three runs, dosimeters of appropriate size were charged and placed in the blockhouse to be irradiated from the appropriate source area. The dosimeter locations for irradiations for the three successive runs are as shown in Figures III-4-6, III-4-7, and III-4-8.

3) For each of the three runs, the source was pumped through the tubing at a constant rate of speed, so that, since the tubing in each area was laid out at constant spacing, a uniformly distributed fallout field was simulated. (Operation of the pumped source system, including all safety precautions, is described in detail in Reference 1.) The operation was controlled and observed from a safe distance (about 500 feet).

4) After each run was completed, the dosimeters were recovered and measured. Data was reduced, the "far field" correction was applied, and comparisons were made with theory.

f) Theory.

1) The reduction factor for a point in the middle of the first floor of the blockhouse may be obtained by adapting a method in Spencer's Monograph (Reference 5) which provides the following formula, slightly modified to suit the present case:

$$R_f = (4)\ (0.9)\ W(X,d)\ W_{al}(X,d,\omega) \quad ,$$

where

$$W_{al}(X,d,\omega) = b(X)\ W_a(d,\omega) + 1.15\ (1 - b(X))\ P_a^s(\infty, \omega) \quad ,$$

and

$$b(X) = P^{(o)}(X)/P(X) \quad .$$

In the above expressions, W(X,d) represents the barrier factor for a wall; $W_{al}(X,d,\omega)$ represents the geometry factor, split into two parts in proportion to the amount which penetrates in unscattered fashion, (b(X)), and that which is the scattered component, (1 - b(X)). The factor 4 in the above expression takes care of the four walls.

The Engineering Manual (Reference 6) provides a formula which is somewhat different in detail, but in principle is the same approach as that previously given:

$$R_f = B_w(X,d)\ G_g \ ,$$

where

$$G_g = (G_s(\omega_l) + G_s(\omega_u))\ S_w\ E + (G_d(\omega_l) + G_a(\omega_u))\ (1 - S_w) \ .$$

In the Architect-Engineers' Guide (Reference 7), all factors are combined so that the reduction factor for the middle of the first floor against ground contamination is obtained from a single graph with wall thickness and floor area as arguments. For the basement center, a similar graph is provided, with an additional chart to give the attenuation factor for the basement ceiling.

For a detector position in the middle of the basement, the Engineering Manual provides the following formulas:

$$R_f = B_w B'_o\ G_g \ ,$$

where

$$G_g = (G_s(\omega'_u) - G_s(\omega'_l))\ S_w E + (G_a(\omega'_u) - G_a(\omega'_l))\ (1 - S_w) \ .$$

It might be noted that the data given in the Engineering Manual and the Architect-Engineers' Guide are for fallout radiation 1.12 hours after fission, whereas the experiment reported on herein uses cobalt-60. However, a comparison of the fundamental curves in

Spencer's Monograph upon which the information in the Manual and the Guide is based indicates little variation between the fallout data and the equivalent data for cobalt-60, at least with respect to those pertinent to the formulas displayed above. Consequently, it is adequate to compare theoretical values based on the fallout attenuation computations with experimental values based on the use of cobalt-60 as a simulant.

2) In determining the experimental values of the reduction factor, one should, after correcting the data by means of calibration charts provided, account for the fact that the simulated field did not completely surround the structure but only a quarter(or an eighth)of the perimeter was surrounded. This is readily done, for example, by multiplying the center values by four. Readings for eccentric positions can be obtained by adding readings for corresponding positions in the four quarters of the structure. In case the field only went an eighth of the way around the structure, the sum of the four values must be multiplied by two.

After this step, the contributions from the three field areas must be added together for the same detector positions. This however, leaves unconsidered the possible contribution beyond the limits of the finite fields actually covered with the simulated fallout. This so-called "far field" contribution can be estimated in the following way. For every detector point, one would expect the ratio of the "far field" contribution to the contribution from Area 3 to be almost the same. We can readily estimate this value for the center of the blockhouse, 3' above the plane on contamination, and this

factor will be used as a multiplier of the Area 3 contribution, in each case, to estimate the "far field." The factor is readily seen to be:

$$C.F. = \frac{\int_{160.03}^{\infty} B(\mu r)\, e^{\mu r}\ (1/r)\, dr}{\int_{80.06}^{160.03} B(\mu r)\, e^{-\mu r}\ (1/r)\, dr}$$

where μ is the total attenuation coefficient for cobalt-60 gamma rays in units of $ft.^{-1}$. In this expression, $B(\mu r)$ can be approximated by the following formula (Reference 8):

$$B(\mu r) = 1.11 + .529\mu r \ ,$$

which is reasonably valid over the distances involved in the above expression. (Although the above formula for B is not expected to be very accurate beyond a thousand feet, the contribution to the integral beyond this distance is small, and the error is minor in using it.)

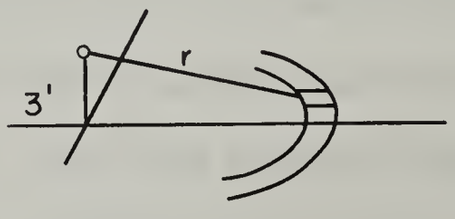

Figure III-4-9

g). Preliminary calculations.

1) Theoretical values at first floor center position, from Spencer's Monograph.

$\epsilon = 0.4$, $\eta = 1.0$, $\omega = 0.17$

First floor above ground at 4' level -- center:

$D/D_o = 0.9\ W(x,d)\ W_{al}(x,d,\omega)4$

where $W(x,d) = 0.1$

$W_{al}(x,d,\omega) = b(x)\ W_a(d,\omega) + 1.15\ (1-b(x))\ P_a^s(\infty,\omega)$

Therefore,

$D'D_o = (0.9)\ (0.1)\ (0.5)\ (4.0) = \underline{0.18}$

2) Theoretical values at center positions, from Engineering Manual.

	ω_u	ω_l	$\omega_{u'}$	$\omega_{l'}$
ϵ	1	1	1	1
η	0.53	0.32	1.3	0.5
ω	0.58	0.73	0.24	0.6
G_d	-	0.63	-	-
G_a	0.080	-	0.095	0.078
G_s	0.345	0.262	0.45	0.335

$B_w = 0.18$

$S_w = 0.67$

$B'_o = 0.06$

$E = 1.41$

First floor at 3' level--center:

$$R_f = \left\{(G_s(\omega_l) + G_s(\omega_u))\ S_w E + (G_d(\omega_l) + G_a(\omega_u))\ (1 - S_w)\right\} B_e$$

$R_f = \underline{0.145}$

Basement at the 3' level--center:

$$R_f = \left\{(G_s(\omega_{u'}) - G_s(\omega_{l'}))\ S_w E + (G_a(\omega_{u'}) - G_a(\omega_{l'})\ (1 - S_w)\right\} B_e B'_o$$

$R_f = \underline{0.001}$

3) Theoretical values at center positions, from Architect-Engineers Guide.

On first floor, $X_w = 69$ psf and area = 400 ft.^{2};

therefore $R_f = \underline{0.16}$, from Chart 3.

For basement, same data; and $X_o' = 55$ psf; therefore, $R_f = .015 \times .07 = \underline{.001}$, from Charts 4 and 1.

4) Theoretical values at middle of wall, from Engineering Manual.

Theoretical dose against wall, 1st Floor, 3' level, from Engineering Manual.

$R_{f1} = \frac{1}{2} G(\omega = 1) \cdot B_w = 0.09$

	ω_u	ω_l
L	37.8	37.8
W	18.9	18.9
ϵ	0.5	0.5
Z	5.0	3.0
η	.265	.159
ω	.65	0.78
G_s	0.31	0.23
G_a	.074	--
G_d	--	.59

$S_w = 0.67$

$(1 - S_w) = 0.33$

$E = 1.34$

$B_w = .18$

$G_s = (G_s(\omega_u) + G_s(\omega_l)) S_w E = .485$

$G_D = (G_a(\omega_u) + G_d(\omega_l)) (1 - S_w) = .219$

$G_g = G_s + G_D = .704$

$G_g/2$ = actual situation, since G_g is based on a structure of double size,

Therefore: $R_{f2} = \frac{1}{2} \times 4.707 \times .18 = 0.0634$

$R_f = R_{f1} + R_{f2} = .09 + .063 = \underline{.153}$

5) Calculation of the "far field" correction factor.

$\mu = 1/525$

$\mu \cdot 80.06 = .1525$

$\mu \cdot 160.03 = .3048$

$$\int_{80.06}^{\infty} (1.11 + .529\ \mu r)\ e^{-\mu r}\ \frac{dr}{r}$$

$$= 1.11\ E_1(.1525) + .529\ e^{-.1525}$$

$$= 2.064$$

$$\int_{160.03}^{\infty} (1.11 + .529\ \mu r)\ e^{-\mu r}\ \frac{dr}{r}$$

$$= 1.11\ E_1(.3051) + .529\ e^{-.3051}$$

$$= 1.382$$

$$C.F. = \frac{1.382}{2.064 - 1.382} = 2.03$$

h) Data and data reduction.

Area 1--Ground Floor (First Run)

Instrument Number	Meter Size	Position x, y	Position z	Zero Reading	Corrected Reading	Dose (r.)	Normalized Dose (r.)
0060	2r	18, 10	3	0	27	.306	2.27
148	200mr	18, 18	3	3	140	.140	1.04
0048	2r	10, 18	3	0	24	.275	2.04
0050	"	2, 18	3	0	18	.2	1.49
0054	"	2, 10	3	0	86	.99	7.36
0051	"	2, 2	3	0	180	2.065	15.34
143	20r	2,2	3	0	2.1	2.1	15.60
0047	2r	10, 2	3	0	82	.94	6.98
0045	"	18, 2	3	0	24	.275	2.04
0059	"	10, 10	0	0	57	.650	4.83
0053	"	10, 10	3	0	56	.640	4.76
0055	"	10, 10	3	0	50	.575	4.27
0056	"	10, 10	3	0	48	.550	4.09
0063	"	10, 10	6	0	49	.560	4.16
0064	"	10, 10	6	0	44	.5	3.72
0062	"	10, 10	8	0	41	.470	3.49

Time of run = 22 minutes

$$R = \frac{A}{C\ T} = D\ \frac{281}{103 \times .367} = 7.43\ D$$

Where

A = 281 sq. ft.

C = 103 curies

T = 22 min. = .367 hr.

D = Corrected dose readings.

R = Normalized values, (r/hr.) / (curies/sq. ft.)

Area 1--Ground Floor (Second Run)

Instrument Number	Meter Size	Position x y	Position z	Zero Reading	Corrected Reading	Dose (r.)	Normalized Dose (r.)
0060	2r	18, 10	3	0	29	.330	1.70
77	200mr	18, 18	3	0	210	.21	1.08
0048	2r	10, 18	3	0	31	.35	1.81
0053	"	2, 18	3	0	29	.33	1.70
0054	"	2, 10	3	0	130	1.49	7.69
0057	"	2, 2	3	0	off scale	2^{+}(?)	10.3^{+}(?)
144	20r	2, 2	3	0.2	2.7	2.7	13.93
0045	2r	10, 2	3	0	119	1.365	7.04
0055	"	18, 2	3	0	25	.29	1.50
0056	"	10, 10	0	0	60	.68	3.51
0062	"	10, 10	3	0	68	.775	4.00
0063	"	10, 10	3	0	76	.865	4.46
0064	"	10, 10	3	0	68	.775	4.00
0047	"	10, 10	6	0	67	.77	3.97
0059	"	10, 10	6	0	68	.775	4.00
0051	"	10, 10	8	0	72	.82	4.23

Time of run = 31 minutes 42 sec.

$$R = D\frac{A}{CT} = D\ \frac{281}{103 \times .5283} = 5.16\ D$$

Where

A = 281 sq. ft.

C = 103 curies

T = .5283 hrs.

240-816 O-67--48

Area 1--Basement

Instrument Number	Meter Size	Position x y	Position z	Zero Reading	Corrected Reading	Dose (mr.)	Normalized Dose (mr.)
121	200	2, 2	7.5	8	53	53	273
9	10	2, 2	7.5	0	off scale	?	?
149	200	2, 2	6	22	22	22	114
14	10	2, 2	6	0	off scale	?	?
96	200	2, 2	3	1	11	11	56.8
4	10	2, 2	3	0	137	14.1	72.8
111	200	18, 2	7.5	8	2	2	10.3
23	10	18, 2	7.5	0	56	5.7	29.4
120	200	18, 2	6	8	3	3	15.5
12	10	18, 2	6	0	48	4.9	25.3
151	200	18, 2	3	1	5	5	25.8
27	10	18, 2	3	0	38	3.9	20.1
83	200	18, 18	7.5	2	7	7	36.1
16	10	18, 18	7.5	0	33	3.35	17.3
110	200	18, 18	6	8	1	1	5.2
6	10	18, 18	6	0	29	2.95	15.2
152	200	18, 18	3	8	3	3	15.5
20	10	18, 18	3	0	27	2.75	14.2
112	200	2, 18	7.5	5	5	5	25.8
24	10	2, 18	7.5	0	off scale	?	?
150	200	2, 18	6	3	3	3	15.5
19	10	2, 18	6	0	54	5.5	28.4
93	200	2, 18	3	1	2	2	10.3
18	10	2, 18	3	0	31	3.16	16.3

Instrument Number	Meter Size	Position x y	Position z	Zero Reading	Corrected Reading	Dose (mr.)	Normalized Dose (mr.)
84	200	10, 10	7.5	9	3	3	15.5
5	10	10, 10	7.5	0	81	8.25	42.6
148	200	10, 10	6	4	12	12	55.1
8	10	10, 10	6	0	136	12.9	66.6
89	200	10, 10	3	3	11	11	56.8
25	10	10, 10	3	0	150	15.5	80.0
95	200	10, 10	3	9	9	9	46.4
87	200	10, 10	3	1	9	9	46.4
26	10	10, 10	3	0	144	14.8	76.4
11	10	10, 10	3	0	129	13.2	68.1

R = 5.16 D, as for 1st Floor

Area 2--Ground Floor

Instrument Number	Meter Size	Position x y	Position z	Zero Reading	Reading	Dose (mr.)	Normalized Dose (mr.)
089	200mr	18, 10	3	3	59	.059	4.07
120	"	18, 18	3	9	53	.053	3.65
0054	2r	10, 18	3	0	11	.110	7.58
0060	"	2, 18	3	0	12	.125	8.61
0058	"	2, 10	3	0	16	.180	12.40
152	200mr	2, 2	3	4	off scale 218	.218	15.02
0063	2r	2, 2	3	0	14	.160	11.02
148	200mr	10, 2	3	3	124	.124	8.54
095	"	18, 2	3	0	53	.053	3.65
127	"	10, 10	0	4	79	.079	5.44
084	"	10, 10	3	7	96	.096	6.61
111	"	10, 10	3	1	96	.096	6.61
0051	2r	10, 10	3	0	11	.110	7.58
149	200mr	10, 10	6	2	95	.095	6.55
109	"	10, 10	6	2	104	.104	7.17
083	"	10, 10	8	5	92	.092	6.34

Time of run = 39 minutes 15 sec.

$$R = D\frac{A}{CT} = D\ \frac{4643}{103 \times .654} = 68.9\ D$$

Where

A = 4643 sq. ft.

C = 103 curies

T = .654 hrs..

Area 2--Basement

Instrument Number	Meter Size	Position x y	Position z	Reading	Dose (mr.)	Normalized (mr.)
42	10	2, 2	7.5	41	4.20	289
3	10	2, 2	6	17	.75	51.7
4	1	2, 2	3	30	.49	33.8
12	10	18, 2	7.5	15	1.55	106.8
18	10	18, 2	6	5	.53	36.5
39	1	18, 2	3	30	.49	33.8
8	10	18, 18	7.5	16	1.65	113.7
6	10	18, 18	6	7	.73	50.3
29	1	18, 18	3	27	.44	30.3
20	10	2, 18	7.5	11	1.15	79.2
16	10	2, 18	6	5	.53	36.5
41	1	2, 18	3	27	.44	30.3
9	10	10, 10	7.5	13	1.35	93.0
5	10	10, 10	6	12	1.23	84.7
30	1	10, 10	6	76	1.25	86.1
23	10	10, 10	3	16	1.66	114
28	1	10, 10	3	71	1.17	80.6
31	1	10, 10	3	71	1.17	80.6

R = 68.9 D, as for 1st floor.

Area 3--Ground Floor

Instrument Number	Meter Size	Position x y	Position z	Zero Reading	Corrected Reading	Dose (r.)	Normalized Dose (r.)
112	200mr	18, 10	3	5	16	.016	1.23
84	"	18, 18	3	1	18	.018	1.38
095	"	10, 18	3	5	19	.019	1.46
121	"	2, 18	3	0	30	.03	2.30
089	"	2, 18	3	3	35	.035	2.69
149	"	2, 2	3	2	30	.03	2.30
148	"	10, 2	3	7	13	.013	1.00
083	"	20, 2	3	1	8	.008	0.61
111	"	10, 10	0	3	9	.009	0.69
109	"	10, 10	3	3	24	.024	1.84
147	"	10, 10	3	0	140	.14	10.75
096	"	10, 10	3	2	22	.022	1.69
152	"	10, 10	6	9	23	.023	1.77
120	"	10, 10	6	5	27	.027	2.07
127	"	10, 10	8	9	22	.022	1.69

Time of run = 57 minutes 11 sec.

$$R = D \frac{A}{CT} = \frac{D \times 7540}{103 \times .953} = 76.8\ D$$

Where

A = 7540 sq. ft.

C = 103 curies

T = .953 hr.

Area 3-- Basement

Instrument Number	Meter Size	Position x y	Position z	Reading	Dose (mr)	Normalized Dose (mr)
16	10	2, 2	7.5	3	.33	25.3
4	10	2, 2	6	6	.64	49.2
41	1	2, 2	3	5	.08	6.1
8	10	18, 2	7.5	off scale	?	?
3	10	18, 2	6	5	.54	41.5
31	1	18, 2	3	9	.15	11.5
18	10	18, 18	7.5	2.8	.30	23.0
9	10	18, 18	6	4	.43	33.0
30	1	18, 18	3	13	.21	16.1
20	10	2, 18	7.5	3	.33	25.3
5	10	2, 18	6	4	.43	33.0
39	1	2, 18	3	6	.10	7.7
6	10	10, 10	7.5	7	.73	56.1
23	10	10, 10	6	9	.95	73.0
12	10	10, 10	3	10	1.05	80.6
29	1	10, 10	3	16	.26	20.0
28	1	10, 10	3	17	.28	21.5

R = 76.8 D, as for 1st Floor.

i) Results. Experimental reduction factors are listed herein, as computed from the foregoing data. It is pointed out that a certain amount of smoothing and selection of the data were necessary, since some of the data appeared quite erratic, especially in the basement. The resulting values, since they contain this judgment factor, are not entirely objectively arrived at. However, it is believed that they are roughly valid; and evidence of this may be seen in the degree of internal consistency among the separately arrived at computations for results from the three separate areas.

1) Experimental data (corrected to full circle source) for first floor, and normalized to a source strength of 1 curie/sq. ft. for 1 hour.

Location	Area 1 (r.)	Area 2 (r.)	Area 3 (r.)	Far field (r.)	Total (r.)	R_f
Ht. 0'6" Center	14.0	21.6	5.5	11.2	52.3	.107
Ht. 3' Center	16.0	26.3	14.2	28.8	85.3	.174
Ht. 6' Center	16.0	27.4	15.4	31.3	90.1	.184
Ht. 8' Center	16.9	25.2	13.5	27.4	83.0	.169
Ht. 3' Corner	18.2	30.8	13.2	26.8	89.0	.182
Ht. 3' Side	18.2	32.3	12.8	26.0	89.3	.182

In this table, the values of R_f are obtained by dividing the total normalized dose to the reference dose in the open, under the same conditions, which amounts to 490 r./hr.

2) Experimental data (corrected to full circle source) for basement, and normalized to a source strength of 1 curie/sq. ft. for 1 hour.

Location	Area 1 (mr.)	Area 2 (mr.)	Area 3 (mr.)	Far Field (mr.)	Total (mr.)	R_f
Ht. 3' Center	250	325	172	349	1096	.0022
Ht. 6' Center	256	349	585	1188	2378	.0049
Ht. 7.5' Center	281	377	449	911	2018	.0041
Ht. 3' Corner	111	129	63	128	431	.00088
Ht. 6' Corner	182	177	314	637	1310	.0027
Ht. 7.5' Corner	345	595	198	402	1540	.0031

j) Summary, discussion, and conclusions. The comparison between experimental results and the predictions of various theoretical approaches is indicated in the following table.

Position	Theoretical			Experimental
	Spencer's Monograph	Engineering Manual	Arch.-Eng. Guide	
		First Floor		
Ht. 3' Center		.145	.16	.174
Ht. 4' Center	.18			
Ht. 6' Center				.184
Ht. 3' Side Wall		.153		.182
		Basement		
Ht. 3' Center		.001	.001	.0022

It is seen that the theoretical and experimental values are within fairly reasonable agreement, considering the approximations inherent in the theoretical approach as well as the scatter in the experimental results.

There is one important exception, however, and that is in the basement. Here it appears that the experimental reduction factors are on the order of twice the theoretical. This is consistent with a remark by Eisenhauer (Reference 8) to the same effect, and therefore it is believed to be a genuine discrepancy and a failure of the theoretical prediction methods for such a case.

It is interesting to note from the results that the dose-rates on the first floor vary very little from point to point. What appears to be a low value at the height of 6" above the floor is unquestionably a peculiarity of the experimental site, in that an appreciable portion of Area 3 contribution is missing because of the fact that the ground is not quite level, and that part which skims close to the ground is shielded out by the ground contours. This affects the far field estimate also, since it is based on Area 3 measurements.

In the basement, the situation is different. The dose-rate increases with height, at least up to a point a few feet from the first floor slab. In this region, it appears to be about constant or even decrease slightly with height. The corner has a much smaller dose-rate than the center, and it is obviously the safest place in the structure.

The following suggestions are made with a view toward improving the quality of the data in future experiments of this type.

1) The basement collects rain water and is exceedingly damp. This causes serious problem with dosimeter leakage. Measures should be taken to prevent water from entering the basement of the blockhouse, and to reduce the amount of moisture in the air which naturally tends to be present.

2) Because of the high intensity of the source, it is not very suitable for instrument calibration, and thus the instruments and source are not compared against one another. This requires that both source and the instrumental calibration be very carefully checked to provide an absolute, rather than a relative, calibration; or else some means of checking the calibration of one against the other should be devised.

Editorial note added in proof: Mr. Russel O. Lyday, Jr., in reviewing these experiments, has pointed out that a certain amount of self-shielding of the pumped source occurs. Aside from a small amount of intrinsic self-absorption, two other factors may be significant: one is the absorption caused by adjacent tubing (3/8" O.D.) in the field for radiation emitted in a direction which almost grazes the ground; the other is the greater self-absorption occasioned when the source (cylindrical in shape) is traveling in a radial direction from the detector. These factors and the correction for them are discussed in Technical Operations, Inc., Report TO-B 62-58, "The Effect of Limited Strips of Contamination on the Dose Rate in a Multistory Windowless Building," by J. F. Batter, A. W. Starbird, and N. York (1962). Precise estimates of these correction factors are probably best obtained by experiment; however approximate estimates can be fairly easily obtained. Improved accuracy in these experiments, especially for the contributions from the more remote fields, could be obtained by use of such a correction, even though estimated. It must be noted, however, that the percentage of time for radial travel of the source is very small in case of the KSU Summer Institute experiments, contrasted with a more substantial proportion of time for the Technical Operations, Inc., experiments. Also, the degree of absorption to be considered by adjacent tubing depends upon geometric factors such as tube-spacing, building height, and source distance. Comparison of the KSU experimental configuration with that of Technical Operations, Inc., and review of their correction factors seems to imply that for the KSU experiments, the correction required in overall results for these self-shielding factors is of the order of or less than ten percent,

except for dosimeters placed near floor level. The low results in this experiment for the dosimeter at 0'6" above the first floor level are certainly due in part to these factors.

5. Model Experiment

a) Purpose. To carry out a shielding experiment on a scaled model basis; to compare results with similar results on a full-scale prototype, thereby determining the efficiency of this approach.

b) References and bibliography.

1) A. W. Starbird, J. F. Batter, and H. A. Mehlhorn, "Modeling Techniques as Applied to Fallout Simulation on Residential-type Structures, and Some Preliminary Results," Technical Operations, Inc., Report TO-B 61-35 (1961).

2) P. M. Frazier, C. R. Buchanan, and G. W. Morgan, "Radiation Safety in Industrial Radiography with Radioisotopes," U. S. Atomic Energy Commission Report AECU-2967 (1954).

3) R. E. Rexroad and M. A. Schmoke, "Scattered Radiation and Free Field Dose Rates from Distributed Cobalt-60 and Cesium-137 Sources," Nuclear Defense Laboratory Report NDL-TR-2 (1960).

4) J. Batter, "Cobalt and Iridium Buildup Factors Near the Ground/Air Interface," Trans. of Amer. Nucl. Soc. 6, No. 1, 198 (1963).

c) Facilities and apparatus used.

1) Steel model of blockhouse, one-twelfth full-scale, with walls, roof and floor scaled to approximately the same mass per unit area as the concrete blockhouse of Experiment No. 4 of this series. (See Figure III-5-1.)

2) Cobalt-60 gamma source, 9.1 curies (± 5%).

3) Motor, pump, hose, and associated equipment necessary to circulate the source over the ground contamination area which simulates that designated area 3 in Experiment No. 4. (See Figure III-5-2.)

4) Fourteen (14) pen-type pocket dosimeters of 200-mr. size.

5) Nine (9) 10-mr. dosimeters.

6) Charger-reader.

7) Two stopwatches.

d) Background. Considerations of time and expense make scale-model experimentation highly desirable in predicting radiations levels within proposed new structures which might be subjected to fallout gamma radiation. Contributing to the attractiveness of model studies, in these considerations, are the extent of contaminated field and the strength sources which would be required with full-scale buildings.

While it is to be expected that the first requirement in similitude is the true scaling of overall dimensions, considerable importance must be assigned to the maintenance of similarity in gamma ray behavior. The model roof, walls, partitions, and floors should exhibit the same scattering, absorption, and buildup as shown by corresponding sections of the prototype.

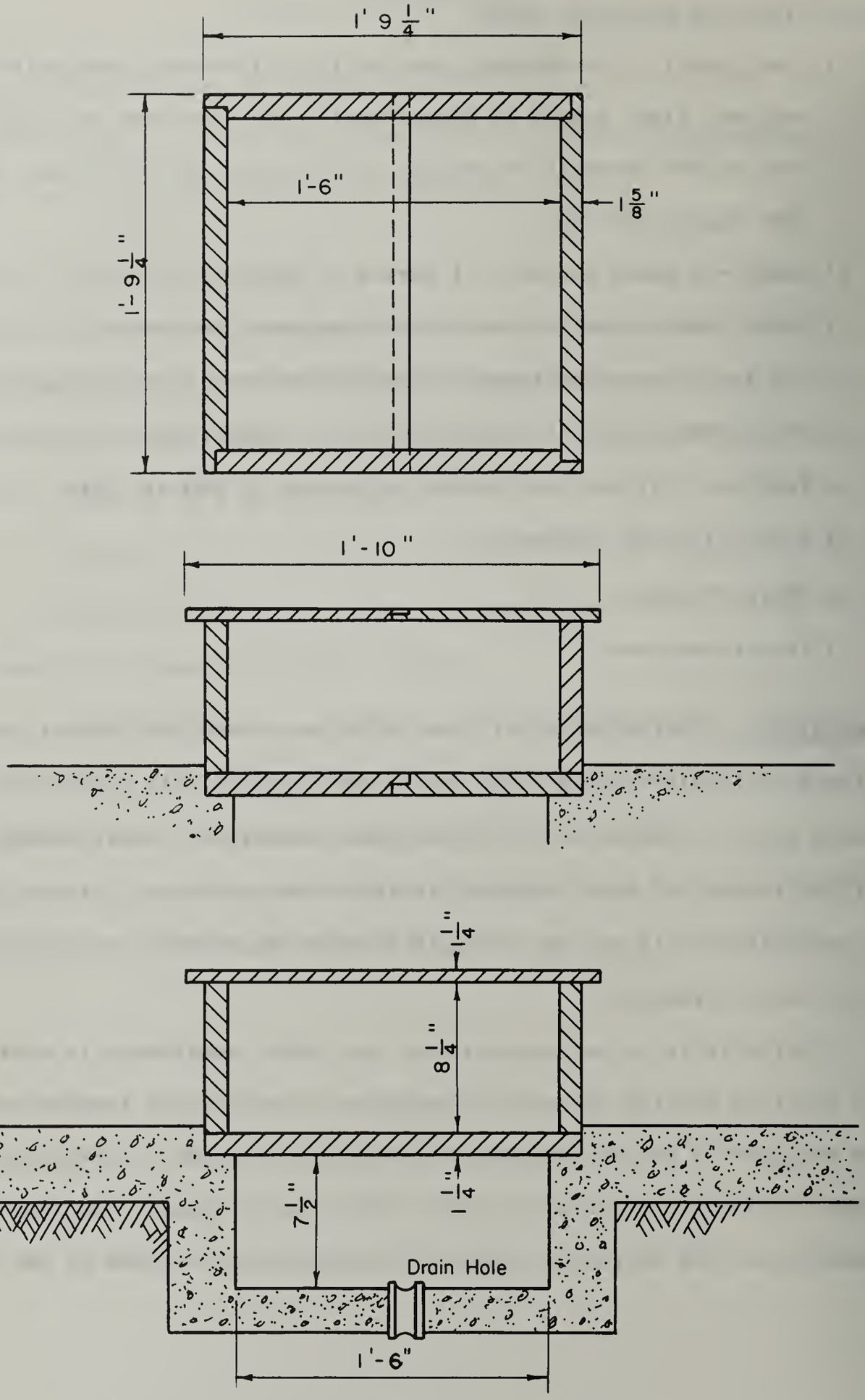

GENERAL ARRANGEMENT OF MODEL
FIGURE III-5-1

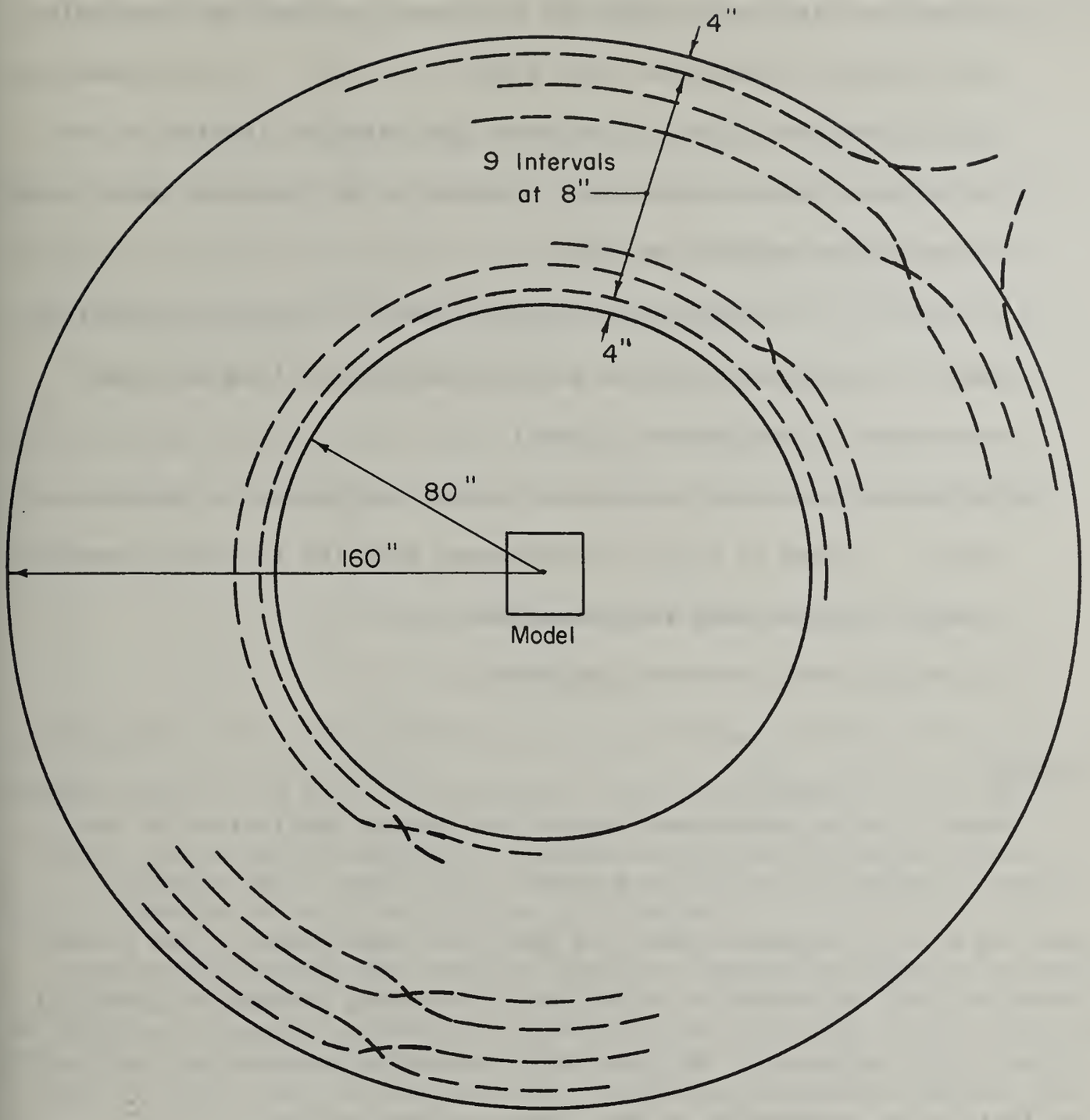

TUBING LAYOUT AROUND MODEL STRUCTURE FOR MODEL AND COMPARTMENTATION EXPERIMENTS

FIGURE III-5-2

240-816 O-67—49

e) Procedure.

1) The model was assembled at the site (see Figure III-5-1). A grid pattern was laid out around the structure to represent Area #3 in the blockhouse experiment (see Figure III-5-2). A scaling factor of 1:12 was used. Tubing was laid in a circular fashion on the established grid, beginning at a radius of 80" from the model center and extending outward to 160".

2) Dosimeters were charged and placed on end in locations as near as possible to those positions established in the blockhouse for Experiment 4 (see Figure III-5-4).

3) The Cobalt-60 source was pumped through the tubing at constant speed. Time of entry of the source into the field was recorded, as well as exit time, with stopwatch.

4) Dosimeters were recovered and read.

f) Theory.

Model scaling techniques require the proper application of two concepts: geometric scaling and dynamic similitude. The physical scaling of all dimensions satifies the first requirement. The second requires that the behavior of the radiation being studied be identical in model and prototype, implying that scattering, absorption, and build-up factors be independent of the linear scaling factor.

These requirements would apply theoretically, not only to the building materials themselves, but as well to the field of contamination, and to the surrounding earth and atmosphere.

The concrete of the blockhouse was simulated with iron in the model. This substitution yields the approximate mass thickness but results in an

overscale wall thickness in the model. It is considered, however, that little error would be introduced by this deviation, since the total model wall thickness was less than 10% of the interior room width in the model.

The atmosphere surrounding the model experiment was not scaled. As a result, skyshine is not properly reproduced in the modeling. This effect is accounted for in the analysis of this experiment by the formulation of a correction factor for non-scaled air.

The gamma ray interaction with the respective materials of model and prototype should be the same. From the viewpoint of attenuation, three methods of comparison may be employed. These require individually the equating of:

(1) mass thicknesses

(2) broad-beam absorption data for flat slabs

(3) electron density.

To illustrate these three comparisons, we note that 8 inches of lightweight concrete (69 psf) is equivalent in mass thickness to 1.68 inches of iron. By absorption criteria, the required thickness is 1.7 inches; and for electron density equivalence, 1.8 inches.

The cross-sections for concrete are very similar to those of aluminum, the various components of which are shown on the next page (Figure III-5-3). It will be noted that the photoelectric component dominates Compton scattering below 0.05 Mev. The interactions that take place with gamma rays below 0.05 Mev are those of absorption. While the Compton cross-section remains constant with changes in atomic number, the photoelectric cross-section goes up at a rate somewhat greater than $Z^{5.00}$. Since iron has a "Z" of 26 and aluminum has a "Z" of 13, the Compton scattering cross-section of iron per atom is at least twice as large, for a given energy, as that of aluminum.

As is shown in Figure III-5-3, the crossover point from dominance of photoelectric effect to that of Compton scattering occurs at approximately 0.05 Mev, and noticeable effect of the absorption phenomenon continues slightly beyond 0.1 Mev. Thus, the use of iron in models to simulate concrete causes gamma rays below 0.1 Mev to be omitted in dose measurements. Since the source used in this experiment averages 1.25 Mev per photon, a great number of interactions were required to degrade the energy to 0.1 Mev, and thus no large error should have resulted in this substitution. See Reference 1 for general discussion of this subject.

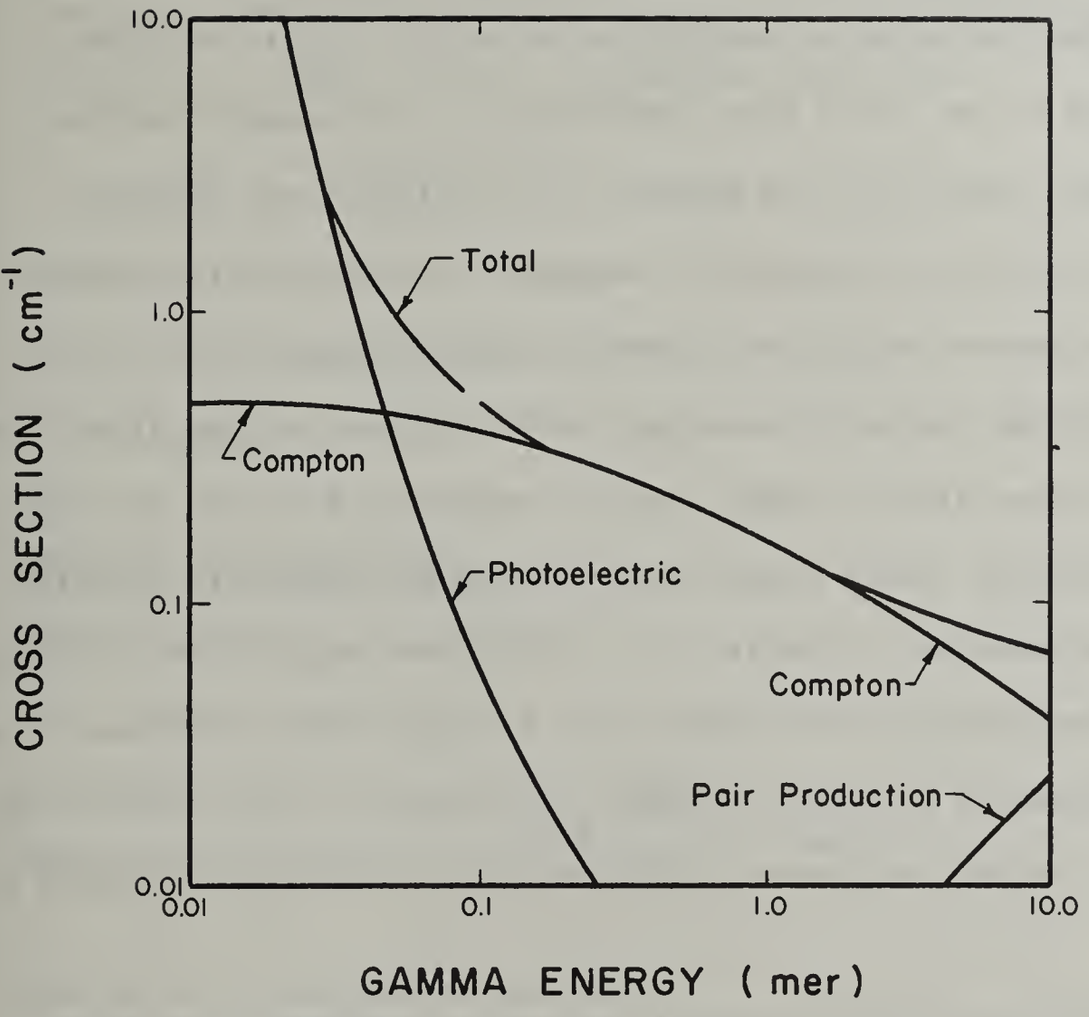

GAMMA RAY MICROSCOPIC CROSS SECTION FOR ALUMINUM.
(SIMILAR TO THAT OF CONCRETE)

FIGURE III-5-3

g) Preliminary calculations.

1) Correction factor due to mismatch in wall thickness. Assuming that modeling on basis of mass thickness is proper, there is a slight mismatch between model and phototype. The thickness of steel equivalent to 69 psf is 1.68", whereas the model only has wall thickness of 1.625". According to Reference 2, this causes a variation of about 4% in a cobalt-60 dose. Thus for radiation penetrating the walls, a correction factor of 0.96 is required. Since most of the first floor radiation is that penetrating the walls, this factor will be applied to all first floor readings.

For radiation entering the basement, an additional correction is needed because of the fact that 55 psf corresponds to 1.35" of steel, whereas the model only has 1.25" thickness in the first floor slab. It must also be noted that the radiation into the basement, being scattered, has a lower photon energy and therefore is more readily attenuated. Finally, it is noted that much of the radiation penetrating the floor slab does so at an angle from the normal. For these reasons an estimate of about 10% is made for this effect, which implies a correction factor for basement dose readings of 0.90 x 0.96, or 0.86.

2) Correction factor due to lack of scaling in atmospheric density. Because of this fact, the radiation in the model situation has less air to penetrate than for the prototype blockhouse experiment. To get a correction factor, one can assume that the average radiation goes a distance equal to the average radial distance from the

structure center to the contaminated area. The relative absorption in such a case gives the correction factor:

$$\text{Factor} = \frac{B(120') \cdot e^{-120/525}}{B(10') \cdot e^{-10/525}}$$

B (120') can be estimated from an experimental curve in Reference 3, for a situation in which the source is on the ground and the detector is a foot above the ground, and equals 1.24. The value of B (10') is best obtained from Reference 4, for a detector height of one foot, and equals 1.16. Thus the correction factor is:

$$\frac{1.24}{1.16} \times \frac{.795}{.981} = 0.87$$

3) Combined correction factors.

For first floor readings: 0.96 x .87 = .83.

For basement readings: 0.86 x .87 = .75.

h) Data and data reduction.

Source strength = 9.1 curies

Area covered = 419 sq. ft.

Duration of run = 32.9 min. = .548 hr.

$$\text{Normalization factor} = \frac{419}{9.1 \times .548} = 84.0$$

"Corrected Normalization Factor" =

correction factor times normalization factor:

For first floor readings, C.N.F. = 84 x .83 = 70.

For basement readings, C.N.F. = 84 x .75 = 63.

200-mr. dosimeter numbers

95	148	84
	109	
89	120	83
	111	
149	127	152

First Floor

10-mr. dosimeter numbers

9	14	6
5	3	12
8	23	4

Basement

Instrument Plan

Figure III-5-4

Instr. No.	Readings (mr.)			Normalized and Corrected (mr.)
	After	Before	Net	
		First Floor		
95	187	4	183	12810
84	176	2	174	12180
152	174	4	170	11900
149	172	9	163	11410
109	179	0	179	12530
120	183	6	177	12390
111	173	7	166	11620
148	151	3	148	10360
83	152	8	144	10080
127	168	7	161	11270
89	161	0	161	11270
		Basement		
	(Instr. Rdg.)		(mr.)*	
9	15		1.55	97.6
6	12		1.25	78.7
4	13		1.35	85.0
8	16		1.65	104.0
14	24		2.45	154.0
12	20		2.05	129.0
23	18		1.85	116.0
5	16		1.65	104.0
3	21		2.15	135.0

*From calibration data provided

i) Results. Because of symmetry, the dosimeters in corresponding positions in the four quarters of the structure should read the same. Therefore, where appropriate, values are averaged over four readings in equivalent locations.

Location	Normalized values	
	Corrected Model	Prototype (Exp. 4)*
	First Floor (r.)	
Center	12.2	14.2
Side	10.7	12.8
Corner	12.1	13.2
	Basement (mr.)	
Center	135.0	172.0
Side	126.0	—
Corner	91.0	63.0

*Taken at 3' Height.

j) Summary, discussion, and conclusions.

It appears from the results obtained and the comparison with the prototype results that fairly good agreement exists, at least within the probable accuracy of the experiments. On the first floor, the discrepancies are of the order of 20% or less. In the basement, the discrepancies appear to be greater; however, the scatter of experimental results in the basement, both in the model and in the prototype, make it difficult to determine whether the discrepancies are the result of failure of the modeling relationships or measurement errors. It appears quite certain that the modeling technique has great promise, if not for obtaining exact answers applicable to prototype structures, at least for getting an approximate answer for many situations and a good understanding of dose variations with position.

The one difficulty that must be expected, and one which probably played a part in the present experiment, is the difficulty of getting a measurement indicative of dose at a point using chambers whose size is substantial compared to the dimensions of the room in the model structure in which it is placed. Under circumstances in which the dose gradients are small, this is no great problem; but under many circumstances there are large gradients, and the measurements can be considered no more than general averages over substantial regions of space in the prototype. In the model experiment reported herein, the instruments on the first floor were "pocket" or "pencil" type dosimeters, stood on end; and in the prototype they would represent an average dose almost from zero to six feet height above the floor. They were compared to prototype results at 3' height, which is presumed to provide a reasonable

mean value. In the basement, the instruments used were 10-mr. chambers, which are not as high, but are several centimeters in diameter, and thus cannot accurately measure the substantial variation in the basement found in the full-scale blockhouse.

This situation can be improved, of course, by using smaller (and presumably less sensitive) instruments, exposed for a longer period of time. Alternatively, one might consider exposure for short time periods, but with a stronger source.*

---

*Footnote: See note added in proof for Experiment 4.

6. Compartmentation Experiment

a) Purpose. To examine by experimental means the adequacy of each of two schematizations for determination of shielding effectiveness of structures with moderately thick internal partitions.

b) References and bibliography.

1) "Shelter Design and Analysis, Vol. 1, Fallout Protection," Office of Civil Defense Compilation (Revised ed., 1962). (This is a revision of an OCD draft document commonly referred to as the "Engineering Manual.")

2) L. V. Spencer, "Structure Shielding against Fallout Radiation from Nuclear Weapons," National Bureau of Standards Monograph 42 (1962).

c) Facilities and equipment used.

1) Steel model of blockhouse, as used in Experiment No. 5 (Model Experiment), with additional assemblies to simulate interior partitions. (See Figure III-6-1.)

2) Cobalt-60 source, 11.0 curies.

3) Pumping apparatus and associated equipment (see Experiment 4).

4) 2 dosimeters, 200-mr.

5) Stop watch.

d) Background. Adequate analytical techniques for analyzing complex, highly-compartmented structures are lacking. There are various possible methods of approach, involving usually some simplification of the geometry of the structure. Two of these which appear simple and reasonable involve the following ideas:

1) One may determine, for each radial direction outward from the detector point, the normal thickness of all slabs intercepted by such a radial line. The outer wall at the point of its intersection with the radial direction line may be considered to have a thickness equal to sum of the normal thicknesses of all slabs intersected. Determination of the dose reduction factor for a simple structure with variable thickness outer walls and no internal compartmentation is a straight-forward calculation.

2) One may consider that the total structure can be replaced for analytical purposes by an idealized material having the same outside configuration as the structure and the same total weight, but with the masses of the structure homogenized to give a constant density of material within the overall dimensions.

Evaluation by simple model experiments should provide information as to the adequacy of each of these ideas for determining dose reduction factors.

e) Procedure.

1) The basic model structure was assembled at the site. The tubing was laid out in a circular ring between 80" and 160" from the center of the model blockhouse. (See Figure III-6-2.)

2) Two reliable dosimeters were placed in a vertical array at the center of the model structure, after charging.

3) The source was pumped through the tubing at a steady rate of speed. Time of entry of the source into the simulated fallout field was accurately recorded, as well as the time of leaving.

4) Dosimeters were recovered and read.

5) The experiment was repeated for the first variation in the assembly.

6) The experiment was repeated for the second variation in the assembly.

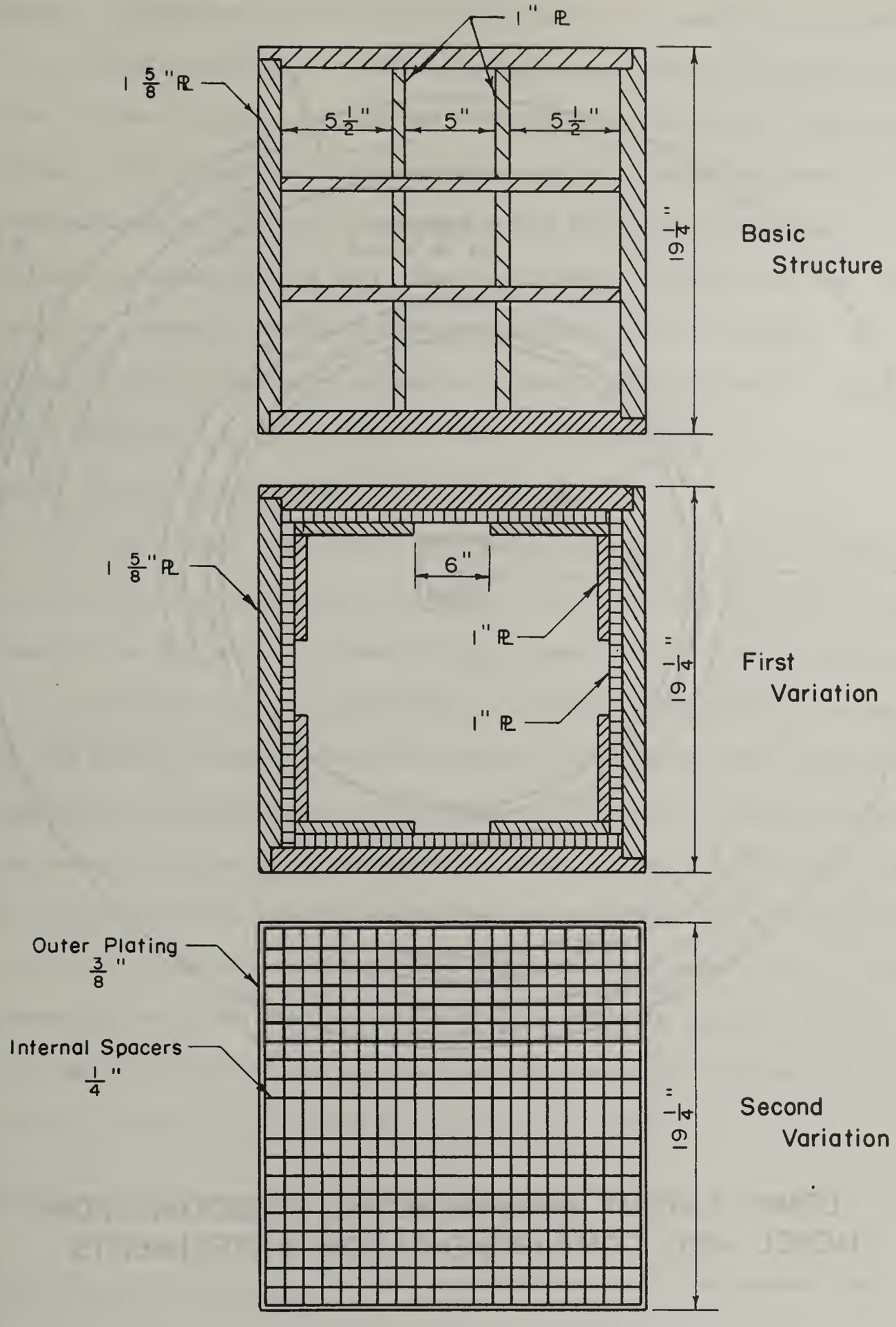

FIGURE III-6-1

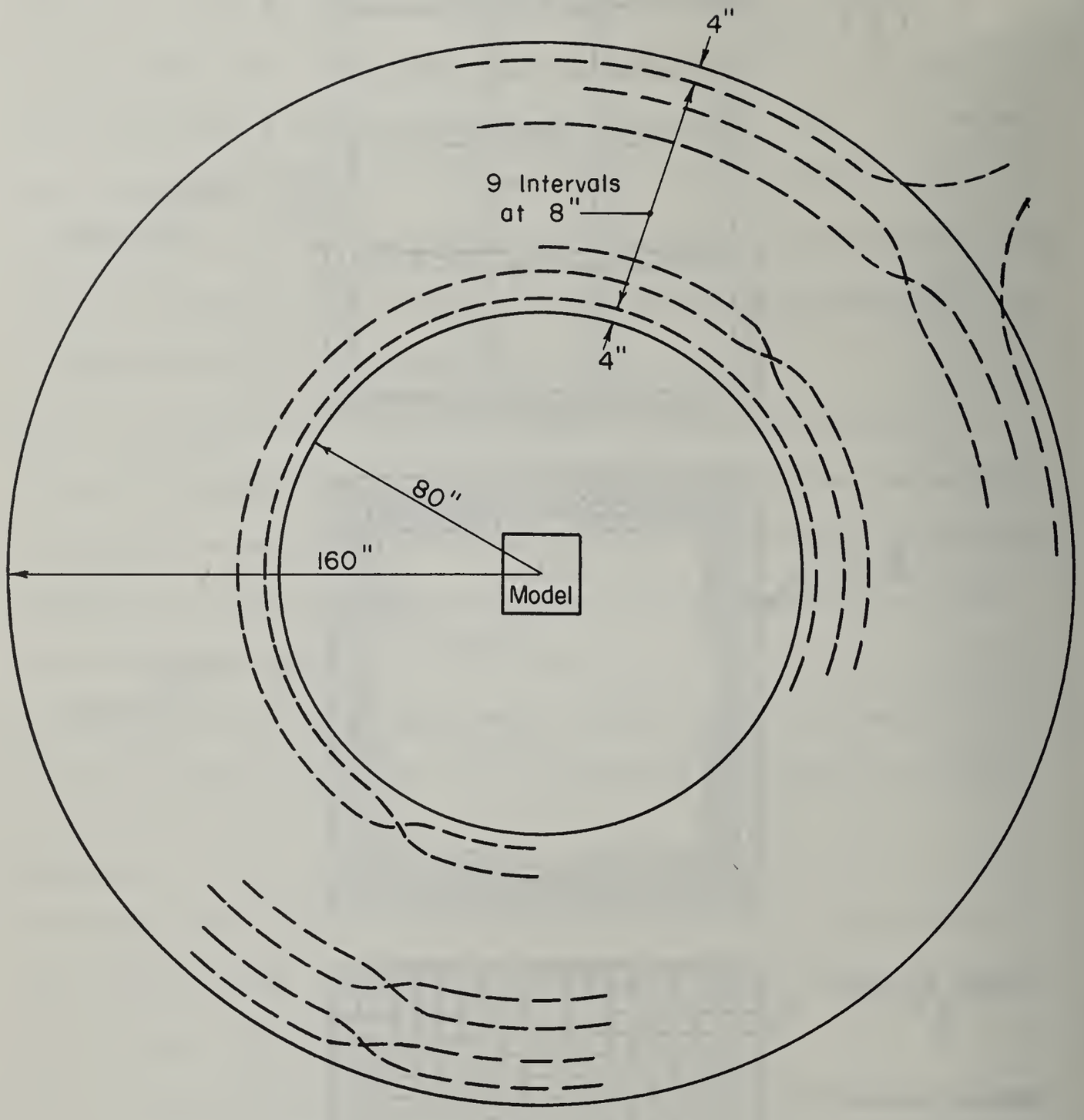

TUBING LAYOUT AROUND MODEL STRUCTURE FOR MODEL AND COMPARTMENTATION EXPERIMENTS.

FIGURE III-6-2

f) Theory. No precise, simple theory yet exists which adequately accounts for the attenuation in a structure which is substantially compartmentalized, that is, has a appreciable amount of interior partitioning. Established methods (References 1 and 2) generally handle the problem either by considering that all partitions in a solid angle sector attenuate in fashion corresponding to their normal thickness, or assuming that the material composing the structure is spread uniformly throughout the volume of the structure. The latter approach is recommended by Spencer (Reference 2) when the structural walls and partitions are less than about 40 psf. in thickness.

In the present experiment, the walls are about 65 psf and the interior partitions are about 40 psf. This then would represent a case somewhat on the border of that in which "smearing out" might be appropriate.

It is not considered desirable to amplify the theoretical background to any further extent. Present schematizations which permit analytical approaches are based more on experience and intuition than on theory, and the experiment presently described is to help justify or deny the validity of the intuitively possible approaches for this experiment already noted. It is also pertinent to remark that since for this experiment the area of contamination is an annulus rather than an infinite plane, existing engineering methods which are designed for practical problems are not greatly suited for analyzing this particular case.

g) Preliminary calculations. None are needed for this experiment.

h) Data and data reduction. In each of the three runs, two pocket type

dosimeters (200-mr.) were placed in the center of the structure, one above the other.

Experimental Configuration	Instrument Number	Readings (mr.)			Exposure Time (hrs.)
		After	Before	Net	
Basic	074 (top)	58	1	57	.494
	083 (bottom)	40	1	39	"
First variation	074 (top)	59	1	58	.467
	083 (bottom)	44	2	42	"
Second variation	074 (top)	23	0	23	.447
	083 (bottom)	20	2	18	"

The area is 419 sq. ft. The source strength was given as 11.0 curies.

Normalization factors to provide equivalent results in mr./hr. at 1 curies/sq. ft. contamination strength are :

For basic configuration, 419/(11 x .494) = 77.1 ;

for first variation, 419/(11 x .467) = 81.6 ;

for second variation, 419/(11 x .447) = 85.2 .

i) Results. Normalized dose-rate readings in middle of model structures.

The normalized dose-rate readings, mr./hr. for contamination of 1 curie/sq. ft. are obtained by multiplying the results by the computed normalizing factors.

Location of Instrument	Basic Configuration	First Variation	Second Variation
Center, top	4.39	4.73	1.96
Center, bottom	3.01	3.43	1.53

j) Summary, discussion, and conclusions. It is quite evident that the first variation gives results much closer to the basic case than the second variation, and we can conclude that the technique of homogenization is not a very good technique for the moderately thick walls encountered in compartmented structures such as this model portrays. Although the experimental data may be subject to some error, the results are sufficiently consistent to make this conclusion quite definite.*

---

*Footnote: See note added in proof for Experiment 4.

Vol. V

LECTURE NOTES, OCD SUMMER INSTITUTE

Charles Eisenhauer

National Bureau of Standards

Development of the Engineering Method and Some Simplified Methods of Structure Shielding Analysis

Development of the Engineering Method and Some

Simplified Methods of Structure Shielding Analysis

Table of Contents

Table of Contents

A. Brief History

1. Before 1958 -

My lecture this morning will be primarily a brief history of the fallout shielding program. While you are here you probably will hear several different histories from several different people and hopefully where they overlap, the picture will be consistent. I will emphasize the events with which I have been most closely associated. In particular, I would like to trace the development of some of the present theory and some of the early experiments.

My discussion begins with March of 1954 when the dangers of radioactive fallout first became apparent. It was the date of the nuclear detonation in the Pacific which showered fallout particles on a group of Pacific Islanders. From then on we realized that fallout was an important aspect of nuclear weapons. Shortly after this, in about 1955, discussions were initiated between FCDA (the Federal Civil Defense Agency), the National Bureau of Standards and the Atomic Energy Commission to discuss what could be done about protecting citizens from this hazard. The main persons involved in these discussions were Mr. Pat Gallagher from FCDA, Dr. Lauriston Taylor of the National Bureau of Standards and Commissioner Willard Libby from the Atomic Energy Commission. The key question was "how much protection is afforded by existing structures?" That was in June 1955. In June 1957, the first experiment designed specifically to measure the penetrability

of fallout radiation was performed by Dr. Frank Titus who was then with the National Bureau of Standards. This experiment was suggested by Lew Spencer. It was an attempt to get some basic data on the penetration of fallout radiation through concrete. The scheme was to try to pick an area where, during one of the nuclear tests, fallout was expected to be deposited. A number of horizontal concrete slabs were buried in the ground, the top surface of the pile being flush with the ground. Sandwiched between these concrete slabs were detectors of gamma radiation. Hopefully, fallout would be distributed on the ground over the slabs. From the measurements at various depths of concrete, the penetration of radiation from a plane isotropic source of actual fallout could be obtained. Fortunately, in this case, fallout was deposited over the slabs and the experiment was a success.

2. Experiments at Nevada Test Site, 1958 -

Things began to pick up in 1957. In November of 1957, Commissioner Libby approached Governor Hoegh, who was then head of the FCDA, and offered the services of the Atomic Energy Commission in seeking solutions to the problems of shielding from fallout radiation. This resulted in a meeting in December between FCDA, the National Bureau of Standards, and the Atomic Energy Commission to try and agree on an approach to the problem. Now, at that time Dr. Libby wanted to see some kind of a mobile vehicle which could go into a community and measure protection in homes. He suggested Battle Creek, Michigan, which was the civil defense headquarters at that time, as the site of such an experiment. The civil defense organization was less than lukewarm to this suggestion. Their

public image was not too good at that time, anyway, and if any of you have had any experience in trying to bring a radioactive source of the order of a Curie into a residential area you can well imagine what the opposition to a plan like this would be. Therefore, the people at Civil Defense tried to modify the plan for a mobile vehicle and perhaps to divert it into what they considered constructive channels. This resulted in a big meeting at NBS in January 1958. Since I had just come to NBS I was asked to attend this meeting. The purpose was to discuss specific experiments. The outcome of this meeting was the decision to do some experiments on residences at the Nevada Test Site. The Nevada Test Site had several advantages. Since it was a restricted area there was no danger to the public of being exposed to any radiation. Since there were no nuclear testing programs at that particular time, there were facilities such as transportation and housing available to the experimenters. Finally, there were already in existence a number of typical residences which had been built primarily for blast studies from nuclear weapons. The experiment was performed in May of 1958. There were about 10 of us who participated in the month-long experiment. It was the first systematic experiment on structure shielding ever performed in this country. Since there was virtually no theory existent at the time, it was an exploratory type of experiment.

The two structures on which most of the experiments were made were a two-story wood frame house and a two-story brick veneer house. Experiments were also made on a rambler-type residence and a precast concrete home of a type which is fairly common out West. Right now there is a

renewed interest in these experiments, because OCD is thinking of running a survey on residential structures in this country. In order to demonstrate that the current calculations give sufficiently accurate estimates of protection,comparisons are again being made with the experimental data from these residences. In fact, the AEC is now sponsoring further experiments on these same structures to obtain more detailed data.

The first experimental program on these structures had several purposes. One purpose was to measure the relative effect of the roof sources and ground sources. At that time no one had much feeling for what the relative effects of the two components would be. Another purpose was to test out some of the emergency procedures that OCD had recommended - procedures such as sandbagging basement windows - to see if they really were effective in improving protection. Still another purpose was to examine the dependence of radiation protection on the source energy of the radiation since there is a wide distribution of energies in the fission product gamma ray spectrum associated with fallout. Artificial radioactive sources of Co-60 and Cs-137 were used to test the sensitivity of the results to the energy of the source. Another purpose was to test so-called "reciprocity". Reciprocity holds if the position of source and detector can be interchanged without changing the detector reading. The situation of interest in structure shielding is one in which the sources are outside of the structure and a detector is in a shielded position inside the structure. However, if sources

could not be distributed in the streets in a residential area, perhaps the source could be placed inside and the detectors outside the structure; this presumably being a less objectionable way of operating in actual residential areas. The question was, "how closely would the results for the reciprocal situation correspond to those for the original situation?" The technique of handling the sources was rather amusing. As you know, most experiments are now conducted with radioactive sources which are pumped hydraulically through plastic tubing. However, at that time the sources we used were small Cobalt sources imbedded 2 feet apart in plastic tubing. These tubes of plastic were then laid out in circles around the structures. The difficulty arose in "turning off" the source. The sources had to be removed from the vicinity of the structure as quickly as possible to minimize radiation received during the transient period. The method which was used to tie a long string to the end of one of these hot pieces of tubing, each of which contained about a Curie. As soon as the experiment was finished someone had to grab the end of the string, run around the house unwinding the tube, and then run out into the desert. We almost lost Neal FitzSimons one night when he kept running and did not hear anybody yell "Stop!"

There were quite a few important conclusions that came out of this experiment with regard to shielding in residential structures. First, we found that in the wood frame structure, the protection factor was only about 2 on the first story of the structure. In the brick veneer house it was more like 5 or 6, which is better, but still not very appreciable. This, of course, is due entirely to the extra shielding of the brick. We also found out that the protection factors in basements

of structures tended to be about 30 and did not seem to depend on whether the upper stories were made of brick veneer or of wood. The two basements were a little different in construction, but generally this was the order of magnitude of the protection factor in the basements.

In the two-story wood frame structure we found the rather surprising result that about 10 times as much radiation reaching a detector on the first story came from ground sources as from roof sources. Although the roof sources are relatively close, the cumulative effect of the many sources on the ground tends to outweigh the effect of the roof. In the brick veneer house the relative contribution from the ground sources would be less since the walls provide greater shielding.

On the subject of reciprocity, we found that if a source is placed inside of the structure and a detector outside and then they are reversed, the readings may be significantly different for a single source-detector configuration. However, if the structure is surrounded with a ring source so that an average is performed over all compass points or azimuthal directions, then the results, surprisingly enough, agreed within about 20%. This implies that - at least for light structures - if a point source is placed in the middle of a building and surrounded with about 20 detectors, equally spaced around a circle, and then the sum of the readings of these dosimeters is taken, it will correspond to the reading obtained by distributing a source of the same intensity around the structure and placing the detector at the center of the structure. The individual readings will vary greatly because of the number of joists or wall studs between the

source and the detector fluctuates greatly. But, when these effects are averaged over the azimuth, the reciprocal situation seems to give similar results. I think the main reason that no one has exploited this phenomenon is that the uncertainties are just large enough to make the procedure of dubious value. But I think that reciprocity worked a little bit better than we might have expected beforehand.

Another surprising result of these experiments was that the basement shelters did not yield as much protection as had been estimated beforehand. The estimate was based on the following line of reasoning. Suppose we start with a protection factor of, let us say, 30 at the center of the basement. Suppose now we move to the corner of the basement, the protection there ought to be as much as a factor of 4 better, because in the center of the basement a detector receives from all directions overhead, while in the corner it receives only from 90°, or one quarter of the azimuth. Suppose, finally, we are inside of a shelter in the corner of the building with 8-inch solid cinder-block walls and ceiling. An additional factor of 10 was expected inside of the shelter. The expected protection factor inside of the shelter was therefore 30 x 4 x 10 = 1200. However, the experimentally measured protection factor in these corner basement shelters was only about 150 to 200, which was disappointing. I don't think we understand all the reasons yet why the PF is so low in these basement shelters. However, we know that the PF does not increase by a factor of 4 when you move to the corner, but more like 2-1/2 or 3. But, it was mainly the factor of 10 inside of the shelter that did not materialize. I think the unexpectedly low PF in the shelter

must be attributed to in-scattering effects. For example, although the shelter ceiling increases the protection against radiation from roof sources it may decrease the protection against radiation from ground sources because its presence enables this radiation to scatter into the direction of the detector. The concept of in-scattering will be more fully discussed in a later lecture.

These experiments were performed during the month of May 1958. John Auxier of Oak Ridge was primarily responsible for the success of the experiments. The experimental results are reported in an AEC Report CEX 58.1. My analysis of these experiments is reported in NBS Report 6539.

3. Other Experiments -

In November 1958, a second series of experiments was done by Technical Operations, Inc. They repeated some of the measurements on the residences with slightly stronger sources and, in general, verified the results we had obtained earlier. They also examined some large structures because by this time the shielding afforded by commercial structures began to be of concern.

Another important experiment was begun in 1957 at the U.S. Army Chemical Center, in Edgewood, Maryland. It involved a square concrete blockhouse 12 feet on a side and 8 feet high, now usually referred to as the NDL blockhouse. The experiment again had been suggested by Lew Spencer and was an attempt to get some measurements on a very simple structure in order to understand the calculations that were being performed and how well they corresponded to reality. This experiment has been a continuing one. It was very helpful at the time we were devising the

Engineering Method because it enabled us to compare our calculations with experiment.

Since 1958 there have been many experiments on structures. I am not going to go into detail on them. There have been experiments both on full scale structures and on model buildings. Perhaps Art Chilton will cover some of the more recent experiments. Most of the experiments have been designed to test some aspect of the engineering method. During this period the basic radiation calculations reported in NBS Monograph 42 were completed and the engineering method was beginning to evolve. The engineering method was developed primarily by Neal FitzSimons of the Office of Civil Defense, Lew Spencer and myself. The problem was to take the results for idealized situations which were reported in NBS Monograph 42 and to incorporate them into detailed calculations which would apply to actual buildings. The calculations were successfully developed, but they were tedious. If any of you have done engineering manual calculations, you know that the basic calculation is simple enough but an attempt to calculate all the various contributions becomes very tedious. Furthermore, many of the contributions, when finally calculated, turn out to be negligible. Consequently, there was pressure at the time to develop a simplified method. The result of the pressure was the method described in the Guide for Architects and Engineers - the first of several simplified methods that have been developed since that time.

4. National Fallout Shelter Survey

In September 1961, the National Fallout Shelter Survey (NFSS) was initiated. I would like to say a few words about the magnitude of the survey. The data processing turned out to be an enormous job. It was

240-816 O-67—51

handled by the computation laboratory at the National Bureau of Standards. This group is entirely separate from the one with which Lew Spencer and I are associated. Having had a great deal of experience in dealing with large amounts of data, this group set up the method by which this data was to be handled. It was really quite complex. I do not know whether any of you took part in this survey, but the general procedure was the following: In all parts of the country architects and engineers went out to their local buildings and filled out so-called FOSDIC forms, on which they noted wall thicknesses, building dimensions, and all the parameters that were needed to calculate shielding. Then, whole booklets of these FOSDIC forms were sent to Indiana, where the Bureau of Census has a microfilming installation. The microfilmed forms were then sent to the Bureau of Census in Washington, D. C. where they were interpreted by scanning the microfilm optically and translating this information onto tapes. Since these tapes were not compatible with the data processing system at the National Bureau of Standards they had to be sent to the David Taylor Model Basin in Washington, D. C., where the information was transferred from one type of tape to another. They then were sent to the National Bureau of Standards where they were put through a very elaborate check to see whether the data was consistent. For example, suppose a ten-story building height was reported as 20 feet. It would then be assumed that the data were internally inconsistent and they would be sent back for correction. If the data were consistent, they were subjected to a protection factor analysis. Lew Spencer and I had written the first version of the computer program of

the PF analysis. It was rewritten in machine language by the NBS Computation Laboratory and streamlined in order to minimize the calculation time. The National Fallout Shelter Survey cost in the neighborhood of 50,000,000 dollars, most of which went to the architects and engineers who recorded the extensive compilation of input data. The actual data processing part of it was a small part of the total cost. The total number of buildings examined in the survey was about 350,000, distributed throughout the country. Most estimates of potential fallout shelter in this country are based on this National Fallout Shelter Survey.

In setting up the PF calculation for the NFSS we were forced to think about contributions from finite contaminated planes. Up until that time, we tended to think mostly about buildings surrounded by infinite planes of contamination. This survey focused our thinking on buildings surrounded by finite planes of contamination at different levels and the techniques for handling more than one contaminated plane came into existence during this survey.

In planning for a large survey it became evident that a large number of people who knew at least the rudiments of protective shielding would be needed. Consequently, courses were instituted, the first of which was held at Ft. Belvoir, Va., in the summer of 1961. The courses were taught primarily by Army personnel at the Ft. Belvoir Engineering Installation. It was during these courses that the concept of azimuthal sectors was incorporated into the engineering method. Until that time calculations for detectors not at the center of a structure were made by constructing

four hypothetical buildings. For example, for the contribution from the wall in quadrant A of Figure 1,* the calculation was made as if the detector were located at the center of a hypothetical building indicated by the dashed lines. The result was then divided by 4 to obtain the contribution from quadrant A. No recommendations were given for cases in which the height of the contaminated plane had more than one value along the length of the building. The instructors at Ft. Belvoir found that buildings were never very simple and in particular that the surroundings of a building might not be very simple. They therefore made a logical extension of the existing method. They divided the azimuth into parts and treated each one of these separately. For example, if in Figure 2 the area C represents an adjoining high building, the contribution from A would be weighted by the relative azimuthal angle φ_1, while the contributions from B and D would be weighted by φ_2. I mention this because there is a real problem in the engineering method of how far one can refine the technique of azimuthal sectors. The main shortcoming is that the technique applies barrier factors which were not designed for that particular type source.

5. Simplified Engineering Methods -

In 1962 the first OCD Summer Institute was held at Kansas State University. At about this time, the equivalent building method was being developed by Jack LeDoux. He felt that the engineering method was too involved and thought that a simpler method could be devised which was better than that in the Guide for Architects and Engineers. The simplified methods than began to proliferate. First of all, the method used in the NFSS did not correspond exactly to that in the Guide for Architects and

---

* All figure references in this volume apply to figures in this volume, e.g., Figure 1 refers to Figure V-1.

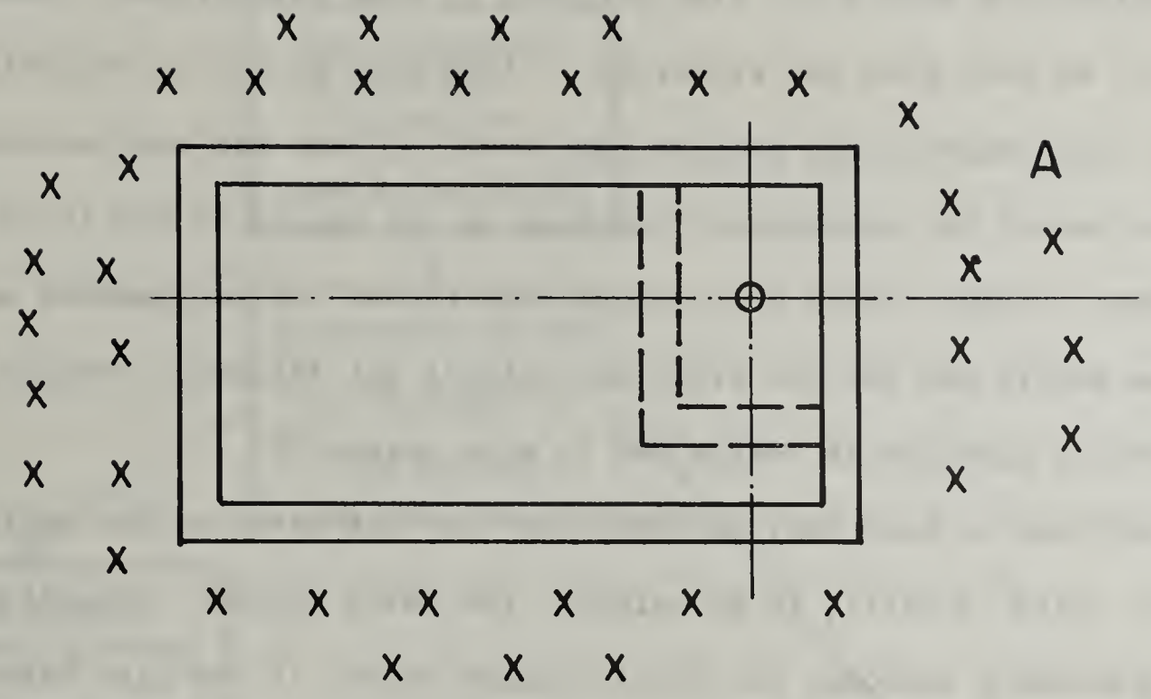

Fig. V-1. Hypothetical building used to calculate the contribution through the wall in quadrant A to an off-center detector.

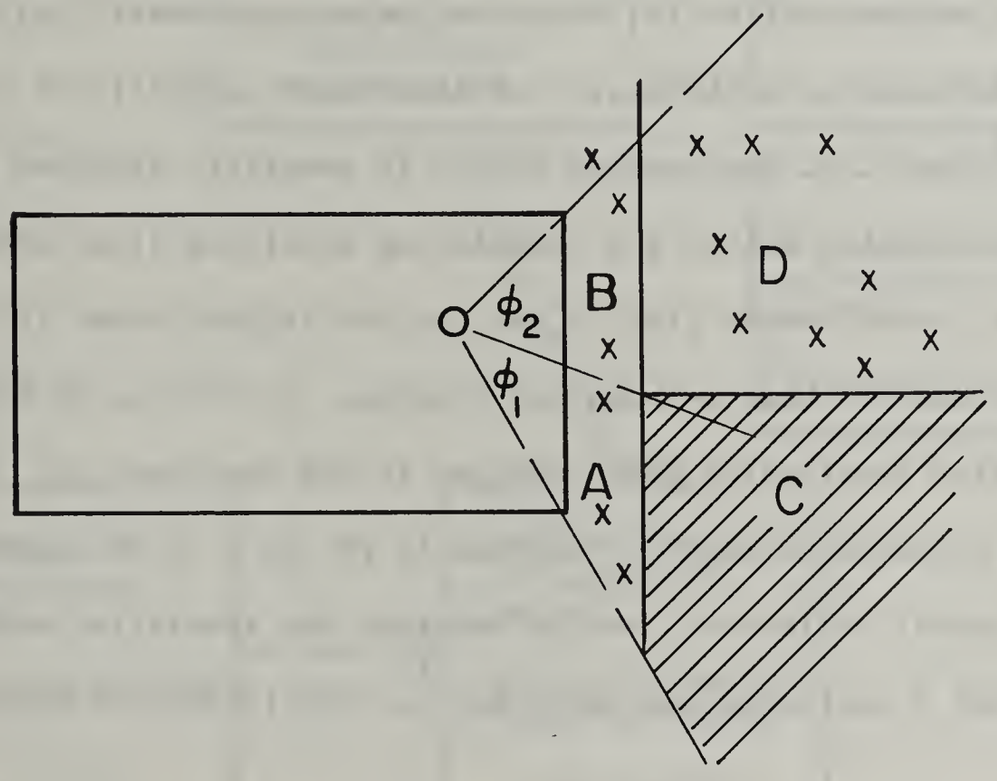

Fig. V-2. Division of the surroundings of a building into azimuthal sectors.

Engineers. Also, each new method was not only a simplification of the engineering method but also differed in some assumptions. Consequently, we went from the situation in 1958 when we had no methods at all to approximately the present time where we have too many methods. I think one of the operational problems of the people in OCD is to define how these methods differ and perhaps even choose one recommended method. Because people who use the different methods get different results, the obvious question is "which one is more correct?"

Although we have many methods, they are all based on the engineering method. This is still, in my opinion, the basic method. In addition to our approximate methods, the British point scheme is now also based on the engineering method. The British had a method of calculation earlier than we did, but in 1963 they incorporated our technical data into their method. Theoretically, the British point scheme results should correspond to the results obtained by the engineering method. In practice, however, the methods differ in detail and do not necessarily give equal results. The Canadian methods are now also based generally on the engineering method. The U. S. Engineering Method is generally accepted in Europe as the best available method for calculating shielding from fallout.

At this point I would like to use the box diagram shown in Figure 3 to show how some of these methods are related. At the top we have the basic radiation penetration data reported in NBS Monograph 42. Below it we have the engineering method, reported in PM 100-1 which applies these results to actual buildings. Now we consider the simplified methods. The first that I mentioned was the Guide for Architects and Engineers.

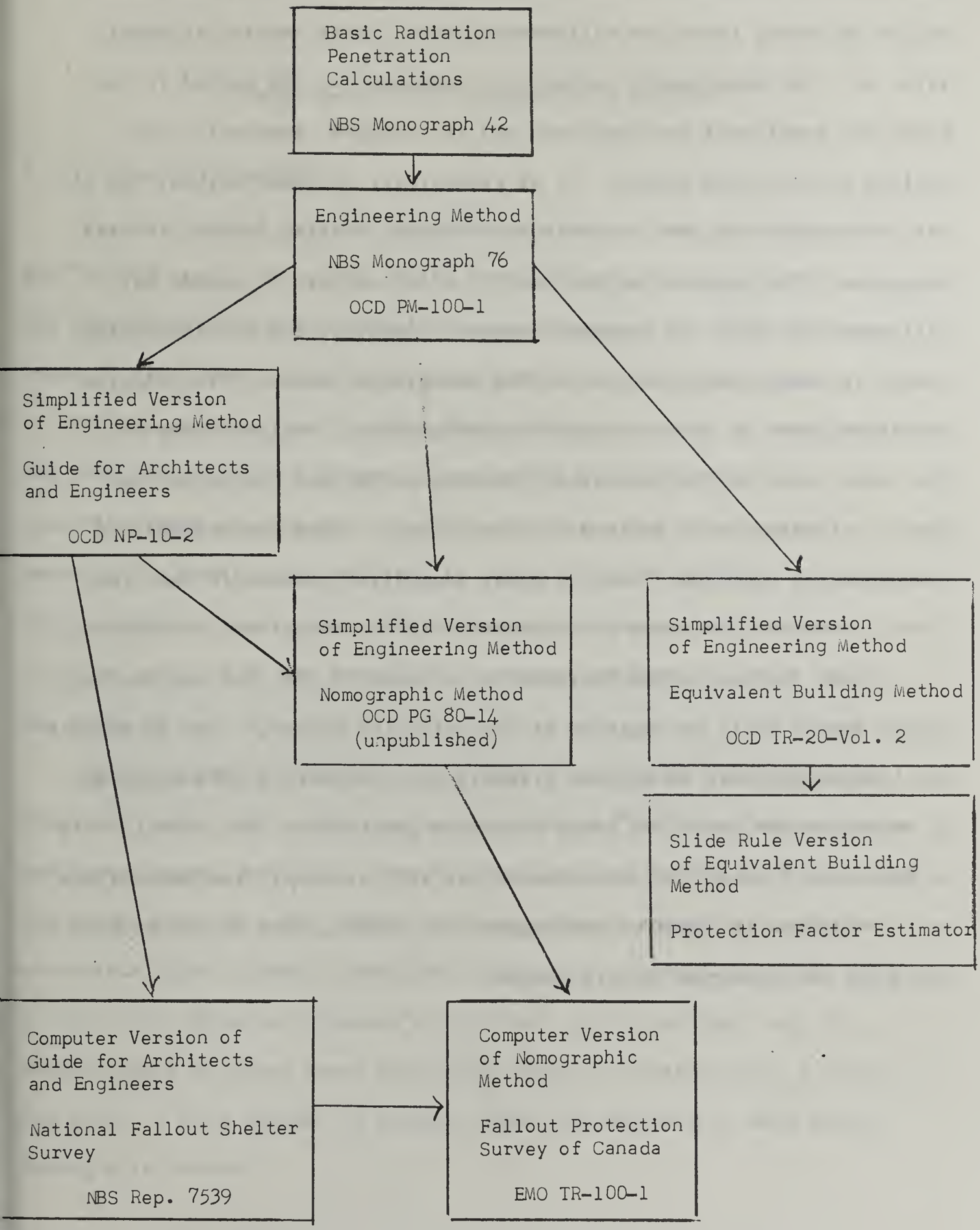

Fig. V-3. Diagram showing the relationship among the various methods of shielding analysis.

This was the first simplification of the engineering method. From that came the National Fallout Shelter Survey. Although it was based on the AE Guide, there are differences which I will mention in detail later on. The nomographic method is a successor to the method in the Guide for Architects and Engineers and is intended, eventually, to replace the AE Guide method. It is essentially the same method, but it has been updated in some respects and instead of using curves, it uses nomograms. The computer method used in pilot surveys in Canada was influenced by the U. S. computer program. However, the PF calculation itself is most closely related to the nomographic method. The diagram therefore shows it to be related to both methods. The two boxes on the right refer to the equivalent building method and the protection factor estimator, both devised by Jack LeDoux. These two methods are fundamentally different from the other simplified methods in that they treat corrections in terms of adjustments to the actual wall thickness.

My own feeling on the hierarchy of methods is that the engineering method should still be regarded as the "official method." Any substitute for this method must be derived directly from the data in NBS Monograph 42 or some other source of basic radiation penetration data. Until this is achieved, I think that the accuracy of all the simplified methods has to be evaluated in terms of the engineering method, even though we know there are shortcomings in this method.

B. Development of the Engineering Method

1. Introductory Remarks -

In the field of fallout radiation shielding I have been sort of the "middle" man. It was my job to take the data that Lew Spencer had calculated for certain idealized geometries and fit them into an engineering recipe for calculating protection in actual buildings. In order to do this I had to know what problems occurred in practice and just what type of information was needed by the engineer. Neal FitzSimons was the man who did an excellent job of making me aware of the problems encountered in practice and of prodding me into doing something about them. The Engineering Method we will discuss in these lectures is the result of a constant exchange of ideas among the three of us.

In developing the Engineering Method I have found a few concepts which have been very helpful to me in getting a "feel" for how radiation penetrates into a building. One of these concepts is the analogy between the penetration of gamma radiation through matter and the transmission of visible light through translucent barriers. Another concept is what I would call taking a "detector's eye view" of the problem; that is, concentrating on those gamma rays which reach the detector and ignoring the rest. I will attempt to develop these two concepts in more detail during this lecture.

I would also like to spend some time on the directional distribution of radiation, with particular emphasis on the directional distribution above an infinite plane, uniformly contaminated with fallout. I think a thorough understanding of the directional distribution, with no buildings present, is necessary in order to understand the shielding effects of buildings.

In my later lectures I will present the reasoning by which we arrived at the Engineering formulas for calculating shielding in buildings. I will develop the formulas for very simple buildings and for radioactive sources on the roof and on the ground surrounding the building. I'll also present a few examples. Finally, I will give a brief discussion on some specialized types of sources and geometries, such as skyshine radiation and limited strips of contamination.

This, then, is a brief review of the material I hope to cover.

2. Analogy between gamma radiation and light -

We return now, to the first concept I would like to discuss, namely, the analogy between the penetration of gamma radiation through matter and the transmission of visible light through slabs of translucent glass.

In Figure 4 we see a diagram of gamma rays from a point source penetrating a barrier. Three types of events can occur: Some gamma rays will penetrate through the barrier without interaction and, consequently, no change of direction. We refer to this radiation as direct, or unscattered radiation. Some gamma rays will be stopped in the barrier by undergoing a photoelectric absorption. Other gamma rays

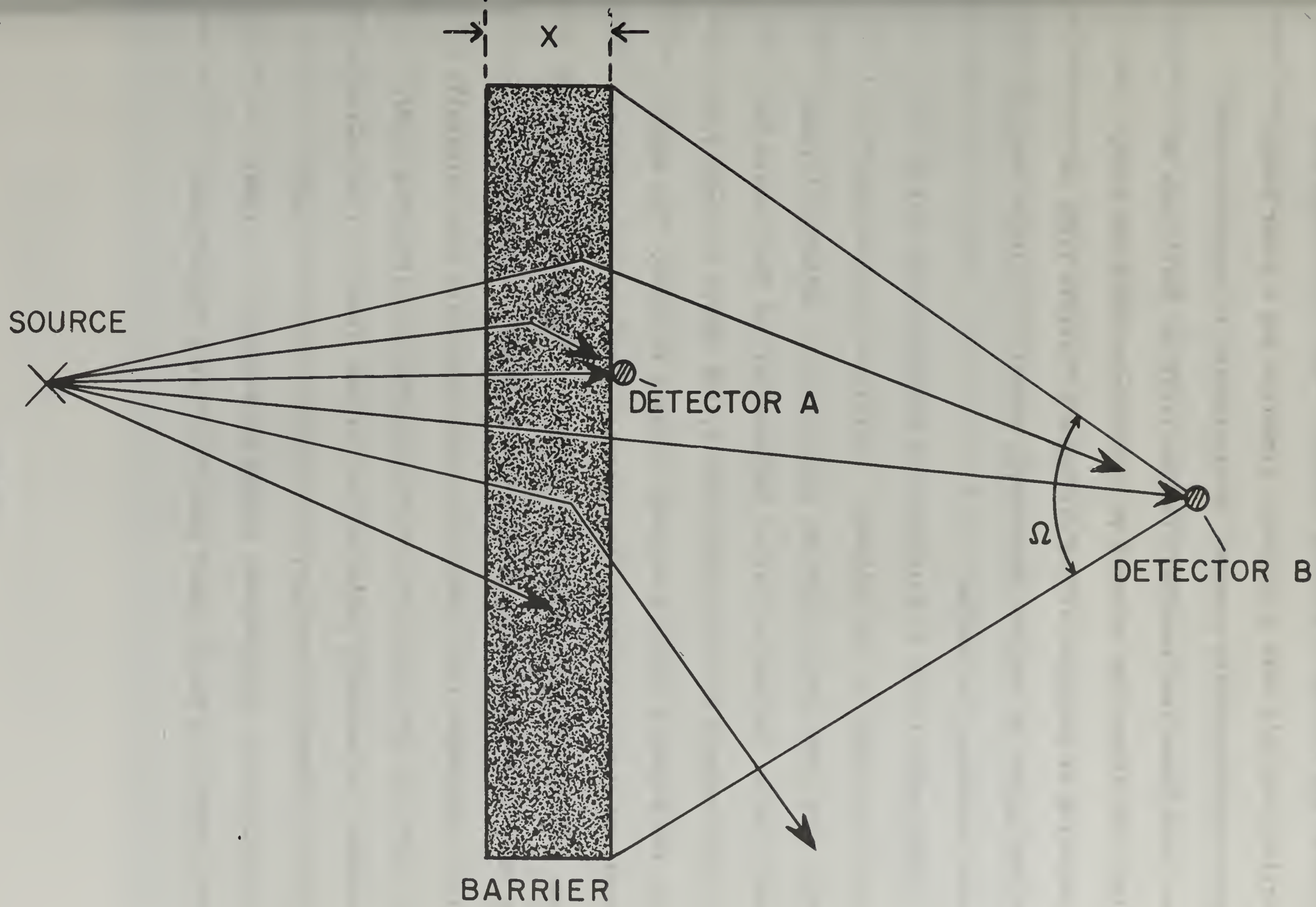

Fig. V-4. PENETRATION OF GAMMA RAYS THROUGH A BARRIER

may penetrate the barrier after undergoing one or more changes of direction by the Compton scattering process. When they emerge from the barrier they will have a different direction and a lower energy than when they entered the barrier. A distinction is sometimes made between those gamma rays emerging from the right and left sides of the slab. The latter are referred to as backscattered gamma rays. The scattering is analogous to the diffusion of visible light in translucent glass, in that the rays do not travel in a single straight line when traversing the medium.

At this point I want to introduce the second concept of the "detector's eye view" of the problem. Until now, we have been standing off to one side viewing the penetration of radiation through the slab. Let us now put our eye at the detector and look toward the slab. Let's examine the intensity, that is, the number of gamma rays reaching the detector with and without the slab in place. The main effect of the slab is to reduce the intensity. This is due primarily to gamma rays lost by absorption. In addition, some gamma rays scatter out of the direct beam and never reach the detector. These are partially compensated for, however, by gamma rays which were originally headed away from the detector but then scattered in a direction toward the detector. A secondary effect of the barrier, then, is the generation of gamma rays, emerging from many other points of the slab beside that on the line of sight between source and detector. If these rays were visible it would appear that the barrier had diffused

the source. It no longer looks like a point source but a smeared-out source. I would like to illustrate this analogy further by the use of some photographs.

Figure 5 shows a picture of a point source of light taken from behind slabs of varying degrees of translucency. The left view is through transparent glass. The analogous case in gamma radiation is a point source and a point detector with a barrier of zero thickness, that is, no barrier between them. The second view is through a lightly frosted slab of glass. In addition to the original point source, we see a haze of scattered radiation around it. This corresponds to the distribution of radiation "seen" by a detector when a thin slab is interposed between source and detector. I would like to emphasize that this slide illustrates only the diffusive effect of slabs. It does not reproduce the true behavior of the intensity. If it were a faithful illustration, the intensity of light emerging from the second slab would be less than that from the first. Unfortunately, the figure does not convey this decrease in intensity. The right view is through heavily frosted glass. The point source is almost indistinguishable from the haze of scattered radiation around it. This means that most of the radiation emerging from the slab has been scattered at least once in the slab. The haze is analogous to the distribution of gamma radiation "seen" by a detector when a thick slab is interposed between source and detector. Here again, however, the intensity emerging from the bottom slab should be the smallest; that is, it should appear dimmest.

Fig. V-5 POINT SOURCE OF LIGHT VIEWED THROUGH GLASS PLATES HAVING VARYING DEGREES OF TRANSLUCENCY

In summary, the presence of the barrier reduces the intensity of radiation reaching the detector and also changes the angles from which the radiation arrives at the detector. For a point source the distribution varies from a point of light, in the case of a thin barrier, to a haze of light, in the case of a thick barrier.

The preceding discussion applies when the barrier lies between the source and the detector. Another important configuration to consider, however, is the case when the barrier does not lie between source and detector. The lower half of Figure 6 shows a diagram of this situation for the case of visible light. (An opaque material is assumed to lie between the source and the eye.) If the barrier is of zero thickness and if the line-of-sight between source and detector is heavily shielded no radiation will reach the detector. If we now put in a barrier of about one mean free path thickness, some radiation will reach the detector because of what we will call "in-scattering". In this case, the radiation intensity is actually increased when a barrier is added. The qualification, of course, is that the barrier does not lie on the line from source to detector. As the barrier is made thicker, the radiation reaching the detector will eventually decrease. There is some intermediate thickness of barrier which will produce a maximum intensity at the detector. The thickness will vary with geometry but will be of the order of one mean free path, or about 3 inches of concrete.

Resorting again to our optical analogy, we can think of the detector as the eye of a person in a foxhole on a dark night. If a bright light is placed some distance away, and he is down far enough, he will see

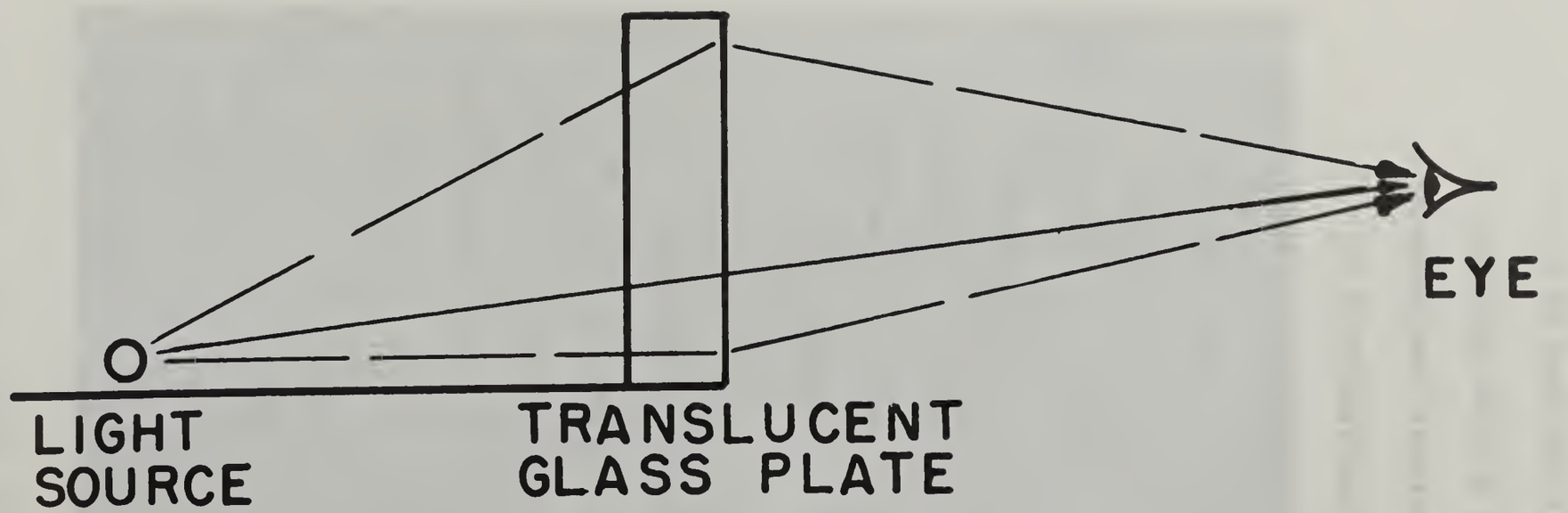

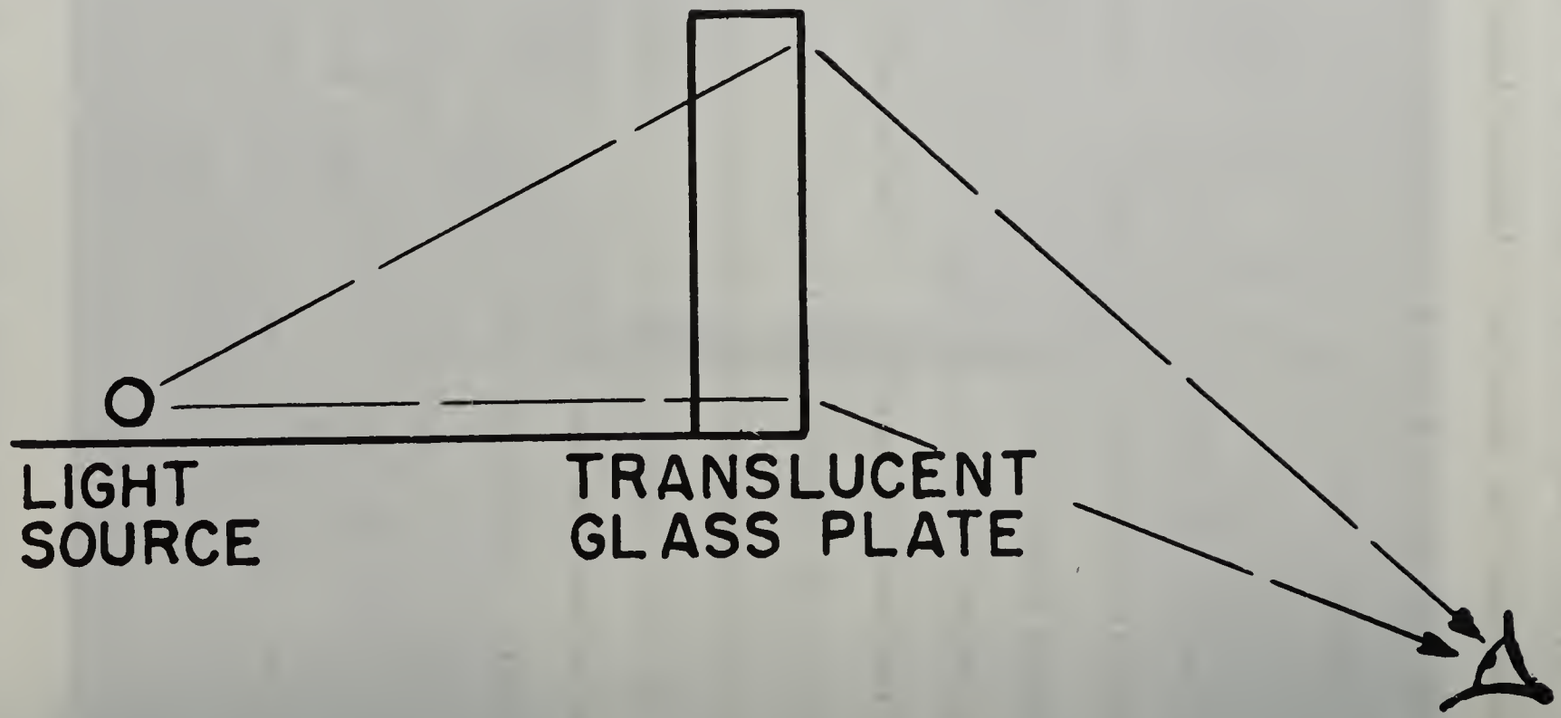

Fig. V-6 CONFIGURATIONS IN WHICH THE BARRIER LIES ON THE LINE-OF-SIGHT BETWEEN SOURCE AND DETECTOR (TOP) AND IN WHICH NO PART OF THE BARRIER LIES ON THE LINE-OF-SIGHT (BOTTOM)

no light. If a translucent wall is erected around the hole, he will then see some light scattered down by the wall. Indeed, this is the main mechanism by which radiation penetrates into a basement lying completely below grade: it scatters down from the walls of the building.

Pursuing the optical analogy one step further, the problem of calculating the radiation intensity in a structure due to fallout is similar to calculating the intensity of light in a building constructed of glass walls of varying degrees of translucency. The sources of light are distributed on the roof and on the ground around the building. Heavily frosted slabs are analogous to thick barriers. The eye or a photometer is analogous to the detector. The problem of the shield designer is to minimize the intensity of radiation inside of the structure.

3. Directional Distribution

a. General

I would like to spend some time discussing the directional distribution of radiation reaching the detector. I might say, first, that knowledge of the directional distribution of radiation in the various configurations associated with fallout shielding constitutes the main advance over earlier attempts to treat this problem. Earlier attempts usually utilized buildup factors. These factors give the total amount of radiation emerging from a slab but no indication of its directional distribution. We will see why knowledge of the directional distribution is necessary in structure shielding.

Figure 7 shows the directional distributions appropriate to three different shielding situations. On the left are three configurations and on the right are plotted the corresponding directional distributions of radiation at the detector. S represents the source and D the detector. The angle θ is the polar angle relative to the direction DS. We will assume azimuthal symmetry about the line DS. The top configuration represents the case of no barrier. Radiation reaches the detector only from the direction $\theta = 0$. Thus, the plot of the corresponding directional distribution is a δ-function with the spike at $\cos\theta = 1$. Negative values of $\cos\theta$ represent radiation reaching the detector from the right-hand side. The next configuration shows a thin circular disk barrier, B, interposed between source and detector. Now radiation can reach the detector from all angles $\theta \leq \theta_o$. In general, however, the greatest intensity exists at $\theta \sim 0$. The corresponding plot of the directional distribution, therefore, shows a peak at $\cos\theta = 1$ and a continuous decrease in intensity down to $\cos\theta_o$ and zero intensity elsewhere. The lowest configuration shows a thick barrier between source and detector. In addition, a barrier has been placed behind the detector. This barrier will backscatter some radiation to the detector. The corresponding plot shows a less peaked distribution between $\cos\theta_o$ and +1 due to the disappearance of much of the direct radiation. In addition, some intensity from radiation backscattered from the second slab reaches the detector from angles between θ_1 and π. In the Engineering Method we generally neglect the backscattered contribution since it usually contributes less than 10% relative to radiation reaching the detector from the primary barrier The <u>concept</u> of backscattered radiation, however, is important in the development of the Engineering Method, as we shall see.

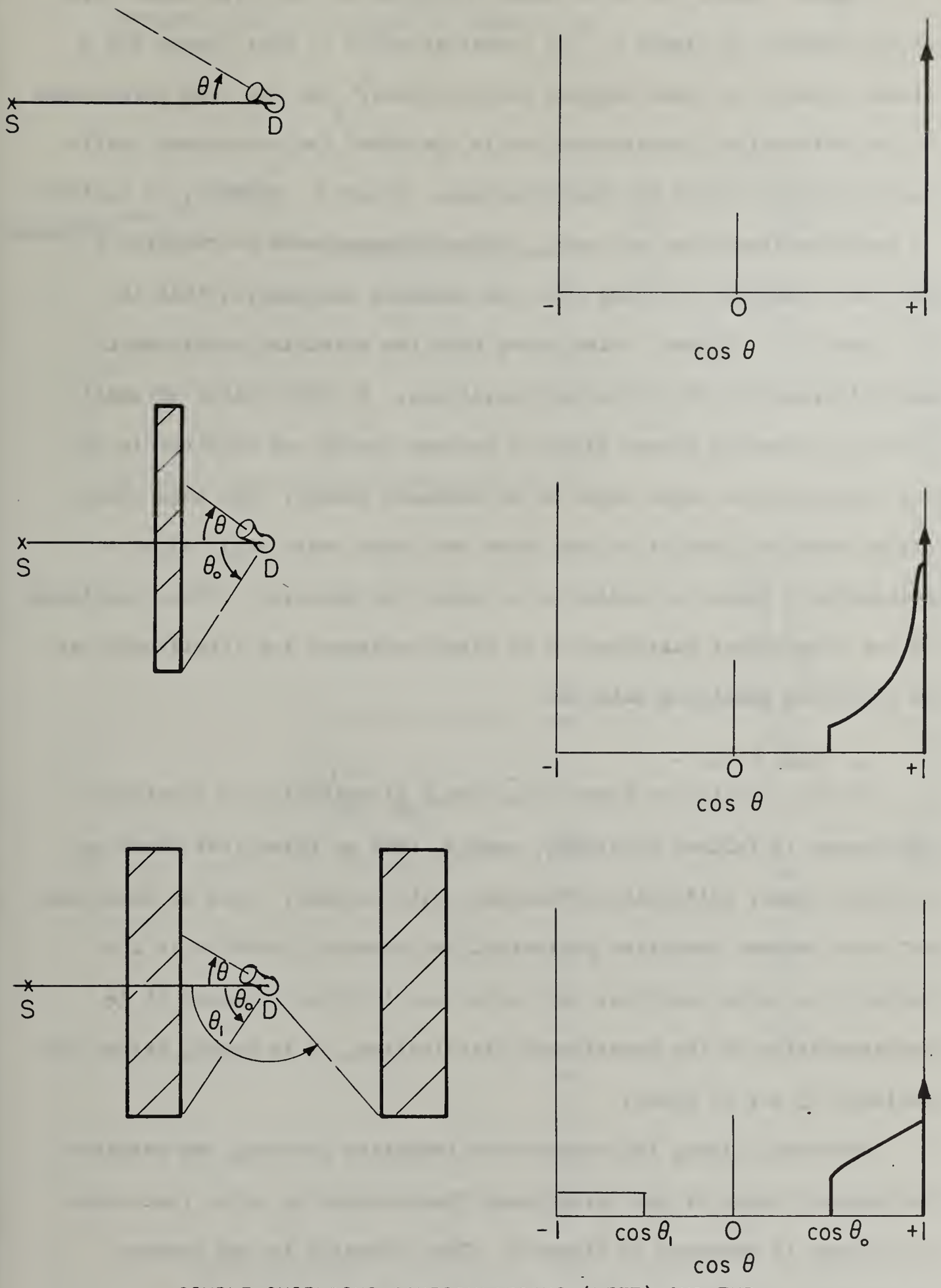

Fig. V-7 SIMPLE SHIELDING CONFIGURATIONS (LEFT) AND THE CORRESPONDING DIPECTIONAL DISTRIBUTION AT THE DETECTOR (RIGHT)

Figure 7 shows the directional distribution for three cases which we saw earlier in Figure 5 . We therefore refer to that figure for a visual picture of those angular distributions. The top view corresponds to the δ-function distribution, while the other two correspond qualitatively to the other two distributions. Figure 5 , however, is limited to positive directions of $\cos\theta$. Another figure would be required to show any radiation arriving from the backward hemisphere, that is, $-1 \leq \cos\theta < 0$. Figure 5 also shows that the shielding requirements are different for the three configurations. A thick shield of small lateral dimensions placed directly between source and detector in the top configuration would serve as an adequate shield. The same shield placed near the barrier in the other two cases would still allow a considerable amount of radiation to reach the detector. Thus, knowledge of the directional distribution is often necessary for intelligent use of available shielding material.

b. Open Field -

We turn now to the first directional distribution of practical importance in fallout shielding, namely, that at three feet above an infinite plane, uniformly contaminated with fallout. This is important not only because radiation protection is expressed relative to the intensity at this position, but, even more important because it is representative of the unperturbed distribution, so to speak, before the building is put in place.

Consider, first, the unscattered radiation reaching the detector. The general shape of the directional distribution at a few feet above the ground is sketched in Figure 8 The intensity is the product of exponential absorption in air and a $\cos\theta$ factor due to the

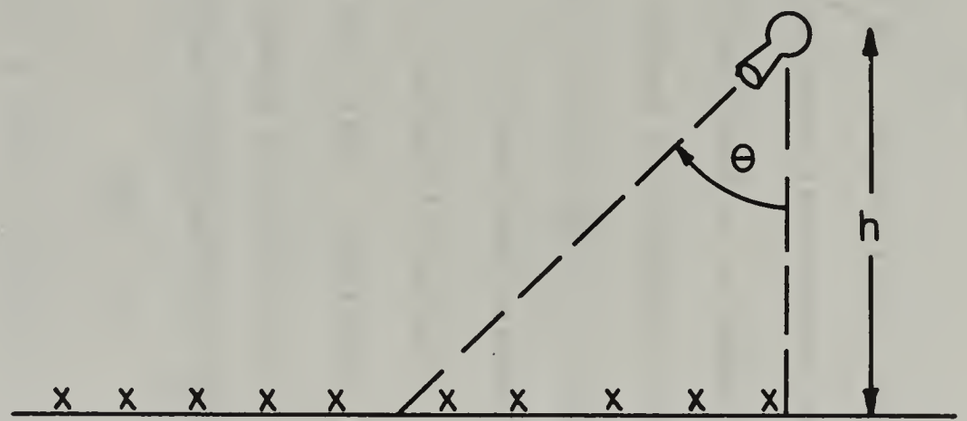

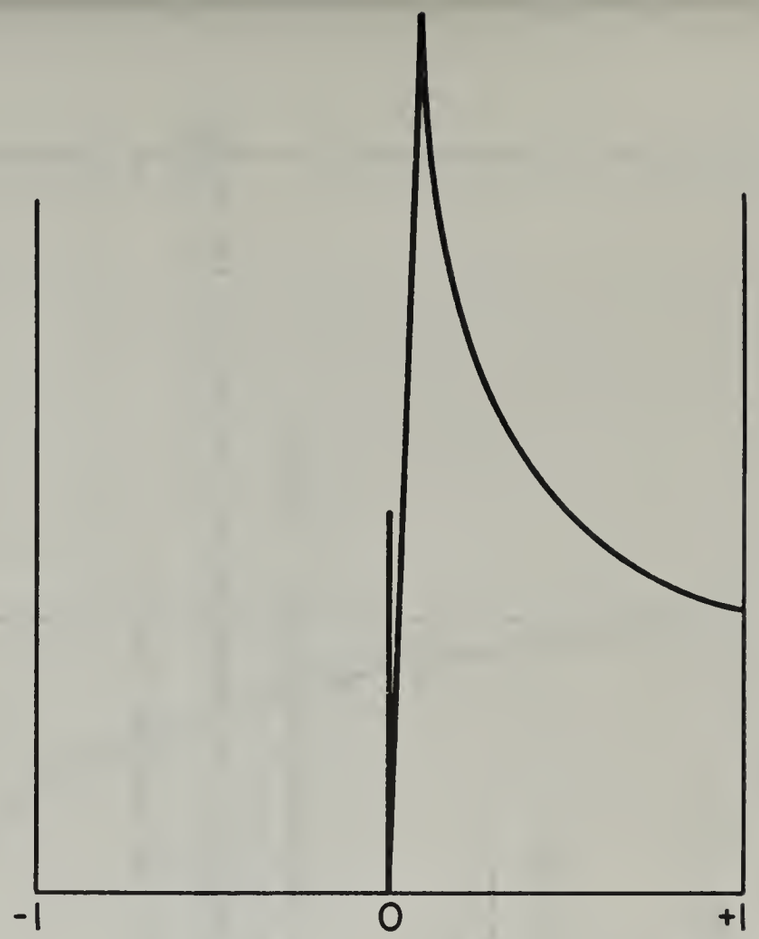

$$\ell^{\circ}(\cos\theta) \sim \frac{e^{-\mu h/\cos\theta}}{\cos\theta}, \quad 0 \leq \cos\theta \leq 1$$

Fig. V-8. GENERAL SHAPE OF THE DIRECTIONAL DISTRIBUTION A FEW FEET (IN AIR) ABOVE A PLANE ISOTROPIC SOURCE

obliquity of the source plane. The total intensity, given by the integral over this expression, is

$$I = \int_0^1 d(\cos\theta) \frac{e^{-\mu h/\cos\theta}}{\cos\theta} ,$$

where h is the height of the detector above the ground.
Let $r = \mu h/\cos\theta$. Substituting in this equation we can derive the more familiar exponential integral expression for I:

$$I = \int_{\mu h}^{\infty} \frac{e^{-r} dr}{r} = E_1 (\mu h) .$$

Returning to the directional distribution, the factor $1/\cos\theta$ dominates near $\cos\theta = 1$ and the exponential absorption in air, $e^{-\mu h/\cos\theta}$ dominates near $\cos\theta = 0$. The result is a distribution with a sharp maximum at $\cos\theta \tilde{=} \mu h$. At greater heights the maximum shifts to higher values of $\cos\theta$. For small values of h the direct radiation determines the main features of the distribution for $\cos\theta > 0$.

When radiation scattered in the air is added to this distribution, the result shown in Figure 9 is obtained. This result was calculated for h = 3 ft by Lew Spencer. We see that the general shape of the curve is the same as that for direct radiation for positive values of $\cos\theta$. In addition,

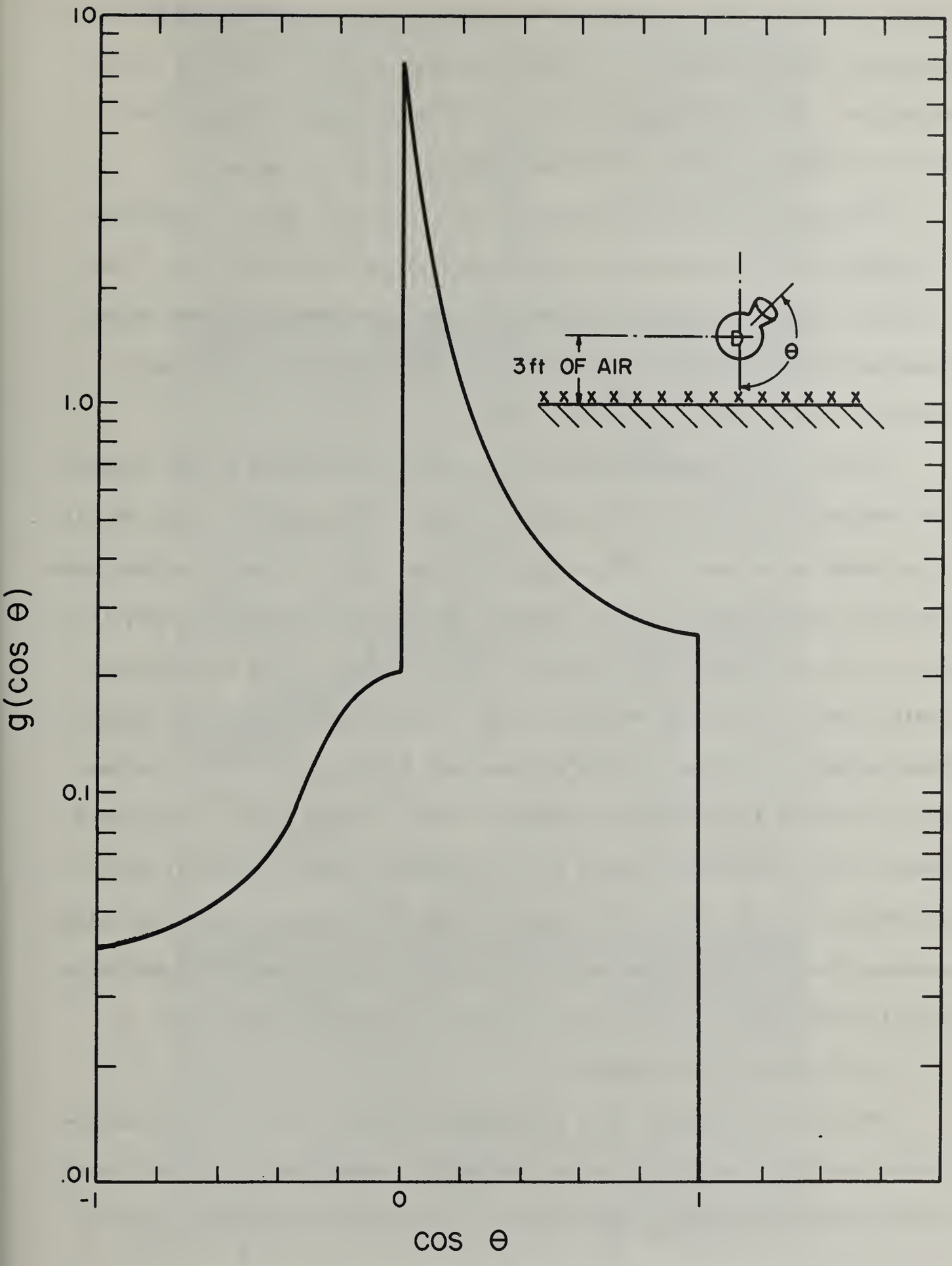

Fig. V-9. DIRECTIONAL DISTRIBUTION OF RADIATION AT THREE FEET (IN AIR) ABOVE A PLANE ISOTROPIC SOURCE OF FALLOUT RADIATION

however, radiation now reaches the detector from directions above the detector, that is, $\cos\theta < 0$. This component is often referred to as skyshine. The total skyshine, which is the integral over negative values of $\cos\theta$, is about 10% of the integral over all angles.

The integral over all angles of this distribution is normalized to unity and all dose rates are expressed relative to this one. The REDUCTION FACTOR is defined as the ratio of dose rate at a particular location to that at three feet above an infinite plane, the source intensity being the same in both cases.

Figure 10 shows directional distributions calculated by Lew Spencer for various heights above an infinite plane. The main effect we see is a decrease in intensity with height. We see that for small heights this decrease is due mainly to the decrease in the spike near $\cos\theta = 0$, that is, in the direction of the horizon. The intensity from radiation arriving from beneath the detector ($\cos\theta = 1$) decreases much more slowly. This is due, of course, to the exponential factor, $e^{-\mu h/\cos\theta}$. We see also the shift in the peak to greater values of $\cos\theta$ which I mentioned before. Increasing the height of the detector, then, gradually shifts the peak intensity from the horizon to the nadir. In terms of our light analogy, the intensity pattern would change from one which was brightest near the horizon to one which was brightest directly below.

c. Inside of Structures -

Now we will consider in a qualitative way the intensity and directional distribution of radiation inside of a structure. We might start with the optical analogy, by plotting the intensity of light inside of

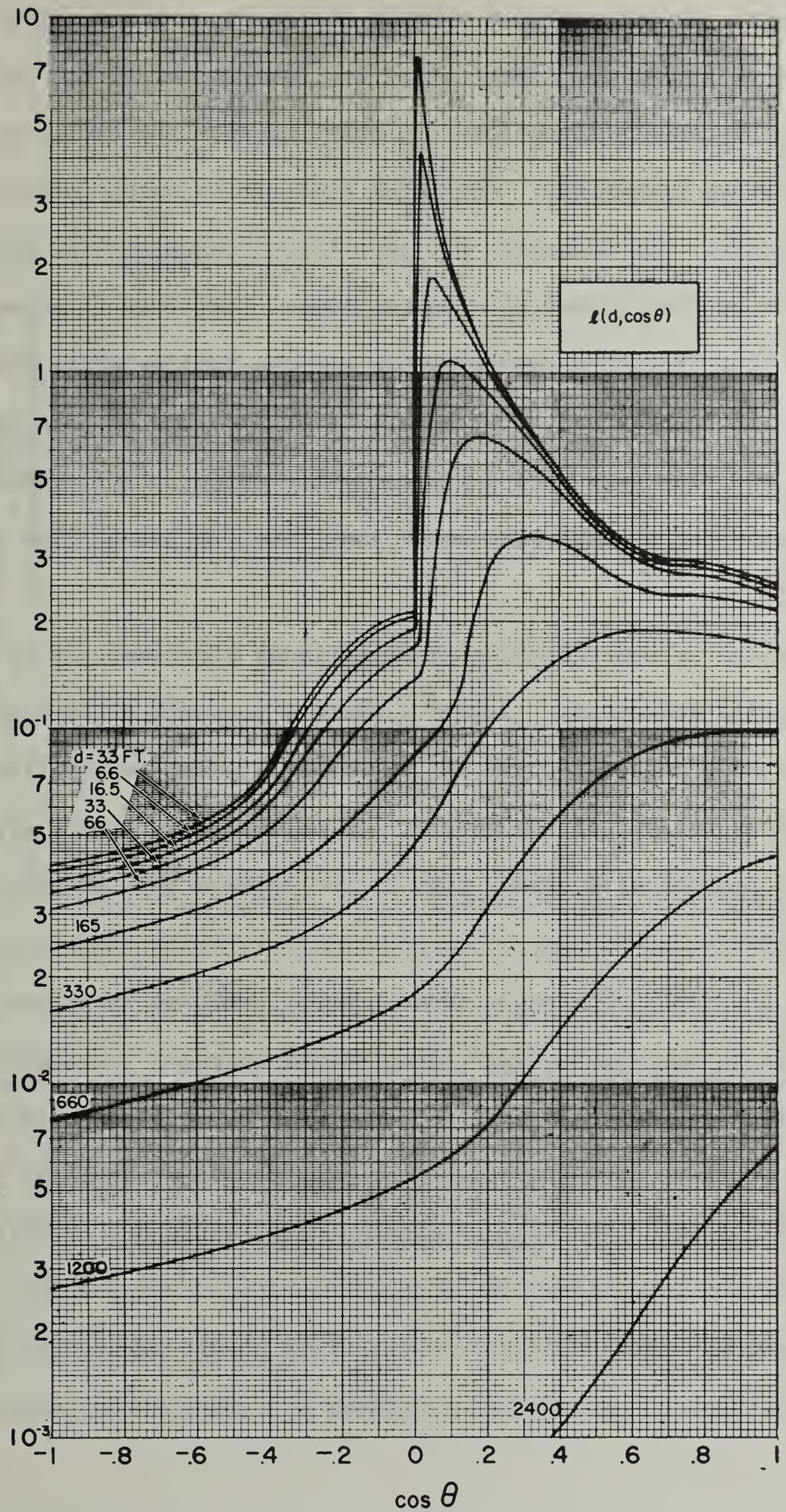

Fig. V-10. DIRECTIONAL DISTRIBUTION OF RADIATION AT VARIOUS HEIGHTS IN AIR ABOVE A PLANE ISOTROPIC SOURCE OF FALLOUT RADIATION

this classroom. In our previous example of the directional distribution in an open field, the distribution was independent of the azimuth, that is, of the compass direction. In the classroom, however, we must specify a compass direction. Let's pick a direction which includes a lighting fixture. The intensity of light looks something like that shown in Figure 11. At $\cos\theta = 1$, that is, looking toward the floor, the intensity of light is low. The walls are brighter and the ceiling still brighter. The ceiling lights, however, are the brightest and show up as a spike near $\cos\theta = -1$. If there were a window in the azimuthal direction we have chosen, the distribution would look like the dashed line added in Figure 8 .

We turn now to some examples of directional distributions of radiation within structures. Figure 12 shows a possible directional distribution at a detector above the window-sill level in a building with very thick walls. If the detector is on the first story, practically no radiation will arrive from directly below the detector. As the detector is swept toward the horizon it sees some radiation penetrating the wall below the window. When it reaches the direction corresponding to sill level there is an abrupt increase in intensity since radiation can travel directly from source to detector with no intervening barrier. Thus, the detector sees the same intensity as if it were out in the open field. Hence, the directional intensity corresponds to the open field intensity which appears as a dashed line on Figure 12. When the detector is raised toward the zenith it encounters first the wall above the windows and finally the ceiling

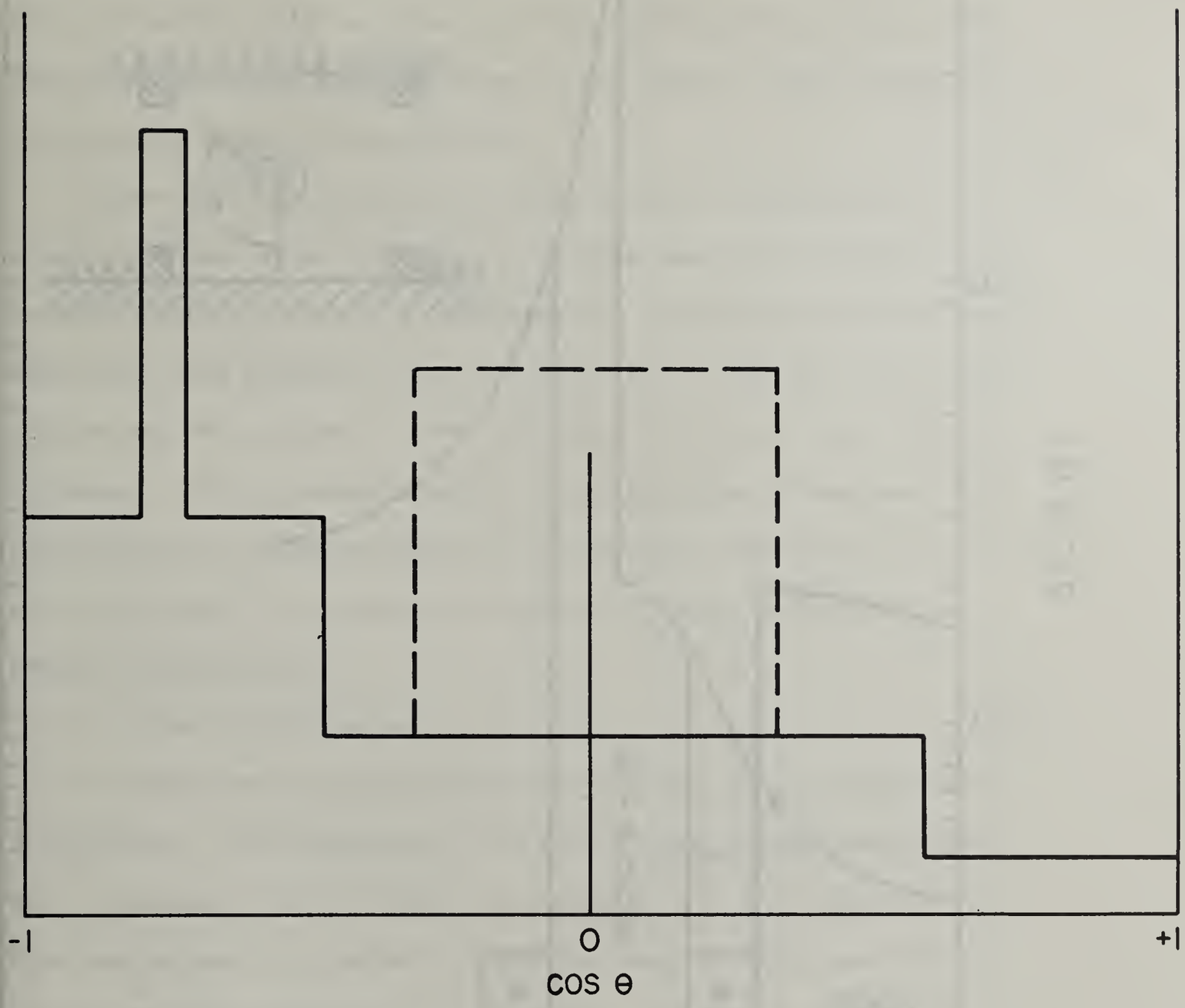

Fig. V-11. HYPOTHETICAL DIRECTIONAL DISTRIBUTION OF VISIBLE LIGHT IN A ROOM. DASHED LINE CORRESPONDS TO THE PRESENCE OF A WINDOW.

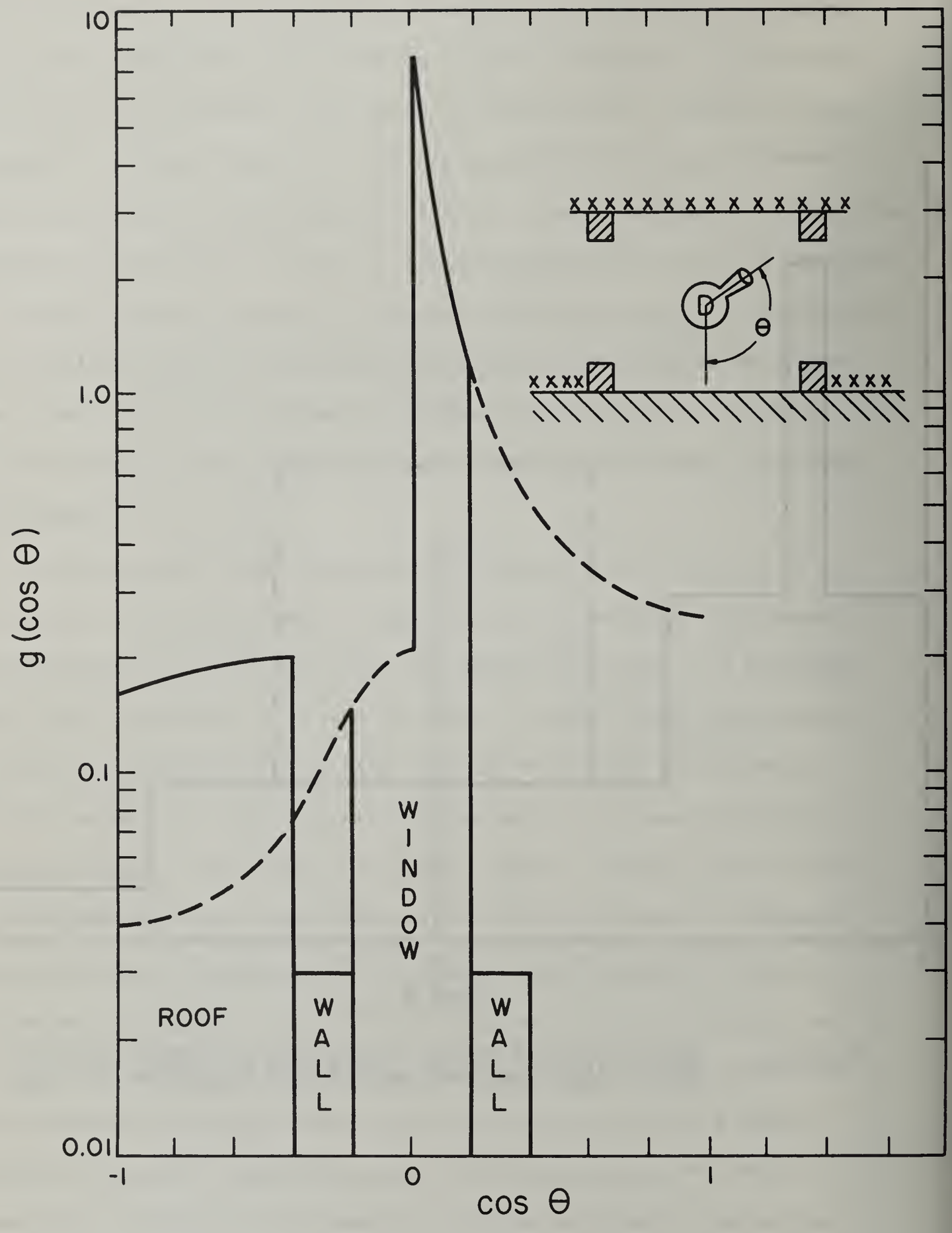

Fig. V-12. HYPOTHETICAL DIRECTIONAL DISTRIBUTION AT A DETECTOR ABOVE WINDOW-SILL LEVEL IN A THICK-WALLED BUILDING

where the intensity is again increased due to the presence of sources on the roof. If this were a cylindrical building, so that the distribution shown in Figure 12 were the same for all azimuths, then the total intensity would be given by the integral under the solid curve. The reduction factor would be given by the ratio of this integral to the integral under the dashed curve.

Figure 13 shows a directional distribution representative of a detector located below sill level. In this case the intensity is low for all positive values of $\cos\theta$, since the radiation through the window comes only from negative values of $\cos\theta$. We can see from this illustration why the dose rates above and below sill level may be quite different. In the present example the sharp spike in the open field distribution is attenuated while in the previous example of a detector above sill level, radiation from part of the spike arrived at the detector unattenuated.

d. Types of Sources -

We have seen how the direction distribution may vary inside of a structure. The problem now is to give a quantitative description and to present a simple method of evaluation. As the first step in this development we consider the types of sources which contribute to the radiation intensity in a structure. We find it convenient to divide the sources into three types, as shown in Figure 14. The first type of source is due to fallout distributed on the roof of the structure. For a flat roof we assume that it constitutes a plane isotropic

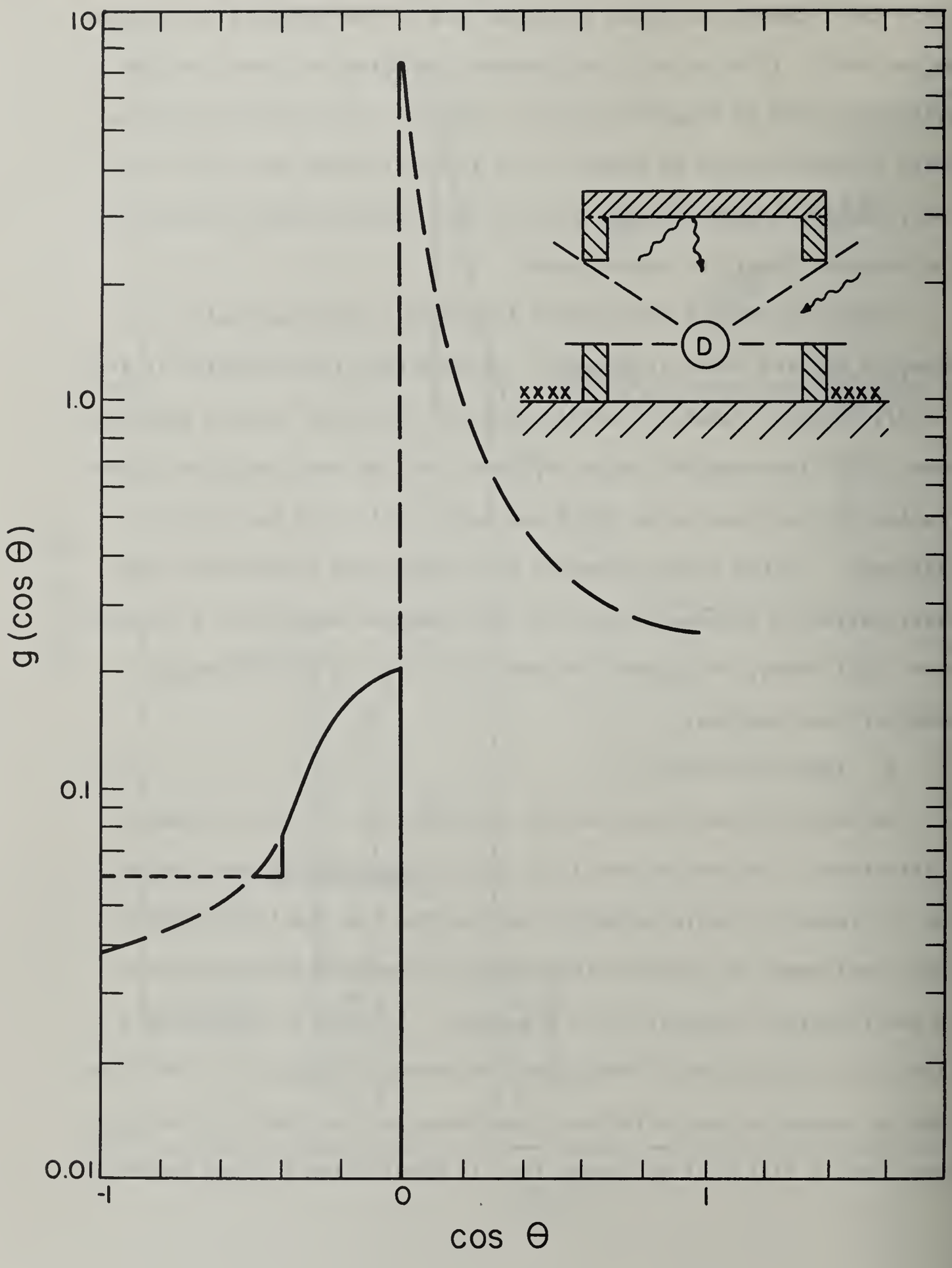

Fig. V-13. HYPOTHETICAL DIRECTIONAL DISTRIBUTION AT A DETECTOR BELOW WINDOW-SILL LEVEL IN A THICK-WALLED BUILDING

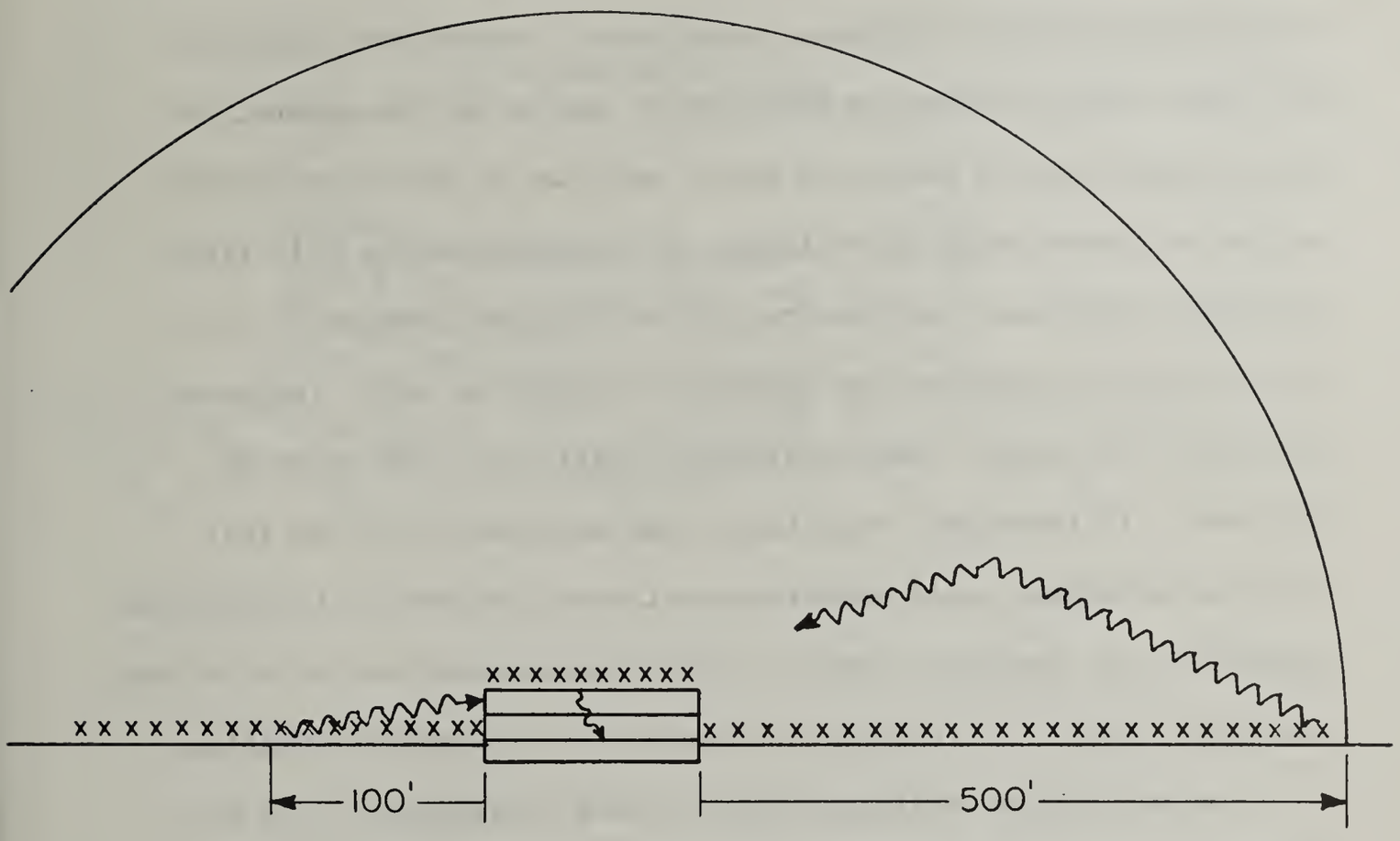

Fig. V-14. SCHEMATIZED VIEW OF THE THREE TYPES OF SOURCES TREATED IN THE ENGINEERING METHOD

source of fallout radiation. The second type of source is due to fallout distributed on the ground around the structure. The radiation from this type of source travels directly from source to the wall of the structure. Since about 3/4 of the intensity is due to sources within about 100 feet of the building we indicate 100 feet is representative of the distance within which sources are important. The third type of source is also due to sources on the ground, but it is constituted of radiation which has made at least one scatter in the air surrounding the building and impinges on the wall from an upward direction. It is often referred to as "skyshine". We can picture the structure as immersed in a bath of air. The mean free path for fallout gamma radiation in air is of the order of 500 feet. It turns out, therefore, that sources out to 500 feet from the structure still make important contributions to the skyshine radiation. An important result is that decontamination is not a very practical method for reducing the intensity of skyshine radiation.

The schematized building which we have considered in the development of the calculations described in this report is shown in Figure 15. It is a cylindrical pillbox, divided into horizontal layers, each of which represents a story of the structure. Since most buildings of interest in shielding are several times longer and wider than an average story height, the radius of our cylinder is several times greater than the height of each layer. Each layer may contain apertures of uniform size and location. This uniformity is

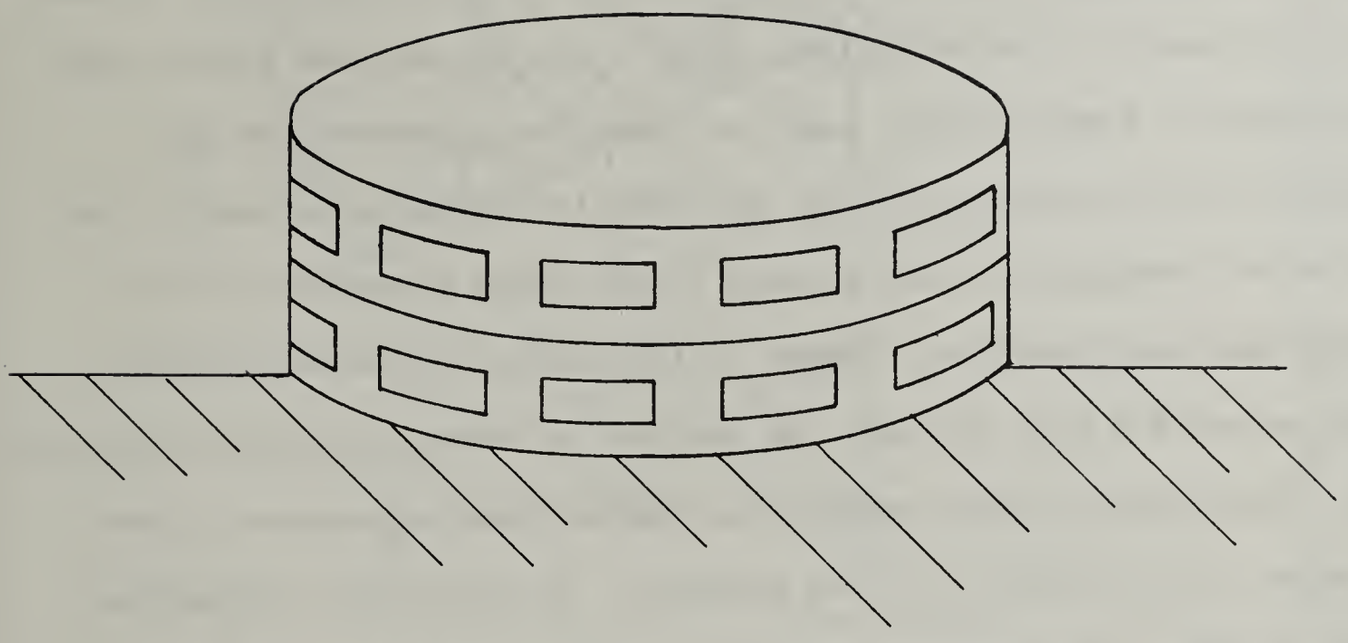

Fig. V-15. SCHEMATIZED VERSION OF A BUILDING USED IN THE DEVELOPMENT OF THE ENGINEERING METHOD

240-816 O-67—53

apt to be present in upper stories of actual buildings, but not perhaps in the first story. We will now discuss these three main types of sources and methods for evaluating their contribution.

4. Roof Source -

We consider first the dose rate due to sources distributed on the roof of a building. Since most buildings are fairly complicated affairs we resort again to SCHEMATIZATION, that is, we replace the actual configuration by a much simpler one. In doing this, however, we must specify certain parameters which determine the shielding capability of the actual configuration and we must relate these parameters to the schematized configuration. Figure [16] illustrates the schematization which we use for roof sources. On the left is shown a typical rectangular roof covered with fallout particles. The roof has a thickness X_o and subtends a solid angle ω_o at the detector. On the right is shown the schematization. The sources are now distributed on a circular area subtending the same solid angle at the detector. Also the barrier material is now uniformly distributed between source and detector, but its total mass thickness remains the same as on the left side. In this schematization, we tacitly assume that once we fix the total mass thickness between source and detector and the solid angle subtended by the source at the detector, the dose rates will be approximately the same.

We can use the curves shown in Figure 10 to obtain reduction factors for the roof schematization. Consider the integral

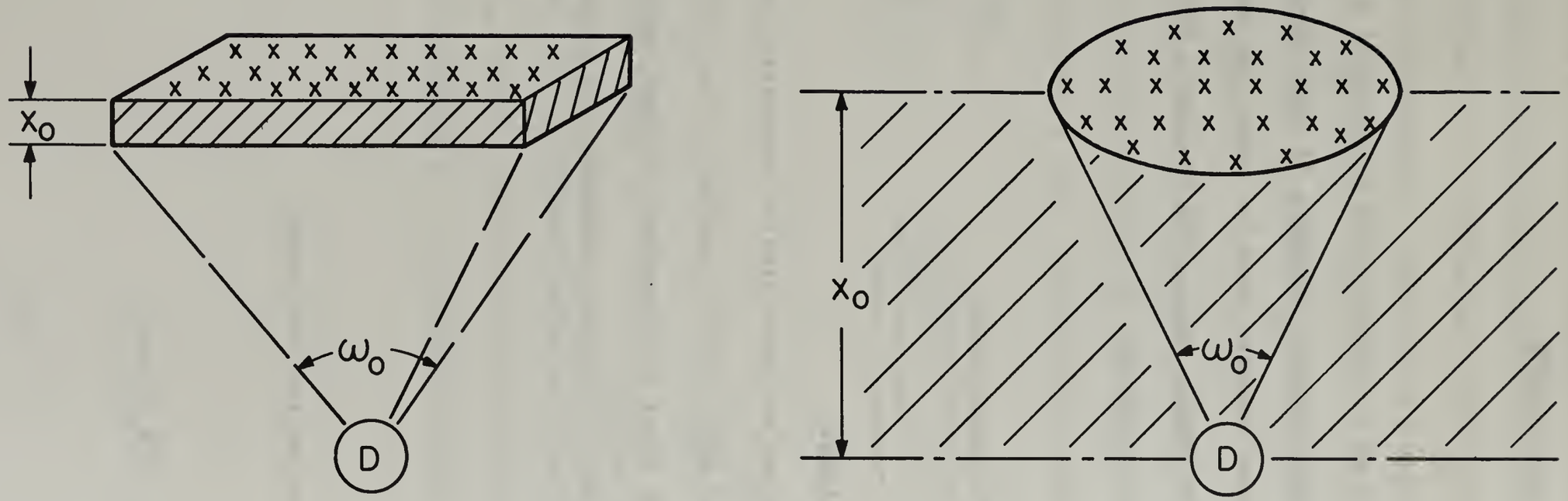

Dig. V-16. RELATION BETWEEN ACTUAL CONFIGURATION (LEFT) AND A CONFIGURATION (RIGHT) SCHEMATIZED TO COMPUTE RADIATION FROM ROOF SOURCES

$$L(d) = \int_{-1}^{1} \ell(d, \cos\theta)\, d(\cos\theta) .$$

It represents the dose rate at a perpendicular distance of d feet of air from a plane isotropic source. However, it also represents the dose rate above a circular cleared area for which the slant distance, r_o, to the nearest source is d. The dose rate from a circular source is therefore given by

$$L(d) - L(d/\cos\theta_o), \quad \cos\theta_o = d/r_o$$

where d is the detector height.

If we assume that concrete and air have similar scattering properties we can convert from feet of air to psf of concrete. The conversion factor is 13.3 ft. of air ≈ 1 psf of concrete. We then convert the parameter θ_o to the solid angle fraction parameter ω by means of

$$\omega = 1 - \cos\theta_o$$

and obtain a new expression for the dose rate:

$$B(X_o, \omega) = L(X_o) - L[X_o/(1-\omega)] .$$

Therefore, we can use the curves in Figure 10 to obtain the function $B(X_o, \omega)$ which gives the reduction factor from a disk source subtending a solid angle fraction of ω at the detector and separated from the detector by a mass thickness X_o. But this is precisely the result we asked for in our schematization. This function is plotted as a series of contour curves in Chart 4 of the Engineering Manual.

Example 1: (See Diagram 1).

If we assume that the density of concrete is 150 pcf then the mass thickness of the roof slab is $150 \times \frac{4}{12} = 50$ PSF.

The solid angle fraction ω can be obtained from Chart 3.

$$n = 2Z/L = \frac{20}{50} = .4$$

$$e = W/L = \frac{30}{50} = .6$$

$$\omega = .56$$

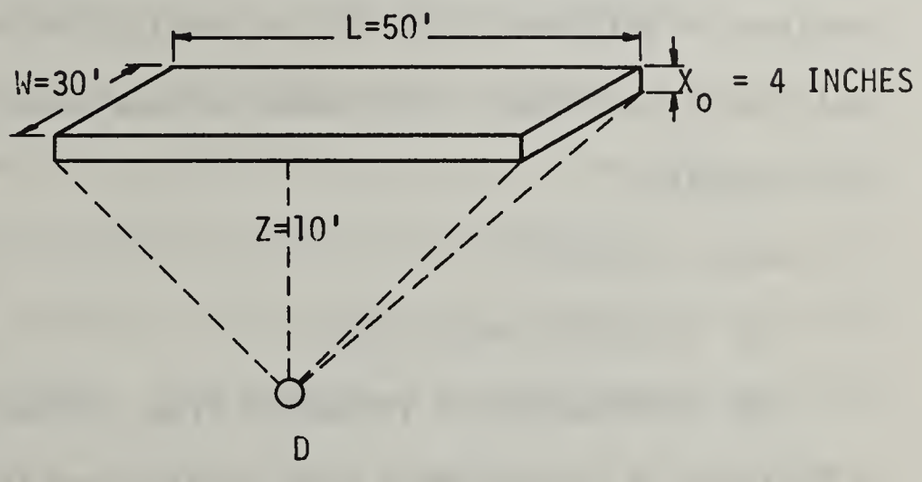

Diagram 1

From Chart 4:

$$B(X_0,\omega) = B(50, .56) = .07$$

The errors inherent in the schematization by circular disk sources and by barriers uniformly distributed between source and detector are discussed in NBS Monograph 76. The maximum error due to smearing

out the barrier is about 40%. The error due to the circular disk approximation is less than 25% for rectangles with length-to-width ratios of less than five. Although the error due to smearing the barrier is fairly large, we should keep in mind two facts. First, Lew Spencer has calculated results for two other configurations, namely, the case of barrier material concentrated near the source and the case of barrier material concentrated near the detector. In situations where the roof sources make an important contribution, one of these two alternatives may provide a closer estimate of the actual reduction factor. Second, in most situations where reasonable shelter is afforded, that is, in middle stories or in basements of multistory buildings, the ground sources make the predominant contribution.

5. Ground Source -

a. Detector above Grade -

The calculation of radiation from sources on the ground surrounding a building is considerably more complicated than the calculation of radiation from roof sources. The basic difficulty is that the radiation from ground sources must penetrate a barrier which is perpendicular to the plane of the source material. Thus, we are confronted with two possible reference directions, namely, the direction normal to the source plane and the direction normal to the barrier. If we choose the latter as our reference direction and consider a detector opposite the center of a rectangular wall we may choose our origin of coordinates

at the detector and our polar axis as the line through the detector and perpendicular to the barrier. But, then we find that the angular distribution of radiation emerging from the wall is no longer azimuthally symmetric about an axis perpendicular to the wall as it was in the case of radiation from the roof. For example, more radiation arrives from below the detector than from above it. Furthermore, walls are often about 10 feet high per story, but over 50 feet long. Thus, it is inaccurate to approximate these highly eccentric rectangles by circular disks. Since we have no information on responses from highly eccentric rectangles radiating with anisotropic azimuthal angular distributions, all angular distributions are referred to the (vertical) direction normal to the source plane. This has the added advantage that we maintain the vertical direction as an axis of symmetry. It has the disadvantage that some correction must be made for the azimuthal dependence of radiation. The azimuth in this system of coordinates is represented by the points of the compass. For example, in a long narrow building there will be a greater intensity arriving from the longer walls than from the shorter walls. No matter which direction we pick for our direction of symmetry, however, we must face a more important shortcoming, and that is that no calculations have been made for the angular distribution of radiation emerging from the inner walls of a building. We have been forced to use angular distributions calculated by Lew Spencer for some idealized configurations.

Before discussing the method we have developed for calculating dose rates from ground sources, I would like to introduce two concepts, namely, barrier factor and geometry factor. Suppose we have an angular distribution $g(X,\cos\theta)$ emerging from a slab of thickness X and suppose we rewrite g as

$$g(X,\cos\theta) = \{\int_o^1 g(X,\cos\theta)d(\cos\theta)\} \; X \; \{[g(X,\cos\theta)/\int_o^1 g(X,\cos\theta)d(\cos\theta)]\}$$

or

$$g(X,\cos\theta) = B(X)g'(X,\cos\theta)$$

where B and g' are condensed notation for the first and second factors, respectively. From the definition of g' it can be seen that

$$\int_o^1 g'(X,\cos\theta)d(\cos\theta) = 1 \; .$$

We could then express the dose rate at a detector with collimating half-angle of θ_o as:

$$R = \int_{\cos\theta_o}^1 g(X,\cos\theta) = B(X) \int_{(1-\omega)}^1 g'(X,\cos\theta) = B(X)G(X,\omega) \; .$$

The first factor, the barrier factor, depends only on the mass thickness, while the second factor, the geometry factor, depends primarily on the solid angle fraction and only weakly on the mass thickness. It is a correction for the fact that the detector receives radiation from within a limited solid angle.

It is convenient to make this separation when the directional distributions are nearly constant in shape or, even more important, when it is necessary to approximate unknown directional distributions. It is for the latter reason that we have used this separation in the treatment of radiation from ground sources.

We consider first the dose rate inside of a cylindrical structure with vanishingly thin walls. We find it convenient to use solid angle fractions $\omega_u \equiv 1 - \cos\theta_u$ and $\omega_\ell \equiv 1 - \cos\theta_\ell$. The angle θ_ℓ is the polar angle relative to the downward vertical direction and θ_u is the polar angle relative to the upward vertical direction. The dose rates from radiation through the walls can be expressed as

$$R = \int_0^{\cos\theta_\ell} \ell(3', \cos\theta)d(\cos\theta) + \int_{-\cos\theta_u}^{0} \ell(3', \cos\theta)d(\cos\theta) ,$$

or

$$R = G_d(\omega_\ell, 3') + G_a(\omega_u, 3')$$

The first equation uses the nomenclature of Lew Spencer's Monograph and gives the mathematical expression for the geometry factors for radiation through the walls. The second equation uses the nomenclature of the Engineering Manual. The subscripts d and a refer to direct and air-scattered, respectively.* In physical terms we consider all radiation which arrives at the detector from directions which intersect the walls of the structure. Since the walls of the structure are of zero thickness, the directional distribution is the same as that for the open field.

For thin walls we write the dose rate as:

$$R = B(X_w)[G_d(\omega_\ell, 3') + G_a(\omega_u, 3')]$$

where the barrier factor $B(X_w)$ accounts for the attenuation of the walls. This barrier factor has been computed by Lew Spencer for a wide range of wall thicknesses. Note that we have simplified the geometry factor by ignoring its dependence on X_w. This is equivalent to assuming that the barrier does not distort the shape of the

---

*Actually $G_a(\omega_u, 3')$ also includes a correction for ceiling shine and is given by $G_a = G_a'[1+5(.1-G_a')]$ where G_a' is given by the second term on the RHS of Spencer's equation.

directional distribution. This assumption can only be justified insofar as it predicts dose rates to within an accuracy satisfactory to the shield designer. The geometry factors G_d and G_a are plotted in Chart 5 of the Engineering Manual.

We turn now to the opposite extreme of a structure with very thick walls. In this context, the work "thick" means much greater than about 40 psf (about 3 inches of concrete). In this case, virtually all the radiation emerging from the inner side of the wall will have scattered at least once in the barrier. The problem then was to assume some directional distribution for this radiation, since no calculations existed at the time. We chose the directional distribution of air-scattered radiation as an approximate distribution. The implicit reasoning behind this choice is that the distribution of scattered radiation behind a barrier will resemble the equilibrium distribution of scattered radiation in air. We therefore calculate the geometry factor for wall-scattered radiation as:

$$G_s(\omega_i) = 5 \int_{-\cos\theta_i}^{0} \ell(3', \cos\theta) d(\cos\theta),$$

where the subscript i refers to either upper or lower angles.

Since the integral from -1 to 0 is 0.1 and since we assume that the distribution is the same in the upper and lower hemisphere, the factor of 5 is required for proper normalization. In physical terms we assume that the radiation scatters so many times that the up-down asymmetry in the original distribution washes out. Figure 17 shows the distributions assumed for thick walls.

Having obtained an expression for the geometry factor we seek one for the barrier factor. The barrier factor calculated by Lew Spencer applies to a detector located between two parallel walls of infinite extent, as shown on the right side of Figure 18. Our geometry factor, however, is based on a cylindrical structure, since we have ignored any variation of intensity with azimuth. This conflict of rectangular and cylindrical geometries is the main disadvantage of the approach used in the Engineering Method. We have welded the two geometries together by means of a shape factor. This factor is an attempt to correct for the fact that the dose rates in the two configurations of Figure 18 are expected to be different, even though the barrier thicknesses are identical. The shape factor is based on the assumption that the dose rate from a straight wall varies as $\cos\phi$ where ϕ is the azimuthal angle. ($\phi = 0$) is defined by a line from the detector, perpendicular to the wall. The reduction factor is then expressed as

$$R_f = B(X_w)E[G_s(\omega_\ell) + G_s(\omega_u)] .$$

The shape factor E is plotted in Chart 8 of the Engineering Manual.

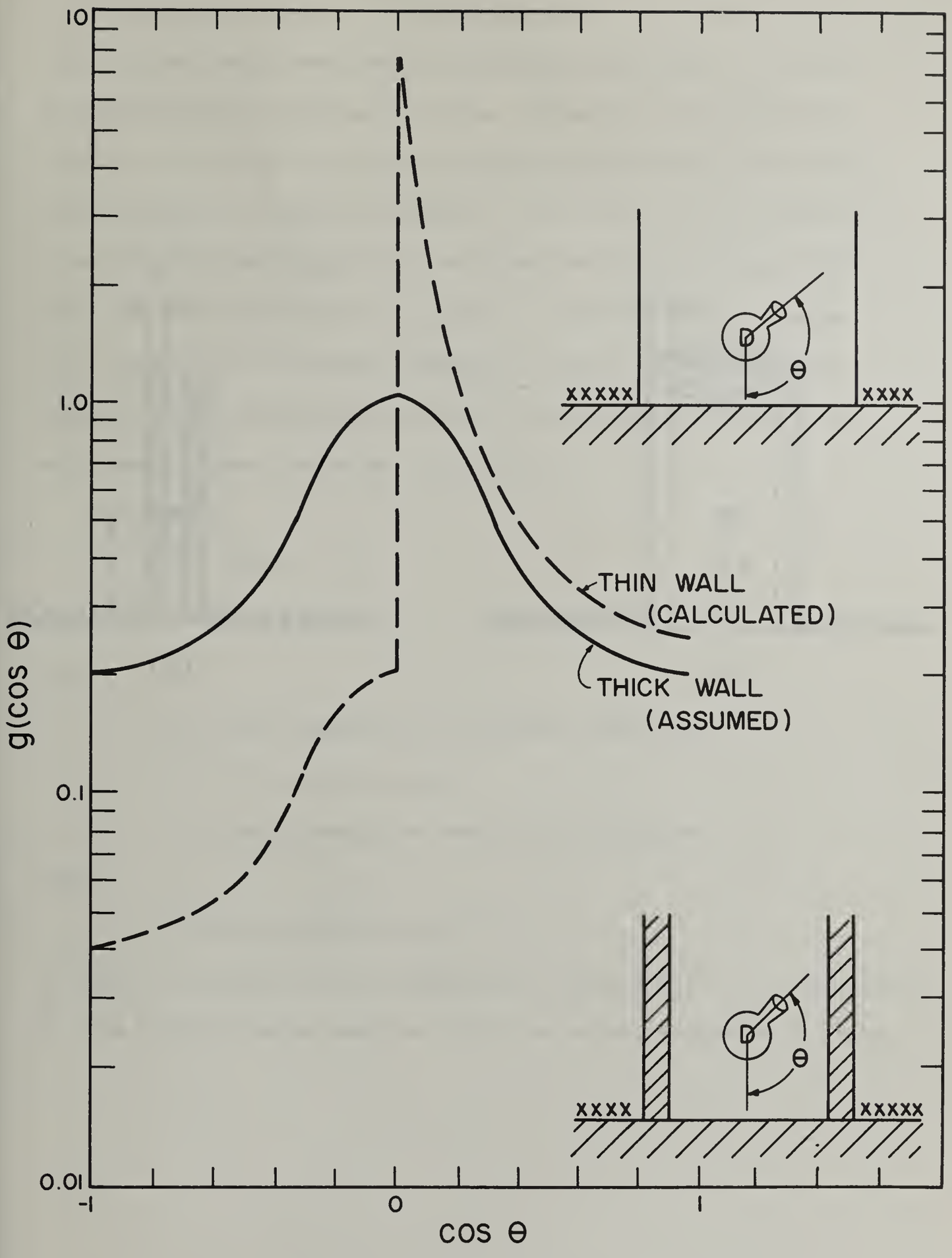

Fig. V-17. DIRECTIONAL DISTRIBUTION OF RADIATION INSIDE OF STRUCTURES WITH THIN AND THICK WALLS

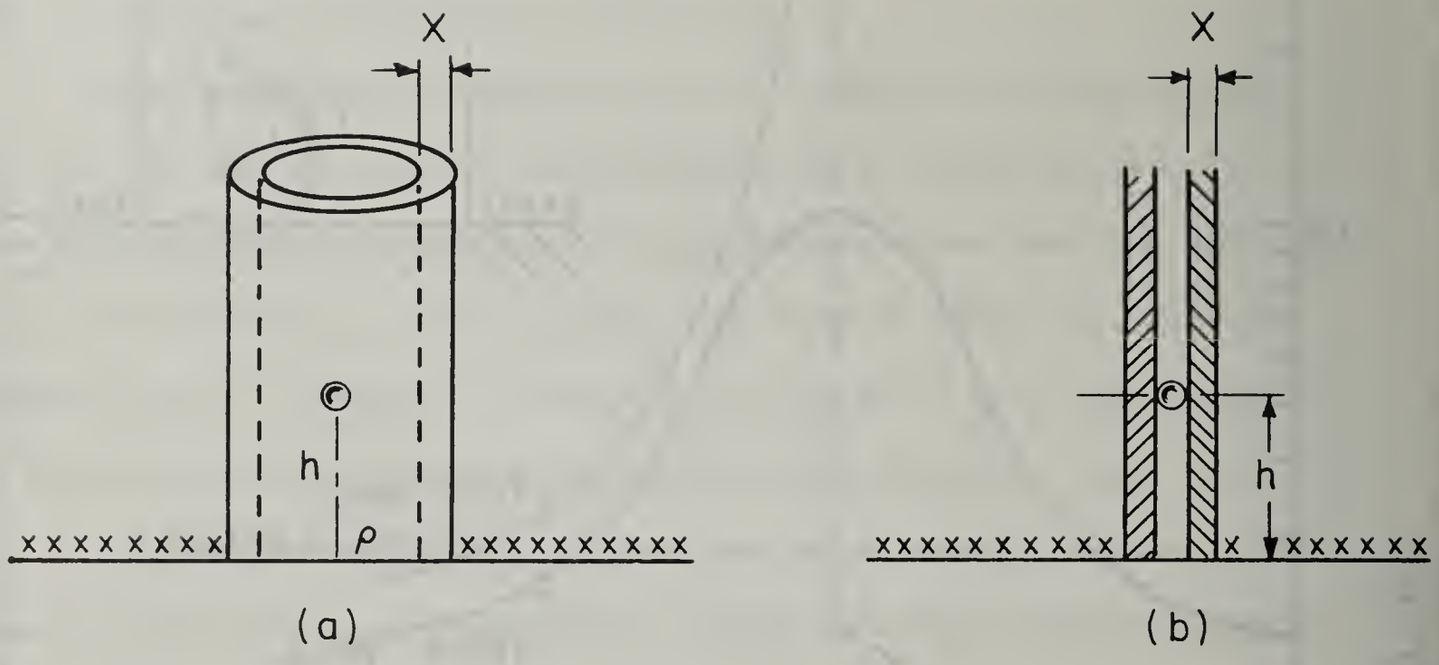

Fig. V-18. CYLINDRICAL STRUCTURE (LEFT AND LONG, NARROW RECTANGULAR STRUCTURE (RIGHT)

We have now discussed the formulas to be used in the case of very thin and very thick walls. Most practical cases of interest fall somewhere in between, of course. Since the two extremes are based on the absence of scattered radiation (thin wall) and on the preponderance of scattered radiation (thick wall), each result may be weighted by the fraction of scattered radiation emerging from a wall of some intermediate thickness. What we require, then, is the fraction of the emerging radiation which is scattered. This fraction can be obtained from buildup factor data. The ratio of scattered to total radiation is given by

$$\frac{SC}{T} = \frac{T-U}{T} = 1 - \frac{1}{B}$$

where

SC is the intensity of scattered radiation

T is the total intensity

U is the intensity of unscattered radiation

and

B is the buildup factor.

We call the fraction SC/T of scattered radiation $S_w(X)$. We calculated it from buildup factor data for Co-60 and normal incidence on slabs.

It turns out, as discussed in NBS Monograph 76, that the $S_w(X)$ curve obtained in this way is not very different from one obtained by using point source data for fission product radiation. The reduction factor for walls of intermediate thickness is given by

$$(1) \quad R_f = B(X_w) \{ES_w(X)[G_s(\omega_\ell) + G_s(\omega_u)]+[1-S_w(X)] [G_d(\omega_\ell)+G_a(\omega_u)]\}$$

Example 2: (See Diagram 2).

We consider the reduction factor for radiation penetrating the walls of a blockhouse with 40 psf walls. For simplicity we place the detector at a height of 5 feet so that the upper and lower solid angle are equal.

First we find the value of the solid angle fraction. The eccentricity ratio is e = 40/100 = 0.4 and the "normality" ratio is n = 10/100 = 0.1

From Chart 3, $\omega_\ell = \omega_u = .835$

From Chart 5, $G_d(\omega_\ell) = .54$

$G_a(\omega_u) = .047$

$G_s(\omega) = .18$

From Chart 7, $S_w(X) = .53$

From Chart 8, E(0.4) =1.3

and finally, from Chart 1 $B(X_w) = .38$

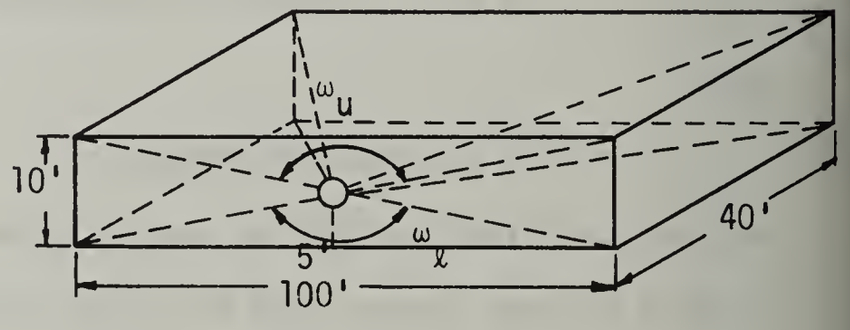

Diagram 2

Therefore

$$R_f = B(X_w)\{ES_w(X)[G_s(\omega_\ell)+G_s(\omega_u)]+[1-S_w(X)][G_d(\omega_\perp)+G_a(\omega_u)]\}$$

$$= (.38)\{(1.3)\ (.53)[.18 + .18]+(.47)[.54 + .047]\}$$

$$= (.38)\{.25 + .28\} = .20 \qquad \text{ANSWER}$$

b. Detector Below Grade

The previous discussion has applied to the case when a horizontal plane through the detector (the "detector plane") intersects the wall of interest. In many cases, however, such as a detector located below grade, the wall of interest lies entirely above or entirely below the detector. In such cases we have to modify the expression for the reduction factor.

240-816 O-67—54

Consider a detector located below grade as in Figure 19 . If we neglect albedo from the walls and floor below the detector plane we can delete any terms in equation (1) involving ω_ℓ . On the other hand, the wall is now defined by two upper solid angle fractions, ω_u and ω_u'. In order to obtain the response from such a wall we must <u>difference</u> the geometry factors for the two solid angle fractions. The resulting expression is

$$(2) \quad R_f = B(X_w)\{ES_w(X)[G_s(\omega_u')-G_s(\omega_u)]+[1-S_w(X)]X[G_a(\omega_u')-G_a(\omega_u)]\} .$$

This expression predicts a phenomenon which is worth discussing in a little detail. Suppose we do a hypothetical experiment in which we start with a building whose walls are of zero thickness and measure the dose below grade as we increase the thickness of the walls. If we examine the various factors in equation (2) we see that the barrier factor decreases with increasing values of X_w. The thick-wall geometry factor (the first term inside of the braces) increases with X_w, while the second term decreases. For some configurations the first term may increase so rapidly that it outweighs the decrease in the other term and the barrier factor. The dose may therefore increase with X_w, go through a maximum, and then decrease with X_w. Although such an increase has not been demonstrated experimentally, it is certain that

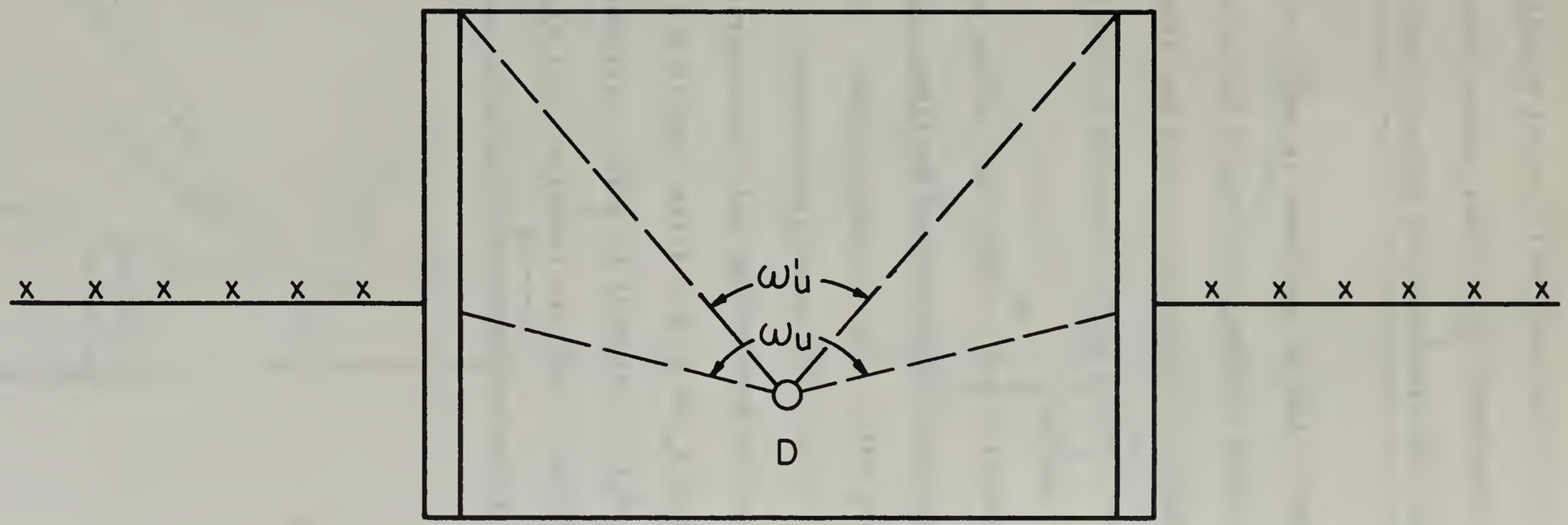

Fig. V-19. ELEVATION VIEW OF A STRUCTURE IN WHICH THE DETECTOR IS LOCATED BELOW GRADE

the first 40 psf added to the first story wall do not significantly decrease the dose rate at detectors below grade, and may possibly increase it. This concludes the discussion on ground sources.

6. Skyshine -

The third type of source which we mentioned is skyshine. Skyshine is ordinarily a secondary effect in that it accounts for only 10% of the dose in an open field. However, in situations where the direct component of radiation is absent due to heavy shielding of some sort, skyshine must be taken into account.

Two situations where skyshine may be important are the case of a detector located below windows in a thick walled building, and a detector in the basement of a building with a light superstructure. The first situation is shown in Figure 20 a. This actually represents a special case of equation 2. Since we are considering only the contribution through apertures the value of X_w is 0, the first term in the brackets disappears, and $[1-S_w(X)]$ is equal to unity. Furthermore, $B(X_w) = 1$. If the windows occupy a certain fraction P_a of the perimeter, then the expression for the reduction factor for radiation received through the apertures is

$$R_f = [G_a(\omega_u')-G_a(\omega_u)]P_a .$$

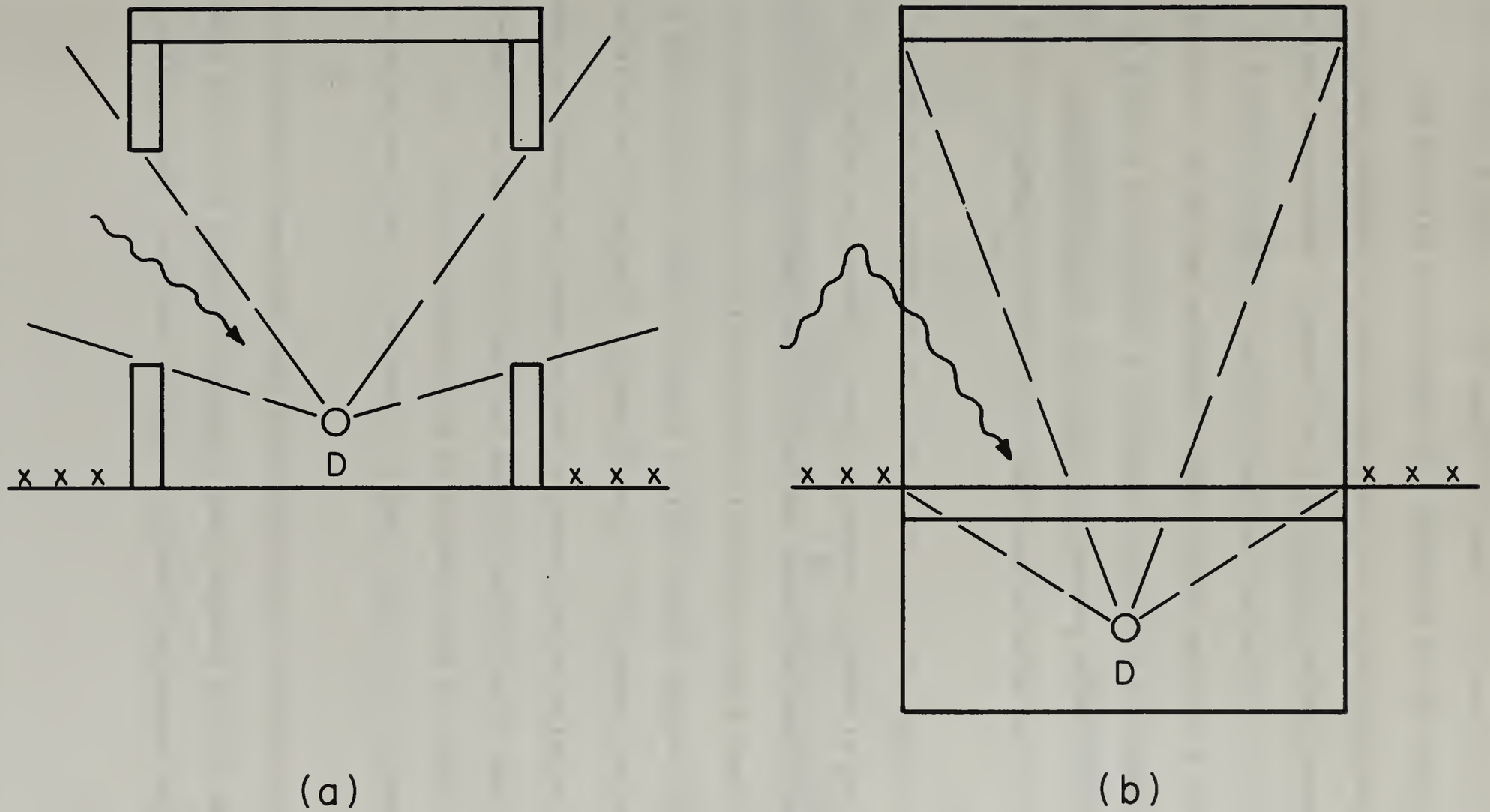

Fig. V-20. SITUATIONS IN WHICH SKYSHINE MAY MAKE AN IMPORTANT CONTRIBUTION TO RADIATION DOSE: DETECTOR BELOW WINDOW-SILL LEVEL IN A THICK-WALLED BUILDING (LEFT) AND DETECTOR IN BASEMENT OF A BUILDING WITH LIGHT SUPERSTRUCTURE (RIGHT)

In the second situation, shown in Figure 20b, we wish to calculate the reduction factor in the basement. In order to do this, we must first derive a barrier factor for the penetration of skyshine radiation. This barrier factor can be calculated if we consider the schematization shown in Figure 18. The actual configuration is a detector located at a depth X_o' below a clearing whose radial dimension may be of the order of 25'. The schematized situation represents a detector at a depth X_o' below a source which emits photons only into the upward hemisphere. All photons counted by the detector must have crossed the interface an odd number of times.

The main difference between the actual and schematized situations is that the actual situation contains a clearing above the detector whereas the schematized configuration contains an infinite plane isotropic source. It has been demonstrated both theoretically and experimentally, however, that the sources lying within a radius of about 50 feet from a point contribute only about 10% to the intensity of skyshine at that point. Therefore, the skyshine in the actual situation should be about the same as that in the case of an infinite plane isotropic source at a ground-air interface. But this, in turn, should be approximately equal to the schematized situation of a plane isotropic source in a uniform infinite medium.

The barrier factor for the schematized case has been calculated by Lew Spencer, and for the reasons just discussed we apply it to the penetration of fallout radiation through a basement ceiling. This barrier

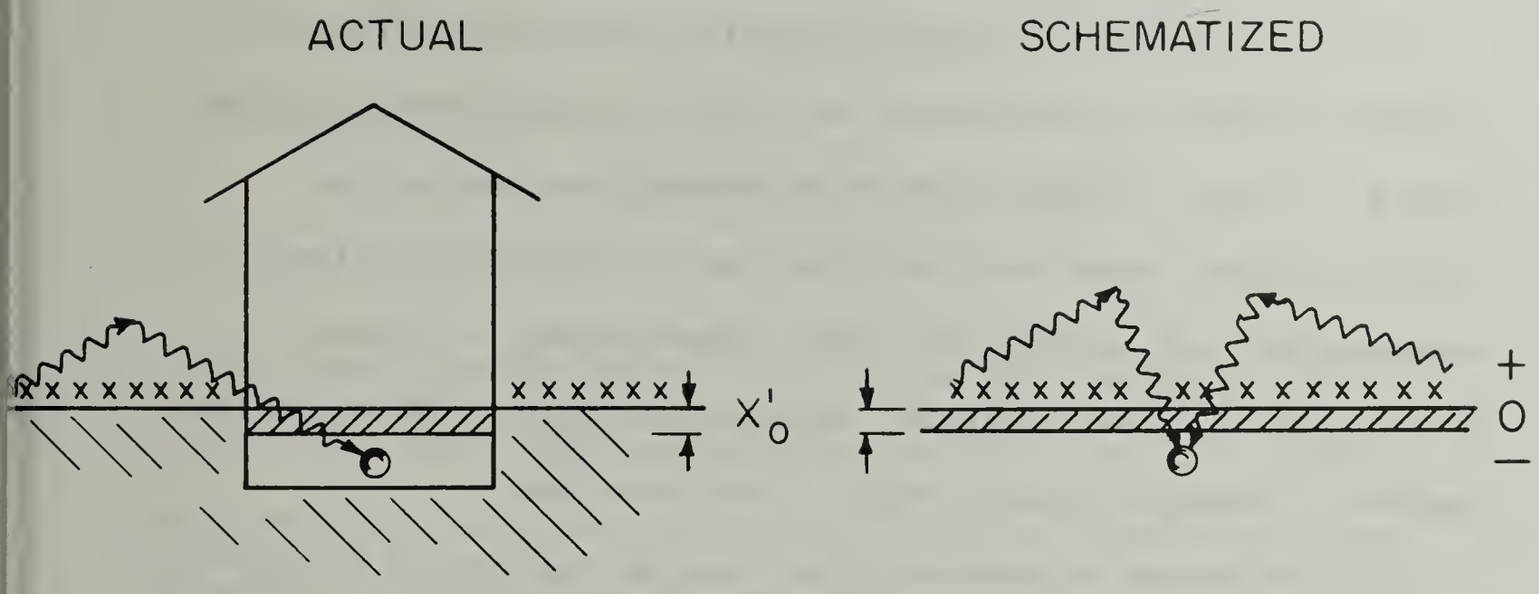

Fig. V-21. RELATION BETWEEN ACTUAL CONFIGURATION (LEFT) AND A CONFIGURATION (RIGHT) SCHEMATIZED TO COMPUTE PENETRATION OF SKYSHINE RADIATION

curve is labeled $B_o'(X_o')$ and is shown as Case 3 in Chart 1. The reduction factor in a basement due to skyshine radiation is given by

$$R_f = B_o'(X_o')[G_a(\omega_u')-G_a(\omega_u)].$$

7. Limited Strips of Contamination -

Up to this point our entire discussion has been concerned with isolated buildings, surrounded by an infinite plane isotropic source. However in urban, or even in suburban, areas where most of our existing shelter space lies, buildings are surrounded by strips of contamination such as lawns and roads whose extent is limited by the presence of other buildings. Calculations must therefore include some way of handling limited areas of contamination.

When we reduce the semi-infinite field on one side of a long wall to a finite area,we reduce the dose on the other side of the wall for two reasons. First, the dose is decreased because the intensity incident on the wall is decreased by virtue of our having removed some of the sources. But, secondly, the barrier factor is reduced because we have altered the directional distribution incident on the wall. By eliminating those sources at great distance we have removed much of the radiation which was perpendicularly incident on the barrier.

The remaining incident radiation therefore contains a higher fraction of radiation incident at slant angles and not as likely to penetrate.

Although limited areas of contamination are apt to be rectangular in practice, we have only Lew Spencer's calculations for semicircular areas of contamination of radius ρ and detectors at height h. (See Figure 22.) The correspondence between the rectangle and the semicircles was determined by equating solid angles at the detector:

$$\omega = (1-\cos\theta) = \frac{2}{\pi}\tan^{-1}\frac{e}{n\sqrt{n^2+e^2+1}}.$$

Thus, for a given detector height H and a rectangular strip of width W and length L, the solid angle subtended by the strip can be calculated. This solid angle and the wall thickness are the input numbers required for Lew Spencer's calculations for semicircular sources. The calculated curve $B_{ws}(X_w,\omega)$ is plotted as a series of contour curves in Chart 9 of the Engineering Manual.

In these few lectures I have tried to indicate how the Engineering Method was developed for a simple type of building such as a blockhouse. My discussion has been limited to detector locations on the first story or in the basement.

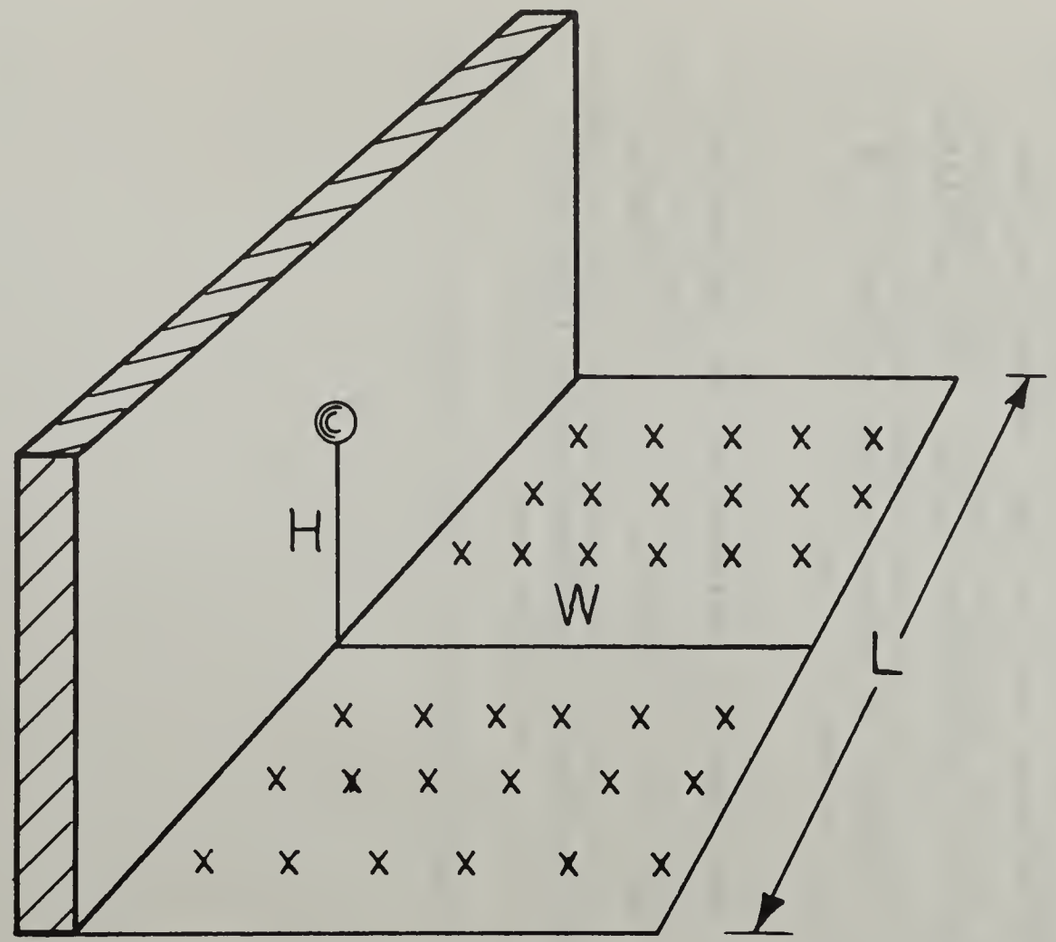

$e = 2W/L$, $n = 2H/L$

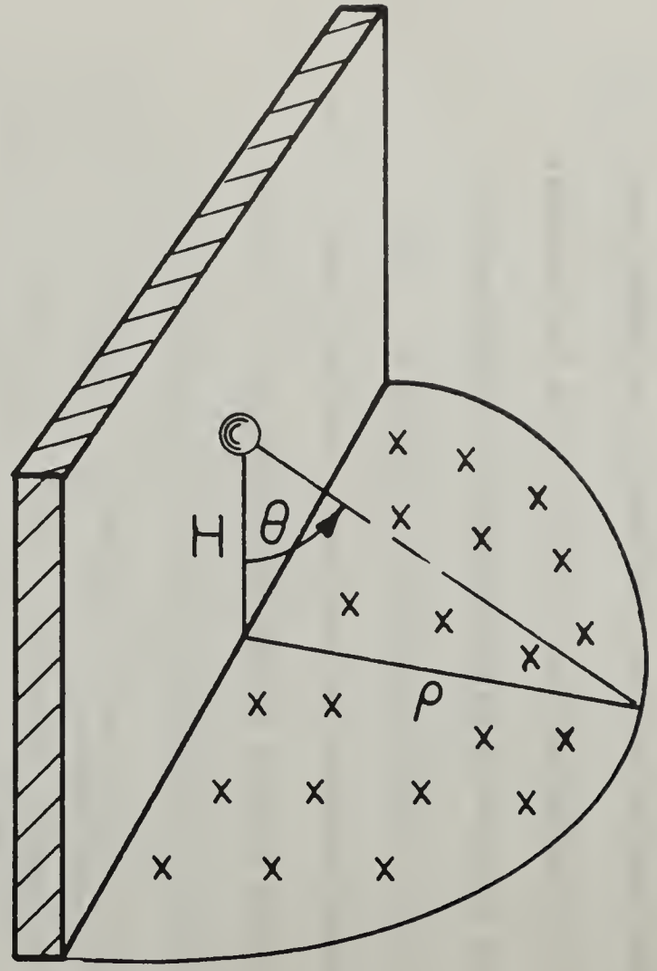

$\text{Tan } \theta = \rho/H$

Fig. V-22. RELATION BETWEEN ACTUAL CONFIGURATION (LEFT) AND THE CONFIGURATION (RIGHT) SCHEMATIZED TO COMPUTE PENETRATION OF RADIATION FROM FINITE RECTANGULAR SOURCES, THROUGH THE WALLS OF A STRUCTURE

Although I have tried, in some cases, to justify the procedures we have developed, the ultimate justification depends on experimental confirmation. The results of experiments to date indicate that some changes will have to be made in the basic charts and some minor changes in procedures. However, experimental results are not always conclusive. The next big step in the development of the Engineering Method seems to be a detailed analysis of existing experiments to determine in what ways the calculational procedures should be modified.

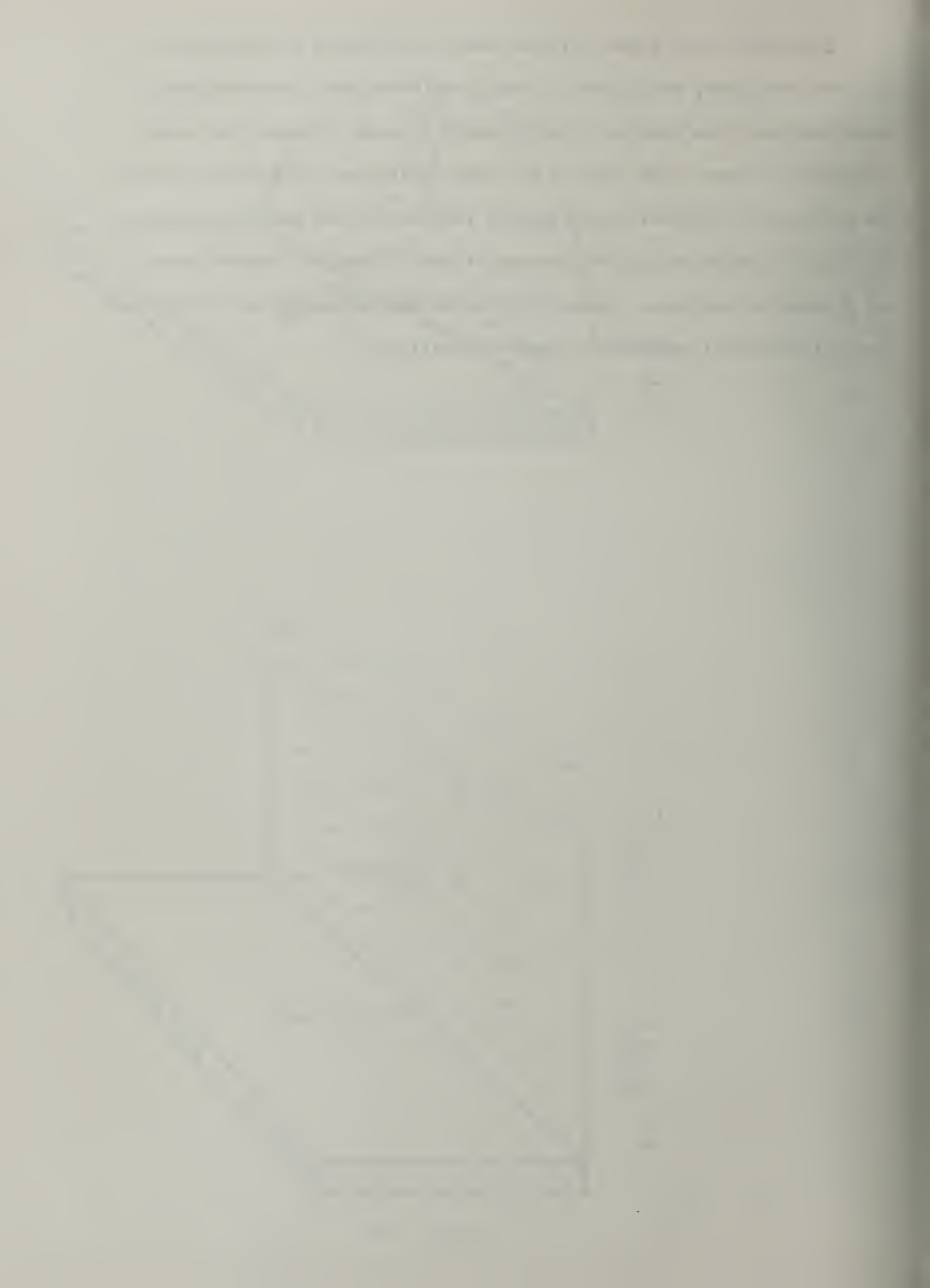

C. Simplified Engineering Methods

1. Simplified Method in Guide for Architects and Engineers -

I would like now to give a somewhat detailed discussion of the Guide for Architects and Engineers which I will refer to as the AE Guide. As I mentioned, there was pressure early in the development of the engineering method to come up with a simplified method. We therefore tried to develop a method suitable for surveys. I will call it the survey method. The philosophy of this method, in general, is as follows: It was designed primarily for statistical application. Since it was a simplified method with fewer variables than the engineering method we had less faith in the accuracy of the calculations. We therefore felt it should be used only on a large number of buildings where some kind of statistical estimate is required. It was not designed to obtain detailed information on individual buildings. It was hoped that the engineering method would be used in the latter case.

The main difference between the AE Guide method and the engineering method in terms of parameters was that we eliminated the use of solid angles. It was felt at the time that a solid angle was a concept that most engineers did not use in everyday practice and that eliminating it as a parameter would simplify the calculations. We therefore assumed a square building, and

fixed the detector height. Once that was done, the solid angle parameter could be translated into an area parameter which was much more familiar to the people who would be using the survey method. Another simplification was the elimination of separate calculations for barrier and geometry factors. The charts in the AE Guide are the result of calculations in which the geometry and barrier factors have been combined beforehand.

Besides the assumption of a square building, the survey method also assumed that the detector position above grade was fixed at 3 feet above grade. This height does not necessarily correspond to 3 feet above the first floor. However, when the two are different, the calculation actually applies to 3 feet above grade. For below grade, the detector position was arbitrarily selected at 5 feet below the first floor. Again, if the first floor is not at grade level, the detector height will correspond to some height other than 5 feet below grade. Since the main contribution to below-grade detectors may come from radiation which enters the walls of the story above and scatters down, some assumption had to be made about the height of the story above, that is, the first story of the building. This was assumed to be 12 feet in height. These numbers are rather arbitrary. At the time we did this calculation we were probably thinking more of typical story heights in large commercial structures, rather than residences. In any case, the results are not very sensitive to the height of the first story.

At this point I would like to discuss the survey method by reviewing the charts in the AE Guide. I will examine each of the Charts and relate them to the engineering method. These charts are reproduced at the end of the section.

Chart 1, on page 33 of the AE Guide, shows barrier shielding effects. It was included primarily to present visually the shielding effects of three different cases of barrier configurations. The curve for Case 3 is the only one used explicitly in the calculations. Case 1 represents fallout on the roof. The corresponding barrier factor is given by the solid line. The result, obtained directly from NBS Monograph 42, was calculated for a plane isotropic source of gamma radiation from 1.12 hour fission products. It is normalized to unity at a depth of 0.22 psf which corresponds to 3 feet of air. Case two represents fallout on the ground next to an external wall. The barrier factor for penetration through the walls is shown by the dashed line. Actually, the diagram for Case 2 is not quite accurate. To be strictly correct, that diagram ought to depict a detector sandwiched very closely between two vertical walls, with an infinite plane of contamination on either side. This barrier factor is the ratio of the dose rate at a height of 3 feet and a depth X to the dose rate at 3 feet above an infinite plane. As the wall thickness shrinks to zero, this ratio approaches

unity. When you go through an example in this method, you do not have to refer to either of these curves specifically. They are here mainly for instructive purposes. Case 3 represents fallout adjacent to a horizontal barrier. In order for radiation to reach the detector it has to start out in the upward direction, scatter in the air or the structure and penetrate down through the floor. The dotted curve is the barrier factor calculated for this case. Its main application is to detectors in basements. I will go into a little more detail on that when I discuss the details of the engineering method, and how these curves were derived. But the main point here is that it is used for penetration through horizontal barriers inside the building - penetration in and down so to speak - and its main application is to detectors in the basement.

Chart 2 is the roof contribution, presented in terms of a contour curve. The principle variable is the total overhead mass thickness, X_o, between the detector and the roof source. In this method the roof contribution is calculated separately from the ground contribution and combined at the end of the calculation. In that respect, it follows the Engineering Method. If there are a number of floors between the detector and the roof source, X_o is the sum of the mass thicknesses lying between the detector and the source. The other variable in Chart 2 is the adjusted roof area.

An adjusted area is necessary because Chart 2 was calculated for a fixed detector distance of 10 feet. However, if all linear dimensions are multiplied by the same factor, the solid angle and therefore the dose rate remains the same. The adjusted area in Chart 2 is the area which subtends the same solid angle at a detector with Z = 10 as does the real area at the real detector location. In other words, if the solid angle is fixed and the mass thickness is fixed the same dose rate is obtained. The adjusted area is obtained by multiplying the real area by $(10/Z)^2$. Each contour curve corresponds to a unique reduction factor. Generally as X increases the reduction factor of the dose decreases. This is very reasonable. Generally as the roof area increases, the reduction factor increases. As you can see, for large areas these contours approach a vertical slope which means that for a given mass thickness, if the roof area is increased beyond a certain amount, the additional sources do not contribute, because they are so far away and have to come through an extreme slant thickness of roof.

Chart 3 is a series of contour curves used for the ground contribution for detectors above grade. Just as in Chart 2, the reduction factor decreases as the wall mass thickness increases. Here, increasing the area is equivalent to moving the wall farther and farther away from the detector. Therefore, the reduction factor

240-816 O-67—55

decreases with increasing area. This can be interpreted as an r^2 effect, since removing the walls farther and farther away corresponds to removing the effective source. Knowing the wall mass thickness and the adjusted area of the building the ground reduction factor can be obtained from this Chart. These reduction factors are based on a detector height of 3 feet above grade.

Now, Chart 4, I think, is probably the most interesting. This gives the ground contribution to a detector below grade. This Chart is used only for radiation through the first story walls which comes down to the detector. There are two types of radiation which are included in this contribution. One is radiation which comes directly from a ground source, scatters in the wall, and heads down to the detector. The other component is skyshine - that is, radiation which is emitted into the upper hemisphere - scatters in the air, and comes down straight towards the detector. As I said earlier, the detector is understood to be 5 feet below the first floor. Suppose we look at the dose rates for fixed area, let us say, 4000 feet and then examine the reduction factor as a function of the wall mass thickness. This method predicts that when the wall thickness increases from X = 0 to X = 15 psf, a slight increase in reduction factor will occur. Notice that this is not very dramatic and certainly the calculations are not really accurate enough to say that this is a real physical effect. I think the best that can be said is that the reduction factor is nearly

constant between X = 0 and X = 40 psf. Technical Operations has made some measurements recently on the wall-scatter component. Since there is no wall-scatter for zero thickness walls, this component has a much more dramatic behavior. If the wall-scattered component were plotted against wall thickness the contribution would start from zero at X = 0 and then build up to a maximum at X ~ 30 psf and then decrease. That much has been verified by a scale model experiment. However, it is more difficult to measure the other component, the skyshine, because about one third of the skyshine component comes from sources beyond 500 feet. It is extremely difficult even with kilocurie sources to get measurements when the sources are so far away. I do not think we have definitive measurement yet. Personnel from Edgerton, Germeshausen & Grier have just reported some measurements on penetration of skyshine through vertical and horizontal barriers. It is possible that their measurements may yield the attenuation of the skyshine component. At any rate, what we can say generally, is that the first 40 psf of shielding on the first story does not contribute in any important way in improving protection in the basement. It certainly improves the protection on the first floor, but it does so by scattering the radiation downward.

Another interesting feature of Chart 4 is the variation of the R_f with area. If you consider a fixed mass thickness, say

20 psf, and ask what happens as the building varies in size, you find that the reduction factor has a maximum at an area of about 4000 square feet. For very large areas, the effective sources lie farther from the detector. Therefore, for fixed mass thickness, the reduction factor would be expected to decrease. However, the surprising thing is that when the building is smaller than about 4000 square feet, the reduction factor again decreases. The reason for this, basically, is that the angular distribution coming out of the wall, is peaked in the horizontal direction. As the building gets very small, the detector is sampling a part of the angular distribution, where there are not many photons. Accordingly, the reduction factor decreases. Knowing the first story wall thickness and the area of the building, one can obtain the ground contribution from the first story walls from this Chart.

Chart 5 is a correction for height dependence, and is taken directly from NBS Monograph 42, Figure 28.2a. It is intended to correct the reduction factor when detectors are not at three feet above grade, but at some greater height. This correction would be quite good, if the position of interest were on the outside of a building, because in that case the detector views radiation coming from all directions. However, in a multistory building with thick

floors, the detector sees radiation only from a limited cone of direction near the horizon. But the dependence on height of radiation traveling parallel to the horizon is significantly different from the height dependence of radiation integrated over all directions.

An estimate of the height dependence of the radiation traveling parallel to the horizon can be obtained from examining $\ell(d,\cos\theta)$ near $\cos\theta \sim .01$ (see Fig. 26.1 of NBS Monograph 42). The value of these curves near $\cos\theta = 1$ decreases by a factor of 10 as the height increases from 3 feet to 16 feet. On the other hand, the intensity of the radiation integrated over all directions, L(d), decreases only by about 30% between 3 feet and 16 feet (see Fig. 28.2a of NBS Monograph 42).

Chart 6 is one that in practice has not been used too much. It was designed primarily for application to commercial structures with large glass-wall areas, very often on the first floor. I will not go into detail on this Chart primarily because it does not appear in the newer methods. I would suspect that the main reason that it has not been used is that protection is too poor in these situations to be of practical interest.

This ends the discussion of the Charts in the AE Guide. There are three tables on page 44 which provide correction factors. These are definitely of less accuracy than the Charts we have been discussing. They were intended to account for what we felt were some important effects for which we did not have very good methods of attack.

Table CF-1 provides a correction for apertures. A distinction is made between above- and below-sill level. The calculations in the AE Guide apply to a detector above sill level with zero thickness floors. Therefore, the correction factors for thin floors above sill are all equal to unity. The remaining three columns of this Table are based on some calculations we had made earlier for the OCD headquarters building at Battle Creek, Michigan. For thick floors, the correction factor for a detector below sill was about 0.2, independent of the story height, while the correction factor for a detector above sill varied as shown in the second column. For detectors below sill in a building with thin floors, the reasoning was as follows: On the first story the correction factor should be the same as that for thick floors. On upper stories the factor should be greater than 0.2 since there is some contribution from the lower stories. On the other hand, the correction factor should be less than 1.0 since the reduction factor is generally lower below sill level than above sill level. The correction factor was therefore arbitrarily assumed to be equal to those for the above-sill case for thick floors.

A correction for skyshine contribution through the roof is given in Table CF-2. Its main purpose is to estimate the skyshine contribution when the roof sources have been removed by decontamination or natural blow-off. Decontamination has long been discussed as a possible way of improving protection in structures. At one time elaborate wash-down systems were considered seriously. There are many problems connected with decontamination. If the sources

are to be washed off the roof they must be handled in such a way that they do not become concentrated somewhere else around the building. Also, I think that before the importance of skyshine was realized, it was felt that decontaminating the roof removed all the radiation. That is not true. If we consider the radiation which comes through the solid angle subtended by the roof, the sources on the roof certainly do make the main contribution. However, there is also a considerable amount of skyshine which comes down through that roof, which comes, not from the sources on the roof, but from the sources on all the horizontal surfaces within several hundred feet of the building. Even in an urban area these sources, which may be distributed at various heights, can all shine up into the air and shine down upon the building in question. It can be seen that for X near zero the skyshine represents an appreciable percentage, about 15% of the contribution, from the roof sources themselves.

Table CF-3 was an attempt to correct for what is now generally called mutual shielding. When we first developed this method, we thought of isolated buildings surrounded by infinite planes of contamination. As I mentioned earlier our work in planning for the National Fallout Shelter Survey forced us to consider seriously the very practical case of finite fields in urban areas. At the time the AE Guide was written, however, we had not yet focused on this problem.

The mutual shielding factor in Table CF-3 was based primarily on the following type of reasoning. Suppose you have a detector at the center of a building and assume that the building has an effective radius of about 50 feet and that it is surrounded by an annular source of width W_c. The correction factor is the ratio of the dose rate from a source annulus of this width compared to one where the sources extended out to infinity. This is the sort of simple reasoning on which Table CF-3 is based. The most important weakness in the AE Guide is that mutual shielding is not at all adequately handled.

Question: Could the combined behavior of wall-scatter and skyshine as a function of wall thickness be measured with models?

Answer: It would be difficult. The air would have to be scaled by using polystyrene or some similar material. Although the effect is academically interesting, the uncertainties are small compared with other shielding problems. It is therefore not a critical experiment from the standpoint of OCD.

Question: How are the curves in Chart 4 affected by the presence of a basement barrier?

Answer: These curves do not include the ceiling barrier. Since the survey method treats the attenuation in the ceiling as a multiplicative factor, the shape of the curves is not altered by the presence of the ceiling. We have found, however, that this simple treatment of ceiling attenuation is inadequate and that the shape of these curves really does vary with ceiling thickness.

Charts from

Fallout Shelter Surveys:
Guide for Architects and Engineers

NP-10-2 Department of Defense, Office of Civil Defense, May 1960

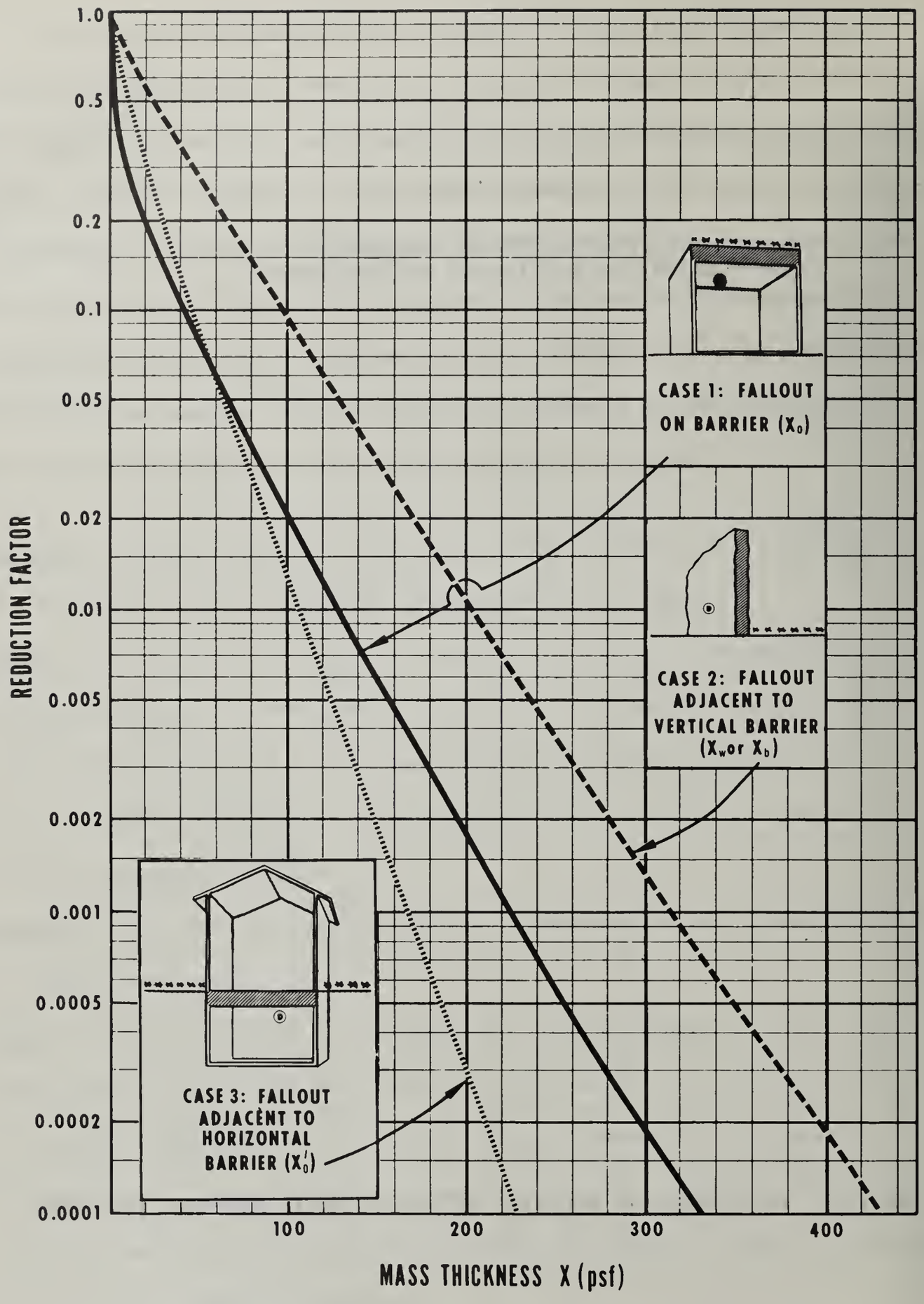

BARRIER SHIELDING EFFECTS

CHART 1

Reduction Factors for Combined Shielding Effects

ROOF CONTRIBUTION

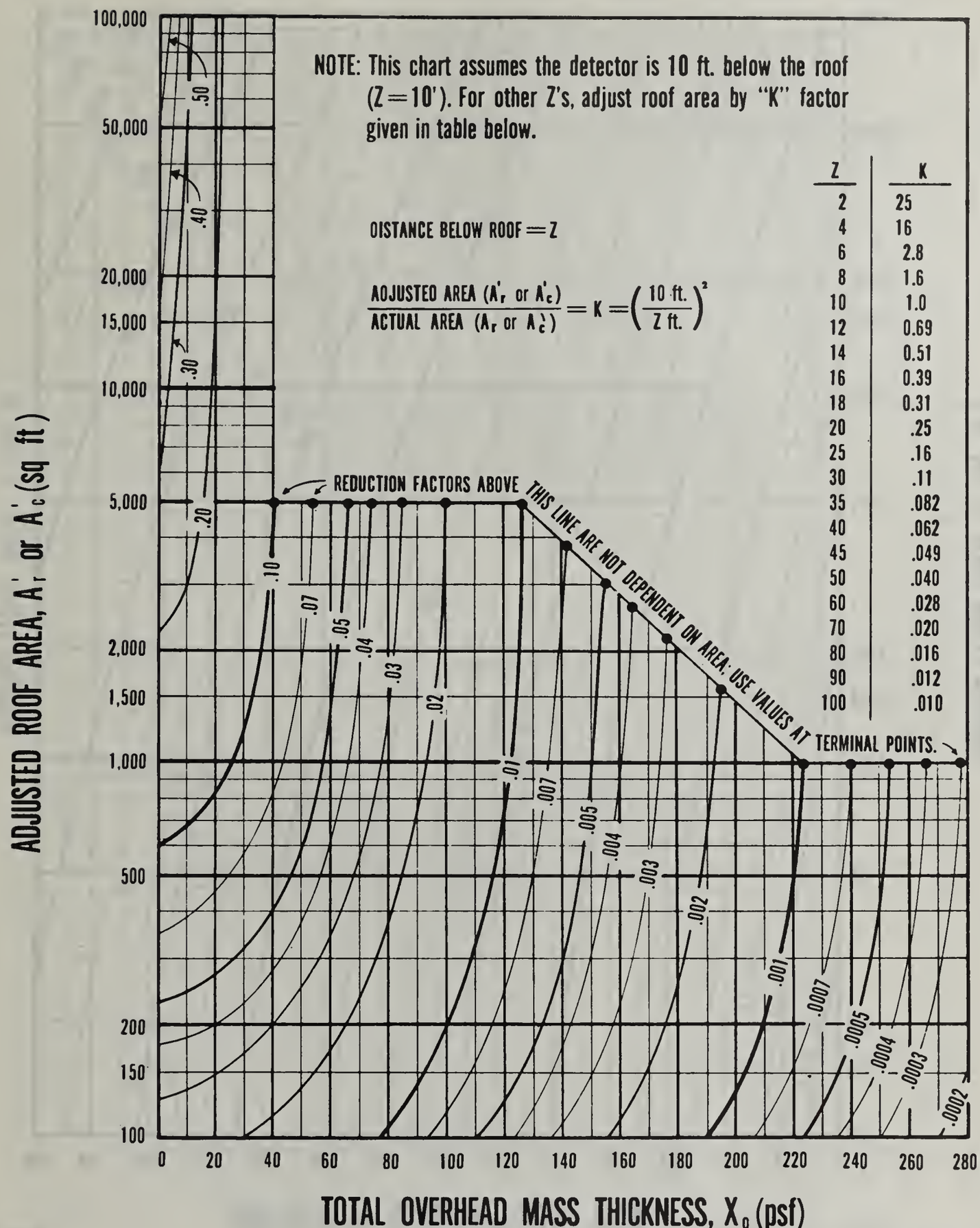

CHART 2

Reduction Factors for Combined Shielding Effects

GROUND CONTRIBUTION – ABOVEGROUND AREAS

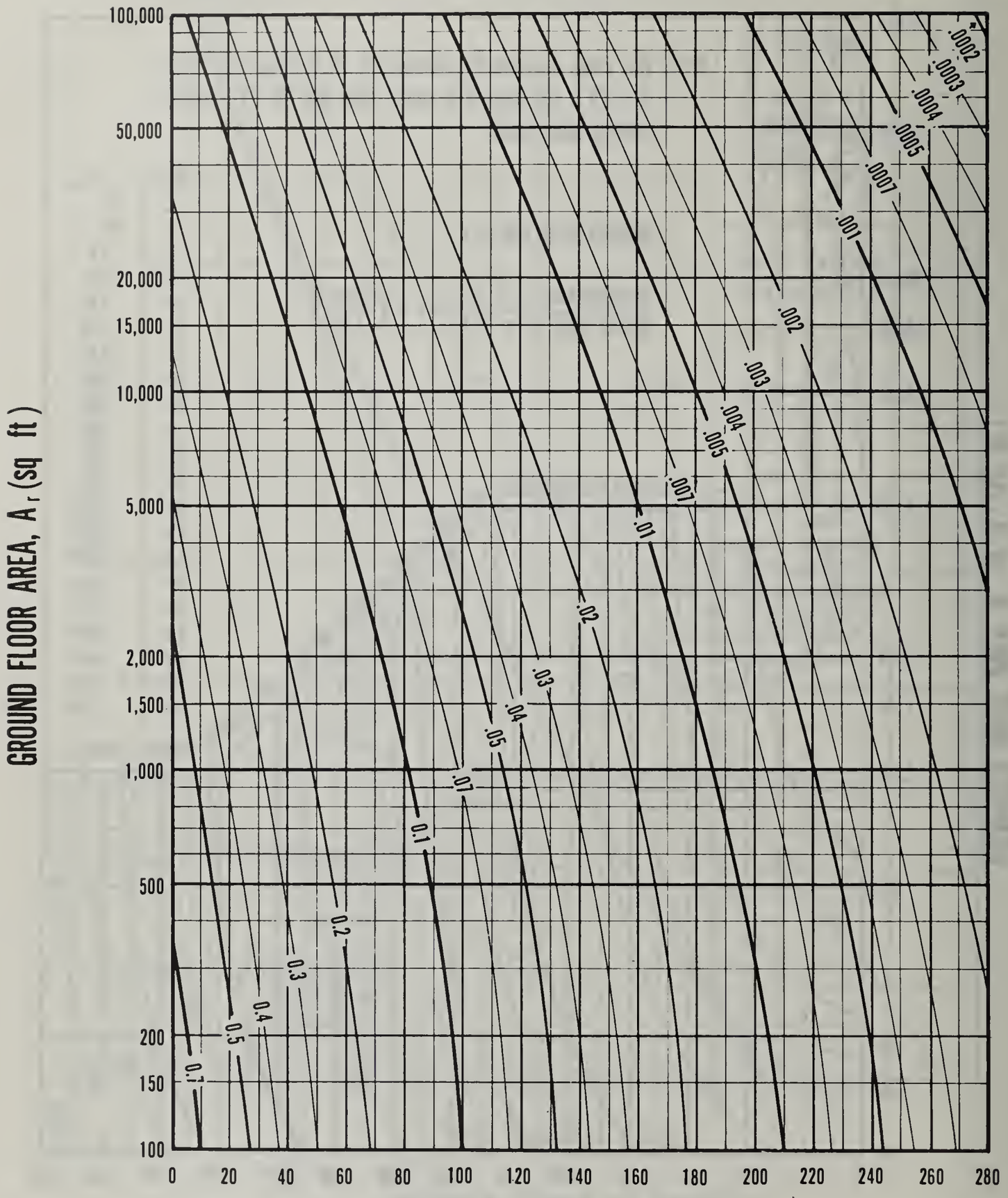

CHART 3

Reduction Factors for Combined Shielding Effects

GROUND CONTRIBUTION - BELOWGROUND AREAS

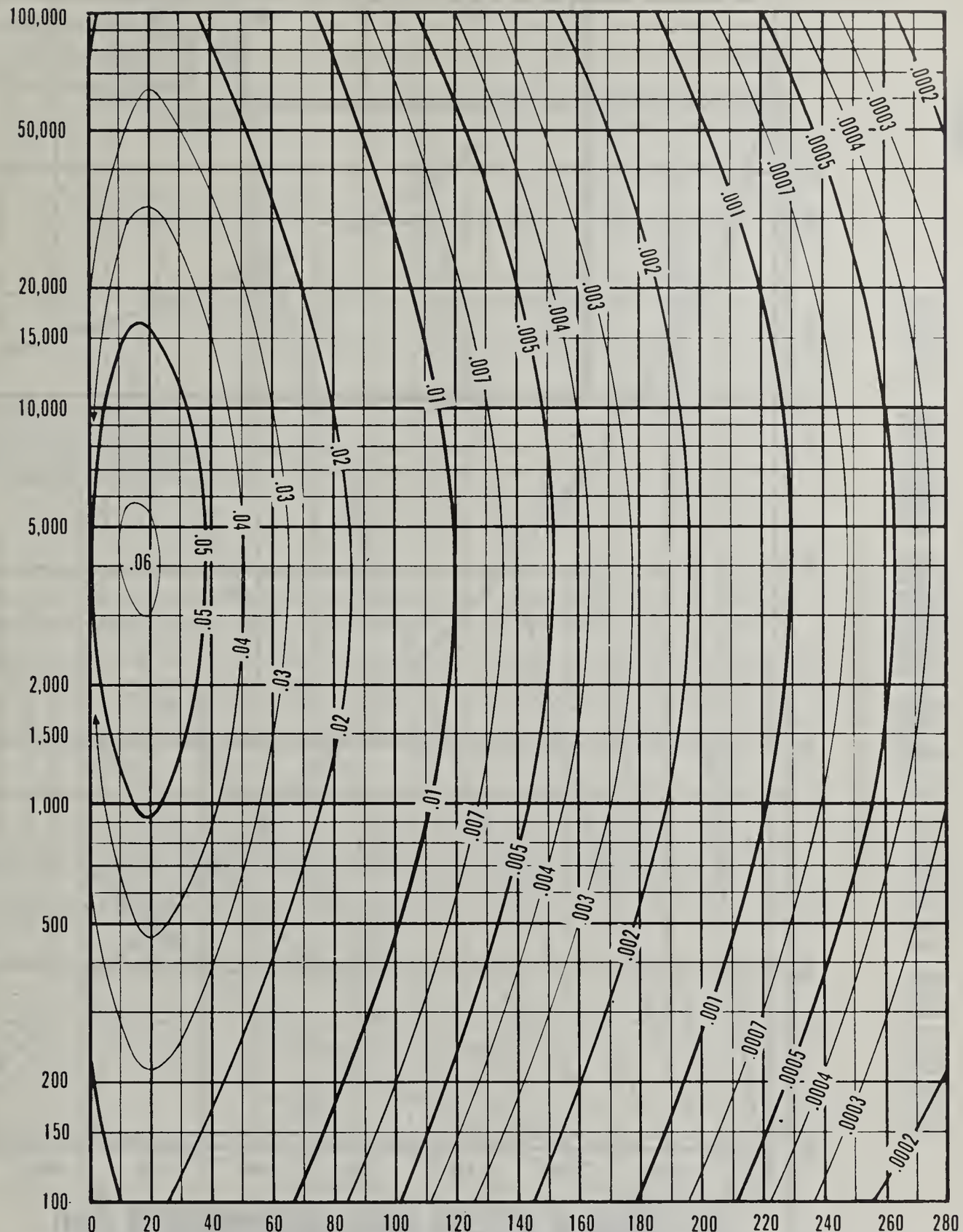

CHART 4

SHIELDING EFFECTS OF HEIGHT

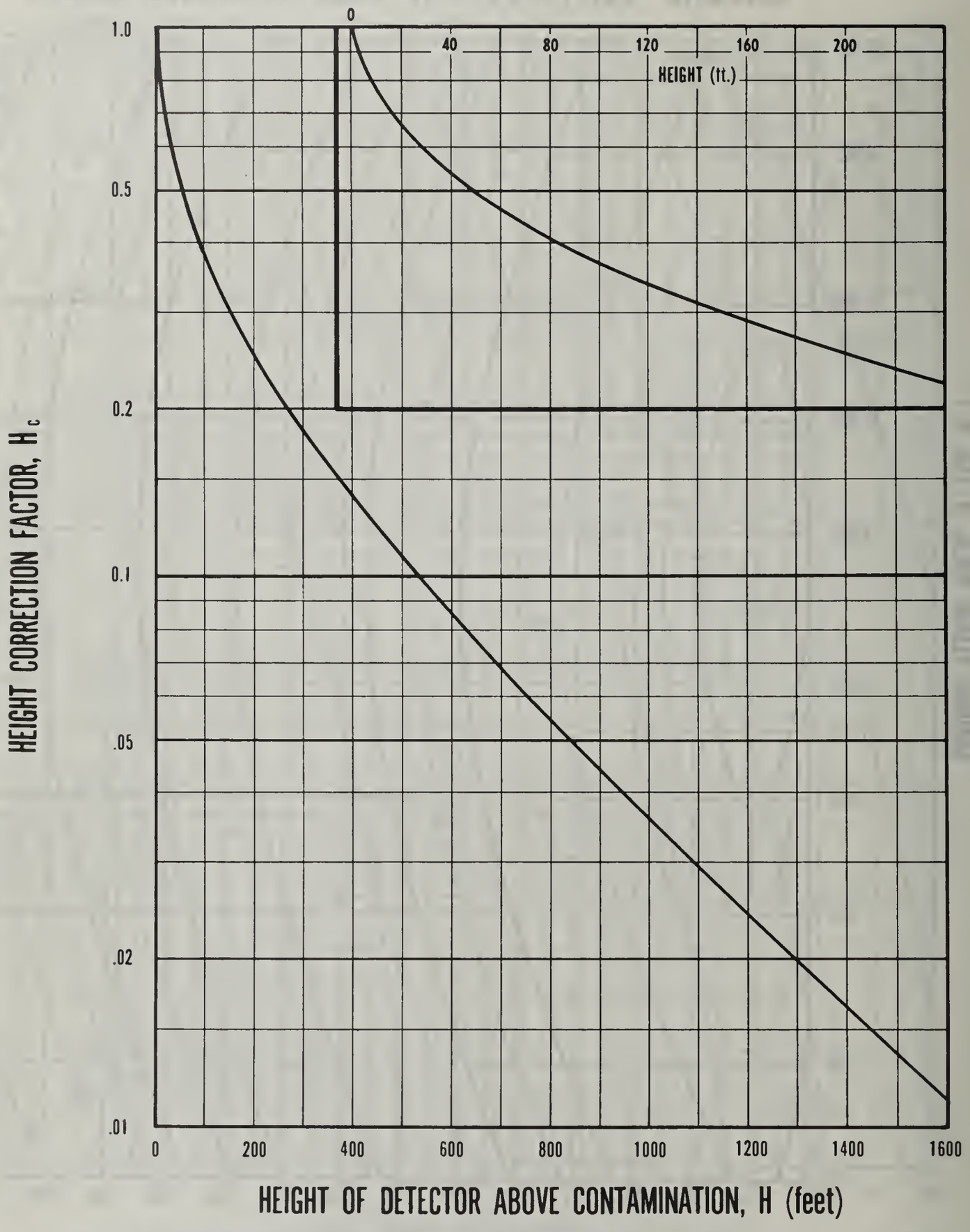

CHART 5

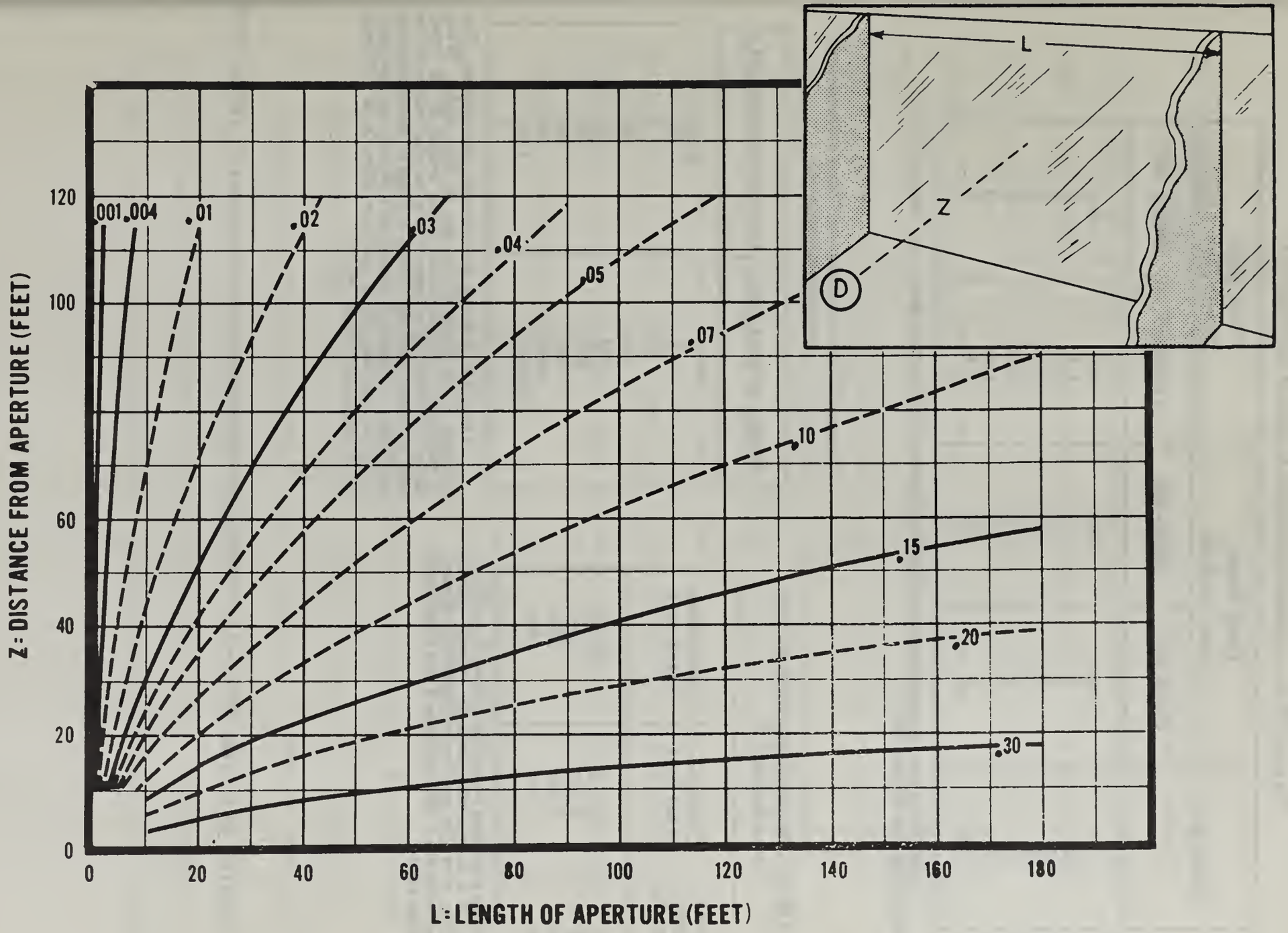

REDUCTION FACTORS FOR APERTURES, GROUND FLOOR

CHART 6

TABLES OF CORRECTION FACTORS

TABLE CF–1.—*Aperture correction to ground contribution* [1]

Floor No.	Thick floors (*X greater than 40 psf*)		Thin floors (*X less than 40 psf*)	
	Above sill	Below sill	Above sill	Below sill
1	1.0	0.2	1.0	0.2
2	.7	.2	1.0	.7
3	.6	.2	1.0	.6
4	.5	.2	1.0	.5
5	.4	.2	1.0	.4
6	.3	.2	1.0	.3
6+	.2	.2	1.0	.2

[1] Table CF–1 may be used for either simple or complex (wall-by-wall) cases. See example 2 for chart 5 for use of this table.

TABLE CF–2.—*Skyshine correction to roof contribution* [1, 2]

Total overhead mass thickness, X_o	Contaminated roof	Decontaminated roof
0	1.15	0.15
50	1.08	.08
100	1.04	.04
200	1.01	.01

[1] Applied to reduction factor from chart 2 (p. 35).
[2] Table CF–2 is generally used for cursory checks only. However, it is also used to evaluate the efficacy of roof decontamination. See examples 4 and 5 for chart 2 for use of this table.

TABLE CF–3.—*Mutual shielding correction to ground contribution* [1]

Width of field (W_o)	Correction factor (M_s)
feet	
0	0.00
10	.08
20	.10
50	.20
100	.40
200	.60
500	.80
1000	.90
Infinite	1.00

[1] Table CF–3 is for wall-by-wall calculations. See example 2 for chart 6 for use of this table. When a condensed computational form (supp. E) is used, make the following adjustments in tabular values in the case of urban buildings (those in areas of predominantly multistory commercial buildings): Streets on one side, × ¼; on two sides, × ½; on three sides, × ¾. (Streets on all sides, use values "as is.")

These tables are from NP-10-2: "Guide for Architects and Engineers", OCD, 1960.

2. Equivalent Building Method -

Now I would like to discuss the equivalent building method. Jack LeDoux who is now with the Bureau of Yards and Docks is the person who derived the equivalent building method. The philosophy of this method is the same as that of the original AE Guide. It was designed to replace the tedious calculations of the engineering method with a quick method which would give essentially the same results as the engineering method for most shielding situations occurring in practice. Originally it was a very simple method. However, as the pressure to handle more detailed problems was increased, more charts were added. Now it is a fairly complex method in the sense that there are 24 charts and 3 tables in the equivalent building method. Only a few of them are used, however, in any one calculation.

The essence of the method is to replace a complicated building by an equivalent blockhouse with just one wall thickness and one roof thickness. All corrections for mutual shielidng, height, area, and basement exposure are treated by adjusting barrier thicknesses. The hypothetical roof thickness is now a function of several variables: the area of the building, the height or distance of the detector from the source, and the thickness of interior partitions. Corrections for all three of these variables are treated by adjusting the overhead

240-816 O-67—56

roof thickness. The equivalent exterior wall thickness is a function of the actual wall thickness, the aperture ratio in the walls, the thickness of the interior partitions, and several other variables associated with mutual shielding and height effects. Now, I would like to discuss the figures in the equivalent building method. The figures are reproduced in Volume III of this book.

Figures 1 to 4* are the basic charts that would be used in a simple calculation. They give the protection factor for a detector location three feet above grade. The ordinate is the protection factor (P_f) and the abscissa is the wall mass thickness. There are various curves for different overhead roof thicknesses. For a given wall thickness it can be seen that as the roof thickness increases the protection factor increases. Furthermore, the curves begin to approach a constant value for large values of the wall thickness and small values of the roof thickness. This shows that for a very thin roof overhead, let us say, $X_o' = 0$, making the walls thicker does not improve the protection because the predominant contribution comes from sources on the roof. In this situation greater protection can be obtained only by making the roof thicker. Figures 1, 2, 3, and 4, correspond to four different areas of buildings. Consequently, one feature of this method is that it is limited to calculations for just four areas, ranging from 100 to 100,000 square

* Figures referred to with respect to the Equivalent Building Method can be found on Pages III-22 through III-40.

feet. In working out an actual problem, this turns out to be a bit of a disadvantage because the area seldom corresponds to precisely the areas for which these charts are calculated. At least two calculations and an interpolation are therefore generally necessary. Since the P_f is not a strong function of area, linear interpolation is generally accurate enough.

Figures 5 through 9 are the corresponding figures for calculating dose rates in basements. The reason there are five of these instead of four is that the sensitivity to area is somewhat greater than for detectors above grade. The extra figure gives curves for an area of 4,000 square feet. For large values of the wall thickness, the general nature of the curves is the same as that for the above-ground case. For a fixed wall thickness, the protection factor increases with increasing roof thickness. As in the above-grade case, the curves approach a constant value for large wall thicknesses and small roof thicknesses. As before, this indicates that in this region the roof contribution is the main one. For small values of X_w, the peculiar shape of the curves is due to the same phenomenon that we saw in the AE Guide, namely, that for first story wall thicknesses below about 25 psf, removal of shielding material may actually increase protection in the basement. This is because there is less wall material from which radiation can be deflected to a detector below grade. The minima in these P_f curves are therefore due to the same effect as the maxima in the R_f curves of the AE Guide. Figures 5 through 9

apply to a basement with no exposure. They are analogous to the below grade chart in the survey method except that here the roof contribution is included.

Figures 10a through 10d on page 25 present corrections for apertures. In using these figures one looks for the actual wall thickness on the abscissa and reads an equivalent wall thickness on the ordinate. The equivalent wall thickness is generally less than the actual wall thickness because the apertures reduce the shielding effectiveness of the wall. For heavy wall thicknesses, of around 200 and 300 psf, the behavior of the equivalent wall thickness as a function of the percent of apertures is straightforward. As the aperture percentage increases, protection decreases, and the equivalent wall thickness therefore decreases. Small equivalent wall thicknesses here mean low protection factors. On the other hand, for small exterior wall thicknesses there is a cross over point in these curves. For wall thicknesses of about 20 or 25 psf, increasing the number of apertures increases the equivalent wall thickness, and therefore increases the protection. It is important to remember that in the equivalent building method the protection factor is calculated for detector locations just below window sill level. In this case, therefore the apertures are always above the detector. Varying the aperture thickness produces the same effect

on an above-grade detector as varying the first story wall thickness does on a basement detector. Each of the four curves correspond to a different building area. Similar corrections for the effect of apertures on a detector below grade are given in Figures 11a through 11e. Although the corrections apply to a basement detector, the wall mass thicknesses in these figures refer to the first story walls. Here again, for large wall thicknesses increasing the aperture percentage decreases the protection. On the other hand, for small mass thicknesses, this trend reverses resulting in some peculiar contours for small values of X_e. The peculiar nature of the curves is due to the fact that the curves in Figures 5 through 9 are double valued functions when P_f is regarded as the independent variable. For example, for X_e between 0 and 25 psf in Figure 11a, the curves could have been drawn so that they all passed through the origin. This is because $X_e' = 0$ and $X_e' = 80$ yield the same P_f in Figure 5. Figure 11e is included for an area of 4,000 square feet.

Figure 12 provides a correction for detector height. The four curves in Figure 12 apply to four different areas. These curves are designed to correct for shielding effects of the floors above and below the detector. In other words, the detector is assumed to be in a multistory building with thick floors. For the higher stories the apparent shielding is increased primarily because the radiation intensity decreases with height above the ground. As the area of

the building is increased the floor and ceiling subtend larger solid angles and are thus more effective in attenuating radiation from walls of other stories. Therefore, in Figure 12 larger areas correspond to larger increments in the equivalent wall thickness. However, this dependence on area cannot be assumed for all mass thicknesses. If the wall is very thin, a relatively greater contribution comes from the stories below. The floor is therefore even more effective in increasing the protection than in the case of thick walls. Thus, the table $X_e = 0$ indicates that a number of psf should be added to the values which were obtained from the curves. The general interpretation here is that the shielding effect of floors is relatively greater in thin-walled buildings.

This prediction is a property of the engineering method that is reproduced in the equivalent building method. In some extreme cases it can be shown to lead to spurious results. For example, consider a limited source terminated by a large adjoining building. The question is how much radiation would get to a detector in the center of an upper story with window walls, that is, $X_e = 0$. According to the engineering method, if the source strip is narrow enough, a thick floor will remove all direct radiation. On the other hand, the wall-scattered radiation is weighted by the $S_w(X_e)$ function and $S_w(0) = 0$. Because the wall is of zero thickness, there is no mechanism for in-scattering. Consequently, the engineering method indicates that the detector receives

no radiation. In reality, there are mechanisms such as ceiling shine and perhaps scattering off of the neighboring building which could in the real physical situation, enable radiation to reach the detector from the finite strip source. This is the reason why the engineering method was recently revised to include the skyshine contribution to a detector even though neighboring buildings block out skyshine. It was felt that the fictitious skyshine contribution would compensate for the absence of the unknown contributions, such as ceiling shine.

Let us now return to the discussion of the equivalent building method. In Figure 13, we have the mutual shielding factor calculated by the equivalent building method. It is important to note that the equivalent building method (1964 version) is based on curves from the AE Guide. The mutual shielding correction for the protection factor estimater is based on experimental data. To complicate matters even more, in the 1965 version the present plan is to use the mutual shielding correction calculated by the engineering method. Therefore, although all three of these approximate methods are based on the engineering method approach, they may yield different answers for specific problems. This illustrates the disadvantage of producing simplified methods which are based on modified versions of the engineering method. I think fundamental changes should be made first in the engineering method and later in the various approximate methods.

otherwise, it makes it very difficult to compare the accuracy of the methods. For example, suppose you go through a detail calculated by, let us say, the nomographic method and then you do a detailed calculation by the equivalent method, if they do not agree you are told that it is because they each use a different correction for mutual shielding. This is obviously not a very satisfactory state of affairs.

Corrections for basement ceiling barriers are given in Figure 14a. There are two curves on Figure 14a indicating some sensitivity to the wall thickness. However, this sensitivity is a bit artificial for the following reason: The wall barrier factor as a function of the wall thickness which is now used in the engineering method is concave upward on semilog graph paper. It is shown as Case 2 in Chart 1 of the AE Guide (Page V-82). In the equivalent building method, an attenuation of say 1/10, produced by a ceiling barrier of about 50 psf, is translated into an equivalent wall thickness. Near zero wall thickness, where the curve decreases more steeply, a relatively small equivalent wall thickness is needed to produce a factor of 10 in attenuation. On the other hand, for large wall thicknesses where the curve decreases more slowly, a larger equivalent wall thickness is required to obtain an attenuation of a factor of 10. The two curves in Figure 14a represent average estimates of this effect for X_w near zero and X_w near 150 psf. Consequently, the dependence on wall thickness in Figure 14a is due to the peculiarities of the

equivalent building method rather than any inherent dependence of ceiling barrier on wall thickness. The same explanation accounts for the two floor barrier curves in Figure 14b. These curves give the equivalent mass that must be added to the wall barrier to account for the attenuation in the floor barrier.

Figure 15 is an attempt to correct for basement exposure. It is used with above grade charts, that is, the basement is treated as if it were a partly submerged above-grade structure. Less exposure implies greater protection which, in turn, requires a larger correction to the equivalent wall thickness. Figure 16 is used to obtain an equivalent overhead mass thickness. This parameter is necessary in order to use the basic figures, 1 through 9. The first procedure is to find the adjusted roof area corresponding to the actual detector distance z. This is done by means of a nomogram. Entering the figure with a certain adjusted area, say 170 ft^2, and the actual overhead mass thickness, let us say 150 pfs, an R_f of .0031 can be obtained. At this point the equivalent building method is a little artificial because the method ignores the reduction factor which has been obtained and seeks only an effective mass thickness which can be used in one of the first nine charts to find the combined P_f for roof and ground sources. I personally think one disadvantage of the method is that it mixes the roof and wall contributions.

I prefer to see them separate. However, I think that arguments can be made in favor of it too. Examination of the first nine charts does give a feeling of how important roof contributions are relative to ground contributions. For example, the results for infinite roof thickness give the P_f for the ground contribution alone.

There are a couple of other corrections to the overhead mass thickness included in Figure 16*. If you want to know what effect interior partitions have on the equivalent overhead mass thickness, you can use Chart C* to obtain the increment in the effective mass thickness. Chart D* is included to correct for the effect of highly eccentric rectangular buildings. The method in these pages was originally derived for square buildings.

* See Page III-40.

Question: Can Figure 14a be used on upper stories?

Answer: Yes. Although Figure 14a is labeled "basement" it would probably be better to discuss 14a and 14b in terms of a detector in an upper story. Figure 14a would apply to radiation which has to come down through the ceiling barrier and 14b would apply to radiation which has to come up through the floor barrier. In the engineering method, it was assumed that the attenuation of the floor barrier is different from the radiation coming down through the ceiling barrier. Therefore, the curves in 14a for basements is a special but very important application.

3. NOMOGRAPHIC METHOD

The nomographic method is intended as a successor to the method described in the Guide for Architects and Engineers (A. E. Guide). The main differences between the two methods are that the nomographic method is quicker than the older method, it has a more accurate treatment of mutual shielding corrections, and information is calculated from nomograms rather than read from contour curves. Although the nomograms contain similar information as the Charts in the A. E. Guide, they have been rederived directly from the engineering method.

The nomographic method is based on many of the same assumptions as the A. E. Guide, namely:

1. Square building
2. Detector position 3' above floor, for above-grade detectors
3. Detector position 5' below basement ceiling, for below-grade detectors

However, the detector is assumed to be at or below sill level. The roof and ground contributions are computed separately. Details of the method can best be seen by reviewing the nomograms individually.

Nomogram 1 is used to compute the roof contribution. It is a two-step calculation. Knowing the area of a structure, which is generally rectangular and the detector distance, a normality ratio, N, is calculated as if the building were square. The ratio N is related to the solid angle subtended by a square. Knowing N and the

mass thickness X_o, the roof contribution is calculated as if the roof were circular. Use of calculations for circular roofs is common to all methods based on the engineering method. If there are interior partitions of thickness X_i, the peripheral roof contribution is calculated from Nomogram 1 using a roof thickness of $X_o + X_i + 10$ psf.

Nomogram 2 is used to calculate the ground contribution to above-grade detectors. The results of nomogram 2 apply for an infinite field and a detector height of 3 feet. The minimum area listed on the nomogram is 400 square feet. For buildings with smaller area the geometry factor is near unity and the ground contribution is given by $B_o\ (X_w)$ for an infinite field or $B_{ws}\ (\omega,\ X_w)$ for finite fields.

Nomogram 3 is used to calculate the ground contribution to below-grade detectors. This chart requires special discussion. Consider first the simplest case of a basement with no exposure. The nomogram is applicable to buildings with areas between 400 and 14,000 square feet. We first note, however, that the area of the building does not appear as one of the variables of the nomogram. This means that the variation with area has been neglected in making up this nomogram. We can see from Chart 4 of the A. E. Guide that this could introduce as much as a 50% error for $X_w = 20$ psf, since the dependence on area extends from $C_g\ (4000,\ 20) = .06$ to $C_g\ (500,\ 20) = .04$. Secondly, the nomogram for X is double-valued. The arrow on the left scale indicates the direction on increasing X_w. This is the nomographic interpretation of the fact, for example, that $X_w = 0$ and $X_w = 67$ yield the

same ground contribution. To obtain the ground contribution you merely lay a straight edge between the value of the first story wall thickness, X_w and the value of the basement ceiling thickness X'_o and read off the value of C'_g.

The procedure just described gives the contribution through the first story walls. If the basement is partially exposed, another term must be added to account for the radiation penetrating the exposed basement walls. This is obtained as follows. Using the thickness of the basement walls for X_w and setting X'_o equal to zero, read off C'_g. Then multiply this value of C'_g by the K_b obtained from Table II. If the exposure is greater than 5', but the detector is below grade, use the K_b obtained for an exposure of 5'. If the detector is above grade, regardless of the exposure, it should be treated as an above-ground case and the basement wall thickness with Nomogram 2 should be used.

If there are apertures in the exposed basement wall, the following procedure is recommended. If the basement wall thickness is less than 50 psf, ignore the apertures. If it is greater than 50 psf, add 2% of the calculated contribution through the exposed walls for each psf of basement wall thickness over 50 psf, regardless of the aperture percentage. For example, if the basement wall thickness were 75 psf, the calculated ground contribution would be multiplied by 1.5.

Nomogram 4 is used to correct for detector height and finite fields of contamination. Unlike the engineering method and the method of the A. E. Guide, these corrections are based on experimental data

rather than calculations. Whenever this nomogram is used, therefore, calculations cannot be directly compared with the other two methods. The results of Nomograms 2 or 3 are multiplied by the MS factor obtained from this nomogram in order to obtain the ground contribution from finite sources. A straight line between the width of the contaminated field on the W_c scale and the detector height on the H scale intersects the middle scale at the MS factor. For $W_c < 300$ ft, we distinguish between two cases. The scale called "case B" is used if the detector is on an upper story of a building with thick (> 50 psf) floors. Case A is used for all other situations. For $W_c > 300$ ft, the results for $W_c = 300$ and case A are used for all situations. This latter rule is an approximation designed to avoid a complicated procedure for very large fields.

Nomogram 5 is used to calculate the ground contribution through horizontal passageways such as entrance ducts or tunnels. A straight line on the nomogram between the d scale (the distance from the opening) and the W scale (width of the opening) gives the reduction facotr. This nomogram is based on calculations made by Dr. Eric Clarke of Technical Operations Research during the National Fallout Shelter Survey.

I would like to illustrate the use of this method by doing problem 4-7 in the Engineering Manual (PM 100-1) by the nomographic method. The detector is located on the fifth story of a ten story building. The detector is 43 feet in height. The width of this building is 80 feet. The length is 140 feet. The exterior wall thickness is 80 psf.

The floor thicknesses are assumed to be uniform at 60 psf. In the nomographic method, the first thing we have to know is the area of the building, which in this case is 11,200. The exterior mass thickness is 80 psf. There are no interior partitions mentioned. Using Nomogram 2 for the ground contribution and putting a straight edge on the area 11,200, and mass thickness of 80 psf, you should come up with a ground contribution of .042. This would be the ground contribution on the first story of this building. However, the detector is on the fifth story at a height of 43 feet. To obtain the height correction, Nomogram 4 is used. Two cases, A and B are given in this nomogram. Strictly speaking, the nomogram says that if the floor thickness is greater than 50 psf, use case B. However, the method recommended for an infinite field, is to use the 300 feet point for case A as one entry and the height of 43 feet as the other entry. If we lay a straight edge between those two numbers, we come up with a height correction of 0.39. Therefore, the reduction factor is equal to .042 x .39 which is equal to about .0164 and we get a P_f equal to about 61. That is the calculated value by the nomographic method. Now, if you look at example 4-7 in the Engineering Manual, you see that the protection factor comes out about 60. You will note that the agreement is partly fortuitous because, as I explained before, this method uses different data from the engineering method in correcting for mutual shielding. However, the agreement in this case, is good.

240-816 O-67—57

Nomograms from

Simplified Method of Shielding Analysis

PG 80-14 Department of Defense, Office of Civil Defense
(not distributed)

REDUCTION FACTORS FOR COMBINED SHIELDING EFFECTS

ROOF CONTRIBUTION

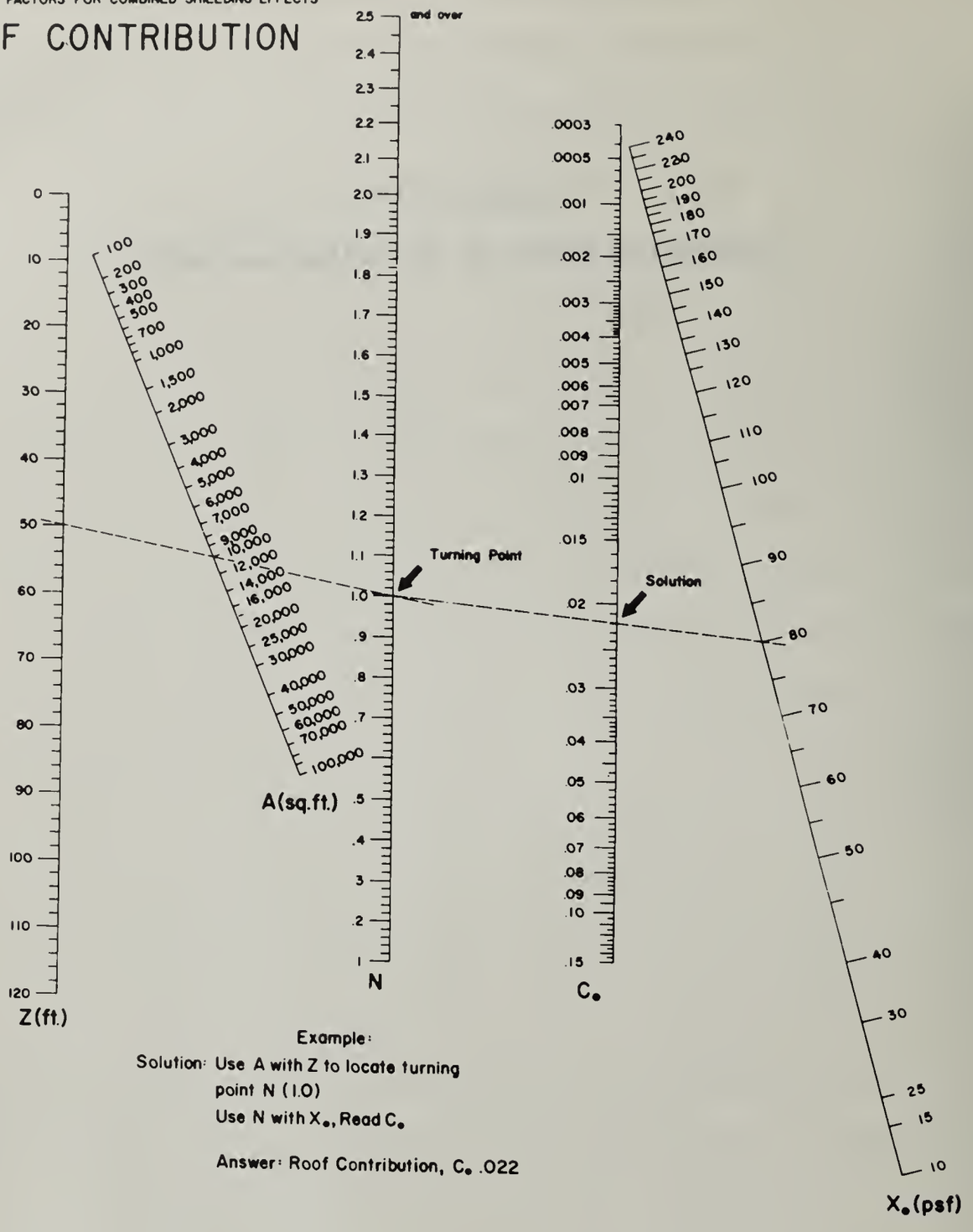

Example:

Solution: Use A with Z to locate turning point N (1.0)
Use N with X_o, Read C_o

Answer: Roof Contribution, C_o .022

Nomogram–I

Nov. 1963

REDUCTION FACTORS FOR COMBINED SHIELDING EFFECTS

GROUND CONTRIBUTION-ABOVEGROUND AREAS

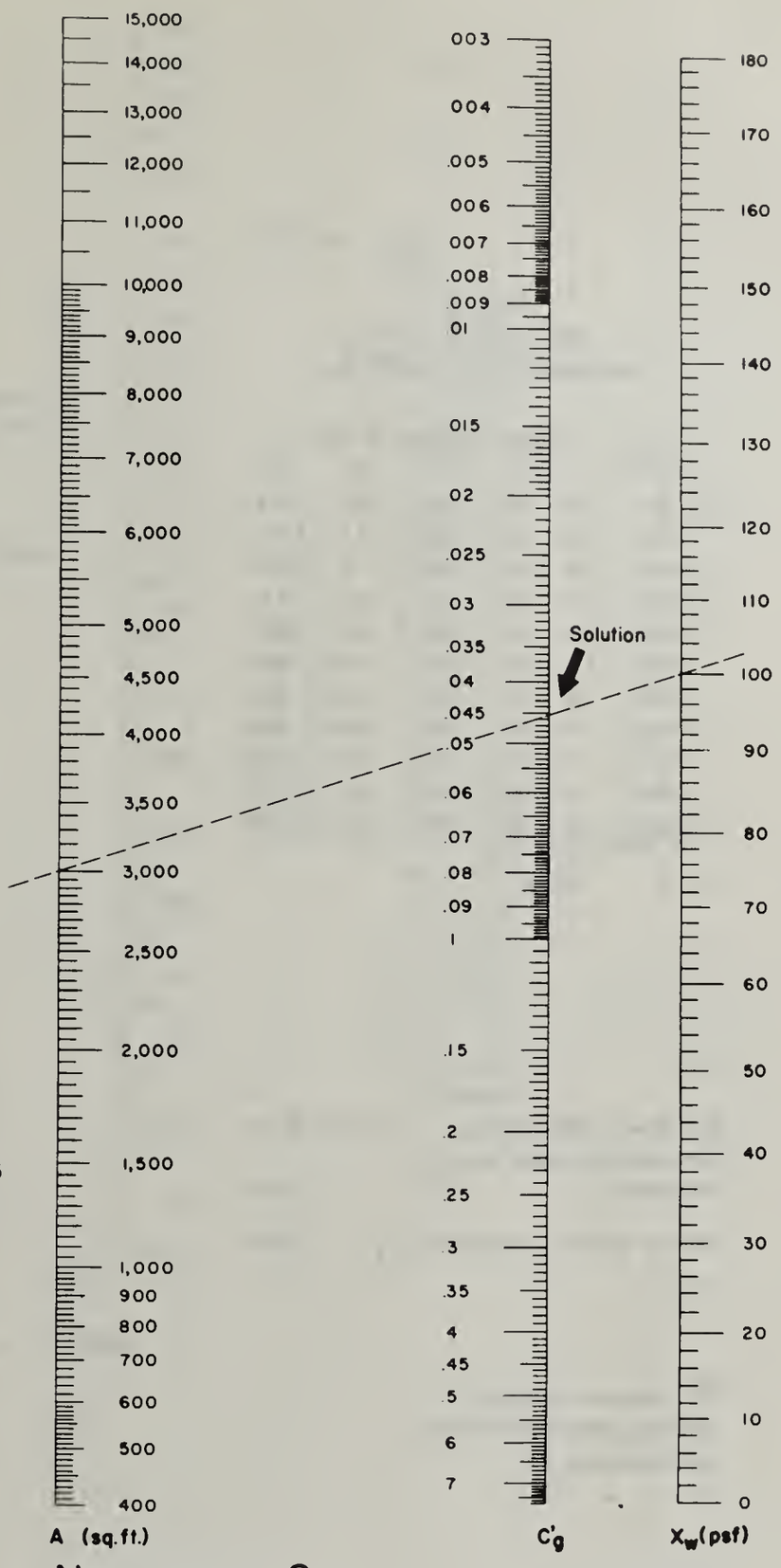

Example

Ground Floor Area, A = 3000 sq.ft.

Wall Mass Thickness, X_w = 100 psf

Solution: Ground Contribution, C'_g .0455

Nomogram -2

Nov. 1963

GROUND CONTRIBUTION - BELOWGROUND AREAS

Toble II

MULTIPLIER FOR

BASEMENT EXPOSURE (K_b)

Areo sq. ft.	Exposed bosement in feet 1'	2'	3'	4'	5'*
up to 400	.35	.70	1.05	1.40	**1.75**
1000	.32	.64	.96	1.28	**1.60**
2000	.28	.55	.83	1.10	**1.38**
3000	.24	.47	.71	.95	**1.19**
4000	.21	.42	.63	.84	**1.05**
5000	.19	.38	.57	.76	**.95**
6000	.18	.35	.53	.70	**.88**
7000	.17	.33	.50	.66	**.83**
8000	.16	.31	.47	.63	**.79**
9000	.15	.31	.46	.61	**.77**
10000 or over	.15	.30	.45	.60	**.75**

Exomple:

Wall Mass Thickness, X_w	80 psf
Immediote Overhead Moss Thickness, X'_o	50 psf
Solution: Ground Contribution, C'_g	.00146

*For exposures which put detector obove ground level, use Nomogrom 2.

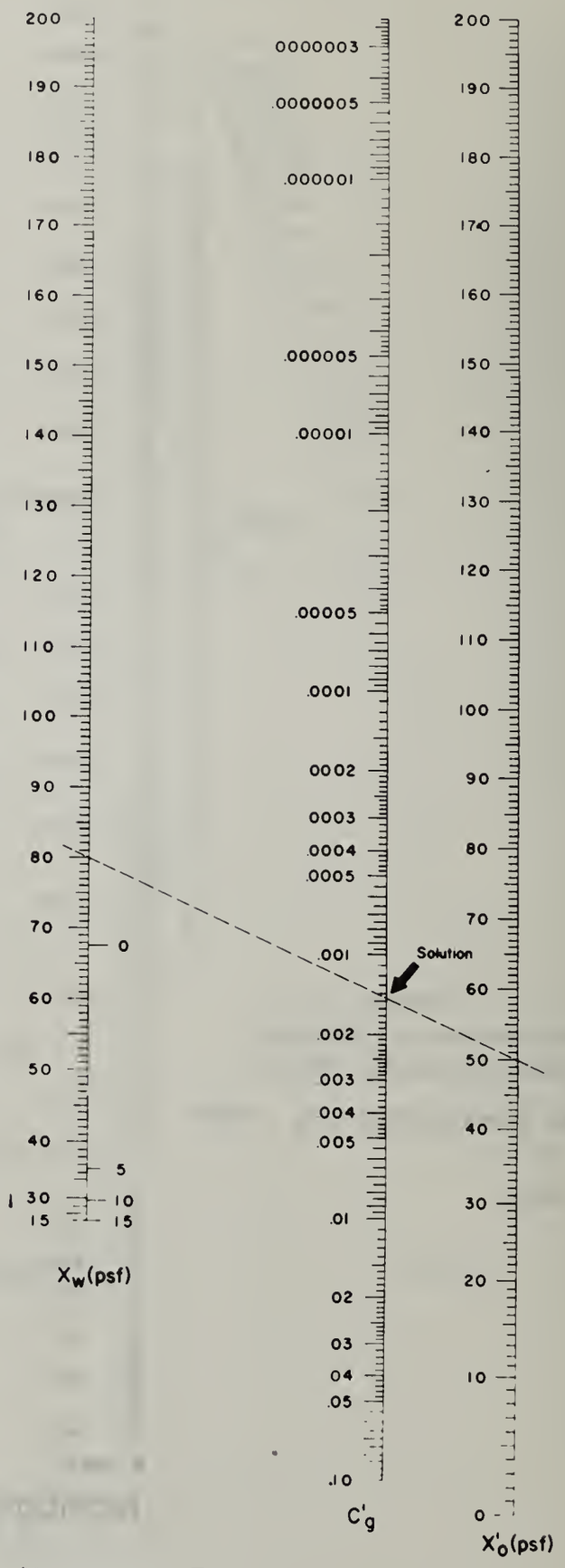

Nomogram-3

Nov 1963

MS, FRACTION OF FIRST STORY INFINITE FIELD DOSE FROM A FINITE RECTANGULAR FIELD

Case A - Upper Stories, Thin Floors ($X_f \leq 50$ psf), and First Story, Thin or Thick Floors.

Case B - Upper Stories, Thick Floors ($X_f > 50$ psf)

Example

First Story Detector, H = 3 ft.,
W_c = 100 ft.
Use Case A
Solution: MS = .825

Fourth Story Detector, H = 40 ft.,
X_f = 80 psf, W_c = 60 ft.
Use Case B
Solution: MS = .025

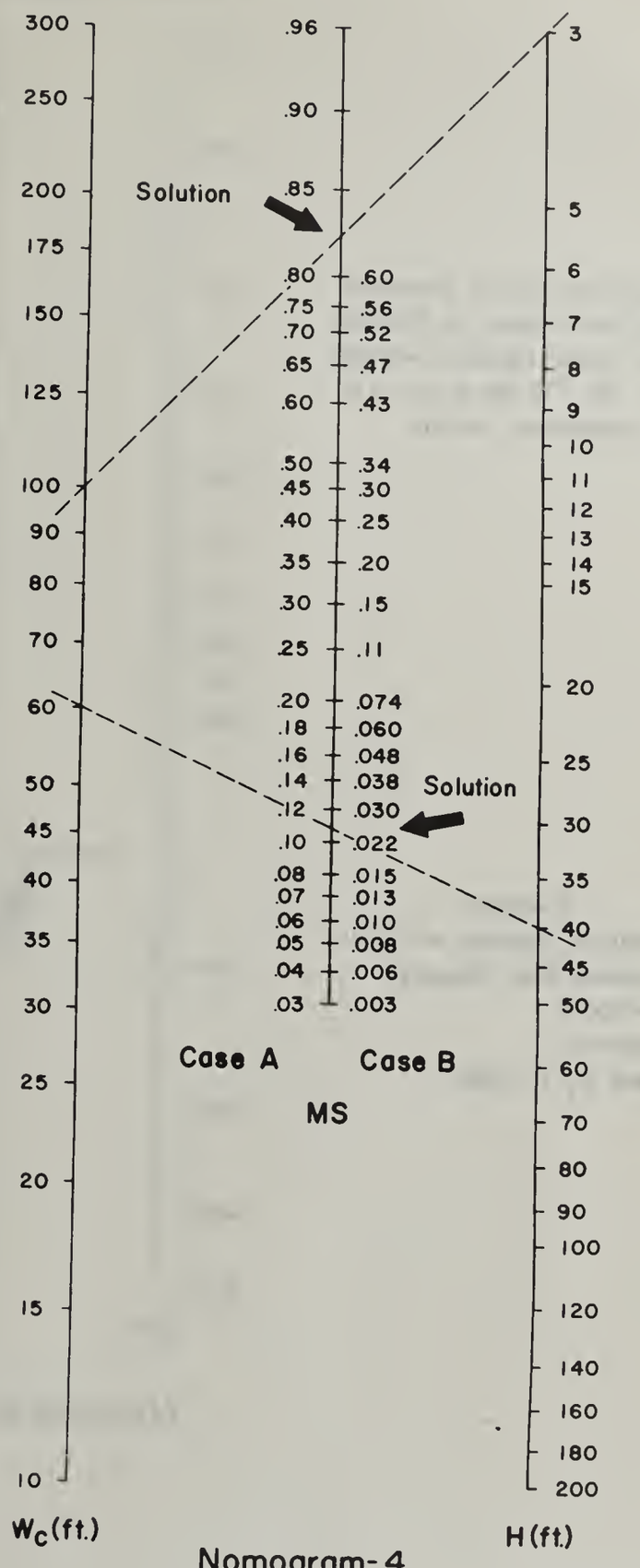

Nomogram-4

Nov. 1963

Reduction Factors for

HORIZONTAL PASSAGEWAYS

(Single Opening)

Reduction Factor Computed for 10 ft. Height of Opening. For Other Heights, Increase "d" by 1% for Each 2 ft. of Additional Height.

Example

Width of Opening, W = 20 ft.;
Distance from Opening, d = 200 ft.
Solution:
Read R_f = .00187

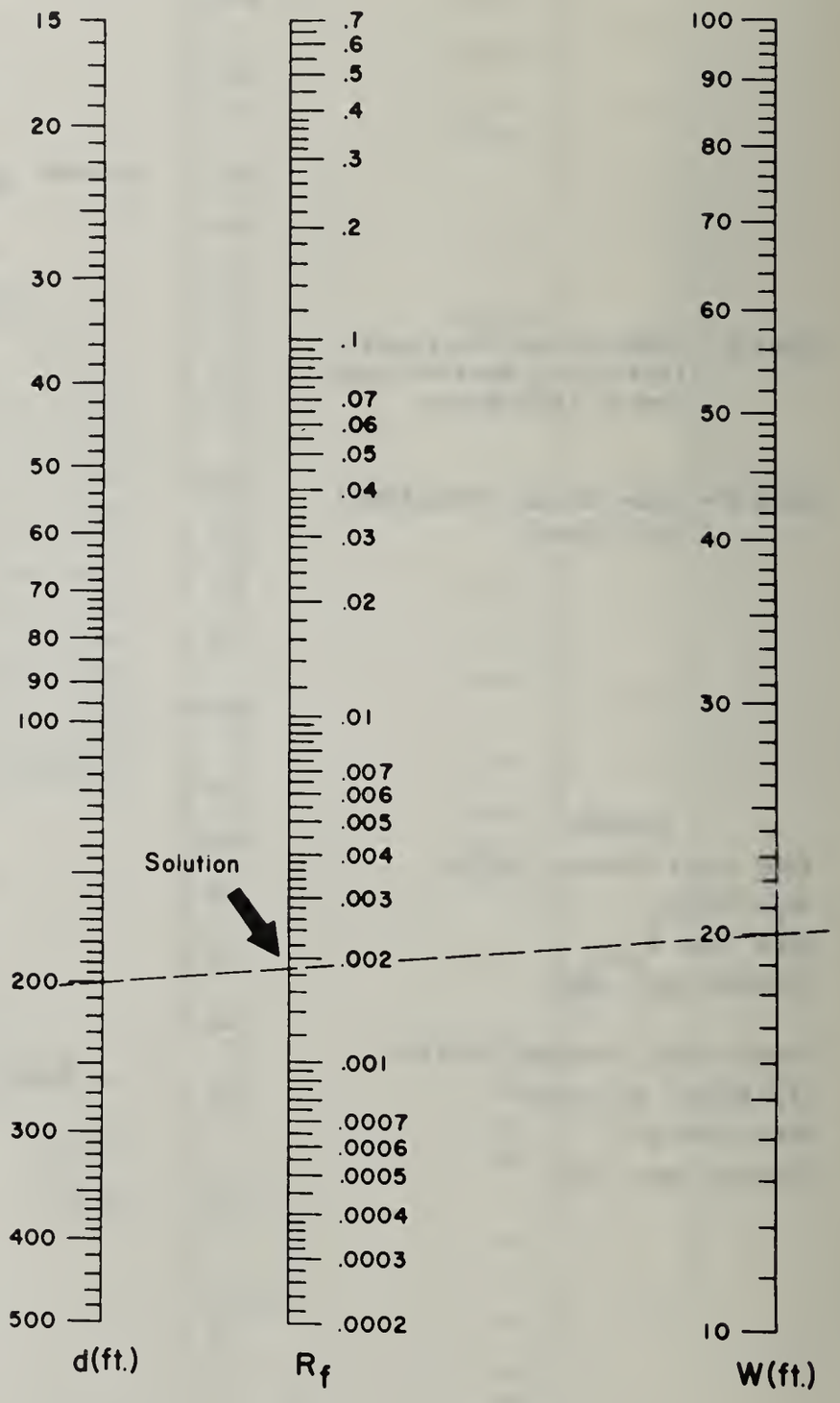

Nomogram-5

Nov. 1963

U.S. GOVERNMENT PRINTING OFFICE : 1967 O—240-816